THE TENTH SCANDINAVIAN INTERNATIONAL CONFERENCE ON FLUID POWER

PROCEEDINS OF THE CONFERENCE

Volume 1

MAY 21-23, 2007

TAMPERE, FINLAND

Editors: Jani Vilenius and Kari T. Koskinen

Technical editor: Janne Uusi-Heikkilä

ISBN 978-952-15-1757-0
978-952-15-1758-7 (Vol. 1)
978-952-15-1759-4 (Vol. 2)
978-952-15-1760-0 (Vol. 3)
978-952-15-1761-7 (CD-ROM)
978-952-15-3272-6 (PDF)

ORGANISING COMMITTEE

Professor Matti Vilenius, TUT / IHA, Conference Chairman
Professor Kari T. Koskinen, TUT / IHA, Conference Vice Chairman
Senior Researcher Jani Vilenius, TUT / IHA, Conference Manager
Secretary Virpi Multanen, TUT / IHA, Conference Secretary
Professor, Senior Adviser for Board of Manag. Matti Kleimola, Wärtsilä Corp.
Professor Aarne Halme, TKK / ATL
Manager, Research and Rock Drills R&D Erkki Ahola, Sandvik UGHRM
Director Technology and Engineering Seppo Taatila, Ponsse Oyj
Managing Director Kalle Tuohimaa, Bosch Rexroth Oy
Technical Director Jussi Hanski, Parker Hannifin Oy Lokomec
General Manager Risto Käkelä, Avant Tecno Oy
Vice President R&D Juha Mäkitalo, Finn-Power Corp.
R&D Manager Merja Lämsä, AarhusKarlshamn Ab Technical Products
Vice President Ilari Orpana, Polarteknik PMC Oy Ab / Chairman of FHPA
Section Manager Olli Pohls, Hytar Oy Water Hydraulics
Professor Kalevi Huhtala, TUT / IHA
Professor Petteri Multanen, TUT / IHA
Professor Jari Rinkinen, TUT / IHA
Professor Tapio Virvalo, TUT / IHA

SICFP'07 Secretariat
Chairman Prof. Matti Vilenius

Institute of Hydraulics and Automation (IHA)
Tampere University of Technology (TUT)
P.O.Box 589
FI-33101 Tampere, Finland

Tel. +358 3 3115 2264
Fax +358 3 3115 2240

PREFACE

This year we really have reason to celebrate! This is the *tenth* time SICFP is organized.

The first international conference on fluid power in Tampere was held in 1987. That was the start of the series of Scandinavian fluid power conferences. In 1993 it was decided that the name of the conference is Scandinavian International Conference on Fluid Power. At the same time it was also decided that SICFP will be held every second year alternately in Tampere and Linköping. So we have already a 20 years' tradition, which is also worth of celebration.

This conference is organized by Institute of Hydraulics and Automation (IHA) at Tampere University of Technology (TUT) together with network of Fluid Power Centres in Europe (FPCE).

This tenth anniversary conference includes various traditional themes like mobile hydraulics, water hydraulics and industrial hydraulics. However, in addition this time there are many more new areas included like digital hydraulics, intelligent mobile machines and teleoperation. They are reflecting well the situation, where electronics, modern information and communication technology is integrating with traditional hydraulics and automation.

We received about 125 interesting and high-level proposals. In addition to five invited speakers, about 80 papers were selected for the final programme. We believe that the conference will give the participants fine opportunities to listen interesting presentations, to exchange opinions and strengthen of old contacts and to establish new ones.

This time the conference proceeding will be published as a printed book and also as a cd-rom. We hope that this proceedings will serve you well during the conference but also far in the future as a source of reference.

We would like to express our sincere appreciation to everybody who has contributed to the success of the conference.

Tampere, 4th of April, 2007

Kari T. Koskinen, Professor
Vice-Chairman, SICFP07

Jani Vilenius, Dr. Tech.
Conference Manager, SICFP07

TABLE OF CONTENTS – Volume 1

PLENARY SESSION P1

SESSION A1: Power Transmissions

SESSION B1: Water Hydraulic Systems

SESSION C1: Aircraft Hydraulics

SESSION A2: Digital Hydraulics

SESSION B2: Pumps

Revolution in Dynamics and Force: New Drive Technology For Proportional & Servo Valves

Dipl.-Ing. Hansgeorg Kolvenbach
Parker Hannifin GmbH & Co. KG
Hydraulic Controls Division Europe
Gutenbergstrasse 38
41564 Kaarst, Germany
Phone +49 2131 513 225, Fax +49 2131 513 285
E-mail: hansgeorg.kolvenbach@parker.com

ABSTRACT

This paper introduces a new, patented drive technology for hydraulic proportional control valves. A comparison of currently utilized technology in today's industrial product offerings of torque motor and solenoid operated first stage control devices leads to requirements and recommendations for a new technology. The practical realisation and possible applications are shown by examples.

KEYWORDS: Electro hydraulics, Servo valve, Proportional valve, VCD Technology, Voice Coil Drive

1 INTRODUCTION

Since proportional technology was introduced to hydraulics in the mid-1970's, all valve developers and manufacturers have continuously strived to deliver more precise and more dynamic valves in order to match the growing demands of the markets. The need for higher accuracy in closed loop positioning applications, increased load stiffness in conjunction with high volumes of flow or pressure drops and higher resolution in pressure controls, have been driving innovation in this area.

Up to now, mainly two types of electromechanical transducers have established themselves: The torque motor drive, used since the 1950's, and the proportional solenoid.

Today, the proportional solenoid is being used in most of the products, as it is more robust and more cost-effective than the torque motor drive. But the solenoid is also less dynamic.

Either of these drive technologies provides specific advantages as well as disadvantages. These are discussed in this paper and result in the requirement for a " better" drive technology, the realisation of which will ultimately be described .

2 STATE OF THE ART

Figure 1 shows a comparison of the most commonly known electromechanical drive principles, of which torque motors and proportional solenoids are the primary principles in use today.

elektrom. Wandler	piezostriktive Wandler	Tauchspule	Proportionalmagnet	Schaltmagnet	Linearmotor	Torque-Motor
Ausführungsbeispiel	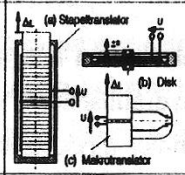	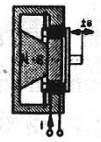	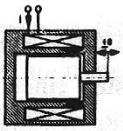	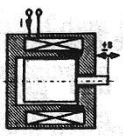	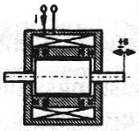	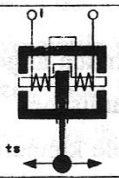
Kennfeldcharakteristik	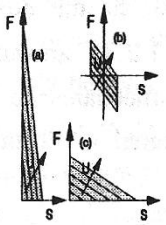		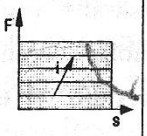	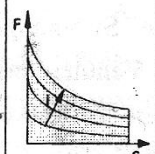	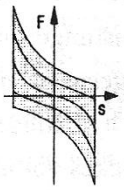	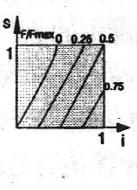
erreichbare Hübe	(a) < 0,18 mm;	(b) < 0,2 mm;	(c) < 1 mm	> 2 mm	2 ... 4 mm	3 ... 8,5 mm	0,7 ... 2 mm	
zugeh. Maximalkräfte	3500 N;	35 N;	50 N	> ± 10 N	55 N ... 180 N	55 ... 200 N	±100 ... ±300 N	
Hubarbeit	>400 Nmm;	7 Nmm;	50 Nmm	> 40 Nmm	80 ... 320 Nmm	75 ... 800 Nmm	140 ... 780 Nmm	
Hubarbeit/Bauvolumen	ca. 5;	0,25;	1 N/mm/cm^3	ca. 0,5 Nmm/cm^3	1,4 ... 1,8 Nmm/cm^3	2,1 ... 2,6 Nmm/cm^3	1,5 ... 2,5 Nmm/cm^3	
Hysterese	nur mit Lageregelung gering			gut	gesteuert < 4%	k.A.	k.A.	k.A
Linearität	nur mit Lageregelung gut			auch gesteuert gut	gut	Korrekturregelung erf.	ohne Regelung mäßig	gut
Resonanzfrequenz	>2000 Hz;	1100 Hz;	100 Hz	typ. 200 Hz	<190 ... 80 Hz	k.A.	ca. 260 Hz	100 ... 300 Hz
Eingangsleistung	typ. 50 W			30 W	18 ... 32 W	16 ... 38 W	7,2 ... 65 W	0.02 ... 4 W
Bauaufwand	hoch (präzise Teile erford.)			teurer Permanentmag.	mäßig (Steuerkonus)	ohne Regelung gering	teure Permanentmag.	teure Permanentmag.
Druckfestigkeit	-			druckfester Stecker erf.	Standardausführung	Standardausführung	ja	ja
Bemerkung	teuer und (a) baut lang			geringe Kraftdichte	kein fail-safe	kein fail-safe		

Figure 1: Electromechanical Transducer [1]

The proportional solenoid was developed based on ON/OFF Solenoid Technology. By influencing the magnetic flux in the air gap (**Figure 2**) the stroke vs. force curve is linearised in a certain stroke range. The force level there is proportional to the coil current. The force acts unidirectionally (i.e. pushing only) due to the principle, i. e. for retraction, a spring, or any other active element, is needed. A typical force vs. stroke curve is shown in **Figure 3**.

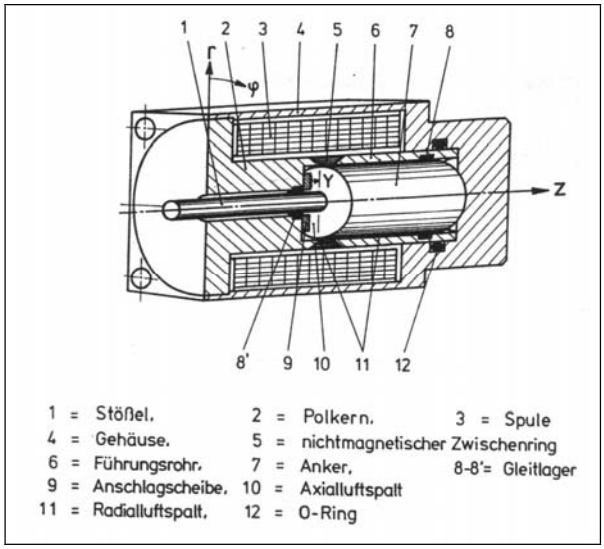

Figure 2: Proportional Solenoid [1]

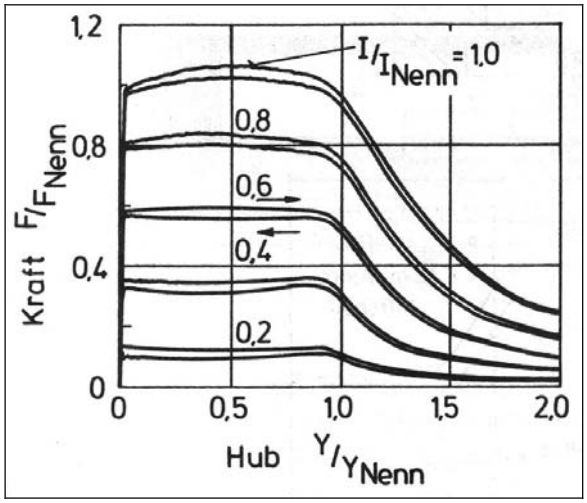

Figure 3: Force vs. Stroke Curve Proportional Solenoid [1]

Today's proportional solenoids can generate forces of up to 180N but have the disadvantage of a relatively large space envelope. Lift work of up to 320Nmm corresponding to lift work per volume (density of force) of 1.8N/cm³ can be achieved.
Hydraulic valves of nominal size 6 (CETOP 3) normally work with coil diameters of 45mm and therefore achieve a maximum force of approximately 100N.
Typical 90° phase shift frequencies at small command signal input are 200Hz.[1]

Torque motors are mainly used in so-called servo valves. The term "servo valve" was originally used to describe all kinds of highly dynamic valves. Along with the improved dynamics of solenoids the term "servo valve" today stands only for torque motor driven valves.

Due to their design principle, torque motors do not generate forces comparable to those of solenoids. Therefore, they always require a kind of amplification stage like nozzle-flappers or jet pipe designs to use the hydraulic forces for moving the valve's spool. This makes them dependent on the supply pressure, which has to be kept at much more constant levels compared to proportional solenoid driven valves.

The principle of torque motors is based on a rotary anchor with two coils placed in a permanent magnetic field. When no current is applied to the coils, this results in an unstable equilibrium to the torque of a spring. When current is led through the asymmetrically wound coils, the anchor itself generates a magnetic field that, together with the permanent field, produces a momentum. The anchor rotates to a position at which a stable equilibrium between its own torque and the torsion spring force has been reached. **Figure 4** shows a typical stroke vs. current curve, **Figure 5** shows the mechanical principle.

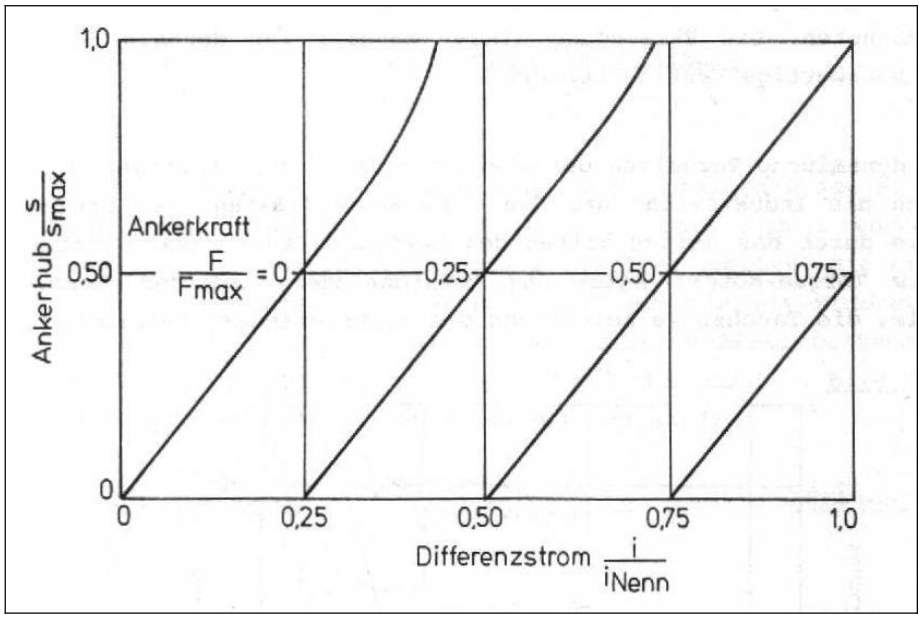

Figure 4: Stroke vs. Current Curve Torque Motor [2]

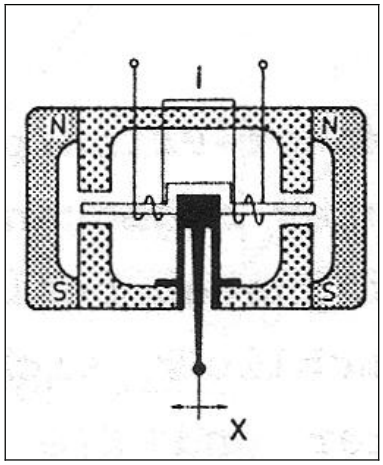

Figure 5: Mechanical Principle of a Torque Motor [2]

Torque motor driven valves achieve 90° phase shift frequencies at small command signals of up to 500Hz.

Now the major differences between these two technologies become evident:
Proportional solenoids generate high forces with limited dynamics,
while torque motor drives generate high dynamics but low forces.

The force of a drive has a major influence on the performance of a valve.

High differential pressures excite higher flow speed and therefore higher flow forces that tend to move the valve's spool in the closing direction.
These forces are added to the forces of the springs in the valve that hold the spool in equilibrium to the solenoid force. Obviously a high percentage of the solenoid force is needed to overcome the spring force, leaving only a small amount to compensate for the flow forces and to generate dynamics. This produces the flow limit curve of a standard proportional valve, which defines the maximum differential pressure above which the solenoid is no longer able to keep the spool positioned. The valve will start to close itself, regardless of whether it is closed-loop-controlled or not.

Torque motors do not act directly on the spool but through indirect, hydraulic amplification and therefore do not have a flow limit curve. Hydraulic amplification, however, requires a permanent pilot oil flow and generates losses. Each variation of the pilot oil pressure immediately influences stiffness and accuracy of the spool position. Even an electronic closed loop control cannot eliminate this influence. Additionally, the mechanics of a torque motor are much more sensitive and more expensive than those of proportional solenoids, which offsets their dynamic advantage to some extent.

3 REQUIREMENTS

The comparison of chapter 2 leads to requirements to be met by "new" drive technology:

1. It should provide dynamic data like torque motor drives combined with the force levels of proportional solenoids.
2. Hysteresis due to friction should be avoided.
3. A linear correlation between current and force has to be achieved.
4. The drive should be able to work bidirectionally, i. e. push and pull, in order to avoid "investing" force into a spring.
5. As a minimum, the robustness of proportional solenoids should be achieved and power consumption and cost should not exceed those of proportional solenoids.

Requirements number 1 and 2 are focused on achieving highly dynamic performance. Numbers 3 and 4 should achieve good closed loop control performance and high load stiffness. Number 5 is necessary for applications in rough, industrial environments.
At first glance, these requirements seem to be mutually exclusive, but a closer look at the principle shows that a voice coil fulfills most of them. Merely the force level and the costly permanent magnets seem to conflict with these requirements, according to current literature.

4 VCD® Technology

Voice **C**oil **D**rive (VCD®) technology is based on the loudspeaker principle and has been modified and optimised in order to meet all the requirements named in chapter 3.

The VCD® Drive works according to the electrodynamic principle: Inside a magnetic field a force is exerted on an electric conductor proportional to the current in it. [3]

If the magnetic induction B and the current I in the electrical conductor are oriented vertically to each other, then the vector product is transformed to a scalar product and the resulting force is again perpendicular to I and B:

$$F = n \cdot i \cdot l \cdot B \qquad (1)$$

The force generated is directly proportional to the current, the length of the electrical conductor in the magnetic field and to the magnetic induction.
The current should not exceed 4A at 100% up-time in order to achieve the same parameters as today's proportional solenoids.
The length of the conductor, i. e. the length of one coil winding, is limited by the outer dimensions of a NG6 valve body to max. 46mm length of one side.
Therefore the number of windings n and the magnetic induction B remain the only variable parameters to achieve the highest possible force per volume. A compromise will have to be found between the overall length of the actuator and the cost for permanent magnets.
The major progress that has been achieved in recent years in the area of rare earth magnets has a positive impact on this compromise.
Supported by simulations, the optimum combination of windings and induction to achieve a force level of 100N has been calculated and resulted in lift work of 300Nmm, corresponding to a force per volume of 1.2Nmm/cm³.
These values are comparable to proportional solenoids.

Figure 6 shows the cross section of a VCD® actuator:

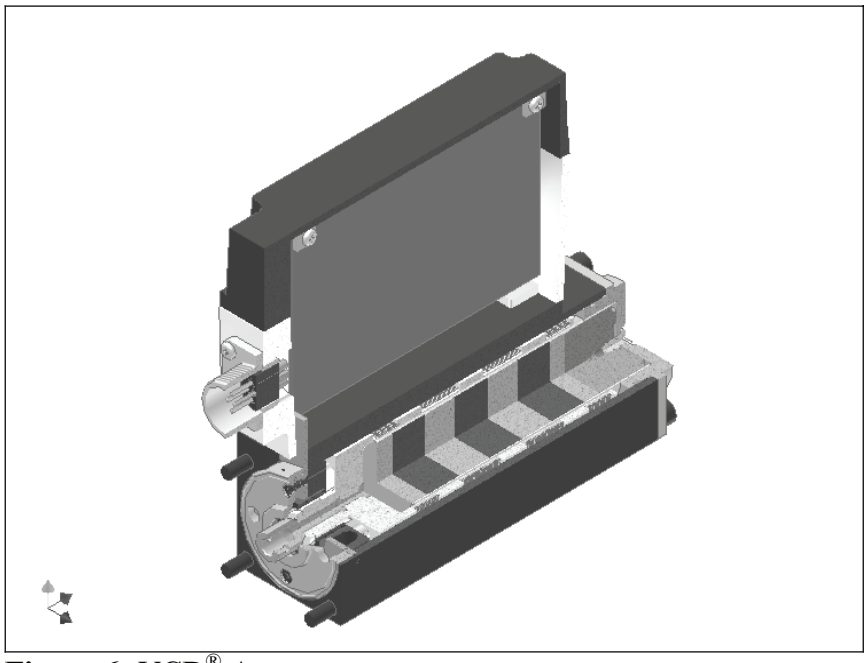

Figure 6: VCD® Actuator

A permanent magnetic rod in the center creates a vertically oriented magnetic field in the radial air gap. A coil wound onto a plastic molded carrier can freely move inside the air gap. The windings of this coil are perpendicular to the field so that, depending on the direction of the current, either a pushing or a pulling axial force is generated. The carrier transmits the force directly to the valve's spool inside a bushing. This is the only bearing in the complete valve. Therefore, the actuator itself does not create any friction

and is free of hysteresis. Additionally, this kind of actuator does not generate lateral forces due to the orientation of windings, current and magnetic field. The drive is able to push and pull depending on the current's direction and can thus operate without any spring inside.
At the connection between the carrier and the spool a position feedback system could be integrated into the actuator, allowing a precise closed loop position control of the actuator to be achieved.
The minimal amount of moving mass combined with the afore-mentioned advantages of zero friction and zero hysteresis results in dynamics of the VCD® actuator comparable to torque motor drives. The force of 100N is nearly completely available to accelerate the drive and to work statically against the flow forces on the spool.
This means that the objective of combining the advantages of proportional solenoids and torque motors while eliminating all the disadvantages of both technologies has been achieved.

5 Comparison of Simulation and Measurements

The system equations to simulate the drive are

$$u(t) = z \cdot B \cdot \pi \cdot d \cdot n \cdot \frac{d}{dt} \cdot x(t) + z \cdot L \frac{d}{dt} \cdot i(t) + z \cdot R \cdot i(t) \qquad (2)$$

and

$$z \cdot B \cdot \pi \cdot d \cdot n \cdot i(t) = m \cdot \frac{d^2}{dt^2} \cdot x(t) + b \cdot \frac{d}{dt} \cdot x(t) + f(x) \qquad (3)$$

Equation (2) describes the sum of all voltages with the respective terms for voltage induced by motion, self-induced voltage and ohmic voltage drop.
The equation of dynamic motion (3) describes the balance between electrodynamically generated force (see equation (1)) and inertial force, damping force and load force.
Figure 7 shows a comparison between simulated and measured step response of 100% stroke at a pressure of 350bar.

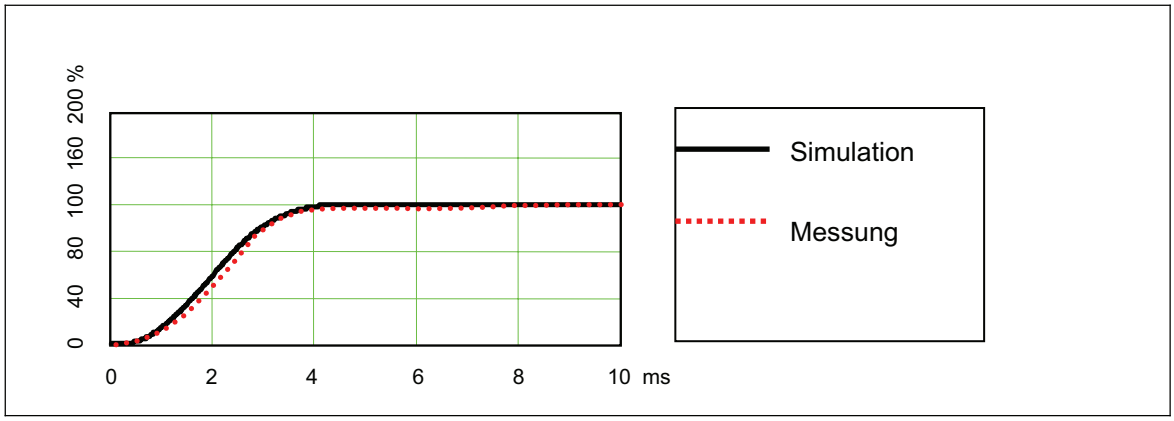

Figure 7: Comparison between Simulated and Measured Step Response

6 Features of DFplus® Valves with VCD® Technology

VCD® technology has been successfully applied to the valve series DFplus®.

DFplus® valves are control valves available in sizes 6 (CETOP 3) and 10 (CETOP 5). The size 6 valves are characterized by a 90° small signal natural frequency of 350Hz, no flow limitation up to 350bar pressure drop, a bidirectional working spool with 100N chip shear force and an absolutely robust industrial construction.
The 90° natural frequency is twice as high as with solenoid driven valves and even outperforms many standard servo valves.

Therefore DFplus® valves provide extremely high accuracy in closed loop controls.
Setup and tuning of closed loop controls becomes less critical as DFplus® valves allow higher gains and provide linear flow curves. Spark-eroded windows in the bushing ensure reproducible high resolution of flow.
Especially with very small cylinders that take over the dynamics of the controlling valve due to their low natural frequency, precision can be significantly increased.

7 Summary

A comparison of the most commonly used electromechanical transducers for hydraulic valves points out the dilemma of today's proportional hydraulics: The advantage of high dynamics in torque motor driven valves is offset by high costs and sensitivity to inconsistent pressures as well as dirt. The robustness advantage in proportional solenoid driven valves on the other hand limits dynamics. The unidirectional function requiring a spring results in loss of force and limits the scope of applications.
The solution is a drive that combines high levels of actuating force with high dynamics in bidirectional operation.
Such a drive is now available as part of the DFplus® valve series with VCD® technology made by Parker Hannifin GmbH & Co. KG. This technology meets all the requirements mentioned in this paper and expands the limits for the use of voice coils in hydraulics in terms of lift work and lift work per volume as stated in current literature [1].

References

[1] Backé, W. ; Murrenhoff, H.
Steuerungs- und Schaltungstechnik II (Proportionaltechnik)
IFAS RWTH Aachen, Umdruck zur Vorlesung, 4. Auflage 1993

[2] Backé, W.
Servohydraulik
IHP RWTH Aachen, Umdruck zur Vorlesung, 6. Auflage 1992

[3] Ameling, W.
Grundlagen der Elektrotechnik I
Vieweg, 4., berichtigte Auflage, 1988

Nomenclature

B	magnetic induction	T (Vs/m²)
b	damping coefficient	kg/s
d	coil diameter	m
F	force	N
f	load force	N
i	current	A
l	length of one winding	m
L	inductance	H
m	mass	kg
n	number of windings	-
R	resistance	Ohm
t	time	s
u	voltage	V
x	stroke	m
z	number of modules	-

DYNAMIC MODEL OF CVT POWER TRAIN

M.Sc. Mikko Erkkilä
Tampere University of Technology
Institute of Hydraulics and Automation
P.O.Box 589
33101 Tampere, Finland
Phone +358 3 2115 3286, Fax +358 3 3115 2240
E-mail: mikko.erkkila@tut.fi

ABSTRACT

The paper presents a simulation model for a CVT Power train, consisting of sub models for diesel engine, hydrostatic, CVT gearbox and clutches, wheel-road-connection and vehicle. The main design features and verification of the sub models are presented. The model is designed for virtual design and testing of the CVT control unit. The main control function requirements are presented. The power rain model can also be used in "Hardware in the Loop" simulation for testing the designed CVT control unit. The Hardware in the Loop special requirements for simulation model is briefly mentioned. Simulation examples are presented and analysed in the paper.

KEYWORDS: CVT, Modeling, HIL, Driveline

1 MODELLING OF SYSTEM COMPONENTS

1.1 Purpose

The dynamic model of the complete power train starting from diesel engine to the driving wheels was developed for stability examination of the system and for development of the control unit and control algorithms.

1.2 Design and features

In the beginning of this work individual models of most of the components were already available, and the first idea was to build the complete system using the existing components. During this work stability and compatibility problems did occur, so it was not possible to get the complete system working in the CVT working area, with those models.

A new design was started in order to develop the model components as simple as possible, including only most significant time constants and characteristics, to enable compatibility and to allow the use of the model in real time.

Figure 1 shows the dynamic model of the power train. The prime mover of the hydrostatic unit and planetary gear is the diesel engine. The input signals for the diesel engine are speed setup value and load torque. The hydrostatic unit is controlled with the displacement command signal and it creates the variable speed n_v to the planetary gear. The CVT areas 1and 2 can be chosen with the $M_{(C1)}$ and $M_{(C2)}$ torque command values, which are created in the clutch actuator models. On the base of output speed n_o and other input signals, the planetary gear and couplings model, creates output torque M_o**,** mechanically transmitted torque M_m and the load torque M_v for the hydrostatic unit. The final drive model calculates from the output torque M_o and the traction effort the wheel speed n_w and output speed n_o for the planetary gear. Finally the vehicle model creates the vehicle velocity and the traction effort on the base of wheel speed n_w**,** wheel slipping factor and load**.**

From the model all interesting data can be recorder and read. In this model configuration the vehicle velocity and acceleration, traction force, sliding, running speed and torque of the planetary gear output and pressure difference in the hydrostatic circuit can be observed.

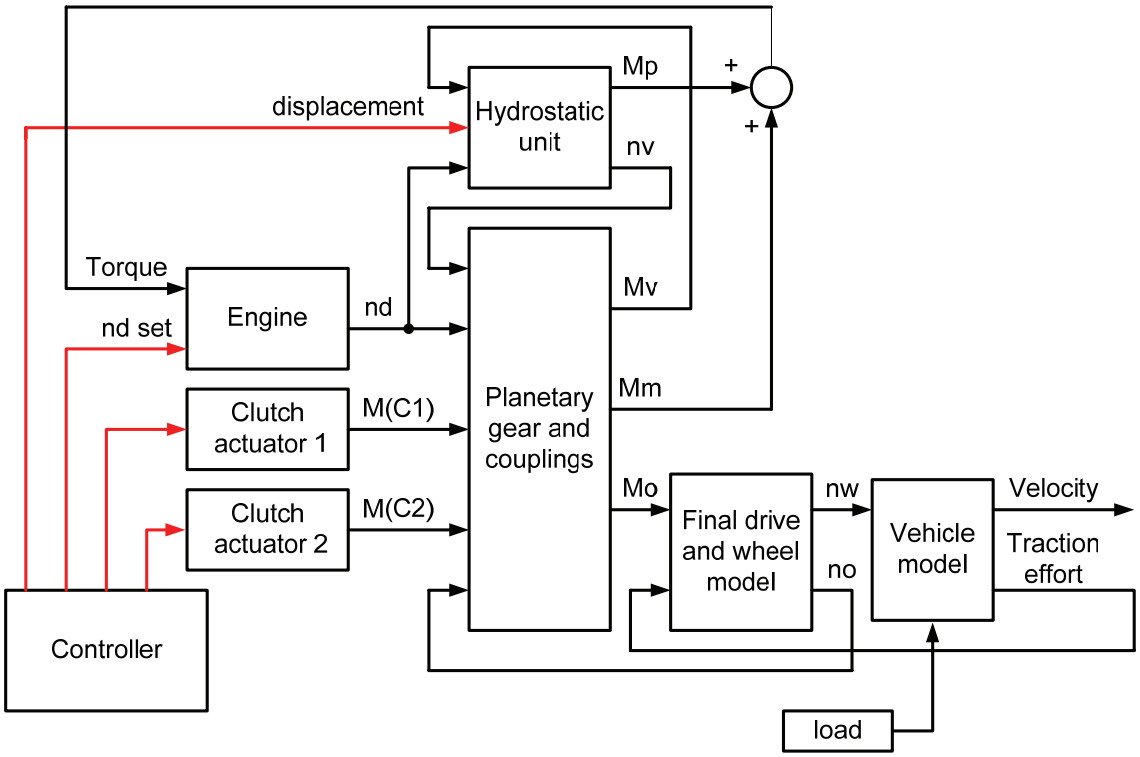

Figure 1 Dynamic power train model

1.3 The model of the hydrostatic drive

The design of the model is based to Huhtala`s dynamic model [1], consisting of models of pump, motor, inertia mass and the compressible oil volume in the circuit, see figure 2. The volumetric and hydromechanical losses of the pump and the motor are the same as used in the steady state calculation model [2].

The control servomechanism of pump is a modeled as second order transfer function.

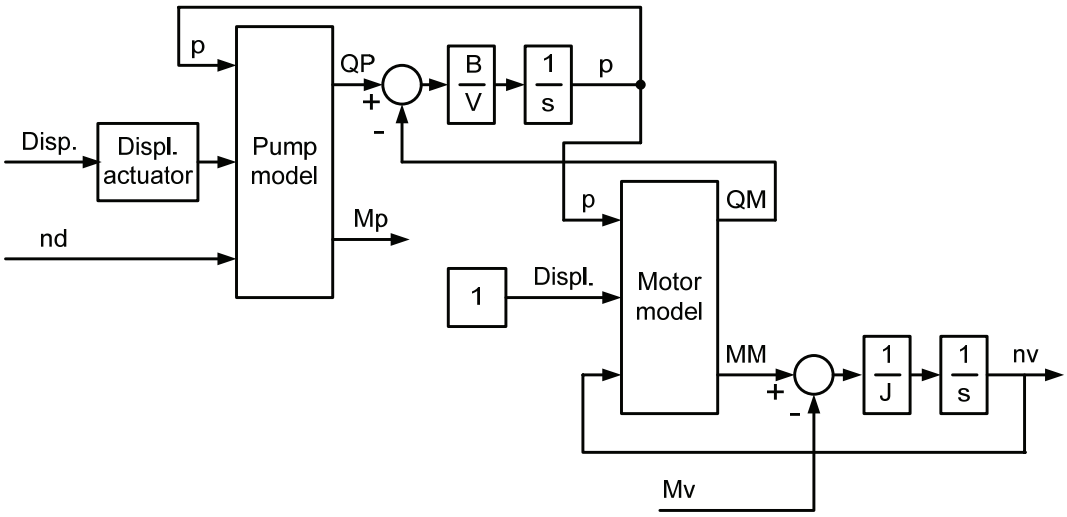

Figure 2: Dynamic hydrostatic model

Figure 3 shows the simulated and measured step responses of the output speed when displacement control signal is changed. The system pressure response, recorded during the same measurement, is shown on figure 4 for the time period starting from 3.4 s to 4.8 s.

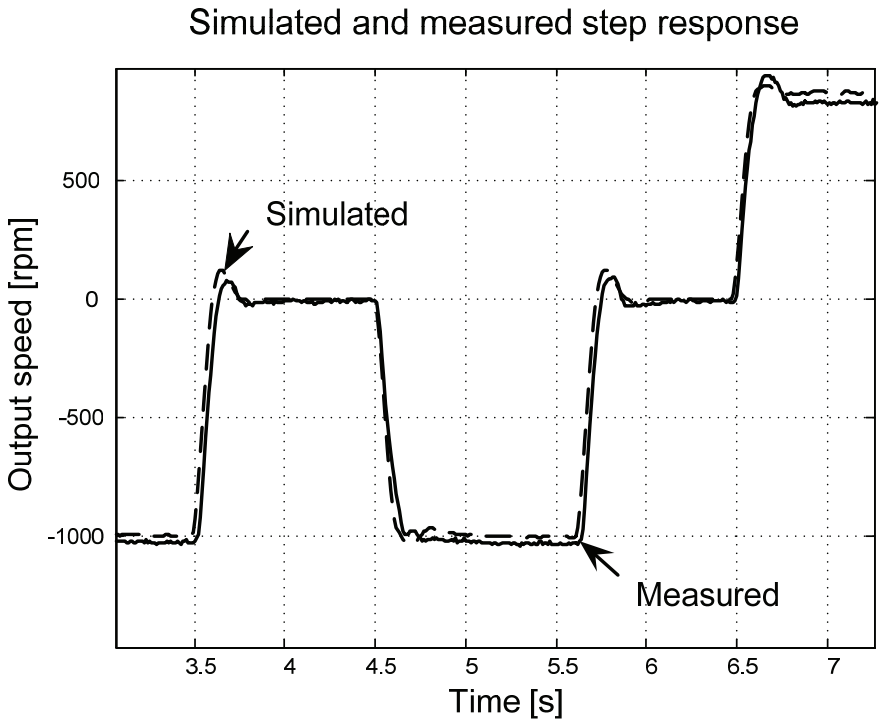

Figure 3: Output speed step response

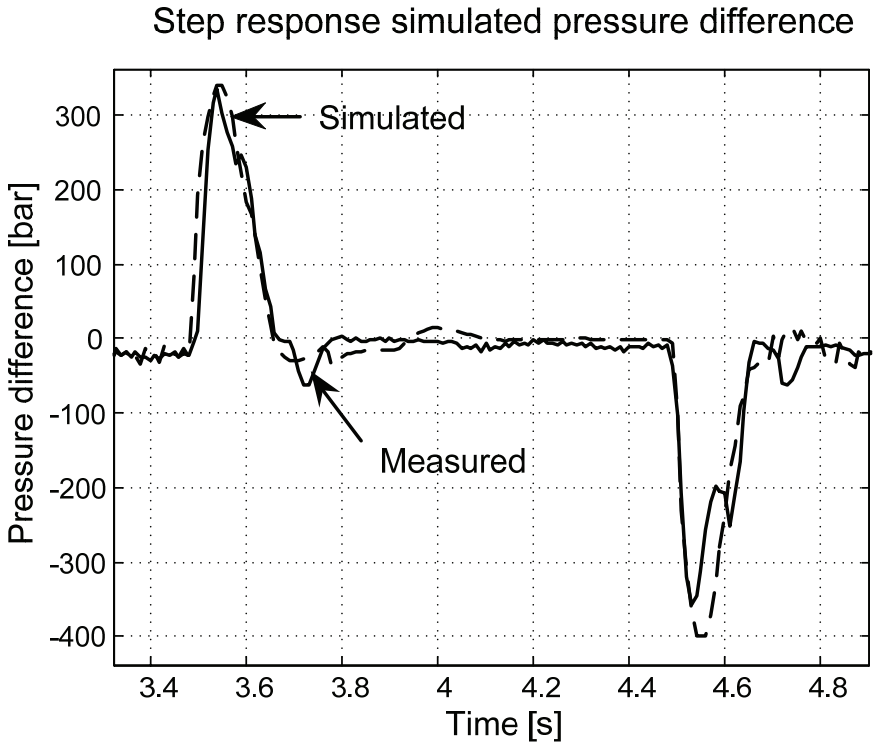

Figure 4: Pressure difference step response

1.3 The clutch model

The required functions for the clutch are following:

- Determine from the input and output speed deviation, the effective torque, and transmit it up to holding torque without sliding
- Limit the output torque to holding torque and allow a continuously speed difference between input and output shafts.
- By exciding the holding torque let the clutch to start to slide.
- When the torque goes below the holding torque the sliding should first stop and then transmit the effective torque.
- For opening and closing the clutch the holding torque should be adjustable.

The lumped clutch model of Farshidianfar, Ebrami and Bartlett [3] presents the holding torque for the clutch as following Laplace transformation:

$$M = \frac{C_d}{s}\left[\omega_o(s) - \omega_i(s)\right] + C_t\left[\omega_o(s) - \omega_i(s)\right] \qquad (1)$$

The holding torque can be seen as a function of the tension angle α of the clutch by marking:

$$\dot{\alpha} = \omega_o - \omega_i \qquad (2)$$

The holding torque differential equation can now be written as:

$$M = C_d \alpha + C_t \dot{\alpha} \qquad (3)$$

is valid for a closed clutch, when the torque M is lower than the clutch holding torque M_c. When the clutch starts to slide, an additional speed difference, the clutch sliding speed ω_s, increases the speed difference between the input and the output speed of the clutch.
In the case of pure coulomb friction the tension angle of the clutch can be assumed to remain the same value in the beginning and during the sliding. By adding the sliding to the equations, it can now be written as follows:

$$\dot{\alpha} = \omega_o - \omega_i - \omega_s \qquad (4)$$

$$M = C_d \alpha + C_t \dot{\alpha} \qquad (5)$$

The sliding of the clutch can be modeled according to the empiric rules:

- The clutch is holding, when the absolute value of the required torque M is less the the holding torque M_c, and it can not start to slide
- The clutch starts to slide, when the required torque M is higher as the holding torque M_c

- If the clutch is sliding and the required torque M is higher then the holding torque M_c the sliding speed will increase, if lower the sliding speed decreases
- The same rules are valid in both directions

The sliding of the clutch can now be described as follows:

$$\dot{\omega}_s = \begin{cases} C_s(M - M_c), \omega_s > 0 \\ C_s(M - M_c), \omega_s = 0, M > M_c \\ 0, \omega_s = 0, -M_c < M < M_c \\ C_s(M + M_c), \omega_s = 0, M < -M_c \\ C_s(M + M_c), \omega_s < 0 \end{cases} \quad (6)$$

Figure 5 shows the simulated behavior of the coupling. The output shaft is loaded with a constant load of 150 Nm and an inertia mass of 2,7 Kgm^2. The dash-and-dot-line is the command signal of the clutch [Nm] and the solid line is the actual value [Nm]. The dotted line is the ω_o rotation speed of the load [rad/s] and the dashed line the ω_s sliding speed [rad /s].

In the begin the load is accelerated with a torque of 300 Nm by reaching the end speed the torque falls to the constant torque load value of 150 Nm. By opening the clutch the load begins to decelerate until it stops. On time point 6s the coupling is closed and after that during the acceleration of the load, the command value coupling is reduced.

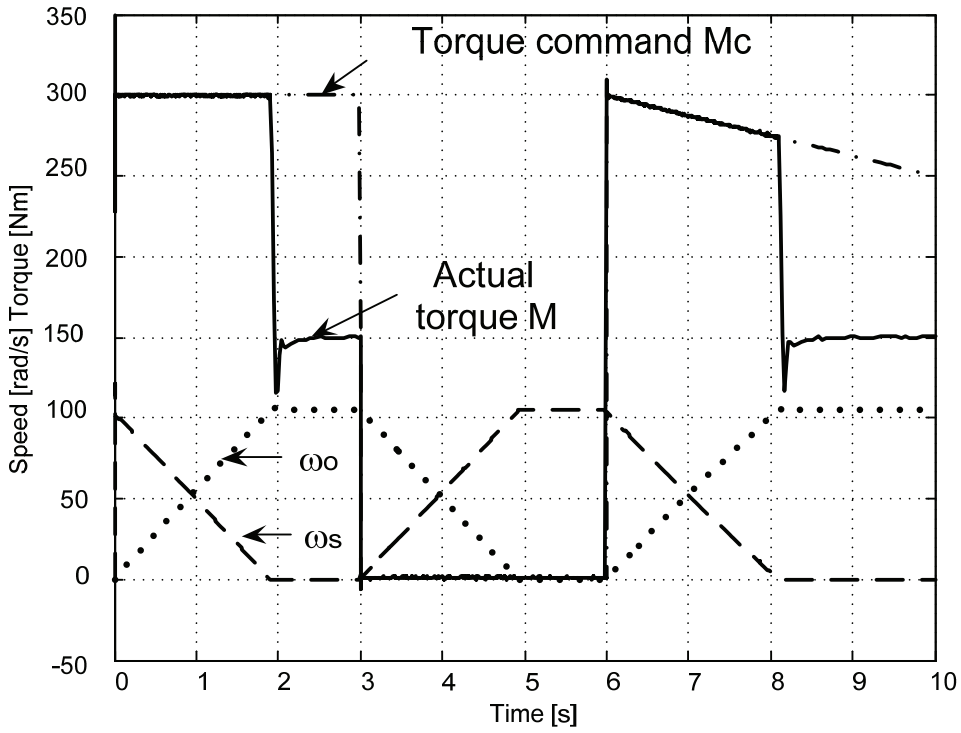

Figure 5: Clutch torque response to command torque

Varied interactive is created when the input shaft speed is changed; figure 6 shows the model response. Dashed line is the input speed, dash-dotted line the output speed, dotted line the sliding and solid line the torque. The mass of inertia was 2.7 kgm^2 and constant load 50 Nm.

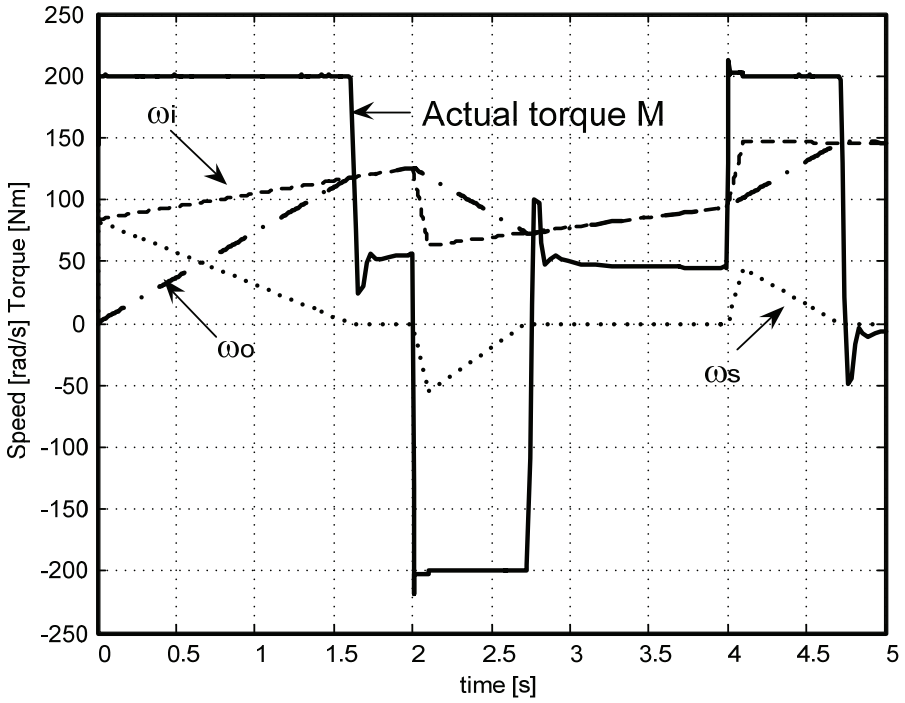

Figure 6: Clutch torque response to input speed.

1.5 Clutch actuator model

The clutch actuator model is based to Viitasalo's [4] Power Shuttle model, see figure 7. In the valve block p_v is the pressure control valve output pressure and Q_v the flow from the pressure control valve to the channels between the valve and cylinder. The Channel block calculates on the base of cylinder pressure p_c and valve flow Qv the valve output pressure pv and cylinder flow Q_c**.** The cylinder position s and velocity **v** and the Shuttle torque M_o are calculated in the Shuttle block on the base of the cylinder force, which is defined in the cylinder block.

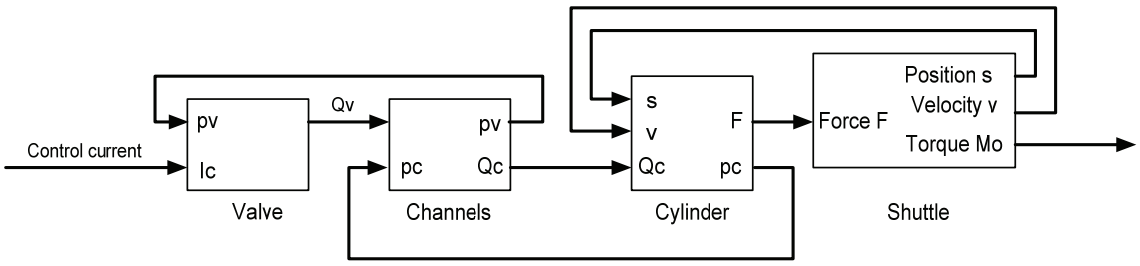

Figure 7: Power Shuttle actuator model

1.6 Tire Road Connection

According to Gustafsson [5] the slip between tire and road can be defined as:

$$s = \frac{\omega_w r_w - v_w}{v_v} \tag{7}$$

The friction coefficient is defined by means of traction force F and normal force N:

$$\mu = \frac{F}{N} \tag{8}$$

The dependence between traction force and slip is presented in a general form:

$$F(s) = D\sin(C\arctan(B(1-E)s - \frac{E}{B}\arctan(Bs))) \tag{9}$$

The tire road model curve on figure 8 is generated using this equation. For the simply modeling of the completely driveline only the rising slope is used, the function can be replaced with:

$$F(s) = N * \tanh(ks) \tag{10}$$

Figure 8 shows the measured friction coefficient vs. slip points and trough the measured point's adjusted curves.

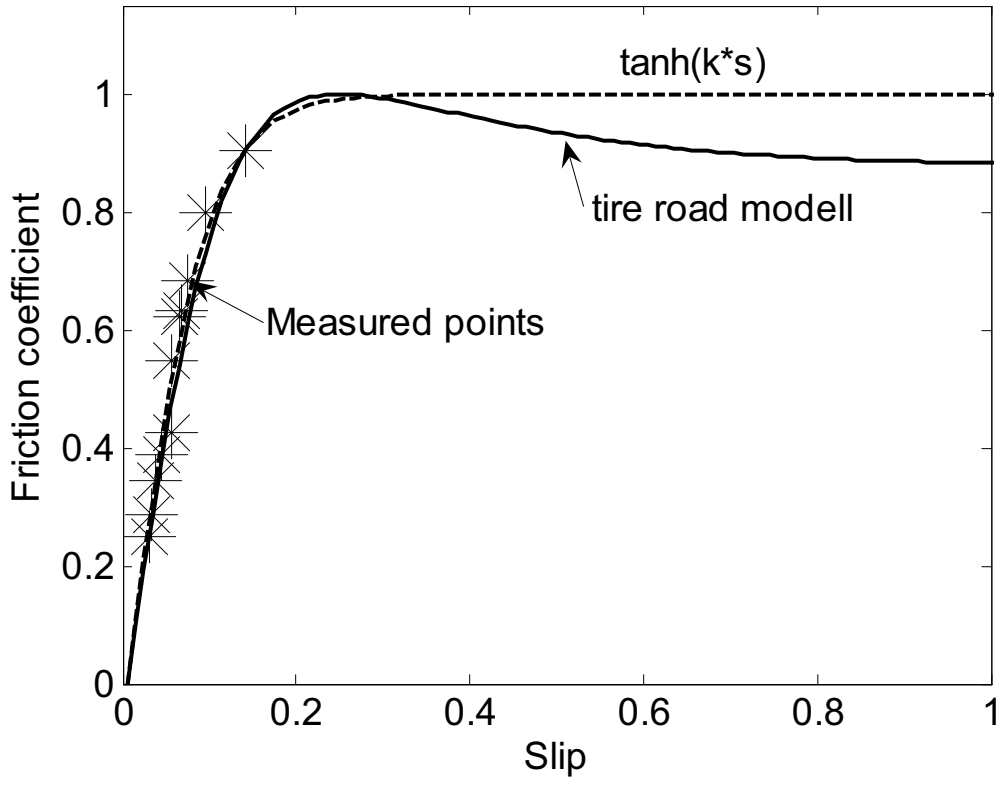

Figure 8: Friction coefficient vs. slip

1.7 Diesel Engine

The model of Tsal and Goyal [6] was selected because it uses the engine mass of inertia as an independent factor. It is easy to add to the model all masses of inertia, which are directly coupled to the engine. The model design is made on the base of the real engine components and it is simply and has a good stability.

The control principle is a PI+D type. The input on PI controller is the speed error signal. The D controller is used only to accelerate the engine by speed command signal changes.

The dynamics of the injection rank actuator is described with second order transfer function:

$$Gi(s) = \frac{1}{\frac{s^2}{\omega_n^2} + 2b\frac{s}{\omega_n} + 1} \tag{11}$$

and the dynamics of the engine torque as first order model:

$$Ge(s) = \frac{1}{0.65T_c + 1} \tag{12}$$

where T_c is defined by Tsal and Goyal as:

$$T_c = \frac{20}{N_c} \tag{13}$$

where N_c is the engine speed in rpm.

Block diagram of the diesel engine model is shown in figure 9.

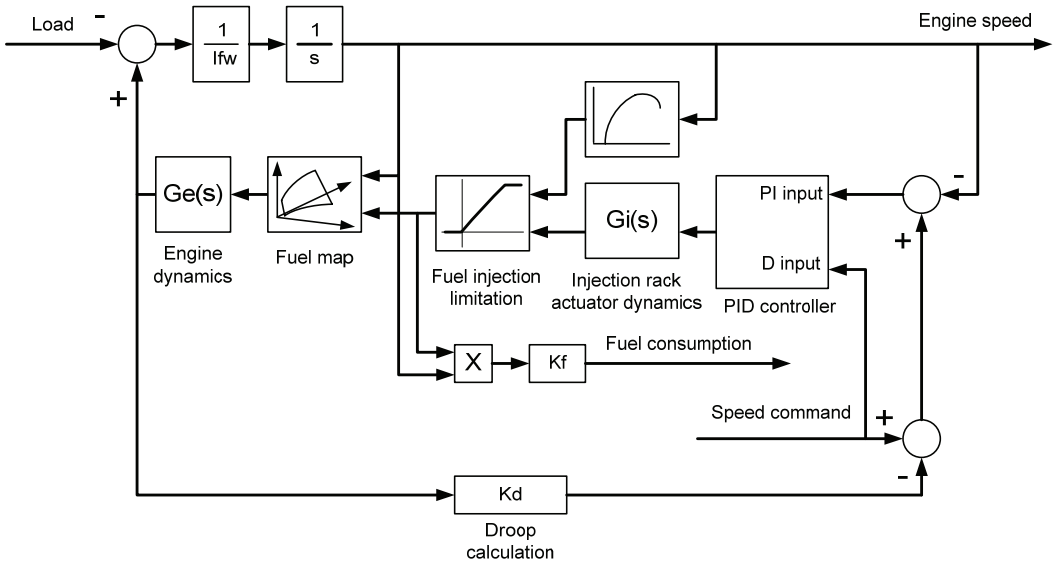

Figure 9: Diesel engine dynamic model

The dynamic model, based on the introduced method, was created for a Sisudiesel 66 CTA diesel engine. Figure 10 shows the measured and simulated speed command step responses from 1000 rpm to 1800 rpm and back to 1000 rpm. The solid line is the measured engine speed and dashed line is the simulated speed. Measurement was made using "on side simulation", where the simulation model is running during the measurement as "Hardware in the loop" model, using the same control signals as the measured unit. The measured load torque of the test system is used as load for the simulation model.

On figure 11 the corresponding results of load step responses are presented. The dash dotted line is the load of the engine. Solid line is the measured engine speed and the dashed line is the simulated engine speed.

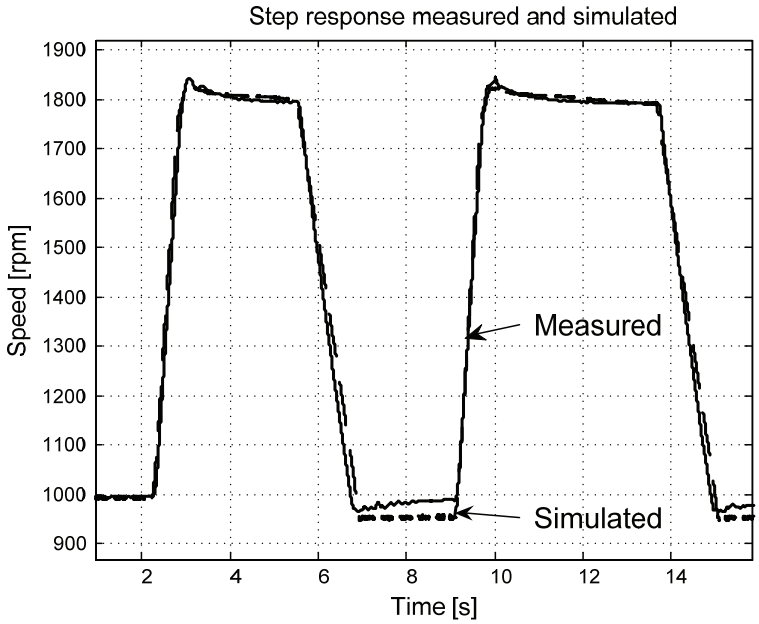

Figure 10: Speed command signal step response

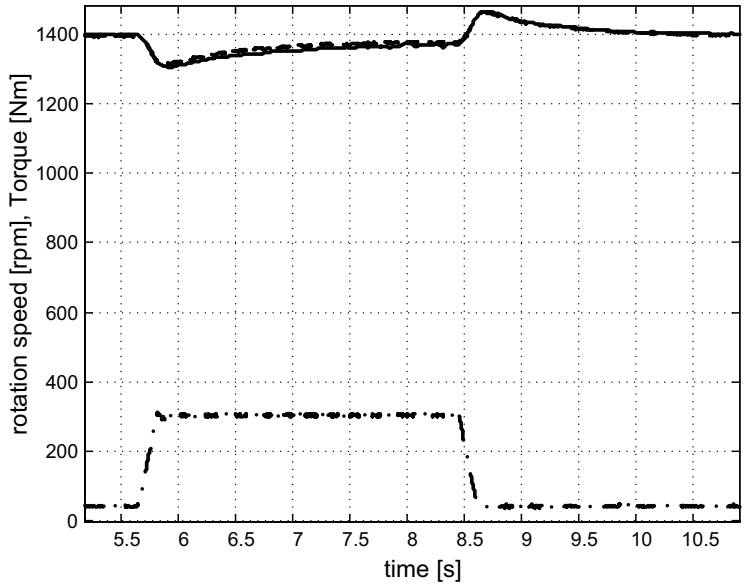

Figure 11: Load torque step response

2 DESIGN OF THE CONTROL UNIT AND ALGORITMS USING DYNAMIC SIMULATION AND HARDWARE IN THE LOOP METHOD

The development of a control system for a new power train design is time-consuming, expensive and it can be dangerous. Because the influence of dynamics of the power train and the vehicle has to be considered, only the complete machine can be tested. Testing a vehicle with unknown characters can lead to dangerous situations for the equipment and testing personnel. It is difficult to repeat the tested conditions exactly.

By means of “Hardware in the loop” [7] it is possible to cut off development cost and time. The basic principle of HIL is that a part of a real system is replaced with the real-time simulation model. The Hardware in loop method can be used for design of controllers where the model of the controller is running as real-time simulation model and the measurement and control signals are transferred between the real system and PC via I/O cards. It is also possible to replace the controllable system with simulation model and test the real controller with it.

2.1 Hardware in the loop simulation of three stage Semi-Power-Shift Transmission

Normally the simulation model is developed and verified on the base of the existing system. In this case this method was not possible, because the new system did not exist. For testing and verification, first an existing three stage semi power shift transmission was modeled and controlled with its own control unit.

Figure 12 shows the design of three-stage-semi power shift. The three different transmission ratios can be chosen with clutches C1, C2 and C3.

First stage is straight. Couplings C1 and C2 are closed and C3 open. All the axes of the planetary gear are rotating with the same speed.

On second and third stage the coupling C3 is closed and the planetary carrier remains stationary. Second stage is selected with closing the coupling C2. The gear ratio increases the output speed. Highest output speed is reached with the third stage, when coupling C1 is closed. The increase of the output speed is about 24 % pro stage.

The couplings are hydraulic operated disc couplings. The driveline control unit controls the couplings via proportional pressure valves with control current. The controller measures from the transmission the input and the output speeds and uses closed loop control to generate load independent soft ratio change.

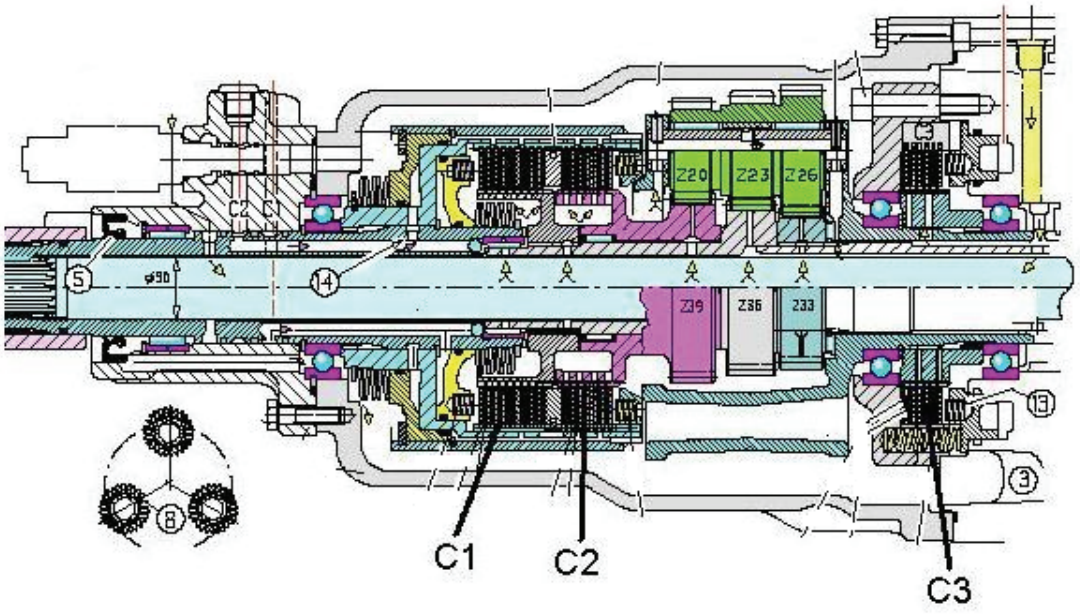

Figure 12: Three stage semi Power Shift transmission

The dynamic model of the power train with three stage semi-power-shift transmission for hardware in loop simulation is shown on figure 13. It includes the models for diesel engine, transmission control block, clutch operating blocks, final drive and wheel model and vehicle model. In the real vehicle the driveline consist also power shuttle, but in this model it is not included. In the HIL simulation a real transmission controller is used as driveline control unit and the rest of the model is running as real-time simulation model.

The driveline control unit reads from the system the engine gas pedal position (n_d set), rotation speed n_d, output speed n_o from the final drive and the vehicle velocity. It creates the control signals for the three clutches on the 3-stage planetary gear. The controller creates also control signals for the power shuttle, but it was not included to the investigated system.

3-stage planetary gear and couplings block calculates, on the base of engine speed n_d, output speed n_o from the final drive and C1-C3 couplings control signals, the engine load torque M_i and the input torque M_o to the final drive.

The wheel model calculates on the base of wheel speed n_w from the final drive and wheel model and the external load signal the vehicle velocity and the traction effort.

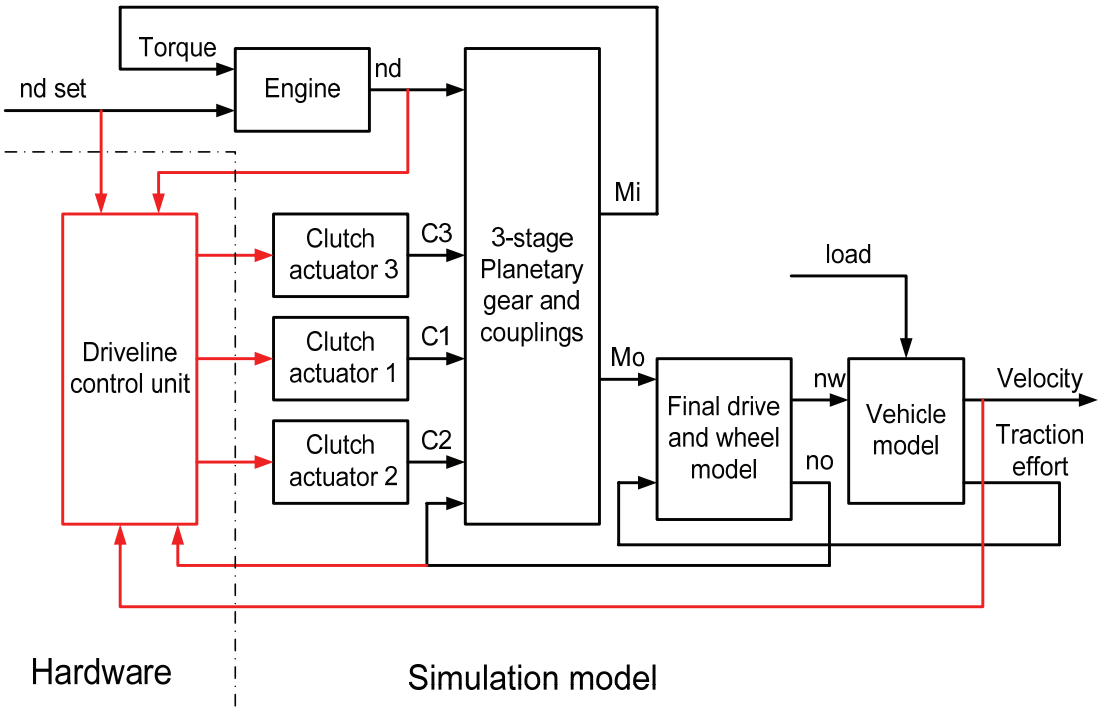

Figure 13: Hardware in the Loop simulation model for the 3 Stage Semi Power Shift Transmission

2.3 Description of the hardware in the loop system

The used HIL hardware is delivered by dSPACE GmbH and consists of a DSP-processor board and I/0 boards with CAN-Bus for connecting the driveline controller. Special adaptation electronics was developed, to adapt the output current signals to the dSPACE input voltage and to create for the driveline controller the input frequency running speed signals. The design of the adapter electronics is shown in Figure 14.

The Matlab Simulink model can be translated and directly used in real-time in the dSPACE DPS processor. The most critical design requirement for the simulation model is, that it has to be able to run in real time.

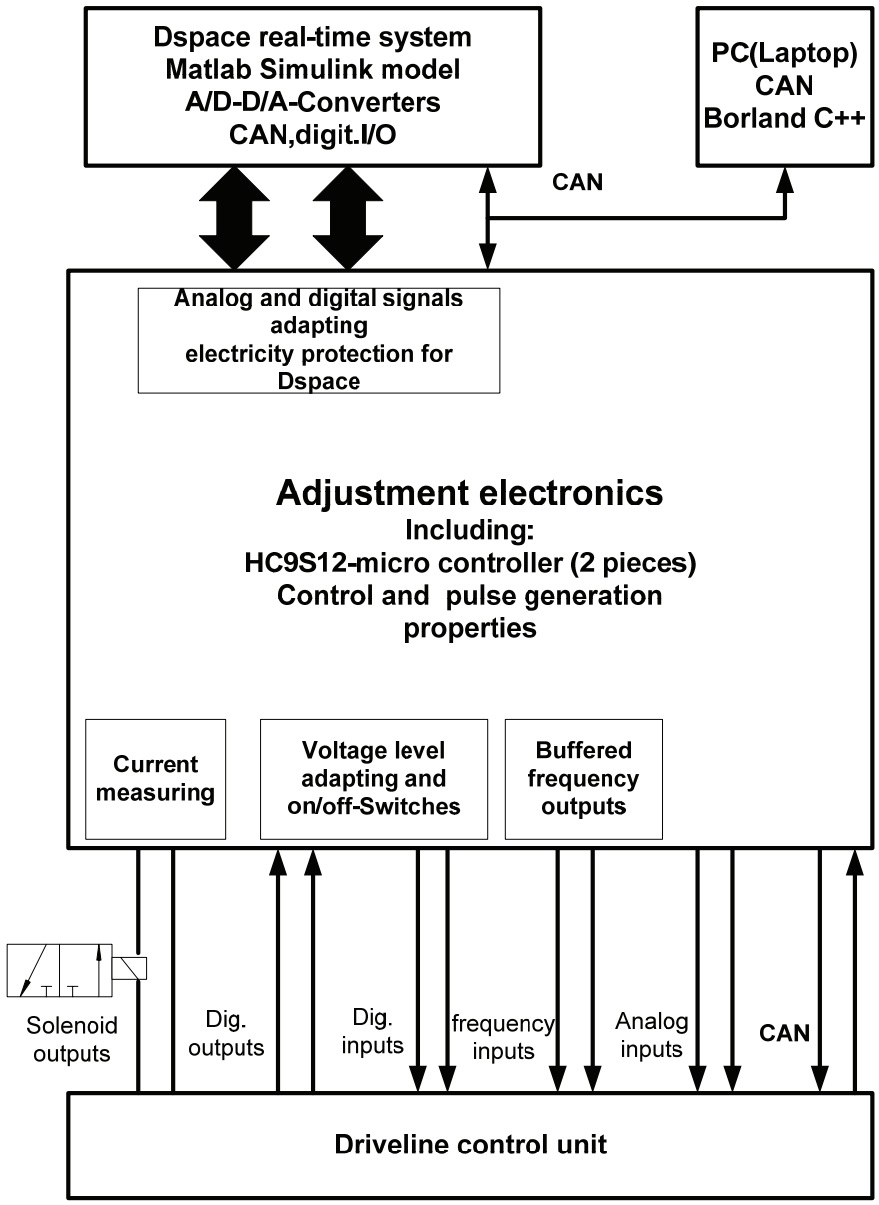

Figure 14 Hardware in loop Adjustment Electronics

3. DESIGN REQUIREMENTS FOR A CVT DRIVELINE CONTROL UNIT

Optimal CVT control consists of multiple separate control features. The driver shall be able to control the vehicle comfortably softly, accurate and if needed aggressively and he needs to have the feeling to control directly the vehicle. The control system shall react automatically to the load changes and protect engine against overloading and stalling. When multi stage CVT Drive is used, the area changes should be automated.

One possible CVT - Engine control system design is shown as a block diagram by Kim and Kim [8] in figure 15.The shown control system is mainly developed for laboratory testing and it includes all the basic components which have to be considered in the design of a real control unit for a CVT drive.

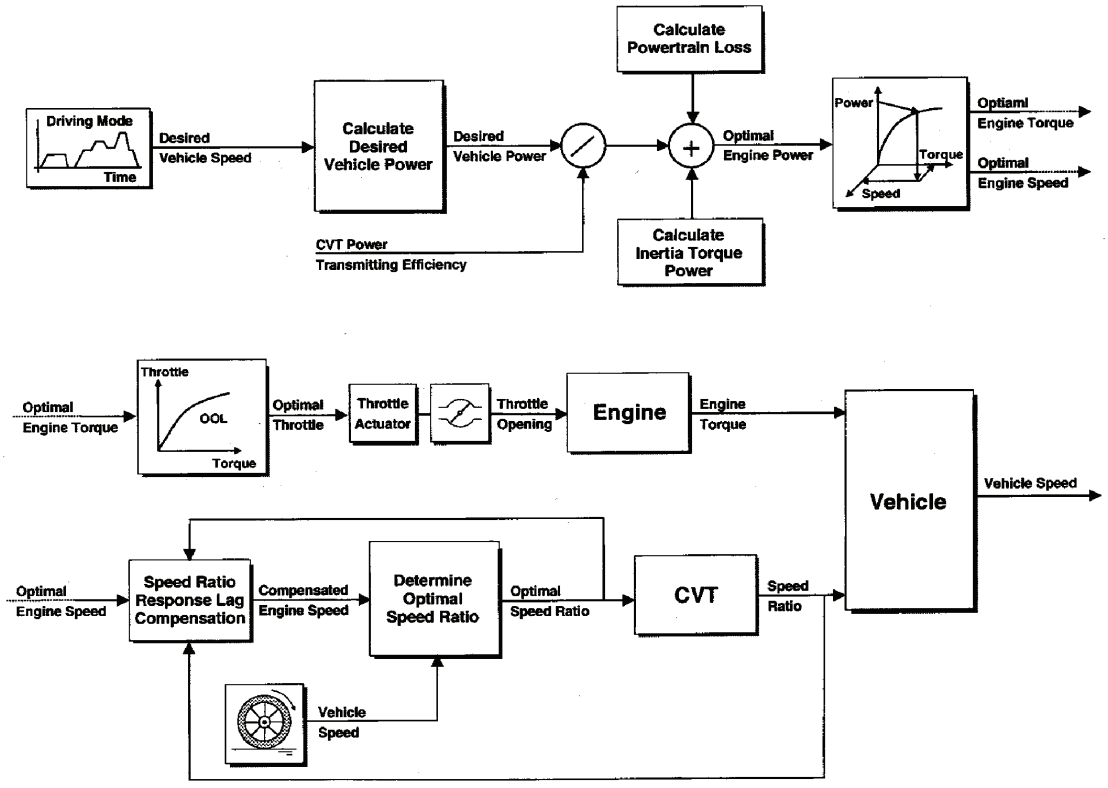

Figure 15 Block diagram of integrated engine-CVT control algorithm

4. POSSIBILITY TO IMPROVE FUEL ECONOMY

The efficiency of the hydrostatic CVT is always lower as the efficiency of a rigged stepped driveline. But the use of CVT driveline, offers the possibility to improve fuel economy by using the engine on its best efficiency area. Because the efficiency of the engine is the lowest one in the driveline and its variation is high in the operation area, it is possible to improve the overall efficiency significant

In the figure 16 there is presented the example of optimal engine operation as presented by Matson [9]. In the figure the typical characteristic of torque vs. rotation speed of an internal combustion engine are shown. Level lines for equal specific fuel consumption (sfc) are included, as well as hyperbolas for equal engine power. The dashed line marks the most efficient combinations of torque speed that produce the required power.

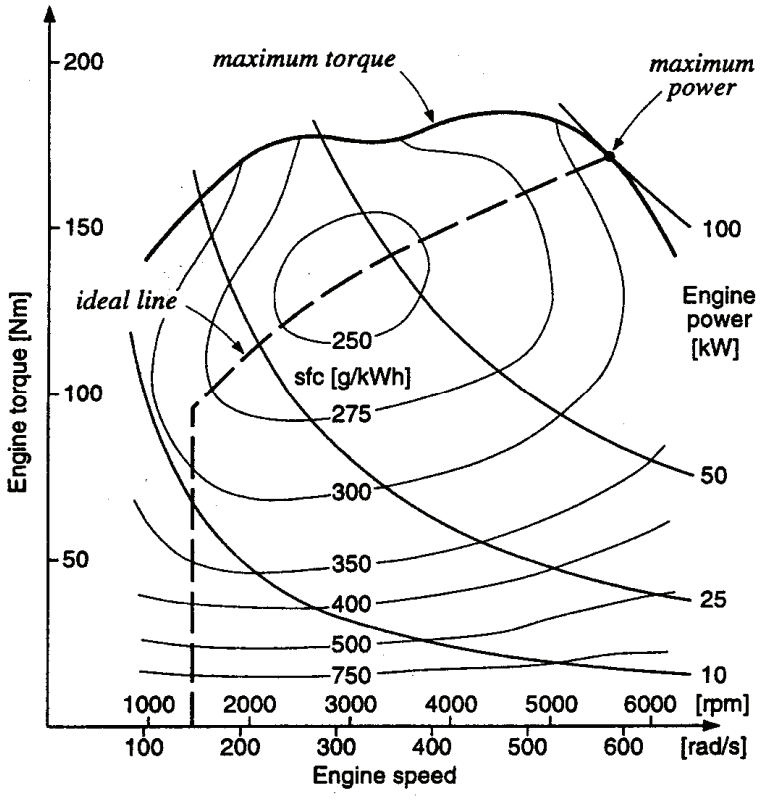

Figure 16: Improved fuel economy. Characteristics of torque vs. rotational speed of a 100 kW internal combustion engine with ideal line for CVT indicated

5. SIMULATED BEHAVIOR OF THE CVT POWER TRAIN

3.1 Response to gas pedal and load

Figure 17 shows a simulated drive diagram of the two-stage-CVT drive with automotive drive control. This means that the driver controls the transmission only using the gas pedal. On the shown example, dashed line is the engine command signal given by the gas pedal and the solid line the actual engine speed. Dot-dashed-line is the velocity of the vehicle; dense-dashed-line is the control signal of the hydrostatics and solid line the load.

First the diesel engine is on low idle and the vehicle is standing still. On the time point two seconds the control signal of the engine is increased to 1100 rpm. The controller starts to stroke the hydrostatic unit to accelerate the vehicle. On the time point about 4 seconds the CVT range is changed and the hydrostatic unit is stroked to the opposite direction for further increase of the velocity. On time point 15 second engine command signal is increased to 1800 rpm. The CVT ratio is decreased to allow the engine revolution to rice fast, and after that the vehicle is accelerated with full power. After the vehicle has reached the maximum speed, the pulling load of the vehicle is suddenly increased to 20 kN. CVT control system reacts by letting the vehicle to decelerate and by changing the transmission ratio respectively to generate the required traction effort.

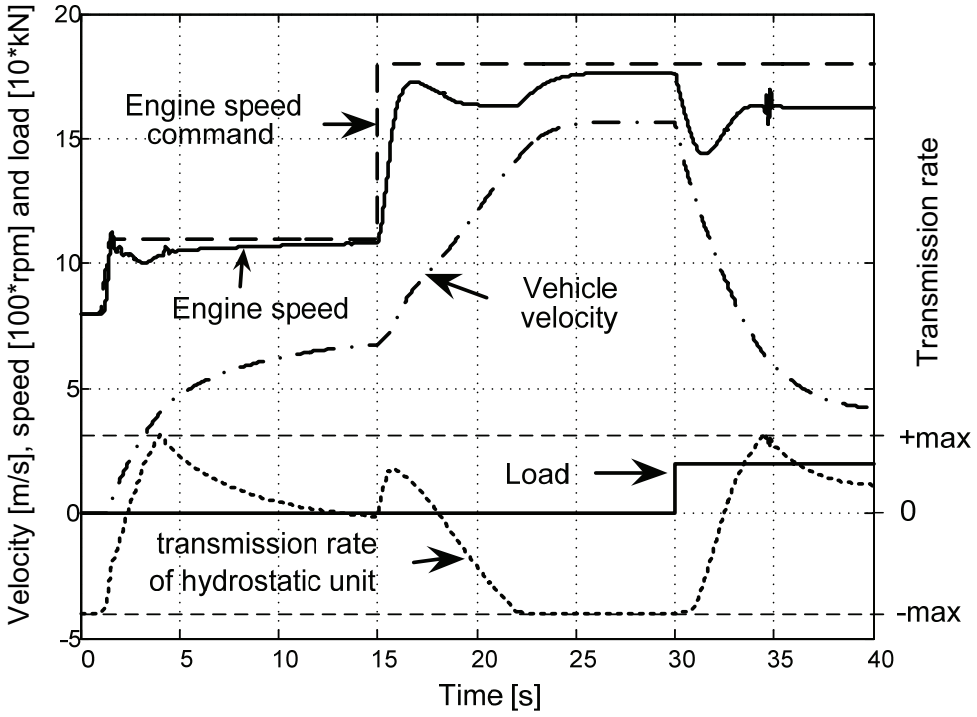

Figure 17: Simulated Drive diagram of an CVT Driveline

5.2 CVT rang change

One challenged task for the driveline control system is the range change on a multi stage CVT transmission. The range gear rations are chosen so, that on the range change situation, the speeds of the both couplings are the same, so that the range change can be done theoretically jerky free. In practical case, by using hydrostatic variator, the volumetric losses affect load dependent speed variation, which has to be compensated during the range change operation.

In the ZF-Eccom CVT transmission used strategy for range change is presented by Polhlenzen and Gruhle [10]. During the range change following actions have to happen synchronized:

- Closing the next stage clutch.
- Adjusting the transmission ratio of the hydrostatic units.
- Opening the currently used clutch

An optimal CVT Range change is shown on figure 18 and the corresponding simulated traces on figure 19. The simulation shows that the presented gear change strategy enables soft and jerky free operation by using ideal control for clutches and hydrostatic unit. The influence of real control parameters, static and dynamic load changes can be tested using this model.

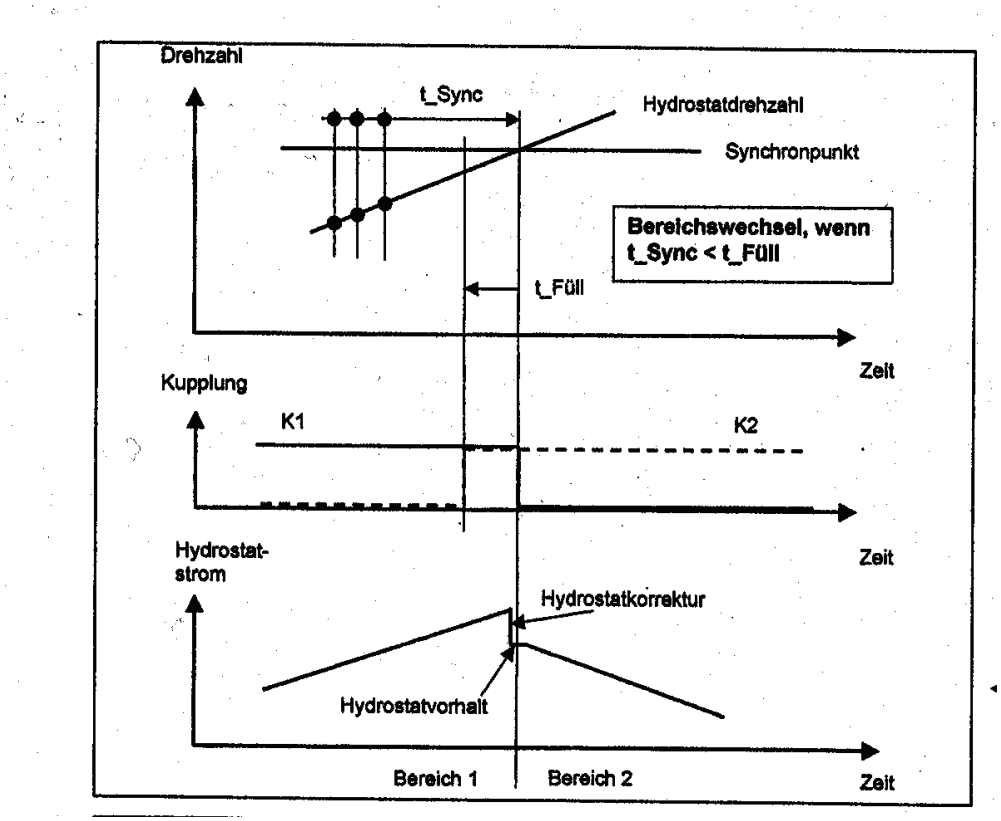

Figure 18: CVT Range change

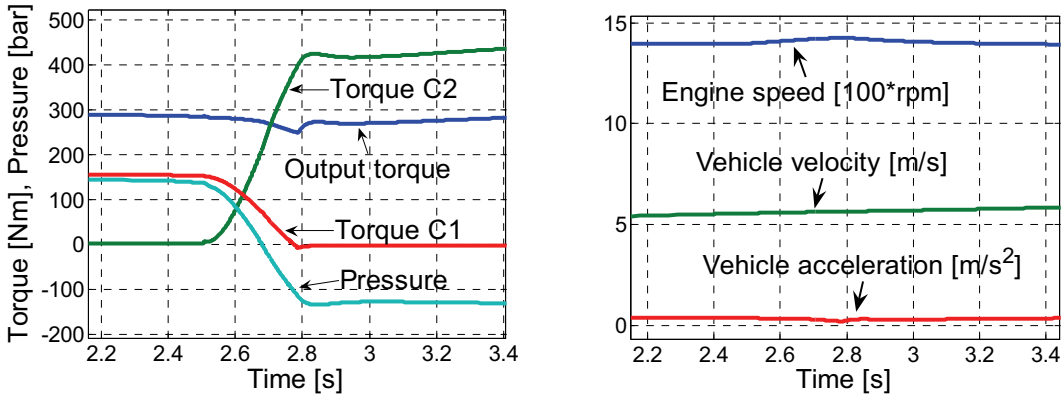

Figure 19 Simulated CVT range change

6. CONCLUSIONS

Dynamic model of a CVT power train offers an interesting and powerful tool for the development work of control logic and algorithm. It offers the possibility to observe the behavior and characteristics of the power train. All the basic functions can be tested in a safe environment. If the accuracy of the model is sufficient, it is even possible to determine the control parameters for the control unit using the model.

The model components have to be selected and designed carefully to prevent stability and compatibility problems. By modeling complete big systems like power trains the

sub models have to be kept as simple as possible to avoid interference and to keep the simulation time reasonable. This is especially important if the model should be used for real time simulation.

The sub models should be individual systems, which can be tested and verified separately. The used parameters should as far as possible be based to physical values, so that design changes can be tested without measure or calculation based parameter determination.

During the design and using the model it is important to keep in mind that there are always differences between the behavior of the model and real system. It is difficult or impossible to simulate all possible driving conditions.

REFERENCES

1. Huhtala, K.: Modelling of Hydrostatic Transmissions – Steady State, Linear and Non-Linear Models. Dissertation. Acta Polytechnica Scandinavia mechanical engineering series No.123 Helsinki 1996
2. Erkkilä, M., Ijas, M., Huhtala, K., Vilenius, M., Pöysti, T.: Hydrostatischer Antrieb mit CVT- Getriebe: Entwicklung eines Kompressorantriebs mit Überlagerungstechnik- teil1, O+P Ölhydraulik und Pneumatik, 05/2006
3. Farshidianfar, A., Ebrahimi, M., Bartlett, H.: Hybrid modelling and simulation of the torsional vibration of vehicle driveline systems. D13599 ©IMechE 2001 Proc. Instn Mech Engrs Vol 215 Part D: Journal of Automobile 2001
4. Viitasalo, V.: Traktorin suunnanvaihtajan simulointi [Simulation of the power shuttle in a tractor] in finish, Master of Science theses, Tampere University of Technology, Tampere 2001
5. Gustafsson, F.: Slip – based Tire – Road Friction Estimation, Automatica Vol.33 No. 6 pp 1087-1099, 1997
6. Tsal. S-C., Goyal M.R.: Dynamic Turbocharged Diesel Engine Model for Control Analysis and Design, SAE paper no. 860455, 1986
7. Linjama, M. Virvalo, T., Gustafsson, J., Lintula, J., Aaltonen, V., Kivikoski, M., Hardware-in-the-loop environment for servo system controller design, tuning and testing, Microprocessors and Microsystems 24, 2000
8. Kim, T., Kim, H.: Performance of an Integrated Engine-CVT Control, Considering Powertrain loss and CVT Response Lag, Vaughan, N., D.: Integrated Powertrains and their Control, Professional Engineering Publishing 2000, ISBN 1 86058 334 2
9. Mattson, P,: Continuously Variable Split – Power Transmission with Several Modes Dissertation, Chalmers University of Technology, Goteborg Sweden 1996
10. Pohlenz, J., Gruhle, W-D.: Stufenloses hydraulisch- mechanisch leistungsverzweigtes Getriebe, O+P Ölhydraulik und Pneumatik 03/2002

LATEST DEVELOPMENT OF CRANKSHAFT DESIGN RADIAL PISTON HYDRAULIC MOTORS: HIGH TORQUE HIGH SPEED VARIABLE DISPLACEMENT MOTORS FOR HYDROSTATIC TRANSMISSIONS

Authors: Mr. Vittorio Pecorari , Mr. Giovanni Pecorari
SAI S.p.A. Hydraulic Motors
Via Olanda, 51, 41100 Modena, Italy
E-Mail : vittorio.pecorari@saispa.it , giovanni.pecorari@saispa.it
Phone : + 39 059 420 229, Fax : +39 059 451260

Author: Mr. Davide Pecorari
R.&D. s.r.l.
Via Olanda, 71/A, 41100 Modena, Italy
E-Mail : info@rd-srl.com
Phone : + 39 059 420 229, Fax : +39 059 451260

ABSTRACT

The paper will describe the enhancements in the overall efficiency of a construction machine that can be obtained by using a dual displacement crankshaft design radial piston hydraulic motor capable of running at very high speeds. Different products have been examined in order to cover a wide range of applications and working conditions. Most of the results are the outcome of significant application studies, which led to the development of prototypes. The common essential feature of all the prototypes was a dual displacement system applied to a crankshaft design radial piston hydraulic motor suitable for very high speeds. Some of the prototypes are currently used by major world-wide construction industries. A typical system to be developed was a dual speed hydraulic transmission. Most of the construction machines in fact, are being designed for having two operational modes: the slow mode, when the machine is under heavy loads and moves with a relatively low speed, and the fast mode, when the machine is virtually unloaded and moves faster on the work ground. The variation of the motor displacement is obtained by a variation of the eccentricity of the crank of the shaft. Hence, the motor can shift in a continuous manner from the maximum to the minimum displacement, with a smooth variation in terms of torque and speed. The wide operational range coupled with very high efficiency both in minimum and in maximum displacement, allows the hydraulic system to adjust the engine working conditions in a smaller range closer to that of the maximum efficiency. The major consequences being less exhaust emissions, less thermal losses, longer machine life, without forgoing the performances of the equipment, rather improving them. The objectives of the analysis were to capture the essential benefits of the application of these hydraulic components referring in particular to the overall efficiency in order to determine the enhancements with respect to the traditional hydraulic motors. The ultimate aim was to identify

candidates for optimal application in terms of performance and design. The results obtained show that with the use of such a component, thanks to its high starting toque, even in minimum displacement, and its very high maximum speed, the system gains elasticity, performance and overall efficiency.

KEYWORDS: radial piston motor, variable displacement, high speed, high efficiency, thermal losses, construction machine.

1. INTRODUCTION

Our aim in designing radial piston motors is to improve efficiency, reliability and also increasing the total power output by converting more fluid power into mechanical power by means of increasing the working pressure and working speed. Another important feature of a hydraulic motor however, is the capability of controlling the power output in terms of torque and speed. The variation of the displacement allows the motors to have the same power output with different values of toque and speed. When this control of torque and speed is achieved without a reduction of the motor efficiency, the performances of the whole transmission increase considerably in terms of functionality and overall efficiency of the transmission.

2. LIMITATIONS OF STANDARD RADIAL PISTON HYDRAULIC MOTORS

The motor examined in this study (see fig.1 below) is a crankshaft design radial piston hydraulic motor. In the past, this class of motors was known as High Torque Low Speed motors. This was because most of the motors with this architecture could not run at high speed. The limit was the inability of the central hydrostatic bearing, when rotating at high speed, to sustain the con-rod (or directly the pistons in case of swivelling cylinders) in contact with the crankshaft. Another limit to the power output of this class of motor was the very high loads on the central bearing when the motor was working at high pressure. Nowadays, the latter limit is commonly recognised to be overcome, since most of the motors on the market can work above 300 bar as a peak pressure. Different is the situation concerning the high-speed capabilities of these motors. As stated before it is not the structure to represent a limit for the maximum speed, but the inadequate characteristics of the central bearing. An improvement in the performances in terms of power output moves necessarily through the enhancement of the performances of the central bearing regardless the kind of bearing that it is used.

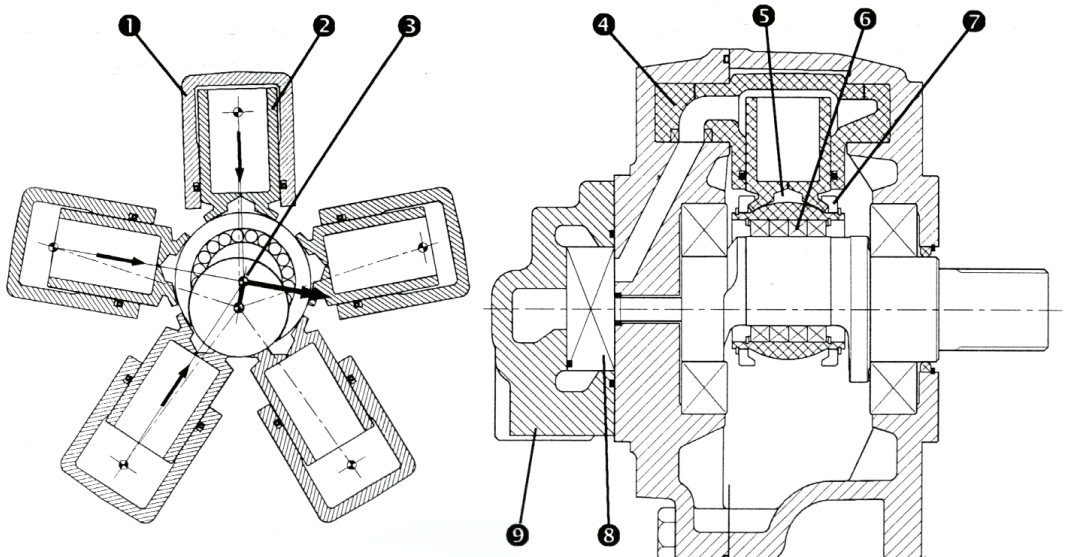

1. Cylinder
2. Piston
3. Crank
4. Trunnion
5. Hydrostatic bearing
6. Central roller bearing
7. Piston retaining ring
8. Rotary axial distributor
9. Interchangeable distributor

Fig. 1: *Radial piston motor*

3. DEVELOPMENT OF CENTRAL BEARING

A first step forward in the performances of the central bearings has come by the use of hydraulic bearings capable of combining hydrostatic and hydrodynamic effects. However, the improvements have not been substantial, a major limit being the difficulty of the sliding surfaces to tolerate oil contamination.

A second and more substantial step forward in the performances of radial motors has come by replacing hydraulic bearings with roller bearings, right onto the crank of the shaft. In this way, it is possible to guarantee extremely low relative velocities between coupled moving parts, and consequently, to increase the maximum speed of the motor. The outer race of the eccentric bearing experiences only an orbital motion and no rotation at all. This condition reduces the contact velocities by 90% compared to those occurring when the shaft itself represents the central sliding bearing. The maximum speed achievable with this solution is definitely higher. Moreover the capacity of the roller bearings is much higher than that of hydrostatic bearings; in addition, they offer a better efficiency of the piston-crankshaft (or connecting-rod-crankshaft) coupling.

Bearing cages mounted into the central roller bearing, and low friction material applied to the sliding bearings represents the latest and more considerable developments towards the high speed.

The low friction material helps the motor to reduce the resistances to be won both when starting-up and when running at maximum speed, therefore the sliding contact can reach higher speeds.

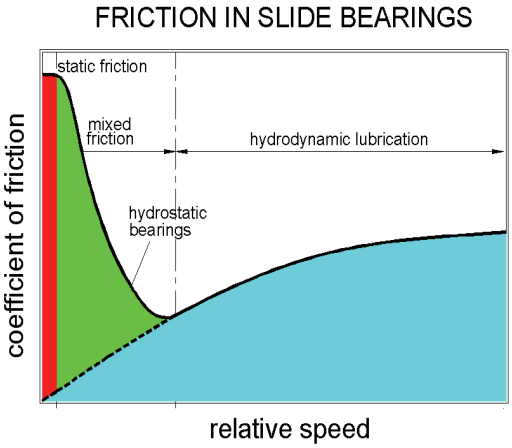

Fig. 2: *Friction in slide bearings*

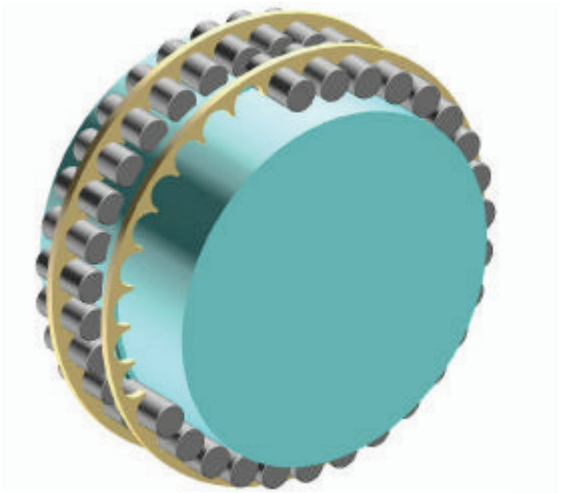

Fig. 3: *Disc bearing cage*

The role of the bearing cage on a roller bearing is to prevent each roller to collide with the adjacent ones when rotating. This function is much more necessary when the bearing is mounted eccentric with respect to the axis of rotation. For this reason, the use of the bearing cage allows the bearings to perform extremely better, thus to reach higher speeds, or alternatively, to extend the component lifetime.

Thanks to this enlargement of their operational range, together with their well-known high efficiency, the radial piston motors have now become attractive for many applications out of the question few years ago.

4. VARIABLE DISPLACEMENT MOTORS

The development in the technology of the central bearing has accelerated the development of Variable displacement radial motors. When the restrictions in speed were significant the variable displacement motors could have very limited displacement reduction ratio, typically 1÷2, 1÷3. Now that the speed limit is much higher the motors can achieve reduction ratios down to 1÷10, still showing excellent values of efficiency.

A variable displacement motor can be infinitely variable, when is capable of working with every single displacement value included between the minimum and the maximum

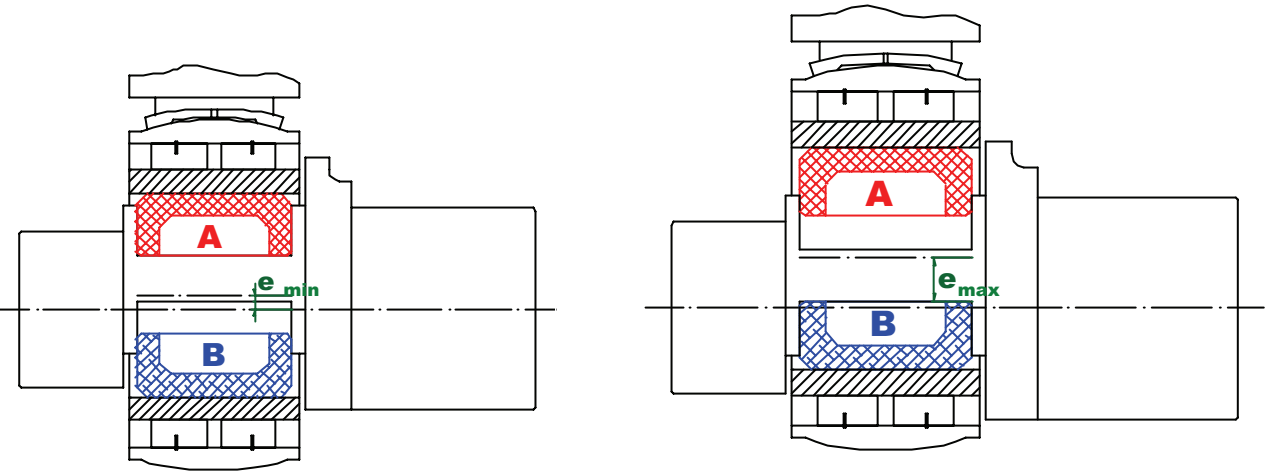

Fig. 4 *Variable displacement control system*

displacement. Alternatively, it can be a dual (or double) displacement motor, when it can work either with its minimum or with its maximum displacement, but no midway values are allowed.

5. DEVELOPMENT AND WORKING OF A VARIABLE DISPLACEMENT MOTORS

This section of the papers describes the concept behind development of the Variable Displacement Motor, control of the working conditions of the motor, dependence of the displacement on the eccentricity and variable eccentricity crankshaft.

5.1 Concept behind development of the Variable Displacement Motor

When using a machine, as well as when designing it, particular attention is paid to the utilisation of the installed power. A good exploitation of the installed power of the machine induces a series of positive effects such as less fuel consumption, reduction of the exhaust emissions better productivity etc. The possibility of varying the displacement of the motor would help in good exploitation of the installed power by operating the motor in a wide range inline with the working conditions of the machine thereby improving the overall efficiency of the machine.

In various mobile equipment the power transmission is made through a fluid system which first transform the power generated by the primary source (the engine) from torque and speed into pressure and oil flow. Then, the various actuators transform the energy they receive from the fluid power generator back into mechanical power capable of overcoming the resisting loads.

From a theoretical point of view, if the system wouldn't have any limitations, the more the external forces were, the more the increase in pressure of the system. For this reason the fluid power generator can sometimes be asked more power than what it can generate. In other words the pump is requiring more power than that of the engine. If the pressure variation of the system could be limited, to some extent, by the possibility of adjusting the fluid actuator according to the resisting loads, then in many cases the pump wouldn't overcome the power limit of the engine which normally is visible as a deceleration (overload).

Thus , the basic concept behind developing the variable displacement motor was if a great amount of the transmission variation is given by the change of the characteristics of the actuators, the fluid power generator pack and hence the engine would work within a limited range of conditions thereby certainly increasing the efficiency of the machine.

5.2 Control of the working conditions of the motor

When speaking about a hydraulic motor the ability of adjusting its actions to the external load is depending on the possibility of adjusting the power outlet (P) in terms of torque (T) and speed (n).

$$P = T * n \quad (1)$$

The rotational speed of the motor is depending on the oil flow (Q) and on the displacement (D) according to the:

$$n = Q / D \quad (2)$$

Besides the torque of the motor (T) is depending upon the pressure (p) and the displacement (D) according to:

$$T = p * D \quad (3)$$

As a result it can be seen that the power outlet is not depending on the displacement of the motor but only on the oil flow (Q) and on the pressure (p):

$$P = T * n = Q / D * (p * D) = Q * p \quad (4)$$

This means that we can change the working condition of the motor adjusting its displacement without changing the power asked to the fluid power generator (engine + pump).

5.3 Dependence of the displacement on the eccentricity

In a crankshaft design radial piston motor the displacement is depending on the bore of the cylinders (b) the stroke of the pistons (s) the number of cylinders (N) according to the:

$$D = N * (\pi(d^2/4) * s) \quad (5)$$

The stroke of the pistons is related to the eccentricity of the crank of the shaft (e):

$$s = 2 * e \quad (6)$$

By combing the equations (5) and (6) we obtain:

$$D = n * (\pi(d^2/4) * 2 * e) \quad (5)$$

Hence we find out that the displacement is proportional to the eccentricity of the crank of the shaft., number of cylinders and diameter of piston.

Therefore the parameters we can play with to adjust the displacement are n, d, and e. This means that we can increase or decrease the displacement by increasing or decreasing the number of cylinders, by enlarging or reducing the bore of the pistons, or by increasing or decreasing the eccentricity of the crank of the shaft.

When modifying the bore or the number of cylinders the change cannot be continuous, hence the change in the displacement is inevitably non-continuous whereas when playing with the eccentricity, it is possible to obtain a step-less variation.

In this paper the third system is described.

5.4 Variable eccentricity crankshaft

In order to obtain a variation of the eccentricity of the crank of the shaft it is necessary to locate a mobile bushing on the crank acting as support for the pistons (in the case of swivelling cylinders) or for the connecting rods (in the case of fixed cylinder architecture). In order to control the position of that bushing an actuator has to be placed inside the crank providing the force to shift the bushing outwards and inwards. Basically, an hydraulic cylinder is put inside the crank. Then, a control has to be added to the system in order to govern the position of the crank. This is obtained by the used of a directional valve connecting the either top or the bottom chamber of the cylinder inside the crankshaft to the high pressure line. By controlling the position of this directional valve, the position of the mobile bushing is controlled, hence the eccentricity consequently the displacement.

6. SALIENT FEATURES OF VARIABLE DISPLACEMENT MOTORS

6.1 Smooth transmission

An important feature of a system with variable displacement motor is the smooth transmission variation achieved by the use of a hydraulically controlled configurable crankshaft, which permits the crank to move continuously between the minimum and the maximum eccentricity. This system allows continuous speed adjustments, which reflects in a smooth, jolt-free behaviour of the machine throughout the entire speed range. The reaction times of the displacement control system are very short, typically some tenths of second. The variation neither during acceleration, nor during deceleration, is bouncy or uncomfortable. Other types of radial motors such as the cam motors cannot vary their displacement in a continuous manner. The most they can achieve is a non-continuous dual displacement motor obtained by cutting-off some of the pistons. They require an additional control to prevent jolts and even when this system is present the operation of the motors is not as smooth as when he variation is continuous. The smooth transmission also improves the drivers safety by providing a smooth , jolt free ride even with the vehicle completely loaded

6.2 Wide operational range:

Thanks to the developments described above this class of motors has extraordinarily extended its operational range and is now entering working fields typical of other classes of hydraulic motors, such as orbital motors and axial piston motors.

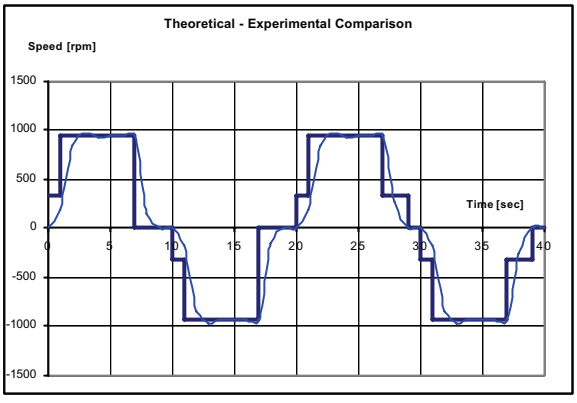

Fig. 5: *In house testing comparison*

6.3 High efficiency

Another important feature of this system is the high efficiency in a wide range of working conditions. The crankshaft design radial piston motors are second to none for having very high mechanical efficiency especially when starting-up, and very high volumetric efficiency. The architecture of this kind of motors is very favourable because the resulting force acting on the shaft forms a right angle with crank throughout most of the shaft rotation. Thanks to this structural design, the mechanical efficiency remains high even when the eccentricity of the crankshaft is small. In other words, even when the motor is in minimum displacement.

6.4 Performance

The overall performance of the system improves because of the fact that it provides a smooth power transmission with a wide operating range in terms of load capacity and operating speed with a low fuel consuming engine operating at its optimum efficiency

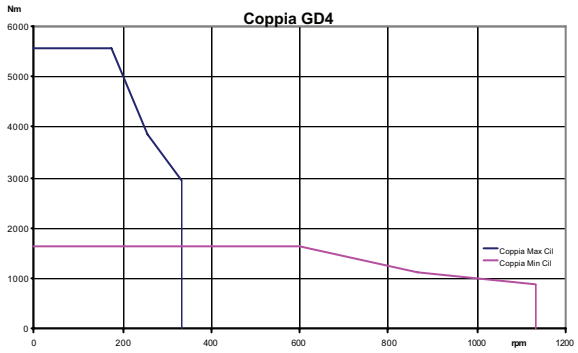

Fig. 5: *Dual speed motor characteristic*

6.5 Cost

There is an overall benefit in cost as it reduces the operating costs as well as maintenance cost due to the fact that the entire system is working at their best operating range hence increasing the lifetime of components.

6.6 Environment friendly

The fact that the system reduces the noise levels and also less polluting as the engine can be tuned to perform for maximum efficiency makes it environment friendly.

7. ADVANTAGE OF A VARIABLE DISPLACEMENT HYDRAULIC MOTOR TO A FIXED DISPLACEMENT MOTOR FOR HYDROSTATIC TRANSMISSION

When considering an hydraulic motor used in a hydrostatic transmission its primary function is to drive the machine in different working conditions where the main variables are the weight of the machine, the speed required, the terrain conditions, the slope to be overcome, the possible obstacles that can be found along the way, the draw bar pull attached to the machine. The motor must provide the wheels with the adequate torque and speed for every condition so that the machine can move and do the job it is supposed to do.

When using a fixed displacement motor the only control that the system can have is away from the motor. Typically it is a control on the pump. If a variable displacement motor is present, then a large amount of the adjustment of the working condition of the machine can be passed on to the motor. The possibility of adjusting the displacement lightens the duty of the power generator which can be working within a narrower range of conditions, those closer to the high efficiency area.

8. APPLICATIONS FOR USING THE VARIABLE DISPLACEMENT MOTOR

The majority of industrial equipments and vehicles require excellent levels of starting efficiency and controllability when they are heavily loaded and subjected to high stresses. Power transmission users are increasingly demanding components that are faster, quieter and more efficient.

A faster speed when on road shortens journey times and offers improved productivity hence lowering the total cost of ownership. Quieter components reduce noise and vibration of the whole machine thereby providing higher safety standards for operators as well as a quieter environment. Improved efficiency reflects in drastically reduced fuel consumption and heat generation, together with increased transmission lifetime.

The variable displacement motors are capable of meeting the wide demands as mentioned above keeping the efficiency at high levels throughout the entire speed and load range. These motors are capable of running efficiently and smoothly at low speed down to 3 rpm and at the same time, when in minimum displacement, the maximum speed allowable is above 3000 rpm, still showing extremely high efficiencies compared to the existing standard. Displacement shifting is hydraulically controlled through a low-pressure pilot line.

A typical system using the variable displacement motor is an on off-road vehicles. By regulating the engine to work in a smaller range of speeds and torque, the task to adjust the power output in terms of torque and speed according to the machine needs can be passed on to the transmission.

Another innovative way of using the variable displacement motors on moving vehicles is to use it on the differential axles (Fig. 6 below)

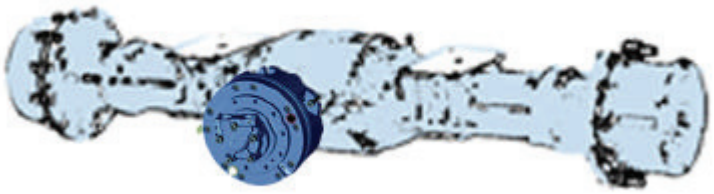

Fig 6: *variable displacement motors on differential axles*

9. VARIABLE DISPLACEMENT MOTOR USED AS DUAL DISPLACEMENT MOTOR

A variable displacement motor which is varied across 2 displacements so that the motor can run at either the maximum or in the minimum displacement is a Dual displacement motor. When considering a crankshaft design variable displacement radial piston motor based on crankshaft with variable eccentricity, the way to achieve such a functionality is rather easy and it can be done by developing a system where the mobile bushing mounted on the crank of the shaft can either operate when completely outwards or when completely inwards with respect to the axis of rotation of the shaft. Therefore the eccentricity of the crank can be the maximum or the minimum and accordingly the displacement and no midway values are allowed. This solution is suitable in most of the hydrostatically driven machines.

In fact, in various applications the working conditions of a machines are essentially two: one in which the machine is working against rather heavy loads at a relatively low speed and the other one when the machine is virtually unloaded and it must run at higher speeds. This kind of applications are particularly suitable for a dual displacement motor. When the machines requires high torque at a relative low speed, the motor can work in maximum displacement and when the machine is not overcoming particularly heavy loads but it is requiring higher speed, the motor can work in minimum displacement.

The dual displacement is achieved by the use of a mobile bushing mounted on the crank of the shaft capable of varying its eccentricity with respect to the axis of rotation of the shaft. Inside the crank, in fact, there are two high-pressure-operated pistons supplied by the high pressure line shifting the bushing outwards or inwards hence changing its eccentricity, therefore the displacement. The control system is placed inside the motor case and is regulated by a low-pressure signal coming from the control line. This simple reliable mechanism allows the motor to greatly expand its operational field, with a minor modification in its dimension and design.

Fig 7: *Typical examples of SAI dual displacement motors*

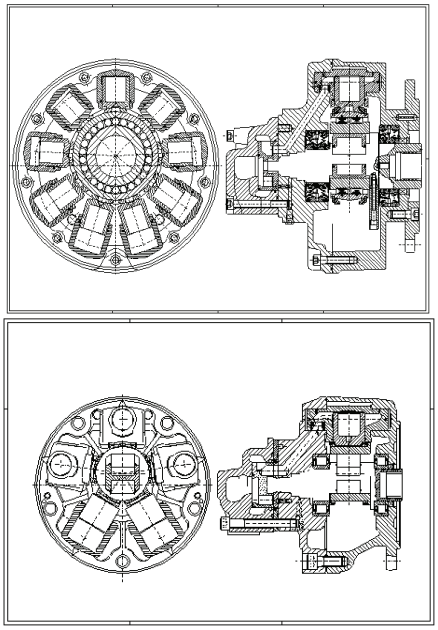

10. TYPICAL APPLICATION OF DUAL DISPLACEMENT MOTOR - CONSTRUCTION EQUIPMENT

Most of the construction equipment is likely to have two running modes: the slow mode, when the machine is under heavy loads and moves with a relatively low speed, and the fast mode, when the machine is virtually unloaded and moves faster on the work ground. This is the case of the material handler, for instance, or the excavators as well as the front loaders. A dual displacement mode combined with very high levels of overall efficiency permits to improve the performances of the machine. By regulating the engine to work in a smaller range of speeds and torque, the task to adjust the power output in terms of torque and speed according to the machine needs can be passed on to the transmission.

Fig. 8: *Front loader*

Fig. 9: *Loader*

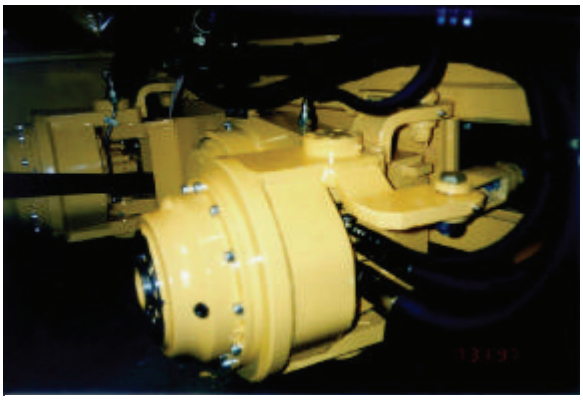

Fig. 10: *Wheel hub*

11. CONCLUSION

By the details mentioned in the above sections of the paper , it can be understood how with the use of a variable displacement crankshaft design radial piston hydraulic motor, the system gains elasticity, performance and overall efficiency.

The most important feature of the variable displacement system is that it offers advantages through maximum functionality and outstanding overall efficiency. It caters to the needs of the ever demanding industry by offering a continuously variable speed over a high speed range and load capacity. It also enhances the overall efficiency of the power transmission system. An optimally designed system with the variable displacement motor provides low fuel consumption with low exhaust emissions and also increases the overall lifetime of the system.

To put things in a nut shell, its a win win solution in which the system is highly flexible with an enhanced overall performance over a wider operating range provided at lower operating cost and at the same time is environment friendly.

The future of the variable displacement is very promising with rapid progress being made in development of a electro-hydraulically controlled variable displacement motor ultimately leading to a fully variable unit.

References

[1] Scheffels, G. 1999. *Mission: reducing emissions.* ITV Europe, issue 7, UK & International Press, Dorking, UK

[2] Aitzetmuller, H. 1999. *Next-generation CVT.* Steyr Daimler Puch AG, Austria issue 7 ITV Europe, UK & International Press, Dorking, UK

[3] Guaglione, E. 2000. *I nuovi ritmi del motore.* Oloeodinamica e Pneumatica, numero 8, Tecniche Nuove, Milano, Italy

RESEARCH ON CONTROL STRATEGY AND WORK POINT OPTIMIZATION OF POWER SYSTEM IN HYBRID HYDRAULIC EXCAVATOR

Qing Xiao, Qingfeng Wang, Yanting Zhang
Zhejiang University
The State Key Laboratory of Fluid Power Transmission and Control
310027 Hangzhou, China
Phone +86 571 87951314-6204, Fax +86 571 87951941
E-mail: xqzju98@163.com

ABSTRACT

Aimed at the hybrid system in hydraulic excavator, engine constant work point and double work points control strategies are proposed. A hybrid hydraulic excavator experiment system is established and experimental researches on these two control strategies have been done. And then, a method which is used to optimize the work point of engine is put forward and researched theoretically and experimentally. The research results indicate that when the work point of the engine is optimized, the double work points control strategy can effectively increase the efficiency of the whole system and keep the SOC (State of Charge) of the capacitor stable in set range.

KEYWORDS: Hybrid power, Hydraulic excavator, Control strategy, Optimization

1 INTRODUCTION

As the load power of hydraulic excavator varies periodically and in large range, the work state of engine also changes periodically, so the engine cannot always work in high efficiency state. Equipping hybrid system in hydraulic excavator is one effective way to solve this problem.

Hybrid system, which has been used successfully in automotive industry and can increase the fuel economy and decrease the emission effectively, was invented at the end of 19th century. In this system, there are two or more power sources and one or

more accumulators. Nowadays, hybrid system is classified into three kinds: series, parallel and series-parallel hybrid system, according to the compound mode of mechanical and electrical energy.

Currently, researches on structure, control strategy and energy saving effect of hybrid system in hydraulic excavator have been carrying through widely [1-4]. Among them, control strategy, which determines the work state of components in the power system directly and affects the energy consumption of hydraulic excavator ultimately, becomes one of the research emphases [5-6].

When adopting hybrid system, the fluctuation of load power can be absorbed by the accumulator of the power system, so the engine only outputs the average of the load power. Thus the control strategy of working at constant high efficiency point can be applied to the engine, which benefits to increase the efficiency of the engine and the system.

But under the control strategy of working at constant high efficiency point, as the chosen work power of the engine cannot be exactly same with the average of the load power, SOC of the accumulator will rise or drop after one work cycle. After long time work, SOC will exceed its work range, and then the system can work normally no longer. To eliminate this limitation, the engine can employ the double work points control strategy. That's to say, the engine can work at one high power point and one low power point in the high efficiency area. When SOC of the accumulator exceeds the set upper limit, the engine switches to the low power point. When SOC comes to the set low limit, the engine switches to the high power point. In this work mode, the engine efficiency keeps high and SOC of the accumulator won't exceed its work range.

The efficiency of hybrid system is mainly determined by the efficiencies of engine, electric motor and accumulator. And the work state of the component decides its efficiency. When the engine adopts the double work points control strategy, the work states of the electric motor and accumulator lie on the work point of the engine. So the efficiency of the whole system is determined by the work point of the engine. To optimize the engine work point reasonably will improve the efficiency of the system.

2 RESEARCH ON CONTROL STRATEGY OF THE POWER SYSTEM

2.1 Constant work point control strategy

Figure 1 is the schematic of parallel hybrid hydraulic excavator (hereinafter HHE) using capacitor as the accumulator. Engine E and electric motor M drive hydraulic pump in parallel. The hydraulic pump outputs pressure and flow rate required by the hydraulic system.

The principle of constant work point control strategy is to stabilize the engine work point at its high efficiency point by adjusting the absorbed or output power of the electric motor when the required power of the hydraulic system changes continuously.

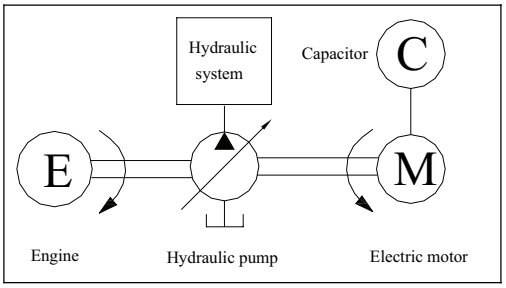

Figure 1: Schematic of HHE

As the engine, hydraulic pump and electric motor are connected coaxially, the rotational speed of them is constant and same with each other when constant work point control strategy is used. So engine work point can be stabilized at constant work point by controlling the absorbed or output torque of the electric motor through changing its synchronous rotational speed. Figure 2 presents the block diagram of the system.

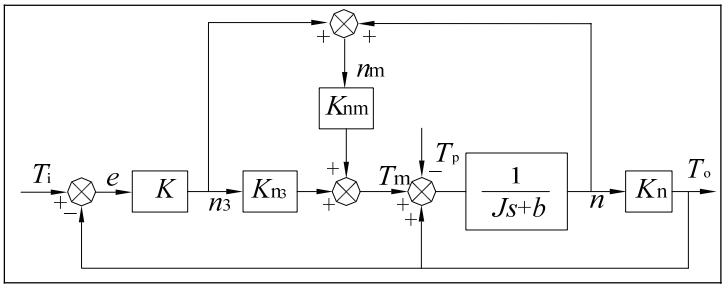

Figure 2: Block diagram of the system

where T_i—— Target torque of the engine
T_o—— Output torque of the engine
T_p—— Driving torque of the hydraulic pump
n—— Actual rotational speed of the system
n_m—— Synchronous rotational speed of the electric motor
K—— Proportional coefficient between torque deviation e and n3
K_{n3}, K_{nm}—— Linearized torque coefficient of the electric motor
K_n—— Linearized torque coefficient of the engine
J, b—— Rotational inertia and viscous damp of the hydraulic pump

A simulation experiment bench, which is illustrated in Figure 3, was established in our lab to study the performance of the work-point control system. Considering the convenience of control, we use one 37kw variable-frequency electric motor M_1, which is controlled by inverter Inv_1, to replace the engine in Figure 1. Variable-frequency electric motor M_2, with the power of 22kw, is controlled by inverter Inv_2. M_1 and M_2 are connected in parallel to drive the hydraulic pump. A set of capacitor, with the capacity of 25F and maximum voltage of 400V, is used as the accumulator of the experiment system.

The controller, which is composed of one industry control computer, one data acquisition card and one data control card, is the main control unit of the system. The sensors are used to measure the output pressure P_p , the rotational speed n and the flow rate Q of the pump, torque T_1 of M_1 and T_2 of M_2, the voltage U and current I of the capacitor, etc. The controller collects and processes data from the sensors and outputs the signals frequency F_1 of Inv_1, frequency F_2 of Inv_2, displacement D_c of the hydraulic pump and pressure P_c of the relief valve, to control the speed of the electric motors and flow rate and pressure of the hydraulic system.

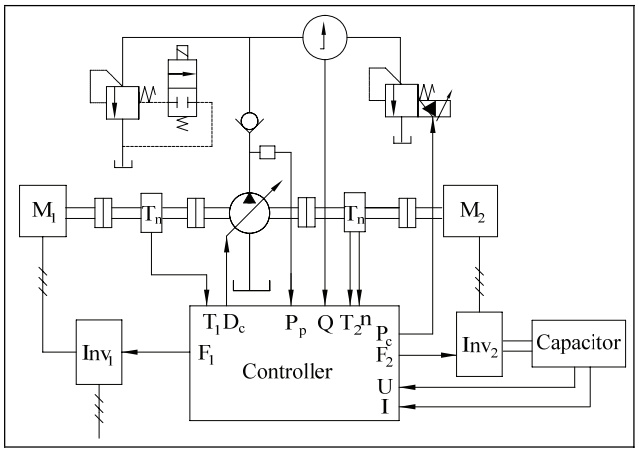

Figure 3: Schematic of the experiment system

Based on the block diagram shown in Figure 2, the engine constant work point control strategy is researched. Figure 4 shows the output power of the hydraulic pump in one work cycle (the data is derived from actual work cycle of hydraulic excavator). Figure 5 presents the comparison of output power of M_1 and M_2. It can be seen that the output power of M_1 fluctuates little during the work, which shows the work point of the engine is almost constant. And Figure 5 also shows that the output power of M_2 is always lower than that of the capacitor, and the difference of them is the transformation energy loss of between the electric motor M_2 and the capacitor.

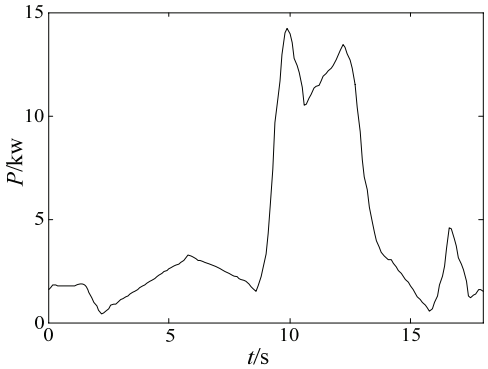

Figure 4: Output power of the hydraulic pump

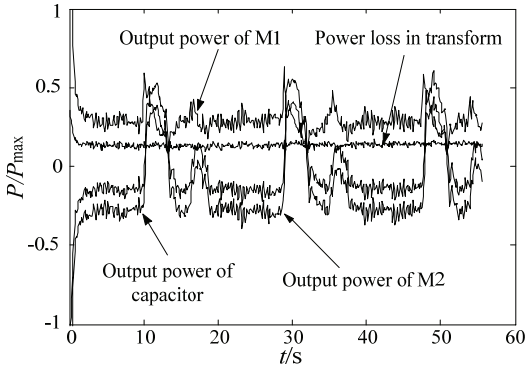

Figure 5: Comparison of the output power

But as the chosen work power of the engine cannot be exactly the same with the average of the load power under this control strategy, SOC of the capacitor will exceed its work range after long time work. This limitation can be eliminated by adopting engine double work points control strategy.

2.2 Double work points control strategy

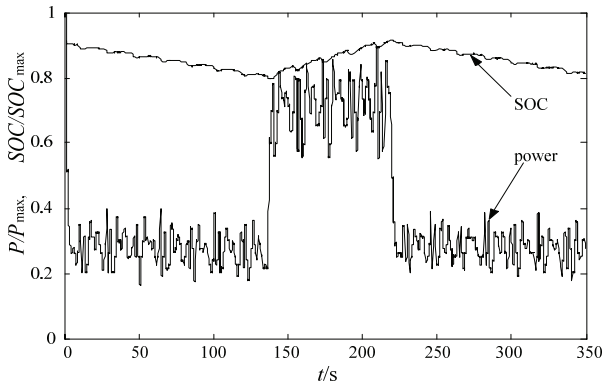

Figure 6: SOC of the capacitor and power of M_1

The principle of double work points control strategy is that the engine can work at one high power point P_h and one low power point P_l in the high efficiency area. When SOC of the capacitor exceeds the set upper limit, the engine switches to P_l. When SOC comes to the set low limit, the engine switched to P_h. In this work mode, the engine efficiency keeps high and SOC of the capacitor won't exceed its work range.

The double work points control strategy is studied in the experiment system mentioned above and the experiment curves are shown in Figure 6. It can be seen the work points of M1 switch between P_l and P_h according to the SOC, which indicates the feasibility of this control strategy.

To improve the efficiency of the whole system, it needs to optimize the engine work point besides employing feasible control strategy. Then the engine can work at high efficiency point, and at the same time the other components can also work at their high efficiency states.

3 OPTIMIZATION OF ENGINE WORK POINT

3.1 Theoretical analysis

As the hydraulic excavator always works periodically, the efficiency of the system is equivalent to that in one work cycle. In one work cycle T, the input energy of the system is:

$$E_i = \int_0^T n_e T_e / \eta_e \, dt \tag{1}$$

where n_e—— Rotational speed of the engine
T_e—— Torque of the engine
η_e—— Efficiency of the engine

The output energy of the system is:

$$E_o = \int_0^T pQ dt + \Delta E_c \tag{2}$$

where p—— Pressure of the hydraulic pump
Q—— Flow rate of the hydraulic pump

ΔE_c —— Energy consumption of the capacitor

The energy consumption of the capacitor is:

$$\Delta E_c = \int_0^T n_m T_m (\eta_m \eta_c)^s \, dt \tag{3}$$

where
n_m—— Rotational speed of the electric motor
T_m—— Torque of the electric motor
η_m—— Efficiency of the electric motor
η_c—— Efficiency of the capacitor
s—— State of the capacitor. When the capacitor is charged, s is 1; When the capacitor discharges, s is -1.

From equations (1)-(3), the complete efficiency of the system is:

$$\eta = \frac{E_o}{E_i} = \frac{\int_0^T pQ dt + \Delta E_c}{\int_0^T n_e T_e / \eta_e \, dt} = \frac{\int_0^T [pQ + n_m T_m (\eta_m \eta_c)^s] dt}{\int_0^T n_e T_e / \eta_e \, dt} \tag{4}$$

It can be seen for equation (4) that the factors affect the efficiency are the engine work point $P_e(n_e,T_e)$, efficiency η_e, the pressure p and flow rate Q of the hydraulic pump, the work point $P_m(n_m,T_m)$ of the electric motor, efficiency η_m, and efficiency η_c of the capacitor.

In equation (4), efficiency η_e of the engine is corresponding to its work point $P_e(n_e,T_e)$, which is determined by the efficiency map. As the power system is parallel, the work point P_m of the electric motor is correlative with the pressure and flow rate of the hydraulic pump and engine work point P_e. So $P_m=f(p,Q,P_e)$. Like the engine, $\eta_m=f(P_m)$. The state s and the efficiency η_c of the capacitor are relevant to P_m. They are functions of P_m.

In one certain work condition, pressure p and flow rate Q of the hydraulic pump are definite values. According to the analyses, other variables are functions of P_e. So the system efficiency η is only correlative with P_e, says $\eta=f(P_e)$.

When the engine is under double work points control strategy, n_e and T_e are fixed values in one work point. According to the system schematic shown in Figure 1, n_m is equal to n_e but T_m changes with the load. Thus, n_e can be firstly chosen based on the efficiency maps of the engine and the electric motor. Our former experiment results show that η_c varies little in various work conditions. So we only consider η_e and η_m in our research.

It can be seen from Figure 4 that the output power of the hydraulic pump fluctuates quickly and in large span. When P_e is chosen, the power fluctuation of hydraulic pump transforms to that of the electric motor. To improve η_m, the work area of the electric motor should be in highest possible efficiency area. But it's difficult to realize as the power of the electric motor change largely. One feasible way is to analyze the power

distribution of the hydraulic pump firstly and then choose proper P_e to make the electric motor working in high efficiency at most time.

Firstly, we optimize the high power work point P_h of the engine. Figure 7 and 8 are efficiency maps of the engine and electric motor. According to the two maps, the rotational speed of P_h can be chosen 1800rpm. At this rotational speed, the high efficiency areas of the engine and electric motor are overlapped. As the rotational speed is constant, the power distribution of the hydraulic pump can be transformed to the torque distribution, which is shown in Table 1. It can be seen from Table 1 that 72% of T_p is distributed within the range of 0-20N·m and 10% is in 60-70N·m. So we choose the torque of P_h is 120N·m as the triangular point shown in Figure 7. Under this circumstance, 72% work time (the long line in Figure 8) of the electric motor is in high efficiency area and 10% (the short line in Figure 8) is near high efficiency area. And if the rotational speed is chosen higher, η_m will be improved. But the power of the electric motor will exceed its work range.

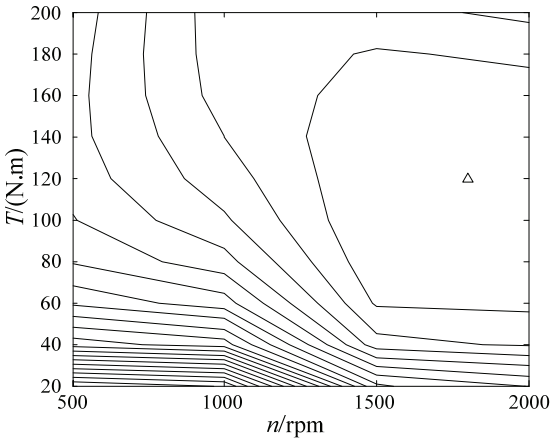

Figure 7: Efficiency map of the engine

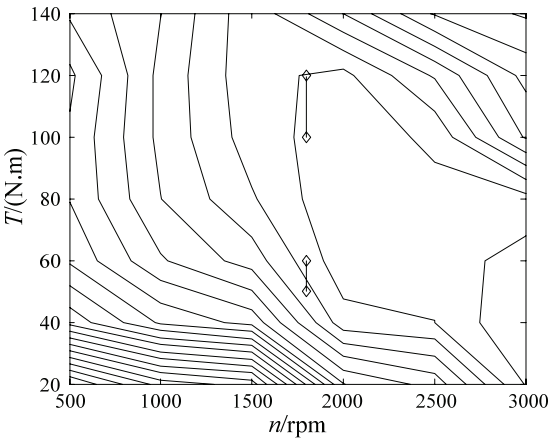

Figure 8: Efficiency map of the electric motor

Table 1: Distribution of driving torque of the hydraulic pump

Torque(N·m)	Percent
0-10	34%
10-20	38%
20-30	4%
30-40	2%
40-50	1%
50-60	4%
60-70	10%
70-80	6%

The torque of P_l should be lower than the average driving torque of hydraulic pump, which is about 22N·m. But η_e and η_m are both very low when T_e is between 0 and 22N·m. So we choose the torque of P_l 0N·m, that's to say, the electric motor drives the hydraulic pump alone.

Based on the experiment system presented in Figure 3, experiment studies have been done to examine the feasibility and effect of this optimization method.

3.2 Experiment study

During the experiment, the controller set the rotational speed of M_1 to the preset value and outputs control signals to hydraulic pump and proportional relief valve. The torque of M_1 keeps the set constant value through adjusting the torque of M_2 by changing its synchronous rotational speed. When SOC comes to the set upper limit, the set torque of M_1 is switched to low value. The experiment ends when SOC drops back to the initial value.

We test the efficiencies when T_l is 0N·m and T_h is 75N·m, 85N·m, 100N·m, 120N·m in this experiment. The results, which are shown in Table 2, are consistent with the analyses trend. When T_h is 120N·m and T_l is 0N·m, the complete efficiency η is 0.419. But when the engine works at other work points, the efficiencies are not so high. The reason is as the above analyses. So it indicates that the optimization method is feasible.

Table 2: Experiment results

T_l(N·m) \ T_h(N·m)	75	85	100	120
0	0.374	0.390	0.4	0.419

Figure 9 presents the torque of M_2 and SOC of the capacitor when T_l is 0N·m and T_h is 120N·m in this experiment. It can be seen that when the torque of M_1 is T_h, the torque of M_2 is in the area from -100 to -120N·m, which is in the high efficiency area. And when SOC rises to upper limit, M_1 switched to low power work point and M_2 outputs the power needed, which indicates the feasibility of this optimization method.

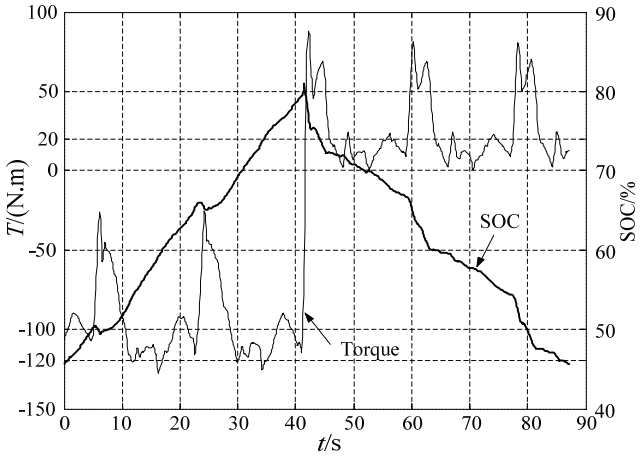

Figure 9: Torque of M_2 and SOC of the capacitor

But theoretical analyses and experiment study both indicate that the optimized engine

work point cannot keep the electric motor in high efficiency area during all working time restricted by the efficiency maps of the engine and the electric motor. So it is necessary to match the parameters of the engine and the electric motor in order to improve the complete efficiency of the system.

4 CONCLUSIONS

(1) Engine constant work point control strategy is proposed. Experiment results indicate that this control strategy can keep the engine working in high efficiency area by adjusting the electric motor, but cannot ensure SOC of the capacitor in work range after long time work.

(2) Engine double work points control strategy is developed. This control strategy overcomes the deficiency of constant work point control strategy. Experiment results indicate that this control strategy can keep SOC in work range after long time work.

(3) An optimization method based on power analysis is presented. Experiment study indicates that this method is feasible and can improve the complete efficiency of the system.

(4) Study also indicates that the optimization of the engine work point cannot keep the electric motor in high efficiency area during all working time. So it is necessary to match the parameters of the engine and the electric motor in order to improve the complete efficiency of the system.

REFERENCES

[1] Zhang YT, Wang QF, Xiao Q. Simulation research on energy saving of hydraulic system in hybrid construction machinery. PROCEEDINGS OF THE SIXTH INTERNATIONAL CONFERENCE ON FLUID POWER TRANSMISSION AND CONTROL, 2005:509-513

[2] Wang Qingfeng, Zhang Yanting, Xiao Qing. Evaluation for energy saving effect and simulation research on energy saving of hydraulic system in hybrid construction machinery. CHINESE JOURNAL OF MECHANICAL ENGINEERING. 2005, 41(12): 135-140

[3] Matsubara M, Matoba N. Hybrid construction machine. JP2004011256. 2004-01-01

[4] Naruse M., Oji N. Hybrid type construction machine. JP2004011502 . 2004-01-15

[5] Naruse M., Tamaru M., Kimoto K. Hybrid construction equipment. US6708787B2. 2004-03-23

[6] Masayuki kagoshima, Toshio Sora, Masayuki Komiyama. Development of hybrid power train control system for excavator. PROCEEDINGS OF JSAE, 2003, 119: 1-6

FAULT CLASSIFICATION BASED ON SELF-ORGANIZING MAPS IN WATER HYDRAULIC FORKLIFT

Krogerus T., Sairiala H., Saarinen M. and Koskinen K.T
Tampere University of Technology
Institute of Hydraulics and Automation
P.O.Box 589
33101 Tampere, Finland
Phone +358 3 365 4432, Fax +358 3 365 2240
E-mail: tomi.krogerus@tut.fi

ABSTRACT

The goal of this paper is to study typical fault situations from water hydraulic valves and cylinders where the Self-Organizing Maps (SOM) with unsupervised learning is used to classify measurement data. Before classification feature extraction is performed to extract relevant and discriminating information from the measurement data and also to reduce data dimensionality. This way it is possible to reduce the amount of measurement data points and improve their interpretability. The extracted features are then used for training and testing the SOM. Feature extraction method used in this paper is wavelet analysis. Operation of the fault classifier is tested in a test system of water hydraulic forklift where the lift movement from the forklift is used.

KEYWORDS: Water hydraulics, Fault classification, Self-Organizing Maps, Condition Monitoring, Forklift

1 INTRODUCTION

The main advantage of hydraulics in the mobile machines is large force to weight or size ratio. Oil is usually used as a pressure medium in these machines but the use of oil hydraulics can cause environmental disadvantages. Oil leakages from the machines are quite common and the leaking oil is obviously polluting the environment. Environmental friendliness of hydraulic systems can be increased by using different fluids instead of oil. By replacing the oil in the hydraulic systems with water the environmental impact of leakages in the system can be minimized. There are only few earlier studies where the possibilities of using water hydraulics in mobile machines are investigated [2, 21]. This study joins as a part to basic research project under way in

IHA where the use of water hydraulics in mobile machines is studied. In this study forklift is used as a research platform where the oil hydraulic components from the work hydraulics of the forklift have been replaced with water hydraulic ones and the main focus is in two work movements which are lift and reach. The driving transmission is electric.

Since this type of forklifts is mainly used in indoor environments the use of tap water in hydraulic system minimizes the loss of handled products in case of leakage. Also there are places in which the use of oils is not allowed because of demanded cleanliness or risk of fire or explosion. In these kinds of places normally forklifts with electrical actuators are used but the problem with these is the limited lifting power when compared to hydraulic forklifts.

Despite of its good properties water hydraulics have some challenges which need to be taken into consideration. The component technology is rather undeveloped when compared to oil hydraulics. This means that all the necessary components to realize traditional type of hydraulic circuits may not be available but different kind of hydraulic circuits and more efficient control need to be used.

The durability of components is not as good as with oil hydraulic components. The high flow velocities in valves lead to high erosion and cavitation. Also the lack of proper lubrication creates potentially high wear of components if material pairs are not selected properly and the construction of the parts is not well designed. Because the viscosity of the water is low the clearances in the components need to be extremely small. Small clearances lead to the possibility of sticking of the valves if the water in the system has impurities. [11, 19]

Because of these reasons sophisticated on-line condition monitoring of the components and also the fluid is required. On-line condition monitoring of hydraulic components allows the forecast of needed maintenance to avoid further damages in the system and the maximization of the component life time. Intelligent condition monitoring allows also the tuning of the control parameters when changes in the component properties are identified. For this purpose proactive condition monitoring system has been developed [9, 10, 15].

Neural network research has been very active for several years and there has also been interest in neural network applications to fault diagnosis problems [1, 3, 12, 13, 14, 17]. Neural network is one possible method which is suitable for classifying different system states of the water hydraulic system. If all the damages are not assumed to be known before diagnostics, ordinary neural network with supervised learning for their detection can not be used [12]. Usually this is the real case and therefore, in this study, neural network method Self-Organizing Maps are used with unsupervised learning. Since this type of neural network can perform non-linear functional mapping between sets of variables they can be used to classify the raw input data directly [14]. However, sometimes the performance of the network can be decreased if high measurement frequency and/or large number of measurements variables are used and therefore it is important to preprocess any raw and/or dynamic data before classifying them to improve the network performance. Wavelet analysis is used to extract information-rich features for use in classification.

2 TEST SYSTEM OF THE FORKLIFT

The forklift (reach stacker) and the water hydraulic test system used to test the condition monitoring of water hydraulic forklift are presented in Fig 1. The test system has a lifting cylinder with load mass and a 4/3-way proportional valve. The size of the cylinder in the test system is 32/16-500 while in the actual forklift the lifting cylinder is 63/40-1000. The maximum load mass in these tests is approximately 200 kg and the supply pressure is 70 bar while in the forklift the maximum load will be approximately 1000 kg. The load in the test bench is smaller than in the forklift due to the limitation of the test bench and this has been compensated with smaller cylinder. The control valve is a proportional spool valve [19].

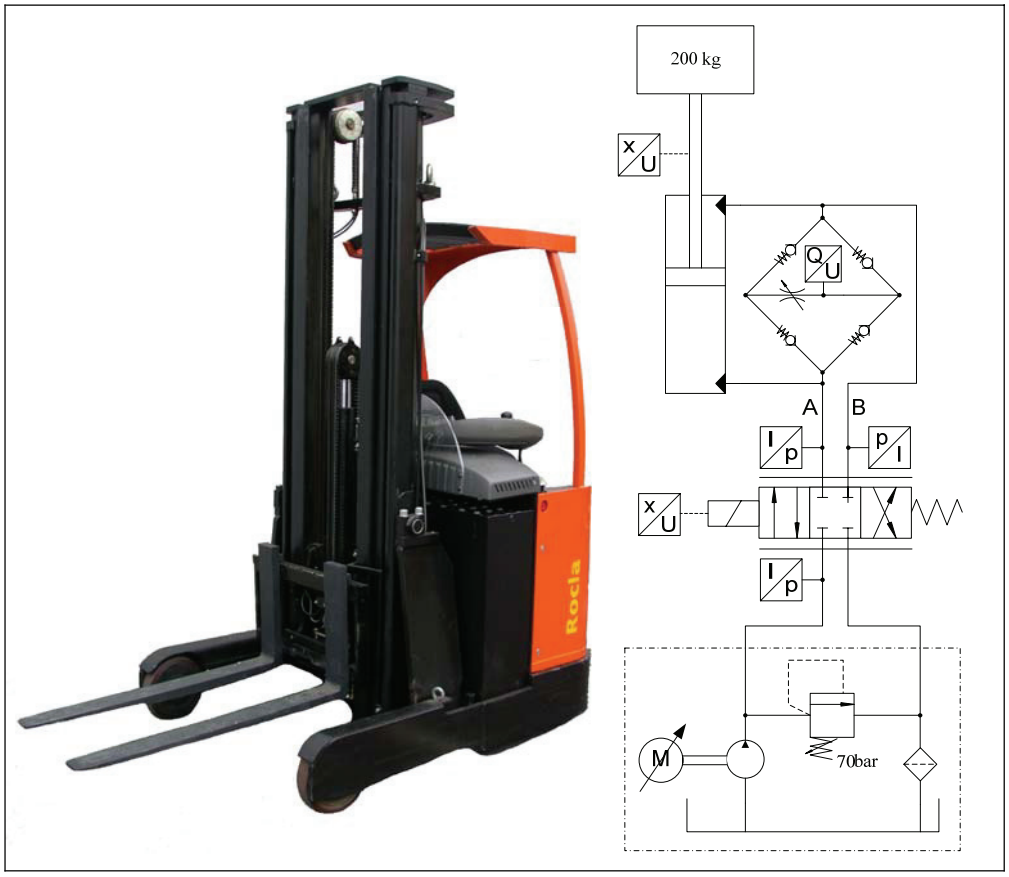

Fig. 1: *Forklift (reach stacker) and its test system (lift).*

The lifting cylinder is driven in a specified sequence. The cylinder is fully retracted when the sequence starts. The upper limit used in the test system is 350mm and lower limit 230mm when the cylinder is retracting and a specified ramp is used in acceleration and deceleration of the cylinder. The deceleration ramp starts after the limit is exceeded. The used limits are programmable. In Fig. 2 is presented an example of the driven sequence and control signal of the proportional valve from normal situation. This type of work sequence is typical with forklifts.

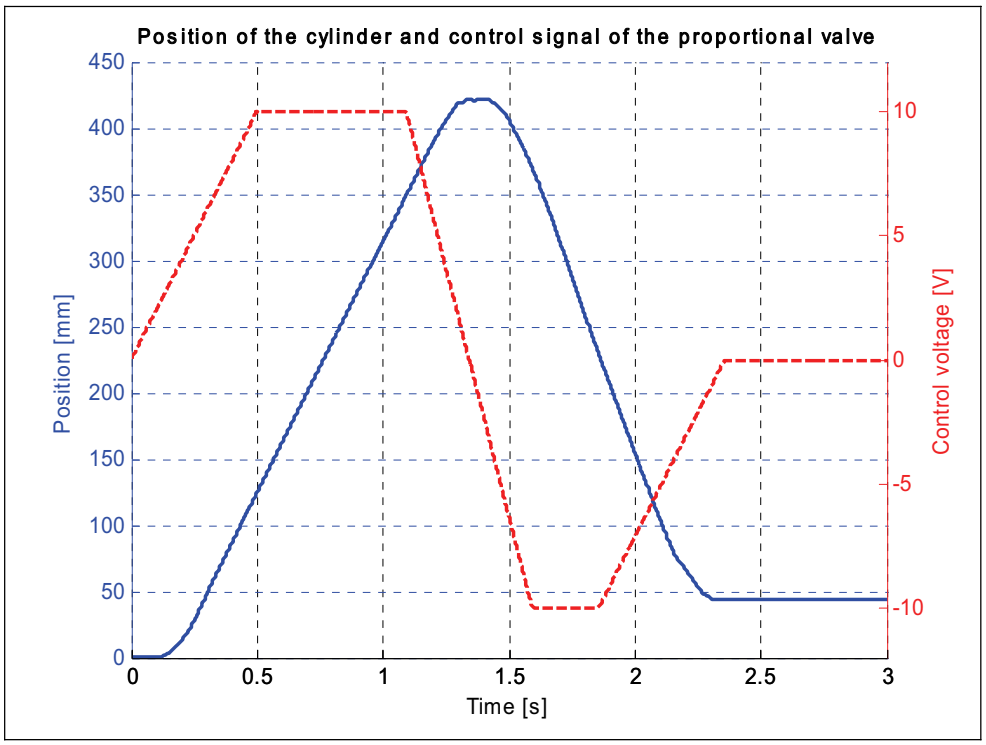

Fig. 2: *Position of the cylinder and control signal of the proportional valve (from normal situation).*

2.1 Fault types

The two monitored components in the test system are the cylinder and the control valve. In this study sealing faults which cause internal leakage in these components are studied. These types of faults are emphasized in water hydraulic systems because of the low viscosity level of the water.

2.1.1 Valve

The potential fault type in control valve is increased internal leakage. The leakage can be increased because of two reasons: seal cracks and wear of the spool. The construction of the valve is such that the spool is inside a sleeve that is mounted in the body of the valve and between the sleeve and the body are o-ring sealings [19]. If these o-rings are damaged the result is increased internal leakage between the ports of the valve. How this is effecting in the function of the system is depending on which sealings are damaged and how big the damage is. Similar damages can occur if the spool is wearing because of the erosion and cavitation in the valve. Also this is causing increased internal leakage.

In this study seal crack in the spool sleeve of the valve has been used as a fault case. The used proportional valve has a spool sleeve that has six seals and four of them are of interest in this study. The valve has external drain line and the outermost seals are only for sealing the drain line from the tank line and do not affect the behavior of the system so that is why they are not used in this study. The effects of seal cracks in these seals are investigated one at a time.

This kind of fault type can be caused by deterioration of the seal material or poor assembling of the spool sleeve into the valve. The used spool sleeve with seals and an example of seal crack are shown in Fig. 3.

Fig. 3: *Spool sleeve of the valve and a seal crack.*

2.1.2 Cylinder

The potential faults in the cylinder are internal leakages through the sealings. This can be caused by the wear of the sealings or damage in the cylinder barrel. Typical cylinder faults have also been studied in [3, 13, 14, 23, 24].

The sealing faults are used here as a fault case. The life time of the sealings of water hydraulic cylinders is much lower than the life time of oil hydraulic cylinders because of the bad lubrication which is caused by the small viscosity of water.

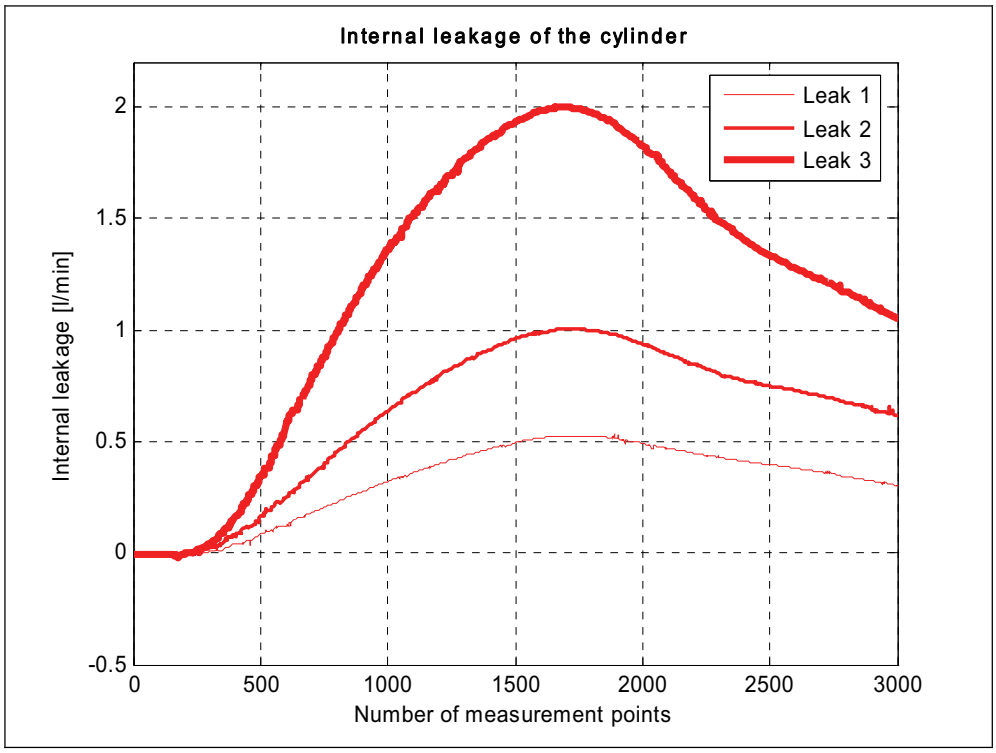

Fig. 4: *Different internal leakage levels of the cylinder.*

The worn/damaged cylinder causes internal leakage which changes behavior of the system. The leakage between the annulus and piston sides of the cylinder is created here by opening a bleed valve between the actuator ports. Three different leakage levels which are used are shown in Fig. 4. The leakage levels used in this paper are determined by the maximum leakage value of the driven sequence. These levels are approximately 0.5/1.0/2.0 l/min. A flow meter is used to set the desired leakage values.

2.2 Training and testing data

Training and testing data for use in fault classification are measured from the test system. The test system is run in normal and two fault situations (internal leakage of the cylinder and the valve). The measured variables are pressures A and B from the actuator ports. The measured pressures are preprocessed and used in training and testing the SOM.

There are eight different system states to measure which are normal state and seven different fault states. The same sequence is measured 100 times in each case so the total amount of sequences is 800. The measurement frequency is 1 kHz and the measurement time is three seconds so 3000 measurement points are recorded in every sequence. Multiple sequences are driven because this way it is possible to improve the generalization of the network when new data is presented to the network and to also get adequate resolution in results.

First only half of the normal state measurements are used in training and other half is used in testing. Also half of each fault state measurements are used in testing. When the fault state is identified properly then the other half of the fault state measurements can also be used in training.

In Fig. 5-8 are shown examples from the measurements. From the figures can be seen how some of the normal and faulty measurement points are very close to each other. That is why the whole sequence is classified here as a normal or fault state instead of classifying each measurement point like in [12, 13].

In Fig. 5-6 are shown pressure signals A and B from the actuator ports in the cylinder leakage case and its coefficients extracted from the original data using wavelet analysis. Normal situation and three different fault cases (cylinder leakage) are shown. Changes in pressure levels are quite small but the effect of leakage can be clearly seen because leakage slows down the lifting state.

The pressure signals A and B from the normal and four different seal crack situations and their coefficients are shown in Fig. 7-8. In this case same clear slowing down of lifting state do not exist but some deviation between the normal and fault situation can be found with every seal crack case. Especially in pressure B there are clear changes in the beginning and at the end of the sequence.

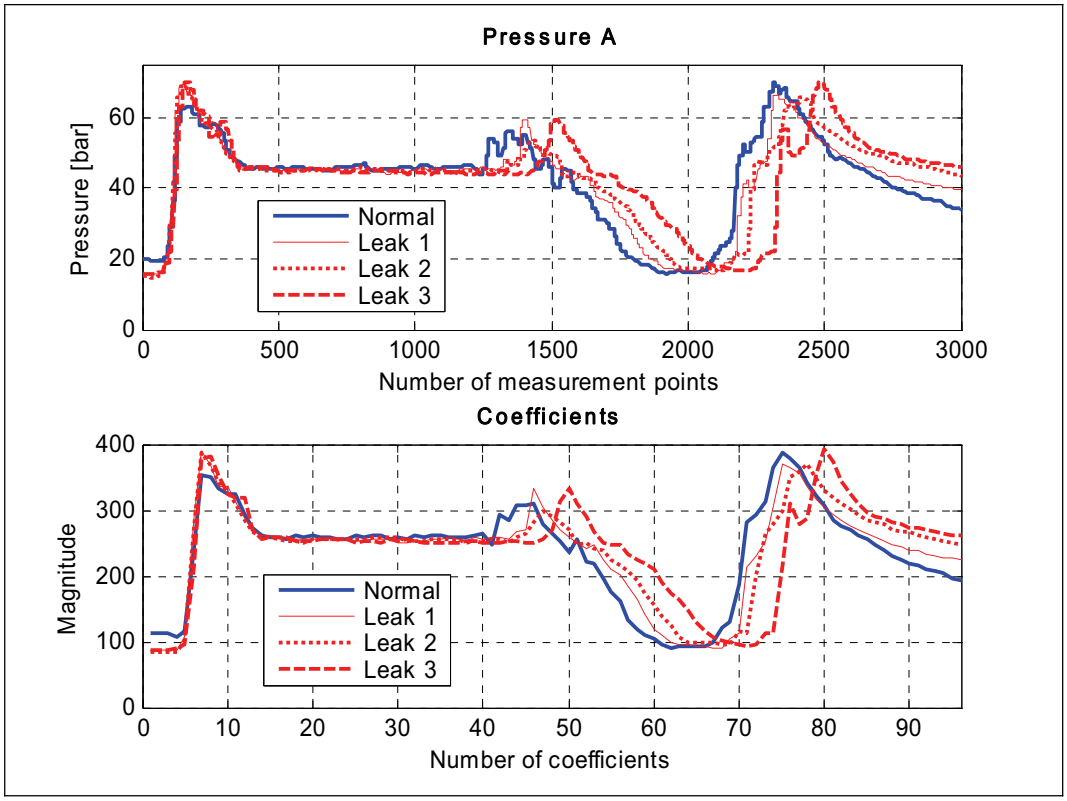

Fig. 5: *Example of pressure A and its wavelet coefficient in normal and three different fault situations (cylinder leakage).*

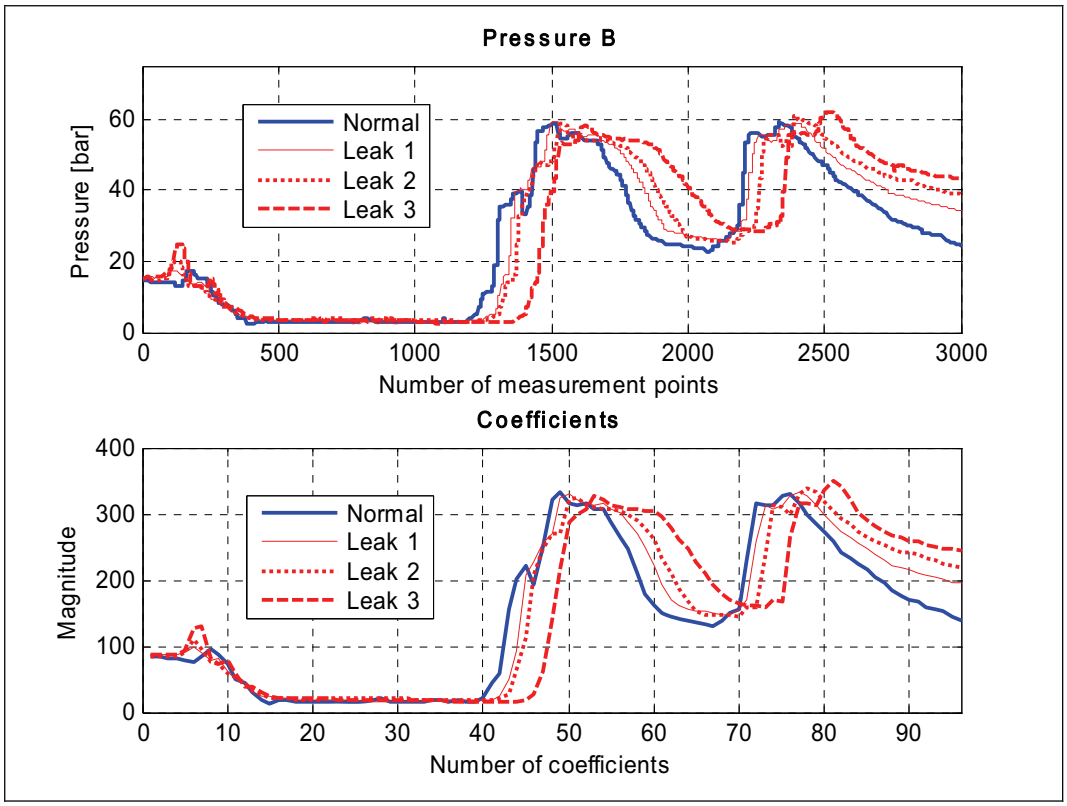

Fig. 6: *Example of pressure B and its wavelet coefficient in normal and three different fault situations (cylinder leakage).*

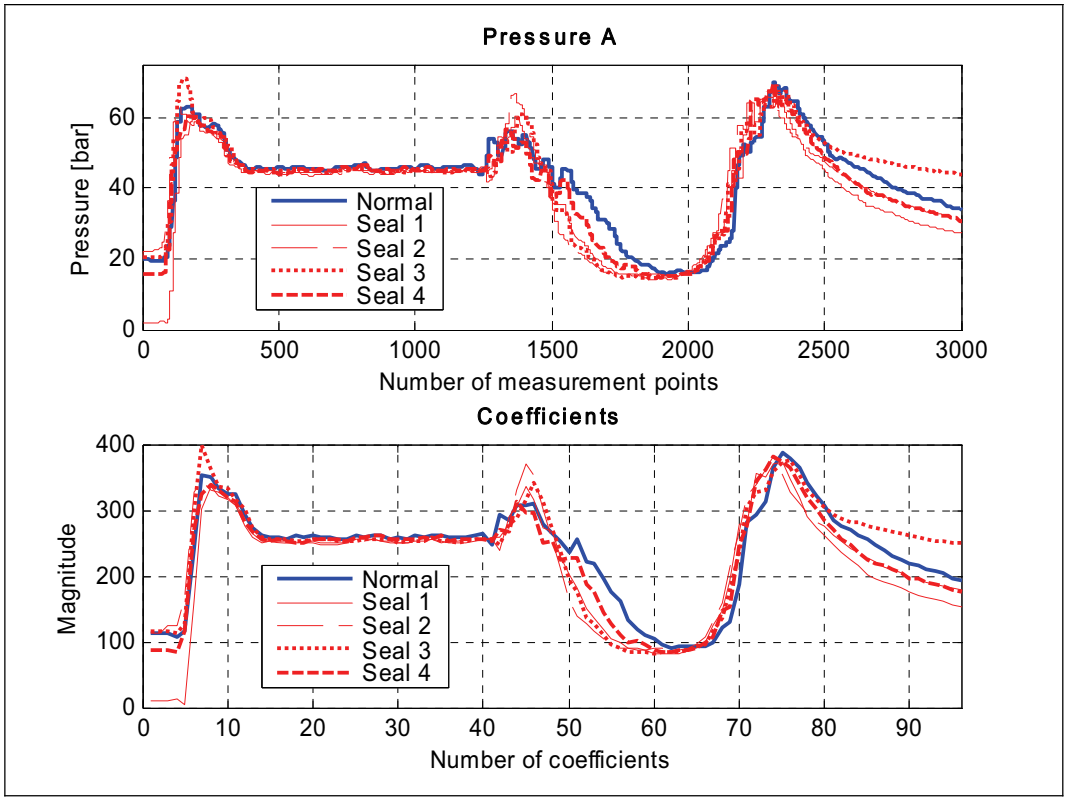

Fig. 7: *Example of pressure A and its wavelet coefficient in normal and four different fault situations (seal crack).*

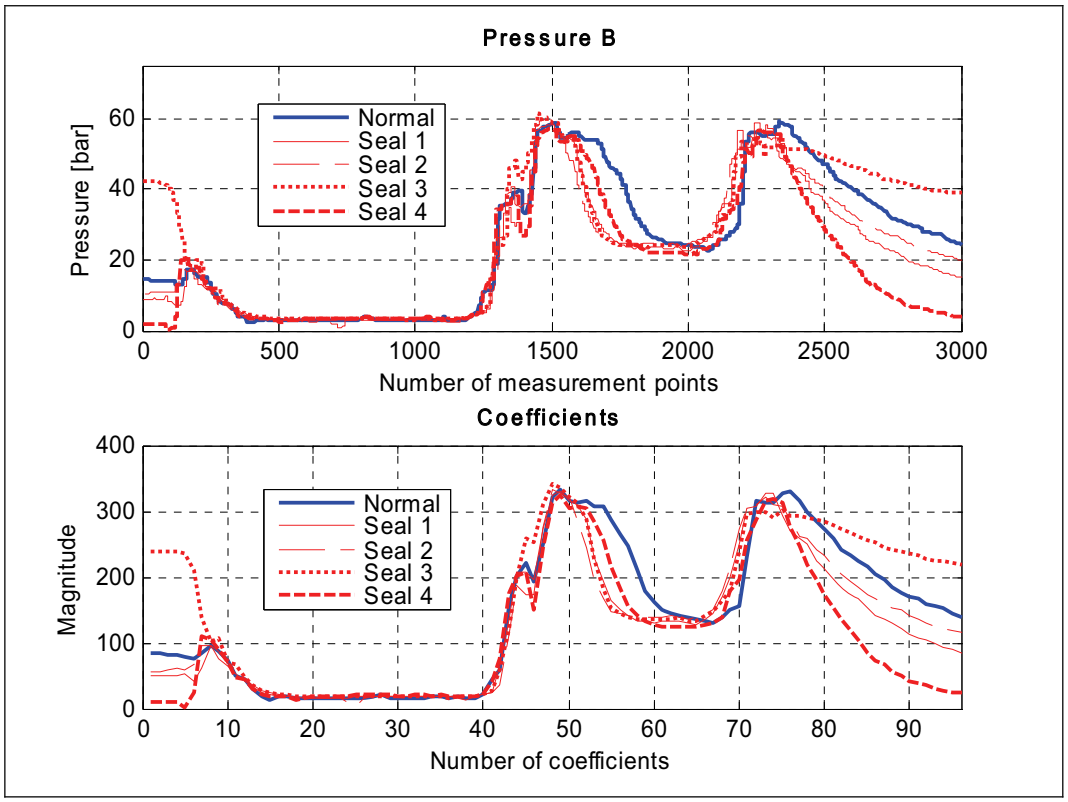

Fig. 8: *Example of pressure B and its wavelet coefficient in normal and four different fault situations (seal crack).*

3 FEATURE EXTRACTION

Preprocessing of the measurement data usually involves extracting relevant and discriminating information and in so doing reducing data dimensionality. This process is often called feature extraction. The feature extraction is a method to transform the original signal into other preferably more descriptive one. Variables that are used to discriminate different system states from each other are called features. [7, 18]

Sometimes the performance of the network can be decreased if high measurement frequency and/or large number of measurements variables are used and therefore it is important to preprocess any raw and/or dynamic data before classifying them to improve the network performance. In these kinds of situations it becomes necessary to decrease the number of variables and/or measurement points to a manageable size and also retain as much discriminatory information as possible. The basic idea is to reduce the dimensionality and optimize the discriminatory information. The discrete wavelet transform is used to extract wavelet coefficients which are then used for classification.

3.1 Wavelet analysis

Wavelet analysis is capable of revealing aspects of data that other signal analysis techniques fail to discover, aspects like trends, breakdown points, discontinuities in higher derivatives, and self-similarity. Furthermore, because it affords a different view of data than those presented by traditional techniques, wavelet analysis can often compress or de-noise a signal without appreciable degradation. By using wavelet analysis it is possible to extract information-rich features for use in classification. [16]

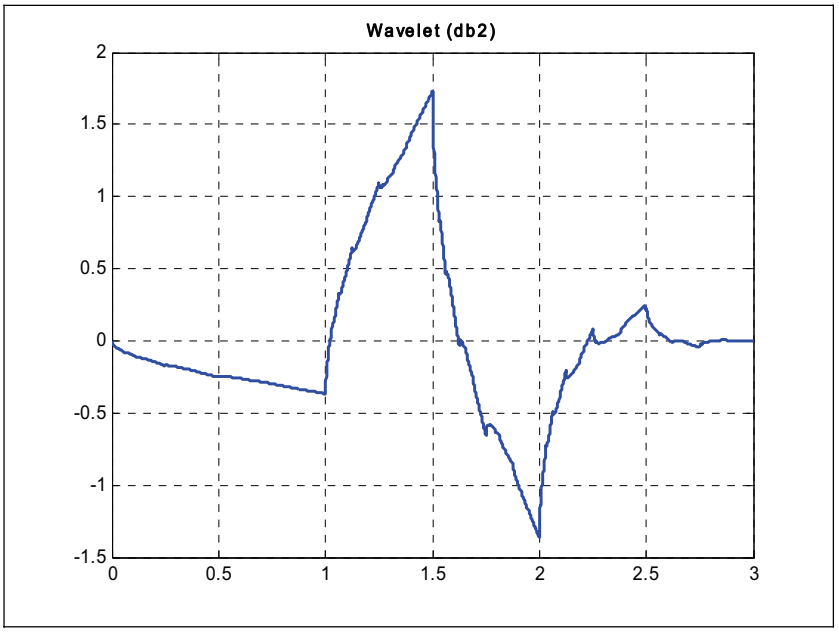

Fig. 9: *Approximation of the Daubechies wavelet function (db2).*

The basic idea of wavelet analysis is to adopt a wavelet prototype function, called an analyzing wavelet or mother wavelet [4]. A wavelet is a waveform of effectively limited duration that has an average value of zero. In the wavelet analysis original measured

signal is broken up into shifted and scaled versions of the analyzing (or mother) wavelet. In Fig. 9 is presented the used analyzing/mother wavelet (db2).

Because the original signal or function can be represented at certain accuracy using only approximation coefficients, data analysis can be performed using just the wavelet coefficients [4]. The wavelet coefficients are extracted from the measured data and used as inputs to the Self-Organizing Map in the classification. Examples of the coefficients are shown in Fig. 5-8 where 96 approximation coefficients are extracted in each case from the original pressure data (3000 data points).

In Fig. 10 is presented the measured pressures A and B from the actuator ports and reconstructed signals using approximation coefficients extracted from the pressure signals. When 96 coefficients are used the original and reconstructed signals are almost identical. The pressure signals are from normal situation.

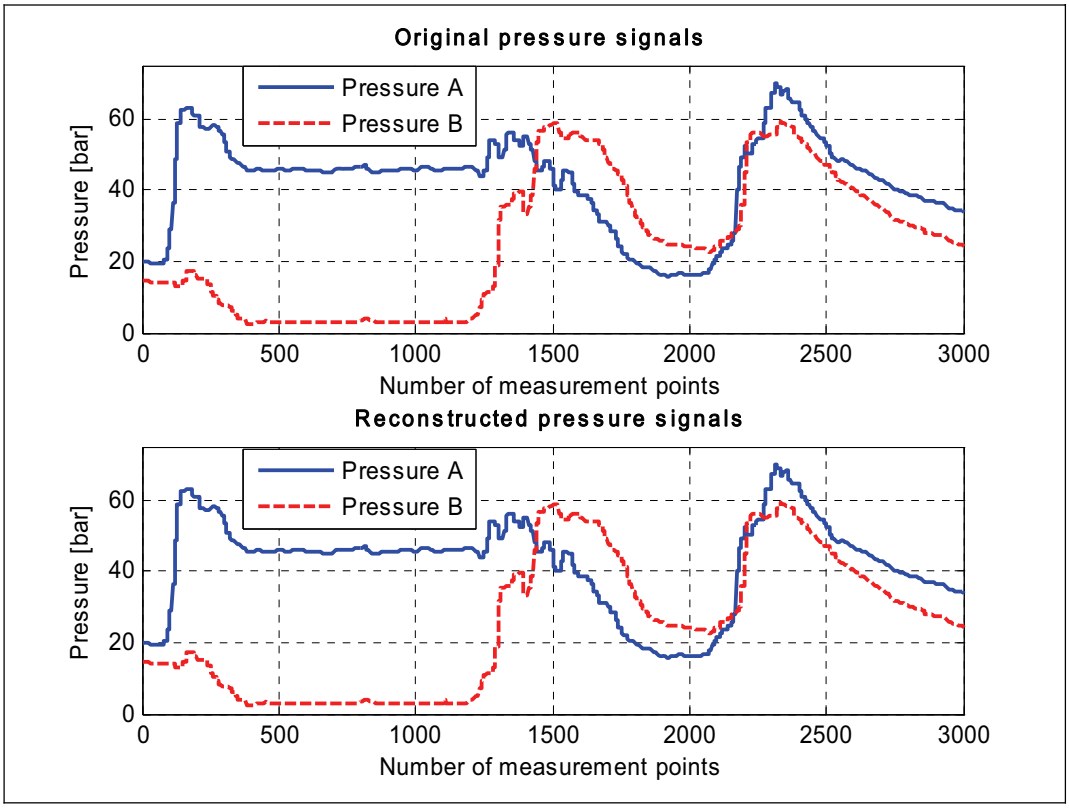

Fig. 10: *Original pressure signals and reconstructed pressure signals using approximation coefficients.*

4 FAULT CLASSIFICATION

Different system states (normal and different fault states) are classified using extracted coefficients from the pressure signals A and B. One sequence is described using 192 (both pressures) data points so the used neural network has 192 inputs. The fault classification is performed using Self-Organizing Maps.

4.1 Self-Organizing Maps

The Self-Organizing Map uses unsupervised learning. In unsupervised learning, the network is not trained towards specified outputs. Networks that are trained without outputs learn by evaluating the similarity between the input patterns presented to the network. Most of the algorithms, which use unsupervised learning, perform some kind of clustering operation where they categorize the input patterns into a finite number of classes [5].

In order to detect abnormal behavior the SOM is trained first only with data from the normal situation. The learned map is used to detect abnormalities in new data by monitoring the shortest distance of these new samples from the learned SOM codebook (all the weight vectors after training). The neuron whose weight vector is closest to the input vector **x** is called the Best-Matching Unit (BMU). The map units which are hit during the training are labeled after the training as a normal situation. Term hit means that neuron in the map has been chosen (at least one time) as a BMU in the training phase. After this a certain threshold is set. This determines the greatest distance on which recognition occurs. This way it is possible identify the state of the system. So the analysis is concentrated on finding the properties of the normal data and the appropriate means to identify the deviations from the normal situation. [6, 8, 22]

Training of the network goes as follows. First the extracted coefficients are scaled from 0 to 1. After that 50 normal sequences are fed to the network each containing 192 data points. Training algorithm is iterative and in each training step, one sample vector **x** (containing scaled values of coefficients) from the input data set is chosen randomly and the distances between it and all the weight vectors of the SOM are calculated. Weight (codebook) vectors of the SOM are updated so that the BMU and its neighbors are moved closer to the input vector in the input space. After many presentations neighboring neurons will have learned vectors similar to each other.

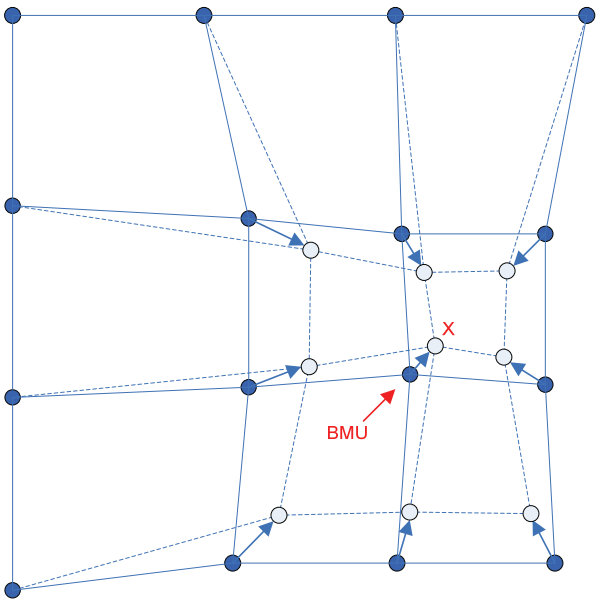

Fig. 11: *Basic structure of the Self-Organizing Map and updating the best matching unit and its neighbors [20].*

The SOM consists of neurons organized on a regular low-dimensional grid. These neurons are organized so that similar neurons are near and different ones far away each other. The basic structure of the Self-Organizing Map and updating the best matching unit and its neighbors are shown in Fig. 11. More details of the Self-Organizing Maps and the whole algorithm are presented in earlier publications [11, 12].

In testing we are just simply searching the smallest distance between input and all the weight vectors of the SOM. If the shortest distance is smaller than the set threshold then it is treated as a normal case but if distance is bigger then it is a fault case.

When fault states are identified properly and the fault levels are known then semantic labels are attached to certain units of the topological map so that fault levels can also be identified.

5 RESULTS OF THE CLASSIFICATION

The SOM is first trained to detect the state of the system. It is either normal or fault. After the fault states of the system has been identified and the fault levels are known then the network can be used to identify fault levels from the measurement data. In both cases unsupervised training is used.

5.1 System state identification

The number of map units in this situation is 7 x 5. The size of the map is quite small but it is not necessary to use a bigger one because it does not make the results any better and it also slows down the calculation. 50 sequences from normal situation are used in training and 50 sequences from each system state (normal + 7 x fault) are used in testing. In Table 1 are presented classification results of the system state. From the results can be seen that used classification method was able to classify all the sequences correct.

Table 1: *System state identification*

		Identified system state	
System state		Normal	Fault
Normal		50	0
Cylinder	Leak 1	0	50
	Leak 2	0	50
	Leak 3	0	50
Valve	Seal 1	0	50
	Seal 2	0	50
	Seal 3	0	50
	Seal 4	0	50

5.2 Fault level identification

The number of map units in this situation is 14 x 7. 50 sequences from each system state are used in training and other 50 from each system state in testing. In Table 2 are presented classification results of the fault level.

From the results can be seen that only one normal sequence is classified wrong. The sequences with cylinder leak 3 (2.0 l/min) are all identified correctly but with smaller leakages there are some errors in classification. With leak 1 (0.5 l/min) there are two sequences that are mix with leak 2 (1.0 l/min). All other errors are due to that empty map unit is chosen. Internal cylinder leakages under 0.5 l/min are very hard to detect using only pressure measurements. Seal cracks in seals 1, 2, 3 and 4 are separated from other faults very well but in some of the sequences empty map unit is chosen.

Selecting the number of map units is a sensitive parameter because when it makes some classification result better it can also deteriorate other cases. This could be prevented by using multiple networks instead of one.

Table 2: *Fault level identification*

		Identified system state								
System state		Normal	Cylinder fault			Valve fault				Empty
			Leak 1	Leak 2	Leak 3	Seal 1	Seal 2	Seal 3	Seal 4	
Normal		49	0	0	0	0	0	0	0	1
Cylinder	Leak 1	0	47	2	0	0	0	0	0	1
	Leak 2	0	0	49	0	0	0	0	0	1
	Leak 3	0	0	0	50	0	0	0	0	0
Valve	Seal 1	0	0	0	0	44	0	0	0	6
	Seal 2	0	0	0	0	0	45	0	0	5
	Seal 3	0	0	0	0	0	0	50	0	0
	Seal 4	0	0	0	0	0	0	0	45	5

In Fig. 13 is shown the distribution of neurons in both classification cases according to the state. System state identification on the left where only normal situation is used in training and fault level identification on the right. The numbers in the figure are 0 = normal, 1 = cylinder leak 1, 2 = cylinder leak 2, 3 = cylinder leak 3, 4 = seal crack in seal 1, 5 = seal crack in seal 2, 6 = seal crack in seal 3 and 7 = seal crack in seal 4. These numbers are used in classification.

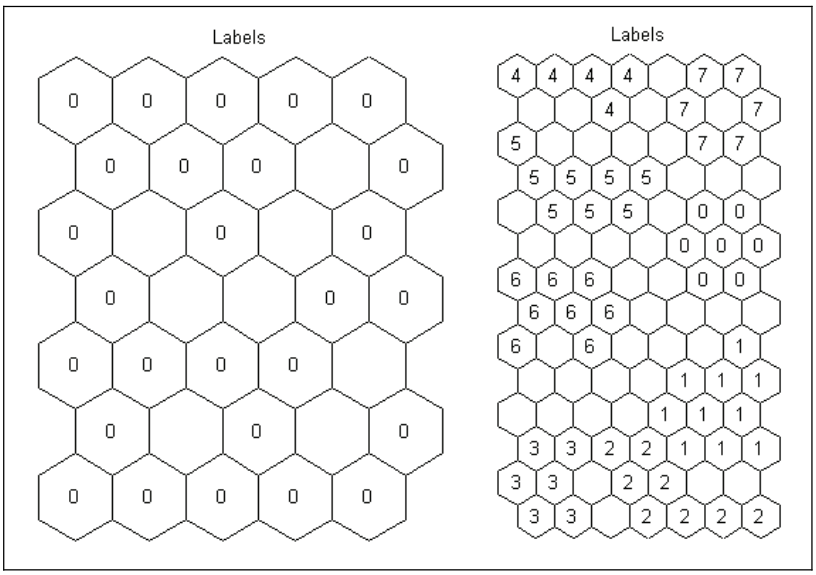

Fig. 12: *Distribution of neurons according to the state of the system. System state identification on the left where only normal situation is used in training and fault level identification on the right.*

6 CONCLUSION

The main goal of this research was to study typical fault situations from water hydraulic valves and cylinders where the Self-Organizing Maps (SOM) with unsupervised learning is used to classify measurement data. The faults used in this paper were internal leakages of the valve and the cylinder.

Wavelet analysis was used to extract approximation coefficients from the measurement variables pressure A and B which were then used in classification of the system state.

The SOM is first trained to detect the state of the system. When only normal state was used in classification and state were classified either normal or fault then the network was able to classify all the sequences correct.

After the fault states of the system were identified and the levels were known then it was possible to use the network to identify fault levels from the measurement data that have not been presented to the network before. In this case also data from the fault situation were used in the training of the network. The classification percent was 88-100% so every used fault level could be detected and separated from other levels.

The performance of the network is determined by how well it works with data that have not been trained to it. It does not bring any extra value to the classification system, if network works fine in a single trained situation. More important is the generalization capability of the network. In this study it was demonstrated that neural network method, Self-Organizing Maps (SOM), is suitable for detecting changes in the state of the water hydraulic system using only approximation coefficients from two pressure signals.

REFERENCES

1. Alhoniemi, E.; Hollmén, J.; Simula, O. and Vesanto, J. 1999. Process Monitoring and Modeling Using the Self-Organizing Map. *Integrated Computer-Aided Engineering*, Vol. 6, No. 1, pp. 3-14.

2. Cassens, L.; Thomas, M. and Krutz, G. 2003. Water Hydraulic Energy Savings Vehicle. *The Eighth Scandinavian Conference on Fluid Power, SICFP'03.* Tampere, Finland.

3. Crowther, W.; Edge, K.; Burrows, C.; Atkinson, R. and Woollons, D. 1996. Fault Diagnosis of a Hydraulic Actuator Circuit Using Neural Networks – A State Space Classification Approach. *Proc IMechE, Part I, Journal of Systems and Control Engineering*, Vol. 212.

4. Graps, A. 1995. An Introduction to Wavelets. *IEEE Computational Science and Engineering*, Vol. 2(2).

5. Hagan, M.; Demuth, H. and Beale, M. 2002. *Neural Network Design*. PWS Publishing Company, Boston, 1st edition.

6. Hiirsalmi, M. 2001. *Abnormality Detection Using SOM Modeling.* Version 1.1-1, VTT Information Technology. 55 p. Research Report TTE1-2001-16.

7. Hiirsalmi, M. 2005. *Design of a Feature Extraction and a Fault Classifier System Using Data Mining Techniques.* T4Liikkudia. Version 1.0-1, VTT Information Technology. 16 p. Research Report TTE1-2005-29.

8. Kohonen, T. 2001. *Self-Organizing Maps.* Springer-Verlag Berlin Heidelberg, New York, 3rd edition.

9. Krogerus, T.; Vilenius, J.; Liimatainen, J. and Koskinen, K.T. 2006. Applying Self-Organizing Maps to Condition Monitoring of Fluid Power Systems. *4th FPNI-PhD Symposium Sarasota/Florida 2006.* Florida, USA.

10. Krogerus, T.; Vilenius, J.; Liimatainen, J. and Koskinen, K.T. 2006. Self-Organizing Maps with Unsupervised Learning for Condition Monitoring of Fluid Power Systems. *SAE 2006 Commercial Vehicle Engineering.* Chicago, Illinois, USA.

11. Krutz, G. and Chua, P. 2004. Water Hydraulics – Theory and Applications 2004. *Workshop on Water Hydraulics, Agricultural Equipment Technology Conference, AETC'04.* Louisville, Kentucky, USA.

12. Kuravsky, L. and Baranov, S. 2001. Application of Self-Organizing Feature Maps for Diagnostics of Vibroacoustic Systems. *International Conference on Condition Monitoring.* St. Catherine's College, Oxford, UK.

13. Le, T.; Watton, J. and Pham, D. 1997. An artificial neural network based approach to fault diagnosis and classification of fluid power systems. *Proc IMechE, Part I, Journal of Systems and Control Engineering,* Vol. 206, 215-214.

14. Le, T.; Watton, J. and Pham, D. 1998. Fault classification of fluid power systems using a dynamics feature extraction technique and neural networks. Proc *IMechE, Part I, Journal of Systems and Control Engineering*, Vol. 212, 87-97

15. Liimatainen, J. 2006. *Dynamic User Interface for Proactive Condition Monitoring of Proportional Valve.* MSc thesis, Tampere University of Technology, Finland. (In Finnish)

16. Mathworks Inc. 2006. http://www.mathworks.com/ [Referred 20.12.2006]

17. Ramdén, T. 1998. *Condition Monitoring and Fault Diagnosis of Fluid Power Systems – A Approaches with Neural Networks and Parameter Identification.* PhD thesis No. 514. Linköping University, Sweden.

18. Rinta-Runsala, E. 2000. Drive System Monitoring: Requirements and Suggestions. MODUS-Project, Case Study ODT2. Version 1.0, VTT Information Technology. 24 p. Research Report TTE1-2000-19.

19. Sairiala, H.; Koskinen K.T.; Vilenius, M.: Jauhola, P.; Jauhola, L. and Selkosmaa, J. Control of a Water Hydraulic Cylinder Drive with New Proportional Valve. *The Eighth Scandinavian Conference on Fluid Power, SICFP'03.* Tampere, Finland.

20. SOM Toolbox. 2006. http://www.cis.hut.fi/projects /somtoolbox/ [Referred 20.12.2006]

21. Tessel, F. 2000. Wasserhydraulische Antriebssysteme in fahrenden Arbeitsmachinen mit Hub- und Neigeeinrichtungen. *2. Internationales Fluidtechnisches Kolloquium in Dresden.* Dresden, Germany.

22. Vesanto, J. 2002. *Data Exploration Process Based on the Self-Organizing Map*. PhD thesis, Acta Polytechnica Scandinavica, Mathematics and Computing Series No. 115, Helsinki University of Technology, Finland.

23. Vidqvist, Ville; Tervo, Jyrki. 2006. Data Mining Enhancement in Model Based Fault Classifiers of a Hydraulic Cylinder Drive. *4th FPNI-PhD Symposium Sarasota/Florida 2006.* Florida, USA.

24. Wue, T.; Chua, P. and Lim, G. 2004. On-line Fault Detection and Analysis of Modern Water Hydraulic System. *Journal of The Institution of Engineers, Singapore*, Vol. 44, Issue 4.

ADAPTIVE CONTROL OF WATER HYDRAULIC SERVO MOTOR SYSTEM –ROTATIONAL ANGLE AND SPEED CONTROL–

Kazuhisa ITO, Hidekazu TAKAHASHI, Shigeru IKEO
Fluidics Engineering Laboratory
Department of Mechanical Engineering
Faculty of Science and Technology
SOPHIA University
Kioicho 7-1, Chiyoda-ku, Tokyo 1028554, Japan
Phone & Fax +81-3-3238-3606
Email: kazu-ito@me.sophia.ac.jp

ABSTRACT

With the recently increased concerns on global environmental problems, the water hydraulic technique using pure tap water as a pressure medium has become a new drive source comparable to electric, oil hydraulic and pneumatic drive systems. However, the main problems for precise control of a water hydraulic servo motor system are steady state errors and overshoot due to its large friction torque in the low speed range. These accounts for the development of a strategy to compensate for uncertainties in the system and to ensure a closed-loop system maintain its specified performance.

In this paper, a model reference adaptive control (MRAC) was applied to a water hydraulic servo motor system. The MRAC system can admit parameter uncertainties by tuning the controller parameters depending on the error between a plant output and the reference signal given by the designer. The experimental results show that while the MRAC proved not to be applicable to the rotational angle control, this controller achieves good speed control performance.

KEYWORDS: Water hydraulics, Motor control, Adaptive control, Rotational angle control, Rotational speed control

1 INTRODUCTION

In a last decade, water hydraulic applications have increased and continue to increase. Water as a pressure medium gives many benefits compared to mineral oil, including lower environmental load, easy maintenance, good availability and so forth. In the early stage of development, many literatures reported the comparison between water and oil on physical and dynamical properties in use while these days' reports give us

the results of control techniques of water hydraulic devices. Linjima *et.al.* studied the position control of water hydraulic cylinder taking advantage of the low compressibility of water and low-cost low-pressure valves[1]. In [2], the displacement and speed control of water hydraulic cylinder are realized introducing the profile generator which generates smooth control signal to attenuate a large overshoot. The rotational angle control and the speed control of water hydraulic servomotor are also tested with conventional PID controller in [3],[4]. These results are mainly based on the conventional technique used for mineral oil hydraulic system. These days some nonlinear robust control methods are applied to hydraulic devices, but almost all such papers are on a control of the mineral oil hydraulic systems. An adaptive controller, which compensates uncertainties of inertia load and some physical parameters, is also proposed in [5]. A feedback linearization method and backstepping design of mineral oil hydraulic motor are proposed in [6] while the parameter uncertainty treatment are open question in the paper.

Recently several papers meet these requests with the application of modern control theory. In [7], the controller for water hydraulic pressing machine was constructed by applying the solution for H_∞ mixed-sensitivity problem to compensate parameter uncertainties for the spool clearance and the coefficient of flow rate of servo valve and the bulk modulus of water.

In this paper, the rotational angle and speed controller designs for water hydraulic motor using the adaptive control theory were discussed. The model reference adaptive control (MRAC) system can admit the parameter uncertainty by tuning the controller parameters depending on the error between plant output and the reference signal specified by the designer. MRACS is ordinary applied to a system assumed to be linear; therefore strong nonlinearity and time varying parameters of the water hydraulic servo system were much influenced on its stability. In fact, instability could be often observed in experiments on rotational angle control. In speed control, on the other hand, the experimental results showed good control performance regardless of inertia load fluctuation. In Section 2, first of all, we derive mathematical model of water hydraulic servomotor by linearizing the nonlinear flow equation which contains control variable. Then we define the problem to be solved. In Section 3, we construct an adaptive controller for uncertain parameters and load fluctuation. We showed the experimental results using the proposed controller in Section 4. Finally we summarized the results.

2 MODELING OF WATER HYDRAULIC SERVO MOTOR

Fig.1 shows the schematic diagram of water hydraulic servo motor system. Introducing the load pressure $P_L = P_1 - P_2$ as a new variable, the system dynamics which is linearized at the neutral spool position of servo valve is given by

$$\begin{bmatrix} \dot{\theta} \\ \dot{\omega} \\ \dot{P}_L \end{bmatrix} = \begin{bmatrix} 0 & 1 & 0 \\ 0 & -c_e\frac{D\mu}{2\pi I} & \frac{D}{2\pi I}(1-c_f) \\ 0 & -\frac{KD}{\pi V_0} & -\left(c_s + \frac{2Kk_P}{V_0}\right) \end{bmatrix} \begin{bmatrix} \theta \\ \omega \\ P_L \end{bmatrix} + \begin{bmatrix} 0 & 0 & \frac{2Kk_X K_U K_S}{V_0} \end{bmatrix}^T u \qquad (1)$$

where θ, ω are rotational angle and speed and u is input voltage to be designed.

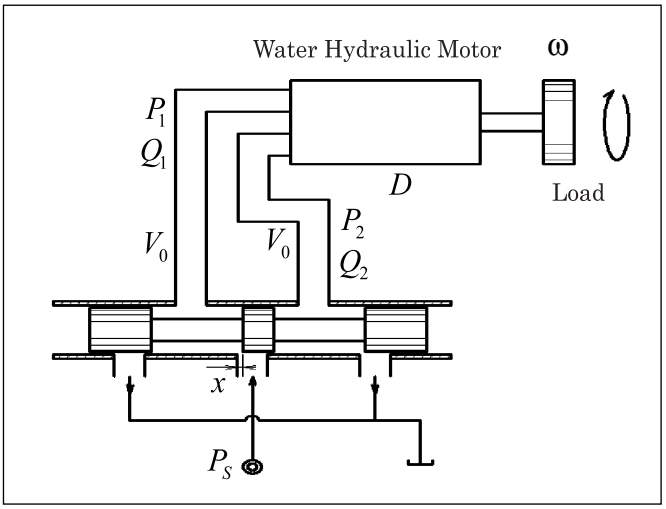

Figure 1: Model of water hydraulic motor

Since the time constant of the load pressure is sufficiently small compared with that of whole system, a nominal model for rotational angle control system can be reduced to the second order system

$$\dot{x} = Ax + bu \tag{2}$$

where $x = [\theta, \omega]^T$ and

$$A = \begin{bmatrix} 0 & 1 \\ -\omega_n^2 & -2\zeta\omega_n \end{bmatrix}, \quad b = \begin{bmatrix} 0 \\ \omega_n^2 \end{bmatrix}$$

The parameters ω_n, ζ are the natural angular frequency and damping coefficient of the system which are, respectively, defined by

$$\omega_n = \sqrt{\frac{Dk_X K_U K_S K_P}{2\pi I k_P}}, \ \zeta = \frac{1}{2}\sqrt{\frac{D^3}{8\pi^3 I k_P k_X K_U K_S K_P}}$$

On the other hand, for speed control, we consider the following nominal model by ignoring the dynamics of rotational angle θ in eq.(1), *i.e.*, the state vector and system description are $\bar{x} = [\omega, P_L]^T$ and $\dot{\bar{x}} = \bar{A}\bar{x} + \bar{b}u$, respectively, where

$$\bar{A} = \begin{bmatrix} 0 & \frac{D}{2\pi I} \\ -\frac{K}{V_0}\left(\frac{D}{\pi} + 2k_X K_U K_S K_P\right) & -2\frac{KK_P}{V_0} \end{bmatrix}, \quad \bar{b} = \begin{bmatrix} 0 \\ 2Kk_X K_U K_S K_P \end{bmatrix} \tag{3}$$

For given each reference signal, that is rotational angle or speed, the control objective is to design an adaptive controller making the output to track the reference regardless of load fluctuation, nonlinear friction and leakage.

3 CONTROLLER DESIGN

In this section, we construct the adaptive controller for unknown plant parameter. Consider a second order model of water hydraulic system;

$$A(z^{-1})y(k) = z^{-1}B(z^{-1})u(k) \tag{4}$$

where $u(k)$, $y(k)$ are input and output signal at step k, respectively. In this research, y corresponds to the rotational angle θ or speed ω. A symbol z stands for the time-shift operator and polynomials $A(z^{-1})$, $B(z^{-1})$ are given by

$$\begin{aligned} A(z^{-1}) &= 1 + a_1 z^{-1} + a_2 z^{-2} \\ B(z^{-1}) &= b_0 + b_1 z^{-1} \end{aligned} \tag{5}$$

The nominal system parameters a_1, a_2, b_0, b_1 in eq.(5) are given by discretization of eq.(2) with proper sampling time. On the other hand, we specify the reference model $G_M(s)$ for the control and discretize it as

$$A_M(z^{-1}) y_m(k) = z^{-1} B_M(z^{-1}) r(k) \tag{6}$$

where signal $r(k)$, $y_m(k)$ are input and output of the reference model and

$$\begin{aligned} A_M(z^{-1}) &= 1 + a_{m1} z^{-1} + a_{m2} z^{-2} \\ B_M(z^{-1}) &= b_{m0} + b_{1m} z^{-1}, \quad b_{m0} \neq 0 \end{aligned} \tag{7}$$

Defining the output error between plant and reference model as

$$e_1(k) = y_m(k) - y(k), \tag{8}$$

the adaptive control objectives then can be expressed as follows; construct an adaptive control input $u(k)$ and parameter update law which makes $e_1(k)$ converges to 0 as $k \to \infty$ ensuring all of the signal in the system are bounded. Based on the results [8][9], the adaptive control input is given by

$$u(k) = \frac{1}{\hat{\theta}_1(k)} \left[D(z^{-1}) y_m(k+1) - \hat{\bar{\theta}}^T(k) \bar{\phi}(k) \right] \tag{9}$$

where $D(z^{-1})$ is second order stable polynomial filter, and controller parameter $\bar{\theta}(k)$ and regressor vector $\bar{\phi}(k)$ are defined by

$$\begin{aligned} \hat{\bar{\theta}}(k) &= [\hat{\theta}_2(k),\, \hat{\theta}_3(k),\, \hat{\theta}_4(k)]^T \\ \bar{\phi}(k) &= [u(k-1),\, y(k),\, y(k-1)]^T \end{aligned}$$

With this adaptive control input, output error defined by eq.(8) can be described as

$$e_1(k) = \tilde{\theta}^T(k) \phi(k-1) \tag{10}$$

where

$$\begin{aligned} \tilde{\theta}(k) &= \hat{\theta}(k) - \theta \\ \hat{\theta}(k) &= [\hat{\theta}_1(k),\, \hat{\bar{\theta}}(k)]^T, \quad \phi(k) = [u(k),\, \bar{\phi}(k)]^T \end{aligned} \tag{11}$$

For derived error system, eq.(10), the control law and parameter update law

$$\hat{\theta}(k) = \hat{\theta}(k-1) + \Pi(k-1) \phi(k) e_1(k) \tag{12}$$

$$\Pi(k) = \frac{1}{\lambda_1(k)} \left[\Pi(k-1) - \frac{\Pi(k-1) \phi(k) \phi^T(k) \Pi(k-1)}{\sigma + (k) \phi^T(k) \Pi(k-1) \phi(k)} \right] \tag{13}$$

$$\lambda_1(k) = 1 - \frac{\|\Pi(k-1) \phi(k)\|^2}{\sigma + \phi^T(k) \Pi(k-1) \phi(k)} \frac{1}{\mathrm{tr}\Pi(0)} \tag{14}$$

ensure that the output error converges to 0 as $k \to \infty$ where the initial value $\Pi(0)$ of gain update law is a constant positive definite matrix and $\sigma > 0$, $\lambda_1(0) > 0$. The boundedness of the regressor vector ϕ is derived from the key technical lemma [8],[9]. Note that this controller adopted an fixed-trace gain update law eq.(14), it has certain robustness for plant parameter change. Therefore the choice of this parameter update law is more realistic.

The block diagram for whole system is shown in Fig.2. And designed parameters will be explained in the following section.

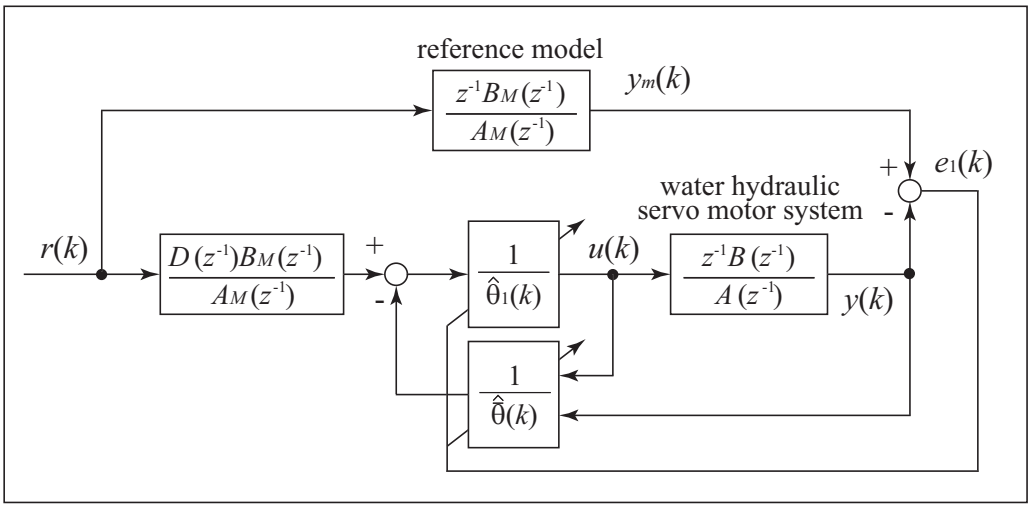

Figure 2: Block diagram of adaptive control system

4 EXPERIMENTAL RESULTS

4.1 TEST RIG

Table 1, Fig.3 and Fig.4 show the basic specifications of the experimental rig, system configuration and the schematic diagram of experimental system. The motor is an axial piston type, and its shaft is connected to the encoder and removable inertia load (0.10, 0.20, 0.31 kg·m^2). The encoder feedbacks the rotational angle to the controller and the control input drives the water hydraulic servo valve. The valve adopts a nozzle-flapper structure. In this research, the controller was realized using dSPACE system (DS1104) installed in PC. The sampling time of all experiments was 1ms.

Table 1: Specification of the experimental set-up

module	specification
power unit	14 MPa, max
	21×10^{-3} m^3/min
motor displacement D	15×10^{-6}m^3/rev
servo valve	1.7×10^{-4} m^3/s @7 MPa
rotary encoder	5400ppr
water temperature	30±1°C (tap water)

For all experiments, we set the reference dynamics as follows:

$$G_M(s) = \frac{\omega_r^2}{s^2 + 2\zeta_r\omega_r s + \omega_r^2} \tag{15}$$

where design parameters ω_r, ζ_r are specified depending on control objectives.

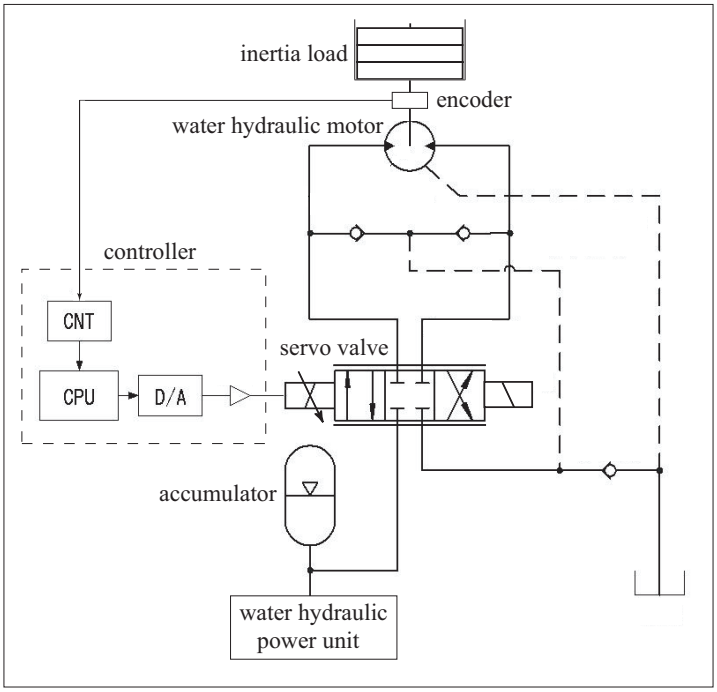

Figure 3: Schematic diagram of water hydraulic system model

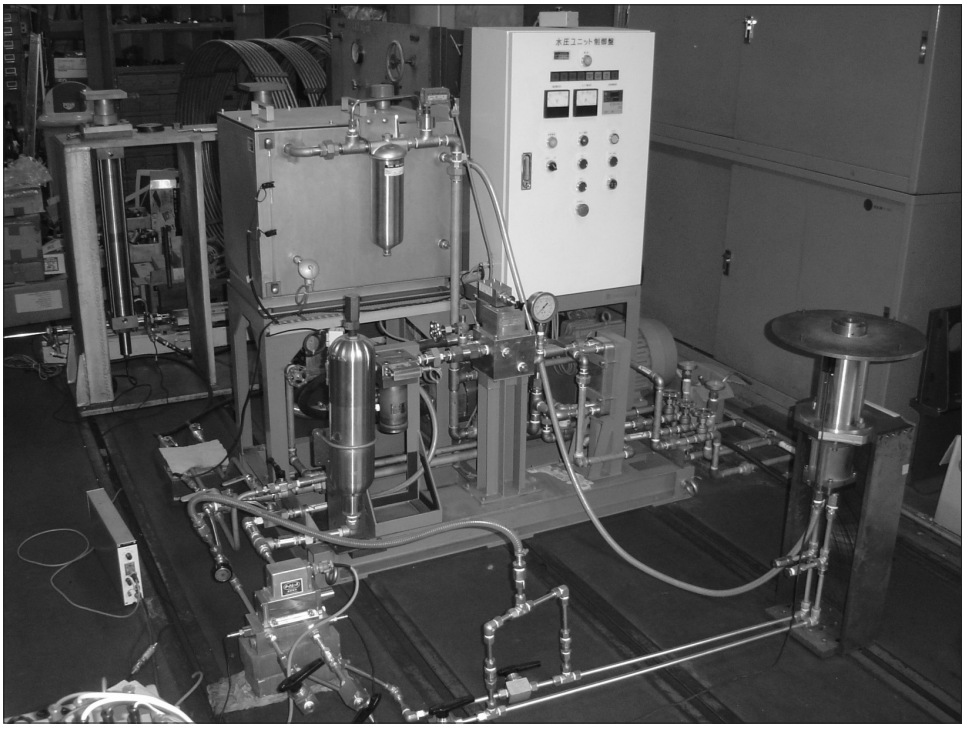

Figure 4: Test rig for water hydraulic servo motor system

4.2 Experimental results for rotational angle control

The experiments on rotational angle control were examined under the condition shown in Table 2. Note that the reference model shows no overshoot.

Table 2: Experimental physical parameter setup for rotational angle control

parameter		value
supply pressure		5 MPa
inertia load I		0.20 kg·m^2
reference angle r (rectangular wave in 20s period)		0-30°
reference model	natural angular freq. ω_r	5 rad/s
	viscous damping coefficient ζ_r	1.2

In eq.(9), the stable polynomial are chosen as $D(z^{-1}) = (1 - 0.1z^{-1})^2$ by trial and error. The initial values were set as $\hat{\theta}(0) = [1, 0, 0, 0]^T$, $\Pi(0) = 10^{-6} I_4$, $\sigma = 50$ where I_4 stands for the 4-th identity matrix. These initial values did not depend on any information about the system state variables.

The control results and its controller parameters were shown in Fig.5 and Fig.6, respectively. In Fig.5, the control performance with other control methods (2DOF-H_∞ control, disturbance-observer-based 2DOF control, sliding mode control) were also plotted. At first glance, the proposed controller could drive the rotational angle θ to the reference angle θ_{ref} quickly because this method tuned control parameter directly based on the output error. The steady state error was also very small (about

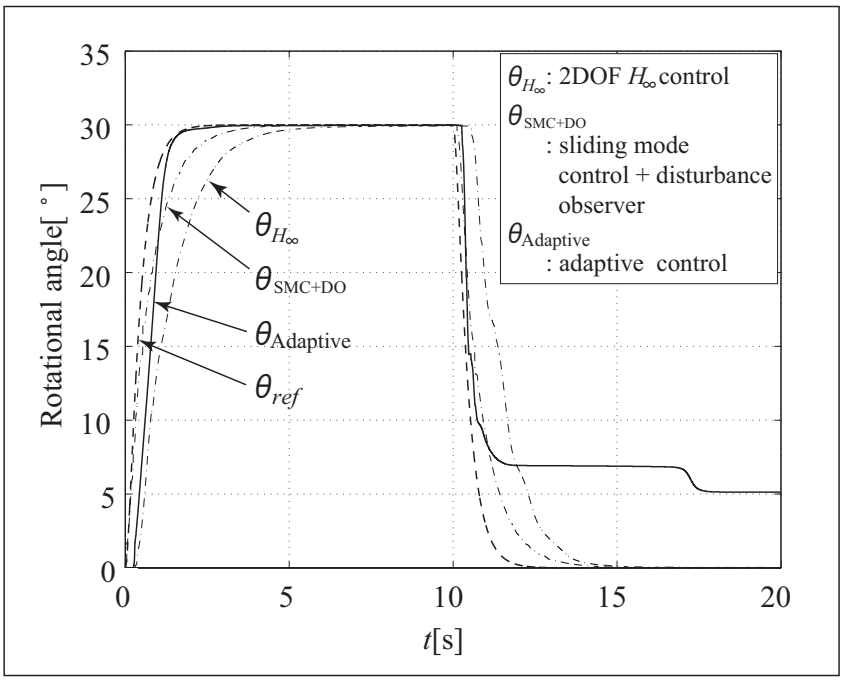

Figure 5: Experimental results of angle control with adaptive controller (r =0-30°, I=0.20 kg·m^2)

0.017°), these results showed good control performance. Moreover the controller parameters converged to almost constant values. But, after the reference angle had been once changed from 30° to 0° at $t = 10\,\mathrm{s}$, tracking performance was lost around $t = 12\,\mathrm{s}$ and large steady state error remained. The controller parameters also diverged at the same time. This result is explained as follows: shortly after the reference angle is changed to the opposite direction, the controller begins to try to make angle θ converge to 0. This means that the controller should tune the parameters from the initial values which were for $\theta_{ref} = 30°$ compensating leakage flow and large friction acting on the motor shaft. The robustness of the adaptation is not enough to overcome large error and these nonlinearities. This situation is far severe than that of the control started from 0° because controller parameter is initialized at $t = 0$. In fact, same phenomenon could be observed when the reference angle was inverted, that is, started from 0° to −30°, then returned to 0°. This shows that even if no load fluctuation and no supply pressure change, the adaptive controller assuming the water hydraulic motor system to be a linear system can not achieve good rotational angle control performance for inherent strong friction and large leakage flow depending on the driving point. With some other robust control or nonlinear control strategy, these may be compensated as shown in Fig.5.

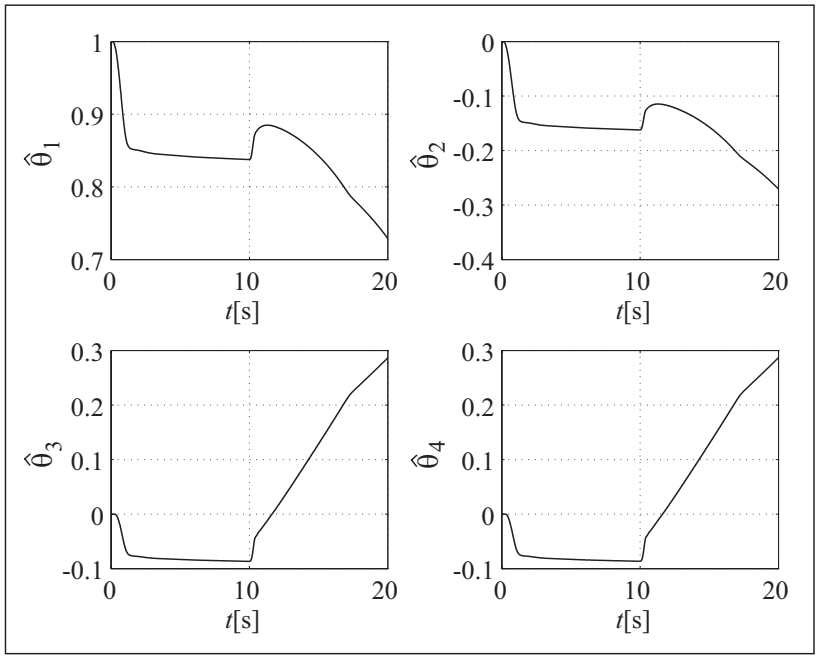

Figure 6: Estimated controller parameters

4.3 Experimental results for speed control

The experiments on speed control were also examined under the condition shown in Table 3. Note that inertia load changes as a step wise or a rectangular wave in this experiments. The filter polynomial $D(z^{-1})$ and all of the initial values of controller parameters $\hat{\theta}(0)$, $\Pi(0)$, σ were set as in the case for the rotational angle control.

Table 3: Experimental physical parameter setup for speed control

parameter		value
supply pressure		7.5 MPa
inertia load I		0.10, 0.20, 0.31 kg·m^2
reference angle	step wise	40 rad/s
	rectangular wave in 10 s period	20-40 rad/s
reference model	natural angular freq. ω_r	5 rad/s
	viscous damping coefficient ζ_r	2

The control results and its controller parameters were shown in Fig.7 and Fig.8, respectively. The experimental results showed a robust speed tracking performance with inertia load fluctuation for step wise reference. The settling time was about 4s and small overshoot was observed with larger inertia load. For speed control, nonlinearities such that coulomb/viscous frictions and leakage flow are almost constant under given driving point. The system can be assumed to be a linear and the adaptive controller compensate with linear structure. The controller parameters updated properly during transient response and converged to almost constant values with no deviations.

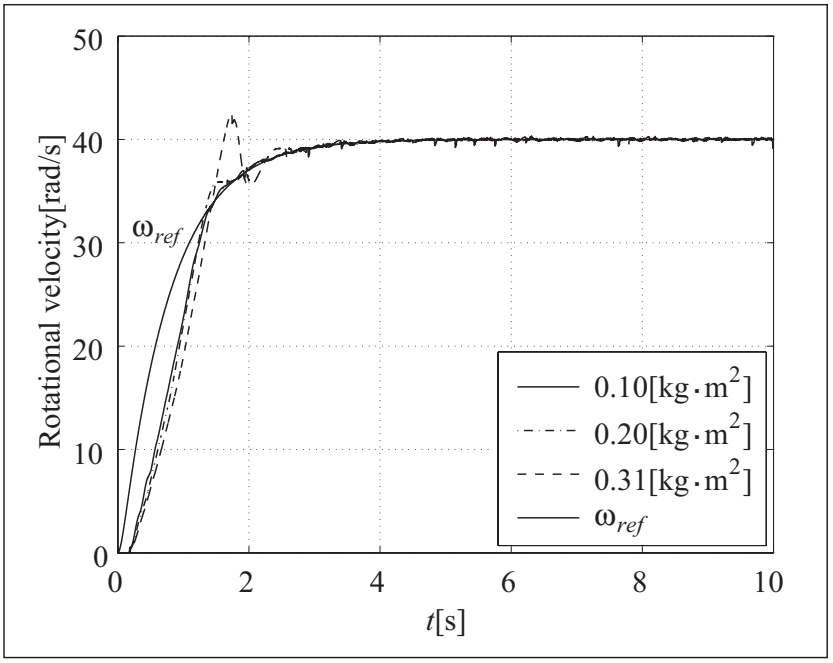

Figure 7: Experimental results of speed control with adaptive controller ($r = 40$ rad/s)

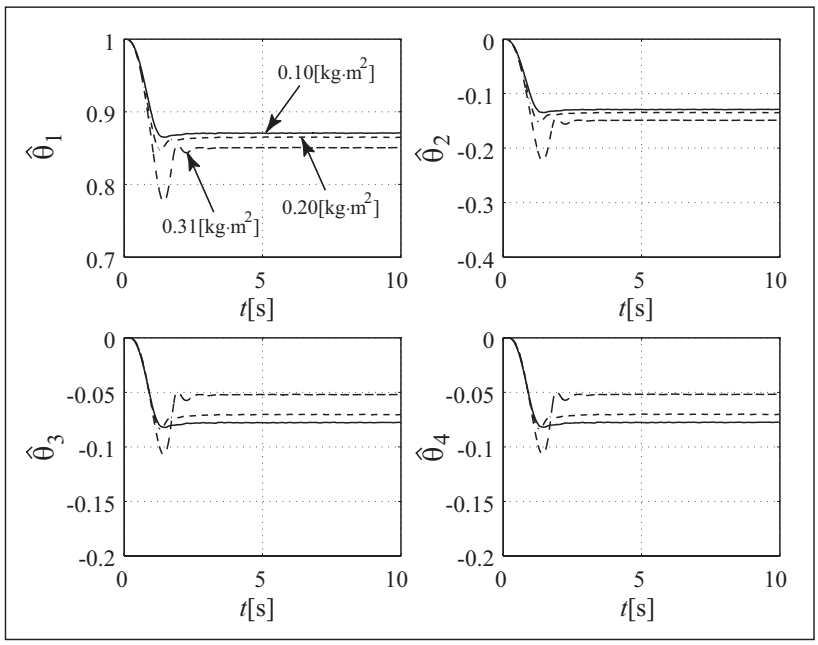

Figure 8: Estimated controller parameters

As a next step, the control results for rectangular wave, 20-40 rad/s with 10 s period and its controller parameters were shown in Fig.9 and Fig.10, respectively. However these results also showed some overshoot with larger load, the tracking performance

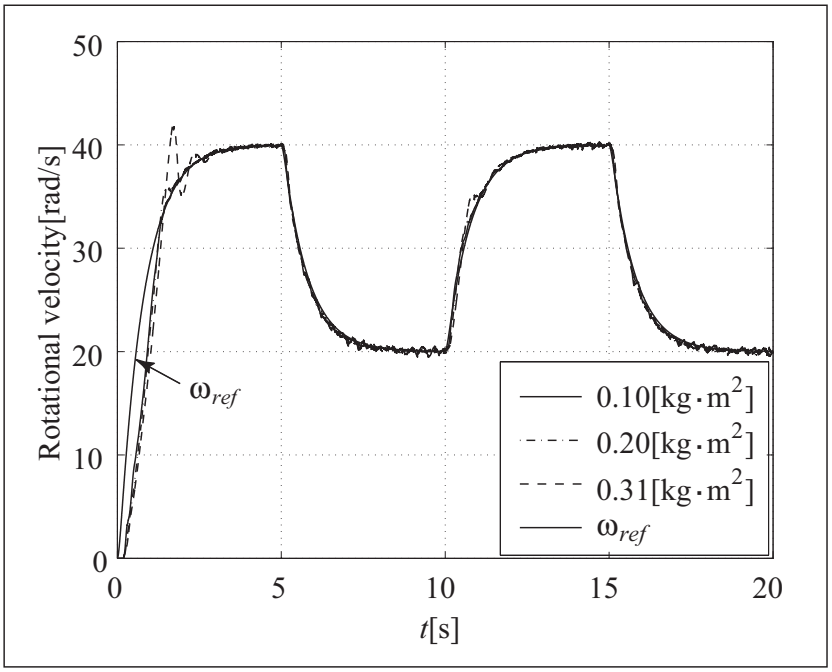

Figure 9: Experimental results of speed control with adaptive controller (r =20-40 rad/s)

was fairly good regardless of the inertia load fluctuations. The settling time was almost same in step wise reference case.

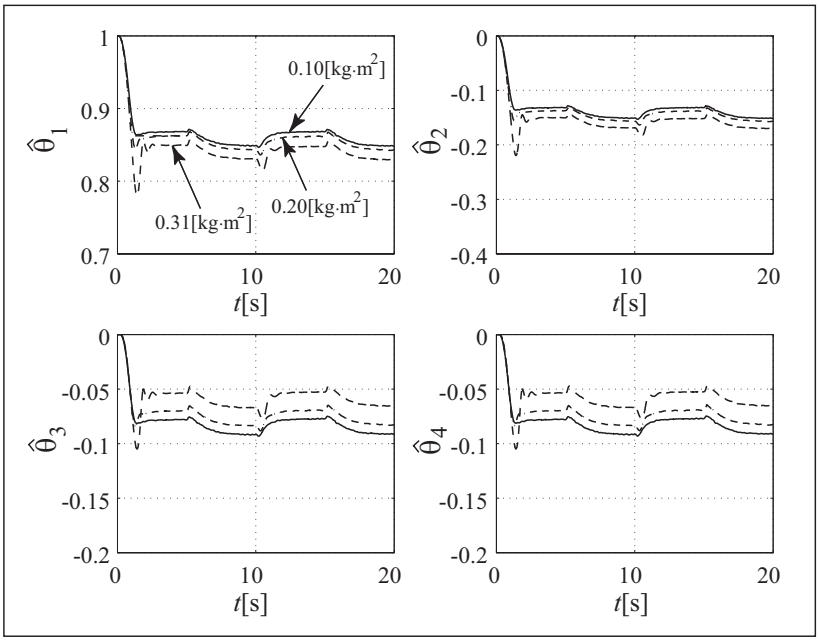

Figure 10: Estimated controller parameters

5 Conclusions

In this paper, we reported the control performance of adaptive control for the rotational angle and speed control of the water hydraulic servomotor system. The adaptive controller failed to compensate some nonlinearity such as parameter change, viscous and coulomb friction and leakage of the motor system because these are much strong and change widely. On the other hand, the control results of the speed control of the motor were very good for these nonlinearities become milder. Moreover this speed controller showed robustness for initial load fluctuation.

NOMENCLATURE

c_e	viscous friction coefficient of water hydraulic motor
c_f	coulomb friction coefficient of water hydraulic motor
c_s	inner leakage coefficient of water hydraulic motor
D	displacement of water hydraulic motor
I	inertia load
K	bulk modulus of water
K_P	inner feedback gain of servo valve
K_S	amplifier gain of servo valve
K_U	gain from input voltage to spool displacement of servo valve
k_P	linearized pressure gain of servo valve
k_X	linearized flow gain of servo valve for spool displacement

P_1, P_2	inlet and outlet pressure
P_L	load pressure, $P_L = P_1 - P_2$
Q_1, Q_2	flow rates
r	reference input (angle or speed)
μ	viscous coefficient of water
θ	rotational angle of water hydraulic motor
θ_{ref}	reference rotational angle of water hydraulic motor (output of reference model in rotational angle control case)
ω	speed of water hydraulic motor
ω_n	natural angular frequency
ω_r	natural angular frequency of reference model
ω_{ref}	reference speed of water hydraulic motor (output of reference model in speed control case)
ζ	damping coefficient
ζ_r	damping coefficient of reference model

References

[1] M.Linjama, J.Tammisto, K.T.Koskinen and M.Vilenius: Pseudo-Prpportional Position Control of Water Hydraulic Cylinder Using On/Off Valves, Proceedings of the 5th JFPS International Symposium on Fluid Power, Vol.1, pp.155-160, November 12-15, Nara, Japan, 2002

[2] E.Mäkinen and T.Virvalo: On the Motion of a Water Hydraulic Servo Cylinder Drive, The proceedings of 7th Scandinavian Internatinal Conference on Fluid Power, SICFP'01, Vol.1, pp.109-123, May 30-June 1, Linköping, Sweden, 2001

[3] Y.Mochizuki and C.Yamashina: Servo Control of a Water Hydraulic Axial Piston Motor, Ebara engineering review (in Japanese), No.184, pp.17-23, 1997

[4] Dai Terasaka, Kazuhisa Ito and Shigeru Ikeo: PID-Control of Water Hydraulic Servomotor System, Proceedings of the 5th JFPS International Symposium on Fluid Power, Vol.1, pp.143-148, November 12-15, Nara, Japan, 2002

[5] B.Yao, F.Bu and G.T.C.Chiu: Non-linear adaptive robust control of electro-hydrailic systems driven by double-rod actuators, International Journal of Control, Vol.74, No.8, pp.761-775, 2001

[6] M.Jovanović, Nonlinear Control of an Electrohydrailic Velicity Servosystem, Proceedings of the 2002 American Control Conference, pp.588-593, 2002

[7] K.Sanada: A method of designing a robust force controller of a water-hydraulic servo system, Proc. Instn. Mech. Eng. Vol.216, Part I:J Systems and Control Engineering, pp.135-141, 2002

[8] G.C.Goodwin and K.S.Sin: Adaptive Filtering Prediction and Control, Prentice-Hall, 181/182 (1984)

[9] G.C.Goodwin, P.J.Ramedge, P.E.Caines: Discrete-Time Multivariable Adaptive Control, IEEE-AC, 449/456 (1980)

CONTROL SYSTEM DEVELOPMENT FOR THE WATER HYDRAULIC 6-DOF MOTION PLATFORM

Rokala M., Palonen T., Sairiala H., Koskinen K.T.
Tampere University of Technology
Institute of Hydraulics and Automation
P.O.Box 589
33101 Tampere, Finland
Phone +358 3 3115 3438, Fax +358 3 3115 2240
E-mail: markus.rokala@tut.fi

ABSTRACT

Stewart platform is commonly used 6-DOF (Degree Of Freedom) motion platform in the driving and flight simulators. There is a research going on for using water hydraulic actuators in Stewart platform in Institute of Hydraulics and Automation. This paper describes the control system of the first water hydraulic Stewart platform.

The motion platform has six water hydraulic cylinders which are controlled by proportional directional valves. The valves are controlled by MathWorks xPC Target real-time software. The measurement and control is realized with standard PC with two analogue input cards and one analogue output card. Control signal is calculated from measured information and from the reference position of the cylinders. Cylinder position, spool position and cylinder pressures are measured. Reference position for the cylinders is calculated through inverse parallel kinematics when the desired position and orientation of the top plate is known.

The real-time simulator with the motion platform requires fast and accurate response from the motion platform. The controlling of the valves is the most important part of the tuning because of the valves is the slowest part of the system. In this paper the measurement results of the platform responses is presented.

KEYWORDS: Water hydraulics, 6-DOF motion platform, platform control

1 INTRODUCTION

In addition of research of water hydraulics and virtual technologies, research and implementation of water hydraulic motion platform has been started in Institute of Hydraulics and Automation. This is the first try to make water hydraulic motion platform and the goal is not to compete against oil hydraulic platforms. The goal is to research how water as a medium and the properties of the water hydraulic components affect to the characteristics of the platform. The project is extremely challenging because both control of the water hydraulic systems and water hydraulic components are not very sophisticated at the moment.

Motion platform will be used in real-time simulator construction that allows simulation of different vehicles with minimal changes. Figure 1 shows the construction of simulator. There are four standard PCs, one for simulation of vehicle (PC 1), one for control and position measurement of platform (PC 2), one for generating graphics (PC 4) and optional PC for main loop (PC 3). System is distributed through local area network (LAN), using UDP (User Datagram Protocol) for communications.

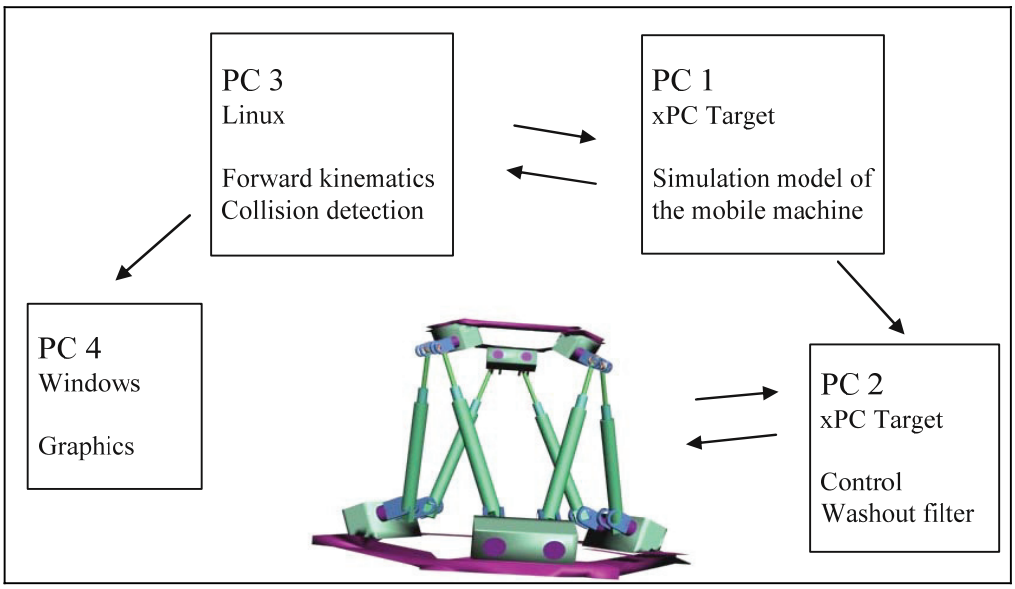

Figure 1. Structure of the simulator.

In the simulator the simulation model works in real-time on MathWorks xPC Target software. The simulation model is distributed in the two standard PCs. Distribution makes easy to change the virtualized machine because of the simulation model and the platforms control system is separated. PC 1 calculates the dynamics of the mobile machine and transfers the necessary information to the other simulation computer (PC 2). Also the interaction between the mobile machine and the terrain is modeled on the PC 1. The control of the platform is done with PC 2.

The main loop is mostly for adding more counting power for the forward kinematics of simulated vehicle and for simulating more realistic collisions than graphics software is capable. Three dimensional graphics for the simulator will be generated in Windows-environment. More information about the concept of the simulator and the tuning of the washout filters is described in reference [1] and to be published.

2 SIMULATOR SOFTWARE

As a minimum requirement, software of the simulator has to be capable to generate a graphical environment, detect collisions and to calculate collision forces. It also has to be able to generate right response to the driving control of the simulated vehicle and to generate the reactions between ground and the tires of the vehicle, thus creating a motion cue to the motion platform.

At simplest, graphical environment can be two-dimensional image in example of the road or terrain, using perspective for creating three-dimensional effect. While this technique is widely used in driving simulators, immersion is rather poor. One of the reasons for poor immersion is absent side image, letting the driver see real world instead of virtual. A better immersion can be achieved by creating the virtual environment from the three dimensional models of the used objects, trees, houses, ground etc. Instead of traditionally projecting the image to canvas, head mounted display (HMD) is better option because of moving platform. There is also available reasonably priced HMDs with internal gyroscopes to track the rotations of viewers head. To create this kind of virtual environment, use of a special application programming interface (API) for computer graphics is essential. Most common APIs for three-dimensional graphics are OpenGL and Direct3D.

Since the simulator has virtual environment with human driven vehicle, collisions are bound to happen at some point. Collisions can happen with solid or with movable objects. Most important issue of collision detection is amount of objects that can be collided with the vehicle. If there are several (over 100) collisions possibilities, selection of the collision detection and collision force computing method should be considered carefully. Amount of data needed to implement collision detection and collision force computing is also essential, because high usage of the run-time memory tends to slow the software.

2.1 Distribution of the simulator software

In a simple driving simulator using kinematic collisions, it is possible to drive whole software in one computer. This requires the all data processing power of single CPU and graphic controller, and can still cause some problems, like lowering of framerate or delays in collision response.

The dynamic simulation models of the vehicle require continuous calculating of the collision forces. Discreet changes in collision forces can dissolve simulation of the mechanics of the vehicle. Because of this, calculating time has to be near integration step of the simulation model of the vehicle mechanics. This means computing cycle frequency from 500 to 1000 Hertz for collisions. If the graphics are generated in same software cycle, frequency slows down to 60 to 100 Hz. By distributing the collision force calculating to different computer, it is possible to keep up higher rate of computing cycles. The position data of the vehicle parts is generated by the simulation model, it is not efficient to send this data to several computers. As the collision computing requires this data, it is convenient to calculate the forward kinematics of the vehicle at the same computer.

2.2 Disadvantages of the software distribution

Because of the distribution of collision force computing and graphics generating, exact shape of the objects of virtual world is not known when computing collisions. Most collision detection algorithms use basic shapes (cylinders, boxes, spheres) in collision force computing and collision detection. Original shape of colliding object is approximated by filling with several smaller collision geometries. This are surrounded with larger bounding geometry, which is used in collision detection. Approximation of objects shape can be done either by dimensions and basic geometry of object or by using initialization files. First method is only applicable to regularly shaped objects, like hay bale or wall. Creating the needed collision data without graphical data can be time consuming, difficult and it is susceptible to programming errors.

Distribution of the software complicates software. It is more prone to programming errors, but this can be avoided with good documentation, efficient debugging and well planned construction of the software.

2.3 Used distribution method in the driving simulator

The driving simulator developed by IHA has been distributed to gain better performance in collision detection. Graphics generation is separated from forward kinematics and collision computing. The collision detection is realized with object oriented bounding boxes (OBB). OBBs are slower to the test and take more memory than spheres as bounding objects, but OBB's are more tight-fitting for rectangular collision objects, like hay bales. Collision force and momentum are computed with spheres as collision geometry. Colliding objects are filled with spheres, collision forces between spheres are calculated and summed up to objects. With vehicle parts, initialization files were used to load collision geometries after those were created in 3D-designing program.

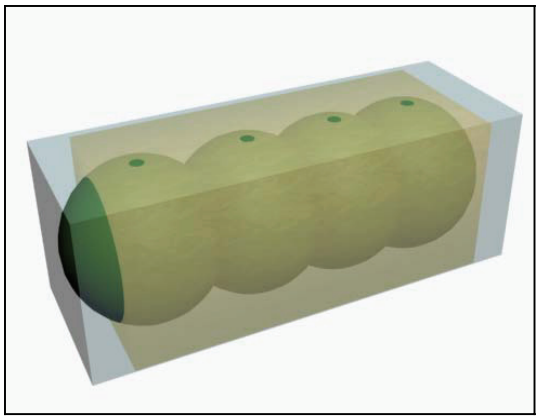

Figure 2. Hay bale filled with four collision spheres and surrounded with object oriented bounding box.

Distribution has been implemented through local area network (LAN) with UDP-protocol. UDP allows fast sending for packages, but no guarantees of delivery. Because of this, extra measures (check number and re-sending) were used to ensure the delivery of critical packages.

3 MECHANICS AND HYDRAULICS OF THE MOTION PLATFORM

The structure of the platform is a common Stewart platform with six actuators [2]. Basic sizing of the mechanical dimensions and hydraulic components are made by simulation model of the Stewart platform. The diameter of the bottom plate is 1.2 meters and the diameter of the top plate is 1.0 meters. Actuators are 0.777 meters long on the shortest length. Distance between connection points is 0.16 meters and the mass of the top plate is about 100 kilos.

The actuators are water hydraulic cylinders which are connected to valves with hoses. Power pack and directional valves are also connected with hoses. The valves are set on the centre of the platform to the lower plate. Pressure medium is tap water. Figure 3 presents circuit diagram for the motion platform.

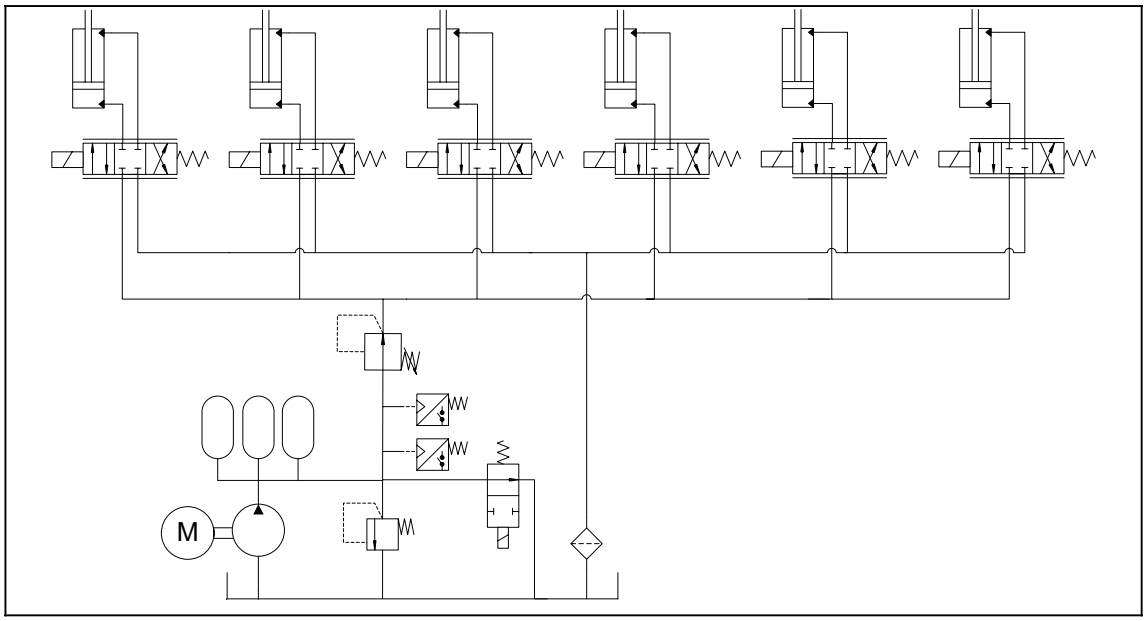

Figure 3. Hydraulic circuit of the water hydraulic motion platform.

3.1 Valves

The directional valves are the most critical part of the hydraulic system of the platform. The characteristics of the valves are very significant for control. The problem is that the range of the water hydraulic proportional valves is very limited at the moment.

The valves chosen for the platform were modified Sitek L22 4/3 proportional direction valves. Maximum supply pressure to these valves is 70 bar and they operate with tap water. Spool position is measured with LVDT-sensor and it is controlled by PI-controller. Original internal leak channels were replaced with external leak channels, which stabilized valve operations. Control voltage for valve is –10 … 10 volts. Figure 4 presents dynamic step response of the valve. Build up time of the step response between 0 … 90 % is from 20 to 200 milliseconds. The valves are very slow compared to proportional valves in oil hydraulics. There is a pressure reducing valve in supply line before directional valves to restrict supply pressure.

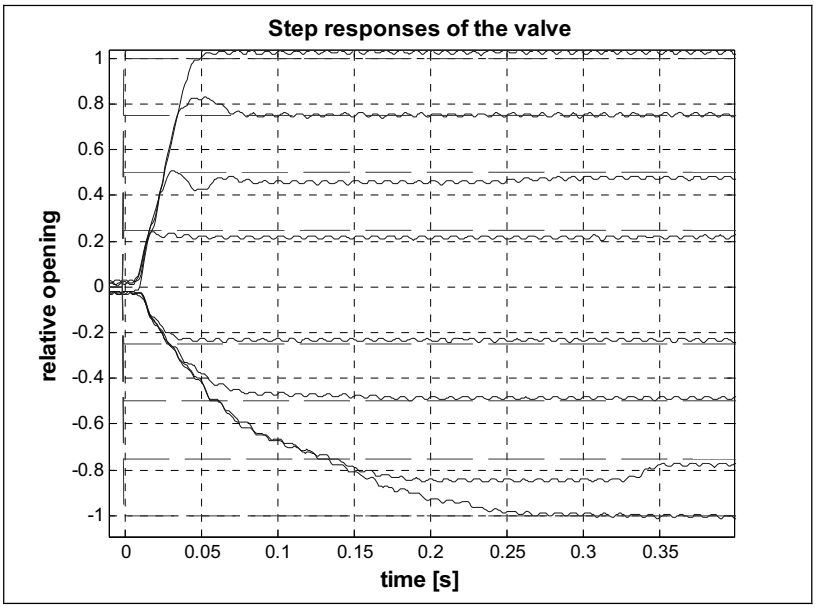

Figure 4. Step responses of the proportional directional valve.

3.2 Cylinders

The platform under research is Stewart platform with six cylinders. Cylinders are 40/25 water hydraulic cylinders with 400 millimeter stroke. Linear transducers are integrated on the cylinders which make the cylinders about 100 mm longer than the standard ones.

The characteristic of the one valve-cylinder pair were measured in test arrangement described in reference [1]. Frictions of the cylinders are known based on the measuring results at velocity of 0.03…0.4 m/s. Kinetic friction is 900…1100 N during the stroke and 1350…1550 N during the return stroke. Frictions are high compared to oil hydraulic cylinders. This causes many problems when generating the pure motion. Oscillations of the cylinders are strong especially in slow motion. It is obvious that in standard cylinders the frictions of the seals make the control of the system very challenging for that kind of application.

3.3 Power pack

Pump flow of the power back of the system is 90 l/min and the maximum pressure level is 140 bars. Volume of the tank is 300 litres and the power back includes 10 µm return filter. The power pack also includes three 35 litres accumulators with preloading pressure of 40 bars.

Pump flow is lead to the system and simultaneously accumulators are loading. When the pressure rises up to the upper pressure switch and the pump is unloaded. When the pressure fall under the settling pressure of the lower pressure switch the pump flow is lead to the system again. When the pump is unloaded the required flow is taken from accumulators.

4 CONTROL OF THE PLATFORM

Control of the platform is realized with one standard PC. PC include Intel Pro/100M network card, two analogue input cards and one analogue output card. Analogue input cards have 13 and 12 inputs connected. One input card is connected to pressure sensors (13) and the other one is connected to cylinder position sensors (6) and the spool position sensors (6). Output card is connected to the valves, which are controlled by voltage. Figure 5 shows the incoming and outgoing data signals of the PC 2.

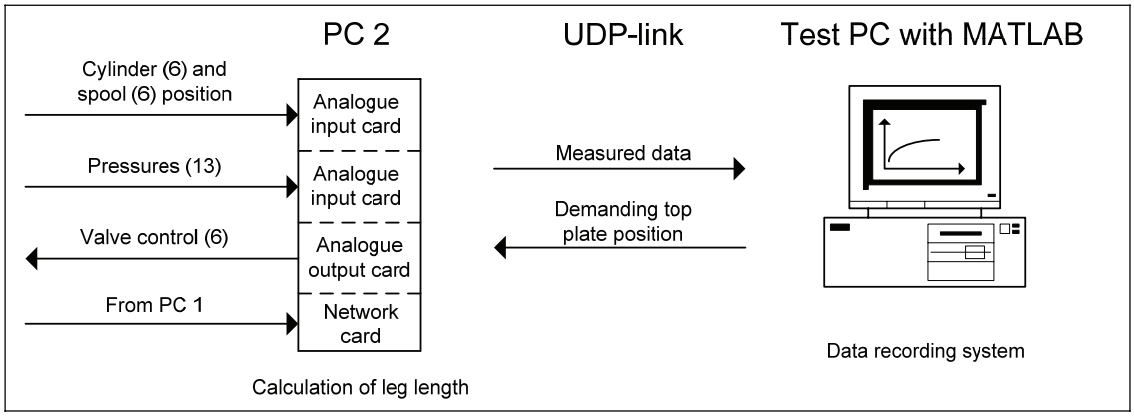

Figure 5. Signals of the PC 2 and structure of the platforms test system.

4.1 Sensors

There are three different kind of sensors used on the motion platform. Pressure in both chambers in every cylinder is measured with pressure transmitters. Pressure transmitters range is 0…250 bars and output signal is 4…20 mA. Also the supply pressure is measured with identical pressure transmitter.

The position of the spool is measured with inductive transducer. The output of inductive transducer is 5.5…9.5 V.

Cylinder positions are measured with linear transducers integrated in cylinders. Output of the linear transducer is 4…20 mA.

4.2 Software of the PC 2

Operating system of the PC 2 is DOS 6.22. Real-time control loop is realized with MathWorks xPC Target 2.8 software. Simulation model in PC 2 is made by MATLAB® Simulink®. Simulation model consists of the calculation of the desired cylinder position and the valve control part. Sample time of the system is 2 milliseconds.

In simulator use angular speeds and tangential accelerations come from PC 1, where the simulation model of the mobile machine and the terrain located. Data is fed to washout filters which give the demand position and the orientation of the top plate. Through inverse parallel kinematics the reference position of each cylinder is calculated.

Calculation of the inverse parallel kinematics is done with the Simulink block made by MathWorks [3]. In test period demanded top plate position can be manually fed to the system and washout filters are not used.

Errors of the cylinders positions are calculated when the reference positions as well as the measured positions of the cylinders are known. Based on error the values of the reference control voltages of the valves are calculated and again based on reference control voltage and the measured spool position the control voltage is calculated for each proportional directional valve. Structure of the controller is shown in figure 6. Both P-controller and feed forward controller were tested for control cylinders positions. Control of the spool position was realized with PI-controller.

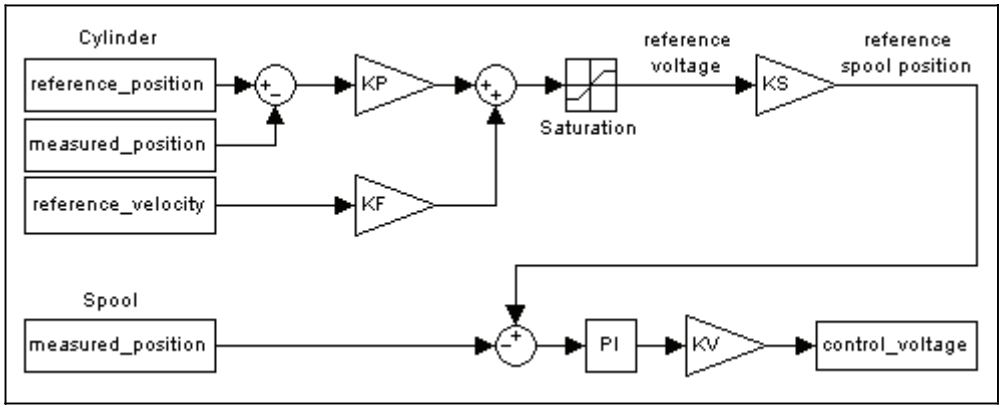

Figure 6. Structure of the controller.

Maximum change of velocity reference signal and the maximum speed of the cylinders are limited. The maximum speed of the cylinders is calculated through flow of the power back. The acceptable workspace of the motion platform is limited by washout filters. If the washout filters give too high values there are also saturation blocks in the simulation model as backup. Workspace and the used coordinate system of the platform are shown in figure 7.

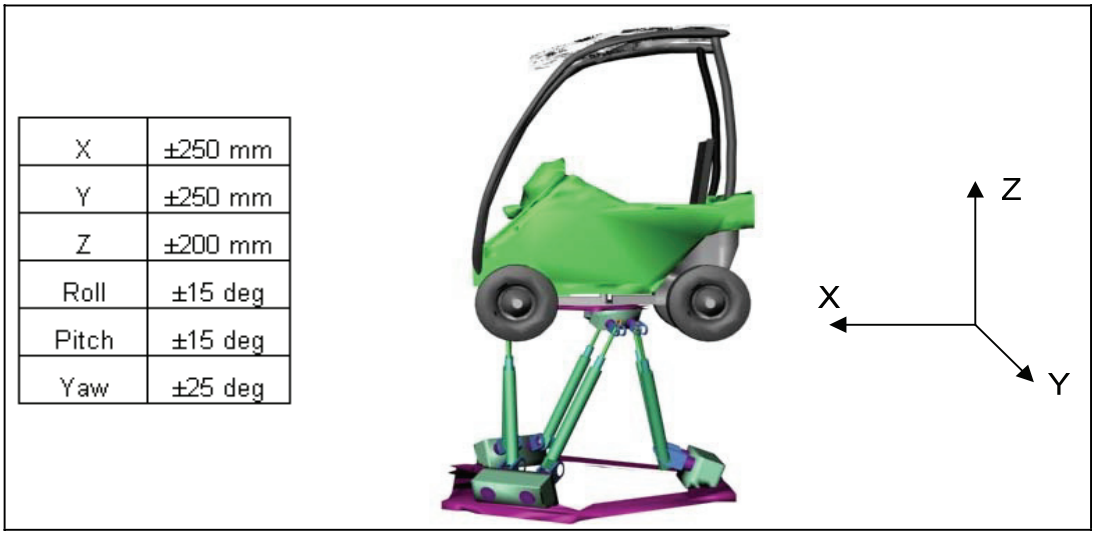

Figure 7. Workspace and the coordinate system of the platform.

Different error situations are recognized in the software and after any error the system is instantly stopped. Error occurs if the pressure in some cylinder chamber is over the limit value or if some of the measurement signals disappear. System is also stopped if the emergency-stop button is pushed.

Every cylinder valve pair is different than the other ones. Zero point of the spool of the valve is tuned up with help of the chamber pressures. Control voltage is slowly raised and the offset of the spool is set so that the pressure changes at same time in every cylinder. By using spool offsets each cylinder can be in theory controlled by equal voltage in step responses. After the valves work simultaneous also the motion of the cylinders could be synchronized.

The problem is that the offsets slightly changes during the using of the platform because of temperature changes. That means that offsets are not exactly correct although the tuning is done regularly. Different frictions cause varieties in cylinders motion although the pressure rises up at same time.

5 TEST RESULTS

Characteristics between different kinds of Stewart platforms vary a lot according to dimensions of the platform and the properties of the actuators and the control part. Common demands to the motion platform can not be done. The main demands depend on the requirements of the application. Responses of different hydraulic motion platforms are represented in references [4], [5] and [6].

The platform is uniformly loaded with test mass of 180 kg. Maximum payload of the platform is limited to 400 kg. Maximum supply pressure is limited to 60 bars by pressure reducing valve. In fact supply pressure varies a lot from 30 bars to 60 bars. Properties of the platform were measured with three different inputs and with two different controllers.

5.1 Step response

Step responses of the platform are measured for direction of Z-axis. Figure 8 presents the motion of the all six cylinders.

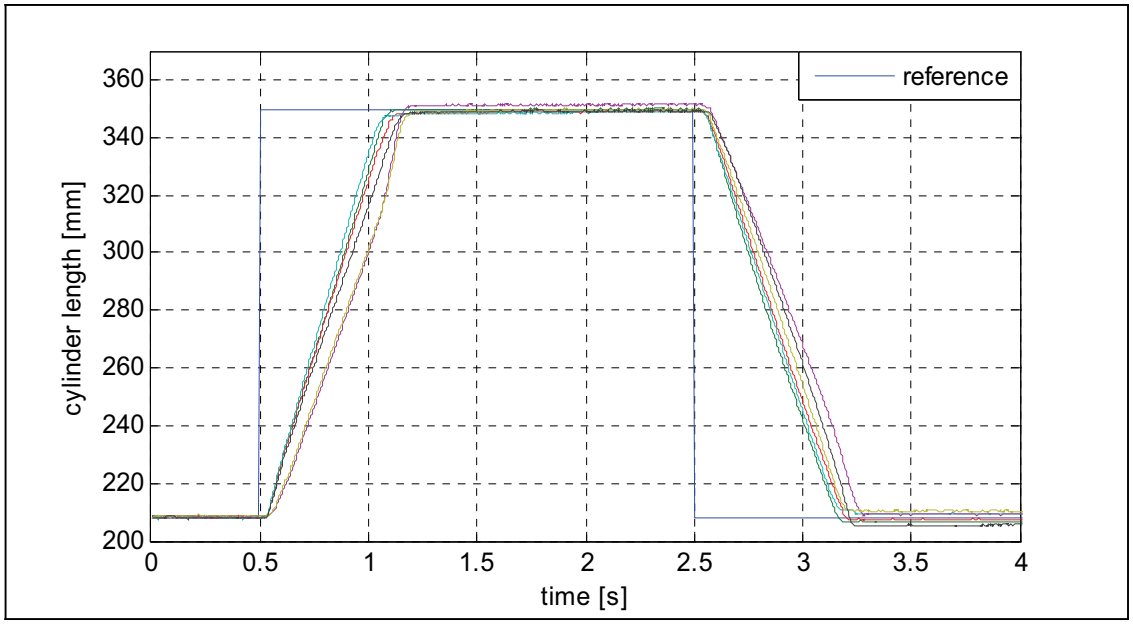

Figure 8. Step response of the platform.

Steps are 150 mm up from zero position of the platform and back to the zero position. The zero position was the platform position of [X, Y, Z] = [0.0 0.0 200.0]mm. Step responses of the platform shows that used proportional valves are quite slow. There is about 25 ms delay before the cylinders start to move. To the downward delays are even longer, about 45 ms.

Figure 8 also shows that with feed forward controller cylinders motion is not simultaneous because in fact feed forward controller is only P-gain for steps. P-gain is so high that all the valves are fully open and the differences between valves and frictions of the cylinders heave into view. After the steps maximum error between cylinders are 4.5 mm at time of 4 seconds. Step response of the platform tells the initial data but there are not steps in real use so different ramps and sinusoidal inputs give more useful information.

5.2 Maximum ramp responses

To make sure that every cylinder gets enough flow in every situation, the maximum change of the reference value is limited to 200 mm per second for each cylinder. Figure 9 and figure 10 show limited step response thus maximum ramp response of the system both feed forward controller and P-controller. Ramps are 150 mm in directions of Z-, X-, Y-axis and 15 degrees in roll, pitch and yaw in that order. Every cylinder has it own trajectory and figure 9 and figure 10 shows trajectories and errors of cylinders 3 and 4. Cylinder 4 located in front of the platform and the simulated machine and cylinder 3 on the right side of the platform and the machine.

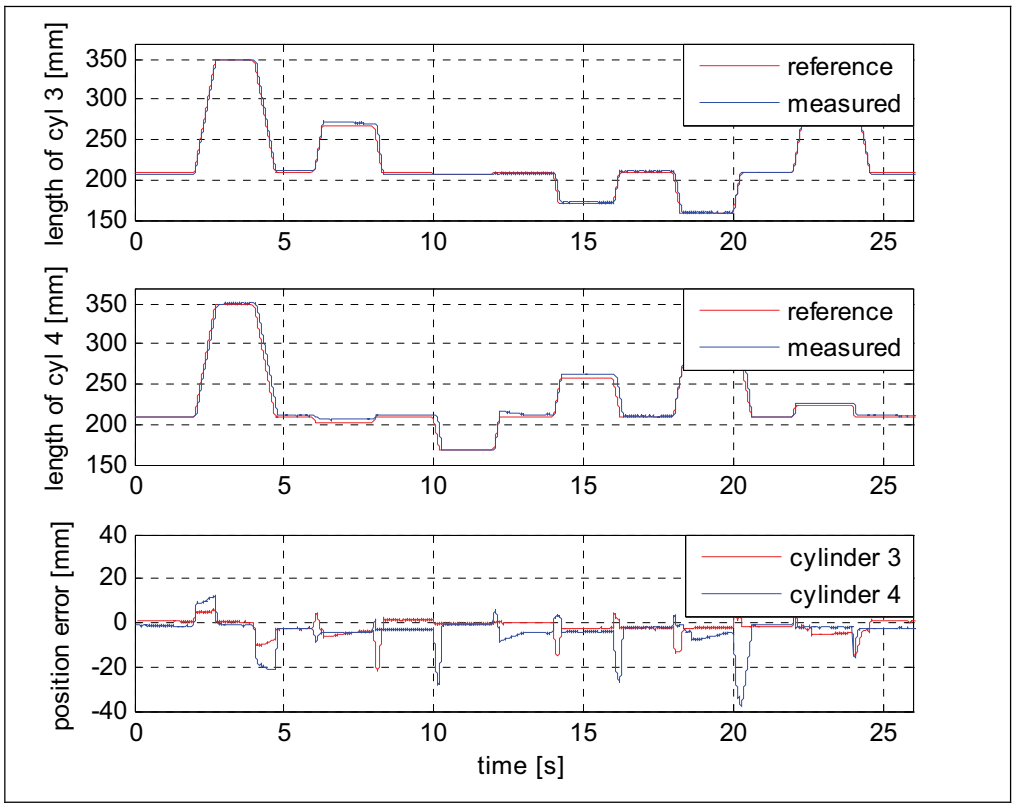

Figure 9. Maximum ramp response of the platform with feed forward controller.

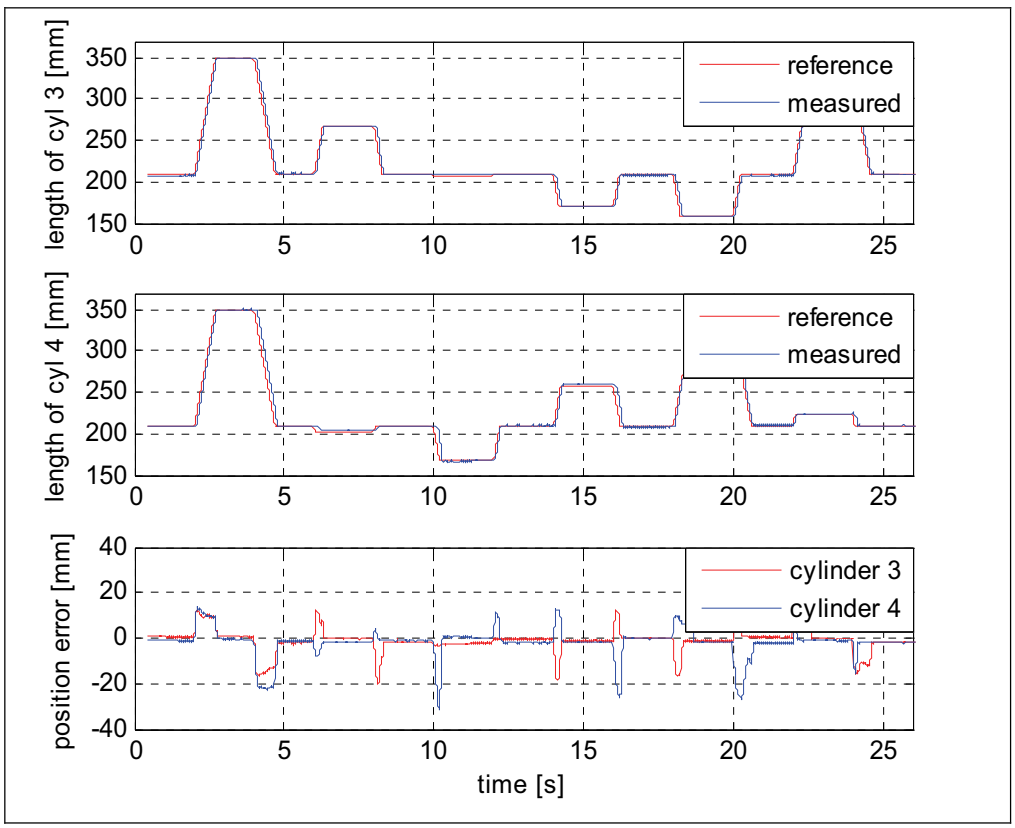

Figure 10. Maximum ramp response of the platform with P-controller.

Figure 9 and figure 10 shows that cylinders move quite well at high speeds. P-controller works very well with maximum ramps. P-gain is set so that there is no overshoot in responses. P-gain is high enough to keep steady state error small, maximum is about 2.5 mm.

Figure 9 and figure 10 shows that maximum error during the cycle is higher with the feed forward controller because of overshoots. However P-gain is so small in the feed forward controller that steady state errors are higher than with P-controller. It is possible to make response better but same gains are used both ramp and sine responses on the feed forward controller which set certain limits.

5.3 Sine wave responses

In actual use most references are either sinusoidal or polynomial signals. Characteristics of the water hydraulic platform are measured with sine signal. Two different frequencies are used, the slower one is 0.2 rad/sec and the faster one is 3.0 rad/sec. Main challenge is to get motion of the cylinders smooth in all velocities under 0.2 m/s. Amplitude of the sine wave is 80 mm in direction of Z-axis. Figure 11 shows the properties of the platform with feed forward controller.

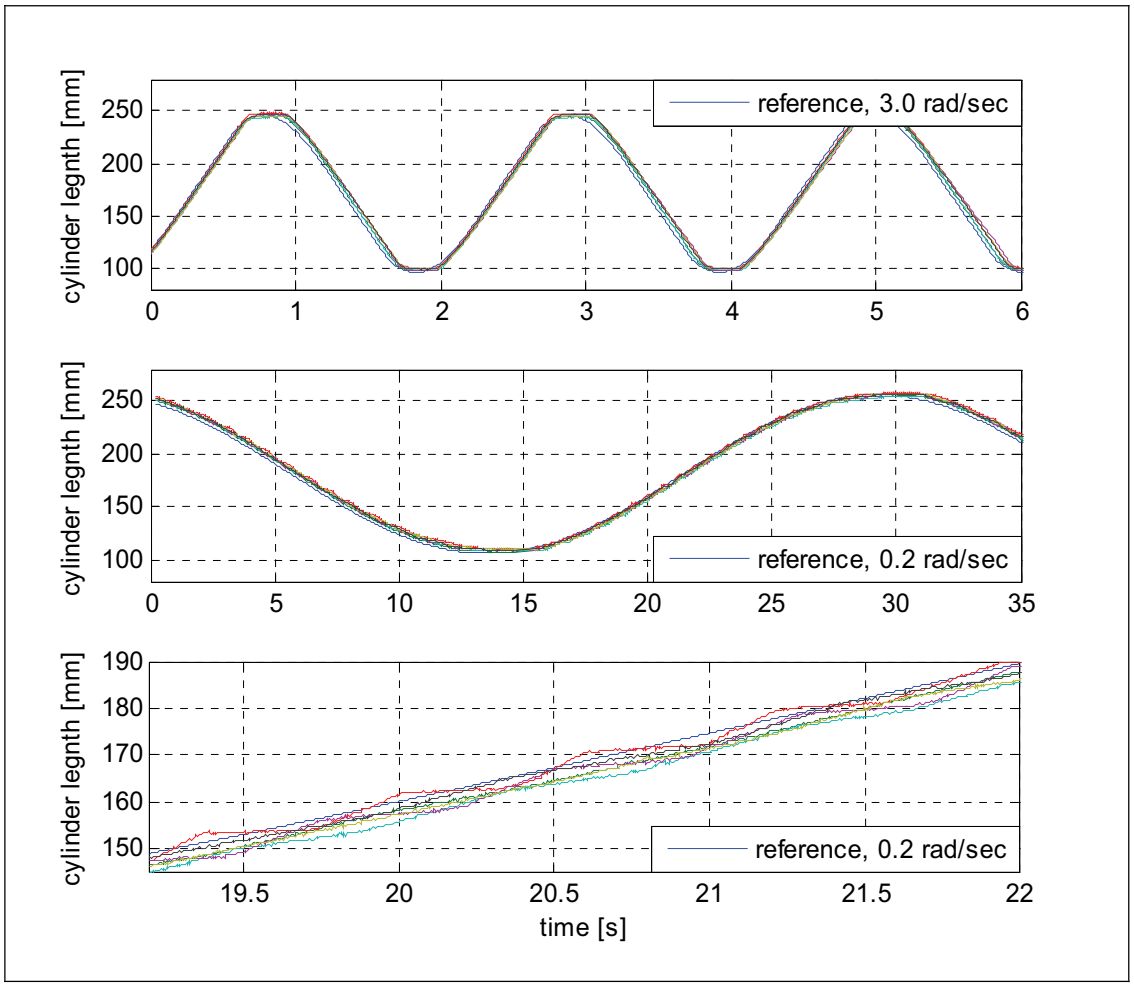

Figure 11. Sine response of the platform with feed forward controller.

With higher frequency difference between input and the response is acceptable. Motion of the cylinders is smooth. During the reversal cylinders stopped and the friction of the cylinders is so high that some error occurs.

With low frequency the problem becomes very clear. Figure 11c shows that the oscillations in the cylinders motion and the high frictions of the cylinders are obvious. By reducing P-gain velocity oscillation could be avoided but the error between reference and the real value rise too high. With nonlinear feed forward controller it is possible to make motion smoother.

With 0.2 rad/sec sine wave P-controller is not suitable because of oscillation of the cylinders motion is very strong. With high frequency and higher speed also P-controller is competitive.

6 CONCLUSIONS AND DISCUSSIONS

In this research is shown that it is possible to build water hydraulic motion platform. Platform is made from commercial components which causes some problems. Frictions of the cylinders are too high for accurate motion. Different types of seals could be a considerable improvement and also the higher pressure level would help. Valves are slightly modified and swiftness of the valves is not adequate. Water hydraulics can be used also in demanding applications with certain limitations and it is noticed that more component development is needed.

The idea and the structure of the control part of the platform are described. Hardware part consist of one standard PC with analogue output card and two analogue input cards and different sensors. The control software of the system is the real-time simulation model.

Characteristics of the motion platform are represented with step, ramp and sine responses. Two different control algorithms are tested and the results show that in normal use feed forward controller works well. Feed forward controller is chosen to first controller to the simulator.

Different kinds of controllers will be tested to get more accurate response. Especially slow motions are problem because of high frictions of cylinders. Accurate synchronization of the cylinders motion is also done in the future. The body of the mobile machine will be attached on the motion platform. The tuning of the parameters has to be made accurately to achieve right feeling. Simulation computers have to be connected and also the main computer and the graphics should be integrated in the package. In the future the structure of the simulator can be simplified as dual-core processors are becoming more common and efficient in personal computers, it is possible to re-unite graphics generation and collisions detection again. This can be done by two parallel software threads, both executed in their own processor core. This allows collision detection to use knowledge of graphical geometry, adding collision computing algorithm selection.

7 REFERENCES

[1] Design and implementation of water hydraulic 6-DOF motion platform for real-time simulators, PTMC06, Bath 2006.
Tuija Palonen, Markus Rokala, Harri Sairiala, Janne Uusi-Heikkilä, Kari Koskinen. Institute of Hydraulics and Automation, Tampere University of Technology

[2] A platform with six degrees of freedom. Proceedings of the Institution of Mechanical Engineers 1965. 180(1):371-386. D. Stewart.

[3] MathWorks MATLAB Central. Stewart Platform Mechanical System. Jeff Wendlandt. 27.10.2006.
http://www.mathworks.com/matlabcentral/fileexchange/loadFile.do?objectType=file&objectId=2334

[4] Modeling, Simulation, and Control of a Hydraulic Stewart Platform. Proceedings of the 1997 IEEE International Conference on Robotics and Automation. D. Li and S. E. Salcudean. Department of Electrical Engineering, University of British Columbia.

[5] A six Degree-of-Freedom, Hydraulic, One Person Motion Simulator. Proceedings of the 1994 IEEE International Conference on Robotics and Automation, 2437-2443. S. E. Salcudean et al. Department of Electrical Engineering, University of British Columbia.

[6] Modal control for a class of multi-axis vibration table. UKACC Control 2004 Mini Symposia. 2004. A.R. Plummer.

SELF PROPELLED WATER HYDRAULIC VEHICLE.

José M. García.
Gary W. Krutz
John Lumkes Jr.
Purdue University
225 South University Street
West Lafayette, IN 47907
USA
Phone**:** +1(765) 494-1179, Fax: +1(765) 496-1115
E-mail: jmgarcia@purdue.edu
krutz@purdue.edu
lumkes@purdue.edu

ABSTRACT

This project determined the amount of energy saved after the conversion of the first all water hydraulics vehicle. A Jacobsen Greens King VI lawn mower was converted from oil to water hydraulics; the hydraulic circuit was divided into two systems, one controlling the propulsion and the steering of the vehicle, and the second one to handle the motion of the grass cutters. The experimental results gathered from the prototype were used as input data for a simulated system using MSC EASY5™. The simulation system was run using water and SAE 50W oil. The simulated pressure drops for both fluids were compared to estimate the power and fuel savings from the vehicle's conversion. The calculated power saved for the hydrostatic drive system was 200 Watts and an additional 810 Watts was calculated to be saved for the reel drive system. The total calculated system savings was 1010 Watts. This power savings could be translated into savings of nearly 220 USD per year assuming the vehicle runs an average of 1000 hours per year.

KEYWORDS: water hydraulics, water powered vehicle, power savings, EASY5, simulation.

1 INTRODUCTION

An environmentally concerned society demands engineering solutions that do not disturb earth's natural equilibrium; for this reason water hydraulics emerges as an alternative to replace petroleum based oil in hydraulic systems.

Water is non-toxic and therefore suitable to be used in applications like those needed in the food industry and many other situations where oil is not acceptable. Additionally, water is non-flammable, an important feature for systems running in locations that have a high risk of catching fire. While the use of water hydraulics is just starting to grow, it is worth mentioning that there is no references to a vehicle whose hydraulic systems are all 100% water driven. The converted lawn mower developed at Purdue University is an attempt to show the scientific community future trends in the field of fluid power and mobile hydraulics.

Beck [1] commented on some of the advantages of converting today's mobile equipment to water hydraulics, water costs 0.0072 USD/liter as opposed to hydraulic oil which is 4.65 USD/liter. Consider Purdue's vehicle that was redesigned to use around 22 liters of water compared to the original 19 liters of oil in the hydraulic reservoir. The difference in cost to fill the hydraulic system would be 88 USD. According to Beck [1], the estimated savings in volume for vehicles in Europe partially running water hydraulic components is about 12 liters of oil per year per vehicle, about 56 USD for every vehicle in a year.

Krutz and Chua [2] acknowledged at least five reasons why using water hydraulics deserves consideration as an alternative in today's industry:

1. Increased safety awareness
2. Improved environmental protection
3. Health of product consumers
4. Long term manufacturing costs which affect profits
5. Advancement in technology

Moreover, physical properties of water make it ideal for applications where oil has been traditionally used as the pressure medium. Table 1 is a compilation of those characteristics that make water preferable when compared to oil.

Table 1 Comparison of the Characteristics of Water with Other Hydraulic Fluids (Trostmann [3] 1996).

Characteristic	Mineral Oil	Water	Proportion
Kinematic viscosity at 50ºC (cSt)	15 - 70	1	15-70
Compression modulus (N/m^2)	$1 – 1.6x10^9$	$2.4x10^9$	2
Thermal conductivity at 0ºC (W/m.ºC)	0.11 - 0.14	0.598	5
Bunsen's Absorption coefficient	0.06	0.02	3
Specific heat at 20ºC and constant pressure (kJ/kg.ºC)	1.89	4.18	2

In addition, components in water hydraulics are smaller compared to their oil counterparts. Because water has a reduced viscosity, pressure drops throughout the system conditions are smaller, decreasing the operating cost of the system using water. The simulation presented in a later section will quantify the savings of water versus oil.

The major disadvantages of using water in hydraulic systems are listed in Table 2.

Table 2 Disadvantages of water hydraulics (Krutz et al [4] 2006).

Disadvantages	**Remedy**
Oxidation and Rust	Use of rust resistant materials
Poor lubricity	Improve surface finish and hydrodynamic design
Lower viscosity	Tighter tolerances
Bacterial growth	Used treated or deionized water
Particles contaminants present	Use 5µm or better filtration

A mobile water hydraulic vehicle was developed at Purdue University. In this project the original oil hydraulic system was replaced with one using water hydraulic components. This vehicle was primarily developed in order to provide an alternative different than oil for the equipment used for maintaining the expensive and delicate grass of golf courses. This vehicle had two independent hydraulic systems, making an efficient use of the power coming from the 19 HP Diesel engine. One of the advantages of having two separate systems is that the hydraulic system is easier to connect and control, another major advantage is the use of fewer hydraulic lines and connectors, which can be directly translated into less friction losses and optimal working pressures. The objective of this research was to estimate the cost savings of operating a converted to water hydraulics vehicle by means of a computer simulation and the experimental validation of the estimated calculation with the field test data taken from the vehicle.

Figure 1 Self-Propelled water hydraulic vehicle

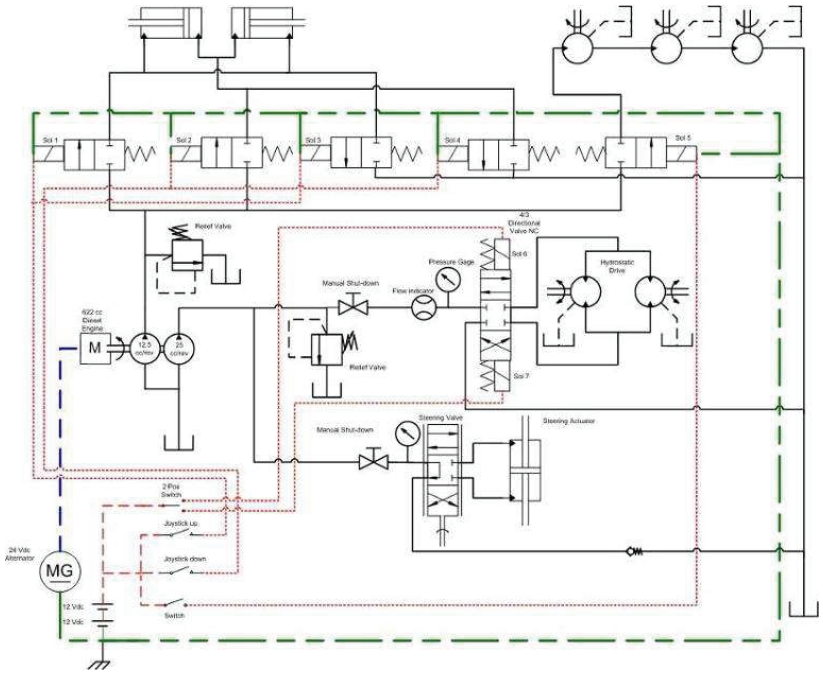

Figure 2 Hydraulic Schematic of the vehicle

2 VEHICLE SPECIFICATIONS AND DATA ACQUISITION:

Table 3 Lawn mower specifications.

J .Greens King VI [5]		
Manufacturer Specifications	Tires	10/10/20
	Nominal Tire Width	0.254 m
	Mass with blades mounted	575 kg
Measured	Minimum Arm Radius	0.0889 m
	Cylinder Stroke	0.1333 m
	Kingpin Offset	0.0127 m
Assumed	Rolling radius	0.254 m
	Net tractive coefficient on Concrete*	0.8
	Friction between tire and concrete*	0.7

*Values taken from Goering et al [6].

National Instruments©' LabView© software was used with the NI DAQ Pad 6015 to create a virtual instrument panel for collecting the information digitally in to a laptop computer. The frequency signal from the flow meters was conditioned using an inverting amplifier with a gain of 1000.

Table 4 Data acquisition instruments.

Component	Model	Quantity
Turbine flow meter	AW TRG 11875	2
Pressure transducer	Webster LPT 3000PN MA	2
Power supply	SHENZHEN HY3003D3	1
Resistors	1MΩ,1 kΩ,470 Ω	2 of Each
Solderless circuit board		2
Operational Amp	National semiconductor LM 741	2
DAQ card	NI DAQ Pad 6015	1
Laptop computer	Dell® Inspiron 4000 series	1
Seamless tube	3/8 and 1/2 OD 316 steel tube	

Calibration data showed that the water turbine flow meters used for this project were able to measure the flow with an accuracy of ±0.26 L/min, the pressure transducers had an accuracy of ± 1.4 bar.

3 EXPERIMENTAL DATA:

3.1 Pressure and flow readings from the hydrostatic drive motors

The Nessie Danfoss PAH 25 pump used to power the hydrostatic drive should deliver 34.02 L/min at a speed of 1500 rpm; the maximum measured flow going to the motors was 37.16 L/min, and 32.39 L/min at the outlet. The combined leakage from the motors was estimated to be 4.77 L/min. The maximum pressure drop at full flow was 30.93 bar. The total hydraulic power delivered to the motors at full flow was 1.92 kW.

Table 5 Data from the drive motors in 2006 Water hydraulic vehicle

Flow IN	Flow OUT	Press IN	Press OUT	Press Drop
L/min	L/min	bar	bar	bar
Turning & running				
17.65	13.08	22.86	4.90	17.97
18.26	12.97	20.99	5.21	15.78
25.86	20.90	35.35	6.30	29.04
26.38	20.41	31.27	5.57	25.70
27.33	22.42	28.69	6.42	22.27
26.08	21.17	29.14	5.90	23.24
Running full flow				
33.57	26.27	58.08	7.26	50.82
37.16	32.39	39.50	8.57	30.93
34.32	30.62	39.43	8.32	31.12

3.2 Inlet and outlet pressure and flow readings for the motor in the rear cutter

Table 6 shows the data collected from the pressure transducers and water flow meters installed on the inlet and outlet port of the hydraulic motor in the rear cutter. The average flow going in was 24.19 L/min and average flow at the outlet port was 23.96 L/min, the difference between these two measurements corresponds to the flow going through the case drain of the motor (0.22 L/min). The pressure on the inlet port showed a fixed value of 47.79 bar, the average pressure on the outlet port is 45.37 bar, the average pressure drop was 2.41 bar. The estimated torque was 9.02 N-m.

Table 6 Data from the rear reel motor

	Flow IN L/min	**Flow OUT L/min**	**Pressure IN bar**	**Pressure OUT bar**
Test 1	24.76	23.81	47.79	41.45
	24.57	24.04	47.79	48.56
	23.78	23.85	47.79	39.15
Test 2	25.36	25.10	47.79	42.37
	25.10	25.29	47.79	50.79
	25.52	25.25	47.79	37.74
	25.14	25.14	47.79	50.79
	24.95	24.99	47.79	41.34

3.4 Vehicle‘s average speed:

The average speed of the vehicle was determined by timing the vehicle when cruising on two different surfaces. On grass while mowing the vehicle traveled a distance of 11.28 m in 18.22 sec, for an average ground speed in grass of 2.22 km/h; the engine speed was 1800 rpm. On asphalt the total distance of 35.0 m was traveled in 44.93 sec, the average speed in asphalt was calculated to be 2.80 km/h; for this last measurement the reels were lifted and the reel motors were not rotating, the approximate engine speed was 1800 rpm.

4 SIMULATION WITH MSC EASY5™:

The MSC EASY5™ software package allows engineers to simulate dynamic systems and perform an analysis of control loops involving complicated or extensive calculations. One of the libraries of this computer program is entirely dedicated to hydraulic components such as, valves, pumps, actuators, etc; every component can be modeled in terms of its flow characteristics and geometry. EASY5 combines variable step integration algorithms with algebraic steady-state methods to resolve hydraulic circuits, both in steady state and with transients. One feature of this program is that the user does not need to develop complicated transfer functions to model the hydraulic circuit, instead, the components can be connected together by following color coded ports that later allow the designer to select and plot the point in the circuit where the information is desired.

4.1 Water hydraulics vehicle simulation:

The steering system was modeled according to the specifications listed in Table 1. The pump and motors characteristics were obtained from the manufacturer datasheets (Nessie Danfoss [7]). The displacement of the pump was 25 cc/rev, and the speed of the input shaft was held constant at 1800 RPM. The volumetric efficiency was set to 0.90 and the overall efficiency to 0.87 for this component (calculated from the datasheet). Figure 3 shows that at high shaft speeds the efficiencies do not change by more than 2.5% at different pressure levels.

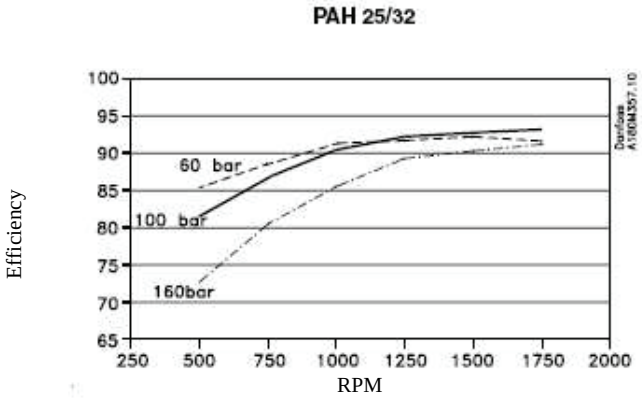

Figure 3 Efficiency of Nessie Danfoss PAH25 pump (Danfoss [7], 2006)

4.1.1 Hydrostatic drive simulation:

A four-port three way, closed center directional valve was used for this model and there was no leakage assumed between ports. The valve gain was modeled at 37.80 L/min flow for a pressure drop of 8.50 bar between the supply and the output port. The valve opening time was 110 ms.

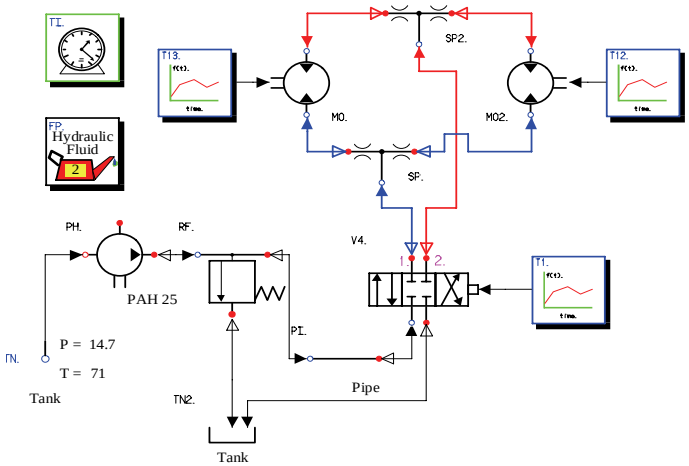

Figure 4 Hydraulic schematic of the hydrostatic drive.

Figure 4 shows the schematic used in EASY5 to simulate the hydrostatic drive of the vehicle. The starting torque required by the motors was set to 85.00 N.m as per Danfoss

specifications. The friction torque was calculated from the reported pressure drop at 1800 rpm. The calculated friction torque was 32.22 N.m. Both motors had a displacement of 160 cc/rev. Two tables were used to account for the torque load on the shaft. The load was estimated from the experimental data to be 46.86 N.m.

The two tee junctions connecting the drive motors in parallel have a hydraulic diameter of 12.7 mm. A tube with an internal diameter of 12.7 mm and 1270 mm long was used to account for the pressure drop from the tubing in the real vehicle; the surface finish used for the model was 32 micron.

The model was initially run using water as the pressure medium, the flow and pressure values were plotted against the same system using SAE 50W oil. No parameters were changed in the model.

4.1.2 Hydraulic reel drive system:

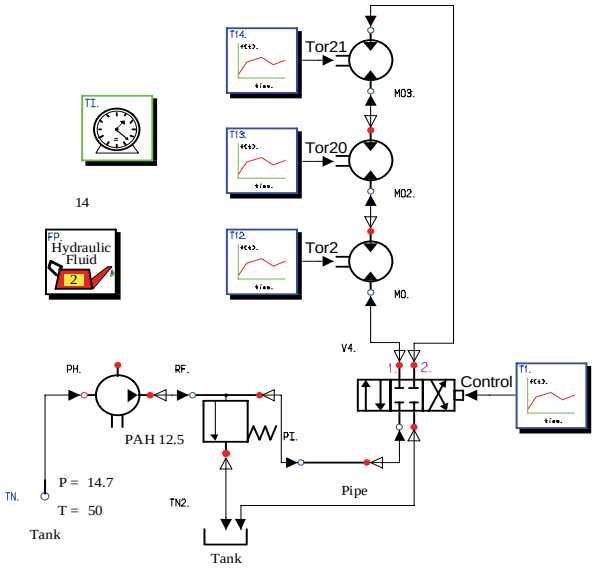

Figure 5 Hydraulic schematic of the reel drive

Figure 5 depicts the hydraulic schematic of the reel drive system used with EASY5. The hydraulic system driving the reels has three motors installed in series, each having a displacement of 10 cc/rev. The breakaway torque of the motors was 10.00 N.m (Danfoss, [7]). The moment of inertia of the rotor was specified as 1.7×10^{-4} kg.m^2, and the Coulomb friction was 0.56 N.m. The total contained volume of the motor's case was 655 cc.

Finally, the Viscous damping coefficient used in the model was 0.01 N.m/(rad/s). The tube between the relief valve and the tube from the return line was assumed to have a diameter of 0.95 cm, the internal roughness coefficient was 32 micron, and the tube's length was 6.35 m. All other components' parameters were assumed to be the same as those in the other simulations. The pump's displacement was 12.5 cc/rev. The overall efficiency was assumed to be 87.5% and the volumetric efficiency was assumed to be 90%.

5 SIMULATION RESULTS:

5.1 Hydrostatic drive system:

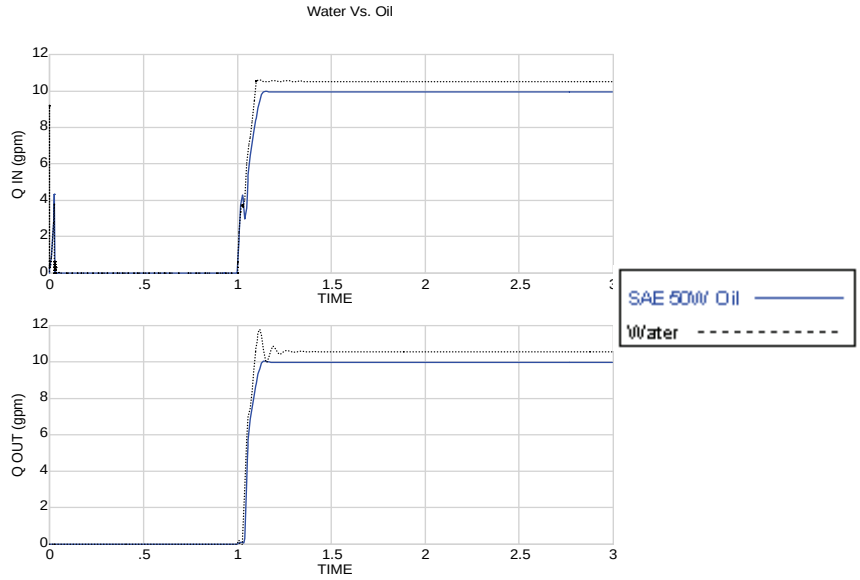

Figure 6 Flow comparison between Water and SAE 50W for the hydrostatic drive

The simulated flow going into the motors remained constant as no leakage was specified for the motors. All losses were assumed to be frictional. The flow across the motor with water was 39.87 L/min, and 37.69 L/min for oil. The average flow input measured in the prototype was 35.02 L/min and 29.76 L/min at the outlet.

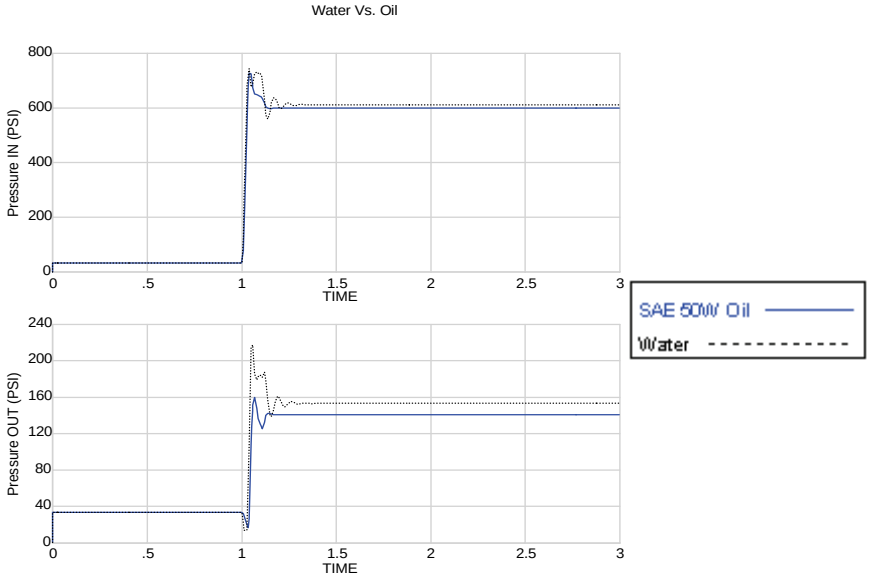

Figure 7 Pressure comparison between Water and SAE 50Wfor the hydrostatic drive

The simulated pressure drop across the motor was 31.45 bar for water and 35.17 bar for oil. In the prototype the average pressure drop running at full flow was 37.62 bar.

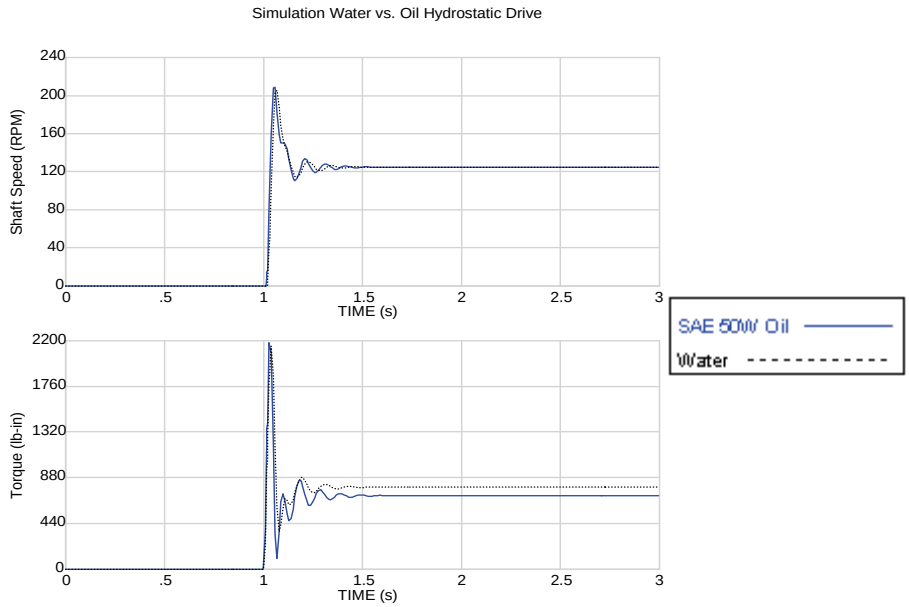

Figure 8 Comparison of motor performance between Water and SAE 50Wfor the hydrostatic drive

Figure 8 shows the output characteristics obtained from the two simulations. The simulated motor shaft speed was 121.0 rpm. The output torque per motor with water was 80.59 N.m and 91.86 N.m for the oil model.

Table 7 Simulated hydrostatic drive system quantities

	Pressure In [bar]	Pressure Out [bar]	Flow/ motor [L/min]	Torque [N.m]	Shaft Speed [RPM]	Hydraulic Power/motor [kW]
Water	42	10	40/20	81	121	2.1/1.04
Oil	46	11	40/20	92	121	2.3/1.16

The oil pump would have to provide 200 Watts more of power than the water pump in order to maintain the same flow, and consequently, the same shaft speed. This loss in power between oil and water is due to the friction losses of the fluid running through all the components in the simulated system. The viscosity of water at 10ºC was assumed to be 1 cSt and the viscosity of the oil at the same temperature was 100 cSt. The hydraulic power calculated from the measurements taken from the prototype vehicle was 1.92 kW.

5.2 Reel drive system

Figure 9 shows the simulated inlet pressure for the rear reel motor using water and SAE 50W oil. The simulated flow for both fluids was 23.06 L/min. The average measured flow input was 24.8 L/min. See Table 8 for a summary of results.

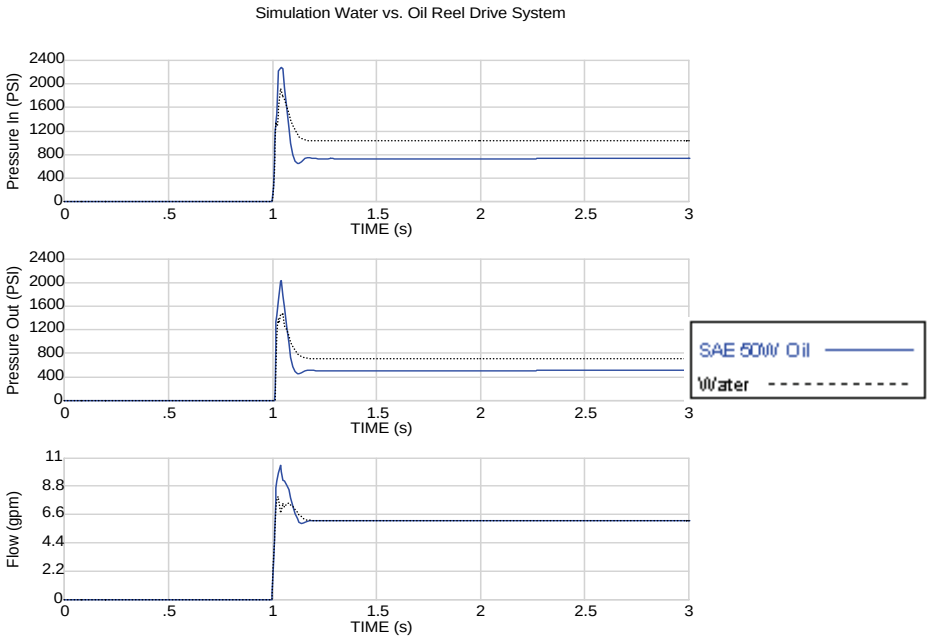

Figure 9 Comparison between Water and SAE 50Wfor the rear reel drive

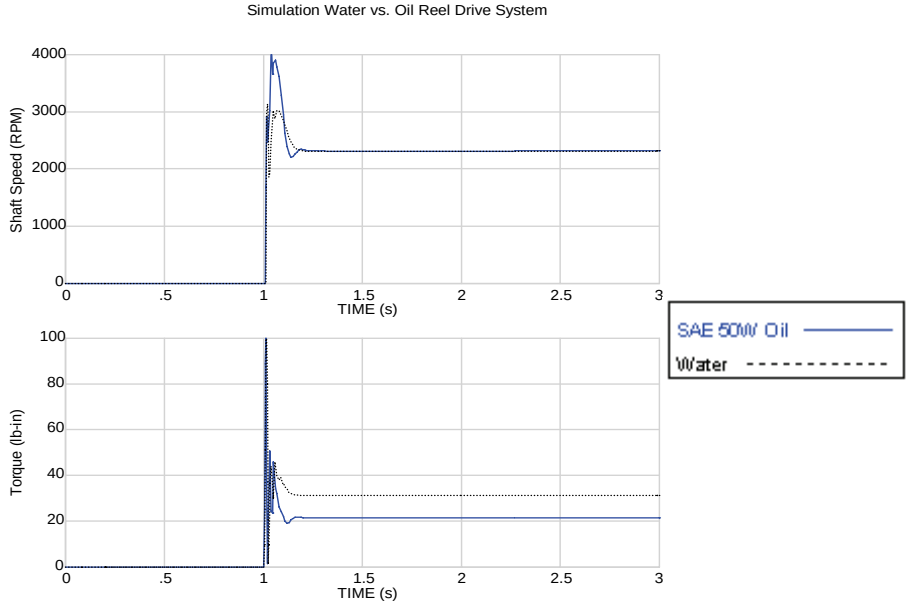

Figure 10 Comparison between the performance of Water and SAE 50Wfor the rear reel drive

Table 8 Simulated reel drive system quantities

	Pressure In [bar]	Pressure Out [bar]	Flow [L/min]	Torque [N.m]	Shaft Speed [RPM]	Hydraulic Power [kW]
Water	50.1	35.4	23.1	2.26	2324	0.59
Oil	71.7	49.4	23.1	3.39	2324	0.86

Table 8 shows that the required hydraulic power to maintain the identical reel speed is 270 Watts. That is, without changing any of the parameters in the simulation except for the fluid. The vehicle is originally designed to have three reels; this means that the necessary hydraulic power to run with oil is increased to 810 Watts.

The hydraulic steering and lifts systems were also modeled using the same fluids. However, no significant change in the required hydraulic power was found.

6 DISCUSSION

The power savings from running a water hydraulic circuit instead of a traditional hydraulic system can be determined using the pressure difference and the flow rate. Using these two figures obtained from the hydrostatic drive simulation it was calculated that a total of 1010 Watts could be saved from running the system with water instead of oil.

The specific fuel consumption for the Kubota Diesel engine mounted on the vehicle is 3.18×10^{-4} liters per W.hr (Kubota [8]). Assuming the average landscaping vehicle runs 1000 hrs per year the estimated savings on fuel would be 322 liters. Given that the current price of Diesel is 0.68 USD/liter, this results in a cost savings of 219 USD per year.

In conclusion, smaller engines may be used in water hydraulic systems or less energy may be spent. Not only the industry's impact on the environment will be decreased by changing from oil to water hydraulics, but there may be long term costs benefits from implementing water as the working fluid.

Continued research is ongoing concerning this topic as many parameters may vary when attempting to develop a more complete model using EASY5 or similar software package. Several variables including temperature effects, spool dynamics, and minor losses were neglected in this model and are being studied. More complex and detailed simulations are easily done with EASY5 in order to acquire a better understanding of the transient states that a hydraulic system undergoes, especially when referring to a fluid as incompressible as water.

7 REFERENCES.

1. Beck, M. E., & Krutz, G. W. (2005). A Power Steering Valve for a Water Hydraulic Lawn Mower. Unpublished M.S.E. Thesis, Purdue University, West Lafayette, IN.

2. Krutz, G., & Chua, P. (2004) Water- Hydraulics – Theory an application. ASAE Agricultural Equipment Technology Conference. Louisville, Kentucky.

3. Trostmann, E. (2001). Tap water as a hydraulic pressure medium. New York, Marcel Dekker.

4. Krutz, G., & Garcia, J. (2006) Self Propelled water hydraulic vehicle. Unpublished M.S.E. Thesis, Purdue University, West Lafayette, IN.

5. Textron/Jacobsen. (2005) “Jacobsen Golf & Turf: Greens King VI.” http://www.jacobsengolf.com.

6. Goering, C. E., M. L. Stone, et al. (2003). Off-road vehicle engineering principles. St. Joseph, MI, American Society of Agricultural Engineers.

7. Danfoss. (2006) “Danfoss High-pressure water solutions”. http://nessie.danfoss.com/Index.asp

8. Kubota Engine (2006). “Kubota engine performance”. http://www.kubotaengine.com

PUMP SUPPLY PRESSURE FLUCTUATIONS IN THE SEMI-CLOSED HYDRAULIC CIRCUIT WITH BOOTSTRAP TYPE RESERVOIR

Jussi Aaltonen, Kari T. Koskinen, Matti Vilenius
Tampere University of Technology
Institute of Hydraulics and Automation
P.O.Box 589
33101 Tampere, Finland
Phone +358 3 365 4433, Fax +358 3 365 2240
E-mail: jussi.aaltonen@tut.fi

Kalle Vaaraniemi
Finnish Air Force Headquarters
Armaments Division (A10)
Aircraft Sector
P.O. Box 30
41161 Tikkakoski, Finland

ABSTRACT

Hydraulic systems of modern aircraft are structurally very complex and closely interlinked to other subsystems of the aircraft. Therefore troubleshooting causes for operational abnormalities is a complicated task. Studying the system operation by test flights is difficult and expensive to realise due to flight safety issues and ground tests do not usually give the useful data to study in-flight operation. Without access to functional simulator (i.e. iron bird) troubleshooting on the basis of measurements is looking needle from the hay stack. Thus an alternative approach on troubleshooting is needed.

This paper presents the approach, combining simulation and in-ground measurements, for studying the causes of cavitation erosion encountered in the hydraulic pump of the fighter aircraft. Hydraulic system operation was studied using detailed analytical simulation model of the hydraulic pump and the hydraulic reservoir. In-flight accelerations affecting on the system were taken into account by using real in-flight acceleration data and operational and environmental extremes were studied. In-ground measurements were planned and carried out on the basis of simulations to verify results.

KEYWORDS: Axial piston pump, aircraft, bootstrap, self-pressurizing

1 INTRODUCTION

Hydraulic system is usually considered to be a separate aircraft subsystem among the others, but it actually is an inseparable part of most of the other subsystems, as in modern aircrafts nearly all power stages of various actuating systems are hydraulic.

Hydraulic system does not operate independently from other subsystems but its operating point is always defined by other subsystems. For example typical 4^{th} generation fighter (for example: F-15, F-16, F-18, AV8, MiG-29, MiG-31, Su-27 etc) has over ten independent flight control surfaces each actuated by hydraulic actuators on basis of flight control system commands. Besides of flight control system actuators, there are also hydraulic actuators in auxiliary systems (weapons system etc) which are controlled by their own control systems.

Even though power-by-wire has been discussed for a long time and its benefits have been proven thoroughly most of military aircrafts in operational service today (up to 4.5^{th} generation) use traditional central hydraulic system. Due to lifespan of aircraft in service now that will be the case for several decades in future also. In central hydraulic system the hydraulic system of the aircraft is divided in two or more separate systems which each are divided in multiple separate circuits. Each system and circuit is not dependant on operation of the others. Systems and circuits are also redundant to give the aircraft adequate fault tolerance and tolerance to battle damage.

Specifications for configuration of military aircraft hydraulic systems are given in design standards such as SAE AS 5440. However reliability and damage tolerance issues are mostly defined by flying quality requirements specified by other standards such as MIL-F-8785. Typical requirement for fixed wing aircraft is that damage in one component or circuit, including the power source, should not cause loss of certain level manoeuvrability and even with two damaged circuits or components a complete loss of manoeuvrability is not allowed.

Semi-closed hydraulic circuits are often used in aircrafts to achieve high power to weight ratio. In semi-closed circuit the system return flow directly supplies the pump and the reservoir is used only for compensating fluid volume changes.

Hydraulic pumps used in aircrafts are typically variable displacement axial piston units with constant pressure regulator. Rotational speed of pumps is usually very high in order to enable using as small and light units as possible. Due to high rotational speed there are some small differences in pump design in comparison to generic hydraulic pumps.

Hydraulic fluid reservoirs in aircraft hydraulic systems differ a great deal from generic mobile hydraulic applications. Reservoir volumes are significantly smaller due to weight savings requirements and reservoirs are always pressurised. Reservoir pressurisation is necessary to guarantee adequate fluid supply for the hydraulic pump independent from the aircraft alignment, acceleration etc. In military aircrafts reservoirs are typically either self-pressurising (i.e. bootstrap) type or charged with some inert gas, typically nitrogen.

Hydraulic pumps and reservoirs with their accessories form the backbone of aircraft's hydraulic system and they are therefore the single most critical components of the system. Most of the power of the hydraulic system is consumed by the flight controls.

Flight control system commands to flight control actuators depend on both pilot command and current flight state. This means that an instantaneous load of hydraulic system is mainly a function of flight state, pilot command and ambient conditions. Thus an arbitrary operating point of the pump and the whole system can not be reproduced in ground tests due to different ambient conditions, lack of aerodynamic loads and limitations of the flight control system. This makes studying the system operation by simple ground tests impossible.

Traditional approach on studying the hydraulic system behaviour in an arbitrary in-flight operating point is laboratory tests on the functional simulator (*ironbird*) or test flights with suitable test instrumentation installed in the aircraft. Test flights are technically very challenging to realise and thus extremely expensive. On the other hand the aircraft manufacturer usually keeps the ironbird available as long as the aircraft remains in operational service, however it still does not mean that the ironbird is kept constantly available for research and development. Therefore a systematic and efficient approach on studying the behaviour of aircraft hydraulic systems without an ironbird or flight testing is needed. This paper presents cost effective and efficient method which combines simulation and ground testing.

2 THE HYDRAULIC SYSTEM STUDIED

The hydraulic system studied belongs to a twin engine fighter aircraft. Schematic diagram of the system structure around hydraulic pumps is shown in figure 1. The aircraft has two separate hydraulic systems which both have two independent hydraulic circuits.

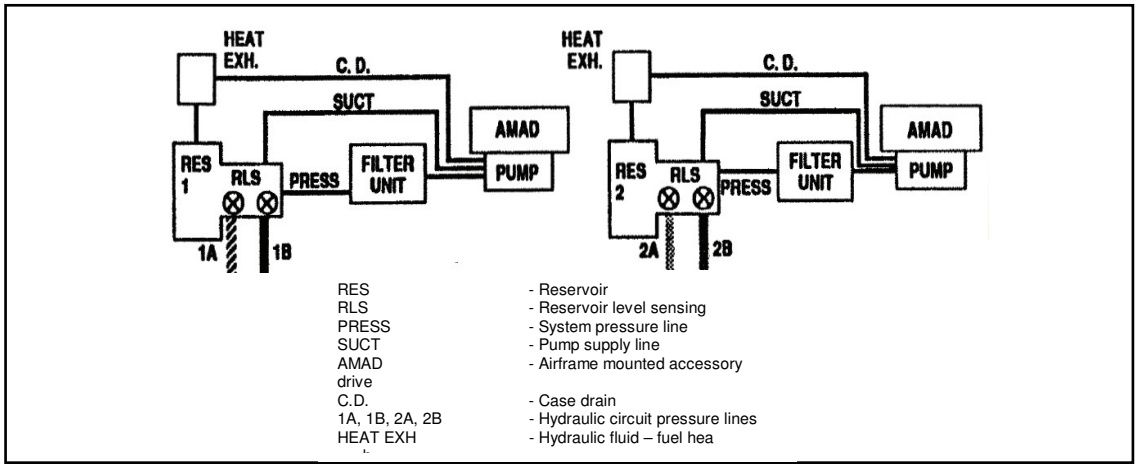

Figure 1. Schematic diagram of the hydraulic system studied

Hydraulic systems are completely separated from each other during normal operation. Reservoir level sensing is used for controlling hydraulic circuit cut-off in case of fluid loss.

Hydraulic systems are semi-closed type with bootstrap type reservoirs (Fig 2). Reservoirs are connected parallel to system return lines which directly supply hydraulic

pumps. Hydraulic pump case drain line is connected to reservoir via heat exchanger and filter. Thus continuous flow through reservoir is equivalent to case drain flow.

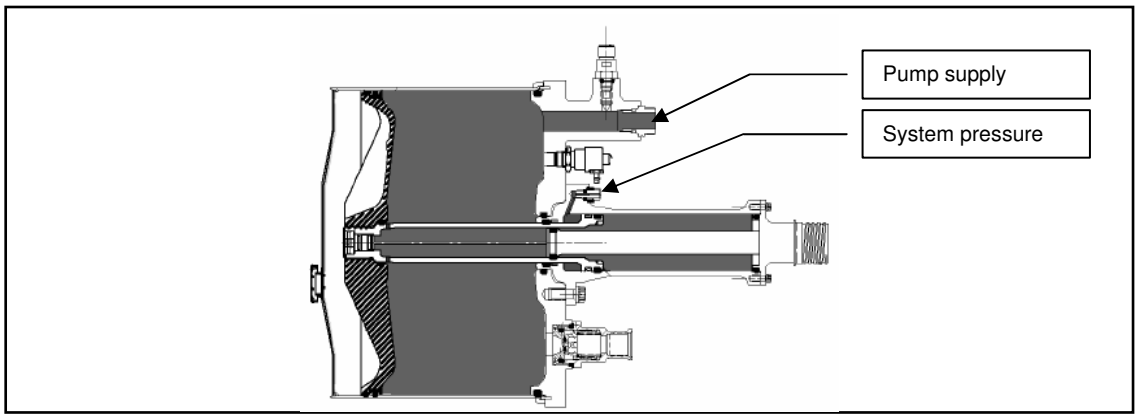

Figure 2. Bootstrap type reservoir

Majority of the actuators in hydraulic systems are symmetrical (i.e. motors etc) or very close to symmetrical (i.e. tension rod cylinders etc) (Fig 3), there are very few asymmetric actuators (i.e. conventional cylinders). Hydraulic systems are used to drive all flight controls and auxiliary systems.

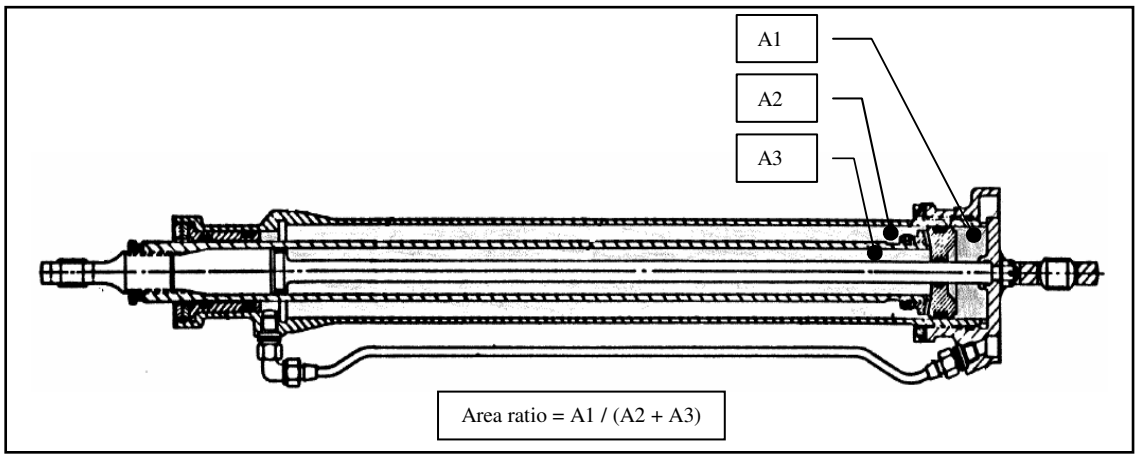

Figure 3. Tension rod cylinder

Hydraulic pump in both circuits is an axial piston pump with hydro-mechanical constant pressure controller. Both pumps are driven by engine via airframe mounted accessory drive.

Lifetime of hydraulic pumps in both hydraulic systems has been found to be shorter than what was expected. Pump failures have not been catastrophic thus they have not been critical flight safety issues but they have caused a significant increase in maintenance costs. Two main failure mechanisms were observed in pump overhauls:

- Seizing: Slipper shoes, swash plate
- Erosion (cavitation): Piston bores, port plate

Failure mechanisms suggest that possible reasons for short lifetime, besides the construction of the pump itself, are inadequate supply pressure and too high case pressure.

It is fairly obvious that reasons for pump failures can be found from hydraulic system in-flight operation. In normal in-flight operation both the load on the system and load variations are the highest. In ground operation flight control system limits speed of most of flight control actuators and also there is only a minimal aerodynamic load on surfaces. Ground operation, consisting mostly of system checks, also forms insignificant portion from the over all use of the system.

Even though both reasons proposed relate mostly to system level phenomena the actual failures in the pump relate mostly to internal phenomena of the pump, thus thorough study of the case with detailed analytical component and system models is needed. This can be seen also as a typical situation for aircraft hydraulic systems in operational service. As systems are already proven flight worthy and usually also have been used for long times problems encountered generally relate to small design details or user specific issues arising from the use of the system.

Experimental research methods can not be used for studying in-flight operation without significant costs and a certain inevitable flight safety risk. Therefore a systematic method for studying the system operation is needed.

3 RESEARCH METHODS

Approach chosen for studying the hydraulic systems was a four stage process described in Figure 4.

Stages of process consist of:

1. Preliminary system analysis
   - System and component structure
   - Interconnections to and interaction with other systems and environment
   - Simplifications

2. Analytical system model
   - Analytical component submodels
   - Analytical system model
   - Interface and interaction models

3. Simulation
   - Detail analysis of the system and components
   - System operation
   - Critical operating points for laboratory / ground testing

4. Laboratory / ground tests
   - Ground and / or laboratory tests of the system in critical operating points

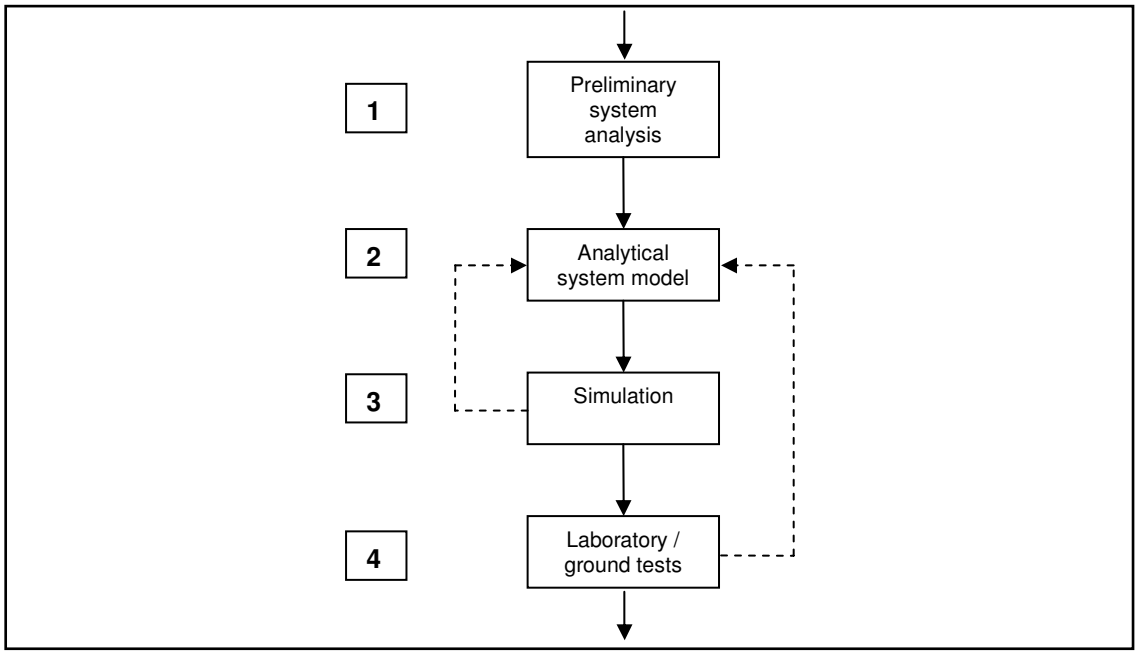

Figure 4. Research process

In the first stage the system and its operation are analyzed on the basis of available material such as manuals, recorded user experience and failure analysis data. Component and system structure are both analyzed to the finest detail. On the basis of this analysis the basic model structure and necessary interfaces and interactions are defined. Also simplifications are defined during this stage.

Submodels of components are generated according to definitions made in the first stage. The system model is composed from component submodels and interfaces to interacting systems and environment are added to the system model. Detailed analytical models are needed to access component detail level behavior. Also in many cases there is no data available to establish empirical or semiempirical models. Due to lack of data establishing model parameters must rely on real physical dimensions and experience. The objective is to establish models that can be used for qualitative analysis, to find phenomena itself, not to find the exact amplitude of it.

Component submodels can usually be adequately tested and verified the same way their real life counter parts are tested. Aircraft component workshop manuals usually contain test requirements and specifications for component performance. Simulating these tests allow tuning parameters which can not be determined from physical dimensions, such as friction etc.

Simulation is done on basis of system operation analysis of the first stage. As wide variation as possible of operating points is simulated. Detailed behavior of each component of interest as well as behavior of the whole system is analyzed to define critical operating points. When critical operating points are defined the system simulation model is used for defining operating points possible in ground or laboratory testing which correspond to critical operating points as closely as possible.

Ground or laboratory testing is done to verify and to further specify simulation results. Objective of this stage is to find the same phenomena in both simulation and test data and to point out the reasons on basis of both simulation and testing.

Both simulation and testing stages can be iterative processes leading back to model generation phase in case of simulation and testing results not converging adequately or simulation models found dissatisfactory during simulation stage. Iteration is not however an end in itself but merely an optional feedback loop in the process.

Simulation models and simulation can be considered as advanced engineering calculations, a handy tool but not sole purpose. There are certain known errors and inaccuracies that can be accepted. Actual model verification and validation process is not necessary if the model is used in combination with testing.

4 PRELIMINARY SYSTEM ANALYSIS

Structure and operation principles of hydraulic system and its components were analyzed on basis of available data, such as manuals and available design documentation. Failure rate data and individual failure mechanisms were analyzed. On basis of these the area of interest in the system and the model detail level were decided. Analyzing failure rates and mechanisms showed that it was unnecessary to study both systems since both failure rates and mechanisms were same on both systems.

Hydraulic systems were simplified to the level where studying pumps, reservoirs and their accessories is possible, but the system in its entirety is as simplified as possible. Hydraulic system (Fig 1.) was broken down to block diagram of Figure 5. Each block in diagram represents a submodel level function in the system model.

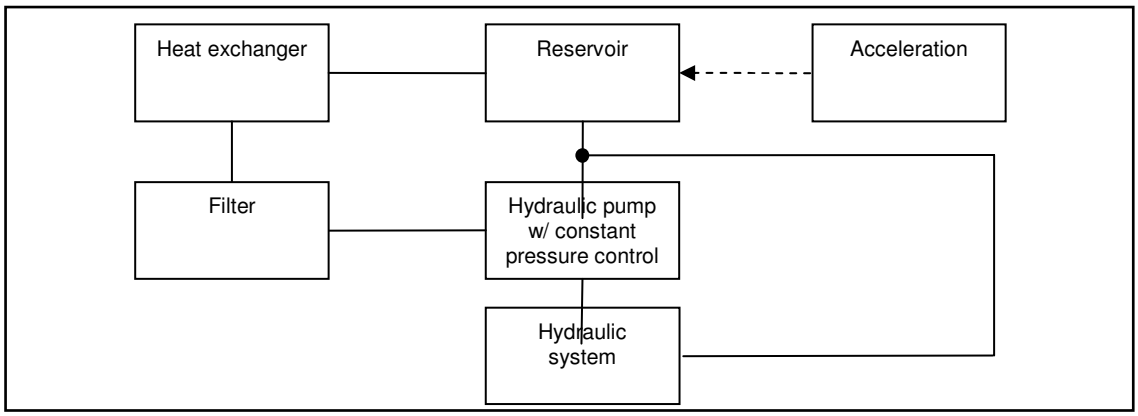

Figure 5. Hydraulic system block diagram

There are numerous interactions with other subsystems and environment but the only interaction possibly affecting on the supply pressure is the aircraft acceleration. Even though acceleration affects on all moving parts in the system it was assumed that its effect on reservoir piston and hydraulic fluid is the only significant interaction. Assumption made was based on recorded maximum accelerations in direction of main axles, masses of moving parts and mounting directions of components.

Actuators of the hydraulic systems can be simplified to simple orifices with logical functions causing in-flow and out-flow imbalance in case of asymmetricity. This simplification is justified by the nature of flight control system and other systems. All flight control actuators are symmetric or nearly symmetric, thus there are no larger in/out-flow imbalances because of flight control system operation and on the other hand many actuators working simultaneously in different phases equalize possible imbalances. However there are certain actuators which have area ratio that causes significant flow imbalance. In normal operation power taken from a single pump varies from nearly zero to nearly 100%. Due to leakages it never drops to zero and on the other hand there is a safety margin in the other end. An instantaneous system power is more or less arbitrary, depending on vast variety of different parameters. Being a constant pressure system the only parameter changing as power changes is system flow, therefore the actuating system can be, with an adequate accuracy, modeled only as a system that causes arbitrary flow demand changes and produces arbitrary system in-flow and out-flow imbalance relative to certain component dimensions.

Most of the accessories, such as filters and heat exchangers, can be modeled as simple orifices with certain pressure difference – flow behavior which can be obtained from component workshop testing data. Heat exchanger and heat balance of the system has an effect on the failure mechanisms observed in pumps, but it was known that system runs in relatively stable temperature and thus modeling the heat exchange in between fuel system and hydraulic system could be ruled out.

5 ANALYTICAL SYSTEM MODEL

Even though the system to be modeled is simplified as far as possible an analytical model of this scale is very complex and contains multiple levels of hierarchy which each need attention. Hydraulic system block diagram (Fig 5.) in its entirety represents the top level system model. Below the top level there are multiple levels of hierarchy: Component and interaction submodels and models of individual basic elements (i.e. restrictors, volumes etc.). As described earlier the object is not to generate a model and to study it in itself, but to generate a model and use it in combination with testing to point out how and what to test and to explain test results. This combination sets rather unique demands to model generation process and model itself.

Simulation model of the system is needed at early stage of the process, thus the generation process has to be fast. On the other hand high level of detail is needed even in the lowest level hierarchy. Information flow and interaction must be seamless in between different levels of hierarchy, to allow finding causal connections. Thus there has to be an efficient and advanced simulation tool to allow fast generation of highly detailed models and allow keeping model structure consistent through out the hierarchy.

Simulation software chosen for the task was AMESim, which is very efficient tool for generating detailed analytical models. Its interface supports hierarchical model structure without limiting the information flow to user. It also has multi domain submodel libraries which offer vast variety of ready made component and basic element submodels for model generation. User interface allows model generation by using

simple causal block diagrams which frees the user from cumbersome and time consuming working with simulation code and allows concentrating in essentials.

In following chapters principles of generation and model structure are discussed. Actual detail construction of models and their governing equations are not discussed but can be found in given references.

5.1 Hydraulic pump

The hydraulic pump in the system studied is swashplate type axial piston pump. Pump has hydro-mechanical constant pressure control. Controller pressure connection is internal and controller return flow is directed to pump case. Pump utilizes so-called secondary swashplate angle perpendicular to primary angle to improve its controller response.

Principal structure of the pump model as a block diagram is shown in the figure 6. Modeling of axial piston units has been discussed in many references in various extents [1] [2] [3] [4] [5]. Rapid modeling of axial piston units in aerospace applications has also been studied [6]. Typical rapid and simplified modeling techniques are however not applicable in this case since the level detail required is high.

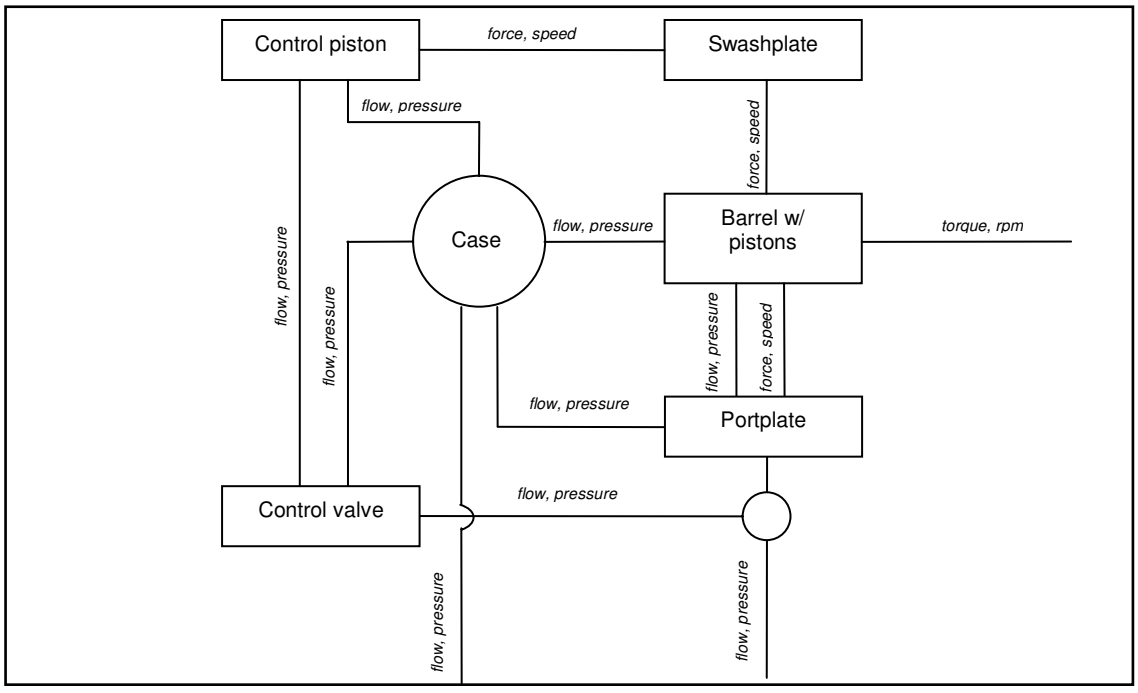

Figure 6. Principal structure of the pump model

The pump was modeled mainly on the basis of references [4] and [5]. Some assumptions and simplifications were made in order to ease the model generation. Assumptions and simplifications were:

- All gap widths are constant
- Mechanical structures are rigid

- Port plate alignment is inclined towards the barrel since the pressure field in between them is imbalanced. Inclination angle is constant.
- Friction in between portplate and barrel is constant
- Slipper shoe friction is constant
- Piston friction does not depend on piston position in the bore
- Bores, pistons, slides, sleeves etc are perfectly circular and situated 1/3 eccentrically.

Due to secondary swashplate angle the top and bottom dead centers are a function primary swashplate angle, thus dead centers move as the pump delivery changes. This causes also change in control torque requirement and change in support reaction forces as a function of swashplate primary angle. Although moving dead centers and changing control torque requirements are very essential the change in support reaction forces was assumed insignificant even though it has definite effect on swashplate friction due to swashplate bearings being of very large diameter.

Even though pump model was simplified it became relatively large and cumbersome model. In the figure 7 a model of single piston with slipper shoe and portplate can be seen.

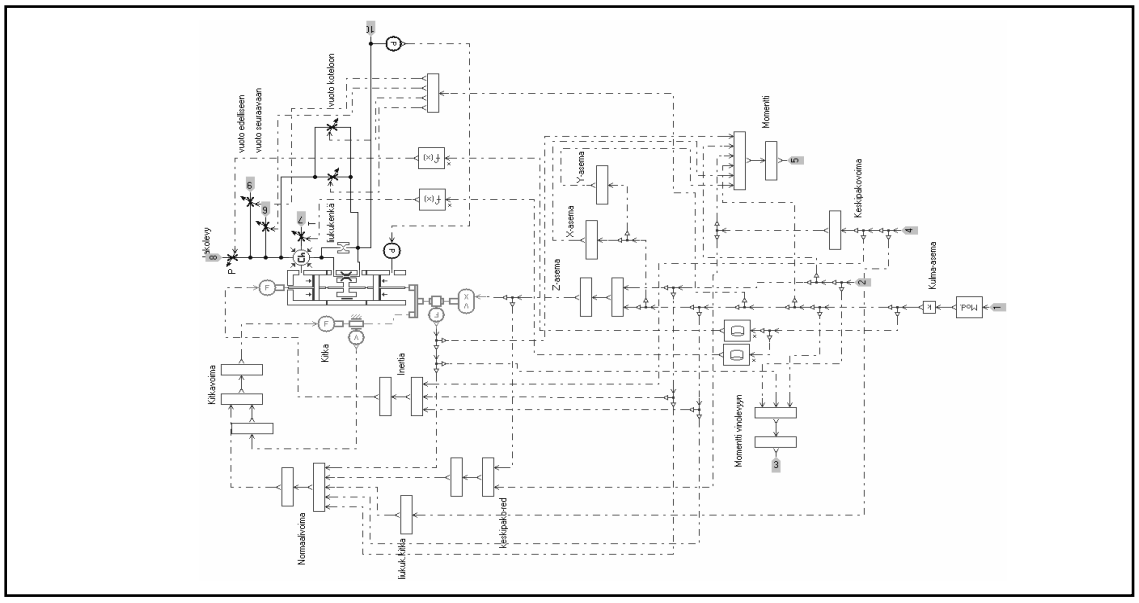

Figure 7. AMESim block diagram of a single piston with slipper shoe and portplate.

The pump controller valve and control piston were modeled with same level of assumptions and simplifications as the pump basic structure. Model is based on the AMESim elemental models [7]. AMESim block diagram of the control valve and piston can be seen in the figure 8.

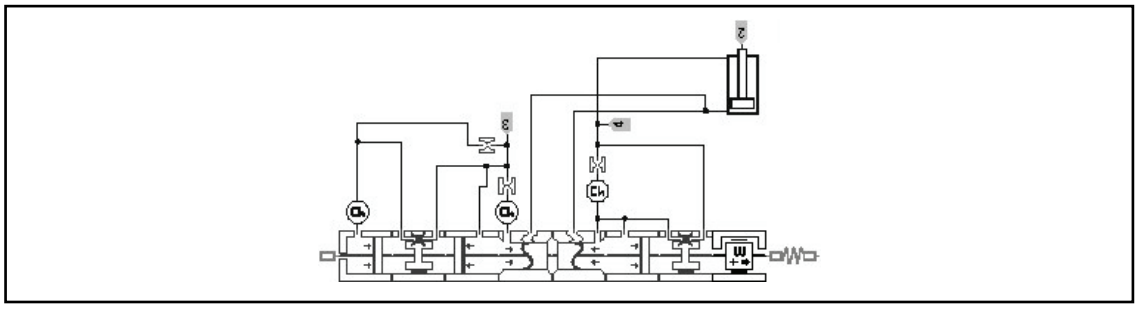

Figure 8. AMESim block diagram of control valve and piston models

Pump model was validated and verified against performance tests given in workshop manual and also against workshop test data of individual pumps. Validation done in this level enables setting most of parameters relatively accurately. It is however obvious that there are lot of parameters which give satisfactory results with numerous different combinations of settings. These parameters have to be set on the basis of experience and it has to be accepted that there is certain error.

5.2 Reservoir and Accessories

Simplifying assumptions made in modeling the reservoir submodel mostly related reservoir level sensing system. The purpose of the RLS-system is to close circuits and eventually the whole system in case of fluid loss. During normal operation RLS-system effects on the system operation only by increasing friction on the reservoir piston. Therefore RLS-system can either be left out from the reservoir model or can be modeled very coarsely. In this case RLS was modeled and included in the submodel for future use, but it was not verified or validated. Model was based on the AMESim elemental models [7].

Acceleration was supplied to reservoir as a simple time dependant data. Data used was real test flight acceleration data sampled on relatively low frequency due to aircraft databus limitations. Time dependant acceleration data does not necessarily exactly match instantaneous operating points of the hydraulic system, but supplying acceleration to reservoir does anyhow give some perspective to behavior of the operating system under acceleration.

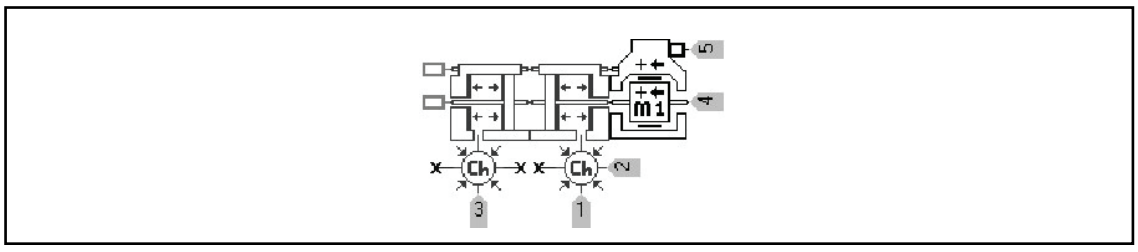

Figure 9. AMESim block diagram of reservoir model without RLS

Accessories, such as heat exchanger and filters, were modeled using AMESim elemental submodels [7]. Models were very simplified, basically simple restrictors with flow – pressure drop map of the real component. Filter by-pass valve was completely left out from the model.

5.3 System Model

The system model was generated by connecting all submodels by either directly or by suitable connectors such as pipe submodels.

As previously mentioned the actuator system was modeled as a series of variable throttles of different maximum openings and time constants. Each throttle representing an actuator was either connected directly to system return to make it act like a symmetric actuator or it was connected to system return via logical function block causing it to return less flow or more flow than system supplied into it, which causes it act like an asymmetric actuator. The subsystem of throttles was constructed to roughly represent the real actuator system, but not as an exact match due to necessary simplifications and because it was not seen necessary for accurate enough results.

6 SIMULATIONS

Simulation runs were targeted for finding critical operation points of the system during normal peace time flight operation. They consisted of series of runs in various temperatures and system flow conditions. Instantaneous acceleration values varied in between -0.5 to 0.5 G in the direction of the reservoir piston axis.

Simulation results were studied on both component level and system level, of which both are reviewed by an example but the latter is further discussed in this paper.

Acceleration was found to have insignificant effect on the pump supply even if the acceleration values were doubled. This was expectable on basis of simple static calculations. Combined mass of hydraulic fluid in the reservoir and reservoir piston is small as well as is the acceleration on piston's axis direction. Also the frequency of acceleration variations is low and does not fall into range of natural frequency of the reservoir volume. Mostly the instantaneous acceleration is in the level where generated force is even lower than static friction of reservoirs moving parts.

Simulation runs showed that supply pressure variations in the system are large. Nominal level of supply pressure is approx. 6 bar and according to simulations supply pressure varies in between 15 bar and vacuum. Seizing encountered in the pump's slipper shoes and swashplate is likely to be connected with fluctuating supply and case pressures as well as is also the cavitation encountered in piston bores and port plate. In general the pressure fluctuation is caused by fluid inertia and time constants involved in the system operation. As the flow demand of the system changes the fluid volumes in both sides of the pump have certain mass flow rate. Generally the valve causing the change in flow demand is much faster than the pump's controller which causes pressure transients in system pressure line due to sudden change of the fluid column speed and on the other hand due to the fact that pump is also not able to reduce flow as fast as needed. In supply side same phenomena occur: Sudden changes in fluid column speed and a difference in time constant of reservoir and valves cause pressure transients. Reservoir sluggishness is caused by both high friction and other mechanical properties but also pipelines connecting it to pump supply line. Even though variation in supply pressure is

high it could clearly be seen that that both minimum and maximum are only encountered only in certain operating conditions.

Both minimum and maximum instantaneous supply pressures are encountered when asymmetric actuators are operated. Figure 10 shows a simple case which represents a situation where a single conventional hydraulic cylinder, controlled by a relatively slow valve, is operated in operating point where the system flow is otherwise fairly constant. As most of actuators are perfectly or nearly symmetric this is relatively rare case, but yet possible to occur on every flight.

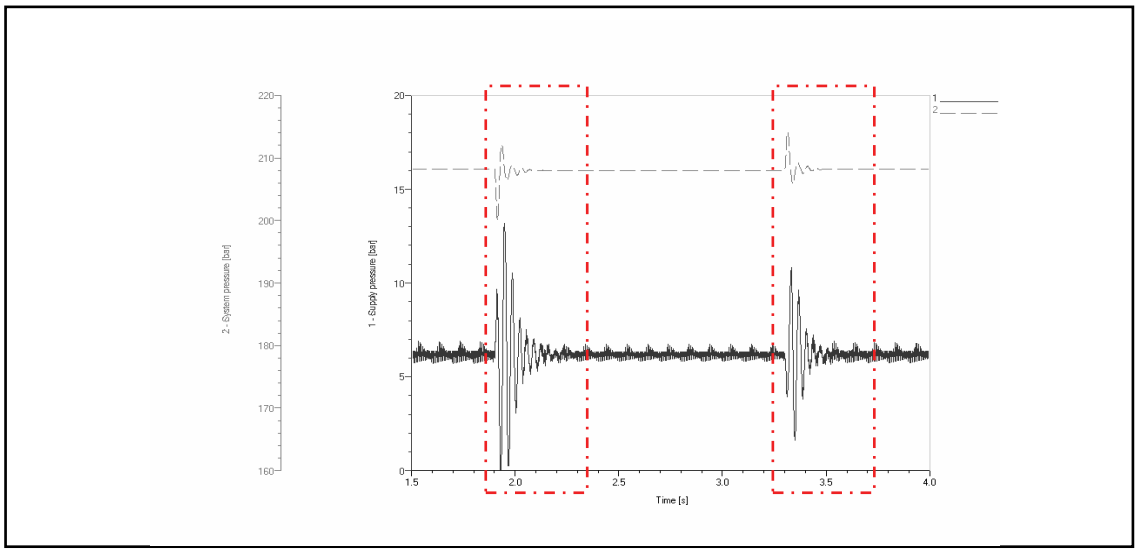

Figure 10. Supply pressure fluctuations caused asymmetric actuator

Figure 11 shows behavior of pumps controller during a relatively large flow change. According to simulations there is large amplitude vibration which suddenly looses its amplitude but frequency remains. Sudden loss of amplitude is caused by phase shift in vibration of control systems moving parts. Phenomenon was found in model verification against pump workshop tests and it occurs very rarely in simulation and is naturally very sensitive to parameters. In the real aircraft as well as in the system simulation model this phenomenon is rare; due to constantly changing flow demand this scale of flow demand changes are rare. However any large amplitude vibration occurring in the controller has an effect on both the case pressure and the supply pressure. Case drain flow fluctuations have an effect on supply pressure fluctuation since the case drain is connected directly to the reservoir.

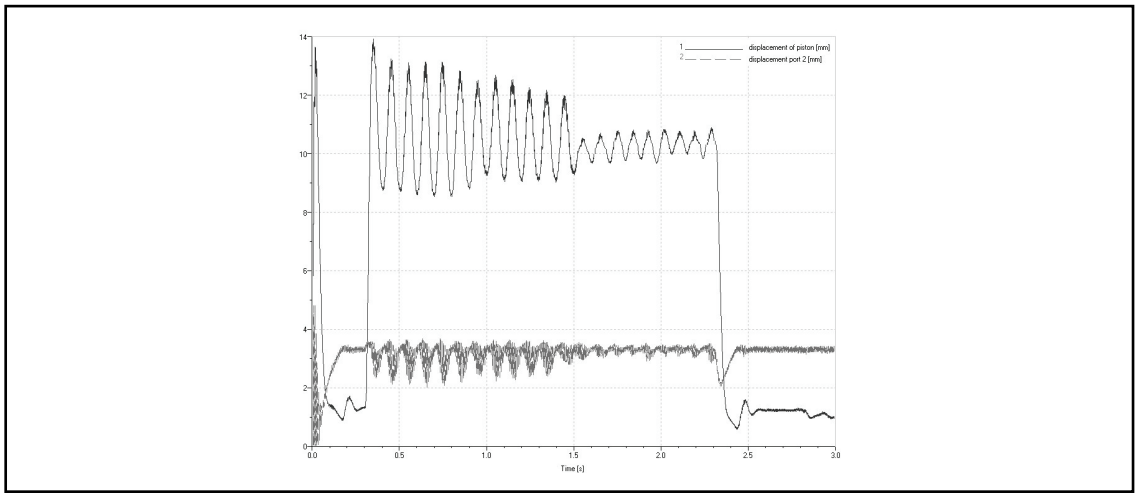

Figure 11. Control piston (1) and control valve (2) displacement in a fast flow change 170 – 70 l/min

7 GROUND AND LABORATORY TESTS

To verify and validate phenomena found in simulations ground and laboratory tests were planned and carried out.

Supply pressure fluctuations could most easily be found by actuating undercarriage, but obviously it is not possible in an aircraft running in test hangar. High power servoactuators of flight controls can not be controlled separately and therefore they are also useless for testing the occurrence of fluctuations. Only feasible option is using the airbrake actuator for testing. Airbrake can be actuated independently from any other actuators and even though it has a tension rod cylinder and actuation is relatively slow speed it is possible to generate flow imbalance that can cause fluctuation.

Figure 12 shows the situation where the airbrake is actuated separately from any other actuators. Even though no other actuator are not deliberately actuated the flow rate on the pump naturally is not zero in the beginning of cycle since there are leakages in the system and some actuators are kept live by dither signal.

Figure shows the same phenomena even in approximately same scale than what was found in simulations. This confirms that one of the reasons for erosion found in pumps is caused by supply pressure fluctuations induced by actuators.

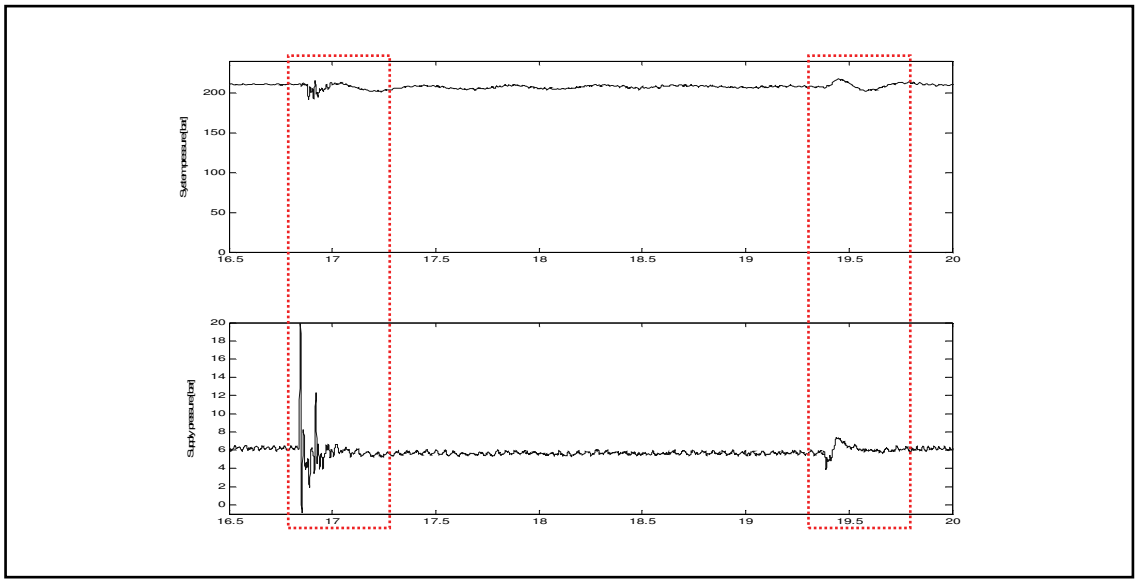

Figure 12. System pressure and supply pressure measured during airbrake actuation in the ground tests

The hydraulic pump was also tested separately in laboratory environment. These tests were done in order to verify and validate some phenomena found inside the pump. The pump was not modified for testing, but all instrumentation was external. It was assumed that for example pump's controller vibrations can be detected by adequate accuracy from system flow rate, drain flow rate and system pressure. Figure 13 shows system pressure and drain flow rate in the situation where flow demand is suddenly (<25 ms) changed from 170 l/min to 70 l/min. The same phenomena than in simulation results of Fig 11 can clearly be identified. Vibration could not be detected in ground tests due to limited possibilities to generate exactly known operating points. Figure 14 shows system, drain line and supply pressure in the operating point where pilot moves stick erratically to generate maximum possible control surface deflections and movement speeds. High variation in all pressures can be seen clearly. There are points where high frequency vibrations can be detected from the system and supply pressure curves, but on the other hand these vibrations can not be detected from drain line pressure curve, which indicates they are not induced by pump's controller. How ever this does not prove that controller vibrations could not occur in the aircraft also.

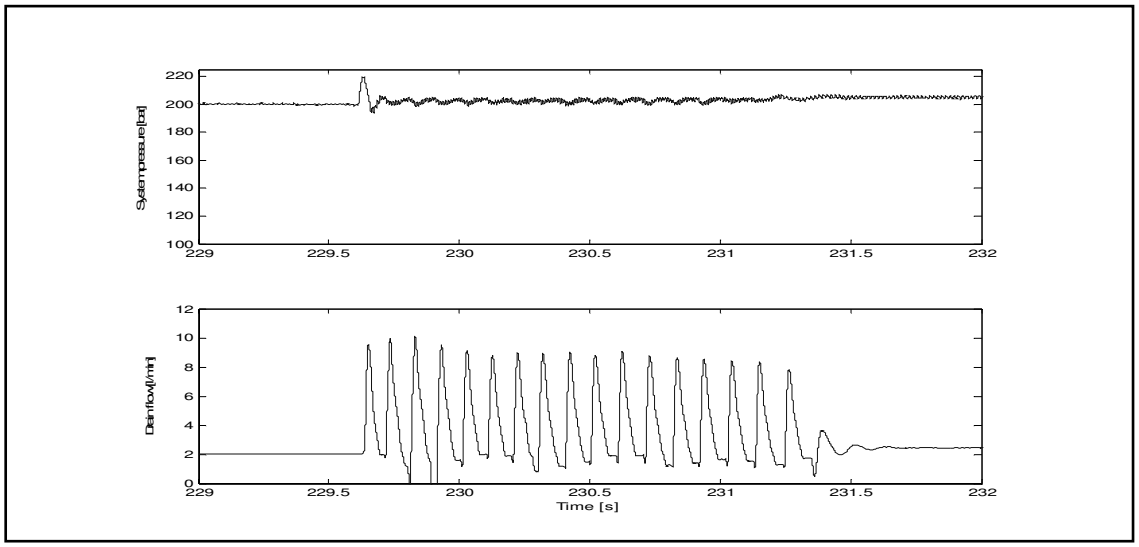

Figure 13. System pressure and drain flow in a fast flow change 170 – 70 l/min

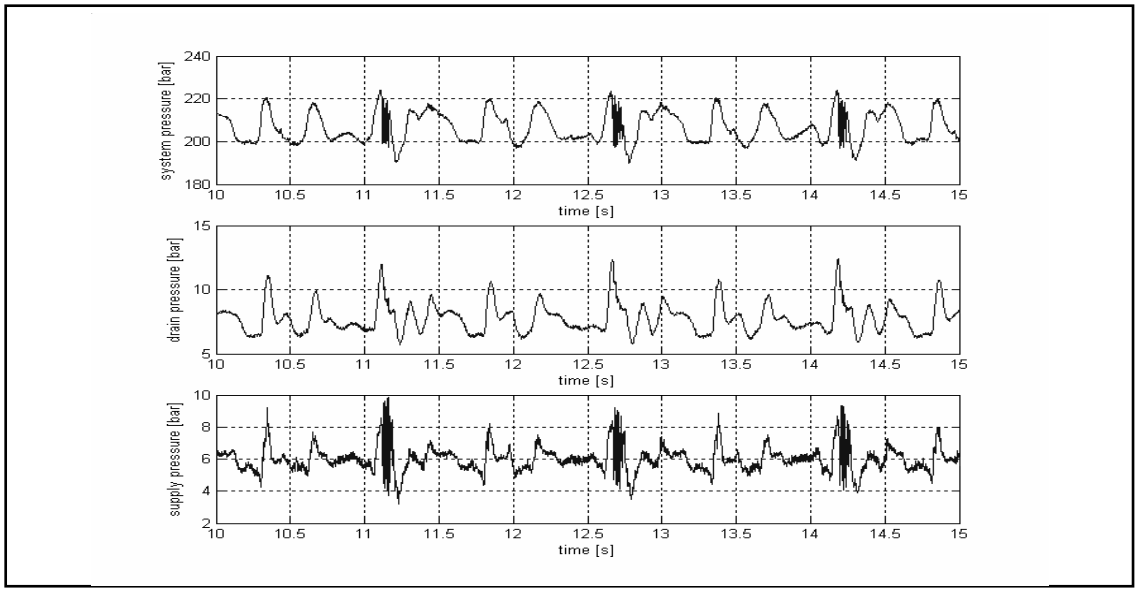

Figure 14. System, drain line and supply pressure during erratic flight surface actuations

8 CONCLUSIONS

The research method used was found to be a success. Combining simulation and testing provided possibility to pinpoint what should be tested and how it should be done. Even though generating simulation models of high detail level is even with efficient tools a cumbersome task it is the only way to find interconnection between system level phenomena found in the aircraft to component detail level phenomena actually causing problems. It is obvious that simulations can not give exact answers, as described in previous chapters, but the whole process is merely for finding reasons for certain behavior or certain problems in a complex system.

Detailed simulation models once generated also provide help in solving future problems. Also if a reason for system or component modification is found, simulation models can be used in modification design. This however requires further verification and validation of models.

During long life span of a fighter aircraft general technical development can open numerous possibilities to improve small details within the system and its components. Also development can make it possible to study and understand behavior of the system in depth not possible the days it was designed. To utilize these possibilities, to improve aircraft's reliability and to reduce its maintenance costs there must be tools and methods for doing it. It is obvious that aircraft manufacturers have these capabilities, but their resources might be limited and tied to commercial interests which small user specific problems might not fulfill. How ever from the end-user point of view sometimes even a very small improvement can be crucial in improving overall quality. Systematically developed model library containing detailed analytical models of aircrafts components used in combination with experimental test methods can be used as a tool for both finding components and system parts needing modifications and it also offers basis for actual modification design and tool for modification testing.

9 REFERENCES

[1] Edge K.A., Darling J., The Pumping Dynamics of Swashplate Piston Pumps, Journal of Dynamic Systems Measurement and Control, ASME Vol 111, 1989

[2] Manring N.D. Modeling and Designing a Variable Displacement Open Loop Pump, Journal of Dynamic Systems Measurement and Control, ASME Vol 118, 1996

[3] Schönau G.J., Burton R.T., Kavanaugh G.P., Dynamic Analysis of Variable Displacement Pump, Journal of Dynamic Systems Measurement and Control, ASME Vol 112, 1990

[4] Ivantysyn J., Ivantysynova M., Hydrostatische Pumpen und Motoren : Konstruktion und Berechnung, Vogel, Wu̇rzburg, 1993

[5] Manring N.D., Zhilin D., The Impact of Using a Secondary Swashplate Angle within an Axial Piston Pump, Journal of Dynamic Systems Measurement and Control, ASME Vol 126, 2004

[6] Mare J.C., Simplified Model of Pressure Regulated Variable Displacement Pumps for the Sizing of Complex Hydraulic Systems, http://fluid.power.net

[7] AMESim Hydraulic Component Design Library, User manual and online documentation, 2005

Advanced Sealing Solutions for modern Commercial Aircraft Hydraulic Systems

Courtesy G Krebs

Torben Andersen
Global Director, Aerospace Segment
Trelleborg Sealing Solutions
TSS Helsingør
Fabriksvej 17
3000 Helsingør
Denmark
Phone +4549270209
E-mail: torben.andersen@trelleborg.com

ABSTRACT

This paper describes the evolution of hydraulic flight control systems for military and civil aircraft as well as the influence of this development on the sealing systems applied in the hydraulic actuators. Introduction of Fly-By-Wire, and unstable aircraft designs, controlled via a flight computer, has increased the stroke frequency, while the demands for long maintenance free service life of new aircraft has increased the expected service life of the sealing system. The corresponding evolution in the sealing systems for military and civil aircraft is discussed.

KEYWORDS: Seals, Turcon® Plus Seal®, Turcon® Double Delta®, Turcon® Hatseal®, Turcon® Variseal ®, Turcon® VL seal, Sealing system, Sealing solutions, Trelleborg, Busak+Shamban, Dowty, Impervia, EHB, EBHA, FBW.

1 Trelleborg Sealing Solutions, Company presentation

1.1 Trelleborg Sealing Solutions,

or for short TSS, is a division of the Swedish company Trelleborg. Trelleborg has more than 100 years of experience in elastomers and Trelleborgs products seals, dampens and protect people and machinery all over the world. TSS develops, designs, produce and market sealing systems for all industries. With a rich aerospace heritage, from well known companies like Dowty Seals, Impervia and W S Shamban, we are market leading in seals for hydraulic actuation systems.

2 Historical overview & Specifics of Aircraft Hydraulics

2.1 Seal grooves

The seal groves we are using today, on 90% or more of all western aircraft dates back to the standards developed for the American aerospace industry during the Second World War. Production of military aircraft in the US was relatively low before the war, but when the war started the US industry swiftly changed to mass production of arms, including aircraft for the war effort of the US and its allies. To encourage the use of common design standards, and to reduce the number of spare parts, a number of standards were issued for seal grooves, hydraulic fluids, materials and many other things. These standards or derivatives of them still guides the aerospace industry today

2.2 Mil F 5514 G

The Mil-F-5514-G is the most important document for the design of the seal grooves for aircraft hydraulics. It is inch based and advises on seal sizes for static and dynamic use as well as hardware tolerances and geometry. Successive versions of this standard have been widely used in the Western aerospace industry since the war. Only recently has it been replaced by AS4716, which is a similar document, but now controlled by the SAE.

2.3 Temperatures

The standard temperature requirement is –54 to +135 deg Celsius, and the components of the sealing system have to operate reliably within this temperature range.

2.4 Aircraft fluids

The fluids used in aircraft hydraulics have low density; wide temperature range and generally two fluids types are in use:

2.4.1 Mineral oil

“Red Oil”, originally based on mineral oil, now often a synthetic version of the same. This is widely used on military aircraft and in landing gears. For these oils we typically use Nitrile O-rings according to Mil-P-25732 or Mil-P-83461

2.4.2 Phosphate Ester fluids

Phosphate Ester fluids are known under a number of trade names like Skydrol originally developed by Monsanto (now supplied by Solutia) and Hyjet that is a similar fluid developed by Exxon. These fluids were originally developed to be fire resistant, to

minimize the risk of fire due to leaks from the hydraulic system. The fluids are widely used on civil aircraft and on some naval aircraft too. For these fluids we typically use Ethylene Propylene O-rings according to NAS 1613.

2.4.3 Hardware surfaces

Rods with hard chrome coating has long been the established solution for hydraulic rams, but due to environmental concerns and in search for extended lifetime of the rods, Ceramic coatings have been widely tested. The A340 and the A380 use ceramic (HVOF) coated rods in several actuators with very good results. It would be too time consuming to enter into a discussion about rod surface finishes here, but generally it can be said about ceramic coatings that the finer the surface finish the better. A standard Ra measurement is not enough to determine if the surface is suitable, and care should be taken that the bearing ratio is high.

3 Trends, military aircraft

Although the title of this presentation refers to civil aircraft, we have to look at the developments in the hydraulic systems for military aircraft to understand the evolution of the systems.

3.1 FBW in military aircraft

Fly-By-Wire, or FBW was originally developed for use in missiles and military fighter aircraft. FBW means that the mechanical links or wires used earlier is replaced by electric wiring. It brings a number of advantages, some of which I will describe in more detail in the following. For obvious reasons it makes sense to control a missile remotely by electric signals and the first FBW systems were used on anti-aircraft missiles in the 1950s. However, as jetfighters replaced piston engine driven aircraft, it became clear that man, the pilot, could not fly these aircraft to their full potential unassisted. Alone the forces resulting from the high speeds and the short reaction times required, made the task impossible for the pilot. Some of the most important advantages of using FBW are:

- Increased aircraft agility and faster reaction times
- Easier installation and maintenance due to the reduction of the number of mechanical parts
- Freedom of design and increased damage resistance as wiring can be routed almost anywhere in the airframe and easily separated
- Weight reduction
- Force and control laws are not directly dependent of pilot input
- No “slack” in the system as in a mechanical system
- Increased service life through simpler systems
- Possibility of including aerodynamic protection against excessive angle of attack or acceleration in the laws of the flight control system

Apart from these almost trivial advantages, FBW opens up completely new possibilities for aircraft design: Where older aircraft had to be designed with a high degree of static stability to reduce the workload on the pilot, FBW allows the design of aircraft with reduced stability leading to increased maneuverability, a highly desirable feature of a combat aircraft. In very simple terms, the on-board computers and the FBW actuators fly the aircraft in a straight line or preprogrammed from A to B, and the pilot only controls deviations from this artificially stable situation. By controlling the laws of the

control system it is possible to limit the influence of the pilots input, so he cannot accidentally fly the aircraft outside safe limits. The reduced workload also means that the pilot can concentrate the military aspects of his job.
While FBW has many good characteristics in general, it has been a big challenge to the sealing industry, as the stroke frequency and total length of travel of the pistons and rods in the flight control cylinders have increased tremendously going from a manually controlled system on a stable aircraft to a computer controlled system on an unstable aircraft.

3.2 Service life increase

At the same time the demands for mission readiness and efficiency, means that the an actuator is expected to work for many more flight hours than before, the following example shows this development.

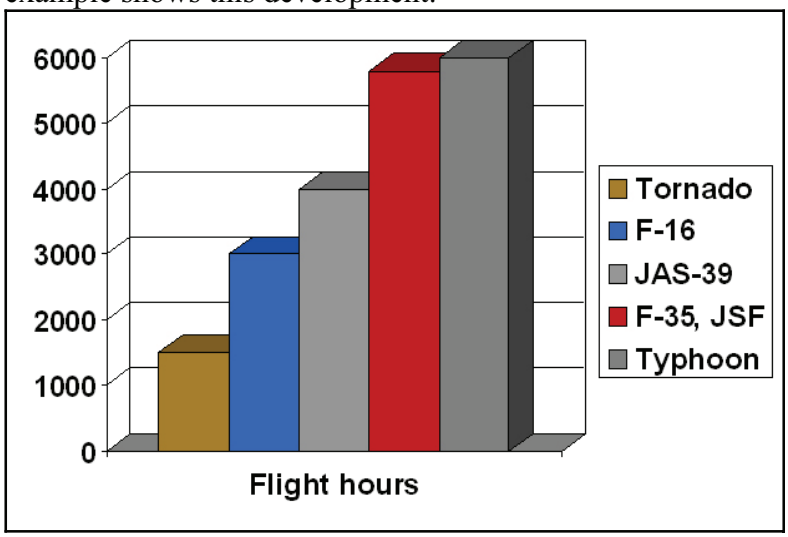

Fig.1 Actuator, expected flight hours

3.3 Pressure increases

In order to handle the larger loads experienced at high speeds and at the same time reduce system weight, the operating pressure of the hydraulic systems have increased radically.
Previous generation aircraft with 21 MPa systems: Hawk, Tornado, F-15, F-16,
In production aircraft with 28 MPa systems: Typhoon (EFA), JSF F35
In production aircraft with 5000psi system: V-22 Osprey
Aircraft with variable pressure system, 21/35MPa: F-18 E/F

Pressures up to 55Mpa were tested, but found to be impractical, so at the moment 35Mpa seems to be the accepted limit. Still, this puts very high demands on the sealing system, when the increase in movement speed and frequency is also considered.

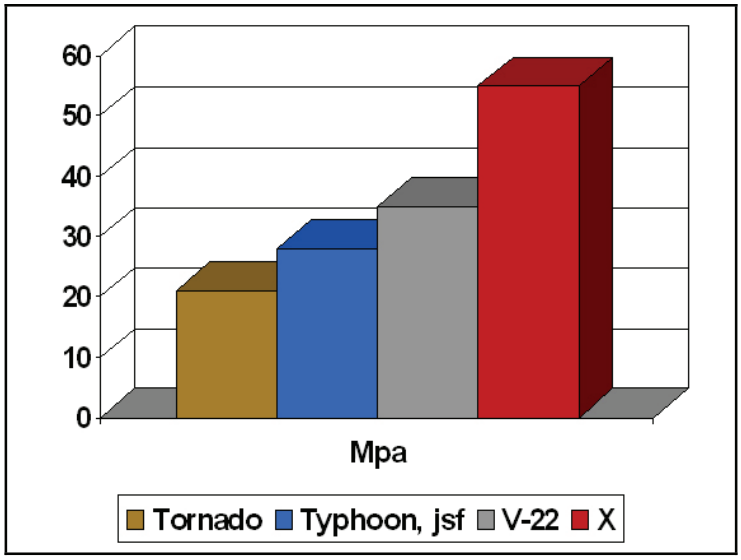

Fig.2 Hydraulic system pressure, military aircraft

4 Trends Civil aircraft

Technologies from the military industry often migrate into civil use and in this case the FBW technology triggered a revolution in aircraft hydraulic systems, as we shall see in the following.

First of all, another technology coming from military use, composites, made it possible to extend aircraft service lives considerably.

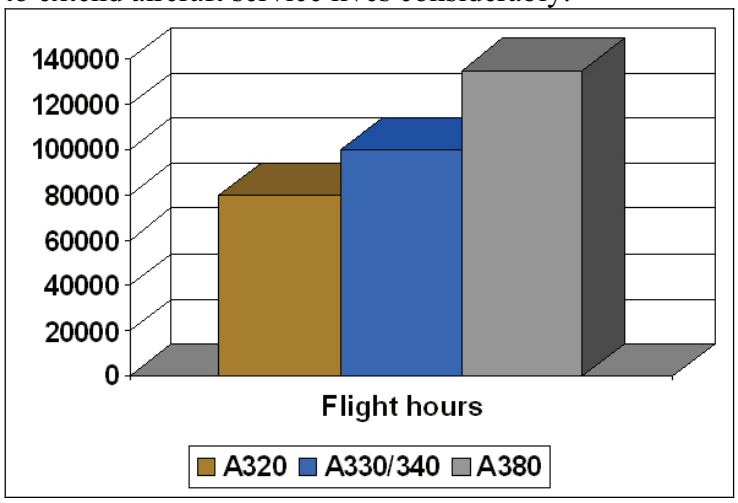

Fig.3 Expected airframe flight hours

This, and the general request for more reliable systems with less down time, has resulted in a drastic demand for increased service life of the hydraulic actuators.

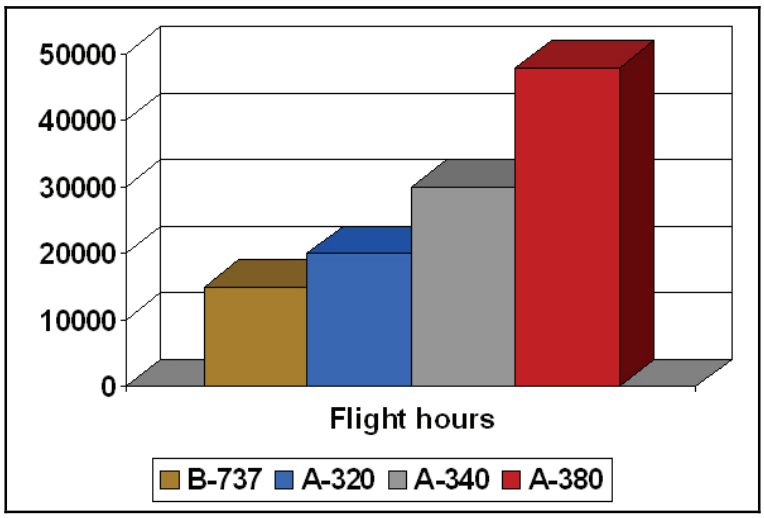

Fig.4 Expected service life of actuators

Please note that 48.000 hours equals 5.5 years of continuous work!

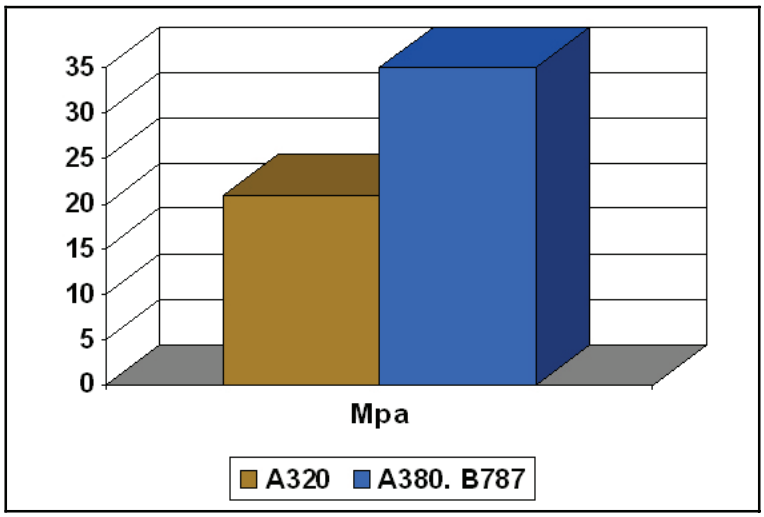

Fig.5 Hydraulic system pressure, civil aircraft.

Aircraft with 21Mpa hydraulic system: MD-80, B-737, A320, A340, and A350
Aircraft in production with 35Mpa system: A380
Future projects with 35MPa: B787

4.1 FBW in civil aircraft

The A320 was the first civil aircraft with full FBW flight control system and many of the advantages experienced in the military aircraft also are interesting for civil aircraft. However, due to the high frequency of movements it results in higher temperatures around the seals, and less cooling of the fluid due to the reduced circulation.
While the actuators have been thoroughly tested and fully qualified both at minus 54 deg C and in hot weather campaigns, these changes made the task of the sealing systems much more difficult.

4.2 EHAs and EBHAs

Traditional hydraulic servo-actuators have been replaced by de-centralised complete individual units called Electro Hydrostatic Actuators (EHAs) that contains all the components of a traditional hydraulic system: Reservoir, motor, pump, accumulator and manifold, thus eliminating the need for these components centrally and eliminating hydraulic lines all over the aircraft.

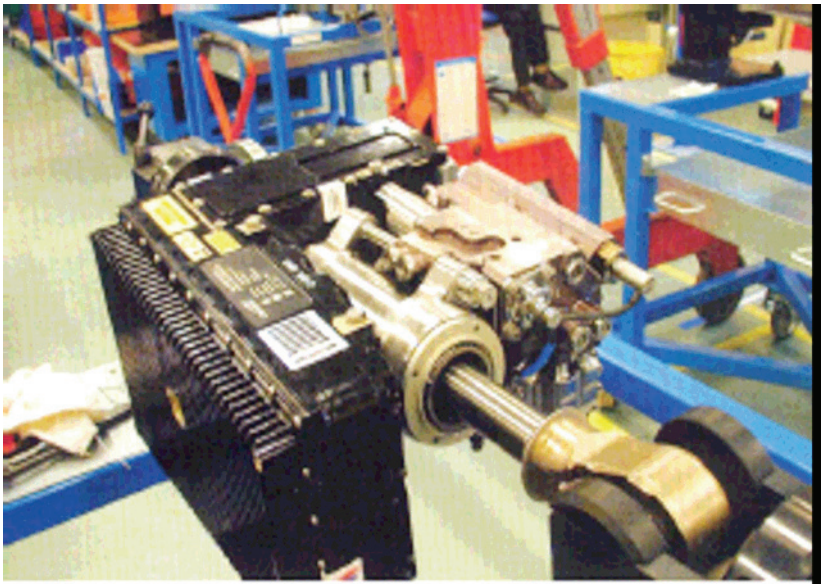

Fig.6 A380 EHA

Advantages of EHAs:

- Line removable units (no system bleeding)
- Weight reduction
- Energy output suited to need = energy saving
- Re-configurable
- More redundancy due to dissimilar systems
- Reduced risk if aircraft is damaged

4.3 Traditional hydraulic system

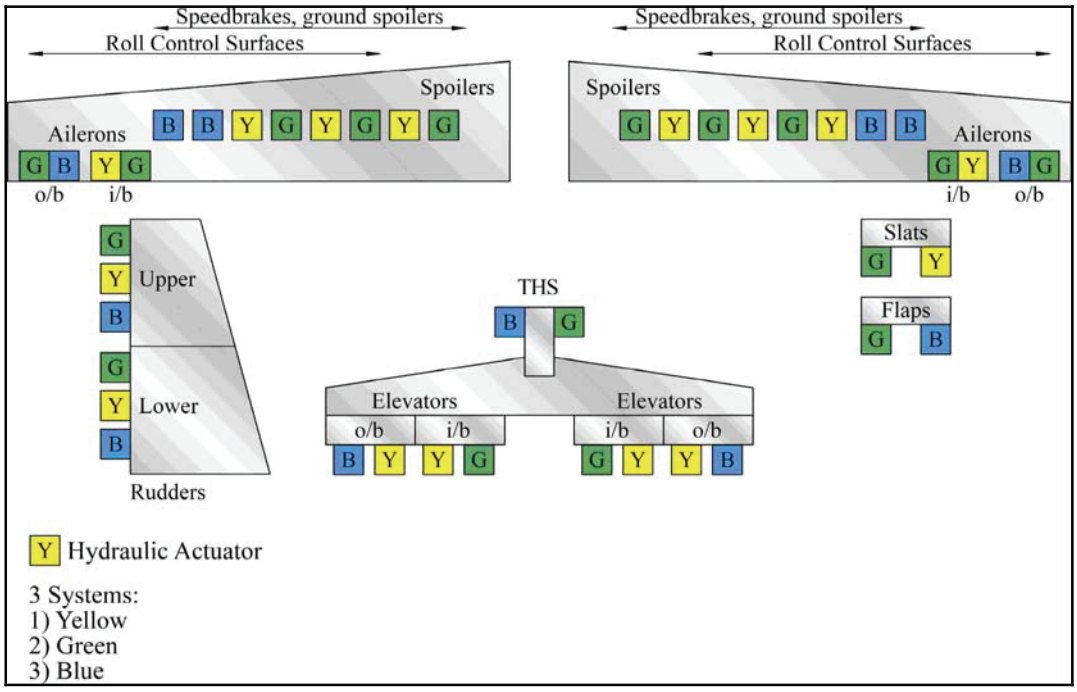

Fig.7 Traditional hydraulic system with 3 separate circuits

For safety reasons most larger aircraft have three separate hydraulic systems. Two of them operate the control surfaces under normal conditions and the third system can be used in emergency. While this has proved it worth many times over the years there are some drawbacks:

- The hydraulic lines for the three systems should normally be separated in the airframe to avoid accidental damage to more than one system at the time. However this can be difficult to obtain in real life when practical concerns come into play.
- Because the three systems largely consist of the same components, it is possible that a systematic mistake is repeated during the build or maintenance of the aircraft, despite training, manuals and routines to avoid it. This can cause all three systems to fail in the same way.

4.4 The A380 hydraulic system [1]

I assume that all here in the audience are familiar with the composition of a normal hydraulic system; with central generation of oil at high pressure, which is distributed out to hydraulic actuators through pipes. An electrically operated servo valve then controls the movement of the actuator.
However Airbus have taken a radical step away from this, by introducing the EHAs on the A380. Here the power is generated at the point where it is needed, by a motor driving a pump directly at the actuator. This eliminates hydraulic lines, as both signal and power now comes to the actuator in the form of electricity.
Another new component is the EBHA, which is a hybrid between the hydraulic actuator and the EHA. The EBHA works as a hydraulic ram under normal working condition. But it can be electrically driven in case of an emergency (provided that the oil is isolated in the EBHA).

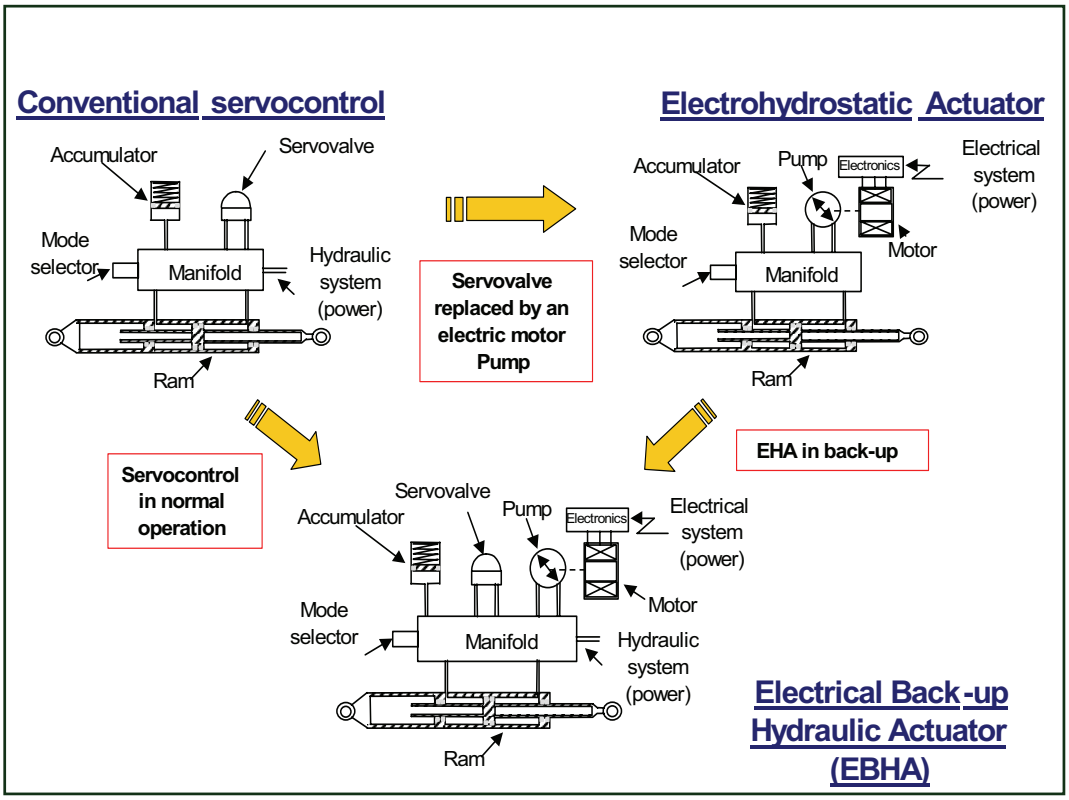

Fig.8 Overview of Servo control types and EHA and EBHA principles

Utilizing the new technology Airbus has replaced the usual 3 hydraulic systems by 2 hydraulic systems (green & yellow) and 2 electrical systems (red). This replaces one set of hydraulics with a weight saving of around one ton. It directly increases the redundancy from 3 to 4 times, by adding a system.

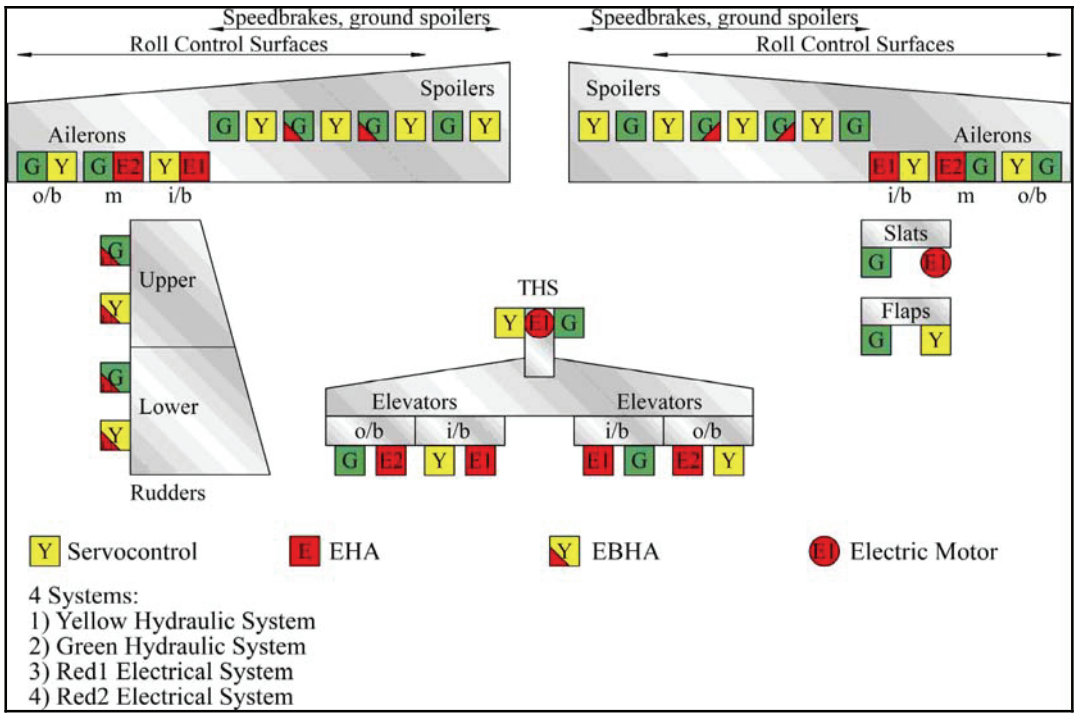

Fig.9 A380 hydraulic system with 4 circuits

In addition to this there is the increased inherent safety coming from the use of dissimilar systems; a maintenance malpractice could affect the two hydraulic systems, but that would still leave two electric systems intact. As proof of the concept, the A380 has been flown, using only the two electric systems with the hydraulic systems switched off. The pilot reported a similar feel of the aircraft as with all systems operative.

5 Trends sealing systems for Military aircraft PFC

In the following we will look at the sealing systems used in several generations of aircraft. The main focus is on the rod sealing systems, as this is the most demanding task, any leakage here will immediately show up on the hangar floor. Piston seals typically have oil on both sides and a certain leakage is allowed or even encouraged as this contributes to long seal life.

The F16 was the first FBW aircraft to go into production. It was designed as an unstable aircraft to allow the extreme agility of a first class supersonic air-superiority fighter. A necessary consequence was that the flight of the aircraft had to be controlled at all times by a computerized flight control system.
For the sealing system this means that instead of occasional corrections to the flight path coming from the pilots input, there now is a stream of constant minute correction from a digital system, increasing the number of movements by several orders of magnitude.

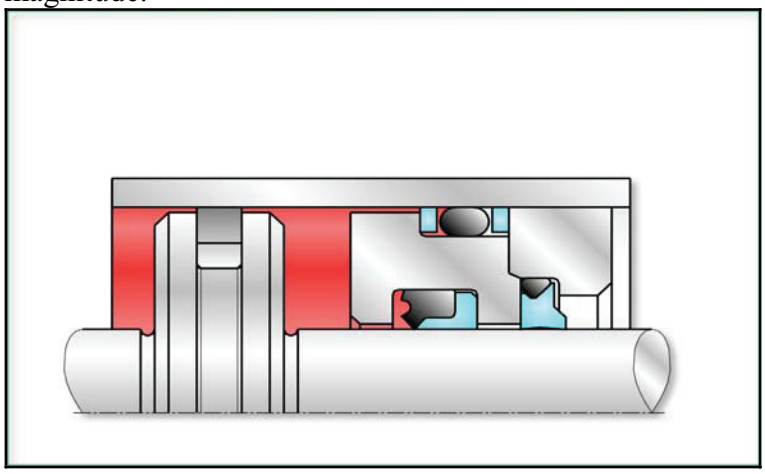

Fig.10 F16 PFC sealing system

Working Conditions:
Control system: Full FBW, no mechanical back up
Requirement: 1.500 Flight hours
Pressure: 21MPa
Fluid: Red Oil, MIL-H-5606 or MIL-H-83282
Temp. : -54°C to +135°C (static down to -60°C)
Rod sealing system: Single combined elastomer contact/slipper seal (Turcon® Hatseal®).
Surface: Hard Chrome

The JAS 39 is also fully FBW, but the with the specification calling for 4000 flight hours a tandem sealing system is needed.

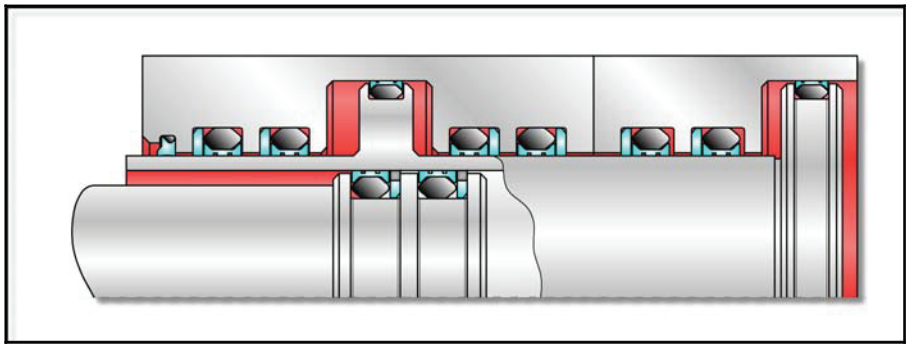

Fig.11 JAS 39 Gripen PFC sealing system

Working Conditions:
Control system: Full FBW, no mechanical back up
Requirement: 4.000 Flight hours
Pressure: 28MPa
Fluid: Red Oil, MIL-H-5606 or MIL-H-83282
Temp. : -54°C to +135°C (static down to -60°C)
Rod sealing system: Dual unvented slipperseals (Turcon® Plus Seal®)
Surface: Hard Chrome

A similar system was first employed on the Typhoon, but inter-stage pressure build up between the seals lead to the development of a venting primary seal.

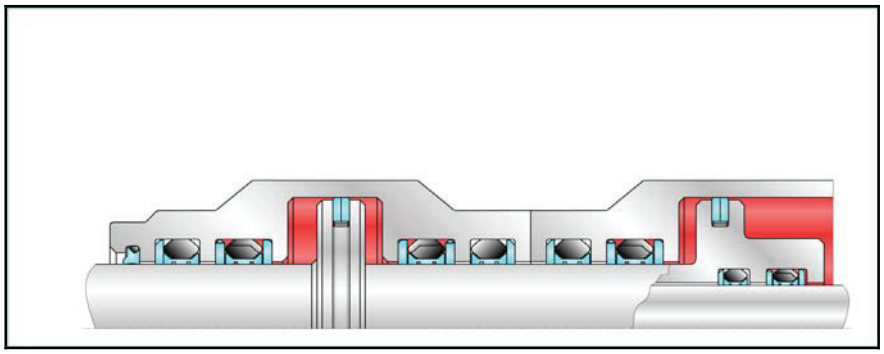

Fig.12 EFA Typhoon PCF sealing system

Working Conditions:
Control system: Full FBW, Out/Inboard Flaperon, no mechanical back up
Requirement: 6.000 Flight hours
Pressure: 28MPa
Fluid: Red Oil, MIL-H-5606 or MIL-H-83282
Temp. : -54°C to +135°C (static down to -60°C)
Rod sealing system: Dual slipperseals with pressure relieving primary seal (Turcon® Plus Seal®)
Surface: Hard Chrome

6 Trends in sealing systems for civil aircraft PFC

While introduced for different reasons, the FBW system has also changed the sealing systems employed in civil aircraft. In earlier aircraft single or vented dual seals were used, as it was necessary to keep seal friction low in systems with manual reverse. This was dropped in favor of a full FBW actuation system in the A320 and consequently a dual un-vented sealing system is used in the PFC rod sealing system.

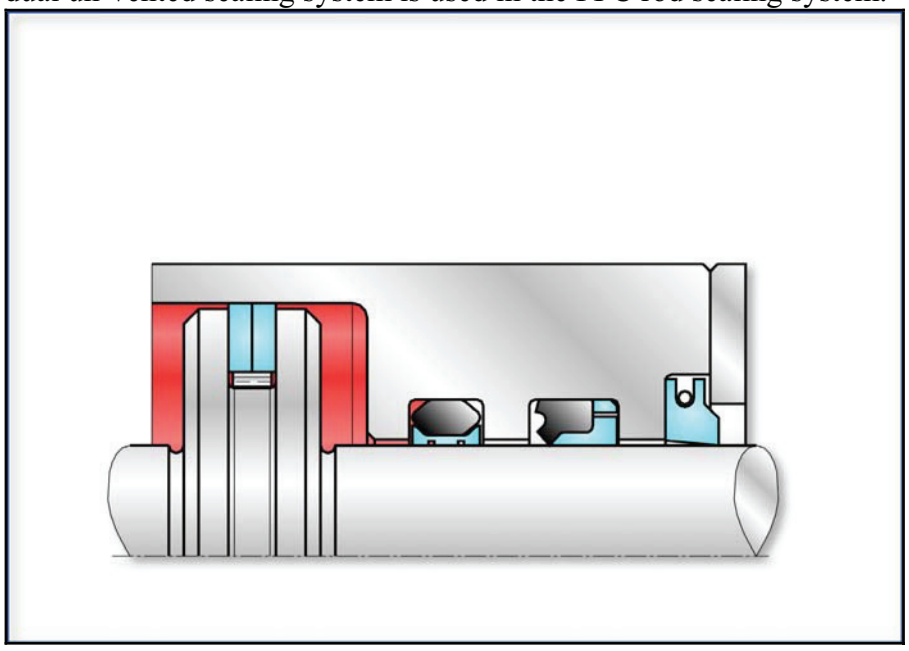

Fig.13 Airbus A320 PFC

Working Conditions:
Control system: Full FBW, no mechanical back up
Requirement: 20.000 Flight hours
Pressure: 21MPa
Fluid: Phosphate ester
Temp. : -54°C to +135°C (static down to -60°C)
Rod sealing system: Primary seal: Slipper seal (Turcon® Plus Seal®), Secondary seal: Combined elastomer contact/slipper seal (Turcon® Hatseal®).
Surface: Hard Chrome

Large diameter cylinders and weight reduction efforts means that some “ballooning” is experienced as the cylinders breathe during operation. Special back-up rings have been introduced to protect the seal against extrusion in this situation as on the A340.

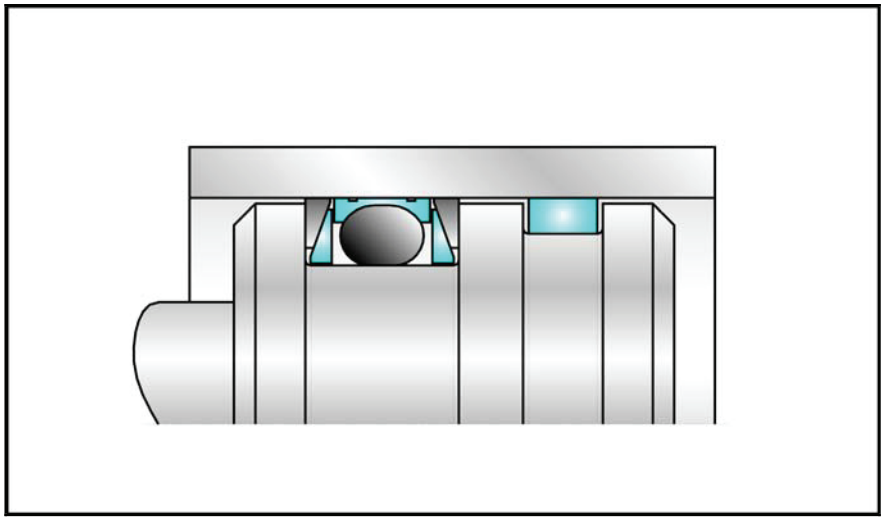

Fig.14 Airbus A340 PFC Piston sealing system

Working Conditions:
Control system: Full FBW, no mechanical back up
Requirement: 30.000 Flight hours
Pressure: 21MPa
Fluid: Phosphate ester
Temp. : -54°C to +135°C (static down to -60°C)
Piston sealing system: Single slipper seal with staged back-up rings to allow high clearance (Turcon® Double Delta®)
Surface: Steel 15-5PH, hardened

Another new development on the A340 PFC was the introduction of seals with back-pumping effect, eliminating leakage and pressure build up between the seals.

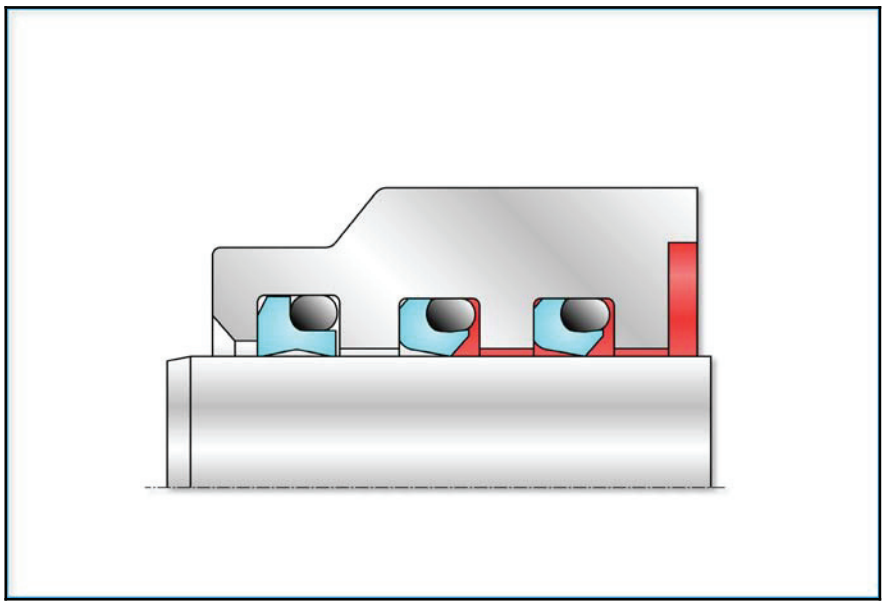

Fig.15 Airbus A340 PFC, rod-sealing system

Working Conditions:
Control system: Full FBW, no mechanical back up

Requirement: 30.000 Flight hours
Pressure: 21MPa
Fluid: Phosphate ester
Temp. : -54°C to +135°C (static down to -60°C)
Rod sealing system: Tandem slipper seal, with back pumping effect (Turcon® VL seal)
Surface: HVOF (Ceramic coated steel rods)

The A380 PFC sealing system is similar to that of the A340, but the rod seals have back-up rings for additional extrusion protection, in order to achieve the long lifetime.

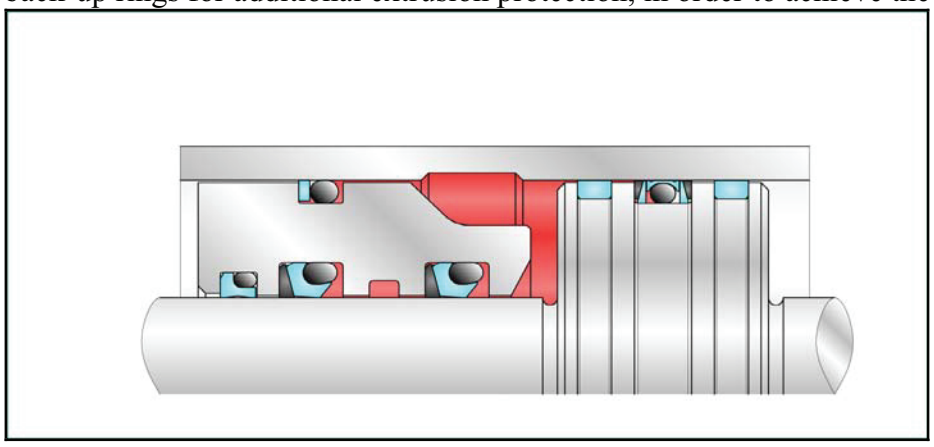

Fig.16 Airbus A380 PFC, Sealing system reinforced with BURs

Working Conditions:
Control system: Full FBW, no mechanical back up
Requirement: 48.000 Flight hours (Current status approx. 25.000 hours completed)
Pressure: 21MPa
Fluid: Phosphate ester
Temp. : -54°C to +135°C (static down to -60°C)
Rod sealing system: Tandem slipper seal with back pumping effect and back-up rings in high modulus plastic (Turcon® VL seal). Piston sealing system as A340 (Turcon® Double Delta®).
Surface: Ceramic (HVOF) coated steel rods and cylinders of steel 15-5PH, hardened

7 Future trends?

While the pressure in the hydraulics systems have been increasing over the last decades, it seems that mid sized aircraft will continue to use 21Mpa systems for a foreseeable future, as the weight reduction from higher pressure systems is limited for smaller aircraft. Other factors like service life of pumps and valves also play a role.
Perhaps a more interesting discussion topic is, if there will be hydraulics on future aircraft at all? Advances in electronics and electric power generation means that for some applications electric actuators have become attractive replacements of hydraulic components, especially on smaller aircraft and UAVs where the forces on the control surfaces are small. However for larger aircraft, all types currently in design, still have hydraulic actuation as their main system, so hydraulics is likely to remain with us for a foreseeable future.

Sealing technology is likely to continue to develop with the demands from the aerospace industry. A number of the new projects are testing spring-energized seals, at

least as a part of the sealing system. In some respects the spring-energized seals are superior to slipper seals and elastomer contact seals, as they are insensitive to fluid types and temperature variations. However installation can be tricky, especially at smaller sizes and the demands to the hardware surfaces are higher. Perhaps more important is that the failure mode is typically a sudden large leakage instead of a slower weepage that can be detected in time and reacted upon. So it is likely that if spring energized seals are applied, they will be part of a hybrid sealing system, again using dissimilar concepts to obtain the highest possible safety.

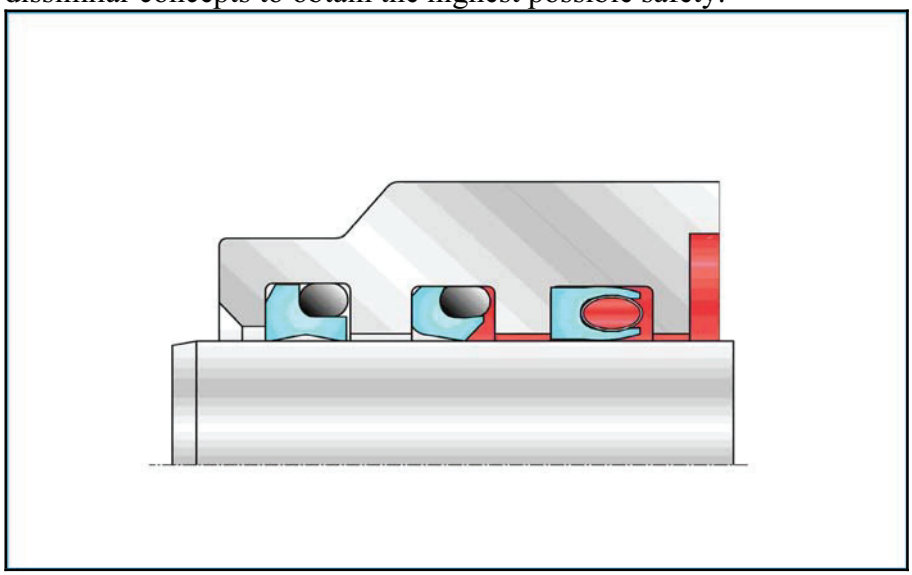

Fig. 17 Hybrid sealing system with spring energized seal and slipper seal, (Turcon® VL seal and Turcon® Variseal ®).

8 Conclusion

Going from simple hydraulic systems to Fly-By-Wire increased the demands on the sealing systems dramatically. In addition to this, the long lifetime expected of the hydraulic components in modern aircraft, further increased the demands. As a result we have seen the seal change from something that was changed regularly, when a leak was discovered, to complex sealing systems, that are an integral part of FBW or EHA units, expected to sit on the aircraft for many years without the need for service. This development means that while the initial value of the installed sealing system has increased, the need for spare parts and service hours has decreased, reducing the total cost for the operators.

9 References

[1] The A380 PFC actuation system, Dominique Van Den Bossche, Airbus

Flow Controlled Variable Displacement Hydraulic Motors for Highly Efficient Aircraft Actuation Systems

Giovanni Jacazio
Politecnico di Torino
Department of Mechanics
Corso Duca degli Abruzzi 24
10129 Torino - Italy
Phone +39 0110906940, Fax +39 0110906999
E-mail: giovanni.jacazio@polito.it

ABSTRACT

This paper first presents a brief outline of the general characteristics of hydraulic actuation systems based on variable displacement hydraulic motors (VDHMs), then it describes the architecture of an innovative solution proposed for the actuation of the cargo door of an aircraft for which a control technique was developed to further exploit the advantages of such hydraulic motors. The merits of this solution are outlined and a comparison is made with the performance of a conventional system using fixed displacement hydraulic motors.

KEYWORDS: Hydraulic motors, actuation systems, system control, energy saving

1 INTRODUCTION

Variable displacement hydraulic motors (VDHMs) can be effectively used in several aircraft hydraulic actuation systems to reduce the flow and energy requirements. Possible applications are: secondary flight control systems, trimmable horizontal stabilizers, cargo doors, engine nozzle control systems. Although they require a more complex control, actuation systems based on these hydraulic motors provide overall benefits to the entire hydraulic aircraft system when a large actuation power is required, and for this reason they were recently used in the secondary flight control system of a large commercial aircraft.

This paper presents the results of a study performed in view of a possible application of VDHMs to the actuation system of a cargo door of an aircraft for which an innovative

control technique was developed to further exploit the advantages of such hydraulic motors.

By fusing all information available from the sensors normally present in a VDHM based hydraulic actuation system it is possible to appropriately control the flow in order to actually build a constant power system. Such system uses at the best the available hydraulic power, thereby reducing the flow requirements with benefits on the size and weight of the hydraulic system components. An additional advantage provided by this solution is the possibility for the actuation system to provide large forces when necessary, such as the case of operation at extremely low temperatures, without the burden of large flow consumption under normal operating conditions, as it would be the case of a conventional solution.

2 THE VARIABLE DISPLACEMENT HYDRAULIC MOTOR

2.1 The Hydraulic Motor Configuration

The variable displacement hydraulic motor considered for aerospace applications is an inline, piston type, hydraulic motor, schematically shown in figure 1. The VDHM consists primarily of a rotating cylinder block containing pistons that can slide in parallel chambers ending as ports in the cylinder block face. Each piston terminates with a shoe assembly running on a shoe bearing plate installed in the recess of a yoke (also known as wobbler). The yoke is held by bearings allowing it to swivel about an axis perpendicular to the motor drive shaft. By changing the angular position of the yoke, the stroke of the pistons within the cylinder block is changed and thus the volume of fluid transferred from the high pressure port to the low pressure port at each motor revolution. The variation of the angular position of the yoke therefore determines a variation of the theoretical ratio between flow rate and speed, which is known as the motor displacement. A wafer plate with appropriately machined slots provides the appropriate connections between the cylinders and the inlet and the outlet ports.

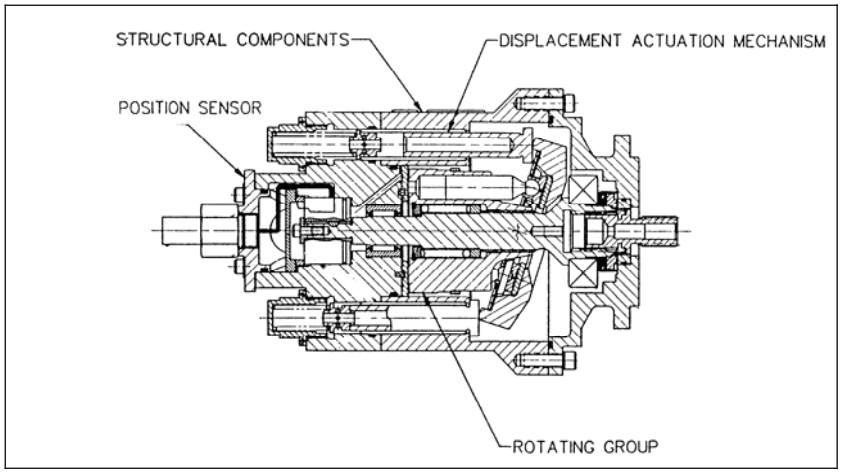

Figure 1: Schematic of a variable displacement hydraulic motor

The position of the yoke, and thus the motor displacement, depends on the balance between the spring force and the pressure force developed by the actuating piston. The spring force acts in the direction of moving the yoke to the maximum angle, whilst the actuator pressure force acts in the opposite direction. Therefore, if the actuating piston is subjected to the minimum system pressure (the return pressure of the hydraulic system), the yoke is at the maximum angle, which is the condition of maximum torque provided by the motor. As the pressure on the actuating piston is increased, the balance between the spring and the actuating piston force is obtained at lower yoke angles, with a corresponding lower displacement of the hydraulic motor, and thus the motor produces lower torque.
In some applications the yoke swiveling can be obtained only from zero to a maximum angle, thus the hydraulic motor can develop a variable torque, but always in the same direction. In other hydraulic motors the yoke can swivel from a maximum negative to a maximum positive angle about the neutral position and they can thus produce a variable torque in both directions of rotation. These variable displacement hydraulic motors are generally referred to as *overcenter motors*.

2.2 Motor Characteristics

The hydraulic motor is a volumetric machine that develops a torque, which in an ideal case is proportional to the applied pressure differential and to the motor displacement. Because of the power losses due to the pressure drops in the internal passageways and to the viscous and Coulomb frictional losses of the sliding parts the actual torque developed by the hydraulic motor can be written as:

$$T = \frac{(p_s - p_r)\Delta}{2\pi} - k_m \frac{(p_s + p_r)}{2} - k_\omega \omega^\alpha - T_0 \qquad (1)$$

In the above relationship T is the motor torque, p_s and p_r are the motor inlet and outlet pressures, Δ is the motor displacement. The second term $k_m(p_s+p_r)/2$ takes into account the frictional losses proportional to the average motor pressure; the frictional loss coefficient k_m decreases from a maximum value at zero speed (static friction condition) to a lower value when the motor picks up speed. The third term $k_\omega\omega^\alpha$ takes into account the losses due to viscous friction and the internal pressure losses, which are a function of the flow rate and thus of the speed; the exponent α of the angular speed ω actually depends on the motor operating conditions, but it was found in our analysis of several hydraulic motors to be generally close to 1.7. The last term T_0 is a mechanical loss due to the frictional effects that are independent of pressure and speed; it actually is the hand torque that one has to provide to the motor shaft to cause a slow rotation of an unpressurized motor.
The above equation (1) can be rewritten as:

$$T = \eta_m \frac{(p_s - p_r)\Delta}{2\pi} \qquad (2)$$

where η_m is the mechanical efficiency of the motor, that of course is a function of the terms making up the right-hand side of equation (1).

The hydraulic motor speed ω is approximately proportional to the flow rate Q. When the internal leakage of the hydraulic motor is considered the flow rate Q entering the hydraulic motor can be written as:

$$Q = \frac{\Delta\omega}{2\pi} + k_L \left(p_s - p_r\right)^{\beta 1} + k_F \left(\frac{p_s + p_r}{2}\right)^{\beta 2} \qquad (3)$$

In this equation the term $k_L(p_s-p_r)^{\beta 1}$ corresponds to the cross-port internal leakage of the hydraulic motor, while the last term $k_F[(p_s+p_r)/2]^{\beta 2}$ corresponds to the internal leakage towards the motor drain. As for the torque, it is useful to introduce a volumetric efficiency η_v and rewrite equation (3) as:

$$Q = \eta_v \frac{\Delta\omega}{2\pi} \qquad (4)$$

When equations (2) and (4) are considered simultaneously, it becomes evident that a reduction of the motor displacement Δ leads to a reduction of both the torque developed by the motor and of the flow rate used by the motor at a given angular speed. Therefore, a control system based on the control of the hydraulic motor displacement provides an efficient way of controlling the mechanical power generated by the hydraulic motor, since the hydraulic flow required by the motor decreases about proportionally with the reduction of the mechanical power requirement at the motor shaft.

2.3 Past Work on Variable Displacement Hydraulic Motors

Variable displacement hydraulic motors have been used for years in the hydrostatic transmissions both for industrial and aerospace applications with the purpose of controlling the angular speed of a mechanical component. One typical aerospace application area of VDHMs has been that of the constant speed drives, where the continuous modulation of the motor yoke is used to maintain a constant speed independent of the load variations. On the other hand, almost very few applications exist for VDHMs in position control servoloops, where the motor displacement has to be modulated to eventually control the position of a mechanical actuator.

The first work on variable displacement hydraulic motors for position servoloops was performed by Abex at the end of the 70's (references [1] and [2]), which also manufactured an overcenter motor for the DIVADS gun turret drive. The DIVADS program however was stopped and that system never went into production. That gun turret drive had a large inertia and a low friction load, thus a large torque was required to accelerate the gun turret, but only a small torque was necessary during the remainder of the actuation, which made a VDHM the optimum solution to minimize the flow consumption.
In the following years Microtecnica, Liebherr and Sundstrand developed technological demonstrators of position servoloops using VDHMs. Although the results of the tests were encouraging, no actual application followed up. At the beginning of the 90's Sundstrand developed a VDHM based system to actuate the leading edge surfaces of

the YF23 fighter aircraft. The system was based on a single hydraulic motor. The system actually operated in the two demonstrator aircraft that were built, but never went into production since the YF23 lost to the F22 the US air force competition for a new fighter aircraft. Some of the work performed on these demonstrators is available in the literature (reference [5]). Meanwhile, studies on microprocessor-based controls of VDHMs were performed by Vickers (references [4] and [6]), and a research activity on secondary flight controls with VDHMs was performed at the University of Duisburg; such research was essentially aimed at determining a robust control for the variable displacement hydraulic motors used in position servoloops [7], [8] and [9].

More recently, actuation systems using VDHMs found an important application on the Airbus A380 and A400M, where they are used to drive the trailing edge flaps of these aircraft. The main characteristics of these systems are described in [10].

3 TYPICAL ARCHITECTURE OF A POSITION SERVOLOOP USING A VDHM

The control of a conventional hydraulic servoloop using a fixed displacement hydraulic motor, as well as a hydraulic linear actuator is based upon a controlled throttling of the fluid flow by means of a servovalve. On the othe hand, the control of the output position of an actuation system using a VDHM is based upon varying the displacement of the hydraulic motor depending on the actuation system needs. A functional diagram of a VDHM actuation system is shown in figure 2.

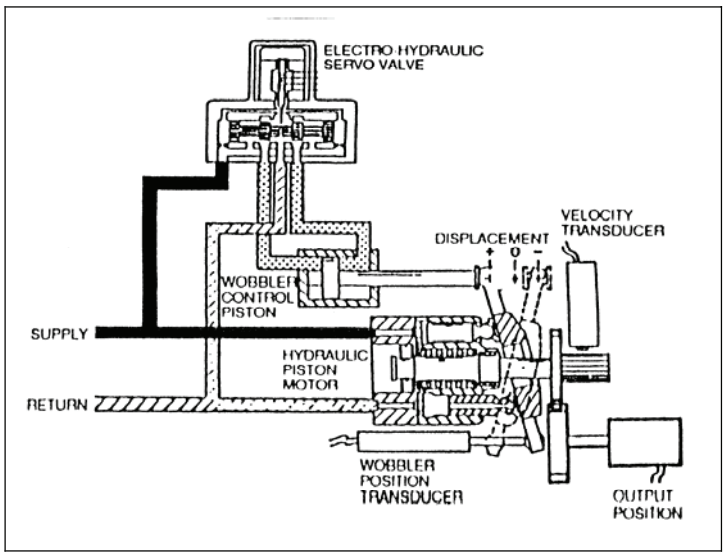

Figure 2: Functional diagram of a variable displacement hydraulic motor (reference [5])

The VDHM inlet and outlet ports are directly connected to the supply and return lines of the aircraft hydraulic system, while a servovalve located in parallel to the hydraulic motor controls the flow to the hydraulic piston, internal to the VDHM, which moves the hydraulic motor yoke to the required position. An either rotary or linear transducer measures the angular position of the yoke, while the motor speed is measured by a tachometer. As an alternative, the motor motor speed can be determined by computing

the time derivative of the position of the controlled output, providing that an appropriate computing algorithm is used for this process. Another alternative for the VDHM control is to use a modified servovalve with a dual internal mechanical feedback spring. One of the two springs provides the mechanical position feedback from the second to the first stage of the servovalve, as normally done in servovalves; the second spring provides a direct mechanical feedback from the piston of the actuator controlling the VDHM yoke to the servovalve first stage. This solution has the advantage of not requiring a yoke angular position transducer, with its associated electronics and control routines, but presents the drawbacks of a special servovalve and motor design and difficulties in matching two hydraulic motors in a dual redundant hydraulic system.

No matter which specific yoke control procedure is followed, it is important to notice that the motor torque is not controlled by throttling the flow in and out of the hydraulic motor, and no power loss is therefore created. It is further important to emphazise that the absence of a servovalve throttling the flow upstream of the hydraulic motor is beneficial also when the maximum motor power output is required. It is a fact that in order to guarantee adequate stability margins, the servovalve flow gain for a conventional fixed displacement hydraulic motor cannot exceed a given limit, which results in a pressure loss being created through the servovalve also in the fully open condition. As a result, the maximum displacement of a VDHM necessary to provide a given maximum output torque is generally 15% lower than that of a conventional fixed displacement hydraulic motor since it can use the entire available pressure differential. Moreover, when torques lower than the maximum are required and hence the motor displacement is lower than maximum, the motor internal losses of the VDHM are lower than those of a corresponding fixed displacement hydraulic motor. This is because the lower rate of flow through the VDHM originates lower internal losses.

Figure 3 shows the block diagram of a position servoloop which uses a VDHM; this block diagram corresponds to a control architecture that can be referred to as "*speed control architecture"*. This term derives from the fact that the variation of the displacement of the hydraulic motor is controlled in order to obtain a given speed of the motor itself. As it can be seen in Fig. 3, the control of a VDHM actuation system presents three nested control loops: an outer position control loop, an intermediate speed control loop and an inner displacement control loop. Since the motor displacement is related to the torque provided by the hydraulic motor, the control architecture of a VDHM actuation system has some similarities with that of an actuation system using a dc electric motor, which normally consists of nested position, speed and current control loops.

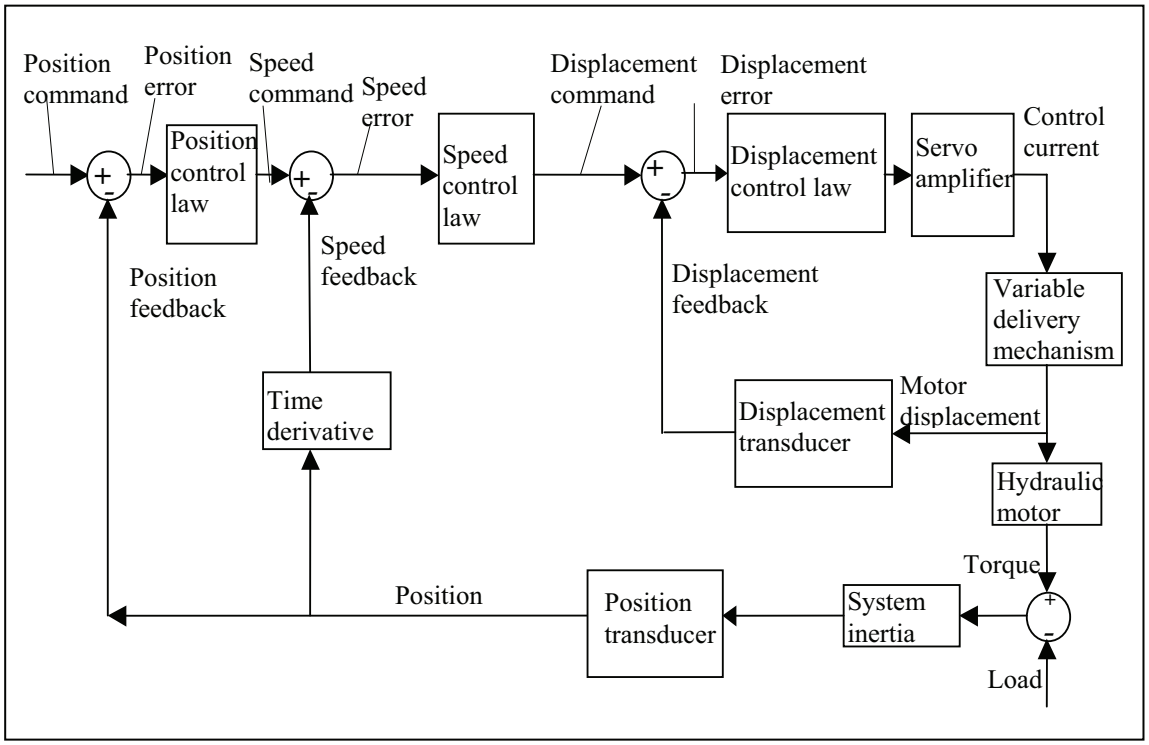

Figure 3: Block diagram of aVDHM control and actuation system with a speed control architecture

4 PERFORMANCE OF A VDHM ACTUATION SYSTEM WITH A SPEED CONTROL ARCHITECTURE

In order to show the performance attainable from a position servoloop based on a VDHM, the results are shown for a system sized to the requirements of a leading edge flap system of a modern fighter aircraft. A hydraulic power supply of 28 MPa was available and the maximum loads were such to require a maximum displacement of 6.5 cm^3/rev for the hydraulic motor.

The control parameters of the system were set to obtain adequate stability margins for all the three control loops (displacement, speed and position). Appropriate control laws were selected, which included a zero-pole compensation to improve the dynamic performance. Furthermore, the control loops were closed within a digital controller having a recursion rate of 500 Hz for the displacement loop and of 250 Hz for the speed and the position loops. As a result, the bandwidth (-90° phase) of the three control loops was the following:
40 Hz for the displacement loop
17 Hz for the speed loop
2.5 Hz for the position loop

The following figures 4, 5 and 6 show the experimental closed loop frequency responses of the displacement, speed and position loops. The corresponding open-loop gain of the position loop was 15.7 s^{-1}. Such dynamic performance would be too slow for a primary flight control system, but is acceptable for a secondary flight control system. It must also be noted that a relatively simple control law was used. A more so-

phisticated control would enable an improvement of the system dynamic response; it was shown in fact in [5] that a bandwidth of 7.5 Hz for the position loop can be achieved with a motor of 4 cm^3/rev displacement.

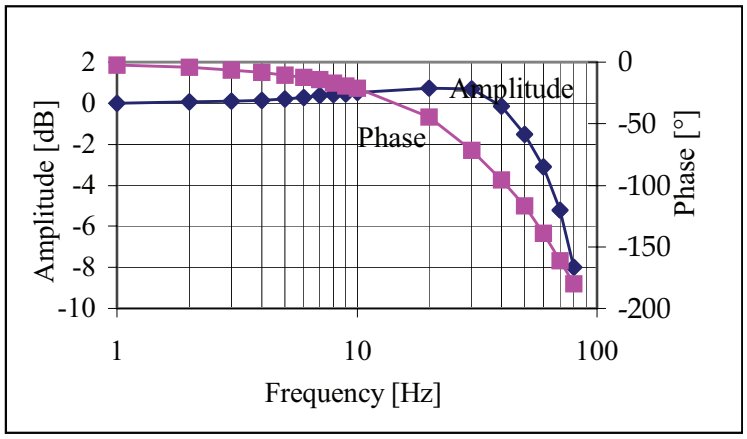

Figure 4: VDHM control and actuation system: frequency response of the displacement loop

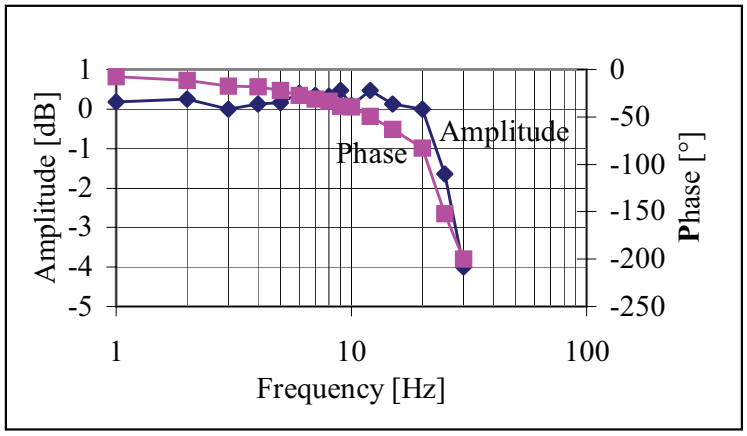

Figure 5: VDHM control and actuation system: frequency response of the speed loop

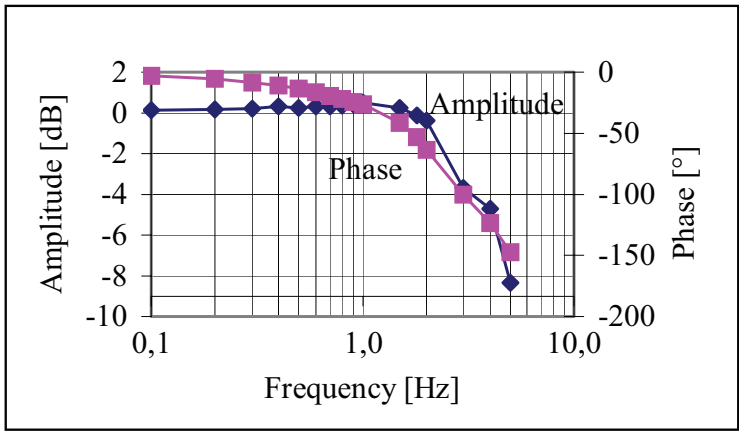

Figure 6: VDHM control and actuation system: frequency response of the position loop

For the case which is herein considered, the displacement necessary to operate the system in a no-load condition is 0.975 cm^3/rev; this displacement is what is required to provide the torque necessary to overcome the motor internal losses and the tare losses of

the mechanical system downstream of the hydraulic motor. The typical duty cycle of the leading edge flaps of a modern fighter aircraft is a sequence of several actuations of different amplitudes performed under different loads. However, if all these actuations are integrated and averaged, the typical averaged duty cycle can be roughly represented by 15-20 actuations of 2 seconds each per flight hour, under an average load equal to 20% of the maximum load. For the maximum number of actuations indicated above, and for the actuation system herein considered, the following table I of comparison for the flow and energy requirements of VDHM versus FDHM actuation systems was prepared. The flow rates shown in this table were computed considering a volumetric efficiency of the hydraulic motors equal to 0.95.

Table I: Flow and energy requirements of VDHM and FDHM actuation systems

Quantity		Fixed Displacement Hydraulic Motor	Variable Displacement Hydraulic Motor
Rated speed		6000 rpm	6000 rpm
Maximum load condition	Displacement	7.65 cm^3/rev	6.5 cm^3/rev
	Flow rate	48.3 l/min	41.1 l/min
Average load condition	Displacement	7.65 cm^3/rev	2.63 cm^3/rev
	Flow rate	48.3 l/min	16.6 l/min
No-load condition	Displacement	7.65 cm^3/rev	0.975 cm^3/rev
	Flow rate	48.3 l/min	6.2 l/min
Requirements for 1 flight hour	Volume of fluid	32.2 liters	11.1 liters
	Energy	901 600 J	309 800 J

As it can be seen from this table, the maximum flow rate required by a VDHM actuation system for a typical secondary flight control system utilizes a maximum flow rate which is about 85% of that for a conventional FDHM. The large saving, however, is that the VDHM system uses only about 1/3 of fluid volume and thus about 1/3 of energy when compared to a FDHM actuation system. The total energy saving shown by the above table is of about 600 000 J, that corresponds to about 0.1 kg of fuel when the efficiencies of the hydraulic power generation system and of the engine are taken into account. This amount is little but not negligeable, since it is the saving for one flight hour only. For the total life of 5000 to 6000 hours often considered for this type of aircraft the total fuel saving becomes 500 to 600 kg.

Although this fuel saving is certainly a positive feature, the major energy saving obtainable from the use of a VDHM lies in the fact that the lower flow required very likely leads to the selection of a smaller pump for the aircraft hydraulic system, and a smaller heat exchanger is also probably required. Smaller pump and heat exchanger mean lower system weight, which, as it is well known, is of paramount importance for all aircraft applications. A possible additional weight saving could also result from a slightly lower size necessary for the hydraulic lines supplying the hydraulic fluid to the VDHM.

5 INNOVATIVE CONTROL ARCHITECTURE FOR A VDHM BASED ACTUATION SYSTEM

The performance of a VDHM driven actuation system outlined in the previous paragraph was determined on the basis of a control architecture in which the speed is maintained at an established constant value whenever the position error resulting from the outer position loop reaches a limit value. As discussed above, the displacement of the hydraulic motor is continuously controlled in such a way to maintain the speed constant, thus reducing the flow consumption with reducing loads. There are applications, however, for which a constant actuation speed is not necessary, but it is only required that the actuation time for the full travel be lower than an established maximum. In such a case, the VDHM can be used in a different control mode providing a constant power. Since the pressure differential available at the VDHM ports is constant, a constant power control implies a constant flow control for the VDHM, as shown in the block diagram of Figure 7.

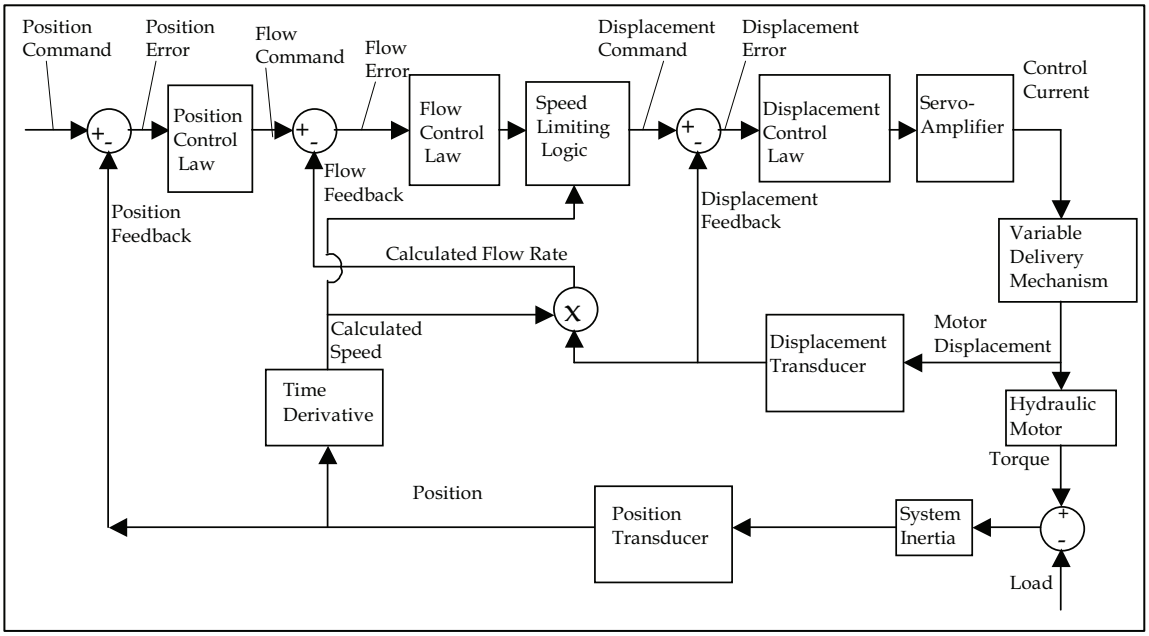

Figure 7: Block diagram of a VDHM control and actuation system with a flow control architecture

The error of the position control loop, after being processed by the appropriate control law, determines a flow command instead of a speed command as for the speed-control architecture. The flow command is compared with the actual motor flow, which is proportional to the product of the motor displacement times the motor speed. Since the VDHM contains both displacement and speed sensors, the actual motor flow can be computed using the information provided by these two sensors. It is also possible not to have a speed sensor, but to obtain the speed information by making the time derivative of the actuation system position. This control technique is instrumental in further exploiting the characteristics of a VDHM, providing a weight saving, a reduction of the maximum flow demand and in the end an optimization in the use of the hydraulic power.

We can consider, as a typical example, a case in which the load increases with the travel. For the case of FDHM the flow is constant when the system is commanded at the rated speed. For the case of a VDHM/speed control, the actuation speed is maintained constant throughout the travel and the flow consumption increases with the increasing load up to a maximum, which is slightly lower than that of a FDHM. For the case of a VDHM/flow control, the actuation speed varies along the travel. At the beginning of the travel, when the load is low, and thus the displacement is low, the actuation speed is high and equal to the maximum that is structurally allowable for the actuation system components. As the actuation travel progresses and the load increases, the motor displacement increases with a corresponding decrease of the actuation speed, since the flow is maintained constant. Such process continues until the minimum speed is obtained at the end of the travel. If the total actuation time has to be maintained, the average speed must be equal to the constant speed of the case of VDHM/speed control mode. Furthermore, for a given external load, the actual torque to be developed by the hydraulic motor increases with the speed due to the increasing tare losses of the actuation system components, therefore the maximum load at the end of the travel for the case of VDHM/constant flow mode is lower than that for the case of VDHM/constant speed mode. This implies that the maximum displacement required for the case of constant flow control mode is lower than the maximum displacement required for the case of constant speed mode. The resulting advantages are clear: a smaller hydraulic motor is required with lower envelope and lower weight, and the maximum flow consumption is much smaller, while the total energy requirement for the actuation is approximately the same for the two cases.

The actual weight saving obtainable with the flow controlled VDHM depends from the specific application. As an example we can refer to the application considered while examining the performance of a speed controlled VDHM. For constant flow control architecture we can allow the actuation speed to vary from a minimum of 3000 rpm to a maximum of 9000 rpm. If the operation against the maximum load occurs at 3000 rpm rather than at 6000 rpm, there is an additional benefit resulting from the increase of the efficiency associated to the reduction of the internal losses of the actuation system components rotating at a lower speed. The actual load torque required to the VDHM output shaft to drive the actuation system rotating at half of the rated average speed can be estimated to be about 15%. The maximum displacement reported in table I for the speed controlled VDHM was 6.5 cm^3/rev. The resulting maximum displacement required for the flow controlled VDHM is thus $\Delta_{M2} = 0.85 \times 6.5 = 5.525$ cm^3/rev based on the above assumption on the load torque reduction. Since this maximum displacement is obtained when the speed is of 3000 rpm, the flow consumption, considering again a flow efficiency of 0.95, is 16.6 l/min, much lower than the 41.1 l/min required by the speed controlled VDHM. Of course, such a large reduction of the maximum flow required by the actuation system is made possible only if the actuation system speed is allowed to vary in the range from 3 to 1 about the average speed. However, since the available flow in the aircraft hydraulic system is often a scarce commodity due to the need of limiting the overall system weight, the possibility of using such control architecture in association with a VDHM is a very attractive option.

A further advantage provided by a flow controlled VDHM is the possibility of driving the actuation system at very low temperature without an increase of the flow consumption. When a mechanical actuation system has to be driven in a very cold environment, which is typical of several aircraft systems after a cold temperature soak, the reduction

of the system efficiency leads to an increase of the torque to be developed by the hydraulic motor. There are applications in which such torque increase is large, reaching up to 25-30% of the rated torque. To make the hydraulic motor capable of developing the torque necessary to drive the actuation system under those conditions, a sufficiently large maximum displacement must be selected. However, when the system is commanded to move, a speed controlled VDHM system runs at the established speed and draws a maximum flow which is determined by the maximum motor displacement multiplied by the rated motor speed. For a flow controlled VDHM system, when a greater than normal torque is required under maximum load/minimum temperature conditions, the actuation speed is automatically reduced to prevent an excessive flow consumption. This speed reduction does not lead in general to a significant increase of the total actuation time, since the maximum loads generally occur only over a limited part of the travel, and the greater speed attained when the loads become smaller makes up for the increase of the actuation time when the loads are large.

A VDHM based actuation system using this control technique is being proposed for commanding the opening/closing of the cargo bay door of an aircraft. Figure 8 shows the time versus door position and flow consumption for operation at standard ambient temperature, while figure 9 shows the same quantities plotted for the case of very low temperature operation.

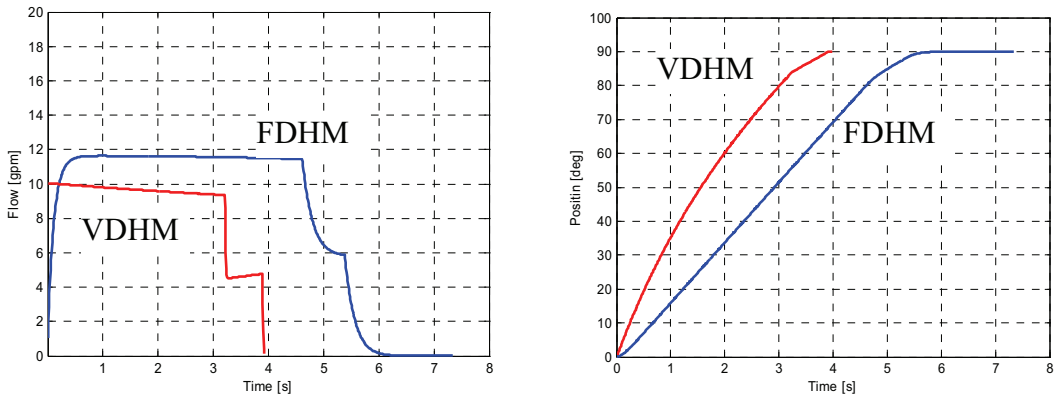

Figure 8: Time history of flow consumption and position of a flow controlled VDHM actuation system for a cargo bay door system at standard temperature

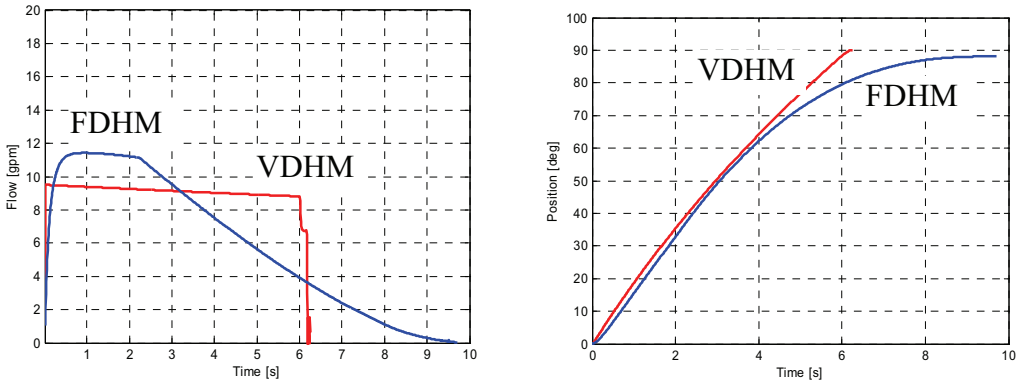

Figure 9: Time history of flow consumption and position of a flow controlled VDHM actuation system for a cargo bay door system at very low temperature

6 CONCLUSIONS

The main characteristics of a position control system, using a variable displacement hydraulic motor for driving an actuation system are presented. The merits of a VDHM based actuation system are outlined, with particular reference to their use in the aerospace applications. Two different control techniques for the VDHM are examined: one based on controlling the motor speed, the other based on controlling the flow consumption. The performance of the two solutions are compared, both for operation at normal ambient and very low temperatures. Results relevant to a specific application are presented.

LIST OF SYMBOLS

k_F = motor drain leakage coefficient
k_L = motor cross-port leakage coefficient
k_m = frictional losses coefficient
k_ω = viscous losses coefficient
p_r = motor outlet pressure
p_s = motor inlet pressure
T = motor torque
T_0 = motor hand torque
α = speed exponent for the viscous losses
β_1 = exponent for the cross-port leakage
β_2 = exponent for the drain leakage l
Δ_{M1} = maximum hydraulic motor displacement (speed control case)
Δ_{M2} = maximum hydraulic motor displacement (flow control case)
η_m = mechanical efficiency
η_v = volumetric efficiency
ω = motor angular speed
FDHM = Fixed Displacement Hydraulic Motor
VDHM = Variable Displacement Hydraulic Motor

REFERENCES

[1] Kubilos C.A.: "Energy Conservation With Variable Displacement Hydraulic Motors"; SAE Paper 791054; 1979.

[2] Lawhead P., Kubilos C.A.: "Servo Controlled Motors Study Project 858671" - Progress Report Number II (Internal Abex Report); 1982.

[3] Jacazio G., Bozzola P.: "Azionamenti per comandi di volo con motori idraulici a cilindrata variabile"; Proceedings of the Symposium of the Italian Association for Aeronautics and Astronautics (pages 105-114), Torino, Italy, 1983.

[4] Tovey P.: “Microprocessor Control of Aerospace Hydraulic Pumps”; SAE Paper 871863; 1987.

[5] Durtschi W.G., Kandil M., Kilroy D.: Design, Development and Demonstration of a Hugh-Pressure, Overcenter, Variable-Displacement Hydraulic Motor; SAE Paper 901794; 1990.

[6] Halat J., Case R.: “Operating Envelope Expansion of Aerospace Hydraulic Pumps and Motors Using Microprocessor Control” - Vickers Report; 1993.

[7] Berg H.: “Robust Position and Speed Control of Variable Displacement Hydraulic Motors”; Proceedings of the 4th IFAC Symposium Robust Control Design RO-COND ’97, Budapest, Hungary, 1997.

[8] Berg H.: “Robust Control of Variable Displacement Hydraulic Motors”; Proceedings of the first Bratislavian Fluid Power Symposium (pages 13-20), Casta Pila, Slovakia, June 1998.

[9] Ivantysynova M.: “Potential of Secondary Control for Hydraulic Drives Used in Modern Flight Control Systems”; Proceedings of the Congress on Recent Advances in Aerospace Hydraulics (pages 67-71), Toulouse, France, November 1998.

[10] Hauber B., Fleddermann A.: “Variable Displacement Hydraulic Motors in the A380 High Lift System”; Presentation given at the SAE A6 Committee in San Diego, October 2005.

HYDRAULIC FLUID QUALITY IN AIRCRAFT HYDRAULIC SYSTEMS

Jussi Aaltonen, Kari T. Koskinen, Matti Vilenius
Tampere University of Technology
Institute of Hydraulics and Automation
P.O.Box 589
33101 Tampere, Finland
Phone +358 3 365 4433, Fax +358 3 365 2240
E-mail: jussi.aaltonen@tut.fi

Kalle Vaaraniemi
Finnish Air Force Headquarters
Armaments Division (A10)
Aircraft Sector
P.O. Box 30
41161 Tikkakoski, Finland

ABSTRACT

Ambient temperature variation aircraft hydraulic systems have to withstand can be nearly 90ºC. Besides of the ambient temperature the hydraulic systems have to withstand very high variation in system temperature. Due to small fluid volume, limited heat exchanger capacity and high system peak power these systems usually run exceptionally hot and fluid may have to withstand a temperature variation as high as nearly 180 ºC. Violent ambient conditions and extreme conditions in the system itself cause hydraulic fluid to be under very exceptional stress in comparison to typical mobile hydraulic systems. Also hydraulic system maintenance and servicing practices in aircraft differ a great deal from practices used in other mobile hydraulic systems.

Fluid contamination and deterioration are normal consequences of the system operation and ambient conditions. Performance, lifetime and reliability of hydraulic components are very sensitive to the quality of the hydraulic fluid used in the system and thus is of great importance to know the overall quality of the fluid in the system and to understand how the quality is affected by maintenance and servicing.

This paper presents results of the fluid quality monitoring study made in two different types of aircraft using different types of hydraulic fluid (mineral oil based and synthetic hydrocarbon). Four individual aircrafts were selected for research and fluid from each

aircraft was sampled periodically. Typical parameters describing the fluid quality (TAN, viscosity, water content etc.) were analysed from samples. Also the level of particulate contamination was determined. Results give an explanation to many typical problems encountered in aircraft hydraulic systems and also point out short comings of typical maintenance servicing procedures used in aircraft hydraulics.

KEYWORDS: Fluid quality, aircraft, MIL-PRF-83282, MIL-PRF-5606

1 INTRODUCTION

A mineral oil-based MIL-H-5606 has been the most widely used type of hydraulic fluid in military aviation since 1940's and it was widely used also in commercial aviation until 1970's. It provides excellent operational properties over the temperature range of –54°C to 135°C. It has one major deficiency, which was recognised early in its use, is its high degree of flammability.

Recognition of fire hazards associated with MIL-H-5606 fluids, resulted in the commercial aircraft industry to develop hydraulic fluid based on phosphate esters. However, the phosphate ester based fluids were not adopted by the military because they were not compatible with MIL-H-5606 fluids, nor with elastomer materials used in MIL-H-5606 hydraulic systems. There was also a view that the use of two incompatible hydraulic fluids could result in significant problems if fluids were ever inadvertently mixed.

The commercial aircraft industry found a significant reduction in the number of hydraulic fluid fires since the adoption of phosphate ester hydraulic fluids, and now-a-days all large civil transport aircraft use this type of fluid in their hydraulic systems. Although the military did not move to phosphate ester type fluids they did identify the need for a fire resistant fluid as a direct replacement for MIL-H-5606. As a result a synthetic hydrocarbon-based fluid, MIL-H-83282 was developed. This fluid is completely compatible with MIL-H-5606 fluids and MIL-H-5606 hydraulic system materials. All physical properties of MIL-H-83282 (new designation MIL-PRF-83282) were equivalent or superior to those of MIL-H-5606 (new designation MIL-PRF-5606) except low temperature viscosity. In particular all fire resistant properties of MIL-PRF-83282 are superior to those of MIL-PRF-5606. More recently MIL-PRF-87257 was introduced in order to offer a fluid which has better low temperature viscosity than MIL-PRF-83282.

Hydraulic fluid contamination and deterioration are normal consequences for hydraulic systems. The most common hydraulic fluid contaminants are entrapped air and water, along with particles of metal, rubber or dirt.

Fluid deterioration can be more appropriately called "additive deterioration". Additives give oil its particular characteristics. These additives are most susceptible to chemical and physical change often caused by chemical reactions with contaminants or high temperatures.

Aircraft hydraulic systems usually have very small fluid volume and limited heat exchanger capacity, which lead to high operational temperature. Also environmental temperature extremes can be very violent. Thus hydraulic fluid is under a very high stresses caused by temperature.

Level of the particulate contamination in the system is kept low by fine filtration and periodic flushing of the system. However hydraulic fluid typically is never completely renewed, but the system is topped up with new fluid as needed. Topping up is a common practice also in hydraulic units used for flushing and system testing. Due to mixing new and used fluid the chemical quality, i.e. stage of deterioration, of the fluid in the system is unknown.

The performance, life and reliability of hydraulic components are very sensitive to the quality and maintenance of the hydraulic fluid used in the system.

2 FLUID SAMPLING PROGRAM

To study hydraulic fluid chemical quality a periodic fluid sampling program was planned. Program included 10-12 fluid samples taken on regular intervals from hydraulic systems of:

- Two jet fighters (MIL-PRF-83282 fluid)
- Two jet trainers (MIL-PRF-5606 fluid)
- Two portable hydraulic test stands for each aircraft type

From each fluid sample following physical properties were tested:

- Viscosity at 40°C and 100°C
- Viscosity index
- Total acid number
- Water content

Samples taken from test stands were also tested for foaming. Reason for not testing samples from aircrafts for foaming was high fluid volume needed for test.

Random samples went also through spectrometric analysis to study if it is possible to trace additive deterioration from samples. Some samples went also through particle counting, but results of particle counting were known to be unreliable because of sampling (bottle samples) and long storage time before counting [1].

Samples of new barrel clean fluid were analysed for reference. Analyses made are further explained in following chapters.

2.1 Viscosity and Viscosity Index

Viscosity is commonly considered to be the single most important property of a hydraulic fluid. Decreased viscosity is generally a sign of additive deterioration. However oxidation and some contaminants can also increase the viscosity of the fluid.

Viscosity index is a measure of fluid's change of viscosity with temperature. The higher the viscosity index, the smaller the relative change in viscosity with temperature.

Viscosity was determined according to ASTM D 445. Viscosity index was determined according to ASTM D2270.

2.2 Total Acid Number (TAN)

Total acid number is the quantity of base, expressed in milligrams of potassium hydroxide, which is required to neutralize all acidic constituents present in 1 gram of sample.

TAN depends on both the base oil and additives. Increase in TAN is usually due to oxidation which on the other hand can be caused by several different factors (air, temperature, water etc). Typical TAN values for new hydraulic fluids are 0.02…0.5 mgKOH/g. TAN value of two times the value of a new fluid is commonly considered to the maximum value acceptable.

Total acid number was determined according to ASTM D 664.

2.3 Water Content

Because of its affinity for other liquids, water is present in some concentration in most hydraulic systems. The hygroscopic nature of liquids causes them to pick up a certain amount of water simply from contact with humid air.

Each fluid has its own saturation level for water. Below the saturation level, water will be completely dissolved in the fluid. For oil-based hydraulic fluids, the saturation level is likely to be in the range of 0.01% to 0.1% (100 to 1,000 ppm) at room temperature. At higher temperatures, the saturation level is greater. Above the saturation level, water takes the form of relatively large droplets, which is also called free water. It is also possible that, due to mixing action, undissolved water is emulsified so that it exists as very fine droplets suspended in the oil.

Water reacts with almost everything in a hydraulic system. Water promotes corrosion through galvanic action by acting as an electrolyte to conduct electricity between dissimilar materials. Water reacting with antioxidation additives produces acids. At operating temperatures above 60° C, water reacts aggressively with zinc-type antiwear additives (For example, zinc dithiophosphate (ZDTP) is a popular boundary lubricant added to hydraulic fluid). When this type of additive is depleted by its reaction with water, abrasive wear will accelerate rapidly. Water can also act as an adhesive which causes particles to clump together in a larger mass.

Water content was determined according to ASTM D 1744

2.4 Spectrometry

There are several different methods of spectrometric hydraulic fluid analysis. Basically these methods can be divided in atomic spectrometry and molecular spectrometry.

According to their names the first one is for determining atomic concentrations and the latter one for molecular concentrations. Both methods need a great deal of expertise in analysis, but can give very accurate results. Spectrometric analysis can be used for tracing wear metals, contamination and additives.

Method used in these analyses was atomic spectrometry.

2.5 Foaming

Foam depressants are usually a part of the additive packages in many oils. Additive deterioration and contamination are the usual causes of foaming.

The foaming test consists of three temperature sequences, 24°C, 93.5°C, then back to 24°C, using the same sample for the last two sequences. At each temperature sequence, air is blown into a cylinder containing the oil through a diffusion stone for five minutes. At the end of five minutes, the amount of foam generated is measured. At the end of 10 minutes settling time, the amount of foam remaining is again reported. Quality lubricants generally have 0 ml foam after about 5 minutes.

Foaming was determined according to ASTM D 892.

3 RESULTS

Results for one of each aircraft type are presented in this paper.

3.1 Jet Fighter

The hydraulic fluid used in the system is MIL-PRF-83282 type. During test period the aircraft systems were topped up several times due to maintenance, repairs and system deaeration. Total usage of new fluid can not be determined.

Total FH during program 135.2 FH

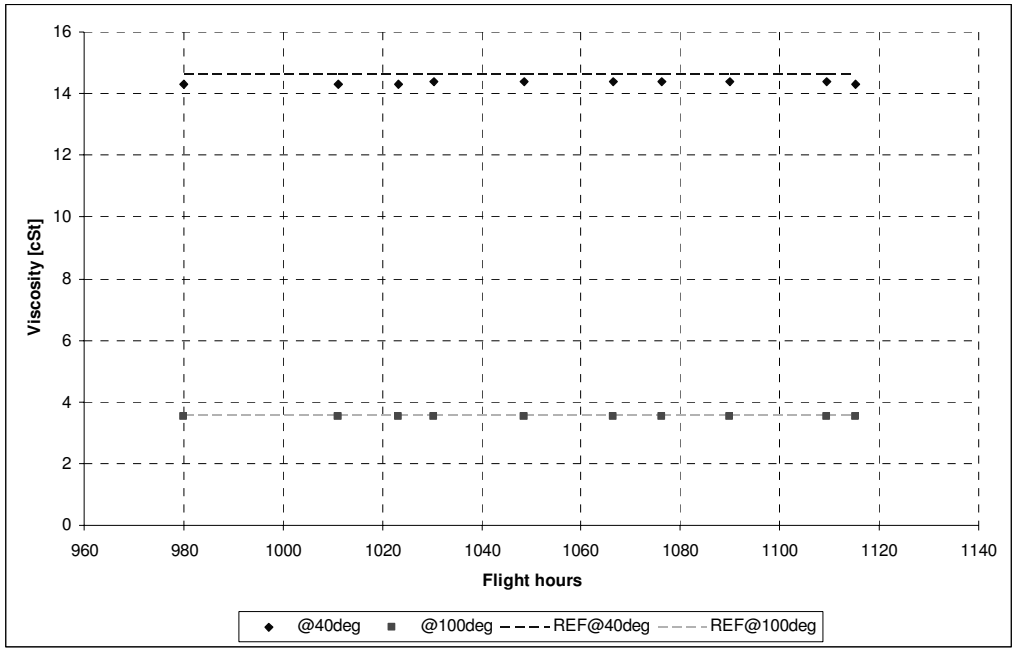

Figure 1. Hydraulic fluid viscosity [cSt], reference curves – new fluid

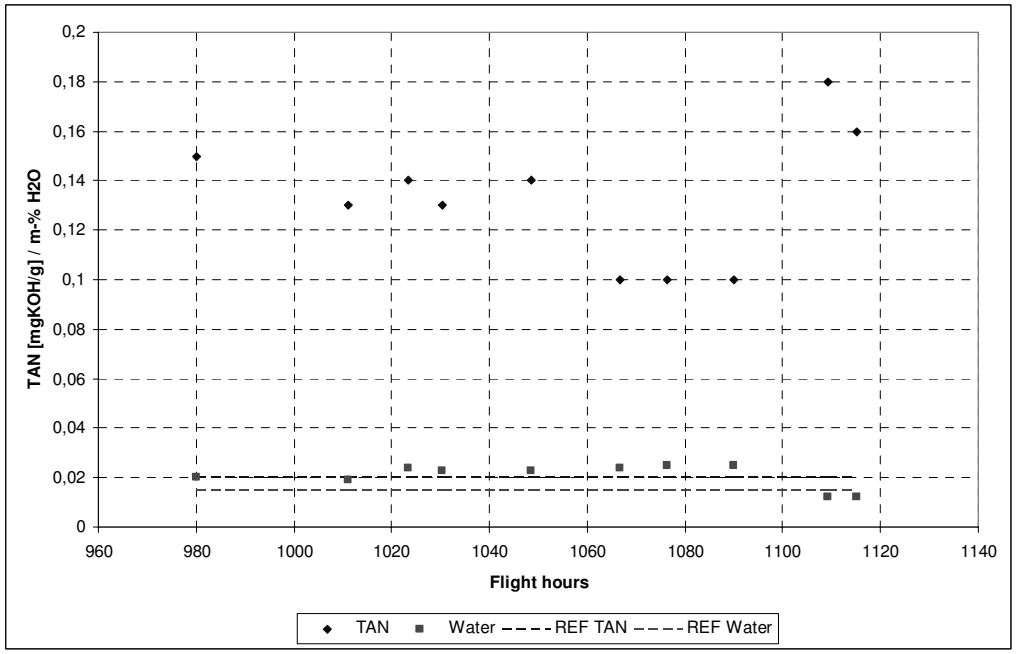

Figure 2. Total acid number [mgKOH/g], reference curves – new fluid. Water content [weight %], reference curves – new fluid

3.2 Jet Trainer

The hydraulic fluid used in the system is MIL-PRF-5606 type. During test period the aircraft systems were topped up several times due to maintenance, repairs and system deaeration. Total usage of new fluid can not be determined.

Total FH during program 159.15 FH

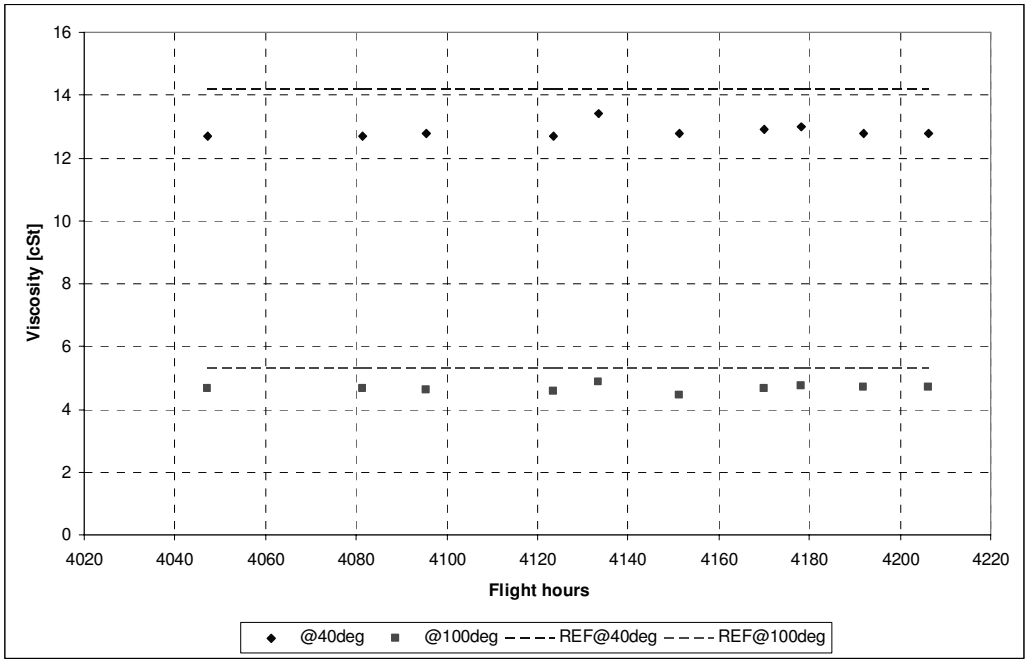

Figure 3. Hydraulic fluid viscosity [cSt], reference curves – new fluid

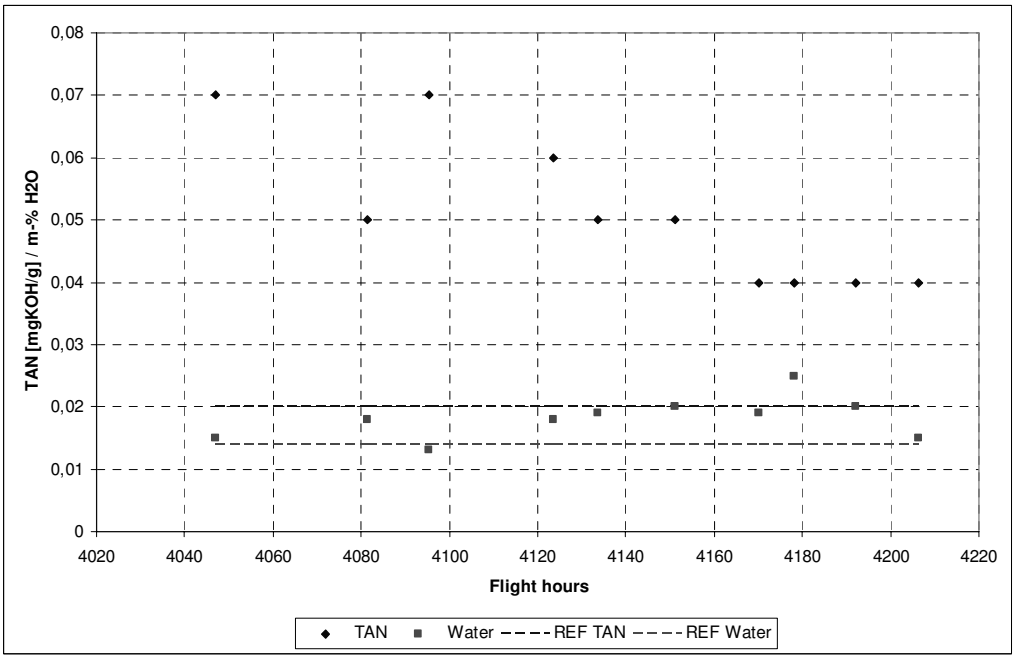

Figure 4. Total acid number [mgKOH/g], reference curves – new fluid. Water content [weight %], reference curves – new fluid

3.3 Portable Hydraulic Test Stand for Jet Trainer

The hydraulic fluid used in the system is MIL-PRF-5606 type. During test period the system was topped up several times. Total usage of new fluid can not be determined.

Total running hours during program: 14 h

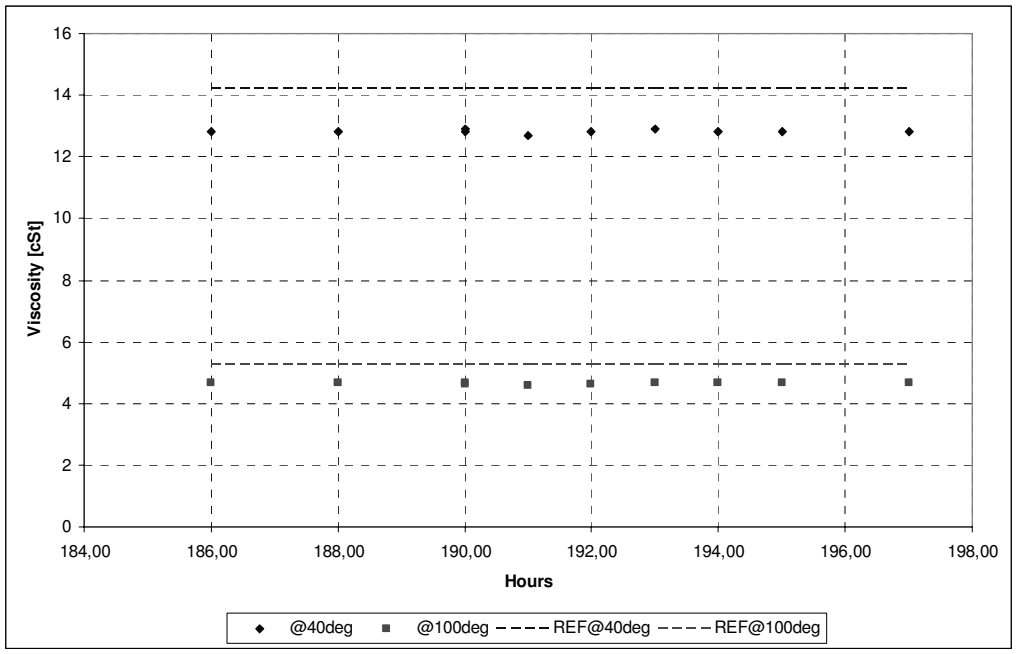

Figure 5. Hydraulic fluid viscosity [cSt], reference curves – new fluid

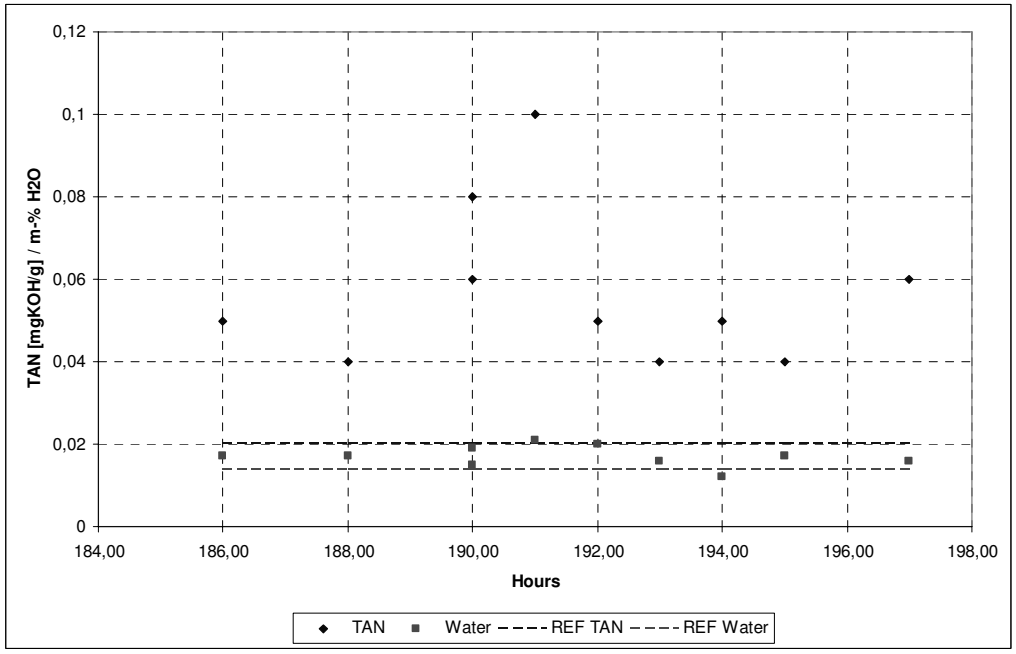

Figure 6. Total acid number [mgKOH/g], reference curves – new fluid. Water content [weight %], reference curves – new fluid

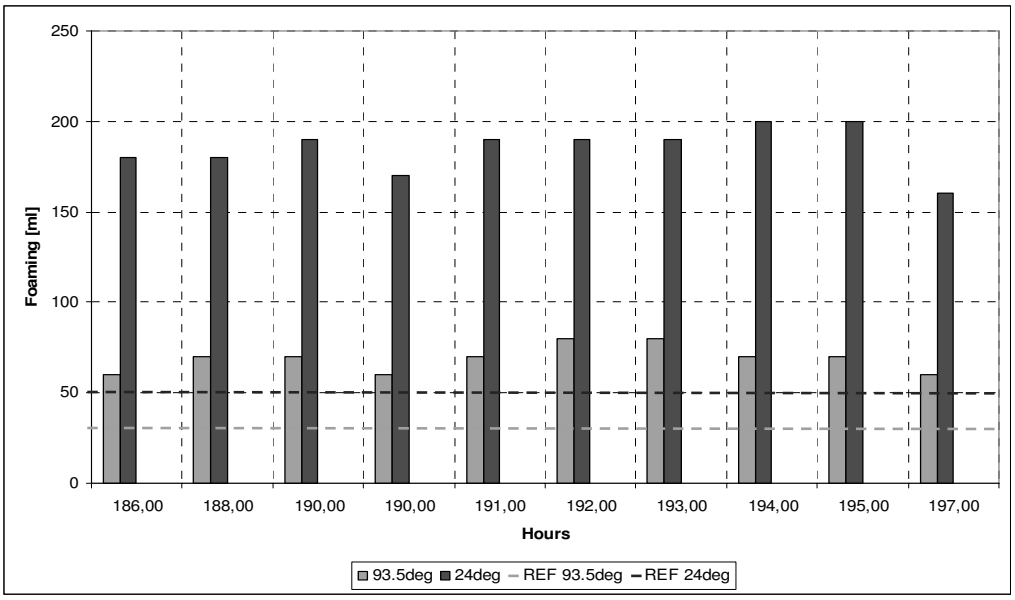

Figure 7. Foaming [ml], reference (red lines) - new fluid

In figure 7 foaming values are presented only for first two phases of test, third phase value is omitted in figures because its values are identical to the first phase. Visible bars present the foam after air mixing, foam after settling time is zero and thus not visible.

3.4 Portable Hydraulic Test Stand of Jet Fighter

The hydraulic fluid used in the system is MIL-PRF-5606 type. During test period the system was topped up several times. Total usage of new fluid can not be determined.

Total running hours during program 31 h

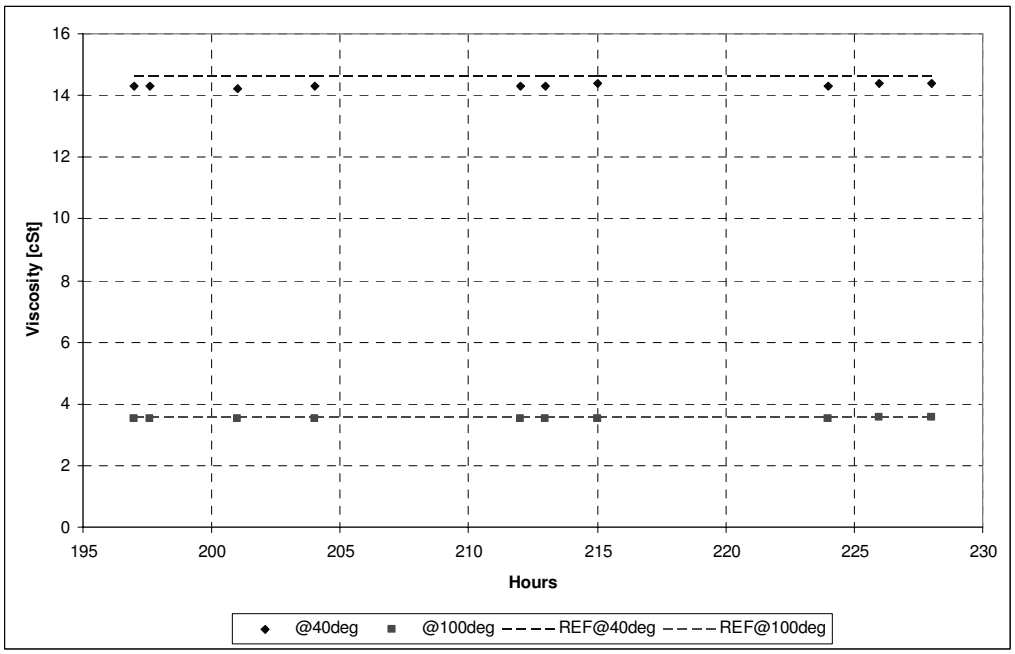

Figure 8. Hydraulic fluid viscosity [cSt], reference curves – new fluid

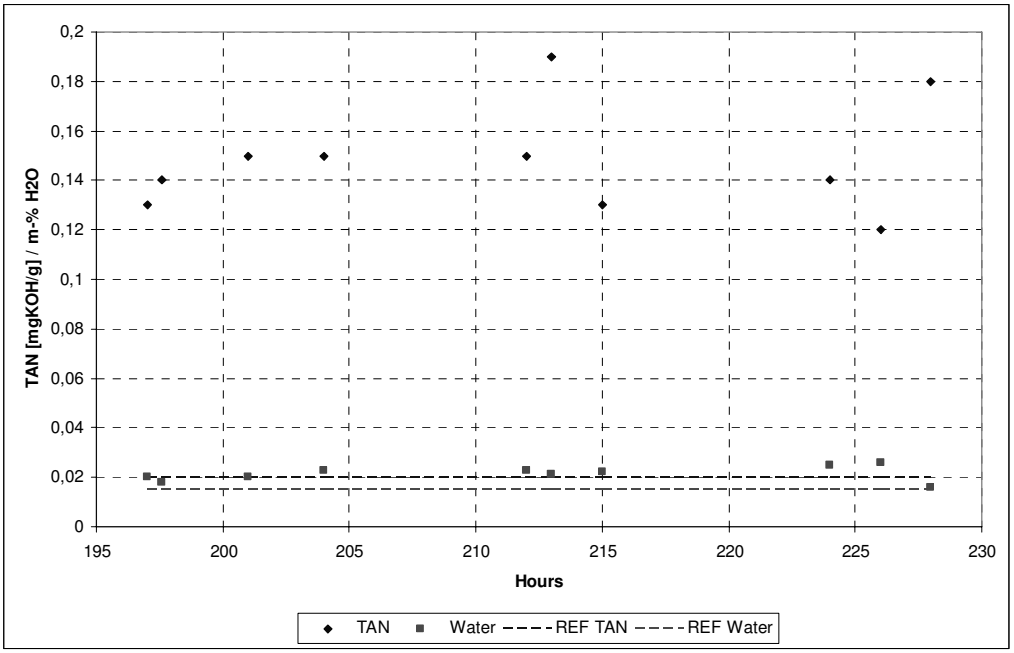

Figure 9. Total acid number [mgKOH/g], reference curves – new fluid. Water content [weight %], reference curves – new fluid

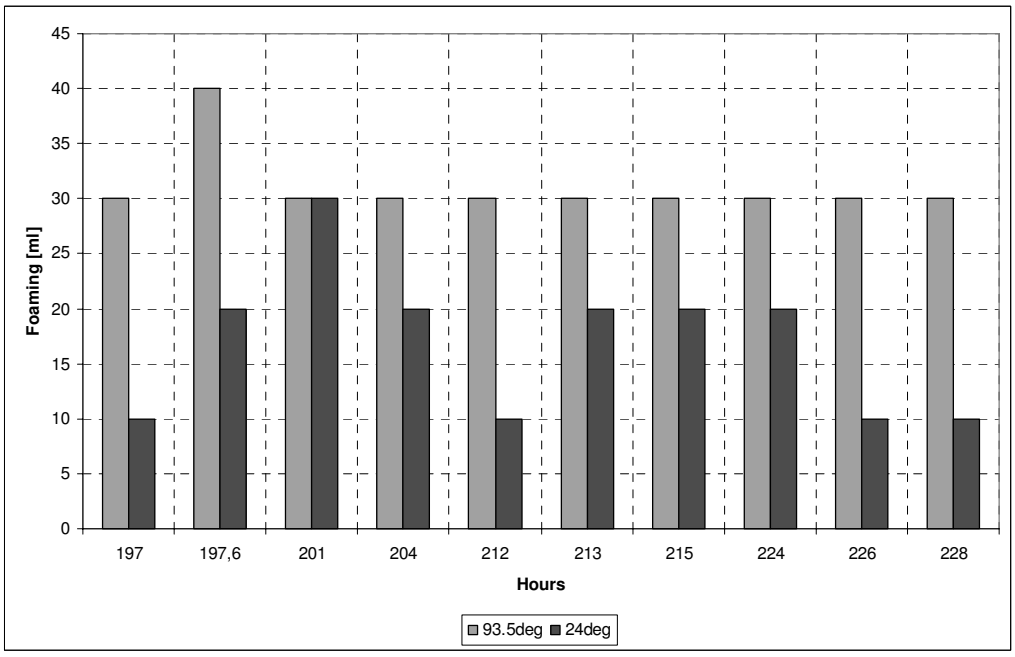

Figure 10. Foaming [ml], reference (red lines) - new fluid

In figure 10 foaming values are presented only for first two phases of test, third phase value is omitted in figures because its values are identical to the first phase. Visible bars present the foam after air mixing, foam after settling time is zero and thus not visible.

3.5 Results of Spectrometry

Spectrometry analysis results for the first batch of samples are shown in figure 11. All other analyses gave similar results.

Possible origins of traces found in samples are:

Ca (Calcium)	Oil additives, water, grease, dirt
P (Phosphorus)	Additives
Si (Silicon)	Dirt intrusion, seal material, additive
Sn (Tin)	Additives, wear metal
Zn (Zinc)	Neoprene seals, additives, wear metal
Ba (Barium)	Additives, water and grease
Cu (Copper)	Wear metal

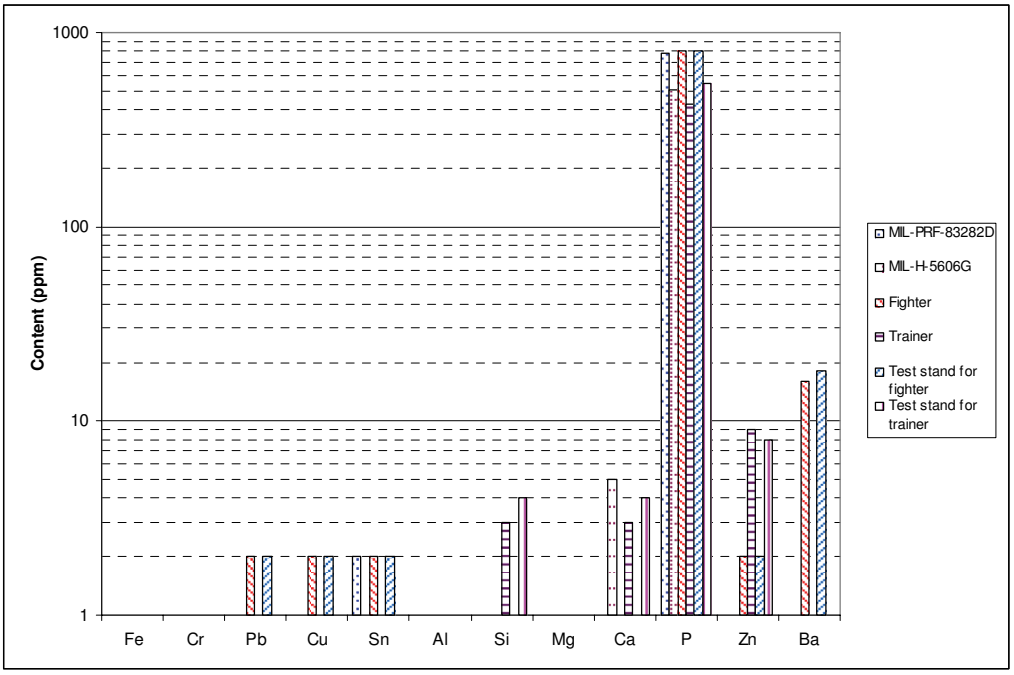

Figure 11 Spectrometry results for the first batch of samples

3.6 Particle Counting

Particle counting was done on several fluid samples during the test. As was expected results were inconclusive. This is mostly due to long storage time of samples before the counting could be done, but also sampling itself could have some effect on results.

In aircraft the sampling point is typically in the system return line before filters. Due to systems being constant pressure systems with variable displacement pump there is almost no flow in the system when system is on idle. Even though it is possible to drain a sample good enough for chemical analysis it is not possible to get a good sample for particle analysis.

Results showed cleanliness of NAS 1638 class 7 – 9, whilst the target cleanliness is class 6. This gives a reason to expect that cleanliness is not on level it should be, but does not prove it. However without system modifications or somehow taking sample from a system running on full flow this is impossible to confirm

4 DISCUSSION

Results of analyses show no signs of time dependency in the deterioration of hydraulic fluids. This was an expected result since it was known that new fluid is constantly introduced to systems and old fluid is bled out, thus it is natural that an equilibrium state in fluid quality is formed.

An equilibrium is also formed in between the fluid quality of test stands and aircrafts due to mixing of fluids when units are used.

From results it can be clearly seen that the synthetic fluid retains its viscosity better than the mineral oil based fluid. Viscosity changes in MIL-PRF-83282 are minimal in comparison to ones found in MIL-PRF-5606, even though the system using MIL-PRF-83282 fluid is known to have much higher operating temperature.

Possibly because of the hydraulic system operating temperature TAN values of fluid in fighters and their test stands are very high (approx. seven times the value of a new fluid). Also the foaming tendency values are in used MIL-PRF-83282 are very high in comparison to level of the new fluid, however as an absolute value they still are below the level of the new MIL-PRF-5606 fluid. Increased foaming tendency can be interlinked with air problems encountered in hydraulic system of fighters.

Used fluid of trainers and their test stands have TAN values of approx 3-4 times the value of the new fluid. Foaming tendency values of used fluid are significantly higher than value of the new fluid.

Water content of fluids in all systems is relatively close to starting values. This however does not necessarily mean that water is not introduced to systems but only that the amount of dissolved and undissolved water is low.

Results of spectrometric analysis were inconclusive. There are some traces of possible additives visible, but they can not be unambiguously identified as additives. For example zinc, phosphorus, calcium and barium are all common constituents of oil additives, but they also can be traces of contamination. To be able to clearly identify additives and contamination a molecular spectrometry should be used instead of atomic spectrometry.

All results indicate depletion of additives in fluid. Additive depletion can be in some extent interlinked with all wear problems encountered in systems and also with system deaeration problems encountered in fighters.

5 CONCLUSIONS

There is nothing to be done in maintenance procedures and schedules of aircraft to improve the quality of hydraulic fluid. System constructions do not make it possible to implement same procedures (i.e. periodic fluid renewal, flushing, reservoir cleaning etc) used in other hydraulic systems to maintain the fluid quality. However the fluid quality could be improved by introducing new maintenance procedures for test stands and by improving test stands themselves. Test stands have much higher fluid volume than aircraft and thus their effect on the fluid quality is relatively high.

Fluid quality could be improved by:

- Introducing periodic fluid renewal and reservoir cleaning to maintenance schedule of test stands
- Improving breather filtration in ground units
- Improving filtering of ground units by offline deep filtering system capable to remove water and resins from fluid
- Periodic fluid sampling (particle count, chemical analysis)

Air in aircraft hydraulic systems is a very common maintenance problem for many aircraft types, especially modern fighters which almost all use MIL-PRF-83282 fluids or equivalent. Results showed that foaming tendency of fluid in aircraft and their test stands is significantly higher than the one of new fluid. Therefore test stand reservoirs should be designed extremely carefully to allow fluid to deaerate in the reservoir and not to introduce more air into the fluid in reservoir.

Bad fluid quality in one aircraft can only cripple one aircraft - Bad fluid quality in one test stand can cripple the whole squadron.

6 REFERENCES

[1] Stecki J.S.(ed), Total Contamination Control, Fluid Power Net Publications, 1998

DIGITAL HYDRAULICS – TOWARDS PERFECT VALVE TECHNOLOGY

Academy Research Fellow Matti Linjama & Professor Matti Vilenius
Tampere University of Technology
Institute of Hydraulics and Automation
P.O.Box 589, FI-33101 Tampere, Finland
Phone +358 3 3115 2690, Fax +358 3 3115 2240
E-mail: matti.linjama@tut.fi

ABSTRACT

Digital Hydraulics is a recently developed alternative for traditional control with servo or proportional valves. The key principle is to use parallel-connected two-way on/off valves together with intelligent control. This paper analyses characteristics of different digital valve systems. It is shown that valve system having equally sized valves is in many senses optimal solution. The feasibility and achievable performance of this approach is discussed. It is shown that the technology has potential for ten times faster response than existing valves and good fault tolerance. Miniaturization is shown to be essential method in implementation of this kind of valve systems.

KEYWORDS: Digital hydraulics, on/off control, miniaturization

1 INTRODUCTION

1.1 Background

Great majority of hydraulic systems are based on analogue control components, such as proportional valves and variable displacement pumps. Benefits of analogue systems are e.g. simple and smooth control. On the other hand, analogue components may be expensive and sensitive to contamination, temperature, vibration etc. Analogue systems have been superseded by digital systems in many fields. Some examples are cameras, displays, computers and music. Digital technology is not limited to electronics but it can be applied in any field of technology. Old examples are DNA code, smoke signs and Morse code, and modern examples are ABS brakes and fuel injection of modern cars [1, 2].

By definition, digital systems utilize discrete value components. Some general principles of digital technology are plurality of similar components (e.g. pixels), AD and DA conversion and intelligent control. Important benefits of digital technology are robustness, repeatability and fault tolerance. The most common solution is to use binary components and it is easy to determine if the signal is ON or OFF. This makes digital systems repeatable and insensitive to noise. Plurality of similar components makes digital systems redundant. For example, failure in single pixel of digital camera causes only a negligible reduction in performance. Digital components are also easier to optimize for performance because there are no requirements for linearity or hysteresis. Digital component is either ON or OFF but nothing between.

Challenges of digital technology are large number of components and/or risk for jerky control. Good controllability requires proper design together with sufficient number of components or extremely fast components. Digital systems have always been more expensive at the beginning but mass production has made them cheaper than analogue counterparts. Also, increased performance, programmability and flexibility (e.g. MP3 player compared to LP disk) have helped to tolerate increased price.

1.2 Classification of Digital Principles in Hydraulics

Digital technologies in hydraulic systems can be divided into three major classes as shown in Table 1. The simplest one is traditional on/off technology, in which the output of the system has only two discrete values, such as motor/pump rotating or stopped, cylinder moving or stopped, pressure high or low. Hydraulic cylinder controlled to one or another end can also be included in this class. The second major class is switching techniques, which mimic principles of electric switching systems. The most popular variant is pulse width modulated (PWM) on/off valve. Switching techniques rely on extremely fast switching and the main benefit is simple hydraulic hardware. The purpose is to produce analogue-like output via high-frequency modulation and filtering. The third class is the utilization of parallel-connected components. The systems are truly digital because the output has only discrete values. Output level is defined as a sum of outputs of ON components. Essential difference to switching techniques is that no switching is needed to maintain any of discrete output values. This technology is called here Digital Hydraulics.

1.3 State of the Art

Basic on/off technology is not studied much nowadays. This is probably because the technology is considered as old-fashioned. However, the on/off control is the best solution for cases in which its control characteristics can be tolerated, and the approach is very popular in pneumatic systems. A short survey on on/off control is given in [4].

Switching techniques have been under active research already for decades. Scheidl and Manhartsgruber [5] give a good overview of switching techniques and this material is not repeated here. Some discussion can also be found in [4]. The biggest challenge of switching techniques is the development of extremely fast, reliable and energy efficient on/off valve. Traditional valve technology seems not to be able to satisfy these requirements, but the resonance valve concept [6] seems promising approach. The most

important commercial applications of switching techniques are ABS brakes and fuel injection systems of modern cars [1, 2]. Switching controlled pump (Table 1 (f)) has been studied in [7].

*Table 1. Classification of digital principles in hydraulic circuits and some example circuits. (*Lower picture of (j) from* [3])

	On/Off Technology	**Switching Technologies**	**Digital Hydraulics**
Valves	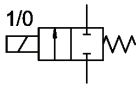 (a)	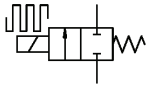 (e)	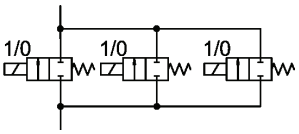 (h)
Pumps	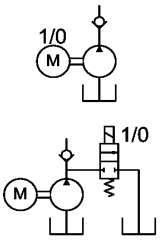 (b)	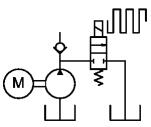 (f)	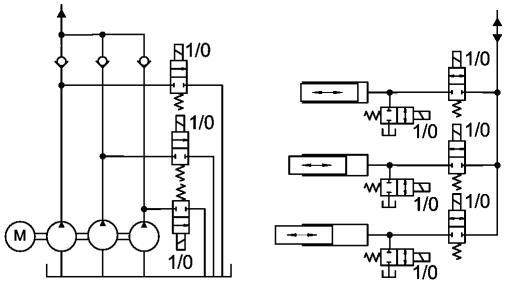 (i)
Cylinders	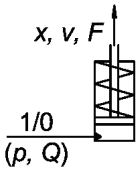 (c)	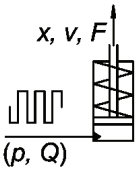 (g)	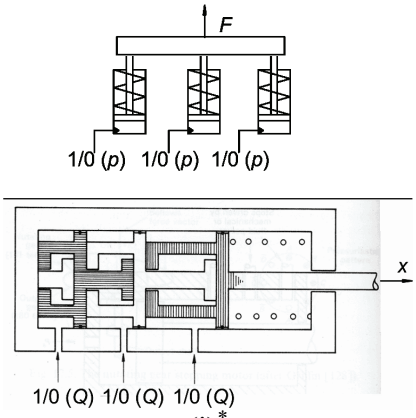 (j)*
Capacitances	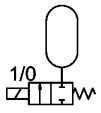 (d)		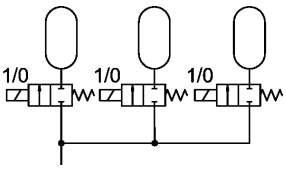 (k)

Parallel connected on/off valve series of Table 1 (h) is an old invention [8, 9], but it has been applied quite seldom in 20th century [10–12]. The development of valves and control techniques has resulted in extensive research and development of this technology since 2000 [13–21]. The results of this research can be summarized as:

- Digital hydraulic valve systems can significantly save energy similarly as analogue distributed valve systems [13]

- The valve system is fault tolerant and failure in single valve does not prevent the use of actuator [14, 15]
- Performance is comparable or better to analogue counterparts [13, 16, 17]
- Rather complicated controllers are needed [13, 18–20]
- Proper design is needed in order to avoid pressure peaks [21]

Parallel connected pumps (Table 1 (i), left) are routinely used in many applications. Another way to implement digital pump is so called digital displacement technology shown in right side of Table 1 (i) [22, 23]. The idea is to actively control operation of each piston of the pump by on/off valves. Each piston can be independently in idle mode, pump mode or motor mode. This results in better efficiency and controllability but for some reason, the approach is not widely adopted.

1.4 Definition of Terms Used Together with Digital Hydraulics

Most of this paper deals with digital valve systems, such as Table 1 (h). The terminology is not well-established and following definitions are used in this paper (see also Figure 1):

DFCU (Digital Flow Control Unit) – Group of two-way two-position on/off valves connected in parallel.
Digital valve system – Configuration of several DFCUs. For example, four-way digital valve system.
Digital Hydraulics – Hydraulic systems, which utilizes parallel-connected binary components. Output has only certain discrete values. See Table 1.
Coding or **Coding scheme** – Coding determines flow rates of valves of DFCUs expressed relative to the smallest valve. Some coding schemes are binary coding (1, 2, 4, 8, 16, … , 2^{N-1}), Fibonacci coding (1, 1, 2, 3, 5, 8, … , $P_{N-2}+ P_{N-1}$) and Pulse Number Modulation (PNM) coding (1, 1, 1, 1, … , 1).
N-bit DFCU – DFCU with N parallel connected valves. For example, four-bit DFCU, seven-bit binary-coded DFCU.
PNM-coding (PNM = Pulse Number Modulation) – Coding scheme in which all valves have the same flow capacity.
PNM control – Control method in which output is changed either by opening or closing valves. This means that simultaneous opening and closing of valves never happen in DFCU.
State of DFCU – Binary vector with N elements or integer number between 0 and 2^N–1. State determines open and closed valves of DFCU. For example, state [1 0 1 0] or 5 means that the first and third valves are open and the second and fourth valves are closed.
Step size – Change in output of DFCU when the state is changed by one. Ideally, equals to flow rate of the smallest valve of DFCU.

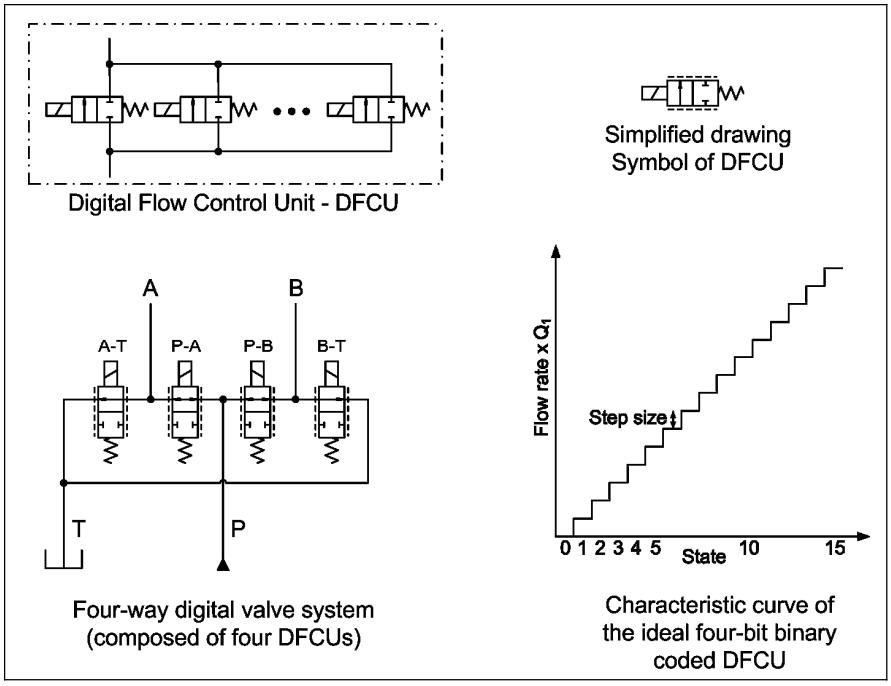

Figure 1. Some definitions of digital valve systems.

1.5 Objectives of the Paper

The main objective is to find out, which kind of performance is possible with digital valve technologies, such as shown in Table 1 (e) and (h). At first, the availability and characteristics of existing on/off valves is introduced. Then requirements set by different digital valve technologies are analyzed and performance of some valve systems is presented.

2 CHARACTERISTICS OF ON/OFF VALVES

2.1 Commercial Valves

Commercial on/off valves are widely used in simple tasks, such as switching hydraulic motor on or off. The response time is not critical in these applications and slow response is many times advantageous in order to reduce pressure peaks. These facts have caused that commercial valves have only moderate performance. Fortunately, characteristics can be significantly improved with proper control electronics and slight modifications [24]. Table 2 presents measured characteristics of some commercial on/off valves. Problem with directly operated valves is that they cannot tolerate high pressure differentials. Pilot operated valves do not have this problem but they have longer and more varying delay.

Table 2. Measured characteristics of some commercial on/off valves [16, 24].

Valve type	Direct operated spool (NS4)	Direct operated spool (NS6)	Direct operated seat valve with dynamic seal (Screw-in cartridge)	Pilot operated seat valve (Screw-in cartridge)
Valve manufacturer & type	Bosch Rexroth 4WE420/EG24N9K4	Moog WE43P06… E03PC0BN	Hydac WS08W-01	Sterling Hydraulics GS0205
Control electronics & modifications	Opening and closing booster, structural modifications	Opening and closing booster, structural modifications	Opening and closing booster	Closing booster
Response time	8-10 ms	8-12 ms	5-8 ms	10-40 ms
Nominal flow Q_N @ 3.5 MPa	75 l/min	200 l/min	36 l/min	52 l/min
Max. pressure differential	3.5 MPa	6 MPa	3.5 MPa	21 MPa
Size excluding connectors	168×37×39 mm	208×45×48 mm	ϕ36.3×95 mm	34×40×91.5 mm

2.2 Special Valves and Valve Prototypes

Standard hydraulic on/off valves are not optimized to be used together with modern digital technologies. This is why many on/off valve prototypes have been developed [25–28]. Automotive industry utilizes also modern on/off valves in fuel injection, brakes and valvetrains [1, 2]. Table 3 presents characteristics of some of these valves.

Table 3. Characteristics of some special valves and valve prototypes.

Valve type	Direct operated bistable spool	Direct operated spool (NS10)	Direct operated bistable seat	Pilot operated seat
Valve manufacturer & type	Sturman Industries SI-1000 [2]	Linz Center of Mechatronics GmbH [25]	Tampere University of Technology [26]	Tokio Institute of Technology [27]
Response time	0.45 ms	2 ms	1.5-3.5 ms	1-2 ms
Nominal flow Q_N @ 3.5 MPa	32 l/min	120 l/min	10 l/min	~6 l/min
Max. pressure differential	n.a.	14 MPa	21 MPa	14 MPa
Size excluding connectors [mm]	Approx. 110×35×35*	Approx. 90×90×110*	ϕ31×28.2	Approx. ϕ50×150*

*Partial or no data available. Size estimated from figure.

3 CHARACTERISTICS OF DIGITAL VALVE SYSTEMS

This chapter analyses characteristics of PWM controlled valve and different digital valve systems. Characteristics are analysed in terms of uncertainty in output, response time, flow capacity, number of valves and fault tolerance.

3.1 PWM Controlled Valve

The output uncertainty of PWM controlled valve can be defined as difference between target duty ratio and true duty. Uncertainty depends on both the switching time and flow uncertainty as shown in Figure 2. Uncertainty depends also on switching frequency. Relative error e_τ caused by variation in valve delay can be expressed as:

$$e_\tau = \frac{(\tau_{\max} - \tau_{\min})f}{Duty} \tag{1}$$

where τ_{max} and τ_{min} are maximum and minimum delay, f is switching frequency and $Duty$ is duty ratio. Equation 1 shows that error increases with frequency and decreases with duty. This means that relative error becomes very big at small duty. Situation is even worse in practice because valve opening is highly unpredictable at very short pulses [2].

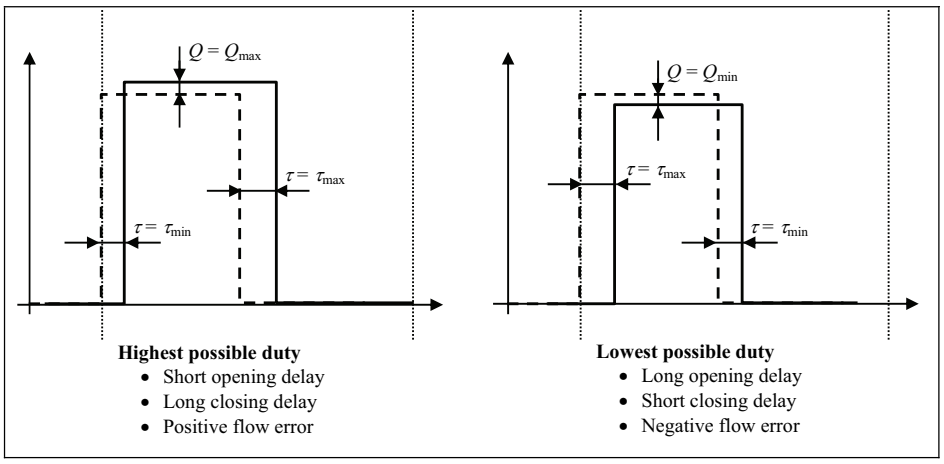

Figure 2. Uncertainty of PWM duty cycle.

Response time of PWM controlled valve depends on valve dynamics and switching frequency. Valve response time must be a small fraction of switching period for successful duty control. A rule of thumb is that switching frequency is at maximum ten percent of inverse of valve response time. The basic principle of classical PWM approach is to filter output such that ripple at switching frequency remains reasonable. This means that output bandwidth is a small fraction of switching frequency, usually less than ten percent. Thus, it can be concluded that response time of the output of the PWM valve is at least 100 times longer than response time of the valve.

Good feature of PWM controlled valve is that only one valve is needed. Side effects are that the valve must pass all the flow and that fault tolerance is poor. Durability requirements are also high because of continuous high frequency switching.

3.2 Binary-Coded DFCU

A binary-coded DFCU consists of N parallel connected on/off valves such that their flow capacities are [1 2 4 8 16 32 etc.]×Q_1 where Q_1 is the flow capacity of the smallest valve. The operation principle of the binary-coded DFCU is similar to DA converter

and output has 2^N discrete values depending on which valves are open. The open valves are defined via *state vector*, which has N elements. For example, "three-bit" binary-coded DFCU has states [0 0 0], [1 0 0], [0 1 0], [1 1 0], [0 0 1], [1 0 1], [0 1 1] and [1 1 1]. Important difference to PWM approach is that no switching is needed in order to maintain any of these output values.

Steady-state output uncertainty depends on output uncertainty of open valves only. This means that relative uncertainty is constant, which allows exact control also at small openings. However, it is important to remember that DFCU can deliver only certain discrete flow rates and flow rate increases stepwise. Another steady-state uncertainty is step size uncertainty, which depends on state transition executed. Step size uncertainty is equal to sum of uncertainty of all valves, which change their state. For example, step size uncertainty of state transition [0 1 0]↔[1 1 0] is equal to output uncertainty of the smallest valve while step size uncertainty of transition [1 1 0] ↔[0 0 1] is equal to sum of output uncertainty of all three valves. Assume for example that flow rate of the two smallest valves is two percent too big and flow rate of the third valve is two percent too small. The flow rate of state [1 1 0] is $3.06\times Q_1$ instead of $3\times Q_1$ and flow rate of state [0 0 1] is $3.92\times Q_1$ instead of $4\times Q_1$, which gives 14 percent too small step. Practical systems have five or six valves, which means that step size uncertainty can exceed step size for certain state transitions in the binary-coded DFCU. This phenomenon has been observed also in practice; see [29] and Fig. 3. Figure 3 shows also clearly that uncertainty caused by viscosity change is proportional to flow rate.

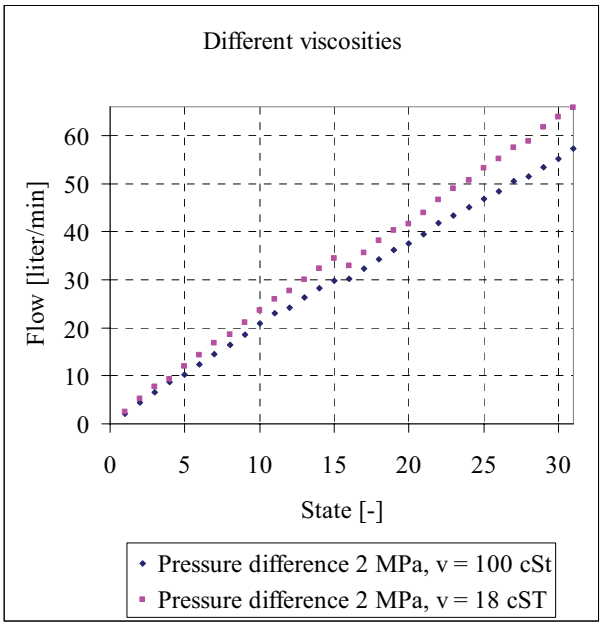

Figure 3. The effect of viscosity on characteristics of a five-bit binary-coded DFCU. Note big change in step size of state transition 15↔16. [29]

Response time of the binary-coded DFCU is equal to response time of individual valves and amplitude has no effect on response time. One special feature of the binary-coded DFCU is transient uncertainty. This is caused by the fact that certain state transitions require simultaneous opening and closing of valves. Variation in response times causes that some valve may close before another opens or vice versa. The result is short term uncertainty in the effective opening. This phenomenon has been studied in detail by Laamanen et al. [21]. Figure 4 presents transient uncertainty for a four-bit binary-coded

DFCU when its state increases linearly. Uncertainty is huge in state transition [1 1 1 0]→[0 0 0 1]. The only ways to reduce uncertainty is to use valves with very small uncertainty in response time or to part with binary coding.

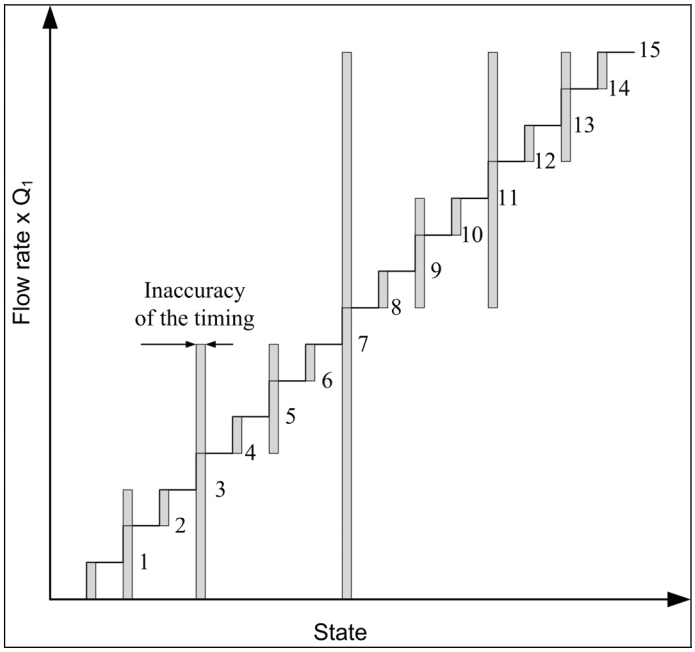

Figure 4. Theoretical transient uncertainty of a four-bit binary-coded DFCU when state increases linearly.

The binary-coded DFCU requires five or six valves for good controllability. Flow capacity of the DFCU is approximately twice the flow capacity of the biggest valve. The flow capacity of the smallest valve is 1/16 (N = 5) or 1/32 (N = 6) of the flow capacity of the biggest valve. Thus, implementation of binary-coded DFCU requires different valve sizes or extensive choking of flow rate.

Fault tolerance of the binary-coded DFCU is good when compared to the PWM valve or any traditional analogue valve. Fault in any of the smaller valve has only a small effect on performance while bigger valves are more critical. It is important to detect faults in order to maintain controllability. Figure 5 presents controllability in the case of five-bit DFCU. [14]

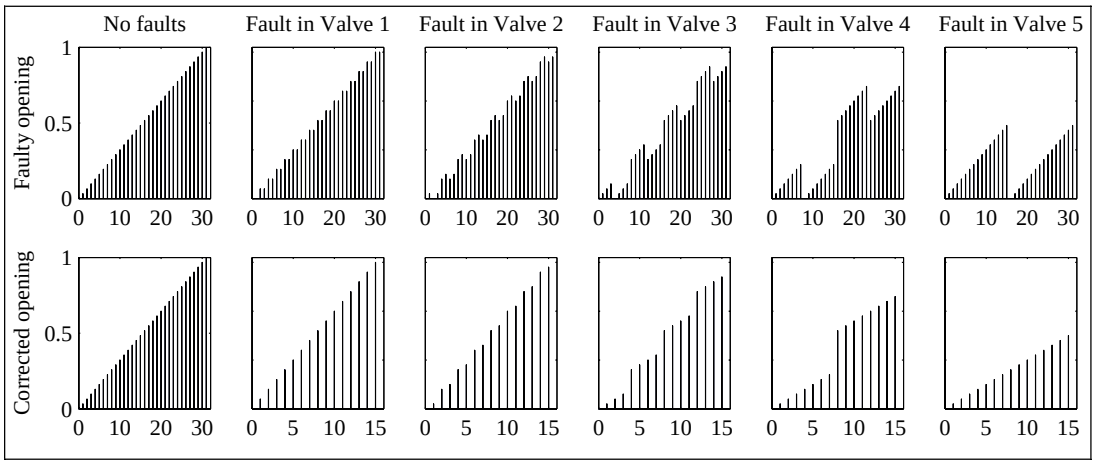

Figure 5. Fault tolerance of five-bit binary-coded DFCU [14].

3.3 PNM-Coded DFCU

The binary-coded DFCU has the highest possible number of output levels but also some problems as described in the previous section. Pulse Number Modulation (PNM) coding is another extreme in which all valves have the same flow capacity. The number of output values is only N+1, which means that a large number of valves is needed in order to achieve high resolution. Control principle is to open more valves when more flow is needed and close valves when less flow is needed, and there never exist simultaneous opening and closing of valves. The PNM-coded DFCU does not have problems of binary-coded DFCU, i.e.:

- Step size uncertainty is small, relative to step size and independent on state transition
- There is no transient uncertainty but opening is between initial and final opening during the state transition.
- There is no need for different valve sizes because all valves have the same flow capacity
- Fault tolerance is much better than in binary-coded DFCU. The only effect of failure in one valve is that flow rate does not increase in one state transition.

The only problem of the PNM-coded DFCU is the big number of valves. For example, 31 valves are needed in order to achieve the same resolution than with five-bit binary coding. On the other hand, only one type valves are needed and mass production may be used. The required flow rate per valve is small ($1/N$), which helps to achieve very fast response.

3.4 Mixed PNM-Binary Coding

Mixed PNM-binary coding tries to combine good characteristics binary and PNM-coding. Targets are set as follows:

- In normal conditions, control strategy must be PNM control, i.e. there are never simultaneous opening and closing of valves.
- In fault situation, binary-like control is allowed if transient uncertainty remains small.
- Number of valves must be reduced significantly from PNM-coded system
- Control resolution can be reduced at bigger openings

The last fact is based on analysis results of [18, 30], which shows that high resolution is needed only at small openings in four-way valve applications. Five-bit binary and 31-bit PNM-coded DFCUs are used as an example. For simplicity, it is assumed that step size is 1 l/min. Flow capacity of all valves is 1 l/min in pure PNM-coding. The number of valves can be almost halved if one 1 l/min valve is used together with fifteen 2 l/min valves. In order to improve fault tolerance and resolution, it could be better to have two or three 1 l/min valves. Several alternatives can be derived from this principle:

1) 3×1 l/min + 14×2 l/min (17 valves)
2) 3×1 l/min + 4×2 l/min + 5×4 l/min (12 valves)
3) 3×1 l/min + 2×2 l/min + 2×4 l/min + 2×8 l/min (9 valves)

Figure 6 depicts flow curves when PNM control is used. Note that all alternatives can deliver all 31 flow rates if binary like control is allowed.

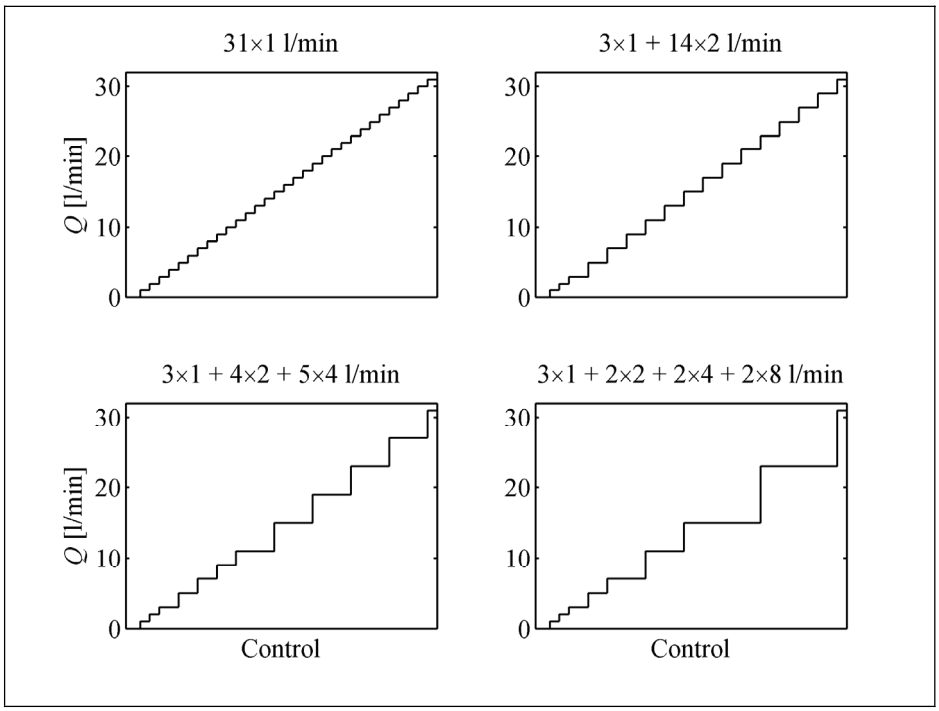

Figure 6. Characteristic curves of pure PNM-coding and different mixed coding schemes when PNM control is used.

3.5 Summary

Table 4 summarizes characteristics of digital valve systems together with valve requirements. PWM Valve requires big, fast and durable valve as well as small uncertainty in switching time. Binary-coded DFCU requires also relatively large valve (the biggest valve) and exact timing. Response time itself is not critical but uncertainty in response time must be small in order to reduce transient uncertainty. PNM-coded DFCU has the best characteristics but the cost is strongly increased number of valves.

Table 4. Summary of characteristics of digital valve systems studied.

	PWM controlled valve	Binary-Coded DFCU	PNM-Coded DFCU	Mixed- Coded DFCU
Number of valves	Small	Moderate	Very large	Large
Steady-state uncertainty	Large	Small	Small	Small
Step size uncertainty	n/a	Big	Small	Small
Transient uncertainty	n/a	Big	Small	Small
Dynamic performance	Poor	Good	Best	Very good
Fault tolerance	None	Good	Best	Very good
Requirements for valves	- High flow - Extremely fast - Extreme durability - Exact timing	- High flow - Exact timing - Small size	- Small size	-Small size

4 MINIATURIZATION AND PNM – TOWARDS PERFECT VALVE

4.1 Definition of Perfect Valve

Well known design rule is to strive for impossible in order to obtain best possible solution. This kind of impossible "perfect valve" could be defined as follows:

- Infinite bandwidth, no oscillations or overshoot.
- No uncertainty, perfect repeatability
- Unlimited durability
- Characteristics independent on fluid, temperature, pressure, wear etc.
- Fully programmable characteristics for optimal fit to any system
- Low costs and small size
- No variants, same valve can perform all necessary tasks

Practical intermediate objectives could be:

- Response time is small compared to pressure wave propagation speed in the system. Propagation speed is usually below 1400 m/s or 1.4 m/ms, which means that response time of 0.1 ms could be considered as fast enough.
- Few percent gain variation may be acceptable if outer-loop feedback is used. It is not enough to have small absolute uncertainty but relative uncertainty must also be small.
- Durability must cover lifetime of the system.
- Valve variants for different number or ports and different flow ranges are allowed.

4.2 Is There Need for Perfect Valve?

A natural question is which the benefits of perfect valve are. If the price of the valve is low, the high performance does not matter. High performance allows new functions, such as:

- Active noise reduction
- Compensation for pump ripple
- Attenuation of pressure shock waves
- Emergency functions
- Bumbless transfer between different modes, such as inflow-outflow vs. differential mode or flow vs. pressure control mode.

The vision is that single high performance programmable valve allows *all* hydraulic functions of an actuator to be implemented with the same valve.

4.3 Miniaturization as a Method to Improve Digital Valves

Consider simple needle valve shown in Figure 7. Let assume that maximum needle lift x is proportional to diameter d, i.e. $x = Kd$. Assuming small opening ($K << 1$) and neglecting flow forces, the flow rate Q, closing force F and opening work W_{open} can be estimated as:

$$
\begin{aligned}
A &= \pi x \sin\alpha\left(d - \frac{x}{2}\sin(2\alpha)\right) = d^2 K\pi \sin\alpha\left(1 - \frac{K}{2}\sin(2\alpha)\right) \\
Q &= \mu A\sqrt{\frac{2(p_{in} - p_{out})}{\rho}} = d^2 K\pi\mu \sin\alpha\left(1 - \frac{K}{2}\sin(2\alpha)\right)\sqrt{\frac{2(p_{in} - p_{out})}{\rho}} \\
F &= d^2\pi(p_{in} - p_{out})/4 \\
W_{open} &\approx Fx = d^3 K\pi(p_{in} - p_{out})/4
\end{aligned}
\tag{2}
$$

These equations show that flow rate and closing force are proportional to square of diameter while opening work is proportional to cube of diameter. For example, if one valve is replaced with four smaller valves with half diameter, the result is same flow but halved opening work. The effect is even bigger in practice because smaller valve has lighter armature (mass is proportional to d^3) and because shorter actuation time is needed (lighter armature and shorter stroke). It can also be assumed that volume of valve is proportional to d^3. Thus, *replacing big valve with several smaller valves results in smaller total volume, faster response and smaller total switching energy.*

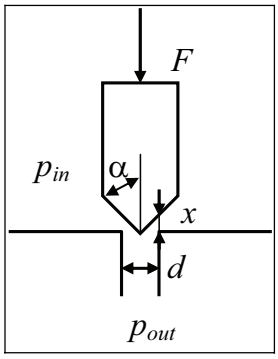

Figure 7. Simple needle valve

Although simplified calculations of a simple seat type valve are used, the benefits of miniaturization seem to be general. An example can be found in [2], in which characteristics of three highly optimized spool type on/off valves are presented. Volume of valve can be assumed proportional to spool travel and square of spool diameter, and flow rate is proportional to flow area. The data of [2] together with two efficiency numbers are presented in Table 5. Comparison show that switching time and relative power consumption decreases with decreasing size and that relative volume reduces or at least remains at the same level.

Table 5. Comparison of three same type high performance on/off valves [2].

Name	Spool diameter d [mm]	Spool travel x [mm]	Flow area A [mm^2]	Switching time [ms]	Switching energy W [J]	$\frac{A}{d^2 x}$	$\frac{A}{W}$
Pilot	3	0.16	0.75	0.19	0.011	0.52	68
SI-1000	6.4	0.38	10	0.45	0.30	0.64	33
SI-1500	9.5	0.64	23	1.0	0.70	0.40	33

4.4 PNM-Coded Miniaturized Four-Way Digital Valve System

Analysis of Chapter 3 shows that PNM-coded digital valve systems give the best characteristics. Miniaturization also goes together well with PNM-coding because PNM calls for plurality of small valves. Let us assume that mass production makes on/off valves so inexpensive that PNM-coded valve systems are feasible. A four-way PNM-coded digital valve system is next outlined. The target nominal flow rate is selected 100 l/min at 3.5 MPa per edge and the target flow resolution is 50:1. This requires 50 valves per edge or 200 valves in total. Each valve passes 2 l/min at 3.5 MPa, which means flow area of 0.6 mm^2. If pilot valve of Table 5 is used to implement this kind of valve package, its characteristics will be:

- Response time 0.2 ms independently on amplitude
- Nominal flow rate 100 l/min at Δp = 3.5 MPa per edge
- Flow resolution 50:1, actuator velocity resolution over 100:1 [18]
- Relative uncertainty of flow rate few percent
- Highly fault tolerant valve system
- Durability of each valve over 10^9 cycles [2]
- Programmable characteristics and possibility for differential connection [13]

Clearly this is towards perfect valve in terms of response time, uncertainty, reliability and programmability. Best existing analogue servovalves have several milliseconds response time from -100 to 100 percent and hardly any fault tolerance. The big number of valves is the biggest obstacle for implementation of this kind of valves, but mixed coding of Section 3.4 can be used to reduce number of valves.

5 DISCUSSION AND CONCLUSIONS

Analysis results of this paper show that digital valve systems based on parallel-connected on/off valves can provide unique features in terms of performance, accuracy and fault tolerance. Miniaturized PNM-coded digital valve systems have the best characteristics and there are no technical obstacles for implementation of 100 l/min valve (at Δp = 3.5 MPa) with 0.2 ms full-amplitude response time. High performance allows all hydraulic functions to be implemented with same type of digital valves, which allows huge reduction of the number of different valve variants. Vision is that only one type of on/off valve with some different sizes are mass-produced and assembled into some different programmable packages.

Essential question is can this kind of valve packages be produced in sufficiently low costs. The price of individual valve should be about 1 € in the four-way digital valve system of Section 4.4. It is clear that this can be achieved only in very big series. It is possible that completely different operation principles and manufacturing methods are needed. One possibility is valve matrix based on active materials, such as piezo [31]. Mixed coding seems an effective way to reduce the number of valves 50-70 percent. This requires bigger valves but may be feasible way to reduce price.

Miniaturization and corresponding increase of number of components seems to be effective method for improving characteristics of digital valves. Important questions,

which are not studied in this paper, are how far miniaturization gives benefits and which the effects of miniaturization on valve actuator design are. It is clear that there is a limit for the degree of miniaturization because Reynolds number decreases as a result of miniaturization. The effects of miniaturization on valve actuator may be positive or negative. At least, the relative surface area increases, which helps to prevent overheating of actuator.

ACKNOWLEDGEMENT

The research was supported by the Academy of Finland (Grant no. 80411).

REFERENCES

1 Wennmacher, G. 1996. Untersuchung und Anwendung schnellschaltender elektrohydraulischer Ventile für den Einsatz in Kraftfahrzeugen. Dissertation D 82 RWTH Aachen, 183 p. (Verlag der Augustinus Buchhandlung, 1996).

2 Johnson, B., Massey, S. & Sturman, O. 2001. Sturman Digital Latching Valve. Proceedings of the Seventh Scandinavian International Conference on Fluid Power, May 30 – June 1, 2001, Linköping, Sweden, pp. 299–314 (Vol. 3).

3 McCloy, D. & Martin, H. 1973, The Control of Fluid Power. 367 p. (Longman Group Limited, London).

4 Linjama, M., Laamanen, A. & Vilenius, M. 2003. Is it time for digital hydraulics? Proceedings of the Eighth Scandinavian International Conference on Fluid Power, May 7–9, 2003, Tampere, Finland, pp. 347–366.

5 Scheidl, R. & Manhartsgruber, B. 2005. State of the Art in Hydraulic Switching Control – Components, Systems, Applications. Proceedings CD-ROM of the Ninth Scandinavian International Conference on Fluid Power, June 1–3, 2005, Linköping, Sweden, 12 p.

6 Manhartsgruber, B. 2006. A Hydraulic Control Valve for PWM Actuation at 400 Hz. **In:** Johnston, D. N., & Edge, K. A. (eds.) Power Transmission and Motion Control, PTMC2006, pp. 373–385 (Hadleys Ltd, 2006).

7 Mansouri, G., Misovec, K., Johnson, B., Babbitt, G. & Sturman, O. 2001. Variable Flow Supply Using Switched-Mode Control of a Fixed-Displacement Pump. Proceedings of the Seventh Scandinavian International Conference on Fluid Power, May 30 – June 1, 2001, Linköping, Sweden, pp. 361–376 (Vol. 1).

8 Rickenberg, F. 1930. Valve. US Patent No. 1757059.

9 Bower, J. 1961. Digital Fluid Control System. US Patent No. 2999482.

10 Virvalo, T. 1978. Cylinder Speed Synchronization. Hydraulics & Pneumatics. Dec 1978, pp. 55–57.

11 Liu, R., Wang, X., Tao, G. and Ding, F. 2001. Theoretical and Experimental Study on Hydraulic Servo Position Control System with Generalization Pulse Code Modulation Control. **In:** Lu, Y., Chen, Y. & Xu, L. (Eds.) Proceedings of the Fifth International Conference on Fluid Power Transmission and Control (ICFP'2001), pp. 176–179 (International Academic Publishers, Beijing, China).

12 Tanaka, H. 1988. Electro-Hydraulic PCM Control. Journal of Fluid Control, Vol. 18, No 1, pp. 34-46.

13 Linjama, M., Huova, M., Boström, P., Laamanen, A., Siivonen, L., Morel, L., Waldén, M. & Vilenius, M. 2007. Design and Implementation of Energy Saving Digital Hydraulic Control System. Accepted for publication in the Tenth Scandinavian International Conference on Fluid Power, May 21–23, 2007, Tampere, Finland.

14 Siivonen, L., Linjama, M. & Vilenius, M. 2005. Analysis of fault tolerance of digital hydraulic valve system. **In:** Johnston, D. N., Burrows, C. R. & Edge, K. A. (eds.) Power Transmission and Motion Control, PTMC2005, pp. 133–146 (John Wiley & Sons, Ltd., 2005).

15 Siivonen, L., Linjama, M. & Vilenius, M. 2007. Fault Detection and Diagnosis of Digital Hydraulic Valve System. Accepted for publication in the Tenth Scandinavian International Conference on Fluid Power, May 21–23, 2007, Tampere, Finland.

16 Laamanen, A., Siivonen, L., Linjama, M. & Vilenius, M. 2004. Digital Flow Control Unit – an Alternative for a Proportional Valve? **In:** Burrows, C. R., Edge, K. A. & Johnston, D. N. (eds.) Power Transmission and Motion Control, PTMC2004, pp. 297–308 (Professional Engineering Publishing Ltd, 2004).

17 Ahola, V., Linjama, M., Mäkitalo, J. & Vilenius, M. 2007. High Performance Digital Hydraulic Servo System for Linear Cyclic Motion. Accepted for publication in the Tenth Scandinavian International Conference on Fluid Power, May 21–23, 2007, Tampere, Finland.

18 Linjama, M. & Vilenius, M. 2005. Improved Digital Hydraulic Tracking Control of Water Hydraulic Cylinder Drive. International Journal of Fluid Power, Vol. 6, No 1, pp. 29–39.

19 Linjama, M. & Vilenius, M. 2005. Digital Hydraulic Tracking Control of Mobile Machine Joint Actuator Mockup. Proceedings CD-ROM of the Ninth Scandinavian International Conference on Fluid Power, June 1–3, 2005, Linköping, Sweden, 16 p.

20 Boström, P., Linjama, M., Morel, L., Siivonen, L. & Waldén, M. 2007. Design and Validation of Digital Controllers for Hydraulic Systems. Accepted for publication in the Tenth Scandinavian International Conference on Fluid Power, May 21–23, 2007, Tampere, Finland.

21 Laamanen, A., Linjama, M. and Vilenius, M. 2007. On the Pressure Peak Minimization in Digital Hydraulics. Accepted for publication in the Tenth Scandinavian International Conference on Fluid Power, May 21–23, 2007, Tampere, Finland.

22 Ehsan, Md., Rampen, W. & Salter, S. 2000. Modeling of Digital-Displacement Pump-Motors and Their Application as Hydraulic Drives for Nonuniform Loads. Transactions of the ASME, Journal of Dynamic Systems, Measurement, and Control, Vol. 122, pp. 210–215.

23 http://www.artemisip.com

24 Mikkola, J., Ahola, V., Lauttamus, T., Luomaranta, M., Linjama, M. & Vilenius, M. 2007. Improving Characteristics of On/Off Solenoid Valves. Accepted for publication in the Tenth Scandinavian International Conference on Fluid Power, May 21 – 23, 2007, Tampere, Finland.

25 Winkler, B. & Scheidl, R. 2006. Optimization of a Fast Switching Valve for Big Flow Rates. **In:** Johnston, D. N., & Edge, K. A. (eds.) Power Transmission and Motion Control, PTMC2006, pp. 387–399 (Hadleys Ltd, 2006).

26 Uusitalo, J.-P., Lauttamus, T., Linjama, M., Söderlund, L., Vilenius, M. & Kettunen, L. 2007. Miniaturized Bistable Seat Valve. Accepted for publication in the Tenth Scandinavian International Conference on Fluid Power, May 21–23, 2007, Tampere, Finland.

27 Park, S.-H., Kitagawa, A., Kawashima, M., Lee, J.-K. & Wu, P. 2002. A Development of Water Hydraulic High Speed Solenoid Valve. Proceedings of the 5th JFPS International Symposium on Fluid Power, Nov. 13–15, 2002, Nara, Japan, pp. 137–142.

28 Aaltonen, J. & Vilenius, M. 2002. Electrohydraulic System For High Speed Gas Exchange Valve Actuation. Proceedings of the 5th JFPS International Symposium on Fluid Power, Nov. 13–15, 2002, Nara, Japan, pp. 775–780.

29 Laamanen, A., Linjama, M. & Vilenius, M. 2003. Characteristics of a Digital Flow Control Unit with PCM Control. CD-ROM Proceedings of Seventh Triennial International Symposium on Fluid Control, Measurement and Visualization, August 25-28, Sorrento, Italy, ISBN 0-9533991-4-1, 16 p.

30 Linjama, M. & Vilenius, M. 2004. Digital Hydraulic Control of a Mobile Machine Joint Actuator Mockup. **In:** Burrows, C. R., Edge, K. A. & Johnston, D. N. (eds.) Power Transmission and Motion Control, PTMC2004, pp. 145–158 (Professional Engineering Publishing Ltd, 2004).

31 Reynolds, G. 1989. Fluid Power Control Apparatus. US Patent No. 4,842,017.

A CAVITATION AVOIDANCE STRATEGY IN HYDRAULIC SWITCHING CONTROL BASED ON A NONLINEAR OSCILLATOR

By R. Scheidl*, H. Kogler**, and B. Manhartsgruber*

* Institute of Machine Design and Hydraulic Drives, Johannes Kepler University Linz

** Linz Center of Mechatronics GmbH

Both: Altenbergerstrasse 69, A-4040 Linz, Austria

E-mail: rudolf.scheidl@jku.at

ABSTRACT

In hydraulic switching control a cavitation critical phase is the switching from the pressure to tank line. A high tank line pressure can generate a fast onset of the flow from the tank line into the system and can avoid cavitation in this way. But for energetic reasons the tank pressure should be kept low. In this paper a method to boost the tank pressure considerably by applying a nonlinear oscillator is presented. Its performance is studied in combination with a `Hydraulic Buck Converter`. The mechanisms of generating cavitation are explained and rules for a proper dimensioning are derived by simplified mathematical models. Due to the nonlinearity a complex system behaviour may occur, like for instance a non periodic response of the oscillator.

KEYWORDS**:** Switching control, Nonlinear oscillation, Cavitation avoidance

1 INTRODUCTION

Hydraulic switching control is seen as a promising new technique to increase energy efficiency, robustness, and cost of hydraulic drives [4], [6]. Like in modern electrical machines control, on-off valves are applied and the power flow is controlled by PWM type actuation of the valves in combination with the hydraulic inductivities and capacities instead of using variable resistances like in resistance control. Very fast on-off valves are necessary to obtain a reasonable performance of such switching systems in terms of size of the components realising inductivities and capacities and in terms of dynamic response.

Less or more periodic switching to low an high pressure lines occurs in such switching systems leading to cavitation critical phases when switching from the pressure line to

the tank line. A low tank line pressure may be unable to generate a fast onset of the flow from the tank line into the system which results in cavitation in the system with high noise, energetic losses, and eventually a destruction of components.
The tank line is pre-pressurised to a pressure level p_T. To avoid cavitation in the valve off phase, an accumulator C_1 could be placed just after the valve (see Figure 1). Such an arrangement has been studied in [1]. The nonlinear characteristics of gas filled accumulators has the advantageous property that if the pressure falls below p_T there is still capacity to provide fluid until a sufficient flow is delivered from the tank line itself. But this arrangement endangers the energetic efficiency, which relies on the fluid being sucked from the tank line. Furthermore, a parasitic inductivity in the switching valve in combination with a fast switching creates a negative pressure difference and in this way may lead to cavitation at the metering edge.
In this paper an alternative arrangement according to Figure 2 with an accumulator C_1, two non return valves NRV_1, NRV_2, and a hydraulic inductivity (L_T) is investigated. The working principle of this `Buck Converter` is as follows. When switching the valve on high pressure acts on the pipe and accelerates the flow therein. When swichting the valve off, the pipe's inductivity makes the flow to move on, although in a decelerating manner. This ongoing flow sucks oil from the accumulator C_1 via the check valve NRV_2. In this way the good energetic efficiency is achieved, because despite a high consume pressure p_C part of the hydraulic fluid is coming from the low pressure line (pressure p_T). Due to switching oscillations in this accumulator/inductivity system arise, which can boost the pressure in the accumulator C_1 above the p_T –level. In the critical phase, just when the valve is switched off, this boosted pressure is able to provide sufficient flow to prevent cavitation for both pressures, p_1 and p_{val}.
There are several parameters that have to be adapted in order to get an optimal result: The size of the non return valves (their nominal flow rate Q_{NRV}), their response time, the inductivity L_T, and the accumulator's capacity (V_0) and filling pressure (p_0). The nonlinear characteristics of the accumulator is of help also in this arrangement since the feasible boost pressure is higher than of an accumulator with a linear behaviour.
The system may behave erratically. At least periodic doubling may arise then. Thus, an additional constraint on system design has to be considered in order to avoid this technically unwanted behaviour.
In this paper a theoretical study is presented which elucidates several aspects of such a cavitation avoidance system.

2 THE CAVITATION PROBLEM IN SWITCHING CONTROL

The cavitation problem in switching control and the proposed countermeasure are studied by the model problem `Hydraulic Buck-Converter`. This converter as shown in Figure 1 is the hydraulic pendant of an electrical switching converter and is studied for instance in [1, 2]. It comprises two switching valves, one for the pressure line and one for the tank line, a hydraulic inductivity L_H in form of a long transmission line, and an accumulator C_2 to suppress pressure pulsation. The cavitation critical process is the switching from high to low pressure. A quickly decreasing flow rate at the parasitic inductivity L_P needs a corresponding large negative difference pressure $p_{val} - p_1 < 0$. Cavitation just after the metering edges of the valve occurs if the absolute pressure p_1 behind L_P is smaller than this required difference pressure. Cavitation also can occur due to p_1, i.e. between the parasitic inductivities and L_H, if the flow rate build-up from the tank line is too slow to deliver sufficient fluid in the whole switching transition

phase. An important system parameter for cavitation avoidance is the tank line pressure p_T. A typical required value for the currently fastest switching valves is 15 to 20 bar.

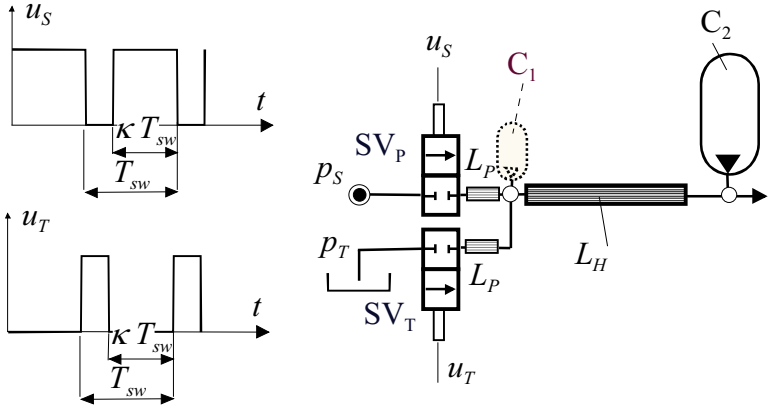

Figure 1: The elementary `Hydraulic Buck-Converter`

From an economic viewpoint this should be reduced, first, to increase the span between high and low pressure line for a higher power density of the hydraulic drive and, second, to save the energy for pre-pressurising the tank line. The latter could be avoided if a pressurised tank is used. But such a solution is technically only feasible if the tank pressure is only a few bars in order to keep the wall thickness of the tank in an acceptable range.
The explanation of the cavitation problem in switching control as given above shows that it is related to dynamical effects. This suggests to apply specific circuits which themselves exploit dynamical effects to provide additional flow during the switching transition phases in order to keep pressures at any point in the system above the vaporisation pressure of the hydraulic fluid.

3 A NONLINEAR OSCILLATOR FOR CAVITATION AVOIDANCE

It is well known that an undamped linear oscillator is dynamically doubling its static displacement if the load is applied instantaneously. This property can be used in hydraulics for pressure amplification. Higher amplification is achieved if oscillators with a progressive nonlinearity are used. In fact, the well known hydraulic ram also exploits nonlinear effects exhibited by the check valves for the conversion of kinetic energy into potential energy, even though without any elastic effects. Thus, there is a variety of principles for pressure amplification by dynamical effects. Of course, such principles are also exploited in an analogue way in electrical engineering.

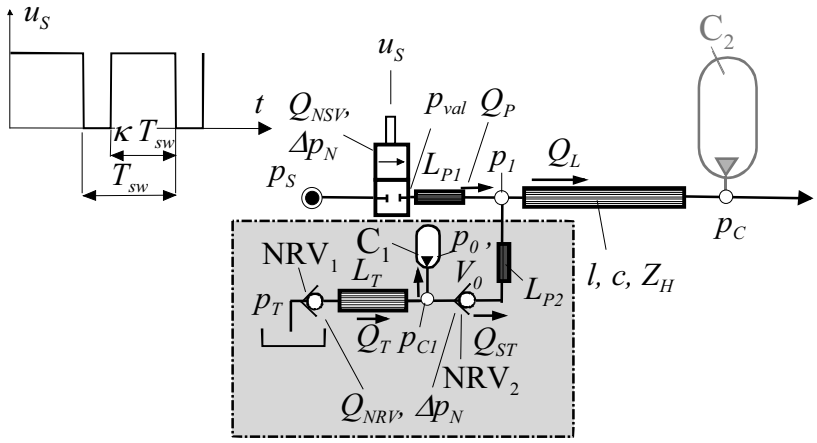

Figure 2: A nonlinear oscillator for cavitation avoidance applied to a `Hydraulic Buck-Converter`

The proposed nonlinear oscillator (further on called oscillator) is shown by its schematic in the grey rectangle in Figure 2. It consists of a hydraulic accumulator C_1, a hydraulic inductivity L_T realised by a pipe, and two non-return valves NRV_1 and NRV_2. L_{P1} and L_{P2} are parasitic inductivities. As pointed out in Section 2, L_{P1} is a major originator of cavitation and should be kept as small as possible by an appropriate design of the switching valve and its hydraulic connection to the system [3, 4]. For simplicity reasons, the pressure p_C at the accumulator C_2 is assumed to be constant. In opposite to the schematic of Figure 1 only one switching valve is present in the converter of this study, since the tank line is connected by the non-return valves of the oscillator. Of course, this allows only a positive power flow to the consumer and no energy recuperation as is feasible with the `Hydraulic Buck-Converter` according to Figure 1. Qualitative pressure and flow rate signals when the valve is switched off without a detailed consideration of the nonlinear oscillator are shown in Figure 3. p_{val} is the pressure just after the metering edges of the valve. A fast switch-off of the valve (signal V_S) creates a negative pressure difference $p_{val} - p_1$ and may cause cavitation at the metering edges of the valve.

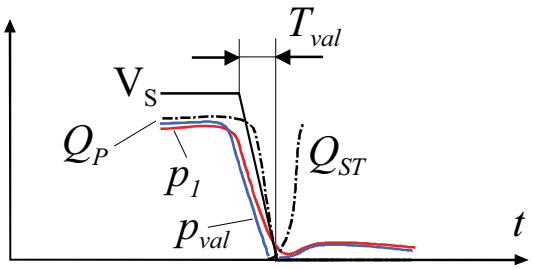

Figure 3: Qualitative pressure and flow rate signals when switching the pressure valve off

3.1 Study of the oscillator by a mathematical model

To better understand the role of the system parameters for this process a simple mathematical model is set-up. It comprises discrete models of all components shown in Figure 2 with exception of the pipe-line which constitutes the converter inductivity L_H.

This component is represented by an inviscid wave propagation model (l, c, Z_H). The system of differential and algebraic equation reads as follows

$$\dot{Q}_P = \frac{1}{L_{P1}}\left(\underbrace{p_S - \Delta p_N \left(\frac{Q_P}{Q_{NSV}}\right)^{\hat{2}} \frac{1}{y_{SV}{}^2}}_{p_{val}} - p_1 \right), \quad (u)^{\hat{2}} = u|u| \tag{1}$$

$$\dot{Q}_T = \frac{1}{L_T}\left(p_T - p_{C1} - \Delta p_N \left(\frac{Q_T}{Q_{NRV}}\right)^2 \right) \tag{2}$$

$$\dot{Q}_{ST} = \frac{1}{L_{P2}}\left(p_{C1} - p_1 - \Delta p_N \left(\frac{Q_{ST}}{Q_{NRV}}\right)^2 \right) \tag{3}$$

$$\begin{aligned} Q_L &= \frac{1}{Z_H}\left(p_r(t) + p_r\left(t - \frac{2l}{c}\right) - p_C \right) \\ p_r(t) &= p_1(t) - p_C + p_r\left(t - \frac{2l}{c}\right) \end{aligned} \tag{4}$$

$$p_{C1} = p_0 \left(\frac{V_0}{V_0 - V_{oil}}\right)^n \tag{5}$$

$$\dot{V}_{oil} = Q_T - Q_{ST}$$

Q_P, Q_T, Q_{ST} are the flow rates over the switching valve, from the tank line, and from the oscillator into the converter. p_S and p_T are the supply line pressures and are assumed to be constant for the sake of simplicity. Q_{NSV} and Q_{NRV} are the nominal flow rates at a pressure loss of Δp_N of the switching valve and the non-return valves respectively. Both non-return valves are considered to have infinitely fast response, hence the flow rates Q_T and Q_{ST} are never negative. p_1 , p_{C1} are the pressures at two points of the system (see Figure 2), $y_{SV} \in [0..1]$ is the nondimensional opening of the switching valve, V_{oil} is the volume of oil in the accumulator, V_0 its nominal volume, p_0 its filling pressure, and n the polytropic exponent of the state changes in the accumulator's gas chamber. The three hydraulic inductivities are designated L_T, L_{P1}, L_{P2}. The fluid friction in the inductivities is neglected even though it has negative effect on the intended performance for the oscillator. The flow rate Q_L enters the converter pipe which has length l, impedance Z_H , and wave propagation speed c. Its value according to (4) is based on the assumption of a constant consumer pressure p_C at the pipe exit and a periodic switching process meaning also that any other pressure and flow rate transients have faded away. p_r is the pressure characteristic propagating rightwards. In the sequel we make use of the further assumption that the converter pipe is a $\lambda/4$ resonator. This requires $4l/c=T_{sw}$ (T_{sw} is the switching period) and $p_1(t-2l/c) = p_C - (p_1(t)-p_C)$ and reduces (4) to $Q_L = p_1(t)/Z_H$.

The converter system notices two phases regarding the effect of the oscillator

- Phase 1: no flow from the oscillator $Q_{ST} = 0$
- Phase 2: a positive flow from the oscillator $Q_{ST} > 0$

A negative flow is prohibited by the non-return valve NRV_2 which throughout this analysis is considered an ideal valve with an infinitely fast response.

Phase 1:

As long as cavitation is not present $Q_P = Q_L$. Then, the behaviour of the converter is described by the nonlinear, time dependent differential equation

$$\dot{Q}_P = \frac{1}{L_{p1}}\left(p_S - \Delta p_N \left(\frac{Q_P}{Q_{NSV}} \right)^{\hat{2}} \frac{1}{y_{SV}{}^2} - Q_P Z_H \right) \tag{6}$$

$$y_{SV} = 1 - t / T_{val}$$

An analytic solution could not be found, but to obtain a good understanding of the qualitative properties of the solution, it is useful to consider the limit case $L_{P1} \to 0$ and its perturbations by small values of the parasitic inductivity L_{P1}. The limit case solution $L_{P1} \to 0$ reads

$$Q_P = \frac{y_{SV} Q_{NSV}}{2\Delta p_N}\left(\sqrt{(Z_H Q_{NSV} y_{SV})^2 + p_S \Delta p_N} - Z_H Q_{NSV} y_{SV} \right) \tag{7}$$

A parasitic inductivity L_{P1} tries to preserve an existing flow rate Q_P, thus the corresponding solution curve is initially more flat and finally declines to zero quite rapidly when the valve reaches its closed position.

In order to keep the two pressures

- p_{val} and
- p_1

positive in this phase, the following relations must be valid

$$p_{val} = p_S - \Delta p_N \left(\frac{Q_P}{Q_{NSV}} \right)^2 \frac{1}{y_{SV}{}^2} > 0 \tag{8}$$

$$p_1 > 0$$

The second criterion (8) is not violated in the very special case that the pipe length is a quarter of the wave length as assumed above to obtain a simple mathematical model. But cavitation at p_1 may occur in other cases.

The qualitative solution properties of (6), (7) and the inequality relations (8) can be studied with a diagram according to Figure 4.

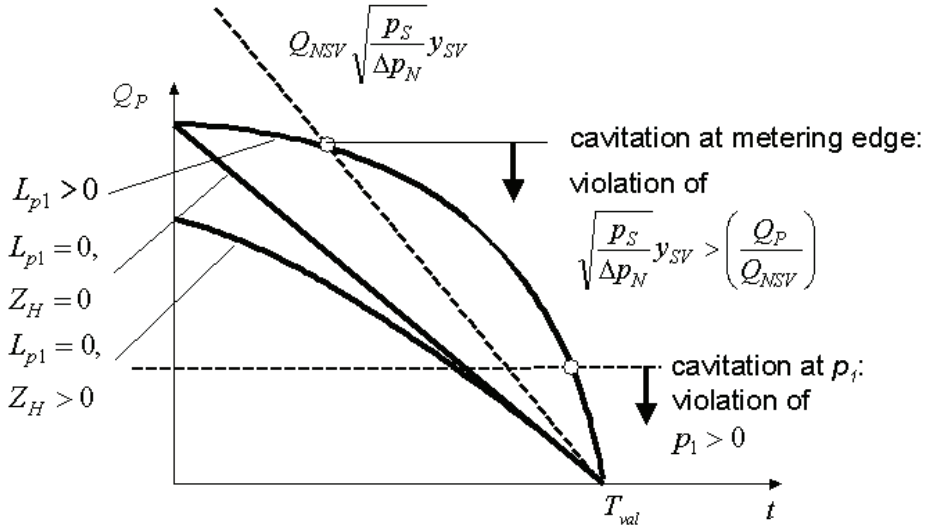

Figure 4: Qualitative solution of (6) and cavitation criteria

The results shown in this Figure indicate very clearly that parasitic inductivities should be kept small in order to avoid cavitation at the metering edges of the valve. Of course, the solutions shown are only valid as long as no flow from the oscillator enters the converter. Such a flow is a must in a generic switching system to avoid cavitation after the inductivity L_{P1}. Generic switching means that the system in the actual operating condition (flow rate, pulse width κ, consumer pressure p_C) is able to suck oil from the low pressure line.
The role of the oscillator is to provide a pressure high enough to submit fluid to the converter before one of the two cavitation avoidance criteria (8) is violated. From Figure 4 one concludes that a higher pressure provided by the oscillator reduces the risk of cavitation because it rises p_1.

3.2 Behaviour of the oscillator

From a design point of view it is important to know the essential system parameters by which the oscillator can be adapted for a certain converter and how the performance depends on these parameters. Since the oscillator couples with the converter there are numerous system parameters influencing the system behaviour. Since a closed form solution for the system of nonlinear equations is most unlikely to obtain, further simplifications are made which are partly driven by some idealised understanding of the converter and the oscillator.
The first simplification is to replace the converter by an assumed pressure curve $p_1(t)$ in order to concentrate on the oscillator's behaviour. The assumed ideal pressure characteristic consists of periodic rectangular pressure pulses with the two pressure levels p_S and $p_{1,0}$ respectively (see Figure 5). The oscillator model of above has the three states Q_T, Q_{ST}, and V_{oil}. But if we omit the inductivity L_{P2}, Q_{ST} is determined by an algebraic equation only, hence only two states are left and the system behaviour can be studied in a phase plane.
With the following scales

$$Q_T = q_T Q_{NRV};\ Q_{ST} = q_{ST} Q_{NRV};\ V_{oil} = v_{oil} Q_{NRV} T;\ V_0 = v_0 Q_{NRV} T;\ \frac{T\Delta p_N}{L_T Q_{NRV}} = \frac{1}{l_L};$$
$$p_0 = \psi_0 \Delta p_N;\quad p_T = \psi_T \Delta p_N; p_1 = \psi_1 \Delta p_N;\quad p_{C1} = \psi_{C1} \Delta p_N;\ t = \tau T;\ \frac{d}{d\tau} = (\,)' \tag{10}$$

the system equations in nondimensional form read

$$q_T' = \frac{1}{l_L}\left(\psi_T - \underbrace{\psi_0 \left(1 - \frac{v_{oil}}{v_0}\right)^{-n}}_{\psi_{C1}} - {q_T}^2 \right);\quad q_T \geq 0$$
$$v_{oil}' = q_T - \sqrt{\underbrace{\psi_0 \left(1 - \frac{v_{oil}}{v_0}\right)^{-n} - \psi_1}_{\geq 0}} \tag{11}$$

The effect of the ideal non-return valves is represented by the two inequalities in (11). A typical steady state behaviour of the system is shown in Figure 5 by the phase diagram and by a time plot. In this diagram v_{oil} is replaced by the nondimensional accumulator pressure ψ_{C1} (see first equation in (11) how both values are related to each other) because this enables a more immediate hydraulic interpretation of the results. There are 3 distinguished phases:

Phase 1 (P_4-P_1): The pressure p_1 drops from p_S to $p_{1,0}$. Oil is delivered from the accumulator to the converter, the pressure in the accumulator ψ_{C1} decreases.

Phase 2 (P_1-P_3): ψ_{C1} has fallen below the tank pressure ψ_T. A flow q_T from the tank over the inductivity L_T is setting on. ψ_{C1} firstly decreases, but when q_T exceeds q_{ST} it increases. P_3 is a stationary point which is reached by the system asymptotically. For a high pulse width κ or when the natural frequency of the oscillator is not high compared to the switching frequency $1/T_{SW}$ the system may fail to come close to this stationary point P_3.

Phase 3 (P_3-P_4): Pressure p_1 switches to p_S. The flow q_{ST} stops immediately and the inductivity L_T is driving a flow q_T against a rising pressure ψ_{C1} in this way boosting ψ_{C1} above ψ_T.

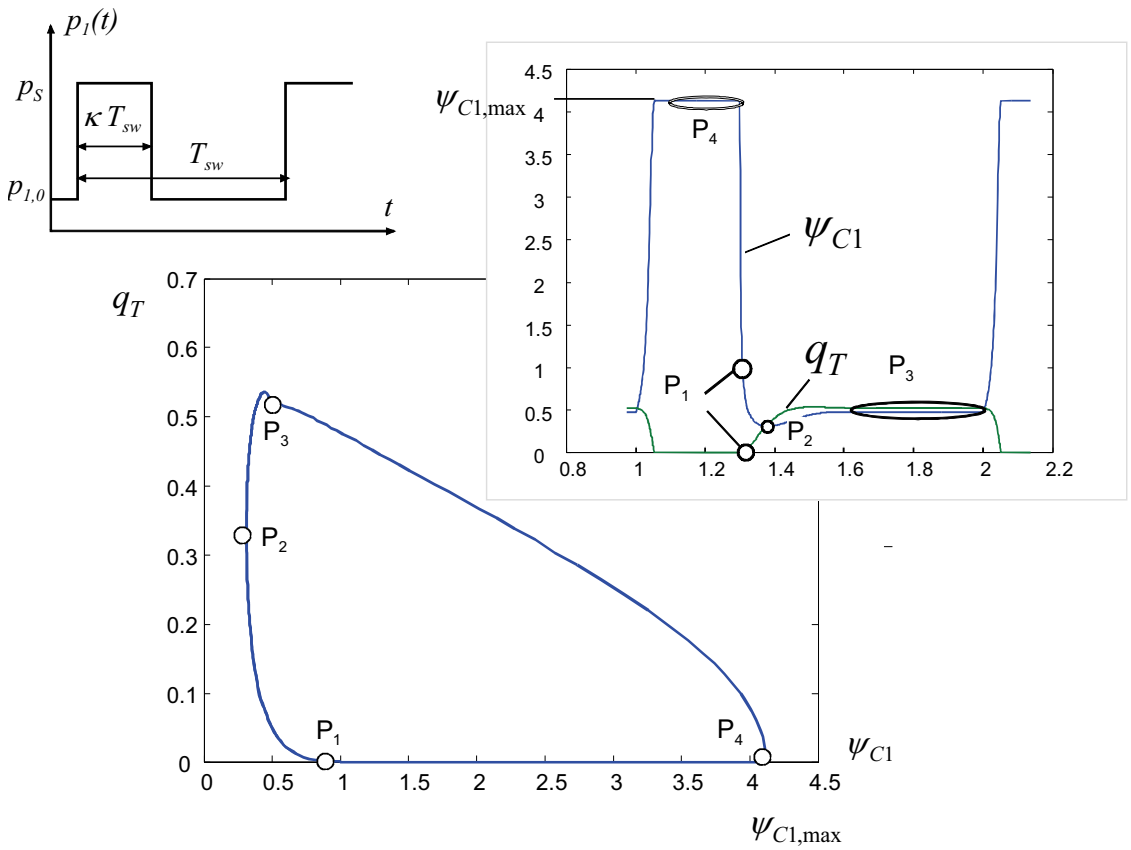

Figure 5: Typical steady state solution of (11)

It has been outlined in Section 3.1 that a high boost pressure is helpful for avoiding cavitation. Furthermore, it helps also to increase the flow from the tank-line into the converter which is important to optimise the energy efficiency.
In the following a rough estimate for the achievable boost pressure $\psi_{C1,max}$ (ψ_{C1} at P_4) is derived. From (11) the state values of the stationary solution P_3 can be easily computed.

$$P_3:\ q_T = \frac{\sqrt{2}}{2}\sqrt{\psi_T - \psi_{1,0}}\ ; \quad v_{oil} = v_0\left(1 - \left(\frac{2\psi_0}{\psi_{1,0} + \psi_T}\right)^{\frac{1}{n}}\right) \tag{12}$$

If in phase 3 any friction is neglected (by omitting the term q_T^2 in the first equation of (11)) and because $v'_{oil} = q_T$ is valid, (11) constitutes a Hamiltonian system. Then a first integral of (11) is given by the energy content H.

$$H = \tfrac{1}{2} q_T{}^2 - \frac{1}{l_L}\int_0^{v_{oil}} \left(\psi_T - \psi_0\left(\frac{1}{1 - u/v_0}\right)^n\right) du \tag{13}$$

In other words, the phase curve P_3- P_4 is approximated by a curve $H=H_0=Const.$ The value of H_0 is computed by inserting the solutions of (12) into (13). The pressure value or value of v_{oil} respectively of P_4 can be computed by setting $q_T = 0$ and $H=H_0$ in (13) and solving for v_{oil}.

The respective equation can be brought into the following form which allows to assess the role of the main system parameters on the boost pressure.

$$\delta(n-1)+\underbrace{\frac{y_0}{\delta^{n-1}}}_{\psi_{C1,\max}/\psi_T}=\frac{l_{Lv0}}{4}\psi(n-1)(1-y_{1,0})-\tfrac{1}{2}\left(\frac{2y_0}{1+y_{1,0}}\right)^{\frac{1}{n}}(y_{1,0}+2n-1)$$
$$\delta=\frac{v_0-v_{\ddot{o}l}}{v_0};\quad y_0=\frac{\psi_0}{\psi_T};\quad y_{1,0}=\frac{\psi_{1,0}}{\psi_T};\quad l_{Lv0}=\frac{l_L}{v_0} \tag{14}$$

To achieve a high $\psi_{C1,max}$ δ must be small. If this holds true, the first term on the left hand side of (14) can be omitted against the second and an explicit relation for $\psi_{C1,max}$ is obtained. It is nearly proportional to l_{Lv0} and increases with a lower accumulator filling pressure ψ_0 and a lower converter entrance pressure $\psi_{1,0}$. Of course, the quotient of ψ_0 and $\psi_{C1,max}$ must not drop below a certain value for reasons of durability of the accumulator's membrane or bladder. Also $\psi_{1,0}$ must stay above some value in order to avoid cavitation securely.
A condition for the validity of this result is that the system comes close to the stationary point P_3. If the inductivity is too high, this will not be true and a lower pressure will arise. To keep the above considerations valid the response time of the oscillator must not exceed the time for Phases 1 plus 2. Practically only Phase 2 counts because Phase 1 lasts only a comparatively short time. A reasonable estimate of the response time can be derived by the following argument: In Phase 2 - which starts when ψ_{C1} falls below ψ_T - ψ_{C1} can be roughly estimated by its stationary value at P_3. If this estimated value is inserted in the first equation of (11) the following nonlinear differential equation for q_T results.

$$q_T'=\frac{1}{l_L}\left(\psi_T-\psi_{C1,P_3}-{q_T}^2\right) \tag{14}$$

It has the solution

$$q_T(\tau)=\tanh\left(\frac{\sqrt{\psi_T-\psi_{C1,p_3}}\,\tau}{l_L}\right)\sqrt{\psi_T-\psi_{C1,p_3}} \tag{15}$$

with an approximate response time $l_L/\left(\psi_T-\psi_{C1,P_3}\right)$.
What is the limiting or optimisation criterion for the accumulator size v_0 ? It is mainly responsible for keeping the minimum pressure (at point P_2) reasonably above the cavitation level for all operating conditions. To evaluate this criterion the converter's dynamics must be incorporated in the study. The last model with a replacement of the converter by a rectangular pressure curve for $p_1(t)$ cannot give answer to this question.

3.3 A numerical study

The system equations (1) to (5) have been cast into a Matlab/Simulink model to study the behavior of the nonlinear oscillator in combination with the simple converter model.

In this numerical study most of the simplifying assumptions of the analytical investigation are replaced by more realistic assumptions. Switching and non-return valves are no more ideal but have finite response times. In Figure 6 to Figure 8 some results are shown, indicating the improvement potential of the oscillator for cavitation avoidance but also some difficulties regarding the oscillation behavior of the whole system.

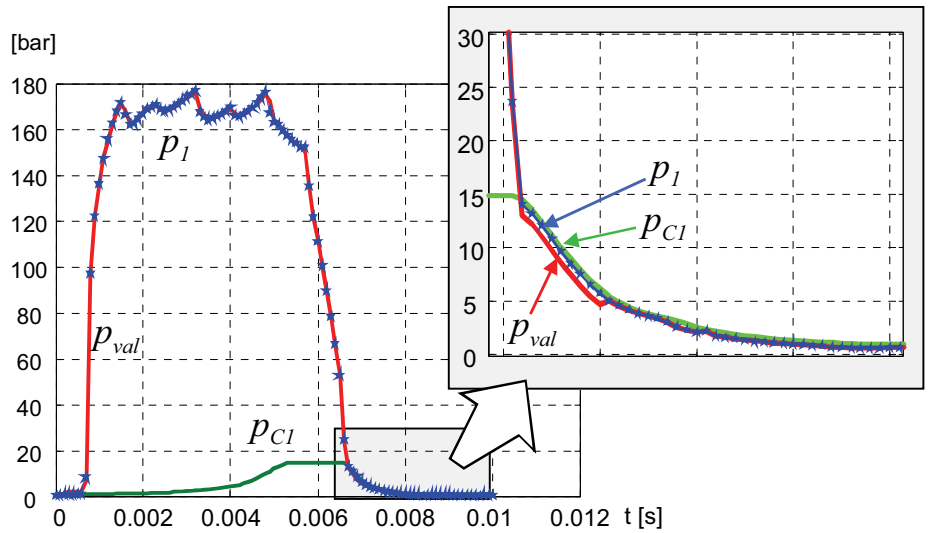

Figure 6: One period of a steady state solution of system (1) – (5); (data: Q_{NSV} = 50 l/min, Δp_N =5 bar, L_{P1} = 43000 kg/m^4 (pipe of length 5 mm and cross section of 1 cm^2), l = 2.658 m, Z_H = 0.218 10^{11} kg/(m^{4}s), L_{P2} =0, Q_{NRV}=360 l/min, V_0 = 2cm^3, p_0 = 1 bar, L_T = 0.219 10^7 kg/m^4, (pipe of length 0.2 m and diameter of 1 cm), T_{SW} = 0.01 s, T_{val} = 0.002 s, κ = 50%, p_S = 180 bar, p_T = 3 bar p_C = 90 bar; Simulation parameters: Simulink R 12.1, Integration: variable step, ode23s (stiff/Mod. Rosenbrock), max. step size: 10^{-5}, min step size: 10^{-9}, initial step size: 10^{-6}, relative tolerance 10^{-4}, absolute tolerance: auto).

This result shows clearly the enormous boost capacity of the nonlinear oscillator. It is able to rise a tank pressure of only 3 bar to a boost pressure of 15 bar and contributes in this way considerably to cavitation avoidance. The depression of p_{val}, to be seen in the magnification, results from the parasitic inductivity and lasts till the valve is totally closed. The faster the valve closing and the higher the inductivity, the higher this depression which can lead to cavitation at the metering edge. A high boost pressure at p_1 can avoid this cavitation if it is higher than the pressure difference needed for the deceleration of the flow rate in this closing phase.

Figure 7 demonstrates the cavitation resulting from a too high parasitic inductivity L_{P1} in case of a fast switch-off. A deceleration of the flow rate requires a pressure difference of about 40 bar which, despite the high boost pressure of the nonlinear oscillator of about 15 bar, creates negative pressure in the simulation model because this model does not account for the cavitation phenomenon.

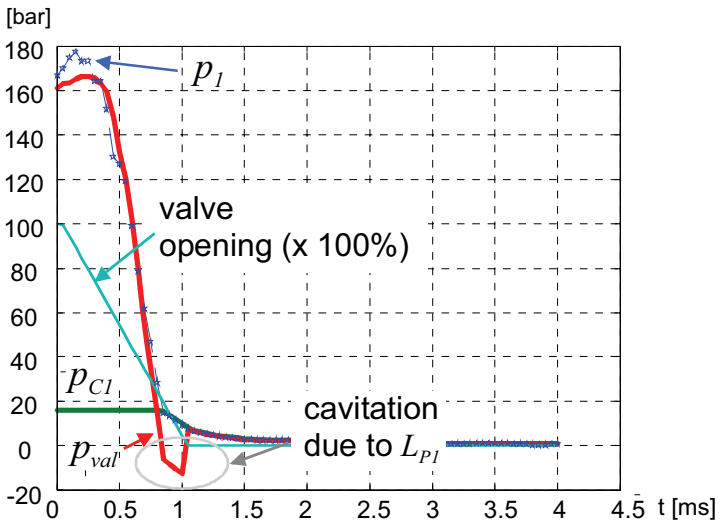

Figure 7: One period of a steady state solution of system (1) – (5); (data: L_{P1} = 430 000 kg/m^4 (pipe of length 50 mm and cross section of 1 cm^2), T_{val} = 0.001 s; all other data as in Figure 6).

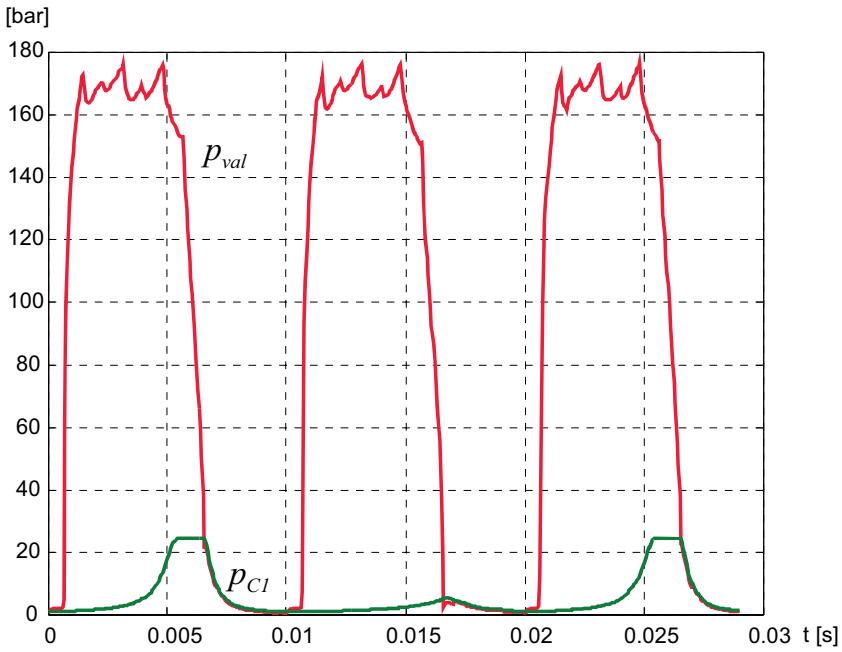

Figure 8: Three periods of a quasi steady state solution of system (1) – (5); (data: V_0 = 3.5 cm^3; all other data as in Figure 6).

The system behaviour according to Figure 8 results from an increased accumulator size and shows a double periodicity of the nonlinear oscillator. In terms of bifurcation theory this corresponds to a so called flip-bifurcation (see, e.g., [5]), resulting from an unstable periodic solution of a periodically excited nonlinear dynamical system. Currently it is an open question if an even stronger irregular system response such as chaotic behaviour may occur.

Comparing these numerical results with the findings of the analytical investigation which had to be based on several simplifying assumptions one can say:

- The oscillator is performing as expected
- Those imperfections of the system which are not included in the analytical model, like the finite response times of the valves and the additional parasitic inductivities, do not degrade its performance in a very significant way
- The most severe problem results from the complex system dynamics which may lead to phenomena like periodic doubling

4 CONCLUSION AND OUTLOOK

A periodically excited nonlinear oscillator consisting of a hydraulic inductivity in form of a pipe, a gas filled accumulator, and two non return valves can be used to boost a relatively low tank pressure to considerably higher values. This capability is of high interest in hydraulic switching control particularly to avoid cavitation occurring in the phase of switching off the pressure valve. Even in case of the relatively simple `Hydraulic Buck Converter` a remarkable complexity of the system behaviour arises. This could be seen from a few numerical studies. In the analysis presented, simplified models have been applied to figure out the main functioning principles and characteristics of the oscillator and also some modes of interaction with the converter. A few rules for a proper dimensioning have been derived and presented.
So far, no experimental validation of such a nonlinear oscillator as a hydraulic pressure boost device has been made. Experimental investigations and a more extended analysis of the behaviour of the full system, comprising the oscillator and the converter, will be made in the future.

ACKNOWLEDGEMENT

The authors gratefully acknowledge the sponsoring of this work by the 'Linz Center of Competence in Mechatronics' in the framework of the Kplus program of the Austrian government. This program is funded by the Austrian government, the province Upper Austria and the Johannes Kepler University Linz.

REFERENCES

[1] R. Scheidl, B. Manhartsgruber, H. Kogler. Hydraulic Switching Control with a Nonlinear Converter" , Proceedings of the 5th MATHMOD Vienna, in I. Troch, F. Breitenecker, 2006.

[2] H. Kogler, B. Winkler, R. Scheidl,. Flatness based Control of a Fast Switching Hydraulic Drive. 2nd International Conference on Computational Methods in Fluid Power, FPNI'06, August 2-3, 2006, Aalborg, Denmark.

[3] R. Scheidl, B. Steiner, B. Winkler, G. Mikota. Basic problems in fast hydraulic switching valve technology. 6th Intern. Conf. on Fluid Power Transmission and Control (ICFP' 2005), April 5-8, Hangzhou, China, 2005.

[4] R. Scheidl, B. Manhartsgruber, G. Mikota, B. Winkler, State of the Art in Hydraulic Switching Control – Components, Systems, Applications, Proc. Ninth

Scandinavian International Conference on Fluid Power (SICFP'05), June 1-3, 2005, Linköping, Sweden.

[5] J. Guckenheimer, Ph. Holmes, Nonlinear Oscillations, Dynamical Systems, and Bifurcations of Vector Fields. Spinger Verlag, New York, Berlin, Heidelberg, Tokyo, 1983.

[6] R. Scheidl, M. Garstenauer, B. Manhartsgruber, Switching Type Control of Hydraulic Drives - A Promising Perspective for Advanced Actuation in Agricultural Machinery, Proceedings of International SAE Off Highway and Powerplant Congress, September 2000, Milwaukee, WI, USA.

FAULT DETECTION AND DIAGNOSIS OF DIGITAL HYDRAULIC VALVE SYSTEM

Lauri Siivonen, Matti Linjama, Mikko Huova and Matti Vilenius
Tampere University of Technology
Institute of Hydraulics and Automation
P.O.Box 589
33101 Tampere, Finland
Phone +358 3 3115 4439, Fax +358 3 3115 2240
E-mail: lauri.siivonen@tut.fi

ABSTRACT

Fault detection and fault diagnosis is the key into fault tolerance of components. Interest on this area has increased a lot lately when measurement systems have developed and hydraulic systems have gotten more complex. Although reacting into faults has not been studied so much, research on fault adaptive systems has increased a lot also. The limitation for this has so far been the lack of components that are capable of operation in case of a failure. Previously only possible solution has been doubling of components but in practice this has been used only in extreme applications. Digital hydraulics has some good features concerning fault tolerance. The system is capable for acting in fault situation with only a small degradation in performance without having to add expensive and troublesome extra components into he hydraulic circuit. This paper concentrates on detecting different kind of valve faults and reacting into them by re-configuring the controller. The fault detection is done by using control electronics internal diagnostics signals and by measuring voltage differences over the valve coils. The signals are diagnosed and the control code is then re-configured according to the fault. The detection and reacting into faults is done on-line and the results show that the system is capable of acting without significant degradation in performance even if rather severe faults occur.

KEYWORDS: Fault detection, diagnosis, digital hydraulic valve system, fault tolerance

1 INTRODUCTION

Fault detection and diagnosis (FDD) is the key into fault tolerance of components [1]. Possible fault must be detected and the effect of it diagnosed so that control can be re-

designed [2]. The area has been researched a lot from several different point of views [3, 4]. In hydraulics, the main area is fault tolerance, detection and monitoring of complete hydraulic systems [5, 6, 7, 8, 9]. Research has also been done in component level e.g. with actuators [10], with hydraulic fluids [11] and with pumps [12].

Hydraulic flow control valves are used to control actuators. As a component, valve is somewhat critical part of the system. Monitoring, fault detection and fault diagnosis of hydraulic valves has also been researched a lot. Probably the most critical systems are in aerospace and nuclear applications where faults may cause extreme consequences [13, 14, 15]. Also in more common systems, valves are still critical components since without parallel connection of several valves they are single point of failure (SPoF) items in serial system [14]. Neural networks has been used in many applications to analyze the difference between normal operation and faulty acting valve [16, 17].

Fault detection and diagnosis is not enough to fulfill the demands of fault-tolerant system. After the fault is found and located, it must be either repaired or taken into account so that the effect is minimized and normal operation is possible. Usually small degradation in performance can be accepted [3, 4, 18]. Reacting into valve faults is difficult in traditional proportional or servo systems. Usually only possible thing to do is to increase or decrease current e.g. in PWM controlled proportional pilot valve. In critical systems, such as aerospace applications, valves can be doubled and in case of a failure the faulty acting valve is isolated from the rest of the hydraulic system and back-up valve is taken into action. This on the other hand demands two valves and increases price, size and complexity of the hydraulic system and therefore has not become a general solution. Siivonen et al. [19] presented a digital hydraulic valve system that can react into faults by re-configuring the valve controller. The results were promising since the system is able to operate with only a small degradation in performance even if one of its valves is acting faulty. Still the system is not doubled and no back-up valves are needed.

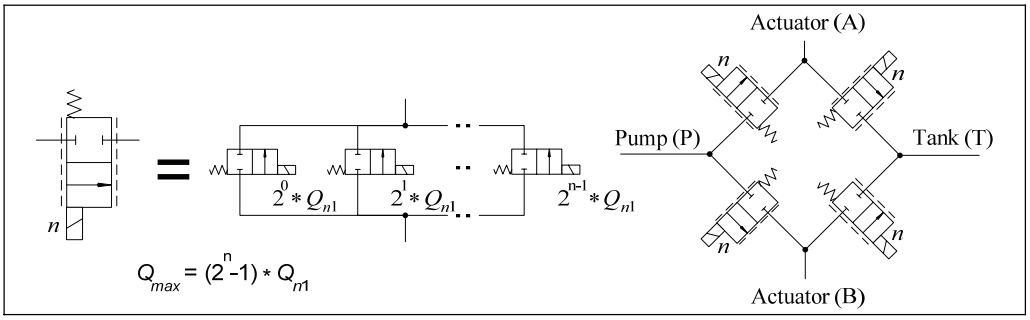

Figure 1. Digital flow control unit and digital hydraulic valve system

Digital hydraulic valve system is basically a four-way hydraulic flow control valve capable for controlling all four flow paths separately. The system consists of four valve series all containing simple on/off valves that are connected in parallel according to certain coding scheme [20]. The parallel connected valve system is called a digital flow control unit (DFCU) [21]. The drawing symbol and internal structure of a DFCU is presented in Figure 1. Passive fault accommodation of the system is relatively good since only simple and reliable on/off valves are used. The system is also not so sensitive to oil contamination since the filtration requirements for on/off valves are not so strict [22, 23]. Some another advantages are simple structure, good performance and small

number of different valve variations [24]. The digital hydraulic valve system is controlled with fully programmable controller. The control code includes all the functions that the valve system is capable of doing. This includes for example anti-cavitation function, counter balance function and energy saving functions [25]. The programmability and parallel connected valves also allow the fault-tolerant control of the system.

2 FAULT TOLERANCE OF DIGITAL HYDRAULICS

Parallel connection of hydraulic on/off valves makes fault tolerance possible. Single point of failure does not cripple the digital hydraulic valve systems since none of the individual valves are vital for valve operation. If a fault occurs and system detects it the controller can be re-configured according to fault diagnosis information. The re-configuration procedure depends on fault type and magnitude.

Table 1. Possible fault situations of an on/off valve

Fault	Opening of valve when control signal is off	Opening of valve when control is on	Case
Normal situation	0	1	-
Valve jammed closed	0	0	I
Valve jammed open	1	1	II
Valve jammed in an intermediate position	x	x	III
Valve does not open fully or valve throughput reduced for another reason	0	x	IV
Valve does not close fully	x	1	V
Valve does not close nor open fully	x	y	VI

Table 1 shows six different fault situations. All possible faults that can occur in a valve are not listed in this table since only static faults are studied at this point. For example some dynamic faults such as increasing of opening or closing delay are not included except if the increasing is so long that it seems static to sensors.

Fault tolerance of digital hydraulic valve system has been previously studied by Siivonen et al. and the results have been promising. The possibility for adapt into type I fault (See Table 1) has been tested in real system and controller re-configuration works well in fault situations. If small degradation in system performance can be accepted, the system is capable of operating under influence of fault. The test results also show that in binary coded system, big valves have greater effect for controllability than small valves. Figure 2 presents a binary coded system with 5 valves connected in parallel. In the upper row the fault has not been detected and in the lower row the controller has been re-configured. The main difference is that in lower row the amount of possible openings is smaller but the opening of DFCU is clearer when throughput of the valve system increases if the control signal is increased. [19, 26]

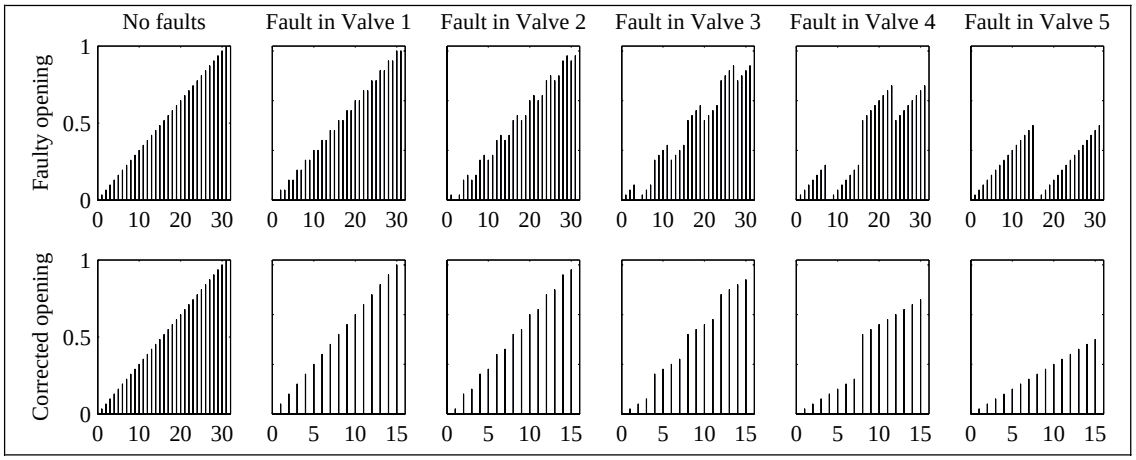

Figure 2. DFCU performance and fault compensation in type I fault.

The analysis of digital hydraulic valve system under fault type II (See Table 1) showed that it is also possible to adapt in this kind of problem. The rest of the fault types in Table 1 are more or less combinations of types I and II. [19]

The coding method has also an effect on fault tolerance of the system. Laamanen et al. has been studying the use of different kind of coding schemes to avoid pressure peaks in state transitions [27, 28]. The same principle also works with fault tolerance. For example Fibonacci coded series has the advantage that certain flow rate can be achieved with several different valve opening combinations. The best coding method for fault tolerance would be pulse number modulation (PNM) where all valves have same flow rates. In order to achieve good performance and small size for the system, the number of valves is too big.

3 FAULT DETECTION AND DIAGNOSIS

Fault must be detected so that it can be taken into account. Faults can be searched in both on- and off-line, during normal operation and stoppages. The best possible case would be on-line FDD that could detect and analyze all possible faults without any sensors. In real life this is however not possible and some compromises must be made. In general the system needs a sensor or multiple sensors to detect abnormalities in behavior. In case of hydraulics, the characteristics of the studied valve must also be known relatively well. The on-line fault detection is more efficient since possible fault does not necessary have time to influence the process itself. However this is dependent on the application. In critical systems, such as aerospace or marine hydraulics, faulty behavior may cause severe damage whereas in some other applications faulty acting does not necessarily affect the result significantly.

The behavior of a single valve can be monitored in many different ways. Perhaps the most commonly used methods are coil current measurement and spool displacement. Spool position measurement is an effective way to detect unwanted behavior in valve actuation. On the other hand this also demands a position sensor to be installed in valve and therefore some changes in mechanical structure may be mandatory. Pressure sensors are also often used for fault detection since they quite often already exist in hydraulic system.

The hydraulic system is not limited only into hydraulic valve and therefore in some applications there is a possibility to use e.g. actuator position, velocity or angle to define the current status of the hydraulic valve. This is strongly dependent on the application and the use of this kind of measurement is case-specific. In digital hydraulics, the fault detection is relatively simple since the functioning of a single on/off valve is relatively easy to check.

3.1 Electrical measurements based FDD

Electrical measurements are the most simplest to include into digital hydraulic valve system. For example current or voltage measurements from valve coil are relatively simple and inexpensive to apply. Also if some electrical components have diagnostics signals of their own, the amount of extra sensors is decreased. The sensors shouldn't be too sophisticated since they demand more complex measuring system, better filters and protection against different kind of disturbances. Accurate sensors also cost more and might not be as reliable as simple ones.

The digital hydraulic valve system that is used in this study has a control electronic system with an integrated fault diagnostics sensor. The sensor is located in DRV102T PWM controller in booster circuit. Normally the component is used to create a boost voltage for valve opening and then hold voltage to keep the valve open. This control method is introduced in detail by Mikkola et al. [29]. The component has internal diagnostics for high temperature, over- and under-current. The diagnostics signal is not omniscient and therefore some extra sensors are needed. The current of all valves in digital hydraulic valve system could be measured but that would require many sensors, a/d converters and more complex code. An easier way is to measure only 1 bit information of the current. In this study this is realized with optocoupler and a couple of resistors. The connection is very simple and easy to apply into any control electronics. The price in mass production is also an issue and with this kind of solution it can be kept low as well. Fault diagnostics still remains simple with these sensors.

Figure 3 presents the fault diagnostics of one valve during one sample time. At first the present control signal is checked. Then the PWM driver diagnostics signal is measured and in case of 0, fault exists. The voltage difference information provided by optocoupler is then used to identify this fault or to seek for failures that were undetected by PWM driver. When this same diagnostics is applied into all valves in digital hydraulic valve system on-line, faults such as cable breaks or broken components, can be found. This method is also tested in this study.

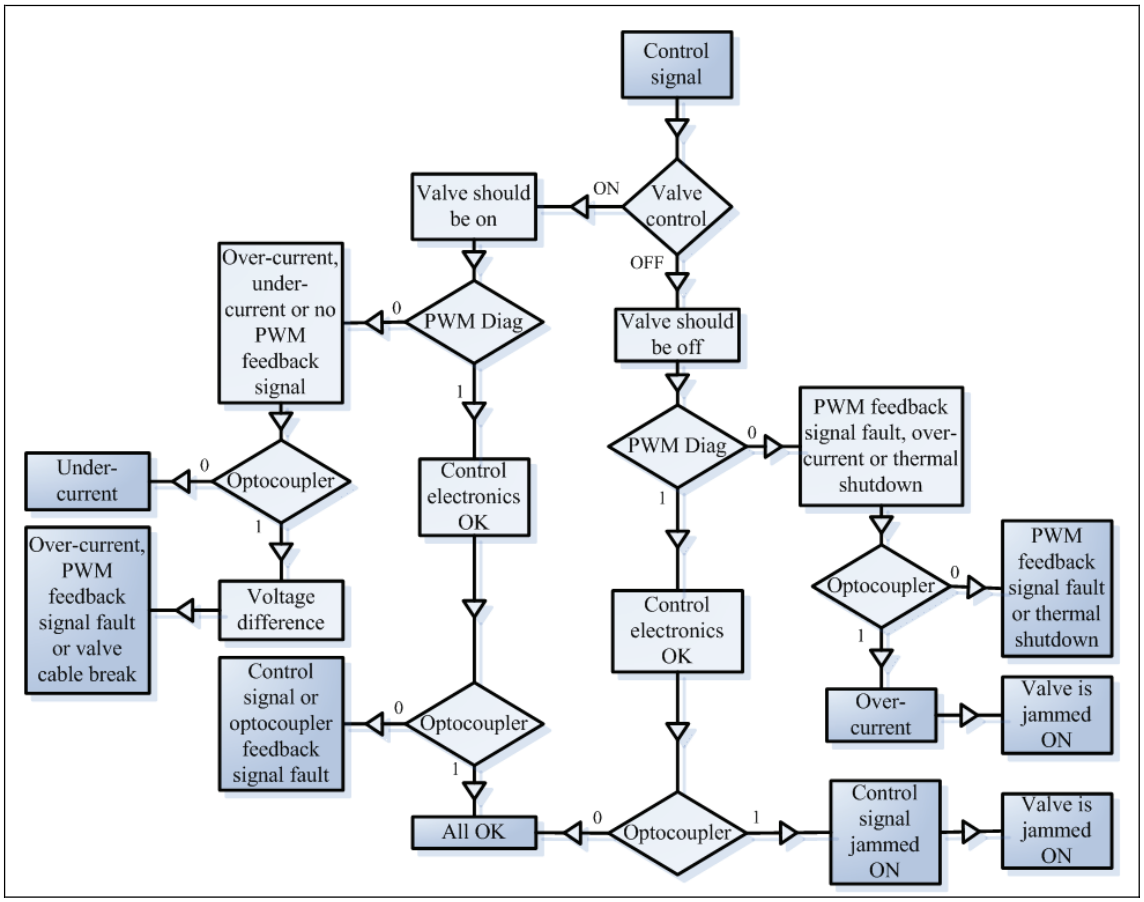

Figure 3. Fault diagnostics of one on/off valve with two sensors

4 TEST SETUP

The studied fault detection and diagnosis method is tested in a hydraulic boom equipped with a digital hydraulic valve system. Several different kinds of faults are caused into the system and functioning of FDD capabilities among with fault reaction techniques of controller are studied.

4.1 The digital hydraulic valve system

The studied digital hydraulic valve system consists of four DFCUs which are in modified binary series. The binary series is done with orifice disks mounted on the bottom of the cavity between the valve block and the valve. Each DFCU has five Hydac WS08W-01 directly controlled seat type screw-in on/off valves with 12 VDC solenoids. The orifices are set so that the two biggest valves are the same size and smaller ones are set to binary series. This is done in order to increase the maximum flow rate of the DFCU so that it fits to the cylinders installed into the boom. This decreases control performance slightly but is still necessary to achieve reasonable velocity with the boom tip. The modified binary sequence has also an effect to the fault tolerance of studied system. This reduces the effect of a fault in case of the biggest valve since the maximum flow rate is smaller and thereby improves the fault tolerance of the valve system. The exact hydraulic circuit of the valve system, flow rates and performance are better described by Linjama et al. [25]. The valves are controlled with 20 channel control box

based on PWM voltage modulation. The control box has internal opening and closing boost in order to improve valve dynamics. The valve system is controlled with AMD Opteron –based dSPACE DS1006 microcontroller board and the valve control box is controlled via DS4003 I/O card.

4.2 Fault detection hardware

The faults are detected with two different methods. Currents from each solenoid are measured as Boolean signals (current on or current off). The measurement is done with Vishay SFH6156-2T optocoupler by connecting it in parallel with the valve coil. The optocoupler senses voltage difference over the coil. The sensor is protected with 10kΩ series resistor and the output signal is TTL type.

The internal diagnostics of DRV102T PWM driver can tell if the output corresponds to the input signal of the driver. Possible faults that can be detected are over-current, under-current and thermal shut-down. The diagnostics signal only tells the existence of the fault but not the type of it. The signal is pull-down type so TTL signal 1 means that input corresponds to the output and 0 means a fault. Figure 4 presents a simplified circuit diagram of the fault detection hardware and locations where faults are caused.

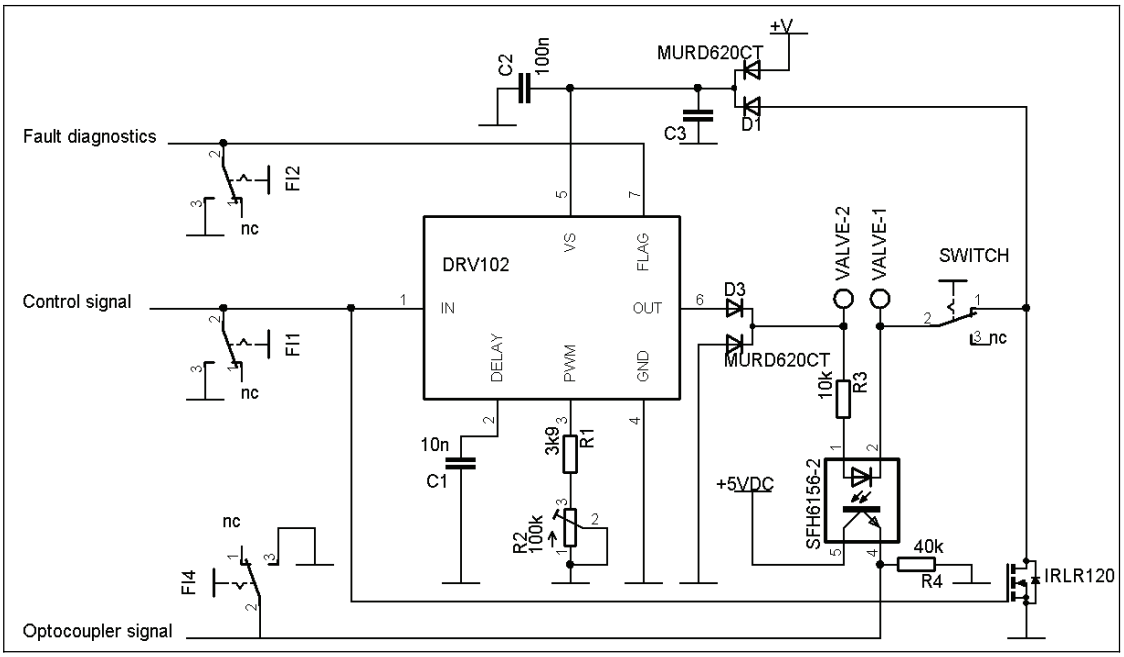

Figure 4. Simplified circuit diagram of the fault detection hardware and fault injection points

4.3 Controller

The controller is basically the same as was used by Linjama et al. in energy saving research [25]. The energy saving functions however are not used in these measurements to avoid unnecessary interference and to study FDD features of the system better. Same controller parameters are used also in this study. The fault detection and diagnostics

features are added to the controller and no extra parameters are needed. The sampling time for the controller is 24 ms and for the measurements 12 ms.

4.4 The test boom and hydraulic circuit

The valve system is tested with a hydraulic boom that has similar dynamics as with a boom used in middle sized mobile machines. The same boom has also been used by Linjama et al. [25]. The boom is four meters long and it is pivoted from the centre. The transmission ratio between boom tip and cylinder piston is about 10. The test system is presented in Figure 5. The load masses are set to almost balanced load (Mass 1: 200 kg, Mass 2: 50 kg, Mass 3: 150 kg). The supply pressure is controlled with Bosch Rexroth DBEME 10-5X/200YG24NK31M proportional pressure relief valve by using a closed-loop non-linear PI-controller and by utilizing measured characteristic curve and feedforward from flow rate. The supply pressure control mimics a LS-system and the load is measured with pressure sensors. The boom is controlled with two parallel connected 63/36-200 hydraulic cylinders and port pressures are limited with pressure relief valves for safety reasons to 25 MPa. The hydraulic accumulator shown in Figure 5 is disconnected during the measurements.

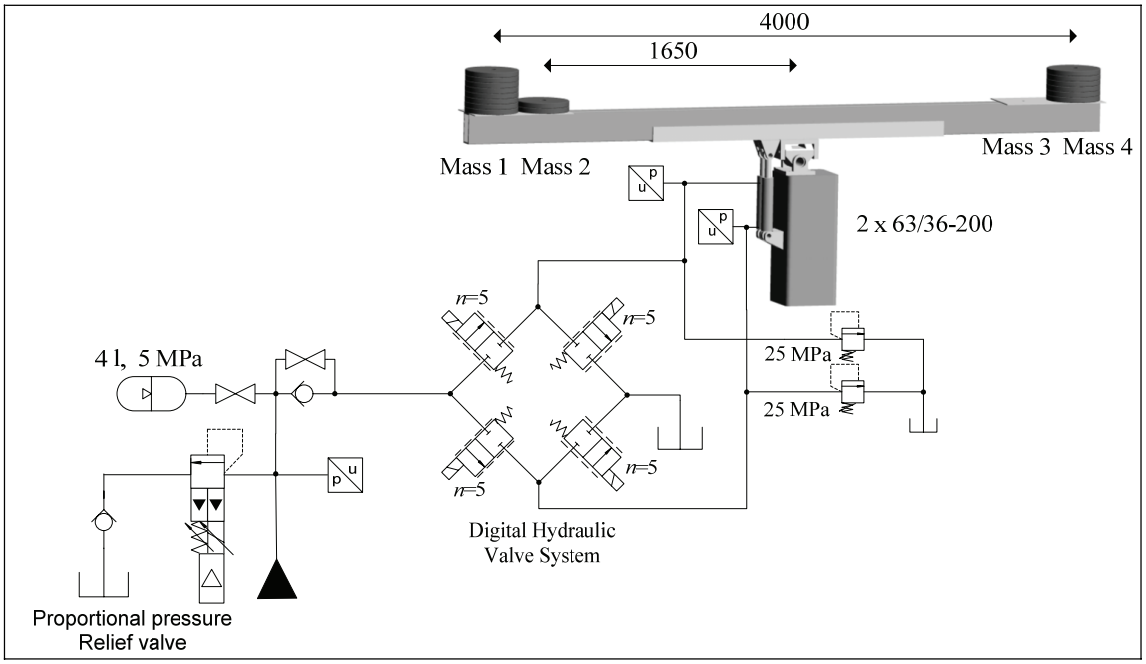

Figure 5. Hydraulic circuit of the test system

4.5 Trajectory and tested faults

The cylinder is controlled with a simple extend and retract movement. The system is tested for control signal faults, valve cable break faults and feedback-signal faults. The cable break fault is generated with a hand controlled 2-channel switch. The cable break time is measured from one channel and the second channel disconnects the valve from control electronics manually. The measured cable break time is not used in FDD. The fault is generated during the extend stroke. The sensor cable and control signal cable breaks are generated with software by disconnecting the control signal at the middle

point of the extend stroke of the cylinder. The time of the fault is 1.125 s from the beginning of the measurement in all sensor and controls signal measurements. Both PWM driver diagnostics signal and optocoupler diagnostics signal faults are tested. Only one fault is tested at a time.

5 EXPERIMENTAL RESULTS

The results are presented in Figures 6-9 where most important signals are plotted. Each figure has measured piston position, piston position reference, velocity reference and calculated velocity. The pressures of supply line and both actuator ports are presented below velocity measurements. The states of each DFCU are also plotted so that control signals can be seen. In control signal faults, the difference between real control signals (solid line) and signals selected by the controller (dashed line) can be seen because the fault is caused with software. In other measurements the signals are equal. The fault detection signals are plotted to the lowest part of the figures. The signals are PWM driver diagnostics signal, optocoupler signal and cable break signal (CB). In cable break measurements the cable is detached with a hand switch at the time of the signal drop. The FDD logic follows Optocoupler signal and PWM drivers diagnostics signal online and in case of a fault, the valve is switched off and the controller is re-configured. The effect of the fault can be examined from pressures, piston velocity and from piston position. The controller re-configuration can be seen in valve states because the faulty valve is not used anymore. Same information can also be obtained from measured optocoupler signal.

The valve cable faults were produced with hand switch during the lift of the boom. The faults in small valves can hardly be seen in pressures or in velocity and position signals. The FDD logic detects all tested cable breaks instantly when the faulty valve is used for the first time. The fault is detected from the PWM-drivers signal and immediately after it the valve is switched off. The diagnostics that can be seen on the Figure 3 shows that the reason of the valve cable break fault is broken valve cable, PWM-driver feedback signal break or over-current. The exact diagnosis can not be obtained with the sensors used but the fault is limited into small number of possibilities and the counter-actions can be made.

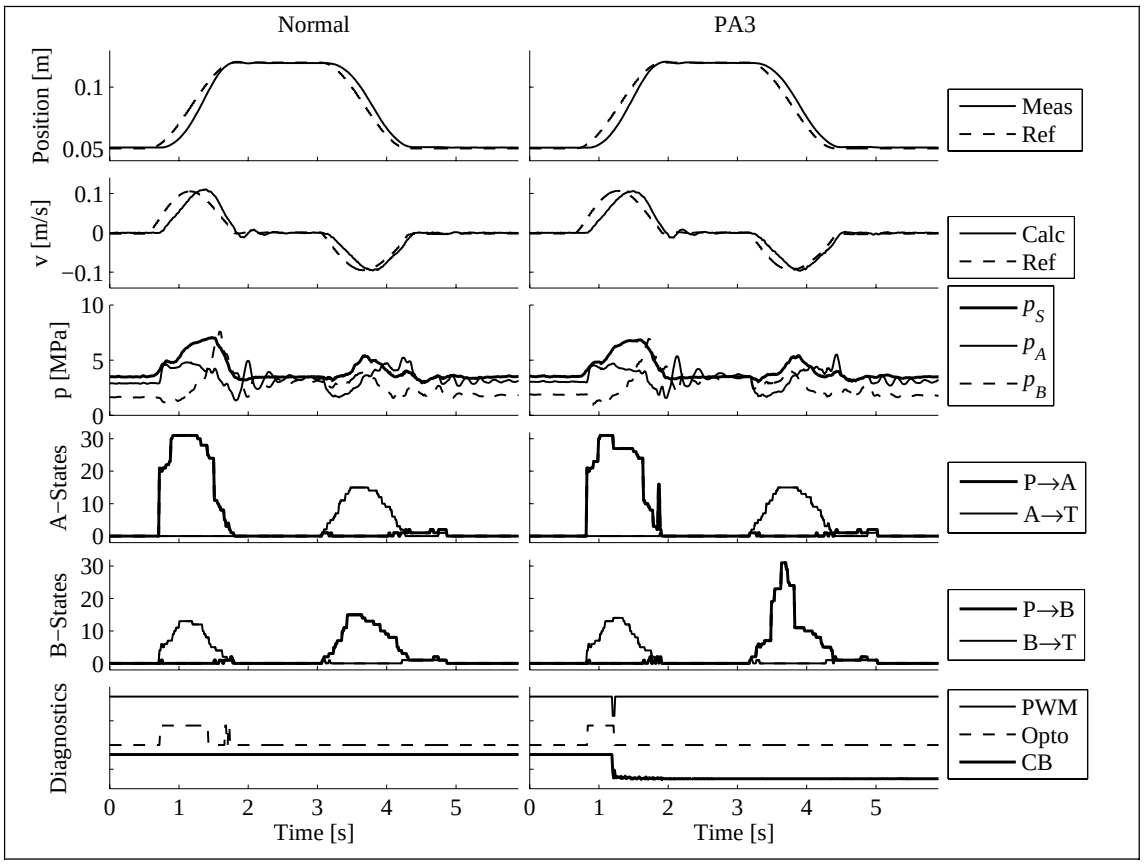

Figure 6. Normal operation and cable brake in valve PA3

Figure 6 presents a normal run without any faults and a run with $DFCU_{P\rightarrow A}$ valve 3 fault. The pressure measurements show only small variations in pressures but nothing that would effect on piston velocity or position so that the change could be seen. The fault in valves PA4 and PA5 are more effective since the opening is at the maximum during the lift. The pressures do not settle to correct level and some problems in velocity can be seen. Same behavior can also be seen in control signal break measurements which are presented later.

The response time of the fault detection and diagnosis logic is closely related to the control signals of the valves. The fault cannot be found before the valve is used for the first time. This can be seen in Figure 7 where cables of valves 2 and 5 from $DFCU_{P\rightarrow B}$ are disconnected during the cylinder extend stroke. The valve 2 is used in the braking of the cylinder movement and therefore it is also detected much sooner than valve 5 fault where the fault first appears during the retract stroke of the cylinder. Still the severe fault in the biggest valve of the $DFCU_{P\rightarrow B}$ does not have notable effect on velocity or position of the cylinder rod. Also in both of these cases the fault is diagnosed correctly.

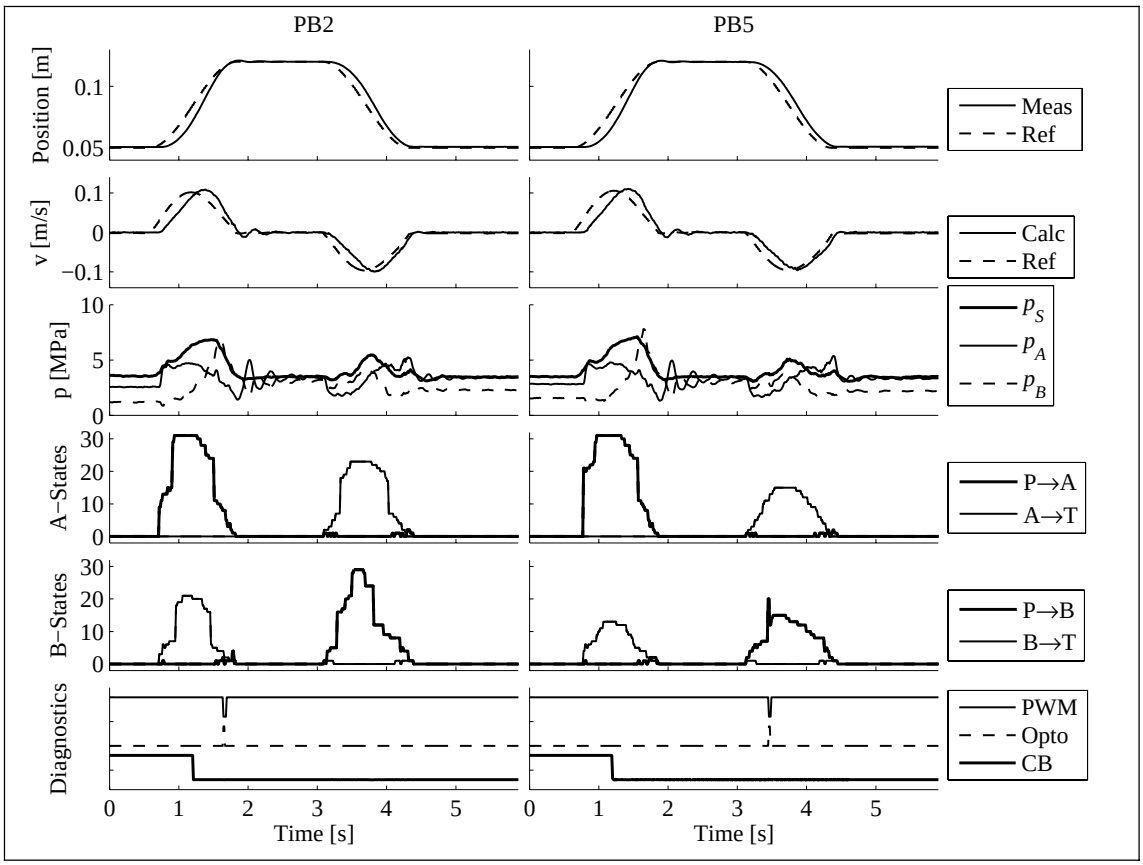

Figure 7. Cable brakes in valves PB2 and PB5

The pressure side DFCU valve cable breaks did not have noticeable effect on the response. The effect of tank side DFCU fault is in theory bigger because of higher pressure difference over the valves. Cable break in one of the smaller valves still has practically no effect at all to the piston velocity or position but in the bigger valves some changes can be seen. Figure 8 presents two faults in tank side DFCUs. Fault in second biggest valve in A-side, the effect is relatively small and can only be seen in pressure curves but in extend stoke the B-side valve 4 creates a pressure peak in B-side chamber and a small notch can be seen in velocity curve. After the compensation the effect disappears.

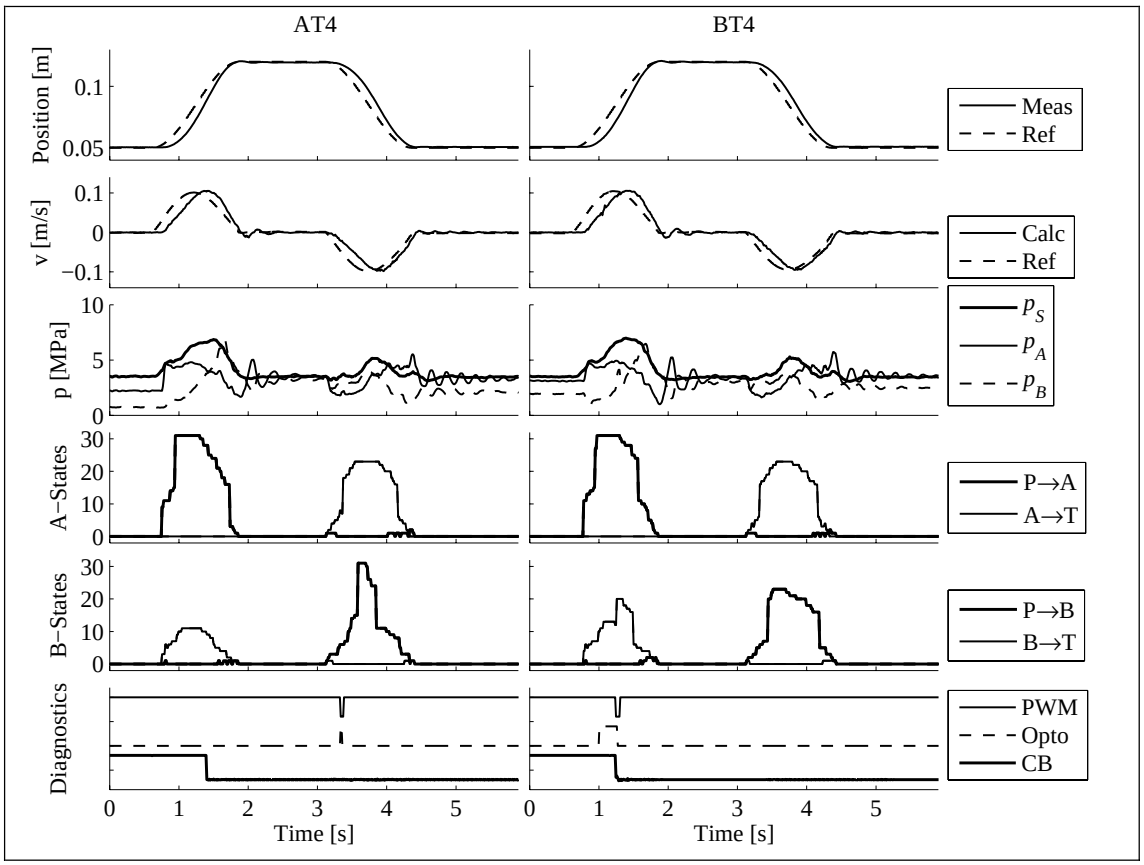

Figure 8. Cable brakes in valves AT4 and BT4

The sensor faults and control signal cable breaks were tested by setting the signal to 0 during the extend stroke. Both control signal and optocoupler faults seem same in diagnostics and therefore give the same diagnostics information. Figure 9 presents control signal break in valve PA4 and optocoupler feedback signal fault in valve AT4. The effect of control signal break is very similar to valve cable breaks and the results are also similar. Faults in small valves have only small effect on the system. In tank side DFCUs and in $DFCU_{P\rightarrow A}$ the faults in bigger valves can be seen in pressures but the effect in velocity or position is small. The control signal faults in valves PA4 and PA5 have also effect on velocity because the maximum flow rate of the DFCU is decreased and the DFCU is fully open. The fault diagnose is the same for both control signal and optocoupler feedback signal faults and the effect of the faults are similar in all studied cases.

The PWM-drivers diagnostics signal faults differ from the rest of the faults because they are detected immediately although valve is not used at the time. This causes different kind of diagnosis result e.g. with valves PA5 and PB4 because PA5 was on when the fault was initiated and PB4 was not. The effect of the fault in PA5 was similar to fault in optocoupler feedback signal fault presented in Figure 9 while the fault in PB4 can only be seen in pressure curves when close to maximum opening is needed. In case of PWM-driver feedback fault in PB4 the diagnose is more accurate while the fault in PA5 is mixed with cable break fault. In all cases however the faulty acting valve-sensor combination was disabled and the controller was re-configured correctly.

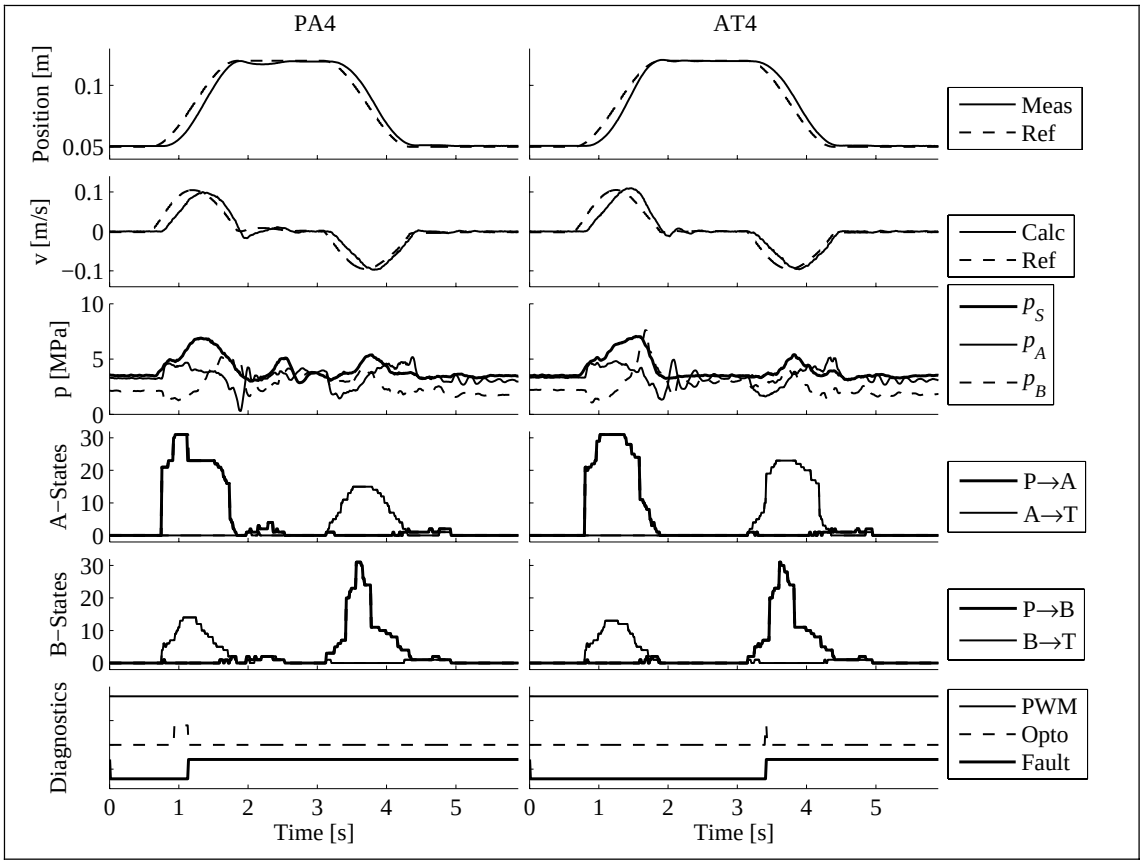

Figure 9. Control signal break in valve PA4 and optocoupler feedback signal fault in valve AT4

CONCLUSIONS

Fault detection and diagnosis (FDD) is the key to fault tolerance. Fault must be found and analyzed so that correct response can be made. FDD has been researched in many different applications including complete systems and also components. Fault tolerance of hydraulic valves is a difficult challenge to achieve because they are usually serial connected systems where single fault may cripple the whole system. Digital hydraulic valve system is an on/off valve based proportionally acting flow control valve capable for accurate trajectory tracking even in demanding conditions. The system has good features in fault tolerance because of parallel connection of its internal components and possibility for online re-programming of the controller.

This paper studied FDD and fault reaction with digital hydraulic valve system. Certain pre-defined faults were caused to the system and the valve controller was re-configured online based on the FDD information obtained from simple on/off diagnostics signals. The fault detection was done by using control electronics internal diagnostics signals and by measuring voltage differences over the valve coils. The results show that the system is capable of acting in fault situation with only a small degradation in performance. The system was able to continue normal operation even in most serious faults that were caused to the system. The fault tolerance features of digital hydraulic valve system combined with active online fault detection and diagnosis seems very effective and unique on area of hydraulic flow control valves.

ACKNOWLEDGEMENTS

The research was supported by the Academy of Finland (Grant no. 80411)

REFERENCES

1. Zhang, Y. and Jiang, J. 2003. Bibliographical review on reconfigurable fault-tolerant control systems. *Proceedings of the 5th IFAC Symposium on Fault Detection, Supervision and Safety for Technical Processes*, June 9-11, 2003, Washington, D.C., USA, pp. 265-276.
2. Blanke, M., Kinnaert, M., Lunze, J. and Staroswiecki, M. 2003. Diagnostics and Fault-Tolerant Control. Springer-Verlag, Berlin, Germany, ISBN 3-540-01056-4.
3. Isermann, R. 1997. Supervision, fault-detection and fault-diagnosis methods – an introduction. *Control Eng. Practice*. Elsevier Science Ltd, UK, Vol 5, No 5, pp. 639-652.
4. Isermann, R. and Ballé, P. 1997. Trends in the application of model-based fault detection and diagnosis of technical processes. *Control Eng. Practice*. Elsevier Science Ltd, UK, Vol 5, No 5, pp. 709-719.
5. Yingjie, G. and Patton, R. J. 2003. Fault tolerant control of hydraulic AGC systems. *Proceedings of the fourth international symposium on fluid power transmission and control* (ISFP'2003). Beijing, China, pp. 666-671.
6. Rinkinen, J., Laukka, J. and Ahola, E. 1997. Condition Diagnosis of Servo Valve in Oil Hydraulic Servo System of Hot Strip Mill. Proceedings of the 5th Scandinavian International Conference on Fluid Power, SICFP '97, 1997, pp. 429-444.
7. Hindman, J., Burton, R. and Schoenau, G. 2002. Condition Monitoring of Fluid Power Systems: A Survey. *Proceedings of the 49th National Conference on Fluid Power* (NFPA'02), March 19-21, 2002, Las Vegas, USA.
8. Murrenhoff, H. 2004. Online condition monitoring (OCM) in fluid power technology. *Proceedings of 4th International Fluid Power Conference*. March 25-26 2004. Vol. 2, Dresden, Germany, pp. 219-244.
9. Ramdén, T.; Krus, P.; Palmberg, J-O. (1995). Fault diagnosis of complex fluid power systems using neural networks. *Proceedings of The Fourth Scandinavian International Conference on Fluid Power* (SICFP'95), September 26-29, 1995, Tampere, Finland, pp. 706-718.
10. Garimella, P. and Yao, B. 2005. Model based fault detection of an electro-hydraulic cylinder. *Proceedings of American Control Conference*. June 8-10 2005, Portland, OR, USA, pp 484-489.
11. Park, R.W. 1997. Contamination control – a hydraulic OEM perspective. *Workshop on Total Contamination Control*. August 1997, Centre for Machine Condition Monitoring, Monash University, Australia.
12. Johnson, M.A. 2005. Pump monitoring and diagnosis. World Pumps, January 2005, pp. 34-36.
13. Jiang, J. and Zhang, Y. 2006. Accepting performance degradation in fault-tolerant control system design. *IEEE Transactions on Control Systems Technology*. March 2006. Vol 14, No 2, pp. 284-292.
14. Kopp, C. 1996. System reliability and metrics of reliability. Slides for lecture series. http://www.csse.monash.edu.au/~carlo/SYSTEMS/Reliability-PHA.pdf (Visited 11.1.2007).

15. Schreurs, J. and Bednar, F. 1990. On-line valve monitoring and diagnosis. *Computer Applications in Power*, IEEE, January 1990, Vol 3, Issue 1, pp. 25-29, ISSN 0895-0156.
16. Liangcai, Z., Kuisheng, C. and Guozheng, S. 2003. Characteristic curves based faulty model identification for electro-hydraulic servo-valve neural networks. *Proceedings of the fourth international symposium on fluid power transmission and control* (ISFP'2003). Beijing, China, pp. 672-675.
17. Mourre, D. and Burton, R. 2001. Investigation of a neural network/statistical condition monitoring technique for a proportional solenoid valve. *Proceedings of the Bath Workshop on Fluid Power Transmission & Motion Control*, September 2001, Bath, UK, pp. 119-134, ISBN 978-1-86058-326-1.
18. Blanke, M. (1999). Fault-tolerant Control Systems. *Advances in Control. Highlights of ECC'99*, Duisburg, Germany, Springer-Verlag London Limited, pp. 171-196.
19. Siivonen, L.; Linjama, M.; Vilenius, M. (2005). Analysis of fault tolerance of digital hydraulic valve system. *Proceedings of the Bath Workshop on Fluid Power Transmission & Motion Control* (PTMC'05), September 7-9 2005, Bath, UK, pp. 133-146, ISBN 13 978-0-470-01677-0.
20. Bower, J.L. 1961. Digital Fluid Control System. US patent no. 2999482.
21. Laamanen, A., Siivonen, L., Linjama, M. and Vilenius, M. 2004. Digital Flow Control Unit - An Alternative for Proportional Valve? *Proceedings of the Bath Workshop on Fluid Power Transmission & Motion Control*, September 1-4 2004 (PTMC'04), Bath, UK, pp. 297-308, ISBN 1 86058 466 7.
22. Anon. Poppet type 2 position 2 way normally closed GS02 05 on/off valve. http://www.sterling-hydraulics.co.uk/files/pdf/gs02_01_02_05_06.pdf (last visited 12.1.2007)
23. Anon. 2001. Sauer-Danfoss PVG 32 Proportional valve technical information. Sauer-Danfoss. www.sauer-danfoss.com (visited 10.3.2004).
24. Linjama, M., Laamanen, A. and Vilenius, M. 2003. Is it Time for Digital Hydraulics? *Proceedings of the Eighth Scandinavian International Conference on Fluid Power*, May 7-9 2003, Tampere, Finland, pp. 347-366.
25. Linjama, M., Huova, M., Boström, P., Laamanen, A., Siivonen, L., Morel, L., Waldén, M. and Vilenius, M. 2007. Design and implementation of energy saving digital hydraulic control system. *To be published in the proceedings of the Tenth Scandinavian International Conference on Fluid Power*. May 21-23 2007, Tampere, Finland.
26. Siivonen, L., Linjama, M. and Vilenius, M. (2005). Fault tolerance of digital hydraulic valve system with separately controlled flow paths. *Proceedings of 4th FPNI – PhD Symposium*. Vol 2. June 13-17. Sarasota, FL, USA, pp. 331-343, ISBN 1-4243-0500-4.
27. Laamanen, A., Linjama, M. and Vilenius, M. 2005. Pressure peak phenomenon in digital hydraulics - a theoretical study. *Bath Workshop on Power Transimission and Motion Control* (PTMC'05), September 7-9. 2005, Bath, UK, pp. 91-104, ISBN 13 978-0-470-01677-0.
28. Laamanen, A., Linjama, M. and Vilenius, M. (2005). The effect of coding method on pressure peaks in digital hydraulic system. *Proceedings of 4th FPNI – PhD Symposium*. Vol 1. June 13-17. Sarasota, FL, USA, pp. 285-295, ISBN 1-4243-0499-7.
29. Mikkola, J., Ahola, V., Lauttamus, T, Luomaranta, M., Linjama, M. and Vilenius, M. 2007. Improving characteristics of on/off solenoid valves. *To be published in the*

proceedings of the Tenth Scandinavian International Conference on Fluid Power. May 21-23 2007, Tampere, Finland.

DESIGN AND VALIDATION OF DIGITAL CONTROLLERS FOR HYDRAULICS SYSTEMS*

Pontus Boström[1], Matti Linjama[2], Lionel Morel[3], Lauri Siivonen[2], and Marina Waldén[1]

[1] Åbo Akademi University, Department of Information Technologies
Turku Centre for Computer Science
Joukahaisenkatu 3-5, 20520 Turku, Finland
{pontus.bostrom,marina.walden}@abo.fi
[2] Tampere University of Technology, Institute of Hydraulics and Automation
P.O. Box 589, FI-33101 Tampere, Finland
{matti.linjama,lauri.siivonen}@tut.fi
[3] INRIA - Campus universitaire de Beaulieu
35042 Rennes Cedex, France
morel.lionel@gmail.com

ABSTRACT

In order to increase the flexibility and performance of hydraulically actuated machines there is a demand for more intelligent controllers. This leads to a rapid increase in complexity of the control systems. To manage the complexity and to ensure reliability of these systems, adequate software development methods are needed. In this work, we propose a methodology for structured design of digital hydraulics controllers in Simulink/Stateflow. A model architecture based on mode-automata is introduced to separate control and data processing. Furthermore, *design by contract* is advocated as a method for system development. The contracts can be used to mathematically reason about correctness of Simulink/Stateflow models and thereby increase the safety and reliability of the developed systems. The usefulness of these concepts are demonstrated on a larger case study from the area of digital hydraulics.

KEYWORDS: Controller Architecture, Mode-Automata, Simulink/Stateflow, Design by Contract, Reliability

* This work is carried out in the context of the ITCEE (Improving Transient Control and Energy Efficiency by digital hydraulics) project funded by TEKES (Finnish Funding Agency for Technology and Innovation)

1 INTRODUCTION

There is a trend toward adding more intelligent controllers in hydraulically actuated machines in order to increase their flexibility and performance. The trend is also to replace hydromechanical functions - such as load-sensing - with sensors, electrically controlled valves and intelligent control. An extreme example is the Digital Hydraulics technology [1] , in which simple on/off valves are used together with intelligent control. The result of these trends is that complexity of control systems increases rapidly. Modern systems also have high requirements on performance, safety and reliability. To handle these requirements, appropriate software development and validation methods are needed.

This paper presents development techniques used for a digital hydraulics controller with energy saving [2]. Since high reliability of the controller software is desired, formal software design methods are beneficial. These methods enable mathematical reasoning about correctness of models. They also enable mathematical proofs that certain properties are satisfied in the system. Among these properties, the focus will mainly be on safety properties, which establish that some *bad* behaviour will *never happen*. The work is carried out using Simulink[4]/Stateflow[5], which have become a widely used tool for model based design of control systems. Our propositions articulate around two main points. First, we advocate a particular software architecture for developing mode-based systems in Simulink. Second, formal techniques for increasing the confidence that the system works correctly are presented. Related techniques have previously been successfully applied to safety-critical systems e.g. [3]. What we propose here is to adapt those techniques to the development of systems where safety issues are less critical and developers are not formal methods experts. The aim is here to maximise the efficiency and ease of use of these methods.

The rest of the paper is structured as follows. In Section 2 the digital hydraulics application is presented. Section 3 describes the development of controllers in Simulink/Stateflow, while Section 4 gives an example and outlines the controller architecture. Design by contract of models is introduced in Section 5 and analytical verification of mode switching based on this method is presented in 6. Section 7 gives the conclusions of the paper.

2 THE DIGITAL HYDRAULICS SYSTEM

The idea of digital hydraulics is to use simple on/off valves [1] together with an intelligent controller to achieve desired performance. Figure 1 shows an overview of such a system. The hydraulic cylinder is controlled by four *digital flow control units* (DFCU) with five on/off valves each (PA_i, PB_i, AT_i, BT_i, $i = 1..5$). The configuration of a DFCU gives the open and closed valves and thereby controls the flow of fluid through it. The configuration of the first DFCU (u_{AT}) controls the flow from A to tank, the second controls the flow of fluid from the pump to A (u_{PA}) , the third (u_{PB}) from pump to B and the last (u_{BT}) controls the flow from B to tank.

[4] Simulink, Mathworks Inc, `http://www.mathworks.com`
[5] Stateflow, Mathworks Inc, `http://www.mathworks.com`

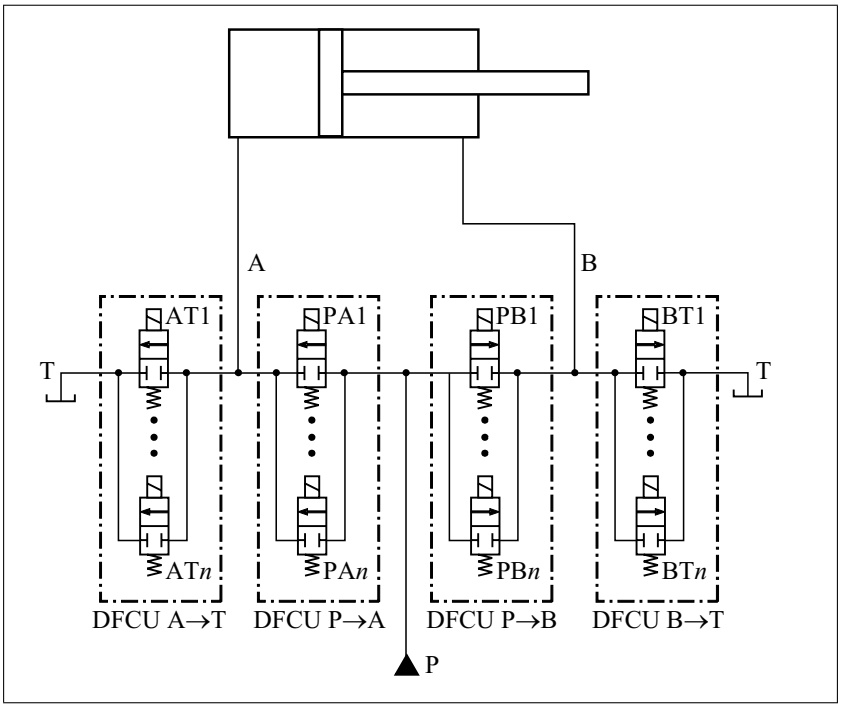

Fig. 1. Overview of a hydraulic cylinder controlled by a set of digital control flow units [1]

To control the speed of the piston, suitable combinations of valves are opened. The controller computes optimal valve configurations at each sampling time, taking into account pressure limitations. The controller has different running modes for normal motion and energy saving motion. Energy efficient modes should then be used whenever possible. Due to the complex calculations needed, the software for the controller is large and involves both signal processing and discrete control logic to handle the switching of modes.

3 CONTROLLER DEVELOPMENT IN SIMULINK/STATEFLOW

A controller usually consists of two parts; signal processing and control logic. Simulink is used to describe the signal processing and Stateflow is used to describe the control logic. In this paper the control logic consists of switching between control modes.

Stateflow is a state-machine implementation for Simulink similar to Statecharts [4]. It is a sequential and deterministic language for creating the supervisory control logic in control applications. Consider the Stateflow chart in Figure 2. The square boxes are *states* and the circles are *junctions*. An arrow is referred to as a *transition segment*. Stateflow supports hierarchical state-machines containing both or-state and and-states. In an or-state (s_2) only one sub-state is active modeling sequencing of transitions, while in a and-state all sub-states are active modeling parallelism. Transition segments in Stateflow can be labelled by *events* (e), *guards* (g_1, g_2, h_1, h_2), and *actions* (act).

The action language of Stateflow is very expressive and contain many advanced features for defining behaviour. However, some of these features have counter intuitive semantics and are difficult to use correctly. Therefore, to aid verification and to only use constructs

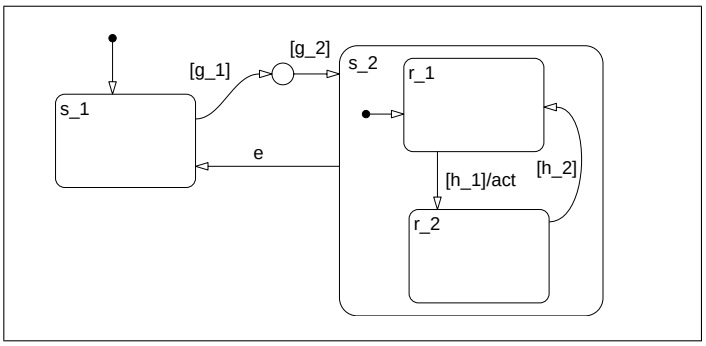

Fig. 2. A schematic example of a Stateflow chart

with a simple semantics, only a subset of Simulink/Stateflow should be used. Guidelines for development of controllers using Simulink/Stateflow have been developed to increase the readability and maintainability of models [5]. In order to have efficient code generation suitable for safety critical systems, even stricter guidelines need to be followed [6, 7].

Even when the guidelines above are followed formal verification is difficult in Stateflow, due to the large number of features for defining behaviour. When considering ease of verification, Simulink often offers a better choice for defining behaviour. Additionally, Simulink/Stateflow models can be analysed by graph checking if textual descriptions are avoided, whenever it is possible. The following restrictions to Stateflow are used in this paper:

- *Activities* inside states are not allowed in Stateflow. Simulink is instead used to define all behaviour inside states (modes).
- Transitions that cross composite state boundaries are not allowed.
- *Events*, *actions* and *condition actions* are not allowed on transition segments.
- Transition segments are restricted to only be labelled by a guard (condition) name, e.g., g_1, g_2 in Figure 2. A guard name is always an input port name in the Stateflow block. In practise we often also need the negation $\neg g$ if guard g is used. Therefore guards of the type $[g]$ or $[\sim g]$ are allowed on the transition segments. Conjunction (and) and disjunction (or) of conditions can be implemented using junctions.

These constraints restrict Stateflow to a safe subset that is easy to analyse, and yet sufficiently powerful to be used in practise.

3.1 Semantics of the considered subset of Stateflow

To get an understanding of how a Stateflow chart is executed a short introduction to the Stateflow semantics is needed. Due to the restrictions in this paper, transition segments can be labelled by a guard condition of the form $[g]$ or $[\sim g]$. A *transition* is a sequence of transition segments connected by junctions that starts and ends in a state. The guard of a transition is given as the conjunction of the guard conditions on the individual transitions segments, e.g., $g_1 \wedge g_2$ for the transition between s_1 and s_2 in Figure 2. A transition is enabled, if its guard evaluates to true. Transitions with the source state higher in the state hierarchy have higher priority, while the ones with the same source either have a fixed priority given by the developer or a priority given by the internal rules of Stateflow. The

internal rules in Stateflow for assigning priorities depends on the graphical layout of the diagram and is therefore not safe to use. The explicit ordering mechanism should therefore always be used.

During the execution of the Stateflow chart, a subset of the states are active. The transitions between states describe how the set of active states changes. When the chart is executed, the enabled transitions from the currently active states are computed. The enabled transition with the highest priority is then executed and the active states are changed to the destination of the transition. If an and-state is active several transitions can be executed concurrently. If the destination of a transition is a composite state, then the corresponding *default transitions* are also executed to initialise the state.

4 CONTROLLER ARCHITECTURE EXAMPLE

A good architecture is needed in order to structure the controller. This guarantees that the controller is maintainable, extensible and the control logic is easy to understand. The architecture proposed here separates control logic from signal processing. The mode specific behaviour is also isolated from the parts common for all modes.

4.1 Controller overview

The controller presented here is used for energy saving digital hydraulics in [2]. The focus in this paper is on architecture and verification of the system, while [2] presents the functionality of the system. An overview of the different parts of the controller is given in Figure 3. Most of the controller functionality is common for all modes. The mode specific behaviour is given in subsystem *Selection of control mode*.

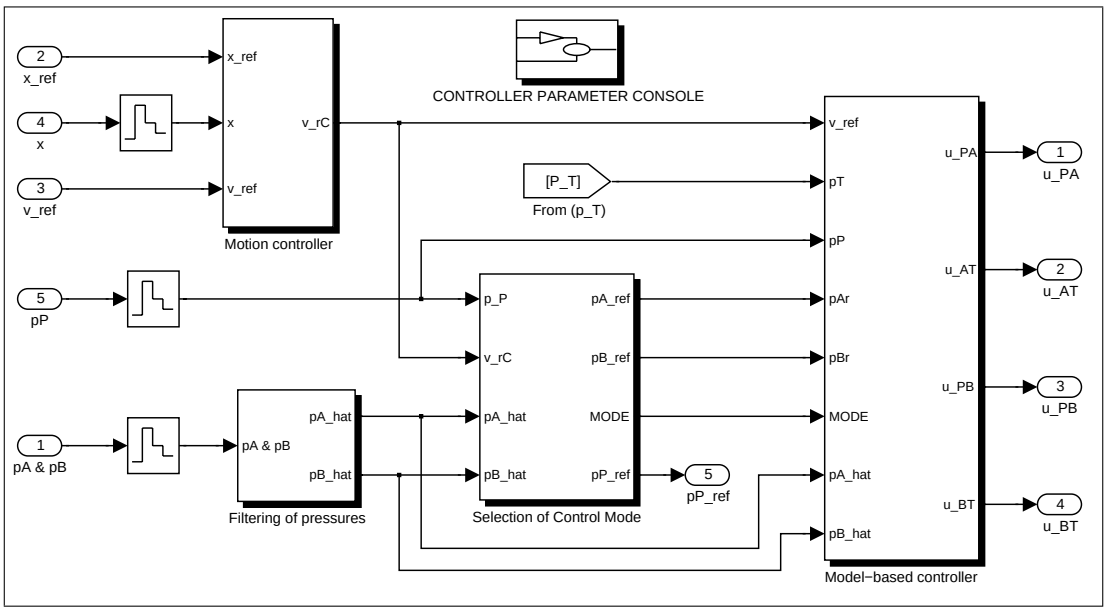

Fig. 3. Overview of the controller

The inputs to the controller are position, x, reference position, x_{ref}, and reference speed, v_{ref}, of the piston, as well as pressure provided by the pump p_P and the cylinder chamber pressures, p_A and p_B. Based on this information, the controller then computes the optimal valve configurations u_{PA}, u_{AT}, u_{PB} and u_{BT}. The subsystem *selection of control mode* computes optimal pressure references for the pump (p_{Pref}) and for the chamber pressures (p_{Aref} and p_{Bref}) based on the reference speed v_{rC}, (filtered) chamber pressures ($\hat{p}_A$ and $\hat{p}_B$) and pump pressure (p_{Pref}). Furthermore, it provides mode specific parameters in the signal $MODE$. The signals from the mode selection block are then used for the *model-based controller* to determine the optimal valve configuration independent of the running mode.

4.2 Mode switching

To increase readability and ease verification of the mode switching system an appropriate design has to be used. Mode-automata [8–12] is such an architecture for developing mode-based systems. It is used for systems that consist of a set of running modes, where each mode is associated with mode-specific signal processing. The switching between modes is described using a state-machine (here a Stateflow chart), where each transition is guarded by a condition. Each non-composite state in the Stateflow chart is connected to an enabled subsystem in Simulink giving the mode specific behaviour.

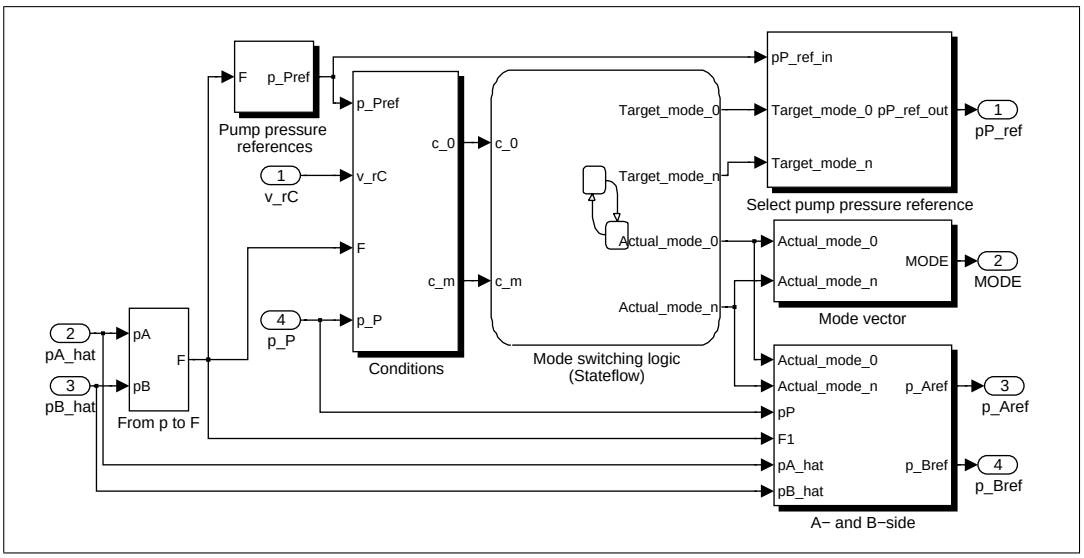

Fig. 4. Simplified view of the Selection of control mode subsystem

Figure 4 shows a simplified version of the core of the mode switching logic. The subsystem *Conditions* computes the conditions $c_0, \ldots, c_m$ that are used to decide when modes should be switched (these corresponds ultimately to the guards $[g]$ that are used in the Stateflow chart). Each output from the subsystem is a boolean stating whether the condition holds or not. The Stateflow chart outputs which modes are currently active. The active modes then triggers enabled subsystems giving the mode dependent behaviour. There are two parallel modes (i.e. sub-states of an and-state) *Target mode* and *Actual mode*. The enabled subsystems activated by target mode are first used for computing the pressure reference (p_{Pref}) for the freely adjustable pump pressure. The best actual mode

is then determined based on the actual pump pressure p_P. The subsystems enabled by the actual mode then compute chamber pressure references (p_{Aref} and p_{Bref}), as well as mode specific parameters ($MODE$).

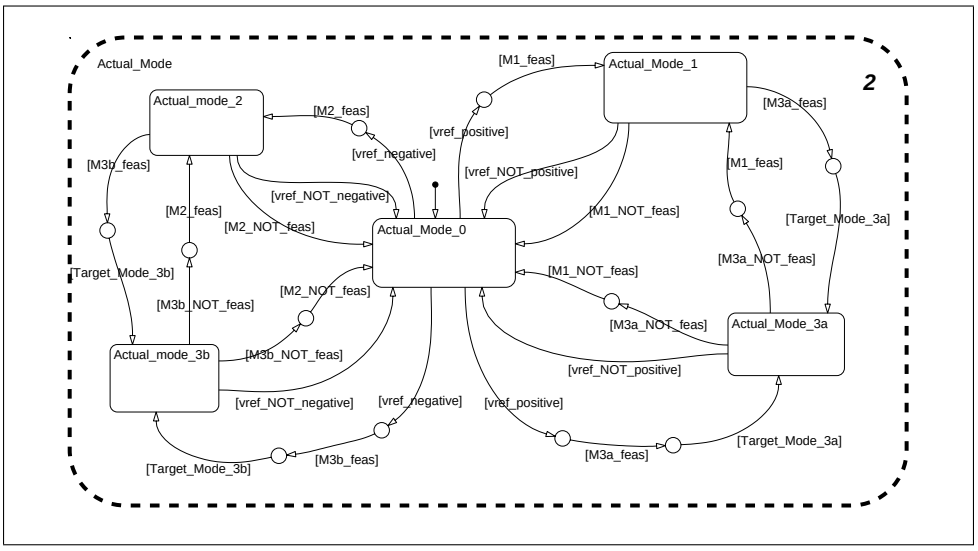

Fig. 5. Switching of the actual mode

The Stateflow chart determines the running mode of the system. Figure 5 shows the switching of the *actual mode*. The switching of the target mode is similar. The actual mode consists of the following submodes [2]:

- 0 *Stopped motion*. If the reference speed is close to zero ($\mathrm{vref\_NOT\_positive}(v_{rC}) \wedge \mathrm{vref\_NOT\_negative}(v_{rC})$) or no other mode is feasible ($\neg \mathrm{Mi\_NOT_feas}(F, p_P, \Delta p_{min})$) this mode is used.
- 1 *Normal extending motion*. This mode is selected if the reference speed is greater than a threshold value ($\mathrm{vref\_positive}(v_{rC})$), the mode is feasible ($\mathrm{M1\_feas}(F, p_P, \Delta p_{min})$) and energy saving should not be used ($\neg(\mathrm{M3a\_feas}(F, p_P, \Delta p_{min}) \wedge Target\_mode\_3a)$). The last condition is derived from the priority of the transitions.
- 2 *Retracting motion*. This mode is similar to mode 1
- 3a *Extending energy saving motion*. If the reference speed is greater than a threshold value ($\mathrm{vref\_positive}(v_{rC})$) and energy saving can be used ($\mathrm{M3a\_feas}(F, p_P, \Delta p_{min}) \wedge Target\_mode\_3a$), this mode is selected .
- 3b *Retracting energy saving motion*. This mode is similar to mode 3a.

Due to noise in the input signals there is a problem with excessive mode switching when the signals remain close to a switching condition. To remedy this problem, e.g. the condition $\mathrm{vref\_NOT\_positive}(v_{rC})$ is not the negation of $\mathrm{vref\_positive}(v_{rC})$, but it contains extra conditions to inhibit switching between modes, when signal values remain close to this switching condition. The conditions $\mathrm{vref\_NOT\_positive}(v_{rC})$ and $\mathrm{vref\_positive}(v_{rC})$ can, hence, evaluate to false at the same time. A further measure to prevent excessive switching is that some conditions also have to evaluate to true for a certain amount of time in the Simulink diagram before they become true in the Stateflow chart. For example, the conditions $\mathrm{Mi\_NOT\_feas}$ are the delayed conditions $\neg \mathrm{Mi\_feas}$.

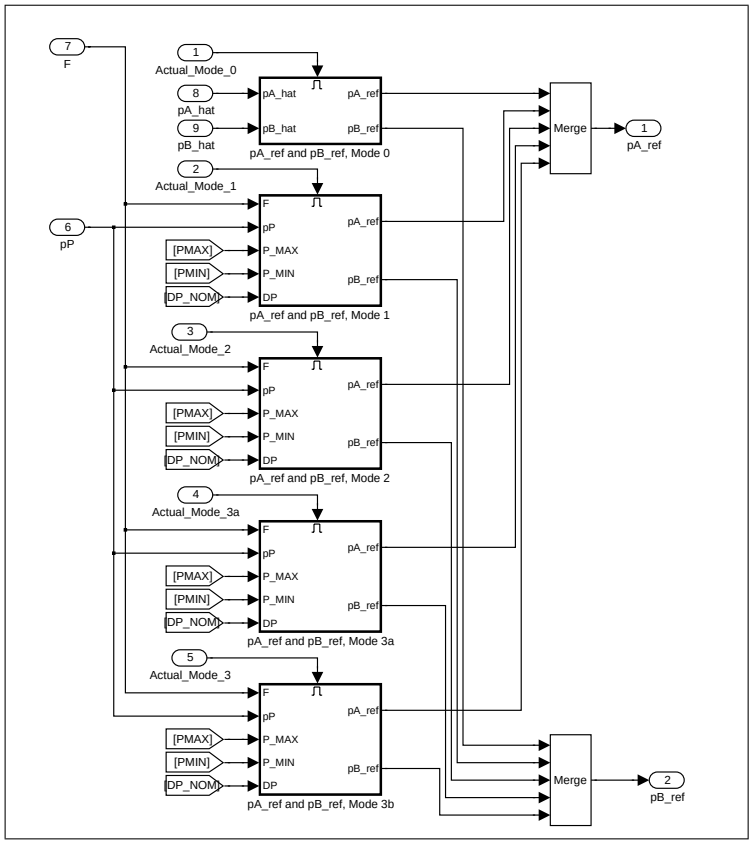

Fig. 6. Definition of chamber pressure references p_{Aref} and p_{Bref} in each mode inside subsystem *A- and B-side*

The actual modes are used to compute the optimal chamber pressures references p_{Aref} and p_{Bref}, which is illustrated in Figure 6. The final pressures are computed with *merge*-blocks that take the latest value computed by an enabled subsystem.

4.3 Mode Dependent Behaviour

The mode-automata architecture puts restrictions on the way the system designer can describe behaviour. The first restriction concerns the memory inside enabled subsystems and the second the connection of enabled subsystems to merge blocks.

Consider the case when a memory block inside a mode enabled system stores a signal value. When the mode is exited and then re-entered the signal value stored in the block refers to possibly a very old value. This can lead to problems in the control algorithms. For example, if the mode dependent behaviour is a PI-controller the integrator might have a value not relevant anymore. The mode dependent behaviour should, therefore, either not contain blocks with memory or the memory should be reset whenever the mode is entered in order to ensure predictable behaviour.

The mode selection system should also define the value of all output signals all the time. Furthermore, each signal value should be uniquely defined. Hence, every enabled subsystem should be connected to merge blocks to obtain the final result and every merge block should have exactly one enabled input at all times.

5 DESIGN BY CONTRACT

The term *design by contract* was first used by B. Meyer in the Eiffel programming language [13]. The idea of design by contract is that software should have precise checkable interface specifications. Each component should state explicitly what conditions on the inputs it require from the environment and what conditions on the output it ensures. Optionally, the component can also state what internal conditions it will always maintain. The theory behind contracts is discussed in [14]. Design by contract ideas are implemented in e.g. Eiffel [13], JML [15] for Java and in Spec# [16] for C#. These languages are accompanied by various tools for compiling, static checking and dynamic checking (testing).

Design by contract can be used for *assume-guarantee reasoning*. The idea behind assume guarantee style reasoning about system correctness is that each component only guarantee that it functions correctly as long as its assumptions about the environment are satisfied. This enables compositional reasoning, since components can be verified individually. Assume-guarantee reasoning about embedded and hybrid systems have been investigated by several authors [17–20].

5.1 Design by Contract in Simulink

A Simulink subsystem can be viewed as a tuple (i, o, p, f), where i is a set of input signals, o is a set of output signals, p is a set of parameters and f is a function that update the output signals based on the parameters and input signals $o = f(p, i, x)$, where x is the memory contained in blocks inside the subsystem. To use Design by Contract and enable assume-guarantee reasoning about correctness in Simulink we need to be able to state what a subsystem assumes of its environment and what it guarantees. To express these kinds of constraints we need two types of conditions: *assume* conditions and *guarantee* conditions. Assume condition violations and guarantee condition violations are interpreted in different ways. Assume violations are not the responsibility of the subsystem the condition belongs to, while guarantee violations are the responsibility of that subsystem. Four types of conditions can be identified for stating properties about different aspects of a subsystem.

- *Initialisation condition* $R(p)$. This is an *assume*-condition for stating properties describing the parameter values the subsystem expects.
- *Pre-condition* $P(p, i)$. This conditions is an *assume*-condition for stating pre-conditions on the input values from the environment.
- *Invariants* I. These conditions are *guarantee*-conditions for stating internal conditions (invariants) that the subsystem should maintain.
- *Post-condition* $Q(p, i, o)$. This is again a *guarantee*-conditions giving the conditions on the output that the subsystem guarantees.

The parameter values cannot depend on the signals in the subsystem and, therefore, the condition describing the parameters depends only on the parameter values. The environment cannot see anything inside the subsystem block. Hence, the pre-condition

can only state properties about the input signals. The invariant condition can state properties about inputs, outputs and all internal signals. Since a post-condition again guarantees a condition for the environment, it can only state properties about the input and output signals of the block. Note that it is here assumed that all signals used in the conditions have the same timing. Contracts over signals with different timing is more complicated and require special treatment.

To illustrate how contracts can be used to define the interfaces of components, a contract is defined for the subsystem enabled by actual mode 1 in Figure 6. The subsystem uses constants A_A and A_B giving the areas of the A and B sides of the piston. The input signals are p_{min}, p_{max}, F, p_P and Δp, while the output signals are p_{Aref} and p_{Bref}. The following conditions can be given.

$$\begin{array}{l} \mathrm{R}_{M1}(A_A, A_B) \hat{=} (0 < A_B < A_A) \\ \mathrm{P}_{M1}(p_{min}, p_{max}, F, p_P, \Delta p) \hat{=} \\ \quad (p_{min} < p_{max} \wedge p_{min} > 0 \wedge \Delta p > 0 \wedge \mathrm{M1\_feas}(F, p_P, \Delta p_{min}) \\ \mathrm{Q}_{M1}(p_{min}, p_{max}, p_P, p_{Aref}, p_{Bref}) \hat{=} \\ \quad (p_{min} \leq p_{Aref} \leq p_{max} \wedge p_{min} \leq p_{Bref} \leq p_{max} \wedge \\ \quad p_P - p_{Aref} \geq \Delta p_{min} \wedge p_{Bref} \geq \Delta p_{min}) \end{array} \quad (1)$$

The initialisation condition states that the piston area on the A side is greater than the piston area on the B side, while the pre-condition states that actual mode 1 is feasible with positive pressure values. Furthermore, the post-condition states that p_{Aref} and p_{Bref} are within limits p_{min} and p_{max}. Finally, in order to ensure controllability of the system the pressure over the valves should not be smaller than Δp_{min}.

There are several benefits in using design by contract in Simulink. Model reuse is becoming more important and the contracts are useful for this purpose, since they state the exact environment where the component is intended to work. Since each component is accompanied by a contract, assumptions components make about each other are clearly stated. This means that responsibility for error handling becomes clearer. The developer is also forced to think more about the interfaces of components and thereby inconsistencies can be identified earlier in the design process. Erroneous components can be identified by finding components that first broke a contract. The conditions used in the design by contract gives concrete condition that can be checked during testing and validation to ensure that the models work as intended. Design by contract also makes compositional verification possible, since we only need to show that each component satisfies its contract and that the contracts between different connected components are compatible.

Note that contracts (which are specifications) should not be confused with error handling (which handles exceptional behaviour). A contract violation always means that the system is incorrect. Error handling should be used to ensure that the contracts can be maintained regardless of possible errors that can occur.

5.2 Correctness of Models

Contracts can be used to define correctness of models. A model is correct if it is impossible for contract violations to occur. Consider a subsystem block C with assumption about parameters R_C, pre-condition P_C, invariant I_C and post-condition Q_C. Assume there are

n blocks $B_1, \ldots, B_n$ connected to the inputs of C with assumption about parameters $R_{B1}, \ldots, R_{Bn}$, pre-conditions $P_{B1}, \ldots, P_{Bn}$ and post-conditions $Q_{B1}, \ldots, Q_{Bn}$. The correctness conditions can be defined as follows:

Correctness of the Parameters of C. The parameters of C are correct if R_C holds for the parameter values.

Correctness of C. The block C is correct iff when R_C holds for the parameter values and P_C holds for all input values so far, then I_C and Q_C also hold.

Correct connection between components. The connections between blocks $B_1, \ldots, B_n$ and C is correct if, whenever the initialisation condition holds for the parameters and the blocks B_i are assumed correct then the precondition of C holds.

$$R_C \wedge \bigwedge_{1 \leq i \leq n} (R_{Bi} \wedge P_{Bi} \wedge Q_{Bi}) \Rightarrow P_C \tag{2}$$

Signals from a subsystem to itself should be avoided, since $P_C \Rightarrow P_C$ is trivially true. The condition P_{Bi} is also only needed, if Q_{Bi} refers to the input of B_i.

Note, that this notion of correctness does not ensure that the model behaves as desired, since contracts often do not capture all properties of the system. It can also sometimes be difficult to derive contracts from the system requirements. However, many types of errors can be found using contracts, such as interface errors between subsystems and safety condition violations.

5.3 Implementation of Design by Contract in Simulink

Design by contract can be implemented using the *model validation blocks* in Simulink, which consists of different types of assertion blocks. These assertion blocks can be used to give the contract conditions. The different types of conditions need to be identifiable, since violations of them are interpreted in different ways. One way to distinguish a block is to prefix the name of the block with either *Assume* or *Guarantee*. Verification of assume conditions for parameters are best implemented as a preprocessing step in Matlab.

Scalability suffers since, adding assert blocks to the model can make it more cluttered and harder to read. To remedy this problem, the pre- and post-conditions can be added to a separate contract library. Using the Matlab model constructions commands a *validation model* can be created from the original model and the contracts. This model contains the pre- and post-conditions inserted into the model in the appropriate places. Efficient and user friendly implementation of contracts is still ongoing research.

To ensure that a model is correct, the correctness constraints have to be satisfied. It is straightforward to ensure that no parameter assumption violations exists. Since all parameters are constants, it is sufficient to check that these constant values satisfy the conditions directly after they have been defined. The most challenging problem is to show that a subsystem always satisfies its invariant and post-condition. Tools such as *ss2lus*[6]

[6] ss2lus, VERIMAG, `http://www-verimag.imag.fr/~synchron/`

[21, 22] and the validation tools for Lustre [23, 24] can be used. If no tool for for static verification exist the substystem need to be validated by testing. Valid test cases consists of any input that satisfies the pre-condition. The post-condition and invariant are then used as the acceptance test. The final condition is the correctness condition for connections between subsystems, which consist of a logical formula. This means that it is easier to verify the composition of subsystems than the correctness of subsystems themselves.

6 ANALYTICAL VALIDATION OF THE MODE-SWITCHING SYSTEM

Design by contract is used to describe the assumption the subsystem *selection of control mode* makes about its environment and what it guarantees. If the subsystem conforms to the mode-automata architecture and the mode dependent behaviour does not contain memory, it is possible to derive simple conditions for the correctness. The memory requirement might seem very restrictive, but often the memory is more naturally placed as a common part of all modes. If no memory is present in mode specific behaviour it can also potentially reduce problems with transients when switching modes.

6.1 Correctness conditions

To prove that the mode transition subsystem (i, o, p, f) satisfies its contracts we derive conditions based on the behaviour in each mode and the transitions between modes. Assume that mode m has behaviour given by the enabled subsystem (i_m, o_m, p_m, f_m). Since the enabled subsystem m does not have memory, the output is a function of the input and the parameters. The following correctness condition is then derived (see correctness of subsystems in Subsection 5.2).

$$R_m(p_m) \wedge P_m(p_m, i_m) \wedge (o_m = f_m(p_m, i_m)) \Rightarrow Q_m(p_m, i_m, o_m) \tag{3}$$

The condition states that if the assumption about constants, the pre-condition of the enabled subsystem and the function from input to output signal holds, then so does the post-condition.

The transitions between modes are correct, if they guarantee that the pre-conditions of the enabled subsystems associated with each mode holds. Assume that there are l transitions with guards $g_1, \ldots, g_l$ into the mode m, and k outgoing transitions with guards $h_1, \ldots, h_k$. The pre-condition of a mode dependent behaviour in mode m need to be guaranteed when the mode is entered and when the mode is not exited. The condition for correct entry into a mode is given as:

$$R_m(p_m) \wedge (\bigvee_{1 \leq j \leq l} g_j(i)) \Rightarrow P_m(p_m, i_m) \tag{4}$$

This condition states that if a transition into the mode can be taken then the pre-condition of the mode dependent behaviour holds. Note that the condition is sufficient, but not necessary. The transition described by g_j is not necessarily taken if it is enabled, since there might be enabled transitions with higher priority. The condition for correct stay in the mode can be given as follows:

$$R_m(p_m) \wedge \neg(\bigvee_{1 \leq j \leq k} h_j(i)) \Rightarrow P_m(p_m, i_m) \tag{5}$$

This condition states that if no transition leaving mode m can be taken, then the pre-condition of the mode dependent behaviour holds. This condition can be shown to be necessary and sufficient.

The post-condition Q of the entire mode switching block should be guaranteed independently of the mode m the system is in. This can be stated as the condition:

$$\bigwedge_m R_m(p_m) \wedge P_m(p_m, i_m) \wedge Q_m(p_m, i_m, o_m) \Rightarrow Q(p, i, o) \tag{6}$$

All these conditions can be proved with a theorem prover such as e.g. PVS[7]. However, automatic proofs often require that all conditions are linear inequalities $c_1x_1+\ldots+c_nx_n \leq d$ or linear equalities $c_1x_1+\ldots+c_nx_n = d$ combined with the logical connectives $\neg$, $\wedge$ and $\vee$. Satisfiability of other types of formulae are in general not decidable. However, many model-checking techniques based on abstractions or other validation techniques based on approximations can solve other types of problems, as well. Usually these techniques are sound, but not complete. This means that if they state that a property is true, it is guaranteed to be true. If they state that a property is false, it can be either true or false.

6.2 Example

As an example of how conditions can be derived from the Stateflow chart consider *actual mode 1* in Figure 5. The contract for the subsystem enabled in this mode was given in Subsection 5.1, while the function computed by it is described in detail in [2]. The function is here denoted by $p_{Aref}, p_{Bref} = \mathrm{f}_{M1}(F, p_P, p_{min}, p_{max}, \Delta p_N)$ for brevity. The correctness of this enabled subsystem is defined as follows.

$$\begin{array}{l} \mathrm{R}_{M1}(A_A, A_B) \wedge \mathrm{P}_{M1}(p_{min}, p_{max}, F, p_P, \Delta p_{min}) \wedge \\ (p_{Aref}, p_{Bref} = \mathrm{f}_{M1}(F, p_P, p_{min}, p_{max}, \Delta p_N)) \\ \Rightarrow \mathrm{Q}_{M1}(p_{min}, p_{max}, p_P, p_{Aref}, p_{Bref}) \end{array} \tag{7}$$

Every transitions into actual mode 1 should establish the pre-condition P_{M1} of the corresponding enabled subsystem. The correctness of transitions into actual mode 1 is defined by the following condition as can be seen from Figure 5 by examining the guards of the transitions entering the mode.

$$\begin{array}{l} (\mathrm{vref\_positive}(v_{rC}) \wedge \mathrm{M1\_feas}(F, p_P, \Delta p_{min})) \vee \\ (\mathrm{M3a\_NOT\_feas}(F, p_P, \Delta p_{min}) \wedge \mathrm{M1\_feas}(F, p_P, \Delta p_{min})) \\ \Rightarrow \mathrm{P}_{M1}(p_{min}, p_{max}, F, p_P, \Delta p_{min}) \end{array} \tag{8}$$

When there is no enabled transition leaving actual mode 1 then the precondition of the enabled subsystem should also hold. When actual mode 1 is not exited the following conditions can be derived by using the guards of the transitions leaving the mode:

$$\begin{array}{l} \neg(\mathrm{vref\_NOT\_positive}(v_{rC}) \vee \mathrm{M1\_NOT\_feas}(F, p_P, \Delta p_{min}) \vee \\ (\mathrm{M3a\_feas}(F, p_P, \Delta p_{min}) \wedge \mathit{Target\_mode\_3a})) \\ \Rightarrow \mathrm{P}_{M1}(p_{min}, p_{max}, F, p_P, \Delta p_{min}) \end{array} \tag{9}$$

[7] PVS specification and verification system, SRI International, `http://pvs.csl.sri.com`

Here $Target\_mode\_3a$ denotes that the target mode of the system is mode 3a. It is possible to derive the condition corresponding to the system being in this mode using the information about transitions to and from the mode. The condition is for brevity not shown here, but guard conditions for the transitions can be found in [2].

The conditions have been checked with the PVS theorem prover. The conditions are not linear if p_{min}, p_{max} and Δp are considered to be variables. However, they are actually constants in the application. If the constant values are used the conditions are linear and the validity of the conditions can be automatically proved.

7 CONCLUSIONS

This paper presented a controller architecture for mode based systems and techniques for reason about correctness of Simulink/Stateflow models. The techniques were introduced using a controller for a digital hydraulics system. First, an architecture based on mode-automata that separated signal processing from control logic was introduced. Signal processing was implemented in Simulink, while control logic was implemented in Stateflow. To reason about model correctness the concept of design by contract was used. Each subsystem in the Simulink model can be specified by a contract in order to describe its interface to the environment. Assume guarantee reasoning about the correctness of the system using the contracts were then presented. Finally, a technique to analytically derive correctness conditions for the mode switching system based on the contracts was presented.

The contracts encourage the developer to more carefully design the interface between different subsystems, as well as explicitly write down assumptions that the subsystems rely on. This makes the models more robust and easier to reuse. The assume-guarantee style reasoning gives precise rules for how subsystems can be connected to each other. The contract also provides conditions that each component should satisfy. This gives acceptance conditions when creating unit tests for the subsystems.

As future work, the design by contract method will be extended to consider refinement [25] of Simulink models. This will provide a comprehensive framework to reason about model correctness. Refinement also enables development of models in smaller manageable parts. Tools that support this process and improve usability of design by contract are also under development.

Safety and reliability of the software used for control of machines are very important properties. To achieve high quality of the software in a timely fashion, adequate software development techniques are needed. This paper presented techniques for structuring a mode based controller, as well as reasoning about correctness of the Simulink/Stateflow models. Using these methods and ideas the quality and reliability of the software can be significantly improved.

REFERENCES

1. M. Linjama and M. Vilenius. Improved digital hydraulic tracking control of water hydraulic cylinder drive. *International Journal of Fluid Power*, 6(1):29–39, 2005.

2. M. Linjama, M. Huova, P. Boström, A. Laamanen, L. Siivonen, L. Morel, M. Waldén, and M. Vilenius. Design and implementation of energy saving digital hydraulic control system. In *The 10th Scandinavian International Conference on Fluid Power*, 2007. To appear.
3. F. Badeau and A. Amelot. Using B as a high level programming language in an industrial project: Roissy VAL. In H. Treharne, S. King, M. Henson, and S. Schneider, editors, *4th International Conference of B and Z Users: ZB2005*, volume 3455 of *LNCS*, Guildford, UK, 2005. Springer Verlag.
4. D. Harel. Statecharts: A visual formalism for complex systems. *Science of Computer Programming*, 8(3):231–274, 1987.
5. Mathworks Automotive Advisory Board (MAAB). Controller style guidelines for production intent using Matlab, Simulink and Stateflow. `http://www.mathworks.com/matlabcentral/fileexchange/`, 2001.
6. M. Beine, U. Eisemann, and R. Otterbach. Transforming a control design model into an efficient production application. In *Proceedings of the 2006 IEEE Conference on Computer Aided Control System Design*, pages 3019–3023, 2006.
7. U. Eisemann. Modeling guidelines for function development and production code generation. Distributed on the occasion of Embedded World Conference 2006, 2006. `http://www.dspace.de/ftp/papers/dspace_embWorld_0602_e_p344.pdf`.
8. F. Maraninchi and Y. Rémond. Mode-automata: About modes and states for reactive systems. In *European Symposium on Programming*, volume 1381 of *LNCS*. Springer Verlag, 1998.
9. F. Maraninchi and Y. Rémond. Mode-automata: a new domain-specific construct for the development of safe critical systems. *Science of Computer Programming*, 46(3):219–254, 2003.
10. J.-L. Colaço, B. Pagano, and M. Pouzet. A conservative extension of synchronous data-flow with state machines. In *EMSOFT '05: Proceedings of the 5th ACM international conference on Embedded software*, pages 173–182, New York, NY, USA, 2005. ACM Press.
11. O. Labbani, J.-L. Dekeyser, and P. Boulet. Mode-automata based methodology for SCADE. In *Hybrid Systems: Computation and Control: 8th international workshop, HSCC 2005*, volume 3414 of *LNCS*, pages 386–401. Springer Verlag, 2005.
12. P. Boström and L. Morel. Mode-automata in Simulink/Stateflow. Technical Report 772, Turku Centre for Computer Science, 2006.
13. B. Meyer. *Object-Oriented Software Construction*. Prentice-Hall, 2 edition, 1997.
14. R.-J. R. Back and J. von Wright. Contracts, games and refinement. *Information and Computation*, 156:25–45, 2000.
15. L. Burdy, Y. Cheon, D. Cok, M. Ernst, J. Kiniry, G. T. Leavens, K. R. M. Leino, and E. Poll. An overview of JML tools and applications. *International Journal on Software Tools for Technology Transfer*, 7(3):212–232, 2005. `http://www.cs.iastate.edu/~leavens/JML/`.
16. M. Barnett, K. R. M. Leino, and W. Schulte. The Spec# programming system: An overview. In *Proceedings of Construction and Analysis of Safe, Secure and Interoperable Smart devices (CASSIS 2004)*, volume 3362 of *LNCS*. Springer-Verlag, 2004. `http://research.microsoft.com/specsharp/`.
17. M. Abadi and L. Lamport. Composing specification. *ACM Transactions on Programming Languages and Systems*, 15(1):73–132, January 1993.
18. M. Abadi and L. Lamport. Conjoining specifications. *ACM Transactions on Programming Languages and Systems*, 17(3):507–534, 1995.
19. T. A. Henzinger, M. Minea, and V. Prabhu. Assume-guarantee reasoning for hierarchical hybrid systems. In *Proceedings of the Fourth International Workshop on Hybrid Systems: Computation and Control (HSCC)*, volume 2034 of *LNCS*, pages 275–290. Springer Verlag, 2001.
20. T. A. Henzinger, S. Qadeer, and S. K. Rajamani. You assume, we guarantee: Methodology and case studies. In *Proceedings of the Tenth International Conference on Computer-Aided Verification (CAV)*, volume 1427 of *LNCS*, pages 440–451. Springer Verlag, 1998.
21. S. Tripakis, C. Sofronis, P. Caspi, and A. Curic. Translating discrete-time Simulink to Lustre. *ACM Transactions on Embedded Computing Systems (TECS)*, 4(4):779–818, 2005.
22. N. Scaife, C. Sofronis, P. Caspi, S. Tripakis, and F. Maraninchi. Defining and translating a "safe" subset of Simulink/Stateflow into Lustre. In *Proceedings of the 4th ACM international conference on Embedded software*, pages 259–268. ACM Press, 2004.
23. P. Raymond. *LUSTRE-V4 manual*, 2000. `http://www-verimag.imag.fr/SYNCHRONE/tools.html`.
24. P. Caspi, N. Halbwachs, D. Pilaud, and J. Plaice. Lustre, a declarative language for programming synchronous systems. In *14th ACM Conf. on Principles of Programming Languages*, Munich, Germany, 1987.
25. R.-J. R. Back and J. von Wright. *Refinement Calculus: A Systematic Introduction*. Graduate Texts in Computer Science. Springer-Verlag, 1998.

HIGH EFFICIENCY AT 200 – 2000 RPM AND 10 – 30 MPa: VANE-IN-GROOVE PUMPS WITH ADAPTIVE ROTOR

A. Stroganov, L. Sheshin, Y. Volkov, S. Ryadnov, A. Nikiforov
Lumex JSC, St. Petersburg, Russia,
Phone +7 812 251 6989, Fax +7 812 251 6989
E-mail: strog@lumex.ru

ABSTRACT

Paper presents a development aimed at substantial reduction of friction losses and leakages level in vane pumps with a working chamber made in annular groove in a rotor face. Since sealing surfaces of a rotor and a housing are flat and vanes are fixed in the annular groove rigidly working fluid leakages are very small. Thus this type of vane pumps (called Vane-In-Groove) achieves high volumetric efficiency at wide range of rotation speed and operational pressure.

The new rotor design (called adaptive) comprises two parts: working and supporting, and provides Vane-In-Groove pump with good hydrostatic axial balancing of both parts of adaptive rotor. This allows to reduce friction forces between rotor parts and cover plates of the housing. Thus with adaptive rotor design high mechanical efficiency can be reached as well.

Paper describes one type of Vane-In-Groove pump architecture. It has an adaptive rotor located between housing cover plates and is preferable for variable displacement machines.

The tests equipment, schematic diagram and procedure for volumetric and overall efficiency measurement are presented as well as the tests results for 28 cm^3 pump. The test results illustrate high volumetric and overall efficiency at 200 – 2000 RPM and 5 – 30 MPa.

KEYWORDS: high overall efficiency, high mechanical efficiency, high volumetric efficiency, vane pump/motor, Vane-In-Groove

1. INTRODUCTION

Vane pump with a working chamber located in annular groove made in one of rotor faces (called by the authors Vane-In-Groove type of pump architecture) offers a number of advantages compare to a vane pump of conventional architecture.

Vane-In-Groove pump has a working chamber formed by four surfaces: in radial direction – by cylindrical walls of the annular groove, in axial direction – by the bottom of the annular groove and a working cover plate of a pump housing, aligned to a rotor face (see Fig. 1).

Such working chamber allocation defines the following advantages of this pump:
- major working chamber sealing is made by a plane-to-plane clamping of a rotor face to a working cover plate of a pump housing;
- rotor is hydraulically balanced in radial direction due to the fact, that working fluid locked in the high pressure area stresses with the same force to the opposite walls of the working chamber, which are the parts of the rotor.
Both technical features in combination with rigidly fixed in the annular groove vanes provide with the following custom advantages:
- high operational pressure (typical for piston pumps);
- uniform output flow with no kinematical ripple;
- high volumetric efficiency at wide range of rotation speed and operational pressure.

Vane-In-Groove (hereinafter VIG) pump can be done reversible, of variable displacement and can be used as a motor.

In the last case VIG architecture provides a motor with useful custom features such as:
- steady torque at wide range of rotation speed;
- low rotation speed at still high volumetric efficiency.

However, VIG architecture itself does not provide with axial balancing of a rotor. Working chamber sealing requires application of significant force to the side of a working cover plate opposite to a working chamber. This force must exceed the fluid pressure forces acting to a working cover plate from a working chamber. This in it's turn results in significant power losses caused by friction between a working cover plate and a rotor face when using mechanical means of a cover plate pressing. Some improvement can be achieved using working cover plate with a hydrostatically balanced axially movable sealing element but friction losses remain significant and overall efficiency of that pumps does not exceed 60 %.

Detailed analysis of the forces acting on a rotor and a working cover plate with an axially movable sealing element is given in [7].

Real solution of friction forces problem can be achieved with the new rotor design called Adaptive Rotor.

2. VANE-IN-GROOVE PUMP WITH ADAPTIVE ROTOR

The idea of Adaptive Rotor is that a rotor comprises two parts (Fig. 1 and Fig. 2) – working and supporting. Annular groove is made at a face of the working part of the rotor, forming a working chamber. Working part of the rotor is in sliding insulating contact with sealing elements of working cover plate (not shown in Fig.1), where forward and backward transfer limiters are located. Supporting part of the rotor has a set of supporting cavities and functions as movable sealing member being in sliding insulating contact with sealing elements of supporting cover plate (not shown in Fig.1). Working and supporting parts of the rotor are connected to each other so, that they rotate synchronously, but can make small mutual axial shifts and tilts to provide a

sliding insulating contact between the rotor parts and both cover plates as rotation of the rotor. Special force chambers of variable axial length are made between the working and supporting parts of the rotor. Each force chamber is connected to the working chamber and to the supporting cavity of the supporting part of the rotor.

Thus it transmits the fluid pressure from the part of the working chamber to the corresponding supporting cavity making the whole rotor assembly "pressure transparent". The area of the force chamber cross-section is chosen so that the fluid pressure forces, acting to the working part of the rotor from the working chamber and from the force chambers are balanced. Similarly, the area of a supporting cavity based on the force chamber cross-section area is chosen so that the fluid pressure forces, acting to the supporting part of the rotor from the supporting cavities and from the force chambers are balanced. Thus axial balancing of both working and supporting parts of the rotor is achieved. Full pressure force now is applied to the housing rather than the rotor. By choosing the abovementioned areas any pressing forces between the rotor parts and corresponding cover plates can be achieved. These pressing forces can be chosen as small as required for insulating each part of the rotor.

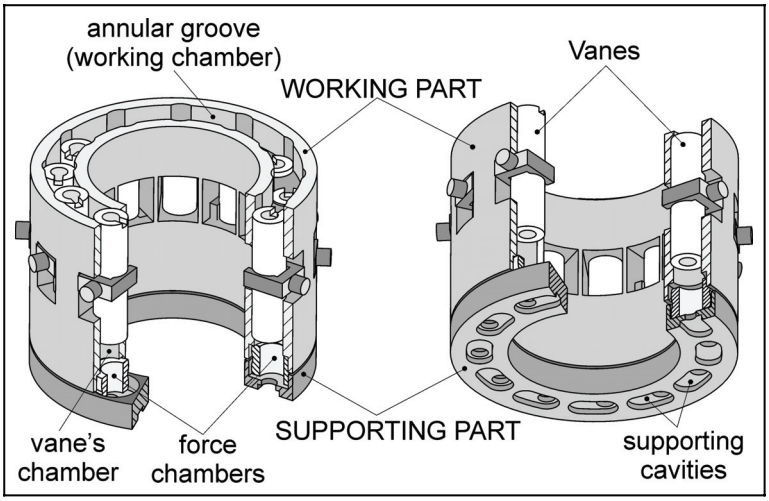

Figure 1: Adaptive Rotor design

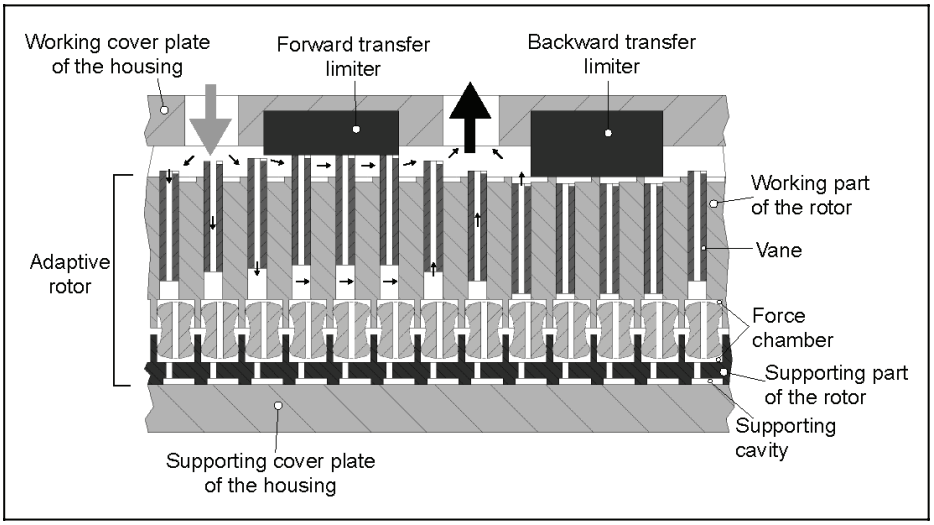

Figure 2: Vane-In-Groove pump with Adaptive Rotor – circular development along the annular groove

Detailed description of Adaptive Rotor design for a VIG machine as well as analysis of the forces acting on a rotor and a working cover plate is given in [7]. The Adaptive Rotor principle offers wide range of a VIG machine embodiments depending on requirements the machine must meet. Some embodiments are described in details in patent application [8].

To verify the idea of Adaptive Rotor in real-life a number of pump prototypes have been designed assembled and tested on our internal testing stand. All they have shown functionality and good performance.

3. TEST INSTALLATION AND PROCEDURE

Figure 3 presents scheme of the internal testing stand and Fig. 4 shows it's photos. The test circuit is closed type without backup. Industrial oil similar to HLP 46 was used as a working fluid. The water cooling system working on counter-current flow principle kept up the fluid temperature within the limits of 30±5 °C. Adjustable orifice was used as a load. Maximal drive power provided by the electromotor was 30 kW. Outlet pressure, oil temperature, pump housing temperature at 2 points were recorded as well as outlet and drainage flow rates were measured by gravimetric method.

The test matrix was defined as follows:
- operating pressure: 10, 20 and 30 MPa
- rotation speed: 200, 800, 1500 and 2000 RPM

Investigated parameters were measured for each value of the rotation speed against the outlet pressure.

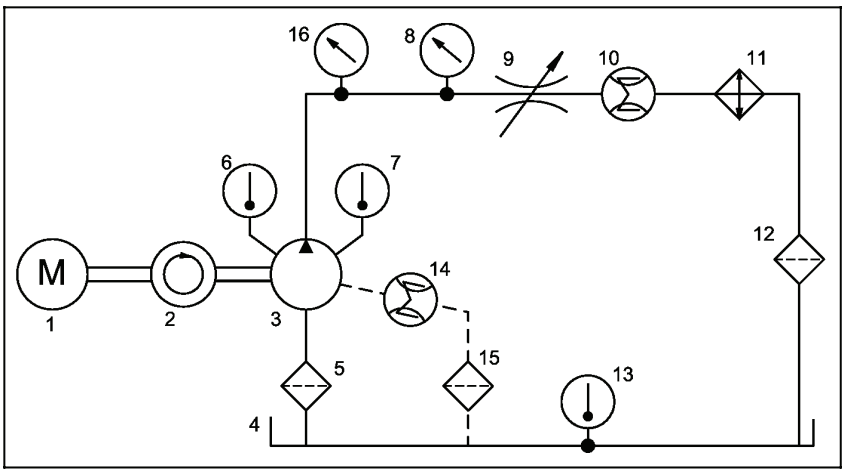

Figure 3: Scheme of the internal testing stand (auxiliary and safety equipment is not shown) 1– electromotor, 2 – tachometer, 3 – tested pump, 4 – tank, 5, 12, 15 – filters, 6, 7, 13 – thermometers, 8 – pressure sensor, 9 – adjustable load throttle, 10, 14 – flowmeter, 11 – counter-current flow cooler, 16 – pressure gauge

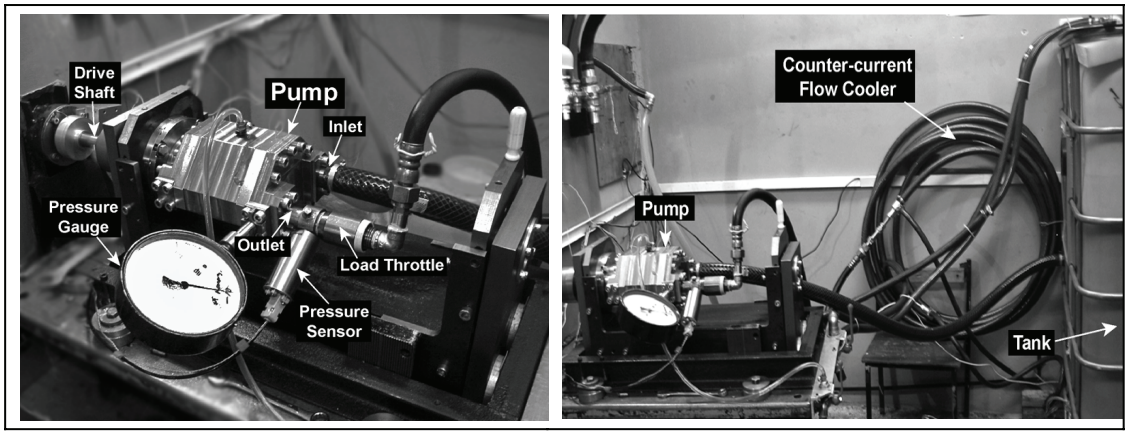

Figure 4: Photos of the internal testing stand (the electromotor is installed in adjacent room)

4. TEST RESULTS

The volumetric efficiency and overall efficiency were evaluated at stationary working points of the test matrix. All findings for each investigated parameter are presented as a set of curves, so that every curve in a set represents one parameter as a function of outlet pressure at constant rotation speed.

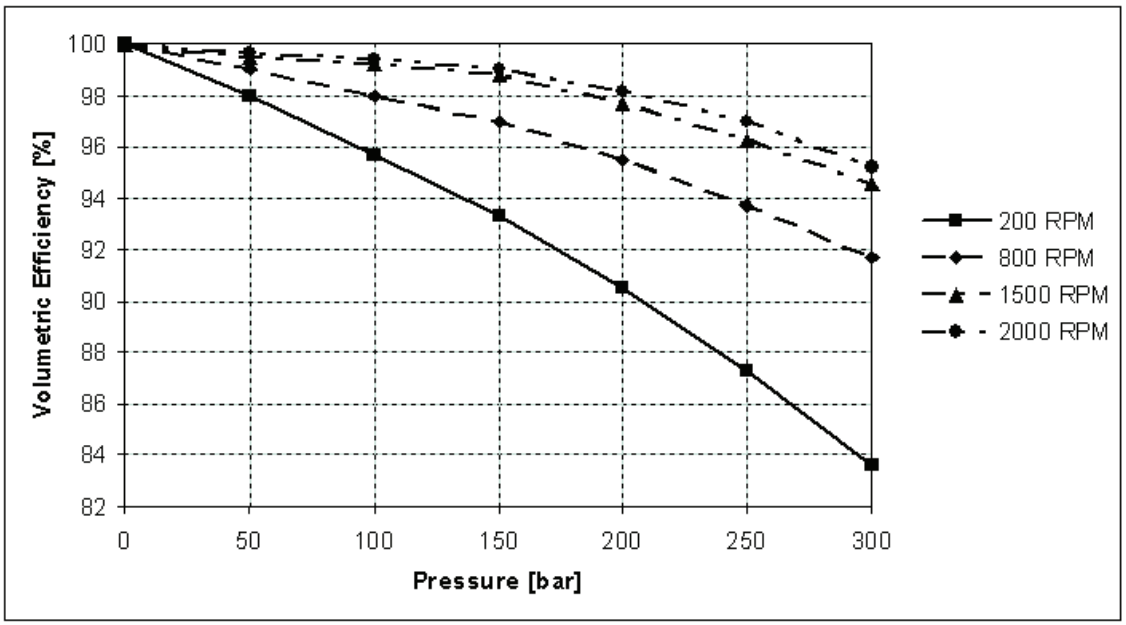

Figure 6: Evaluated volumetric efficiency against outlet pressure for 200, 800, 1500 and 2000 RPM

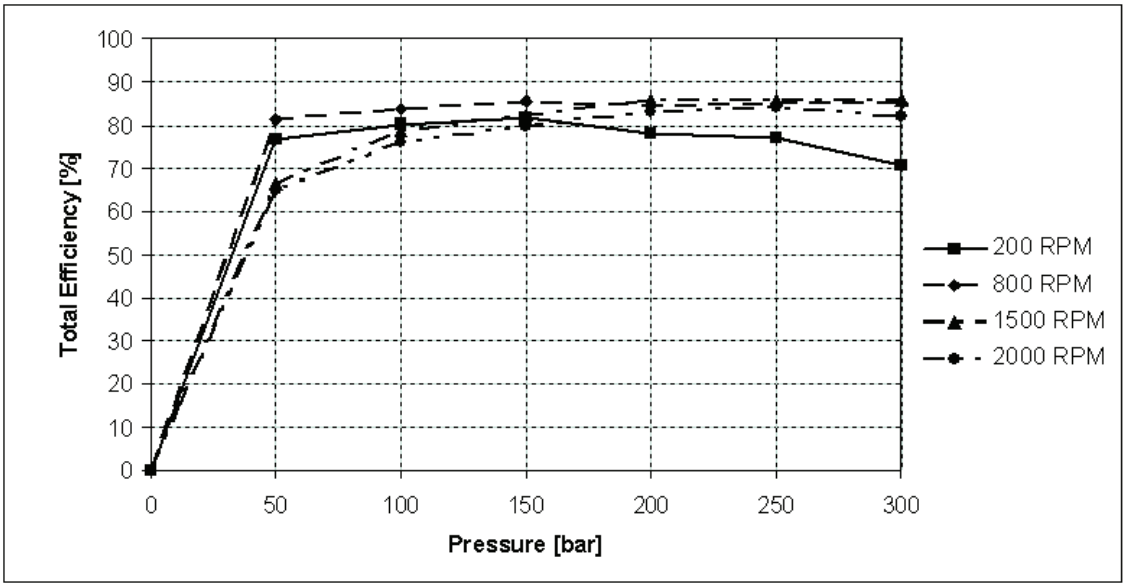

Figure 7: Evaluated overall efficiency against outlet pressure for 200, 800, 1500 and 2000 RPM

5. CONCLUSION

Data presented in 4 show high volumetric and overall efficiency of a VIG pump with Adaptive Rotor at wide range of rotation speed and operational pressure suitable for most of common fluid power applications. In fact a VIG pump with Adaptive Rotor combines high volumetric and overall efficiency proper to a piston pump with uniform output flow proper to a vane pump. When a VIG machine used as a motor it can deliver uniform rotation, constant torque and high overall efficiency at low rotation speed.

6. REFERENCES

1. Eggleton, S.W., and Vaughn, H.S., "Rotary Pump", Patent No.: US 1,096,804, May 12, 1914
2. Fischer, A., "Rotary Piston Machine," Patent No.: US 3,348,494, Oct. 24, 1967
3. Leroy, D., and Maupu, J., "Composant hydrostatique a palettes axiales et a placage axial," Patent No.: EP 0 269 474 A1, Oct. 16, 1986
4. Stroganov, A., Volkov, Y., Zimnikov, A., and Drouzhinin, A., "New Type of Reversible, Invertible, Variable Hydraulic Pump/Motor," Proceedings of the 49th National Conference on Fluid Power, March 19-21, 2002, Las Vegas, Nevada USA, pp 123-128
5. Stroganov, A.A., Volkov, Y.M., and Zimnikov, A.N., "New Type of Reversible, Invertible, Variable Hydraulic Pump/Motor," Proceedings of the Eighth Scandinavian International Conference on Fluid Power, May 7-9, 2003, Tampere, Finland, Vol. 1, pp 239-251
6. Stroganov, A.A., and Zimnikov, A.N., "Rotary Machine," Patent No.: US 6,547,546 B1, Apr. 15, 2003
7. Stroganov, A.A., Volkov, Y.M., "New Adaptive Rotor in the Vane-In-Groove Pumps: Significant Reduction of the Mechanical Losses," Proceedings of the 50th National Conference on Fluid Power, March 16-18, 2005, Las Vegas, Nevada USA

8. Stroganov, A.A., Volkov, Y.M., “Rotor Sliding-Vane Machine”, International Application No.: PCT/RU2006/000162, publication No.: WO/2006/115434

POTENTIALS OF A NUMERICAL TOOL FOR THE SIMULATION OF FLOW IN EXTERNAL GEAR MACHINES

Paolo Casoli, Andrea Vacca, Gian Luigi Berta
Industrial Engineering Department - University of Parma (Italy)
e.mail: paolo.casoli@unipr.it

ABSTRACT

This paper deals with the numerical prediction of the flow in external gear machine. As well known, a crucial aspect of gear machines is the variable offset of the axes of rotation of both gears in operation, as produced by pressure distribution in the chamber: which means that gears work in different positions from the nominal ones, i.e. those deduced from the machine drawings. In this work, on the basis of simulated results, several considerations about the effects of the actual position of gears centres on the main characteristics of the flow in external gear machine are developed.
The model used for the calculations has been developed by the authors and is named HYGESim (HYdraulic Gear machines Simulator). HYGESim permits a detailed evaluation of the flow inside gear pumps and motors, accounting for the main geometrical design parameters (e.g. shape and dimensions of the grooves on the bearing blocks, tooth profile, etc.). HYGESim consists of three different models strictly connected: a geometrical model (developed in the Pro/Engineer® environment), a fluid dynamic model and a module for the evaluation of forces and toques acting on the gears. These two latter are lumped parameters models (implemented in the AMESim® environment), utilizing a high number of parametric sub-models, written directly in C++ language.
Through the latest improvements implemented in HYGESim, the results discussed in the paper – referring to comparisons with data coming from experiments carried out on a stock pump – highlight how this simulation tool can be useful for an estimation of the actual position of both gears as a function of load pressure and shaft speed.

KEYWORDS: gear pump, gear motor, flow visualization, pressure ripple, flow ripple.

1. INTRODUCTION

In many fluid power circuits, a gear pump or motor are often preferred as energy conversion units owing to their simplicity and reliability, despite their unsuitability for variable displacement.
The principle of operation for the fixed displacement external gear units is displayed in fig. 1*a*: the fluid is transferred from the inlet port to the outlet port along the peripheries of the gears. The pressure values at the ports depend on the function of the machine: in case of pump, a lower level (LP) is at the inlet port and a higher level (HP) is

established by the hydraulic circuit at the outlet port; opposite conditions define the typical operation for a motor. The displacing volume is realized in the meshing zone (fig. 1*a*), where teeth enter into mesh, causing rapid changes in the volume of fluid trapped. The unevenness of these variations can determine pressure peaks – significantly above the average value at the HP port, or below the average value at LP port – that are strictly related with the pressure ripple and flow oscillation at the outlet port; therefore an excessively rugged pressure course can lead to noise and instability of the whole hydraulic system. Moreover, overpressures have to be limited to avoid high loading of the gears, mechanical losses and erosion. Vacuum values, due to the insufficient flow into the expanding inter-tooth volumes, are responsible for possible cavitation onset.
These transient pressures, in the most recent gear pumps and motors, have been limited by the introduction of properly designed recesses in the slightly movable bushing or sliding bearings (fig. 1*b*). These recesses prevent the trapped volumes from being fully isolated from both the inlet or outlet ports.

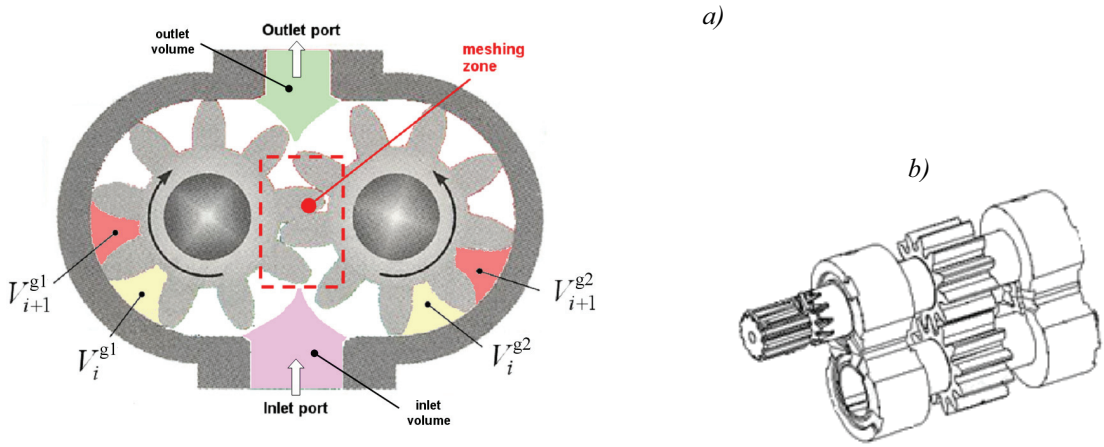

Figure 1 – *a)* Operation of a gear machine; definition of the control volumes for the HYGESim model *b)* detail showing a typical design of bearing blocks

Further, the typical design of the bushings or sliding bearings is complicated by the introduction of grooves (such as blackflow grooves) and other recesses for sealing rings, in order to realize an optimal pressure distribution on the surfaces of all the moving parts, thus permitting force balance and gap control (the latter for the reduction of leakages losses) [1].
All the described aspects have been captivated the interest of many researchers and fluid power industries, providing a significant spin-off for improved designs, in terms of noise emissions, flow oscillations, cost and reliability. Many works in the open literature are focused on a detailed description of the processes characterizing the machine operation, such as [3-7,10,12-14], while others (such as [2,8,9]) propose numerical models for the prediction of the gear machine operation. Moreover, many consolidated design principles are summarized in [1]. Certainly, the ability to simulate the pump or motor operating accounting for the main processes involved is a key requirement, so far as simulations are utilized for design analysis and optimization. The detailed prediction of the flow processes in the meshing zone allows, for example, the comparison of different recess geometries on the bearing blocks, as for their effects on the pressure transients and volumetric efficiency.
However, it is well known that the entire flow dynamics inside the gear machine is affected by the conditions at the inlet and outlet ports, which are dependent on the behaviour of hydraulic system connected to the machine. There is also a strict interaction between the flow through the various elements of the gear machine: for example the pressure history of the tooth space volume during the gear rotation is

significantly affected by blackflow grooves, if present. Therefore, the results provided by an accurate model of the meshing zone may be nullified by unsuitable assumptions made on the boundary conditions.
Considering these aspects, the authors have chosen to model the complete machine operation, developing a code that provides a detailed evaluation of the flow through the gear machine allowing, at the same time, the simulation of a complete hydraulic system. The model, described in [15-17], is named HYGESim (HYdraulic GEar machines Simulator), utilizes a discrete parameter approach, and permits the analysis of the flow under a precise characterization of the shape of the teeth profiles, of the recesses and of the axial (gear sides) and radial (between tooth tip and housing) gaps. Being the fluid dynamic model implemented in the AMESim environment, HYGESim easily permits the study of the machine, when it is used in a generic circuit. This allows a correct prediction of the flow resulting from the interaction between different systems with a single machine, as well as with machines of different design.
This paper reports only a brief description of the HYGESim structure, referring for details to previous works [15-17], while attention is mainly paid to the latest improvements to the model. In the release presented herein, HYGESim can easily evaluate the effects caused by a different offset of both gears on the main flow features. These results deal with an important issue of external gear machine design; as a matter of fact, the forces applied by the fluid onto the gears are responsible for movements of both the centres of rotation. Consequently, the actual position of the gears is, in general, different from the nominal one, which is reported on the drawings of the machine. The control and compensation of these forces yields to a reduction in the offset of gears axes; on purpose, a numerical tool for the evaluation of these forces (as presented in [16,17]) can be useful to the designer. However, it is important to evaluate, on the basis of the instantaneous resulting forces, the position of both gears in order to reproduce the actual conditions, that are dependent on the operating conditions.
Results provided in this work show how, from the comparisons between experimental data and simulation results, it is possible to utilize HYGESim for an estimation of the actual average positions assumed by the gears centres. Predictions concerning a time-varying offset of the gears are also available in HYGESim, even if the analysis of the relationship between the offset and the forces suffered by both gears is still in progress.

2. HYGESIM MODELLING APPROACH

Fig. 2*a* reports the structure of the HYGESim model, which includes three different parts: the model for the analysis of the flow through the machine, the model for the evaluation of the geometrical features required by the fluid dynamic model, and finally the module for the evaluation of forces and toques acting on the gears.

2.1. Fluid dynamic model

The fundamental part of HYGESim is the fluid dynamic model, the other parts being developed on the basis of its specifications. In particular, the flow through the machine is evaluated with a lumped parameter approach, considering the flow domain subdivided in a number of control volumes (CVs), as shown in fig. 1*a*. In each CV fluid properties depend only on time and are assumed uniform.
The model evaluates the flow through the gear machine solving a system formed by a continuity equation for each CV and a laminar, or turbulent, orifice equation for each connection between adjacent CVs. In this way the pressure inside each CV can be predicted.

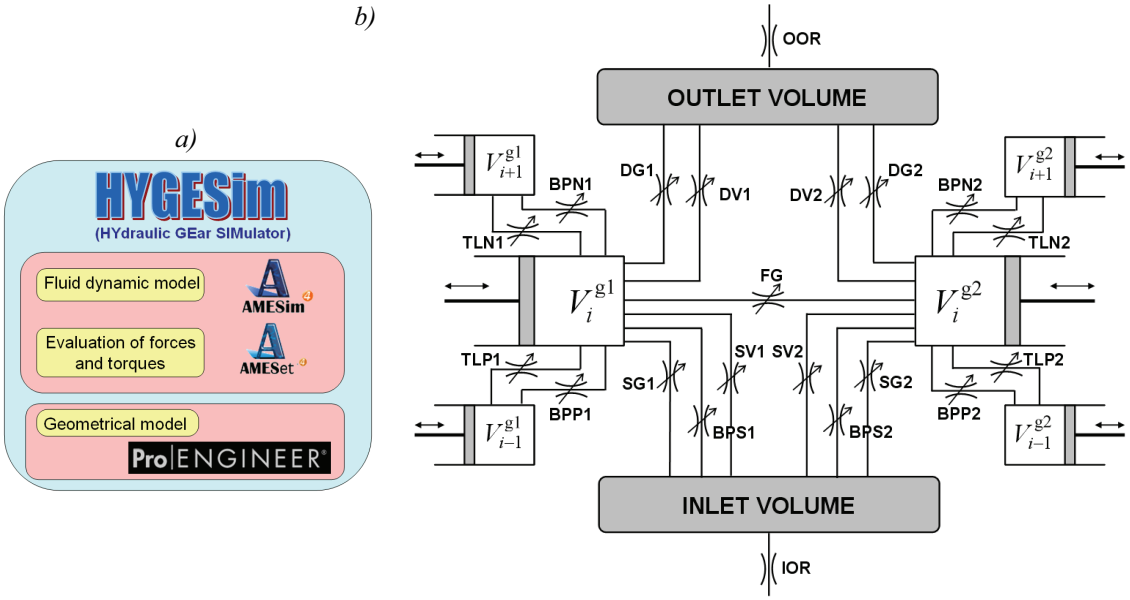

Figure 2 – *a)* The HYGESim structure
b) Hydraulic model for a couple of corresponding teeth space volumes (V_i^{g1}, V_i^{g2})

Connection type (*)	Description	Equation
FG	connection between the two corresponding teeth space volumes, fig. 3*a* (connection closed outside the meshing zone)	$\dot{m}_{i,j} = \frac{(p_i - p_j)}{\lvert(p_i - p_j)\rvert}\rho\left(\overline{p_{i,j}}\right)c_{eq}\left(Re_{i,j}\right)\cdot \cdot\Omega_{i,j}(\theta)\sqrt{\frac{2\lvert(p_i - p_j)\rvert}{\rho\left(\overline{p_{i,j}}\right)}}$ (1) $\Omega_{i,j}$ indicates the flow area of the connection between the CVs *i* and *j*
DV	connection between the TSV and the outlet volume through the gear whole depth (examples are displayed in fig. 3*a*)	
SV	connection between the TSV and the inlet volume through the gear whole depth (fig. 3*a*)	
DG	connection between the TSV and the outlet port through the grooves on the bearing blocks (fig. 3*b*)	
SG	connection between the TSV and the outlet port through the grooves on the bearing blocks (fig. 3*b*)	
BPP BPN	connections representative of leakages between adjacent TSVs due to clearances among gear side faces and bearing blocks internal faces. BPP indicates the leakage between a TSV and the previous one on the same gear (fig. 3*c*); while BPN is used for the analogous flow with the following tooth space volume	$\dot{m}_{i,j} = \rho\left[-\frac{h^3}{12\mu}\frac{p_i - p_j}{L} + \frac{u}{2}\right]b$ (2)
BPS	connection between a tooth space volume and shaft bearing (connected to the drain line), as reported in fig. 5*c*	
TLP TLN	leakages between adjacent TSV due to clearances among teeth tip and casing. TLP refers to the connection with the previous TSV on the same gear (fig. 3*c*); while TLN is for the connection with the following TSV	

Table 1 – Description of connections represented by orifices in fig. 2*b*
(*) the number following the acronym indicate the gear (1 or 2) to which the connection is referred

The connection framework is summarized in fig. 2*b*, which reports the basilar fluid dynamic scheme adopted by HYGESim. The figure refers to a generic couple of corresponding tooth space volumes (V_i^{g1}, V_i^{g2}), that always mesh together, under the hypothesis of same number of teeth per gear. According to this assumption, a suitable description of the basic fluid dynamic model can be provided focusing on the scheme of fig. 2*b*, for a single pair of corresponding TSVs. However, the HYGESim model considers the duplication of such scheme for a number of times equal to the number of teeth per gear. Hence, all the TSVs of the machine are simultaneously simulated, considering for each pair of TSVs a defined angular position ϑ. From this point of view, this approach significantly differs from the one chosen for the simulation model

proposed in [10,12-14], which is conceived for an accurate description of flow only in the meshing zone, while it is analogous to the models proposed in [2,8,9].
Descriptions provided in tab. 1 and fig. 3 clarify the scheme of fig. 2*b*. In detail, tab. 1 reports the equations utilized for the calculation of the instantaneous flow rates through the connections. The typical orifice equation is used for FG, DV, SV, SG connections, considering a dependence of the discharge coefficient on the Reynolds number [18,19]. As concerns the calculation of leakages, the modified Poiseuille equation, that is able to consider the relative motion of walls (in case of BPP, BPN, TLP, TLN) is adopted.
Once the instantaneous flow rates through the connections are known, the time course of the pressure inside every CV is determined by means of the following equation:

$$\frac{\mathrm{d}p_i}{\mathrm{d}t} = \frac{1}{V_\mathrm{i}} \frac{\mathrm{d}p}{\mathrm{d}\rho}\bigg|_{p=p_i} \left[\sum \dot{m}_{in,i} - \sum \dot{m}_{out,i} - \rho\big|_{p=\overline{p}} \frac{\mathrm{d}V_i}{\mathrm{d}t} - \sum \left(\rho\big|_{p=\overline{p}} \frac{\mathrm{d}V_{var,i}}{\mathrm{d}t} \right) \right] \tag{3}$$

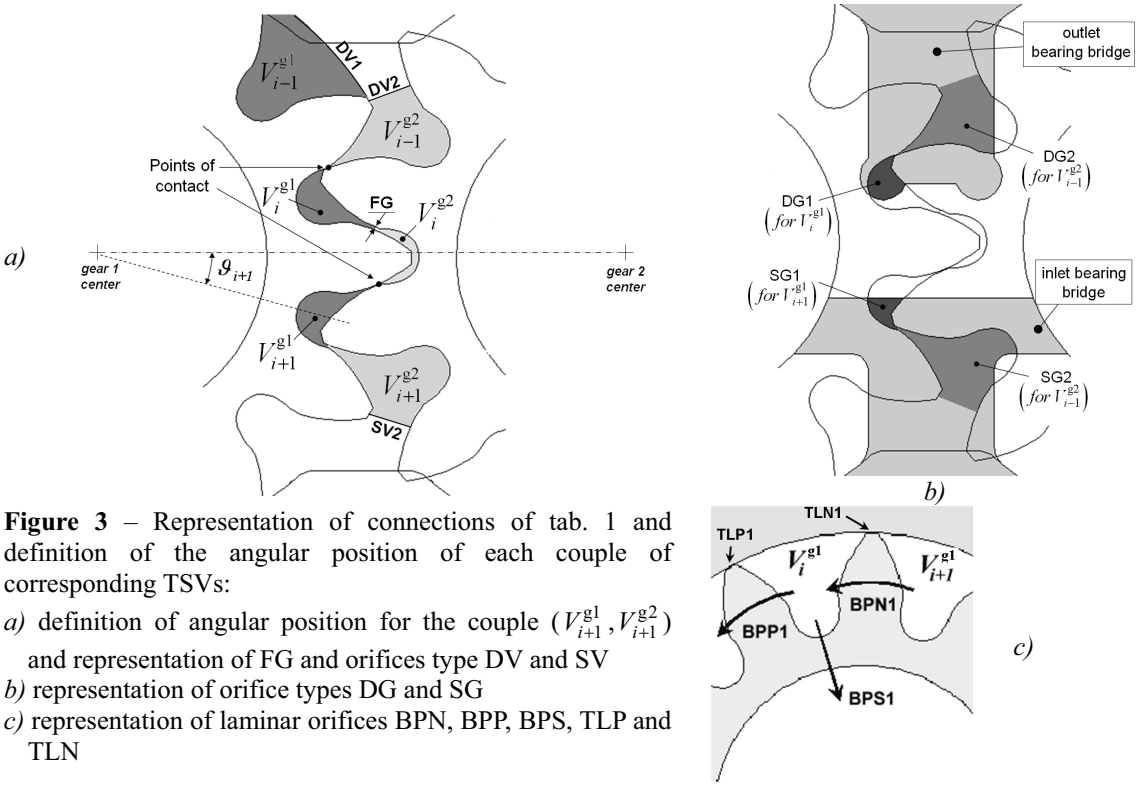

Figure 3 – Representation of connections of tab. 1 and definition of the angular position of each couple of corresponding TSVs:
a) definition of angular position for the couple (V^{g1}_{i+1}, V^{g2}_{i+1}) and representation of FG and orifices type DV and SV
b) representation of orifice types DG and SG
c) representation of laminar orifices BPN, BPP, BPS, TLP and TLN

Eq. (3) combines the continuity equation and the state equation of incompressible fluid. By considering a dependence of fluid density on pressure, the model allows to account, in a simplified manner, for the effects of both gaseous (air release) and vapor cavitation. These effects can strongly influence the characteristics of flow in the expanding inter-tooth volumes of meshing zone, and, consequently, the overall performance of the gear machine. Details concerning the modeling of the fluid properties, with an approach similar to the one proposed for another positive displacement hydraulic machine in [20], can be found in [21].

2.1. Geometrical model

The geometrical features (throat areas, equivalent diameter, volume of each CV) required by the fluid dynamic model are in general dependent on the angular position of the gears. In particular, as regards the connections of fig. 2*b*, many parameters are defined only in restricted intervals of gear revolution, and need to be nullified in the remaining phases.

As a consequence, a precise evaluation of flow is possible only under an accurate evaluation of such features; for this purpose, a parametric CAD model has been developed. Much effort has been made on this model, which takes advantage of the Pro/E facilities, in order to guarantee an adequate evaluation of all the geometric data as a function of the angular position of gears. In particular, the latest version of the geometrical model allows an automatic generation of the input for the fluid dynamic model (ASCII file) starting directly from the drawings of the gears, bearing blocks and casing (fig. 4*a*). The model allows to locate the centres of rotation of both gears in a defined position, leading to the possibility of extending the potentials of HYGESim, as concerns the prediction of the effects due to the movements of gears axes.
The model operating principle is based on the definition of the geometry of the TSVs with assumptions consistent with the fluid dynamic model. Therefore in fig. 4a two corresponding TSVs are considered during a complete revolution of the gears, with an angular step imposed by the user (e.g. 0.1°, for simulations performed in this work).
Particular attention is paid for the definition of CVs delimiting surfaces: criteria of minimum distance between two corresponding profiles of teeth are assumed in the meshing zone, as evident from fig. 3; while the outside circle diameter is considered when the TSVs are not meshing. The assumptions on the geometrical model should avoid unrealistic discontinuities, especially as regards the course of volumes (that are strictly related to the pressure course, according to eq. (3)). For this purpose, the model changes the features used for the definition of each CV when, referring to fig. 4*b*, the area of zones A and B equals the area of zones A and C. Fig. 4*b* refers to a TSV for a gear in the initial interval of the meshing zone, but the same considerations can be extended to the corresponding TSV of the other gear, and for the final part of the meshing zone.
The definitions used for the CV in the meshing zone involve modifications of both the inlet and outlet volumes, well predicted by the geometrical model. As reported in [16], a correct evaluation of flow in presence of these volumes modifications requires the introduction of the derivative term ($dV_{var,i} / dt$) in eq. (3), for all the CVs of the fluid dynamic model.

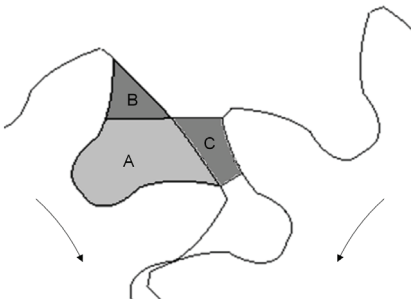

b)

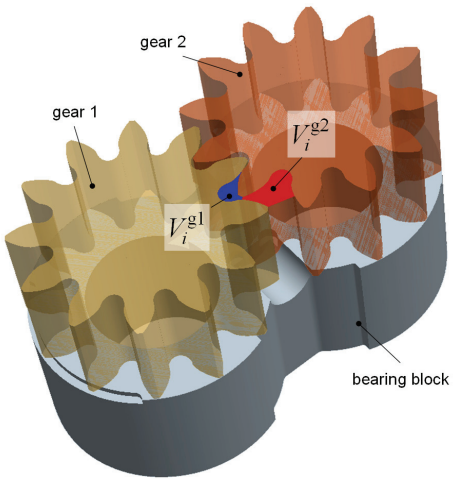

a)

Figure 4
a) Definition of the TSV for the fluid dynamic model at the borders of the meshing zone
b) Detail of elements utilized for the geometrical model, based on Pro/E

2.3. Module for the evaluation of forces and torques

Taking advantage of the results provided by the fluid dynamic model, HYGESim permits the prediction of the forces orthogonal to the axes of rotation (fig. 5). The estimation of these forces suffered by gears allows significant considerations concerning the gears displacement, as a function of the operating conditions of the machine.

The module evaluates the instantaneous forces and torques starting from the distribution of pressures acting on each gear, provided by the calculations performed for each CV by the fluid dynamic model. In detail, the approach followed in this module consists of a subdivision – for each gear – of the cylindrical surface in a number of sub-surfaces corresponding to the CVs defined by the fluid dynamic model. Therefore, a single fluid dynamic CV (thus a single value of pressure) is pertinent to a generic tooth space outside the meshing angular interval, while more CVs (up to three) pertain to the same surface when the tooth space is in the meshing zone, as evident observing the representation of fig. 3*a*. Further descriptions concerning the definition of the surfaces in accordance to the fluid dynamic model for the calculation of pressure forces can be found in [16].
The contribution (pressure in the CV multiplied by its effective surface) of every surface – for each gear – is summed up in order to obtain the total force due to fluid pressure. This is done performing separated calculations in x and y components. In particular, starting from the system of x (or y) forces, it is possible to evaluate an equivalent system given by the resultant $F_{p,x}$ (or $F_{p,y}$) applied at the gear centre and a torque $T_{p,x}$ (or $T_{p,y}$). At last, the overall effect of fluid pressure is given by:

$$\vec{F}_p(\vartheta) = F_{p,x}(\vartheta)\vec{i}_x + F_{p,y}(\vartheta)\vec{i}_y \tag{4}$$

$$T_p(\vartheta) = T_{p,x}(\vartheta) + T_{p,y}(\vartheta) \tag{5}$$

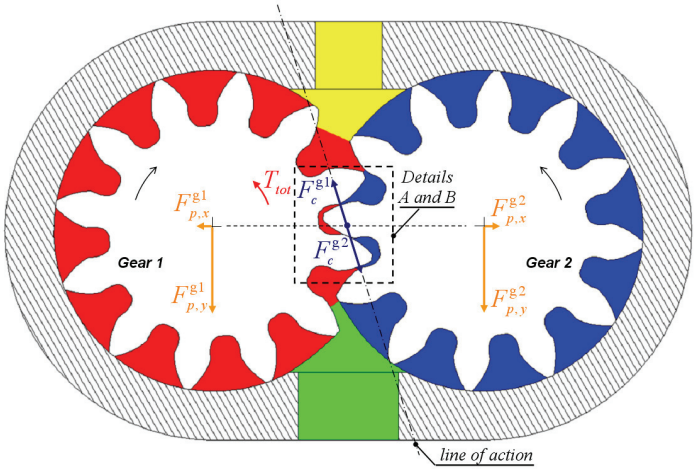

Figure 5
Main parameters calculated by the module of forces and torques, starting from the pressures in each CV provided by the fluid dynamic model. The figure refers to a gear pump

Assuming gear 1 connected to the shaft of the machine (thus the driving gear, in case of a pump), the moments equilibrium for gear 2, under the hypothesis of constant rotational speed, yields:

$$T_p^{g2}(\vartheta) = F_c^{g2}(\vartheta)R^{g2} \tag{6}$$

Eq. (6) simplifies the features that characterize the power transmission between gears, considering the force F_c to be constantly directed along the line of action and always located at the pitch centre. Therefore, effects of teeth deformations, tolerances and friction are neglected. In deeper detail the friction due to sliding teeth profiles has been neglected because of the typical low values of friction forces in gear hydraulic machines; moreover it is known that the sign of this contribution changes in proximity of the pitch point where sliding vanishes [19].
Including the contact force the system of forces and torques acting on both gears is given by:

$$\text{Gear 1: } \left\{F_{p,x}^{g1}(\vartheta)\vec{i}_x; F_{p,y}^{g1}(\vartheta)\vec{i}_y; \vec{F}_c^{g1}(\vartheta); T_p^{g1}(\vartheta)\right\} \tag{7}$$

$$\text{Gear 2: } \left\{F_{p,x}^{g2}(\vartheta)\vec{i}_x; F_{p,y}^{g2}(\vartheta)\vec{i}_y; \vec{F}_c^{g2}(\vartheta)\right\} \tag{8}$$

HYGESim reduces the systems given by Eqs. (7) and (8) into the two equivalents:

$$\text{Gear 1: } \left\{F^{g1}_{tot,x}(\vartheta)\vec{i}_x; F^{g1}_{tot,y}(\vartheta)\vec{i}_y; T^{g1}_{tot}(\vartheta)\right\} \tag{7}$$

$$\text{Gear 2: } \left\{F^{g2}_{tot,x}(\vartheta)\vec{i}_x; F^{g2}_{tot,y}(\vartheta)\vec{i}_y\right\} \tag{8}$$

T^1_{tot} is representative of the instantaneous torque on the shaft, and can be used for the evaluation of the power exchanged between the machine and the fluid. $F_{tot,x}$ and $F_{tot,y}$ express the total forces on the wheels, that are balanced by the journal bearings. Once both intensity and direction of the $\vec{F}_{tot}$ forces are determined, it is possible to estimate the position of the gears centres.

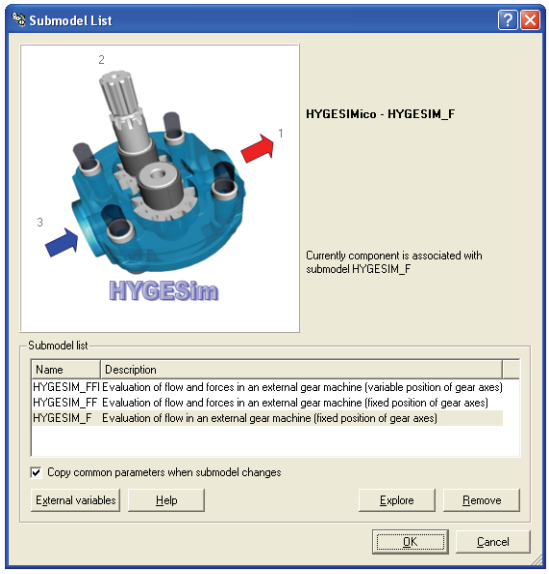

a)

MODEL	Geometrical feature definition
HYGESIM_F	$Gf = Gf(\vartheta)$
HYGESIM_FF	
HYGESIM_FFI	$Gf = Gf(\vartheta, i_c)$

Table 2 – Definition of the generic geometrical feature

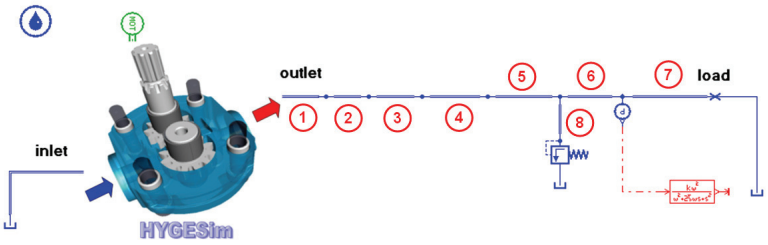

b)

Figure 6 – *a)* HYGESim icons and the three different levels of analysis available
b) Example of utilize of HYGESim in a AMESIM (circuit used for the simulation of experimental tests)

3. HYGESIM IMPLEMENTATION

The latest release of HYGESim permits three different levels of analysis of the machine, through different AMESim® submodels (fig. 6). The simplest and fastest level allows the prediction of the characteristics of flow through the machine; the intermediate level includes also the evaluation of forces and torques involved in the machine operation; while the most complex simulations allow to introduce a variable position of both gears centres axes during the rotation of gears. The AMESim® sketch of HYGESim obviously changes with its different versions. Fig. 7 reports the case of the most complex version (HYGESIM_FFI, tab. 2). The figure highlights the parts of the model used for the calculation of forces and torques acting on both gears (detail A); the submodel for the interaction with the geometrical model (detail B); and the model for the calculation of

the position of gears axes (detail C). This latter utilizes the instantaneous $\vec{F}_{tot}(\vartheta)$ as input and determines the position of gear axes expressed in terms of distance between gears centres, assuming the movement of the centres in a direction related to the forces (fig. 8). Further details concerning the calculation of the displacement of gears will be provided in a future work. Results discussed in this work refer to simulations performed with the simplest versions of HYGESim model (HYGESIM_F and HYGESIM_FF), that require geometrical data pertinent to a fixed position of both gear axes.

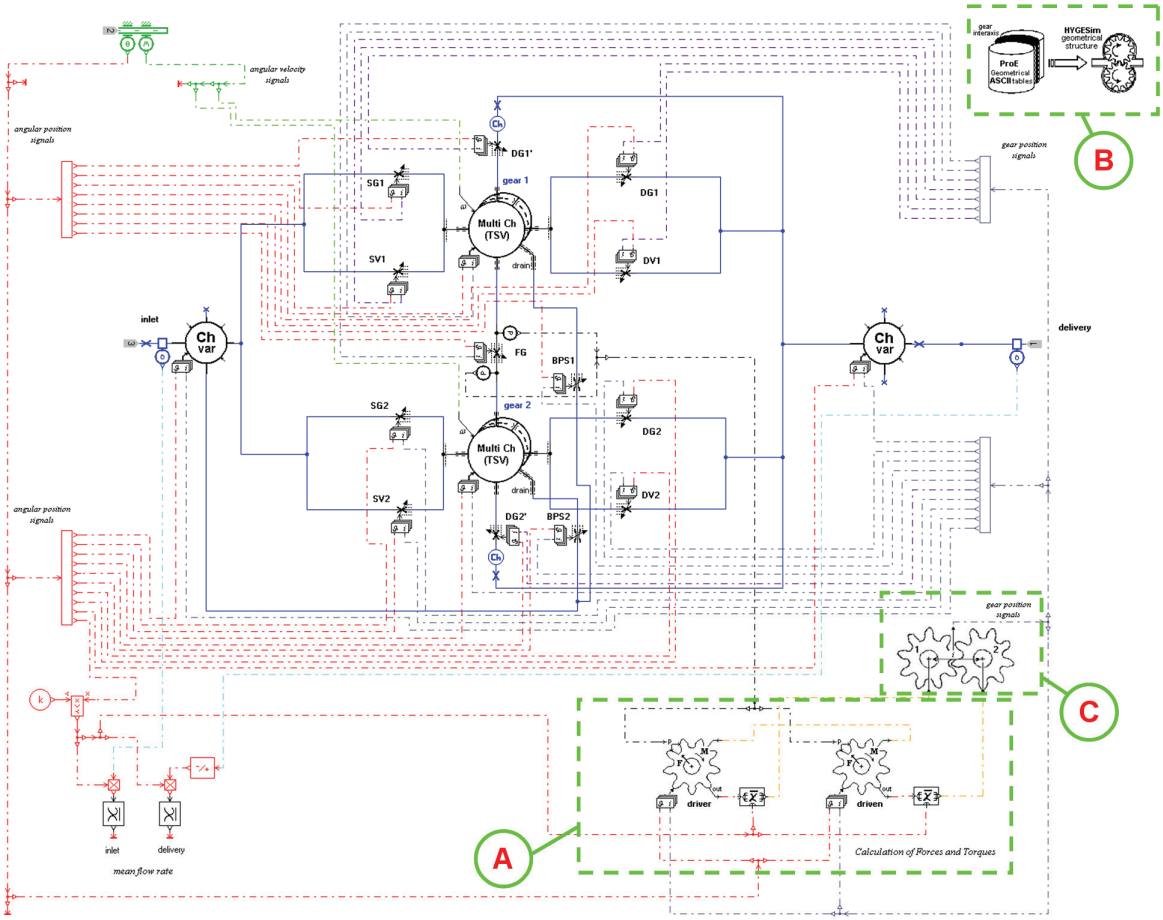

Figure 7 – AMESim® sketch of the most complex HYGESim version

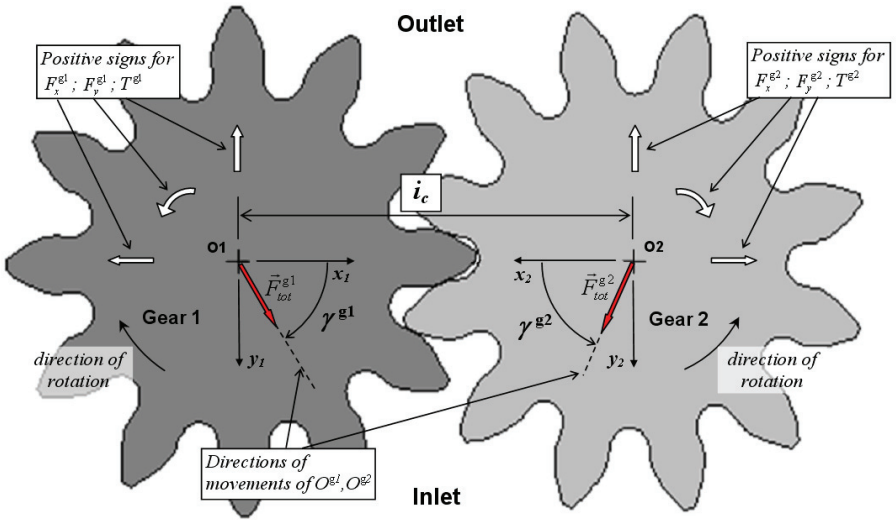

Figure 8 Conventional sign for forces and torques utilized by HYGESim. Definition of distance between gears centres

RESULTS

Numerical results provided by HYGESim have been verified through comparisons with experimental data. As a matter of fact, a test campaign was carried out on a CASAPPA PLP20 stock pump. The machine considered for the experiments has a 11.2 cm^3 nominal displacement and 12 teeth per gear.
Experiments were performed at Casappa laboratories, utilizing a rig similar to the one described in [22]. Fig. 9 reports a ISO simplified scheme of the hydraulic circuit used for the gear pump characterization and a picture of the apparatus utilized.
From fig. 9*a*, it is possible to observe how the transducers placed in the circuits permit the measure of steady state pump characteristics; however, considering the good agreements between the predicted and experimental data in such conditions, the results discussed in this work are mainly focused on the pressure ripple, acquired by the device 7 of fig. 9*a*. Different operating conditions, in terms of load at the delivery (controlled through the variable orifice 8 of fig. 9*a*) and shaft speed, were considered for the verification of numerical results. For the sake of brevity only some relevant conditions are here described.

a)

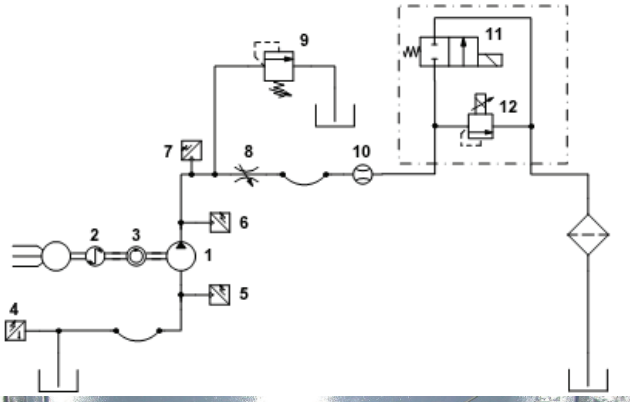

1. Pump under test
2. Torquemeter
3. Rotational speed transducer
4. Temperature transducer
5. Pressure transducer
6. Pressure transducer
7. High bandwidth pressure transducer
8. Variable orifice (load)
9. Pressure relief valve
10. Flowmeter
11. Pressure control valve
12. Solenoid on/off valve

b)

Figure 9
a) ISO representation of the hydraulic circuit used for tests
b) Picture of the test rig

From both the practical experience and the theory of hydraulic line phenomena, it is well known that there is a strong influence of the delivery circuit features on the resulting pressure oscillations. For this reason, the role played by the simulation of the circuit downstream from the delivery end of the pump is comparable to the accuracy achieved by the model of the machine. In this context, many methods have been developed for solving the differential equations that describe the unsteady fluid flow in hydraulic lines [23]. These techniques may be classified into two branches: the linear models (such as the variable separation method, known also as acoustic method, and the impedance method), that assume constant fluid properties, and the nonlinear models

(such as the method of characteristics and some space sampling approaches), that are based on the more realistic assumption of variable fluid properties [24,25]. For the simulation of hydraulic lines AMESim® adopts 1D Finite Elements Method with a variable time step integration, that provides an accurate solution and are best suited for usage with a variable time step [19]. These methods provide a solution acceptable for lumped parameter models. Moreover, the damping for fast dynamics can be under estimated, compared to reality [19]. However, for the cases considered in this work, the accuracy on the simulation of fast dynamics assumes a lower importance, because of:

-) the limited bandwidth typical of the hydraulic components;
-) the limited sampling frequency of transducer 7 in fig. 9*a*;
-) the damping effect introduced by the frequency dependant friction model.

These premises clarify the importance of a proper utilization of the standard models provided by the software [19], in view of both the desired accuracy of the results and the global simulation time requirements. Consequently, after a subdivision of the delivery circuit (length ≈ 17 mm; diameter ≈ 9 mm) between the pump and the variable orifice (fig.9*a*) in an AMESim® sketch consistent with the actual geometry (see fig. 6*b*), the proper submodel for each hydraulic line has been chosen on the basis of the evaluation of the theoretical natural frequencies of the delivery circuit (in comparison to the sampling frequency that characterizes the tests) and of the dissipation numbers. As described in [26-28], the latter parameter permits to evaluate the importance of the frequency dependant friction phenomena.
The contribution of the highest frequencies has been neglected introducing a numerical filter (highlighted in fig. 6*b*). In this way the calculated delivery pressure courses can be used for the comparison with the data acquired during the test campaign.
Once the model for the simulation of the test circuit has been established, many simulations have been considered in this work in order to estimate the average distance between the centres of the gears. For this purpose, different results obtained with HYGESIM_FF version of the model – changing the distance between the gear centres (value of i_c, tab. 3) – have been compared to experimental results. A different set of values for the geometrical features required by the fluid dynamic model pertains to every case of tab. 3. Hence, the geometrical code has been executed separately for each i_c, placing the gears according to the direction of the total forces suffered (see results in the following).

Achronym	Trend for i_c
Int1	*increment of* i_c
Int2	
Int3	
Int4	

Table 3 – List of i_c used for the simulation of tests performed on the CASAPPA PLP20.11,2 pump

Fig. 11 shows the changes of some significant geometrical features for a couple of corresponding TSVs taken as reference. It is evident that only features strictly related to the meshing mechanism are prone to relevant changes with the value of i_c (cases *a* and *b* of fig. 11); while other characteristics are almost unaffected by i_c (cases *c* and *d*).
Figs. 12 and 13 present the comparison between the experimental and the simulated pressure courses at pump delivery. In detail, two different conditions have been considered: fig. 12 shows the comparison in terms of frequency spectra, while fig. 13 pertains to the time course. In all the cases considered, a good agreement between simulation and experiments has been found for the “Int 2” and “Int 3” cases of tab. 4. This justifies also the good predictions discussed in [15,16], in which the nominal geometry of the pump - deduced from quotes and tolerances indicated on the pump drawings and close to the “Int 2” and “Int 3” cases – was considered as for the

evaluation of the geometrical features. “Int 4” well approximates the experimental trend only at the highest values of delivery pressure (fig. 13), highlighting the dependence of i_c on the operating pressure. In all the experimental courses of p_D a low frequency mode is evident, which corresponds to the rotational frequency: this is due to movements of the geometrical centre of revolving gears, as it is caused by imperfections due to dimensional tolerances and wear.

a)

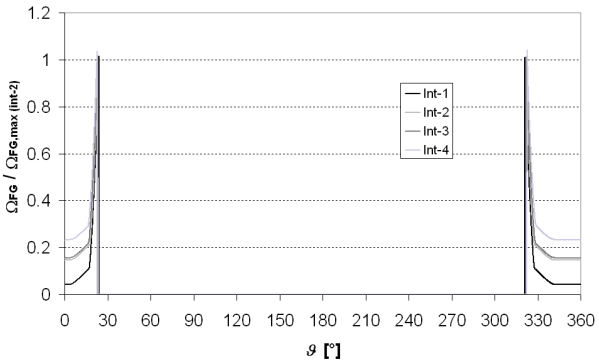

b)

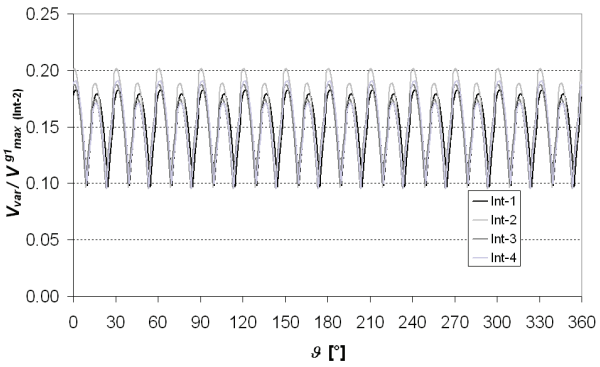

c)

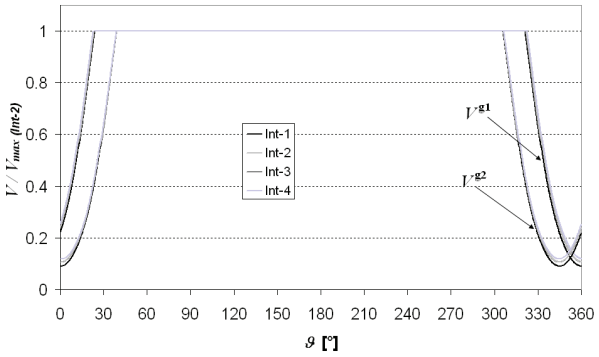

d)

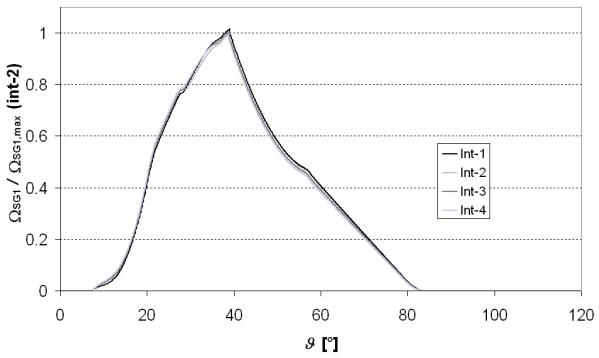

Figure 11
Examples of significant effects on pump geometrical features due to changes on the value of i_c:
a) flow area of connection FG
b) variable volume of the inlet port
c) volume of two corresponding TSVs
d) flow area of connection SG1
Differences are significant in the courses of *a)*, *b)* and are negligible in the diagrams *c)* and *d)*

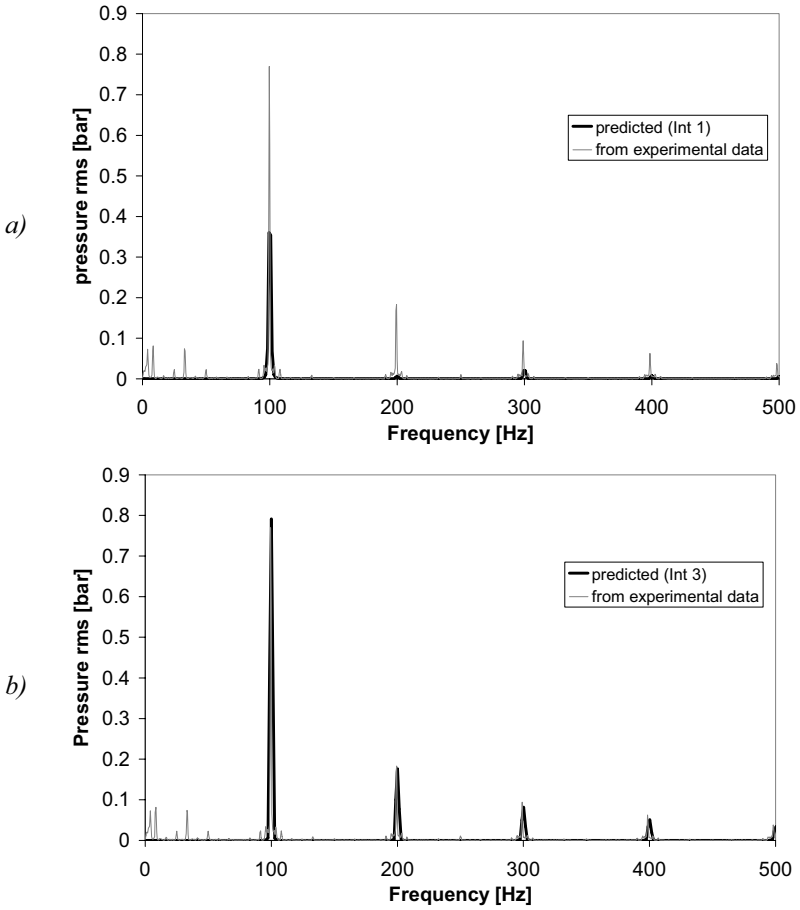

Figure 12
Comparison between the experimental and the predicted FFT courses of delivery pressure (n=500 r/min; $\overline{p_D}/p_{\max} \approx 0.8$):
a) prediction using Int 1 geometrical data
b) prediction obtained utilizing Int 3 geometrical data

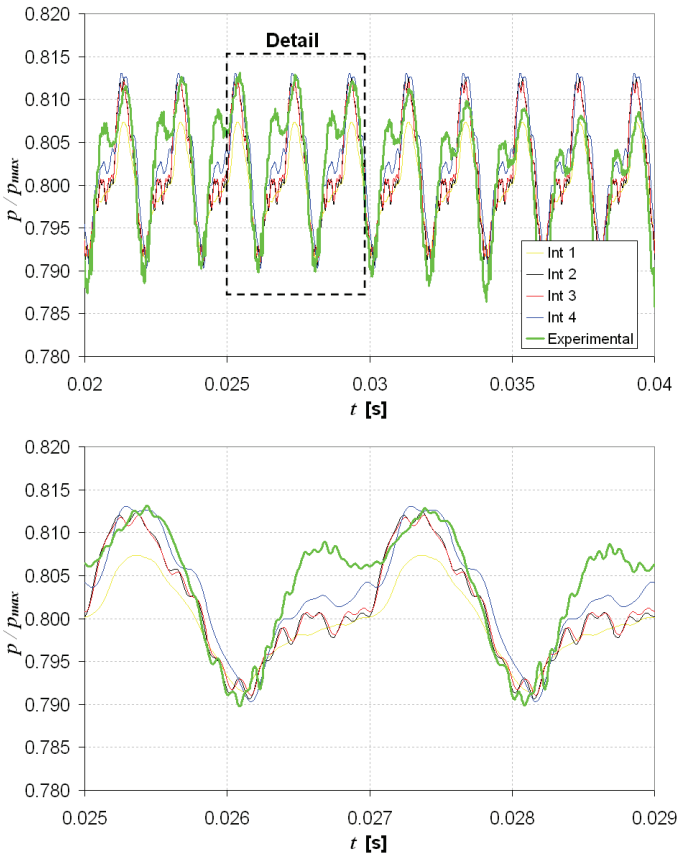

Figure 13
Comparison between the experimental and the predicted time courses of the delivery pressure (n=2500 r/min; $\overline{p_D}/p_{\max} \approx 0.8$)

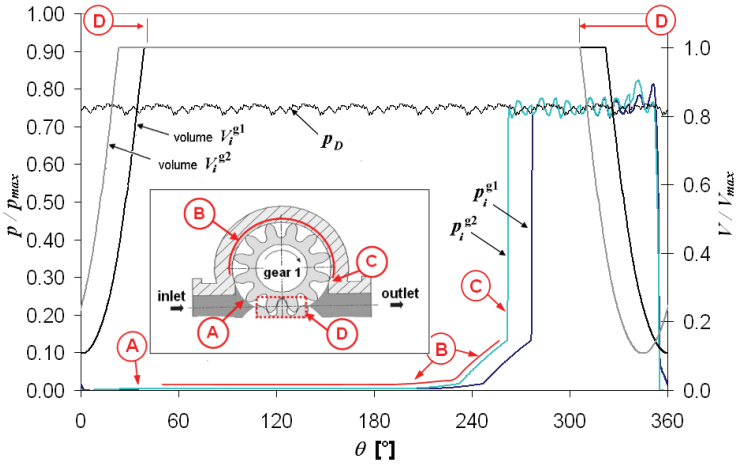

Figure 14
Simulated pressure inside corresponding TSVs (n=2500 r/min; $\overline{p_D}/p_{max} \approx 0.8$):

a) with reference to V_i^{g1}, assuming "Int 3" geometry:

- **A.** The considered CV is outside the meshing zone;
- **B.** Effect of leakages;
- **C.** The considered CV reaches the delivery port
- **D.** Meshing zone

a)

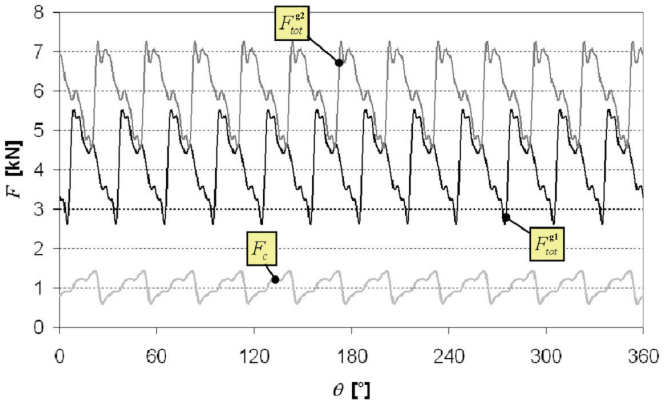

b)

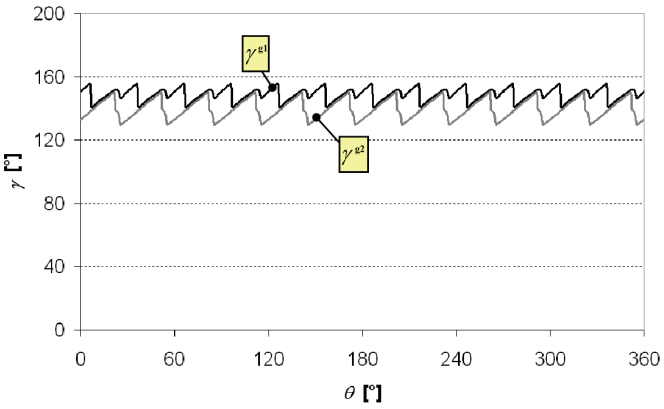

c)

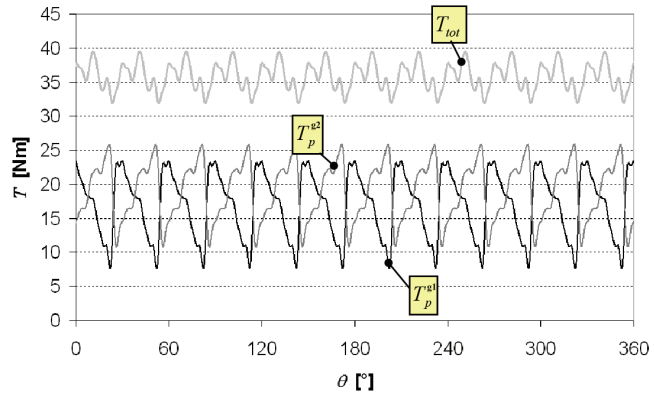

Figure 15
Results obtained for forces and torques changes (Int 3, n =2500 r/min ; $\overline{p_D}/p_{max} \approx 0.8$):

a) force intensity (average values $\overline{F_{tot}^{g1}} = 4.2$ kN; $\overline{F_{tot}^{g2}} = 6.0$ kN; $\overline{F_c} = 1.05$ kN)

b) direction of forces (notation of fig. 8), average values: $\overline{\gamma^{g1}} = 148.7°$; $\overline{\gamma^{g2}} = 138.2°$)

c) torques due to fluid pressure and total torque required at pump shaft ($\overline{T_{tot}^{g1}} = 35.80$ Nm)

The use of HYGESim permits deep analyses of the working concept of the gear machine. Fig. 14 describes the course of the pressure inside a pair of corresponding TSVs, and permits to evaluate the main causes that are involved in the main changes of its value. Results shown in fig. 14 are consistent with those discussed in [3], and are similar to what reported in [16], although in the case considered here backflow grooves are absent from the bearings blocks. Therefore, the developed simulation tool permits the detailed prediction of the highest and lowest pressure value reached by each TSV in the meshing zone, accounting for the dynamics of the hydraulic circuit connected to the outlet and inlet ports. Consequently, HYGESim can be utilized not only for the prediction of flow oscillations at the machine ports, but also as a development tool that permits to evaluate the influence of pump geometry and of the overall hydraulic system on the working conditions of the pump. Moreover, the adoption of a proper model for the evaluation of fluid properties ([21] similar to one of those described in [20]) permits a reliable evaluation of a possible onset of cavitation (detail A of fig. 14).
The last results reported pertain to the HYGESim module for the calculation of forces and torques (fig. 15). With the notation of fig. 8, the figs. 15*a* and 15*b* displays the intensity and the angular direction of the forces acting on each gear. The values assumed by γ_1 and γ_2 confirms the absence of the backflow grooves (if they are present, for the same pump different values are found, as reported in [16]).
The predicted torque required at pump shaft is displayed in fig. 15*c*; the same figure reports also the torques T_p^{g1} and T_p^{g2} that permits to consider the force due to fluid pressure acting on the gear centres. From T_p^{g2} it is possible to derive the force F_c, shown in fig. 15*a*.

CONCLUSIONS

The latest improvements introduced on HYGESim, a lumped parameter code for the simulation of external gear hydraulic units, are presented in this paper. The simulation code consists of three different modules: a fluid dynamic model, a geometrical model and a module for the calculation of forces and torques suffered by the gears. The geometrical model is a CAD pre-processor that permits to account for the complex geometry of gears and recesses on the bearing block; the other two modules are developed in C++ in the AMESim® environment.
The latest version of the simulation model permits different level of analysis of the machine when it is placed in a generic AMESim® hydraulic system: the simplest model solves the flow through the machine assuming a fixed position of gear axes, while the most complex one permits to consider a variable distance between the gears centres during the fluid dynamic calculations.
The potentials of the code, as a tool useful for design and deep analysis of gear machines operation – discussed also in previous works – are highlighted by the results presented in the paper. Moreover, with a particular reference to experiments performed on a stock pump, in this work the simulation tool has been utilised for the analysis of effects due to changes in the distance between the axes of rotation. For this purpose, a number of simulations performed assuming different positions of gears centres have been considered for the comparison with experimental data, thus permitting the estimation of the actual position of gears as a function of the machine operating conditions.
Due to the importance of the hydraulic lines in unsteady flow conditions, the good agreement between simulated results and experimental data shown in the paper – for all the conditions considered – has been reached with a careful utilisation of the AMESim® models provided for the simulation of the wave propagations in hydraulic lines.

NOMENCLATURE

F	Force
L	Clearance length
R	Base circle radius
Re	Reynolds number
T	Torque
V	Volume
b	Clearance width
c_{eq}	Coefficient of discharge
h	Clearance thickness

Subscripts

D	delivery
c	contact
i,j	indexes
in	entering
max	maximum
out	exiting
p	pressure
tot	total
var	variable
x,y	axis of reference

i	Unit vector
i_c	Distance between gear centres
$\dot{m}$	Mass flow rate
n	Angular velocity
p	Pressure
t	Time
u	Peripheral velocity
Ω	Orifice cross sectional area
γ	Angular direction of force
μ	Fluid viscosity
θ	Gear angular position
ρ	Fluid density

Superscripts

g1	gear mounted to the shaft (driver, for a pump)
g2	freewheel gear (driven, for a pump)

Abbreviations

CV	control volume
TSV	tooth space volume

ACKNOWLEDGEMENTS

The authors would like to thank Casappa S.p.A, in particular Dr. Marco Guidetti, for providing test facilities and hardware.

REFERENCES

[1] Ivantysyn J., Ivantysynova M., 2003, *Hydrostatic Pumps and Motors*, Tech Books Int., New Delhi, India.
[2] Fielding D., Foster K., Hooke C.J., Martin M.J., 1977, *Sources of pressure pulsation from a gear pump*, Seminar on "Quiet oil hydraulic systems", The Institution of Mechanical Engineers.
[3] Mancò S., Nervegna N., 1993, *Pressure Transient in an External Gear Hydraulic Pump,* Second JHPS International Symposium on Fluid Power, Tokyo, Japan.
[4] Bonacini C., Borghi M., 1990, *Calcolo delle Pressioni nei Vani fra i Denti di una Macchina Oleodinamico ad Ingranaggi Esterni*,Oleodinamica-Pneumatica, Nov. 1990, Tecniche Nuove.
[5] Poy Ferrer M., Codina E., 2002, *Suction Capability of Gear Pumps*, 2nd Int. FPNI PhD Symposium, Italy, July 2002.
[6] Gutes M., Gamez Monter P.J., Castilla R., Codina E., 2000, *Journal Bearing Performance in Gear Pumps*, 1st Int. FPNI-PhD Symposium, Germany, Sept. 2000.
[7] Manring N. D., Kasaragadda S., 2003, *The Theoretical Flow Ripple of an External Gear Pump*, ASME Journal of Dynamic Systems, Measurement, and Control. Vol. 125.
[8] Eaton, M., Keogh, P.S., Edge, K.A., 2006, *The modeling, prediction, and experimental evaluation of gear pump meshing pressure with particular reference to aero-engime fuel pumps*, Proc. IMechE Vol.220 Part I: J.System and Control Engineering pp. 365-379.
[9] Mancò S., Nervegna N., 1989, *Simulation of an External Gear Pump and Experimental Verification*, JHPS International Symposium on Fluid Power, Tokyo, Japan.
[10] Eaton M., Edge K., 2001, *Modelling and Simulation of Pressures within the Meshing Teeth of Gear Pumps*, Int. Conf. on Recent Advantages in Aerospace Actuation Systems and Components, June 13-15, 2001, Toulouse, France.

[11] Bonacini C., Borghi M., 1990, *Calcolo delle Pressioni nei Vani fra i Denti di una Macchina Oleodinamico ad Ingranaggi Esterni*,Oleodinamica-Pneumatica, Nov.1990, Tecniche Nuove.
[12] Paltrinieri F., Borghi M., Milani M., 2004, *Studying the Flow Field Inside Lateral Clearances of External Gear Pumps*, 3rd FPNI-PhD Symposium on Fluid Power, Spain, June 2004.
[13] Zardin B., Paltrinieri F., Borghi M., Milani M., 2004, *About the Prediction of Pressure Variation in the Inter-Teeth Volumes of External Gear Pumps*, 3rd FPNI-PhD Symposium on Fluid Power, Spain, June 2004.
[14] Borghi M., Milani M., Zardin B., Paltrinieri F., 2006, *The influence of cavitation and aeration on gear pump and motors meshing volume pressures*, IMECE2006, ASME International Mechanical Congress and Exposition, November 5-10, Chicago, IL (USA).
[15] Casoli P., Vacca A., Franzoni G., 2005, *A numerical model for the simulation of external gear pumps,* The sixth JFPS International Symposium on Fluid Power, Tsukuba, Japan, Novembre 07-11 2005.
[16] Casoli P., Vacca A., Berta G.L., *A Numerical Model for the Simulation of Flow in Hydraulic External Gear Machines*, PTMC2006 Power Transmission and Motion Control, 13-15 September 2006, University of Bath (GB).
[17] Berta G.L., Casoli P., Vacca A., *Modellazione del funzionamento di macchine ad ingranaggi esterni*, 61° Congresso Nazionale ATI, Perugia, 12-15 Settembre 2006.
[18] Blackburn J. F., Reethof G.., Shearer J. L.. 1966, *Fluid Power Control*. USA: MIT Press.
[19] IMAGINE S.A., 2004, AMESim® *and* AMESet® *version* 4.2 *User manual*, Roanne, France, September 2004.
[20] Casoli P., Vacca A. Franzoni G., Berta G.L., 2006, *Modelling of fluid properties in hydraulic positive displacement machines*, Simulation Modelling Practice and Theory 14 (2006) 1059–1072 – ELSEVIER.
[21] IMAGINE s.A., AMESim_ Standard fluid properties, – *Indexed elementary fluid properties,* Report FP01, Roanne, France, 2000.
[22] Casoli P., Vacca A., Franzoni G., 2003, *A Numerical Model for Simulation of "Load Sensing" Spool Valves*, The 18th Int. Conf. on Hydraulics and Pneumatics, Prague, Czech Republic, September 2003.
[23] Hoffman J.D., 1992, *Numerical methods for engineers and scientists*, McGraw-Hill, Inc.
[24] Streeter, V. L., and Wylie, E. B., 1974, *Waterhamme*r *and Surge Control*, Annual Review of Fluid Mechanics, Vol. 6, pp. 57-73.
[25] Fletcher C.A.J., 1992, *Computational techniques for fluid dynamic,* 2nd ed Berlin*:* Springer.
[26] Goodson, R. E., and Leonard, R. G., 1972, *A Survey of Modeling Techniques for Fluid Line Transients*, J. Basic Eng. Trans. ASME*,* Vol. 94, pp. 474-482.
[27] Zielke W., 1968, *Frequency dependent friction in transient pipe flow* , Trans. ASME, Journal of Basic Engineering, Series D, Vol. 90, March 1968, pp. 109-115.
[28] Bergant A., Simpson A. R., Vìtkowsky J., 2001, *Developments in unsteady pipe flow friction modelling*, Journal of hydraulic research, vol.39, 2001, No.3.

The Test Rig for Lubrication Properties of Port Pairs in Axial Piston Pump and Preliminary Test Investigation on It

Bin Wang, Hua Zhou, Huayong Yang
Zhejiang University
State Key Laboratory of Fluid Power Transmission and Control
310027 Hangzhou, P.R.China
Phone +86 571 87951659, Fax +86 571 87951646
E-mail: wb3581@163.com, hzhou@sfp.zju.edu.cn, yhy@zju.edu.cn

ABSTRACT

To develop lubrication property tests of port plate in axial piston pump with higher supply pressure, larger flow, and to study the working characteristics of key friction pairs of high performance pump, the new test rig is built up. According to the mechanical model of port pair, principally the two parameters, supply and loading pressure acting on test sealing area, respectively offered by two individual hydraulic circuits, can be controlled availably for interference avoidance and comparative study with theoretical models. Such present main problems as lubrication properties of port pairs, especially test investigation are discussed and the primary coverage of them from theoretical lubrication model are analyzed, and aimed at their technical difficulties, the makeup, characteristics and key techniques of dynamic test rig of lubrication film of port pairs with new electrohydraulic control based on exact position feedback are brought forward. The test data of factual film balance, frictional torque, film height measuring at several points on sealing area, leakage flow and oil temperature by testing on this rig indicate that the supply pressure notably affects the film height and its shape and that they show unequivalent change. The oil temperature, as one of the main factors, which play a part on the leakage flow, does indistinctively at low or middle temperature points.

KEYWORDS: Port pair, Lubrication film, Supply pressure, Film height, Leakage

1 NOMENCLATURE

μ	Kinetic viscosity of fluid
ρ	Density of fluid
U_1	Center speed X-component of friction piece 1(Cylinder block)

V_1	Center speed Y-component of friction piece 1(Cylinder block)
W_1	Center speed Z-component of friction piece 1(Cylinder block)
u_{2x}	Center speed, U_2, X-component of friction piece 2(Port plate)
w_{2x}	Center speed, W_2, X-component of friction piece 2(Port plate)
r_1	Inner circle radius of inside sealing loop of half-circumference groove, double-cavity, interim supply port plate
r_2	Outer circle radius of inside sealing loop of half-circumference groove, double-cavity, interim supply port plate
r_3	Inner circle radius of outside sealing loop of half-circumference groove, double-cavity, interim supply port plate
r_4	Outer circle radius of inside sealing loop of half-circumference groove, double-cavity, interim supply port plate
h	Height of oil film
p_s	Supply pressure
μ	Dynamical viscidity of lubrication oil between port pairs
c_e	Flux correction coefficient result from initial phase laminar flow effect in the gap of port pair

2 INTRODUCTION

As steady performance improvement of hydraulic power unit in, all kinds of industrial equipments and engineering machinery, higher pressure, higher speed and advanced displacement change ways have been the trends of axial piston pump. However, a key factor confining its performance, in these plunger machines, is the failure of their port plate or cylinder after short running. Port pair, one of key frictional pairs, has been hot investigated by many scholars because of its service life restricted by worse conditions and important effects on the whole pump performance. The necessary lubrication condition that proper height lubrication film forms between slipping surfaces of the pair in axial piston pump should been kept, which can work as lubricants. At home and abroad, some related experimental equipments has been set up, but most of them work on static simulations or embedded tests so that it's difficult for main signals to be captured in real time ,and the film height cannot be modulated during testing so that more exact data or conclusions of lubrication experiments cannot be gotten easily. This paper aims at the lubrication test system of port pair in axial piston pump and gives some analysis of technical characteristics and preliminary test results.

3 THEORETICAL MODEL

Figure 1 shows the tribological model of port pair. It can be reduced to the dynamic lubrication film between two frictional surfaces. The formula 1[1] is universal Reynolds lubrication equation on the basis of orthogonal cartesian coordinate system:

$$\frac{\partial}{\partial x}\left[\frac{\rho h^3}{\mu}\frac{\partial p}{\partial x}\right]+\frac{\partial}{\partial z}\left[\frac{\rho h^3}{\mu}\frac{\partial p}{\partial z}\right]=6\frac{\partial}{\partial x}[\rho h(u_{2x}+U_1)]+6\frac{\partial}{\partial z}[\rho h(W_{2z}+W_1)]$$
$$-12\rho\left(u_{2x}\frac{\partial h}{\partial x}+W_{2z}\frac{\partial h}{\partial z}\right)+12\rho\left(V_{2y}-V_1\right) \quad (1)$$

The principle of port pair resembles that of the thrust bearing. While the cylinder rotates, its center circumference speed U_1 works in the same direction as the coordinate, and the port pair revolves about the axis center in the some circumference speed U_2 with U_1, accordingly , $u_{2x}=U_2$. The speed direction V_2 of the plate parallels with the film height, then $V_{2y}=V_2$, so formula 1 can be the following form:

$$\frac{\delta}{\delta x}\left(\frac{\rho h^3}{\eta}\frac{\delta p}{\delta x}\right)+\frac{\delta}{\delta z}\left(\frac{\rho h^3}{\eta}\frac{\delta p}{\delta z}\right)=6\frac{\delta}{\delta x}\left(U_1+U_2\right)\rho h$$
$$-12\rho U_2\frac{\delta h}{\delta x}+12\rho\left(V_2-V_1\right)=6\left(U_2+U_1\right)\frac{\delta\rho h}{\delta x}$$
$$+6\rho h\frac{\delta\left(U_2+U_1\right)}{\delta x}-12\rho U_2\frac{\delta h}{\delta x}+12\rho\left(V_2-V_1\right) \quad (2)$$

Considering the actual piston pump and experimental model of lubrication properties, the cylinder and port plate can be simplified, respectively to a fixed piece and a moveable one. Here the frictional piece 2 is moveable and the frictional piece 1 is fixed. Meanwhile, $\frac{\delta\left(U_2+U_1\right)}{\delta x}=0$, $U_1=V_1=0$, so the formula 3 can be gotten:

$$\frac{\delta}{\delta x}\left(\frac{\rho h^3}{\eta}\frac{\delta p}{\delta x}\right)+\frac{\delta}{\delta z}\left(\frac{\rho h^3}{\eta}\frac{\delta p}{\delta z}\right)=6U_2\frac{\delta\rho h}{\delta x}-12\rho U_2\frac{\delta h}{\delta x}+12\rho V_2 \quad (3)$$

The above formula is differential equation applicable to lubrication properties of port pair deduced from universal Reynolds equation. Surely, their specific form depends on naming to all speed and displacement vector.

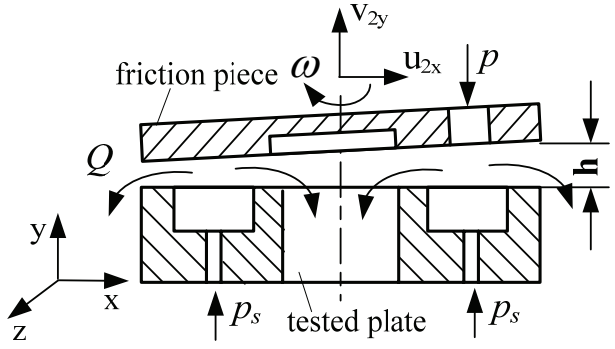

Figure 1. Mechanical model of port pair

Formula 3 shows that the film height of different points, a reflection of lubrication characteristics, varies with their location on the seal area, and the film configuration can be resolved numerically. Moreover, in the view of flowing, because of damper effects on the seal gap [2], lubrication medium will heat after flow, which can induce the change of oil viscidity, so it is also the function of the time. In addition, the factors that the pressure at each point of seal area fluctuates in real time and that it's hard for Bivar

Second Order PDE to be resolved, proceeding with this method, make it so difficult to analyze the specialties of lubrication.

4 EXPERIMENTAL ITEMS

The above deduction shows that lubrication characteristic test of oil film should involve the dynamic acquisition of many parameters instead of single actual film height under the condition of equilibrium. Accordingly, system pressure, leakage flow, oil temperature and frictional torque signals are gathered in real time and multipoint acquisition can be done in the light of their polytropism to characterize the physical impression of actual seal area.

By the lubrication property investigation of port pair on this test system, the following items can be gotten to study its forming and change rule of oil film: Under stated speed and oil temperature, lubrication film height and leakage flow are tested when supply pressure changes[3]; Under stated speed and different pressure, lubrication film height and leakage flow is tested when supply pressure changes; Under stated oil temperature and different pressure, lubrication film height and leakage flow are tested when speed of pair changes; Under stated working condition, lubrication characteristics are tested when structural parameter changes[4], etc..

Particularly, this test system is chiefly characterized by its increase of such parameters as supply pressure and flow rate, and by top test pressure up to 31.5 MPa, top rotate speed up to 3000 rev/min, which can obtain the useful experimental data and conclusions more compatible with actual working condition. This test system provides an experimental platform for design of frictional pairs in high-pressure, high-speed and large-flow axial piston pump.

5 EXPERIMENTAL PRINCIPLES

Two key problems involves in investigation on lubrication properties of port pair with top supply pressure 31.5 MPa and top rotate speed 3000 rev/min: (1) adjustable high pressure power unit; (2) accurate, convenient variable speed operation of port pair. Considering scores of micron lubrication film of port pair[5], the micron electrohydraulic position feedback control is realized by servo control valve in this electrohydraulic power system, so effect study of flow field of port pair seal area on different supply pressure or lubrication properties of different film height (leakage flow, oil temperature, etc.), which are shown in the Figure 2.

As shown in Figure 2, hydraulic drive system, the primary power source, is divided two pieces of main circuit and loading circuit (A, B in Figure 2). Circuit A is the main circuit of lubrication test system while circuit B is the loading circuit. Their circuit principle and buildup listed on the prophase related paper.

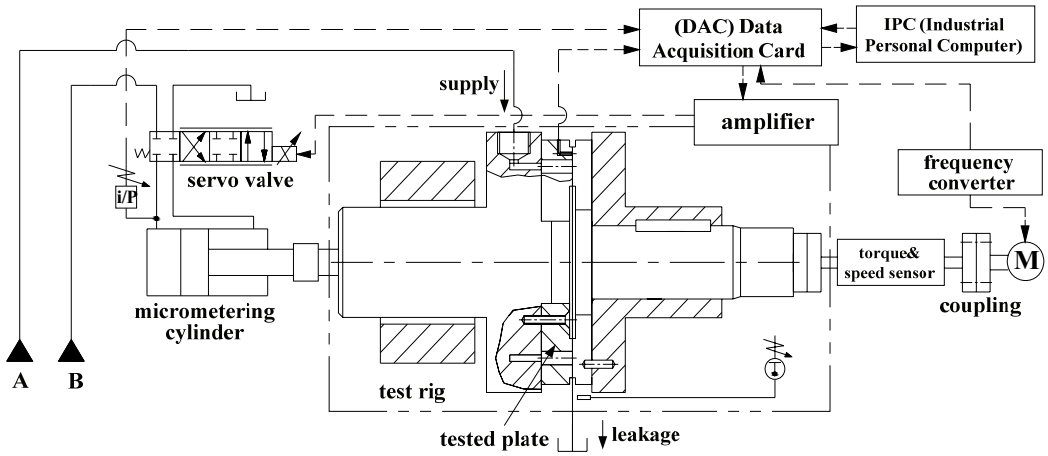

Figure 2 Functional diagram of test system

Investigation on lubrication characteristics of port pair under different operation condition can be made on this test bed of lubrication characteristics, and its monitoring system can supervise real time experimental state, gather multiple parameters in the process of experiment to fulfill the analysis, processing and other tasks of experimental data, and feedback control of micron lubrication film height. Based the separation of input and output, the two circuits in this system, including the main oil circuit and loading oil circuit, are parted to reduce interference of the former to the latter, and to carry out process control easily. High performance system key components selected meets the experimental pressure needs, while rotate speed control by frequency variation ensure the required experimental speed of port pair. Passive loaded style instead of positive loading can make sure the maximum controllability.

6 ACQUISITIONS AND MONITORING OF SIGNAL

Experimental rig of port pairs consists of port plate, thrusting plate, end cover, assembly of high speed shafting, minisize temperature sensor, high-precision current vortex displacement transducer and other main parts. The port plate is fixed under end cover, and high pressure oil enters from supply port, pass through the seal area and leaks from the outer seal loop. High pressure oil in cavity B drives shaft housing and thrusting plate to clamp the port plate. The clamping force reaches equilibrium with hydraulic separating force resulted from flow damping. The oil pressure in cavity B can be adjusted to change the clamping force on port plate, accordingly to modulate the gap of seal area. The experimental rig shows in Figure 3.

Three current vortex displacement transducers measure directly the height of lubrication film in the test, three values specifies a plane, which can get the height numerical value of lubrication film, determine dynamic position and figure. Pressure differential flow and shear flow between high pressure and high speed port pair will heat lubrication oil, which leads to oil temperature between port pair rising faster than that in other place in the test rig. Moreover, viscosity-temperature characteristics can affect the forming of lubrication film between port pair, so here temperature measure is very important. The minisize temperature sensor reviews the effects of lubrication film between port pair by viscosity-temperature characteristics.

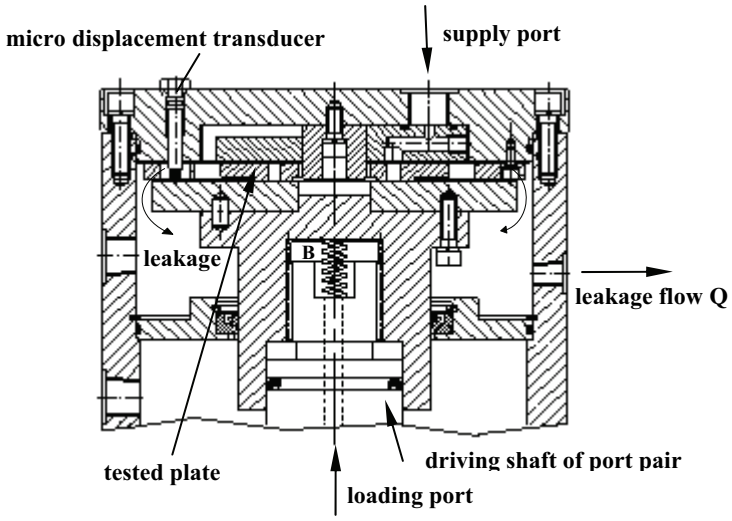

Figure 3. Structural diagram of test rig for port pair

In monitoring system, IPC(Industrial Personal Computer) works as the signal monitoring centre and data processing platform. The data gathered by sensors are input into IPC by data grabbing card, and based on the LabWindows/CVI, one of the virtual device software in measurement and control field, displays the dynamic change in real time. By software analysis, processing lubrication characteristic parameters, for example, the lubrication film height, bearing capacity and leakage flow, comparison with actual ideal values, and control strategy adoption of PID algorithm, feedback control of the lubrication film height is achieved.

7 PRELLIMINARY LUBRICATION EXPRIMENT OF PORT PAIR

7.1 Film equilibrium

In experiment, the intermitted supply port plate in axial piston pump is adopted to be tested under different working condition. Presently, the supply pressure in mian oil circuit reaches more than 20 MPa. Figure 4 shows the real time curve of film height and time during lubrication film forming and equilibrium with normal temperature, 600 r/min rotate speed of port pair motor, different supply pressure.

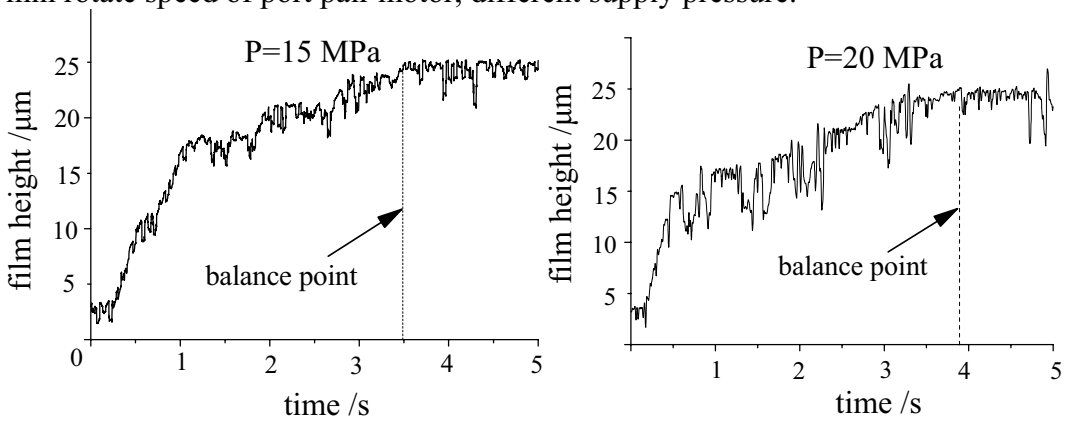

Figure 4. oil film forming curve under 15 MPa and 20 MPa supply pressure

Here are the curves of 15 MPa and 20 MPa supply pressure with fixed other working condition parameter. The curves show that the equilibrium height of lubrication film fluctuate about 25 μm. Under the two supply pressure, oil height with 15 MPa pressure reaches about 23 μm after 3.5 s while oil height with 20 MPa pressure reaches about 23 μm after 3.8 s and has large shake amplitude. It's obvious that within the moderate supply pressure, time of oil film forming differs with each other and tends to increase with the increase of supply pressure, which shows that it's uneasy for oil film to form and that the stability under higher supply pressure is worse, namely, that the rigidity is a bit smaller rather than wide distinction.

7.2 Distributing test of equilibrium film height

Under the same operation condition, change curve of the film height from the three exact displacement transducers, as shown in the Figure 3, puts up good consistency. Figure 5 shows two of them, and respectively the sampling points locate high pressure region and low pressure region.

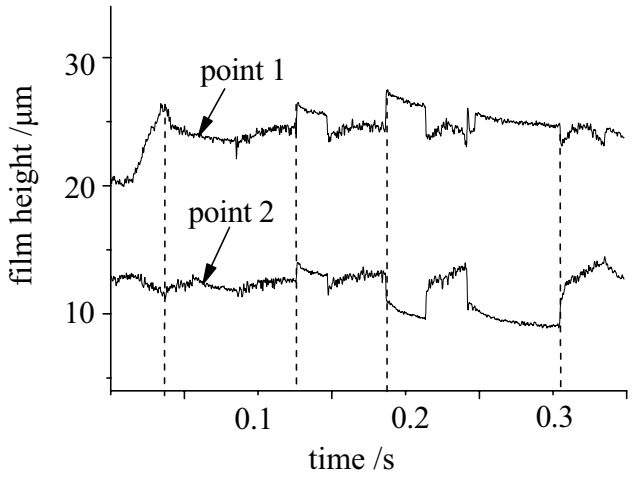

Figure 5. Two curves of oil film height at seal area

For getting the right relative location of the active bearing plane, the transducers positioning is decided to make sure the height of lubrication film between two planes of port pair and their change relations. Since the displacement transducers 1 (testing point 1 in Figure 5) locates high pressure region while the other transducers 3 (testing point 2 in Figure 5) locates low pressure region, the clearance value tested by transducer 1 more than that tested from transducer 3, and actual film height value fluctuates slightly with this relation. Tracking of the two displacement transducers keeps very good. Therefore, tilting angle of loading frictional plane can be ascertained in the light of tested value of oil film height and then the load offset by formulating differential motion of the test rig. The displacement from both displacement transducers has relevant fluctuation, which is caused by heeling torque acted on port plate and the clearance between matching surfaces or motion pairs. Seen from the curve, the oil film can take on the approximate periodicity when equilibrium, which shows the port pair steady operation and in good lubrication condition.

7.3 Leakage test with different film height

Theoretically, the clearance increases as the film height does, namely the leakage flow goes up. Based on the static bearing theory, the approximate leakage formula of inner and outer seal area shows in formula 4:

$$Q = \frac{\pi h^3 p_s}{6\mu c_e \ln\left(r_4 / r_3\right)} + \frac{\pi h^3 p_s}{6\mu c_e \ln\left(r_2 / r_1\right)} \tag{4}$$

Formula 4 demonstrates that leakage flow loss is in direct proportion to the third power of oil film height. Figure 6 is the test curve of leakage flow and film height. By analysis of it, 5～18 MPa test curves are present in exponential growth trend. When the film height is greater than 15 μm and supply pressure changes from 5 MPa to 10 MPa, from 10 MPa to 12 MPa, 18MPa, the port pair produces biggish inner leakage.

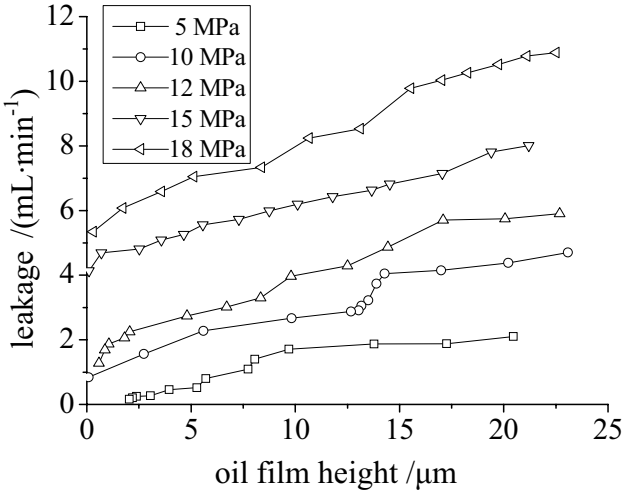

Figure 6. Change curve of leakage and film height

7.4 Frictional torque test with different film height

Rotate speed is the key factor of flow and life increase for axial piston pump and the frictional torque of port pair is the direct parameter affecting it, one of important indexes scaling lubrication state[6]. Figure 7 is the curve of frictional torque and film height.

The curves with different supply pressure are listed in Figure 7. Seen from Figure 7, as a whole, frictional torque increases with the decrease of film height and the amplitude reduction is greater under 15 MPa, 18 MPa. At the same time, when the supply pressure is higher, relative motion resistance of seems increase to enable the tested frictional torque to increase. The cause of it is that the higher pressure makes the test rig carry heavier load, so the frictional resistance increases and the frictional torque does. When the clearance of port pair increases, the steadier state of liquid lubrication film forms and it improves the lubrication pattern and lessen the frictional torque greatly. Consequently, now the curve is sharper than that under lower pressure. The test curves shows that film height control can improve lubrication state of port pair and relieve the heavy wear result from long time bad friction to prolong its life.

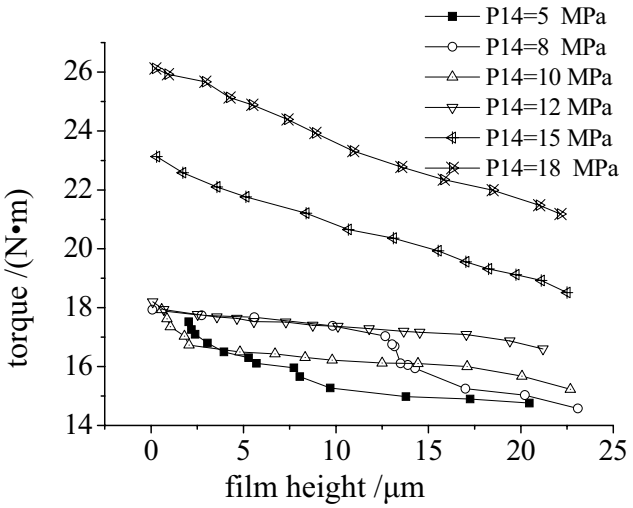

Figure 7. Change curve of frictional torque and film height

Another working parameter affecting the frictional torque and whole pump efficiency is the working temperature, which results from damper effects when lubrication oil flows through the seal area and produces energy loss. It mainly depends on the flow rate and the structure of port pair. The experiment shows that, under specific working condition, when oil reaches its stable temperature, the temperature rise not better than 5 ℃.

8 CONCLUSIONS

(1) New design idea that the main oil circuit and loading oil circuit were severally designed, was adopted in the test system of lubrication characteristics of port pair in axial piston pump, which effectively improves the experimental control system the ability of interference resistance and also offer the physical basis for lubrication properties of frictional pair in pure water hydraulic components.
(2) At the stage of film forming, time of steady oil film forming differs with supply pressure, which validates the cause of low speed startup. It seems that equilibrium film under higher pressure takes more time, so the possibility of wear of frictional pair adds.
(3) The experimental curves shows that actual shape of oil film appears cuneal rather than flat and that when equilibrium, 5 μm difference exists in the direction of film height. Under the same condition, open direction cuneal film is constant. The maximum film height locates near the input oil port rather than high pressure region. The simulation should be done for validation next step.
(4) Leakage flow change distinctly as the clearance of port pair, but in factual application, because of a good many factors of oil, such as impurity, dynamic damping and so on, it can be cut down, which relieve the reduction of pump volumetric efficiency in part.

8 REFERENCES

[1] Zhenqian D., *Design of hydrostatic bearing (in China)*.Shanghai, 1989
[2] E.Koc, C.J.Hooke. An analysis of the lubrication mechanisms of the bush-type

bearings in high pressure pumps. *Tribology International*，1997，Vol. 30, No. 8, pp. 553~560
[3] SergeiB.Glavatskih, Qsten, Uusjtalo, Daniel J. Spohn. Simulta-neous monitoring of oil film thickness and temperature in fluid bearings. *Tribology International*, 2001,No. 34, pp. 853~857
[4] H.R.Le, M.P.F. Sutcliffe. Measurements of friction in strip drawing under thin film lubrication. *Tribology International*, 2002, No. 35, pp.123-128
[5] Yaoming X., Design and experimental study of port and slipper pairs in axial piston pump, *Hydraulic & pneumatics*, 1977, No. 2, pp. 3-12
[6] Noah D. Manring, Chris L. Wray, Zhilin Dong. Experimental Studies on the Performance of Slipper Bearings within Axial-Piston Pumps. *Journal of Tribology*. Vol. 126, No. 3, pp. 511-518

THE SOURCE ADMITTANCE METHOD FOR PUMPS WITH COMPLEX OUTLET CHANNELS

L. Ericson and J-O. Palmberg
Department of Management and Engineering,
Linköpings universitet, Sweden
E-mail: (liselott.ericson, jan-ove.palmberg)@liu.se

ABSTRACT

The source admittance method offers a new way to measure flow ripple. Compared to earlier methods such as the two-microphone method, the main benefit is that there is no need for a model of the outlet channel - the source flow is measured through an additional pressure transducer inside the pump. This makes the source admittance method easier to use and less modelling skill is needed. Furthermore, the method is more reliable because the source flow is measured, i.e. pressure at the creation spot, directly. In earlier studies, the method proved to work very well for pumps with simple discharge channels but less well for pumps with complex discharge channels.

The experimental test object is a pump with a simple outlet channel. Its internal impedance can easily be changed in a controlled manner; complexity can thus be added step by step. The paper contributes to the understanding of how complexity of the pump's discharge channel influences the usefulness of the source admittance method.

KEYWORDS: Flow pulsations, source flow measurements, two-microphone method, source admittance method

1 INTRODUCTION

The noise in hydraulic systems has its origin in the hydrostatic pump, both from flow pulsations and forces. Flow pulsation in the pump is mainly created when fluid is forced from the low pressure side to the high pressure side. Simulation techniques are useful in the early stages of the development process. There are useful and accurate simulation models capable of predicting source flow ripple in hydrostatic pumps and thereby useful for optimization purposes. Simulation results, however, are of little practical use before they are experimentally verified.

To verify real pumps, the flow pulsations have to be measured in real applications. Over the last three decades, researchers have investigated the possibility to measure flow from the pump, called source flow, which is system independent. Some of the measurement methods give very good and accurate results, but the measurements are rather time-consuming and some engineering skills are needed. The different methods are explained in section 1.2.

1.1 The Source Characteristics

In simulation, the source flow is described as the sum of all flow from the cylinders that are connected to the discharge port and measured directly after the valve plate. This flow is more or less a theoretical quantity and completely system independent, which means that source flow is constant for any dynamic load with the same stationary pressure. Also, the source impedance is required to characterize a pump and can be explained as the geometrical compartments in the discharge port, i.e. between the valve plate and the pump flange.

The source flow and source impedance describe the pump's contribution to flow pulsations to the system. If the pump manufacturer records the pump's source flow and source impedance, customers can estimate the influence of the pump in a specific system. If this is going to work the measurement method has to be convenient to use.

Over the years, many methods of measuring fluid-borne noise have been developed. Some of the methods are simple but do not give a complete description of the pump. Others are fairly complicated but give a good description of the pump. A brief summary of some of the source flow measurement methods follows below.

1.2 Different Methods to Measure Fluid Borne Noise

As stated in the section above, some good measurement methods do exist and some of these are explained below with their disadvantages and benefits.

One method for measuring fluid-borne noise is anechoic termination, [1]. The anechoic termination creates a reflection-free system. This means that pressure ripple is the same in the whole system if viscous friction in the pipe can be neglected. The method is simple but does not give the source flow from the pump and is not suitable for model verification. Another method is the blocked acoustic impedance method; this method gives the correct quantity of fluid-borne noise because it is system independent. But the method can only give the product of $Q_s Z_s$ and is not appropriate for verification of flow characteristics from the pump. This method was first developed in 1977 at the University of Bath, and later also adopted as an international standard for rating fluid-borne noise generated in pumps, see reference [2].

One method that separates source characteristics is the hydraulic trombone method and was developed at the University of Bath, reference [3]. The method uses different pipe lengths. The source characteristics can be separated with a mathematical algorithm, but the method is rather time consuming.

Another method is the secondary source method, references [4] and [5]. This method has been adopted as the international standard for high-precision measurements of fluid-borne noise from hydraulic pumps. The method uses a secondary source which produces a broadband spectrum in the region of the measurement unit that is of interest but with harmonics different to the test unit. Another method, which has been developed at Linköpings universitet, is the two-microphone method, reference [6]; it is similar to the secondary source method, but instead of having a secondary source, the main test pump is used to introduce a broadband frequency spectrum. The disadvantage of these two methods is that there is a need for a mathematical model of the pump's outlet channel, and the model can be fairly complicated for pumps with complex outlet channels. Also, the parameters in the model are set by a human tuner.

A new approach to measuring source flow is the source admittance method which is

investigated in this paper and was published for the first time in [7]. This method uses the two-microphone method but instead has to use the model of the pump outlet channel; the pressure pulsations are measured where the source flow is created. The aim of the method is to make the whole process automatic, from the first measurement till the source flow and source impedance are plotted, and all the competence and knowledge that the method needs should be implemented in the measurement algorithm. The method was further tested in [8] and is explained in section 2.

2 METHOD

Earlier investigations, [8], show that the source admittance method works excellently with the fixed bent-axis pump with a fairly simple outlet channel. There is no obvious difference between the well proven two-microphone method and the source admittance method. The location of the transducer is insignificant as long as it is located close to the valve plate. However, an increase in difficulties can be observed when the speed is raised.

In references [7] and [8] a variable 60 cc in-line pump with a more complex outlet channel is tested. The source admittance method does not work perfectly with this pump. There is a region between 1200 Hz and 2000 Hz where the measurements are not reliable, but at lower frequencies the measurements are very accurate. Reasons why the source admittance method does not work well for the variable in-line pump may be: the reciprocity may not be valid for pumps with complex outlet channels; there may not be a linear relationship between flow and pressure; and the discharge channel is time-variant.

The intention of this paper is to add complexity to a simple bent-axis pump to see if the source impedance behaviour is of great importance.

The pump is a 40 cc seven-piston bent-axis pump. The variable source impedance is put into practice through an external variable volume placed in two different locations; Position A at the end of the discharge channel and position B at the pre-compression filter volume entry. The source impedance becomes time-variant at position B. Figure 1 shows the measurement set-up and volume placed at position A and position B is shown in the figure with a dashed rectangle. The pump's source impedance changes in a controlled technique through different sizes of anti-volumes inside the volume. Figure 2 shows the volume and its elements.

The volume sizes are from 9 cm^3 to 39 cm^3 according to table 1. The table shows also the marker and line style for the different volumes through the paper.

The measurements of the source flow are compared to simulations with the program HOPSAN, [9] and [10]. The program was developed at Linköpings universitet and is used mainly for hydraulic simulations. The model's accuracy has been extensively verified by experiments, [11] and [12]. The measurements of the source impedance are compared to the mathematical analysis of the outlet channel in section 2.1.

2.1 Model of the outlet channel

To see if the source impedance is measured correctly, an expected mathematical model is needed for the geometry of the pump's outlet channel. The outlet channel is commonly modelled as a volume, an orifice and a pipe from the valve plate to the pump flange. When the external volume is in use, the channel is more complex and this needs to be taking care

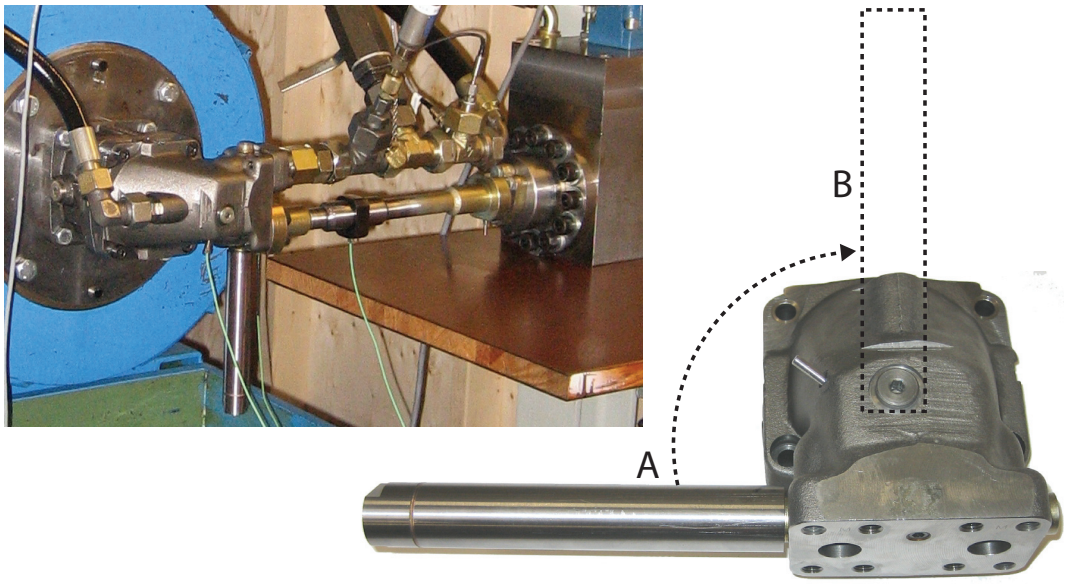

Figure 1: Top left: The test set-up for the source admittance method. Bottom right: The volume placed on the pump at position A at the end of the discharge pipe on the pumps top end. Position B at the pre-compression filter volume entry is shown by the dashed rectangle.

Figure 2: The volume's different parts with the biggest anti-volume.

Volume nr	Volume size	Figure marker	Line style
0	39 cm^3	x	Solid
1	31 cm^3	$*$	Dashed
2	23 cm^3	$\diamond$	Dashed
3	16 cm^3	o	Dashed
4	9 cm^3	$\bullet$	Dashed
-	No volume	$\square$	Dotted

Table 1: The different sizes of the external variable volume end its marker and line style in the figures.

of when modelling the outlet channel. The complete outlet channel including the volume at position A is shown in figure 3(a) and figure 4 shows the volume located at position B. The figure shows the notations for equations 1-9.

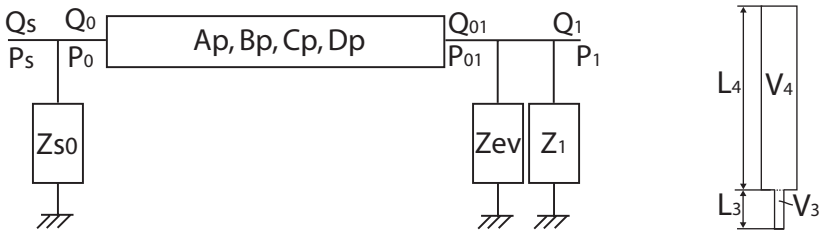

(a) The pump's outlet channel for position A. (b) Helmholz-resonator, Z_{ev}.

Figure 3: The model of the pump's outlet channel including the external volume Z_{ev} at the end of the pipe.

The external volume can be treated as a Helmholz-resonator as equation 1, reference [13]. The notation is shown in figure 3(b).

$$Z_{ev} = \frac{(\frac{s}{\omega_h})^2 + 1}{C_{ev} s} \qquad \text{where} \qquad \begin{array}{l} C_{ev} = \frac{V_3 + V_4}{\beta_e} \\ \omega_h = a\sqrt{\frac{A_3}{L_3 V_4}} \end{array} \tag{1}$$

The pipe in figure 3(a) can be formulated as a four-pole matrix, relating flows and pressures at both ends of the pipe, equation 2. In [13], a derivation of the four-pole matrix is explained.

$$\begin{pmatrix} Q_{01} \\ P_{01} \end{pmatrix} = \begin{bmatrix} A_p & B_p \\ C_p & D_p \end{bmatrix} \begin{pmatrix} Q_0 \\ P_0 \end{pmatrix} \tag{2}$$

If the Helmholz-resonator is placed at the end of the outlet channel and the chain rule is used to incorporate the external volume, Z_{ev}, and the outlet channel, equations 1 and 2 can be rewritten as

$$\begin{pmatrix} Q_1 \\ P_1 \end{pmatrix} = \begin{bmatrix} A_p - \frac{C_p}{Z_{ev}} & B_p - \frac{D_p}{Z_{ev}} \\ C_p & D_p \end{bmatrix} \begin{pmatrix} Q_0 \\ P_0 \end{pmatrix} \tag{3}$$

The impedance Z_{s0} is commonly treated as a volume and an orifice like equation 4. The volume, V_s, represents the sum of all the cylinder volumes which are connected to the outlet channel and the volume between valve plate and pump flange. The laminar restrictor, k_c, represents the total leakage from volume V_s to the surrounding volumes.

$$Z_{s0} = \frac{1}{\frac{V_s}{\beta_e} s + k_c} \tag{4}$$

The upstream circuit of the outlet channel can be formulated with a Norton representation and is obtained as

$$Q_s = Q_0 + \frac{P_0}{Z_{s0}} \tag{5}$$

A combination of equations 3, 4, and 5, gives

$$\frac{1}{Z_1} = \frac{Q_s}{P_1 X_1} - \frac{1}{Z_s} \qquad \text{where} \qquad X_1 = D_p - \frac{C_p}{Z_{s0}} \tag{6}$$

Z_s is the final source impedance and is calculated as

$$Z_s = \frac{D_p - \frac{C_p}{Z_{s0}}}{\frac{A_p - \frac{C_p}{Z_{ev}}}{Z_{s0}} - B_p + \frac{D_p}{Z_{ev}}} \tag{7}$$

When the volume is placed at the pre-compression filter volume entry, position B, the source impedance can be modelled as shown in figure 4. In this case, the impedance Z_{s0}

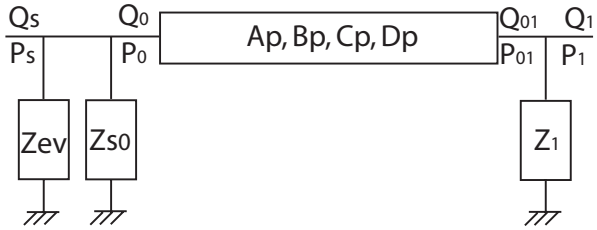

Figure 4: The pump's outlet channel's representation for position B.

is connected in parallel with Z_{ev}, equations 4 and 1 gives

$$Z_{s0ev} = \frac{1}{\frac{1}{Z_{ev}} + \frac{1}{Z_{s0}}} \tag{8}$$

The final source impedance can be calculated as before with equations 5 and 2, where $Z_{s0} = Z_{s0ev}$ and gives

$$Z_s = \frac{D_p - \frac{C_p}{Z_{s0ev}}}{\frac{A_p}{Z_{s0ev}} - B_p} \tag{9}$$

The volume changes the behaviour of the source impedance. Figure 5(a) shows the impedance for all the volume sizes when the volume is at position A. The figure also includes the original pump outlet channel without a volume (dotted line). The first anti-resonance is between 800 - 1600 Hz for the different volume sizes. The second anti-resonance is from the cylinder outlet part and the behaviour of this part is not changed by the volume, which is why no difference can be seen in the figure.

Figure 5(b) shows the source impedance at position B. The first anti-resonance is between 400 - 1200 Hz, the slightly lower frequency interval is caused by the fact that the pipe before the volume is longer than at position A. The second anti-resonance is slightly moved. The big difference between this location and position A is the source impedance changes during one period. When the cylinder connects to the outlet port the volume is in contact with the outlet channel, but when the rotation continues the volume is disconnected and the source impedance behaviour is like the one without the volume (dotted line in figure 5). When the system is time-invariant, i.e. position A, one specific frequency of the input signal affects the output signal only at the very same frequency. However, when the source impedance is time-variant, the input signal at one specific frequency does not only affect the output signal at just the same frequency but more or less at all the output frequencies.

The frequency of the Laplace operator $s = i\omega$ in figure 5 can be chosen at one's own discretion and the number of points is 500 in the figures. However, the frequency of the Laplace operator at measurements is given from the number of pistons and the rotation speed of the pump, $\omega = nz$. At 2000 rpm the available amount of frequencies is 12.

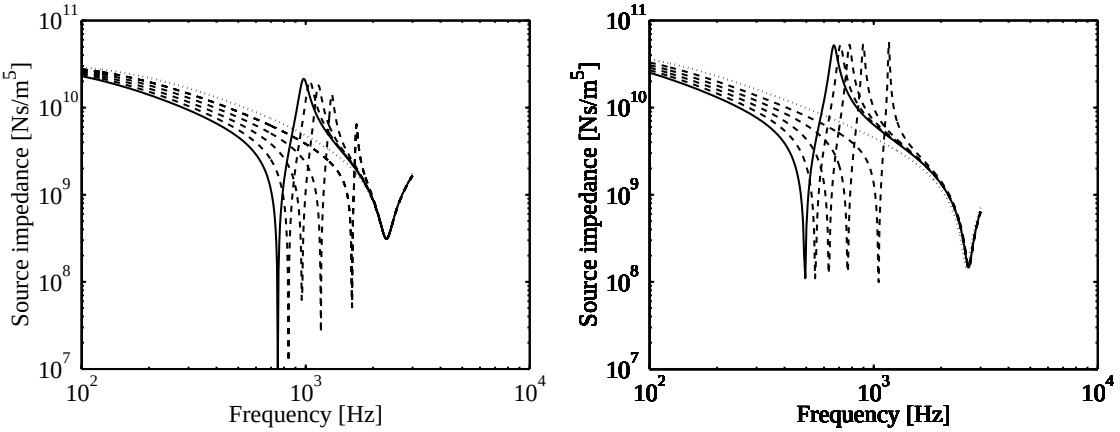

(a) Volume at position A (b) Volume at position B

Figure 5: The source impedance with different volume sizes and locations. The solid line are with volume size zero, i.e. the biggest volume. The dashed lines is from the other volumes and the dotted line is the source impedance without the external volume.

2.2 Calculate the Source Characteristics

It is possible to describe the relationship between dynamic pressures and flows at two points in any hydraulic circuit by an admittance matrix 10. In this equation, h_{11}-h_{22} are frequency dependent and complex functions. Figure 6 gives the notation for matrix 10.

$$\begin{pmatrix} Q_A \\ Q_B \end{pmatrix} = \begin{bmatrix} h_{11} & h_{12} \\ h_{21} & h_{22} \end{bmatrix} \begin{pmatrix} P_A \\ P_B \end{pmatrix} \tag{10}$$

Figure 6: Flow and pressure in equation (10) are correlated with each other through an admittance.

If matrix 10 is transferred to the pump's outlet channel, the matrix can be written as

$$\begin{pmatrix} -Q_s \\ Q_1 \end{pmatrix} = \begin{bmatrix} h_{11} & h_{12} \\ h_{21} & h_{22} \end{bmatrix} \begin{pmatrix} P_s \\ P_1 \end{pmatrix} \tag{11}$$

Q_1 is calculated with the two-microphone method by measuring two pressures along a rigid pipe and uses the four-pole matrix. The two-microphone method is explained in [6]. P_1 is the measured dynamic pressure at the start of the measurement pipe. P_s is the measured dynamic pressure at the origin of source flow, probably close to the valve plate. As can be seen in equation 10 and 11, $-Q_s$=Q_A since the flow is defined into the outlet channel.

Due to reciprocity, h_{12} and h_{21} can be assumed equal. By using the two different load cases, indexing $L1$ and $L2$, from the measurement, the four unknown quantities in matrix 11 can be calculated as shown in equation 12.

$$h_{11} = h_{22}\frac{P_{1L2} - P_{1L1}}{P_{sL1} - P_{sL2}} \tag{12a}$$

$$h_{12} = \frac{Q_{1L1} - h_{22}P_{1L1}}{P_{sL1}} \tag{12b}$$

$$h_{22} = \frac{P_{sL1}Q_{1L2} - P_{sL2}Q_{1L1}}{P_{1L2}P_{sL1} - P_{1L1}P_{sL2}} \tag{12c}$$

$$Q_s = -(h_{11}P_{sL1} - h_{12}P_{1L1}) \tag{12d}$$

The matrix equations 11 can be combined and P_s eliminated, giving equation 13.

$$\frac{1}{Z_1} = \frac{Q_s}{P_1}(-\frac{h_{12}}{h_{11}}) - (\frac{h_{12}^2}{h_{11}} - h_{22}) \tag{13}$$

If equation 13 is compared with equation 6, it is obvious that the source impedance can be calculated as

$$Z_s = \frac{1}{\frac{h_{12}^2}{h_{11}} - h_{22}} \tag{14}$$

As can be seen, the source admittance method calculates the source flow Q_s, equation 12, and the source impedance Z_s for the pump, equation 14, without a mathematical model. A more detailed explanation of the method can be found in [7].

3 RESULTS

Measurements have been performed at different pump speeds as well as static pressure levels. The volume has been placed at two different locations, at the end of the discharge channel (position A) and at the pre-compression filter volume entry (position B).

3.1 Position A

The left graph in figure 7 shows the source impedance for five different volumes at position A. The anti-resonance is not perfectly located but it is difficult to get the measurement point correct with the few available points. The tendency, however, is comparable with analytic results, figure 5(a). It is misleading to connect the measurement points to each other when the available frequencies are few. The right graph in figure 7 shows an example when there are just 16 frequencies in the mathematical model in section 2.1, as there are when the pump speed is 1600 rpm.

To get a better view of the source impedance for the pump, more available frequencies are needed. In figure 8, measurements were performed at 2000 rpm, 1600 rpm, and 900 rpm and were compared to the analytic results in section 2.1. The results are good for all the volume sizes apart from the smallest volume, volume four. This may be due to the volume size being too small to model as a Helmholz-resonator.

The two-microphone method uses the model of the source impedance to calculate the source flow and as can be seen the behaviour of the source impedance is fairly complex and not easy to model. The outlet channel of the pump can be even more complex and even more difficult model mathematically. The source admittance method does not need

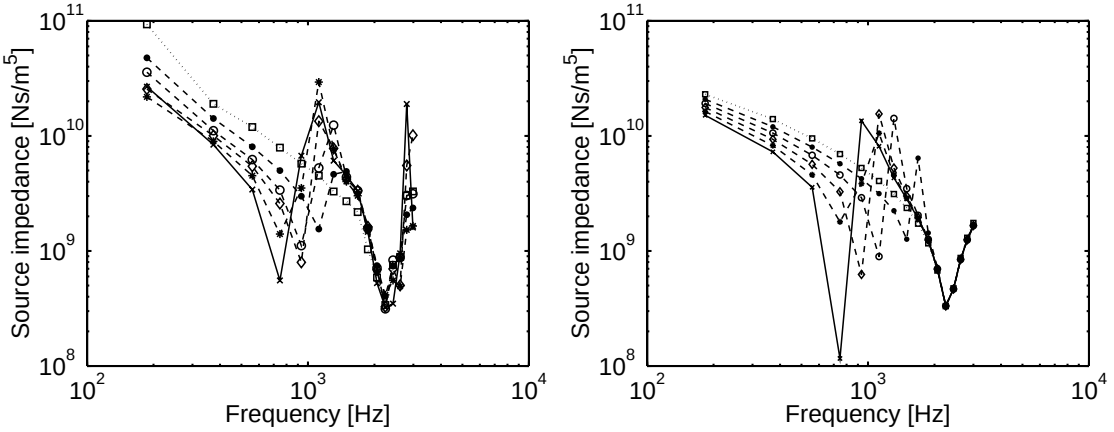

Figure 7: Left: The source impedance from measurements with the different volumes located at position A. The solid line with x's is with the biggest volume, the dashed lines are with smaller volumes, and the dotted line is with no external volume. Right: The mathematical model of the source impedance with 16 available frequencies with the different volumes.

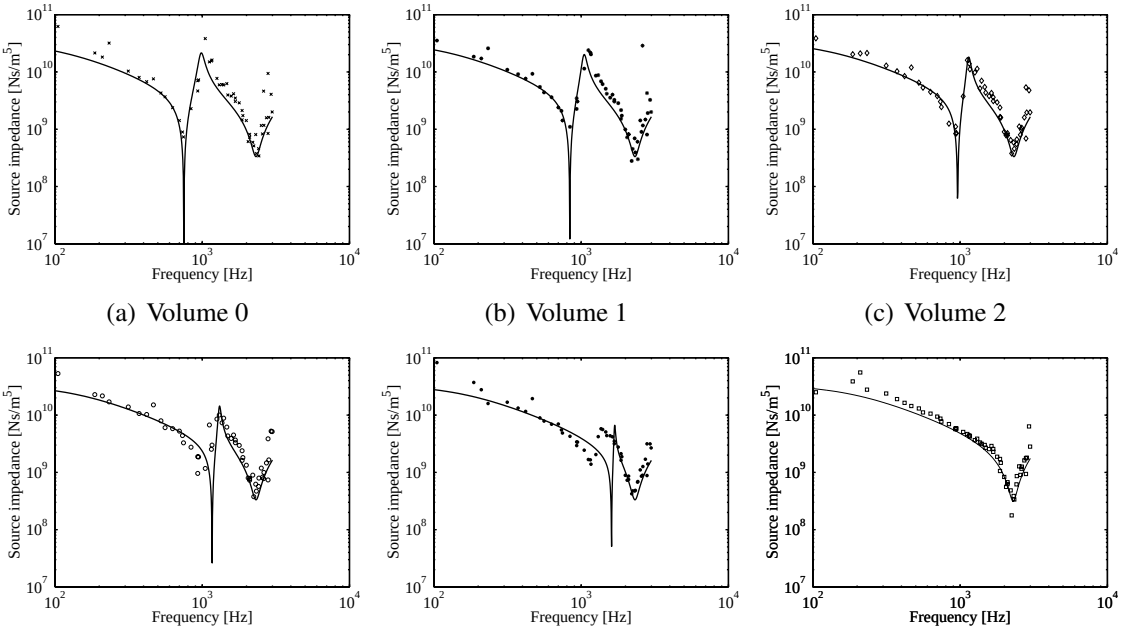

(a) Volume 0 (b) Volume 1 (c) Volume 2

(d) Volume 3 (e) Volume 4 (f) No volume

Figure 8: The source impedance with different volumes at position A. The solid line is the mathematic model and the markers are measurements at 900, 1600 and 2000 rpm.

the model and this problem disappears. The measured source impedance is one of the source characteristics of the pump which is needed for a complete description of the pump.

The source flow for all five volumes and no volume at all at different operation points is shown in figure 9. The measurements were compared to simulation results. As can be seen, the measurements are extremely good for measurements at 900 rpm and 1600 rpm, but at 2000 rpm the measurements have too large amplitude at frequencies over $\approx$ 1500 Hz.

3.2 Position B

Figure 10 shows the source impedance for the pump with the different volume sizes at position B. The measurement results of the source impedance are difficult to predict because the impedance is not constant during one period. As mentioned in section 2.1, one specific frequency of the input signal does not only affect exactly that frequency of the output signal.

The source flow for all five volumes and no volume at all at different operation points is shown in figure 11. The measurements are comparable with the simulation results. The measurements are a little rougher than for position A but if the results are compared with the measurements with the proven two-microphone method in [14], the measurements can not be expected to be better with a pre-compression filter volume. There is no obvious deterioration at 2000 rpm as shown at position A.

4 DISCUSSION AND CONCLUSIONS

The outlet channel's geometric shape is not very crucial. As shown in this paper the source impedance is disturbed but no obvious errors can be seen in the measured source flow.

The question of why is there problem with the measurements on the in-line pump is still not answered. One reason may be that the flow in the measurement pipe is turbulent. The four pole matrix which is used when calculating Q_1 presumes laminar flow. During the experiments, the temperature is kept low, 32°-36°, in order to keep kinematic viscosity high, 35-45 cSt, and Reynolds number low. The Reynolds number in the measurement pipe is changed when the speed of the fluid rises, which it does when the rotation speed of the pump increases. The Reynolds number is calculated as

$$Re = \frac{vd}{\upsilon} = \frac{4Dn}{\upsilon d\pi} \tag{15}$$

It is accepted that the transitional point from laminar flow to turbulent flow is Re $>$ 2300. In the bent-axis pump, the turbulent area starts at $\approx$ 1700 rpm. This can be the answer to the high-speed problem for the bent-axis pump. However, in the in-line pump the turbulent flow starts at $\approx$ 1500 rpm and the measurement problem already at 1000 rpm, as shown in reference [7]. It is not likely that the measurement errors for the source admittance method with high speed and with the in-line pump are the cause of the turbulence in the measurement pipe. Also, the laminar flow solutions can be used over a limited turbulent flow range, if the flow oscillates, [15].

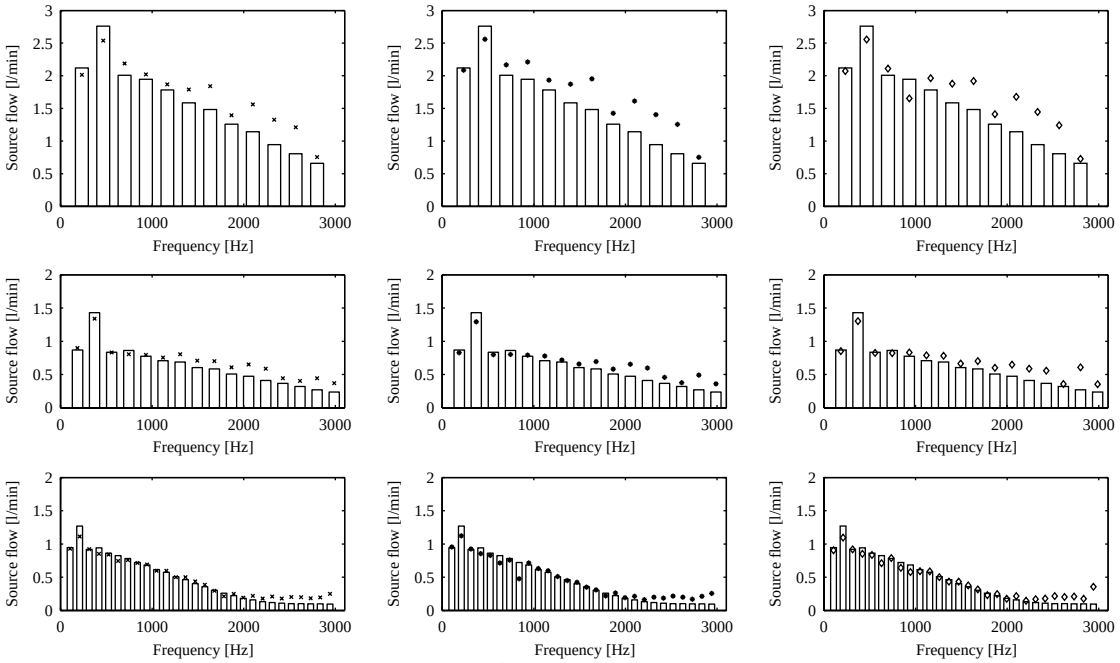

(a) Volume 0 (b) Volume 1 (c) Volume 2

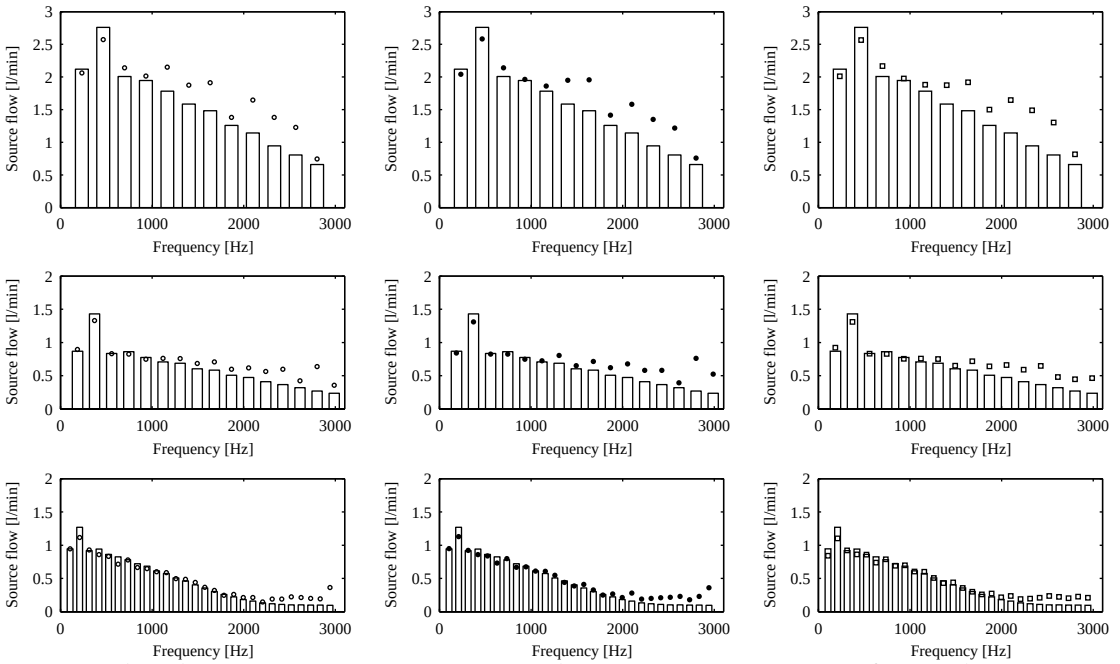

(d) Volume 3 (e) Volume 4 (f) No volume

Figure 9: Source flow at position A, measured (markers) and simulated (bars). Top to bottom in each column gives: 2000 rpm 200 bar, 1600 rpm 100 bar, and 900 rpm 200 bar.

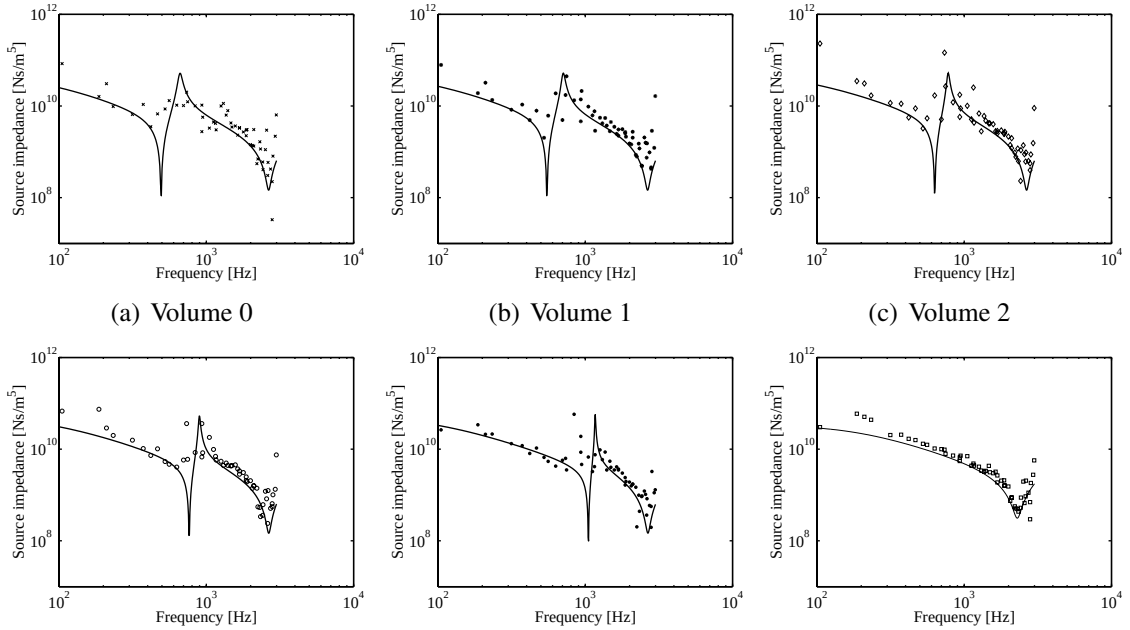

(a) Volume 0 (b) Volume 1 (c) Volume 2

(d) Volume 3 (e) Volume 4 (f) No volume

Figure 10: The source impedance with different volumes at position B. The solid line is the mathematic model and the markers are measurements at 900, 1600 and 2000 rpm.

However, it is more difficult to decide whether the flow in the discharge channel is laminar or turbulent. The flow should be very disturbed right at the cylinder outlet.

After the valve plate, both the pump's outlet channels change from kidney-shaped to circle-shaped. The in-line pump has a 90° bend at the outlet channel whereas the bent-axis pump has a 45° bend. This may cause the problem with the in-line pump, but in earlier studies, the bends are shown not to be crucial for the use of the four pole-matrix approach. There are no obvious reasons why the admittance matrix should be influenced differently.

The bent-axis pump's cross section area from the valve plate to the pump flange grows by 17 %, while the in-line pump's outlet channel first shrinks by 53 % and then grows by 69 %. This can cause the difficulties with the in-line pump.

The in-line and the bent-axis pumps have different length of the outlet channels. Tests have been performed with extended outlet channel of the bent-axis pump and no influence could be seen of the measured source flow.

The investigations will continue by measurements on variable displacement in-line pumps to further answer the question of where the breakpoint for complex outlet channels is and consequently when the source admittance method stops working accurately.

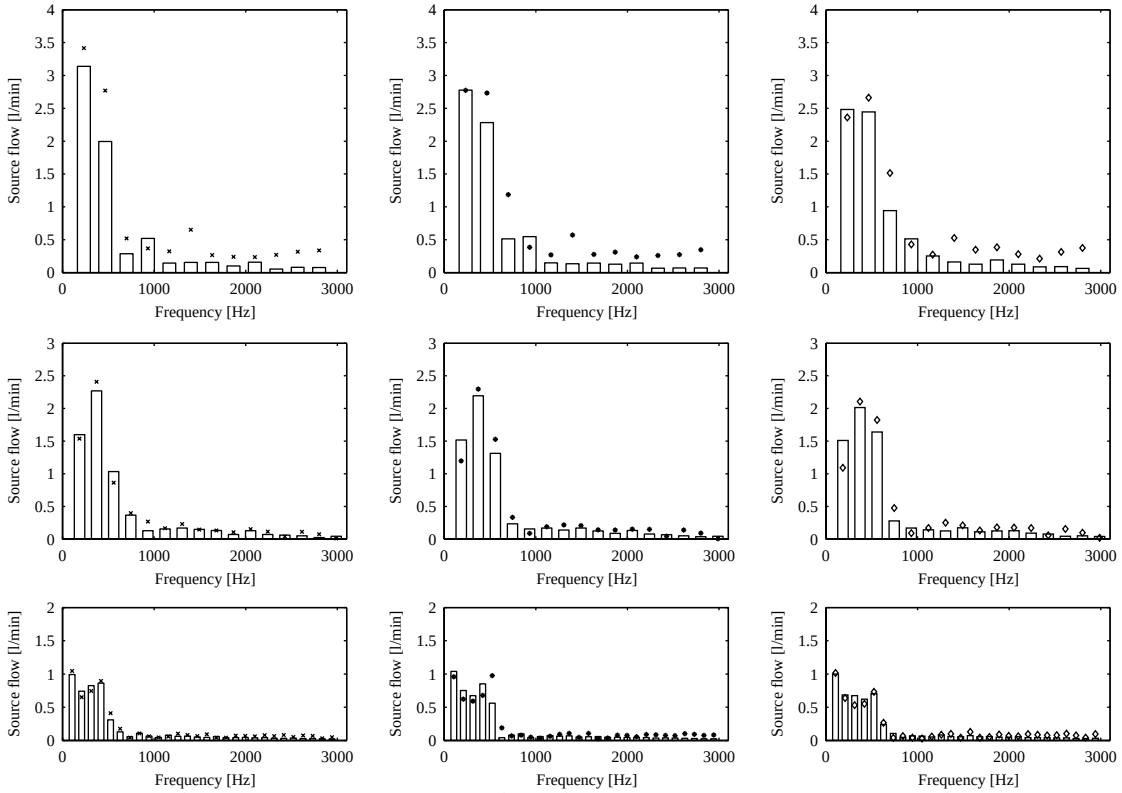

(a) Volume 0 (b) Volume 1 (c) Volume 2

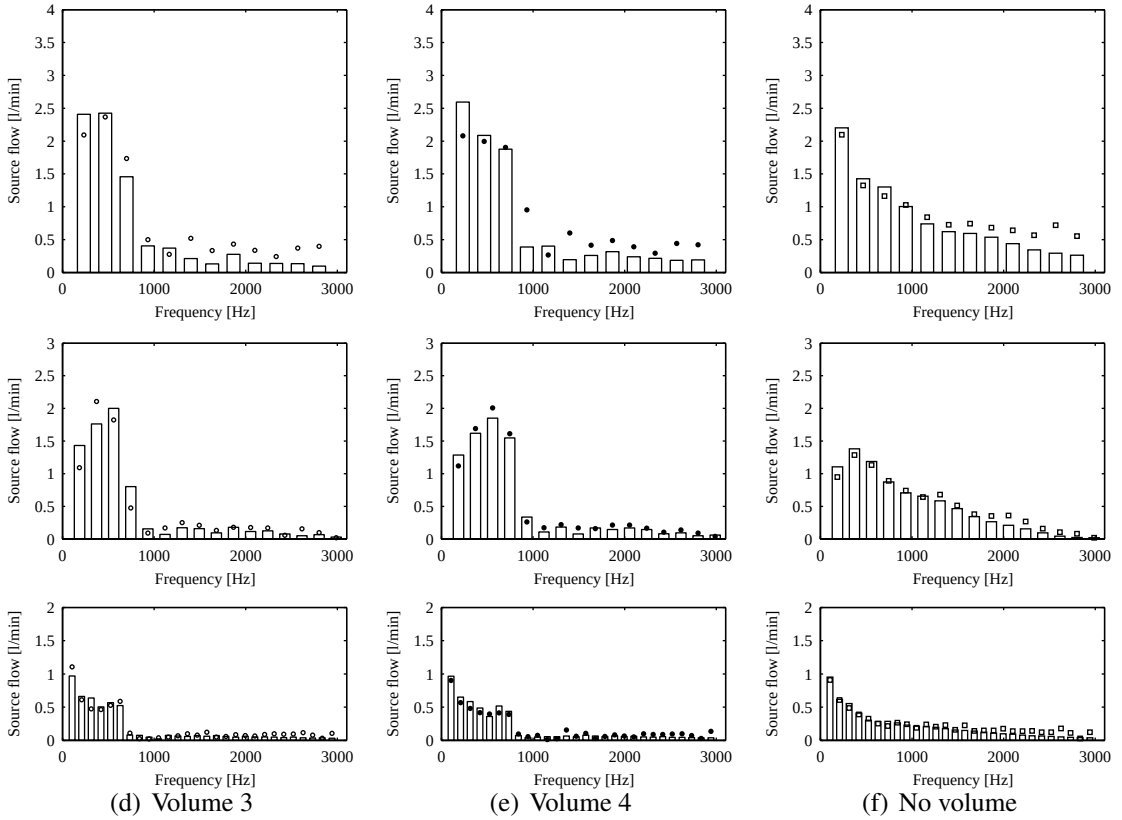

(d) Volume 3 (e) Volume 4 (f) No volume

Figure 11: Source flow at position B, measured (markers) and simulated (bars). Top to bottom in each column gives: 2000 rpm 200 bar, 1600 rpm 100 bar, and 900 rpm 200 bar.

5 NOMENCLATURE

5.1 Variables

A	Four-pole element
a	Wave propagation velocity
B	Four-pole element
C	Four-pole element
D	Four-pole element
D	Displacement
d	Diameter of the measurement pipe
h	Admittance matrix element
i	Imaginary unit
k_c	Linearised flow-pressure coefficient
L	Length
n	Pump speed
P	Pressure
Q	Flow
Re	Reynolds number
s	Laplace operator
V	Volume
v	Fluid speed
Z	Impedance
z	Number of pistons
β_e	Effective bulk modulus
υ	Kinematic viscosity
ω	Frequency

5.2 Subscripts

0	Position
01	Position
1	Position
11	Variable h position
12	Variable h position
21	Variable h position
22	Variable h position
2	Position
3	Part of the external volume
4	Part of the external volume
A	Position
B	Position
ev	External volume
$L1$	Load case 1
$L2$	Load case 2
p	Four-pole for the model
s	Source or volume index
$s0$	Position

REFERENCES

[1] P Larsson, J-O Palmberg, and K Weddfelt. Analysis and measurement of pressure ripple of fluid power pumps. In *Eighth IASTED International Symposium: Measurement, Signal Processing and Control - MECA'86*. Taormina, Italy, September 1986.

[2] International Standard. *Hydraulic Fluid Power - Determination of Pressure Ripple Levels Generated in System and Components*, 1999.

[3] K A Edge and D E Browns. Method for characterizing the fluid borne noise generated by positive displacement pumps. In *39th National Conference on Fluid Power*, pages 37:310–317. USA, December 1983.

[4] K A Edge and D N Johnston. The 'secondary source' method for the measurement of pump pressure ripple characteristics. Part I: Description of method. *Proc IMechE*, 204:33–40, 1990.

[5] K A Edge and D N Johnston. The 'secondary source' method for the measurement of pump pressure ripple characteristics. Part II: Experimental results. *Proc IMechE*, 204:41–46, 1990.

[6] K Weddfelt. Measurement of pump source characteristics by the two-microphone method. In *The second Tampere International Conference on Fluid Power*, Tampere, Finland, March 1991.

[7] A Johansson. *Design Principles for Noise Reduction in Hydraulic Piston Pumps - Simulation, Optimisation and Experimental Verification*. PhD thesis, Division of Fluid and Mechanical Engineering Systems, Department of Mechanical Engineering, Linköpings universitet, Linköping, Sweden, 2005. Dissertation No. 965.

[8] L Ericson, A Johansson, and J-O Palmberg. The source admittance method - a new measurement method for hydraostatic pump flow pulsations. *Proceedings of the 4th FPNI - PhD Symposium Sarasota*, 1:297–309, 2005.

[9] HOPSAN. Hopsan, a simulation package, user's guide. Lith-ikp-r1704, Division of Fluid and Mechanical Engineering Systems, Linköpings universitet, Linköping, Sweden, April, 1998.

[10] R Werndin, A Johansson, and J-O Palmberg. A general model of a multi-displacement machine - using tlm. *The Seventh Scandinavian International Conference on Fluid Power, SICFP'01*, 2:115–130, May - June 2001.

[11] K Weddfelt. *On modelling, simulation and measurements of fluid power pumps and pipelines - with special reference to flow pulsations*. PhD thesis, Division of Fluid and Mechanical Engineering Systems, Department of Mechanical Engineering, Linköpings universitet, Linköping, Sweden, January 1992. Dissertation No. 268.

[12] M Pettersson. *Design of Fluid Power Piston Pumps, with Special Reference to Noise Reduction*. PhD thesis, Division of Fluid and Mechanical Engineering Systems, Linköpings universitet, Linköping, Sweden, September 1995. Dissertation No. 394.

[13] J T Viersma. *Analysis, Synthesis and Design of Hydraulic Servosystems and Pipelines*. ISBN 0-444-41869-5, ISSN 0-444-41872-5. Elsevier scientific publishing company, 1980.

[14] M Pettersson, K Weddfelt, and J-O Palmberg. Reduction of flow ripple from fluid power piston machines by means of a precompression filter volume. In *Tenth Aachen Colloquium on Fluid Power Technology*, Aachen, Germany, March 17-19 1992.

[15] ME Stecki and DC Davis. Fluid transmission lines - distributed parameter models part 1: a review of the state of the art. *Proc Instn Mech Engers*, Vol. 200 No. A4:215–228, 1986.

THE TENTH SCANDINAVIAN INTERNATIONAL CONFERENCE ON FLUID POWER

PROCEEDINS OF THE CONFERENCE

Volume 2

MAY 21-23, 2007

TAMPERE, FINLAND

Editors: Jani Vilenius and Kari T. Koskinen

Technical editor: Janne Uusi-Heikkilä

ISBN 978-952-15-1757-0
978-952-15-1758-7 (Vol. 1)
978-952-15-1759-4 (Vol. 2)
978-952-15-1760-0 (Vol. 3)
978-952-15-1761-7 (CD-ROM)
978-952-15-3272-6 (PDF)

ORGANISING COMMITTEE

Professor Matti Vilenius, TUT / IHA, Conference Chairman
Professor Kari T. Koskinen, TUT / IHA, Conference Vice Chairman
Senior Researcher Jani Vilenius, TUT / IHA, Conference Manager
Secretary Virpi Multanen, TUT / IHA, Conference Secretary
Professor, Senior Adviser for Board of Manag. Matti Kleimola, Wärtsilä Corp.
Professor Aarne Halme, TKK / ATL
Manager, Research and Rock Drills R&D Erkki Ahola, Sandvik UGHRM
Director Technology and Engineering Seppo Taatila, Ponsse Oyj
Managing Director Kalle Tuohimaa, Bosch Rexroth Oy
Technical Director Jussi Hanski, Parker Hannifin Oy Lokomec
General Manager Risto Käkelä, Avant Tecno Oy
Vice President R&D Juha Mäkitalo, Finn-Power Corp.
R&D Manager Merja Lämsä, AarhusKarlshamn Ab Technical Products
Vice President Ilari Orpana, Polarteknik PMC Oy Ab / Chairman of FHPA
Section Manager Olli Pohls, Hytar Oy Water Hydraulics
Professor Kalevi Huhtala, TUT / IHA
Professor Petteri Multanen, TUT / IHA
Professor Jari Rinkinen, TUT / IHA
Professor Tapio Virvalo, TUT / IHA

SICFP'07 Secretariat
Chairman Prof. Matti Vilenius

Institute of Hydraulics and Automation (IHA)
Tampere University of Technology (TUT)
P.O.Box 589
FI-33101 Tampere, Finland

Tel. +358 3 3115 2264
Fax +358 3 3115 2240

PREFACE

This year we really have reason to celebrate! This is the *tenth* time SICFP is organized.

The first international conference on fluid power in Tampere was held in 1987. That was the start of the series of Scandinavian fluid power conferences. In 1993 it was decided that the name of the conference is Scandinavian International Conference on Fluid Power. At the same time it was also decided that SICFP will be held every second year alternately in Tampere and Linköping. So we have already a 20 years' tradition, which is also worth of celebration.

This conference is organized by Institute of Hydraulics and Automation (IHA) at Tampere University of Technology (TUT) together with network of Fluid Power Centres in Europe (FPCE).

This tenth anniversary conference includes various traditional themes like mobile hydraulics, water hydraulics and industrial hydraulics. However, in addition this time there are many more new areas included like digital hydraulics, intelligent mobile machines and teleoperation. They are reflecting well the situation, where electronics, modern information and communication technology is integrating with traditional hydraulics and automation.

We received about 125 interesting and high-level proposals. In addition to five invited speakers, about 80 papers were selected for the final programme. We believe that the conference will give the participants fine opportunities to listen interesting presentations, to exchange opinions and strengthen of old contacts and to establish new ones.

This time the conference proceeding will be published as a printed book and also as a cd-rom. We hope that this proceedings will serve you well during the conference but also far in the future as a source of reference.

We would like to express our sincere appreciation to everybody who has contributed to the success of the conference.

Tampere, 4th of April, 2007

Kari T. Koskinen, Professor
Vice-Chairman, SICFP07

Jani Vilenius, Dr. Tech.
Conference Manager, SICFP07

TABLE OF CONTENTS – Volume 2

PLENARY SESSION P2

SESSION A3: Intelligent Mobile Machines and Systems

SESSION B3: Water Hydraulic Valves

SESSION C3: Digital Hydraulic Systems

SESSION A4: Mobile Hydraulic Valves

SESSION B4: Seals and Filters

SESSION C4: Special Applications and Systems

SESSION A5: Energy Efficient System

SESSION B5: Fluids

SESSION C5: Condition Monitoring

DEVELOPMENT OF MULTI-MACHINE REMOTE CONTROL PLATFORM

Jari Saarinen[1], Mika Hyvönen[2], Jussi Suomela[1], Jani Vilenius[2], Aarne Halme[1], Kalevi Huhtala[2]

[1]Helsinki University of Technology
Automation Technology Laboratory
Otaniementie 17
02150 Espoo
Phone +358 9 451 5146, Fax +358 9 451 3308
E-mail: Jari.Saarinen@tkk.fi

[2]Tampere University of Technology
Institute of Hydraulics and Automation
P.O.Box 589
33101 Tampere, Finland

ABSTRACT

The paper describes the components of a multi-machine teleoperation system. The main components of the system are: work site, work machines, teleoperation/control station and a simulator. The components are joined together with a software architecture that enables the flexible implementation of distributed systems. The control of the system is done via the Internet. As a result the system presents a full featured test platform for multi work machine teleoperation with real work machines at a real work site.

The system acts as a development platform for the Finnish center of excellence in Generic Intelligent Machines research (GIM). The GIM goals are to study the multi-machine teleoperation and develop the future work site concept.

KEYWORDS: Machine Control, Teleoperation, Multi-machine teleoperation, distributed system.

1. INTRODUCTION

Teleoperation and partial autonomy begins to be the reality in the work machine industry. Teleoperation (at some levels) can already be found for example in the mining, forestry and harbor machines. In some cases the machines are already robotic machines working autonomously for most of the work cycle. Only exceptions and some difficult tasks such as loading are teleoperated (e.g. Sandvik AutoMine™ [6] and Kalmar's autonomous straddle carrier system [1]). The teleoperation provides safety in such cases as mining in unsafe areas. Combining partial autonomy with teleoperation, the productivity is improved as the autonomous functions provide more effective running time during the shift and less maintenance time/cost due to the more machine friendly control.

The most primitive form of teleoperation - remote control – refers to operating a machine in its vicinity. Due to several incidents where operator has been crushed by the machine he was operating, laws prohibiting work machine remote control are planned in many countries. The next step is to operate the machine from a distance, away from the dangers. The difference is that now there is no line of sight between the operator and the machine, thus the necessary sensory data must be provided to him. In the traditional sense this is called teleoperation.

In traditional teleoperation the operator always concentrates on controlling one machine at a time. The next step in the development is that one operator would be able to control multiple machines. This step is rather radical, since doing this efficiently requires that the machines have some autonomy functions. Also, the fact that the operator controls multiple different types of machines sets requirements for the machine interfaces as the same control equipment and software should be used with all the machines. The concept of telepresence also gets a new meaning: the operator no longer concentrates to operating a single machine, instead/additionally he needs an overview of the whole situation (situational awareness).

The research topics described above are the focus of the newly founded Finnish Center of Excellence in Generic Intelligent Machines Research (GIM). GIM is a research center focused on intelligent mobile machines and robotics with a background is in the strong research traditions of the participating institutes and the urgent need from industry. In the development of mobile machines the research in intelligent machines/field and service robotics is the leading force of today, which is in a very active state globally at the moment. This anticipates the creation of a fully new intelligent machines industry with a noticeable economic potential in the future. It has become evident that there is an urgent need for a more generic and concentrated research effort in the key areas of future intelligent machines, regardless whether they are related to the new generations of traditional working machines or fully new type of mobile machines, such as service robots.

This paper presents the development of the GIM test platform: the multi-machine remote control platform, which allows the testing and development of a variety of generic systems with real work machines. The platform offers different types of work machines that should be operable from anywhere (on board, locally or remotely). The machines are equipped with on-board computers that allow the development of

autonomy as well as assistive functions for teleoperation. The implemented software architecture is completely distributed, which allows the design of any type of applications varying from the direct teleoperation to fully featured autonomy. The developed software system will serve as a basic infrastructure for future GIM research projects.

The results presented in the paper concentrate on the testing of the base architecture in direct teleoperation over the Internet.

2. SYSTEM DESCRIPTION

2.1.Overall description

The overall goal of the system is to offer a test platform to study generic intelligent machines. The system is realized in cooperation between two universities, Helsinki University of the Technology (TKK) and Tampere University of Technology (TTY). The physical distance between the Universities is about 200km.

In addition to on-site control, the machines should also be controllable from both local and remote control room. The difference between on-site control and local teleoperation is that in on-site control the operator sees and hears the machine. The difference between the local and remote control rooms is that some of the sensor data can be transferred to the local control room with wires (e.g. Camera).

The work machines are small tractors (AVANT^{TM}), which are powered with diesel engines. The power for the subsystems is produced by hydraulics. A small embedded computer is used to control the actuators. The machines are connected to Internet via WLAN and radio modems.

A simulator is embedded as a part of the system. The simulator is a hardware-in-the-loop (HIL) simulator, which uses the same control electronics as the real machine, but the mechanics, hydraulics and the environment are simulated. The simulator provides valuable information in the testing and development phase.

The system communication is based on TCP/IP. Basically the only communication links in the system that do not use the Internet are the radio modem channel between the local network and the work machines and the on board communication, which uses CAN.

The overview of the system components is illustrated in the figure 1.

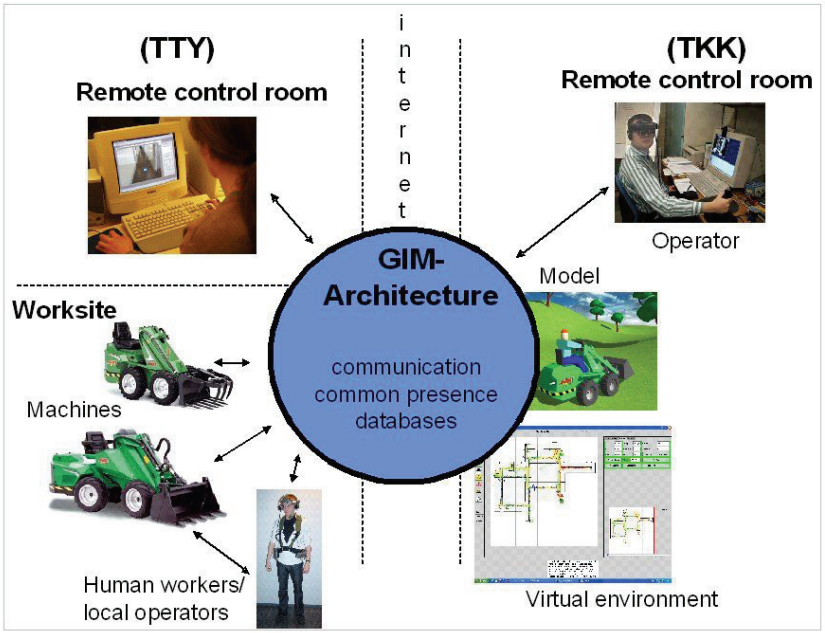

Figure 1: The components of the system

2.2.Communication Architecture

Figure 2 illustrates the network topology and the connection of the components in the system. The topology is based on the physical location of the project partners. The remote control station could be situated anywhere and there is no limitation to the number of remote control stations (at least remote observation is possible from a practically unlimited number of places).

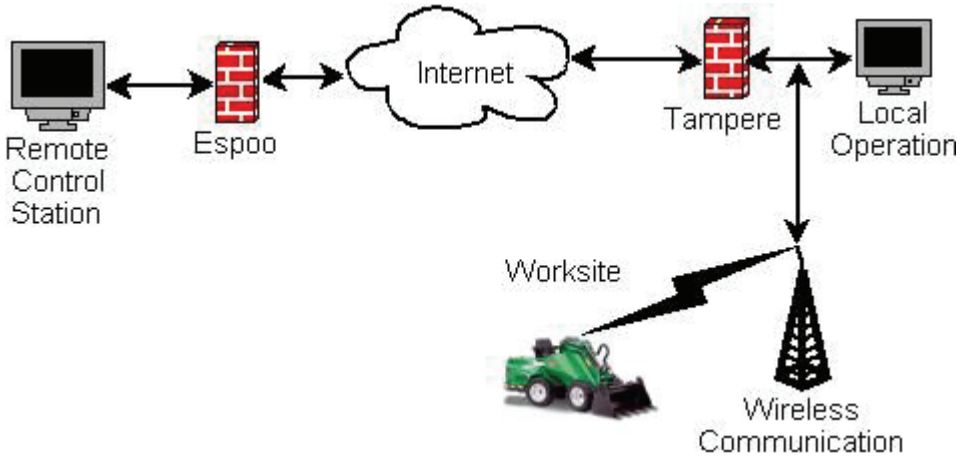

Figure 2: The Network topology

The work site is equipped with two communication channels: radio modems and WLAN. The WLAN is used for general communication between operators and machines. The radio modem is used as a backup for emergency purposes. The setup

allows tests with broadband TCP/IP communication as well as narrow band tests.

The local operator station is situated near the work site. The local operator s4tation and the work site are in the same local network.

TKK/TTY servers are the central connecting points between the operation stations. The role of these servers is to enable the building of the GIM Intranet. The GIM Intranet is a self-developed software which enables the connection of remote softwares between each other despite firewalls. Network security is one of the biggest challenges of distributed software development and therefore it is impossible to think of a completely open system.

The remote operation station will be situated in the network with access to its own local server.

2.3.Remote machines

The remote machines are small skid steered tractors from AVANT TECNO (see fig 3). These off-the-shelf products are modified to be computer controlled. The leading idea in the instrumentation of these machines was to maintain them as real mobile work machines (robust, environment tolerance, etc).

2.3.1 Instrumentation

Figure 3 presents a prototype with three main parts that are important in a computer controlled mobile machine. Number one includes all electronic components, number two is a control and display module which runs the main program and number three is the place of the proportional valve block which is installed to the front of the machine.

An electrically controlled valve was added to control the number of hydraulic pumps in action (one or two). Because of the proportional valves, a pressure filter was needed. Also, all original hoses were changed to type more suitable to be used with the proportional valves. Two electrically controlled valves were added to lock the boom and the bucket if needed. This lock option increases the capacity of the power transmission. In this study proportional valves with load sensing pressure measurement sensors were used. [4]

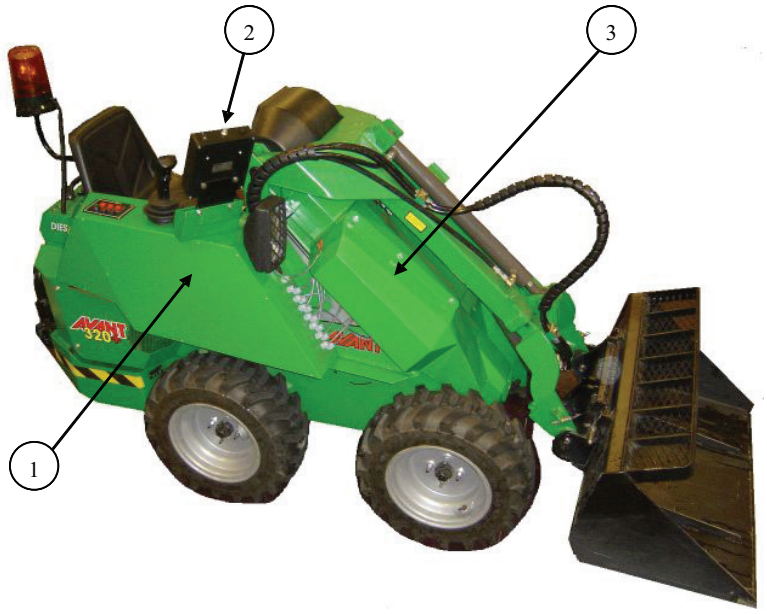

Figure 3: Computer controlled and teleoperated mobile machine.(1) Electronic components (2) Control and display module(3) Proportional valve block

It was challenging to find electronic components which could be suitable for both the final prototype as well as for a commercial product. In some cases also laboratory built components were also used. The use of commercial products sets technical and economical limitations but typically produces more reliable and robust result.

There are two input/output modules which contain analogue, digital and frequency inputs as well as PWM and digital outputs. The analog inputs are used for example to get pressure sensor information and the position of the steering wheel. Joystick button information is collected with digital inputs and frequency inputs are used to get velocity information of each wheel and the diesel engine. The pumps and lock valves are controlled by digital outputs. Proportional valves are controlled by PWM outputs. These IO modules are waterproof and military tested and they are connected by a CAN bus to the control and display module. [5]

The control and display module (fig. 4) is an embedded Linux computer, which is robust and waterproof. The display is a monochrome screen visible in all weather conditions. There are two rotary switches, a power switch and five buttons.

Currently the machines allow on-board control, a small remote controller for short distance remote control and a control room for long distance teleoperation, which includes a camera view from the machine. The connection between the machine and the remote controller is made using radio modems. These modems are commercial products and they are robust and suitable for this application.

Figure 4: Control and display module.(1) A screen handle selector (2) Change value handle (3) Main power switch (4) Selection buttons

2.3.2 On-Board automation

An on-board computer is included in the machine to allow higher level sensory processing and (semi) autonomous control. The on-board computer is connected to the machine through the CAN bus and it has the same communication interface to the machine as the radio modem.

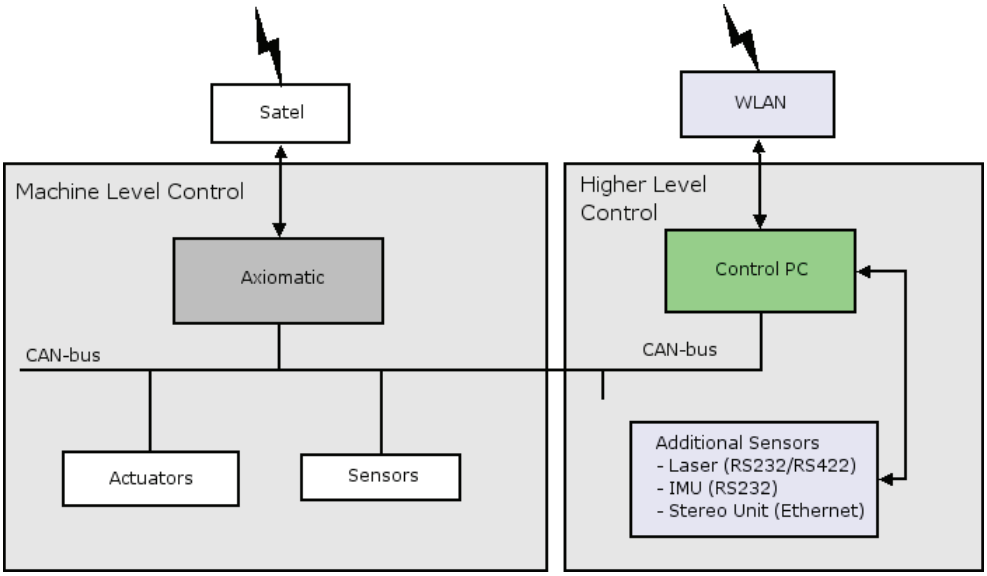

Figure 5: Overall control architecture of the mobile machines

Figure 5 presents the schematics of the overall control architecture. The CPU is connected to the Internet through WLAN allowing higher bandwidth communication

between the world and the machine. The radio modem is still attached to allow the direct remote control of the machine and some safety functions.

The on board computer is connected to various sensors for measuring the state of the machine as well as the environment. The goal is that the machine has sufficient sensors and processing so that it can be localized within the work site, and it can perform some level of 3D mapping in real time.

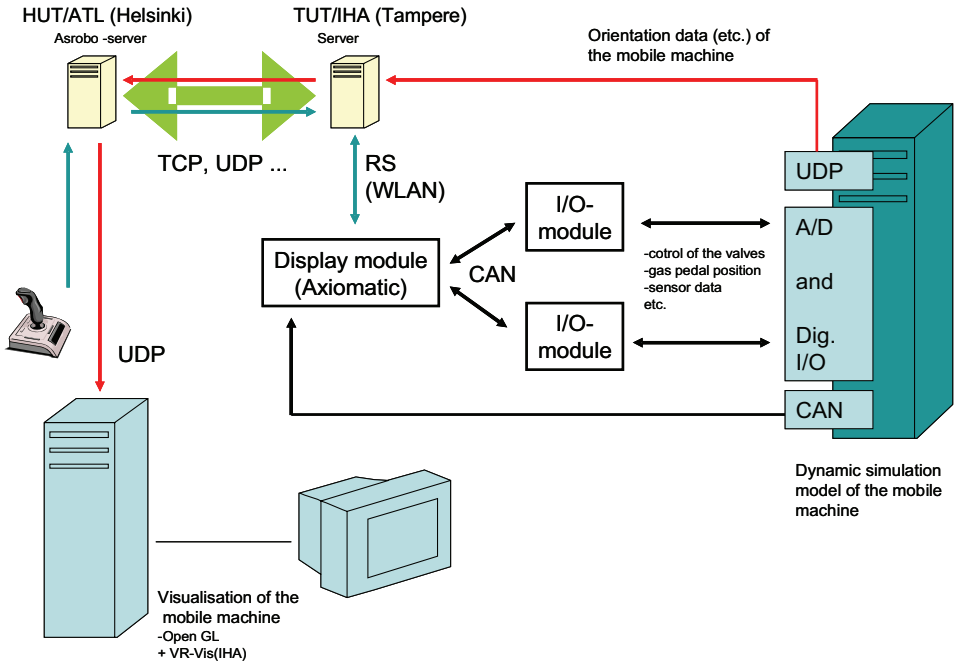

Figure 6: Teleoperated real-time mobile machine simulator with hardware-in-the-loop.

2.4.Simulator

The simulator can be used to test and develop all components of the system. The simulator is a hardware-in-the-loop (HIL) simulator, which uses the same control electronics as the real machine, but the mechanics, hydraulics and the environment is simulated. Thus, from software point-of-view the simulator is just an extra machine in the system. This allows accurate testing from communication to control with the simulator, before implementing them on the real machine.

The location of the real-time simulation computer was at Tampere and the visualization computer at Helsinki. The communication interface of the simulator is the same as with the real machine (see ch. 2.2).

2.4.1 Structure of the simulator

The basic architecture of the mobile machine simulator is presented in Figure 6. Computers used for the calculation of the simulation model and visualization were standard personal computers equipped with fast AMD Athlon 64 processors. The simulation model was made in the Matlab/Simulink environment and compiled to the embedded xPC target kernel. The visualization of the mobile machine was made with OpenGL–based software. The visualization model was created from the laser scan of the mobile test hall at TTY (see Figure 7). Controls were the same as for the real mobile machine.

The hardware connected to the simulator consists of the same hardware setup as the real mobile, except that the radio modem was replaced by direct RS232 cable and the PWM-valve control signal was filtered by passive low pass filter. The control software was exactly the same as in the real machine. Other hardware include a display module (Axiomatic) and I/O valve control modules. The I/O interface between the simulation model and the HIL consists of several AD, DA and Digital I/O connections and a CAN bus card. An Ethernet card was used to transfer the simulated data to the visualization computer.

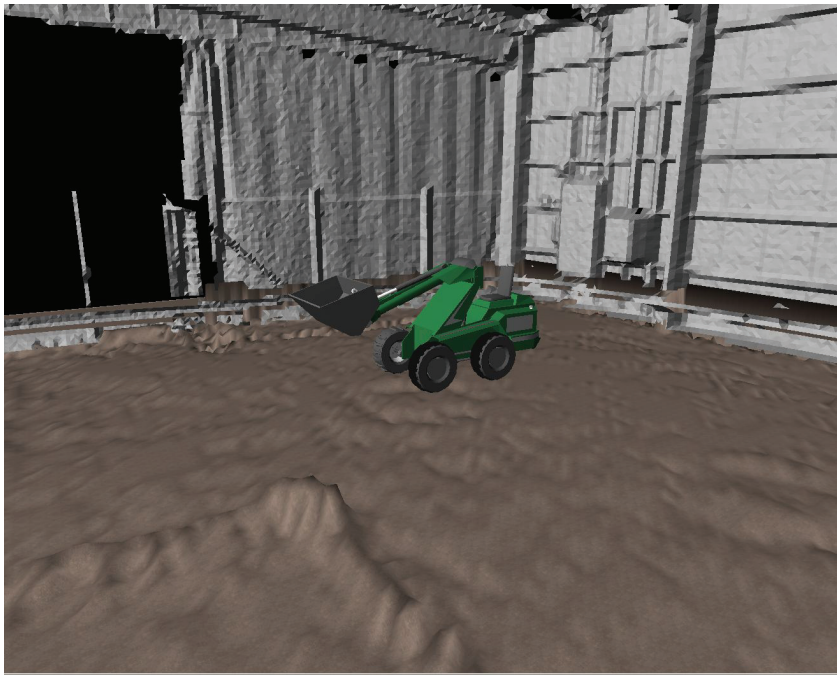

Figure 7: The visualization of the simulated machine. The environment is modeled from 3D laser image of the test hall

In Figure 8 the basic structure of the mathematical model of the mobile machine is presented. The simulation model is a simplification of the accurate offline simulation model of the same mobile machine presented in [3]. For real-time purposes semi-empirical component models are used instead of analytical models. Dynamic friction models are also replaced with simplified friction models.

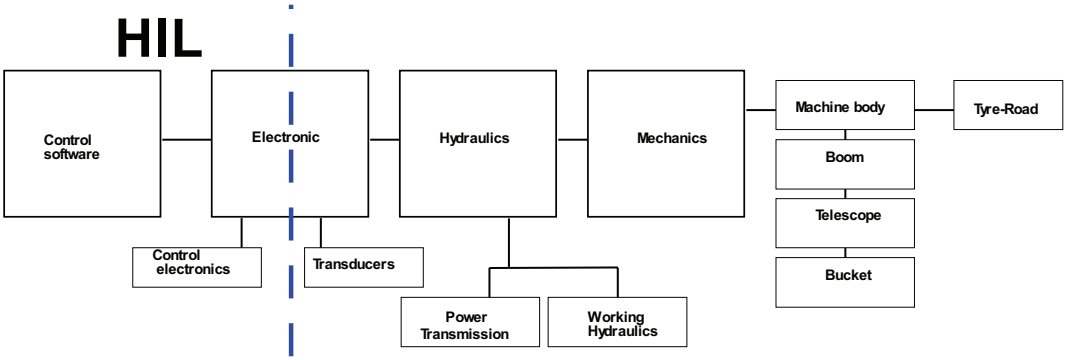

Figure 8: Basic structure of the simulation model of the mobile machine.

2.5.Operation stations

At the present state of the project the machines are operated only in direct teleoperation. The feedback is mainly through fixed overview cameras at the work site. The control of the machines is done with standard computer game controllers (steering wheel, pedals and joystick). The figure 9 illustrates one possible setup.

Figure 9: An operating station

The control software connects to the local (work site) server, which handles the data forwarding to the remote machines. The local connection handler takes care that there can be only one operator at a time. Images are grabbed at the work site and can be subscribed to by the clients. The same applies for the feedback data received from the machines. The setup allows one operator per machine and an unlimited number of observers or supervisors. Also, the setup allows the operator station to be situated anywhere on the Internet.

2.6. Software architecture and design

The project aims at a generic multi machine system that can be controlled remotely, locally, or both. The concept includes components at the machine level, work site level as well as at the global level. This implies that the implementation will be distributed to several locations. One way of implementing such a system is to use a server-client architecture [2]. The strong points of the server-client architecture are that the data access is managed and the authentication is simple. The server-client architecture also helps with firewalls as only the server needs to be accessible. Another extreme is a point-to-point architecture, where each client communicates directly with each other. The point-to-point streams are widely used in streaming and data sharing. This is the most efficient way of sharing data between clients, however with current security policies this is very restrictive and in many cases impossible (e.g. between universities). Additionally, a pure point-to-point network lacks the management facilities which are useful when the system can have various configurations.

GIM software system implements an architecture that is a hybrid of the ones mentioned above. Each client can communicate with each other directly, but the connection is managed. The central piece in the architecture is a software called *tcpHub*. A client connects to it using TCP/IP socket. The tcpHub forwards the data from a sender to a receiver. It maintains a local name (and id) data of each client connected to it. The number of tcpHubs is not limited and the hubs handle the connections between each other. Currently the system supports unicasting, multicasting and broadcasting.

Figure 10 illustrates the principle of the GIM software system. The tcpHub must be in network which has at least one TCP port open to the clients that will connect to it. The same applies to the connections between the tcpHubs. In principle it is enough to have one tcpHub, but having local ones reduces the network load significantly. The applications can see each other by name and ID. For the applications the network is invisible.

The Network Interface in figure 10 is an implementation of the lower level functions and protocols. This module is not even visible for the application, since it is wrapped inside the Generic Intelligent Machine Interface (GIMI). This (C++) interface basically handles all communication related tasks. The idea of this module is to provide a unified interface unified functionality. This implements for example data subscription, application level ping, service discovery and multi-casting. In other words the programmer does not need to be a communication specialist to be able to implement an application using the GIM software system. This is an important aspect since the platform is developed to be used as a research platform for several years.

The current implementation does not restrict the future solutions in any way. The programs can be run completely distributed or they can be built to be centralized.

The data type specification is based on the ID numbering in the system. The specified IDs are global in the system and the same IDs are used as a service specification. For example, one module can provide sensor data. This sensor data will have a unique key, which is used in determining the content of the data. The module that provides the data adds it as a service which can then be subscribed to by others.

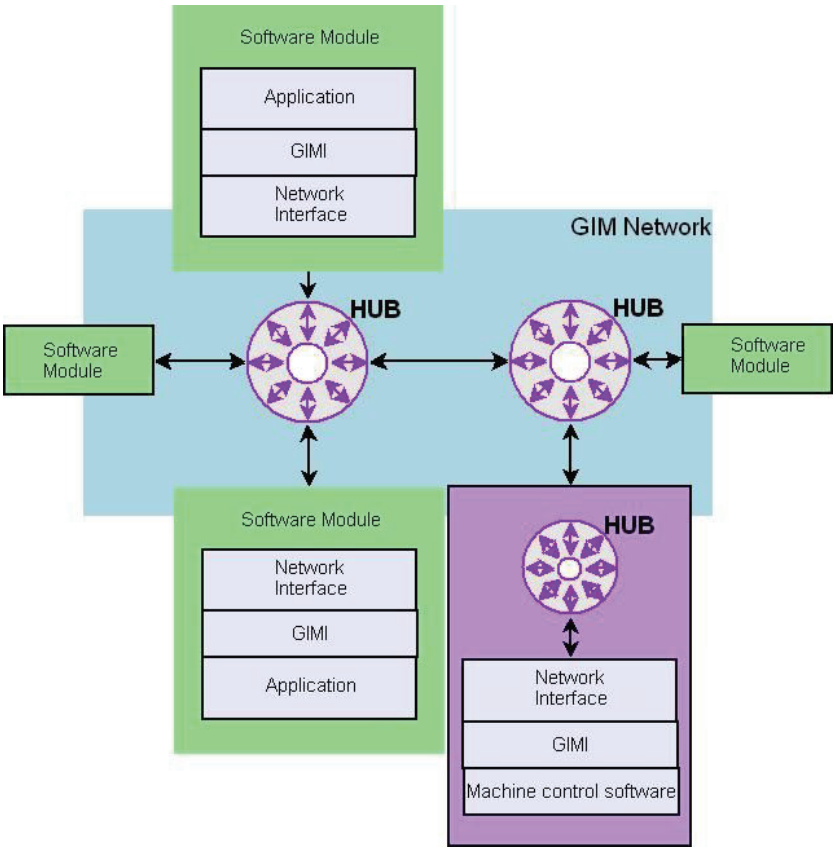

Figure 10: A block diagram of the GIM software system

Figure 11 illustrates an example implementation, where two operators operate remote machines. One operates the real machine and the other operates the simulator. The TeleUI block reads the control commands from controllers, sends them to the appropriate connection handler and receives the feedback data from the same connection handler. The camera data is visualized to the operator by the ImageDisplay. Additionally the ModelUI receives data from the simulator and visualizes the state of the simulated machine to the operator controlling it. The connection handlers forward the data from the operators to the machines and receive feedback from the machines. The feedback can be subscribed to clients as a service. The camera server grabs images and sends them to subscribers.

The blocks in figure 11 can physically be driven under different platforms, but they are connected to the shown hubs. For example both the operators are using different computers and the camera server software runs on its own computer. Also noteworthy is that even in this simple demonstration the reuse of software is relatively high. Besides all the infrastructure code, the UI applications are identical and the connection handlers are identical.

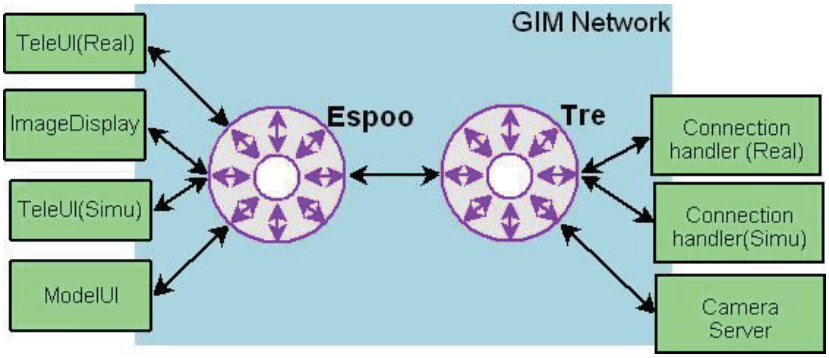

Figure 11: The direct teleoperation of the simulator and real machine

3. INITIAL TESTS AND RESULTS

So far the tests have been concentrating on proving the functionality of the infrastructure. The first tests concentrated on the underlying network. This was done using standard Unix network tools.

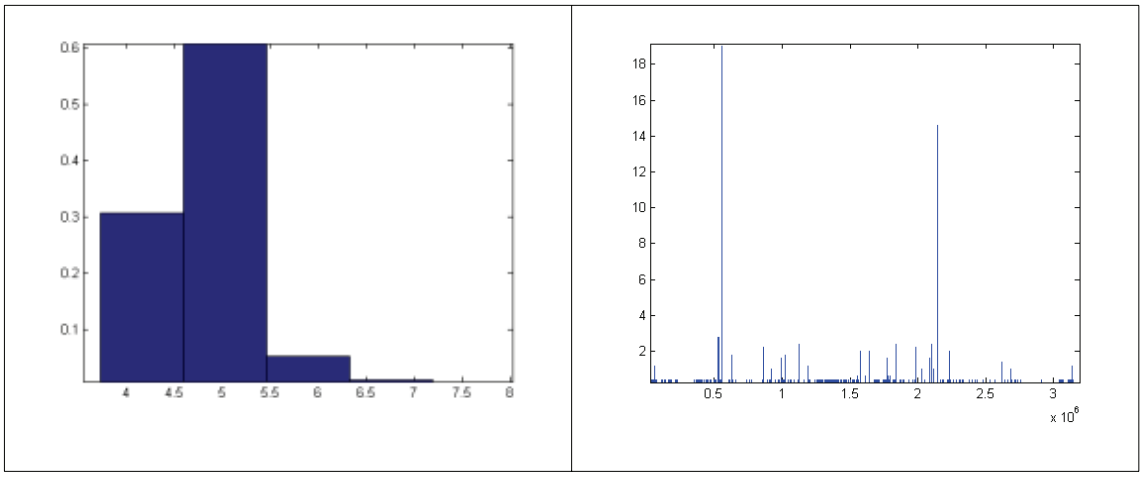

Figure 12: The results of the network tests. On the left is a histogram of the ping times within one week (y-axis is percentages(/100), x-axis is milliseconds). On the right are the network failures during the week (y-axis is seconds and x-axis is samples).

Figure 12 (left) shows the histogram of the round-trip time of the TCP/IP packets sent between Espoo and Tampere. The tests show that 99.5% of the packets will have a round trip time less than 10ms, the average being 4,91ms. Figure 12 (right) shows the times the network has not been responsive (within 200ms). During the weeks test there were two longer periods that the packets were not delivered. The longest time the network was down was 18 seconds and second longest 14 seconds. Even though this happened only a couple of times it is clear that this type of events should be considered in the future.

Similar ttests were also made at the application level. The purpose of these tests was to show that our software does not cause lag or unpredictability in the system. The results

can be seen in figure 13. The left image shows that the local connection is very fast. Almost all the packets have round-trip time less than 0.8ms. This includes the application layer. The second (right) image illustrates the round-trip times of the route client-remote server-local server-client. This is practically the route the data travels when teleoperating. The payload was chosen to be 512 bytes, which is significantly more than the average control data payload however smaller than image stream payloads. The average round-trip time was 7.46ms and almost all the packets were received within 10ms (99.0% within 10.28ms). If the bare network tests and the application level tests are compared, the base infrastructure caused in our tests approximately 1.88ms more delay (client-local server-client time is reduced from total time).

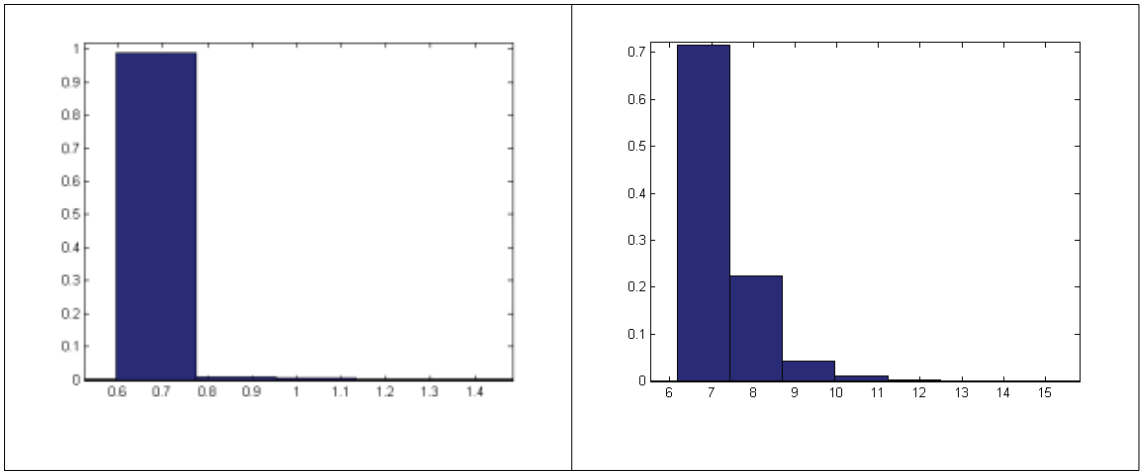

Figure 13: Application level tests. On the left is round-trip time between client and local server. On the right is the histogram of the time spent in route client-remote server-local server-client. Y-axis is percentages (/100), X-axis is time in milliseconds.

Finally, the tests with the whole system. The tests cannot be illustrated here, but the setup described in the section 2.6 and illustrated in figure 11 has been successfully demonstrated several times. During the demonstrations some primitive tasks have been performed such as driving around, picking up sand and unloading sand. However the system does not yet provide enough feedback (telepresence) for performing more detailed work tasks.

4. FUTURE WORK AND CONCLUSIONS

This paper has presented the very early stages of the GIM. The components have been described separately and some initial tests have been discussed and presented. At present the system has been demonstrated with direct teleoperation; operator(s) being in Espoo and the work site in Tampere. These tests/demonstrations have proved that the base infrastructure works and it does not cause lag to the system.

During the demonstrations there has always been one operator for one machine. The next step is to increase the level of autonomy in the machines. Also, the environment

perception and modeling will be improved. Currently the information presented to the operator is not sufficient for working effectively even with one machine. The goal is that one operator will be able to operate multiple machines. For this the operator needs a clear idea of the state of the task as well as the machines. Also, it will be inevitable that the machines will have at least some level of autonomy.

5. REFERENCES

[1] Nelmes, Graeme, Key Note Address, Patric Corporation, The 5th International Conference on Field and Service Robotics, July 29-31 2005, Port Douglas Australia http://www.acfr.usyd.edu.au/FSR/Plenary%20Speakers/FSR%20Patrick.pdf

[2] 2004 Kulich, M., Kout, J., Preucil, L., Mazl, R., Chudoba, J., Saarinen, J., Suomela, J., Halme, A., Driewer, F., Baier, H., Schilling, K., Ruangpayoongsak, N., Roth, H.: PeLoTe – a Heterogeneous Telematic System for Cooperative Search and Rescue Missions. Urban search and rescue: from Robocup to real world applications, in conjunction with the 2004 IEEE/RSJ International Conference on Intelligent Robots and Systems (IROS) Sendai (Japan), September 28, 2004.

[3] Mika Hyvönen, Jani Vilenius, Antti Vuohijoki, Kalevi Huhtala, Mathematical model of the valve controlled skid steered mobile machine, 2nd International Conference on Computational Methods in Fluid Power, FPNI'06

[4] Vilenius J., Raneda A., Hyvönen M., Uusisalo J., Huhtala K., Valve Controlled Teleoperated Skid Steered Mobile Machine, Proc. of IMECE 2004, Anaheim, USA, 2004

[5] Vilenius J., Raneda A., Huhtala K., Characteristics of Teleoperated Skid Steered Mobile Machine, The 3rd FPNI-PhD Symposium on Fluid Power, (Terrassa, Spain)

[6] Woof, M., Technology for Underground Loading and Hauling Systems Offers Exciting Prospects, Engineering and Mining Journal, April 2005

A PNEUMATIC CLIMBING ROBOT FOR INSPECTION TASKS

Professor Enrico Ravina
University of Genoa (Italy)
Dept. Of Mechanics and Machine Design
Via Opera Pia 15 A
16145 Genoa, Italy
Phone +39 010 3532848, Fax +39 010 3532834
E-mail: enrico.ravina@unige.it

ABSTRACT

The paper refers on an application research oriented to the design and realisation of climbing robots able to automously move their selves using pneumatic devices. The purpose is the design implementation of low cost service robots, conceived for inspection tasks on different kind of surfaces. The main characteristics and potentialities of original prototypes designed, realised and tested are focussed and discussed, showing application advantages and operation limits.

KEYWORDS: Robotics, Pneumatics

1 INTRODUCTION

Service robots include a very interesting and diversified spectrum of autonomous machines and vehicles conceived and designed for specific tasks, usually not directly related to an industrial production but oriented to solve functions suitable to users or to machines. The design of an automatic task requires the specification of the desired automation level, of the level of the autonomy and of the characteristics of the environment where the service must be developed. These informations are significant for the definition of the mobility and dexterity of the robot, for its kinematics' configuration and for the level of "intelligence" of the control unit.
A particular typology of service robots is represented by climbing and walking robots: their main characteristic is the ability to move their selves on different kind of surfaces, exceeding obstacles reached during their vertical motion. The state-of the-art in this field suggests experiences based, as reference models, on the motion features of animals (insects, snakes, lizards, geckos, snails,..), proposing simulations and prototypes attempting to mimic their performances. Many of these proposals are very interesting

but often expensive, difficult to realise, and justified only for very specific tasks. The purpose of the study is the development of prototypes of low cost climbing robots, conceived for inspection of different kind of surfaces, and devoted to carry on detection equipments (photo or video cameras, contact or contact less transducers, lasers, microphones, thermal sensors,..) able to acquire and to make available information on the state of the surface or the environment round the robot, predicting defects, failures, or critical conditions.
A wide spectrum of surfaces requires periodic inspections: the surface monitoring is fundamental for diagnosis and for the definition of correct maintenance programs. Field where this type of autonomous unit could be successfully applied are, for instance:

- civil applications, for monitoring of inside and outside walls of buildings, skyscrapers, chimneys, road bridges;
- naval field, for inspections on hulls of ships or offshore platforms, also in presence of critical environmental conditions (holds or bunkers saturated of gas,..);
- aeronautics, for periodic check of wings of aircrafts

and, more in general, when the human inspection must be avoided for dangerous, critical or difficult operating conditions (risk of explosion,..).
Robots for inspection tasks actuated by electric servo-motors are proposed by several researchers: the pneumatic technology in here experimented in order to evaluate the advantages, but also the limits, of a low cost approach to the problem of the remote manipulation.

2 ASPECTS OF THE PNEUMATIC ROBOT DESIGN

The study has been initially focussed on the design of a self-moving unit able to climb on flat or low curvature surfaces, generically oriented. The proposed system is totally pneumatic, with four orthogonal crossed main actuators: each of them carries, at its end, another cylinder able to lift and to lower a couple of suction cups. A general view of the prototype is shown in Figure 1.

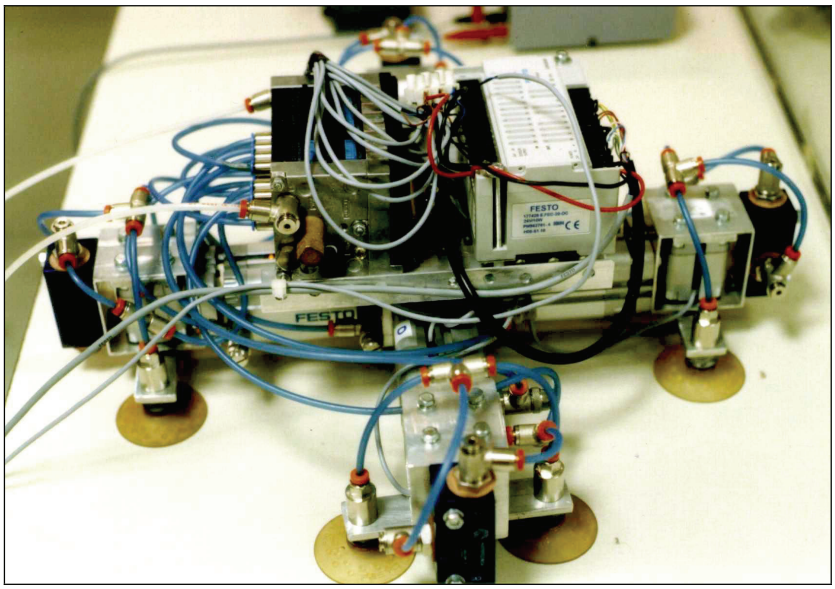

Fig. 1: General view of the pneumatic climbing robot.

2.1 Motion

As shown in figure 1, the essential geometry consists on a "cross" with four main pneumatic actuators, able to make steps on two orthogonal directions on surfaces generically oriented. Thanks to eight suction cups (two for each axis) the single step can be performed following this logic:

- simultaneous grip of all the cups on the surface;
- release of the front couple of cups;
- lift of the front couple;
- first displacement;
- lowering and replacement of the cups;
- release of two couples of cups corresponding to the axis orthogonal to the motion direction;
- second displacement;
- replacement of two couples of cups;
- release of the hind couple of cups;
- lift of the hind couple;
- third displacement;
- lowering and replacement of the hind couple of cups;
- repetition of the step.

The design of the proposed robot is based on a difficult compromise of different features, taking into account:

- the anchorage, based on deformable devices (suction cups);
- the variable behaviour of cups varying the external load distribution and the surface orientation;
- the necessity to generate a local motion of the cups, in order to avoid the slipping between cups and surface;
- the necessity to have the centre of the mass of the robot as near as possible to the surface (for stability problems) but, at the same time, to compensate the static deflection of the cups, variable with the robot position;
- an acceptable ratio between the stroke of the main actuators and the transversal load applied to their rods;
- an acceptable overall payload;
- the necessity of an embedded control system, reducing the physical connections to the frame;
- the necessity of an acceptable structural stiffness, to avoid uncontrolled static deformations;
- the definition of a simple design solution, cheap but reliable.

These requirements are often contrasting, but the proposed prototype seems to be a good solution of compromise.

2.2 Suction cups selection

Performances of the suction cups are fundamental for the correct motion of the climbing robot. The critical drawback consists both on slipping of the cup on the surface and on undesired releases: in any case the motion of the robot is inefficient or, if the worst comes to the worst, the robot can lose adherence and drop.
For these reasons it is very important to evaluate the chemical, physical and mechanical properties of the cup material: in addition to the maximum sustainable load it is necessary to evaluate the maximum lateral load able to produce slipping. A dedicated

test bench has been set up to this purpose: chosen the surface (material, environmental condition,..) the cup is gripped at a selected depression, modifiable by the user. By mean a pneumatic actuator a lateral force on the cup is generated. The consequent deformation is monitored both in the point of force application (by a precision potentiometer) and on the labium of the cup (by an optical fibers sensor). The test consists on the increasing of the pressure to the actuator evaluating, for each pressure, the corresponding deformation of the cup and the limit conditions of beginning of slip and/or complete lose of adherence. Different kind of tests can be implemented changing the size and the geometry of the cups, in presence of surfaces different for material (glass, plastics, wood, metal,..) and for state (clean, wet, greasy, dirty,..).
Figures 2 and 3 show an example of results. The reported data correspond to an average of 30 tests for each cup: this choice allows collecting also information about the repeatability of critical conditions. The response concerns a circular flat silicon cup (55 mm of diameter), in contact with two different flat and clean surfaces (Fig 2 for plastic surface and Fig 3 for aluminium surface) under different depression conditions (0.4, 0.5 and 0.6 bar).

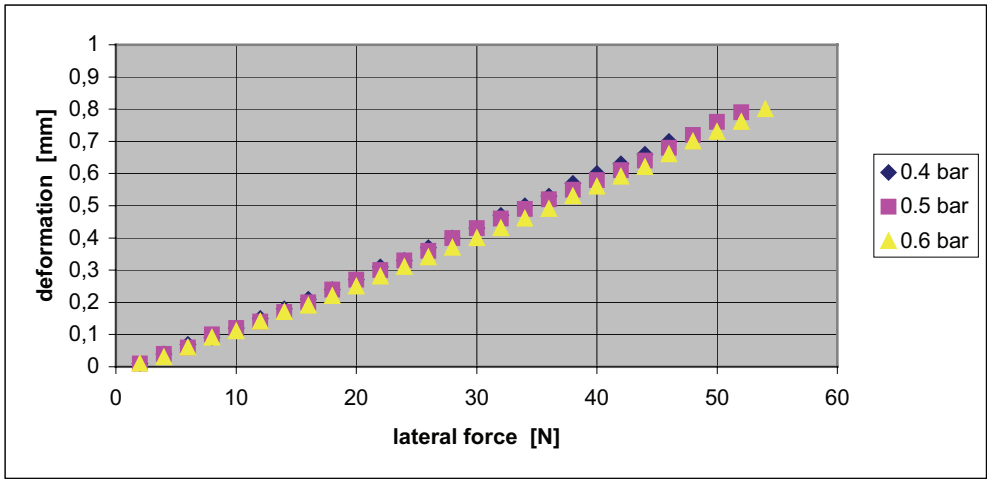

Fig. 2: Silicon cup on flat plastic surface.

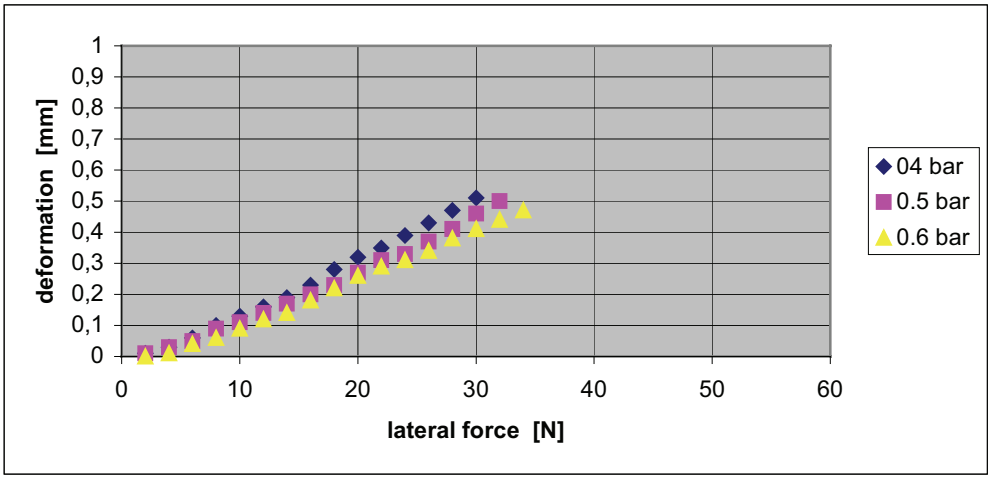

Fig. 3: Silicon cup on flat metallic surface.

On plastic surfaces the cup deformation increases because the release condition occurs for higher lateral forces.

The cup geometry strongly influences the performances under lateral loads: a comparison is reported in figures 4 and 5, where pressure conditions, labium geometry, labium dimension and material are the same but the shape of the cup is modified, from round standard to round bellows. On plastic surfaces, at the same lateral force, the cup deformation increases and the effect of different internal depressions is magnified.

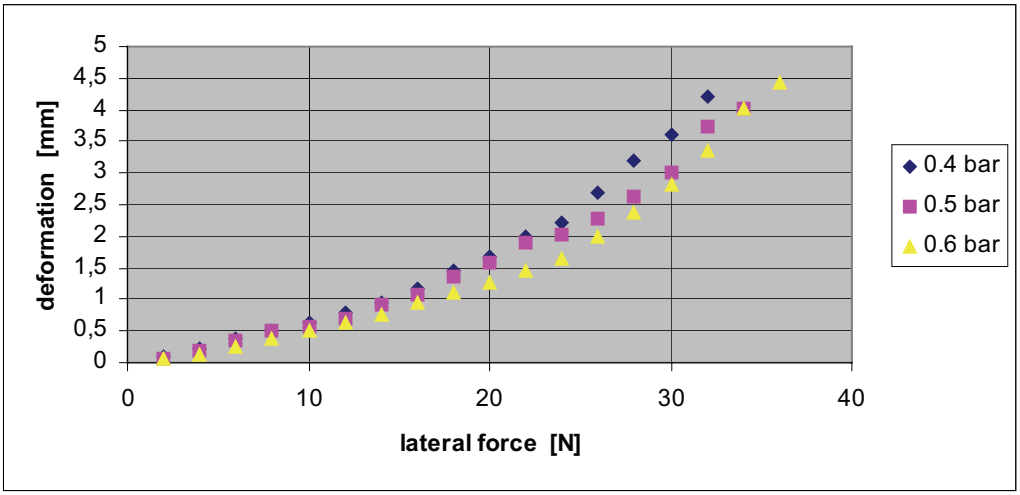

Fig. 4: Round bellows cup on plastic surface.

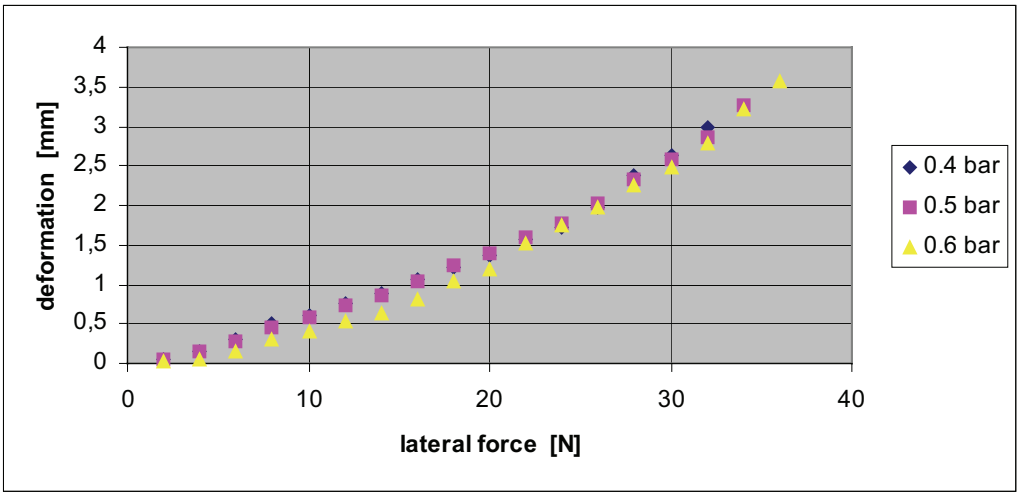

Fig. 5: Round bellows cup on metallic surface.

Considering the logic applied for generate the single step (four cups simultaneously gripped), the design of the robot has been implemented in such a way the external load can be supported by only three cups. The air consumption is 42 Nl/min at 4 bar for one couple of cups. Altogether the air consumption of the unit is less than 200 Nl/min.

2.3 Embedded control

The concept for drive and control is oriented to a low cost and reliable solution. For this reason the motion devices are pneumatic; on/off position sensors equip each axis and digital distributors drive it. Also pneumatic valves drive the ejectors supporting the suction cups: in order to reduce the weigh and to simplify the pneumatic connections, the driving system is realised as a group of compact pneumatic valves controlled by a

micro-PLC. All the components are embedded on the robot: in this way the “umbilical cord” connecting the autonomous system to the frame is reduced to a single hose and to a single electrical wire (24 V power supply), increasing the robot dexterity. In figure 6 the simplified pneumatic layout of the proposed climbing robot is reported: A, B, C, D represent the four main axes and GA, GB, GC, GD the groups of the corresponding suction cups.

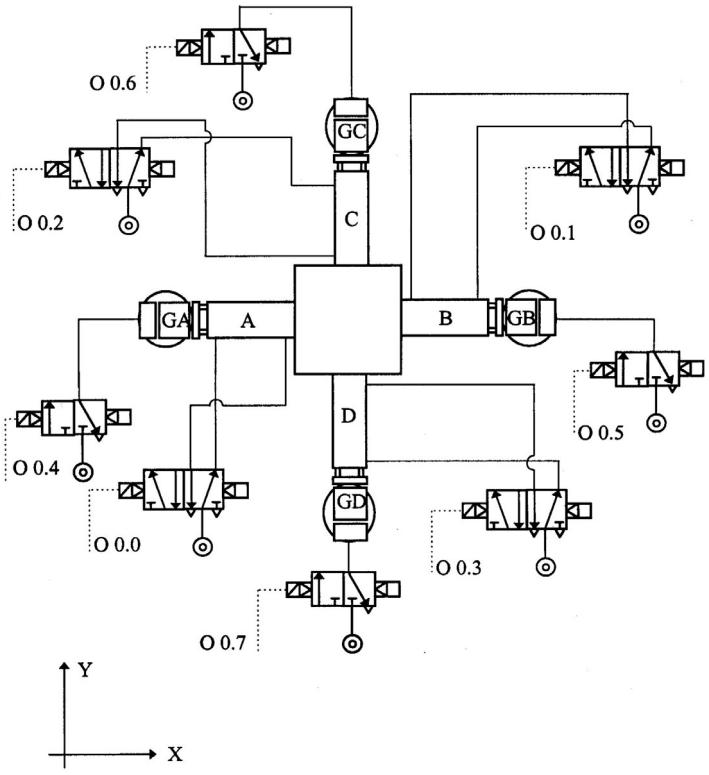

Fig. 6: Schematic layout of the climbing robot.

Figure 7 shows the implemented solution: the group of compact 3/2 distributors in directly interfaced to a micro-PLC, both embedded on board.

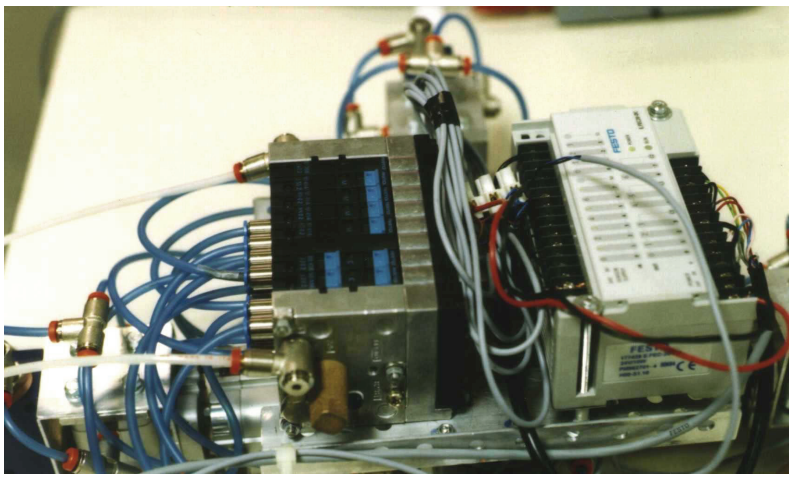

Fig. 7: Compact distributors and micro-PLC, assembled on board.

The micro-PLC makes available 12 input channels at 7 mA and 8 output channels with maximum switch current of 2 A. The programmable motions concern:

- single or multiple steps on X or Y direction;
- alternate single or sequences of steps in X and Y direction (diagonal approximated with zigzag);
- forward and backward motions.

3 RESULTS

Motion tests on different kind of surfaces have been developed: climbing operations on horizontal, tilted and vertical surfaces have been programmed, changing the surface roughness and the motion sequence of the robot. Climbing motions on glass, plastics, rolled wood, plasters have been successfully tested. Figure 8 reports some motion phases of the robot, equipped with a web camera, on rolled wood surface generically oriented.

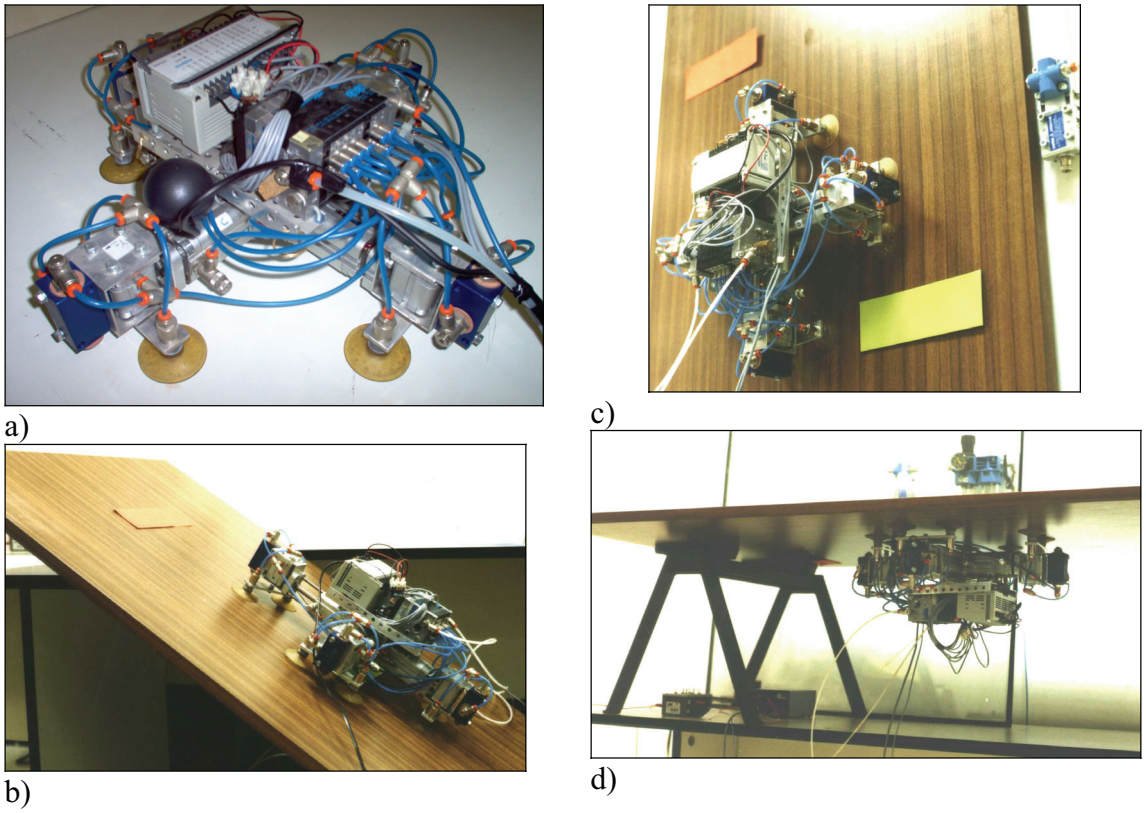

Fig. 8: Motion phases: a) robot with embedded web camera; b) motion on tilted surface; c) motion on vertical surface; d) top-down motion.

The structure of this type of climbing robot is rigid: nevertheless, specific tests have shown the possibility to use it not only on flat surfaces but also on low curvature walls, thanks to the local deformations of the suction cups. The overall dimensions of the proposed prototype are 600 x 600 x 150 mm, and the weight is 5.5 kg.
Step sequences are completely programmable. The gripping is assured by the control of the vacuum level inside the cups: if the level decreases below –0.4 bar the unit stops itself, maintains the position and generates an air-raid warning. The average speed of the unit is about 0.1 m/s.

4 IMPROVEMENTS

The main disadvantage of the previously described unit is its rigid structure: that not allows to the robot climbing operations on surfaces with variable slope. In order to improve the dexterity a modified articulated prototype has been designed and realised: a general view is reported in figure 9.

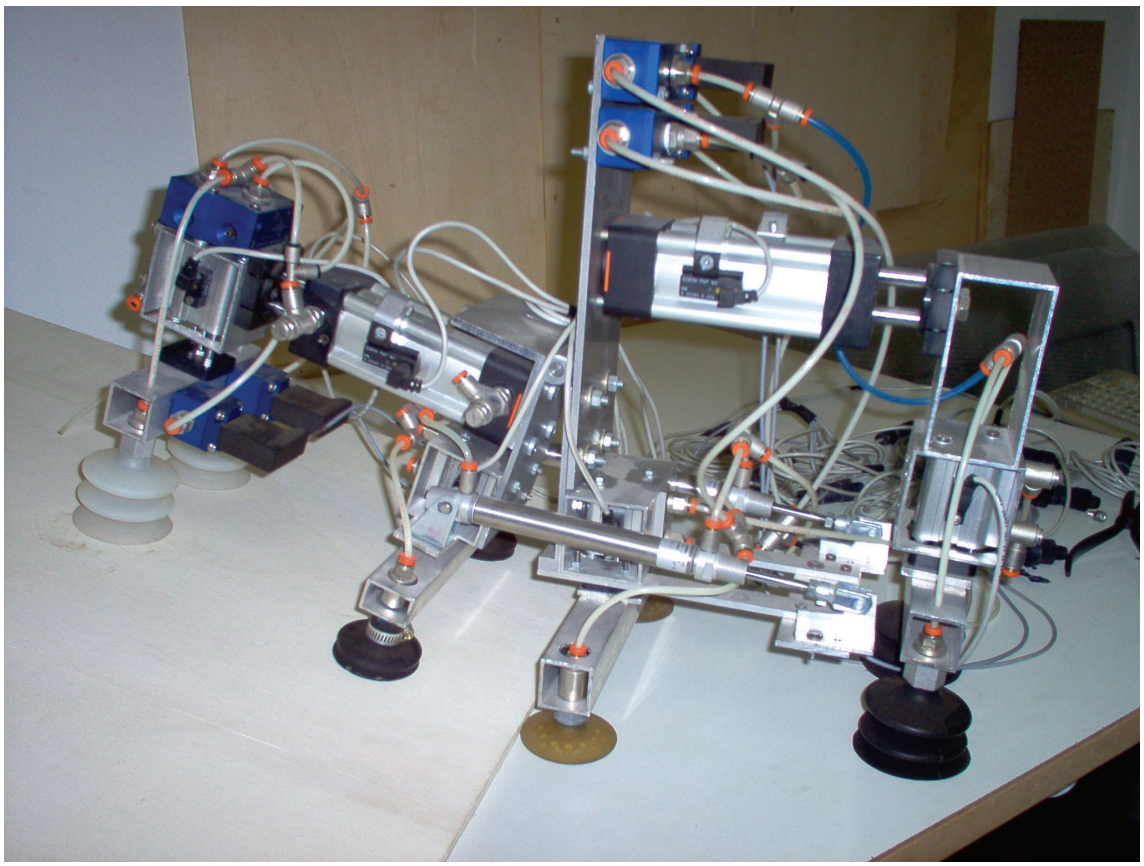

Fig. 9: General view of the articulated pneumatic climbing robot.

At present time the proposed unit is conceived for climbing motions only in a single direction: it consists of two parts (front and back) respectively mounted on articulated frames. If, during the motion of the robot, the slope of the surface varies, a contact less sensor detects this variation and the front part is rotated: this additional motion can be programmed for particular slope variations (e.g. from horizontal to vertical plane) or controlled by a pneumatic servo-system.
In order to eliminate the centralized control on board, a modified solution based on ASI control (Actuator Sensor Interface) has been tested: the weight of the robot decreases, but the umbilical cord remain the same because the electrical wire is used not only for power supply but also for communication signals.
Figure 10 shows some motion phases of this unit, starting from a horizontal plane and approaching a vertical surface. Initially the unit moves itself as a rigid structure: when the proximity sensor detects the presence of the vertical wall the front part of the robot rotates of 90 degrees. The horizontal motion goes on, till the front part is able to begin the climbing phase: after an intermediate condition where the back part moves itself horizontally and the front climbs, the robot reaches the vertical position and the climbing proceeds, in similar way to the previously described unit. The movement from floor to wall is realised generating rotations of 90 degrees between front and back parts

of the robots. Variable angles can be controlled by a pneumatic servo-valve: this technique is, at the preset time, under development.

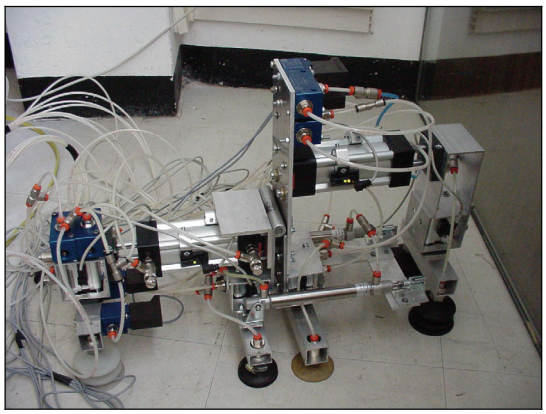

a)

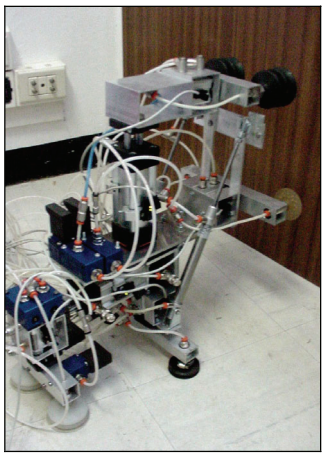

b)

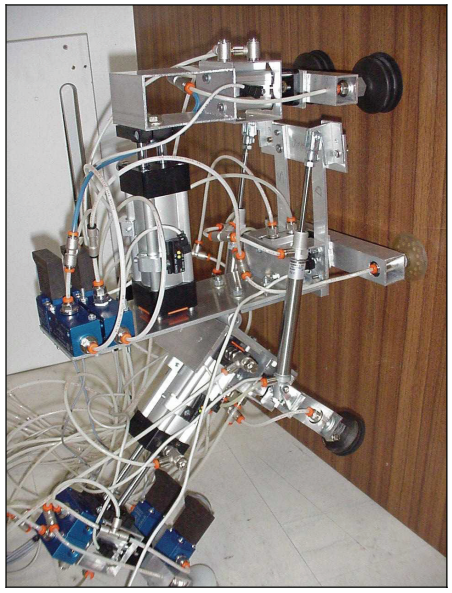

c)

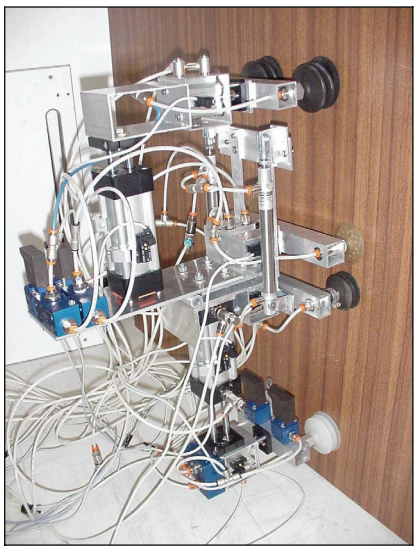

d)

Fig. 10: Motion phases: a) motion on horizontal plane; b) approaching to vertical plane; c) intermediate climbing phase; d) motion on vertical plane.

The variable load conditions on the suction cups force to use different cup geometries: this aspect requires, at present time, further deepening. Another problem, not completely solved, concerns the position of the centre of mass of the robot: the geometry proposed in figure 9 and its stability must be optimised. An accurate analysis of the masses distribution on board in under development, in order to evaluate the actual position of the centre of mass of the robot in any significant position, minimizing its distance from the motion surfaces.
The control based on AS-I technology is organized on a sequence of slave modules interconnected, by means the AS-I cable, to a master unit: figure 11 shows a test phase of this control system, before the assembly of the modules on board. The supervision is managed by IPC (Industrial Personal Computer).

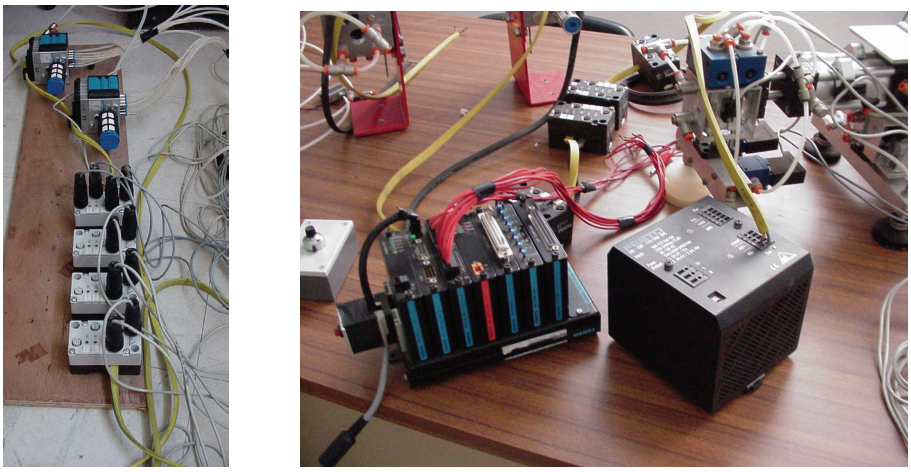

Fig 11: Test phases on AS-I control.

5 SOME CONCLUDING REMARKS

A low cost autonomous climbing robot oriented to inspection tasks is proposed. First rigid prototype shows good performances on flat or low curvature surfaces, but it is not able to move itself on surfaces having variable geometry. An interesting improvement has been designed and tested, substituting the point-to-point control (by PLC) with a distributed control (AS-I). Further developments will be oriented to eliminate the umbilical cord, installing on board a micro-compressor and batteries for electric power supply.

6 REFERENCES

[1] R.D. Schraft "Mechatronics and robotics for service applications", IEEE Robotics and Automation Magazine, Vol. 1, n. 4, 1994.
[2] M.A. Minor, R. Mukherjee, "Under-actuated kinematic structures for miniature climbing robots", Journal of Mechanical Design, Vol. 125, June 2003.
[4] A. Nishi, "Development of wall climbing robots", Computers & Electrical Engineering, Vol. 22, n. 2, 1996.
[5] S. Hirose, A. Nagakubo, R. Toyama, "Machine that can walk and climb on floors, walls and ceilings", Fifth Intl. Conference on Advanced Robotics, Pisa, Italy, 1991.
[6] B.L. Luk, Collie A.A. "Walking and climbing service robots for safety inspection of nuclear reactor pressure vessels", Measurement and Control, Vol. 39, n. 2, 2006.
[7] A. Kochan, "CLAWAR highlights research progress on climbing and walking robots", Industrial Robot, Vol. 33, n. 2, 2006.
[8] J.H. Liu, K. Tanaka, L.M. Bao " Analytical modeling of suction cups used for window-cleaning robots" Vacuum, Vol. 80, n. 6, 2006.
[9] C. Balaguer, A. Gimenez, A. Jardon, "Climbing robots' mobility for inspection and maintenance of 3D complex environments", Autonomous Robots, Vol. 18, n. 2, 2005.
[10] Y.Z. Zhao, Z. Fu, Q.X. Cao, "Development and applications of wall-climbing robots with a single suction cup", Robotica, vol. 22, 2004.
[11] R.L. Tummala, R. Mukherjee, N. XI, "Climbing the walls", IEEE Robot Automation, Vol. 9, n.4, 2002.

ENABLING AUTONOMOUS FUNCTIONS ON HYDRAULIC EXCAVATOR ATTACHMENT

Otso Karhu, Javier Moya, Jarno Uusisalo, and Kalevi Huhtala
Tampere University of Technology
Institute of Hydraulics and Automation
P.O. Box 589
33101 Tampere, Finland
Phone +358 3 3115 4436, Fax +358 3 3115 2240
E-mail: otso.karhu@tut.fi

ABSTRACT

Hydraulic mobile machines are used in various tasks. Many of these are repetitive and boring or even dangerous for human operator. Therefore it would be very convenient if the mobile machine could perform some tasks autonomously. In this work autonomous excavation is discussed. Required control electronics, sensors, and algorithms are studied. Special requirements due to demanding operating conditions and different soil types are considered. An excavator attachment for a hydraulic mobile machine is used to test the ideas. The control system is installed and software is designed. The system is tested. The test system and results are presented and discussed.

KEYWORDS: Excavator, Autonomous, Closed loop control, Mobile hydraulics

1 INTRODUCTION

Many applications of hydraulic mobile machines are uncomfortable or even hazardous to the operator. Vibrations, loud noises, and repetitive tasks are common problems. Working area may be dangerous because of radiation or challenging environmental conditions. Falling accidents, for example, may also happen in safe environments. Teleoperation solves most of these problems but the operator still has to perform the repetitive work cycles. This may be stressful to many operators. Furthermore, one operator could supervise several mobile machines simultaneously if they were able to perform some functions autonomously.

Autonomous machines are a common research topic in robotics. Many projects aim to vehicles that are merely able to drive from one location to another while collecting data. Robots that perform autonomous tasks have been researched but they are often limited to indoor use or light environmental conditions. They are not very robust and typically

have very limited working areas, velocities, and power ratings. Some robot appliances such as a vacuum cleaner and a lawn mower have, however, been successfully commercialized. [1]

In this work autonomous functions of actual hydraulic mobile machines are discussed. Some requirements for autonomous functions are introduced. An excavator attachment for a hydraulic mobile machine is used as an example. The excavator attachment with modifications and control software is presented. A simple operator assisting function that employs closed loop control is implemented and tested. The test setup is described and results are shown. Finally, the results and future work are discussed.

2 REQUIREMENTS FOR AUTONOMOUS FUNCTIONS

An autonomous mobile machine can be developed from the start exclusively for autonomous operation. Another approach is to modify a regular mobile machine. Main benefit in designing an exclusively autonomous machine is that there is no need for a driver's seat or cabin. Therefore, the chassis and motion control of the machine are easier to design since there is no driver comfort to take into account. However, it is usually easier to modify a regular mobile machine because most mechanical components are directly applicable to autonomous operation. Furthermore, the modifications can be done so that the machine can optionally be operated from the original driver's seat which makes the modified machine quite flexible.

In this work a regular mobile machine is modified. Since the machine should remain as robust as possible, mobile hydraulic components should be used as far as possible. In addition, required sensors and control algorithms are discussed in this chapter.

2.1 Hydraulic components

Most hydraulic mobile machines have simple open loop control systems: valve control signals are transmitted either electronically or mechanically directly from joysticks. Most mobile proportional valves are designed to be robust and cost-effective. This usually means that the valves are not very accurate or fast. They are often optimized for open loop control and have large dead bands and nonlinear flow curves.

Autonomous operation typically requires rather accurate closed loop control. The responses should be quick to achieve at least the efficiency of a human operator. These objectives may be challenging to meet using mobile proportional valves. Some research projects have, however, shown promising results [2,3,4,5]. Compensating for the dead band by controller design will most likely prove essential [6].

2.2 Sensors

Very few regular mobile machines have enough sensors for autonomous operation. The required signals depend on application. If the machine is supposed to travel autonomously, it should have a rather reliable and accurate positioning system. Possible

solutions could include real-time kinematic GPS or laser measurements. Machine vision, wheel odometry, inertial navigation, and active beacons can be used as well. [7] Typically two or more different navigational measurements are needed for adequate accuracy and reliability. If the working area of the machine is not a closed environment or there are moving obstacles, some sensors should also scan the immediate surroundings of the machine.

The minimum requirement for autonomous excavation is to measure the joint angles of the excavator. There are different types of sensors for this purpose. Accelerometer-based angular sensors measure angle relative to earth radius. They can be installed anywhere on the measured solid but often have a limited bandwidth. In some applications an extra accelerometer is required on the machine frame to calculate the angle of the excavator relative to the frame. Gyroscopes have a higher bandwidth but they give relative angular data that requires an additional absolute sensor to prevent error accumulation. These sensor types are easy to install and have practically no wearing parts.

An accelerometer-based angular sensor can not be used to measure the lateral movement of the excavator since the direction of the movement is perpendicular to gravity. Therefore a rotary or linear potentiometer or absolute encoder could be used. Some rotary sensors can be mounted directly on the measured axle [8]. This is more robust and simple for angle calculation than using wire reels or toothed bars. If the axle is rotating freely, installation may become more difficult. Linear sensors can be mounted between almost any two points across the joint. It may, however, be difficult to install a linear sensor so that it does not limit the movement of the excavator. If there is a hydraulic cylinder that moves the excavator laterally, the sensor may be installed on the cylinder. The most robust way is to replace the cylinder with one that has an internal position sensor [9]. Potentiometers typically have the most limited life: around 100 million cycles [10]. This may still be enough considering the lifetime of a typical mobile machine. In any case it is important to take into account that dithered valve control signal may result in constant low-amplitude vibration of the cylinder that wears the potentiometer considerably.

2.3 Control algorithms

Autonomous work cycles require advanced control algorithms. The control system typically consists of several layers. Low-level motion controllers may be similar to normal operation. On the next layer autonomously travelling machines usually have a navigation controller that does short range path planning, mainly obstacle avoidance. The top level of control is mission or path planning that is normally coordinated by the operator. [7]

In an autonomous excavator a similar approach is applicable. The motion controllers can be simple position controllers. Depending on the following layer, trajectory tracking properties may be required. Resolved-mode control in mobile machines has been researched in some projects [4,11]. It makes the user interface more intuitive for the operator and helps when straight bucket trajectories are needed. Resolved-mode control is, however, not necessarily required for autonomous operation, at least not at motion control layer. The target trajectories may be continuous but in many cases a phased

position control through a couple of points could be adequate. The work of professional excavator operators could be observed to generate efficient and economical bucket trajectories [12].

If the trajectory points are given in values of joint angles or by manually producing the desired trajectory at first, the control algorithms can be kept rather simple. For more advanced user interfaces with Cartesian coordinates, at least inverse kinematics of the excavator has to be calculated.

The most demanding part in autonomous excavation is probably the interface between the bucket and soil when the bucket is filled. Different soil types, rocks, and varying temperatures affect substantially the behaviour of the excavator. A general solution may be difficult to find. One option is to monitor the velocity of the bucket as it approaches the soil. If the velocity drops enough before the target position is reached, the bucket can be filled, emptied, and the cycle can be repeated. Learning or fuzzy control might improve the efficiency of the bucket filling algorithm and make it suitable for more soil types and conditions.

3 EXCAVATOR ATTACHMENT

A hydraulic excavator attachment is used as an example. The excavator is a commercial product that has been slightly modified. An electronic control unit for the excavator has been designed and built. [13] The attachment is installed to a skid steered mobile machine that has been developed at the Institute of Hydraulics and Automation [14]. The modified excavator attachment installed to the mobile machine is shown in Figure 1.

3.1 Commercial version

The excavator is an Avant Backhoe 205 that has originally mechanically actuated valves. The levers are located so that the operator can reach them from the driver's seat. The mechanics consist of a boom, a stick, and a bucket. There is a hydraulic cylinder for each of these. A fourth cylinder is used to move the excavator laterally. The excavator has a dozer plate that supports the excavator with the rear wheels of the mobile machine when the excavator is operated.

3.2 Hardware modifications

The mechanical valves have been replaced with an electrically actuated sandwich type mobile proportional valve with four spools, Sauer-Danfoss PVG 32. The electrical actuation unit is a low-cost option with large hysteresis and medium accuracy [15]. A valve from the same series, but probably with a better actuation unit, has been used in resolved-mode control [4].

The electronic control unit of the excavator has been installed on the valve block. Control, measurement, and configuration data are transmitted using a CAN bus. The control unit utilises a flexible 56F8323 microcontroller. [13]

A linear potentiometer has been installed on the lateral cylinder. The potentiometer is sealed to make it dust and water proof. The solution is not optimal but it is easy and low-cost compared to a cylinder with an internal position sensor. The position signal is measured with the excavator control unit.

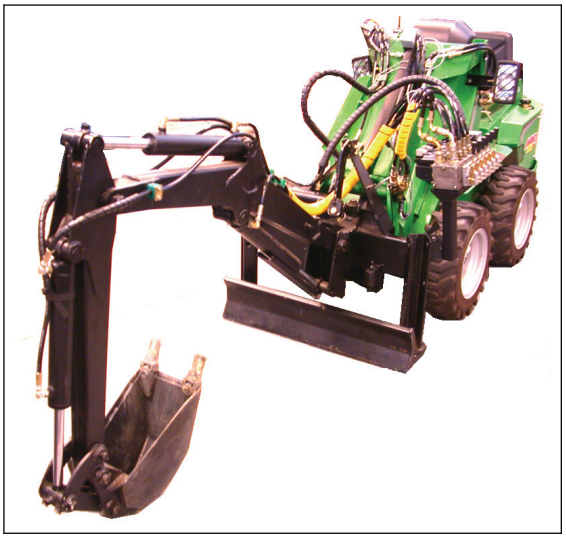

Figure 1. *Modified excavator attachment installed to the mobile machine.*

3.3 Controller and software

A block diagram of the software of the excavator controller unit is presented in Figure 2. The main program is simple because most of the data processing is done in the interrupt handlers. The sample and control interval is set to 1 ms by the timer interrupt. The microcontroller could perform a much shorter interval but considering the dynamics of the excavator the current interval seems sufficient. Every time an A/D conversion is completed, a new average of the lateral position signal is calculated. The length of the averaging window can be configured using SDO messages. Typically 5 to 15 latest samples are used in calculation. This removes almost all the noise from the position signal while causing only little delay. The FlexCAN receive interrupt handler checks the type of the received messages. According to the message type either the parameter values are updated, the open loop input signals are updated, the position of the excavator is stored, or the position controller is activated. The control unit can store up to 15 different excavator positions.

Figure 3 shows the block diagram of the position controller. The boom, stick, and bucket are always controlled in open loop. The control of the lateral movement depends on the commands received from the CAN bus. The excavator can be moved laterally in open loop control to set required target positions, a ditch and a pile, for example. The position controller can then be activated by sending the target number via CAN. The position is controlled using a simple proportional controller with dead band compensation.

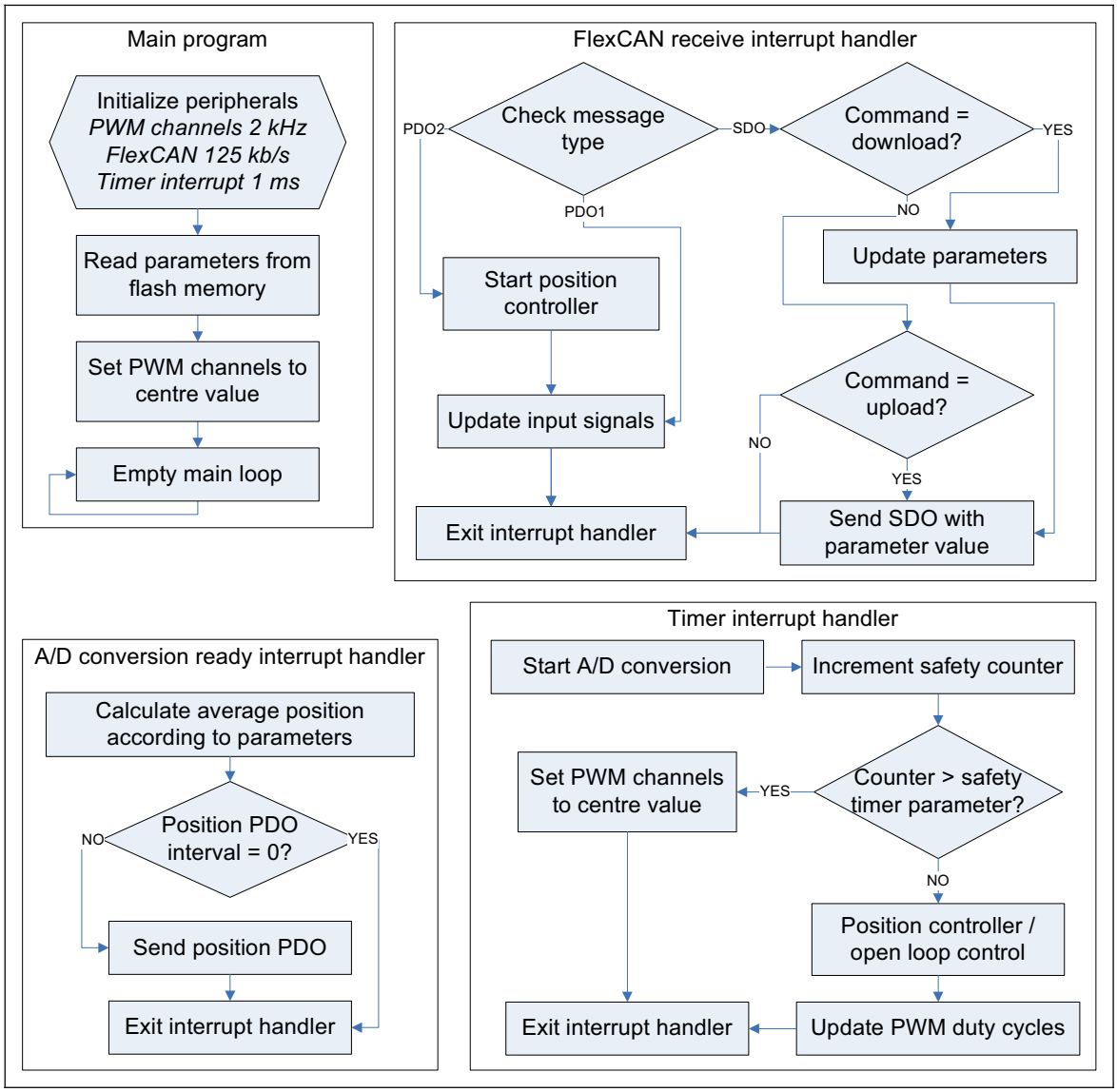

Figure 2. *Software of the excavator control unit.*

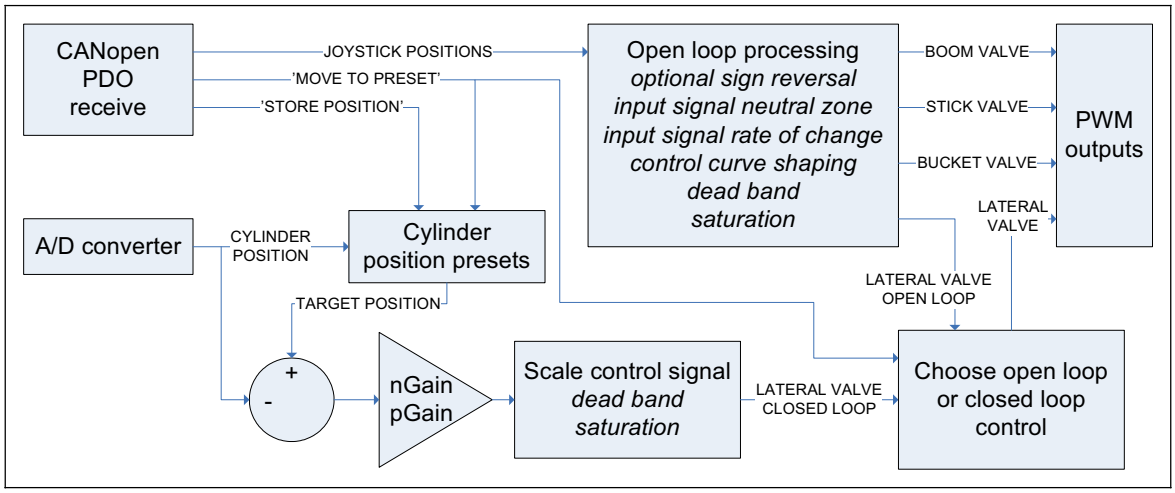

Figure 3. *Position controller.*

The limit values that are used to decide when to switch back to open loop control are presented in Figure 4. *xmax* and *xmin* are the limits of the target zone around the target cylinder position *xd*. When the position signal enters the target zone, a timer is started. If the timer reaches a set limit (*t1 – t0*, typically around 500 ms) while the position signal is inside the target zone, the controller switches to open loop control. If the time limit is not reached, the timer is reset and restarted when the position signal enters the target zone again. There is also a timer that counts the total time from the start of the position control. If the timer reaches its limit before the controller has reached the target position, the controller switches to open loop control. This time limit is set to several seconds and it is only needed if there is an obstacle blocking the excavator.

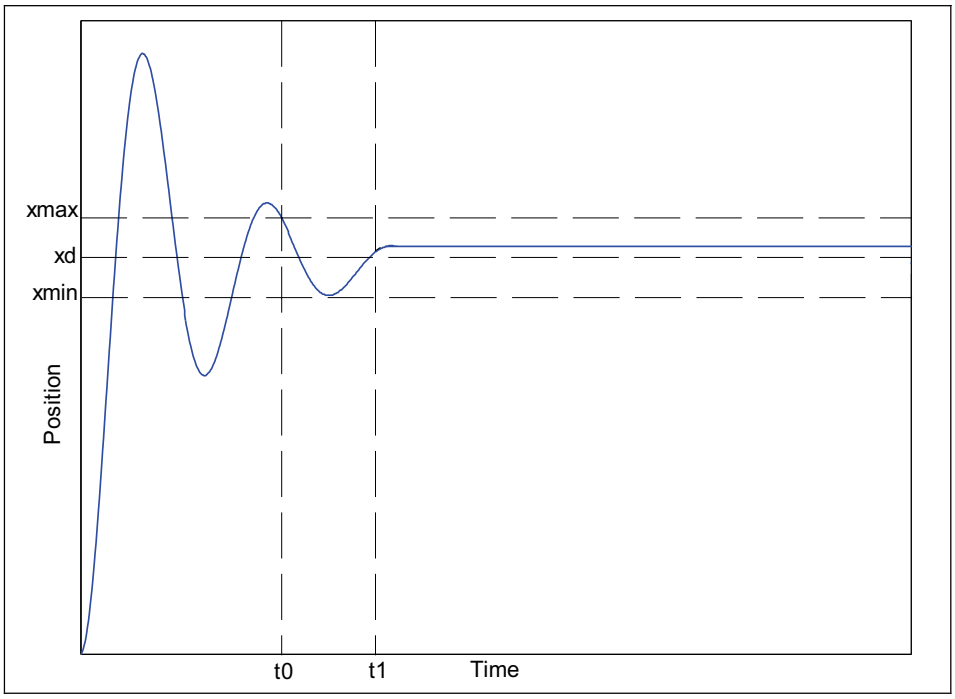

Figure 4. *Limit values for switching to open loop control.*

4 EXPERIMENTAL TESTS

The software of the mobile machine was modified to test the excavator. A trigger button of the joystick was used to send a message 'store excavator position to preset *p*' in store mode and 'move to preset *p*' in move mode. The value of *p* was changed every time between 1 and 2. The excavator control unit was configured to transmit lateral position PDO every 10 ms.

Because the cylinder position was measured instead of the lateral angle of the excavator, some calculation is required to make the results easier to interpret. The mechanical arrangement of the lateral joint is presented in Figure 5. The angle γ is calculated using the law of cosines:

$$\gamma(x) = \arccos\left(\frac{a^2 + b^2 - x^2}{2ab}\right) \tag{1}$$

The lateral angle δ is calculated from vertically opposite angles:

$$\delta(x) = \gamma(x) + \alpha - \beta - 90° \tag{2}$$

Finally, the equation (1) is substituted into equation (2):

$$\delta(x) = \arccos\left(\frac{a^2 + b^2 - x^2}{2ab}\right) + \alpha - \beta - 90° \tag{3}$$

The supply pressure from the mobile machine was set to 100 bar because the pressure compensator of the PVG 32 does not work properly at low pressures [15]. The diesel engine of the mobile machine was set to maximum speed to keep the supply pressure stable.

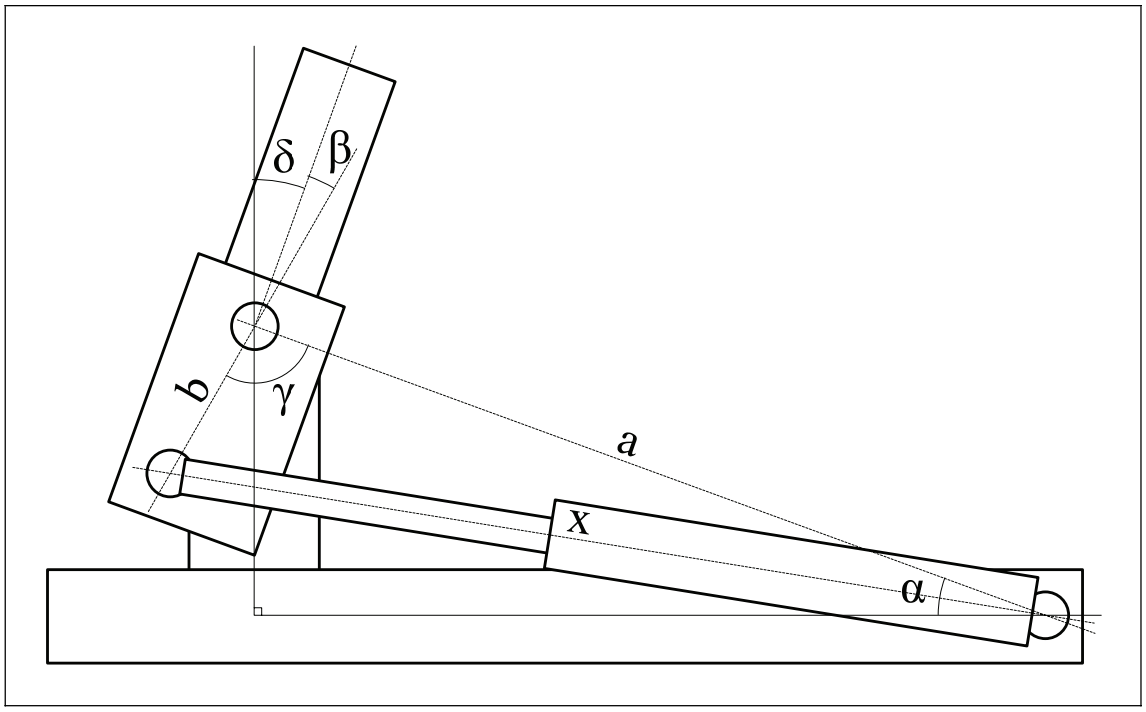

Figure 5. *Joint arrangement for lateral movement.*

5 RESULTS

The performance of the controller was tested with a couple of different cases. Figure 6 shows the angle error signal as the excavator is moved to a target position of -45°. The boom, stick, and bucket are oriented so that the centre of mass is as far as possible, making the control of the excavator demanding.

To test longer movements, the target value was set to 0°. The angle error is shown in Figure 7. The excavator was moved from extreme positions, about ±70°, to the centre position.

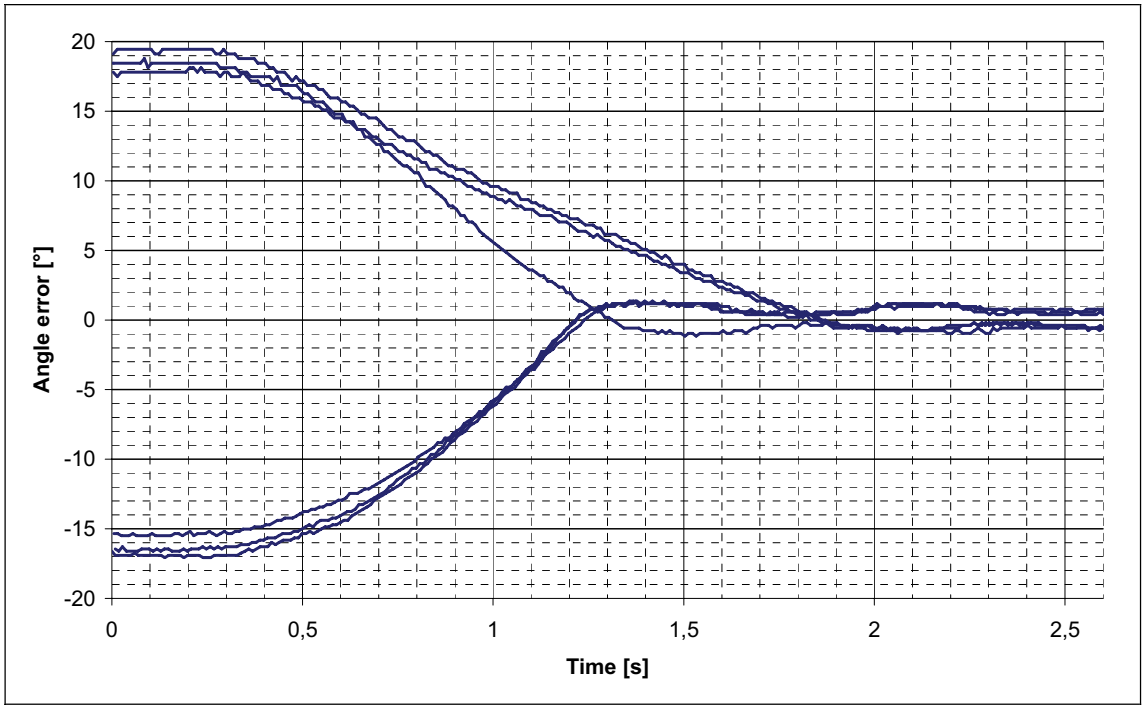

Figure 6. *Angle error when target value is -45°.*

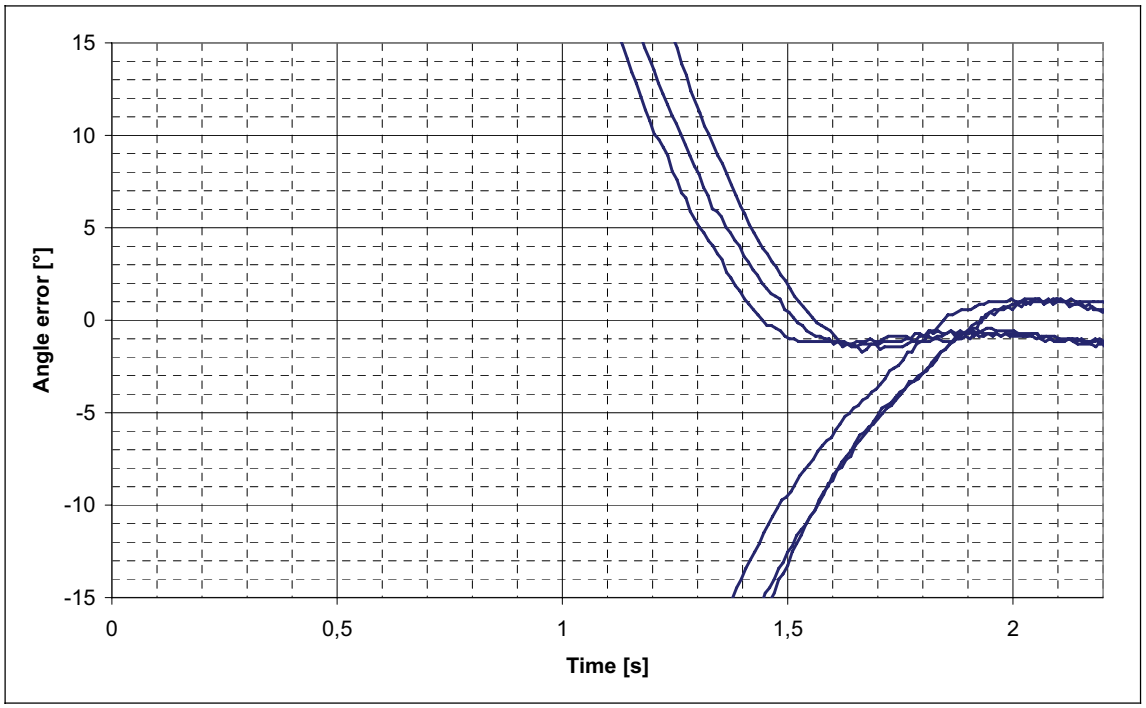

Figure 7. *Angle error when moving from extreme positions to centre.*

As it can be seen from Figures 6 and 7, the steady-state error is about 1°. This results in a position error of about 5 cm when the excavator is fully extended. This is probably sufficient for most applications taking into account the diverse behaviour of soil. Moreover, the repeatability of the steady-state error is very good: about 0.5° when the excavator is moved between two targets. This is the most typical case in excavation.

The proportional gains of the position controller were set rather low to limit the acceleration of the excavator. This prevents the machine from jerking and therefore decreases the absolute position error of the bucket. The settling times are not very constant, probably because of the low-cost valve actuation unit. In addition, the construction of the excavator makes the position controller slightly asymmetric. The valve seems, however, quite suitable to autonomous excavation.

6 CONCLUSIONS

An autonomous mobile machine could make the excavation work safer, more cost-effective, and convenient. There are several solutions to perform the measurements required by autonomous operation. Adapting the mobile proportional valves to closed loop control is one of the key problems related to components.

A commercial hydraulic excavator attachment was modified to perform closed loop position control using cost-efficient mobile proportional valves. The controller was a simple proportional controller with dead band compensation. The results are promising: autonomous excavation might be possible with reasonable accuracy and efficiency using conventional mobile proportional technology.

7 FUTURE WORK

The results encourage adding sensors to all the joints of the excavator. Because of the mechanical limits, angle resolvers or inclinometers might be suitable. First simple application could be autonomous emptying of the bucket. Eventually, a user interface that utilises inverse kinematics of the excavator is going to be required. Efficient work cycles must be investigated. Most work, however, will probably relate to finding a general control solution to the filling of the bucket.

REFERENCES

[1] Trilobite 2.0, user manual. Västervik, Sweden 2004, Electrolux. 23 p.

[2] Bu, F. & Yao, B. Nonlinear adaptive robust control of hydraulic actuators regulated by proportional directional control valves with deadband and nonlinear flow gains. Proceedings of the American Control Conference, Chicago, Illinois, USA, June 28-30, 2000. pp. 4129-4133.

[3] Münzer, M., Jørgensen, F. & Sigurdsson, H. Increasing functionality of an excavator with standard proportional valves. Proceedings of SICFP, Tampere, Finland, May 7-9, 2003.

[4] Münzer, M. & Pedersen, P. Tool centre control of mobile hydraulic manipulators. Proceedings of FPNI-PhD, Modena, Italy, July 3-5, 2002.

[5] Zhou, B. Trajectory-tracking control in a proportional hydraulic robotic excavator. Proceedings of FPNI-PhD, Terrassa, Spain, June 30 - July 2, 2004.

[6] Uusisalo, J., Vilenius, J., Krogerus, T., Karhu, O. & Huhtala, K. Automated bucket stabilizer for hydraulic mobile machine. Proceedings of ISARC, Ferrara, Italy, September 11-14, 2005.

[7] Durrant-Whyte, H. Autonomous land vehicles. Proceedings of IMechE. Part I: Journal of systems and control engineering 219(2005)1, pp. 77-98.

[8] DSP resolver, user manual. Tampere, Finland 2006, Axiomatic Technologies. 52 p.

[9] Hydraulic cylinders with linear positioning systems. Ikkala, Finland 2005, Nurmi Hydraulics. 2 p.

[10] PS6300 linear sensor 50-1000 mm. Uppsala, Sweden 2003, Regal Components. 1 p.

[11] Sepehri, N., Lawrence, P., Sassani, F. & Frenette, R. Resolved-mode teleoperated control of heavy-duty hydraulic machines. Journal of dynamic systems, measurement, and control 116(1994)2, pp. 232-240.

[12] Hall, A. & McAree, P. A study of the interaction between operator style and machine capability for a hydraulic mining excavator. Proceedings of IMechE. Part C: Journal of mechanical engineering science 219(2005)5, pp. 477-489.

[13] Karhu, O., Vilenius, J., Uusisalo, J. & Huhtala, K. Developing intelligent hydraulic excavator. Proceedings of PTMC, Bath, UK, September 13-15, 2006. pp. 265-274.

[14] Raneda, A., Vilenius, J. & Huhtala, K. Development of a teleoperated hydraulic mobile machine. Proceedings of SICFP, Tampere, Finland, May 7-9, 2003. pp. 449-459.

[15] PVG 32 proportional valves, technical information. Lincolnshire, Illinois, USA, 2006, Sauer-Danfoss. 80 p.

DEVELOPMENT OF A PRESSURE-COMPENSATED FLOW CONTROL VALVE FOR WATER HYDRAULICS

Kenji Suzuki and Professor Eizo Urata
Department of Mechanical Engineering
Kanagawa University
3-27-1 Rokkakubashi, Kanagawa-ku, Yokohama, 221-8686, Japan
Phone +81 45 481 5661, Fax +81 45 481 5122
E-mail: suzuki@kanagawa-u.ac.jp

ABSTRACT

This paper describes development of a pressure-compensated flow control valve for water hydraulics. A pressure-compensation valve with two throttles in series was installed to suppress cavitation. The pressure-compensation valve has hydrostatic supports to reduce the wear of sliding parts and has a viscous damper to suppress vibration of the valve. The developed flow control valve has adjustable flowrate range of 2.5-20 L/min within the pressure range of 2-14 MPa. Although the leakage through the hydrostatic supports exists, discharge flowrate is almost constant. Flowrate variation to the average flowrate is about 5 % in the experimental results. The static characteristics show no hysteresis. In addition, the valve does not radiate cavitation noise in the range of experiment.

KEYWORDS: Water hydraulics, Flow control valve, Pressure-compensation

1 INTRODUCTION

A pressure-compensated flow control valve keeps discharge flowrate constant using a flow-detecting throttle and a pressure-compensation valve connected in series in the valve. The pressure-compensation valve works to keep the pressure drop across the flow-detecting throttle constant. The pressure-drop across the pressure-compensation valve increases with the increase of pressure difference between upstream and downstream of the entire valve. Pressure-drop at the flow-detecting throttle is normally small; the most part of the pressure-drop across the entire valve arises at the pressure-compensation valve. A single throttle for a high pressure difference has an inclination to induce cavitation [1] while commercially available valves have a single throttle [2, 3]. In a pressure-compensated flow control valve for water hydraulics, therefore, counter-measures against cavitation at the pressure-compensation valve are important. The valve

also requires countermeasures against problems originated from the low viscosity of water: friction and wear of the sliding parts, large leakage, and low damping.

This paper describes development of the pressure-compensated flow control valve for water hydraulics, which includes countermeasures in the pressure-compensation valve against the cavitation, wear of sliding parts, and vibration of the valve. In the followings, we explain the structure of the developed valve, simulation results of static- and dynamic characteristics of the valve, and experimental results of static characteristics.

2 NOMENCLATURE

A_* : areas (see Eqs. (13) and (15))
c : discharge coefficient [-]
d_p : diameter of damper-piston in pressure-compensation valve [m]
d_s : diameter of bore for pressure-compensation valve [m]
d_b : hydrostatic bearing orifice diameter [m]
d_i : inner diameter of the i-th throttle of pressure-compensation valve [m]
d_t : diameter of flow-detecting needle valve seat [m]
F_{di} : dynamic flow force at the i-th throttle of pressure-compensation valve [N]
F_s : static flow force acting on the pressure-compensation valve [N]
h_t : displacement of flow-detecting needle valve [m]
h_{xi} : axial opening of the i-th throttle of pressure-compensation valve (see Fig. 2) [m]
h_{0i} : initial axial opening of the i-th throttle of pressure-compensation valve [m]
k : spring constant of pressure-compensation valve [N/m]
l_* : length (see Fig. 2) [m]
l_i : damping length of the i-th throttle of pressure-compensation valve [m]
m : mass of pressure-compensation valve including 1/3 of spring mass [kg]
m_f : mass of water moving with pressure-compensation valve [kg]
N_b : number of pockets of hydrostatic supports [-]
p_* : pressures (see Fig. 2) [Pa]
P_m : dimensionless intermediate pressure ($=(p_m - p_d)/(p_c - p_d)$) [-]
q_* : flowrate (see Fig. 2) [m^3/s]
V_* : volume (see Fig. 2) [m^3]
x : displacement of pressure-compensation valve [m]
x_0 : initial displacement of spring for pressure-compensation valve [m]
β : bulk modulus of water [Pa]
δ_i : radial clearance of the i-th throttle of pressure-compensation valve [m]
δ_p : radial clearance between piston and cylinder of damper [m]
δ_s : radial clearance between spool and sleeve [m]
θ_f : jet angle at throttle of pressure-compensation valve [-]
θ_t : half cone angle of flow-detecting needle valve [-]
μ : viscosity of water [Pa·s]
ρ : density of water [kg/m^3]

3 VALVE STRUCTURE

Figure 1 and 2 show a cross-section and illustrative drawings of the developed valve, respectively. The port arrangement is according to ISO Code No. 6263-06-05-0-97. The water enters through the inlet port, passes through the flow-detecting needle valve, the pressure-compensation valve, and exits through the outlet port. Adjusting the displacement of the needle valve enables us to set the flowrate. A tip of the needle valve extends as a pressure-compensation rod; its diameter is equal to the valve seat so as not to increase operating torque of the needle valve by upstream pressures.

To suppress cavitation, it is effective to reduce pressure in steps by multiple restrictors [1, 4]. The developed valve in this study has the pressure-compensation valve that includes two annular throttles with nearly equal diameters. The ratio of the openings of each throttle determines the intermediate pressure at the space between the two throttles. We define *dimensionless intermediate pressure* as the intermediate pressure divided by the pressure at upstream of the first throttle of the pressure-compensation valve. That is, the dimensionless intermediate pressure is 0.5 when the pressure drops across each throttle are equal.

To reduce friction and wear of sliding parts of the pressure-compensation valve, the valve includes hydrostatic supports [4, 5, 6]. To get supporting force for the valve, the pressure-compensation valve is placed at downstream of the flow-detecting needle valve. This enables us to use the pressure difference across the entire valve for actuation of the hydrostatic supports. However, this structure induces increase of leakage through the clearance of the hydrostatic supports. To compensate the leakage, it is ideal to lower the flowrate through the pressure-compensation valve so that the flowrate through the entire valve keeps constant. To realize such characteristics, a precise study on valve parameters will be required.

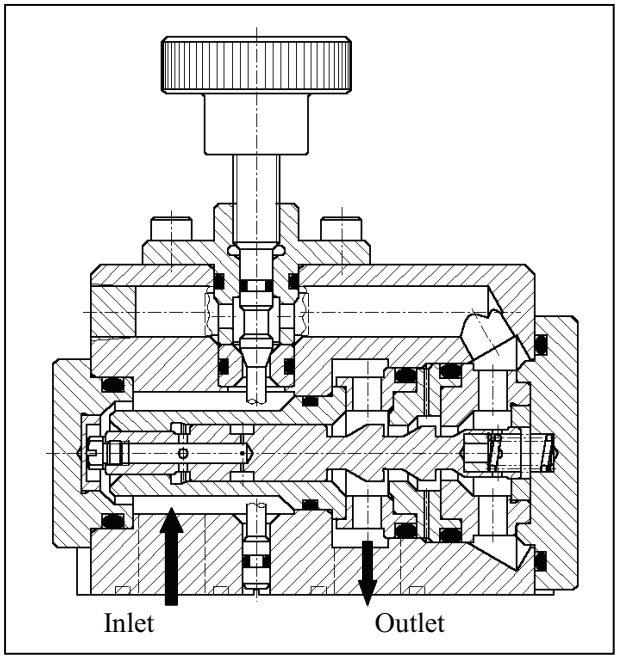

Fig. 1 Cross section of the developed valve

The first throttle of the pressure-compensation valve has slightly smaller diameter than the second throttle. Therefore, when the intermediate pressure is smaller, the resultant force to open the valve becomes smaller, and the flowrate through the valve decreases. Next, radial clearance of the second throttle is made larger than that of the first one. Hence, when the axial opening of the valve is smaller, dimensionless intermediate pressure becomes smaller. Therefore, as the pressure-compensation valve closes with increase of pressure difference across the entire valve, the dimensionless intermediate pressure becomes smaller. Then, the flowrate through the valve decreases. By choosing optimal dimensions for the valve design, the desirable characteristics will be obtained.

For the damping of vibration of the pressure-compensation valve, a viscous damper is placed at upstream of the hydrostatic supports. This damper compensates flow force acting on the pressure-compensation valve because it uses pressure drop across the damper clearance.

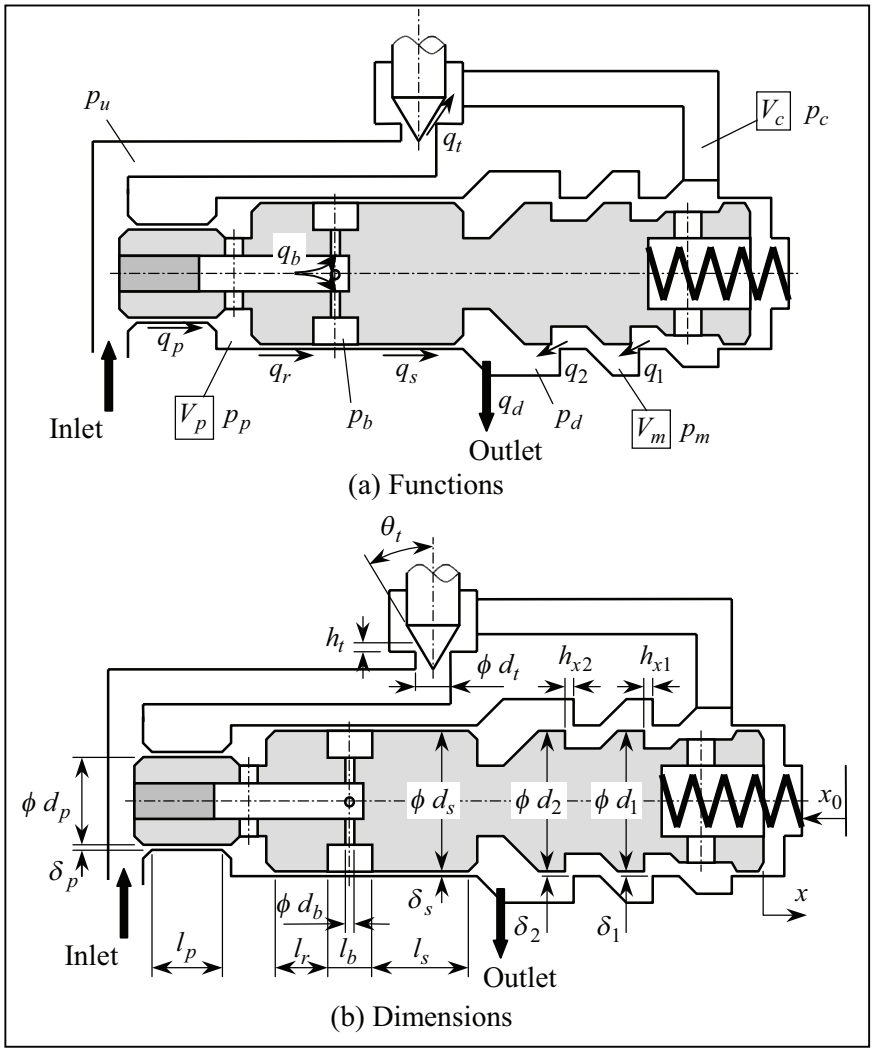

Fig. 2 Valve functions and dimensions

The flow force acts on the valve toward closing direction and its magnitude increases as both of the pressure and flowrate is increasing. To compensate the flow force, namely, to reduce the closing force on the pressure-compensation valve, the pressure drop across the damper clearance is used. Therefore, the damper clearance influences both of the compensatory force and damping force, that is, the static- and dynamic characteristics. The dimensions of the valve are determined by numerical simulation; the dynamic responses are calculated using the Simulink®.

When the valve opening is small, the machining accuracy of the metering edges of the valve considerably influences the intermediate pressure. To improve accuracy of the metering edges, the sleeves of the pressure-compensation valve is built up from accurately machined four pieces. Particularly, the part for the second throttle needs accuracy on the axial length. This dimension strongly influences the intermediate pressure, especially when the valve opening is small because the intermediate pressure is determined by the ratio of openings of the two throttles.

The clearances of the hydrostatic supports and the damper must have high precision. To establish necessary accuracy, some machined pieces of valve body and sleeve are selectively combined.

4 BASIC EQUATIONS

To simplify governing equations, following assumptions are made besides the ordinary assumptions:

(a) In the hydrostatic supports and the damper for the pressure-compensation valve, eccentricity of the valve spool to the sleeve is negligibly small because the supporting force is enough for the centering of the valve.
(b) Pressure variation along circular direction near the pockets of hydrostatic supports is negligibly small compared to pressure in the pockets; that is, pressure around the spool near the pockets is regarded constant.
(c) Compressibility of fluid in the pockets of hydrostatic supports is negligible because their volume is small.
(d) Flow through narrow clearance at the damper and hydrostatic supports is approximated by a laminar flow between two parallel flat walls.
(e) Viscous frictional force acting on the pressure-compensation valve caused by steady flow through the narrow clearance is negligibly small compared to the force caused by the pressure acting on the valve.
(f) Jet angles at the throttles of the pressure-compensation valve are constant (69°).

Equations of flowrate through the restrictors are written as follows.

$$q_t = \mathrm{sgn}(p_u - p_c)\, c\pi h_t \sin\theta_t \left(d_t - \tfrac{h_t}{2}\sin 2\theta_t\right)\sqrt{2|p_u - p_c|/\rho} \tag{1}$$

$$q_1 = \mathrm{sgn}(p_c - p_m)\, c\pi d_1 \sqrt{h_{x1}^2 + \delta_1^2}\,\sqrt{2|p_c - p_m|/\rho} \tag{2}$$

$$q_2 = \mathrm{sgn}(p_m - p_d)\, c\pi d_2 \sqrt{h_{x2}^2 + \delta_2^2}\,\sqrt{2|p_m - p_d|/\rho} \tag{3}$$

$$q_p = \frac{\pi d_p \delta_p^3}{12\mu l_p}(p_u - p_p) + \frac{\pi}{2} d_p \delta_p \dot{x} \tag{4}$$

$$q_r = \frac{\pi d_s \delta_s^3}{12\mu l_r}(p_p - p_b) + \frac{\pi}{2} d_s \delta_s \dot{x} \tag{5}$$

$$q_s = \frac{\pi d_s \delta_s^3}{12\mu l_s}(p_b - p_d) + \frac{\pi}{2} d_s \delta_s \dot{x} \tag{6}$$

$$q_b = \operatorname{sgn}(p_p - p_b) N_b c \tfrac{\pi}{4} d_b^2 \sqrt{2\left|p_p - p_b\right|/\rho} \ , \tag{7}$$

where

$$h_{x1} = h_{01} - x \, , \quad h_{x2} = h_{02} - x \tag{8}$$

are axial opening of the first and the second throttle of the pressure-compensation valve, respectively.

Equations of continuity are as follows:

$$\dot{p}_p = \frac{\beta}{V_{p0} + A_e x}(q_p - q_r - q_b - A_e \dot{x}) \tag{9}$$

$$\dot{p}_c = \frac{\beta}{V_c}(q_t - q_1 + A_1 \dot{x}) \tag{10}$$

$$\dot{p}_m = \frac{\beta}{V_{m0} - A_m x}(q_1 - q_2 + A_m \dot{x}) \tag{11}$$

$$q_r + q_b - q_s = 0 \, , \tag{12}$$

where

$$\left.\begin{aligned} &V_{p0} = V_p\big|_{x=0}, \quad V_{m0} = V_m\big|_{x=0}, \\ &A_e = \tfrac{\pi}{4}(d_s^2 - d_p^2), \quad A_1 = \tfrac{\pi}{4} d_1^2, \quad A_m = \tfrac{\pi}{4}(d_2^2 - d_1^2) \end{aligned}\right\}. \tag{13}$$

In Eq. (10), $V_c >> A_1 x$ was additionally assumed.

Equation of motion of the pressure-compensation valve is

$$(m + m_f)\ddot{x} + c_q \dot{x} + k(x + x_0) = A_p p_u + A_e p_p - A_1 p_c - A_m p_m + F_s + F_{d1} + F_{d2} \, , \tag{14}$$

where

$$c_q = \pi\mu\left\{\frac{d_p l_p}{\delta_p} + \frac{d_s}{\delta_s}(l_r + l_s)\right\}, \quad A_p = \tfrac{\pi}{4} d_p^2 \tag{15}$$

$$F_s = 2c\pi \cos\theta_f \left\{d_1 \sqrt{h_{x1}^2 + \delta_1^2}(p_c - p_m) + d_2 \sqrt{h_{x2}^2 + \delta_2^2}(p_m - p_d)\right\} \tag{16}$$

$$F_{d1} = c\pi d_1 l_1 \sqrt{\rho}\left\{(\dot{p}_c - \dot{p}_m)\sqrt{\frac{h_{x1}^2 + \delta_1^2}{2(p_c - p_m)}} - h_{x1}\dot{x}\sqrt{\frac{2(p_c - p_m)}{h_{x1}^2 + \delta_1^2}}\right\} \tag{17}$$

$$F_{d2} = c\pi d_2 l_2 \sqrt{\rho}\left\{(\dot{p}_m - \dot{p}_d)\sqrt{\frac{h_{x2}^2 + \delta_2^2}{2(p_m - p_d)}} - h_{x2}\dot{x}\sqrt{\frac{2(p_m - p_d)}{h_{x2}^2 + \delta_2^2}}\right\}. \tag{18}$$

5 SIMULATION RESULTS

The representative dimensions of the designed valve are listed in Table 1. The following sections describe various simulation results, where the dimensions in Table 1 are used as the reference values.

Table 1 Representative dimensions of the designed valve

d_p = 8.966 [mm]	d_s = 11.989 [mm]	d_1 = 11.49 [mm]	d_2 = 11.98 [mm]
δ_p = 22 [μm]	δ_s = 10.5 [μm]	δ_1 = 10 [μm]	δ_2 = 15 [μm]
l_p = 11 [mm]	l_s = 14.5 [mm]	l_b = 5 [mm]	N_b = 4 [-]
k = 56.9 [N/mm]	x_0 = 2 [mm]	$h_{01} = h_{02}$ = 1 [mm]	

5.1 Dynamic characteristics

A block diagram was made on the Simulink® from the governing equations in section 4. The influences of the pipelines connected to the upstream and downstream of the valve were not considered. The displacement of the flow-detecting needle valve was set to 1 mm. The downstream pressure was set to zero and a rectangular wave of the upstream pressure was used as the input signal. The upstream pressure, which was 3 MPa initially, changed to 7 MPa at 0 ms, and then returns to 3 MPa again at 10 ms. Corresponding to the pressure change, the pressure-compensation valve moved to the closing direction during 0 to 10 ms, and then moved back to the initial condition during 10 to 20 ms.

Figure 3(a) and (b) shows the responses of the discharge flowrate q_d and the valve displacement x, respectively, where the clearance of the damper δ_p varied ± 5 μm to the reference value, 22 μm. Each waveform was made dimensionless by means of dividing by the initial value so that we can compare the responses directly.

First, the response curves of flowrate and valve displacement are different corresponding to the sign of pressure change. The response is fast in a pressure rise, and slow in a pressure fall. This is caused by the steady flow through the damper clearance.

At the instant the upstream pressure rises, a spike of the flowrate appears. When δ_p = 27 μm, the valve displacement overshoots and the flowrate undershoots, thus it is underdamping. When δ_p = 17 μm, it is overdamping obviously.

Furthermore, the settling values also change with δ_p. In other words, the damper clearance in this valve influences both of the dynamic- and static characteristics. In the next section, we will discuss the static characteristics in detail.

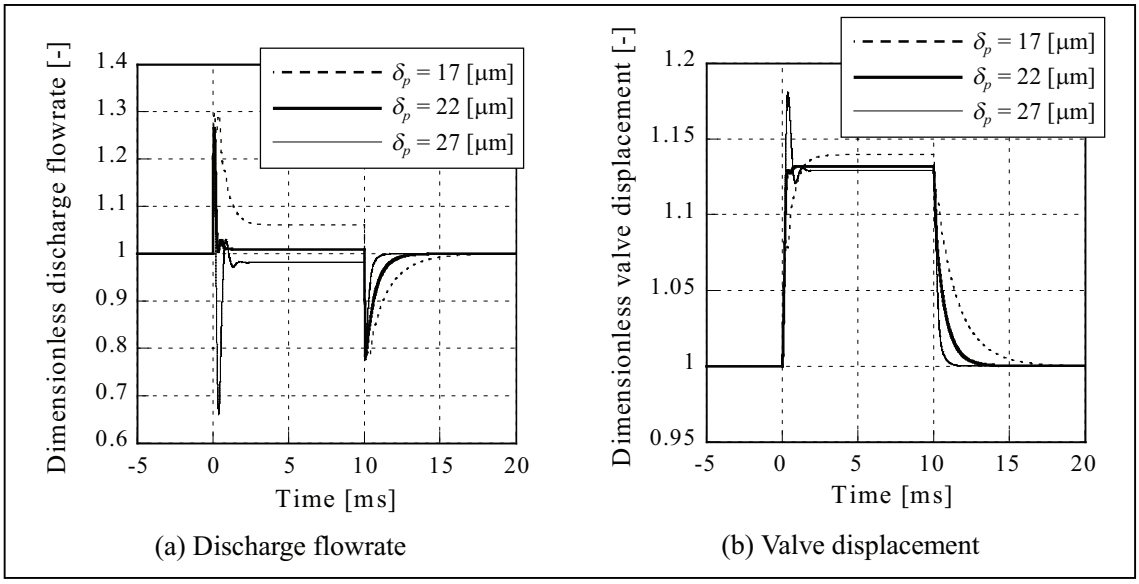

(a) Discharge flowrate (b) Valve displacement

Fig. 3 Step response of the discharge flowrate and the displacement of the pressure-compensation valve

5.2 Static characteristics

To calculate the static characteristics, the time-derivative terms in the governing equations were set to zero. The resultant set of equations was solved numerically. Figure 4 shows the simulation results of the discharge flowrate q_d vs. the pressure difference across the entire valve $p_u - p_d$. The parameter of the graphs is h_t. Regardless of h_t, the discharge flowrate keeps almost constant in the range of pressure difference larger than 2 MPa.

Let us discuss the influence of the dimensions shown in Table 1 to change of the static characteristics. To examine the influence of pre-set flowrate, two cases for little and large flowrate were calculated taking h_t to 0.3 mm and 1.2 mm, respectively.

Figure 5 shows the influence of the damper clearance δ_p with the variation of ± 5 μm. Larger δ_p makes less pressure drop across the damper clearance, thus increases the force to close the pressure-compensation valve and results in a decrease of the flowrate. The change of flowrate due to the variation of δ_p is greater for a greater value of the pre-set flowrate.

Figure 6 shows the influence of the clearance of the hydrostatic supports δ_s with the variation of ± 5 μm. Larger δ_s makes larger leakage and thus higher pressure drop across the damper clearance and results in less force to close the pressure-compensation valve and an increase in the flowrate. Similar to the case of δ_p, the flowrate change due to variation of δ_s is greater for a greater value of the pre-set flowrate. Comparing Figs. 5

and 6 reveals that the change of flowrate is more sensitive to the variation of δ_s than to the variation of δ_p. Therefore, dimensional tolerance of the hydrostatic supports should be smaller than that of the damper clearance.

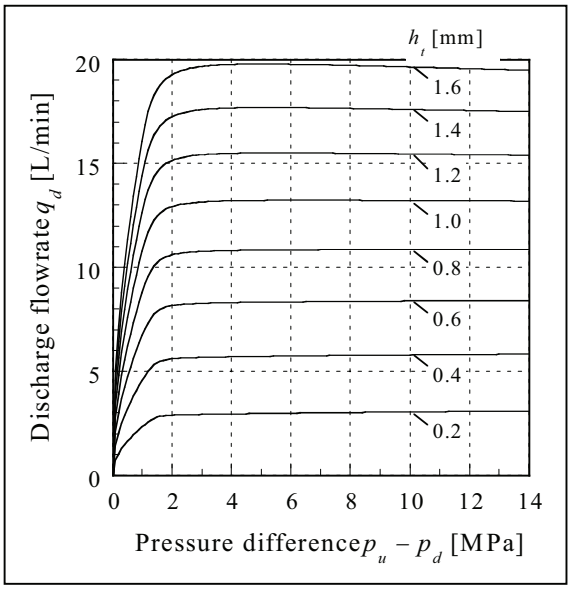

Fig. 4 Simulation results of the discharge flowrate vs. pressure difference across the valve

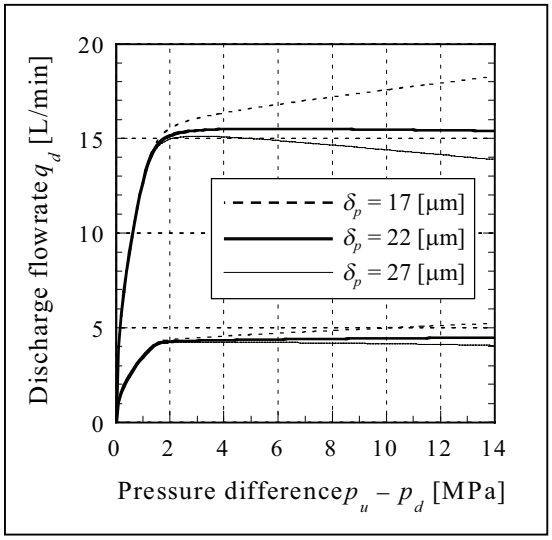

Fig. 5 Influence of clearance in the damper on flowrate

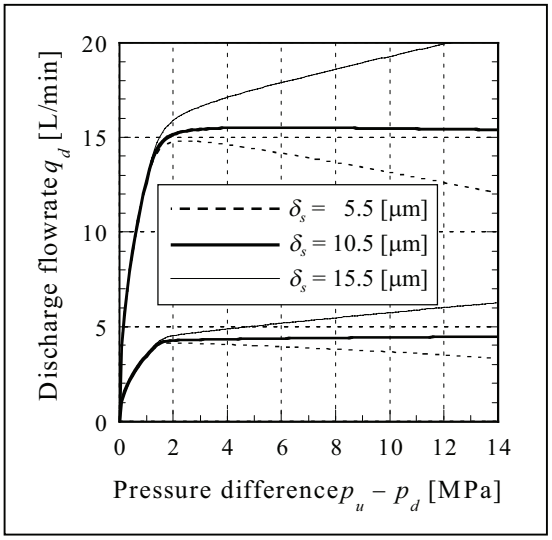

Fig. 6 Influence of clearance in the hydrostatic supports on flowrate

Figure 7 shows the influence of the diameter of the first throttle d_1 with the variation of ± 0.5 mm. Again the variation of the parameter results in a larger change of flowrate at larger pre-set flowrate. When d_1 is nearly equal to d_2, referring to equations (13), (14), and (16), there is no significant influence of the intermediate pressure on the static balance of the pressure-compensation valve. Therefore, the valve opening force does not decrease even if the intermediate pressure decreases. As the result, an increase of the valve opening force induces an increase in the flowrate.

Finally, Fig. 8 shows the influence of the radial clearance of the second throttle δ_2 with the variation of ± 10 μm. The influence of δ_2 on the flowrate is negligibly small especially high pre-set flowrate.

The change of three parameters (δ_p, δ_s, d_1) induces a larger change of flowrate for larger pre-set flowrate; an influence of variation of δ_2 appears in less flowrate range. Adjusting these parameters makes a better constancy of the flowrate.

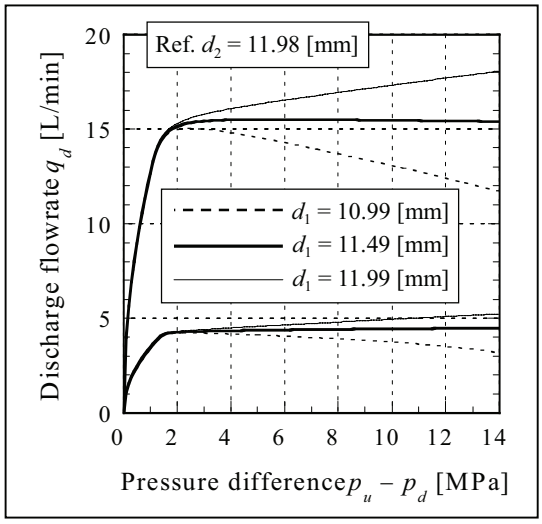

Fig. 7 Influence of diameter of the first throttle on flowrate

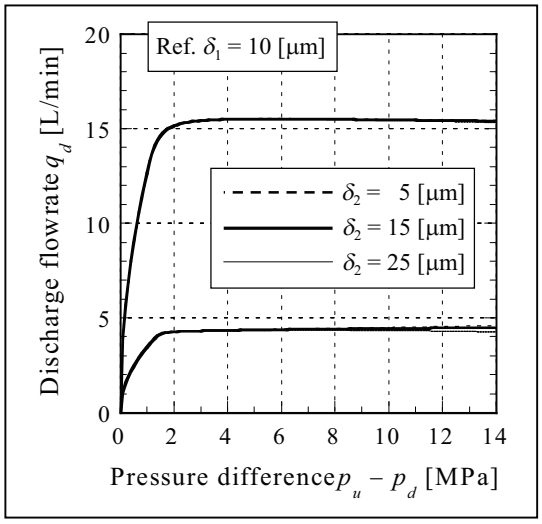

Fig. 8 Influence of radial clearance at the second throttle on flowrate

6 EXPERIMENTAL RESULTS AND DISCUSSION

A three-throw piston pump was used as the water pressure source. The rated pressure is 14 MPa and the rated flowrate is 20 L/min, by which upper limit of flowrate through the test valve was 18 L/min. The upstream pressure was adjusted with a manually handled needle valve. The discharge flowrate was measured by a turbine-type flow-meter connected to a pulse counter. A measuring cylinder was used when the flowrate is less than measuring range of the flow-meter. The water temperature was kept 25-30 °C by a cooler in return-line to a reservoir. In the following experimental results of static characteristics, each abscissa represents the pressure difference between the upstream and downstream of the test valve.

Figure 9 shows leakage through the hydrostatic supports for the pressure-compensation valve. Measurement was made after replacing the flow-detecting needle valve with a plug. The solid line in the graph is a simulation result based on the dimensions listed in Table 1. It seems that the leakage through the clearance kept laminar flow, because the leakage was almost linear to the pressure difference. Reynolds number at the clearance was about 230 at maximum.

Figure 10 shows the discharge flowrate. Flow regulation was made in the pressure range higher than 2 MPa. Although the leakage through the hydrostatic supports exists, the discharge flowrate was almost constant regardless of the pre-set flowrate level. Flowrate

fluctuations to the average flowrate within the pressure range where the pressure-compensation was made were about 5 %. The static characteristics does not show visible hysteresis; this means the pressure-compensation valve moves smoothly by virtue of the hydrostatic supports.

The flowrate slightly decreases with an increase of pressure difference particularly when the pre-set flowrate is large. This decrease is caused by the flow force acting on the pressure-compensation valve. When the pressure difference increased, axial opening of the throttle decreased. A change of throttle induces a change of the jet angle of the flow. Although the jet angle has been assumed constant for simplification at the design stage, more precise treatment on the jet angle will be required for the improvement of the valve.

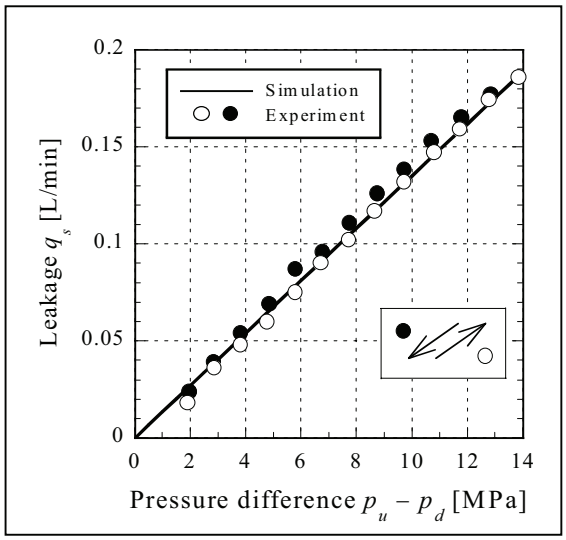

Fig. 9 Leakage through the hydrostatic supports of the pressure-compensation valve

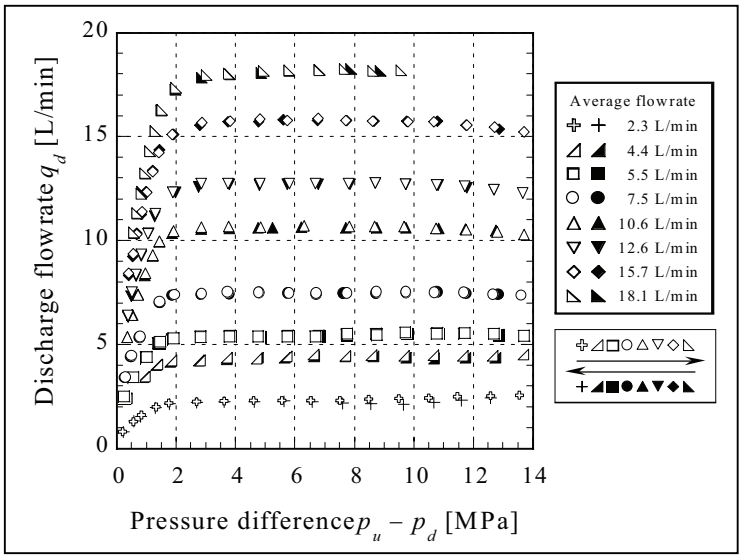

Fig. 10 Experimental results of discharge flowrate vs. pressure difference across the valve

Although the leakage through the hydrostatic supports always exists, the discharge flowrate was almost constant. Let us explain the phenomena. The pressure drops across the flow-detecting needle valve are shown in Fig. 11. At all the pre-set flowrate, the pressure-compensation valve did not work by the pressure below 1.5 MPa. Flow-regulation was made in the pressure range over about 2 MPa, where the pressure drop across the needle valve decreased with the increase of the pressure difference across the entire valve. This means the flowrate through the pressure-compensation valve decreases. In this way, decrement of the flow through the pressure-compensation valve is compensated by the increase of the leakage flow.

The pressure drop across the flow-detecting needle valve suddenly increased at the range over 8 MPa when the pre-set flowrate was 2.3 L/min. This was caused by full closing of the pressure-compensation valve; at this state the valve cannot regulate the flowrate any more.

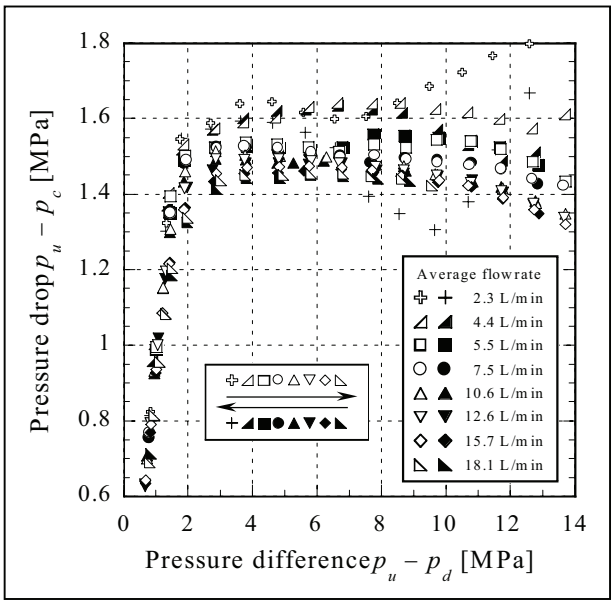

Fig. 11 Experimental results of pressure drop at the flow-detecting needle valve

Finally, Fig. 12 shows the dimensionless intermediate pressure in the pressure-compensation valve. This value is determined by the ratio of the openings of two throttles, where the radial clearance of the second throttle is larger than that of the first one. Therefore, smaller the axial opening of the valve, smaller the dimensionless intermediate pressure. This state appears when the pre-set flowrate is small or the pressure difference is large.

In the pressure range below 2 MPa, the pressure-compensation valve fully opens and does not work. Thus the values within this range has no significant meanings. When the pre-set flowrate was 2.3 L/min, the pressure-compensation valve fully closed at the range over 8 MPa; the dimensionless intermediate pressure shows no change in this range.

In all cases, the two serial throttles reduce the pressure in steps. The valve did not radiate cavitation noise in the range of experiment.

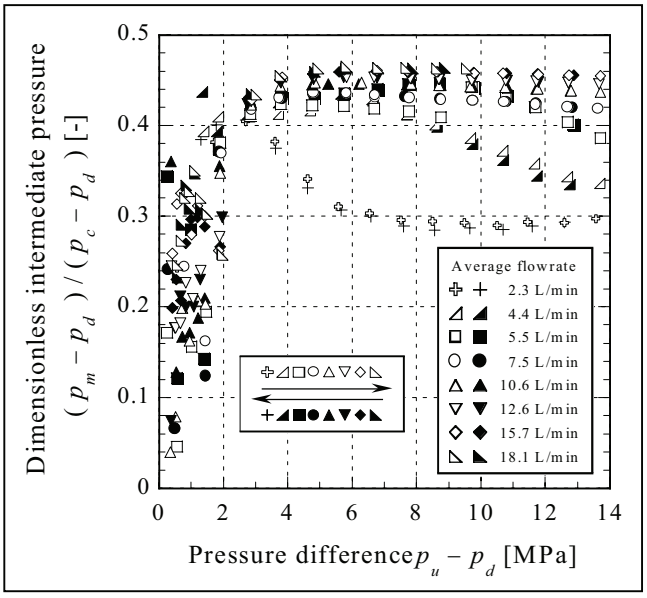

Fig. 12 Experimental results of dimensionless intermediate pressure at the space between the two throttles of the pressure-compensation valve

7 CONCLUSION

A pressure-compensated flow control valve for water hydraulics was developed. The developed pressure-compensation valve has two annular throttles in series, by which pressure drops in steps. The pressure-compensation valve includes the hydrostatic supports and the viscous damper, which reduces the wear of sliding parts and vibration of the valve, respectively.

The developed valve has adjustable flowrate range of 2.5-20 L/min within the pressure range of 2-14 MPa. Although the leakage through the hydrostatic supports exists, discharge flowrate is almost constant. Flowrate variations relative to the average flowrate are about 5 % in the experimental results. The static characteristics show negligible hysteresis. In addition, the valve does not radiate cavitation noise in the range of experiment.

Acknowledgement

The authors thank Mr. C. Kamijo and Mr. D. Tomii for their help in the experimental work.

References

[1] J. Berger, Kavitationserosion und Maßnahmen zu ihrer Vermeidung in Hydraulikanlagen für HFA-Flüssigkeiten, Dissertation der TH Aachen, 1983.
[2] E. Trostmann, Water Hydraulics Control Technology, Marcel Dekker, Inc., 1995.
[3] Danfoss Nessie High-pressure water solutions, http://nessie.danfoss.com/
[4] K. Suzuki and E. Urata, Improvement in Static Characteristics of a Water Hydraulic Relief Valve, The Ninth Scandinavian Intl. Conf. on Fluid Power, Proc. CD-ROM (Linköping, 2005-6).
[5] K. Suzuki and E. Urata, Analysis of Hydrostatic Bearing for Water Hydraulic Servovalve, The Sixth Scandinavian Intl. Conf. on Fluid Power, Vol.1, pp.179-190 (Tampere, 1999).
[6] K. Suzuki and E. Urata, Experimental study on hydrostatic supports of water hydraulic valves, Proc. Fifth JFPS Intl. Symp. on Fluid Power, Vol.1, pp.177-180 (Nara, 2002).

On cavitation characteristics of the shapes in water hydraulic seat valves

Leino, T,. Koskinen, K. T., Vilenius, M.
Tampere University of Technology
Institute of Hydraulics and Automation
P.O.Box 589
33101 Tampere, Finland
Phone +358 3 365 4434, Fax +358 3 365 2240
E-mail: timo.leino@tut.fi

ABSTRACT

The performance of the water hydraulic seat valve with the several different shapes in the cavitating flow conditions has been investigated in this research project. The previous experiments and simulations made with the method of computational fluid dynamics are treated in the light of the recent findings in the simulations. The cavitation modelling is applied to the case where the vapour clouds are seen in the experiments. Essential facts, that have to be borne in mind in the simulation of the seat valve, are proposed. The numerical model does not give realistic result for the pressure distribution in the orifice shape modelled with the absolutely sharp edge. The influence of the sharpness of the edge in the experimental valve is also investigated. According the limited set of measurements, the sharpness does not seem to have such a radical impact on the cavitation production that would be presupposed bases on the simulation.

KEYWORDS: Water hydraulics, Seat valve, Cavitation, CFD

1 INTRODUCTION

The results presented in this paper are part of the wider research project. Even thought the graphs are made concerning only some of the valve shapes and operating conditions, they are compared to the others by words. The publications, where those other cases are published, are identified.

Water has been used through the whole history of hydraulics. First it was the only choice, but was superseded by mineral oil because of some advantageous properties of it. Today, the use of water is again often reasonable because of the environmental or safety reasons [1].

The low viscosity, high mass density, high vapour pressure, corrosive properties and poor lubrication properties of water set special demands to the hydraulic system applied with it. Leakproof constructions, like a seat valve is, are therefore usable [2]. It is, however, prone to the cavitation phenomenon, that is one of the major factors to shorten the life time of the components [3].

This project is partly based on the research done of the cavitation in oil hydraulic seat valves [4] [5] [6]. The experimental arrangement is quite similar with it and the test valve has been machined using the same design.

The reason for applying the method of computational fluid dynamics to model the flow in the valve has been to verify it as a tool for developing new shapes of the valve structures. Because the intention is usually to avoid the cavitation in the valve, the modelling of the cavitation phenomenon is not the purpose of the simulation. The cavitation model is also tried, but it did not give the vapour cloud existence appropriately in this case.

Cavitation in water hydraulic seat valves, applying the cfd-method, has also been made by some other researchers. Gao et al. has varied the poppet angle and use also truncation in the poppet head. The models have been axially symmetric, an unstructured grid has been used and the turbulence has been modelled using the RNG κ-ε model. The cavitation modelling has also used. About the influence of the valve shapes, she states that the increase of the poppet angle increases the potential for cavitation and the truncation decreases it.

2 RECAP ON THE PREVIOUS WORK

The project has begun with the experiments with some of the similar valve shapes than were used in the references [4-6]. The results and the detailed description of the experimental arrangements are presented in the journal paper [7]. The principle of the measurements is based on the half-cut valve where a transparent plate covers the cut plane. The opening of the valve, upstream and downstream pressures and the temperature of the water are possible to adjust. The measured quantities are the flow rate thought the valve, downstream and upstream temperatures, and the sound pressure outside the valve. In some cases, the local pressure has been measured through the transparent plate. The occurrence of the cavitation is detected visually through the plate. The overview of the experimental system is presented in Figure 1.

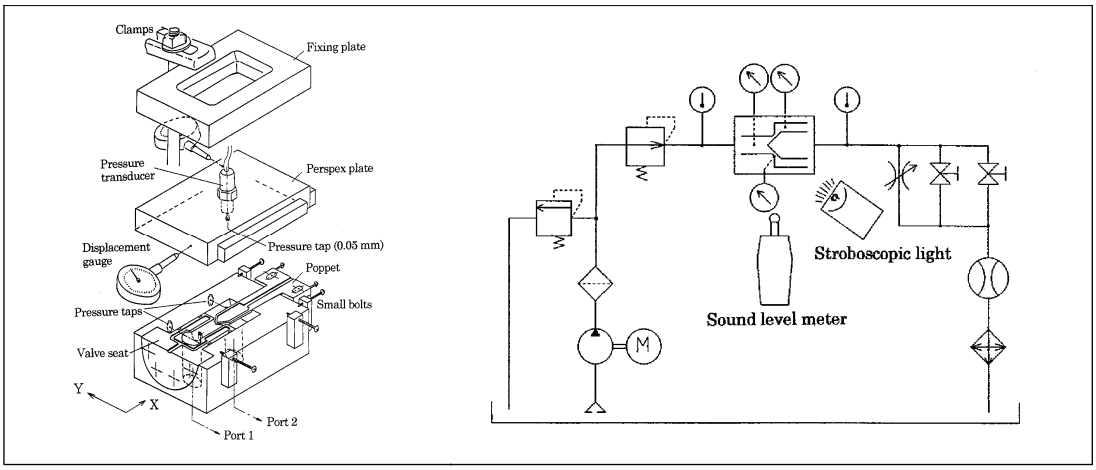

Figure 1. Arrangement of the experimental tests.

The valve shapes in this phase are conical poppet, valve seat with a sharp edge and valve seat with a 1.2 mm chamfer on the edge. The conclusion of this phase is that the valve with the chamfered seat edge is more susceptible to cavitation and thereby also noisier.

The method of computational fluid dynamics is first applied in paper [8]. A three dimensional symmetric model with an unstructured grid is used. Turbulence is taken into account with the RNG κ-ε turbulence model. The flow conditions are constant and the cavitation is not modelled. Thus, the simulations are run as steady state. The point in the simulation are set to the fact that the prerequisite for the cavitation is a local pressure under the vapour pressure in some point in the flow region and the cavitation modelling is not required approaching that point of the flow situation from the direction of the higher pressure. Therefore, the concern has been in the modelling of that point. The results of this phase are very promising. The place, where the cavitation first appears in the diverging flow, is just behind the poppet corner and the simulation gives the same result. In addition, the simulated and measured flow rates are very accurately the same.

The modelling method includes many parameters that are fitting the numerical results to some default experimental or analytically solved case by the empirical factors. In addition, there are several different alternatives for modelling separate phenomena in the flow. One of those is turbulence modelling. In paper [9] are compared three turbulence models (standard κ-ε, RNG κ-ε and RSM) together varying also the grid type between structured and unstructured. The model space is been two dimensional and axially symmetric. The differences in the compared quantities, flow rate, velocity- and pressure field, are not very remarkable. The structures of the velocity fields are similar and the locations pressure minimums and maximums are the same. The flow rates are in all the cases lower than the measured ones having the differences of 0.3-5%. From the results above, it can be concluded that the differences are such a small between the cases of these parameter variations, that it is not possible to judge that some of them would be more correct than the others. In this conclusion, the estimation of the errors in the measurements is taken into account. The other fact led to this conclusion, is that the model with the unstructured grid type should contain more numerical error, but now they are giving the smallest errors. Thus, it must be kept in mind that the errors can compensate each others.

Next a new poppet, having a ball-shaped head with the same radius than the poppet shank, is made. The same seats are used with this poppet than with the conical one. A short comparison between the experimental results of the cases of conical and ball-shaped poppet is made in paper [10]. Also a preview of the cfd-modelling of the ball shaped poppet is given that publication. The results can be summarised so that the differences between the valves with the conical and ball-shaped poppets are not very different. In the modelling, there are some evidences that it is not giving right the decrease of pressure in the valve orifice in circumstances where the cavitation is appearing already in it.

The pressure distributions in the valves with the sharp edge are treated more detailed in paper [11]. It seems clear that the modelling is not working properly right in the orifice region in the circumstances where the cavitation is undoubtedly produced from the there. The situation is the same with both poppet shapes. There is not seen even any decrease of the pressure (under the current downstream pressure) in that area. When studying in graphs how the pressure decreases when moving over the orifice, the simulated pressure does the drop faster than what is observed in measurements.

3 MEASUREMENT AND SIMULATION DETAILS

It's a natural continuum of the previous findings to get straight why the simulation fails in the basically simple solution of the orifice flow. Until now, the attention has been more in the valves with the sharp edge seat. The pressure distribution on the chamfered orifice and how the case behaves in the simulation is analysed in this paper. The other important ambition is to get more extensive results of the simulation. This is made by applying the simulation widely in the different flow conditions with all the valve shapes. From now on the valve shapes are identified as follows:

Valve 1	The conical poppet with the sharp seat corner
Valve 2	The conical poppet with the chamfered seat corner
Valve 3	The ball-shaped poppet with the sharp seat corner
Valve 4	The ball-shaped poppet with the chamfered seat corner

Table 1. Valve identification.

For the reasons of changes in the experimental system, the upstream pressure in the cases of the valve1 and valve2 has been 5 MPa (abs.) and in the cases of the valve3 and valve4 it has been 3 MPa (abs.). The influence of the difference is that the cavitation conditions are reached with the smaller pressure difference values in the cases of the valve3 and valve4. Otherwise, the absolute pressures used here are so small compared to the bulk modulus of water that they are not significant in the non-cavitating conditions. The temperature range in the cases of the valve1 and valve2 has been wider (28-42°C) than in the others where it has been 30±0.5°C. The liquid properties of every current temperature have been used in the simulation.

Based on the previous experiences in the simulations, the axially symmetric model space with the structured grid has been used. Turbulence is modelled using the standard κ-ε model. At least four different conditions of the downstream pressure, keeping the

upstream pressure constant, are modelled for each valve shape, for each opening and for both flow directions. Thus, 96 single simulations have been made. The conditions are selected so that one would be situated in the non-cavitating range, one in the point where the cavitation appeared first and one in the range of strong cavitation. In addition to these, some models are solved also with the modelling of the mass transfer between the liquid and vapour phases – i.e. applying the cavitation model.

4 COMPARISON AND ANALYSIS OF THE RESULTS

The results, comparison of them and the analysis of the results are presented in this section. In 4.1 are the flow rates of all the valve shapes, using both flow directions and all the openings. The 4.2 treats the findings in the microscopic shapes in the seat edge. In the 4.3 are examined the local pressure inside the valve 2. Finally in 4.4 has made a quick enterprise to use modelling of cavitation.

4.1 Flow rate through the valve

The comparison of the flow rates between the different valve shapes, using different openings and flow directions, has been made in this section. The valve 1 and the valve 2 have been tested using the openings of 0.4, 0.6 and 0.8 millimetres. Respectively, the valve 3 and valve 4 has been tested using the openings of 0.2, 0.4 and 0.6 millimetres. Thus, all the valve shapes have been compared together using the openings of 0.4 and 0.6 millimetres. The cavitation modelling is not used in this phase. Thus, the chocking effect would not be possible to see in the simulation values.

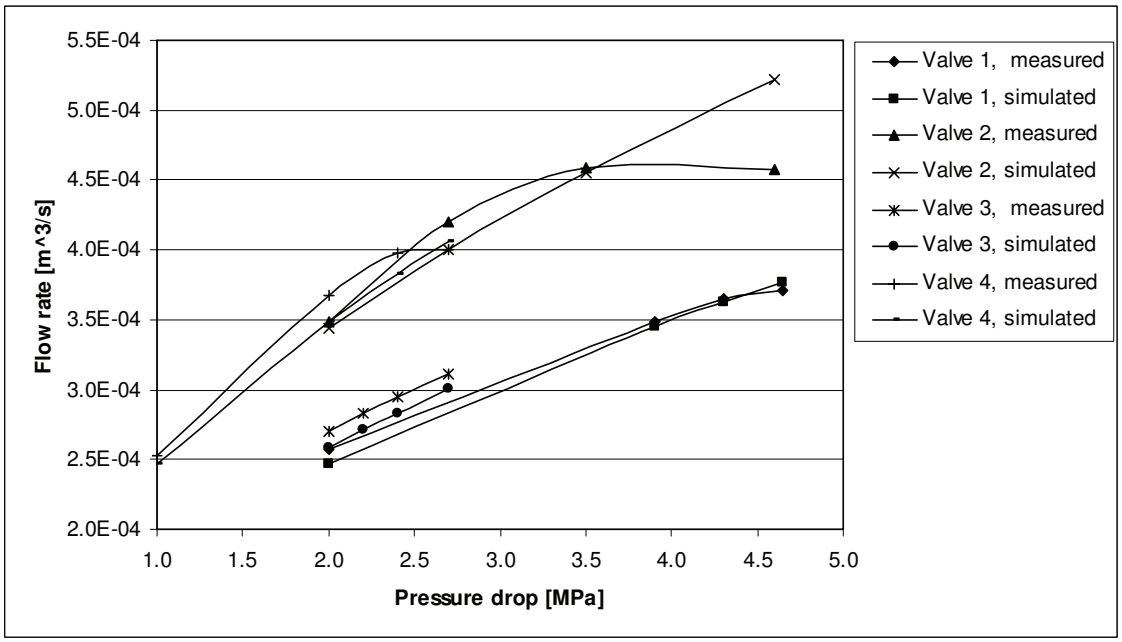

Figure 2. Flow rate, diverging flow direction, opening 0.4 mm.

In the Figure 2 are presented the flow rates through the 0.4 mm opening in diverging direction. The difference caused by the chamfer in the seat is clear. The flow rate

through the valve 2 and the valve 4 is about 1•10-4 m3/s more on an average. The chocking of the flow is seen in the valve 2 after the pressure drop value of 3.5 MPa and in the valve 4 after the pressure drop of 1.8 MPa. The simulated curves are following the measured ones quite well having most often lower values in all the cases. The difference is around 10 % in the cases of the valve 3 and valve 4 and few percents in the cases of the valve 1 and valve 2.

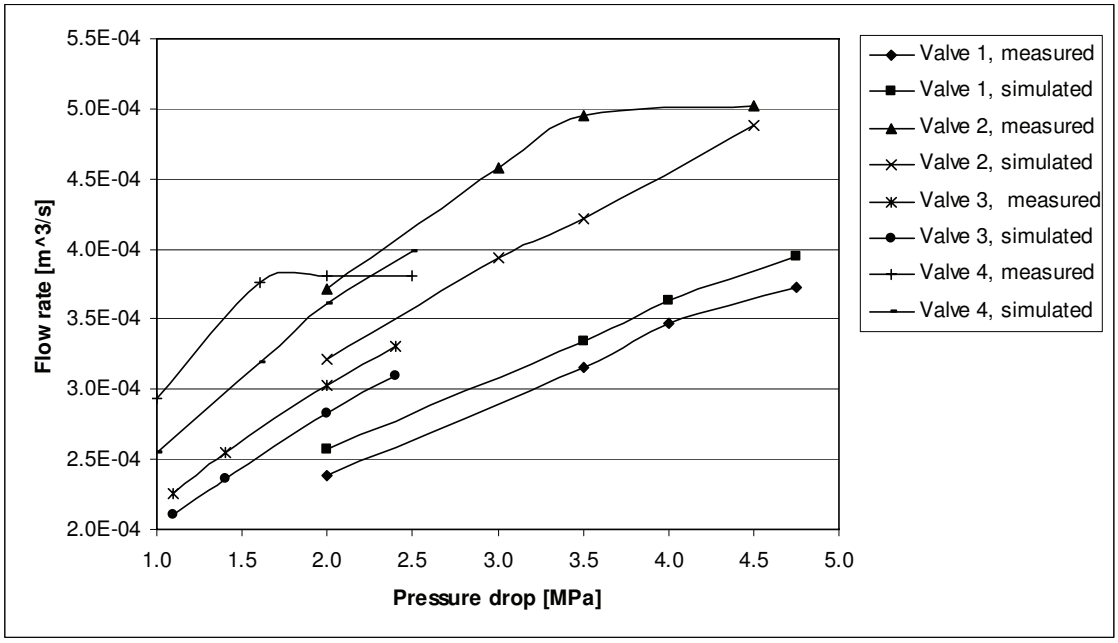

Figure 3. Flow rate, converging flow direction, opening 0.4 mm.

Turning the flow to the converging direction has a remarkable influence to the relation between simulation and measurement in the case of the valve 1. The simulation gives higher flow rate there. The order of the curves in the other cases is not changing – quite the contrary, the difference is increasing.

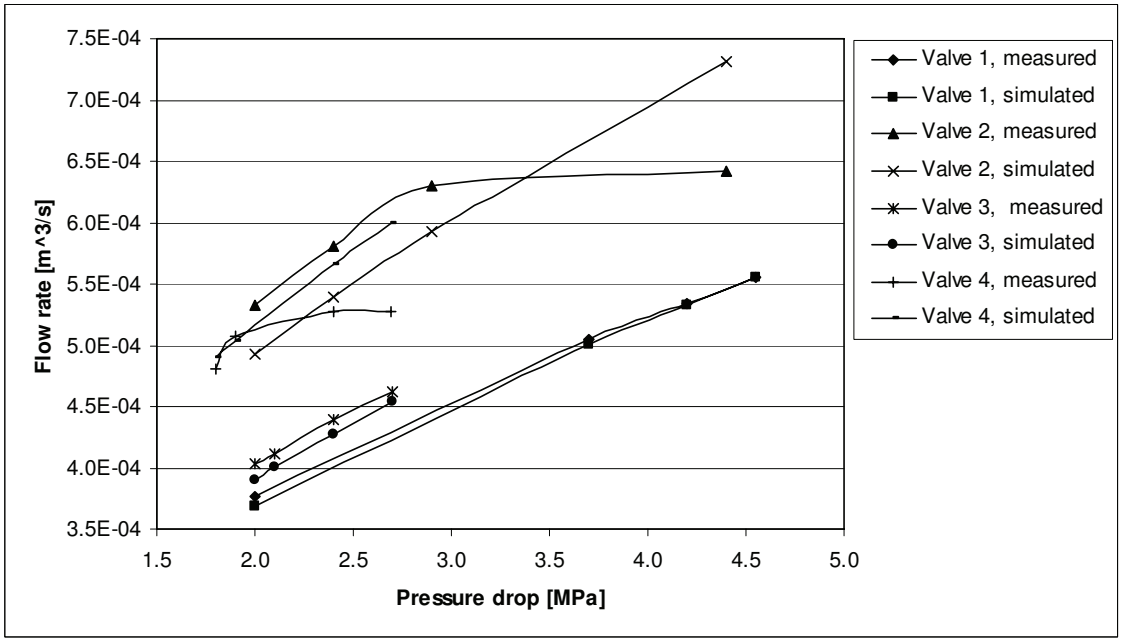

Figure 4. Flow rate, diverging flow direction, opening 0.6 mm.

Using the opening of 0.6 mm, the relative behaviour of the measured and simulated values is not radically changing. The simulation gives lower value except in the cases of the chamfered seat. The simulation fits well in the cases of the valve 1 and valve 3. In valve 2, the simulation gives about 0.5•10-4 m3/s smaller flow rate before the chocking.

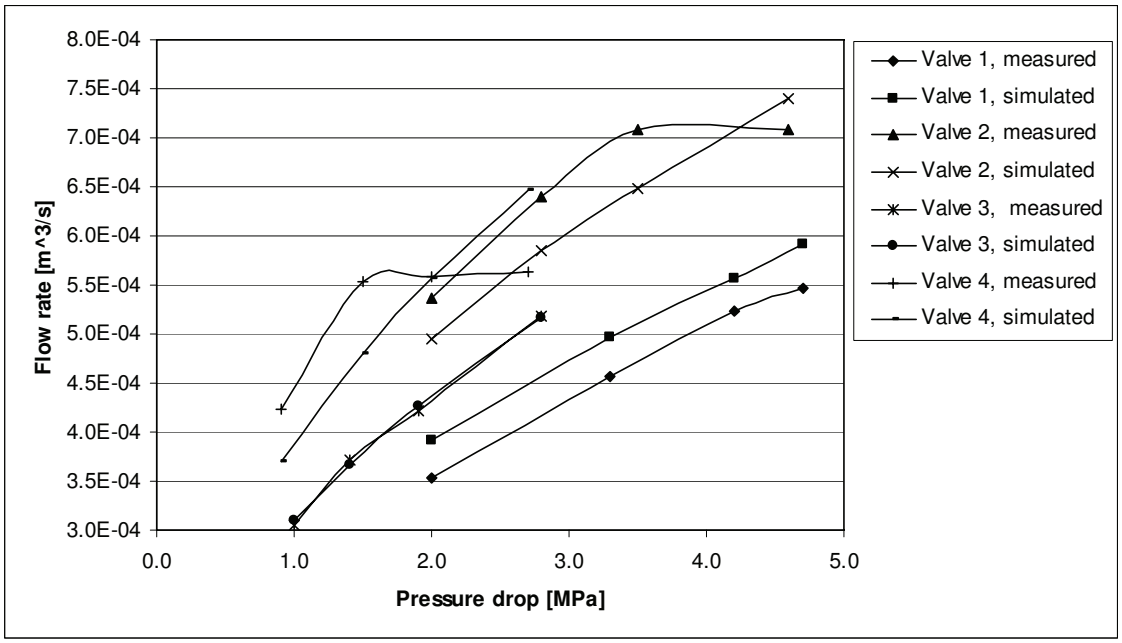

Figure 5. Flow rate, converging flow direction, opening 0.6 mm.

When the opening is increased to 0.6 mm, the situation in the valve 1 remains similar than with the smaller opening. The gap between the curves of the valve 3 is disappeared. The relations of the other cases are the same than preceding cases.

4.2 Effect of the valve seat sharpness

The seat corner, which is previously mentioned to be sharp, was detected to have a small chamfer on the seat edge. This chamfer is probably a consequence of the touch of the poppet. The left picture in the Figure 6 shows the chamfer on the edge. The distance between the arrows in the picture is about 0.03 mm. The shape of the corner truly seems to be chamfer but not rounding, for instance. This has established by alternating directions of two light sources and looking the light reflection off the corner surface.

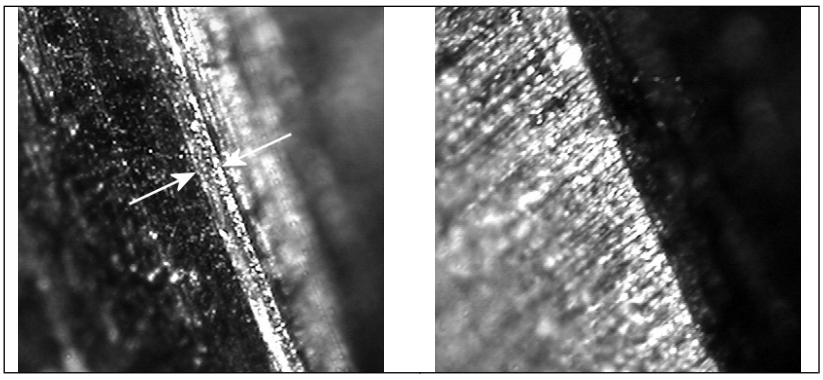

Figure 6. The original(left) and modified (right) sharp seat.

It has found a significant difference in the pressure fields in the simulation when the minor chamfer has been added in the seat corner. Based on this observation, the original sharp seat is ground to make the corner as sharp as possible. The modified seat corner is presented in the right picture in the Figure 6. Both pictures have the same scale. The actual sharpness of the modified seat corner is hard to state, but clearly it is substantially sharper than the original shape. A set of the same experimental testes are made with this sharpened seat than what was made previously with the original shape. It was not found any appreciable difference between the modified and the original valve. The flow rates through the valve were the same and the visually observed cavitation started exactly at the same conditions.

The observation in the modelling that led to the modification of the real structure is shown in the Figure 7.

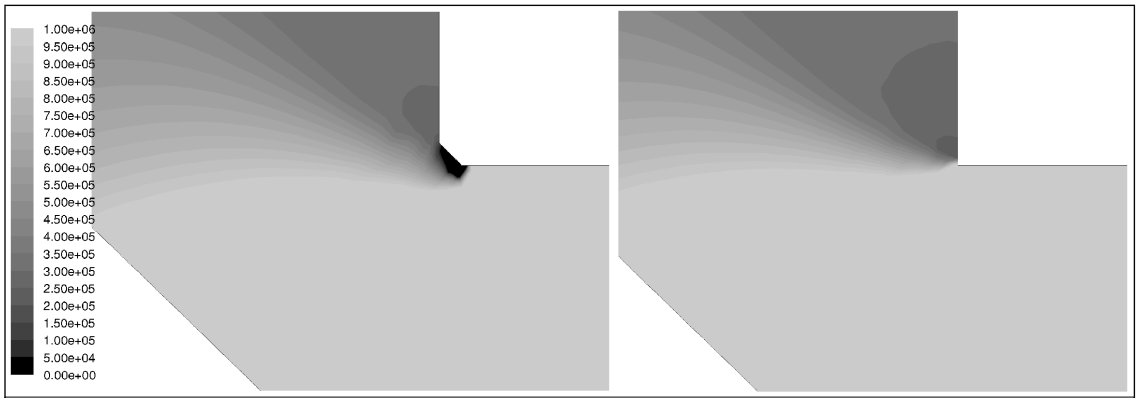

Figure 7. Pressure contour plots of the shape with the 0.03mm chamfer (left) and the sharp edge.

Both pictures are of the same boundary conditions in the diverging flow; the upstream and downstream pressures of 5 MPa and 0.35 MPa and opening of 0.4 mm, where the flow is strongly cavitating and the cavitation is clearly produced from the seat edge. The model with the absolutely sharp edge seems not to be capable of presenting the cavitation potential in the orifice. The situation changes totally when a minor chamfer is added on the edge. Also the variation of the grid size around the sharp edge is tried, but there has not detected differences within the realistic grid size range.

4.3 Pressure distribution on the orifice surfaces

This section treats the surface pressures in orifice of valve 2. The local pressures are measured through the channel in the plate covering the cut plane. The diameter of the hole is about 0.05 mm, that is assumed to be small enough not disturb the flow.

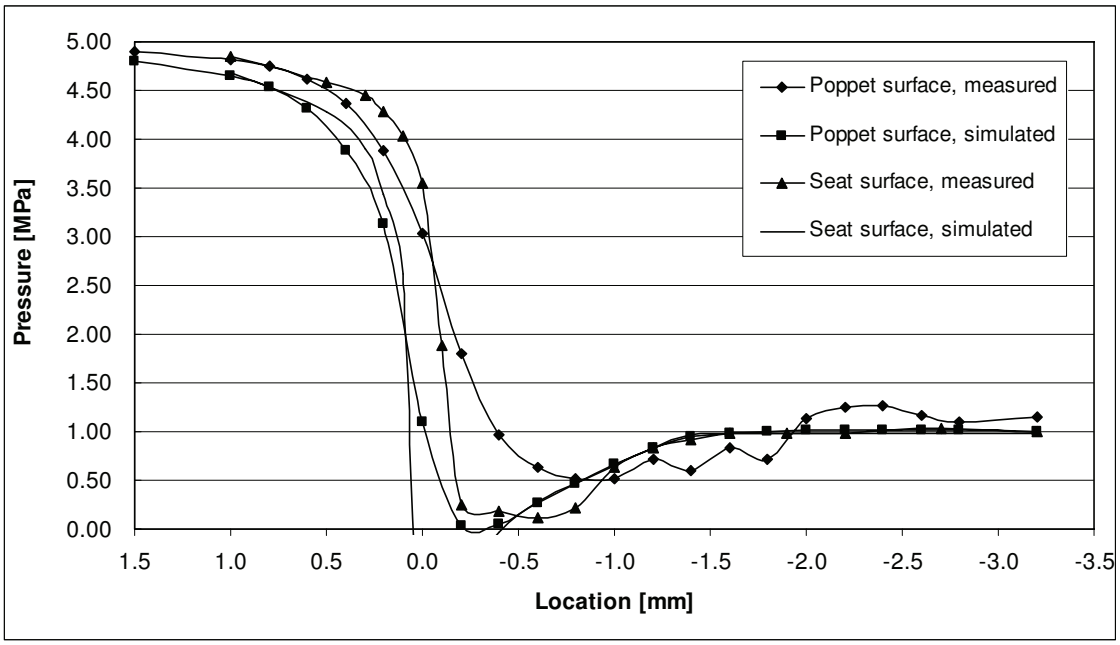

Figure 8. Local pressures on the seat and poppet surfaces in the case of diverging flow in the valve 2. Opening 0.4 mm, downstream pressure 1 MPa (abs.).

In the Figure 8 are shown the simulated and measured pressures on both surfaces using the diverging flow. Quite big differences can be observed in the curves. When moving along the seat surface, the pressure in the model decreases about 0.25 mm earlier than the measured pressure having the same shape of the curve fall. The curves have already difference in the first given point. The simulated pressure drops bellow the absolute zero pressure level because the real conditions are cavitating but the phase change between the liquid is not allowed in the model. The measured pressure leaves approximately on the level 0.2 MPa inside the orifice. The simulated pressure rejoins the measured level in middle of the orifice. After that, both methods give the same pressure values. The simulated pressure drops earlier also on the poppet surface. It is not, however, tending to decrease under the zero level. After the orifice area, it is smoothly reaching the downstream pressure level. The measured pressure on the poppet surface is decreasing until the orifice end. Some oscillation occurs after the orifice. The measured and simulated flow rates are 4.67•10-4 m3/s and 4.87•10-4 m3/s respectively.

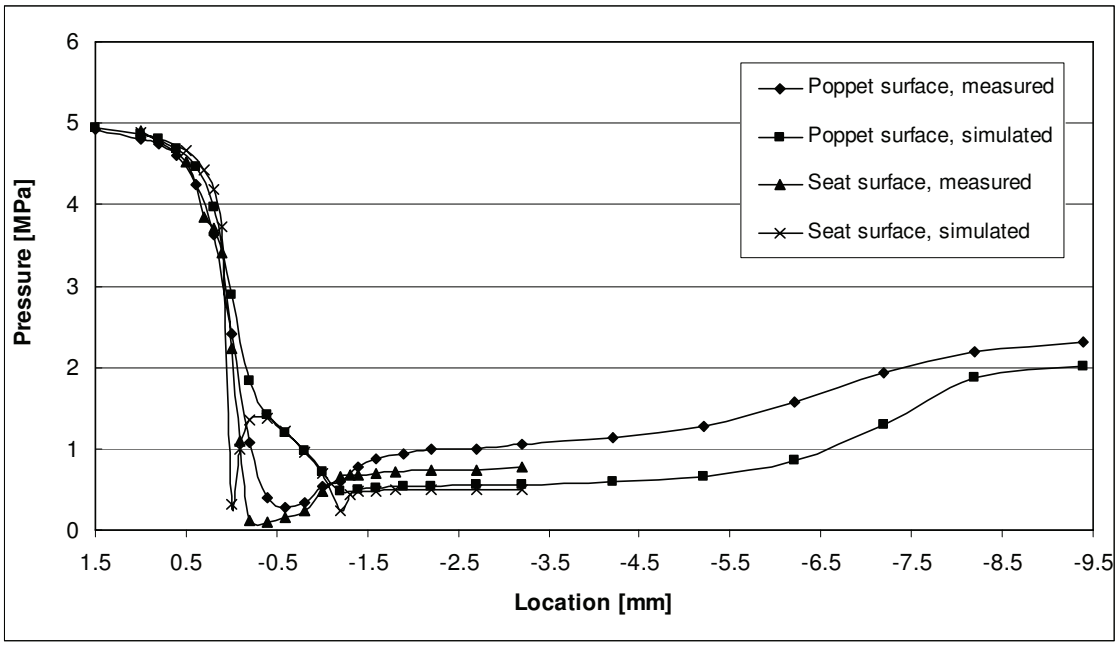

Figure 9. Local pressures on the seat and poppet surfaces in the case of converging flow in the valve 2. Opening 0.4 mm, downstream pressure 1 MPa (abs.).

In the case of the converging flow, none of the pressures is reducing under the current vapour pressure. All the pressures are behaving quite similarly before the orifice upstream edge. Inside the orifice, the simulated pressure on the poppet surface drops slower than the measured. This is opposite situation to what happened in the case of the diverging flow or in the valve 1 with the converging flow. The order of the curves reverses at the end of the orifice and the simulated pressure keeps lower level than the measured one also when going towards the poppet head and the high pressure area. The pressures on the seat surface have remarkable difference. Approaching the orifice upstream corner, the simulated and measured pressures are still behaving similar. When this point is passed, the simulated pressure decreases and follows the poppet surface pressure inside the orifice. After this, the difference becomes smaller. There is also a small downward peak in the simulated pressure at the downstream corner of the orifice. The measured flow rate is 5.00•10-4 m3/s and the simulated 4.53•10-4 m3/s in this case.

In the paper [11] were treated the pressure distribution in the valve 1 and valve 3. If comparing the results of this section with them can be found that the measured and simulated pressures around the orifice behave very differently in valve 1 and valve 2. In valve 1 the simulated pressure kept the level near the upstream value quite near the orifice, but dropped then faster to the level of the downstream pressure. In the case f valve 2, the simulated pressure drops earlier and with the slower slope when approaching the orifice from the upstream direction. After that position, the comparison of the pressure distributions is not anymore meaningful because of the too different structures. The Figure 10 compares the pressure field in the model to the cavitation occurrence in the valve 2.

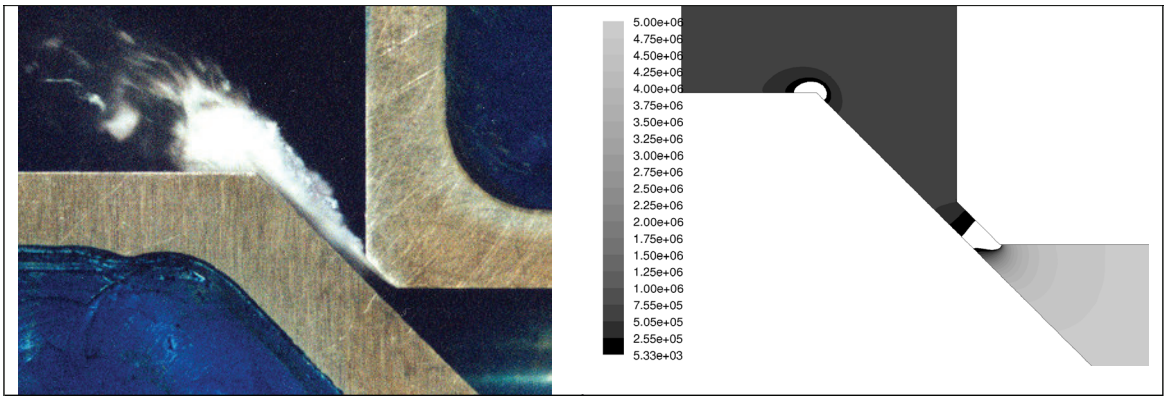

Figure 10. The cavitation situation in the valve 2 in the diverging flow and the corresponding pressure field in the model. Upstream pressure 5 MPa, downstream pressure 0.6 MPa, opening 0.6 mm.

Even if the cavitation is not modelled, the figure shows the model to give theoretical possibility to the cavitation appearance after the upstream corner of the chamfer. In the white are in the contour plot, the pressure tends to go under the vapour pressure in the current temperature.

4.4 Modelling of cavitation

The cavitation model available in the code is developed by Singhal et al. [12]. It should fully account the mechanisms of the cavitation i.e. phase change, bubble dynamics, turbulent pressure fluctuations and non-condensable gases in the liquid. The main force defining the direction of the mass transfer in the model is the local static pressure. The effect of the turbulence-induced pressure fluctuations are taken into account by a modification of the phase-change threshold pressure. The model is assumed to be capable of describing the bubble appearance, transfer and collapsing when the modeling has been made in the unsteady state.

The model including the mass transfer effects is quite an unstable and needs the reduction of the under-relaxation factors during the solution process. In addition, a good initial condition is required. The modelling of cavitation is applied to the case of valve 2, diverging flow, opening of 0.4 mm and the downstream pressure of 0.4 MPa. This condition is strongly cavitating. The steady state solution of the case without the cavitation model is used as the initial condition.

The result of the modelling is not what is expected. It seems not to describe the transfer of the cavitation bubbles from the orifice at all. Several sizes of time steps in the solution has been used – even unrealistic short, but the only place where the model shows the vapour to be existing, is the area inside the orifice where the pressure is under the current vapour pressure. In some examples, however, this model is stated to describe the transfer of the cavitation bubbles. The attention in the project is focused to this problem.

5 CONCLUSION

The main part in this paper was to make extensive viewpoint of the different shapes of water hydraulic seat valves. The comparison between the experiments and computational fluid dynamic simulations were made at the same. The interests were then focused in the valve with the chamfered seat and the microscopic detail in the seat sharpness. The general cavitation model was also tried.

The modelling seems to include uncertainties when modelling the orifice with the high gradients and cavitations existence. The theoretically sharp corner in the orifice is making the model unable to predict the cavitation appearance, because it depends mostly on the static pressure in the model. But, even in the case where the pressure is decreasing under the vapour pressure, the used cavitation model may not give the vapour transfer via the flow correctly. Generally, the simulation is often giving smaller values for the flow rate through the valve.

REFERENCES

[1] Varandili, E., Properties of Tap Water as a Hydraulic Pressure Medium, The 6th Scandinavian Int. Conference on Fluid Power-SICFP'99, Tampere, Finland, [113-127], May 1999

[2] Mauer, J., Proportional, High Pressure Valves for Water Hydraulic System, The 4th Scandinavian Int. Conference on Fluid Power-SICFP'95, Tampere, Finland, [898-909], Septemper 1995

[3] Backé, W., Water- or Oil Hydraulics in the Future, The 6th Scandinavian Int. Conference on Fluid Power-SICFP'99, Tampere, Finland, [51-65], May 1999

[4] Oshima, S., Ichikawa, T., Cavitation Phenomena and Performance of Oil Hydraulic Poppet Valve (1st report, Mechanism of Generation of Cavitation and Flow Performance), Bulletin of JSME, Vol.28 No.244, [2264-2271], October 1985

[5] Oshima, S., Ichikawa, T., Cavitation Phenomena and Performance of Oil Hydraulic Poppet Valve (3st report, Influence of the Poppet Angle and Oil Temperature on the Flow Performance), Bulletin of JSME, Vol.29 No.249, [743-750], March 1986

[6] Oshima, S., Ichikawa, T., Cavitation Phenomena and Performance of Oil Hydraulic Poppet Valve (5st report, Influence of Dimensions of Valve on the Thrust Force Characteristics), Bulletin of JSME, Vol.29 No.251, [1427-1433], May 1986

[7] Oshima, S., Leino, T., Linjama, M., Koskinen, K. T. and Vilenius, M. Effect of cavitation in water hydraulic poppet valves. International Journal of Fluid Power, Vol. 2, No. 3, pp. 5-13, 2001

[8] Leino, T., Linjama, M., Koskinen, K.T. and Vilenius, M. Modelling of a Water Hydraulic Poppet Valve Using CFD Technique. Proceedings of the 2nd International FPNI PhD Symposium on Fluid Power, Modena, Italy, 2002.

[9] Leino, T., Koskinen, K.T. and Vilenius, M. CFD-Modelling of a water hydraulic poppet valve - Comparison of different modelling parameters. The Eight Scandinavian International Conference on Fluid Power, Proceedings of the Conference, Tampere, Finland, 2003.

[10] Leino, T., Koskinen, K. T. and Vilenius, M. Numerical and experimental investigation of cavitating flow in water hydraulic seat valve. Proceedings of The Sixth International Conference on Fluid Power Transmission and Control (ICFP' 2005), Hangxhou, China, 2005.

[11] Leino, T., Koskinen, K. T. and Vilenius, M. Modelling of fluid dynamics in water hydraulic seat valve – investigation of pressure distribution, The 9th Scandinavian International Conference on Fluid Power, SICFP'05, June 1-3, 2005, Linköping, Sweden

[12] Singhal, A. K., Li, H. Y., Athavale, M. M., and Jiang, Y. Mathematical Basis and Validation of the Full Cavitation Model. ASME FEDSM'01, New Orleans, Louisiana, 2001.

STUDY ON WATER HYDRAULIC 2/2 DIRECTIONAL VALVE WITH PLANE PISTON STRUCTURE

Gong Yongjun[1], Yang Huayong[2], Wang Zuwen[1]
1, Dalian Maritime University
The Laboratory of Fluid Power Transmission and Control
Linghai Road No.1,Dalian
116026 DaLian, China
E-mail:sklofp@sohu.com
2, Zhejiang University
The State Key Laboratory of Fluid Power Transmission and Control
310024 Hangzhou, China

ABSTRACT

Due to its fire resistance and environmental compatibility, using water as the working fluid in hydraulic circuits is receiving an increasing attention by both manufactures and users. Water hydraulics that offers components and systems for general commercial use is quite young. The water hydraulic components are being developed thoroughly. Materials, machining technology, structures and so on must be examined for whether or not they are compatible with water when the components are designed.

The internal leakage is normally a harmful phenomenon which should be minimized by the right design. This is emphasized especially in water hydraulics due to the low viscosity of the media. This paper introduce a water hydraulic 2/2 directional valve and its principle (Fig1). The valve is composed of a hydraulically operated seat valve and a magnetic 3/2 direction valve. Aimed at the serious leakage and impact generating easily in reversing suddenly, an improved structure of water hydraulic directional valve is developed. When new water hydraulic directional valve is designed and manufactured, traditional space seal is changed to direct seal, compaction force between main valve spool and main valve pocket was logically designed and damper in pilot valve port is matched with sensitive cavity in main valve (Fig2).

From the view of flow control, the method of cavitation resistance of the directional water hydraulic valve is investigated. The computational fluid dynamics（CFD）

approaches are applied to obtain static pressure distributions and cavitation images in the channel of the main stage of the valve with two kinds of structure(Fig3, Fig4, Fig5, Fig6, Fig7, Fig8).The results show that the method of optimized spout can effectively restrain cavitation. The work provides some useful reference for developing water hydraulic control valve with the lower noise and lower vibration.

The structural parameters are optimized on the basis of information obtained from simulation. The experiments are carried out. Static test, dynamic test and life test are accomplished(Fig9, Fig10). The results show that the water hydraulic directional valve possess good property, its pressure loss is 1.1MPa lower, the switching time is shorter than 0.025s, strike crest is 0.8MPa lower(Fig11, Fig12). The valve possess fine dynamic performance with the characteristic rapidly action and lower impulsion. The life experiments are carried in normal condition. and the primary part aren't shattered(Fig13). The performance of the water hydraulic directional valve has achieved the level of traditional directional valve.

KEYWORDS: water hydraulic, directional valve, Structure Optimization**,** Flow Field Analysis.

1 INSTRUCTIONS

For its abundant transmission media, environmentally friendly, clean and safe, fire resitant and so on, water hydraulic technology has been turned out to be a focus of research in the field of fluid power transmission and control[1].Water hydraulic valve, as one of the key components, is studied extensively.

The traditional oil hydraulic directional valve is of spool pilot valve, rotary valve or cane valve. Although the unbalance force on the rotary valve and the pilot pool valve are weak, hence the force to operate them are weaker, the leakage are usually bigger with a larger tolerance for the relative movement of the valves and valve seats[2].For its low viscosity, the loss of leakage of water hydraulic system is much higher. For the same clearance and pressure, the loss of leakage of the water hydraulic system is several decade times that of oil hydraulic system. In order to maintain a reasonable low leakage the clearance should be extremely small, which may lead to difficulty of machining, and at the same time it is easily for the moving parts to be choked and stuck. As for the cane valve, although has a smaller leakage, unbalanced axial fore on the valve exist, so there need a stronger force to operate it. For its uncompressible and high stiffness, the hydraulic shock of the water hydraulic directional valve is more serious. So how to lessen the leakage, how to realize direction change with low or even no hydraulic shock and how to improve its static and dynamic characteristic are the key issues of study.
So far, there is no report on the study of water hydraulic directional valve. In this paper,

a new serial of water hydraulic valves has been provided based on change of seal pattern, reasonable design of pre-tightening force, and optimization of the flow passage.

2 WORKING PRINCIPLE OF THE WATER HYDRAULIC DIRECTIONAL VALVE

Figure NO.1 is the water hydraulic directional valve. It is electro-hydraulic directional valve.

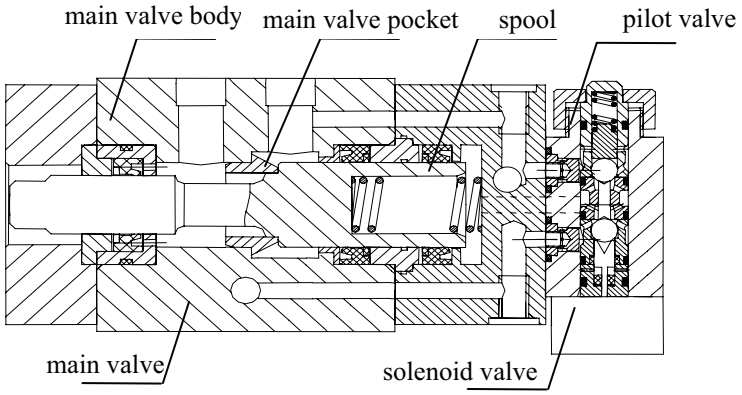

Fig.1Sketch of water hydraulic directional valve structure

The pilot stage is a 2/3 electromagnatic directional ball valve. Being different from traditional oil hydraulic valve, a valve pocket is added to the main valve, and the main valve pocket is over fitted to the valve body. the main valve spool is fitted to the main valve pocket, and the surface sealing is achieved by the plane of the valve. Lip-type packings are set in both ends to achieve no leakage. The spring is for compensation of the frictional force. Both ends of the main valve spool are supported radially by bushes, which are made of wear-resisting materials, so the problem of abrasion is settled in this way.

The structural principle of the valve is as following, there is damper at the valve port, two dampers in series act as half bridge resistant, and the controlling rib connects to the sensitive chamber on the right side of the valve by the central hole. When the electromagnet is out of power, main valve spool is moved to the right under the force of inlet, at the same time water in the sensitive chamber is discharged through the pilot valve, and the main valve is open. when the electromagnet is charged, water for control is inducted to the sensitive chamber, and the main valve spool is compressed on the valve pocket, and the main valve is shut down.

2.1 Design of the pressing force of main valve spool

The contact surface of the main valve spool and the valve pocket is plane, there maintains a certain pressing force between them. The pressing force varies according to the change of control fluid pressure, the higher the pressure is, the bigger the pressing force will be. Therefore, leakage between the main valve spool and the valve pocket is nearly zero. The stress condition of the main valve spool is as following,

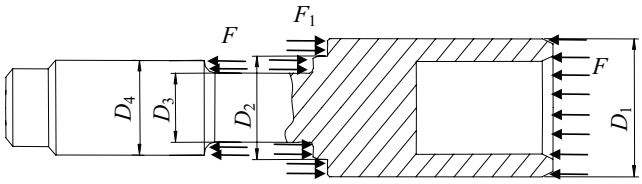

Fig.2 Sketch of axial force of main valve

Supposed that the inlet pressure of the main valve is F, and pressure loss is neglected, so the pressing force of the main valve is F_1

$$F_1 = F \cdot (1 + \frac{D_4^2}{D_1^2 - D_2^2}) \qquad (1)$$

It is obvious that F_1 is positive, which ensures that the main valve spool is pressed against to the valve pocket. If F_1 is too weak, there will be leakage between the main valve spool and the valve pocket, and if F_1 is too high, the force for directional change will be bigger and abrasion between the main valve spool and the valve pocket will occurs. According to our experiments, the facial contact force for the main valve spool and the valve pocket is at best 2 times the inlet pressure F. In the process of design, it is required that,

$$\frac{D_4^2}{D_1^2 - D_2^2} \approx 1 \qquad (2)$$

2.1.1 Matching design of pilot valve damper and sensitive chamber

For the design of directional valve, it is not only necessary for a quick directional change, but also a minimal hydraulic shock. So a damper is set at the inlet of the pilot valve, two dampers in series act as half bridge resistant, a throttle backing pressure is then built up at the end of the main valve, which has a function of retardation and speed-regulation.

Provided at any time, there is even pressure in the sensitive chamber and the compressibility of the fluid is omitted, equations will be acquired as following,

$$(F - f - k \cdot x) - p \cdot A_d = m \cdot a \qquad (3)$$

$$p = \Delta p \qquad (4)$$

$$q_v = c_q \cdot A_0 \cdot \sqrt{(\frac{2}{\rho} \cdot \Delta p)} \quad (5)$$

$$q_v = V \cdot A_d \quad (5)$$

$$a = \frac{1}{2}\frac{dv^2}{dx} \quad (6)$$

$$a = \frac{1}{2}\frac{dv^2}{dx} \quad (7)$$

Where, F is exterior force ,f is frictional force, K is the stiffness of the spring, X is buffer distance, p is pressure of the sensitive chamber, A_d is area of the main valve spool end, M is the mass of main valve spool, α is shock accelerated velocity, Δp is differential pressure between imports and exports of damper, A0: flow area of the damper, V is shock velocity, q is flow of the damper, c_q is coefficient of discharge of inundated port's efflux.

From equation 3 ~ equation 7, the characteristic expression of the pilot valve port can be deduced as following,

$$\frac{d(V^2)}{dx} = \frac{2}{m}(F - f - K \cdot x) - \frac{\rho V^2}{m}(\frac{A_d}{c_q \cdot A_0})^2 \quad (8)$$

the equation can be figured out by numerical method. When shock energy is too big and throttling area is too small, shock is rather strong and can create bigger front-shock hump, and buffer effectiveness is not good; When the shock energy is too big and throttling area is too big, shock is weak, buffering force is smaller, and residual velocity can exist which may create packed oil phenomenon and bigger back-shock hump at the end of the shock. Therefore in the case of proper design, it is required that the damper should match with sensitive chamber, and the damper should have good performance and linearity. According to experience, linearity of the damper should be less than 30%.

3 FLOW FIELD SIMULATION AND ANALYSIS

When designing directional valve, its pressure loss should be as small as possible. Pressure loss of the directional valve usually is determined by experiment. Development of calculated hydromechanics provides a scientific approach to calculate pressure loss of the directional valve with complex flow passage. It turned out to be an effective method to make use of numerical calculation, with which optimization of the movement, flow and structure of the hydraulic component can be done.

3.1 Mesh division

The mesh of water hydraulic directional valve's main valve passage is shown in figure 3. Main valve passage is three-dimensionally symmetrical structure, the passage 's three-dimensional model is used for mesh division and flow field calculation in the study.

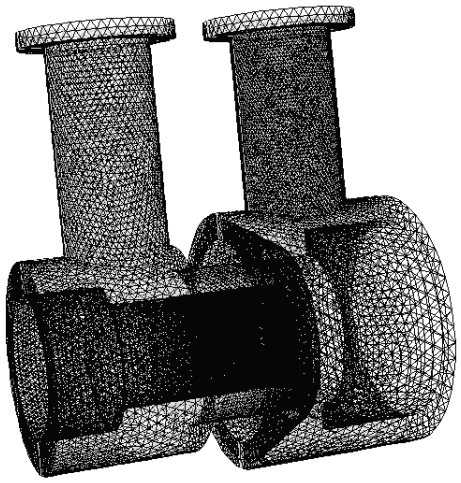

Fig.3 Mesh of main valve flow passage

Because area gradient of flow field of the computational domain varies greatly, in order to improve calculation accuracy, and reduce amount of calculation work, the computational domain has been divided into multiple small sectors. Initial computational mesh is created in Gambit. In high speed domain of the main valve port and nearby, velocity gradient is very big, complex flow pattern exists, finner structuring meshes in this domain and coarser unstructural meshes in other area were applied .

3.2 Mathematic model

3.2.1 Fundamental equation

Assume that fluid is uncompressible, and gravity and inner thermal effects can be ignored, its mass equation is,

$$\frac{\partial \rho}{\partial t} + \nabla \cdot (\rho V) = 0 \cdot \qquad (9)$$

momentum equation is,

$$\rho \frac{\mathrm{d}V}{\mathrm{d}t} = -\nabla p + \mu \nabla^2 V \cdot \qquad (10)$$

in the pillar coordinate system, equation (10) can be simplified as,

$$\frac{\partial v_r}{\partial t} + (V \cdot \nabla) v_r - \frac{1}{r} v_\theta^2 = -\frac{1}{\rho} \frac{\partial p}{\partial r} + \nu \left(\nabla^2 v_r - \frac{v_r}{r^2} - \frac{2}{r^2} \frac{\partial v_\theta}{\partial \theta} \right)$$

$$\frac{\partial v_\theta}{\partial t}+(V\cdot\nabla)v_\theta-\frac{1}{r}v_r v_\theta=-\frac{1}{\rho r}\frac{\partial p}{\partial\theta}+\nu\left(\nabla^2 v_r-\frac{v_r}{r^2}-\frac{2}{r^2}\frac{\partial v_r}{\partial\theta}\right)$$

$$\frac{\partial v_z}{\partial t}+(V\cdot\nabla)v_z=-\frac{1}{\rho}\frac{\partial p}{\partial z}+\nu\nabla^2 v_z$$

Where, $v=1/\mu$

energy equation is,

$$\rho c_v\frac{\mathrm{d}T}{\mathrm{d}t}=k\nabla^2 T+\varphi \quad . \qquad (11)$$

in the pillar coordinate system, equation (11) can be simplified:

$$\rho c_v[\frac{\partial T}{\partial t}+(V\cdot\nabla)T]=k\nabla^2 T+\mu[2(\varepsilon_{rr}^2+\varepsilon_{\theta\theta}^2+\varepsilon_{zz}^2)+\varepsilon_{\theta z}^2+\varepsilon_{rz}^2+\varepsilon_{r\theta}^2] \quad .$$

Where,

$$\varepsilon_{rr}=\frac{\partial v_r}{\partial r} \quad ,$$

$$\varepsilon_{zz}=\frac{\partial v_z}{\partial z} \quad ,$$

$$\varepsilon_{rz}=\frac{\partial v_r}{\partial z}+\frac{\partial v_z}{\partial r} \quad ,$$

$$\varepsilon_{\theta\theta}=\frac{1}{r}\left[\frac{\partial v_\theta}{\partial\theta}+v_r\right] \quad ,$$

$$\varepsilon_{\theta z}=\frac{1}{r}\frac{\partial v_r}{\partial\theta}+\frac{\partial v_\theta}{\partial z} \quad ,$$

$$\varepsilon_{r\theta}=\frac{1}{r}\left[\frac{\partial v_r}{\partial\theta}-v_\theta\right]+\frac{\partial v_\theta}{\partial r} \quad .$$

3.2.2 Anisotropic k-ε turbulent model

Because Anisotropic k-ε model adopt Reynolds stress correlation equation assumed by Launder, the aeolotropism and eddy flow of turbulent current can be well predicted, this paper uses Anisotropic k – ε model to simulate flow pattern of flow field of the relief valve 's main valve, calculation equation of its turbulent kinetic energy k and turbulent dissipated energy ε is,

$$k=\frac{1}{2}\overline{u_i' u_j'} \quad , \qquad (12)$$

$$\varepsilon = \left(\frac{\mu}{\rho}\right)\overline{u_{i,j}^{'}u_{i,j}^{'}} \quad . \qquad (13)$$

calculation equation of turbulent current frequency ω is,

$$\omega = \frac{\varepsilon}{k} \qquad (14)$$

Where, ui' is fluctuation velocity sector in i direction, uj' is fluctuation velocity component in the j direction, ρ is fluid density, μ is absolute viscosity.

3.2.3 Cavitation model

gas phase volume percent equation can be expressed as,

$$\frac{\partial}{\partial t}(\alpha_{\mathrm{a}}) + \frac{\partial}{\partial x_i}(\alpha_{\mathrm{a}} u_{i,\mathrm{av}}) = \frac{1}{\rho_{\mathrm{a}}}\dot{m}_{\mathrm{al}} \quad . \qquad (15)$$

Where, a is gas phase, αa is gas phase volume percent, ρa is gas phase density. l is fluid phase, ρl=998.2kg/m3(fluid phase density), (l-αa) is fluid phase volume percent.

mean density ρ: $\rho = \alpha_{\mathrm{a}}\rho_{\mathrm{a}} + (1-\alpha_{\mathrm{a}})\rho_{\mathrm{l}}$. (16)

$\dot{m}_{\mathrm{al}}$ is mass transfer between gas phase and fluid phase due to cavitation,

$$\dot{m}_{\mathrm{al}} = \frac{3\rho_{\mathrm{a}}\alpha_{\mathrm{a}}}{R}\sqrt{\frac{2(p_{\mathrm{v}} - p)}{3\rho_{\mathrm{l}}}} \qquad (17)$$

Where, pv is vaporization pressure, n is number of bubbles per unit volume, R is bubble radius, $R = \left(\frac{3\alpha_{\mathrm{a}}}{4\pi n}\right)^{1/3}$.

3.3 Simulation results and analysis

3.3.1 Flow characteristic analysis

Numerical calculation is carried out with Fluent software. In the calculation there are some assumptions as follow:
The fluid is uncompressible, flow is of thermal insulation, there is no slip on the wall. Supposed the opening of valve port is 4mm, the inlet flow is 120L/min, and the outlet pressure is the pressure of working water circuit, whose absolute pressure is 1MPa.

Figure 4 shows the static pressure isoline along axial symmetry plane in the flow passage of the main valve. It can be see that at the nozzle between the main valve spool

and main valve pocket, the pressure contour is denser and pressure drop is bigger, which lowered to 0.7MPa.

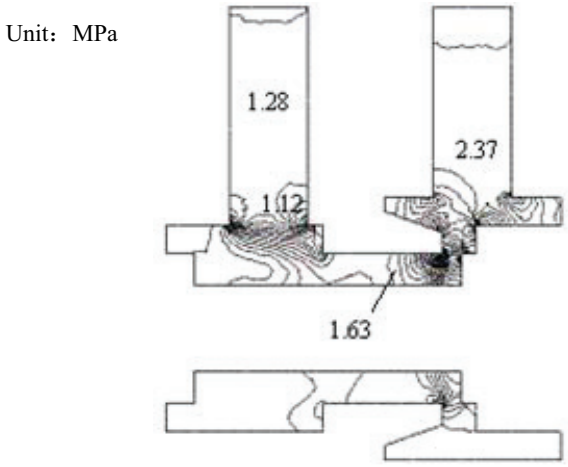

Fig.4 Pressure isoline of main valve flow

Fig.5 shows the velocity vector distribution along axial symmetry plane in main valve flow passage. It can be seen that after fluid enter chamber, spiral vortex is formed near the main valve spool corner, its central pressure is lower, spiral vortex dissipates fluid kinetic energy by viscous friction.

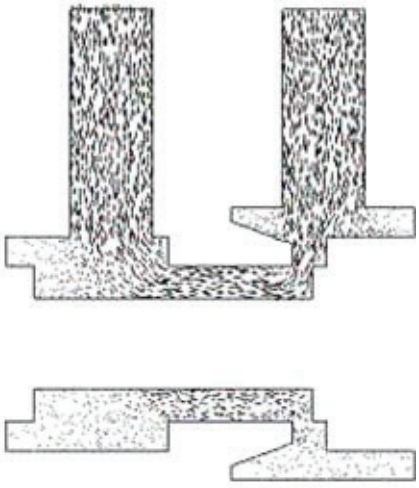

Fig.5 Velocity vector distribution of main valve flow passage

3.3.2 Structure optimization and flow field analysis

Based on the analysis above, at the nozzle formed by the main spool and main valve pocket ,the fluid will diffuse or shrink suddenly as is limited by the structure, which may cause the streamline changing sharply, spiral vortex appeared on the corner point which will dissipate the kinetic energy of the fluid, all of which will cause great pressure loss. In order to improve the performance of water hydraulic directional valve,

the structure of nozzle has to be optimized.

Figure 6 shows the comparison of flow passage between before and after optimization. in order to make the streamline smooth ,the optimized valve spool is manufactured to be arc transitional surface ,which voids appearance of death angle.

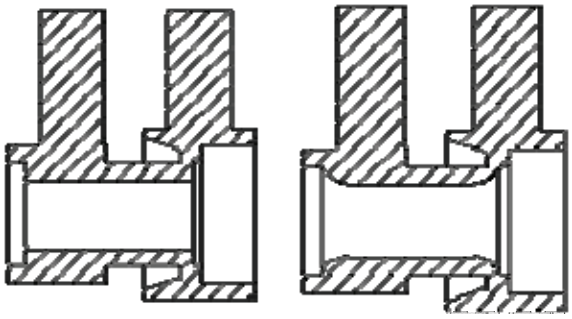

(a) before optimization (b) after optimization

Fig.6 Comparison of flow passage between before and after optimization

Simulation and computation of its flow passage of the optimized main valve have been done under the same condition, the pressure distribution in axial symmetry plane is shown as Fig 7.It can be seen that at the nozzle where fluid flows into the chamber, the density of pressure isoline decreases, pressure gradient reduces, and pressure loss reduces to 0.3Mpa after the structure is optimized.

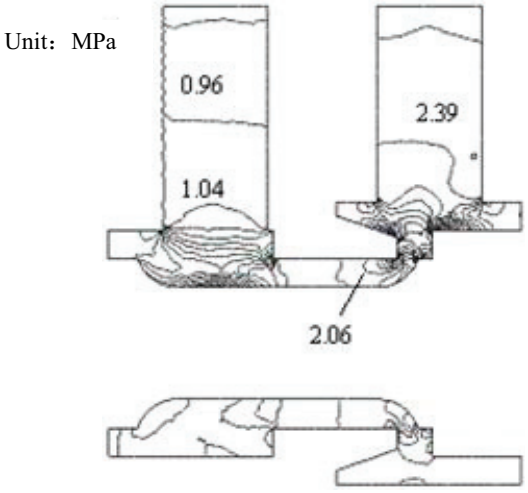

Fig.7 Pressure isoline of flow passage after optimization

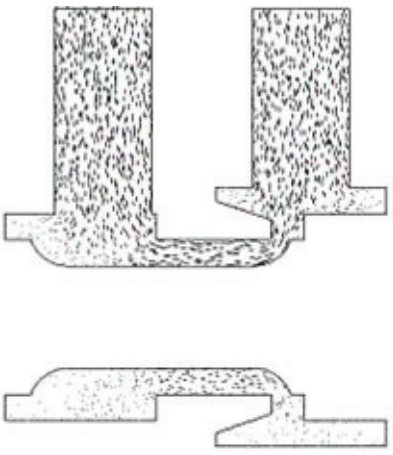

Fig.8 Velocity vector distribution of flow passage after optimization

The distribution of velocity vector after optimization along with axial symmetry plane is shown as Fig 8. There is no spiral vortex on the corner point of main valve near the nozzle, so the optimized structure effectively restrains the appearance of low pressure area in the fluid field.

4 EXPERIMENT AND DATA ANALYSIS

4.1 Experiment device and method

The water hydraulic directional valve designed is made of stainless material, its rated pressure is 14Mpa, and maximum flow up to 120L/min. In order to prove the correction of design principle and simulation results, experiments on both static and dynamic characteristics of the valve has been done .The experiment method refers to related national standard GB8106-87 of similar experiments of oil hydraulic directional valve. The experiment has been done on the test rig of the State Key Laboratory of Fluid Power Transmission and Control of Zhejiang University, as is shown in Fig 9,

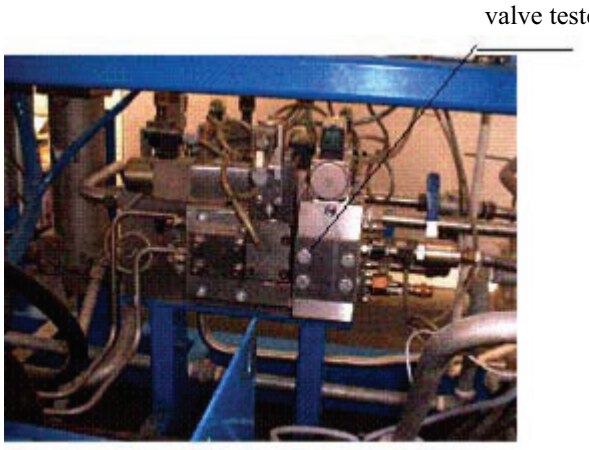

Fig.9 Test rig of water hydraulic components

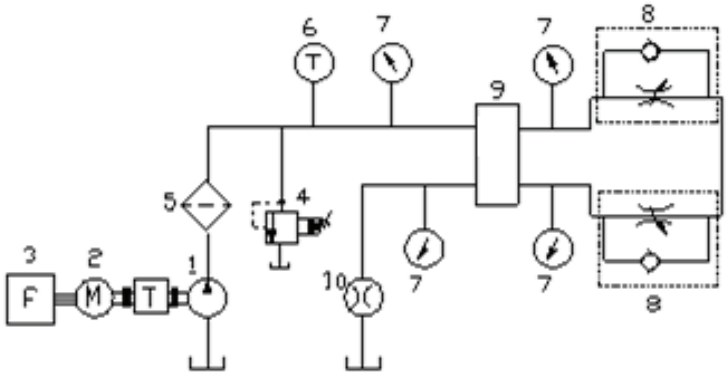

1-tap water hydraulic pump 2-conversion motor 3-convesion
4-relief valve 5-filter 6-thermometer 7-pressure transducer
8-one-way throttle 9-valve tested 10-floemeter

Fig.10 Test principle of water hydraulic directional valve

Fig 10 shows the schematic diagram of this experiment. As the medium of water is strongly corrosive, all components of this system are of stainless materials. During the experiment, relief valve 4 regulates the entrance pressure of the valve being checked ,rotation speed of the variable-frequency electric motor 2 is regulated by frequency-transformer 3 ,which adjusts the discharge flow of water hydraulic pump 1. The outlet backing pressure of the valve 9 is adjusted by one-way throttle valve 8 and is measured by flowmeter.

4.2 Experiment result

4.2.1 Flow-pressure difference experiment of water hydraulic directional valve

In the experiment of pressure loss, relief valve 4 serves as safety valve whose safety pressure is 18Mpa.The valve tested is charged and then its spool is on the position of through-flow. To make the amount of fluid flowing through the valve 9 increase gradually from zero to rated flow by Adjust the discharge flow of water hydraulic pump, and choose several points to measure each point's discharge pressure, based on which the valve's flow-pressure difference performance curve can be achieved. The outlet backing pressure of the valve tested 9 can be adjusted by one-way throttle valve 8. The value of the flow is read out on the flowmeter 10, the pressure of inlet and outlet display on the indicating instrument of pressure transducer 7.

Comparison of the characteristic of flow-pressure difference between the result of simulation and experiment is shown as Fig 11, it can be seen that, for qV<15L/min,the pressure difference between inlet and outlet results from the flow passage of pilot ball valve and increases notably as the flow increases; forqV≥15 L/min, the pressure difference between inlet and outlet results mainly from the main valve passage and increases slowly almost like a linear as the flow increases.

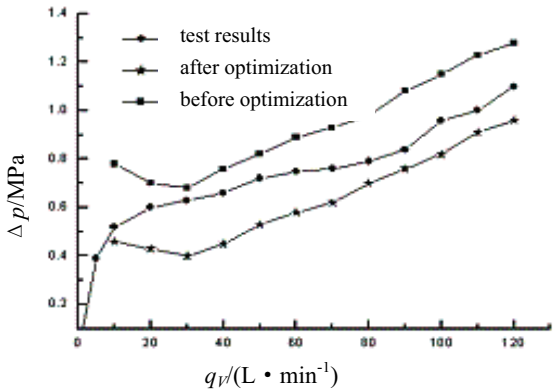

Fig.11 Characteristic curve of q_V - Δp

In addition, the result tested is bigger than the result simulated. This is because the pressure loss in the test is the sum of the pressure loss of main valve and pilot valve,

while the optimized result from simulation and computation only includes the pressure loss of main valve.

From the comparison of the structure of main valve between before and after optimization, it can be noticed that the optimized pressure loss of main valve decreases notably. Attention should be paid that for qV＜30 L/min, the result of simulation shows that the pressure loss between inlet and outlet decreases as the flow increases; however, this case does not appear, which indicates that there is much discrepancy for the simulation when the flow is small.

4.2.2 Experiment of dynamic characteristics of water directional valve

Adjust the overflow valve 4 and one-way throttle valve ,making the pressure of inlet P of the tested valve 9 to be the rated pressure 14Mpa, and the pressure of outlet T to be the given backing pressure, the amount of fluid flowing through the tested valve is 80% of maximum flow. Then charge and discharge the tested valve under rated voltage and the data acquisition system picks the dynamic response curve of the tested water hydraulic directional valve, as is shown in Fig 12.

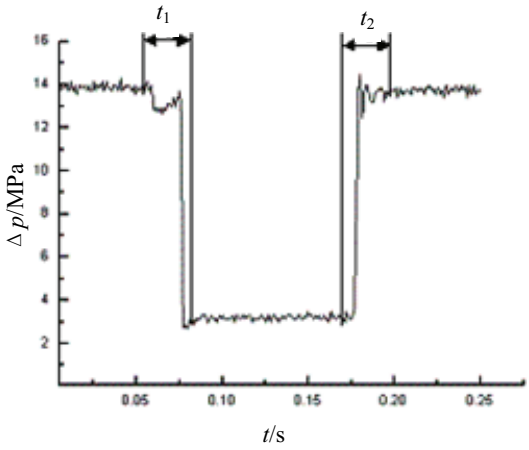

Fig.12 Dynamic response curve of water hydraulic directional valve

From Fig 12,the pressure decreasing time t1 is smaller than 0.05s, the pressure increasing time t2 is smaller than 0.05s ,the charging time and discharging time are almost the same, direction change is quick, the pressure peak △p produced while reversing is decrease 6%, the reversing shock is small, which indicates good dynamic response characteristics.

4.2.3 Experiment on the life of water hydraulic directional valve

Respectively set the pressure of inlet P of the tested valve to be variable value and the

pressure of outlet T to be remained the specified backing pressure and the amount of fluid flowing through the tested valve to be 100L/min, continuously charge and discharge the electromagnet of the tested valve up to 10,000 times, and then check the main components of the tested valve, there should be no damage inordinate wear.

Fig13(a)(b)shows the response curve of continuous directional change under pressure of 12MPa and 14MPa. It is clarified that the dynamic responsive characteristics of the valve are nearly uniform, and direction change is reliable and prompt.

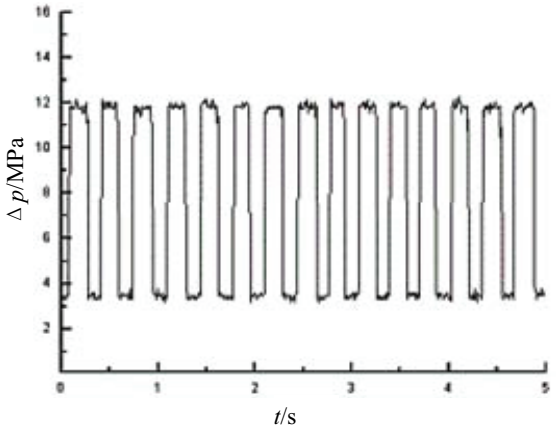

(a) pressure=12 MPa

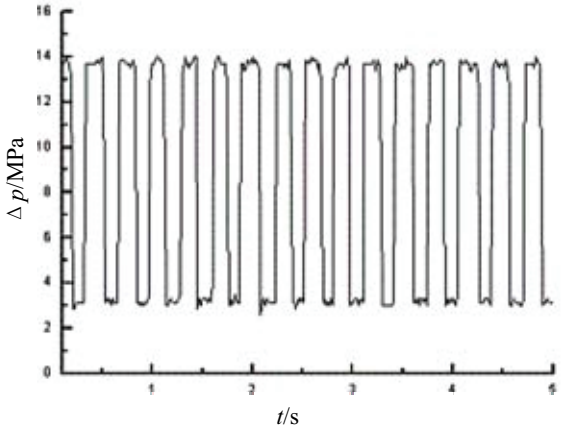

(b) pressure=14MPa

Fig.13 Life test curve of water hydraulic directional valve

4 CONCLUSIONS

(1)This new water hydraulic directional valve's pressure loss is small under rated condition, and its speed of directional change is fast while its hydraulic shock is weak, and good dynamic characteristics are obtained. In its life experiments, the directional valve operates normally, and its direction change is reliable. Its performance of this kind is comparable to the same kind oil hydraulic valve.

(2)AS for its leakage, traditional clearance sealing is taken place by directional sealing. And for the contradiction of requirement of quick directional change and hydraulic shock, the pressing force and the matching of damper and the sensitive chamber are designed, which provide warrantee for its successful design and machine.

(3)Simulation results show that there are pressure loss at the valve pot caused by the main valve spool and the valve pocket. By structural optimization of the valve pot, an effective method is found to decrease the formation of turbulence and pressure loss and to enhance its performance.

References：

[1]YANG Hua-yong, ZHOU Hua. Research condition and development direction of water hydraulics[J]. China Mechanical Engineering, 2000, 11(2): 1430-1433.
[2]SONG Hong-yao, DING Hong-yao. Design and calculation of hydraulic valve[M]. China Machine Press, 1982.
[3]BACKE W. Water-or-Oil hydraulics in the future[C]. Proceedings of 6th Scandinavian International Conference on Fluid Power, Tampere. Finland: Tampere University of Technology, 1999:51-64.
[4]YANG Shu-dong, LI Zhuang-yun. The development and the key basal technology of water transmission[J]. Machine Tool & Hydraulics, 2000(5):6-9.
[5]GAO Dian-rong, WANG Yi-qun. Finite element investigation of flow in hydraulic cone[J]. Machine Tool & Hydraulics, 2000(2):12-14.
[6]JI Hong, FU Xin, YANG Hua-yong. Effects of internal structure on cavitating noise of hydraulic relief valve[J]. Chinese Journal of Mechanical Engineering, 2002, 38(8): 19-22.
[7]GAO Hong, FU Xin, YANG Hua-yong, et al. Numerical investigation of cavitating flow behind the cone of a poppet valve in water hydraulic system[J]. Journal of Zhejiang University: SCIENCE, 2002, 3(4): 395－400.
[8]PAOLUZZI R. Stationary and dynamic analysis of a water Relief Valve[C]. Proceedings of the 4th JHPS International Symposium on Fluid Power, Tokyo: Tokyo Institute of Technology, 1999: 561-566.

EROSION DUE TO IMPINGEMENT OF SUBMERGED CAVITATING JETS IN TAP WATER, BIODEGRADABLE AND MINERAL OILS

Toshiharu Kazama and Kenji Shimizu
Muroran Institute of Technology
Department of Mechanical Systems Engineering
27–1, Mizumoto−cho, Muroran
Hokkaido, Japan
Phone +143 46 5349, Fax +143 46 5349
E–mail: kazama@mmm.muroran−it.ac.jp

ABSTRACT

Using a submerged cavitating jet apparatus, a cavitation erosion experiment was performed. Tap water, synthetic type biodegradable oil, or mineral type hydraulic oils with ISO VG32 and VG46 were alternatively used as test liquids. The liquid temperature was maintained at 40–65°C. The upstream pressure was set at 10–18 MPa and the cavitation number was 0.02–0.04. The standoff distance was varied 10–35 mm. The 15-mm-diameter specimens were made of aluminum alloy. The main conclusions are the following. The mass loss with tap water was markedly greater than losses with any type of oil. The loss with VG32 was larger than the loss with VG 46. As the liquid temperature increased, the mass loss with the biodegradable and mineral oils increased proportionally. The mass loss was approximately proportional to the fourth power of the upstream pressure. The surfaces were eroded as ring-shaped for all tested liquids. The surfaces eroded by tap water were noticeably rough: severe damage was distinctly visible in SEM micrographs and photographs. Comparing the mass loss and processed images of cavitating jets, the correlation between erosion and the jets was partially shown.

KEYWORDS: Cavitation erosion, Tap water, Biodegradable oil, Fluid power systems

1 INTRODUCTION

Cavitation erosion [1,2] is a serious problem that affects hydraulic equipment such as valves, pumps, and motors. It is caused by the collapse of bubbles at or near the solid boundaries. Numerous studies have been made of cavitation erosion, mainly using a vibratory type tester [3−5].

In relation to erosion in hydraulic equipment, impingement of a cavitating jet is the dominant cause. Lichtarowicz [6–8] proposed a submerged cavitating jet apparatus to evaluate materials for erosion. Subsequently, Kleinbreuer [9], Yamaguchi and Shimizu [10–16], and others [17–21] studied jet-cavitation erosion. In 1990s the method has been established and standardized [22]. Aspects of cavitation erosion, however, can be extremely complicated. Therefore, a strong need remains to better understand its mechanisms.

The author and collaborators have investigated cavitation erosion behavior using the jet cavitation rig. The effects of fluids and materials on erosion were examined. The tested parameters included: cavitation numbers, fluid types such as tap water, mineral oils and high-water-content fluids (HWCF), nozzles [15] and specimen configuration [13], pressure pulsation [14] and material properties [16] of the specimens. Additionally, Yamaguchi proposed a method to predict and estimate erosion caused by impingement of cavitating jets [23,24].

Because water is amenable to the natural environment and humans, tap water and biodegradable oils have gradually replaced mineral-based hydraulic oils in some applications. Because of differences in fluids' physical properties, alternative working fluids cause many serious problems related mainly to cavitation and tribology.

Water-hydraulic systems have begun to be developed in recent years. A salient problem is that cavitation erosion by water is more severe than that by oil. The reason for the intense cavitation caused by water is that higher vapor pressure and lower viscosity of water than oil result in easier inception of cavitation and stronger intensity of bubble collapse.

Biodegradable oils are used as working fluids, especially in construction machinery in European countries. Using a vibratory type rig, Meged *et al*. [25] and Pai and Hargreaves [26] investigated the cavitation erosion of biodegradable oils. However, less information on jet cavitation erosion is available and the use of biodegradable oils as an alternative to hydraulic fluids is not yet completely understood.

The objective of this paper is to evaluate the influence of differences in fluids on cavitation erosion experimentally using a jet cavitation rig. Tap water, biodegradable oils and mineral oils were prepared as test liquids, and the effects of the liquid temperature, upstream pressure, cavitation number and the standoff distance on the cavitation erosion were examined in detail.

2 TEST RIG AND EXPERIMENTAL PROCEDURE

2.1 Test method

The vibratory method offers advantages of ready exchangeability of test liquids as well as a compact apparatus; for those reasons, the method is widely used. Cavitation erosion in hydraulic equipment, however, is basically caused by impingement attributable to a submerged cavitating jet and the collapse of bubbles near the walls. Aside from this, the author and collaborators have shown that some discrepancies exist in results between the

vibratory and jet cavitation methods [16]. Therefore, an experiment using the cavitating jet apparatus is fundamentally necessary for examining cavitation erosion in hydraulic equipment.

The apparatus and test procedures used for this work are similar to ASTM standards [22], but with partially differing geometry and test conditions. Deviation of the tests used here relative to these standards is similar to that described in papers by Yamaguchi and Shimizu [10,11].

2.2. Experimental apparatus

The hydraulic circuit for testing erosion by tap water, shown in Fig. 1, included a test chamber, a hydraulic pump with an electric motor, and auxiliary accessories including valves, a cooler, a filter, pressure gages, and a thermometer. The maximum pressure and discharge of the pump were, respectively, 19 MPa and 2.8×10^{-4} $m^3 \cdot s^{-1}$. An online filter with nominal filtration size of 3 μm was used to remove contaminants from the test liquid. A cooler capable of maintaining a desired liquid temperature was installed. The circuit for biodegradable and mineral oils was fundamentally similar to that shown in Fig. 1.

The test chamber arrangement is illustrated in Fig. 2 [10,11]; its geometry and materials for tap water and the oils were the same. The stainless steel chamber included the long-orifice nozzle, its holder, the specimen, its mount, and spacers. The inner geometry of the chamber was cylindrical; its diameter was 80 mm. Two transparent windows were provided at both sides of the chamber such that the cavitating jet was observed and photographed. Annular spacers with various thickness enabled adjustment to an arbitrary standoff distance *L*. The diameter and length of the nozzle were, respectively, 1.0 mm and 4.0 mm. The nozzle was bored cylindrically and the inlet was manufactured carefully to provide a very sharp entry edge. It was fixed by a holder with a hollow core of 3-mm diameter.

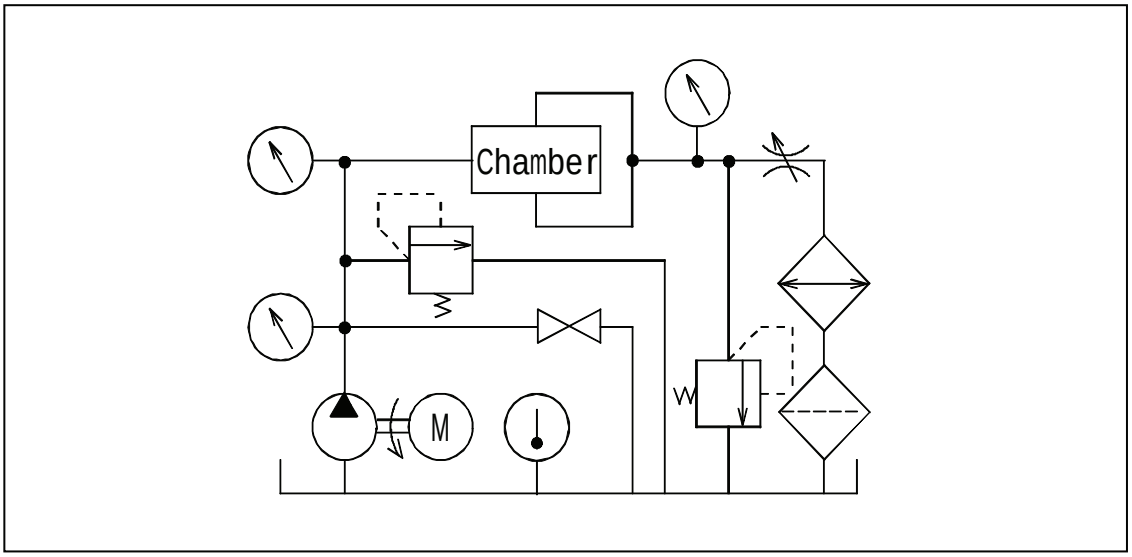

Figure 1 Hydraulic circuit of the test apparatus

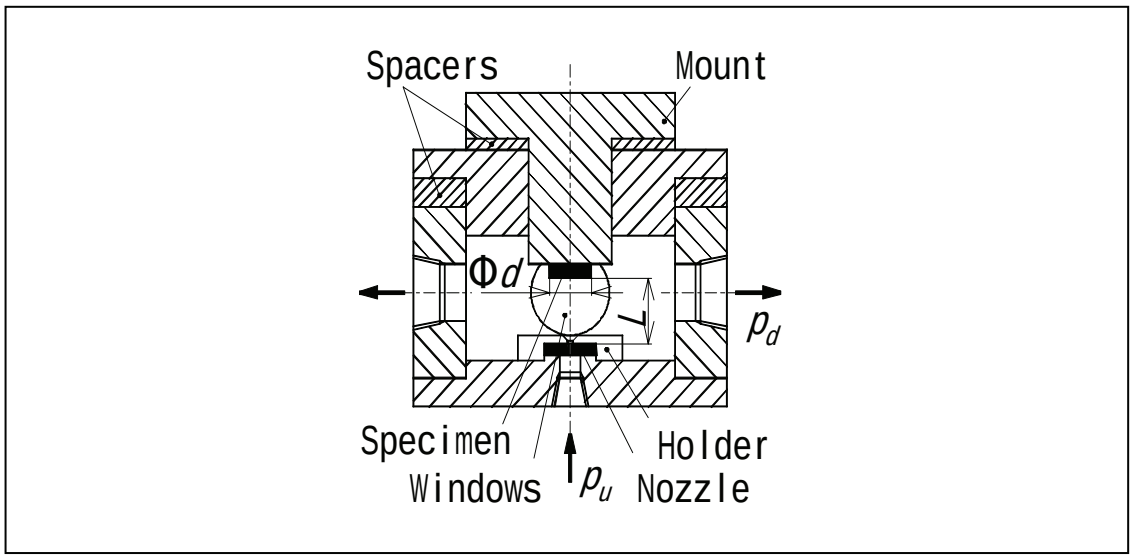

Figure 2 Test chamber

2.3 Test fluid

The liquids tested in this study were: tap water, synthetic ester-type biodegradable oil with the ISO viscosity grade of 46, mineral based hydraulic oils with grades of 32 and 46, which are designated respectively as WAT, BIO, MIN32, and MIN46.

2.4 Specimens

The specimens' diameter d was 15 mm. The specimens were made of aluminum alloy designated as A5056 by Japanese Industrial Standards (JIS) corresponding to AlMg5 in Deutsches Institut für Normung, DIN. The physical and mechanical properties were as follows: the modulus of longitudinal elasticity 69.6 GPa, Vickers hardness 77Hv, micro-Vickers hardness 98Hmv, density of specimens 2730 kg·m^{-3}, yield stress 124 MPa, breaking strength 272 MPa, tensile strength 223 MPa, breaking elongation 30.2% and contraction of area 49.3%. The chemical composition is shown in Table 1.

Table 1 Chemical composition of specimens [%]

Cr	Cu	Fe	Mg	Mn	Si	Ti	Zn	Zr
0.07	0.01	0.09	4.53	0.08	0.08	0.01	0.01	–

2.5 Experimental conditions

The upstream absolute pressure p_u was established as p_u=10.1–18.1 MPa. The cavitation number σ was defined as the ratio of the downstream pressure p_d to the upstream pressure,

i.e. $\sigma=p_d/p_u$; it was set as σ=0.02–0.04. By recirculating the test liquids and installing the coolers online, the temperature T was maintained at T=40–65±1°C.

The standoff distance L was defined by the distance from the edge of the nozzle outlet to the specimen surface, as indicated in Fig. 2. Using the spacers, L was established as L=10–35 mm with intervals of 2.5 mm. The dimensions and conditions are summarized in Table 2.

Table 2 Experimental conditions

Cavitation number	σ	0.02–0.04	
Liquid temperature	T	40–65±1	°C
Liquids	BIO	Biodegradable oil (VG46)	
	MIN	Mineral oils (VG32, VG46)	
	TAP	Tap water	
Nozzle diameter		1.0	mm
Nozzle length		4.0	mm
Specimen diameter		15	mm
Specimen material		Aluminum alloy (A5056 in JIS)	
Standoff distance	L	10–35	mm
Upstream pressure	p_u	10.1–18.1	MPa

2.6 Test procedure of cavitation erosion

The experiment was conducted under the following procedures: At the beginning of each test, the standoff distance L was set and the liquid temperature T was elevated. The specimen was mounted co-axially with the nozzle. The chamber was filled with the liquid. The remaining air and bubbles were then slowly bled from the chamber. The pressurized liquid was supplied from a constant pressure source at p_u. The submerged jet was cavitated through the nozzle and discharged into the chamber at a constant p_d. The cavitating jet was impinged upon the specimen surface. The upstream and downstream pressures as well as the liquid temperature were monitored continuously and controlled precisely to maintain experimental conditions during the tests.

The pump operation was interrupted at regular intervals. The specimen was removed carefully and dried sufficiently for the water test and rinsed with normal hexane for oil tests. The mass was determined using a precision balance with accuracy and sensitivity of 0.1 mg. The sectional profile of the eroded specimen surface was recorded using a contact-type profilometer. Its surface was photographed and observed. These procedures were repeated several times during a specific period of up to eight hours.

2.7 Visualization and picture processing of cavitating jets

The behavior of cavitating jets and the cavitation erosion intensity were correlated experimentally using the same cavitating jet apparatus. The cavity-clouds of the jets were

observed and recorded using video cameras, the existence-probability distributions of the clouds were approximately and simply obtained using the following picture processing techniques. The xenon light source was provided through a mating window by a lamp; consequently, the clouds were illuminated from behind. Using those movies, the pictures were produced using digital capture processes; they were subsequently layered.

3 EXPERIMENTAL RESULTS AND DISCUSSION

3.1 Time evolution of mass loss and the erosion rate

Figures 3 and 4 depict the mass loss M and the erosion rate ER versus exposure time t respectively. The loss M and the rate ER corresponded to the cumulative erosion and the interval erosion rate after ASTM terminology [27,28]. Under identical test conditions, the loss M by tap water was larger on the order of 10^1 than M by both oils; furthermore, ER reached a maximum value within a shorter period of t<1 h. Comparing these two VG46 oils, both M and ER by the mineral oils were slightly larger than those by the biodegradable oil.

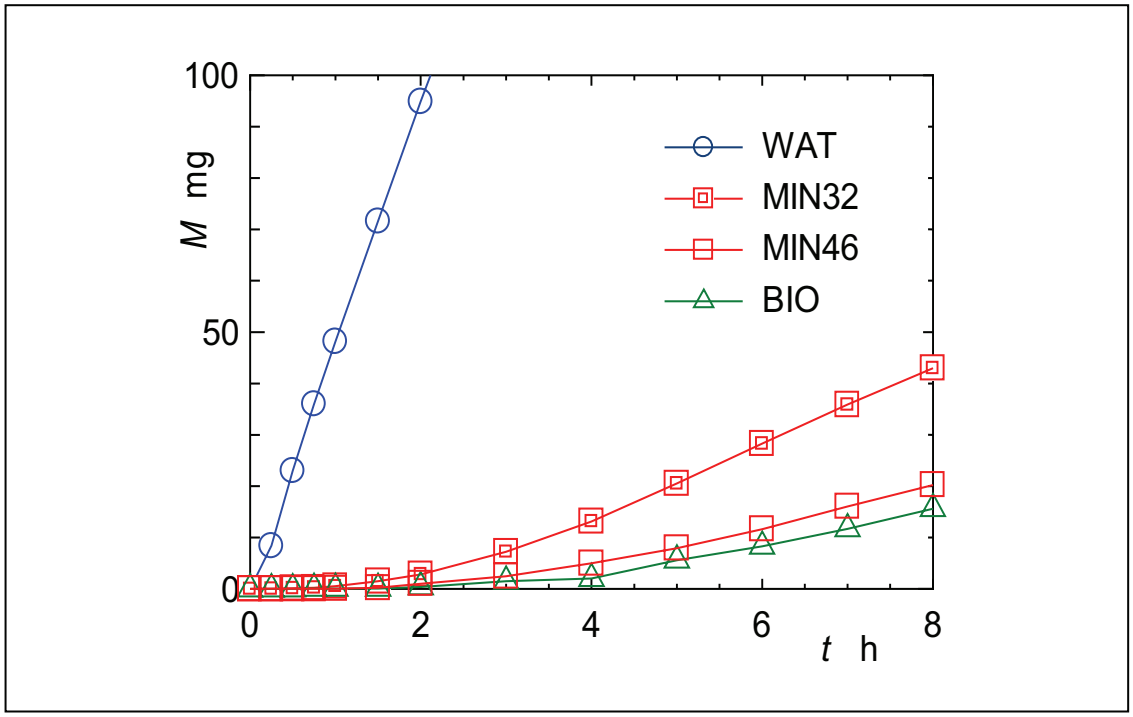

Figure 3 Time evolution of mass loss M (L=25 mm, p_u=10.1 MPa, T=40°C, σ=0.02)

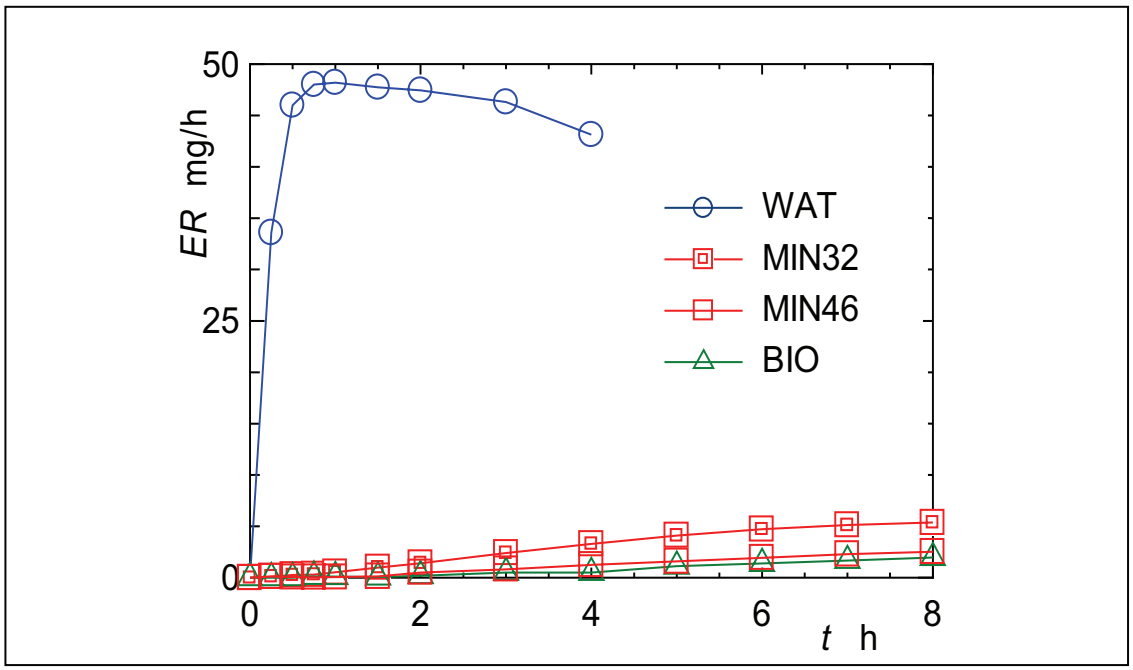

Figure 4 Time evolution of erosion rate *ER* (*L*=25 mm, p_u=10.1 MPa, *T*=40 °C, σ=0.02)

Figure 5 exhibits the loss *M* versus the standoff distance *L* in terms of the cavitation number σ. The tested liquid was the VG32 mineral oil. The maximum loss *M* designated as M_{max}, at the distance *L* of *ca.* 25 mm for the number σ=0.02 and at *L*=20 mm for σ=0.03. For smaller σ, the M_{max} loss was greater and the standoff distance *L* was greater. In addition, uncertainty and repeatability of these data were checked at the standoff distance *L*=25 mm and 30 mm where the mass loss was large; they are plotted in Fig. 5.

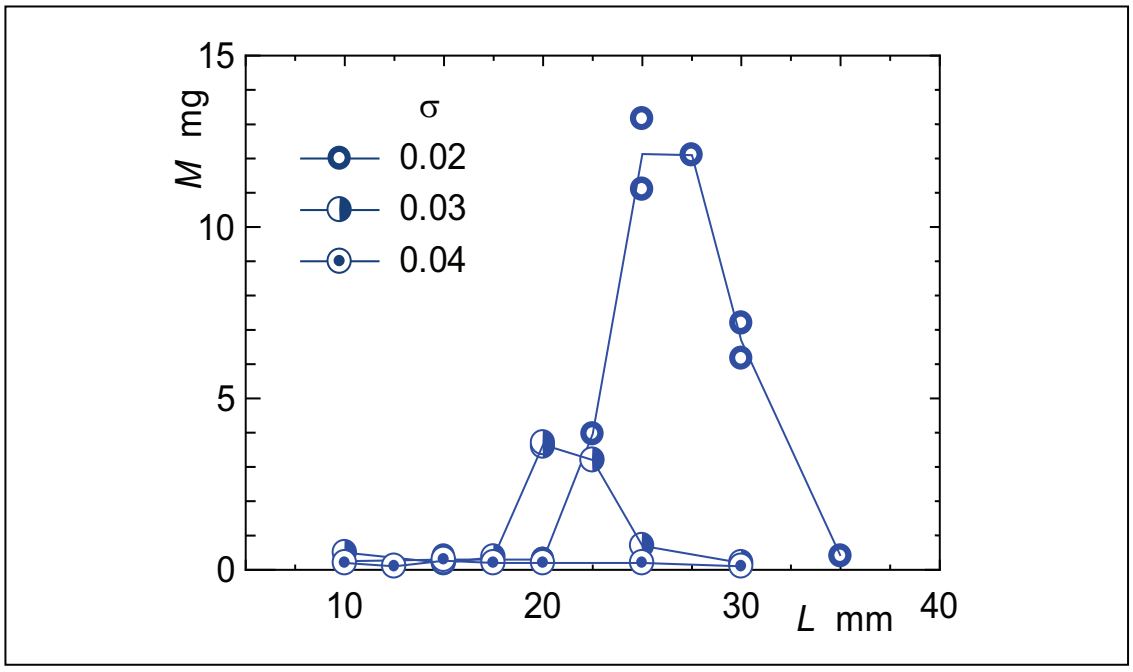

Figure 5 Mass loss *M* vs. standoff distance *L* in terms of cavitation number σ (MIN32, p_u=10.1 MPa, *T*=40°C, *t*=4 h)

A comparison of the biodegradable and mineral oils for the mass loss M at the exposure time t=8 h is shown in Fig. 6. The maximum M_{max} by the mineral oil with VG32 was 2.8 times larger than M_{max} by the biodegradable oil with VG46, but the distances L of these oils mutually coincided. The standoff distances L at which the mass loss (M_{max}) was maximized were 25 mm for all oils.

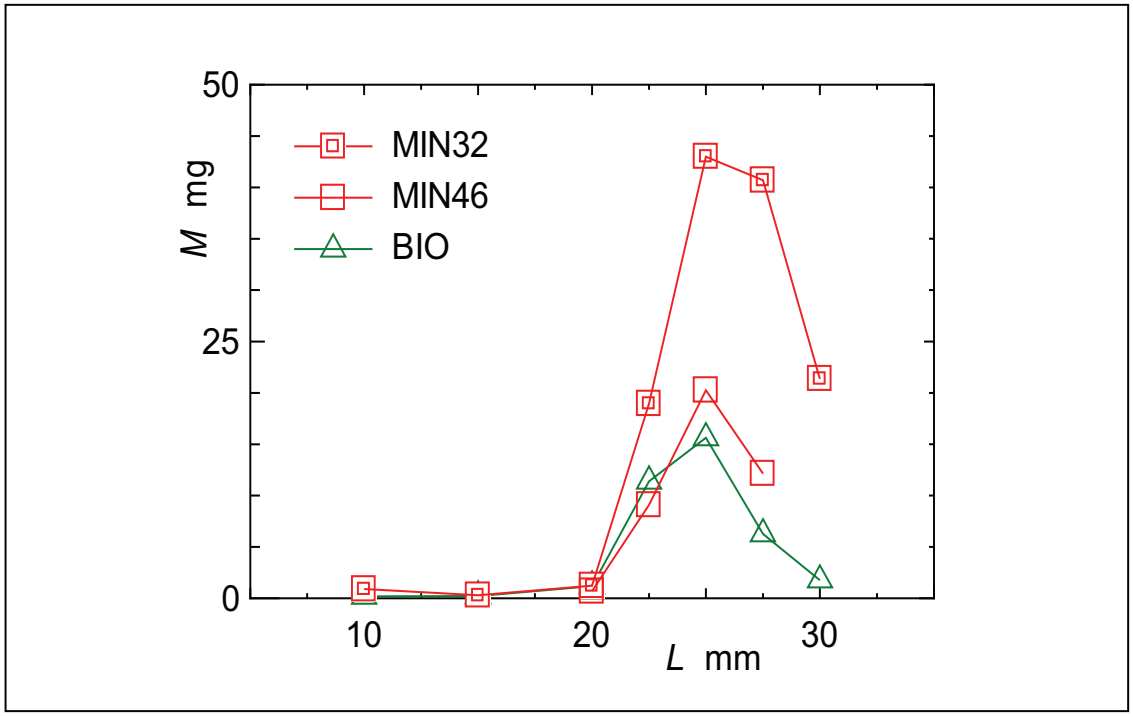

Figure 6 Comparison of mass loss M for standoff distance L (p_u=10.1 MPa, T=40°C, t=8 h, σ=0.02)

3.2 Erosion rings

Plate 1 shows sequential photographs of the surfaces eroded after four hours' periods of exposure in terms of the cavitation number σ. The specimen surfaces were eroded circumferentially: ring-like [10,11]. The diameter at the deepest valley was defined as the erosion-ring diameter D. One can see that the diameter D became small as the number σ increased.

The diameter D versus the standoff distance L for all liquids tested is plotted in Fig. 7. In particular, D with tap water was larger and D with the biodegradable oil was smaller at long distance L (*ca.* 25 mm), which qualitatively coincided with the relation of the mass loss and the standoff distance. In contrast, D with all liquids was closed in a short distance L.

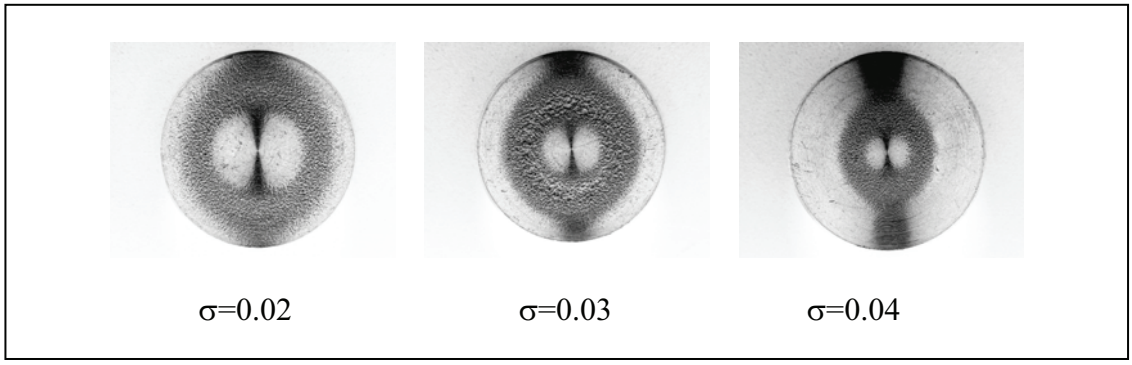

Plate 1 Eroded surfaces of specimens (MIN32, L=20 mm, p_u=10.1 MPa, T=40°C)

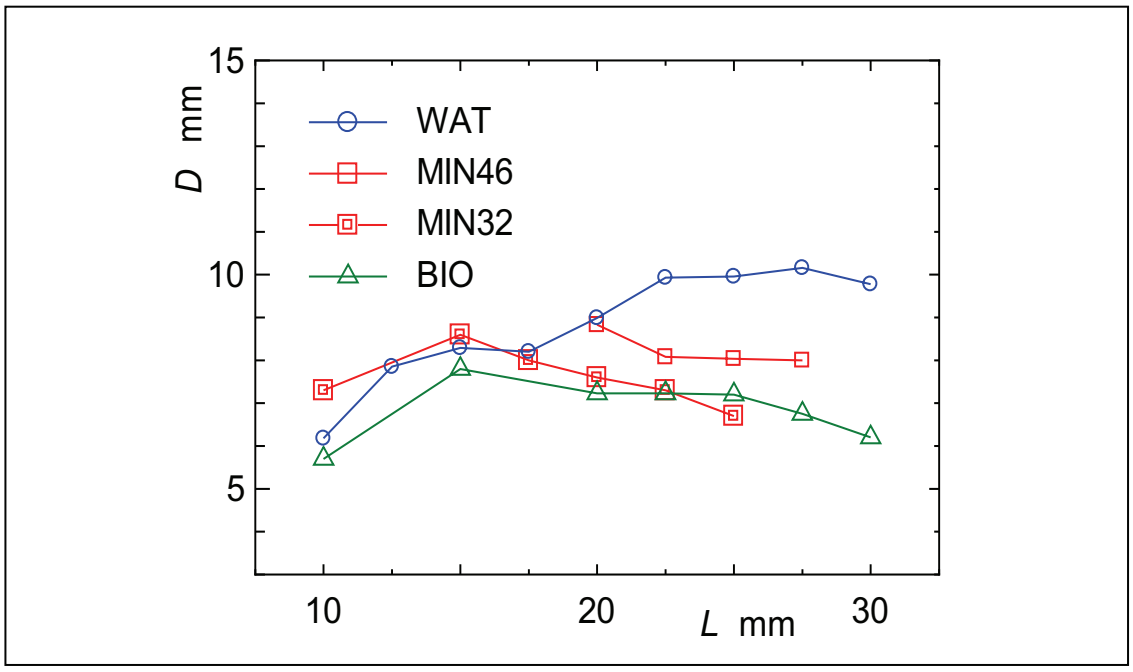

Figure 7 Erosion ring diameter D *vs*. standoff distance L (p_u=10.1 MPa, T=40°C, t=8 h, σ=0.02)

3.3 Comparison of surface damage

Plates 2 and 3 show scanning electron microscope (SEM) fractographs of the eroded surfaces of the specimens for tap water and the mineral oil respectively at four hours' exposure time. The surfaces were visibly damaged because of fatigue fracture, plastic deformation, and striation in these plates. The surfaces had a fine grain look for the case of tap water.

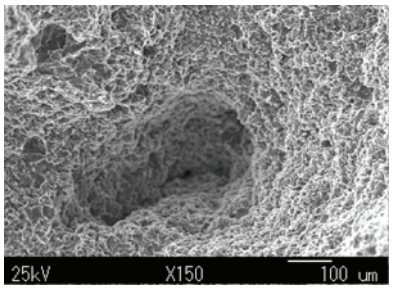

Plate 2 SEM micrograph of the specimen surface (WAT, p_u=10.1 MPa, σ=0.02, L=25 mm, T=40°C, t=4 h)

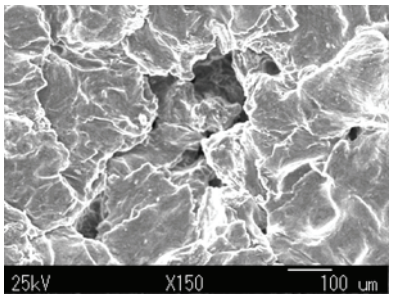

Plate 3 SEM micrograph of the specimen surface (MIN32, p_u=10.1 MPa, σ=0.02, L=25 mm, T=40°C, t=4 h)

3.4 Comparison of cavitating jets

Plate 4 shows processed images of the side-views of the cavitating jet of tap water and the mineral oil (MIN32). At the low cavitation number σ (=0.02), the jets reached far from the nozzle. As the number σ increased, especially for MIN32, the jets were shortened. Over the all number σ, the water jets reached a longer distance than the oil jets.

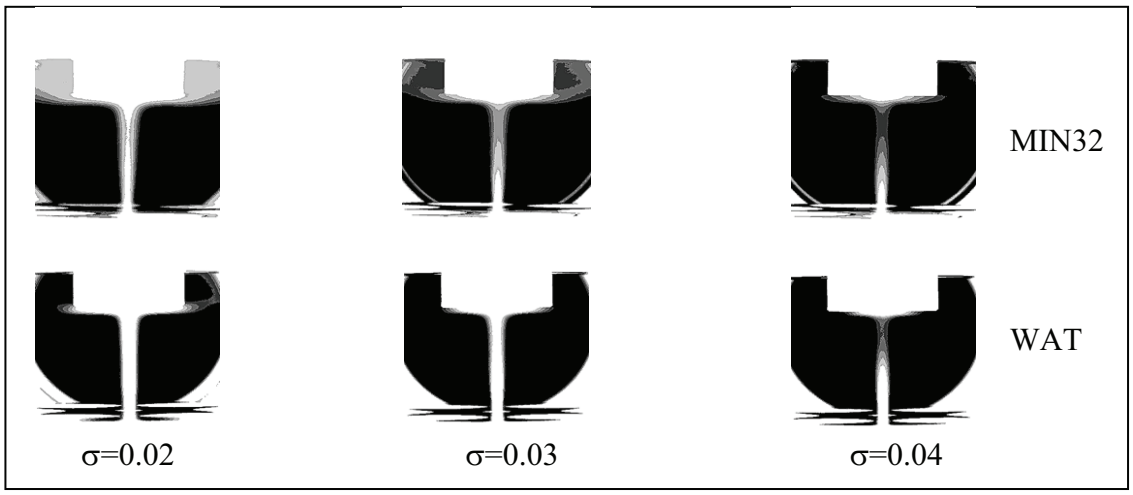

Plate 4 Processed images of cavitating jets of tap water and mineral oil of VG32 (L=20 mm, p_u=10.1 MPa, T=40°C)

3.5 Influence of liquid temperature

Figure 8 demonstrates the effect of the liquid temperature T on the mass loss M of the biodegradable and mineral oils. As the temperature T increased, the loss M became large for all oils, except for M with MIN32 at 60°C. The influences of T on M with MIN46 and BIO were similar, but the influence of T with MIN32 was peculiar.

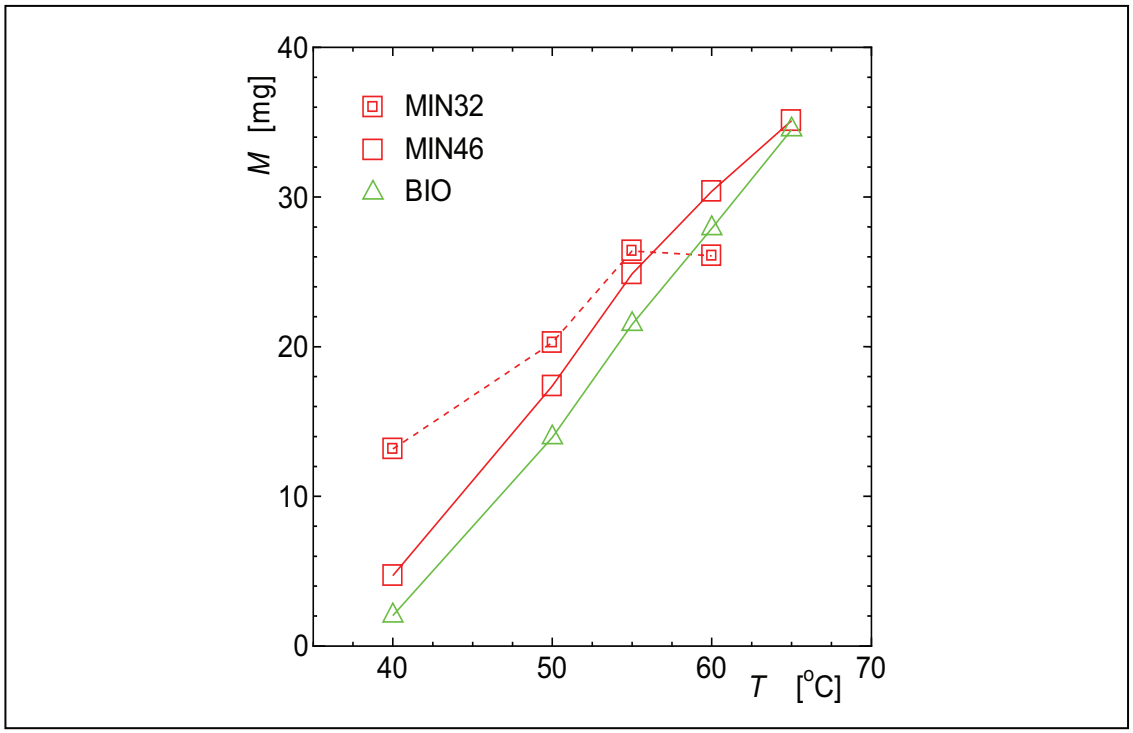

Figure 8 Effect of oil temperature T on mass loss M for biodegradable and mineral oils (L=25 mm, p_u=10.1 MPa, t =4 h, σ=0.02)

3.6 Influence of upstream pressure

Figure 9 provides the maximum of the erosion rate (ER_{max} [mg/h]) within the exposure time $t \leq 8$ h with respect to the upstream pressure p_u [MPa]. Assuming the relation of $ER \propto p_u^n$ and resolving the index n using regression analysis, n=4.4 for the biodegradable oil and n=3.8 for the mineral oil VG32 were obtained.

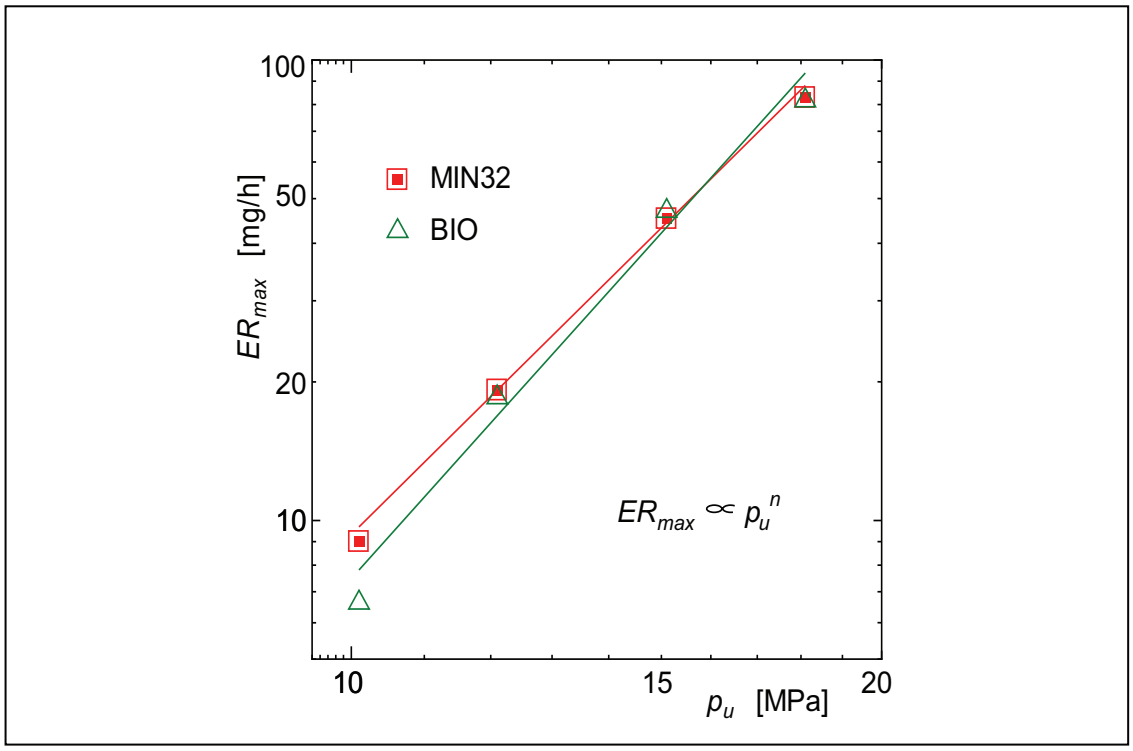

Figure 9 Relation of maximum erosion rate ER and p_u (L=25 mm, T=50 °C, $\sigma \cong 0.02$)

4 CONCLUSIONS

Cavitation erosion experiments were performed using submerged cavitating jets with tap water, synthetic ester-type biodegradable oil, and mineral-based hydraulic oils. In parallel, the cavity-clouds of the jets were observed and recorded with video cameras, and the existence-probability distributions of the clouds were obtained by picture processing techniques. The salient conclusions are the following:

i) The mass loss by tap water was noticeably greater than the loss of all test oils. The loss with the VG32 mineral oil was larger than the loss with the VG 46 oils.

ii) At temperatures of 40–65°C, the mass loss of the oils was greater under higher liquid temperature conditions.

iii) The surfaces were eroded as ring-shaped for all tested liquids. The diameter with tap water was large, but the diameter with the biodegradable oil was small especially at long standoff distances. The eroded surfaces by tap water were markedly rougher than those by oils. The diameter was smaller for larger cavitation number.

iv) The mass loss with the biodegradable oil and the mineral oil was approximately proportional to the fourth power of the upstream pressure.

v) In comparison with the oil-jet, the water-jet reached at the great distance and eroded substantially the specimens. As the downstream pressure decreased, the range of the jet lengthened and the mass loss increased. For the VG32 oil, the correlation between mass loss of the specimens and the processed images of the cavitating jets was obtained.

ACKNOWLEDGEMENTS

The authors express their sincere appreciation to Prof. Emeritus Atsushi Yamaguchi of Yokohama National University and to Prof. Emeritus Mitsuru Fujiwara of Muroran Institute of Technology for their thoughtful encouragement. They also thank Messrs. T. Goto, Y. Fukuchi, J. Yamada, and K. Sanpei of the students of Muroran Institute of Technology for their cooperation in performing the experiment. This research was partially supported by a Ministry of Education, Culture, Sports, Science and Technology of Japan Grant-in-Aid for Scientific Research (C), 2001–2003.

APPENDIX NOMENCLATURE

BIO	Biodegradable oil
D	Erosion ring diameter [mm]
ER	Mass erosion rate [mg/h]
L	Standoff distance [mm]
MIN	Mineral oil
p_d	Downstream absolute pressure [MPa]
p_u	Upstream absolute pressure [MPa]
T	Liquid temperature [°C]
t	Exposure time [h]
WAT	Tap water
σ	Cavitation number $=p_d/p_u$

REFERENCES

[1] M.S. Plesset and R.E. Devine, Effect of Exposure Time on Cavitation Damage, *J. Basic Engineering, Trans. ASME,* 88 (1966), 691–705.
[2] R.T. Knapp, J.W. Daily and F.G. Hammitt, Cavitation, (1970), *McGraw-Hill*.
[3] K. Endo, T. Okada, T. Nakano and M. Nakajima, A Study of Erosion between Two Parallel Surfaces Oscillating in Close Distance in Liquids (Especially on the Failure of Lined Bearing Metal), *Trans. JSME*, 32 (1966), 831–841 (in Japanese).
[4] J.M. Hobbs, Experience with a 20-kc Cavitation Erosion Test, Erosion by Cavitation or Impingement, *ASTM Special Technical Publication*, 408 (1967), 159–185.
[5] ASTM, Standard Method of Vibratory Cavitation Erosion Test, *Annual Book ASTM Standards*, G32–85, 03.02. (1989), 142–147.
[6] A. Lichtarowicz, Use of a Simple Cavitating Nozzle for Cavitation Erosion Testing and Cutting, *Nature: Physical Science*, 239–91 (1972), 63–64.
[7] A. Lichtarowicz, Cavitating Jet Apparatus for Cavitation Erosion Testing, *ASTM Special Technical Publication*, 664 (1979).

[8] A. Lichtarowicz and P. Kay, Erosion Testing with Cavitating Jets, *Proc. 6th International Conference on Erosion by Solid and Liquid Impact*, (1983), 15.1–15.4.
[9] W. Kleinbreuer, Kavitationserosion in Hydraulischen Systemen, *Industrie-Anzeiger*, 99–34 (1977), 609–613.
[10] A. Yamaguchi and S. Shimizu, Erosion due to Impingement of Cavitating Jet, *J. Fluids Engineering, Trans. ASME*, 109–4 (1987), 442–447.
[11] S. Shimizu and A. Yamaguchi, Erosion due to Impingement of a Cavitating Jet, *J. Japan Hydraulics and Pneumatics Society*, 19 (1988), 68–75 (in Japanese).
[12] S. Shimizu and A. Yamaguchi, Cavitation Erosion in Hydraulic Oil, HWBFs, and Tap Water, *Proc. 1st JHPS International Symposium on Fluid Power*, (1989), 261–266.
[13] S. Shimizu, A. Yamaguchi and T. Kazama, Erosion due to Impingement of a Cavitating Jet (2nd Report: Effects of Nozzle Holder and Configuration of Impingement Surface), *J. Japan Hydraulics Pneumatics Society*, 22 (1991), 57–62 (in Japanese).
[14] A. Yamaguchi, X. Wang and T. Kazama, Erosion due to Impingement of a Cavitating Jet (4th Report: Effects of Nozzles Shape and Upstream Pressure Pulsation), *J. Japan Hydraulics and Pneumatics Society*, 28–3 (1997), 353–358 (in Japanese).
[15] T. Kazama and A. Yamaguchi, Effects of Configuration of Nozzles, Outlets of Nozzles and Specimens on Erosion due to Impingement of a Cavitating Jet, *Proc. 48th National Conference on Fluid Power*, (2000), 263–272.
[16] A. Yamaguchi, T. Kazama, K. Inoue and J. Onoue, Comparison of Cavitation Erosion Test Results between Vibratory and Cavitating Jet Methods, *Intern. J. Fluid Power*, 2-1 (2001), 25–30.
[17] T. Momma and A. Lichtarowicz, A Study of Pressures and Erosion Produced by Collapsing Cavitation, *Wear*, 186–187(2) (1995), 425–436.
[18] H. Soyama, A. Lichtarowicz, T. Momma and E.J. Williams, A New Calibration Method for Dynamically Loaded Transducers and Its Application to Cavitation Impact Measurement, *J. Fluids Engineering, Trans. ASME*, 120–4, (1998), 712–718.
[19] J. Steller, International Cavitation Erosion Test and Quantitative Assessment of Material Resistance to Cavitation, *Wear*, 233–235 (1999), 51–64.
[20] B.S. Mann and V. Arya, An Experimental Study to Correlate Water Jet Impingement Erosion Resistance and Properties of Metallic Materials and Coatings, *Wear*, 253 (2002), 650–661.
[21] S. Hattori, Y. Goto and T. Fukuyama, Influence of Temperature on Erosion by a Cavitating Liquid Jet, *Wear*, 260 (2006), 1217–1223.
[22] ASTM, Standard Test Method for Erosion of Solid Materials by a Cavitating Liquid Jet, *Annual Book ASTM Standards*, G134.95 (1995), 529–540.
[23] A. Yamaguchi, Prediction of Erosion due to Impingement of a Cavitating Jet (1st Report: Size and Number of Bubbles at Outlet of Long Orifices), *Trans. JSME*, B 60–577 (1994), 2945–2949 (in Japanese).
[24] A. Yamaguchi, Prediction of Erosion due to Impingement of a Cavitating Jet (2nd Report: Bubble Dynamics and Erosion Rate), *Trans. JSME*, B 60–577 (1994), 2950–2954 (in Japanese).
[25] Y. Meged, C.H. Venner and W.E. Ten Napel, Classification of Lubricants According to Cavitation Criteria, *Wear*, 186–187 (1995), 444–453.

[26] R. Pai and D.J. Hargreaves, Performance of Environment–friendly Hydraulic Fluids and Material Wear in Cavitating Conditions, *Wear*, 252 (2002), 970–978.
[27] ASTM, Standard Terminology Relating to Wear and Erosion, G40–88 (1988).
[28] ASTM, Characterization and Determination of Erosion Residence, (1970), 29–47.

ON THE PRESSURE PEAK MINIMIZATION IN DIGITAL HYDRAULICS

Arto Laamanen, Matti Linjama and Matti Vilenius
Tampere University of Technology
Institute of Hydraulics and Automation
P.O.Box 589
33101 Tampere, Finland
Phone + 358 3115 2197
E-mail: arto.laamanen@tut.fi

ABSTRACT

Non-ideal on/off valves may cause coincidentally pressure peaks in digital hydraulics. The risk of pressure peaks depends on the coding scheme of the digital hydraulic valve system. Traditional Pulse Code Modulation (PCM) control based on the binary coding has high risk for pressure peaks whereas in Pulse Number Modulation (PNM) control pressure peaks does not occur at all. However, PNM is not yet a solution for pressure peak problem in digital hydraulics due to some technical issues. Instead, Fibonacci coding is a compromise between the above systems and it can ease pressure peak problem in digital hydraulics. Together with coding, controller has also an influence on pressure peaks. Cost function based controller can take into account the risk of pressure peaks in different state transitions and the bad state transitions can be avoided. In this study, a cost function for pressure peak minimization is utilized in a binary and Fibonacci coded valve system based on Separate Meter-In and Separate Meter-out (SMISMO) control. Suitability of different coding schemes is evaluated and the effects of controller parameters on pressure peaks are experimentally studied.

KEYWORDS: Digital hydraulics, Pulse Code Modulation, pressure peaks, Fibonacci coding

1 INTRODUCTION

High quality and energy efficient motion control system is possible to implement with digital hydraulic valve system which utilizes only simple on/off valves [1-3]. In spite of the several advantages, digital hydraulic system based on the Pulse Code Modulation (PCM) still has some challenges like the risk of pressure peaks [4,5].

The risk of pressure peaks exists always in PCM control systems where a number of non-ideal on/off valves are connected in parallel and the flow capacities of the different valves are set according to binary series (Figure 1). It is possible to achieve 2^n-1 (Figure 2) different flow rates in the system of this type, but this requires that valves must sometimes be closed and opened simultaneously. Switching times of the available commercial on/off valves are not constant and in the worst case, some valves may close before the next ones open (or vice versa) when the opening of the valves (=state) is changed. As a result, a short period undesired flow rate error occurs which may cause a pressure peak. Flow rate error originates from the uncertainty of the valve timing which causes uncertainty for the opening of the digital flow control unit (DFCU) as shown in Figure 3. Flow rate error is reduced as well as pressure peaks if one or the other of these uncertainties can be minimized, (Figure 3).

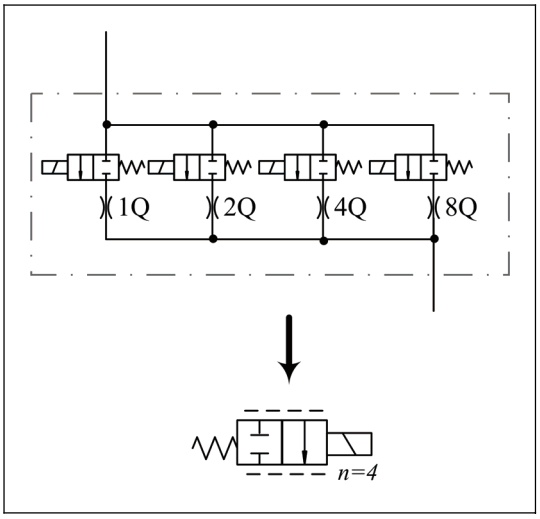

Figure 1. Digital flow control unit (DFCU) and its simplified drawing symbol. Q is one flow unit and *n* is the number of valves.

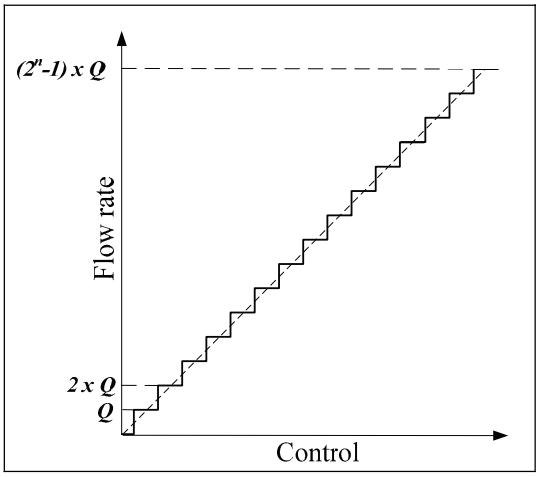

Figure 2. Flow rates of a DFCU.

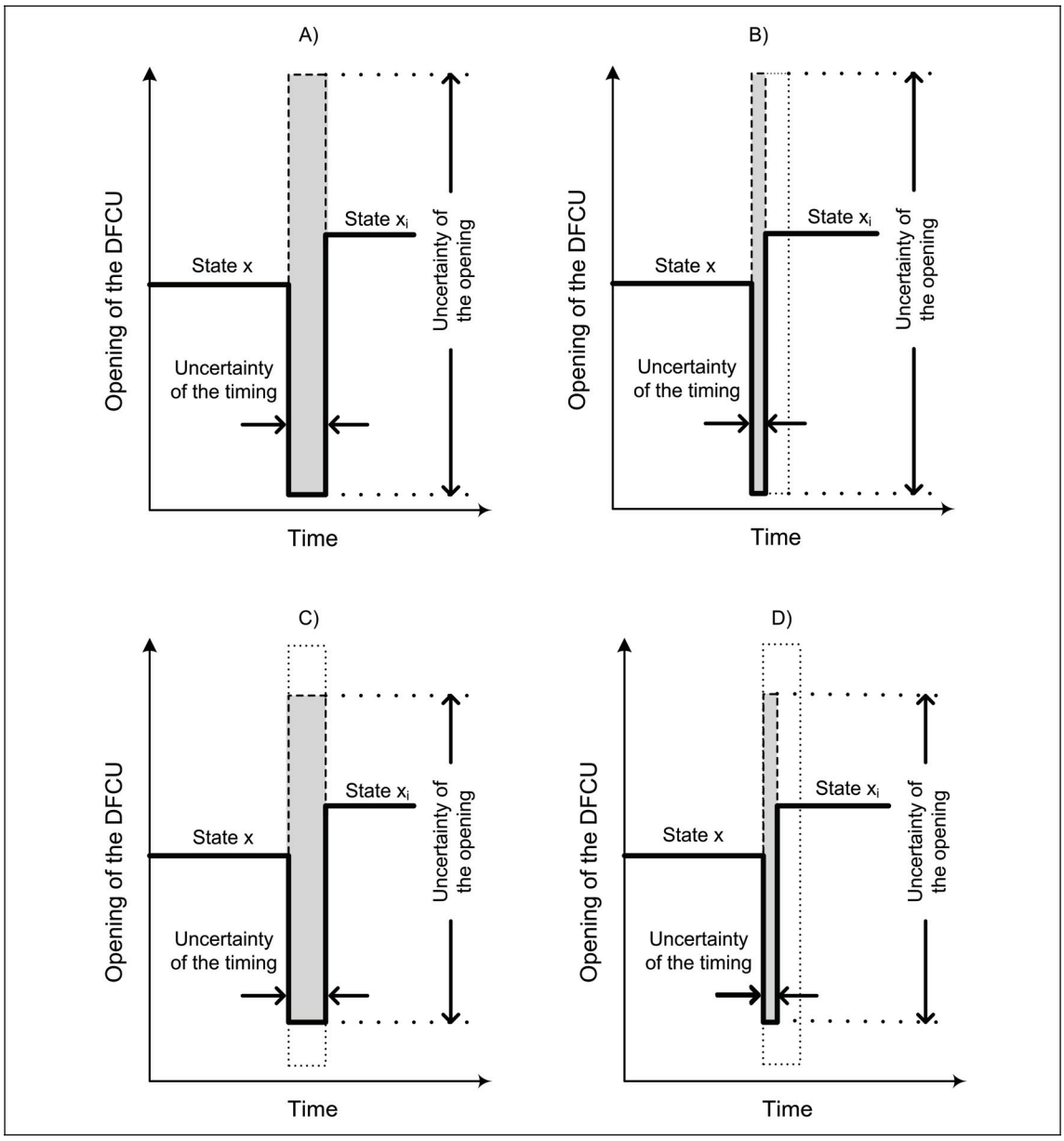

Figure 3. Theoretical state transition x → x_i in a digital hydraulic valve system implemented with extremely fast operating valves. Original flow rate error (A) can be limited by reducing uncertainty of the timing (B) or opening (C) or both (D).

The conventional ways of approaching pressure peak problem are utilization of accumulators or pressure relief valves. Different kind of cushion orifices have been also studied [6], but these solutions cause extra costs or make the dynamic characteristics of the system worse. Certainly, these methods are suitable for digital hydraulics, but it is also possible to take care of pressure peaks by enhancing controller or coding scheme.

Although the first hydraulic PCM control systems are from 1960s [7,8], there are only a few studies published concerning pressure peak analyses and minimization methods in digital hydraulic system. One of them was published by Tanaka in 1988 [9]. He solved the pressure surge problem by employing hysteresis and altering the holding time of the valves. Similar switching time synchronization method has been used also in the recent studies [1-5, 10,11]. This method has shown its effectiveness in oil and water hydraulic

systems, but development work is still needed because it is difficult to implement synchronization perfectly.

Digital hydraulic valve systems are mainly based on the binary coding or its modifications [12], but for example Fibonacci coding could be a solution for pressure peak problem as introduced by Laamanen et al 2003 [10]. In this paper, Fibonacci coded DFCUs are compared to a binary coded valve system in a Separate Meter-In and Separate Meter-Out (SMISMO) controlled system. Controller has important role in digital hydraulics and in this study, it is based on the controller published by Linjama, M. & Vilenius, M. [1]. As a difference, in this study the controller is configured with a pressure peak minimization option [5]. Suitability of the pressure peak minimization methods are evaluated based on the experimental measurements in a mobile hydraulic boom mock-up. Motion control characteristics of the system are not the finest but the main target of this study is to concentrate on the pressure peak phenomenon.

2 MINOR PRESSURE PEAKS BY MINIMIZING UNCERTAINTY OF THE DFCU OPENING.

Pressure peak problem would not exist in digital hydraulics if the ideal on/off valves were used. This is based on the fact that without switching time variation simultaneous valve openings and closings can be synchronized perfectly and flow rate error does not occur in any case. Synchronization is difficult to get completed with the available non-ideal commercial valves and therefore, some alternative ways to limit pressure peaks are worth taken into the consideration. Based on the theoretical study [4], pressure peaks can be minimized by limiting uncertainty of the DFCU opening. This is possible to implement by coding scheme or controller as introduced below.

2.1 Coding Scheme

Flow rates of the different valves in DFCU have been originally based on the binary series, i.e. binary coding (Table 1). The main advantage of binary coding is high resolution, but unfortunately it has a high risk for pressure peaks, too [4,5]. Binary coding is not the only coding scheme, but there are also several other possible coding schemes which could offer solution for pressure peak problem.

Pulse Number Modulation (PNM) is the ultimate solution for pressure peak problem in digital hydraulics. PNM is based on the same sized parallel connected valves and it does not have risk for similar pressure peaks as in binary coded valve system. This is based on the fact that valves are either opened or closed simultaneously but not both. The key technical issue of PNM coding scheme is that the good resolution requires a large number of valves. For example, same resolution as with four valves in binary coded system requires in PNM system 15 valves (Table 1). So far, over ten valves per DFCU are not accepted in most applications due to size problem and thus, some other alternatives are worth thinking. One of them is Fibonacci coding, which is a compromise between binary coding and PNM. It offers more potential to limit pressure peaks than binary coding, but it does not need as much valves as the system based on PNM coding (see Tables 1 & 2).

Table 1. Opening combinations of the valves in a binary coded DFCU and PNM system.

Binary DFCU

Net flow	Valve 1, Q	Valve 2, 2Q	Valve 3, 4Q	Valve 4, 8Q	State
0	0	0	0	0	0
1xQ	1	0	0	0	1
2xQ	0	1	0	0	2
3xQ	1	1	0	0	3
4xQ	0	0	1	0	4
5xQ	1	0	1	0	5
6xQ	0	1	1	0	6
7xQ	1	1	1	0	7
8xQ	0	0	0	1	8
9xQ	1	0	0	1	9
10xQ	0	1	0	1	10
11xQ	1	1	0	1	11
12xQ	0	0	1	1	12
13xQ	1	0	1	1	13
14xQ	0	1	1	1	14
15xQ	1	1	1	1	15

PNM DFCU

Net flow	Valve 1, Q	Valve 2, Q	Valve 3, Q	Valve 4, Q	Valve 5, Q	Valve 6, Q	Valve 7, Q	Valve 8, Q	Valve 9, Q	Valve 10, Q	Valve 11, Q	Valve 12, Q	Valve 13, Q	Valve 14, Q	Valve 15, Q
0	0	0	0	0	0	0	0	0	0	0	0	0	0	0	0
1xQ	1	0	0	0	0	0	0	0	0	0	0	0	0	0	0
2xQ	1	1	0	0	0	0	0	0	0	0	0	0	0	0	0
3xQ	1	1	1	0	0	0	0	0	0	0	0	0	0	0	0
4xQ	1	1	1	1	0	0	0	0	0	0	0	0	0	0	0
5xQ	1	1	1	1	1	0	0	0	0	0	0	0	0	0	0
6xQ	1	1	1	1	1	1	0	0	0	0	0	0	0	0	0
7xQ	1	1	1	1	1	1	1	0	0	0	0	0	0	0	0
8xQ	1	1	1	1	1	1	1	1	0	0	0	0	0	0	0
9xQ	1	1	1	1	1	1	1	1	1	0	0	0	0	0	0
10xQ	1	1	1	1	1	1	1	1	1	1	0	0	0	0	0
11xQ	1	1	1	1	1	1	1	1	1	1	1	0	0	0	0
12xQ	1	1	1	1	1	1	1	1	1	1	1	1	0	0	0
13xQ	1	1	1	1	1	1	1	1	1	1	1	1	1	0	0
14xQ	1	1	1	1	1	1	1	1	1	1	1	1	1	1	0
15xQ	1	1	1	1	1	1	1	1	1	1	1	1	1	1	1

Table 2. Opening combinations of the valves in Fibonacci coded DFCU. States are named according to binary system.

Combination 1

Net flow	Valve 1, Q	Valve 2, Q	Valve 3, 2Q	Valve 4, 3Q	Valve 5, 5Q	State
0	0	0	0	0	0	0
1xQ	1	0	0	0	0	1
2xQ	0	0	1	0	0	4
3xQ	0	0	0	1	0	8
4xQ	0	1	0	1	0	10
5xQ	0	0	0	0	1	16
6xQ	0	1	0	0	1	18
7xQ	0	0	1	0	1	20
8xQ	0	0	0	1	1	24
9xQ	0	1	0	1	1	26
10xQ	0	0	1	1	1	28
11xQ	0	1	1	1	1	30
12xQ	1	1	1	1	1	31

Combination 2

Valve 1, Q	Valve 2, Q	Valve 3, 2Q	Valve 4, 3Q	Valve 5, 5Q	State
-	-	-	-	-	
0	1	0	0	0	2
1	1	0	0	0	3
0	1	1	0	0	6
1	1	1	0	0	7
1	1	0	1	0	11
0	1	1	1	0	14
1	1	1	1	0	15
0	1	1	0	1	22
1	1	1	0	1	23
1	1	0	1	1	27
1	0	1	1	1	29
-	-	-	-	-	

Combination 3

Valve 1, Q	Valve 2, Q	Valve 3, 2Q	Valve 4, 3Q	Valve 5, 5Q	State
-	-	-	-	-	
-	-	-	-	-	
-	-	-	-	-	
1	0	1	0	0	5
1	0	0	1	0	9
0	0	1	1	0	12
1	0	0	0	1	17
1	1	0	0	1	19
1	0	1	0	1	21
1	0	0	1	1	25
-	-	-	-	-	
-	-	-	-	-	
-	-	-	-	-	

Combination 4

Valve 1, Q	Valve 2, Q	Valve 3, 2Q	Valve 4, 3Q	Valve 5, 5Q	State
-	-	-	-	-	
-	-	-	-	-	
-	-	-	-	-	
-	-	-	-	-	
-	-	-	-	-	
-	-	-	-	-	
1	0	1	1	0	13
-	-	-	-	-	
-	-	-	-	-	
-	-	-	-	-	
-	-	-	-	-	
-	-	-	-	-	
-	-	-	-	-	

Table 2 shows that the certain flow rate can be achieved with a number of different valve combinations in a Fibonacci coded valve system. For instance, net flow of combinations Valve 1 + Valve 3, Valve 2 + Valve 3 or Valve 4 is 3×Q. This feature is useful in pressure peak minimization because controller has more options to avoid state transitions where is a higher risk for pressure peaks.

2.2 Cost Function Based Controller for Pressure Peaks Limitation

There are hundreds or even millions of different valve combinations in a four way digital hydraulic valve system. In order to find the most suitable combinations, cost function based controller is useful. The fundamental aim of the cost function in pressure

peak limitation is to eliminate state transitions which may cause pressure peaks. A case of this type is for example state transition where several valves of the DFCU are closed and opened simultaneously, such as in state transitions 7↔8 ([1 2 4 0]↔[0 0 0 8]) or 6↔9 ([0 2 4 0]↔[1 0 0 8]).

Inferiority of the all possible state transition options can be classified by

$$J_{pp} = (\underline{u}_k \vee \underline{u}_{k-1})^T \cdot \underline{Q}_V - \max(\underline{Q}_V{}^T \cdot \underline{u}_k,\ \underline{Q}_V^T \cdot \underline{u}_{k-1}) \tag{1}$$

This can be included for example into the following cost function:

$$\begin{aligned} J = {} & \left(v_{ref} - v_{ss}\right)^2 + W_\kappa \left(\frac{\kappa_r - \kappa}{\kappa_r}\right)^2 \left|v_{ref}\right| + \\ & W_{sw} \sum_{i=1}^{n} \left(Q_{N,PAi} \left|\Delta u_{PAi}\right| + Q_{N,ATi} \left|\Delta u_{ATi}\right| + Q_{N,PBi} \left|\Delta u_{PBi}\right| + Q_{N,BTi} \left|\Delta u_{BTi}\right|\right) + W_{pp} J_{pp} \left|v_{ref}\right| \end{aligned} \tag{2}$$

This cost function has four terms so that the first one sets penalty for difference between target and calculated steady-state velocity. The second term defines penalty for error in inflow-outflow opening ratio. Target value for inflow-outflow ratio κ_r is derived from cylinder areas and it is tried to follow only at higher velocities. The third term of the function is used to reduce superfluous activity of valves by setting penalty for valve operations multiplied by flow capacities. This term is important especially in the case of Fibonacci coding where the controller may find several valve combinations which realize target velocity relatively well. The last term is intended for pressure peak minimization as introduced above. Weighing parameters W_κ, W_{sw} and W_{pp} are used for finding an optimal compromise between different characteristics. Block diagram of the controller is shown in Figure 4.

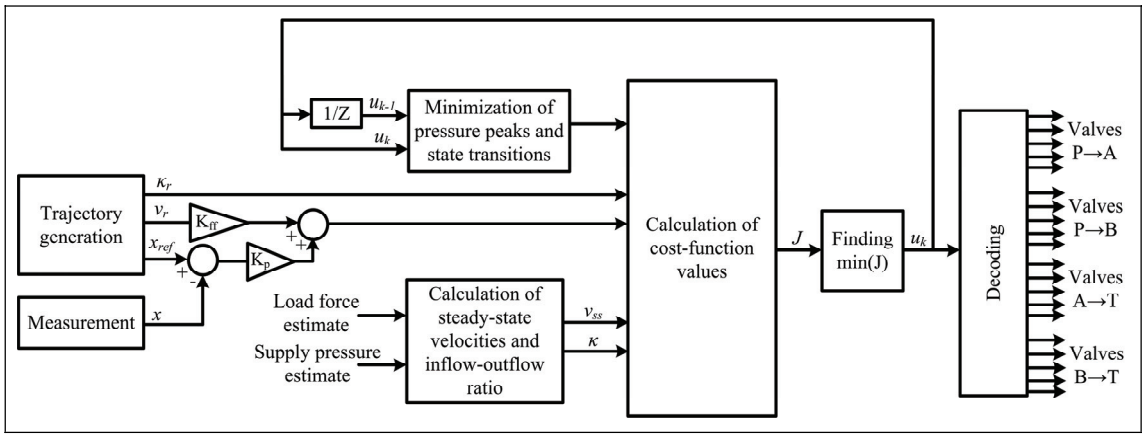

Figure 4. Block diagram of the controller.

3 TEST SYSTEM

3.1 Boom Mock-up

Pressure peak minimization methods are studied in a boom mock-up which mimics the dynamics of the joint actuator of a typical medium sized mobile machine boom. Design as well as static and dynamic characteristics of the system are introduced by Linjama & Vilenius [1]. Test system with the hydraulic circuit diagram is shown in Figure 5.

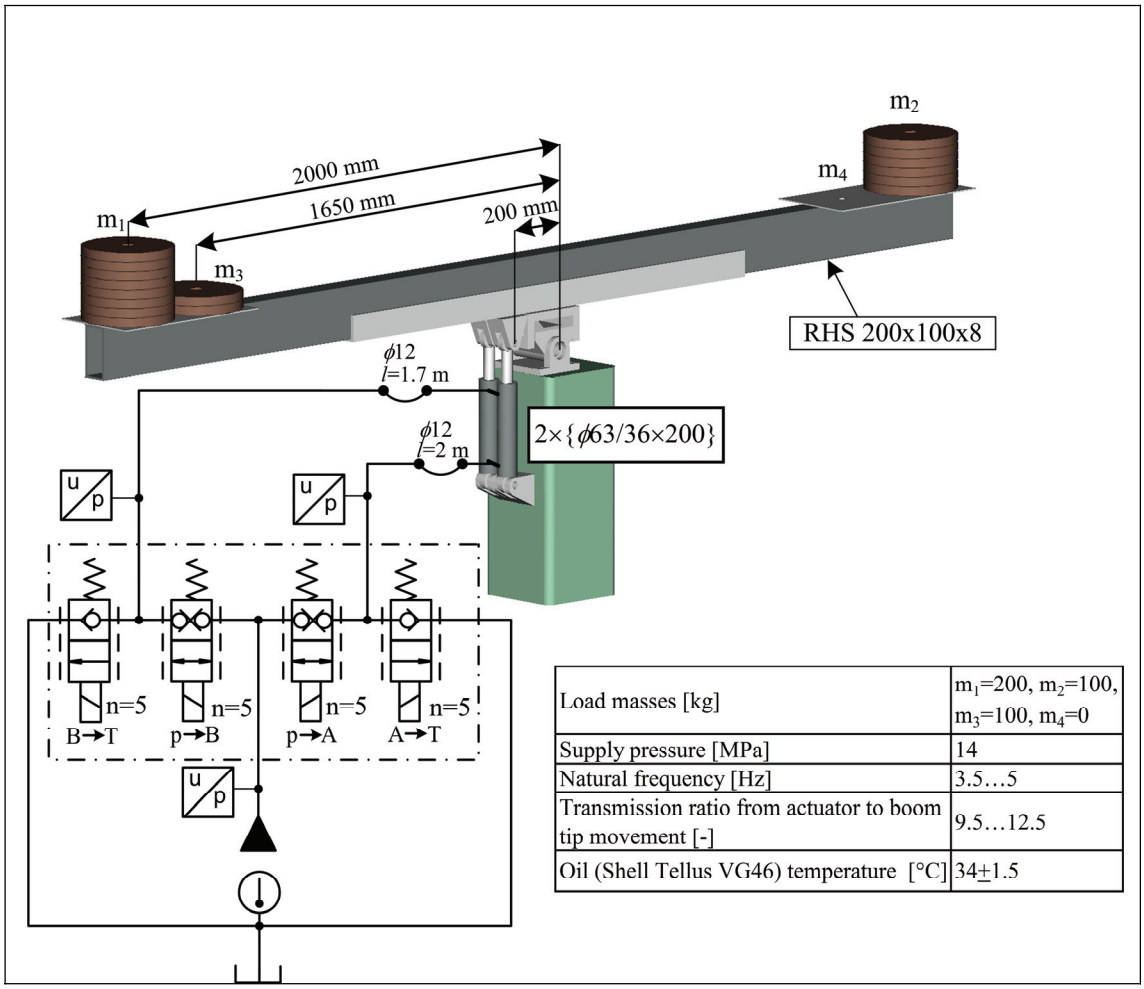

Load masses [kg]	m_1=200, m_2=100, m_3=100, m_4=0
Supply pressure [MPa]	14
Natural frequency [Hz]	3.5…5
Transmission ratio from actuator to boom tip movement [-]	9.5…12.5
Oil (Shell Tellus VG46) temperature [°C]	34±1.5

Figure 5. Joint actuator with a digital hydraulic valve system.

3.2 Valves and Control Electronics

Pilot-operated normally closed screw-in cartridge valves are used in the four DFCUs. Pressure side is implemented with bidirectional valves and the tank side with unidirectional valves as shown in Figure 5. Nominal flow rate of the valves is 19 l/min at 0.5 MPa pressure differential and maximum operating pressure is 21 MPa. Ideal viscosity of the valves is 15-50 cSt. [13]

The control hardware consists of a dSPACE DS1006 controller board with 2.2 GHz AMD main processor. The valve control electronics has been implemented by low-side Smart Power MOSFETs (International Rectifier IPS0151) which are controlled directly by TTL outputs of the dSPACE system.

3.3 Flow Capacities of the Valves in Different Coding Schemes

A fair comparison between binary and Fibonacci coded systems is difficult to complete [4,5]. Flow capacity of the smallest valve fixes resolution (~step size) and the number of valves together with coding scheme determines maximum flow capacity. In the case studied, sizing of the compared DFCUs is based on the same size smallest valves which offer identical step size. Force pulsations caused by the required load acceleration or deceleration depend partly on the step size and accordingly, this arrangement should give a good basis for the fair comparison. However, equal maximum flow capacity cannot be implemented with the same number of valves in binary and Fibonacci coded systems. Four valves offer adequate flow capacity for the binary coded DFCUs, but in the Fibonacci coded DFCUs five valves are needed.

Table 3 introduces flow capacities of the all four DFCUs (P→A, A→T, P→B, B→T) in Fibonacci and binary coded systems. Flow capacities in the pressure side are measured at 2 MPa pressure differentials (p_s=10 MPa, p_T=8 MPa) and in the tank side at 5 MPa pressure differentials (p_s=55 MPa, p_T=0.5 MPa). Diameters of the chosen orifices are in binary coded DFCUs P→A & P→B [1.2, 1.5, 2.4, 3.1] mm, A→T & B→T [1.1, 1.7, 2.2, 3.2] mm and in Fibonacci coded DFCUs P→A & P→B [1.2, 1.2, 1.5, 1.9, 2.5] mm, A→T & B→T [1.1, 1.1, 1.7, 2.0, 2.5] mm.

Table 3. Estimated flow capacities of the valves in binary and Fibonacci coded DFCUs at 0.1 MPa pressure difference.

Binary coded DFCUs

	Optimal net flow	P→A	A→T	P→B	B→T
Valve 1	Q x 1	0,69	0,67	0,70	0,69
Valve 2	Q x 2	1,29	1,35	1,34	1,38
Valve 3	Q x 4	2,62	2,82	2,62	2,87
Valve 4	Q x 8	4,87	5,19	4,87	5,12
ΣQ:	Q x 15	9,48	10,03	9,53	10,06

Fibonacci Coded DFCUs

	Optimal net flow	P→A	A→T	P→B	B→T
Valve 1	Q x 1	0,68	0,66	0,68	0,68
Valve 2	Q x 1	0,69	0,67	0,70	0,69
Valve 3	Q x 2	1,29	1,35	1,34	1,38
Valve 4	Q x 3	1,95	2,12	1,98	2,15
Valve 5	Q x 5	3,32	3,26	3,31	3,25
ΣQ:	Q x 12	7,94	8,07	8,00	8,15

Table 3 shows that the maximum flow capacities of the compared DFCUs are not exactly the same, but close enough. External fixed orifices are used in the outlet side of the valves in order to set required flow capacities. They are available at intervals of 0.1 mm, which means that flow capacities are not in the ideal ratios.

3.4 Switching Times of the Valves

According to information given by the manufacturer, response times of the bidirectional valves are 0.04/0.04 s and unidirectional valves 0.03/0.03 s at nominal pressure and flow rate [13]. Based on the experimental measurements, opening and closing times are not equal [2]. The opening delays seem to vary between 0.010 s and 0.027 s. The closing delays are longer and they vary between 0.015 and 0.040 s. Digital hydraulic valve system usually requires that different opening and closing times of the valves are synchronized with some suitable method. The simplest way is delaying the operation of the fastest valves, but the problem is that switching times of the valves depend on the circumstances. As a result, performance of the basic synchronization method is quite sensitive. In order to avoid any ambiguity for the test results, any synchronization method is not used in this pressure peak study.

3.5 Controller Parameters

Sampling time of the controller is 0.03 s, controller gain K_P 2.5 1/s and feedforward gain K_{FF} 0.8 (Figure 4). Weight for error in inflow-outflow opening ratio is 0.001. The effect of parameters W_{sw} and W_{pp} are studied by altering them.

4 EXPERIMENTAL RESULTS

Evaluation of cost function and coding schemes are based on the test sequence which consists of 90, 100, 110, 120 and 130 mm movements. This sequence is repeated 10 times in each measurement. Initial position of the cylinder piston is 40 mm. Fifth order polynomials are used as position references and movement time is 1.6 s. This gives approximately peak piston velocities of 105, 117, 129, 141 and 153 mm/s.

Figure 6 shows piston position and velocity, force (derived from A- and B-pressures of the cylinder) and states of the different DFCUs during the test sequence. Behavior of binary and Fibonacci coded systems can be compared quite easily, but in the DFCU states there is significant difference. State of the binary coded DFCU correlates with effective opening, but in Fibonacci coded system it is not as clear. States are named according to binary system (e.g. opening [0 0 1 0 1] is state 5) also in Fibonacci coded DFCUs and as a result, in some cases bigger state may even have smaller opening than some lower state.

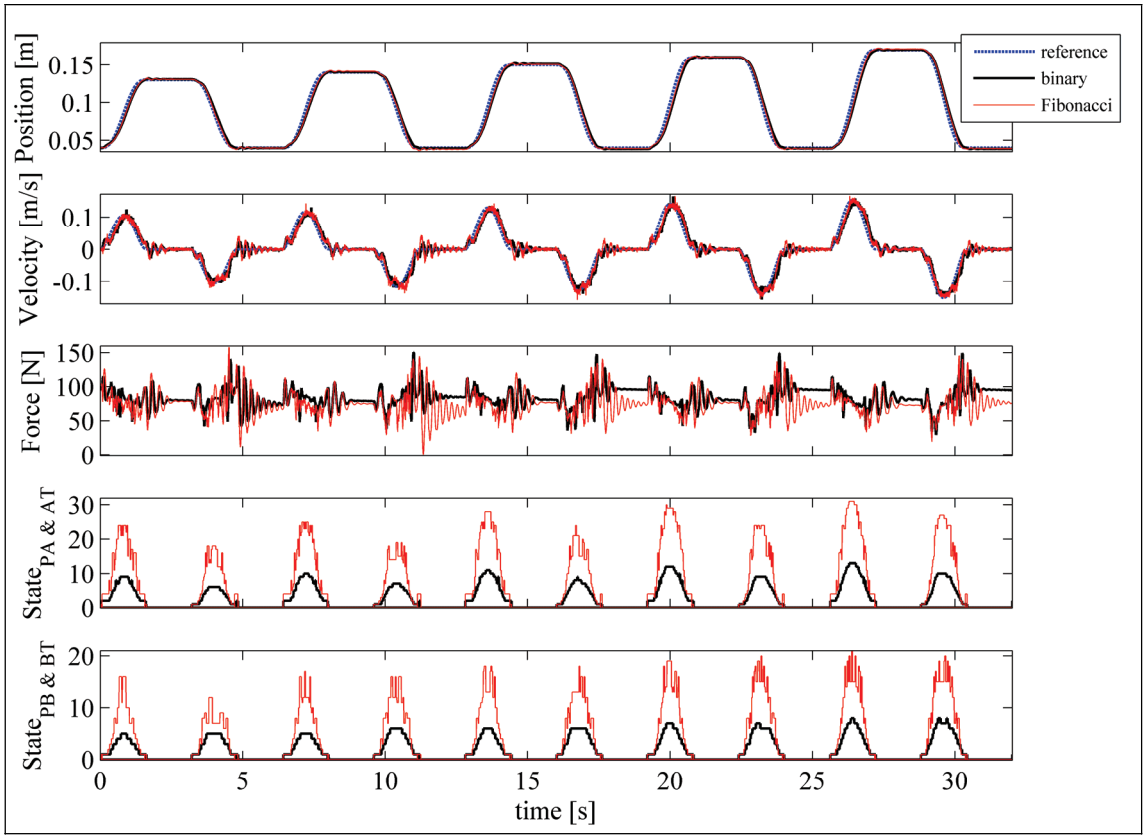

Figure 6. 90, 100, 110, 120 and 130 mm movements in the test sequence. Sampling time is 0.001 s. Force is derived from A and B pressures of the cylinder. W_{pp} and W_{sw} are 0.

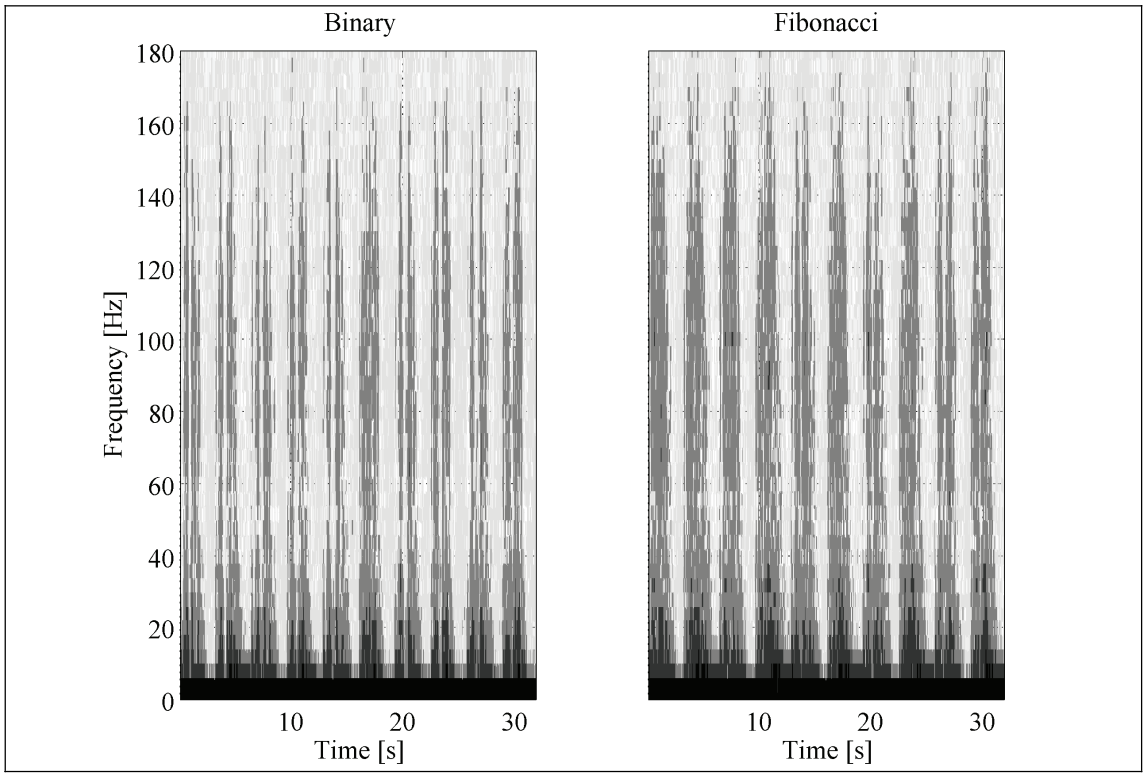

Figure 7. Spectrogram of the test sequence shown in Figure 6. Spectrogram illustrates the energy of the frequency content of the force as it changes over time.

4.1 Nominal Response

Digital hydraulic control system is stochastic and accordingly, there are always several different valve openings which can lead almost into the same result. Three responses of 130 mm movement are shown in figure 8. It can be seen that the valve openings are not equal in each response but nevertheless, repeatability of piston position and velocity is good. Tuning parameters W_{pp} and W_{sw} are 0, i.e. unnecessary valve switching is not reduced or risky state transitions are not tried to avoid. Fibonacci coding offers several valve openings with the almost same flow rates and this explains unreasonable valve switching in Fibonacci coded valve system.

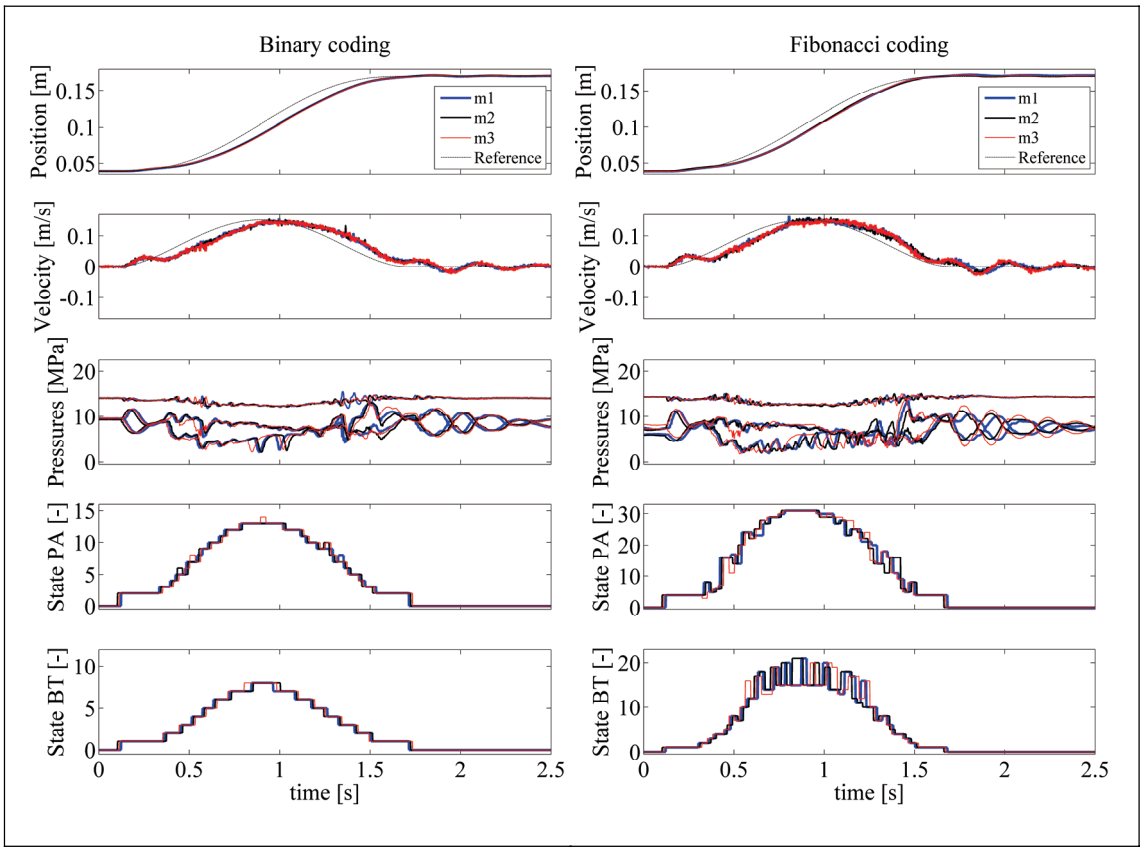

Figure 8. 130 mm stroke repeated three times in binary and Fibonacci coded systems. Valve switching or bad state transitions are not limited, i.e. W_{pp} and W_{sw} are 0.

4.2 The Effect of Cost Function Parameters on Pressure Transients

In order to achieve good controllability, well-designed cost function is essential. In this study cost function has tuning parameters W_{pp} and W_{sw} which are used for finding optimal balance between motion control characteristics, pressure peak limitation and reduced valve activity.

In figure 9, pressure peaks are tried to limit by avoiding unnecessary valve switching and bad state transitions with higher risk for pressure peaks. Weighing factor for valve switching (W_{sw}) is 1 and for pressure peaks (W_{pp}) 10.

It can be seen in the binary coded DFCU (P →A) that in acceleration state transition 7 → 8 does not occur but the controller chooses directly state 9 or 10 instead of state 8. Accordingly, one or two valves are open during the state transitions. In deceleration, controller chooses after state 8 state 5, 4 or 3. This means that any of the valves do not stay open during the state transition which is not the desired phenomenon. Same phenomenon is observed also in Fibonacci coded system, but it is not as bad because the flow capacity of the biggest valve is about 30 % lower than in binary coded system.

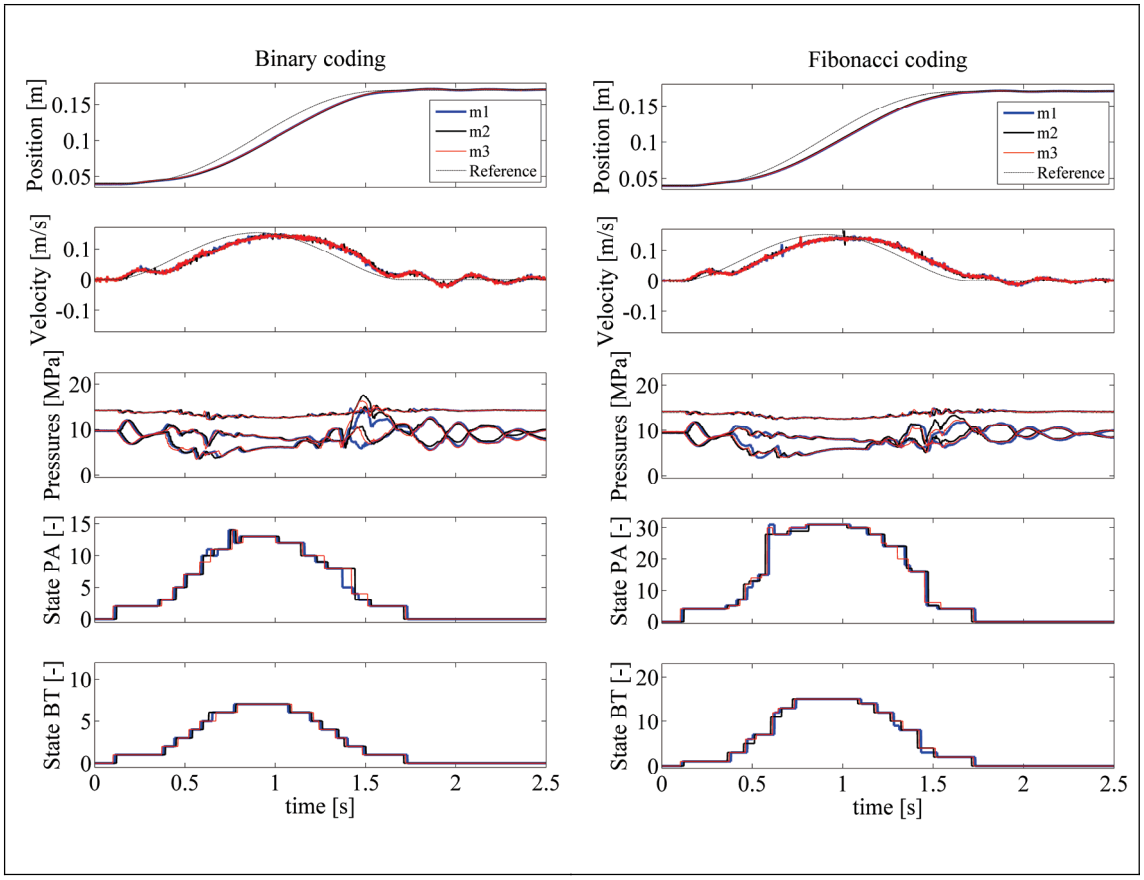

Figure 9. 130 mm stroke repeated three times in binary and Fibonacci coded systems. W_{pp} is 10 and W_{sw} 1.

Figure 10 shows that if W_{sw} is 0 and W_{pp} is 40, results are quite similar as in Figure 9. State transitions are reduced and tracking control is still reasonable. Spectrograms of the test sequence with these weighing factors are introduced in Figure 11.

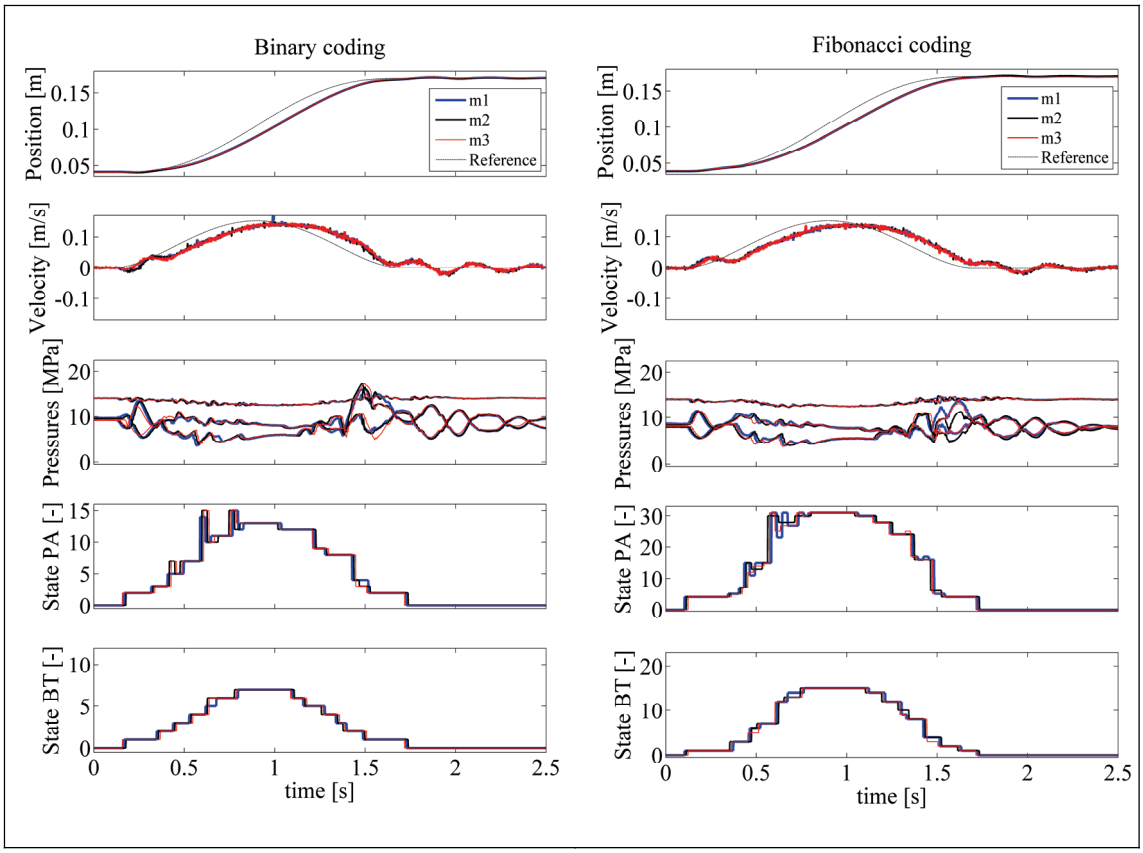

Figure 10. 130 mm stroke repeated three times in binary and Fibonacci coded systems. W_{pp} is 40 and W_{sw} 0.

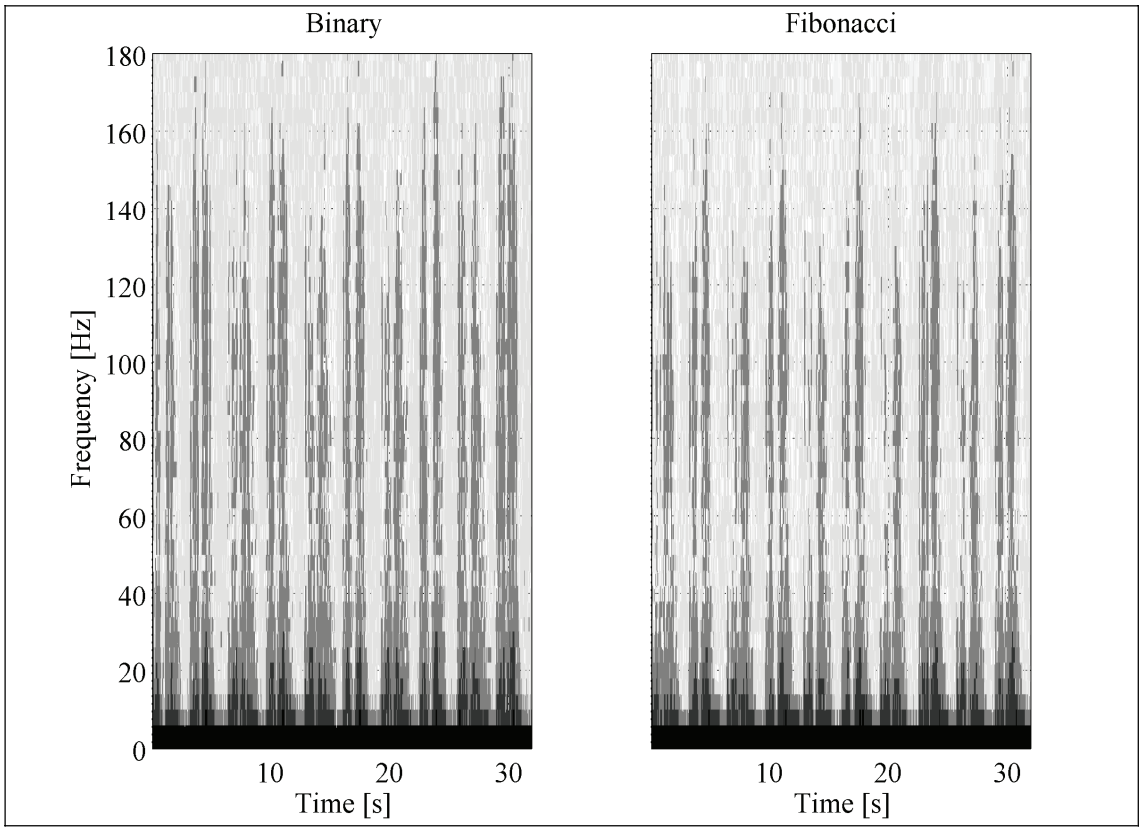

Figure 11. Spectrogram of the test sequence. W_{pp} is 40 and W_{sw} 0.

5 CONCLUSIONS

Pressure peaks are an annoying phenomenon in digital hydraulics. They are undesired in any modern motion control system and hence, some effective pressure peak limitation methods must be used. Traditional pressure peak limitation methods can be used also in digital hydraulic applications, but there are also some other alternative ways to limit pressure peaks. Based on the theoretical study, Fibonacci coded DFCU seems to have lower risk for pressure peaks than binary coded DFCU.

It is difficult to establish in practice that Fibonacci coding really helps to limit pressure peaks. This is due to the fact that pressure peaks occur quite randomly and several factors have an effect on them. Although switching time synchronization method was not used in the experimental tests, binary and Fibonacci coded digital hydraulic valve systems were behaving surprisingly well and nasty pressure peaks were observed seldom. Although pressure peaks were relatively uncommon in this study, results show that with suitable cost function values pressures behaves better in Fibonacci coded system than in binary coded valve system. Cost for bad state transitions limits the risk of pressure peaks but it also reduces unnecessary valve activity. Therefore, additional cost for valve switching can be often ignored and then, the tuning of the cost function becomes easier.

ACKNOWLEDGEMENT

The research was supported by the Academy of Finland (Grant No. 80411).

NOMENCLATURE

n	Number of valves	-
p_A	Pressure in port A	Pa
p_B	Pressure in port B	Pa
p_s	Supply pressure	Pa
p_T	Tank pressure	Pa
$Q_{N,PAi}$	Flow coefficient of the i-th valve of DFCU P→A,	liter/(min·Pa$^{0.5}$)
$\underline{Q}_v$	Flow rates of the valves in DFCU at one Pa pressure differential	liter/(min·Pa$^{0.5}$)
$\underline{u}_k$	Vector of the control of the DFCU	-
$\underline{u}_{k-1}$	Vector of the previous control of the DFCU	-
v_{ref}	Piston velocity reference	m/s
v_{ss}	Calculated steady-state piston velocity	m/s
W_{pp}	Weight for pressure peaks	-
W_{sw}	Weight for state transitions	-
W_κ	Weight for error in inflow-outflow opening ratio	-
Δu_{PAi}, u_{ATi}, Δu_{PBi}, Δu_{BTi}	Changes in control signals of the valves when new control signal is applied.	-

REFERENCES

1. **Linjama, M. & Vilenius, M.** 2004. Digital hydraulic control of a mobile machine joint actuator mockup. Bath Workshop on Power Transmission and Motion Control (PTMC'04), September 1-4, Bath, UK, pp. 145-158.
2. **Linjama, M.; Vilenius, M.** 2005. Digital hydraulic tracking control of mobile machine joint actuator mockup. Proceedings of the Ninth Scandinavian International Conference on Fluid Power, SICFP'05, June 1.-3, 2005, Linköping, Sweden.
3. **Linjama, M. & Vilenius, M.** 2005. Energy-efficient motion control of a digital hydraulic joint actuator. Proceedings of the 6th JFPS International Symposium on Fluid Power, November 7-10, 2005, Tsukuba, Japan pp. 640-645.
4. **Laamanen, A.; Linjama, M.; Vilenius, M.** 2005. Pressure Peak Phenomenon in Digital Hydraulic Systems – a Theoretical Study. Bath Workshop on Power Transmission and Motion Control (PTMC 2005). September 7-9. 2005, Bath, UK. pp. 91-104.
5. **Laamanen, A., Linjama, M. & Vilenius, M.** 2006. The effect of coding method on pressure peaks in digital hydraulic system. In: Ivantysynova, M. (ed.) Proceedings of the 4th FPNI - PhD Symposium, Sarasota 2006, June 13-17, 2006, Sarasota, FL, USA, pp.285-295.
6. **Lee, J.S.; Lee, K.B.; Lee, C.G.** 2001.An experimental study on the control of pressure transients using an orifice. International journal of Pressure Vessels and Piping 78 (2001). pp. 337-341.
7. **Bower, J.** 1961. Digital Fluid Control System. US Patent No. 2999482.
8. **Murphy, R. E.** 1962. Hydraulic control system. US Patent No. 3038449.
9. **Tanaka, H.** 1988. Electro-hydraulic PCM Control. Journal of Fluid Control 18 (1). pp. 34-46. USA.
10. **Laamanen, A.; Nurmia, M.; Linjama, M.; Koskinen, K.T.; Vilenius, M.** 2003. Two different control methods for digital flow control unit. Proceedings of the Eight Scandinavian International Conference on Fluid Power (SICFP´03), May 7-9, 2003, Tampere, Finland. pp. 887-898.
11. **Linjama, M.; Laamanen, A.; Vilenius, M.** 2003. Is it time for Digital Hydraulics? Proceedings of the Eight Scandinavian International Conference on Fluid Power (SICFP´03), May 7–9 2003, Tampere, Finland. pp. 347-366.
12. **Liu, R., Wang, X., Tao, G. and Ding, F.** 2001. Theoretical and Experimental Study on Hydraulic Servo Position Control System with Generalization Pulse Code Modulation Control. In: Lu, Y., Chen, Y. & Xu, L. (Eds.) Proceedings of the Fifth International Conference on Fluid Power Transmission and Control (ICFP'2001), pp. 176–179.
13. http://www.sterling-hydraulics.co.uk

TRANSIENT PRESSURE CONTROL IN DIGITAL HYDRAULIC SYSTEMS

Jyri Juhala, Jyrki Kajaste, Matti Pietola
Helsinki University of Technology
Faculty of Mechanical Engineering
Department of Machine Design
P.O. Box 4400
FIN-02015 TKK
FINLAND
Phone +358 9 451 3330, Fax +358 9 451 4945
E-mail Jyri.Juhala@tkk.fi

ABSTRACT

In digital hydraulics the system is controlled with DFCUs (Digital Flow Control Unit) which consist of several on/off –valves. Due to this operating principle changes in control quantity cause step input excitations which awaken system modes. The solenoid valve types which have been used in digital hydraulic systems suffer from stochastic variation in operating times. Both the delays before the actual motion and the duration of movements may vary. These may lead to failed synchronizations of valve timing. The effective flow area of a DFCU may momentarily drop to zero or reach oversized values. These effects can be reduced by proper control strategy but also hardware solutions may be necessary.

The aim of this study is to demonstrate the ability of pressure accumulator based hydraulic filters to reduce the pressure oscillations. Also the dynamics of a solenoid valve are estimated. The results show that the system behavior can be improved both by using an accumulator with a throttled check valve and with a "digital accumulator" consisting of an accumulator and a digital valve. The orifice diameters of throttle valves and the on/off valve synchronizing times of the digital accumulator can be adjusted for optimal response.

KEYWORDS: Digital Hydraulics, DFCU, Pressure control, Pressure transient

1. INTRODUCTION

The core of the digital hydraulic system control is a DFCU (Digital Flow Control Unit) which is a valve unit consisting of number of two-way on/off valves connected in parallel. The flow capacities for each valve can be chosen many ways but the only practical method is Pulse Code Modulation (PCM). In PCM control system the flow capacities of individual valves are not equal but are set according to certain coding. Traditionally PCM control is based on binary sequence (2^0,2^1,2^2,2^3,…,2^n) but also coding according to Fibonacci sequence (0,1,1,2,3,5,8,…,F_n) has been investigated. The hydraulic circuit diagram of DFCU is presented in Figure 1. [1, 2]

Due to the discontinuous way to control flow rates while changing state a DFCU generates excitations which lead to system dependent pressure transients. The imperfections in the current solenoid valve technology with variation in valve operation times may lead to even more severe operational conditions. During these short time states all of the inlet flow ports of a DFCU may be totally closed. This means a water hammer type of a transient state in which the magnitude of the pressure response is emphasized if the supply piping is long enough and the valve closing times are short. The failure in valve synchronization may also lead to overdimensioned flow area if too many valves of a DFCU are open at the same time. These two transient operational conditions of a DFCU may end in severe pressure transients with positive or negative pressure spikes which may deteriorate the operation of the machine, lead to failures, accelerate fatigue and raise noise levels.

In the field of hydraulic transient and vibration control much work has been done during the few last decades. Also the problems with DFCUs have been observed and some methods for transient control have been introduced.

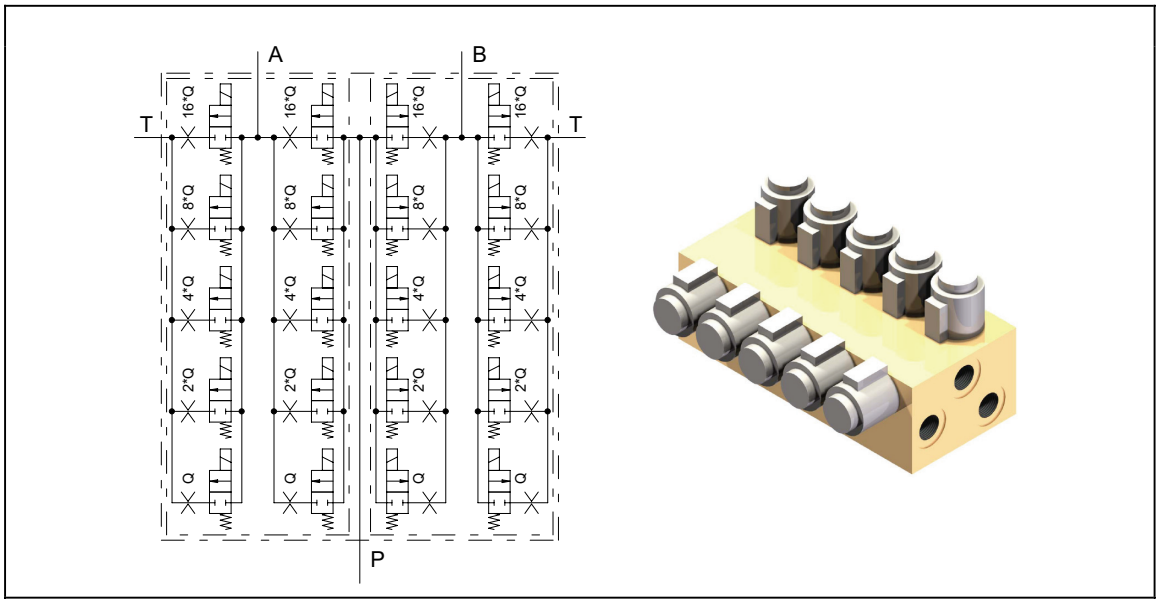

Figure 1. *Circuit diagram of system consisting of four DFCUs and an illustration of a manifold containing two DFCUs and five on/off valves per DFCU*

Laamanen et al. studied pressure peak phenomenon in digital hydraulics. They found that tuning carefully controller parameters, especially switching time and using alternative coding methods such as Fibonacci coding for DFCU, the most harmful pressure peaks can be minimized. Fibonacci coding makes it possible to avoid state transitions where whole valve system is momentarily fully closed but it also has some drawbacks e.g. worse accuracy than with binary coding. [3]

Siivonen et al. compared the characteristics of a digital flow control unit and a commercial mobile proportional valve experimentally in cold conditions. The results showed that both systems have problems in cold conditions. The problems faced included substantially higher response times and decreased maximum flow rates than at normal operating temperatures. The hysteresis was negligible in digital valve system at each temperature level. [4].

Linjama et al. studied the possibility to use a digital hydraulic pilot valve instead of a proportional pilot in a Valvistor flow amplifier. A digital hydraulic pilot valve with eight on/off valves was developed and applied in a commercial Valvistor. The results showed that the digital hydraulic pilot valve reduces hysteresis and makes the Valvistor about three times faster. However, the physical size of the prototype developed was large when compared to proportional pilot valves. Four different small capacity models for pilot-valve were evaluated both statically and dynamically and the results showed good dynamics with relatively short delays. As low working delays as 4-5 milliseconds for valve opening and 1-3 milliseconds for closing were found for some models. The use of the tested models directly in DFCUs is not reasonable due to limitations in pressure levels and flow capacities. [5].

Kajaste et al. studied the use of a pressure accumulator and an in-line suppressor to hydraulic oscillation control. They found that the latter device possessed larger frequency bandwidth for operation. Also the accumulator modeling and the effect of pressure accumulator attaching pipes on the system dynamics were studied. [6].

Both Kajaste and Viersma found that with the use of pressure accumulators in the system especially in systems with pressure controlled pumps and long pipelines there is a risk of low frequency resonances. [7, 8].

Esser developed an adaptive attenuator for flow rate disturbances. The system consists of a pressure accumulator and a metallic membrane equipped with an orifice which connects the main system to the accumulator. Also a new kind of a flow rate pulsation sensor was constructed which is based on the principles of the adaptive attenuator. [9]

The target of this study is to test the ability of passive and semi-active methods and devices to control hydraulic transients in a lengthy supply line caused by abrupt changing states of DFCU. The passive components include a pressure accumulator and a hydraulic filter made of an accumulator with a throttled check valve. Also a semi-active device consisting of a pressure accumulator, an orifice and a solenoid valve is constructed and tested. This “digital accumulator” is aimed to be used only on demand i.e. only under the threat of the most severe transients.

In attaching the additional devices for transient control there is likely to be a trade-off between good dynamics and decent transient behavior. The additional pressure responses due to disturbances should be filtered off but the supply pressure should be able to follow the demand accurately and fast enough. The transient control system should not make system too sluggish or awake new poorly damped vibrational modes.

2 TEST INSTALLATIONS

The following chapter presents the passive and semi-active devices used to filter pressure transients. The hydraulic pressure transient test system is introduced and testing methods are presented.

2.1 Passive device

The adjustable accumulator is based on combination of throttled check valves and membrane pressure accumulators. The basic idea is to find compromise between the ability to absorb high amplitude pressure transients and to minimize the effect on system dynamics.

The device is equipped with two accumulator systems, one for positive and one for negative pressure transients. The check valve sections of throttled check valves are for pressure transients and the orifice sections are for resetting the accumulator pressures back to mean level. The throttled check valves also diminishes the tendency to sluggish the system pressure changes and provide some damping to prevent the emergence of low frequency oscillations, especially in systems where pressure controlled pumps are used.

2.2 Semi-active device

The so called Digital accumulator consists of a digital (on/off) valve system, orifice and an accumulator. The idea is to use accumulator only on demand i.e. when the most severe transients are expected. The schematic picture of the Digital accumulator is presented in Figure 2.

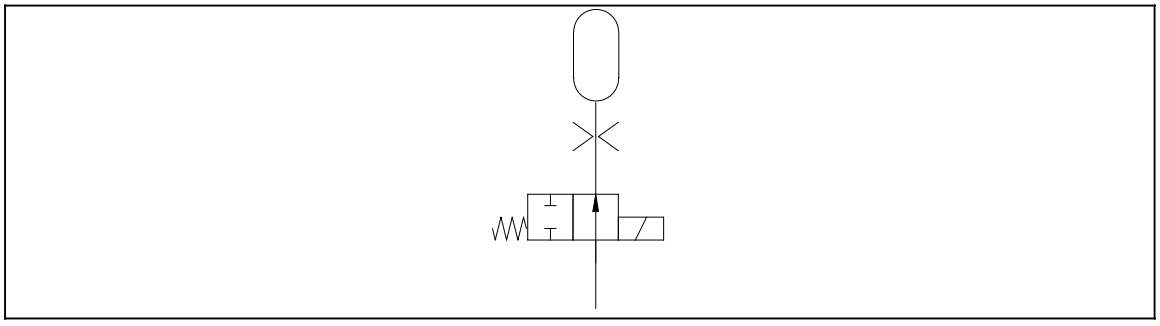

Figure 2. *Digital accumulator consisting of accumulator(s), solenoid valve(s) and orifice(s)*

As an on/off valve the model HYDAC WS08W-01 was used. The nominal volume of the membrane accumulators was $0.16 \cdot 10^{-3}$ m^3 and the pre-loading pressure 60 bars (absolute pressure) both in the adjustable accumulator and digital accumulator tests.

2.3 Test Rig

The ability of pressure accumulator based hydraulic filters to damp DFCU based hydraulic transients were tested with a system consisting of

- Piston pump
- pressure relief valve
- a relatively long supply piping from pump to DFCU to emphasize the effect of transients.

As a substitute for a DFCU a fast acting servo-solenoid valve (High Response Valve, HRV, Bosch 4WRREH6) was used. The magnitude of operating times of this valve type and on/off valves used in DFCUs is roughly speaking the same - approximately 5 ms for total opening/closing.

Figure 3 presents a layout of the hydraulic system which was built to demonstrate the effects of the pipeline dynamics on the system behavior. The system consists of (B) a long pipe with small inner diameter (20 m / 12 mm) and (A) a short pipe section (3,3 m) of hose and a pipe with effective flow area about four times larger than that of section B.

2.4 Testing methods

To clarify the dynamics of current solenoid based on/off valves used in digital hydraulics some measurements were carried out. The response times of HYDAC WS08W-01 two-way on/off valve were estimated two ways. At first the poppet displacement was measured without hydraulic load by laser displacement transducer. Also the coil current and the acceleration of valve body were measured. Then the valve was attached to hydraulic system and the opening times were estimated by coil current and pressure changes.

The pressure transient measurements were done for three filtering methods

- Pressure accumulator(s)
- Throttle check valve - pressure accumulator combination
- Digital accumulator

From each measurement the following variables were measured

- flow rate
- temperature (for viscosity)
- adjustment of pressure relief valve
- pressures near pump and near the source of pressure transients.

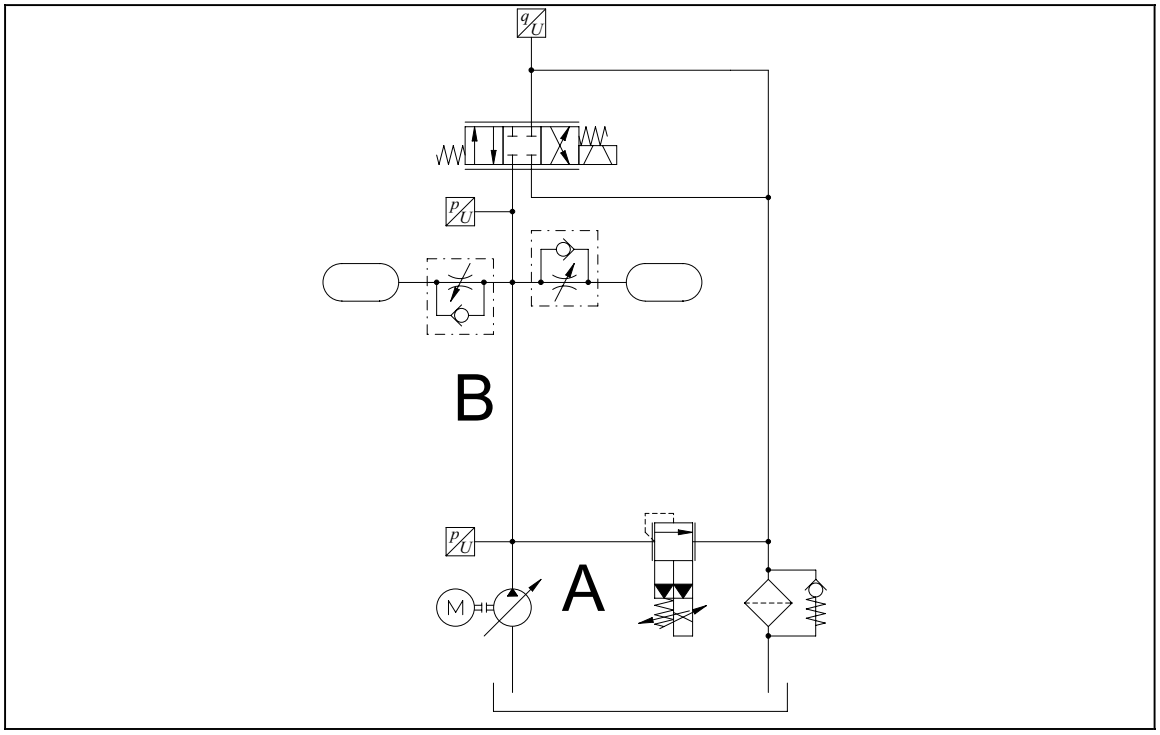

Figure 3. *Hydraulic test system with passive filter*

Figure 3 illustrates the hydraulic test system in adjustable accumulator measurements. The distance from valve inlet to accumulator connection is circa 0.25 m.

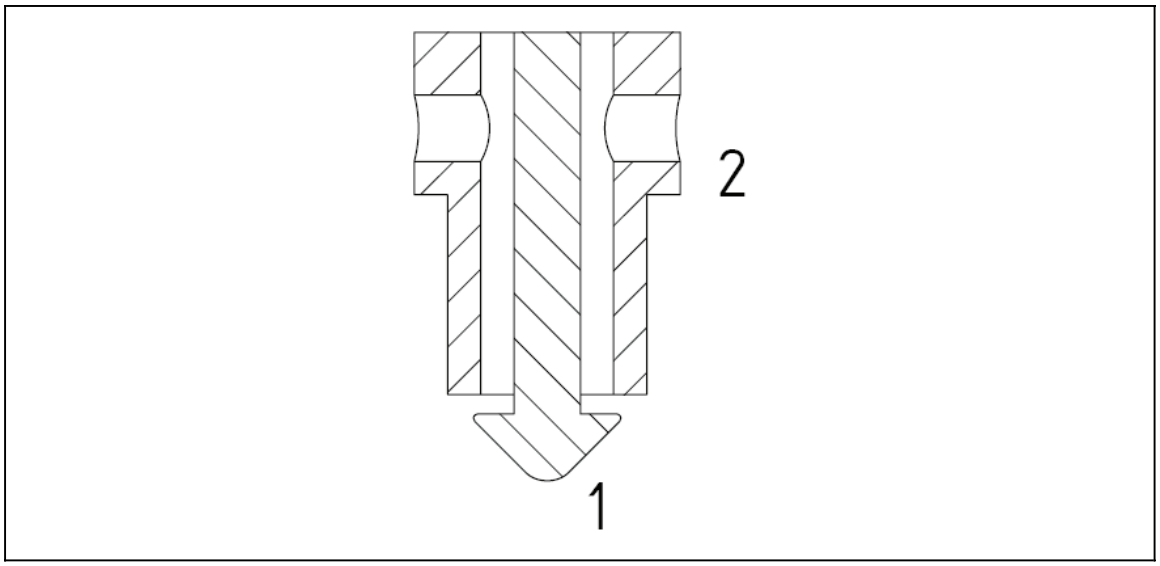

Figure 4. *Sectional draft drawing of on/off -valve*

Figure 4 demonstrates the locations of the flow ports of on/off valves (HYDAC WS08W-01) used in digital hydraulics circuits of this study.

3 RESULTS

3.1 Valve response times

Figure 5 shows the opening/closing times of Hydac on/off valve. The estimated operating times of this type of valve are presented in Table 1. The estimation of valve closing times under hydraulic load was impossible because valves body acceleration was not measured and the closing time can not be estimated from coil current in the test arrangement used. The flow directions in Table 1 are according to Figure 4.

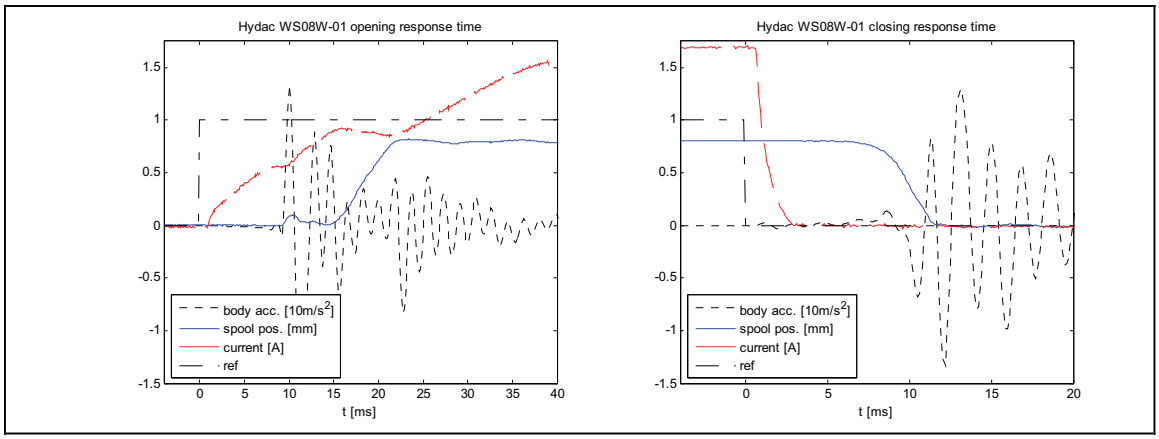

Figure 5. *Opening and closing of HYDAC WS08W-01, valve spool movement, coil current, valve body acceleration*

Table 1. *Estimated operation times of valve (HYDAC WS08W-01)*

	Delay (opening) [ms]	Rise time [ms]	Delay (closing) [ms]	Fall time [ms]
Dry	15	7	7	5
Under hydraulic load (flow 2->1)	16	12	*Not measured*	*Not measured*
Under hydraulic load (flow 1->2)	17	9	*Not measured*	*Not measured*

Figure 6 shows that Bosch HRV is approximately as fast as Hydac on/off –valve without delay. For that reason and the good controllability of it this servo-solenoid valve model is suitable to be as a substitute for DFCU in transient tests.

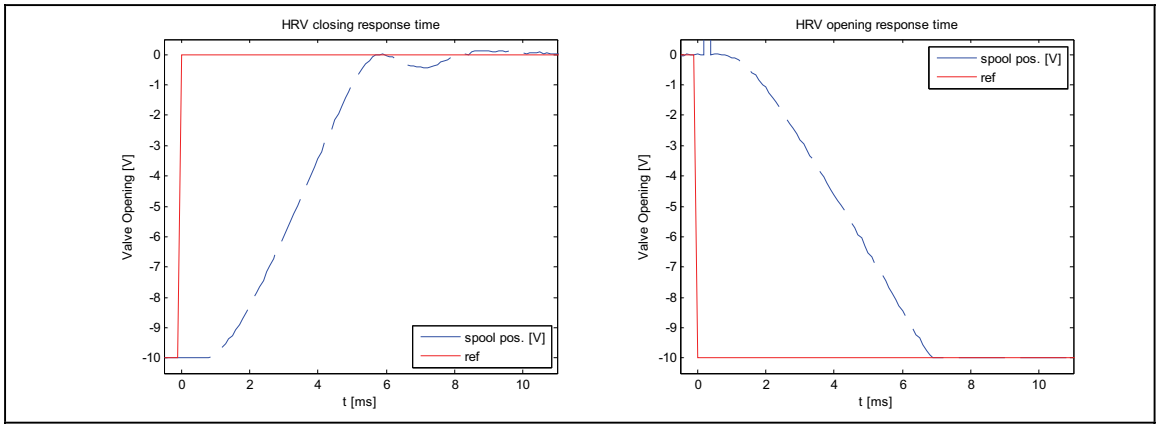

Figure 6. *Opening and closing of an HRV-valve, control signal and the spool displacement output signal (LVDT).*

3.2 Pressure transient measurements

Pressure accumulator system

Pressure transient measurements without, with one and with two accumulator(s) are presented in Figure 7. The tests were carried out by using the closure of servo-solenoid valve as an excitation. The flow rate before the transient was $0.6 \cdot 10^{-3}$ m^3/s (36 l/min).

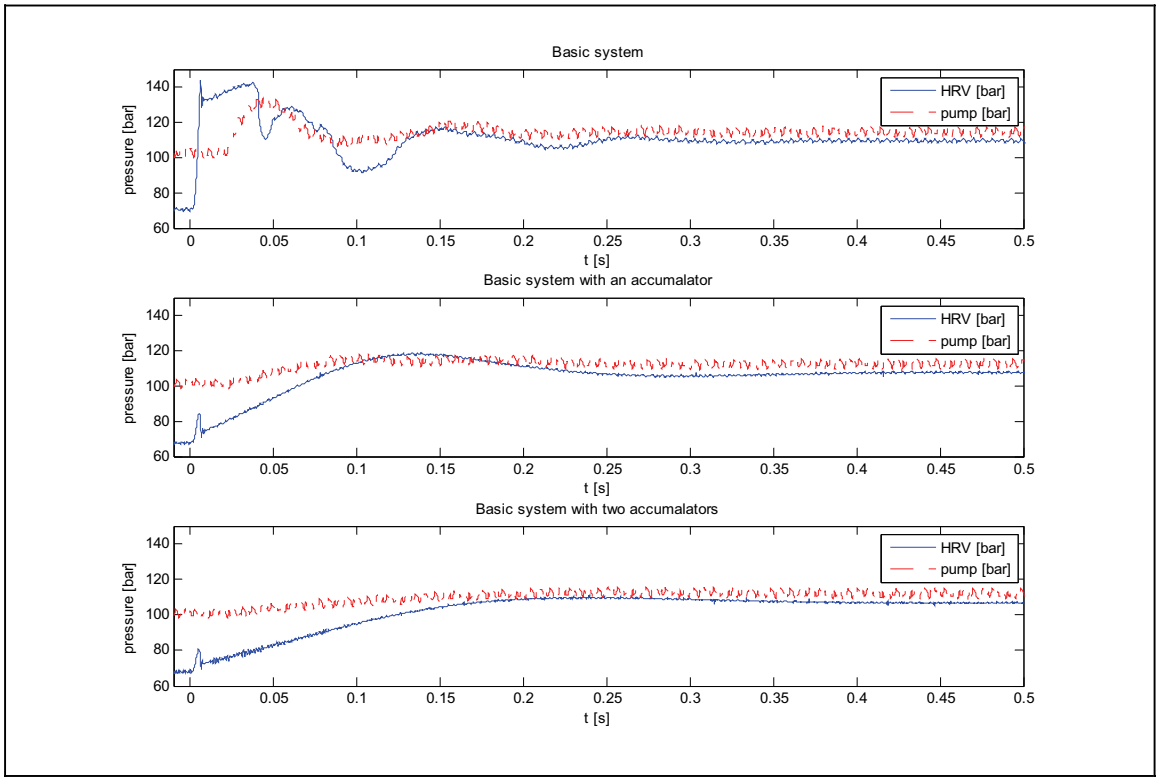

Figure 7. *Pressure transient test (waterhammer) with basic hydraulic system, with one accumulator and with two accumulators*

Adjustable accumulator system

Figure 8 shows the effects of throttled check valve - pressure accumulator on the pressure response. The measurements are made with different throttle valve openings, small, intermediate and wide. The pre-transient flow rate was $0.6 \cdot 10^{-3}$ m^3/s (36 l/min).

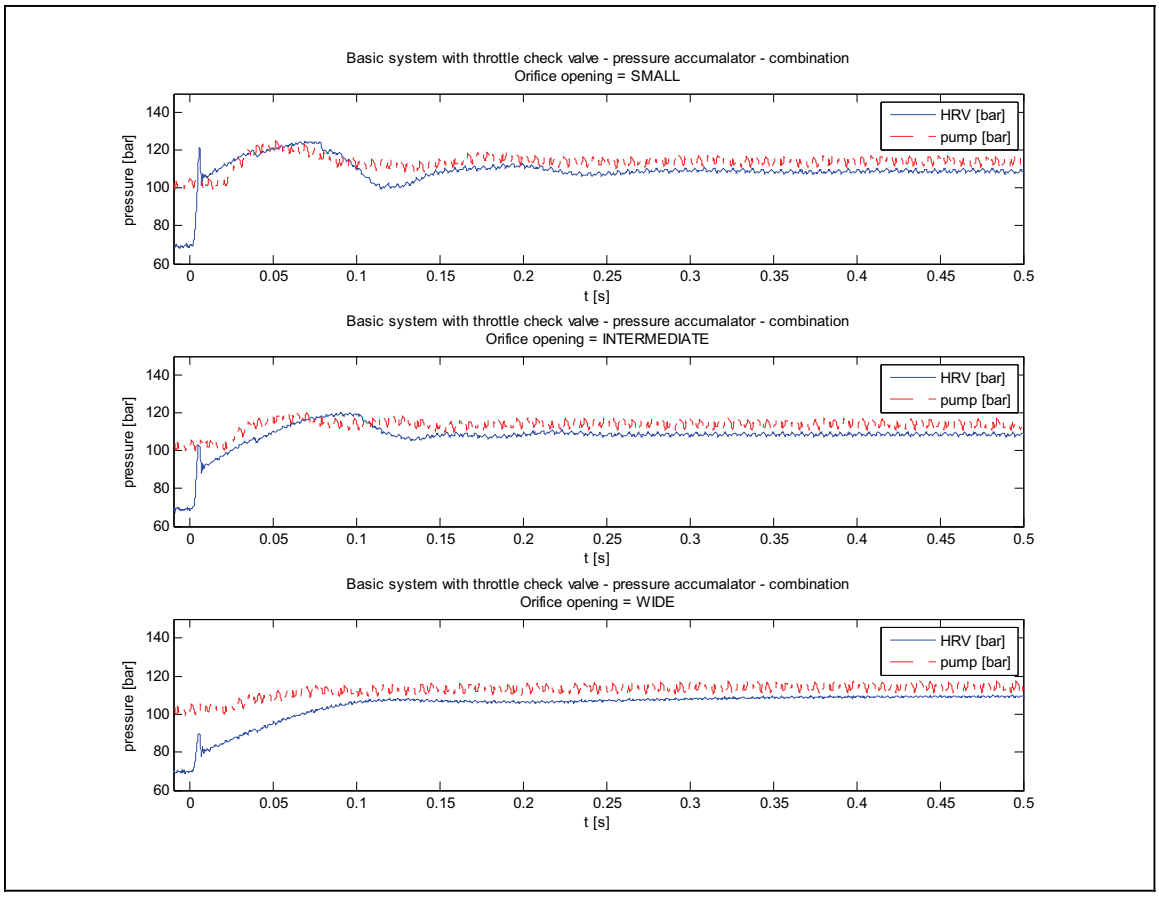

Figure 8. *Pressure transient test (waterhammer) with adjustable accumulator, small opening – intermediate opening – wide opening of throttle valve*

Digital accumulator system

Figures 9 - 12 show the pressure behavior of hydraulic system which is equipped with "digital accumulator". In Figures 9 and 11 the filtering system is deactivated. In figures 10 and 12 different sized orifices are used. The flow rate was circa $0.55 \cdot 10^{-3}$ m^3/s (33 l/min).

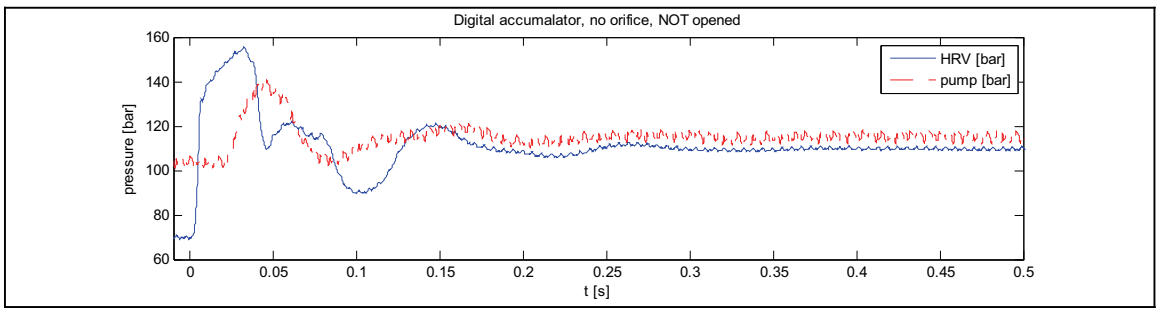

Figure 9. *Pressure transient test with "digital accumulator", accumulator disconnected*

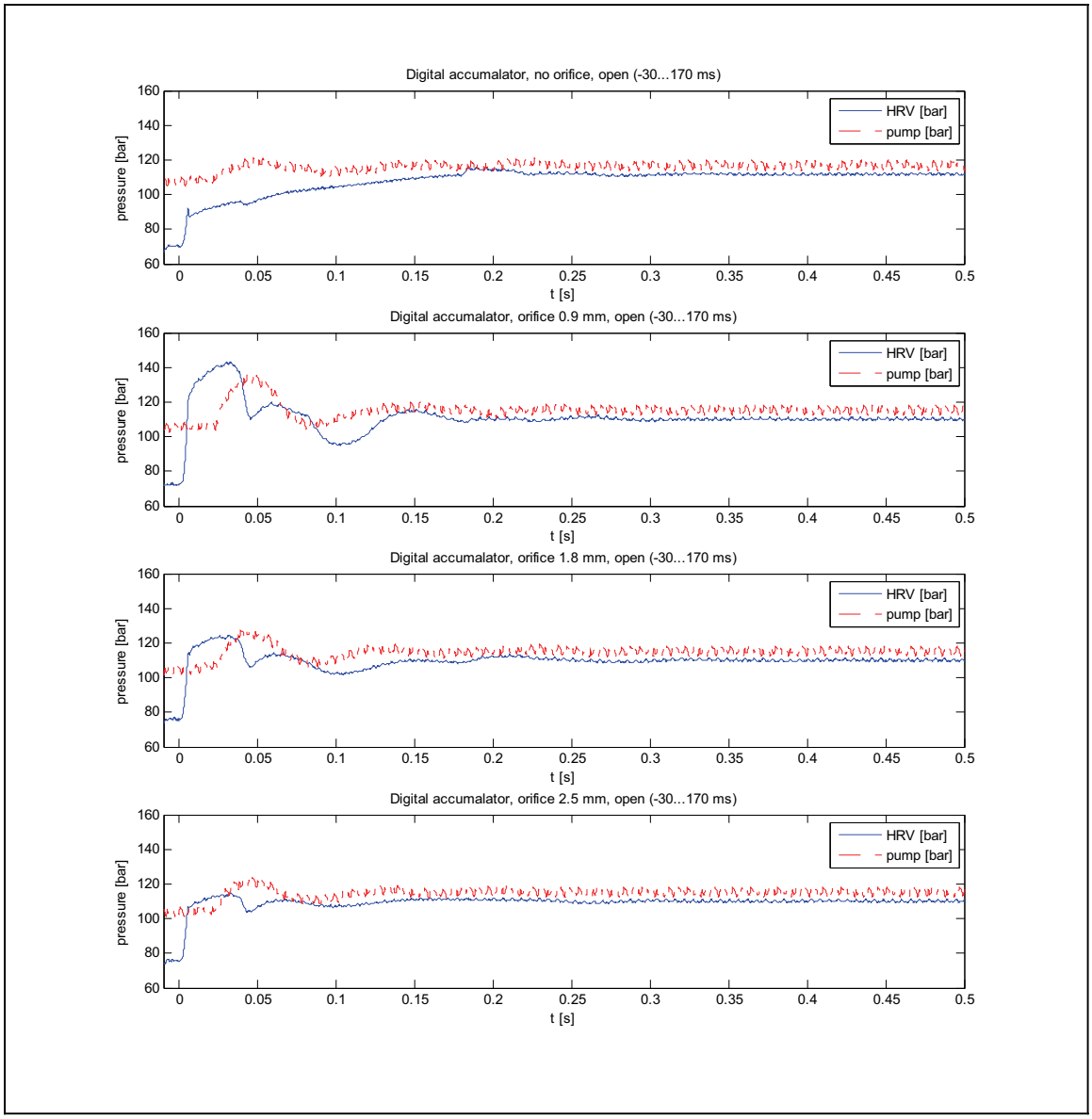

Figure 10. *Pressure transient test (waterhammer) with "digital accumulator" system without orifice and with different sized orifices. Digital valve to accumulator is opened 30 ms before transient and closed 200 ms later.*

Figures 11 and 12 demonstrate the effect of digital accumulator and the different orifices on transient behavior ("negative waterhammer") during large scale opening of the servo-solenoid valve. In measurement associated to Figure 11 the digital accumulator has not been activated. Figure 12 shows the influence of orifice size selection. The flow rate after the transient was approximately $0.55 \cdot 10^{-3}$ m^3/s (33 l/min).

During most of the tests in Figure 12 the transient pressure goes under the pre-loading pressure of the accumulator (circa 59 bars, gauge pressure) and thus eliminates the effect of it on the system dynamics.

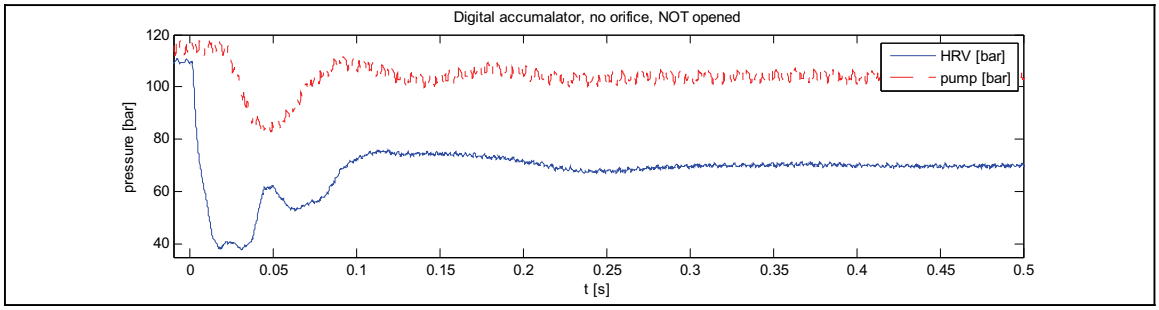

Figure 11. *Pressure transient test ("negative waterhammer") with "digital accumulator" system. Accumulator is disconnected.*

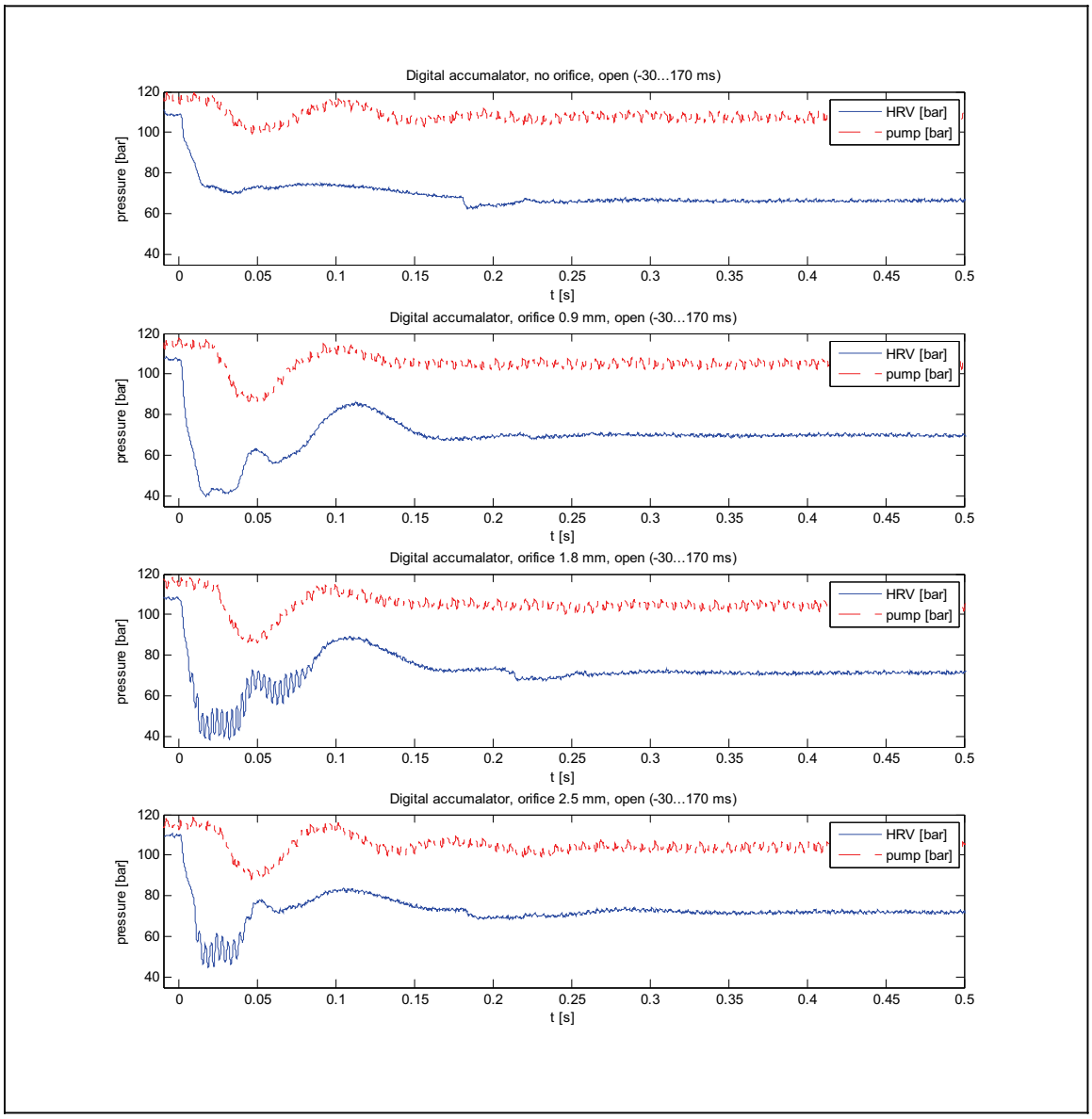

Figure 12. *Pressure transient test ("negative waterhammer") with "digital accumulator"system without orifice and with different sized orifices. Digital valve to accumulator is opened 30 ms before transient and closed 200 ms later.*

4 DISCUSSION

Even though commercial solenoid valves are not considered as extremely fast devices from the control viewpoint the actual movement of the spool or poppet after the latency time is rapid enough to cause severe excitations to the hydraulic system. In systems with lengthy pipelines and digitally controlled DFCUs even a waterhammer type of a transient state is possible. Due to stochastic variation in operation times of valves there is a risk of a short time total closure of the valve system. This is a phenomenon which can be affected by recognition of hazardous valve state changes and proper control of the DFCU. The control system can for example learn to be aware of the risky valve changes and a) try to avoid them or b) switch an active or semi-active transient control system on.

The measurement of solenoid valve operation times showed that the latency time plays an important role in the valve dynamics. The actual movement of poppet was rapid also under the influence of hydraulic load and flow. In this case the operating times differed somewhat from the values measured under no hydraulic load. It was noticed that the operation times and delays of solenoid valves can be estimated also by using coil current or even valve body acceleration measurements.

In the transient tests the pressures differed considerably from each other at the line ends during high flow rate periods due to the long pipelines and the corresponding flow losses. By diminishing the valve opening both the flow and the friction decrease and the valve end pressure rises approaching the pump pressure which stays approximately unchanged due to the pressure relief valve. Without hydraulic filtering an abrupt pressure level alteration at the valve end is a highly dynamic event in which pipe, pressure relief valve and pump dynamics participate. As a consequence large pressure overshoots and oscillations may combine with the steady state pressure level change.

The use of pressure accumulators as hydraulic filters resulted in a mild pressure response with major pressure spikes filtered off and a sluggish pressure change from a steady state to another. The transient starts with a slight and short-term spike due to the small distance which the pressure wave has to traverse between the controlled valve and the accumulator. The high hydraulic capacitance of the accumulator and the low damping of it affect the pressure supply system dynamics considerably. A risk of low frequency oscillation tendency exists particularly in systems with pressure controlled pumps.

If the test results with single or two accumulators are compared with the ones including a throttled check valve as an add-on a change in the system dynamics can be observed. By adjusting the opening of the throttle valve the system can be altered from a version resembling the original system without hydraulic filters to the one equipped with a normal accumulator. With this variability an optimal response which filters the detrimental pressure peaks off and still preserves an adequate dynamic stiffness can be found. As the filter includes two accumulator units different openings for the orifices can be used to tune the unit to act differently for rising and decreasing pressure. Because of the distances between the excitation valve and the adjustable accumulator small scale pressure peaks at the transient start were observed also in the response of the system with this “adjustable accumulator”.

A new kind of “digital accumulator” consisting of a membrane accumulator and a manifold including several solenoid valves equipped with orifices of different size was

manufactured and tested. The accumulator was controlled by “filtering on demand” principle by switching the valve open shortly before the actual actuation of the main valve and closing the connection to accumulator after a certain time window. During steady state operation the connecting solenoid valve was held closed to keep the hydraulic stiffness of the pipe system high. The pressure response of the system with digital accumulator varied as a function of the valve and orifice combination chosen. A fast pressure rise with a minor overshoot was achieved with a relatively large diameter orifice. The time windows of control were of the magnitude of 200 ms. As in the case of adjustable accumulator different effective orifice sizes can be chosen for the opening and closing of digital control valve system. Also the time window length can be altered for optimum performance.

Passive systems which are tuned for certain operating point of a system may deteriorate the system performance at a different operating point. This is true also for vibration control systems. An accumulator may be effective in neutralizing severe hydraulic transients but as a drawback it may make the system too sluggish related to system pressure changes. In practice often a compromise must be found in system tuning.

Semi-active systems for vibration control provide the possibility to optimize the filter for each operating point. In the case of a digital accumulator the means and parameters are related to accumulator opening time window and to the choice of effective orifice diameter. To realize this kind of semi-active system some extra electrically operated valves and an optimization routine for the controller are needed to the DFCU system.

In the future due to valve evolution the response times of digital valves are likely to shorten and the uncertainty related to operation delays will also diminish and make the control easier. However this fastness will also raise the dynamic excitations to a new frequency level which will bring further challenges to system control and maintenance.

Theoretically the awakening of DFCU induced transients could be avoided by stabilizing actively the system transfer function (hydraulic impedance in frequency domain) at the DFCU hydraulic interface. The impedance could be held constant also during switching of valves with an extra integrated device which would compensate the impedance changes due to valve adjustments.

5 CONCLUSIONS

The dynamics of a solenoid valve used in digital hydraulic systems were estimated and the result showed that latency times were relatively long according to actual poppet movement times. The switching times of these valves were found to be short enough to cause severe pressure transients.

The results of transient measurements showed that passive (“adjustable accumulator”) and semi-active (“digital accumulator”) accumulator based filters can be used to improve system behavior.

Further research is needed to optimize the orifice sizes in both passive and semi-active accumulator based filters. Proper and validated simulation models will help in this development. Along with active means for hydraulic damping also other filtering methods could be tested in the near future including in-line suppressors and other

passive or semi-active means. More frequency response orientated results will also be shown.

6 ACKNOWLEDGEMENT

The research was supported by the Finnish Funding Agency for Technology and Innovation and Finnish industry.

REFERENCES

1. Linjama, M., Laamanen, A. and Vilenius, M. 2003. Is it time for digital hydraulics? The Eighth Scandinavian International Conference on Fluid Power (SICFP'03). Tampere, Finland, May 7-9.

2. Laamanen, A., Nurmia, M., Linjama, M., Koskinen, K. T. and Vilenius, M. 2003. Two different control methods for digital flow control unit. The Eighth Scandinavian International Conference on Fluid Power (SICFP'03). Tampere, Finland, May 7-9. s. 887-898. ISBN 952-15-0972-4

3. Laamanen, A., Linjama, M. and Vilenius, M. 2005. Pressure peak phenomenon in digital hydraulics - a theoretical study. Bath Workshop on Power Transmission and Motion Control (PTMC'05). Bath, UK, September 7-9.

4. Siivonen 2005 Siivonen, L., Linjama, M. & Vilenius, M. 2005. The Effect of Fluid Viscosity on Performance of Proportional Directional Valve and Digital Flow Control Unit. The Ninth Scandinavian International Conference on Fluid Power (SICFP'05). Linköping, Sweden , June 1-3.

5. Linjama, M., Tamminen, P., Andersson, B. & Vilenius, M. 2005. Performance of the valvistor with digital hydraulic pilot control. The Ninth Scandinavian International Conference on Fluid Power (SICFP'05). Linköping, Sweden , June 1-3.

6. Kajaste J. 2001. Oscillation reduction by using pressure accumulators and inline suppressors. The Seventh Scandinavian International Conference on Fluid Power (SICFP'01). Linköping, Sweden, May 30th, p. 329 - 343.

7. Kajaste, J., Of the capability of component models to predict the response of a fluid power system with a long pipeline and an accumulator. Acta Polytechnica Scandinavica, Mechanical Engineering Series No. 139, Espoo 1999, 116 p. Published by the Finnish Academy of Technology. ISBN 951-666-517-9. ISSN 0001-687X.

8. Viersma 1980 Viersma, T.J. Analysis, synthesis and design of hydraulic servosystems and pipelines. Amsterdam, The Netherlands: Elsevier scientific publishing company, 1980. 280 p. ISBN 0-444-41869-5.

9. Esser, J. Adaptive Dämpfung von Pulsationen in Hydraulikanlagen. Verlag der Augustinus Buchhandlung. Aachen: 1996. 138 S. (Dissertation.)

DEVELOPMENT OF A FAST SEAT TYPE SWITCHING VALVE FOR BIG FLOW RATES

Bernd Winkler*, Rudolf Scheidl**

*Linz Center of Mechatronics
Altenbergerstrasse 69
4040 Linz, Austria
Phone +43 732 2468 9748, Fax +43 732 2468 9753
E-mail: bernd.winkler@lcm.at

**Johannes Kepler University of Linz
Institute of Machine Design and hydraulic Drives
Altenbergerstrasse 69
4040 Linz, Austria
Phone +43 732 2468 9745, Fax +43 732 2468 9753
E-mail: rudolf.scheidl@jku.at

ABSTRACT

Highly accurate and fast response drives, for instance for fast and precise positioning, currently rely on big servo or proportional valves. Such valves are costly and are applied to resistance control with its inevitable energetic losses. A promising method to get rid of such losses and to reduce the valve costs is to use appropriate switching valves in combination with switching control. Former investigations showed that switching valves with flow rates of about 100 l/min at 5 bar and switching times of 1 to 2 ms can cover a reasonable range of applications. Commercial switching valves don't meet such requirements. In this paper, a novel, hydraulically piloted, seat type switching valve which approximately fulfils the mentioned requirements on switching time and flow rate is presented. The high flow rate is accomplished by multiple metering edges in a plate type valve, just like the well known Hörbiger compressor valve. The fastest switching time which is strongly pressure dependent is about 1.5 ms. Its seat valve properties make it highly suitable for emergency applications and mobile hydraulic applications were absence of leakage is required.

KEYWORDS: switching valves, big flow rate, fast switching, seat type valves

1. INTRODUCTION

Cost reduction and improvement of energy efficiency are of capital importance to keep hydraulic systems competitive with other drive technologies. The application of the hydraulic switching technology is a promising attempt to meet these demands.

Today, fast and precise hydraulic motion control can only be realized by the use of big and costly servo or proportional valves. They are typically applied to resistance principle with its considerable losses. Hydraulic switching control which requires fast and big switching valves can increase energy efficiency and lower costs. A poppet valve based realisation of this principle has been presented in [1, 2]. This spool type switching valve is directly operated by a solenoid and switches on and off within 1 ms at a nominal flow rate of about 45 l/min at 5 bar pressure drop.

Such a directly operated switching valves have two main shortcomings:

- The nominal flow rate is practically limited by the flow forces. Own investigations showed that a flow rate of about 50 l/min is a reasonable limit for a robust performance.
- A leaking valve is unacceptable in some cases, like for instance in many mobile machinery applications.

To avoid these shortcomings of spool valves a seat valve was developed. It is hydraulically piloted and should fulfil the following demands:

- Switching time of about 1 to 2 ms
- Nominal flow rate of about 100 l/min @ 5 bar pressure drop
- No leakage
- Low production costs
- Low electric power consumption of the pilot stage

2. BASIC CONCEPT

High flow rates need a large flow passage area. This can be realised either by a big stroke or by a big diameter of a spool or poppet valve respectively. But, both measures tend to increase the switching time which hinders to achieve the performance data mentioned above.

The new valve presented in this paper utilises the Hörbiger plate valve principle [3,4] which has several annular rings at two opposite valve plates to form multiple metering edges. This principle facilitates a very big flow passage area at a given poppet diameter and stroke. The Hörbiger plate valve which is used since about a hundred years as a compressor valve and a simplified scheme of the presented hydraulic valve are shown in Figure 1. The passage area is controlled by the distance of both plates.

The flow saturates if the plates' distance is approximately one half of the groove width. The smaller this width the smaller the necessary plate stroke and the faster the switching

time of the valve. Exploitation of this measure is limited by the manufacturing process, by oil contamination, or by fluid friction effects which may destroy the positive effect narrow grooves if they become too small.

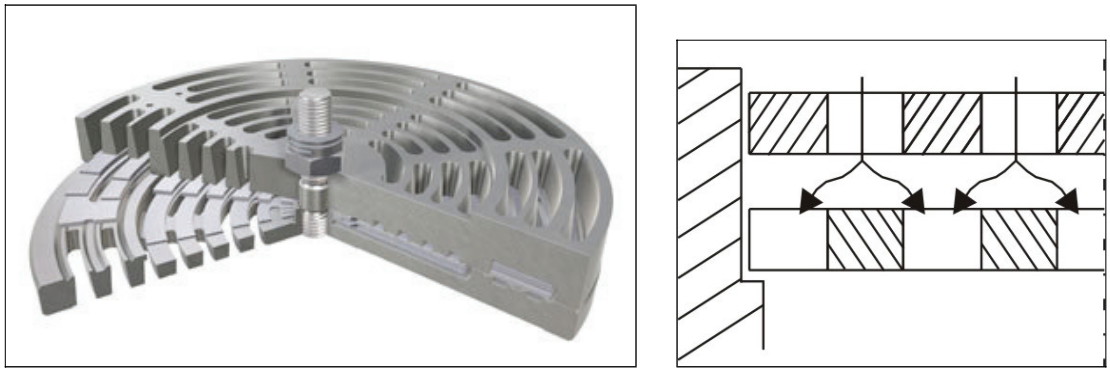

Figure 1: Hörbiger plate valve (left) and simple scheme of the flow path (right)

To make it a fully controllable valve it must be equipped with some actuator to open and close the poppet. For this purpose, the Hörbiger principle is combined with the 2/2 way cartridge valve principle which applies a plunger to control the poppet position. Thus, the new valve can be considered a modified cartridge valve which applies the multiple metering edges plate valve principle instead of the conventional conical seat valve.

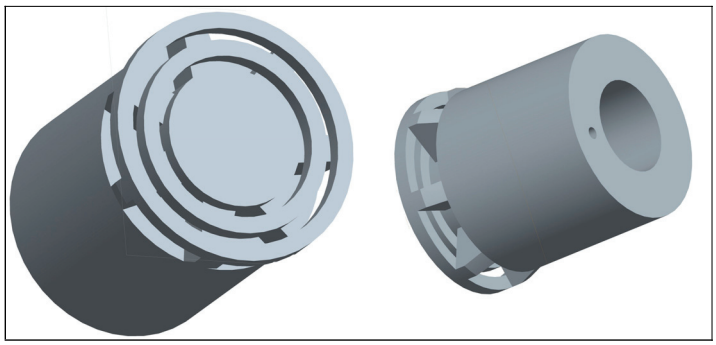

Figure 2: Poppet with coaxial metering edges

Figure 2 shows the realized poppet with its multiple metering edges. The opposite fixed plate is designed accordingly.

3. VALVE DESIGN

As already mentioned, the coaxial rings forming the metering edges are tiny structures to achieve small poppet strokes and, hence, a small switching time. The limitations in the feasible and affordable manufacturing techniques of the prototype valve resulted in a groove width of 1mm. Thus, the saturation stroke limit is about 0.5 mm.

Besides the number of the needed metering edges for a nominal flow rate of 100 l/min at 5 bar it has to be ensured that rigidity and strength of the rings are sufficient and the

surface pressure at the contact areas between poppet and opposite plate is not too high. Stresses and distortions have been analyzed, both, by an analytical model based on curved beam theory and by a Finite Element model.

Figure 3 shows the final design of the valve. As pilot valve a 3/2 way valve developed at LCM years ago for another application was used. The nominal flow rate of this pilot valve is about 3.5 l/min @ 5 bar pressure drop and an oil temperature of 45°C. The switching time of this valve is about 1.6ms (oil temperature: 23°C).

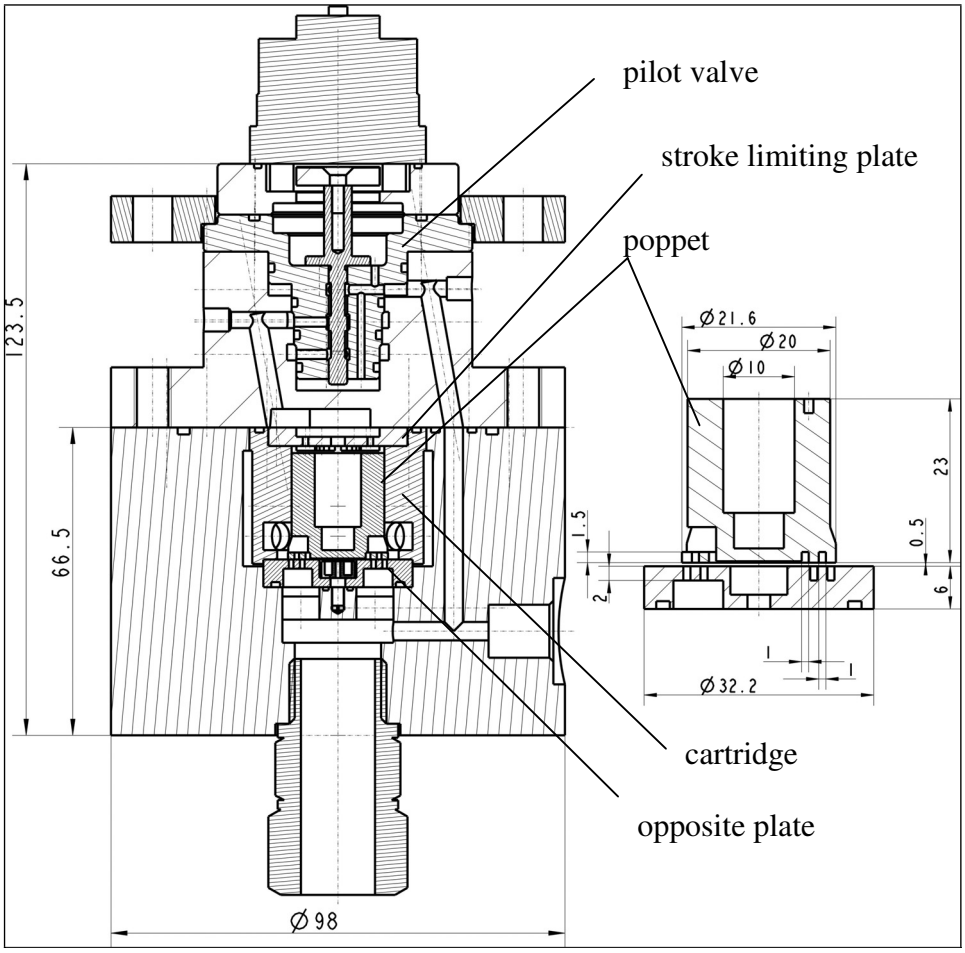

Figure 3: Design of the seat type switching valve

The poppet and its opposite plate are depicted in detail on the right side of Figure 3. In the center bore of the poppet the counterbalancing spring for closing the valve is arranged (not shown in Figure 3).

The poppet is guided within the cartridge which fixes also the opposite plate. Above the poppet a plate for limiting the poppet stroke is arranged.

4. EXPERIMENTAL RESULTS

Both, the pilot valve and the main stage have been measured in detail. The following experimental results are focusing on the main stage, since the pilot valve has not been a proper subject of this development.

4.1. Steady State Flow Characteristics

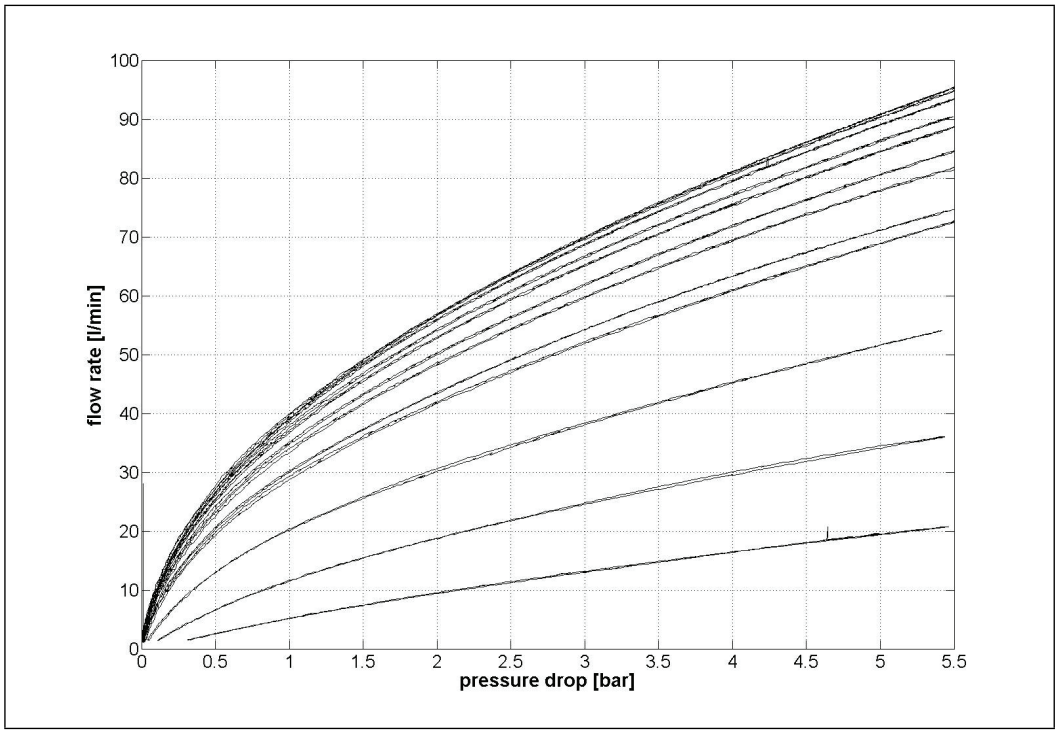

Figure 4: Steady state flow characteristic of the valve at 32°C

Figure 4 shows the steady state flow characteristic of the valve (main stage) for different poppet positions which have been adjusted by a special adjustment device in the range of 0.05 mm to 0.6 mm in steps of 0.05 mm.

The expected nominal flow of 100 l/min at 5 bar is not fully achieved. The maximum measured flow rate is about 90 l/min @ 5bar. This results from additional losses at the metering device which have not been taken into account in the basic dimensioning. Of course, with these experimental findings the model for calculating the nominal flow rate can be updated.

4.2. Dynamic Experiments

It is well known that the switching time of hydraulically piloted 2/2 way valves which exploit the two main stage pressures and don't apply a separate pilot pressure source depend strongly on the pressure drop over the valve. Thus the switching time has to be assessed in conjunction with the pressures at the two ports of the valve.

For this valve the flow rate at 200 bar difference pressure is about 600 l/min. Such high instantaneous flow rates can normally only be realized by very dynamical accumulators right at the ports of the valve (see Figure 5) and with very low parasitic inductivities between these two accumulators.

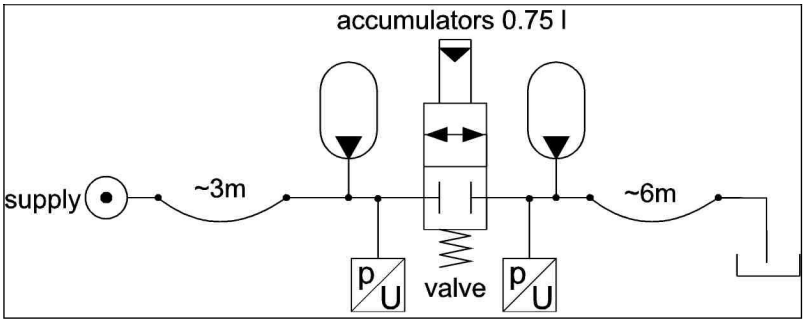

Figure 5: Hydraulic circuit for measurements

In the experiments the accumulators have been attached outside the valve, resulting in some sub-optimal dynamical performance of the system. With integrated accumulators, however, the switching times can be considerably decreased.

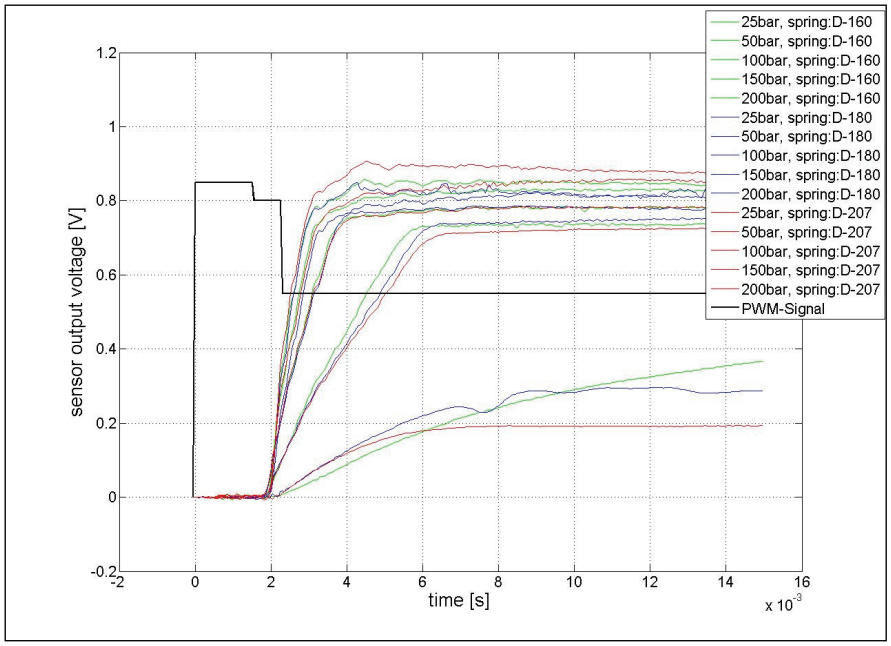

Figure 6: Opening curves of the valve's main stage (consider: switching of the pilot stage after the on signal takes about 1.6 ms)

Figure 6 depicts the results for the valve opening at different supply pressures and with different counterbalancing springs. At time = 0 the PWM-signal for the solenoid of the pilot valve is set (PWM=1 means 24V and PWM=0.5 means 0V). It has to be pointed out that in the diagrams only the voltage signal of the sensor is depicted and not the exact curve of the poppet position. A sound calibration of the position sensor with a reasonable effort was not possible due the special placement of the sensor in the valve. But this shortcoming is acceptable since the switching time is the main performance measure.

It takes almost 2 ms before the main stage starts to move. The switching time depends only marginally on the counterbalance spring stiffness. As expected, the pressure drop over the valve has the most important influence. For low pressures the switching times (which is defined as the time between 5% and 95% of total poppet stroke) are about 4 to 6 ms. For higher pressures (200 bar) the switching time of the main stage is reduced to 1.1 ms in the fastest configuration. But is must be pointed out that the rated pressure difference is only pending as long as the valve is closed. Once the valve starts opening a rapid drop of the pressure difference over the valves takes place which has a strong influence on the further valve motion.

To single out the influence of the supply system the switching times without accumulators have been recorded and are depicted in Figure 7.

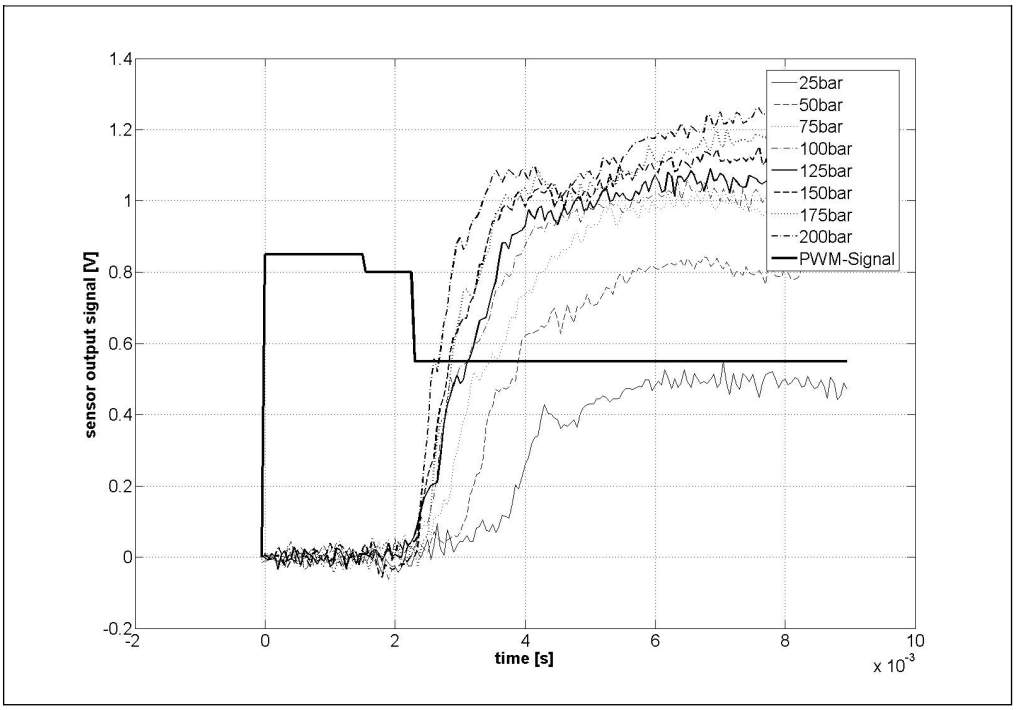

Figure 7: Valve opening curves without accumulators

The pressure evolution and the valve opening and closing motion depend on the dynamics of the whole system unless a perfect decoupling of the switching process from the system is achieved.

Figure 7 shows oscillations in the opening process resulting from pressure oscillations in the hydraulic system. In contrast to switching valves with a separate actuation system this valve has no proper characteristic switching time.

Besides the opening time of the main stage the closing time is a significant performance value. The results of the corresponding measurements are shown in Figure 8. Like for the opening of the valve the influence of the pressure drop over the valve is essential for the closing time. Again, the used counterbalance spring is not significant.

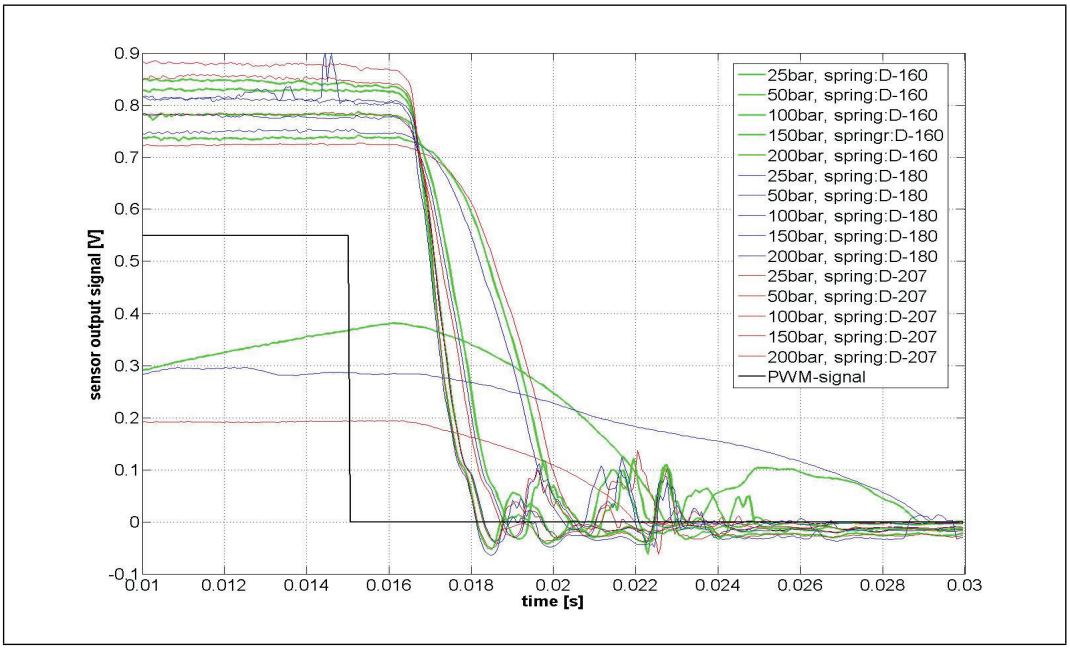

Figure 8: Closing time of the main stage

After the valve is closed one short reopening can be observed. The reason for that are negative pressure differences as can be seen in Figure 9. This valve acts as a check valve in the negative flow direction. When the pressure at the low pressure side rises above the high pressure side, what can easily occur via pressure pulsations in the system, the main stage will open.

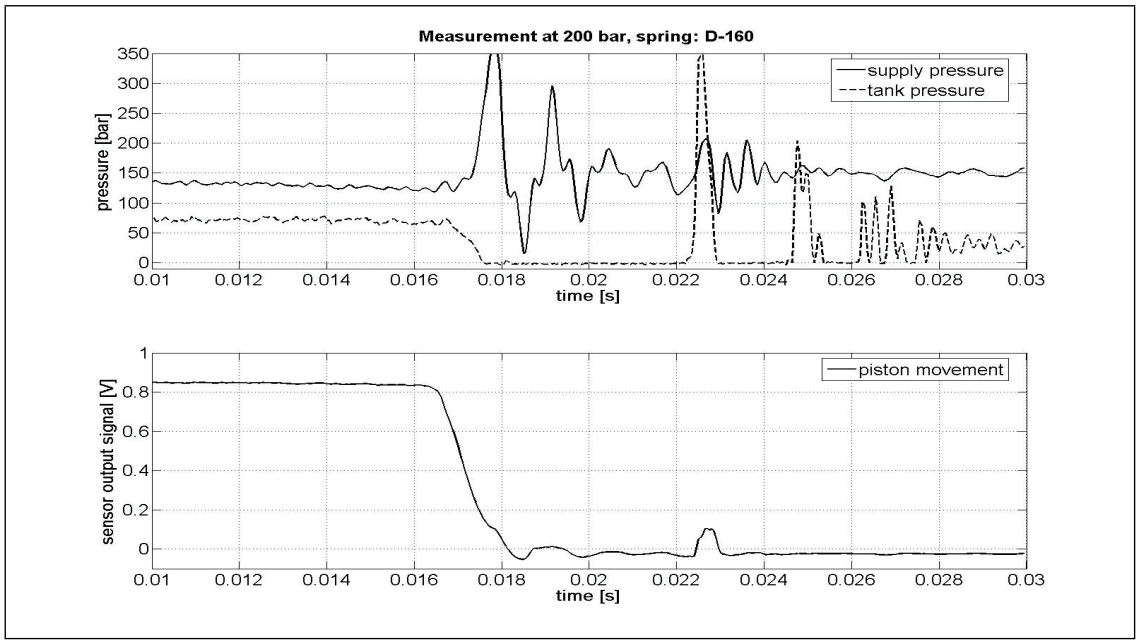

Figure 9: Pressure and poppet position for valve closing at 200 bar supply pressure

For the measurement with 200 bar supply pressure the valve closing and the corresponding pressures before and after the metering edge are depicted in Figure 9. After the closing of the valve (about 2ms) a pressure peak occurs at the low pressure side at about 0.022s. This pressure peak is responsible for the short reopening of the valve as can be seen in the lower diagram.

4.3. Leakage

Seat type valves normally are leakage free in the closed position. But this valve showed some small leakage as indicated in Table 1. For the measurement the inlet port is set under supply pressure and the leakage flow at the outlet port is measured in a measuring beaker. Sealing is provided by several bands along which the poppet and the opposite plate are in contact. The optimal width of these bands must assure a high enough contact pressure to avoid leakage but must avoid a damage of the surface by a too high contact pressure. The quality of this seat has to be improved in further versions of the valve. The main reason for the unexpectedly high leakage flow is that the sealing seat was slightly harmed by some hand grinding carried out to remove some adhesive on top of the position gauge.

Pressure [bar]	Leakage [ml/min]	Oil Temperature [°C]
50	0.45	27
100	0.8	28
200	2.8	28

Table 1: Leakage at different supply pressures

5. CONCLUSION

A new seat type valve has been presented which basically fulfils the demands on switching time (1ms) and nominal flow rate (100 l/min). Due to the dependency of the switching time on to the pressure drop over the valve the demanded switching time of about 1ms can only be achieved with a sufficient pressure drop prevailing at the valve even when it is open. The measured nominal flow rate of this valve (90 l/min) can easily be increased to higher values with some small modifications in the valve geometry.

For the presented prototype of the valve the annular grooves are 1 mm. This design can be realised with standard manufacturing processes like turning and milling without trouble. A thorough manufacturing analysis would be necessary prior to reducing this groove width considerably.

With modern production processes like etching or laser cutting tinier structures can be realised. This could reduce the needed poppet stroke and thus reduce the switching time.

The used pilot valve in the presented prototype is not properly aligned with the main stage. A bigger pilot valve would reduce the valve's switching time.

ACKNOWLEDGMENTS

The authors gratefully acknowledge the sponsoring of this work by the 'Linz Center of Competence in Mechatronics' in the framework of the Kplus program of the Austrian government. This program is funded by the Austrian government, the province of Upper Austria and the Johannes Kepler University Linz.

REFERENCES

1. Winkler, B.; Development of a Fast Low-cost Switching Valve for Big Flow Rates, In the Proceeding of the 3rd FPNI-PhD Symposium on Fluid Power, Terrassa, Spain, 2004

2. Winkler B., Scheidl R.; Optimization of a Fast Switching Valve for Big Flow Rates, In Proceedings of Bath Workshop on Power Transmission and Motion Control, PTMC 2006, Bath, England, UK, 2006.

3. Hörbiger, H. ; Rogler, F.; Patent: Ringventil mit Ventilfänger und Belastungsfedern, ATD5987419110710. June 1913

4. Hörbiger, J. ; Hörbiger, A.; Patent: Automatic Annular Valve, US19360061608 19360130. August 193

DESIGN PRINCIPLES FOR PROPORTIONAL PRESSURE REDUCING VALVES IN MOBILE APPLICATIONS

Dr.-Ing. Dirk Linden
Wandfluh AG
Helkenstrasse 13
CH-3714 Frutigen, Switzerland
phone: +41 33 672 72 72
email: dirk.linden@wandfluh.com
internet: www.wandfluh.com

ABSTRACT

Proportional pressure reducing valves are an important element in modern hydraulics. The applications and their requirements are many and diverse. Not surprisingly, today there are many different design principles available on the market which frequently leave the user helpless in view of this huge diversity.

The paper introduces the different design principles, analyses them systematically in detail and points out their advantages and drawbacks with respect to the application demands. For some widespread applications typical requirement profiles are elaborated. Application requirements as well as the typical performance of a design are graphically represented. By systematically matching these graphs, it is possible to select the optimum valve design for a given application.

KEYWORDS: Proportional, Pressure, Reducing, Control, Valve

1 APPLICATIONS

The applications for proportional pressure reducing valves are many and diverse. They can be found both in industrial as well as in mobile hydraulics. Other important fields are offshore technology and mining.

Here some of the most widespread applications are to be presented and analysed with respect to their specific requirements.

1.1 Hydraulic Motor Drive

The applications for hydraulic motors can be roughly split-up into those where the load is known, i.e. where there is a close association between pressure and speed, and those, where the load varies.

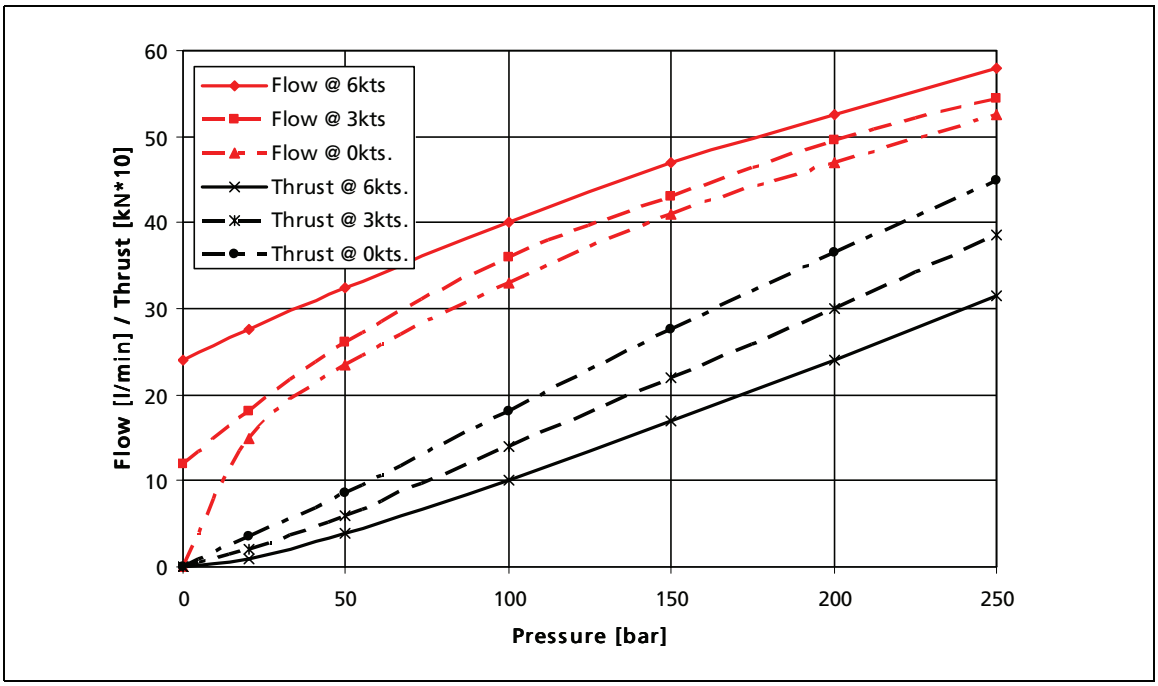

Fig. 1: Characteristic curve of a ROV-Thruster

The first case is applicable, e.g. for fan drives, therefore propellers in air and on thrusters in ships, therefore propellers in water. Similar conditions can also be found for mixing and conveying fittings in the chemical industry, and in extruder drives for injection moulding machines. As is illustrated in Fig. 1, on the basis of a characteristic curve of a thruster of a remote operated submarine vehicle (ROV), there is a close connection between the operating pressure and, in this case, the thrust of the thruster. The situation is similar for the fan drives of construction machines (Fig. 2).

Fig. 2: Hydraulic fan drive in a construction machine

In these applications, pressure reducing valves frequently provide advantages versus flow control valves. In the example of the ROV, e.g., with a flow controller the propeller speed, but not the thrust would be influenced, which actually would be required. Flows above approx. 80 l/min frequently cannot be achieved with flow control valves, because these are only available in direct controlled versions.

In the case of a varying load, such as with a saw motor or a spindle drive of a machine tool, however, a flow control valve has to be used, if the objective is maintaining a constant speed.

1.2 Clamping / Braking

An important field for pressure reducing valves are all the hydraulic clamping or braking applications.

A typical application for clamping can be found in modern machine tools. Complex, filigree components, such as motor blocks are frequently clamped at different points with differing clamping pressures, on one hand in order to prevent a distortion, on the other hand in order to hold the work-piece securely. In modern machining centres up to eight channels are available with proportionally adjustable clamping pressures which are independent one of another.

As an example for braking, the service brake of an cable car can be quoted, where the drive has to be gently braked when traversing a support column or running into the station.

Applications of clamping and braking have the common requirement that the pressure has to be adjustable over a wide range, but that there typically is no volume flow, or only a very low one. In addition, for these applications it is usually necessary to have the possibility to control down to 0 bar, in order to completely release a brake disc for example.

1.3 Pressing / Pressing against

In the case of forest harvesters, the transport rollers for the transportation of the log have to press against it with a precisely defined pressure during the removal of the branches. This is only one of several examples, where in a process a roller or something similar has to be pressed against a work-piece.

Typical pressing applications are to be found in the compressing of waste, or in the compaction of harvested goods in agriculture.

A special pressing application can be found in the paper -, plastics - and steel industries, where foils or tapes run through rollers and are to be rolled to a certain thickness. To compensate for the sag of these very huge and heavy so called calender rollers, they are specifically bent at different

points by means of pressure impingement, in order to achieve a uniform thickness of the rolled goods over the complete width of the roller (Fig. 3).

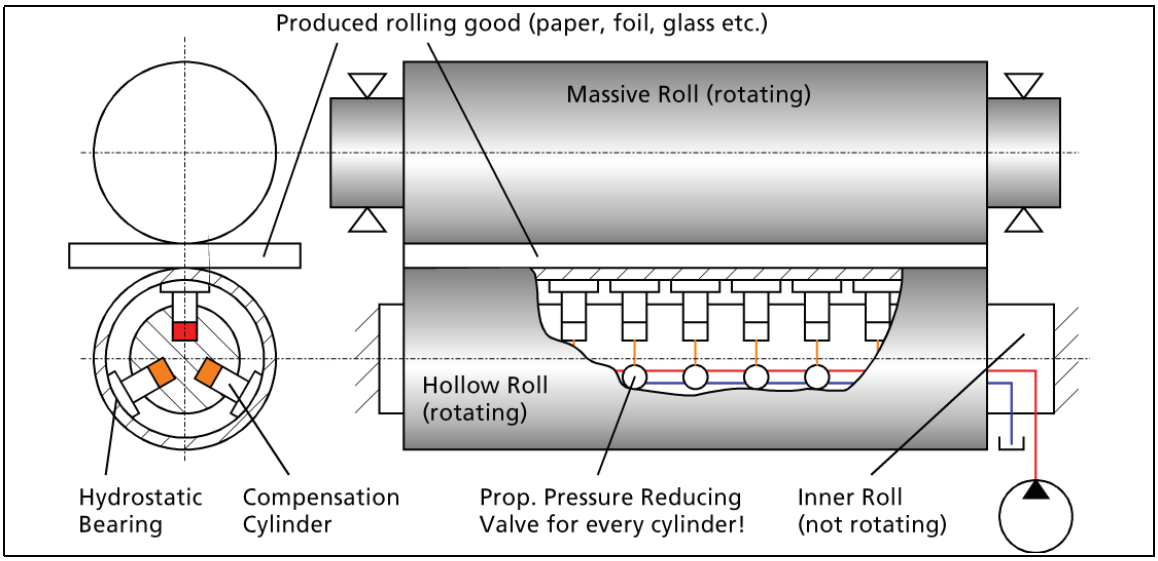

Fig. 3: Sag compensation on calender rolls

In contrast to the applications of clamping and braking, during pressing and pressing against there normally is a movement of the hydraulic cylinder, therefore there is a certain volume flow. The disruptions can be very dynamic - one can imagine, for instance, the sudden giving way of the pressed goods in a waste press. Particularly for industrial applications, frequently a very high precision of the pressure control system is demanded.

1.4 Piloting

Possibly the most frequent application for pressure reducing valves is the pilot operation of larger valves. Finally, also the flapper-nozzle pilot operation of the servo valve is nothing else than a pressure reducing valve.

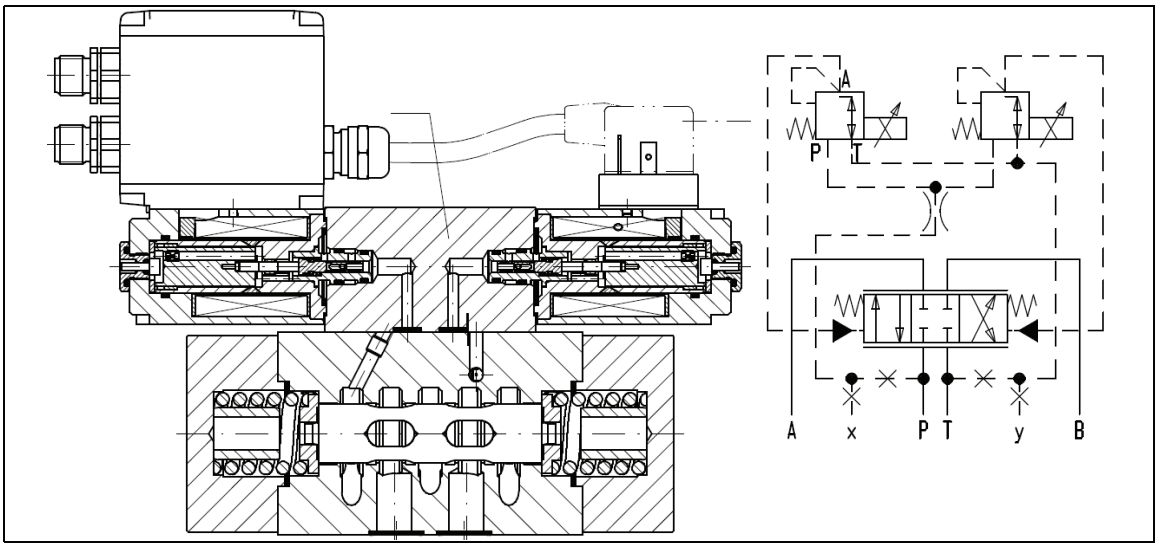

Fig. 4: Proportional directional control valve pilot operated by direct driven proportional pressure reducing valves

Here classical multi-stage valves in spool - or cartridge construction are meant. A large pilot operated proportional directional control valve can very elegantly be designed with one or two pressure reducing valves, without a displacement sensor being necessary for the main stage (Fig. 4).

Apart from the pilot operation of valves the hydraulic adjustment of hydraulic pumps and - motors has to be mentioned, which is closely related.

1.5 Specific Requirements for Typical Applications

Here the attempt shall be made to elaborate specific requirement profiles for the typical applications of proportional pressure reducing valves described above. Of course every application is unique. Nonetheless practical experience has shown, that there are typical requirement profiles for the application fields mentioned.

For the elaboration of the requirement profiles, the following criteria shall be taken into account:

- Maximum volume flow
- Leakage
- Maximum pressure
- Minimum adjustable pressure
- Reproducibility
- Hysteresis
- Dynamics
- Gradient of the volume flow - pressure characteristic curve

Apart from these, there is a multitude of further criteria, such as:

- Contamination tolerance
- Service effort
- Installation effort
- Robustness
- Costs

In contrast to the first group, however, these can hardly be attributed to the application. One example: While for braking applications, be they mobile or industrial, it is absolutely typical, that a low maximum pressure is demanded, so that the braking pads can lift off the brake disc also without a reset spring, the pressure of the cost without doubt is higher for a brake on a mobile vehicle, than, for instance, for a tractive force control system in a rolling mill.

Expressed differently, the criteria of the first group are effectively dependent on the fundamental mechanical function, for which the valve is being used (therefore motor drive, clamping, braking, pressing, etc.), while the second group of criteria is rather more typical for the ambient, in which the valves are used (therefore mobile unit, industrial application, mining, off-

shore, special machine, series machine, etc.). With this consideration, grey zones cannot be avoided of course.

Fig. 5 illustrates how the typical applications mentioned above can be described with reference to their requirements. It becomes visible that, in dependence of the application, completely differing, partly even contradictory requirement profiles are demanded.

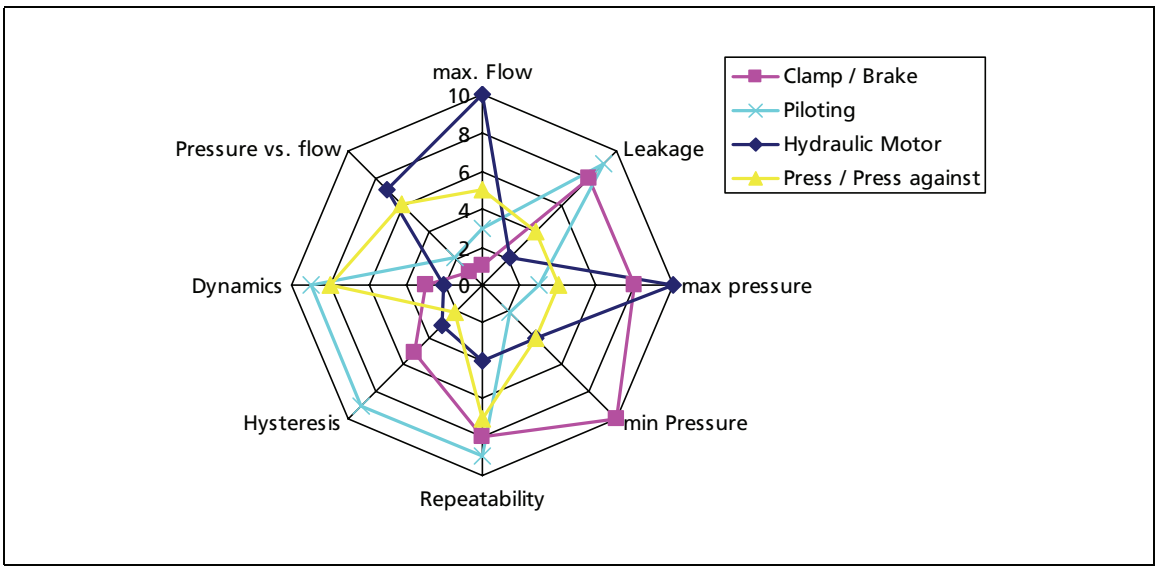

Fig. 5: Requirement profiles of typical applications

While, for example, in pilot applications the leakage is always of decisive significance, this normally is unimportant for driving hydraulic motors. But in the case of the maximum achievable flow throughput, it is exactly the opposite. The flow throughput is decisive for the motor driving, and it is less important for pilot operations in most cases.

2 DESIGN PRINCIPLES

In this section, the design principles for proportional pressure reducing valves available on the market are to be presented and their specific characteristics elaborated.

2.1 Direct Drive

The direct driven proportional pressure reducing valve is the simplest conceivable design for valves of this kind. The design principle is illustrated in Fig. 6.

In this principle, the pressure in the consumer connection acts on the front side of the spool. Acting against it are the spring force and the force of the proportional solenoid. The control edges are arranged radially to the pressure - and tank port. In the non-activated condition (no solenoid force), the

working connection is linked with the tank port. By activating the proportional solenoid, the spool is moved against the spring and a connection A to P is opened. This causes the pressure in A to rise, to work against the solenoid force and to move the spool back. As from a certain stroke, the connection A to P is closed and the connection A to T opened again, so that the pressure is able to sink. The final result is a hydraulically - mechanically controlled equilibrium between the solenoid force (proportional to the solenoid current) and the consumer pressure.

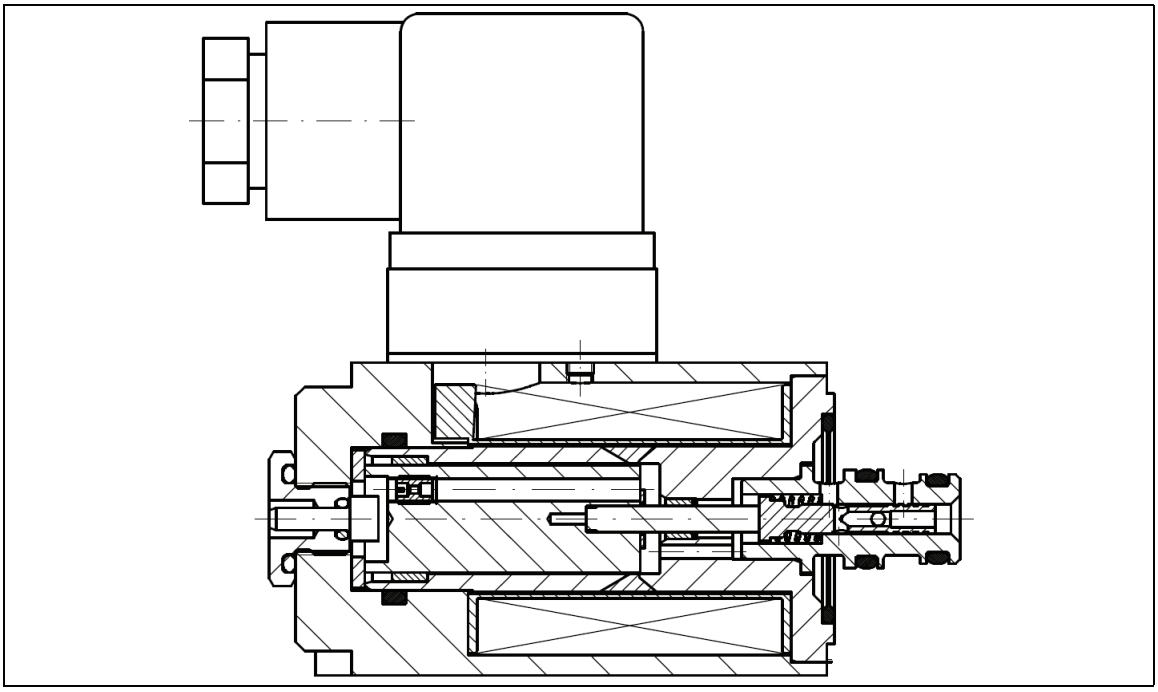

Fig. 6: Sectional view of a direct driven proportional pressure reducing valve (Wandfluh MDPPR11)

With respect to its design, the valve is distinguished by its tremendous compactness, which predestines it as a pilot operating element. In practice, the pressure achievable is limited to a maximum of 40 bar by the available solenoid force, and the minimum spool diameter capable of being manufactured. In addition the maximum volume flow is very limited because of the small spool diameter.

With respect to the requirement criteria defined in the first chapter, this valve construction can be characterised as follows:

- Maximum volume flow: Very small - small
- Leakage: Low
- Maximum pressure: Low
- Minimum adjustable pressure: Very low
- Reproducibility: Very good
- Hysteresis: Very good
- Dynamics: Medium - good
- Gradient characteristic curve: Steep (poor)

2.2 Direct Drive with Pilot Piston

A variant of the direct operated proportional pressure reducing valves are the valves with a pilot piston. The principle is illustrated in Fig. 7. Here the main spool is pressure-balanced. Only the spring force, the force of the pilot piston and the flow forces are acting on it.

The pilot piston is a very thin pin. Typical is a diameter of 1 to 3 mm. On the one front side the consumer pressure A is acting on it, on the other side the solenoid pressure. With this dodge it is possible to directly control high pressures, and nonetheless to achieve volume flows up to a maximum of 20 l/min because of the large diameter of the main spool.

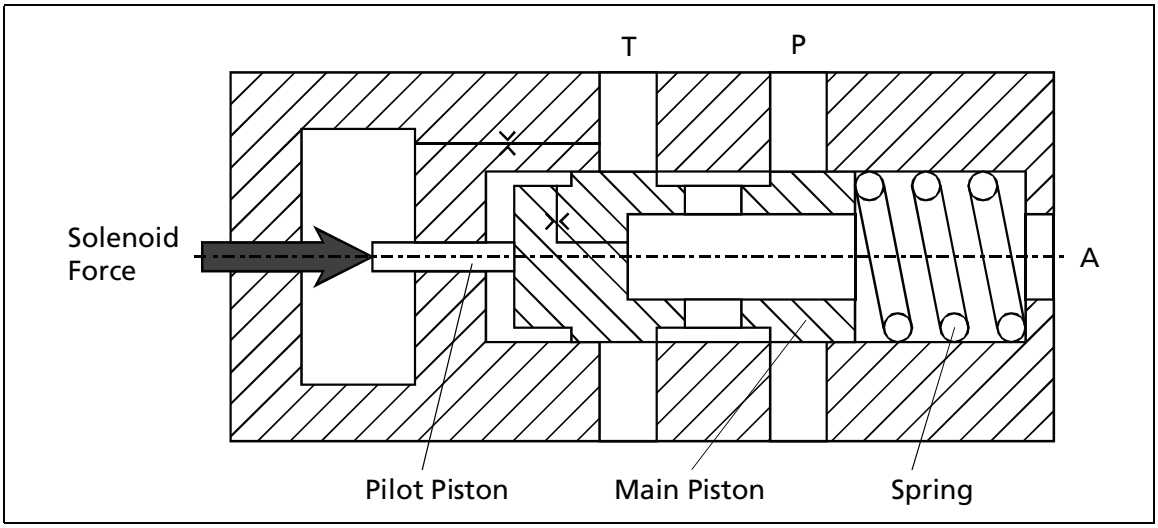

Fig. 7: Valve direct driven by pilot piston (Principle)

In practice, however, this concept has not been able to prevail up to now. On one hand, the guiding of the pilot piston and its alignment to the main spool produces friction problems, which result in a high hysteresis and a poor reproducibility. On the other hand, the very low actuation force available in comparison with pilot operated valves results in a rather steep pressure - volume flow characteristic curve. Also dynamically these valves are weak, because relatively large strokes and actuating forces are faced with only a small surplus of solenoid force.

With respect to the requirement criteria defined in the first chapter, this valve construction can be characterised as follows:

- Maximum volume flow: Medium
- Leakage: Medium
- Maximum pressure: High
- Minimum adjustable pressure: Low
- Reproducibility: Poor
- Hysteresis: Poor
- Dynamics: Poor
- Gradient characteristic curve: Steep (poor)

2.3 Pilot Operated

Fig. 8 illustrates an example of a pilot operated proportional pressure reducing valve. On the front of the main spool the consumer pressure A is acting from the valve nose. On the solenoid side (resp., the rear side) of the main spool the pilot operating pressure and the spring force are acting. The pilot operation itself is implemented as a proportional pressure relief valve. In the example presented, the pilot operation is supplied from the consumer connection A through a nozzle in the main spool. The precise function of the pilot operation will be shown in chapter 2.3.2.

The pressure control on the main spool works similarly to that of the direct operated concept - with the difference, that an equilibrium between the solenoid and the consumer pressure is not directly produced, but between the pilot operation pressure and the consumer pressure. This concept is suitable for very large volume flows (200 l/min and more). The most significant disadvantage, however, is that, due to the nozzles in the pilot operation and the spring on the main spool, a certain minimum pressure cannot be fallen below. In practice, this value is at approx. 10 bar.

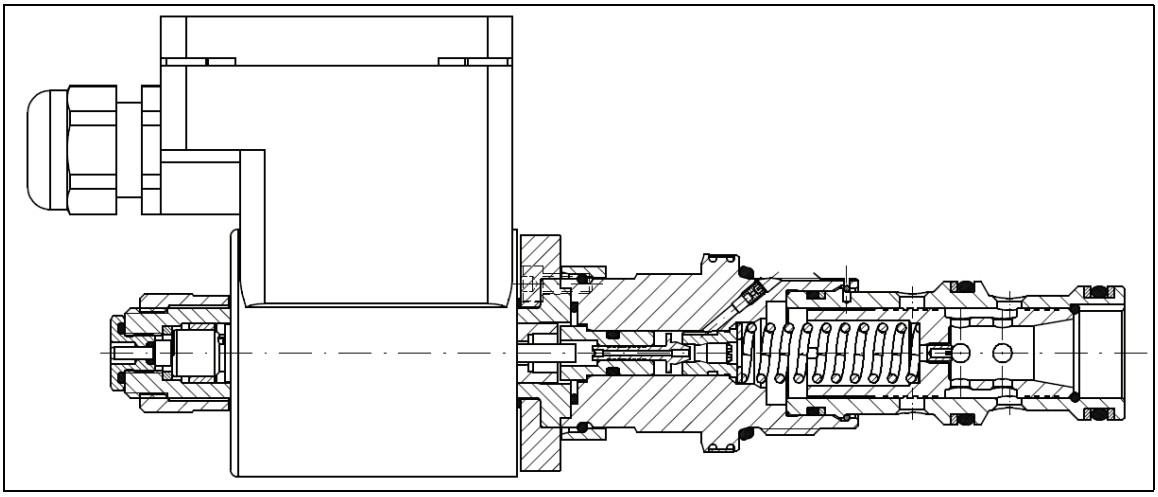

Fig. 8: Pilot operated proportional pressure reducing valve (Wandfluh MVCPM33 - Explosion proof)

With respect to the requirement criteria defined in the first chapter, this valve construction can be characterised as follows:

- Maximum volume flow: Very large
- Leakage: Medium
- Maximum pressure: Very high
- Minimum adjustable pressure: Medium
- Reproducibility: Good
- Hysteresis: Good
- Dynamics: Good
- Gradient characteristic curve: Flat (good)

2.3.1 Source of Pilot Flow

The most significant disadvantage of standard pilot operated pressure reducing valves is the minimum pressure which is only adjustable above a certain level. This can be overcome with a main spool design where, with not operated solenoid, the connection A-T is open instead of the connection P-A. In this case, however, the supply of the pilot operation cannot anymore take place from the consumer connection A. This, because a pressure has to be set on the rear side of the spool which is higher than the consumer pressure. Finally, apart from the consumer pressure also the spring force has to be overcome.

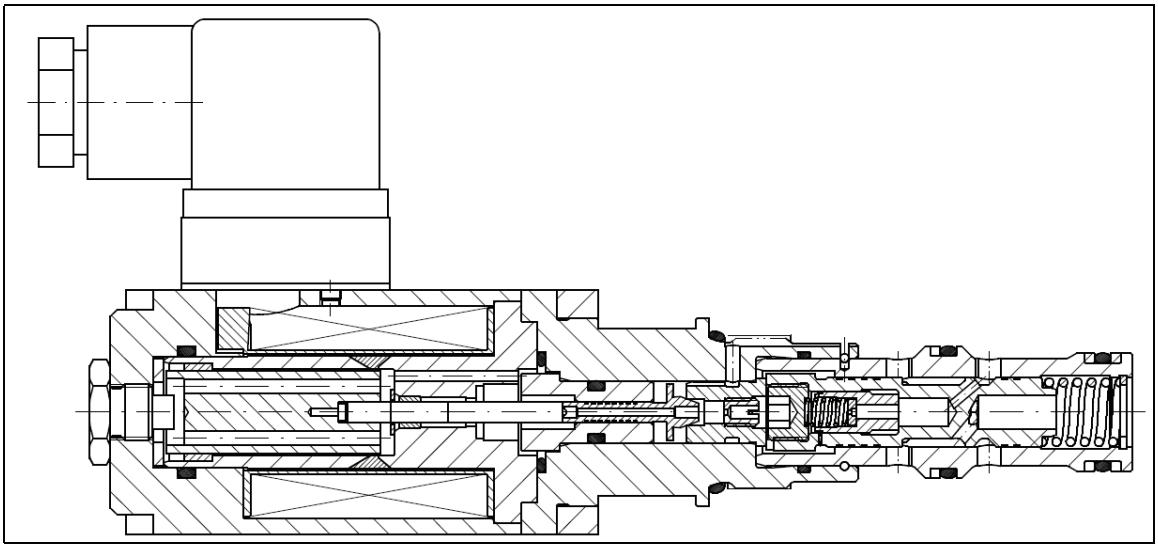

Fig. 9: Pilot supplied from P-Port (Wandfluh MQPPM22)

In the concept described under 2.3, the valve leakage is dependent on the consumer pressure in A. With the supply of the pilot operation from P, however, it is dependent on the system pressure in P, which normally is very high. But as the valve has to be designed in such a manner, that also with low system pressure sufficient pilot operation oil is available for a good valve function, this concept leads to an increased leakage oil flow.

The construction illustrated in Fig. 9 counteracts this with a miniaturised 2-way flow control valve integrated into the main spool. With this, the pilot operation oil flow (therefore the valve leakage) is controlled within tight limits with the effect, that the overall leakage, in the case of high pressures, is even lower than if the pilot operation is supplied from A.

With respect to the requirement criteria defined in the first chapter, this valve construction can be characterised as follows:

- Maximum volume flow: Large - very large
- Leakage: Small - medium
- Maximum pressure: Very high
- Minimum adjustable pressure: Very low
- Reproducibility: Good
- Hysteresis: Good

- Dynamics: Good
- Gradient characteristic curve: Flat - very flat (good - very good)

2.3.2 Pilot Design

For the design of the pilot control itself, different concepts are utilised (Fig. 10). The simplest design consists of a ball with a seat belonging to it. At first sight, this design is very economical, because precise balls are well available at low prices. But in practice an elaborate guiding of the ball with a cage is necessary.

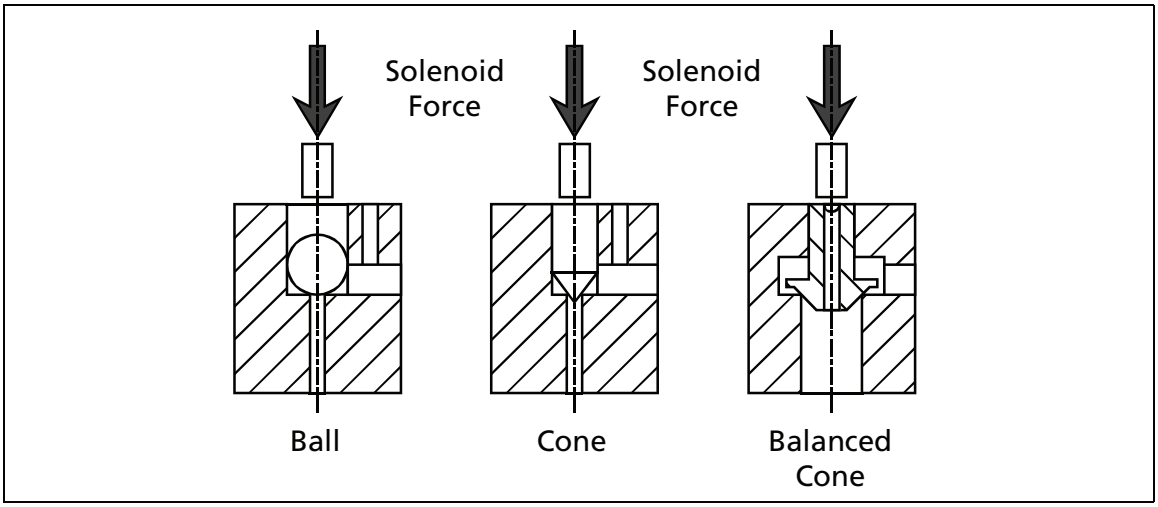

Fig. 10: Design principles of pilot controls

A further design uses a cone instead of the ball. With the conical design, it is much more simple to implement the guiding.

As a further variant, all pilot operated Wandfluh valves have a pressure compensated pilot operation cone in accordance with the differential surface area principle. The essential advantage of this concept is, that it is significantly less susceptible to oscillation than all other known principles. This is because the seat diameter is significantly larger than in the case of a ball seat or of a non pressure compensated (balanced) cone seat. A comparatively small stroke of the pilot operation adjusts itself. With this, the gap the fluid flows through is considerably wider and less high than in other concepts. There is less turbulence in the jet, fewer vortices are formed, and as a result the susceptibility of the valve to oscillation is clearly reduced.

2.4 Electronics / Closed loop control

Every proportional valve requires driving electronics. For this purpose both analogue as well as digital versions, both as on-board as well as standalone versions are available. The advantages and disadvantages of the different versions have already been discussed in detail in literature [1-3], so that they shall not be dealt with more closely here.

Independent of the type of valve utilised, a significant improvement of the dynamic-, and above all of the static control characteristic can be achieved by means of a pressure control in a closed loop control system. For this, an electronic pressure sensor is used. The control electronics compare the actual pressure signal of the sensor with the set-point pressure signal. In function of the control deviation established, the control electronics adjusts the correcting variable (therefore the solenoid current) so that the desired control characteristic is obtained.

Apart from the proportional pressure reducing valves presented here, it is also possible to use directional control valves in control valve - or servo valve versions for the pressure control in a closed loop. However, they are considerably more expensive and, in this particular application, they provide hardly any advantages.

3 APPLICATION SPECIFIC DESIGN CHOICE

The characteristics profiles of the different valve designs elaborated in chapter 2 are illustrated in Fig. 11. Through a comparison with the requirement profiles of typical applications represented in Fig. 5, it is possible to derive which type of valve design is optimally suitable for the corresponding application.

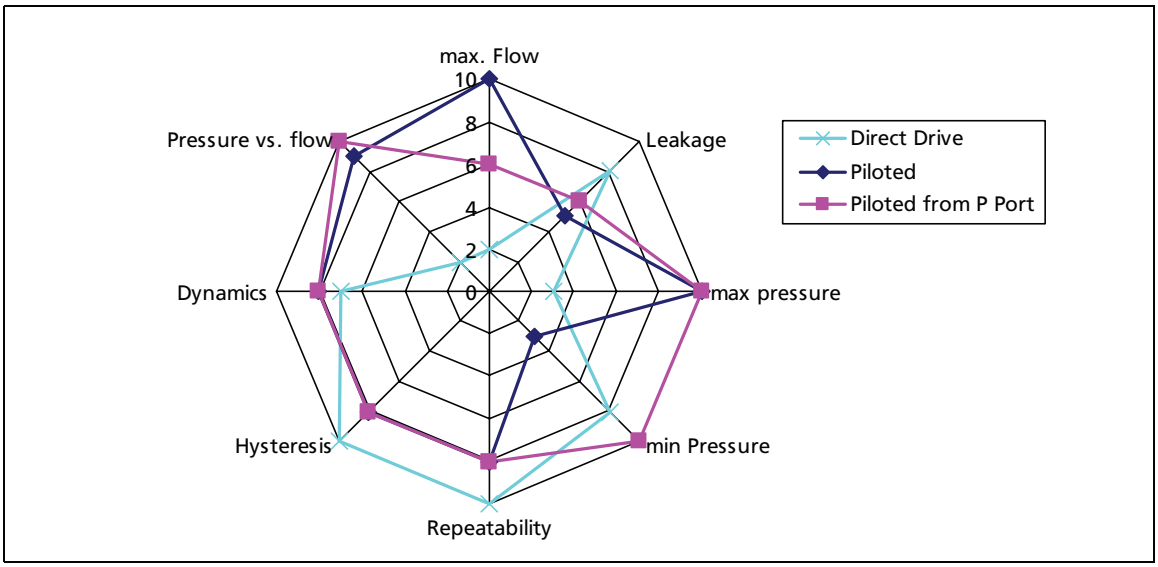

Fig. 11: Characteristics profiles of valve designs

In detail, the following statements can be made:

For pilot control applications, mainly direct controlled valve types are recommended. Requirements profile and characteristics profile are practically congruent. The low leakage rate and the good control characteristics (hysteresis and reproducibility) are the decisive points.

For pressing -, braking - and clamping applications, pilot operated versions with a supplying of the primary stage from the P - connection are especially suitable. The decisive point is the particularly low minimum pressure of this valve design.

For the driving of hydraulic motors and of other applications with a high volume flow requirement, pilot operated valves with a supplying of the pilot control from the working connection are particularly suitable.

4 CONCLUSIONS

It has been demonstrated that "the" proportional pressure reducing valve as such does not exist. Rather more, the requirements of the most differing applications are so diverse and partly even contradictory, that there have to be different solutions.

It is not very surprising that the most diverse versions of proportional pressure reducing valves are to be found on the market, which all have their justification, respectively, their specific field of application.

With the requirement profiles of the valve designs and the requirement profiles of the different applications elaborated within the framework of this article, the user is provided with an decision-making aid, which will show him the way to solve a specific problem.

5 LITERATURE

[1] Linden, D.
Standard proportional valves with digital onboard electronics
Hydraulikdagar i Linköping, June, 3rd-4th, 2003

[2] Linden, D.
A sense of proportion
IVT - International Vehicle Technology 2004
Lift Truck & Materials Edition, pp. 131-133

[3] Linden, D.
Standardproportionalventile mit integrierter Elektronik
O+P Ölhydraulik und Pneumatik, April 2004, pp. 228-230

THE DYNAMIC PROPERTIES OF A POPPET TYPE HYDRAULIC FLOW AMPLIFIER

Björn ERIKSSON, Bo R ANDERSSON and Jan-Ove PALMBERG
Division of Fluid and Mechanical Engineering Systems
Department of Mechanical Engineering
Linköping University
58183 Linköping
SWEDEN
Email: bjorn.eriksson@liu.se

ABSTRACT

This paper examines the dynamic properties of a two-stage flow control valve of the "Valvistor" brand. There are several benefits to this: the valve has a high closed loop bandwidth, the design allows big flow capacities etc. An attractive feature of this two-stage valve is that the pilot flow contributes to the total flow giving higher steady state flow efficiency. This paper presents an analytical model of this particular type of valve. A simplified model with relevant approximations is also presented. Measurements on the valve were made to validate the valve model. The paper also includes a further discussion about the pros and cons of the valve in open and closed loop applications.

KEYWORDS: fluid power, Valvistor, dynamic model

NOMENCLATURE

The quantities used in this paper are shown in tables 1 and 2. Upper-case letters of variables that are also presented in lower-case letters mean that they are in linearized form.

Table 1: Quantities

Quantity	Description	Unity	Quantity	Description	Unity
K_v	Static gain, denominator	$\frac{m^4}{s}$	K_{vY}	Static gain, nominator	$\frac{m^6}{s^2}$
K_{vPA}	Static gain, nominator	$\frac{m^9}{Ns^2}$	K_{vPB}	Static gain, nominator	$\frac{m^9}{Ns^2}$
K_{QM}	Flow gain, main poppet	$\frac{m^2}{s}$	K_{CM}	Pressure gain, main poppet	$\frac{m^5}{Ns}$
K_{QP}	Flow gain, pilot valve	$\frac{m^2}{s}$	K_{CP}	Pressure gain, pilot valve	$\frac{m^5}{Ns}$
K_{QS}	Flow gain, feedback slot, main poppet	$\frac{m^2}{s}$	K_{CS}	Pressure gain, slot, main poppet	$\frac{m^5}{Ns}$
K_M	Spring coefficient, main poppet	$\frac{N}{m}$	K_P	Spring coefficient, pilot poppet	$\frac{N}{m}$
K_{FXM}	Flow force coefficient, main poppet	$\frac{N}{m}$	K_{FPM}	Flow force coefficient, main poppet	m^2
K_{FXP}	Flow force coefficient, pilot poppet	$\frac{N}{m}$	K_{FPP}	Flow force coefficient, pilot poppet	m^2
B_M	Viscous friction, main poppet	$\frac{Ns}{m}$	C_C	Hydraulic capacitance above poppet	$\frac{m^5}{N}$
A_M	Area, main poppet	m^2	m	Mass, main poppet	kg
ω	Break frequency	$\frac{rad}{s}$	δ	Damping, flow angle	$-$, $^\circ$
q, Q	Flow	$\frac{m^3}{s}$	p, P	Pressure	Pa
x_M, X_M	Poppet position	m	y_P, Y_P	Pilot poppet position	m
κ	Area ratio, poppet	$-$	C_q	Flow coefficient	$-$
w	Area gradient	m	ρ	Density	$\frac{kg}{m^3}$
f, F	Force	N	α	Angle	$^\circ$
g	Flow gain	$-$	s	Laplace operator	$\frac{1}{s}$

Table 2: Subindexes

Subindex	Description	Subindex	Description
Y	Pilot stroke	P	Pilot
S	Slot in the poppet	M	Main poppet
PA	Pressure on the A-side of the valve	PB	Pressure on the B-side of the valve
A	A-side of the valve	B	B-side of the valve
C	Chamber above the poppet	s	Steel
q	Flow forces		

1 INTRODUCTION

The Valvistor valve was originally developed at Linköping University in the early 1980s [1]. The Valvistor principle was first produced by Hydrauto, a Swedish valve manufacturer, and used in a directional load-sensing valve, called Rego, for mobile applications where the conventional spool was replaced by four Valvistor poppet valves. The valve was produced during the 1980s until propriety was transferred to Vickers in the USA. Since the early 1990s, Vickers (today owned by Eaton) has been producing Valvistor valves of different types and sizes. One common valve for both mobile and industrial use is their EPV16 valve where the Valvistor poppet and an electrical operated pilot valve are designed into a standardized screw-in cartridge. See figure 1(a).

The pilot valve in the EPV16 valve is proportionally controlled by a proportional solenoid. The force from the solenoid acts on a normally closed pilot poppet against a preset return spring. See figure 1(b). The outlet pressure is also connected to the spring side as well as to the solenoid which makes the pilot valve completely balanced from static pressure. The pilot flow direction is from the side to the nose. The poppet has a very specific shape, where the pilot valve is pressure compensated by using both opening as well as closing flow forces. The flow direction makes it possible to use opening flow forces to reduce the closing flow forces to obtain a net closing flow force that works together with the spring coefficient. Therefor a change in the flow force results in a change of pilot position.

The pressure balance of the pilot valve is essential for the performance of the complete Valvistor valve. If this pressure balance is not understood, as is the case in [2] and [3] where Alleyne et al has made a mathematic model of the EPV16 valve assuming that the pilot valve is not pressure balanced, the steady state performance of the complete valve will be misunderstood. In their investigation they have also drawn some erroneous conclusions about the dynamic performance of the Valvistor valve. One object of this paper is to present a detailed accurate mathematical model of the Valvistor, and in particular the dynamic performance of the main Valvistor valve.

The performance of the Valvistor valve depends on both the pilot valve and the main valve. In all practical applications of the EPV16 valve, the dynamic performance of the pilot valve completely dominates the dynamic performance of the complete EPV16 valve.

The bandwidth of the pilot valve is low because of the slow proportional solenoid where the armature has a large mass and where the coil has a high inductance.

With a pressure drop of 1 MPa or higher, the bandwidth of the EPV16 is therefore limited to about 10 Hz. The bandwidth of the main Valvistor valve itself depends on the pressure drop and has a much higher bandwidth, especially at a higher pressure drop.

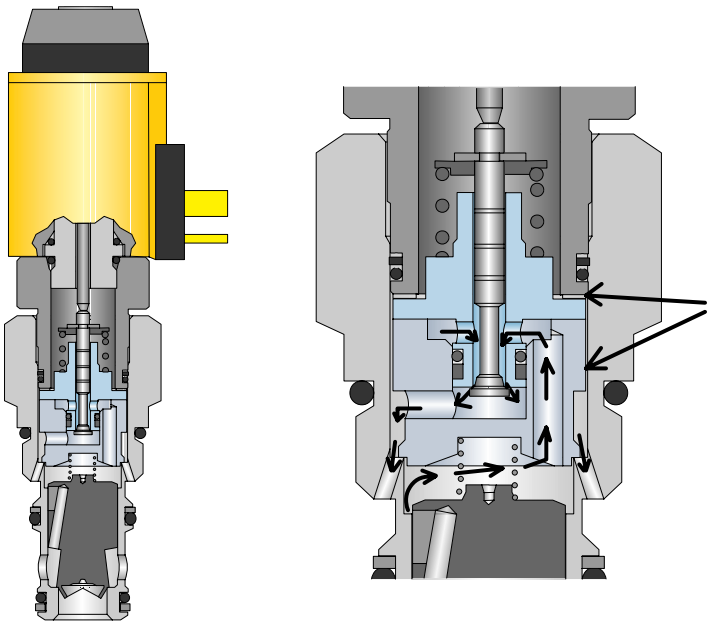

(a) A cross-sectional sketch of the EPV16 valve

(b) Detailed view of the EPV16 valve showing the pilot flow path and the pressure balanced pilot poppet

Figure 1: EPV16, a multi-purpose proportional flow control Valvistor valve produced by Vickers

2 MODEL

The modeled valve can be seen in figure 2. This valve can be described by the equations below, see [4], (1) - (7). The equations are Laplace transformed and linearized on the right hand side.

$$q_{tot} = q_p + q_M \qquad Q_{tot} = Q_p + Q_M \tag{1}$$

$$q_M = C_q w_M x_M \sqrt{\frac{2}{\rho}(p_B - p_A)} \qquad Q_M = K_{QM} X_M + K_{CM}(P_B - P_A) \tag{2}$$

$$q_P = C_q w_P y_P \sqrt{\frac{2}{\rho}(p_C - p_A)} \qquad Q_P = K_{QP} Y_P + K_{CP}(P_C - P_A) \tag{3}$$

$$q_S = C_q w_S x_M \sqrt{\frac{2}{\rho}(p_B - p_C)} \qquad Q_S = K_{QS} X_M + K_{CS}(P_B - P_C) \tag{4}$$

$$q_S - q_P = -\dot{x}_M A_M + C_C \dot{p}_C \qquad Q_S - Q_P = -s X_M A_M + s C_C P_C \tag{5}$$

$$f_q = 2 C_q w_M x_M (p_B - p_A)\cos\delta \qquad F_q = K_{FXM} X_M + K_{FPM}(P_B - P_A) \tag{6}$$

$$p_A(1-\kappa)A_M + p_B \kappa A_M - p_C A_M - f_q = \ddot{x}_M m + \dot{x}_M B_M + x_M K_M$$

$$P_A(1-\kappa)A_M + P_B \kappa A_M - P_C A_M - F_q = s^2 X_M m + s X_M B_M + X_M K_M \tag{7}$$

Transfer functions from pilot stroke, A-side pressure and B-side pressure, Y_P, P_A and P_B respectively, can be determined. The transfer functions end up in three third order

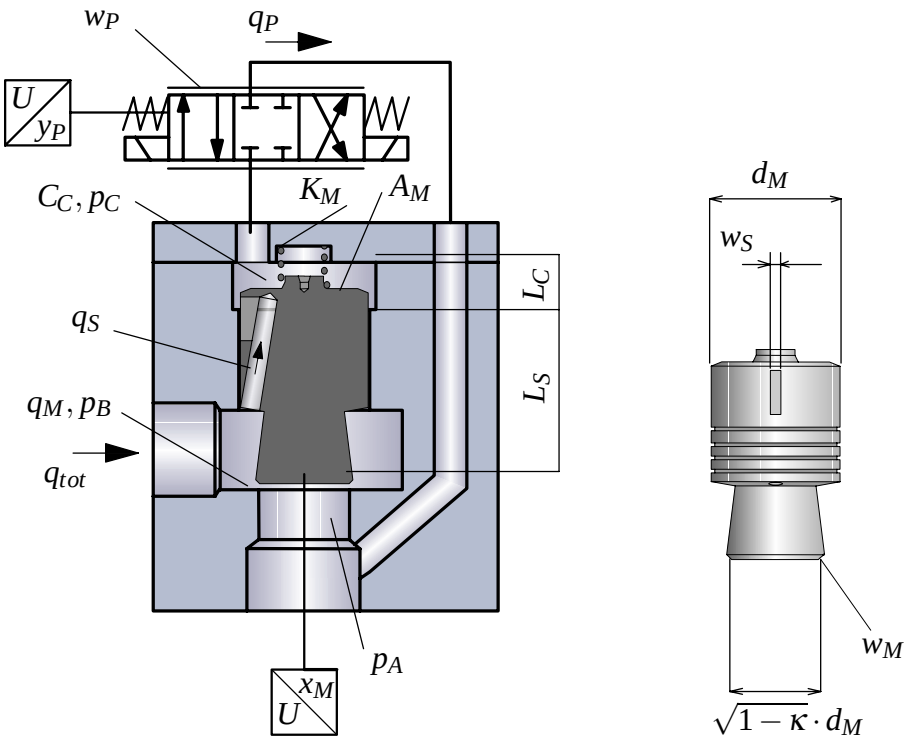

(a) The EPV16 valve under laboratory conditions (b) The main poppet

Figure 2: Sketch of the Valvistor valve

transfer functions, see equations (9), (10) and (11).

$$Q_{tot} = G_Y \cdot Y_P + G_{PA} \cdot P_A + G_{PB} \cdot P_B \tag{8}$$

where
$$G_Y = \frac{d_Y s^3 + c_Y s^2 + b_Y s + a_Y}{Ds^3 + Cs^2 + Bs + A} \tag{9}$$

$$G_{PA} = \frac{d_{PA} s^3 + c_{PA} s^2 + b_{PA} s + a_{PA}}{Ds^3 + Cs^2 + Bs + A} \tag{10}$$

$$G_{PB} = \frac{d_{PB} s^3 + c_{PB} s^2 + b_{PB} s + a_{PB}}{Ds^3 + Cs^2 + Bs + A} \tag{11}$$

Expressions of all coefficients can be found in appendix A.

It is desirable to somehow rewrite the denominator and numerator of these transfer functions as factors of first and second order equations. It is possible to break up the third order equations into the following equations

$$G_Y \approx \frac{K_{vY}\left(\frac{s}{\omega_{bY}}+1\right)\left(\frac{s^2}{{\omega_{hY}}^2}+\frac{2\delta_{hY}}{\omega_{hY}}s+1\right)}{K_v\left(\frac{s}{\omega_b}+1\right)\left(\frac{s^2}{{\omega_h}^2}+\frac{2\delta_h}{\omega_h}s+1\right)} \tag{12}$$

$$G_{PA} \approx \frac{K_{vPA}\left(\frac{s}{\omega_{bPA}}+1\right)\left(\frac{s^2}{{\omega_{hPA}}^2}+\frac{2\delta_{hPA}}{\omega_{hPA}}s+1\right)}{K_v\left(\frac{s}{\omega_b}+1\right)\left(\frac{s^2}{{\omega_h}^2}+\frac{2\delta_h}{\omega_h}s+1\right)} \tag{13}$$

$$G_{PB} \approx \frac{K_{vPB}\left(\frac{s}{\omega_{bPB}}+1\right)\left(\frac{s^2}{{\omega_{hPB}}^2}+\frac{2\delta_{hPB}}{\omega_{hPB}}s+1\right)}{K_v\left(\frac{s}{\omega_b}+1\right)\left(\frac{s^2}{{\omega_h}^2}+\frac{2\delta_h}{\omega_h}s+1\right)} \tag{14}$$

The assumption $|2\omega_b\delta_h| << |\omega_h|$ was used in all nominators and denominators when they were factorized. It is an accurate approximation of the denominator and the nominators of the G_{PA} and G_{PB} transfer functions and a fairly good approximation of the G_Y transfer function. See also the bode plots in figure 4. The working point of the valve can be seen in table 3. It is the same working point as the one used in the measurements.

Table 3: Working point

Quantity	Numeric number	Unit	Description
p_{A0}	0		Pressure on the A-side of the valve
p_{B0}	10	MPa	Pressure on the B-side of the valve
$y_{P0} \cdot w_P$	$1 \cdot 10^{-6}$	m^2	Opening area of the pilot valve

2.1 Stability criterium of the Valvistor valve

All three transfer functions have the same denominator and thereby they have the same stability criterium, $\delta_h > 0$.

Since all coefficients are positive numbers it can be seen from equation (46) that stability is maintained when

$$\frac{m\left(K_{CS}+K_{CP}\right)+B_M C_C}{mC_C} > \frac{\left(K_{CS}+K_{CP}\right)\left(K_M+K_{FX}\right)+A_M K_{QS}}{{A_M}^2+B_M\left(K_{CS}+K_{CP}\right)+C_C\left(K_M+K_{FXM}\right)} \tag{15}$$

B_M and $(K_{FXM}+K_M)$ can often be ignored. Equation (15) then reduces into

$$K_{CS}+K_{CP} > \frac{C_C K_{QS}}{A_M} \tag{16}$$

The critical working point is when K_{CP} and K_{CS} have their minimum and when K_{QS} has its maximum.

K_{CS} and K_{CP} have their minimum when the main poppet are about to leave its seat, then $K_{CP} = K_{CS}$. By substituting equation (16) with $\kappa = \frac{1}{2}$, $K_{CP} = K_{CS} = \frac{C_q w_S x_{M0}}{\sqrt{2\rho(p_{B0}-p_{C0})}}$, $K_{QS} = C_q w_S \sqrt{\frac{2}{\rho}(p_{B0} - p_{C0})}$ and when flow forces are ignored $p_{C0} = \frac{p_{B0}+p_{A0}}{2}$ equation (16) becomes

$$x_{M0} > \frac{C_C (p_{B0} - p_{A0})}{2A_M} \tag{17}$$

The simplified, reduced equation of the stability criterium, equation (17), was also presented in [1].

Equation (17) yields that the main poppet always has to maintain an opening of at least $\frac{C_C(p_{B0}-p_{A0})}{2A_M}$ to guarantee stability. This can be archived by means of an underlap in the slot; this means that when the poppet is closed there still is a small opening in the slot. $p_{B0} - p_{A0}$ is the maximum pressure drop over the valve at all working points.

Note from equation (15) that the viscous friction coefficient B_M will contribute to decrease the demands of x_{M0}. B_M can be increased by having a single slot in the main poppet asymmetrically on one side. Then, there will be an unbalanced force on the cylindrical wall of the valve.

2.2 Simplified model

The equations (45) and (53) show that ω_h and ω_{hY} in equation (36) are approximately equal. However, the relative damping coefficient δ_{hY} is in most cases negative, meaning that there are two conjugating zeros in the right half plane and the system is a non-minimum system. The criterion of when $\delta_{hY} < 0$ is derived from (54) and is shown approximately in equation (18), B_M is ignored.

$$2C_C A_M C_q (1-\kappa)(p_{B0} - p_{A0})(w_{QM} + w_{QS}) > w_{CS} x_{M0} {A_M}^2 \tag{18}$$

Now, equation (12) can be rewritten as

$$G_Y = \frac{K_{vY}\left(\frac{s}{\omega_{bY}}+1\right)\left(\frac{s^2}{{\omega_h}^2} - \frac{2(-\delta_{hY})}{\omega_h}s + 1\right)}{K_v\left(\frac{s}{\omega_b}+1\right)\left(\frac{s^2}{{\omega_h}^2} + \frac{2\delta_h}{\omega_h}s + 1\right)} \tag{19}$$

The two second order terms in the transfer function, equation (19), can be seen as a notch filter with its zeros in the right-side half plane. The negative zeros do not affect the stability of the system as long as the valve is used in an open loop system. However, if the valve is used in a closed loop application the phase lag due to the zeros is still not any problem. The frequency ω_h, were the phase crosses $-180°$, occurs so high that any pilot valve will suppress the peak of the notch in the loop gain. A small capacitance, C_C, of the volume above the poppet also suppresses the notch peak, see equations (54) and (46). So for that reason, the pilot valve should be mounted close to the poppet.

The first order frequency, ω_{bY}, is in all cases relatively high. It is always a positive number, see equation (52), and therefore does not cause any trouble in a closed loop application such as phase lag. Rather, it advances the phase. Due to the high frequency, ω_{bY} can be ignored. If $K_M \approx K_{FXM} \approx B_M \approx 0$ is assumed, equation (52) becomes

$$\omega_{bY} = \frac{K_{QM} + K_{QS}}{A_M} \tag{20}$$

Finally, the transfer function from pilot opening to flow can be fairly well approximated as

$$G_Y \approx \frac{\frac{K_{vY}}{K_v}}{\frac{s}{\omega_b} + 1} \tag{21}$$

How the pressures, p_A and p_B, influence the system is described, by the equations (10) and (11).

In the bode plots in figures 4(c) and 4(b) the static gain is not equal to the asymptotic gain when the frequency goes to infinity, $|G_{PA}(0)| \neq |G_{PA}(\infty)|$ and $|G_{PB}(0)| \neq |G_{PB}(\infty)|$.

From the basic equations (1) to (7) it can be seen that statically, the slot opening is equal to the pilot opening, $w_s x_M = w_P y_P$. Furthermore, if the flow forces and spring constant, K_M, are ignored the flow gain of the valve can be derived as

$$g = \frac{Q_{tot}}{Q_P} = 1 + \frac{\frac{w_M}{w_S}}{\sqrt{1-\kappa}} \tag{22}$$

The frequency response of $|G_{PB}(0)|$ and $|G_{PA}(0)|$ is according to equations (11) and (10)

$$|G_{PA}(0)| = \left|\frac{a_{PA}}{A}\right| = \left|\frac{K_{vPA}}{K_v}\right| \tag{23}$$

$$|G_{PB}(0)| = \left|\frac{a_{PB}}{A}\right| = \left|\frac{K_{vPB}}{K_v}\right| \tag{24}$$

and $|G_{PB}(\infty)|$ and $|G_{PA}(\infty)|$

$$|G_{PA}(\infty)| = \left|\frac{d_{PA}}{D}\right| = \left|\frac{\frac{K_{vPA}}{{\omega_{hPA}}^2 \omega_{bPA}}}{\frac{K_v}{{\omega_h}^2 \omega_b}}\right| \tag{25}$$

$$|G_{PB}(\infty)| = \left|\frac{d_{PB}}{D}\right| = \left|\frac{\frac{K_{vPB}}{{\omega_{hPB}}^2 \omega_{bPB}}}{\frac{K_v}{{\omega_h}^2 \omega_b}}\right| \tag{26}$$

The relation between these responses is

$$g \cdot (|G_{PA}(\infty)| - |G_{PA}(0)|) = |G_{PA}(0)| \tag{27}$$

$$g \cdot (|G_{PB}(0)| - |G_{PB}(\infty)|) = |G_{PB}(0)| \tag{28}$$

The physical interpretation can be described as follows. The total flow difference, Q_{tot}, is described by equation (1). Statically, when a pressure change occurs in P_A the

pilot flow will change as well as the total flow, and the flow gain in equation (22) will be fulfilled. The poppet will statically have the same position as mentioned above.

When the frequency of the pressure change in P_B goes to infinity on the other hand, the mass of the poppet makes it stand still, as in the static case. The difference from the static case is that the pilot flow will not change. This is because of the dynamics of the chamber above the poppet. The pressure P_C will not change due to the volume capacitance despite a change in the flow Q_S. A high frequency change in the pressure P_A behaves in a similar manner. The difference is that P_A changes the pressure drop over the pilot instead of the slot and the pressure P_C is unaffected due to the volume. Therefore, the pressure drop, and the flow, over the pilot are twice as large as in the static case. This argumentation only holds when the flow forces and spring constant, K_M, are ignored since these disturb the force equilibrium of the poppet and thereby the chamber pressure P_C.

The zeros in these transfer functions are positive for almost all cases, $\delta_{hPA} > 0$ and $\delta_{hPB} > 0$, see equations (62) and (70).

ω_{bPA} and ω_{hPB} is in the same range as ω_b. ω_{hPA} and ω_{hPB} are placed close to ω_h. This means that the phase is close to zero. The system has some oscillation around ω_h due to the second order terms. However, because of the high frequency this should not be a problem in reality.

Furthermore, the stationary gains of G_{PB} and G_{PA} should intuitively be equal as near as a minus sign. The equations (67) and (59) shows that $K_{vPB} = -K_{vPA}$.

According to this argumentation, the equations (10) and (11) can be fairly well approximated as

$$G_{PB} = -G_{PA} \approx \frac{K_{vPB}}{K_v} = \frac{-K_{vPA}}{K_v} = \frac{K_{vP}}{K_v} \tag{29}$$

The relation of the frequencies to each other can be derived if some geometrical assumptions are made, see geometry properties in figure 2. Flow forces, viscous friction and the spring constant are ignored, $K_M \approx K_{FXM} \approx B_M \approx 0$.

The volume length of the chamber above the poppet, L_C, can be approximated with the smaller radius of the poppet, $L_C = \sqrt{1-\kappa} \cdot \frac{d_M}{2}$. This is because the maximum opening is approximately the radius $\sqrt{1-\kappa} \cdot \frac{d_M}{2}$. The height of the poppet, L_S, can be approximated with the diameter of the poppet, $L_S = d_M$, since they are usually quadratic. Now, by substituting the equations (45), (53), (44), (52) and (22) with $A_M = \frac{\pi}{4} {d_M}^2$, $V_c = \frac{\pi}{8}\sqrt{1-\kappa} \cdot {d_M}^3$ and $m = \rho_S \cdot A_M L_S$, normalized frequencies can be derived

$$\frac{\omega_h}{\omega_b} = \frac{\omega_{hY}}{\omega_b} = g \cdot \underbrace{\frac{1}{4\sqrt{1-\kappa} \cdot C_q} \sqrt{\frac{\rho}{\rho_s}}}_{\text{constant } (K \text{ in figure 3})} \cdot \sqrt{\frac{\beta_e}{p_{B0} - p_{A0}}} \tag{30}$$

$$\frac{\omega_{bY}}{\omega_b} = g \tag{31}$$

The normalized frequencies are shown in figure 3.

Bode plots of the different models can be seen in figure 4, where model parameters correspond to the measured EPV16 valve.

Note that $K \cdot \sqrt{\beta_e} \approx 5500 \sqrt{\text{MPa}}$. When using the valve in a closed loop application it is favorable to have the frequency $\omega_{hY} >> \omega_b$, let's say $\omega_{hY} \geq \frac{g}{2} \cdot \omega_b$.

This means that the critical pressure drop is as great as $(p_{B0} - p_{A0})_{critical} \approx 5500^2$ Pa $= 121$ MPa, which will quite likely never occur.

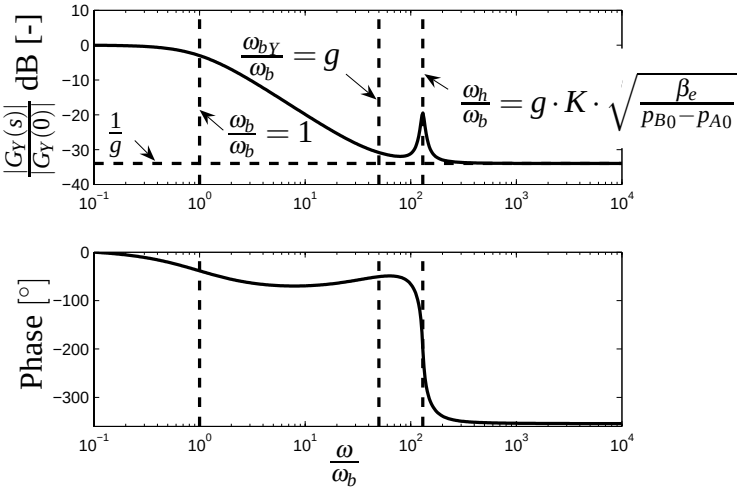

Figure 3: Normalized frequency relations of the Valvistor valve

With this assumed geometry equation (17) reduces to

$$x_{m0} > \frac{(P_{B0} - P_{A0})_{max}}{4\sqrt{2}\,\beta_e} \cdot d_M \tag{32}$$

which usually yields an underlap demand in the range of 0.1 mm.

To sum up, if the criteria in this section are fulfilled, which is the common case, the total flow in a Valvistor valve can be approximated as

$$Q_{tot} \approx \frac{\frac{K_{vY}}{K_v}}{\frac{s}{\omega_b}+1} \cdot Y_P + \frac{K_{vP}}{K_v} \cdot (P_B - P_A) \tag{33}$$

If K_M, B_M flow forces are ignored and $\kappa = \frac{1}{2}$ (51), (43), (44), (59), (67) and (22) reduces (33), $K_{CP} = K_{CS}$ is also valid stationary, this yield

$$\frac{Q_{tot}}{q_{P0}} \approx g \cdot \left(\frac{1}{\frac{s}{\omega_b}+1} \cdot \frac{Y_P}{y_{P0}} + \frac{1}{2} \cdot \frac{P_B - P_A}{p_{B0} - p_{A0}} \right) \tag{34}$$

$$\text{where} \qquad \omega_b = \frac{q_{P0}}{x_{M0} \cdot A_M} = \frac{K_{QS}}{A_M} = \\ = \frac{C_q w_S \sqrt{\frac{p_{B0}-p_{A0}}{\rho}}}{A_M} = Const. \cdot \sqrt{p_{B0} - p_{A0}}$$

The functionality of a Valvistor valve is often placed in the pilot circuit due to the relatively small flows. The pressure compensation of a Valvistor valve can be archived in different ways. Different kinds of pressure compensators can be used, see [1] and [5] for examples. Another rather simple, but not so accurate, method is used in the valve tested in this paper. The flow in the pilot poppet is pressure compensated through flow forces.

In the latter case the linearization of the pilot circuit will be changed as described below. There will be a change of the input variable Y_P into a magnetic force F_P from the solenoid. When the mass in the pilot valve is ignored the linearized flow, force and flow-force equations yield

$$\left.\begin{aligned} Q_P &= K_{QP} Y_P + K_{CP}\,(P_C - P_A) \\ F_P &= (K_P + K_{FXP})\,Y_P + K_{FPP}\,(P_C - P_A) \end{aligned}\right\} \Rightarrow$$

$$Q_P = \underbrace{\frac{K_{QP}}{(K_P + K_{FXP})}}_{"K_{QP_{new}}"} F_P + \underbrace{\left(K_{CP} - \frac{K_{QP} K_{FPP}}{K_P + K_{FXP}}\right)}_{K_{CP_{new}}} (P_C - P_A) \tag{35}$$

The equations of the break frequencies in appendix A show that it is practically not affected by changes in K_{QP} and K_{CP}.

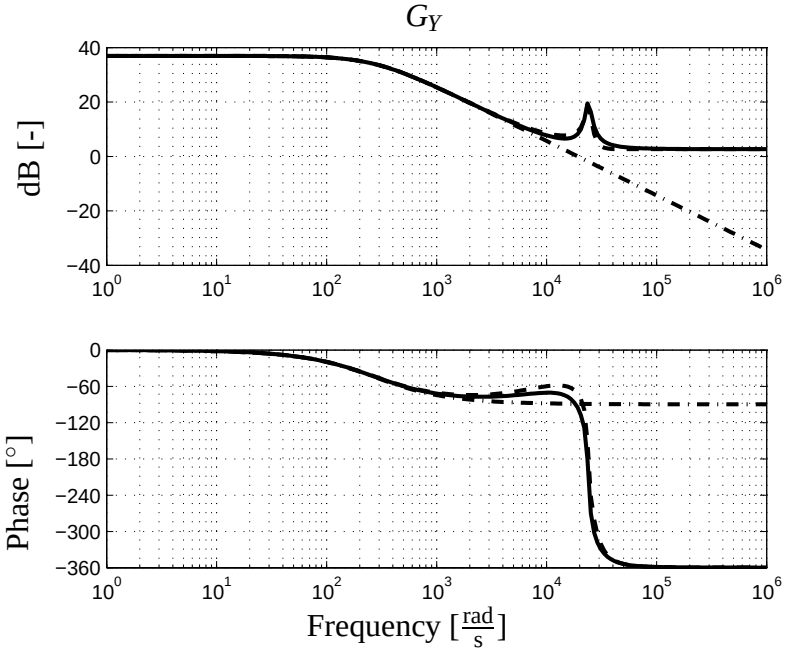

(a) Transfer function from pilot position to main flow

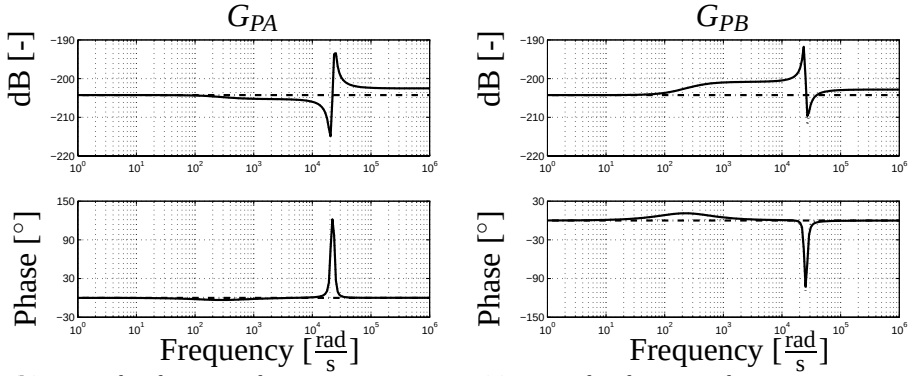

(b) Transfer function from pressure P_A to main flow

(c) Transfer function from pressure P_B to main flow

Figure 4: Transfer functions derived from the model; exact model is solid, factorized model is dotted and approximated model is dash dotted. Data according to EPV16 main stage and table 3 was used

3 EXPERIMENTAL RIG AND TEST METHOD

To validate the theoretical results, experimental tests were made, see figure 2(a) for the test arrangement. A standard Valvistor valve, the Vickers EPV 16, was tested. In order to study the dynamics of the main piston of the Valvistor valve, the standard pilot valve was replaced with a high performance servo-valve. The servo-valve had an external pilot supply.

The servo valve had a main spool position sensor. A position sensor was also mounted on the Valvistor main stage, see figure 2. Large capacitances were connected up- and downstream of the Valvistor to ensure undisturbed measurement conditions. The measurements are in good agreement with those shown in [1].

The input to the servo valve was a sinus with a constant frequency. The amplitude ratio and the phase lag between the opening of the servo valve and the position of the Valvistor main poppet were measured at different constant frequencies. The results were computed and presented in the form of Bode diagrams. Figure 5 shows a typical result.

4 EXPERIMENTAL RESULTS AND DISCUSSION

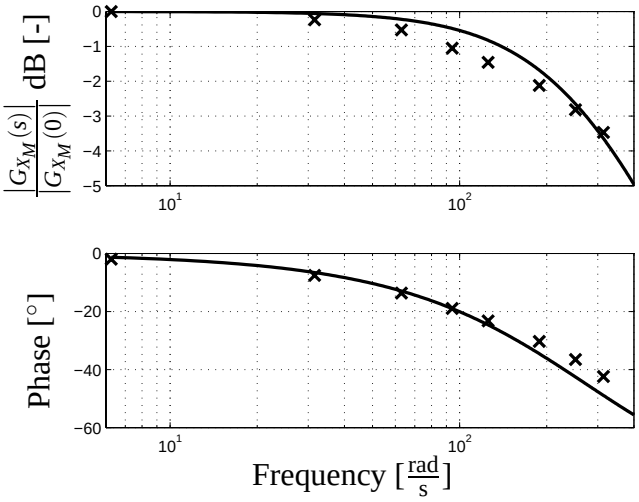

Figure 5: Normalized bode plot from the performed measurements. Measurements are marked by X and the approximated model is solid (a fast servo-valve was used as pilot.)

The experimental results validate the theoretical analysis. The results also show that the dynamics of the main Valvistor poppet for lower frequencies could be simplified as a first order system with a break frequency of ω_b.

5 CONCLUSIONS

A complete linear dynamic model of the Valvistor valve is presented that describes its flow characteristics. By fair simplifications the model ends up in a favorable first order system. The model can be used to size valves and perform analysis of closed loop systems.

The Valvistor may be looked upon as a flow amplifier. The amplification gain, g, is a design variable and is typically 30-70. The Valvistor can be modeled as a first order system with a break frequency, ω_b, which is proportional to the square root of the pressure drop (typically 50 Hz at 10 MPa pressure drop). It is shown that, if the Valvistor is properly designed, higher order dynamics can be neglected. This conclusion is in contrast to some recent publications that claim the opposite, based on incorrect modeling, [2] [3].

As the Valvistor is a true flow amplifier it means that the main stage is mimicking the pilot characteristic but amplified by the factor g. This is often used to create different functions such as pressure compensation on the pilot side, which is a big advantage compared to make it on the main side of the valve. However, pressure compensation of the pilot, the underlap of the slot in the main poppet must be considered. Due to the high bandwidth of the Valvistor the pilot dynamics is often dominating the valve as a whole.

In this paper the emphasis has been directed to the main stage of the valve. A second paper will be published later on studying the pilot stage of the EPV16 valve. Although the EPV16 valve is just one of many variants of the Valvistor principle, we will investigate it closely due to the interest for this valve among others.

REFERENCES

[1] Bo R. Andersson. *On the Valvistor, a proportionally controlled seat valve*. PhD thesis, LiTH, 1984. ISBN 91-7372-748-2.

[2] E. Prasetiawan, R. Zhang, and A. Alleyne. Fundamental performance limitations for a class of electronic two-stage proportional flow valves. In *Proceedings of the 2001 American Control Conference*, pages 3955–3960. IEEE, 2001.

[3] Roger Fales. Stability and performance of a metering poppet valve. *International Journal of Fluid Power*, (2):11 – 17, 2006.

[4] Herbert E. Merritt. *Hydraulic Control Systems*. John Wiley & Sons, New York, 1967. ISBN 0-471-59617-5.

[5] B. Eriksson, J. Larsson, and J-O. Palmberg. A novel valve concept including the valvistor poppet valve. In *The Tenth Scandinavian International Conference on Fluid Power*, 2007.

A COEFFICIENTS

$$G_Y = \frac{d_Y s^3 + c_Y s^2 + b_Y s + a_Y}{Ds^3 + Cs^2 + Bs + A} \approx \frac{K_{vY}\left(\frac{s}{\omega_{bY}}+1\right)\left(\frac{s^2}{{\omega_{hY}}^2}+\frac{2\delta_{hY}}{\omega_{hY}}s+1\right)}{K_v\left(\frac{s}{\omega_b}+1\right)\left(\frac{s^2}{{\omega_h}^2}+\frac{2\delta_h}{\omega_h}s+1\right)} \tag{36}$$

$$G_{PA} = \frac{d_{PA} s^3 + c_{PA} s^2 + b_{PA} s + a_{PA}}{Ds^3 + Cs^2 + Bs + A} \approx \frac{K_{vPA}\left(\frac{s}{\omega_{bPA}}+1\right)\left(\frac{s^2}{{\omega_{hPA}}^2}+\frac{2\delta_{hPA}}{\omega_{hPA}}s+1\right)}{K_v\left(\frac{s}{\omega_b}+1\right)\left(\frac{s^2}{{\omega_h}^2}+\frac{2\delta_h}{\omega_h}s+1\right)} \tag{37}$$

$$G_{PB} = \frac{d_{PB} s^3 + c_{PB} s^2 + b_{PB} s + a_{PB}}{Ds^3 + Cs^2 + Bs + A} \approx \frac{K_{vPB}\left(\frac{s}{\omega_{bPB}}+1\right)\left(\frac{s^2}{{\omega_{hPB}}^2}+\frac{2\delta_{hPB}}{\omega_{hPB}}s+1\right)}{K_v\left(\frac{s}{\omega_b}+1\right)\left(\frac{s^2}{{\omega_h}^2}+\frac{2\delta_h}{\omega_h}s+1\right)} \tag{38}$$

A.1 Denominator coefficients for all three transfer functions

$$A = K_{QS}A_M + (K_{CP}+K_{CS})(K_{FXM}+K_M) \tag{39}$$

$$B = {A_M}^2 + (K_{CP}+K_{CS})B_M + (K_{FXM}+K_M)C_C \tag{40}$$

$$C = (K_{CP}+K_{CS})m + C_C B_M \tag{41}$$

$$D = mC_C \tag{42}$$

$$K_v = A_M K_{QS} + (K_{CS}+K_{CP})(K_M+K_{FXM}) \tag{43}$$

$$\omega_b = \frac{(K_{CS}+K_{CP})(K_M+K_{FXM}) + A_M K_{QS}}{{A_M}^2 + B_M(K_{CS}+K_{CP}) + C_C(K_M+K_{FXM})} \tag{44}$$

$$\omega_h = \sqrt{\frac{{A_M}^2 + B_M(K_{CS}+K_{CP}) + C_C(K_M+K_{FXM})}{mC_C}} \tag{45}$$

$$\delta_h = \frac{1}{2}\left(\frac{m(K_{CS}+K_{CP}) + B_M C_C}{mC_C} - \frac{(K_{CS}+K_{CP})(K_M+K_{FXM}) + A_M K_{QS}}{{A_M}^2 + B_M(K_{CS}+K_{CP}) + C_C(K_M+K_{FXM})}\right) \cdot \sqrt{\frac{mC_C}{{A_M}^2 + B_M(K_{CS}+K_{CP}) + C_C(K_M+K_{FXM})}} \tag{46}$$

A.2 Pilot stroke transfer function coefficients

$$a_Y = K_{QP}(A_M(K_{QM}+K_{QS}) + K_{CS}(K_{FXM}+K_M)) \tag{47}$$

$$b_Y = K_{QP}\left({A_M}^2 + C_C\left(K_{FXM} + K_M\right) + K_{CS}B_M\right) \tag{48}$$

$$c_Y = K_{QP}\left(K_{CS}m + C_C B_M\right) \tag{49}$$

$$d_Y = K_{QP}C_C m \tag{50}$$

$$K_{vY} = K_{QP}\left(A_M\left(K_{QM} + K_{QS}\right) + K_{CS}\left(K_M + K_{FXM}\right)\right) \tag{51}$$

$$\omega_{bY} = \frac{K_{CS}\left(K_M + K_{FXM}\right) + A_M\left(K_{QM} + K_{QS}\right)}{{A_M}^2 + C_C\left(K_M + K_{FXM}\right) + B_M K_{CS}} \tag{52}$$

$$\omega_{hY} = \sqrt{\frac{{A_M}^2 + C_C\left(K_M + K_{FXM}\right) + B_M K_{CS}}{C_C m}} \tag{53}$$

$$\begin{aligned}\delta_{hY} = &-\frac{1}{2}\left(m\left(C_C A_M\left(K_{QM} + K_{QS}\right) - K_{CS}{A_M}^2\right) - B_M\left(C_C {A_M}^2\right.\right.\\ &\left.\left.+ {C_C}^2\left(K_M + K_{FXM}\right) + B_M C_C K_{CS} + m{K_{CS}}^2\right)\right)\cdot\\ &\frac{\sqrt{\frac{{A_M}^2 + C_C\left(K_M + K_{FXM}\right) + B_M K_{CS}}{C_C m}}}{\left({A_M}^2 + C_C\left(K_M + K_{FXM}\right) + B_M K_{CS}\right)^2}\end{aligned} \tag{54}$$

A.3 Pressure P_A transfer function coefficients

$$\begin{aligned}a_{PA} = &K_{CP}\left(\left(K_{QM} + K_{QS}\right)\left(-\kappa A_M + K_{FPM}\right)\right) + K_{CS}K_{QM}\left(\left(1-\kappa\right)A_M + K_{FPM}\right)\\ &- K_{CM}K_{QS}A_M - \left(K_{CM}K_{CP} + K_{CM}K_{CS} + K_{CP}K_{CS}\right)\left(K_{FXM} + K_M\right)\end{aligned} \tag{55}$$

$$\begin{aligned}b_{PA} = &K_{CP}\left(-\kappa {A_M}^2 + K_{FPM}A_M - C_C\left(K_{FXM} + K_M\right)\right)\\ &- K_{CM}\left({A_M}^2 + C_C\left(K_{FXM} + K_M\right)\right) + K_{QM}C_C\left(\left(1-\kappa\right)A_M + K_{FPM}\right)\\ &- \left(K_{CM}K_{CP} + K_{CM}K_{CS} + K_{CP}K_{CS}\right)B_M\end{aligned} \tag{56}$$

$$c_{PA} = -\left(K_{CM} + K_{CP}\right)C_C B_M - \left(K_{CM}K_{CP} + K_{CM}K_{CS} + K_{CP}K_{CS}\right)m \tag{57}$$

$$d_{PA} = -\left(K_{CM} + K_{CP}\right)C_C m \tag{58}$$

$$\begin{aligned}K_{vPA} = &K_{CP}\left(K_{QM} + K_{QS}\right)\left(-\kappa A_M + K_{FPM}\right) - K_{CM}K_{QS}A_M +\\ &K_{CS}K_{QM}\left(\left(1-\kappa\right)A_M + K_{FPM}\right) - \left(K_{CM}K_{CP} + K_{CM}K_{CS} + K_{CP}K_{CS}\right)\left(K_{FXM} + K_M\right)\end{aligned} \tag{59}$$

$$\omega_{bPA} = \frac{\begin{array}{c} K_{CP}\left(K_{QM}+K_{QS}\right)\left(-\kappa A_M + K_{FPM}\right) + K_{CS}K_{QM}\left(\left(1-\kappa\right)A_M + K_{FPM}\right) \\ -K_{CM}K_{QS}A_M - \left(K_{CM}K_{CP}+K_{CM}K_{CS}+K_{CP}K_{CS}\right)\left(K_{FXM}+K_M\right) \end{array}}{\begin{array}{c} K_{CP}\left(K_{FPM}A_M - {A_M}^2\kappa\right) - K_{CM}{A_M}^2 - \left(K_{CM}K_{CP}+K_{CM}K_{CS}+K_{CP}K_{CS}\right)B_M \\ +K_{QM}C_C\left(\left(1-\kappa\right)A_M + K_{FPM}\right) - C_C\left(K_{CM}+K_{CP}\right)\left(K_M+K_{FXM}\right) \end{array}} \tag{60}$$

$$\omega_{hPA} = \sqrt{\frac{\begin{array}{c} K_{CP}\left(\kappa {A_M}^2 - K_{FPM}A_M + C_C\left(K_{FXM}+K_M\right)\right) + K_{CM}\left({A_M}^2 + C_C\left(K_{FXM}+K_M\right)\right) \\ +\left(K_{CM}K_{CP}+K_{CM}K_{CS}+K_{CP}K_{CS}\right)B_M - K_{QM}C_C\left(\left(1-\kappa\right)A_M + K_{FPM}\right) \end{array}}{mC_C\left(K_{CM}+K_{CP}\right)}} \tag{61}$$

$$\delta_{hPA} = \frac{1}{2}\cdot \left(\begin{array}{c} \frac{\left(K_{CP}+K_{CM}\right)B_MC_C+\left(K_{CM}K_{CP}+K_{CM}K_{CS}+K_{CP}K_{CS}\right)m}{mC_C\left(K_{CM}+K_{CP}\right)} + \\ \left(K_{CM}K_{CP}+K_{CM}K_{CS}+K_{CP}K_{CS}\right)\left(K_M+K_{FXM}\right) + \\ \frac{K_{CP}\left(K_{QM}+K_{QS}\right)\left(\kappa A_M - K_{FPM}\right) + K_{CM}K_{QS}A_M - K_{CS}K_{QM}\left(\left(1-\kappa\right)A_M + K_{FPM}\right)}{K_{QM}C_C\left(\left(1-\kappa\right)A_M + K_{FPM}\right) + K_{CP}\left(-\kappa {A_M}^2 + K_{FPM}A_M - C_C\left(K_{FXM}+K_M\right)\right)} \\ -K_{CM}\left({A_M}^2 + C_C\left(K_{FXM}+K_M\right)\right) - \left(K_{CM}K_{CP}+K_{CM}K_{CS}+K_{CP}K_{CS}\right)B_M \end{array}\right) \cdot \sqrt{\frac{mC_C\left(K_{CM}+K_{CP}\right)}{\begin{array}{c} K_{QM}C_C\left(\left(1-\kappa\right)A_M + K_{FPM}\right) + K_{CP}\left(-\kappa {A_M}^2 + K_{FPM}A_M - C_C\left(K_{FXM}+K_M\right)\right) \\ -K_{CM}\left({A_M}^2 + C_C\left(K_{FXM}+K_M\right)\right) - \left(K_{CM}K_{CP}+K_{CM}K_{CS}+K_{CP}K_{CS}\right)B_M \end{array}}} \tag{62}$$

A.4 Pressure P_B transfer function coefficients

$$\begin{array}{c} a_{PB} = K_{CP}\left(\left(K_{QM}+K_{QS}\right)\left(\kappa A_M - K_{FPM}\right)\right) - K_{CS}K_{QM}\left(\left(1-\kappa\right)A_M + K_{FPM}\right) \\ +K_{CM}K_{QS}A_M + \left(K_{CM}K_{CP}+K_{CM}K_{CS}+K_{CP}K_{CS}\right)\left(K_{FXM}+K_M\right) \end{array} \tag{63}$$

$$\begin{array}{c} b_{PB} = K_{CP}\left(\kappa {A_M}^2 + K_{FPM}A_M\right) + K_{CM}\left({A_M}^2 + C_C\left(K_{FXM}+K_M\right)\right) \\ +K_{QM}C_C\left(\kappa A_M - K_{FPM}\right) + \left(K_{CM}K_{CP}+K_{CM}K_{CS}+K_{CP}K_{CS}\right)B_M \end{array} \tag{64}$$

$$c_{PB} = K_{CM}C_CB_M + \left(K_{CM}K_{CP}+K_{CM}K_{CS}+K_{CP}K_{CS}\right)m \tag{65}$$

$$d_{PB} = K_{CM}C_Cm \tag{66}$$

$$\begin{array}{c} K_{vPB} = K_{CP}\left(K_{QM}+K_{QS}\right)\left(\kappa A_m - K_{FPM}\right) + K_{CM}K_{QS}A_M \\ -K_{CS}K_{QM}\left(\left(1-\kappa\right)A_M + K_{FPM}\right) + \left(K_{CM}K_{CP}+K_{CM}K_{CS}+K_{CP}K_{CS}\right)\left(K_{FXM}+K_M\right) \end{array} \tag{67}$$

$$\omega_{bPB} = \frac{\begin{array}{c} K_{CP}\left(K_{QM}+K_{QS}\right)\left(-\kappa A_M + K_{FPM}\right) + K_{CS}K_{QM}\left(\left(1-\kappa\right)A_M + K_{FPM}\right) \\ -K_{CM}K_{QS}A_M - \left(K_{CM}K_{CP}+K_{CM}K_{CS}+K_{CP}K_{CS}\right)\left(K_{FXM}+K_M\right) \end{array}}{\begin{array}{c} K_{CP}\left(-\kappa {A_M}^2 + K_{FPM}A_M\right) - K_{CM}{A_M}^2 - \left(K_{CM}K_{CP}+K_{CM}K_{CS}+K_{CP}K_{CS}\right)B_M \\ +K_{QM}C_C\left(-\kappa A_M + K_{FPM}\right) - K_{CM}C_C\left(K_{FXM}+K_M\right) \end{array}} \tag{68}$$

$$\omega_{hPB} = \sqrt{\frac{\begin{array}{c} K_{CP}\left(\kappa {A_M}^2 - K_{FPM}A_M\right) + K_{CM}\left({A_M}^2 + C_C\left(K_{FXM}+K_M\right)\right) \\ +\left(K_{CM}K_{CP}+K_{CM}K_{CS}+K_{CP}K_{CS}\right)B_M - K_{QM}C_C\left(-\kappa A_M + K_{FPM}\right) \end{array}}{mC_CK_{CM}}} \tag{69}$$

$$\delta_{hPB} = \frac{1}{2}\cdot \left(\begin{array}{c} \frac{K_{CM}C_CB_M + \left(K_{CM}K_{CP}+K_{CM}K_{CS}+K_{CP}K_{CS}\right)m}{mC_CK_{CM}} - \\ \left(K_{CM}K_{CP}+K_{CM}K_{CS}+K_{CP}K_{CS}\right)\left(K_M+K_{FXM}\right) + \\ \frac{K_{CP}\left(K_{QM}+K_{QS}\right)\left(\kappa A_M - K_{FPM}\right) + K_{CM}K_{QS}A_M - K_{CS}K_{QM}\left(\left(1-\kappa\right)A_M + K_{FPM}\right)}{K_{QM}C_C\left(\kappa A_M - K_{FPM}\right) + K_{CP}\left(\kappa {A_M}^2 - K_{FPM}A_M\right)} \\ +K_{CM}\left({A_M}^2 + C_C\left(K_{FXM}+K_M\right)\right) + \left(K_{CM}K_{CP}+K_{CM}K_{CS}+K_{CP}K_{CS}\right)B_M \end{array} \right) \cdot \sqrt{\frac{mC_CK_{CM}}{\begin{array}{c} K_{QM}C_C\left(\kappa A_M - K_{FP}\right) + K_{CP}\left(\kappa {A_M}^2 - K_{FPM}A_M\right) \\ +K_{CM}\left({A_M}^2 + C_C\left(K_{FXM}+K_M\right)\right) + \left(K_{CM}K_{CP}+K_{CM}K_{CS}+K_{CP}K_{CS}\right)B_M \end{array}}} \tag{70}$$

Electronic Flow Control Valve (EFCV) with Pressure Compensation Capability

QingHui Yuan
Eaton Corporation – Innovation Center
7957 Wallace Road
Eden Prairie, Minnesota USA 55344
Email: QinghuiYuan@Eaton.com

Chris Schottler
Eaton Corporation – Hydraulics Division, Controls Group
14615 Lone Oak Road
Eden Prairie, Minnesota USA 55344
ChrisWSchottler@Eaton.com

Jae Y.Lew
Eaton Corporation – Innovation Center
7957 Wallace Road
Eden Prairie, Minnesota USA 55344
JaeYLew@Eaton.com

ABSTRACT

A new concept for an Electronic Flow Control Valve (EFCV) with pressure compensation capability is introduced. Based on its embedded sensors and micro controller, the EFCV can provide flow control without the need of load/displacement/speed information from the power elements, like hydraulic cylinders or hydraulic motors. The flow controller inside the EFCV approximates the actual flow rate by the quasi-steady flow rate equation. Experimental studies show that the analytical model is not accurate enough to cover all operating conditions. Therefore, an experiment-based calibration method is suggested so that the electronic flow controller can provide accurate flow control across the working pressure and flow range. Finally, an innovative application of the EFCV, a self-sensing cylinder, is also presented.

NOMENCLATURE

A	Cap area of the spool	m^2
A_1	Piston area of cylinder	m^2
F_{vc1}	Force produced by the voice coil	N
F_{sp1} F_{s1}	Steady flow forces for pilot and main stage	N
$K_{correction}$	Error-correction coefficient	
K_{sp} K_s	Centering spring constant for pilot and main stage	N/m
K_{vp} K_v	Damping coefficient for the pilot and main stage	Ns/m
M M_m	Spool mass for pilot and main stage	K_g
P_1, P_2	Port pressure	P_a
P_{11} ,P_{12}	Chamber pressures.	P_a
P_s	Supply pressure	P_a
P_t	Return pressure	P_a
Q_1, Q_2	Port flow rate	m^3/s
Q_{11}	Flow rate into the upper chamber	m^3/s
Q_{12}	Flow rate out of the lower chamber	m^3/s
$Q_{1,d}$ $Q_{1,c}$ $Q_{1,m}$	Desired/calculated/measured flow rate	m^3/s
V_o	Volume of chamber 1 as $x_p = 0$	m^3
V_{11} V_{12}	Volumes in the upper and lower chamber	m^3
W_p W	Area gradient for the pilot and main stage	m
i	Current through the actuator coil	A
x_1 x_{v1}	Spool displacement for pilot and main stage	m
x_p	Piston displacement	m
β_e	Bulk modulus of hydraulic fluid	Pa

1.0 INTRODUCTION

Flow control is one of the most critical functionalities in the hydraulic industry. Traditionally, flow control is implemented via a proportional or servo valve. The principle of proportional and servo valves is briefly reviewed in the following. When current is applied in to the coil of a solenoid (proportional valve) or a torque motor (servo valve), a corresponding electromagnetic force is generated. These forces could either directly stoke the spool (single stage configuration) or indirectly move the main stage spool via regulating the hydraulic pressures on the each end of the main stage spool (multiple stage configuration). The motion of the main stage spool leads to the variation of the orifice area. With a given pressure drop, the orifice area is directly associated with the flow rate. Modeling and control of proportional and servo valves is very rich in literature [1] [2] [3]. However, most proportional and servo valves on the market are incapable of providing accurate flow rate control without feedback from the power elements or without the addition of mechanical pressure compensators. For example, consider a double-ended hydraulic cylinder with the piston area equal to 1 [unit]. If the required speed is 1 [unit], then the required flow rate is actually 1 [unit]. Without knowing the displacement/speed information from the hydraulic cylinder, neither the servo valve nor the proportional valve can correctly provide the desired flow. The reason for this is because the flow rate is related not only to the spool displacement (orifice area) but also to the pressure drop across the orifice. Therefore, feedback from the power elements is often required to achieve accurate flow control.

In real world applications, the sensors in the power elements are not often available or are too costly to implement. However, accurate flow control is still required for several applications. For example, in a mobile excavator application the operators are in the loop controlling the motion of machine. The operators use a human machine interface device (like a joystick) to send the flow command to each individual cylinder. By controlling the angle of the joystick on each axis, one may also control the speed of multiple cylinders. Despite the variance in supply pressure of the system and the changing loads on the power elements, it is preferred that a joystick angle provides a corresponding velocity of the cylinder/motor consistently.

The traditional solution for this problem is to regulate the pressure drop across the metering orifice to be constant, so that the flow rate is essentially only dependent on the orifice area. This is the principle of a pressure-compensated flow control valve. **Figure 1** illustrates a typical restrictor-type pressure-compensated flow control valve [3]. The compensator spool has to be added to implement pressure regulation functionality. This methodology adds additional cost and complexity to the system.

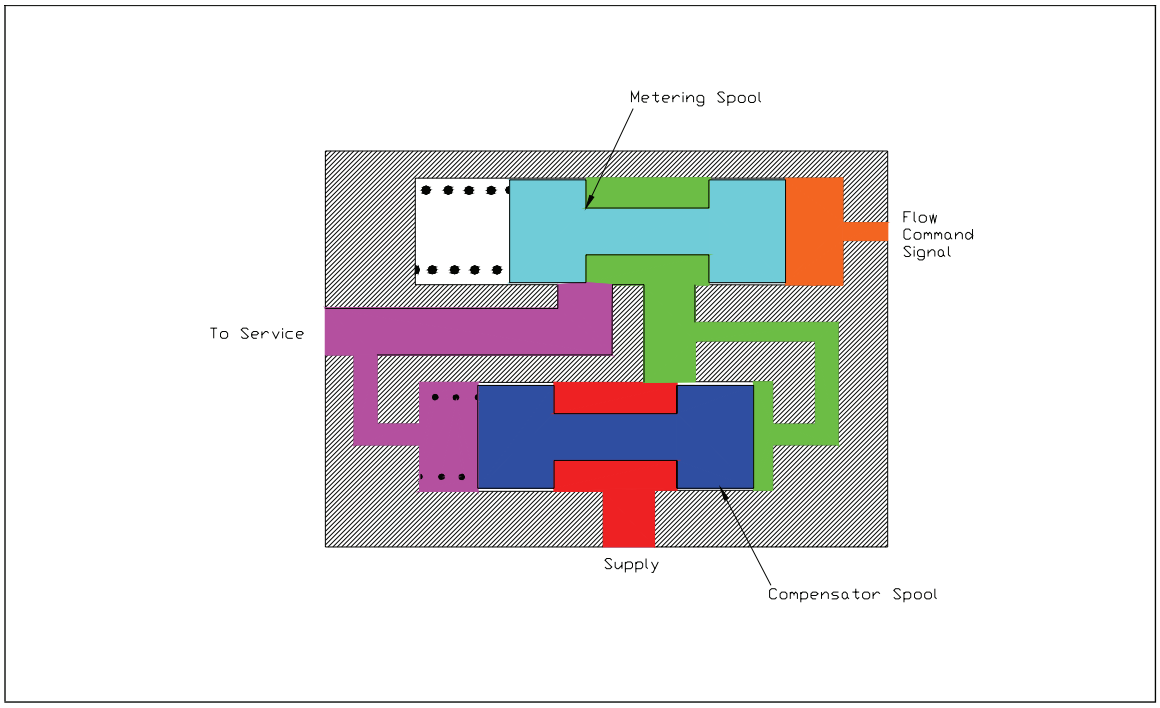

Figure 1 Restrictor-type pressure-compensated flow control valve

In the following paper, an innovative flow control valve with pressure compensation capability, referred to as an Electronic Flow Control Valve (EFCV), is presented. The EFCV distinguishes itself from other traditional flow control valves because of its embedded sensors and micro controller that have been integrated in to the valve. These integrated components make the EFCV "smart" so it can achieve flow control without the need of feedback from the power elements or the addition of a complicated mechanical system to regulate the pressure drop across the metering orifice. The Electronic Pressure Compensated Flow Control Valve is more cost effective and scalable compared to its mechanical counterparts.

The paper is organized as follows. First, the configuration and model of EFCV is developed. Next, the principle of electronic flow control via the EFCV integrated controller is described. Subsequently, the experimental study regarding the flow control accuracy is reviewed. Finally, an application of EFCV for a self-sensing cylinder is presented as well as some concluding remarks.

2.0 ELECTRONIC FLOW CONTROL VALVE

2.1 System Configuration

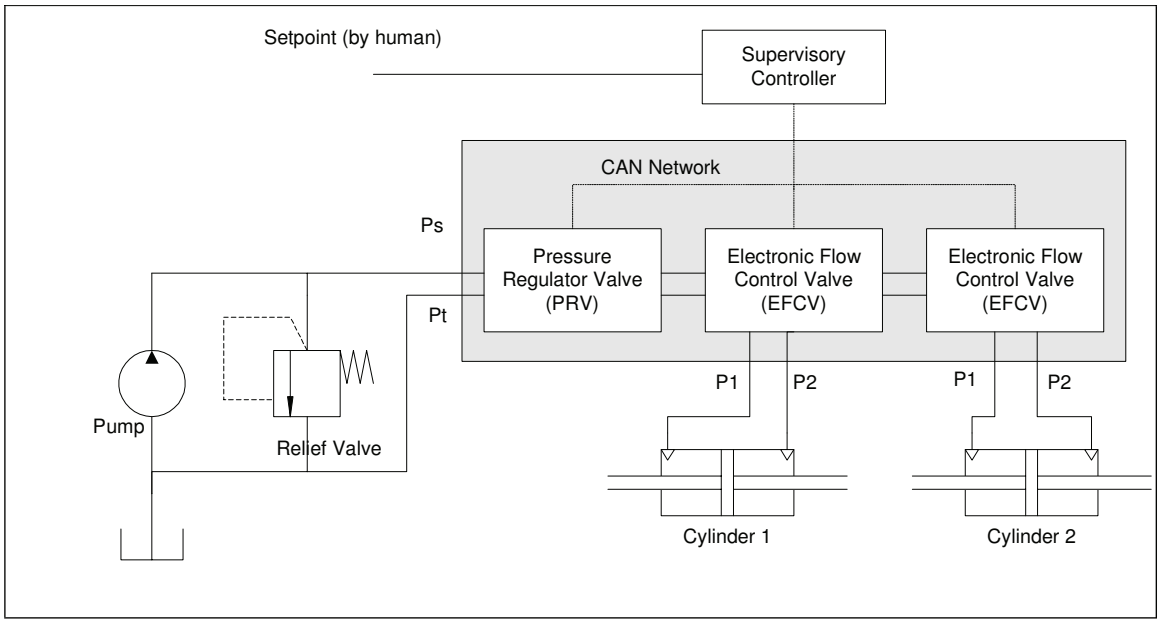

Figure 2 Configuration of hydraulic system with Electronic Flow Control Valve (EFCV)

Figure 2 illustrates the system design of the EFCV. A supervisory controller, which is implemented by an ECU, processes the input from the human as the set point for the flow rate. An EFCV, as well as a Pressure Regulation Valve (PRV), are connected to the supervisory controller via CAN communication. The embedded sensors in the PRV can provide the value of the supply pressure (P_s), and the tank pressure (P_t). The PRV can also control the supply pressure according to the load requirement, which is out of scope for this paper. The embedded sensors in the EFCV include the LVDTs, which measure the main stage spool displacement, and the pressure sensors, which measure the port pressures P_1 and P_2. The ports P_1 and P_2 are connected with hydraulic power elements as shown in **Figure 2**. It is worth mentioning that the system is designed so that multiple EFCVs may be connected with multiple power elements. Finally, the entire valve stack, including PRV and EFCVs, are connected to the hydraulic source (pump and a relief valve as shown in **Figure 2**).

The differentiating characteristic of the EFCV when compared to servo and proportional valves is the pressure feedback from the internal sensors. The pressure feedback combined with the positional feedback from the main stage spool, allows the EFCV to control the flow rate based on the command from the supervisory controller. On the contrary, traditional servo and proportional valves do not have internal pressure feedback inside the valves themselves and therefore cannot accurately control the flow rate across a large pressure drop spectrum.

2.2 Internal model of EFCV

An illustration of the pilot and main-stage spools in the EFCV is shown in **Figure 3**. It is important to note that for complete control of a typical power element, an additional pilot and main-stage spool is required. The embedded electronics performs the internal control, the communication between individual valves, and the communication to the supervisory controller. The EFCV has a two-stage configuration. The pilot stage, stroked by a linear force motor (voice coil), can control the pressures on the end

chambers of the main stage spool while the main stage spool can then control the flow rate to the power element. In addition, the EFCV can be designed to have independent upstream and downstream orifice control for the sake of energy savings and application flexibility. The schematic in **Figure 3** only reflects the configuration of the upstream or downstream portion of the EFCV. Interested readers may refer to [4] for more details about twin spool valves.

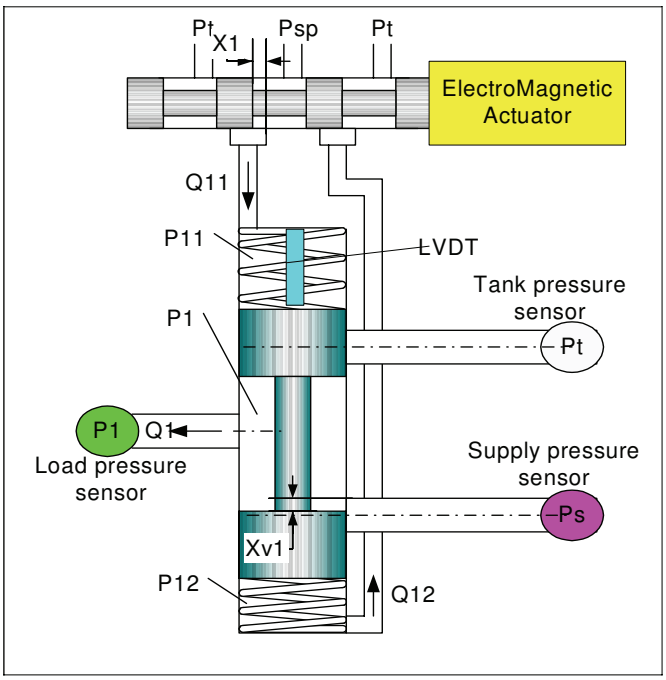

Figure 3 Schematic of Electronic Flow Control Valve (EFCV)

In the next section, the models of the EFCV related to the flow control will be developed.

2.3 EFCV model

2.3.1 Pilot stage spool dynamics

We assume that the transient flow forces applied on the pilot spool are negligibly small. From Newton's Second Law, we have the spool dynamics as follows:

$$M\ddot{x} = F_{vc1} + F_{sp1} - K_{vp}\dot{x}_1 - K_{sp}x_1 \tag{1}$$

in which M is the pilot spool mass, F_{vc1} is the force produced by the voice coil, which is proportional to the current i driven through the actuator coil, K_{sp} is the centering spring constant, and F_{sp1} is the steady state flow induced forces that are governed by:

$$F_{sp1}(x_1, P_{11}, P_{12}) = \begin{cases} -2C_d W_p x_1 \cos\theta \left[P_{sp} - P_t - (P_{11} - P_{12}) \right], & x_1 \geq 0; \\ -2C_d W_p x_1 \cos\theta \left[P_{sp} - P_t - (P_{12} - P_{11}) \right], & x_1 < 0. \end{cases} \tag{2}$$

where C_d is the discharge coefficient, W_p is the gradient area for the pilot stage, θ is the jet angle, P_{sp} is the supply pressure for the pilot stage, and P_t is the pressure of the reservoir. P_{11} and P_{12} are the chamber pressures shown in **Figure 2**. The viscous damping coefficient, K_{vp}, can be computed based on the valve geometry via [1].

2.3.2 Main stage dynamics

Similarly, the main stage spool dynamics can be obtained:

$$M_m \frac{d}{dt}\dot{x}_{v1} = -K_s x_{v1} - K_v \dot{x}_{v1} + (P_{11} - P_{12})A + F_{s1} \tag{3}$$

where M_m is the spool mass in the second stage, x_{v1} is the displacement of the spool, K_s is the centering spring constant, K_v is the viscous damping coefficient, A is the cap area of the spool contacting the end chambers, P_{11} and P_{12} are the chamber pressures. F_{s1} is the steady state flow force.

The steady state flow force, F_{s1} is given by:

$$F_{s1}(x_{v1}) = \begin{cases} -2C_d W x_{v1} \cos\theta (P_s - P_1), & x_{v1} \geq 0; \\ -2C_d W x_{v1} \cos\theta (P_1 - P_t), & x_{v1} < 0. \end{cases} \tag{4}$$

where W is the area gradient for the main stage, P_s is the supply pressure, and the other variables can be referenced from Eq. (2).

2.3.3 Chamber pressure dynamics

The chamber pressure dynamics are determined by the compressibility of the fluid in the chambers between the pilot stage and the main stage spools and are as follows:

$$\frac{d}{dt}P_{11} = \frac{\beta_e}{V_{11}}(Q_{11} - A\dot{x}_{v1}) \tag{5}$$

$$\frac{d}{dt}P_{12} = \frac{\beta_e}{V_{12}}(A\dot{x}_{v1} - Q_{12}) \tag{6}$$

in which P_{11} and P_{12} are the pressures in the upper and lower chambers, respectively, Q_{11} is the flow rate into the upper chamber, Q_{12} is the flow rate out of the lower chamber, β_e is the bulk modulus of hydraulic fluid, V_{11} and V_{12} are the volumes in the upper and lower chamber. On the quasi-steady state flow assumption, Q_{11} and Q_{12} are given by:

$$Q_{11}(x_1, P_{11}) = \begin{cases} C_d W_p x_1 \sqrt{2(P_{sp} - P_{11})/\rho}, & x_1 \geq 0; \\ C_d W_p x_1 \sqrt{2(P_{11} - P_t)/\rho}, & x_1 < 0. \end{cases} \tag{7}$$

$$Q_{12}(x_1, P_{12}) = \begin{cases} C_d W_p x_1 \sqrt{2(P_{12} - P_t)/\rho}, & x_1 \geq 0; \\ C_d W_p x_1 \sqrt{2(P_{sp} - P_{12})/\rho}, & x_1 < 0. \end{cases} \tag{8}$$

2.4 Flow Control of EFCV

The above model shows the EFCV is a highly nonlinear system with six states. However, a reduced model can be obtained from the following facts:

1. The pilot stage has very fast response. Compared to the other dynamics within the system, the transfer function from the current (*i*) to the pilot spool displacement (x_1) can be simplified as a DC gain.
2. Next, the transfer function of the main stage from x_1 to x_{v1} can be written as

$$\frac{x_{v1}(s)}{x_1(s)} = \frac{\frac{2\beta_e K_{qp} A}{V_0}}{s[M_m s^2 + K_v s + (\frac{2\beta_e A^2}{V_0} + K_2)]} \tag{9}$$

where $K_2 = K_s + C_d W \cos\theta (P_s - P_t)$, $K_{qp} = C_d W_p \sqrt{\frac{P_{sp} - P_t}{\rho}}$. In our analysis, the transient flow forces are neglected. The linearized equation has poles located at 0 and are repeated at -160.

In short, the higher order system can be approximated by a second order system in series with an integrator. For this open-loop stable system, a standard PI controller is chosen to assure adequate performance of the closed loop system. Standard PI gain tuning techniques can be used [5].

The flow control diagram is illustrated in **Figure 4**. The desired flow rate $Q_{1,d}$ is given by the supervisory controller thru the CAN bus. The actual flow rate $Q_{1,c}$ is analytically given by [1]:

$$Q_{1,c} = f(P_s, P_1) x_{v1} \tag{10}$$

where the flow mapping $f(P_s, P_1) = \begin{cases} C_d W x_{v1} \sqrt{2(P_s - P_1)/\rho}, x_{v1} > 0 \\ C_d W x_{v1} \sqrt{2(P_1 - P_t)/\rho}, x_{v1} \le 0 \end{cases}$.

In the diagram, the inverse flow mapping is used to convert the desired flow rate $Q_{1,d}$ to the desired spool displacement $x_{v1,d}$. The error between the desired and the actual displacement is imposed on the PI controller, whose output will drive the current into the pilot valve voice coil. The controller drives the displacement error to zero. If the actual flow follows Eq. (10) perfectly, then the flow error goes to zero as well, or $Q_{1,c} = Q_{1,d}$. Otherwise, if the actual flow mapping $g(\cdot) \neq f(\cdot)$, or $f^{-1} g \neq 1$, then the flow error will not converge to zero even when the displacement error is zero. In the following section, we will investigate the flow rate accuracy experimentally.

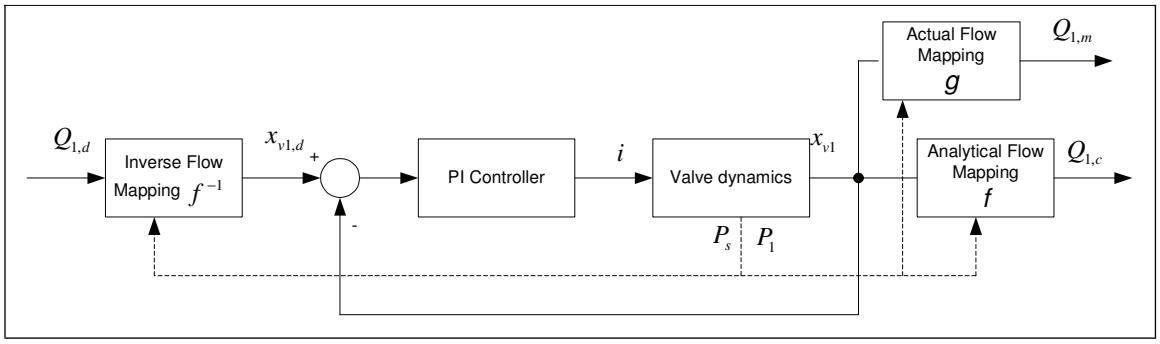

Figure 4 The flow control diagram inside EFCV

3.0 EXPERIMENTAL STUDY OF ELECTRONIC FLOW CONTROL

In the flow controller design, we use Eq. (10) to approximate the actual flow rate. Eq. (10) is a widely acceptable quasi-steady state model for the flow rate across an orifice. In the following section, an experimental study will be discussed that investigated the accuracy of the calculation.

A prototype of EFCV has been built and tested. The mechanical design can be referred to in **Figure 3**. The hydraulic test set up is illustrated in **Figure 5**. As you can see from Figure 5, the valve was set up on a fixed displacement test stand. An adjustable relief

valve (on the right side of **Figure 5**) simulates a load on the valve. A flow meter in series with the "load" relief valve is used to measure the actual flow from that service. The type of flow meter that was used depends on the demanded flow in order to improve the measurement accuracy. For flows below 7 GPM a 0.95 in^3/ rev meter motor (Vickers Model MF3039133061592) was used; while for flows above 7 GPM a flow turbine was used (Max Machinery Model 241-120).

Given a flow command from the supervisory controller, the "load" relief valve is adjusted so that the pressure drop between P_1 and P_s is equal to some predefined value. Then the actual flow rate was measured. **Table 1** displays all of the actual flows [GPM] recorded as a function of the commanded flow [GPM] and the pressure drop [psi] across the service spool.

Note that at steady state, the PI controller in **Figure 4** regulates the error between the flow command $Q_{1,d}$ and the calculated flow rate $Q_{1,c}$ to be zero, or $Q_{1,d} = Q_{1,c}$ only if the flow mapping $f(\cdot)$ and the inverse flow mapping $f^{-1}(\cdot)$ are perfectly inverse. In **Table 1**, the experimental results show that the measured flow rate $Q_{1,m}$ diverts from the analytical calculation $Q_{1,c}$. Another source for the error could also be that the flow mapping is different from what we suggested, or $g(\cdot) \neq f(\cdot)$ as shown in **Figure 4**. For convenience, we will compare the measured flow rate $Q_{1,m}$ and the commanded flow rate $Q_{1,d}\,(=Q_{1,c})$. The error $\dfrac{Q_{1,m} - Q_{1,d}}{Q_{1,d}}$ (unit: %) as a function of the pressure drop is illustrated in **Figure 6**.

Remarks:

1. For small flow commands, the error is significant. For example, when $Q_{1,d}$=1.32 [gpm], the actual flow rate only reaches about 20% of the demanded value. The error is larger than 80% at some pressure drops.
2. When the flow command is larger than 5 gpm, the error is bounded with +/-15%.
3. Given a flow command, the actual flow $Q_{1,m}$ first increases with the pressure drop. However, as the pressure drop is above 500-750 [psi], the flow $Q_{1,m}$ then reduces. This observation is based on the theoretical flow mapping $f(\cdot)$ in Eq. (10).

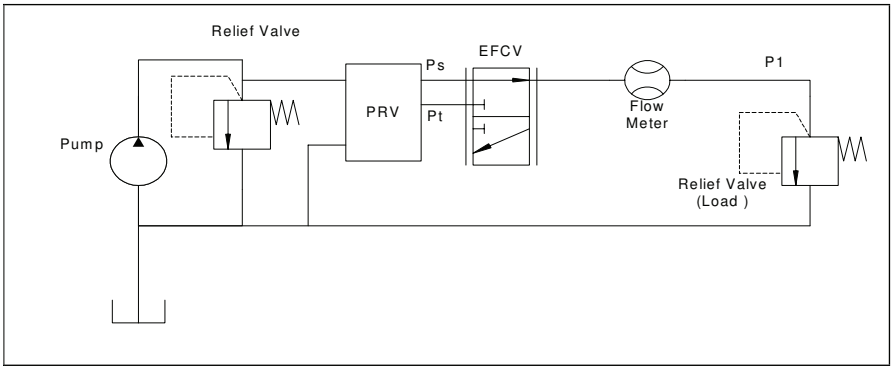

Figure 5 Diagram of the experimental setup

Command Flow	Differential Pressure [psi]									
	150	**300**	**450**	**600**	**750**	**900**	**1000**	**1500**	**2000**	**2500**
1.32	0.4	0.4	0.3	0.2	0.2	0.2	0.2	0.1	0.1	0.1
2.64	2.35	2.5	2.4	2.2	2.1	2	1.9	1.7	1.5	1.4
5	5	5.6	5.5	58	5.8	5.7	5.6	4.65	4.45	4.4
6.6	6.45	6.67	7.25	7.47	7.14	7.03	6.96	6.67	6.38	6.22
13.2	13.92	14.29	14.17	13.85	13.59	13.63	13.51	13.63	14.03	14.33
19.8	19.4	21.13	22.74	22.82	21.57	21.54	21.23	20.62	19.89	20.25
26.4	27.25	27.7	28.55	30.72	29.59	28.76	28.57	27.37	26.74	26.26
30.36	29.08	30.62	31.5	33.13	35.05	34.48	34.02	32.22	32.2	30.91

Table 1 Measured Flow $Q_{1,m}$ vs. Commanded Flow $Q_{1,d}$ $(= Q_{1,c})$ (unit: GPM)

Obviously the observed error demonstrates that the flow rate model in Eq. (10) is not very precise. For simplicity, in our generation of the flow map we assumed the density (ρ) and the discharge coefficient C_d in Eq. (10) to be constant. In reality, the density of the fluid may vary slightly according to the pressure and will change proportionally with temperature. In addition, the discharge coefficient is a very complicated function with respect to the pressure drop, the orifice area, the orifice geometry, and the Reynolds number [6]. To precisely model (using CFD) the discharge coefficient for various operating conditions would be very difficult.

Due to the complexity of the discharge coefficient, a feasible and useful strategy is to experimentally calibrate the flow calculation equation to eliminate the theoretical error. An empirical error-correction coefficient, $K_{correction}$, is defined as:

$$K_{correction} = \arg\left[\min_{K}\left(\left\| Q_{1,c} - KQ_{1,m} \right\|\right)\right] \tag{11}$$

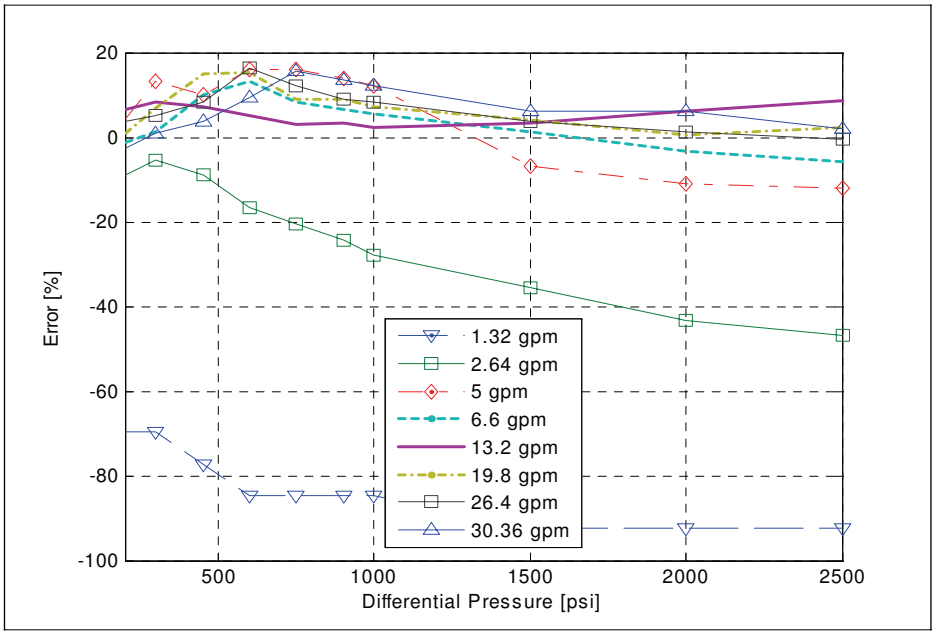

Figure 6 The error of the actual flow compared to the demanded flow, $\dfrac{Q_{1,m} - Q_{1,d}}{Q_{1,d}}$

The solution $K_{correction}$ is shown in **Figure 7**. The correction coefficient is a function of both pressure and flow rate. Curve fitting techniques can be used to get the relationship between $K_{correction}$ and the pressure drop and the flow rate. The following is an example that provides sufficient agreement with the measurement:

$$K_{correction} = c_0 + c_1 x + c_2 \sqrt{P} + c_3 x^2 + c_4 P \tag{12}$$

where c_0=3.1387, c_1=-0.0085, c_2= -0.0383, c_3=-1.03e-5, c_4=9.13e-4.

Due to the flexible system design of EFCV, the correction can be easily applied either inside EFCV or in the supervisory controller.

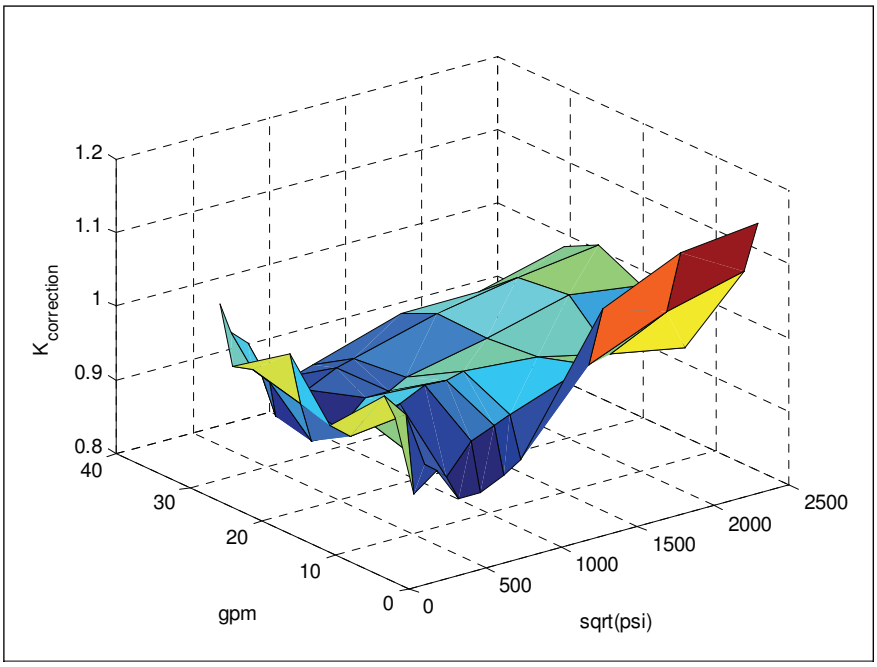

Figure 7 Correction gain for the flow rate calculation in Eq. (12)

4.0 APPLICATION OF EFCV: SELF-SENSING CYLINDER

In the following section we will discuss an innovative application for the EFCV. The application is a self-sensing cylinder, which will estimate the piston displacement of a regular hydraulic cylinder by taking advantage of integrated sensors and flow rate calculation of the EFCV.

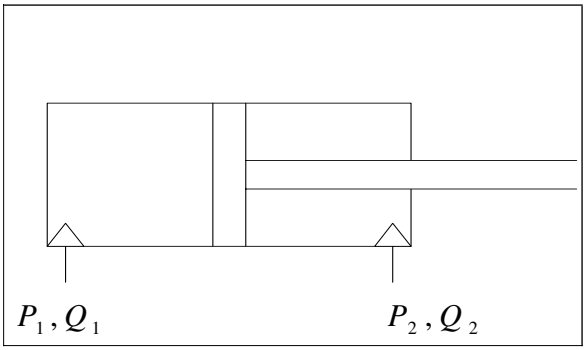

Figure 8 Self-sensing cylinder

The diagram of a self-sensing cylinder is illustrated in **Figure 8**. Two EFCVs connect each chamber respectively. The sensors in the EFCVs measure the pressures, P_1 and P_2. The flow rates, Q_1 and Q_2, are calculated by using the analytical model with the experimental calibration (as described above). In addition, in order to eliminate the integration error some deterministic displacement information is required (an absolute start position). For instance, a latch sensor could be installed so that the output voltage is high when the piston displacement $x_p = 0$ and is low as $x_p \neq 0$.

The pressure dynamics in chamber 1 gives

$$\dot{P}_1 = \frac{\beta_e}{V_0 + A_1 x_p}(Q_1 - A_1 \dot{x}_p) \tag{13}$$

where β_e is the bulk modulus of hydraulic fluid, V_o is the volume of chamber 1 as $x_p = 0$, A_1 is the piston area, x_p is the piston displacement, and Q_1 is the calibrated flow rate.

By manipulating the above equation, an observer of the piston displacement is proposed as

$$\dot{x}_p = \frac{1}{\beta_e A_1}(-A_1 \eta_1 x_p - \eta_1 V_0 + \beta_e Q_1) \tag{14}$$

where $\eta_1 = P_1 \frac{s}{s+p}$, or the low pass filtering of the pressure differential.

The simulation results are shown below in **Figure 9**. Due to the combined effect of the flow rate and the load applied to the cylinder, the actual displacement is the sinusoidal signal with the higher frequency oscillation. The observer in Eq. (14) is a close approximation of the actual displacement. Note that at *t=0.1* [sec], the latch sensor is enabled and then enforcing the error to be zero. Without the latch sensor, the observer will still give the similar displacement profile but with an offset error. In **Figure 9**, the estimate by using the simple kinematic relationship between the flow rate and the piston speed, $\dot{x}_p = \frac{Q_1}{A_1}$, is also plotted. It can be seen that its performance is worse than that in Eq. (14). In short, the integrated pressure sensors and the experimentally calibrated flow rates in the EFCV, together with the proposed observer, make it possible to implement the self-sensing cylinder.

CONCLUSION

A new type of valve, an Electronic Flow Control Valve (EFCV), is presented in this paper. Due to the embedded sensors and micro controller inside the valve, the flow rate can be controlled through the power elements without the need of knowing the load or the displacement condition from the power elements. The flow controller utilizes the well-known quasi-steady flow rate equation to approximate the actual flow rate in the internal closed loop system. Experimental studies show that the one equation model with constant parameters is not accurate enough to cover all conditions. In particular for the low flow rate high-pressure drop case, the flow error calculation is significant. An experiment-based calibration method is then presented. The new flow controller, by

taking into account the error correction coefficient $K_{correction}$, could provide a very accurate flow controller. An innovative application of the EFCV, a self-sensing cylinder, is also described.

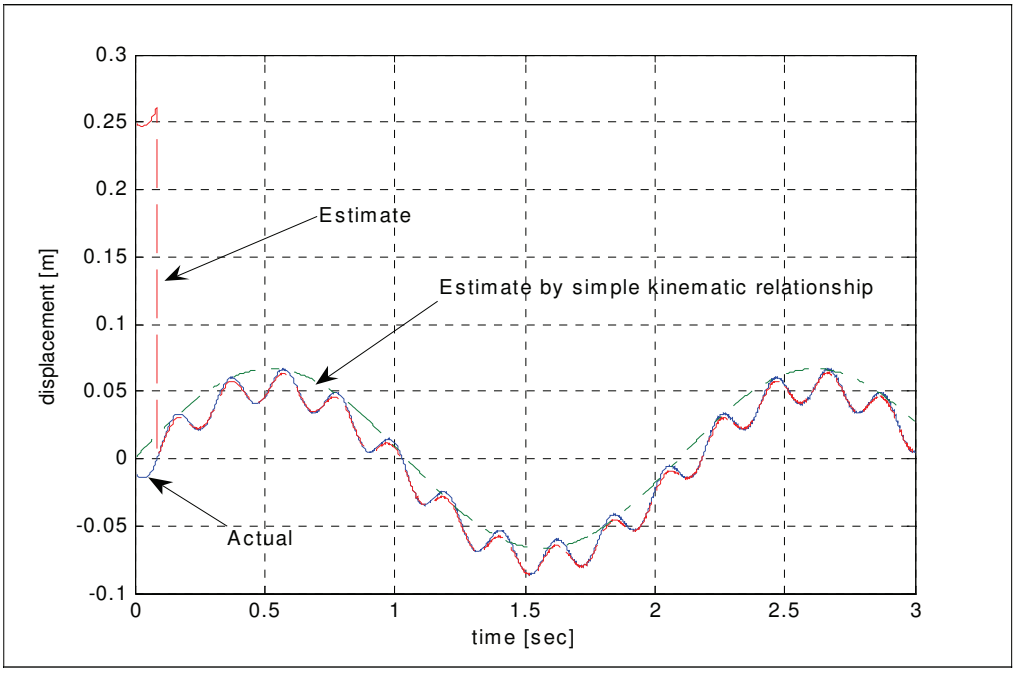

Figure 9 Simulation result: actual displacement and estimates

REFERENCES

1. **Herbert E Merritt**, Hydraulic control system, John Wiley and Sons, 1967

2. **Mohieddine Jelali and Andreas Kroll**, *Hydraulic Servo-systems: Modeling, Identification and Control,* Springer, 2003

3. **Eaton Corp.** *Proportional Valve Manual,* 1999

4. **QingHui Yuan and Jae Y Lew**, *Modeling and control of two stage twin spool servo-valve for energy-saving,* American Control Conference, 2005, 8-10 June 2005 Page(s):4363 - 4368 vol. 6

5. **William S. Levine**, *The Control Handbook,* CRC press LLC, 1996

6. **Duqiang Wu, Richard Burton and Greg Schoenau**, *An empirical discharge coefficient model for orifice flow,* International Journal of Fluid Power, Vol. 4, No. 1, Apr 2003.

Automotive Design for Electro Hydraulic Proportional Valves in Mobile Applications

Dr.-Ing. Harald Geis
Dr.-Ing. Jens Krallmann
Dipl.-Ing. Michael Lutz
Thomas Magnete GmbH
San Fernando 35
57562 Herdorf, Germany
Phone +49 2744 9290, Fax +49 2744 929290
E-Mail: jens.krallmann@thomas-magnete.com

ABSTRACT

The developments in the field of mobile working machines during the last years were characterised by a continuing trend to applications with a higher complexity, progressive processes of automation and uprated requirements on ergonomics and efficiency.

To give consideration to the risen demands, the OEMs are using electro-hydraulic valves to an increasing degree. Especially because of the increasing automation in the use of electro-hydraulic applications there is a need of high precision in the range of micro controlling of the actuators, repeat accuracy, hysteresis and valve-to-valve accuracy. By designing the solenoids in a compact construction, the preciseness of the valves can be increased significantly. Due to the fixed assembly of solenoid and hydraulic part this valves have less variability than systems with removable coils.

The paper shows the advantages and strengths of compact electro-hydraulic valves and shows possibilities to ensure the variability, which is necessary for applications in mobile hydraulics. Because of the design of defined interfaces between electrical and hydraulic part of the valve it is feasible to build up different types of valves from a modular system. Beside valves with different working pressures it is possible to realise valves with different volume flows as well.

KEYWORDS: Electro-hydraulic Systems, Proportional Valves, Pilot Operation, Transmission Control, Modular System

1 INTRODUCTION

In the range of mobile hydraulic applications a strong and continuing trend to the use of electro-hydraulic systems exists for several years now. In the fields of forest machinery (harvester and forwarder) and in agricultural machinery above engine power-classes of 85 kW, electro-hydraulic systems are nearly completely established. The number of machines in lower engine power classes which are featured with these systems is growing steadily. Currently the proportion of electro-hydraulic systems in construction machinery is lower; however an increasing number of applications is expected for the next years as well – legal requirements are one of the drivers of these development. [1]

A part of this growing market is related to cartridge valves which are built in a compact design being used in mobile working machines. More and more these compact valves substitute valves that are used with a removable coil. Advantages of these valves are the smaller installation space, an improved precision in micro controls, decreased hysteresis and a lower price. In contrast to these advantages there are some restrictions in comparison with systems with a removable coil concerning the variability of the valves which is needed in mobile hydraulics due to the large number of different machine types and applications. To compensate this, it is necessary to design the valves with some expedient and standardised interfaces. In this way it is possible to combine the benefits of a high precision with a very high variability.

2 AUTOMOTIVE DESIGN AND MOBILE HYDRAULICS

The term “Automotive Design” is used in this context to describe the special design and assembly of the valves. This design with specialised tools and processes follows experiences from the automotive business. In the broader sense, this is a selection of design principles resp. low-priced production and assembly procedures, which can be used with a high number volume output. Tooling and development costs are significantly higher with this approach, but in combination with the low variable costs this way is economical efficient.
Special design features are:

- Deep-Drawing of housings
- Force-fit connections by interference fit assembly
- Form-fir connections by crimping
- Fastening by flanges
- Stamp-bent-part housings
- Cold extrusion parts

Usually design changes require high investments, because the tooling has to be rebuilt or modified, additional costs for development and testing are necessary.
A special challenge in this context is the mentioned variability in mobile hydraulic applications. A large number of different applications demands many different machine types. Various environments need flexibility in the configuration of the valve charac-

teristics; this means the hydraulic performance as well as the costumer system and the environment. [2]

3 ADVANTAGES OF COMPACT DESIGN WITH STANDARDISED INTERFACES

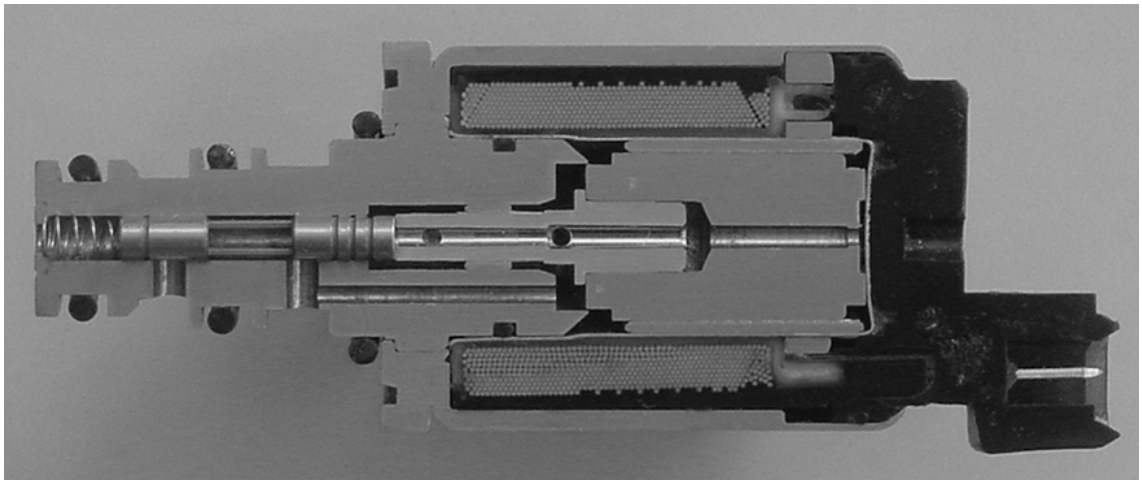

Figure 1: Electro-hydraulic Proportional Pressure Reducing valve in compact design

The most important characteristic of compact magnets resp. compact valves is the inseparability of pole respectively armature tube, coil and hydraulic parts after the assembly of the valve. By form fitted connections an air gap within the magnetic flow can be reduced to a minimum; the tolerances of the complete magnet system become much smaller. This leads to several advantages concerning the hydraulic properties of the valves:

- Higher force-diameter ratio
- Lower hysteresis
- Better control on small signals
- Higher Repeatability (valve-to-valve and shot-to-shot) (figure 2).

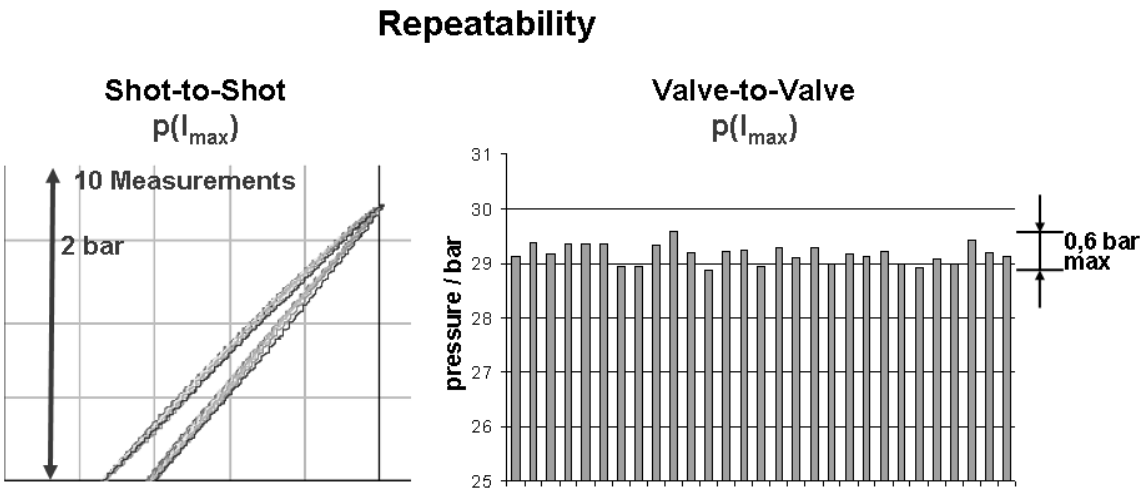

Figure 2: Improved Repeatability of valves in compact design

To assure the variability in the configuration of the valves it is necessary to provide interfaces with a certain standard or specification, which can be used to combine the different modules. Figure 3 shows an example for interfaces of a proportional pressure reducing valve with direct operation.

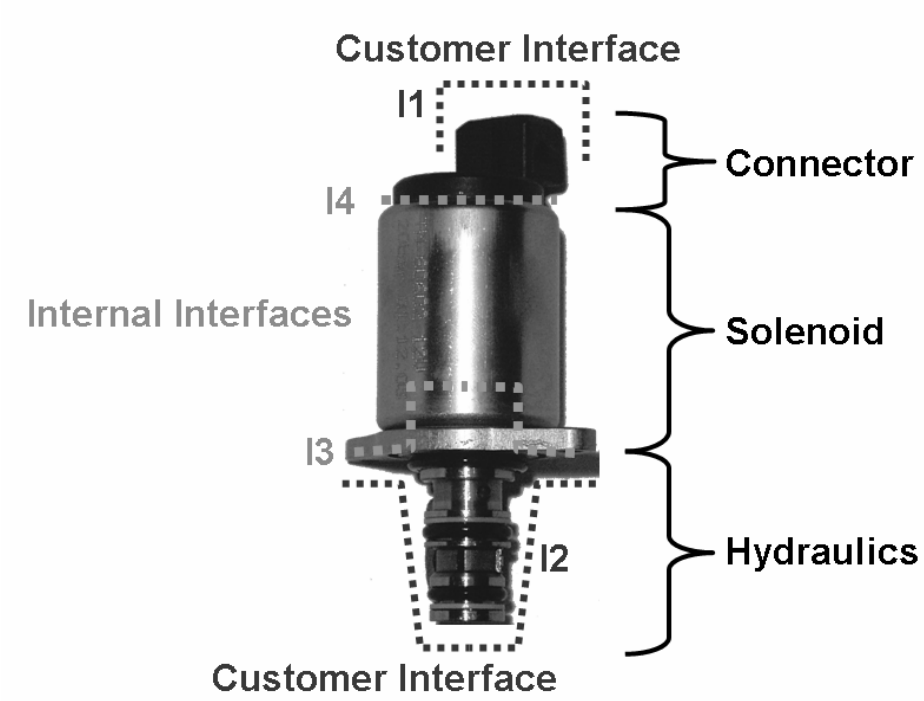

Figure 3: Example of interfaces of a compact valve

As shown in figure 3, two different types of interfaces are integrated. Two of them (I1 and I2) are the outer borders, where the connection to the costumer system is made. They are defined by market requirements or the costumer specification resp. in agreement between customer and manufacturer. The connector builds the interface to the control unit, the valve sleeve realises the adaptation to the hydraulic block, incl. flange mounting. The internal interfaces (I3 and I4) are used to connect the outer parts

with the solenoid and the housing. I3 enables the possibility to modify the geometry of the cone according to the application. Stroke-force characteristic and length of the stroke can be adapted by this.

Figure 4 shows a variety of valve types that are used in field for several years. Changes are only made at the interfaces I1, I3 and I4; the design of the valve sleeve is not affected.

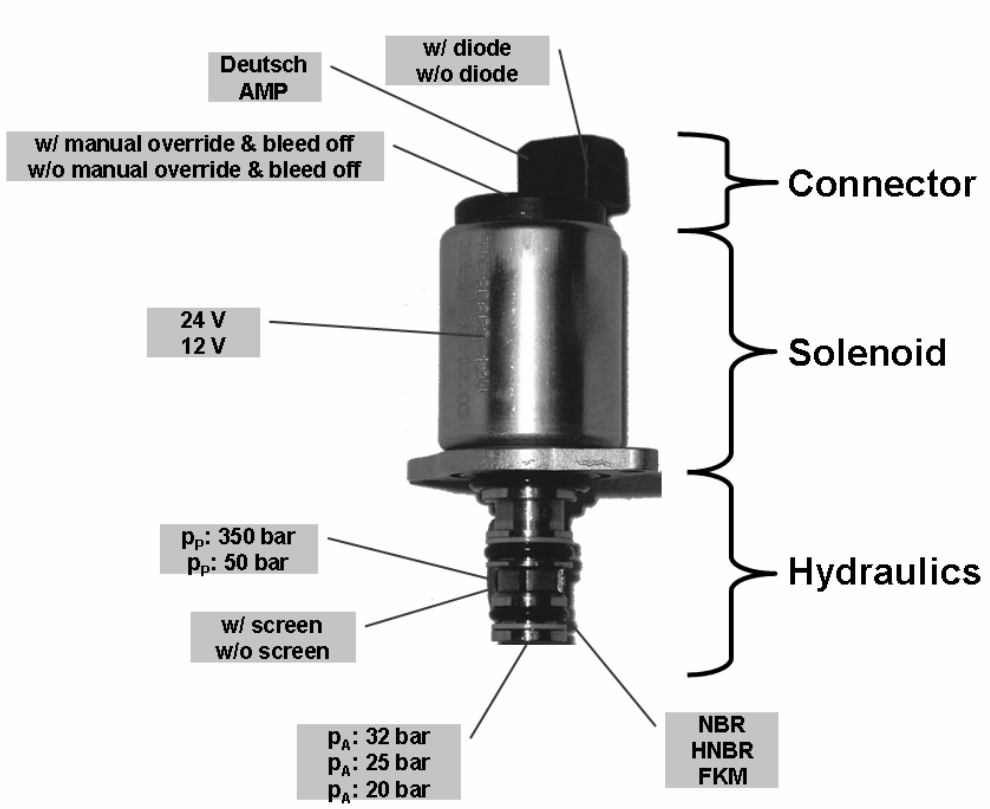

Figure 4: Most common versions of PPCD (size 04)

Base of the possibility to create these variations is that the housing and the solenoid are used for every type. The tooling for these parts is expensive and therefore changes should be made on turn parts or parts with a low effort in tooling.

4 DEVELOPMENT IN AUTOMOTIVE DESIGN

4.1 Development Process

Starting from a costumer request respectively from requirements according to the market a valve concept is made in interaction of design and simulation departments. The modular system is used in the design as various tools for simulation and layout. Defined interfaces and data transfer between various programmes allow a linking of standard software and self development and self-programmed tools. Figure 5 shows the most important tools that are in use at Thomas Magnete.

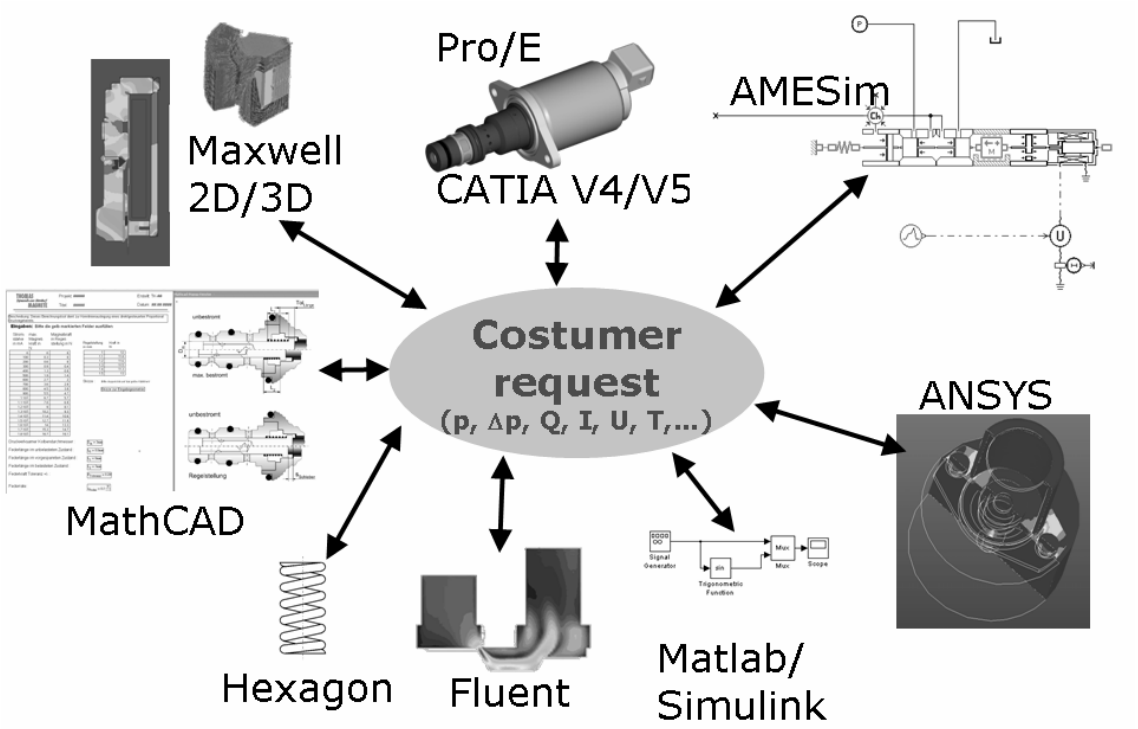

Figure 5: Tools for simulation, dimensioning and layout

A typical development process starts with the layout of the valve including the dimensioning of the geometrical and mechanical values. Subsequent an optimization and vernier adjustment is done; e.g. for single parts and/or the complete system. It is also possible to build a simulation model of the valve which can be given to the customer as a "Black Box" for the simulation of his complete system. A comprehensive analysis includes also a FEM evaluation of valve parts and blocks.
The first prototypes can be designed very exactly by a consequent using of the provided tools and the development time can be reduced considerably.

4.2 Development of Variations

For the developing of a new valve, which is designed in an automotive way, the estimated sales numbers are decisive new layout modifications. A big advantage results from the use of similar parts. If the volume is not very high the use of an existing coil and housing, already produced in high quantity, is required. Nevertheless the opportunity to design a complete family of valves from one solenoid gives a big benefit in terms of cost. Figure 4 showed the variations which can be made within one type of valves, but as shown in figure 6 it is also feasible to build other sizes, e.g. for higher volume flows or different working pressures.
The different valve types are all realized by changing the internal and external turn parts. The valves have different volume flow characteristics according to the diagram 6, and also different strokes and force characteristics.

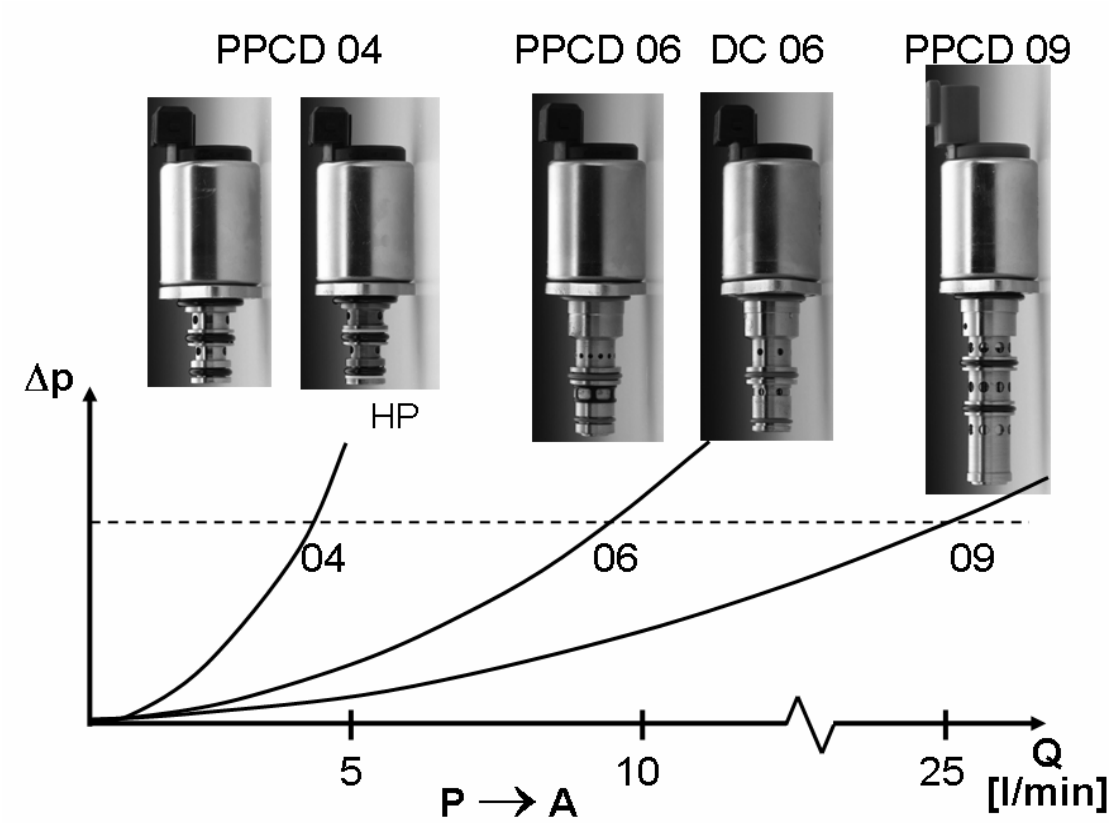

Figure 6: Valve variation by using a modular system

The figure shows different sizes of proportional pressure reducing valves (PPCD – Proportional Pressure Controller – Direct operated) from small valves which are mostly used for pilot operations and pump control to bigger valves which are needed for clutch controls, e.g. in gearboxes. There are also directional switching valves like the DC06 available.

4.3 Development of a New Generation of valves

The other way to develop a valve is to start from sketch on. The PPCD04 like shown in figure 7 is an example for this way. To give the customers most benefit, a complete valve for a challenging high volume market was designed. A detailed market analysis followed by interviews of potential costumers and a value analysis were basis of the development.
Some of the most important items were:

- Smaller dimensions
- Lower price
- Decrease of step response
- Decrease of pressure drop
- Decrease of leakage
- Outer diameter < 30mm
- Better linearity of the p-I-curve

To fulfil all these requirements it needs a lot of effort and all the tools which are shown in figure 5 had been used to reach the target.
By using the CFD simulation tools it was possible to downsize the valve sleeve significantly; as shown in figure 7.

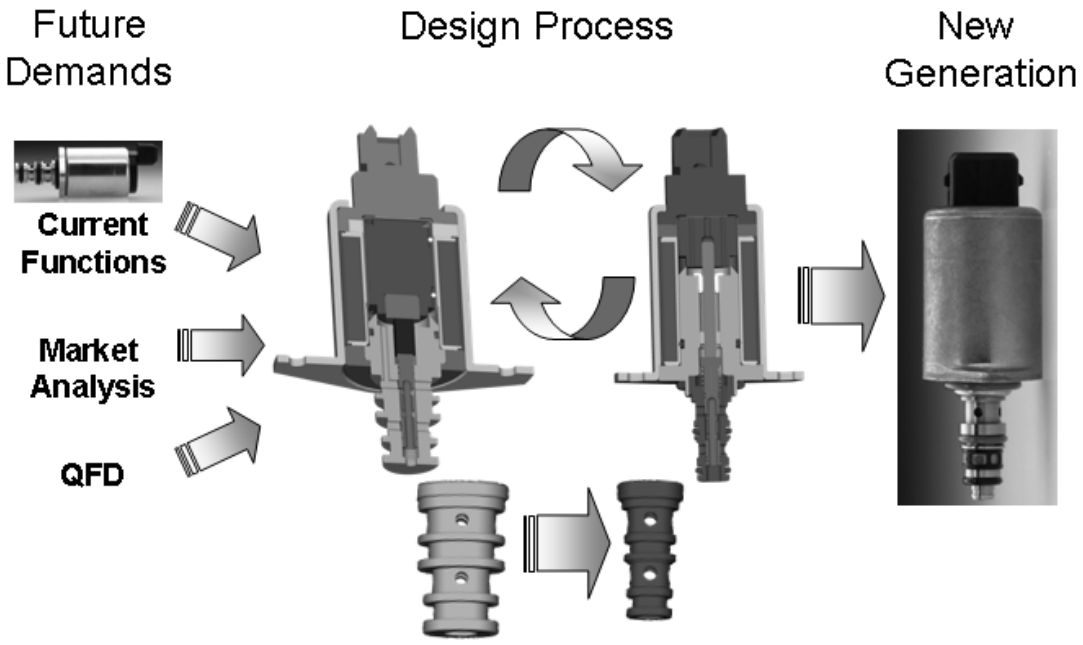

Figure 7: Design process for a New Generation of valves

Other results of the design process were that housing and flange should be made from one deep-drawn part only and the connector has a central position. A filter screen is now standard equipment.
The use of the simulation tools made it possible to reach the targets of a small solenoid diameter with an equal force and better hydraulic performance as compared with the existing valve.

5 ELECTRONIC CONTROL UNIT - ECU

Although electro hydraulic systems have become very common within the last years in the fields of mobile machinery, there are still a lot of applications, where the use is not established yet. One of the main reasons for that is a lack of low priced electronic control units on the market. Therefore Thomas Magnete is developing an ECU including the necessary periphery or equipment. The principle of a modular system was also pursued with the design of the ECU consequently. This leads to the opportunity to treat every client like an automotive costumer and to give him a product that is close to his demands.
The ECU as a central unit assumes the control tasks for the system. Proportional and discrete signals from joystick, pedals and sensors will be processed and forwarded as an analogue signal to the valves. Furthermore the ECU has a serial interface to make a connection to Display, Handheld or PC. A CAN bus interface is available if required.

Core of the ECU is the main board that takes control of the administration of the tasks. Dependent on the number and type of required outputs one up to six modules can be attached to the main board by slots. The actual control job of the valves is done by the modules. Up to four valves can be attached to each module, so that it is possible to provide the signals for 24 valves per ECU.

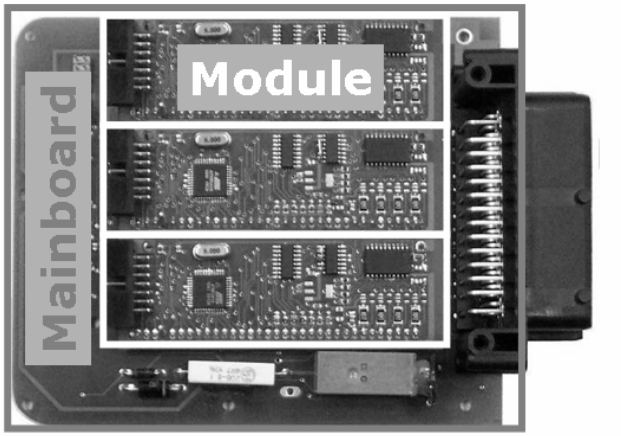

Figure 8: Hardware-concept of the ECU

Beside the proportional valves it is also possible to control directional valves or other types of actuators. Additional to the analogues and digital inputs the ECU has incremental sensors.
A special feature is a heating that is implemented on the main board to preheat the electronic parts at very low temperatures.
The software for the ECU consists of several modules as well, which have to be processed sequential during the initialization process. Examples of parameters that have to be defined within this process are:

- Characteristic lines resp. diagrams
- Null range
- Partially defined ramps
- Logical operations
- Smooth accelaration

Furthermore several typical machine types like tractors, excavators, wheel loaders or cranes are pre-configured to make the installation more comfortable for the customer.

6 CONCLUSION

The sector of mobile hydraulics is still characterized by lots of activities. Whereas the introduction of electro hydraulic systems is nearly completed in some applications, other operative ranges are still at the beginning.
Common over all applications is the continuously growing international competition as well in technical as in economical aspects. The use of optimised production processes and economy of scale effects by high volumes can decrease the cost per unit significantly. The paper shows that the use of compact valves is an advantage even if

there are special requests of variability in the fields of mobile hydraulics. A consequent design of modules that can be combined in a flexible way make it possible to use the parts with high tooling costs for a lot of different valve types. Interfaces that have to be adapted due to the connection to customer systems can de realised by parts which can be changed with low costs.
The idea of a modular system can be transferred to other areas like the development process or electronic units. Prototypes and simulation files can be created within a very short time; the electronic unit can be specially designed for every application so that the customer gets exactly what he needs.

7 LITERATURE

[1] Fedde, T.: Traktorhydraulik – Tractorhydraulics. Jahrbuch Agrartechnik 16 (2004), S. 73-78. Münster: Landwirtschaftsverlag 2004. ISBN 3-7843-3272-2.

[2] Geis, H.; Lutz, M.: Baukasten mir drei Baureihen. fluid 40 (2006) H. 1, S. 34-36

A SUGGESTION OF ARTIFICIAL FILTER TEST DUST

Eizo Urata, Kazuo Tajima, Kenji Suzuki and Tomokazu Suda
Kanagawa University
3-27-1 Rokkakubashi, Kanagawa-ku, Yokohama, 221-8686, Japan
Phone +81 45 481 5661, Fax +81 45 481 5122
E-mail: urata@mech.kanagawa-u.ac.jp

ABSTRACT

This paper describes the preparation of test particles for filtration testing of fluid power filters. The purpose of this work is to eliminate the drawbacks of natural sands as test particles, such as size ambiguity and sedimentation in working fluids. This paper outlines a method for preparing artificial test particles that have the following features: spherical shape, free from sedimentation, of uniform colour, controlled size distribution, and producible in a normal fluid power laboratory.
The principle of dust generation adopted in this report is the injection of liquid styrene monomer (LSM) into water with dissolved surfactant. LSM droplets in the water are polymerised by thermal and mechanical treatment. They are free from sedimentation and their colour is white. An SEM observation proved that the particles are spherical. The size distribution of the generated particles is similar to that of common natural dust. The particles prepared in this way will help accurate testing of the filtration performance of fluid power filters.

KEYWORDS: Contamination control, Filtration performance test, Filter test dust, Polystyrene particles

1 Introduction

This paper reports on a trial for preparing particles for filtration performance tests of fluid power filters. The purpose of fluid power filters is to cleanse fluids going through them. Therefore, to estimate the filtration performance of fluid power filters, we measure the cleanliness level of fluid at filter downstream. For this measurement, we must control the contamination level of fluid at the upstream filter since this is a fundamental parameter determining the fluid contamination level of the downstream filter [1]. To control the contamination level of fluid at the upstream filter, we use test dust or test particles.

What kind of test particles is suitable for the filtration tests? The answer can be found if we consider the desirable properties of particles for the filtration tests. The following are desirable properties of the test particles:

The shape and size of each particle are uniquely determined,
Having constant density and neither settle down nor float up,
Having uniform colour,
Particle size distribution is controllable,
Particle shape and size are stable,
Equally available everywhere in the technological world.

As the filtration performance test, the multi-pass test is internationally used, in which the classified natural sand (ISO ISO-No.16889 [2], ISO-No.12103-1; Arizona test dust [3]) is specified for the test particles. However, no natural sand can satisfy the above-listed requirements; Arizona desert sand is no exception. Therefore, to satisfy the requirements, we decided to prepare some ideal test particles using artificial materials and means.

2 Test particles for filtration performance tests

In the introduction, we listed the desirable properties of particles for the filtration performance test of fluid power filters. Let us discuss each property in this section.

(1) The shape and size of each particle are uniquely determined

Particles of natural sand have irregular shapes. There are many definitions of diameter for non-spherical particles: a volumetric equivalent diameter, Stokes diameter, an equivalent diameter of equal projection area, etc [4], [5]. Although some of them are impossible to apply to a real object, namely, tremendous numbers of particles, the other definitions can be applied to real particles. Even if the diameters following the definitions are found, the measured results depend on the measuring means and calibration methods. For example, a projected area of non-spherical particle changes with direction of projection. Only spheres are free from such uncertainty; the diameter of spheres can be uniquely determined using a microscope. This exact size estimate results in a better counting accuracy. Another advantage of spheres is they may be taken as a base for the permeability of particles through filter media. For example, square particles are more prone to being caught in filter media than spherical particles. A test using spherical particles can be taken as the base level of the permeability assessment.

(2) Having constant density and neither settle down nor float up

The first problem by filtration test is particle sedimentation and adherence to walls inside the test facilities. Since the specific weight of natural sands lies between 2.3 and 3.5, the sands are prone to sediment in oil and water. This characteristic requires particular caution for test facility design and operation, such as to keep flow turbulent, to avoid swirling or stagnation of flow. These requirements induce restrictions on design parameters. Flows in the slurry conduit and on-line counter are usually difficult to make turbulent. Tubing and reservoir shapes must be designed to avoid sedimentation.

If artificial dusts or particles are made with a specific weight similar to that of the fluid,

this problem vanishes; the particles will always float in fluid in a stable state. The specific weight of hydraulic oil is about 0.85 and that of water is unity. Therefore, if we allow a specific weight of 0.9 for test contaminants, we can find many resins and plastics as candidate materials for them. Such small difference of specific weight greatly reduces sedimentation and will not induce practical trouble.

(3) Having uniform colour

Natural sand is often a mixture of particles of various colours; difference in colour hinders the microscope observations that are the foundation of size calibration. Under the microscope, a dark background blurs dark particles but a bright background blurs the boundaries of white particles. Different transparency also affects the determination of particle sizes. Artificial particles can be made to have a single colour with common transparency. Thus, by using artificial particles of a single colour, we can reduce errors by observation.

(4) Particle size distribution becomes controllable

The raw material of natural sand is extracted from deserts, riverbanks etc. The extracted natural sand is adjusted to take a required size distribution using grinding machines, classifiers and blending machines. The quality of the sand produced is sensitive to these machines and their operation as well as the raw material; this situation practically forces us to use a specified product of a specified supplier. Although the multi-pass test of ISO 16889 defines the use of Arizona sand, the sand is by no means representative contamination in fluid power systems all over the world.

At present, there is no theoretical reasoning for necessary particle size distribution. However, the control of particle size distribution for a test dust is necessary to compare the performance of different filters. If we determine a process for preparing particles, the process automatically establishes a size distribution. Therefore, controlling the particle size distribution of artificial particles is easier than adjusting the particle size distribution of natural sands.

(5) Particle shape and size are stable

Change of shape or size of particles due to breakage, coherence or dissolution induces disorder of the test dust characteristics. If particle size distribution changes during a filtration test, the validity of the test result will be questionable. While recognition of particle breakage or coherence is difficult with irregularly shaped particles, it is easy with spherical particles. Plastic particles are usually not cohesive, not soluble in oil or water, and can be made spherical.

(6) Equally available everywhere in the technological world

If we use natural sand in a test, then the test cannot be free from regional restrictions, such as source of the sand, supplier, etc. To be free from regional restrictions, the particles should be made by a clearly defined production or preparation process using defined chemicals and defined preparation devices. We add here our request that fluid power engineers could prepare them in a normal fluid power laboratory. In the next section, we will outline a particle preparation process that was followed in our fluid power laboratory.

3. Experimental apparatus and method of experiment

3.1 Particle generation principle

The process we followed was to extrude liquid state monomer into water through a porous medium. Figure 1 illustrates a simplified image of the process. In Fig.1, water flows along the surface of the porous medium. The liquid state monomer protruding into the water is taken away as droplets by the water flow. The monomer droplets in the water become spheres by their own surface tension. Then the droplets become solid by polymerisation. Our work is to design and build an apparatus to realise this process.

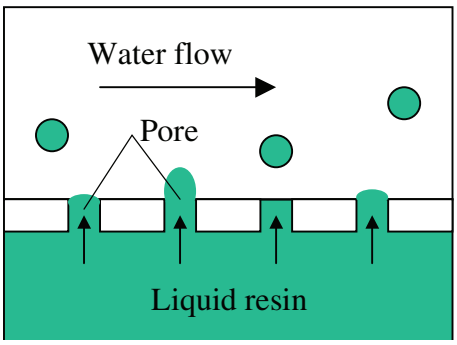

Fig. 1 Particle generation process

3.2 Particle generator

We designed and made the particle generator illustrated in Fig. 2. The casing has a circular hole along its length. A tube made of a porous medium is put in the hole. Thus, an annular cylindrical space is formed between the casing and the tube. The monomer is led to the annular cylindrical space. Water is fed into the tube and run through it. While running the water through the tube, we add pressure to the monomer; thus, we can realise the state shown in Fig.1.

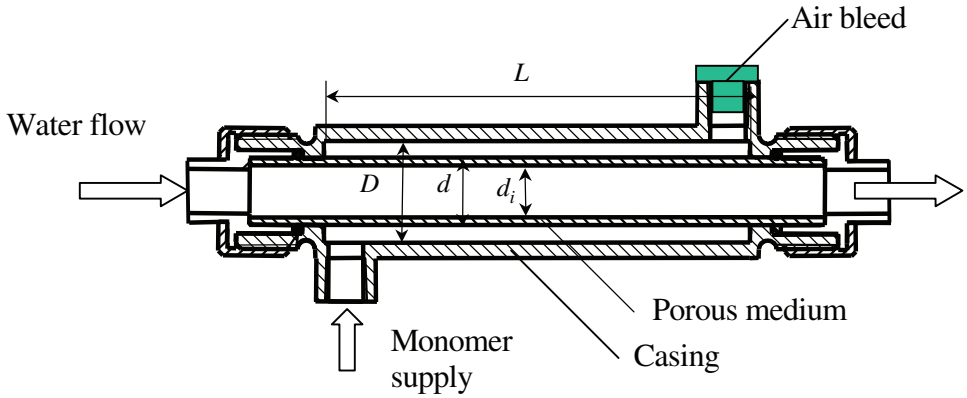

Fig. 2 Particle generator

The porous media selected for this experiment are stainless gauze and sintered bronze. Stainless gauze of specific size or mesh diameter can be purchased as a filter. The specifications of the stainless gauze filter used in this experiment are as follows:

L=125 mm, d=15 mm, d_i=10 mm, nominal size as a filter: 5 μm.

A sintered bronze filter is made applying sintering process to bronze particles. The filter medium can be identified specifying the size of the bronze particles. For this experiment, however, the material was purchased directly from the manufacturer's available stock. The specifications of the sintered bronze filter are as follows:

L=125 mm, d=10 mm, d_i=8 mm, nominal size as a filter: 5 μm.

Figures 3 and 4 are SEM photographs of the surfaces of these porous media. The diameters of the bronze spheres are not equal and spaces between the spheres are irregular. On the contrary, stainless gauze reveals a good regularity of wire diameters and mesh spaces. These photographs suggest that the stainless gauze will be better for reproduction of the same experimental condition in other laboratories.

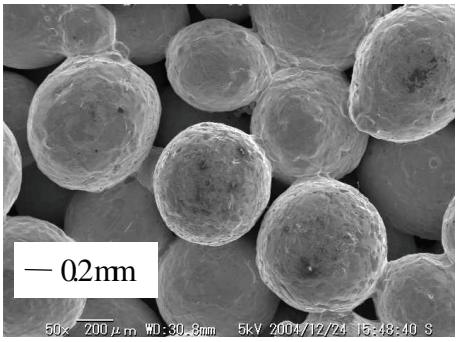

Fig. 3 Sintered bronze filter

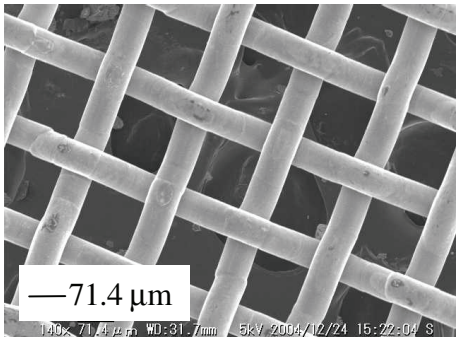

Fig. 4 Stainless steel gauze filter

Figure 5 shows a schematic sketch of the particles generation facility. The facility includes the particle generator, a piston-cylinder pair for extrusion of monomer, a pump, conduits and a beaker. The exit of the cylinder is connected to the particle generator. The pump sends the water to the particle generator; water from the generator returns to the beaker. The electric motor drives the piston via the gear train and the ball screw. An upward motion of the piston supplies the monomer in the cylinder to the particle generator. The piston velocity controls the rate of monomer flow. The cylinder dimensions are as follows:
Ball screw pitch = 5 mm, Piston diameter = 50 mm, Cylinder volume (max.) = 230 mL, Motor power = 30 W.

Let us estimate the amount of contaminants consumed by one filter test. The ISO multipass test uses the Arizona dust. The contamination level in the standard is specified by weight, e.g. 10 mg/L. Assuming that one test requires about 90 min operation and flow rate is 60 L/min, the necessary quantity of sand is

$$m_{\text{sand}} = 10\frac{\text{mg}}{\text{L}} \times \frac{60\text{L}}{\text{min}} \times 90\,\text{min} = 54\ \text{g}.$$

Since the specific weight of the sand is about 2.65, the equivalent quantity of monomer of

specific weight 0.9 is

$$m_{resin} = 54\ \text{g} / 2.65 \times 0.9 = 18.3\ \text{g}.$$

The volume of liquid resin is then

$$V_{\text{resin}} \approx 20\ \text{mL}.$$

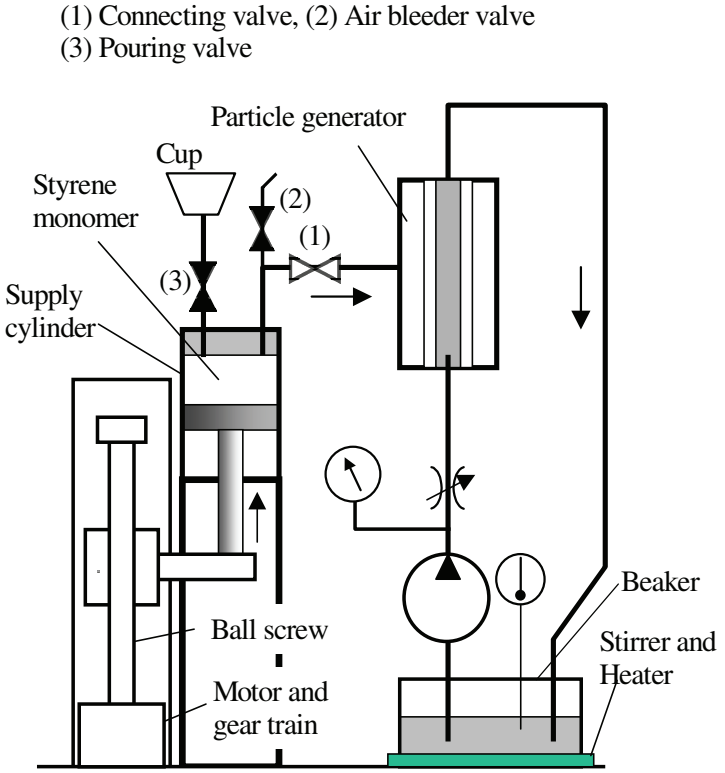

Fig. 5 Experimental rig

The above particle generation apparatus is able to treat up to about 200 mL of monomer; hence, the apparatus has sufficient capacity to produce the particles required by a filtration test.

3.3 Materials and generation process of particles

The chemicals we used in this experiment are the following:

Styrene Monomer ($C_6H_6CH\text{-}CH_2$, molecular weight 104.15),
Surfactant (Sodium Dodecyl Sulphate (SDS), $CH_3(CH_2)_{11}OSO_3Na$, molecular weight 288.38),
Polymerisation initiator (Benzoyl Peroxide (BP), $(C_6H_5CO)_2O_2$, 364.45).
(The surfactant prevents agglomeration of particles in water.)

In this process, first the styrene monomer is converted to droplets suspended in water by a mechanical process, then the monomer droplets polymerise by vibration and heating. The process is as follows. First a mixture of the surfactant and clean water is put into the beaker, and then the pump is run to circulate the water through the particle generator. A

mixture of styrene monomer and BP put in the cylinder is led to the particle generator and extruded into the flowing water. At this stage, the monomer becomes spherical particles suspended in the water. After extrusion is completed, the suspension is kept at a temperature of 75 degrees (C) with vibration continuing until polymerisation completes.

3.4 Procedure of particle preparation

Caution: Put on rubber gloves for this experiment. Good ventilation of the room is necessary since styrene monomer is toxic.

Procedure

[*1] Put the porous medium into clean water and expel any remaining air using an ultrasonic vibrator.
[*2] Measure the clean water volume and defined amount of SDS. Then, put them in a beaker and start heating and stirring. Temperature should be kept between 60-70 degrees (C).
[*3] Mount the porous medium prepared in [*1] on the particle generator.
[*4] Close the valve between the cylinder and the particle generator.
[*5] Put measured styrene monomer and the BP into a beaker. Then, stir it by ultrasonic vibrator for about 5 minutes.
[*6] Put a measured amount of clear water in the cylinder; then pour the above mixture of styrene monomer and BPO into the cylinder. Then, close the pouring port (close valve (3) in Fig.5). The volume of water and SM are equal.
[*7] Open the air bleeder valve (valve (2) in Fig.5) and raise the piston to expel the air from the cylinder and connecting tube to the particle generator. Then, stop the piston and close the air bleeder valve.
[*8] Run the pump.
[*9] Open the valve (valve (1) in Fig.5) connecting the cylinder and the particle generator.
[*10] Drive the piston by operating the electric motor.
[*11] Stop the piston at the upper end. Then close the connecting valve.
[*12] Stop the pump after a few minutes.
[*13] Continue stirring the beaker for about 5-6 hours, keeping the temperature to about 75 degrees (C).
[*14] Store the fluid (water suspending polystyrene latex beads) in a container with cap.

Note 1: Wash the cylinder, pump and particle generator after this process. The remaining styrene should be wiped off using ethanol. Waste fluid must be collected and send to a waste-treatment site.
Note 2: For measurement of usual particle counters, the prepared suspension should be diluted about 10,000 times with clean water.

4 Experimental result and discussion

Figure 6 shows an SEM photograph of generated particles; it proves that their shape is

spherical. Table 1 shows the experimental conditions.
The particle number density of the prepared suspension was measured after 1:10,000 dilution with clean water. The HIAC counter is used for the counting. The cleanliness level of water for dilution must be sufficiently lower than the particle density of the prepared suspension. Figure 7 shows contamination level of the clean water used for the dilution. As shown later, particle number density of the prepared suspension is about 10^6 times higher than that of the dilution water. Hence, the 1:10,000 dilution by the clean water is justified.

Table 1 Experimental condition

Water volume	2000 ml
Piston velocity	50 mm/min
Styrene Monomer	40 ml
Sodium Dodecyl Sulfate	3.3 g
Benzoyl Peroxide	0.9 g
Water temperature	75 ℃
Flow rate	4.4 L/min
Stirring time	5 hours

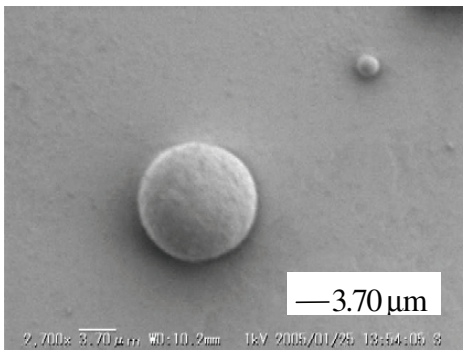

Fig. 6 Produced particles
(Stainless wire gauze)

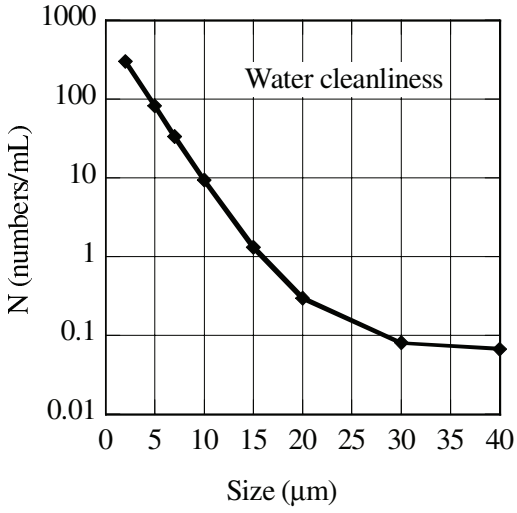

Fig. 7 Cleanliness of water for dilution

Figure 8 shows measured examples of prepared suspension. A specimen is prepared in the following way: take 5 mL of prepared suspension, then dilute it by the clean water of 495 mL, take 10 mL of the diluted suspension, then dilute it by the clean water of 990 mL.

Scatter is relatively large in larger particle ranges. Table 2 shows coefficient of variation (Sample standard deviation/Average value of samples) at each particle size range.

The size distribution curves are normalised by dividing the counted number for each size by the counted number for a fixed size, for example, 10 micrometers. Figure 9 compares the particle size distributions of sands and prepared particles. The distribution curves of the prepared suspensions are similar to those of natural sands and common contaminants in fluid power systems. While the sintered bronze and the stainless gauze show similar distribution, definition of the filter media can be made more exact by stainless gauze filters than by sintered bronze sphere filters. Hence, our study concentrates on the prepation of particles by the stainless gauze filter.

Table 2 Statistics of measurement

D(μm)	2	5	7	10	15	20	30	40
Average	133458	14100	5096	1476	215	47.3	6.60	1.73
STDV	1787	214	205	187	70.7	23.4	3.97	1.04
Coef. var.	0.013	0.015	0.040	0.127	0.329	0.495	0.601	0.599

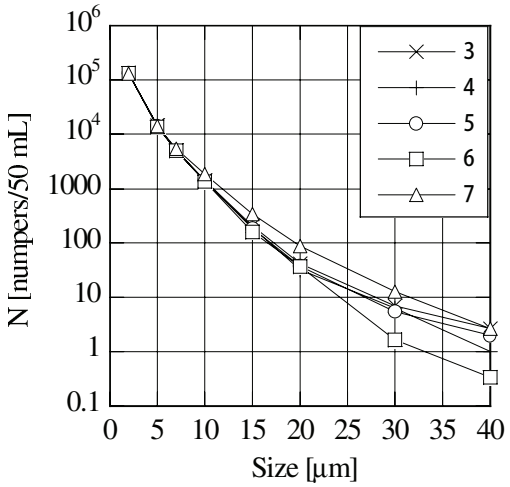

Fig. 8 Example of size distribution of prepared suspension (1: 10,000 dilution)

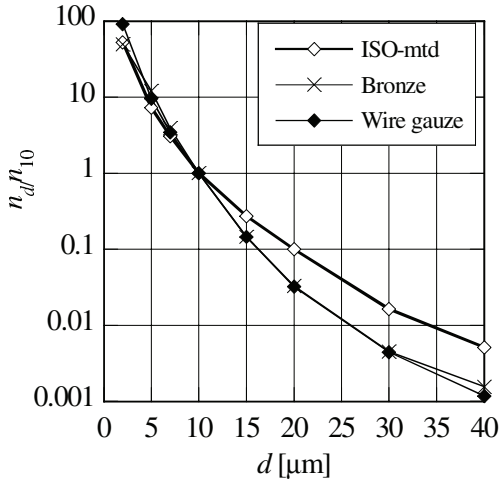

Fig. 9 Particle distribution function

The influence of flow rate on the particle size was also studied. However, in our experimental range, namely, in the range of Reynolds numbers 8,000-15,000, no clear tendency appeared. The prepared suspension did not separate for at least one month after preparation. Therefore, we can prepare the suspension several days before the filter tests.

Since this is our first trial of preparing artificial test particles, there may be some possibilities for improving the preparation process. The suspension prepared by the process is used for the study of filters for water hydraulics. While particles suspending in oil are required for oil hydraulics, some modification of the preparation process will be required to apply it to oil.

5 Conclusions

This paper shows that artificial test particles for filtration performance testing of fluid power filters can be prepared in a fluid power laboratory. We have illustrated the process of preparing suspensions of polystyrene latex and designing the necessary devices. Prepared particles have the following properties:
spherical shape, specific weight of 0.9, white colour, size distribution suitable for filter testing, producible in normal fluid power laboratories.

Acknowledgement

The authors would like to express their thanks to the following people who helped with this study: Associate Professor K. Kudoh took the SEM photographs, graduate students Mr. Akira Nakakamura and Mr. Terutaka Doi, undergraduate student Mr. Tetsuya Inaba helped with the experimental work.

References

1. Stecki, J., Total contamination control, Fluid Power Net (1998).
2. ISO16889, The multi-pass test method for evaluating filtration performance of filter elements.
3. ISO 12103-1, Road vehicles-Test dust for filter evaluation-Part 1: Arizona test dust.
4. Allen, T., Particle size measurement, Vol. 2, Surface area and pore size measurement, Fifth edition, Chapmann & Hall (1997).
5. Lowell, S. Shields, J. E.. Thomas, M. A. and Thommes, M., Characterisation of porous solids and powders: surface area, pore size and density, Kluer Academic Publishers (2004).

EXPERIMENTAL STUDY OF SEALING CAPABILITY OF LARGE DIAMETER ROTARY FACE SEALS FOR FLUID POWER APPLICATIONS IN PROCESS INDUSTRY

Olof Calonius, Henri Hänninen and Matti Pietola
Helsinki University of Technology (TKK)
Machine Design / Fluid Power
P.O. Box 4400
FI-02015 TKK, Finland
Phone +358 9 451 4573, Fax +358 9 451 3418
E-mail: Olof.Calonius@tkk.fi

ABSTRACT

The costs of sealing failure in industrial fluid power systems are likely to be quite high, because costs other than the cost of just replacing the damaged seal are involved. In addition to economic factors, the quest for reliable solutions is driven by environmental legislation factors. In this study, full scale testing of face seals 531 mm and 534 mm in diameter made of filled polytetrafluoroethylene was conducted in a new test rig. The seals were tested by varying both the sliding speed, ranging from 8.3 m/s to 19.6 m/s, and the seal cross-section compression, ranging from 1.2 mm to 2.2 mm. For each set of test variables, three repetitions were made. Leakage values, temperatures near the sealing zone and values of friction and frictional power are reported. With the test rig the operating conditions could be systematically varied and recorded. It was found that increasing in the speed of rotation reduced the leakage. This tendency increased with the amount of compression. It was concluded that in the tested sealing system the leakage oil was partly centrifuged back to the oil side of the sealing lip, such that leakage values represented the equilibrium between flow into and flow out of the sealed space. Least leakage throughout the sliding speed range is likely to be produced with the seal type having a stiffer spring and greatest compression. However, this combination created a high sealing force resulting in high frictional power loss and high operating temperature, which emphasizes the need for arranging good lubrication conditions in sealing systems involving high sliding speeds.

KEYWORDS: Sealing, Face seal, Full scale tests

1 INTRODUCTION

Reliable sealing solutions are of particular importance in industrial fluid power systems. Most seals are relatively inexpensive machine elements, but in a process industrial setting the costs of sealing failure are likely to be much higher than the cost of just replacing the damaged seal. In case of sealing failure, issues such as continuity of the process and protection of the environment will become involved.

The purpose of this study was to investigate the sealing capability of large diameter face seals intended for fluid power systems involved in the operation and lubrication of large rotating components in process machinery. To this end, full scale sealing tests to establish the effect of variation of operational variables on leakage were conducted in a newly developed test rig. In full scale testing both the test equipment and the test specimens are expensive and therefore published data concerning operating conditions and sealing capability of large diameter industrial seals appears to be scarce. In these initial tests with the rig, face seals sealing the space between two vertical disks, one of which was rotating, was conducted. An additional aim of the study was to systematically determine the prevailing conditions in the large diameter rotary seal system simulated in the test rig. The recorded conditions could be of interest for engineers involved in designing of industrial sealing and condition monitoring solutions.

2 METHODS

In this section the test rig, the tested seals and the test program will be described.

2.1 Test rig

The test rig consisted of a hydraulic circuit which implemented the lubrication system, an electric drive motor with a frequency converter to produce the rotary motion and an instrumented test chamber housing the seal and its counterface, **Figure 1**. The operating conditions were recorded with a PC-based data acquisition system (National Instruments NI PCI-6229 and LabVIEW 7.1). The seal was attached to the rotating disk and the counterface (black nitrided, nominal surface roughness: R_a 0.2 μm) to the non-rotating disk. Oil was delivered to the seal-counterface contact zone from six evenly spaced positions along the circumference of the non-rotating disk. Total flow was 8-9 liters per minute. The counterface temperature (10 mm below the contact surface) was recorded with resistive temperature sensors (Pt100, ϕ3 mm) and the relative axial motion between the counterface and the rotating disk was measured with eddy current transducers. The dynamic axial runout of the rotating disk relative to the non-rotating disk was 0.08 mm (p-p; measured at 500 rpm with eddy current transducers). The static radial runout was 0.2 mm (p-p; measured with a dial gauge). Instrumentation to measure the dynamic radial runout was not available.

2.2 Tested seals

The face seal type being evaluated in this study was a spring-loaded large diameter rotary lip seal, **Figure 2**. The profile of the seal is also common in radial lip seals and in rod seals. In this study, the face seal was attached to the rotating disk and sealed against oil on the outside of the seal ring. The seal material was carbon fiber filled polytetrafluoroethylene (PTFE) that can withstand high temperatures produced in the contact zone due to frictional heating, **Figure 3**. Two seal types were tested in a comprehensive test series. The overall dimensions of both seals were identical and are shown in **Table 1**.

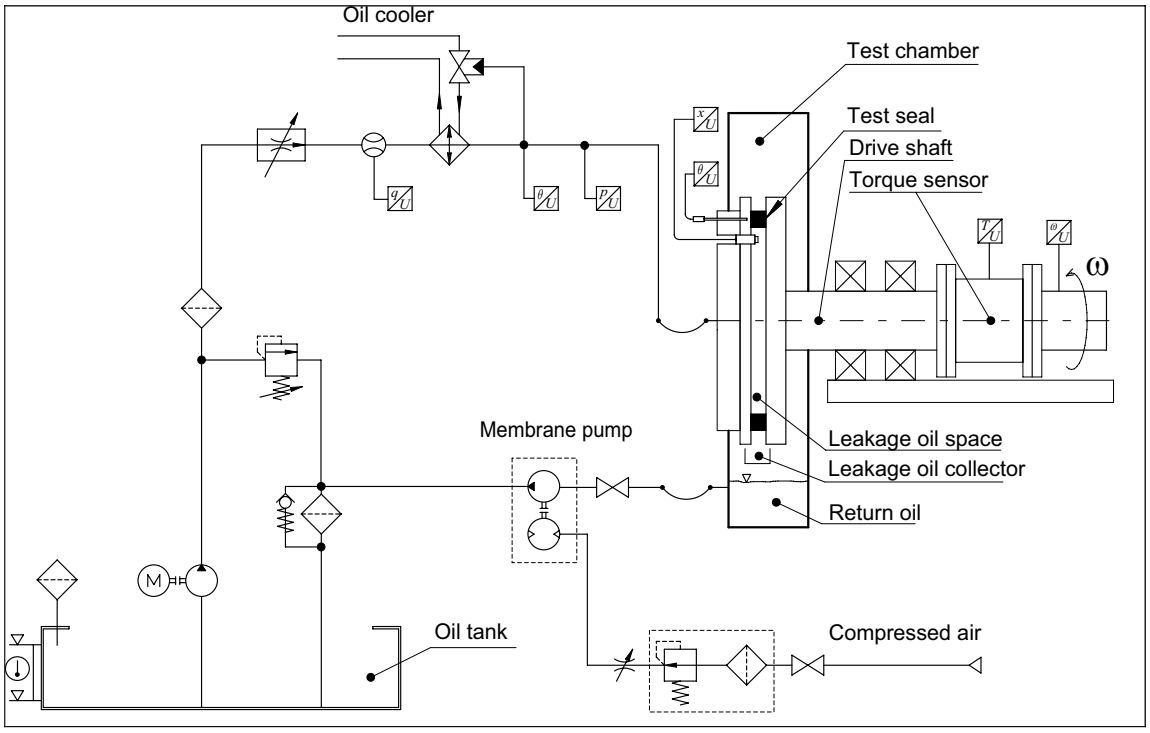

Figure 1. *Test rig.*

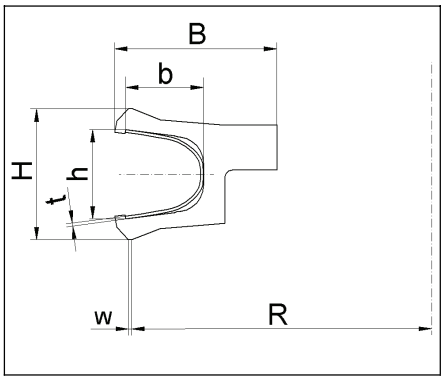

Figure 2. *Seal cross-section. Oil space on the left. Dynamic sealing zone of width w is located on the lower seal lip in contact with the counterface.*

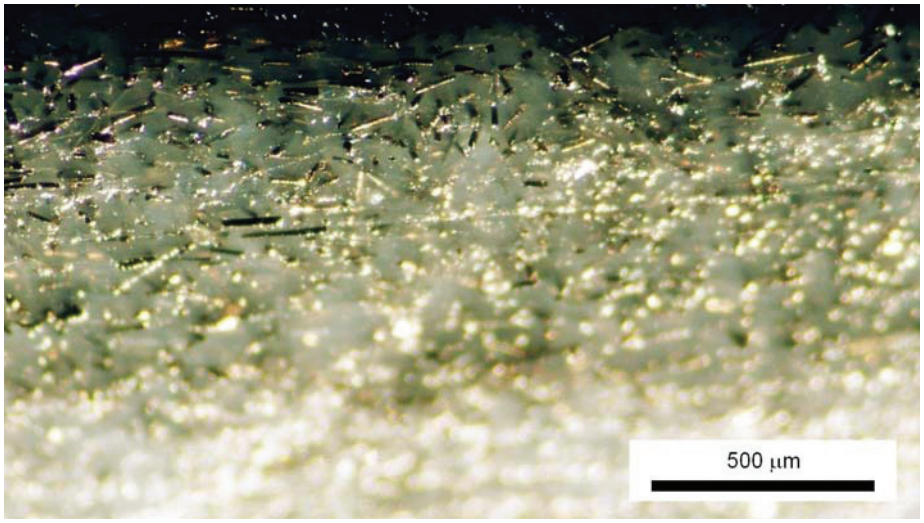

Figure 3. *Micrograph showing seal material containing carbon fibers. View of contact zone of seal lip, sliding direction is horizontal.*

The spring stiffness was considerably different in the two tested seals, Seal A and Seal B. The stiffness of the whole seal (combined stiffness of seal jacket and spring) was measured after the warm-up run when the test rig was driven at 500 rpm and when setting the operating compression of the seal. The stiffness of Seal B (2 kN/mm) was 2.6 times higher than the stiffness of Seal A (0.77 kN/mm). An additional difference was that in Seal B the seal lip was modified into a double lip. Compared to Seal A, Seal B had a small tapered concentric groove on the air side of the original lip and a primary lip with a diameter that was 1.5 mm smaller than for the original lip. The groove allows for some relief of pressure load and better lubrication.

Table 1. *Dimensions of the seals.*

Seal jacket				**Spring**		
Radius R (mm)	Contact width w (mm)	Width B (mm)	Height H (mm)	Width b (mm)	Height h (mm)	Thickness t (mm)
267 (Seal A) 265.5 (Seal B)	0.3	13	9	6	6.3	0.23

2.3 Test program

Both seal types were tested with three speeds of rotation (300 rpm, 500 rpm, 700 rpm) and three values of compression. The compression values (from the point of initial contact of the seal lip with the counterface) were 1.2 mm, 1.7 mm and 2.2 mm. The sliding speeds corresponding to the speeds of rotation were 8.4 m/s, 14.0 m/s and 19.6 m/s for Seal A and 8.3 m/s, 13.9 m/s and 19.5 m/s for Seal B. For each compression value all speeds were tested before increasing the compression. This was done because not more than two

expensive seal samples were available and because first testing all compression values before increasing the speed would have changed the compressive force to a much larger extent than with the present procedure.

Each test run lasted for 2 hours and was repeated three times. The values of leakage, friction etc. are reported as averages of these three tests. The intent was to test all combinations of speeds and compressions for both seal types, but for Seal B the highest values of compression and speed of rotation was not tested because the temperature of the counterface became too high. Therefore, the total number of test runs was $(2 \times 3 \times 3 - 1) \times 3 = 51$.

The measured quantities were the leakage, the counterface temperature, the frictional torque, the force needed to produce the compression of the seals, i.e., the sealing force and the relative axial motion of the rotating seal disk and the non-rotating counterface disk. In addition, the lubrication oil flow rate was recorded. It ranged from 8 to 9 liters per minute in all tests. The lubrication flow was equally divided into six nozzles distributed 60 degrees apart along the circumference of the seal. The hydraulic oil was VG68, with a room temperature density of 870 kg/m^3.

Leakage was measured by moving the counterface out of contact with the seal and letting the leakage space drain into the leakage collector below. Because the leakage collector had to be inserted into the test chamber after the test run, collecting the leakage oil was postponed for one hour after the run to allow dripping of oil from components near the collector to subside.

Prior to each test there was a warm-up run of approximately 45 min. The warm-up run was continued until the temperature change of the seal counterface beneath the contact zone was negligible. After the warm-up there was a 15 min draining period of the leakage space before starting the actual test run.

3 RESULTS

First, values obtained directly by measurements are presented. These include the average values of leakage measured at the end of each test run, counterface temperature, sealing force and torque. Then, the results will be used to derive some additional quantities that describe the test conditions of the seal. These are estimates of the frictional power and the coefficient of friction. Furthermore, the measured leakage values of the two hour test runs are projected to deciliters (one tenth of a liter) per day.

3.1 Measured values

The results include leakage values, counterface temperatures, values of compressive force applied to the seal and torque, **Figure 4** and **Figure 5**. Leakage collected into a measuring cylinder was weighed with a scale immediately after each test run. The change in sealing force (compressive force) during tests (all speeds were tested before increasing the compression) is shown in **Figure 4** (c) and **Figure 5** (c).

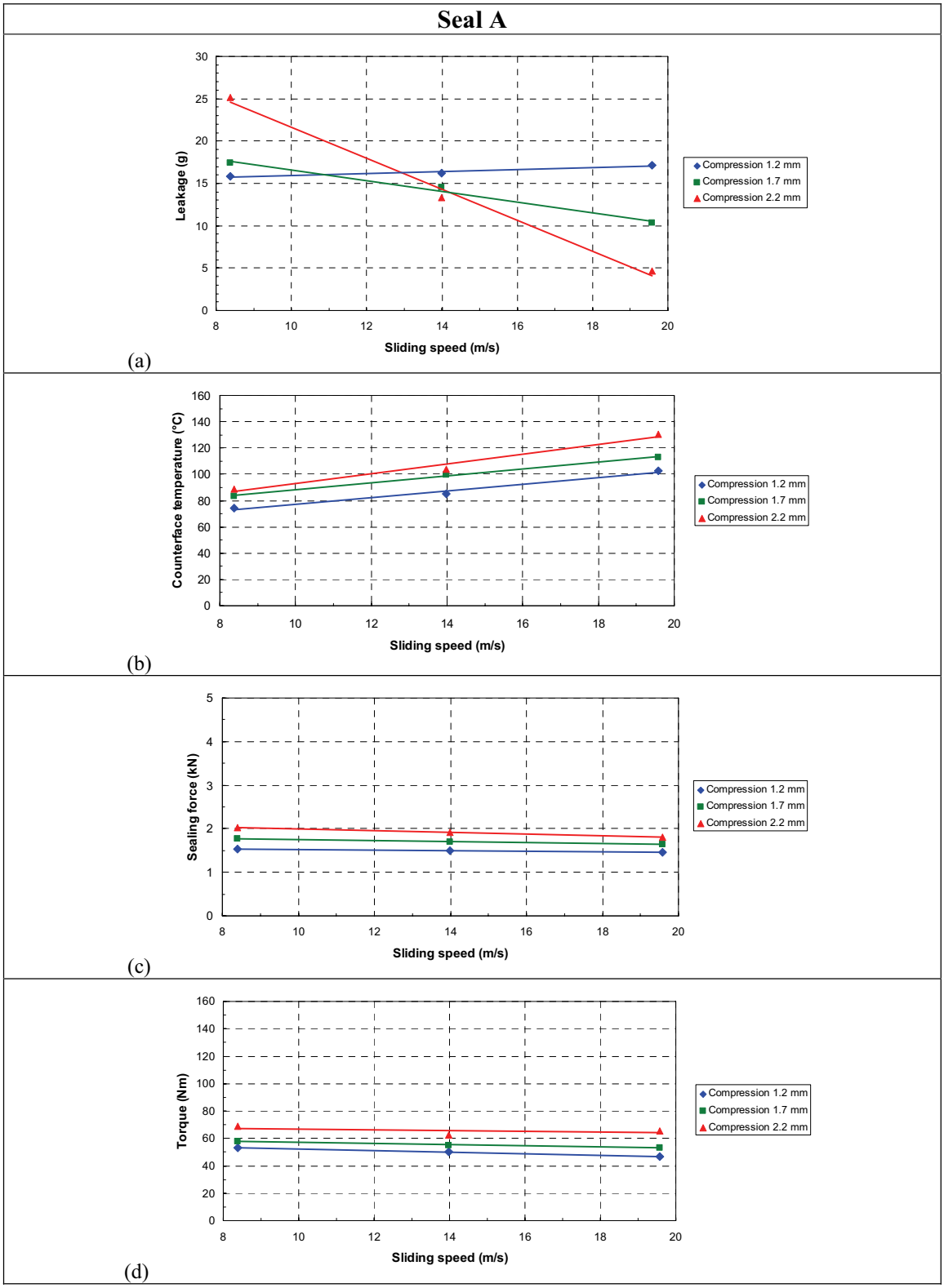

Figure 4. *Results of tests with Seal A. (a) Leakage, (b) Counterface temperature, (c) Sealing force, (d) Torque.*

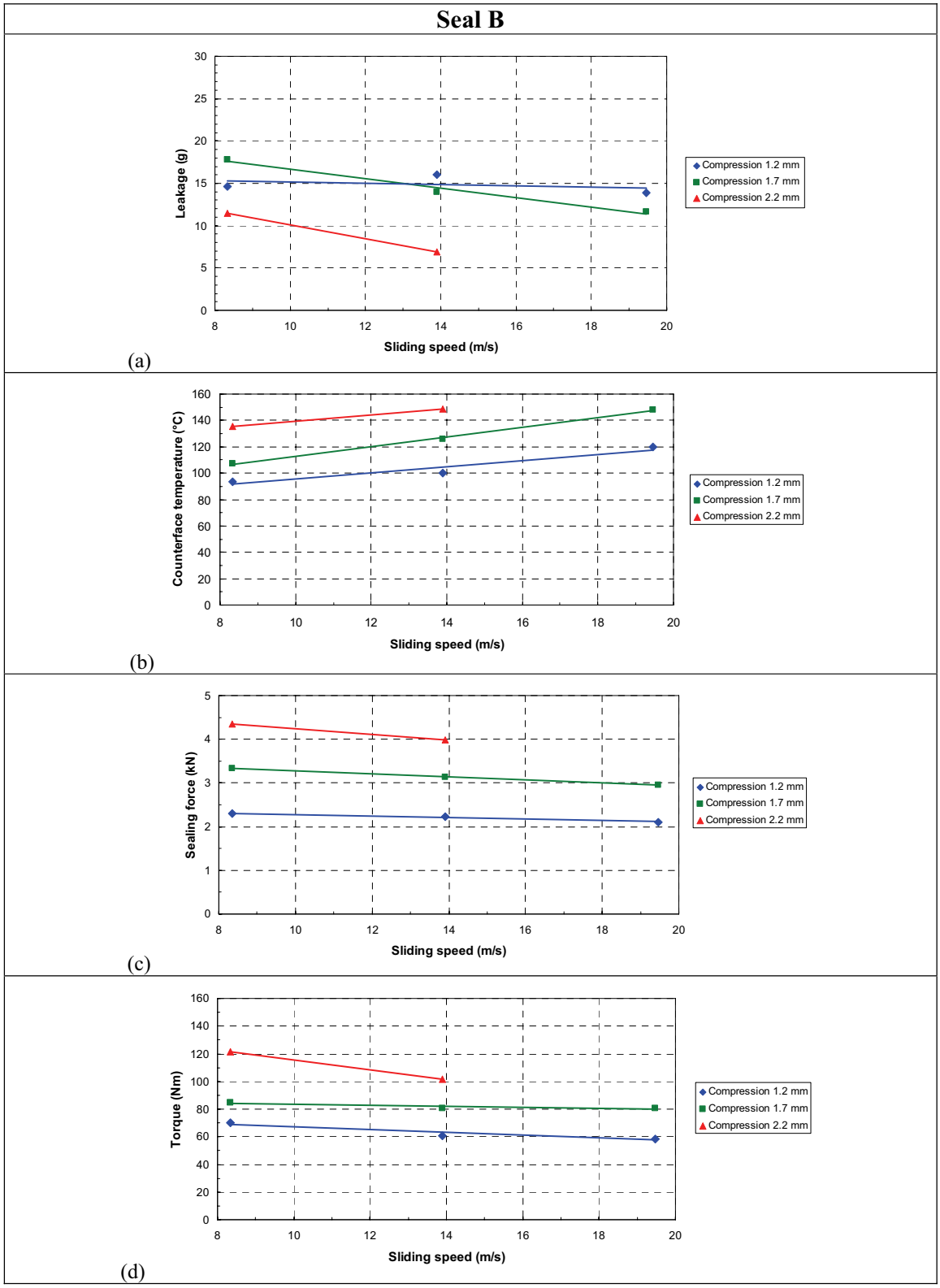

Figure 5. *Results of tests with Seal B. (a) Leakage, (b) Counterface temperature, (c) Sealing force, (d) Torque.*

3.2 Derived values

The frictional power is estimated with the formula $P = M \times \omega$, **Figure 6**. M is the measured drive shaft torque and ω is the speed of rotation. In the test rig, frictional torque dominates the value of measured torque. The frictional torque due to the bearings was found to be unimportant compared to the frictional torque generated by the large diameter seal ring which was loaded with a compressive force of several kN.

Since the torque and the compressive force were measured, the coefficient of friction could be computed with the formula $\mu = M / (F \times r)$, where F was the compressive force and r was the radius of the contact zone of the seal. See **Figure 7**.

Projected leakage data are presented in **Figure 8** and the relation between duty number $G = \eta \times \omega / p_{contact}$ and friction and leakage in **Figure 9**. η is the dynamic viscosity, ω is the angular velocity and $p_{contact}$ is the contact pressure.

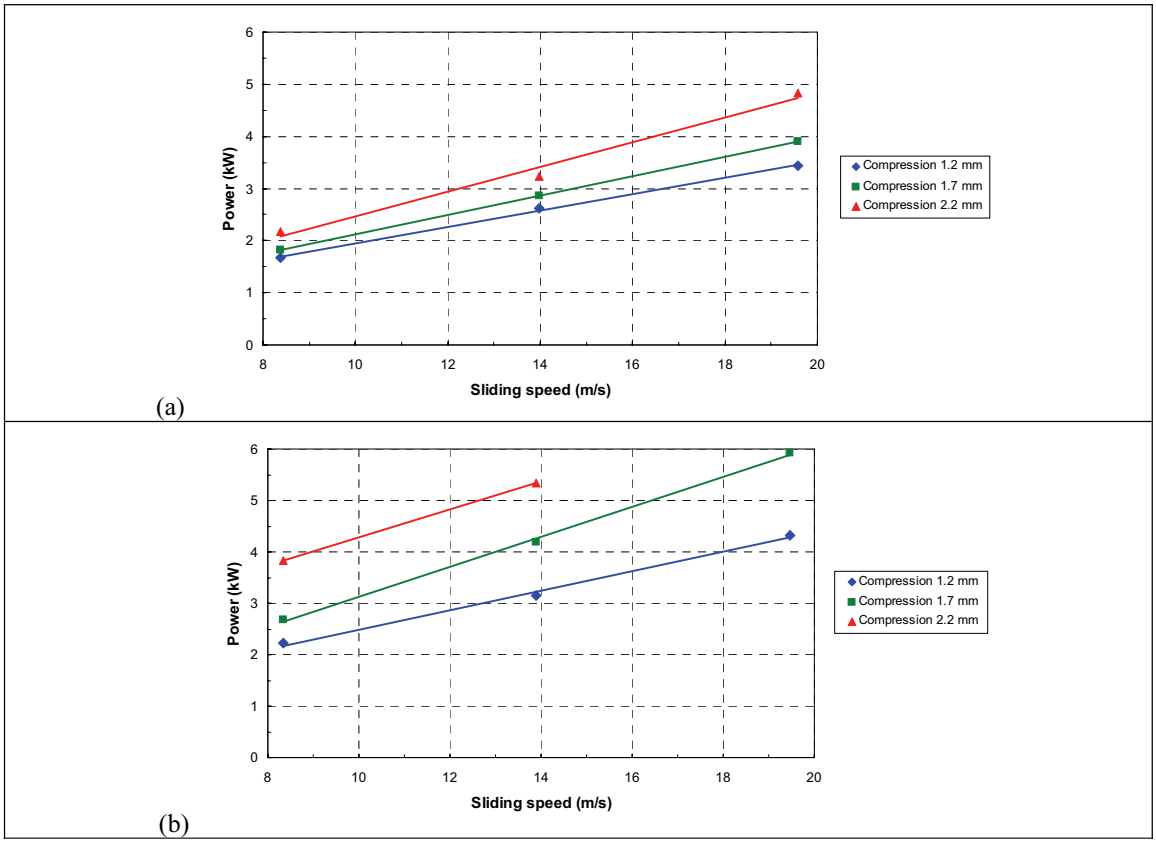

Figure 6. *Frictional power generated by the seals. (a) Seal A, (b) Seal B.*

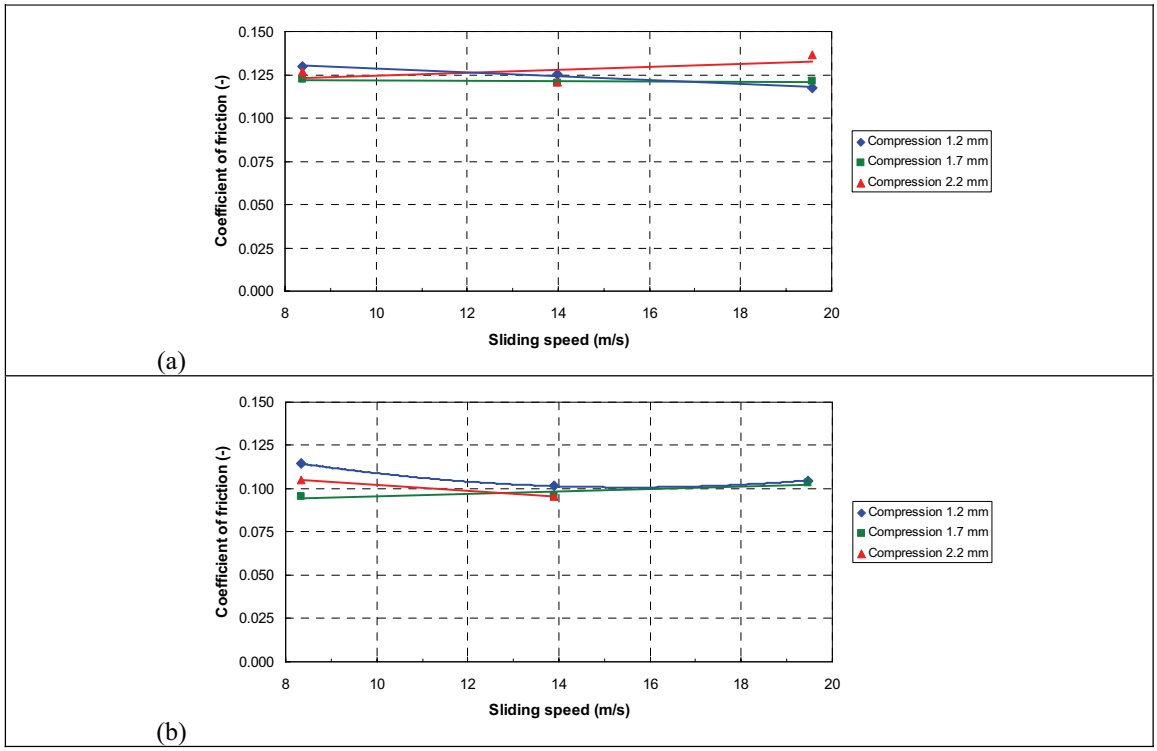

Figure 7. *Coefficient of friction. (a) Seal A, (b) Seal B.*

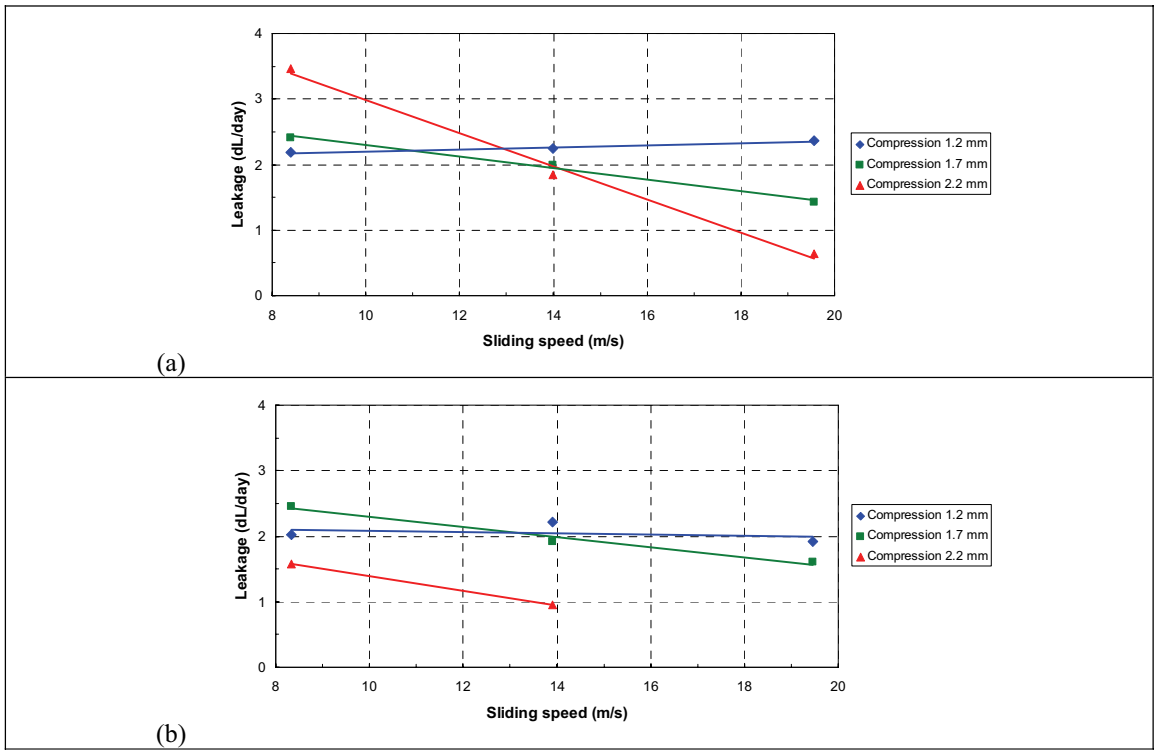

Figure 8. *Projected leakage values; deciliters per day. (a) Seal A, (b) Seal B.*

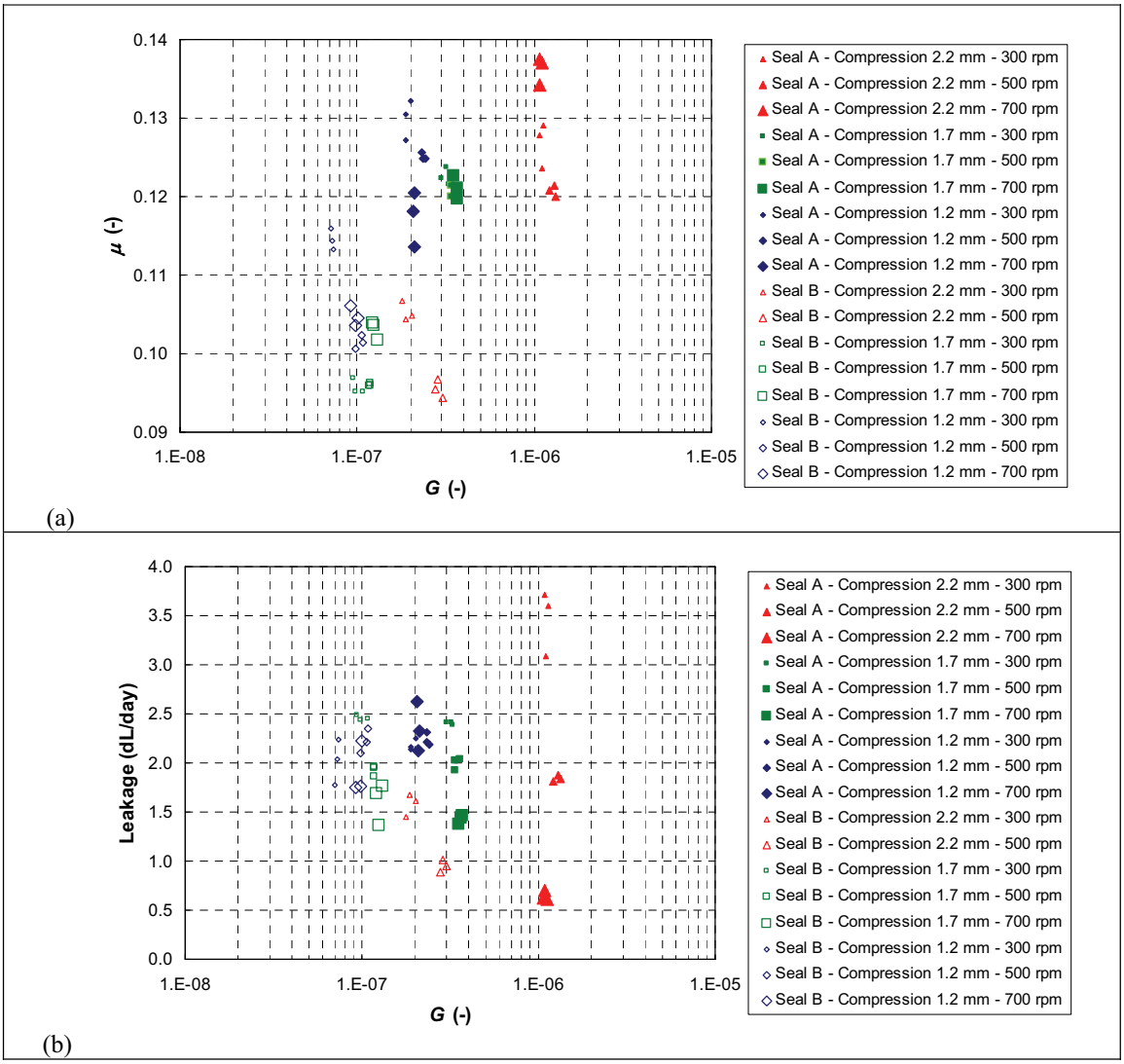

Figure 9. *(a) Duty number vs. friction, (b) Duty number vs. leakage.*

3.3 Seals and counterface after tests

After the tests, the worn regions of the seals have a slightly polished appearance. Corresponding worn regions can be seen on the counterface disk. **Figure 10** and **Figure 11** show Seal A and the counterface after the tests.

Table 2 shows the surface roughness values of the counterface disk (average values of three measurements). In the unworn area measurements were made in both the radial and the circumferential direction so as to verify that the surface properties were initially isotropic. For the wear tracks, the values for the circumferential direction are shown for three positions along the circumference.

Table 2. *Counterface R_a-values.*

Unworn area		**Wear track**		
Radial (μm)	Circumferential (μm)	Top (μm)	Bottom (μm)	Medial (μm)
0.19	0.18	0.15	0.15	0.14

Figure 10. *Seal A after tests. Attachment flange to the left and seal lip to the right.*

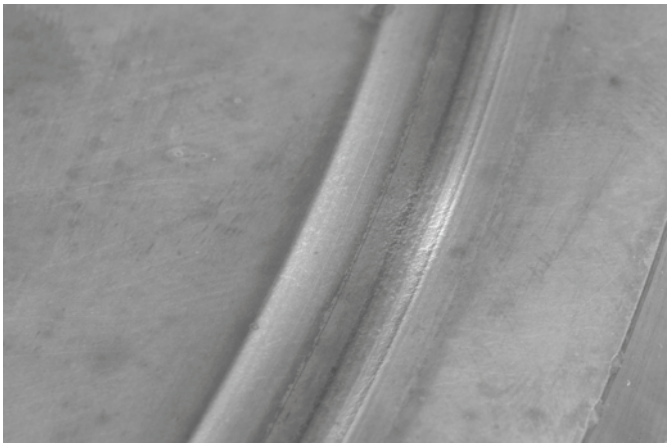

Figure 11. *Wear tracks on counterface after tests. Areas in the figure are in the same plane, except in the lower right corner where the edge of the counterface disk is seen. Wide track to the left produced during maximum compression from part of seal next to attachment flange. Tracks from the lips are in the right half of the contact zone, which shows a thin layer of deposits towards the edge. Deposits are also seen in areas between tracks from the lips and the seal body.*

4 DISCUSSION

The Discussion involves the operating conditions of the seals, the factors influencing the leakage and issues related to further research.

4.1 Operating conditions

Even though the speed of rotation in the tests of this study can be characterized as moderate, the sliding speeds become high due to the large contact diameter of the seal lip. In the study, a sliding speed range from approximately 8 m/s to 20 m/s was covered.

Because of the need for seal compression up to 2.2 mm, the load become quite high. With this compression, line loads of up to 1.2 N/mm were found for Seal A and up to 2.6 N/mm for Seal B. In combination with the high sliding speed this resulted in intense generation of frictional heat. However, the coefficient of friction was limited to the range from 0.10 to 0.14. For radial shaft seals made of PTFE, reported values are clearly higher, e.g., from 0.2 to 0.3 [1].

Another factor that contributed to the high thermal load was that in the initial version of the test rig the lubrication oil flow was not explicitly controlled in the region near the seal lip. After the oil had been pumped through the nozzle to the seal lip, it was allowed to escape due to the action of the rotating disk and due to gravity. Thus, cooling by lubrication was not optimal.

As a result, counterface temperatures in excess of 100 °C were measured for all cases tested at 700 rpm (19.6 m/s for Seal A and 19.5 m/s for Seal B), **Figure 4**(b) and **Figure 5**(b). In particular, for Seal B with 2.2 mm compression the temperatures became inconveniently high. For this seal the combination of 2.2 mm compression and 700 rpm speed of rotation was not tested, because in an initial short run the temperature rose to above 180 °C.

In the tested cases, when the sliding speed of the seal approaches 20 m/s, the frictional power ranged from 3.4 kW to 4.8 kW (Seal A) and from 4.3 kW to 5.9 kW (Seal B), **Figure 6**. The high power consumption could indeed be anticipated based on the results of an earlier computational study of several face seal variants [2].

Frictional torque of Seal A was in the range from 50 Nm to 70 Nm, while for Seal B the range was from 60 Nm to 120 Nm. The high values of frictional torque of Seal B caused some trouble in that the frequency converter controlled drive did not produce enough torque to begin rotating the disk. It was necessary to start up the tests with a smaller compression and then gradually increase it to the desired value.

The difference between the two seal springs can easily be seen in **Figure 4**(c) and **Figure 5**(c). Relatively small differences in the sealing force due to different values of compression were measured for Seal A. All values fall approximately between 1.5 kN and 2 kN. For Seal B, an increase in compression of 0.5 mm increases the sealing force by approximately 1 kN. At a sliding speed of 500 rpm (~ 14 m/s) and compression of 2.2 mm, the sealing force of Seal A was nearly 2 kN, while the sealing force of Seal B was 4 kN.

The decrease in sealing force corresponding to a given compression during the tests can also be seen in **Figure 4**(c) and **Figure 5**(c). The change is small when the compression is 1.2 mm but can be clearly seen when the compression is 2.2 mm, especially for Seal B. It is likely that the change in sealing force was mostly due to decrease in stiffness of the PTFE material at elevated temperatures produced at higher speeds, such that a similar difference in force would have occurred had separate seal specimens been used.

4.2 Leakage

Leakage estimates for seals are often based on laminar gap flow under the action of a pressure difference across the seal. Even though the oil film thickness in the gap could be estimated (based on fluid friction and measured values of torque and speed of rotation [3]), in the tested seal system there was no pressure difference across seal which would act as the driving force for leakage. The situation in the present study was different compared to shaft sealing in which the pressure across the seal is the driving force for leakage and for which counterpumping, not the centrifugal force, is the main effect trying to return the leakage oil once it has escaped from the sealed space.

As the regions near to the seal ring and the counterface disk could not be directly observed (sight blocked by attachment disks), it may be hypothesized that in the tested sealing system the measured leakage value represented the equilibrium between the actual leakage flow (inflow into sealed space) and return flow (outflow to oil side). The former flow was driven by the lubrication oil feed and the latter by centrifugal forces produced by the rotating disk acting on oil in the leakage space. Gravity acts to increase inflow in the upper regions of the counterface and correspondingly to increase outflow in the lower regions of the counterface.

The leakage behavior of Seal A, **Figure 8**(a), appears to be somewhat peculiar. When the compression was small (1.2 mm) the seal functioned consistently over the entire sliding speed range. The leakage was noticeable (projected value above 2 deciliters/day), but it changed very little as the speed was increased. It was, however, surprising to find that when the compression was increased the leakage tendency increased as well. This behavior can be seen in that the slopes of the regression lines were increasing with increasing compression. For both 1.7 mm and 2.2 mm compression the measured leakage at low sliding speeds, i.e., at slow speeds of rotation was higher than when the compression was only 1.2 mm. As the speed of rotation was increased, the outflow increased proportionally. The tendency was accentuated because the operating temperatures increased when the compression increased which decreased the viscosity of the oil.

An explanation to why the leakage tends to increase with compression is that the seal jacket material may undergo partial plastic deformation resulting in loss of tracking capability of the seal lip. When the seal jacket comes into contact with the counterface in regions other than the seal lip (as evidenced by the wear tracks on both seal and counterface), the seal tracking arm may become irreversibly displaced. Loss of tracking capability due to large compression is probably less severe if the spring stiffness is large compared to the stiffness of the seal jacket material.

For the smaller compressions (1.2 mm and 1.7 mm) the leakage behavior of Seal B, **Figure 8**(b), follows the same pattern that was observed for Seal A. The leakage for the highest compression (2.2 mm) is (unlike the situation for Seal A) smaller than for the other values of compression even at the lowest speed of rotation. With the maximum compression the operating conditions of Seal B were much harder than for Seal A. The sealing force of Seal B was more than two times higher than that of Seal A, **Figure 4**(c) and **Figure 5**(c). In addition, the operating temperature of Seal B at 2.2 mm compression and 300 rpm was 135 °C which was approximately 40 °C higher than at 1.2 mm compression and 30 °C higher than at 1.7 mm compression for Seal B at the same speed of rotation. The high sealing force and the stiff spring does indeed reduce the leakage (Seal B at maximum compression shows least leakage of the configurations tested). The penalty is the high frictional power and the resulting high operating temperatures in excess of 130 °C.

The leakage curve of Seal B at maximum compression, **Figure 8**(b), has a negative slope, indicating that outflow plays a role for this seal as well. To confirm the inflow/outflow balance hypothesis an additional test was performed with Seal B (700 rpm ⇔ 19.5 m/s, compression 1.7 mm). 30 grams of oil was injected into the leakage space prior to the test which was otherwise conducted in the same manner as the previous tests. After the test (2 hours), the leakage was measured to 11.8 grams (projected value 1.6 deciliter/day). Earlier (in the normal test with same parameters and without injected oil) the leakage had been measured to 11.6 grams, indicating that a state of dynamic equilibrium will develop. The leakage corresponding to this equilibrium state depends on the speed of rotation, the operating temperature and the operating mode of the seal. The compression of the seal significantly influences the latter two factors.

In the present test configuration, the tendency of the tested face seal system to centrifuge the leakage oil and therefore to nominally leak more at slow speeds of rotation is likely to be observed in situations where there would be many starts and stops. Leakage would appear significant compared to the situation where the seal was running continuously at high speed.

In some cases zero leakage may not be the best solution as leakage does protect the seal from burning and excessive wear. Controlled leakage where the leakage oil can be collected and reintroduced in the circulation could be desirable.

The duty number G (dimensionless quantity) can be used to characterize the lubrication conditions of the seal. Similar parameters (e.g. the Gümbel-number) are used when describing journal bearing lubrication. In Ref. [4] the duty number (number of hydrodynamic similitude) is defined as half the value of G, i.e., $(\eta \times \omega)/(2 \times p_{contact})$. According to [4], boundary lubrication corresponds to values of G up to approximately 4×10^{-7}, mixed lubrication to values between 4×10^{-7} and 1.2×10^{-6} and full film lubrication to values above 1.2×10^{-6}.

It can be seen in **Figure 9** that in this study Seal A was operating both under boundary and mixed lubrication conditions whereas Seal B was operating primarily under boundary lubrication. The lubrication conditions were primarily determined by the compression of the seal because both friction and leakage values (especially for Seal A) were approximately vertically grouped according to compression. Otherwise, no clear

correlation could be found in the present data between, e.g., low leakage and high friction or vice versa. In [5] an inclined dividing line between sealing and leaking seals could be drawn in a μ–G graph. As some leakage was measured in all cases in the present study, the seals were evidently operating in the 'LEAK' part of the μ–G space. In support of this, the present friction values were much lower than those reported for non-leaking seals in [5].

4.3 Further research

One limitation of the study was that the test duration was only two hours. It is possible that fully stable contact conditions between the seal lip and the counterface will need longer time to develop after a change influencing the wear track position. However, with a laboratory test rig the operating conditions were reproducible such that values measured with the same set of test parameters were reasonably well grouped together. In the future, if unmanned testing can be realized, longer tests will be pursued.

In the study, only one counterface was used because of restrictions in funding. Thus, because of the face seal geometry, it was not possible to produce the wear track in a completely unused position for each test. Even though it is expensive, it would be preferable to have a new counterface area for each test run to avoid the risk of confounding effects of wear and deposits from previous tests.

5 CONCLUSIONS

The following conclusions could be drawn:

In the constructed test rig the operating conditions of the face seals could be systematically varied and recorded, enabling comprehensive studies of sealing capability.

As expected, the leakage was influenced by compression of the seal. Additionally, it was found that the speed of rotation had a clear effect on the leakage. The tested sealing system was special in that it was possible for leakage oil to be returned back to the oil side of the sealing lip by centrifugal action. This was manifested as a dependence of measured leakage on speed of rotation. The leakage decreased as the speed of rotation increased. The measured leakage value was not the total quantity of oil that had escaped past the seal lip, but rather the collected leakage oil represented the equilibrium between flow into and flow out of the sealed space at a given speed of rotation and a given compression.

When compression was increased, the tendency of decreasing leakage with increasing speed of rotation increased as well. Apparently the larger values of compression partially damaged the seal so that both inflow and outflow could increase.

On the other hand, for the smallest value of compression leakage was nearly independent of the speed of rotation indicating that the seal lip was operational throughout the speed range. However, leakage was noticeable throughout the speed range.

Both seal types displayed the same leakage tendency, but leakage of Seal B (stiff spring) was less or equal to that of Seal A at a given speed of rotation and a given compression. The penalty was that the higher cross section stiffness of Seal B created a high sealing force resulting in high frictional power loss and high operating temperature.

To limit temperature rise and seal wear good lubrication is important. Lubrication conditions were not ideal in the tested sealing system. Most of the oil was centrifuged away from the seal-counterface contact zone which resulted in inadequate cooling.

Wear of counterface in the sealing zone was moderate. Slightly polished wear tracks in the metal produced by the contact areas of the seal could be clearly seen together with rings of deposits.

The seal material appeared to be wear resistant and possess good ability to withstand high temperatures.

ACKNOWLEDGMENT
The study was financed by the National Technology Agency (Tekes), a public funding organization for research and development, and Finnish industry. The cooperation of Mr. Petri Keski-Honkola, Mr. Jussi Lehtiö and Mr. Antti Sinkkonen at the Laboratory of Machine Design is greatly appreciated.

REFERENCES

1 Müller, H.K. and Nau, B.S., www.fachwissen-dichtungstechnik.de, Kapitel 8 Wellendichtringe ohne Überdruck, p. 22, Accessed 2003-04-19.

2 Calonius, O. and Pietola, M., Explicit Finite Element Analysis of Spring-Energized Rotary Face Seal for Industrial Process Machinery. The 18th Abaqus Users' Conference, 18–20 May 2005, Stockholm, Sweden.

3 Buhl, S. and Haas, W., Reibung im Dichtspalt von Radialwellendichtringen. Berechnung der Fluidfilmdicke. O+P 4/2006, pp. 220-224.

4 Schnürle, F. and Upper, G., Influence of Hydrodynamics on the Performance of Radial Lip Seals. ASLE Transactions, Vol. 16, 4, 1973, pp. 310-315

5 Hirano, F. and Ishiwata, H., The Lubricating Condition of a Lip Seal. Proc Inst Mech Engrs, Vol. 180 Pt 3B, 1965-66, pp. 187-196.

Radiation Effects on Friction and Leakage Properties of Water Hydraulic Seals

Jyrki Tammisto[1], Jouni Mattila[1], Mike Irving[2], Mikko Siuko[2], Matti Vilenius[1]
Tampere University of Technology[1]
Institute of Hydraulics and Automation
P.O.Box 589
33101 Tampere, Finland

EFDA-CSU Garching[2]
Boltzmannstrasse 2
85748, Garching, Germany

ABSTRACT

Remote Handling (RH) is one of the most challenging aspects of the ITER project (International Thermo Experimental Reactor), and the European home team is building a major prototype of the divertor region (the Divertor Test Platform 2) to confirm practically the RH concepts proposed in this area. To handle the 10 Tonne divertor cassette, water hydraulics has been selected because it offers high forces and precise control in a compact envelope, with minimal long-term contamination should a leak develop. Water hydraulic components use mainly stainless steel – unaffected by gamma radiation – but the integral seals and O-rings are known to be sensitive. For radiation testing of these components, a modular approach was adopted, enabling up to 10 seal carriers assemblies to be irradiated simultaneously in the limited space available, with individual carriers being removed at varying total doses up to 10 MGy. Each carrier was then installed in a real hydraulic rig in which friction and leakage can be measured. Tests showed that irradiation has some effect on friction but leakage increases dramatically with doses over 2 MGy. Acceptable dose for tested seal seem to be between 0,5 and 1 MGy.

KEYWORDS: Water Hydraulics, Seals, Irradiation, ITER

1. INTRODUCTION

Remote Handling (RH) is one of the most challenging aspects of the ITER project, and the European home team is presently designing and constructing a major prototype of the divertor region (the Divertor Test Platform 2) to confirm practically the concepts

proposed for the RH systems in this area [1]. The CMM (Cassette Multifunctional Mover, fig. 1) must lift and transport the 10 Tonne divertor cassette around the vessel and down the narrow duct from the vessel to a sealed cask which will carry the cassette to the hotcell. Due to limited access, the cassette must be grappled in a cantilevered manner, and water hydraulics has been selected because the required high forces and precise control are available in a compact envelope, with minimal long-term contamination of the vessel or duct should a leak develop.

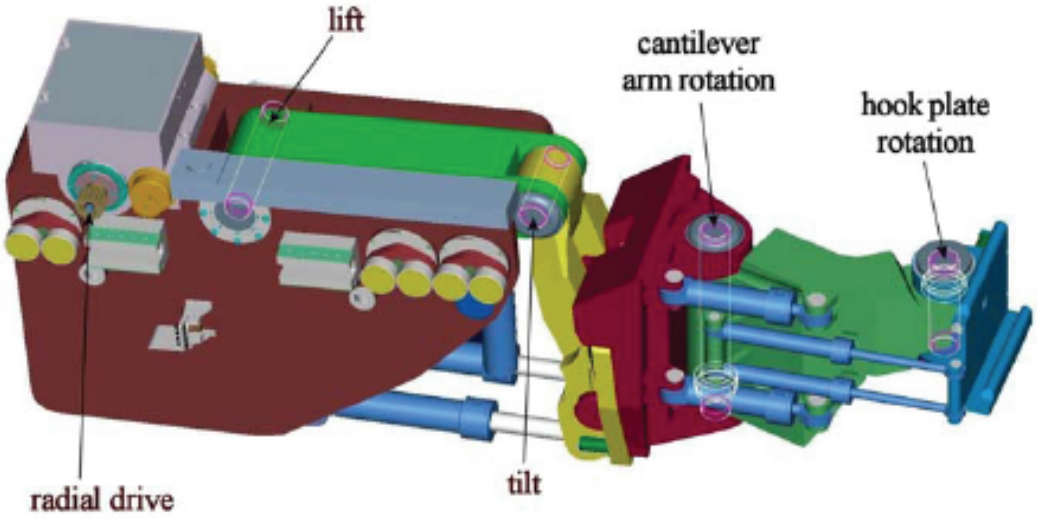

Figure 1. The Cassette Multifunctional Mover (CMM).

Although the main material used in water hydraulic components is stainless steel (and therefore unaffected by secondary gamma radiation), the materials used for seals and O-rings inside these components are known to be sensitive to radiation. ITER has a complementary program to assess levels of radiation in key areas of the vessel at various points in the maintenance schedule, and an earlier study of radiation levels and total doses for typical usage of the CMM over the lifetime of ITER [2] indicates that for 4 shutdowns the total exposure would be of the order of 1.2 MGy. However, the timings upon which these figures are based are very provisional, and for this equipment a total dose of up to 5 MGy is a more realistic target, although some maintenance will certainly be carried out between RH shutdowns.

2. TEST SYSTEM

Testing of the seals was carried out in a purpose-built hydraulic rig (fig.2) developed by the Institute of Hydraulics and Automation at the University of Tampere. This comprises two connected cylinders: one into which the seal carrier was installed, and the other a general purpose oil cylinder acting as a controllable test load. Each cylinder is powered by its own pump, and a PC with a MatLab/dSpace interface controls and monitors the flows and pressures, force and displacement of the rig.

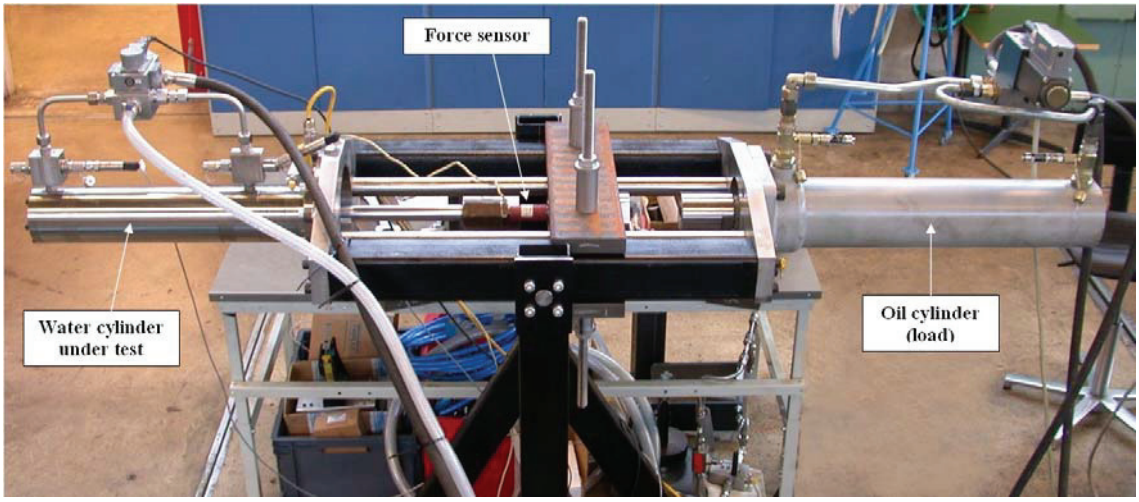

Figure 2. The hydraulic test rig showing key components.

Following previous experience, testing of the cylinder focused on measuring friction and leakage. Friction was calculated by driving the water cylinder with different open-loop steps to achieve a constant velocity, whilst maintaining a preset, constant load with the oil cylinder. When the velocity was constant, the friction is calculated from the chamber pressures and force sensor readings. Although this will inevitably include both piston and piston-rod seals, the latter (being the same throughout) should not differ significantly between the tests, and it is the difference in these values which is of most interest. Leakage is measured by closing the chamber of the water cylinder with a ball valve, providing a constant force with the oil cylinder, and measuring the displacement over a period of time.

2.1. Tested seal

The tested seals are Busak + Shamban's Turcon® Glyd Ring® T Z80 (fig. 3). The seal consists of a profile ring (Seal ring in fig. 3) and an O-ring as the compression element. The profile ring material is Ultra-High Molecular Weight Polyethylene (UHMW-PE) and the O-ring is Acrylonitrile Butadiene Rubber (NBR).

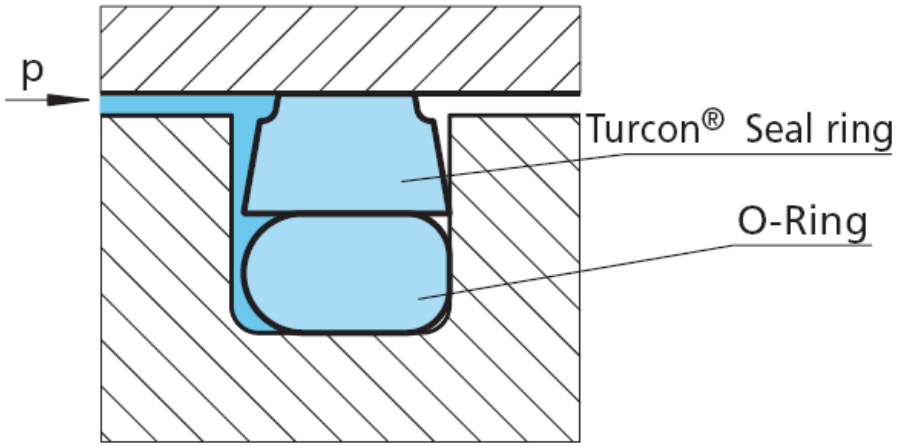

Figure 3. Cross section of Busak + Shamban's Turcon® Glyd Ring® T [3].

3. DESIGN OF THE HYDRAULICS COMPONENTS

Hydraulic seal components are normally fitted to the piston by warming the component and carefully stretching it over the piston crown into the groove below where, with cooling, it returns to its original size and state. However, irradiation gradually hardens the material which does not then soften when heated, leading to damage or even breakage during fitting to the piston. This means that irradiation is best carried out on a complete piston with the seal already fitted, but this is very wasteful of irradiation space and with campaigns typically lasting up to a month, an alternative method was sought. Previous irradiation testing had already used a 'split' piston concept to allow seals, even those made from hard material, to be fitted and removed without damage. This still required the whole piston to be irradiated, and did not simulate the actual cylinder conditions well because without a cylinder wall, the seal components were left uncompressed. A new concept was needed to simulate better the mechanical conditions of the real cylinder, whilst enabling more efficient use of the irradiation chamber space.

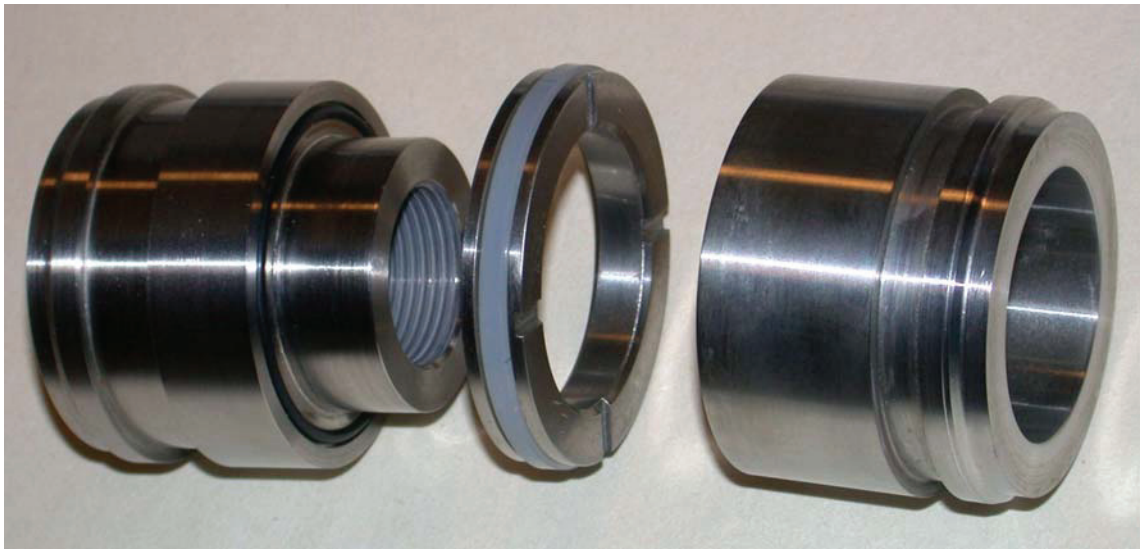

Figure 4. Seal carrier in the middle of two part piston.

Since irradiation was planned to take place in the Nayade facility operated by the CIEMAT in Madrid, the latest concept uses a special designed assembly which fits inside the 60mm diameter x 100mm long irradiation chamber available. This uses another modified piston, but this time only the part which houses the seal is irradiated. This seal 'carrier' (fig. 4) is annular and only 4mm longer than the seal itself, enabling up to 10 carriers to be irradiated simultaneously.

Each carrier is fitted inside a hollow ring of the same internal diameter as the cylinder (fig. 5), and during irradiation, the complete assembly is immersed in deionised water simulating closely the actual conditions of a stationary actuator. Space is also available inside the hollow tube assembly for other material samples for independent mechanical testing and inspection.

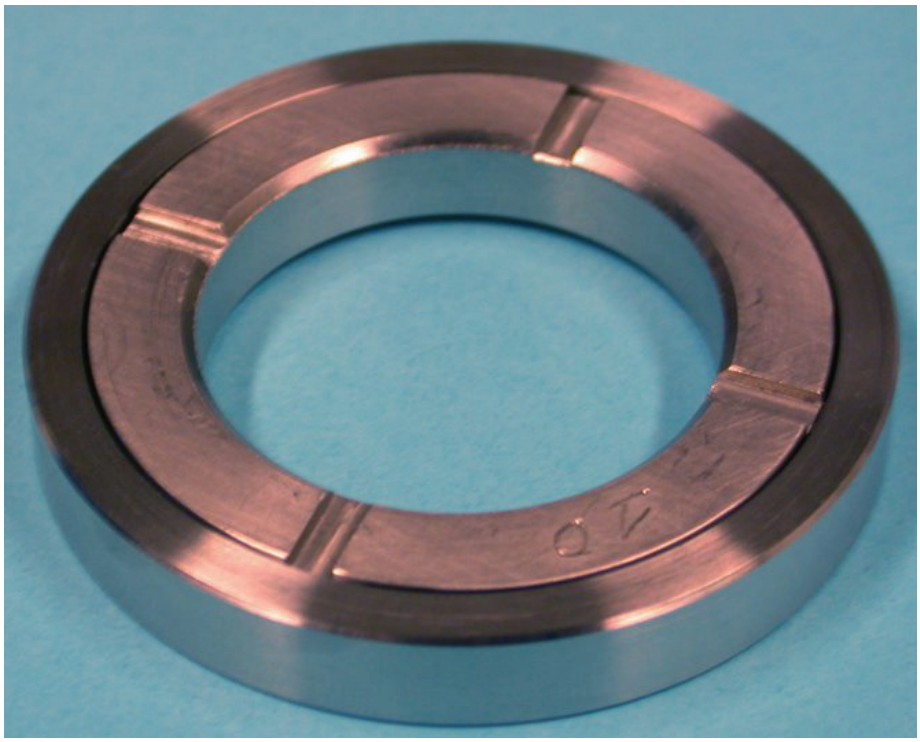

Figure 5. A seal carrier complete with outside ring.

The seal components were all integrated into the carriers and outer rings using special tooling to reduce the seal expansion trauma to a minimum. The seals were in the seal carriers and outer rings during irradiation, with the outer ring removed just before the seal was assembled into the test cylinder.

4. IRRADIATION OF THE SEAL CARRIERS

The seals, with the outer rings fitted, were mounted onto the carrier assembly and sent to CIEMAT's Nayade facility in Madrid. Here the assembly was placed in the chamber, together with other material samples and the container filled with deionised water.

Irradiation to a total dose of 10 MGy was carried out from the 6th to the 31st March 2006 at a dose rate of 5.94Gy/second, with individual samples being removed at total doses of 0.1, 0.2, 0.5, and 1 MGy, and pairs of samples at 2, 5 and 10 MGy. As the seal carriers were removed, they were stored in another vessel containing deionised water.

5. TEST RESULTS

The seals were tested before and after irradiation. Tests before irradiation were made to ensure that the seals are correctly assembled in the seal ring and give also the deviation of the seals in friction and leakage. Also two non-irradiated reference seals were tested: one before, and one after the irradiated seals.

5.1. Preliminary tests before irradiation

Friction tests before irradiation were done with 120 bar supply pressure and 0 kN load force (fig 6).

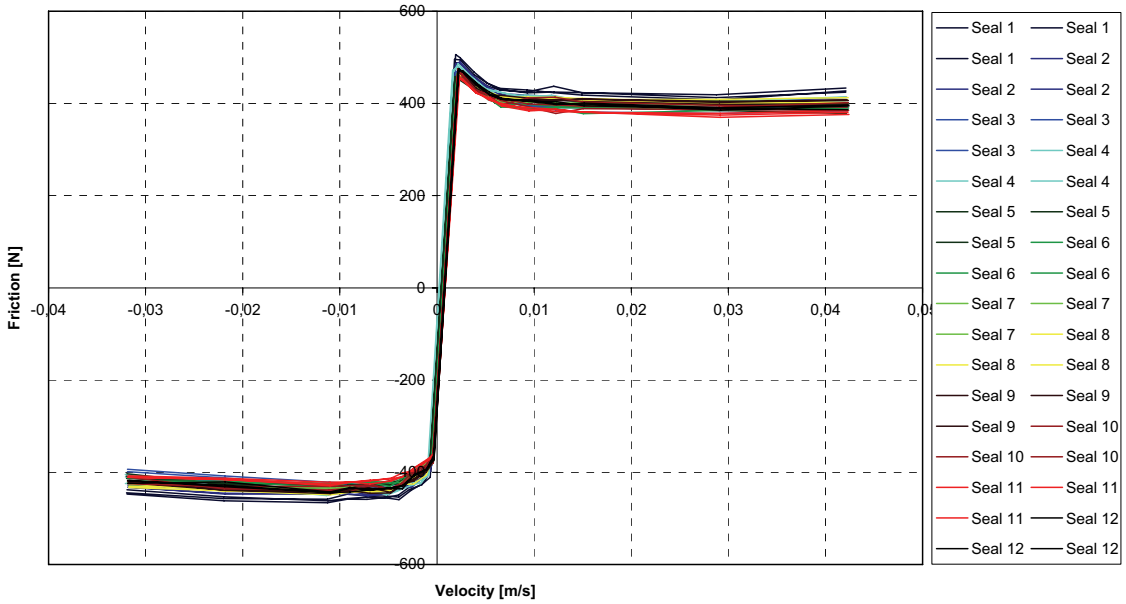

Figure 6. Friction before irradiation.

It can be seen that the variation in friction is small; less than ± 30 N. Low variation means that the seals are very similar when they are new, and indicates that repeatability of the test system is good.

The leakage test before irradiation was carried out with one pressure difference, at a load force of 2 kN i.e. the pressure difference was about 9 bar. In this test it cannot be distinguished whether leakage takes place between the profile ring and cylinder wall, or between the O-ring and piston groove. Leakage before irradiation is low (fig. 7).

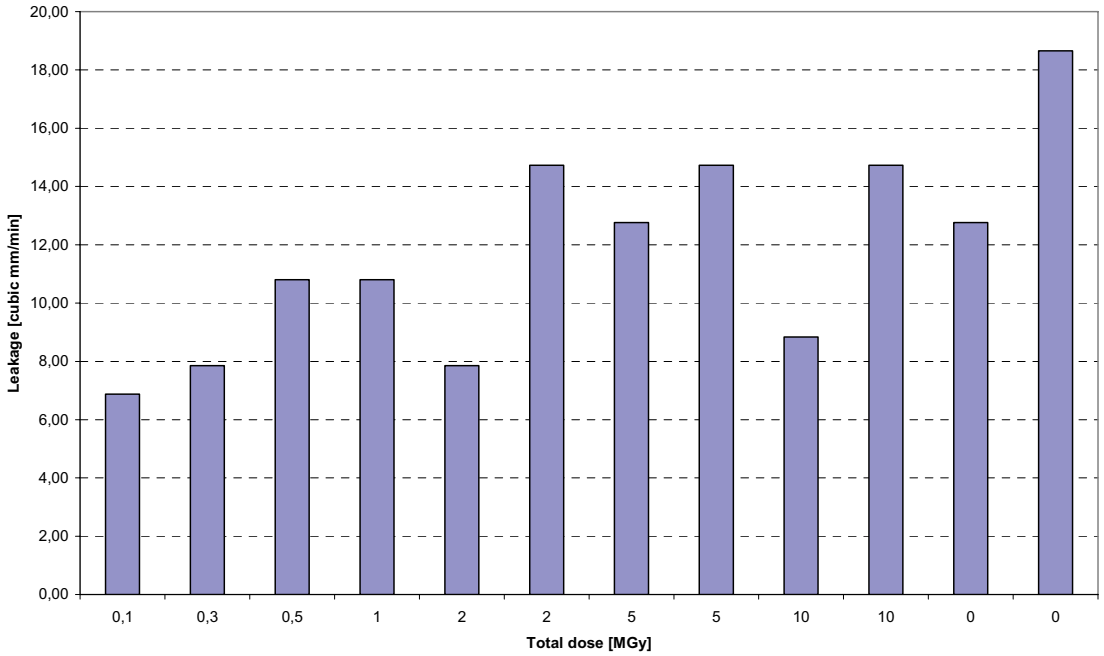

Figure 7. Leakage before irradiation.

It can be seen that leakage varies between 7 and 19 mm^3/min. The leakage was measured twice with seal 1, giving results of 2,95 and 6,9 mm^3/min. This shows that there are some uncertainties which cause variation in the leakage. The piston seal has an axial gap in the seal groove, and when the ball valve is closed and the load is increased, the seal will be pushed by the pressure to the piston rod side of the groove. The seal will probably settle differently depending upon whether it moves or not (or how much it moves) when the pressure rises. Also pressure was little different because the seal settled differently in different cases. The piston side chamber pressure at the beginning of the leakage test was between 8,2 and 9,8 bar, and although variation in leakage was quite large, the level of the leakage was very low.

5.2. Tests after irradiation

Friction tests were done with two different supply pressures (120 and 200 bar), with loads of 0, ±2 and ±5 kN. The friction curves of all seals with 0 kN load and 120 bar supply pressure are presented in fig 8.

Here it can be seen that the friction of seal 1 (0,1 MGy) is slightly lower than seal 12 (ref 1), friction with seals 1 and 2 (0,3 MGy) and seal 12 are similar to those in the preliminary tests, (fig. 6). Friction with seals 3 (0,5 MGy) and 11 (ref 2) is a little higher than the above seals. The difference in friction between two reference seals indicates that friction of the cylinder has changed, probably due to the particles and scratches found in the cylinder after the tests (see below). With higher doses the seal friction continues to increase gradually, although this remains at a moderate level.

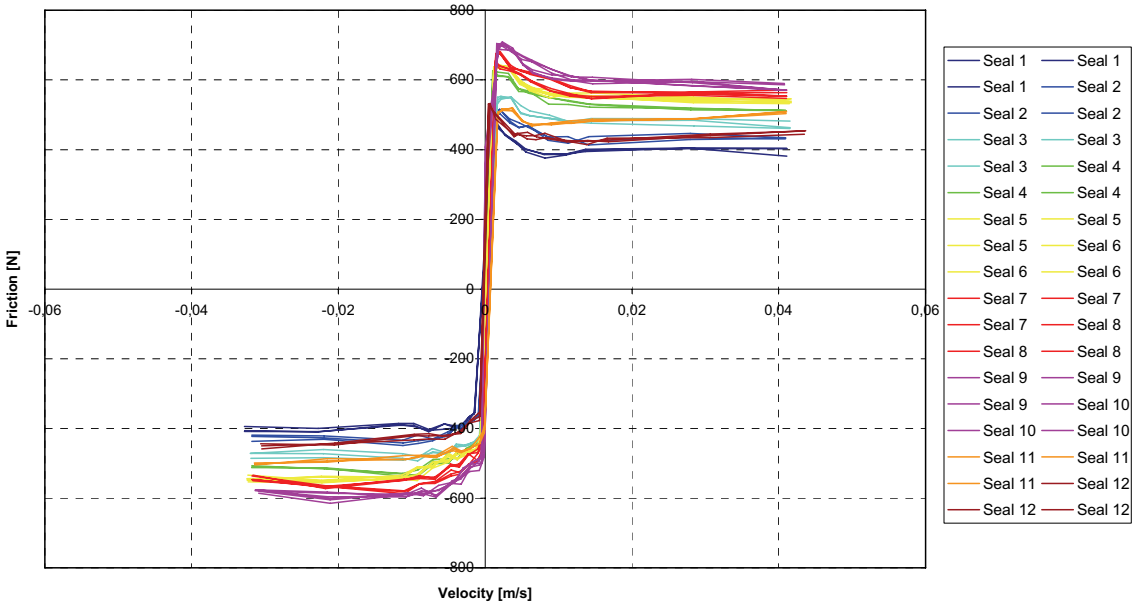

Figure 8. Friction after irradiation.

Leakage tests after irradiation were made with three different pressure differences: 9, 48 and 107 bar (fig 9). Leakage with the irradiated seals changes considerably with different doses and pressure differences.

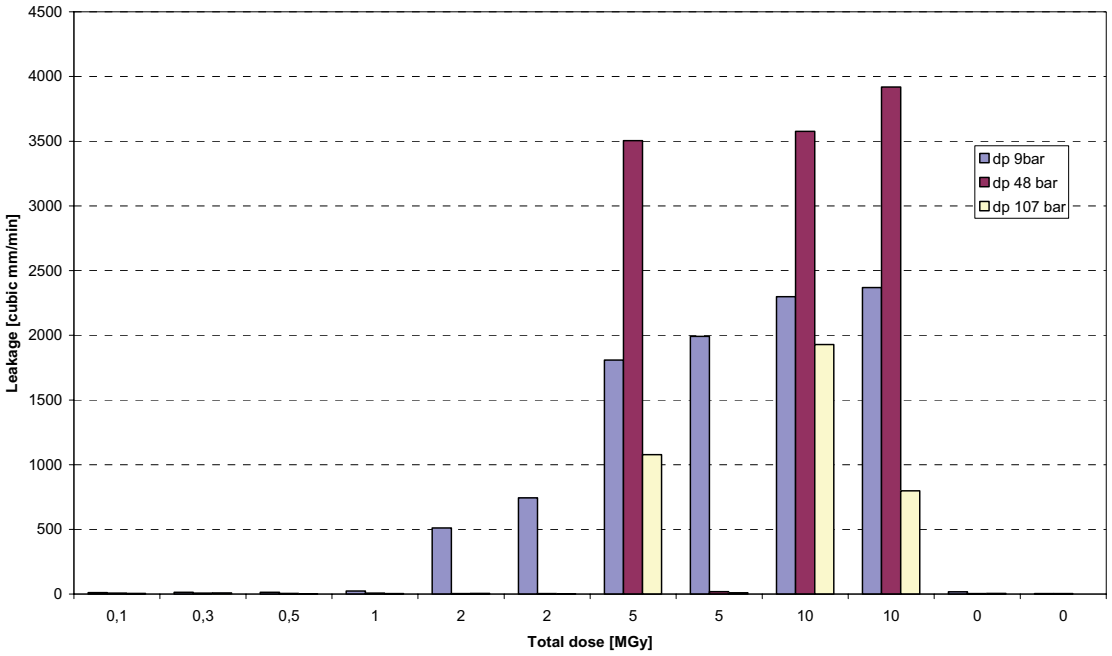

Figure 9. Leakage past the seal with increasing total dose.

Leakage tests showed that leakage starts to increase with the smallest pressure difference when the dose is over 1 MGy, and with 1 MGy dose the leakage is still very small. When the dose is 2 MGy the leakage is much higher with the smallest pressure difference but the leakage decreases to the level of non-irradiated seals when the pressure difference was increased. The reason for this is probably that the hardened profile ring material (UHMW-PE) was still elastic enough to seal the cylinder with the higher pressure difference. It could also be that the O-ring loses its elasticity and therefore there is not enough preload to push the profile ring against the cylinder bore when the pressure is low, whilst with a bigger pressure difference, the pressure pushes the profile ring hard against the cylinder bore. The first 5 MGy seal leaked considerably at all pressure differences but the other 5 MGy seal leaked much less with higher pressure differences. At 10 MGy, both seals leaked considerably regardless of pressure difference. Leakage tests shows also that with high dose, leakage can vary considerably. As an illustration, the cylinder moves about 0,1 mm in 20 minutes when the seal is in good shape, whereas with the worst seal, the cylinder moves about 40 mm in 20 minutes.

Fig.10, showing the seal carrier assembly with all the samples mounted, clearly shows the typical effect of radiation on materials of this type – the higher exposures inducing a brownish discolouring on the original pure white colour. It can also be seen that seals are more scratched as the doses rises.

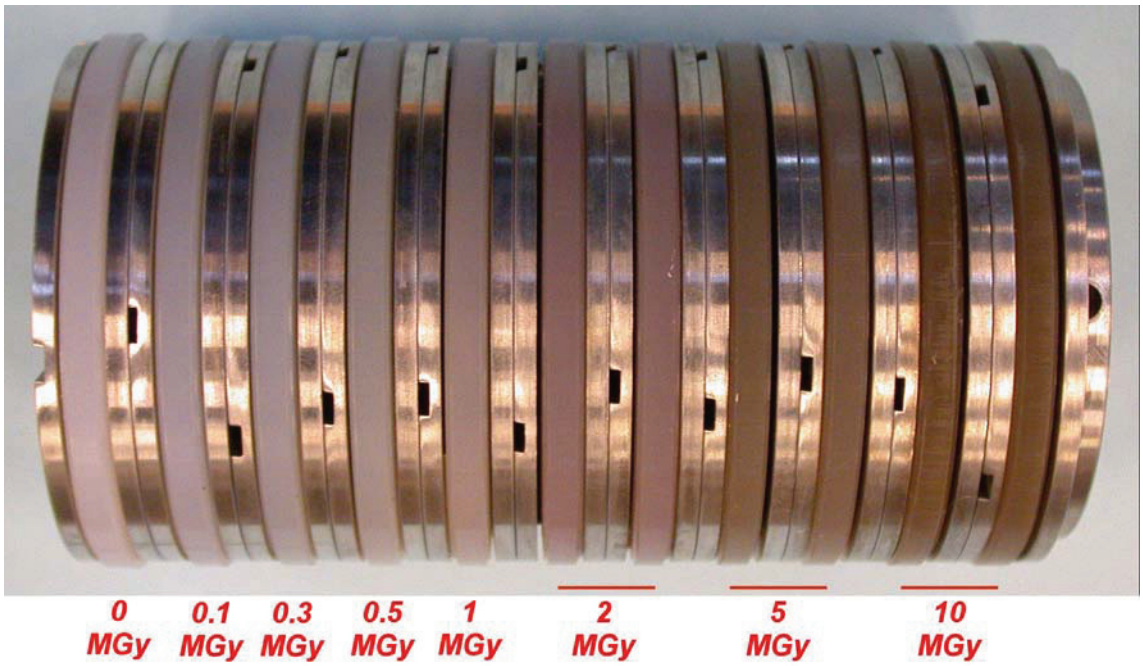

Figure 10. Seals after tests.

After the tests, the seals, glide ring (fig. 11) and cylinder were found to be scratched, and some black impurities were found in the cylinder. The effect of those scratches on the friction is quite small as can be seen in the differences between reference seal 1 (tested at the beginning) and 2 (tested at the end, when the particles were present). Those impurities are probably caused by outside contamination and if so, the parts selected can be considered acceptable. Any way the cause of the particles needs to be clarified later.

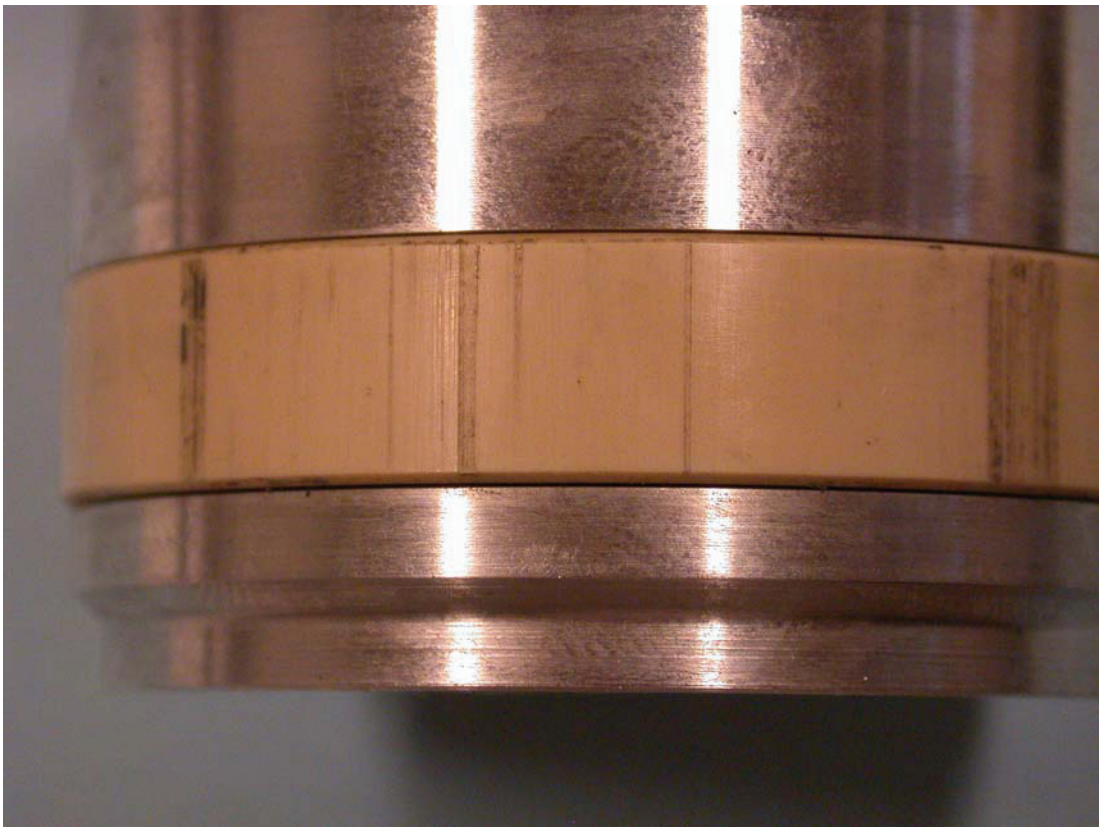

Figure 11. The glide ring showing deep scratches.

6. CONCLUSION

The test concept where the seals are assembled on seal carrier assemblies during irradiation proved to give more reliable results than earlier tests, since this arrangement is close to the situation where a stationary cylinder is irradiated as a whole. This concept also enables a number of samples to be irradiated at the same time in the limited space of irradiation chamber.

The tests showed that leakage, whilst remaining very low up to 1MGy, is a more dominant factor than friction above this value. In this test only the piston seals were irradiated but in the real application, the whole cylinder will be irradiated. Leakage past the piston rod seal means that water will pass out of the cylinder into the environment, and therefore leakage of the piston rod seal is more harmful than leakage of the piston seal itself. It might therefore be useful to construct a leakage channel between the cylinder primary and secondary piston rod seals to tank: this would minimize leakage to the environment and, if the volumes of liquid were measured, could also be used in condition monitoring.

In the friction tests it was found that friction changes little when dose is under 0,3 MGy, and with 0,5 MGy the rise of friction is also quite small. With dose ≥1 MGy the friction continues to rise. In the real application, the piston rod seal is also irradiated and therefore the increase in friction is larger. Assuming that half of the total friction is caused by the piston seal; the increase of friction is about 15-25 % (with different loads and supply pressures) at 0,5 MGy, and about 35-45 % at 1 MGy dose. It would be useful to study the effects of increased friction on the CMM application with a simulation model.

As a result of the leakage and friction tests it can be concluded that acceptable dose with tested seals is 0,5 to 1 MGy. Reason for particles and scratches found in cylinder need anyway be clarified.

ACKNOWLEDGMENT

This work, supported by the European Communities under the contract of Association between EURATOM / TEKES, was carried out within the framework of the European Fusion Development Agreement. The views and opinions expressed herein do not necessarily reflect those of the European Commission.

REFERENCES

[1] J.Palmer, M.Irving, J.Järvenpää, H.Mäkinen, H.Saarinen, M.Siuko, A.Timperi, S.Verho, “The Design and Development of Divertor Remote Handling Equipment for ITER”, Proceedings of the 24th Symposium on Fusion Technology (SOFT)'06, Warsaw, Poland.

[2] M.Pitkääho, M.Siuko, A.Raneda, A.Kopperoinen “Cassette Multifunctional Mover – CMM Design Requirements Document, TW3-TVR-MOVER-D1-IHA-CMM-Requirements-Document”, Appendix 2, Report by IHA to EFDA 5th January 2004.

[3] Busak + Shamban “Hydraulic seals – linear; piston seal” brochure.

LAYOUT PROGRAM IN THE SEALING TECHNOLOGY

Dieter von Borstel
Dr. Guido J. Wüstenhagen
Merkel Freudenberg Fluidtechnic GmbH
Industriestr. 64
D-21107 Hamburg, Germany
Phone +49 (0)40-75306-487, Fax +49 (0)40-75306-6487
E-mail: guido.wuestenhagen@freudenberg.de

ABSTRACT

Sealing elements have become a very important part of our technical world. Nearly all industrial areas these days have the requirement to separate or seal machinery components from the various media available in the market. With so many varied applications existing, with such a large range of requirements, the number of different seal designs and sizes available is vast.

In our global industry, there is a requirement for the constant functionality of seal designs, in all of the different housing types that exist. As a seal manufacturer, Merkel Freudenberg Fluidtechnic delivers seal with geometries that have been generated using a layout program. Through this, Merkel Freudenberg Fluidtechnic has the possibility during the laying out of different seal sizes, from the smallest to the largest diameters and profiles, in metric and inch sizes, to meet the high quality expectations of our customers, as well as enabling us to be able to layouts nearly every seal variation in the quickest possible time.

As an example, here are the procedures carries out when generating a WDR-Radiamatic seal.

KEYWORDS: Layout program, sealing technology, radial shaft seal, Radiamatic

1 ADVANTAGE OF LAYOUT PROGRAMS

In a wide range of applications customers requires seals. These applications are characterized by operation demands such as pressure, temperature, motion-speed, fluid etc.. Based on these values an application engineer could recommend a type of seal. Additionally, the applications demand various diameters and profiles in the housing. If

at this time no article is available on this base, an application engineer needs to define the details of the technical drawing. By using a layout program, new articles according to this technical drawing will suit the following aspects:

- fulfilling functional operating demands
- reduced risk though design errors
- following production demands
- in a short time frame

In view of these advantages several layout programs were designed for various types of seals as shown in figure 1.

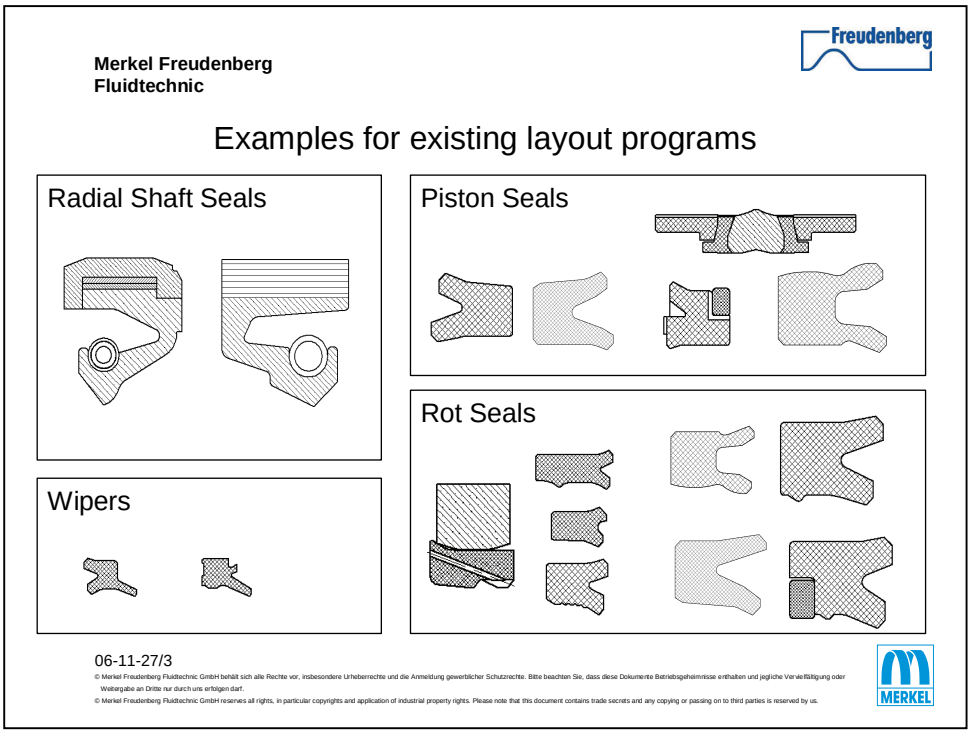

Figure 1: Examples for existing layout programs

2 PROCESS OF PROGRAM DESIGN

A suitable way to create a layout program is shown in the following: Concentrating on one type of seal, the state of the art should be considered. In any case - new design or redesign - three inputs should be accessible: experiences from field application, experiences from test runs in-house or at research institutes and technical designs of precursors. Together with these experiences, the application engineers and the production engineers can integrate with further demands in a new design or redesign. Figure 2 shows examples.

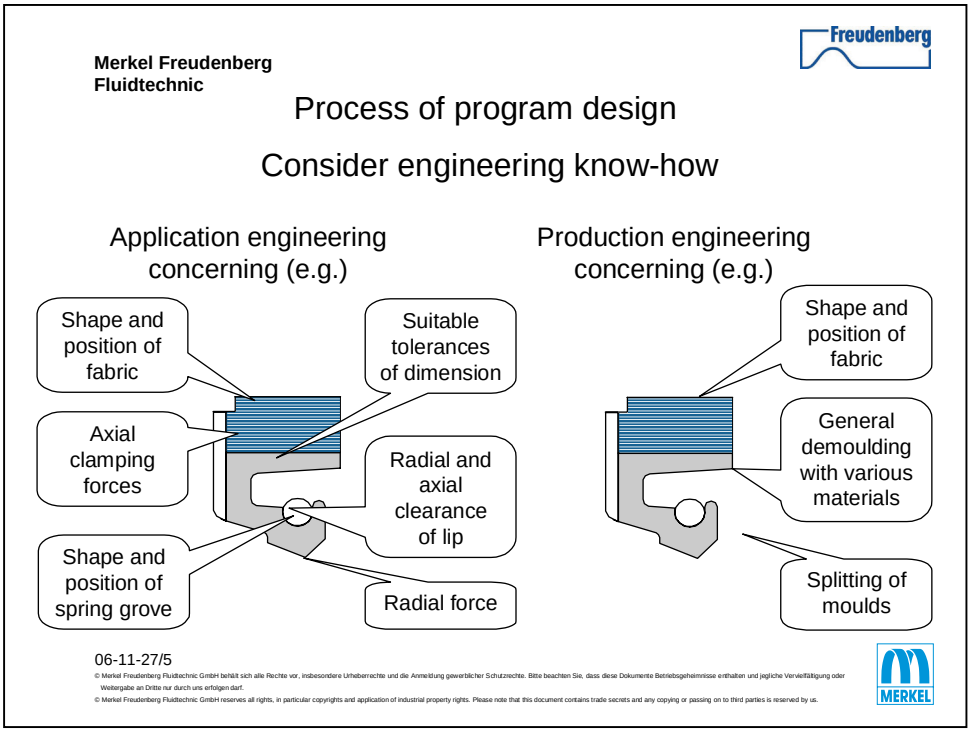

Figure 2: Examples for additional demands to a new design or redesign

On this base the crucial metrics can be defined. Crucial metrics ensure the function of the seal under the given operating conditions by a reliable production process. Figure 3 shows a few examples.

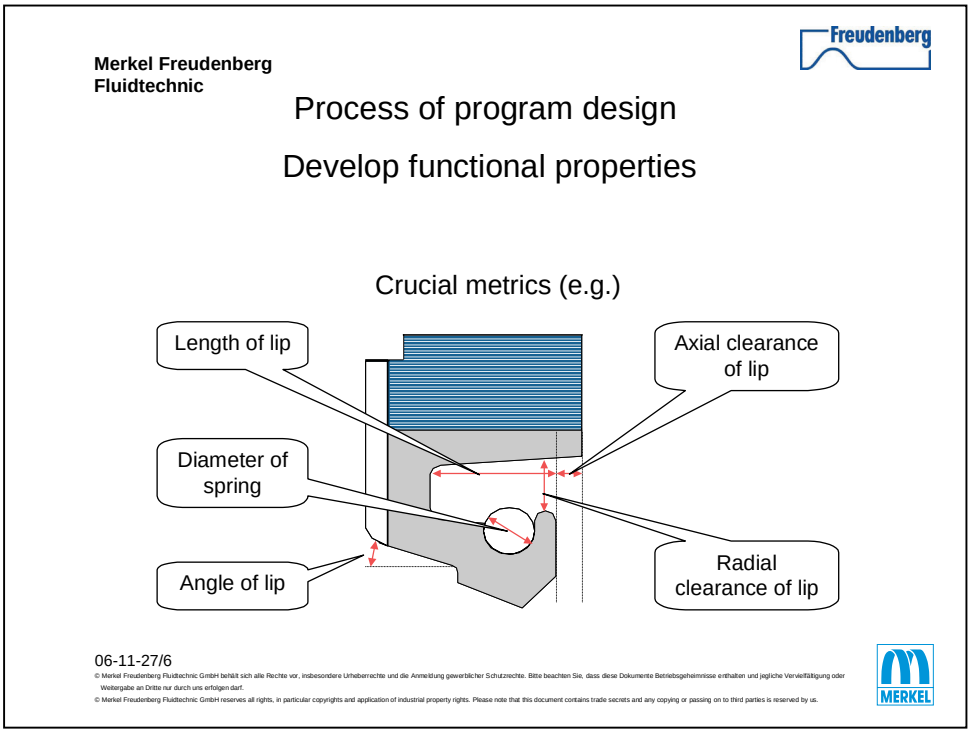

Figure 3: Examples for crucial metrics of a radial shaft seal design

Some aspects concerning the clearance of the sealing lip: In any possible application the sealing lip needs to be free in its movement. Due to the movement the sealing lip should never touch the housing nor the inner diameter of the clamping block of the seal. Therefore, it has to be ensured that at any tolerance of the seal or the housing and at any misalignment of the shaft, contact is avoided.

Figure 4 shows how to define the expected profile range of the layout program. A layout program will not cover all possibilities but still a wide range. Just as the diameter, the profile length and height need to be limited by a minimum and a maximum value. The limitation is influenced by the demands of the application and the technical and production possibilities of the seal. In any way, it might be necessary in single cases to leave the layout program and to design a single article by using e.g. finite-element-analysis.

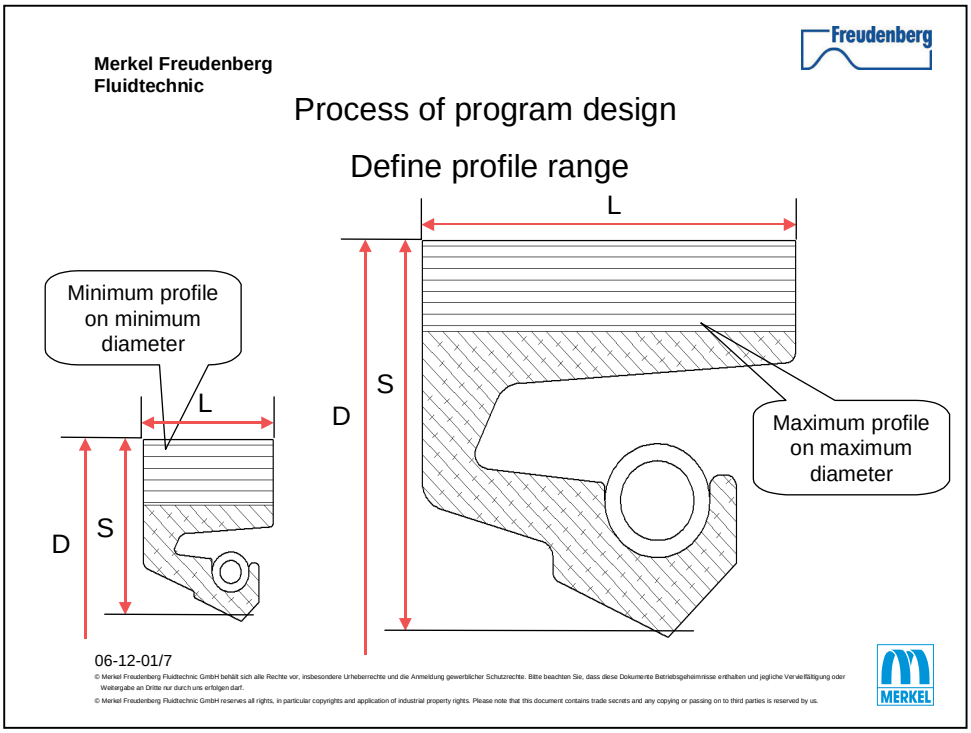

Figure 4: Defining the profile range of the layout program

Finite-element-analysis is already used in the process of designing the layout program. Figure 5 shows an example of several calculations. In the course of the calculation process, various profiles are investigated under various operating conditions. The pure profile is compared to a profile with a mounted spring. The profile is calculated by different misalignments of the shaft. This calculation is superposed by various pressures. In a number of recycles the crucial measures could be defined to fulfill the functional demands, e.g. the pressure distribution in the contact area. Now the crucial measures could be linked in their dependence of the profile range metrics: Diameter, profile length and height - figure 6.

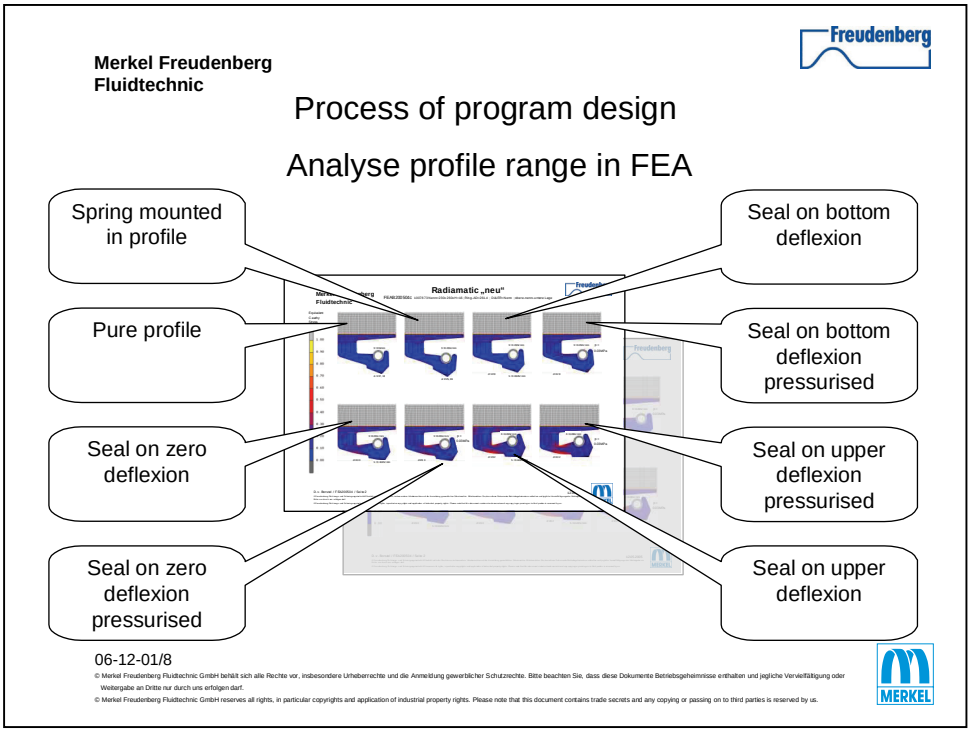

Figure 5: Example for analyzing the profile range by FEA

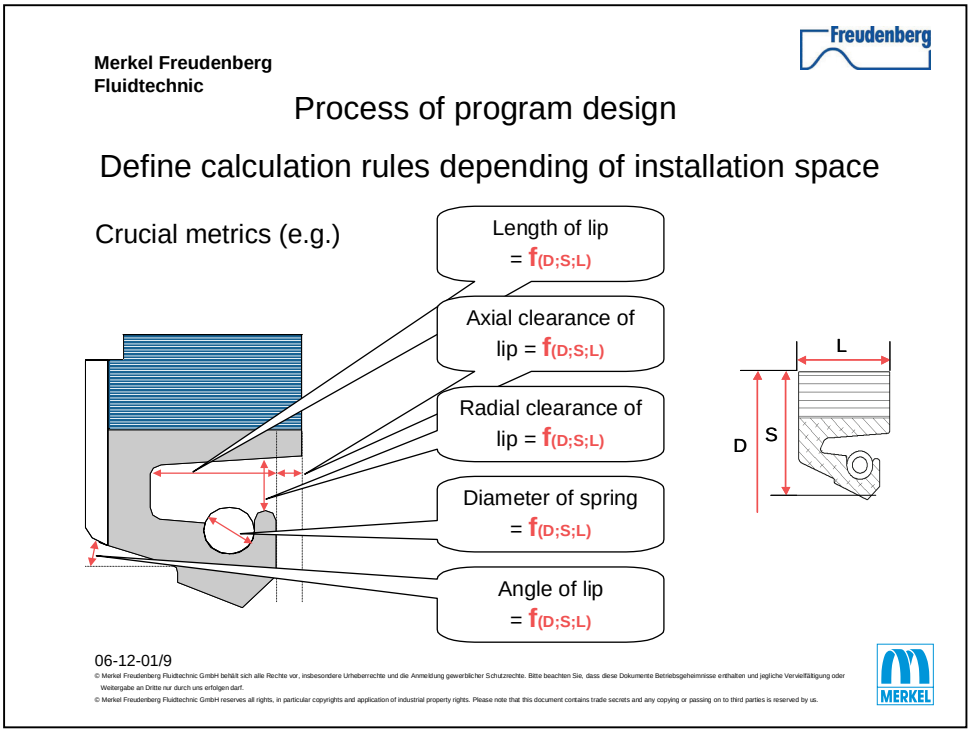

Figure 6: Defining the calculation rules depending upon the installation space

This dependency - the calculation rules - between crucial measures and profile range needs to be optimized. Another number of recycles in the finite-element-analysis is required and gave the base for the writing of the program it self (figures7).

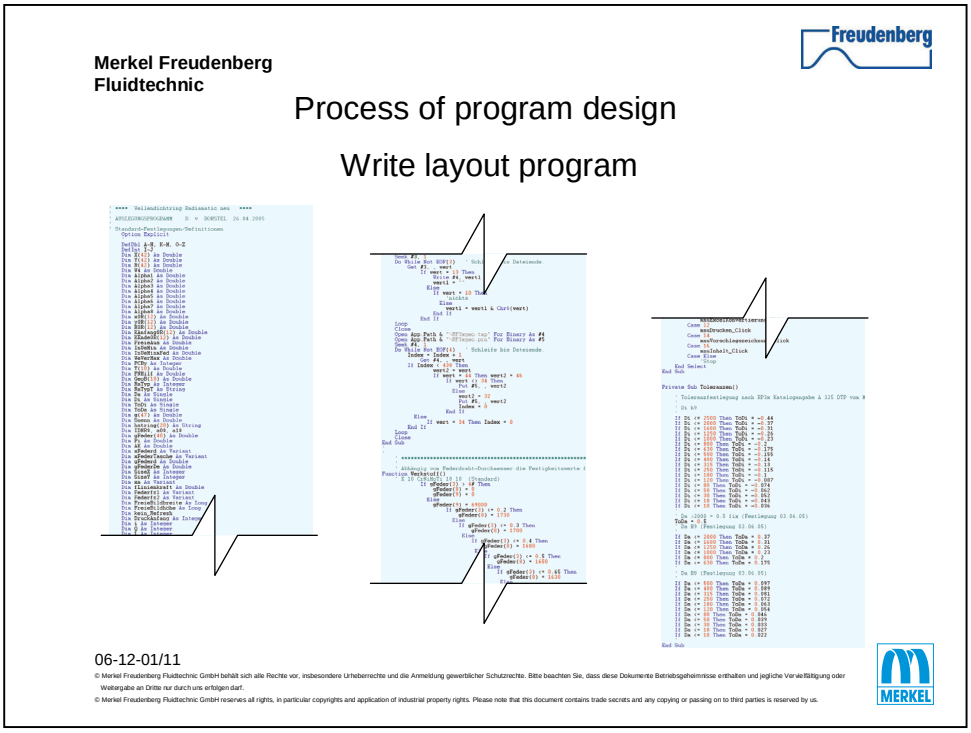

Figure 7: Writing the layout program

Finally the layout program has to be released. Therefore, a few specific seals are designed by using the program and are tested with the help of the finite-element-analysis and on test rigs - figure 8.

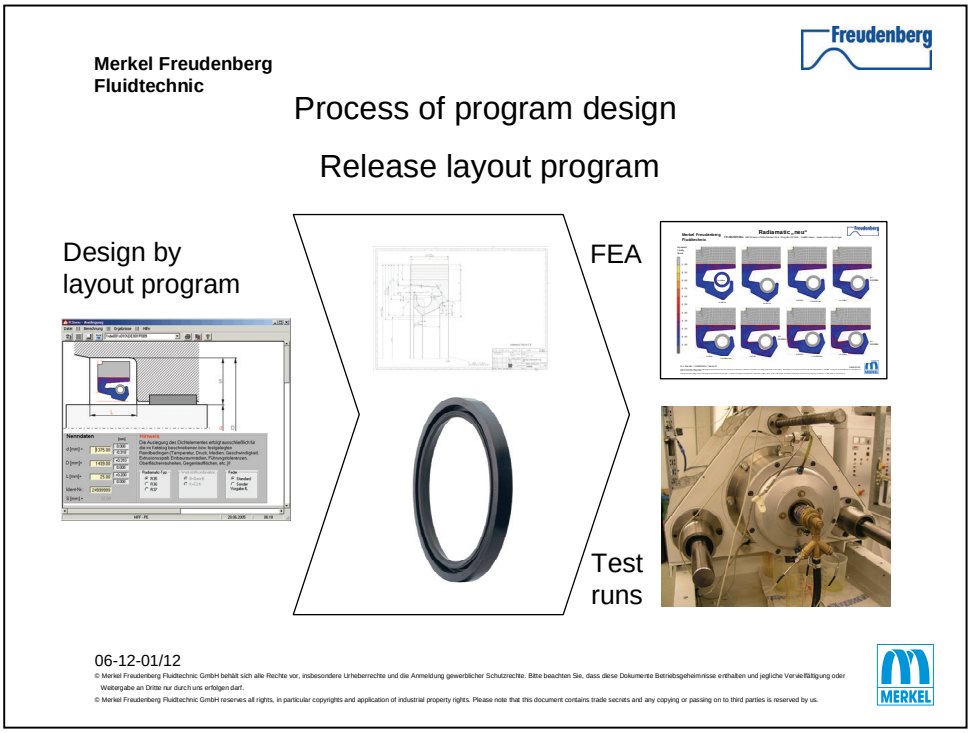

Figure 8: Release of the layout program

3 USING THE PROGRAM

The following steps describe the use of the program. Depending upon the demands of the application, the application engineers have to chose a suitable type of seal. The profile then has to be defined according to the demands of the installation space. Figure 9 shows how to enter the data into the layout program.

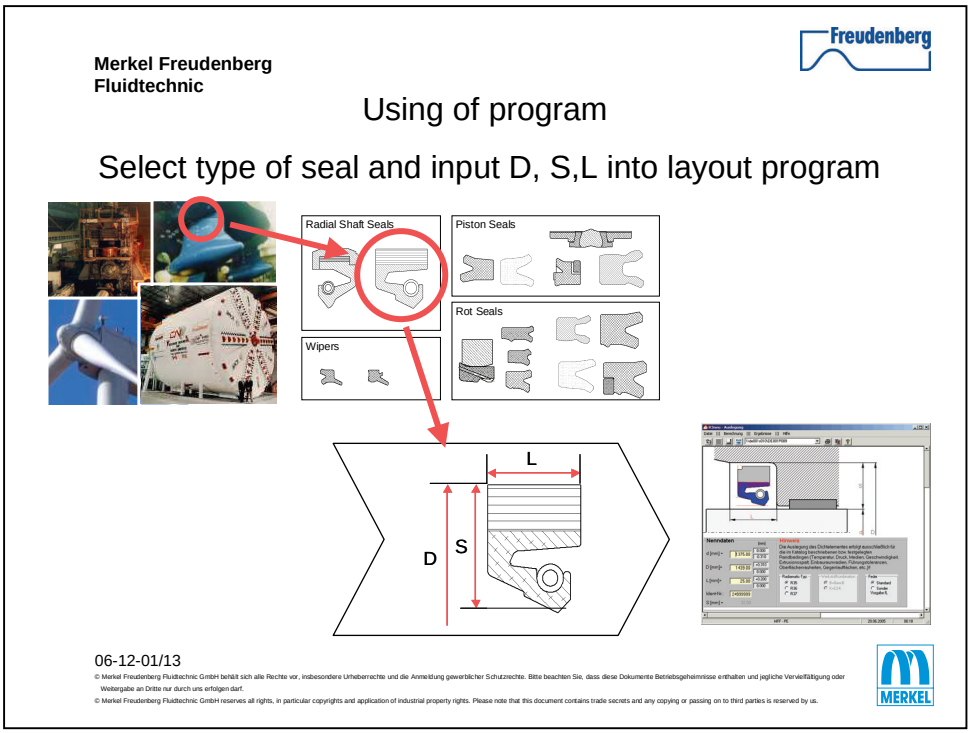

Figure 9: Select type of seal and enter D, S, L into the layout program

If the acceptable range of the layout program has been exceeded, a warning will occur and inform about the available range (figure 10). This warning will lead to a detailed design of the demanded seal. As already mentioned before, the finite-element-analysis of this specific seal could support the design.

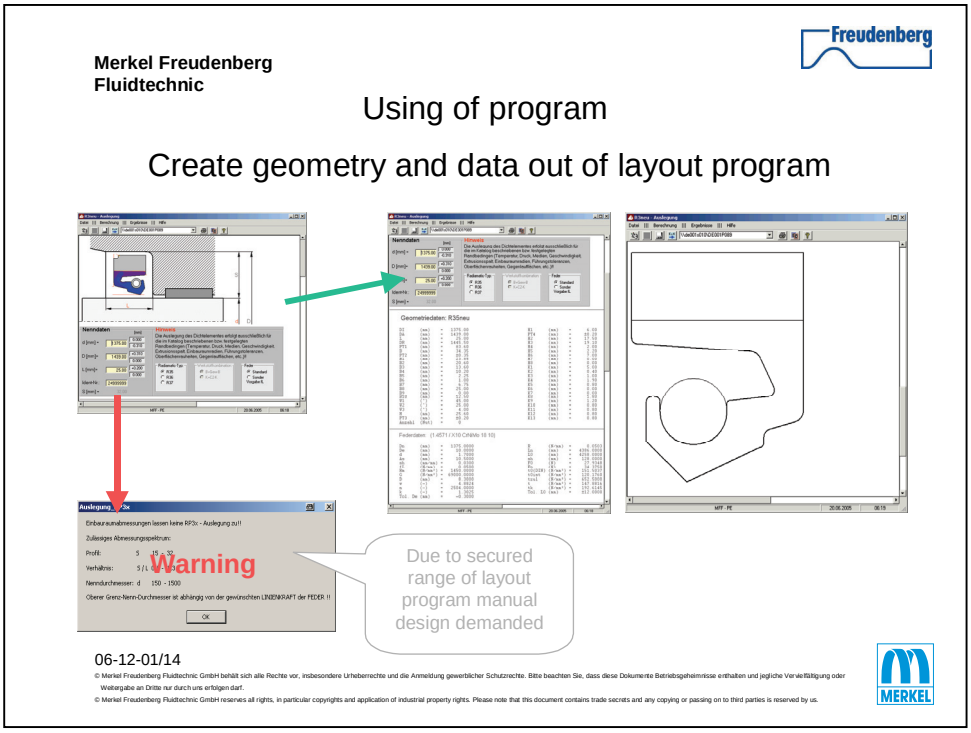

Figure 10: Create geometry and data out of layout program

Usually, the layout program will deliver a shape of the profile to check on the proportions and a set of data for further use. The set of data consists of the crucial metrics and will be imported into a parametric drawing. A macro in the CAD-program creates a technical drawing of the specific seal (figure 11).

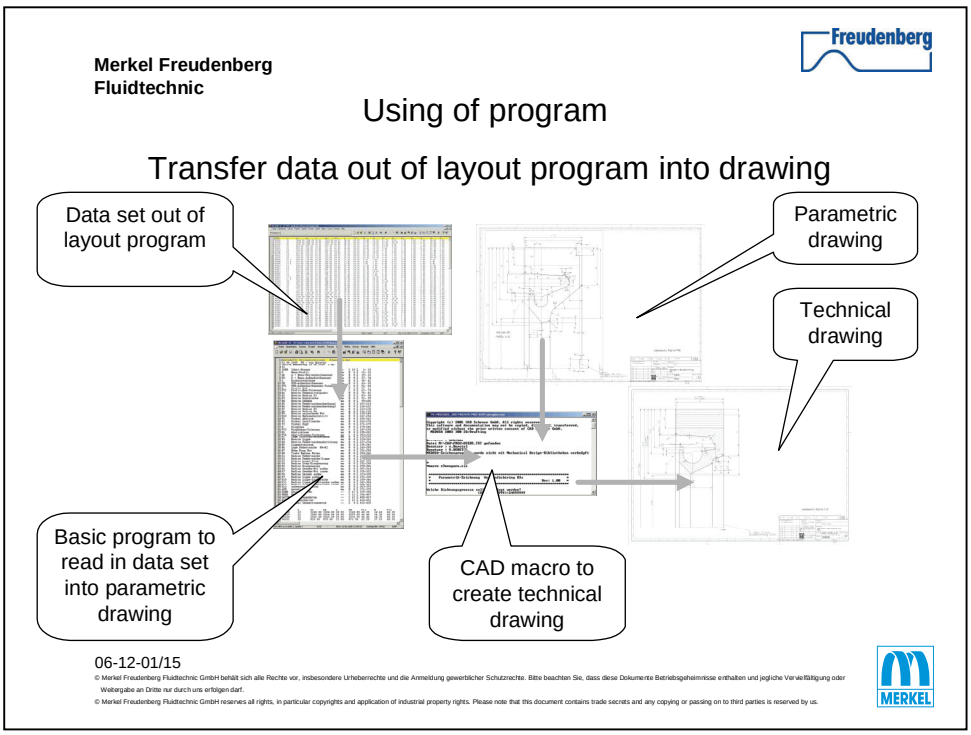

Figure 11: Transfer data out of layout program into drawing

4 CONCLUSION

To design a layout program all kinds of experiences need to be involved: from field application, test runs, technical design of precursor and also from the in-house application engineers and production engineers. By using the finite-element-analysis, final calculation rules for the crucial metrics can be defined and implemented into the layout program. The outcome is a tool which - within a short time frame - helps to design a specific seal that fulfills various operating conditions and dimensions. It reduces the risk of design errors and ensures a reliable production process.

Electropneumatic test bench for aeronautics application : Robust control

Alexis Girin[1], Xavier Brun[2] and Franck Plestan[1]
[1]Insitut de Recherche en Communication et Cybernetique de Nantes, France
[2]LAI, INSA Lyon, Villeurbanne, France
alexis.girin@irccyn.ec-nantes.fr
Xavier.Brun@insa-lyon.fr

Abstract

This paper presents design, modelization and control of an electropneumatic test bench. The test bench was writing for aeronautic application. The model of system is extremely nonlinear, so a nonlinear control based on sliding mode theory is synthesis and compare with scheduling feedback. Interest of higher order sliding mode controller is the finite time convergence and its robustness with respect to uncertainties and parameters variations.

Keywords

Higher order sliding mode, electropneumatic system, robustness, finite time convergence, non linear control.

Introduction

Control of pneumatic actuators is a challenging problem, viewed their increasing popularity (law maintenance cost, lightweight and good force/weight ratio), in spite of their traditional drawbacks (friction, variation of the actuators dynamics due to large change of load and piston position along the cylinder stroke, nonlinearities, ...). The development of high-performance closed-loop linear/nonlinear controllers [1], [2], [3], [4] has shown the feasability of high-level positioning of pneumatic actuator. The knowledge on pneumatic actuator is limited at classical actuator where dynamics are limited. For a flying machine, a new electropneumatic system is design. The aim of this new design is to reproduce the aerodynamics forces. In order to duplicate this force, four springs are coupled on a carriage moved with pneumatic actuator controlled by servodistributor. In this work two aspects of study are presented. In first two models of pneumatic system are presented, simulation model implemented in AMESim software and model used for control synthesis. In second part high order sliding mode control law synthesize and is compare to classical scheduling gain feedback over experimental results.

Nomenclature

y, v, a	position, velocity and acceleration of the actuator $[m][m/s][m/s^2]$
y_d, v_d, a_d, j_d	desired position, velocity, acceleration and jerk $[m][m/s][m/s^2][m/s^3]$
p_X	pressure in the chamber X $[Pa]$
u_P, u_N	servodistributors voltages $[V]$
k	polytropic constant
K_r	springs rates $[N/m]$
V_X	chamber X volume $[m^3]$
b_v	viscous friction coefficient $[N/m/s]$
F_f	friction force $[N]$
M	total moving load mass $[kg]$
T_X	chamber X temperature $[K]$
r	perfect gaz constant $[J/kg/K]$
S	piston area $[m^2]$
q_m	mass flow rate provided from the servo--distributor $[kg/s]$
X	P or N
γ	adiabatic constant
T_r	temperature inside an upstream tank $[K]$
Q	thermal exchange $[J]$
λ	thermal exchange coefficient by conduction $[J/K/m^2/s]$
S_{cX}	total area inside X chamber $[m^2]$
T_{cX}	temperature of the X chamber wall $[K]$
$q_{mX_{in}}/q_{mX_{out}}$	mass flow rate brought inside/outside of a chamber $[kg/s]$
t_F	fixed time convergence $[s]$

1 Electropneumatic System

1.1 Description

The electropneumatic system under interest is a double acting actuator controlled by two servodistributors (see Figure 1) and composed by two chambers denoted P and N. Piston diameter is 63 mm and rod diameter 16 mm. With a source pressure equal to 7 bar, the maximum force developed by the actuator is 1750 N. The air mass flow rates q_m entering in the chambers are modulated by two three-way servodistributors Servotronic (Asco-Joucomatic) controlled by a micro-controller. The pneumatic jack horizontally moves a load carriage of mass M. This carriage is coupled to 4 springs (which restrain the displacement of the carriage and restore the initial position in the middle of the total stroke equal to 50 mm - see Figure 1) for a total of 63000 N/m rate. Additional dry friction is controlled by two skates, with a maximum value equal to 40 N. In case where the maximal displacement of carriage is 16 mm, the maximal spring force is 1008 N. The electropneumatic plant model is obtained from three physical laws: the mass flow rate through a restriction, the pressure behaviour in a chamber with variable volume and the fundamental mechanical

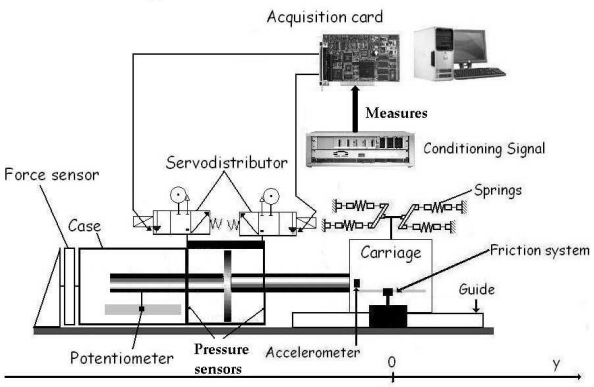

Figure 1: Electropneumatic system

equation. The experimental set-up is simulated with a fluid power systems dedicated software AMESim, and the control law is developped under Matlab/Simulink trade of mathworks, which implies a cosimulation program [5]. In the sequel, two models are displayed

- the first one, which takes into account physical phenomena as temperature variations, experimentals values of mass flow rate delivred by each servodistributors, dynamics of servodistributors, dry friction..., is developed under Amesim.
- The second one, which is simpler than the previous, is used in order to design the nonlinear controller under Simulink.

1.2 Simulation model

In standard version, pneumatic actuator has pneumatic damper for protect the piston. This damper is composed by a restriction which limit the exhaust mass flow rate. In order to obtain maximum performance, this restriction has been deleted. In first the control law is test on cosimulation in order to validate control law algorithm. **Servodistributor model.** The servodistributor model is composed in two parts, a dynamic part and a static one :

- Dynamic part is modelized by a second order transfer function identified from experimental measure of slide displacement.

$$F(s) = \frac{\omega_{ns}^2}{s^2 + 2 \cdot \zeta_s \cdot \omega_{ns} s + \omega_{ns}^2} \quad (1)$$

  with $\omega_{ns} = 246\ rad \cdot s^{-1}$ and $\zeta_s = 0.707$.

- Static part is modelized by an experimental table where mass flow rate is given in function of ratio pressure (upstream/downstream) and control voltage [6].

Pneumatic chamber variable volume model. Each chamber of the pneumatic

actuator is considered as a variable volume, in which the air mass evolves with time. State the classical following assumptions [7]:

A1. Air is a perfect gas ands its kinetic is inconsequential.

A2. The pressure and the temperature are homogeneous in each chamber.

A3. The mass flow is pseudo-stationary.

The first dynamic principle applied to the air mass and the thermodynamic evolution of air in each chamber read as (with $X = P$ or N) [7]

$$\begin{aligned}
\frac{\mathrm{d}p_X}{\mathrm{d}t} &= -\gamma\frac{p_X}{V_X}\frac{\mathrm{d}V_X}{\mathrm{d}t} + \frac{\gamma r T_r}{V_X}q_{mX_{in}} - \frac{\gamma r T_X}{V_X}q_{mX_{out}} \\
&\quad + \frac{(\gamma-1)}{V_X}\frac{\delta Q_X}{\mathrm{d}t} \\
\frac{\mathrm{d}T_X}{\mathrm{d}t} &= -(\gamma-1)\frac{T_X}{V_X}\frac{\mathrm{d}V_X}{\mathrm{d}t} + \frac{rT_X}{p_X V_X}(\gamma T_r - T_X)q_{mX_{in}} \\
&\quad - \frac{rT_X^2}{p_X V_X}(\gamma-1)q_{mX_{out}} + (\gamma-1)\frac{T_X}{p_X V_X}\frac{\delta Q_X}{\mathrm{d}t}
\end{aligned} \tag{2}$$

with γ the adiabatic constant, T_r the temperature inside the upstream tank, $q_{mX_{in}}$ the mass flow rate brought inside the X chamber, and $q_{mX_{out}}$ the mass flow rate brought outside the X chamber. Q_X, the thermal exchange with the X chamber wall, is described by assumption A4.

A4. The thermal exchange is due only by conduction described by

$$\frac{\delta Q_X}{\mathrm{d}t} = \lambda S_{cX}\left(T_{cX} - T_X\right) \tag{3}$$

with λ the thermal exchange coefficient by conduction, S_{cX} the total area inside a X chamber, and T_{cX} the temperature of the X chamber wall.

Mechanical model. The second Newton law gives

$$\begin{aligned}
\frac{\mathrm{d}v}{\mathrm{d}t} &= \frac{1}{M}\left[S\left(p_P - p_N\right) - F_f - b_v v - K_r y\right] \\
\frac{\mathrm{d}y}{\mathrm{d}t} &= v
\end{aligned} \tag{4}$$

With friction force F_f included stiction, Coulomb and Stribeck phenomena.
Samplers and saturation. Samplers are added in AMESim's model in order to take into account samplers of acquisition card; sample time is 1 ms which is very smallest than the natural frequency of this electropneumatic system. So it is not necessary to discretize the model all the control law are synthesize in continuous time. Saturation signal control are added, *i.e.* $|u_{sat}| = 10\ V$.

1.3 Control model

This model is developed in order to design the control law and a simplest version of the simulation one. The following hypotheses are added

A5. The process is polytropic and characterized by coefficient k (with $1 < k < \gamma$).

A6. The leakage between system and atmosphere are neglected

A7. Furthermore, the temperature variations in each chamber are inconsequential with respect to the supply temperature, *i.e.* $T_P = T_N = T$.

Then, pressures dynamics read as

$$\frac{\mathrm{d}p_X}{\mathrm{d}t} = -k\frac{p_X}{V_X}\frac{\mathrm{d}V_X}{\mathrm{d}t} + \frac{krT}{V_X}\left(q_{mX_{in}} - q_{mX_{out}}\right) \tag{5}$$

A8. The leakage between the two chamber and between servodistribuor and jack are negligible.

A9. Supply and exhaust pressure are supposed constant.

By defining $q_m(u_X, p_X) := q_{mX_{in}} - q_{mX_{out}}$, one gets

$$\begin{aligned} \frac{\mathrm{d}p_P}{\mathrm{d}t} &= -k\frac{p_P}{V_P(y)}\frac{\mathrm{d}V_P(y)}{\mathrm{d}t} + \frac{krT}{V_P}q_m(u_P, p_P) \\ \frac{\mathrm{d}p_N}{\mathrm{d}t} &= -k\frac{p_N}{V_N(y)}\frac{\mathrm{d}V_N(y)}{\mathrm{d}t} + \frac{krT}{V_N}q_m(u_N, p_N) \end{aligned} \tag{6}$$

A10. All dry frictions forces are neglected. The friction force are identify on real system. The carriage without springs have a quasi linear friction force at 30 N. But with springs, the friction force is nonlinear and variate between 30 and 170 N. So the polynomial approximation permitt to obtain a dry friction model function of carriage position.

A11. There is no control signal saturation.

A12. Dynamic part of servodistributor is neglected. Using singular perturbation theory, the dynamic of servodistributor (63 H_z) can be neglected compare to the actuator dynamic (4 H_z).

A13. Static part of servodistributor is approximate by polynomial function of pressure and control value.

$$q_m(u_X, p_X) = \varphi\left(p_X\right) + \psi\left(p_X, \mathrm{sign}\left(u_X\right)\right) u_X$$

with φ and ψ defined as 5^{th}-order polynomials with respect to p_X [8] and issued from experimental measures.

A14. Only the position of the actuator is controlled, which means that the problem is a single input-single output (SISO). It implies that $u_P = -u_N = u$.

A15. Springs force is considered to be a perturbation.

Then, with $V_P(y) = V_0 + S \cdot y$ and $V_N(y) = V_0 - S \cdot y$ (V_0 being equal to the half of the cylinder volume), the model used for the design of controller is a nonlinear system reads as

$$\begin{aligned} \dot{p}_P &= \frac{krT}{V_P(y)}[\varphi(p_P) + \psi(p_P, \text{sign}(u))\, u - \frac{S}{rT} p_P v] \\ \dot{p}_N &= \frac{krT}{V_N(y)}[\varphi(p_N) - \psi(p_N, \text{sign}(-u))\, u + \frac{S}{rT} p_N v] \\ \dot{v} &= \frac{1}{M}[Sp_P - Sp_N - b_v v] \\ \dot{y} &= v \end{aligned} \tag{7}$$

Hypothesis use to obtain control model generate uncertainties. These uncertainties are taken into account, in the controller design, through two models

- The so-called "nominal" model (7),
- The so-called "real" model which takes into account the uncertainties on several parameters or functions (Temperature T, functions φ and ψ, mass M)

$$\begin{aligned} \dot{p}_P &= \frac{kr(T+\Delta T)}{V_P(y)}[\varphi + \Delta\varphi - \frac{S}{r(T+\Delta T)} p_P v] \\ &\quad + \frac{kr(T+\Delta T)}{V_P(y)}(\psi + \Delta\psi)u \\ \dot{p}_N &= \frac{kr(T+\Delta T)}{V_N(y)}[\varphi + \Delta\varphi - \frac{S}{r(T+\Delta T)} p_N v] \\ &\quad - \frac{kr(T+\Delta T)}{V_N(y)}(\psi + \Delta\psi)u \\ \dot{v} &= (M^{-1} + \Delta M^{-1})[Sp_P - Sp_N - b_v v] \\ \dot{y} &= v \end{aligned} \tag{8}$$

with $|\Delta T| < T_M$, $|\Delta\varphi| < \varphi_M$, $|\Delta\psi| < \psi_M$ and $|\Delta M| < M_M$ all bounded values.

1.4 Desired trajectory

One of advantage of integral sliding mode is to controlate all over time the maximum velocity and acceleration. The desired position trajectory, named $y_d(t)$, is displayed in Figure 2 and has been designed such that associated velocity and acceleration are continuous functions. The maximum velocity (resp. acceleration) is $0.8\ m \cdot s^{-1}$ (resp. $33\ m \cdot s^{-2}$). This displacement corresponds to 64% of the total stroke around the central position. The initial conditions are such that $[y(0)\ v(0)\ \dot{v}(0)]^T = [0.008\ 0\ 0]^T$.

1.5 Conclusion about models

The use of different models for experiment and for the control design implies that, if high accuracy is required, it is necessary to design robust control law with respect

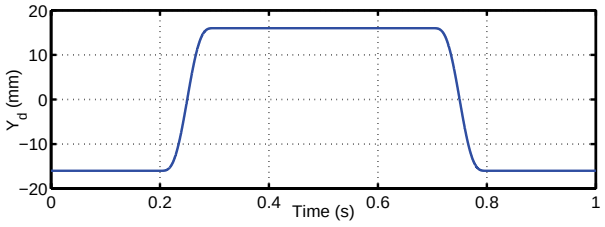

Figure 2: Desired position (mm) versus time (sec)

to uncertainties generated by the difference between these two models. Different nonlinear robust control approach have been implemented in electropneumatic field as [9, 10, 11, 12]. The aim of the following part is to present a new algorithm of nonlinear robust control.

2 Application of integral sliding mode controller

2.1 Controller design

On this paper the application of integral sliding mode controller is presented. The theory of integral sliding mode controller is developped to [13, 14] The objective consists in designing a robust (with respect to uncertainties/disturbances) position controller. Define s the sliding variable as $s = y - y_d(t)$: from (8), its relative degree with respect to u equals 3, which implies that a 3^{rd} order sliding mode controller is designed. The 3^{rd} order controller implies $s = \dot{s} = \ddot{s} = 0$ at $t > t_f$. The validity of the control law depends on the stability of the unobservable subsystem of dimension one, which is supposed. One has

$$s^{(3)} = \chi(\cdot) + \Gamma(\cdot)u \tag{9}$$

with $\bar{T} = T + \Delta T$, $\bar{\varphi} = \varphi + \Delta\varphi$, $\bar{\psi} = \psi + \Delta\psi$, $\bar{M}^{-1} = M^{-1} + \Delta M^{-1}$, and

$$\begin{aligned}
\chi(\cdot) &= kr\bar{T}S\bar{M}^{-1}\left(\frac{\bar{\varphi}(p_P)}{V_P(y)} - \frac{\bar{\varphi}(p_N)}{V_N(y)}\right) - kS^2v\bar{M}^{-1}\left(\frac{p_P}{V_P(y)} - \frac{p_N}{V_N(y)}\right) \\
&-b_v\bar{M}^{-2}\left(S\left(p_P - p_N\right) - b_v v - K_r y\right) - K_r v\bar{M}^{-1} - y_d^{(3)} \\
\Gamma(\cdot) &= kr\bar{T}S\bar{M}^{-1}\left(\frac{\bar{\psi}(p_P, sign(u))}{V_P(y)} + \frac{\bar{\psi}(p_N, sign(-u))}{V_N(y)}\right)
\end{aligned} \tag{10}$$

The control law is defined as $u = \Gamma_{Nom}^{-1} \cdot [-\chi_{Nom} + v]$ with Γ_{Nom} (resp. χ_{Nom}) the nominal value of Γ (resp. χ), *i.e.* derived from (10) with no uncertainties. It is important to note that Γ_{nom} is always strictly positive. So u has the same sign as $(-\chi_{nom} + v)$. By definition, χ_{nom} and v are independent of u. Consequently, the control law is not implicit. This explains the choice of the function φ, independent of u, in the mass flow rate expression of assumption A10. Then, one gets

$$s^{(3)} = \bar{\chi}(\cdot) + \bar{\Gamma}(\cdot)v \tag{11}$$

with $\bar{\chi} = \chi - \Gamma\Gamma_{Nom}^{-1}\chi_{Nom}$ and $\bar{\Gamma} = \Gamma\Gamma_{Nom}^{-1}$. Let $z = [s \;\; \dot{s} \;\; \ddot{s}]^T$. The 3^{rd} order sliding mode control is equivalent to the finite time stabilization of

$$\dot{z} = \underbrace{\begin{bmatrix} 0 & 1 & 0 \\ 0 & 0 & 1 \\ 0 & 0 & 0 \end{bmatrix}}_{A} z + \underbrace{\begin{bmatrix} 0 \\ 0 \\ 1 \end{bmatrix}}_{B} v + \begin{bmatrix} 0 \\ 0 \\ \beta(\cdot) \end{bmatrix} \tag{12}$$

where $\beta(\cdot)$ is defined as $\beta = \bar{\chi} + (\bar{\Gamma} - 1)\, v$. The integral sliding mode controller v reads as

$$v = v_0 + v_1.$$

The first part v_0 is a continuous one which ensures that s, $\dot{s}$, and $\ddot{s}$ converge to 0 at a fixed time t_F; the second one v_1 is a discontinuous one which ensures the previous convergence in spite of uncertainties. The design follows two steps.

Continuous part v_0. From [13]

$$v_0 \;\; = \;\; \begin{cases} -B^T M z(t) + B^T \delta(t) & \text{for } 0 \leq t \leq t_F \\ -B^T M z(t) & \text{for } t > t_F \end{cases} \tag{13}$$

with M and $\delta(t)$ defined by

$$\begin{array}{rcl} \dot{\delta} & = & -(A^T - MBB^T)\, \delta, \\ 0 & = & MA + A^T M - MBB^T M + Q. \end{array} \tag{14}$$

From (14), one gets $\delta(t) = e^{A_m t}\delta(0)$ with $A_m = -\left[A^T - MBB^T\right]$. Then, given $\delta(t)$, one gets $\dot{z} = -A_m^T z + BB^T e^{A_m t}\delta(0)$. Initial condition $\delta(0)$ of $\delta(t)$ is selected in order to satisfy the terminal condition $z(t_F) = 0$.

By multiplying both side of previous equation by $e^{A_m^T t}$, and integrating from $t = 0$ to $t = t_F$, with $z(t_F) = 0$, one gets

$$z(0) \;\; = \;\; -\left[\int_0^{t_F} e^{A_m^T t} BB^T e^{A_m t} \mathrm{d}t\right] \cdot \delta(0) := -H \cdot \delta(0)$$

Matrix H is the partial reachability gramian of linear system $\dot{x} = A_m x + Bv$ and is, viewed the form of A_m, B and $t_F < \infty$, invertible. Then, the initial condition $\delta(0)$ ensuring that $z(t_F) = 0$ can be derived from $\delta(0) = -H^{-1}z(0)$. The matrix H is evaluated using an algorithm from [15] which yields $\delta_1(0) = -3.6034e4$, $\delta_2(0) = -3.6034e3$ and $\delta_3(0) = -1.2002e2$ for $z(0) = [0.024\ 0\ 0]^T$ and a convergence time fixed to $t_F = 0.5\ sec.$ The control u_0 and $\dot{\delta}$ is given by (13) and (14).

Discontinuous part v_1. The switching variable σ reads as $\sigma = \ddot{s} + \zeta_3 + 2\xi\omega_n\left(\dot{s} + \zeta_2\right) + \omega_n^2\left(s + \zeta_1\right)$ with $\zeta_3(0) = -\ddot{s}(0)$, $\zeta_2(0) = -\dot{s}(0)$ and $\zeta_1(0) = -s(0)$, and $\dot{\zeta}_1 = \zeta_2$, $\dot{\zeta}_2 = \zeta_3$, $\dot{\zeta}_3 = v_0$. Then, one gets $v_1 = -\alpha \cdot \mathrm{sign}\,(\sigma)$ with $\xi = 0.7$, $\omega_n = 190\ rad \cdot s^{-1}$ and $\alpha = 10^5$ (in order to compensate the uncertainties due to the difference of experimental and control models, and the variations of mass (+125%)).

2.2 Experimental results

The control law is implemented on DS1005 Board. This card samples the control and measures to 1 ms. Two kind of experiment have been made. The first, named

"Nominal case", consist in considering that the moving mass is $0.8kg$ (*i.e.* the control law has been designed with this hypothesis). The second experiment consist in increasing the moving mass to $1.8kg$, *without changing the structure of the controller and its gains values*. In order to evaluate the performances of integral sliding mode controller, a classical gain scheduling state feedback control, defined as

$$u = K_y(y - y_d) - K_v v - K_a a \tag{15}$$

has been designed by using a linear model around actuator position y [16], and by computing gains K_y, K_v and K_a by Ackerman's approach such that poles placement authorized 4.6% overshoot [17]. The gains are calculated in order to have the maximum of bandwidth compare to actuator position.

Note that for all control law synthesis here, the springs force is unknow. The force $K_{springs}$ is considered as a perturbation.

Nominal case. The actuator position (Figure 3) converges to the desired trajectory in $0.2s$ (which is the stated convergence time t_F) for ISM[1] controller withoutcontrol saturation. With CF controller, the convergence is ensured in $0.15s$, with a theorical control equal to $-30\ V$. The maximum error position in steady state is $0.26mm$ for ISM controller and $0.37mm$ for CF controller. During all trajectory tracking with ISM controller, the velocity and the acceleration is controlled and control input is realistic (Figure 4). For CF, during convergence time, the velocity and acceleration are not controlled, the convegence time is smaller but the control input is more than $10\ V$. After convergence time t_f, the two control input have the same saturation during transitory phase. The design of trajectory permit to control the maximum of velocity and acceleration. Note that, in steady state, the force developped by the actuator, $F = S \cdot (p_P - p_N)$, allows to compensate springs force, as shown in Figure 4-Bottom.

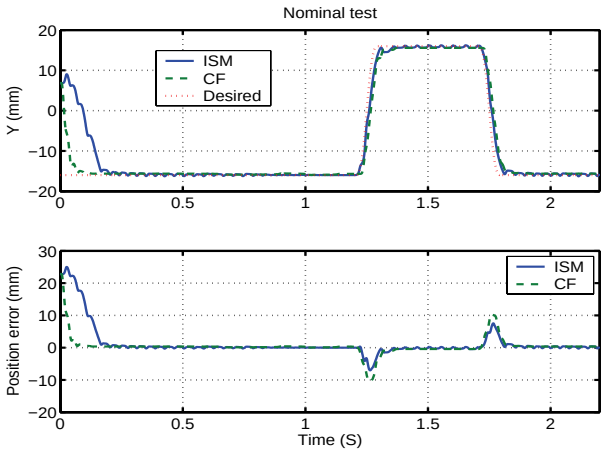

Figure 3: **Top.** Desired and current positions (mm) versus time (sec). **Bottom.** Positions errors (mm) versus time (sec).

Robustness evaluation. The ISM controller still ensures convergence in $0.2s$ without saturation (Figure 5 and 6). With CF controller, saturation is always 200%.

[1]In the sequel, "ISM" denotes Integral Sliding Mode controller, and "CF" denote Classical State Feedback controller

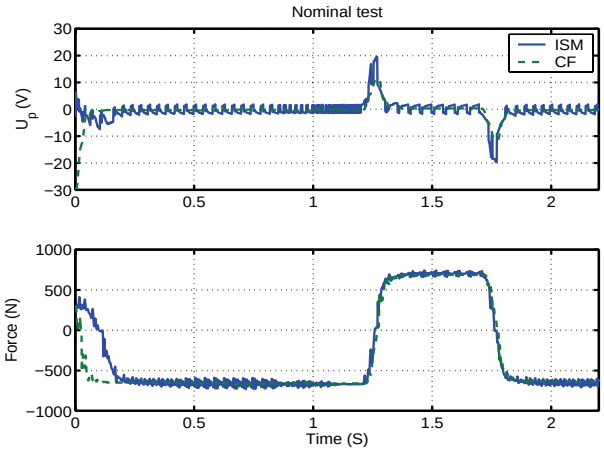

Figure 4: **Top.** Control (U_P) (V) versus time (sec). **Bottom.** Force (N) versus time (sec).

The maximum position error in steady state equals $0.3mm$ for ISM controller and $0.37mm$ for CF controller. This robustness evaluation with respect to mass modification confirms the best efficiency of ISM controller versus CF one in position control.

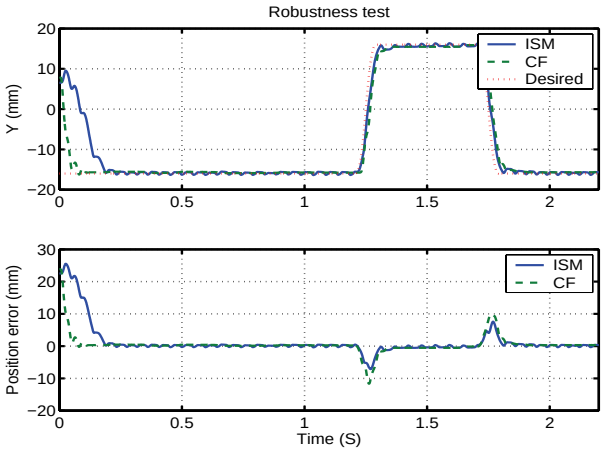

Figure 5: **Top.** Desired and current positions (mm) versus time (sec). **Bottom.** Positions errors (mm) versus time (sec).

3 Conclusions

This paper has proposed the application of a higher order sliding mode controller based on integral sliding mode [18, 19, 13] to the position control of a pneumatic actuator. Design and experimentation have shown the efficiency and applicability of the control approach to the pneumatic area. The further works concern the design of 4^{th} order sliding mode controller in order to improve the trajectories tracking accuracy.

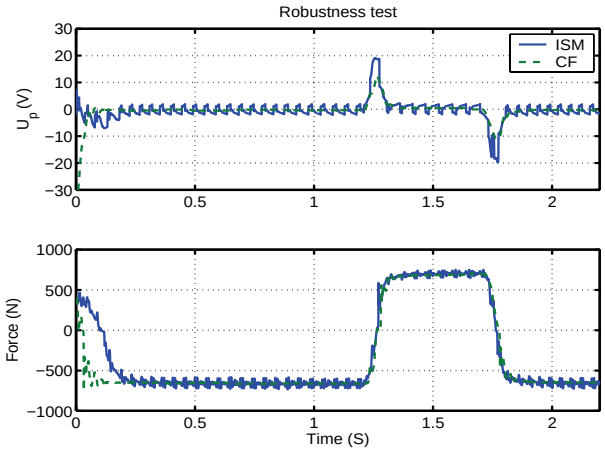

Figure 6: **Top.** Control (U_P) (V) versus time (sec). **Bottom.** Force (N) versus time (sec).

Acknowledgements

This work is supported by Direction Générale de l'Armement (DGA-French Defense Ministry) through the Alexis GIRIN's Ph.D. grant.

References

[1] S. Laghrouche, M. Smaoui, and F. Plestan, "Third-order sliding mode controller for electropneumatic actuators", *IEEE Conference on Decision and Control CDC'04*, Paradise Island, The Bahamas, 2004.

[2] M.Smaoui, X.Brun, D. Thomasset, "A combined first and second order sliding mode approach for position and pressure control of an electropneumatic system", *American Control Conference ACC'05*, Portland, Oregon, 2005.

[3] A. Levant, "Universal SISO sliding-mode controllers with finite-time convergence", *IEEE Trans. Automat. Control*, vol. 49, no.9, 2001, pp.1447-1451.

[4] EDGE, K.A., "'The control of fluid power systems - responding to the challenge"'. *Journal of Systems and Control Engineering*, 1997, Vol 211, N12, p 91-110.

[5] X. Brun, D. Morand, S. Scavarda, D. Thomasset, "Contributions of the cosimulation in the chain of design of an electropneumatic system ", 5th International Conference on Fluid Power Transmission and Control, Hangzhou, China, 3-5 Avril 2001, p 195-199.

[6] S. Sesmat, and S. Scavarda, "Static characteristics of a three way servovalve", *in Conference on Fluid Power Technology*, Aachen, Germany, 1996, pp.643-652.

[7] J.L. Shearer, "Study of pneumatic processes in the continuous control of motion with compressed air", *Trans. Am. Soc. Mech. Eng.*, vol.78, 1956, pp.233-249.

[8] M. Belgharbi, D. Thomasset, S. Scavarda, and S. Sesmat, "Analytical model of the flow stage of a pneumatic servo-distributor for simulation and nonlinear control", *in Scandinavian International Conference on Fluid Power SICFP'99*, Tampere, Finland, 1999, pp.847-860.

[9] S. Laghrouche, M. Smaoui, X. Brun, and F. Plestan, "Second order sliding mode controllers for pneumatic actuators", *in American Control Conference ACC'04*, Boston, Massachusetts, 2004.

[10] S. Laghrouche, M. Smaoui, and F. Plestan, "Third-order sliding mode controller for electropneumatic actuators", *in IEEE Conference on Decision and Control CDC'04*, Paradise Island, The Bahamas, 2004.

[11] M.Smaoui, X.Brun, D. Thomasset, "A combined first and second order sliding mode approach for position and pressure control of an electropneumatic system", *in American Control Conference ACC'05*, Portland, Oregon, 2005.

[12] M. Bouri, and D. Thomasset, "Sliding control of an electropneumatic actuator using an integral switching surface", *IEEE Trans. Control Syst. Technology*, vol.2, no.2, 2001, pp.368-375.

[13] A. Girin, F. Plestan, X. Brun, A. Glumineau and M. Smaoui, "'A 3^{th} order sliding mode controller based on integral sliding mode for an electropneumatic system"', *in IEEE Conference on Decision and Control CDC'05*, San Diego, USA, 2006.

[14] F. Plestan, S. Laghrouche, and A. Glumineau, "Multivariable practical higher order sliding mode control", *in IEEE Conference on Decision and Control - European Control Conference CDC-ECC'05*, Sevilla, Spain, 2005,

[15] C.F. VanLoan, "Computing integrals involving the matrix exponential", *IEEE Trans. Automat. Control*, vol.23, no.3, 1978, pp.395-404.

[16] X. Brun, S. Sesmat, D. Thomasset, and S. Scavarda, "A comparative study between two control laws of an electopneumatic actuator", *in European Control Conference ECC'99*, Karlsruhe, Germany, 1999.

[17] G.F. Franklin, J.D. Powell, and A. Emani-Naeini, *Feedback Control of Dynamic Systems*, Addison-Wesley, Reading, Massachusetts, 1987.

[18] S. Laghrouche, F. Plestan, and A. Glumineau, "Higher order sliding mode control based on optimal LQ control and integral sliding mode", *in IFAC Symposium on Nonlinear Control Systems NOLCOS'04*, Stuttgart, Germany, 2004.

[19] S. Laghrouche, F. Plestan, and A. Glumineau, "Higher order sliding mode control based on integral sliding mode", submitted to *Automatica* (second lecture), 2006.

GENERATING VIBRATION WITH ARTIFICIAL MUSCLES

Petri Keski-Honkola and Matti Pietola
Helsinki University of Technology
Faculty of Mechanical Engineering
Department of Machine Design / Fluid Power Group
P.O.Box 4400
FIN-02015 TKK, Finland
Phone +358 9 451 3280, Fax +358 9 365 2240
E-mail: Petri.Keski-Honkola@tkk.fi

ABSTRACT

This paper presents a study on the applicability of pneumatically actuated McKibben type fluidic muscles for producing mechanical vibrations in heavy machinery. Although McKibben type artificial fluidic muscles have been commercially available for couple of years, they are for the time being not very commonly known and used only in very restricted and special applications.

Fluidic muscles can produce even ten times the force of pneumatic cylinder with the same pressure difference and diameter. They are also practically slip-stick free which enables them to generate smooth movements. Another feature of the muscle is that there is interdependence with force and degree of contraction. Force is reduced while the muscle contracts. This feature enables the muscles to automatically center the position of the load when mounted in reverse-coupled manner and pressurized at the same time.

The artificial muscle actuated vibrator presented in this paper was constructed to replace a pneumatic motor-camshaft vibrator used to produce the vibration movement in a test installation. The muscle vibrator was designed so that the frequency, waveform and amplitude of the vibration could be adjusted. The problems related to the camshaft vibrator, like fluctuation of vibration frequency, difficulty in positioning the vibrated load and realizing an automated system were solved with the new vibrator.

KEYWORDS: Pneumatic artificial muscle (PAM), artificial pneumatic muscles (APM), Fluidic muscle, McKibben type muscles, Generating vibration.

1 INTRODUCTION

McKibben type artificial fluidic muscles have been commercially available from 1980's (Bridgestone Rubber Company of Japan), 1990's (Shadow Robot Group of England) and 2000's (FESTO Company) [1]. However they are not very commonly known actuators and they are typically used only in special applications. Yet these lightweight, easy to assemble and relatively inexpensive pneumatic actuators could replace many conventional actuators in many applications. In this paper the use of this type of artificial muscle is examined in an application where a specific vibration (waveform, amplitude, frequency, duration) has to be produced.

There are many ways to produce vibration. Commonly used actuators are solenoids (as used in acoustic systems), motor-camshafts and hydraulic or pneumatic cylinders. A test installation at TKK/Department of Machine Design was originally equipped with a pneumatic motor-camshaft for producing the vibration needed. However this application had a number of problems. When ending the vibration sequence the camshaft most probably stopped in a wrong position and the load was left displaced. Camshaft could be manually positioned, but that would make automating the test sequence impossible. After a short period of testing there also occurred some wearing in the bearings, which caused more error in the load position.

Another difficulty was the speed control of the pneumatic motor. Motor speed was controlled only by manually adjusting the air pressure of the system. Pneumatic motor was also meant for higher nominal speed so the torque was too low to maintain constant speed in this application. Also when the bearings of the motor heated up and the load varied it influenced the speed of the motor considerably and changed the vibration frequency.

A new vibrator was designed in order to meet the needs of the test installation. After considering different options McKibben type pneumatic artificial muscles (PAMs [2]) were selected as actuators. Other names used of PAM are artificial pneumatic muscles (APM [3]) and fluidic muscle [4]. PAM is relatively cheap, clean and easy to install when pressured air is available. They are also lightweight and service free. These muscles are very application specific and they should be selected very carefully.

In the laboratory test installation a vibration with maximum frequency of 5–20 Hz and maximum amplitude of 2 mm was needed. The vibration actuator was required to produce fifteen seconds long bursts of vibration every second hour.

PAM is an actuator that can only produce pulling force and the amount of force is reduced when the muscle contracts. This means that to produce bi-directional motion in vibrator, muscles have to be organized in reverse-coupled manner. On the other hand, due to the interdependence of force and contraction, when muscles are pulling from both sides they can center the load. This was one of the main reasons why muscles were used in the first place.

2 PAM-VIBRATOR

As described above the vibration was needed in a laboratory test installation. Original motor-camshaft vibrator wasn't sufficient and a new vibrator was needed. To solve the problems McKibben type muscles were selected to be used as new actuators.

Vibrating system couldn't be modeled and simulated in detail at the time because of tight schedule. There were also some variables that couldn't be determined at the time. This meant that some assumptions had to be made and all components were selected to be sufficient in performance.

Vibrating mass is over a hundred kilograms, but it is supported by an axel, so that the vibrator doesn't have to support the whole mass. However the mass is not fully balanced, so there is a static load of some 300 N to the vibrator. Additionally to the mass, different kind of spring loads are also applied to the system, depending what kind of test is being made, **Figure 1.**

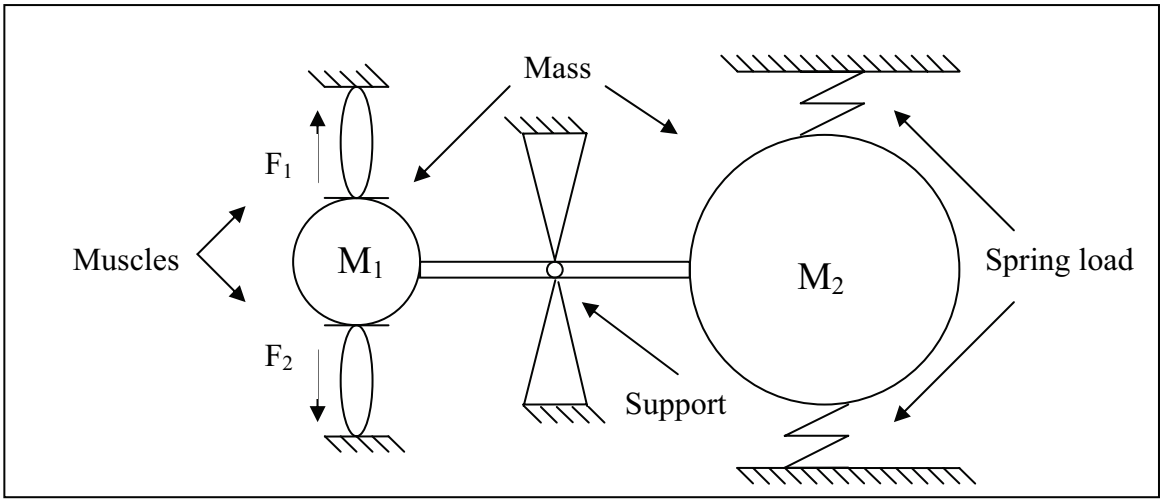

Figure 1. Vibrating mechanism.

2.1 McKibben type artificial muscle actuator

J. L. McKibben invented McKibben type pneumatic artificial muscles (PAMs [2] or APMs [3]) in 1950's as an actuator to be used in prostates. The principle of the muscle is the fact that a network of non-expandable fibers has been inserted around an inflatable rubber tube. Under pressure this tube expands in diameter and shortens in length, **Figure 2.** Fluidic muscle can contract even 25% at the maximum pressure of 600 kPa. [3].

Artificial muscles are commonly operated with pressured air but they can also be operated with hydraulic medium like water. This is the reason why pneumatic muscles are also called as fluidic muscles [4].

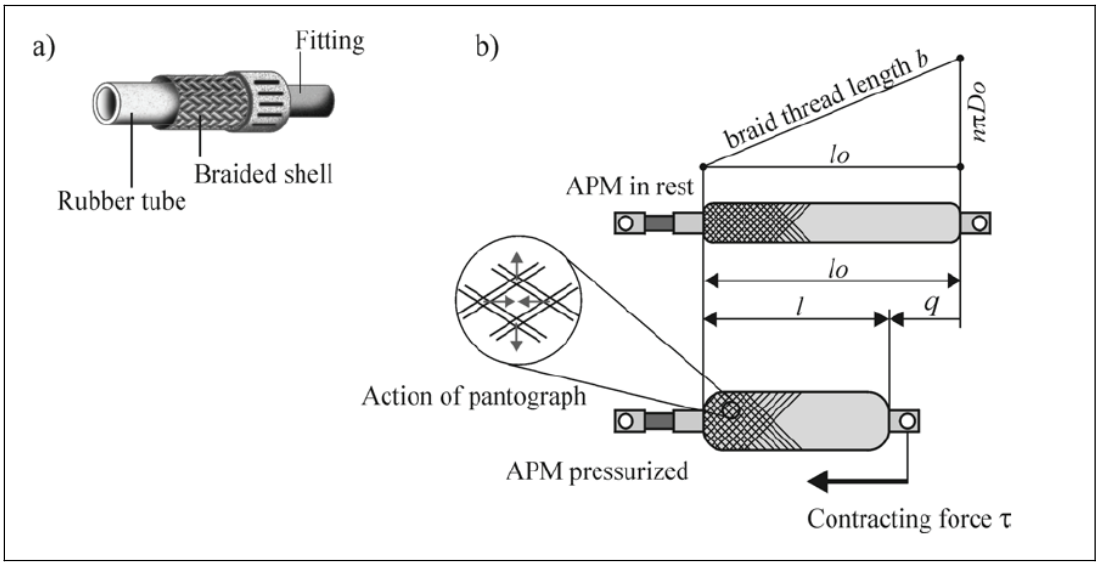

Figure 2. Working principle of McKibben type fluidic muscle actuator [3].

While expanding, the muscle can only produce pulling force ten times stronger than same size conventional pneumatic cylinder. However the amount of force is reduced when the muscle contracts as shown in **Figure 3.** This means that to produce bi-directional motion, muscles had to be organized in reverse-coupled manner. Gravity or a spring can also be used to pull the muscle back to its nominal length. Due to the interdependence of force and contraction, when muscles are pulling from both sides at the same pressure they move to the position where forces are equal at the both sides. This means that if no outside forces applied, muscles move to center position. If there is a constant load force involved, muscles can be pretensioned so that when the muscles are pressurized at the same time the load is centered to certain position. This was one of the main reasons why muscles were selected as actuators in the new vibrator [4].

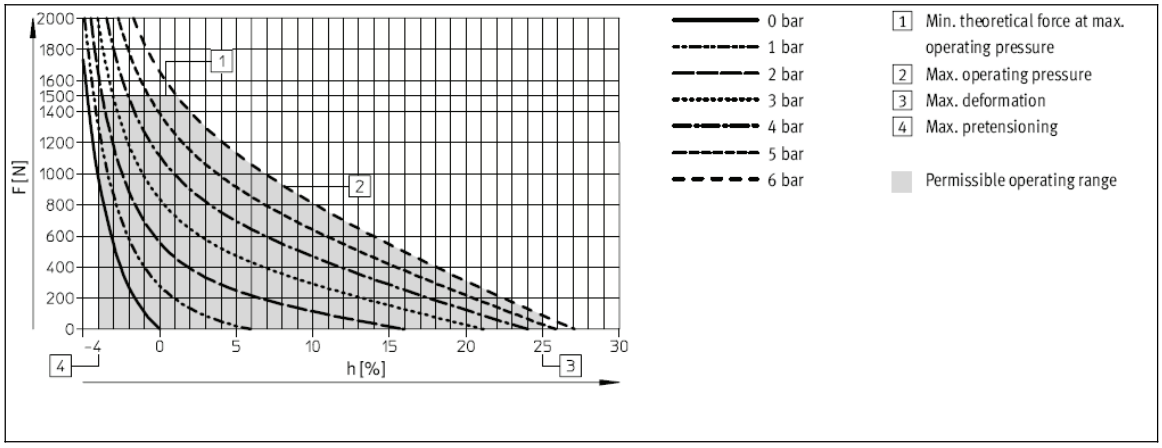

Figure 3. Festo DMSP with diameter of 20 mm. h is the percentage of contraction [5].

Maximum force produced in respect to nominal diameter is represented in **Table 1.** Muscles with nominal diameter of 20 and 40 mm can theoretically produce more force, but it might damage the muscle and is not recommended by vendor.

Table 1. Maximum force of FESTO-DMSP fluidic muscles. [5]

Nominal diameter	Maximum Force
10 mm	630 N
20 mm	1500 N
40 mm	6000 N

2.2 Mechanical Design of Vibrator

Controlled vibration of 5-20 Hz with maximum amplitude of 2 mm was needed in a laboratory testing installation. In machinery, suddenly applying or releasing large loads often causes such vibrations as described. In the tested application the actuator had to produce a fifteen seconds short bursts of vibrations every second hour. Final settings used were 12 Hz and 0.7 mm

These muscles can contract 25 % from its nominal length but only a fraction (0.9 %) of this was used to obtain more force, **Figure 3**. It was calculated that the load mass could be vibrated fast enough with 1200 N of force. Because there was also the extra load caused by the system of springs a construction of two parallel muscles on both sides of the actuator was selected to produce enough force. Muscles were installed in reverse-coupled manner and as pairs, **Figure 4.** Load is attached between the muscle pairs so it can be pulled up and down. These medium sized muscles have a radius of 20 mm and nominal length of 80 mm and they can produce a maximum force of 1200 N each. This means 2400 N of maximum force to one direction. In this application maximum amplitude is limited to 0.7 mm but it could be easily changed and made larger since it was realized with simple adjustable mechanical end-stoppers. If the amplitude is increased then the maximum frequency will naturally be reduced.

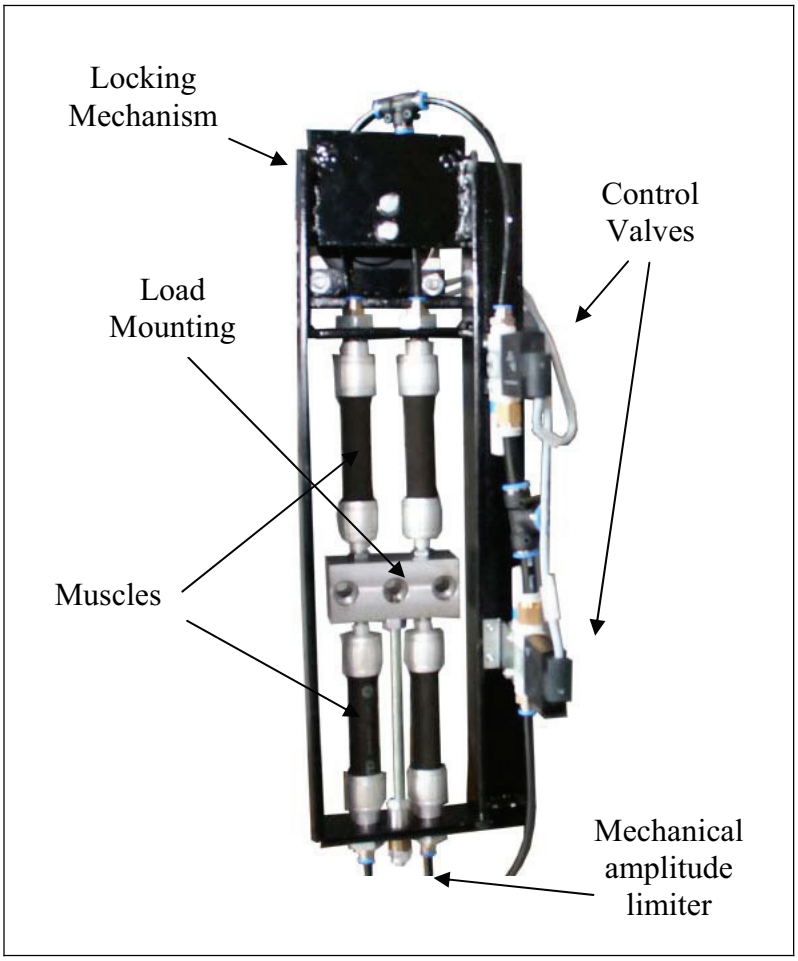

Figure 4. Artificial muscle vibrator.

2.3 Pneumatics

Two Festo 3/2 (MHE4-MS1H-3/20-1/4) fast switching on/off-valves were selected to control the airflow to the muscles, **Table 2**. They are capable of producing ten times the frequency that is needed. Current consumption of the valves is shown in **Figure 5.** These valves ensure adequate airflow and response time. One valve feeds air to one side of the vibrator and another to the other side. This means that two muscles are connected to one valve. By applying pressure to one side at a time the mechanism is made to vibrate, **Figure 6** [4].

Table 2. MHE4 fast switching valves [6].

Opening and closing times	3.5 ms
Maximum switching frequency	230 Hz
Nominal airflow	400 l/min
Operating voltage	24 V

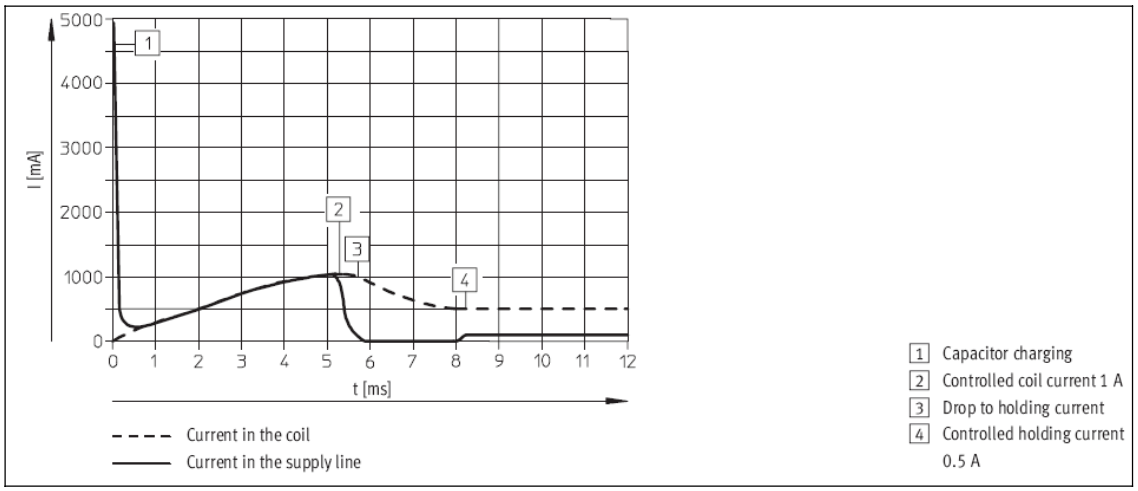

Figure 5. Supply current curve of the control valve [6].

Both control valves have an adjustable choke in their release channel, **Figure 6.** This means that the release speed of the air from the muscles can be adjusted. When release channel is choked, the idle muscles are not emptied immediately and they keep producing force for a while. This allows adjusting the form of the vibration.

System pressure levels were set to 400 KPa. This pressure produces the maximum force that the muscles can endure at this setup.

There is also a third valve (Lock Release Valve) which uses a pneumatic cylinder. This cylinder locks the vibrating mass and ensures that the load stays in a right position while the vibrator is off. Cylinder is spring actuated and the lock opens when pressure is applied trough the Lock Release Valve, **Figure 6.**

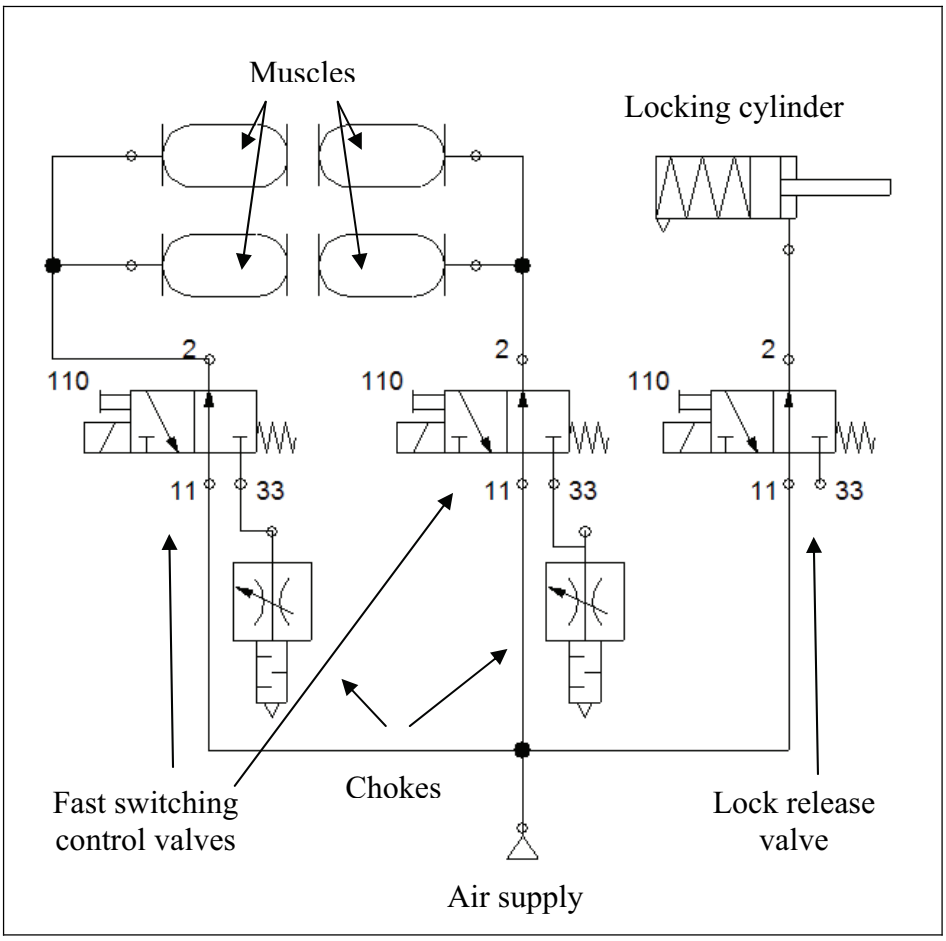

Figure 6. Pneumatic chart of the muscle vibrator.

Pneumatic connections of the system is made so the air doesn't change in the muscle and therefore they could heat up, but while using small amplitude of 0.7 mm heating does not happen. Only with faster vibrations and larger amplitudes, e.g., 20 Hz and 2 mm, the thermal load would be a problem.

Using the connection described in **Figure 7** reduces thermal load. Pressured air is directed through one-way valve in to the muscle. Releasing pressure from the control valve opens the quick exhaust valve and releases pressure from the muscle. This kind of setup allows air to flow through the muscle and carry the excess heat out with it.

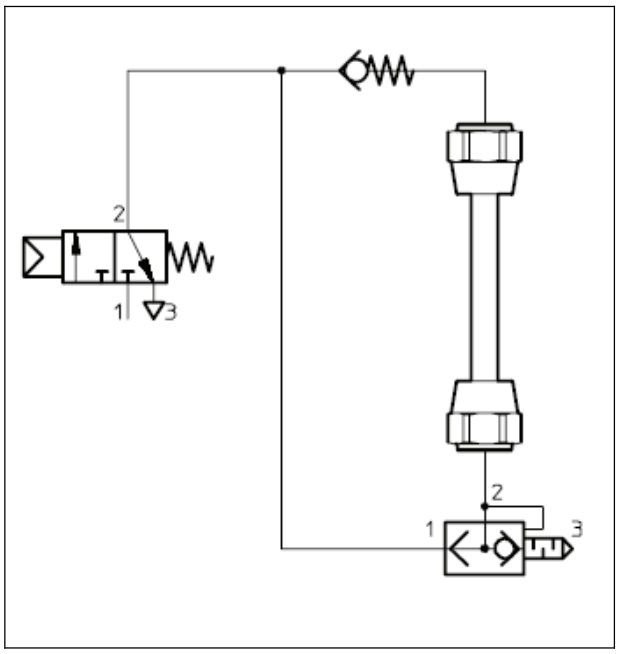

Figure 7. Reducing the thermal load [5].

2.4 PLC (Programmable Logic Control)

Vibration is produced at a certain intervals and it lasts for fifteen seconds. Command to produce vibration is generated in a PC-based measurement computer by a LabView program and delivered to Siemens LOGO! PLC. After receiving command signal, PLC directs power to an oscillator circuit for fifteen seconds. PLC also controls the locking cylinder and releases it while system is vibrating.

2.5 Oscillator

LOGO! PLC relay has a maximum switching time of 0.1 s. This means that it can't be used it to produce over 10 Hz vibrations. For these reason a separate oscillating circuit was made. It can produce square wave signal from 8 to 25 Hz. On and off time of the signal can be adjusted separately. PLC feeds oscillator circuit with 24 volts when vibration is needed, thus controlling the time and duration of vibration. Oscillator circuit feeds current to the two fast-switching valves in turns. This again makes the muscles contract one side at a time and load starts to vibrate.

3 MEASUREMET SYSTEM

In this section the measurement arrangement and sensors will be described in detail.

3.1 Data acquisition system

Measurement system and control system are partly the same. Same PC-based data acquisition system (National Instruments NI PCI-6229 and LabVIEW 7.1) was used to control the intervals of vibration and collect the data. Data was stored at the frequency of 2 kHz, which means that the interval of samples is 0.5 ms.

3.2 Position Sensor

Vibration form was measured near the connection point of the vibrator. A linear potentiometer was used, **Figure 8.** Static values were certified with a manual displacement sensor. When amplitude of the vibration is low (under 1 mm) and maximum frequency is less than 30 Hz, the performance limits of the sensor are not exceeded, **Table 3.**

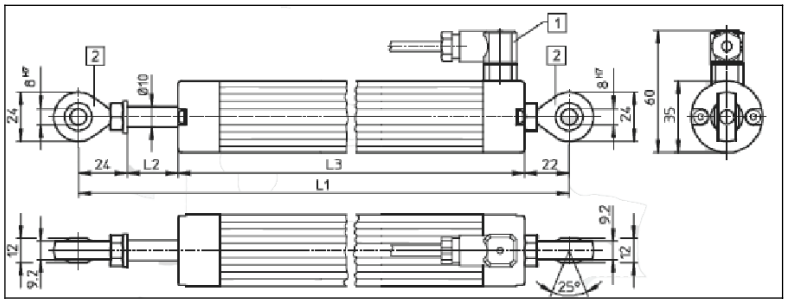

Figure 8. . Potentiometer MLO-POT-100-LWG [7].

Table 3. Datasheet of POT-100-LWG [7].

Maximum Stroke	100 mm
Resolution	0,01 mm
Maximum speed	5 m/s
Maximum acceleration	200 m/s²

3.3 Measurement arrangement

In all measurements there is a spring related force additional to the inertia of the system. Measurement sensor, electronics, mechanism of the vibrated system and the data acquisition system are same while measuring both vibrators.

4 RESULTS

Measurement results are shown in **Figure 9.** They represent the position of load in mm as a function of time. All signals are filtered with same filter and while some phase shift occurs the amplitude and waveform are not affected at a significant level.

There are four different charts titled Fast, Middle, Medium and Original Motor. First three represent the new muscle actuated vibrator at different vibrating frequencies. Original Motor is measured with the original camshaft mechanism which is rotated with pneumatic motor.

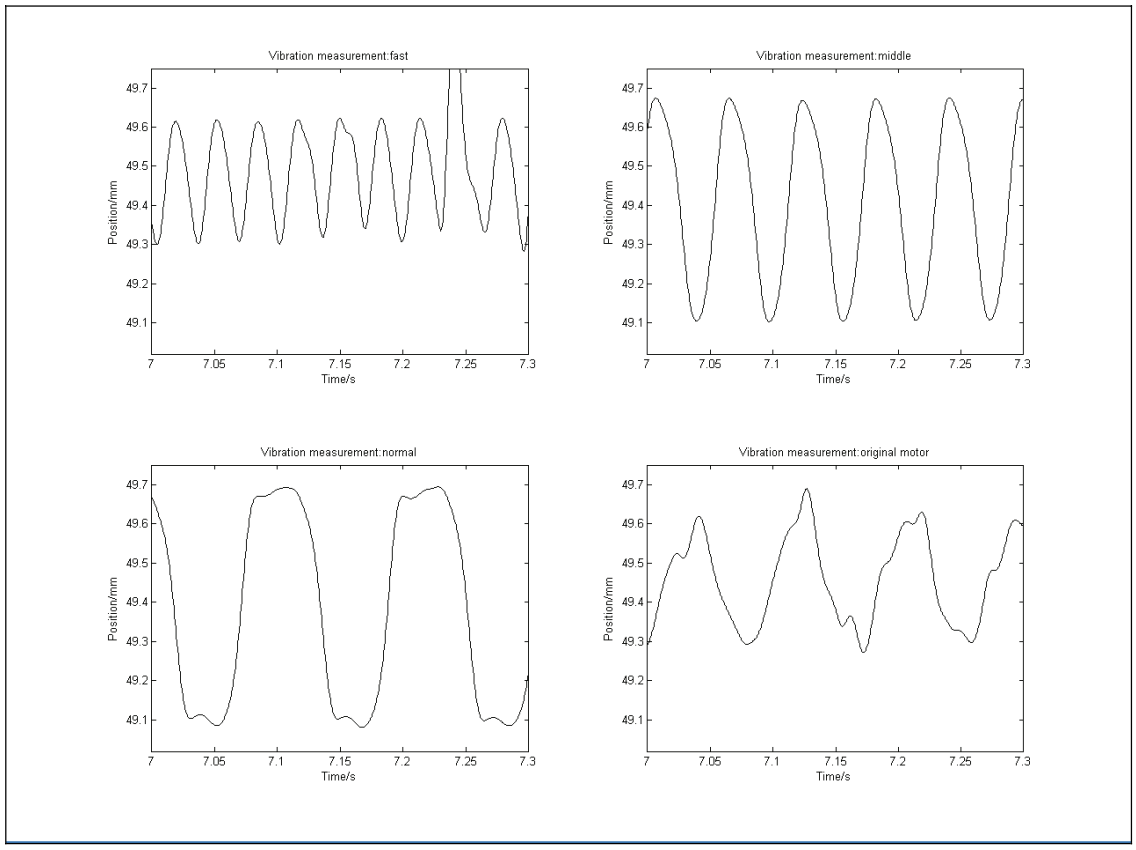

Figure 9. Position of the load in respect to time. Fast, Middle and Normal represent the PAM generated vibrations. Chart titled Original Motor is generated by the camshaft mechanism.

5 DISCUSSION

The vibration produced by the original pneumatic motor-camshaft mechanism is presented in Figure 10, lower right graph. Vibration has an amplitude of 0.4 mm and frequency of 17 Hz in this specific measurement, but during the tests it was noticed that the frequency could vary significantly and go even up to 50 Hz by itself. The waveform is not the sine that it should be. This is probably caused by the wear of bearings and that

there is unnecessary play in the mechanism. This would also explain that the amplitude is smaller than it should be.

First test with PAM actuated vibrator was made with the lowest frequency that the oscillator circuit would allow. The result of this measurement is shown in Figure 10 lower left graph, labeled as Normal. Waveform is near square wave because the valve chokes are fully open and the movement is stopped by the mechanical stopper which limits the amplitude to 0.6 mm. Little bounce caused by the end stopper is also visible.

The measurement result labeled as Middle, **Figure 9** upper right graph, was measured at the frequency of 20 Hz. The amplitude is still at the maximum of 0.6 mm. Load is moving little faster upwards. This is because the load is off balanced to that direction and the muscles must work harder pulling the load down. This result shows that the goal set for the project was achieved.

Third measurement with PAM vibrator, **Figure 9** upper left graph, was to determine the limits of the system. It induced a lot of not wanted vibrations to the system and the results might not be very reliable. There was also a danger of breaking some parts of the larger system. Nevertheless a vibration of some 35 Hz was achieved even if amplitude dropped to 0.3 mm.

The result of the study demonstrates that pneumatically powered fluidic muscles can be used to produce accurate vibrating motion of different waveforms in applications where pressurized air is preferred to oil and the required force is of moderate level. The advantage of pneumatic solutions is that they tend to be cheap and reliable compared to other alternatives. Choking the airflow, changing switching frequency of valves and changing pretension of the muscles mechanically can be used to control dynamics of the movement waveform. With smaller load smaller muscles could use used (diameter of 20 mm and nominal length of 40 mm). This means that the volume of the muscles would be smaller and higher frequencies could be achieved with the same airflow.

6 CONCLUSION

Although the pneumatic motor in the original application was not optimal for this application a different motor would not have solved the problem of stopping the load to right position. Positioning the load in idle state was the main advantage of using pneumatic muscles. Also controlling the waveform by simply adjusting the chokes in control vale release channels was a great asset. Chokes were fully open while measuring the dynamics. In the final setup chokes were used to make vibration form more round.

System has been running for two months and no problems have appeared. More PAM projects have been started inspired by this one. One area of interest is that the vibrator could be used to reduce vibration either by actually producing counter vibration or by changing its stiffness and thus changing the vibrating properties of the system.

7 REFERENCES

[1] University of Washington/BioRobotics Laboratory. McKibben Artificial muscles. [Referenced 10.6.2006] Available: http://brl.ee.washington.edu/Research_Past/Biologically_Based/Device_01_McKibben/Mckibben.html

[2] Daerden, F., Lefeber, D., The concept and design of pleated pneumatic artificial muscles, International Journal of Fluid Power, 2(3):41–50, 2001

[3] Petrovic, P., Modeling and Control Of an Artificial Muscle, Part one: Model building, 10th conference on mechanical vibrations, 47(61), 2002.

[4] Hesse, S., The Fluidic Muscle in Application, Festo AG & Co. KG, 2003

[5] Festo AG & Co., Product catalog 2004-2005. Fluidic Muscle DMSP/MAS. Version: 04/2005 [Referenced 1.9.2006]. Available: http://catalog.festo.com/data/CAT_PDF/001/MAS_EN.pdf.

[6] Festo AG & Co., Product catalog 2006. Solenoid Valves MH2/MH3/MH4, fast-switching valves. Version 03/2006 [Referenced 5.10.2006]. Available: http://catalog.festo.com/data/CAT_PDF/001/FAST-SWITCHING-VALVES_EN.pdf

[7] Festo AG & Co., Product catalog 2006. Displacement encoders. Version 03/2006 [Referenced 5.10.2006]. Available: http://catalog.festo.com/data/CAT_PDF/001/DISPLACE-ENCODER-MLO-MME_EN.pdf

HIGH PERFORMANCE DIGITAL HYDRAULIC SERVO SYSTEM FOR LINEAR CYCLIC MOTION

Ville Ahola, Matti Linjama, Matti Vilenius

Tampere University of Technology, Institute of Hydraulics and Automation
P.O. Box 589, FI-33101 Tampere, Finland
E-Mail: ville.ahola@tut.fi
Tel: +358 3 3115 4430 Fax: +358 3 3115 2240

ABSTRACT

Hydraulic actuation has been popular in linear cyclic motion because of high power-to-weight ratio. Good control performance and good repeatability are important in order to achieve high quality. Therefore, servo valves are usually used as control valves. Problems with servo valve are high cost as well as sensitivity for contamination and vibrations. Required high flow rates and high bandwidth are also difficult to satisfy. These problems could be reduced if fast on/off valves were used instead of servo valve. In this paper, the two-stage servo cartridge valve is replaced with parallel-connected on/off valves. 5+3 valves are used to control inflow and outflow of the cylinder actuator. Controller is developed for this Digital Hydraulic solution and control performance is compared with traditional system. Results show that digital hydraulic valve system gives better control performance and is therefore a potential solution.

Keywords: Digital hydraulics, on/off control, linear cyclic motion

1 INTRODUCTION

Traditionally, linear cyclic motion, accompanied with high force (up to 300 kN) and velocity requirements has been hydraulically actuated. Characteristics of electric drives have strongly developed during last decade and they are replacing hydraulic drives in punching applications, for example. In order to make hydraulic drives competitive, energy efficiency, reliability and performance must be improved. Energy efficiency has been studied in [1] and this paper concentrates on improving reliability and performance.

Conventional hydraulically operated punching machines are controlled by fast servo valves, which are expensive and sensitive to contamination. Alternative control solution is based on Digital Hydraulics, which relies on robust on/off technology and intelligent control [2]. The approach is attractive in punching machines because it makes valve system fault tolerant and less sensitive to contamination [3]. In addition the response time is independent on amplitude [4]. The objective of this paper is to study applicability of digital hydraulics in punching machines and to experimentally compare digital and traditional system.

2 DIGITAL HYDRAULIC CONTROL OF LINEAR MOTION

2.1 Traditional Control Methods

Traditional control methods for punching machine were studied and compared by [1]. Figure 1 shows three different control methods. First one on the left is probably the most common way to control a punching machine and this kind of control method is also used in the compared traditional system. Asymmetric cylinder is used and the direction of the movement is controlled with a 3/2 servo valve. Outward stroke is executed by connecting the supply pressure into the upper chamber. Constant supply pressure on the piston rod side enables the return stroke when the upper chamber is connected to the tank. In the middle system the movement of the asymmetric cylinder is controlled with 4/3 servo valve.

Last system on the right introduces a cylinder with two different surface areas for outward stroke. The idea of this system is to use smaller area for the movement of the piston and when more force is needed the effective area is increased. Direction of the movement is controlled with 3/2 servo valve and available punching force is controlled with pressure sensing pilot operated 3/2 valve. The energy consumption can be reduced with this kind of system but with dual pressure system it can be improved even more [1].

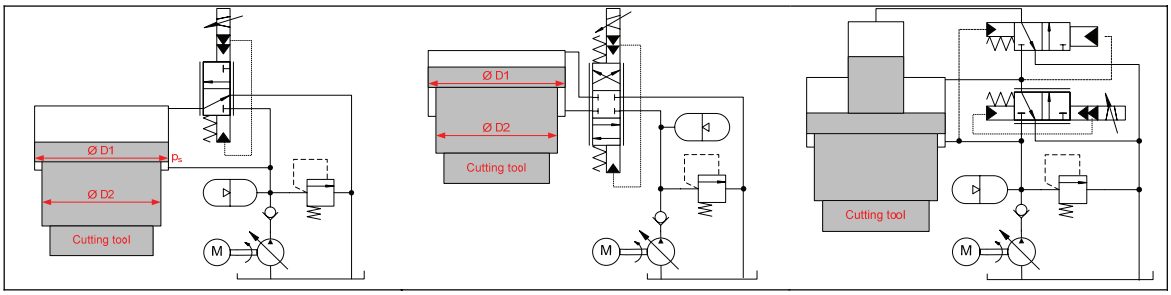

Figure 1. Conventional control methods [1].

2.2 Digital Hydraulic Control Methods

One parallel connected on/off valve series – so called Digital Flow Control Unit (DFCU) – is used for each control edge in digital hydraulic control. This kind of configuration gives independent control over the all control edges, which traditional spool type valves cannot accomplish.

In this application, a 3 way DFCU design is chosen (Fig.2) in order to keep the modifications to the actual test system minimal and to make the comparing to the old system more valid.

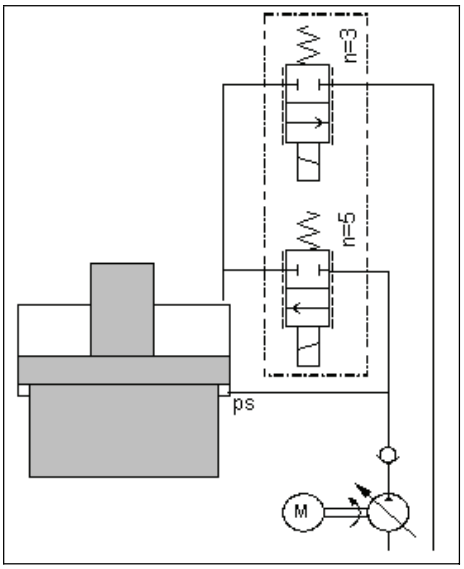

Figure 2. Principled diagram for digital hydraulic system

The simplest possible control method is chosen because of the nature of the work cycle. In a punching machine, the goal is to reach the desired position as fast as possible and still retain enough accuracy. The reference position is in most cases square wave like. P-controller seems to be suitable for these needs.

2.3 Different Coding Methods of Valve Sizes

After selecting the control method, the next focus is on the coding of the valve series. Possible coding methods for this application are binary, Pulse Number Modulation (PNM) or progressive PNM. In binary coding, the flow capacity of each valve is two times higher than previous valve (Fig.3).The amount of available different flow rates can be calculated from 2^N where N is the number of parallel-connected valves. This gives the best possible control resolution but may cause pressure peaks [5]. PNM coding utilizes valves with equal flow capacity and the number of open valves determines flow rate. The number of different flow rates is only N+1 but on the other hand, there is no risk for pressure peaks. PNM can be used when requirements for controllability of velocity are modest. PNM coding (Fig.4, a) is suitable for extremely fast work cycles because every valve is switched on/off usually only once per piston movement.

Progressive PNM (Fig.4, b) is modification, in which flow capacities are not equal but valves are controlled like in PNM control. In this study the selected coding method is progressive PNM and the valve sizes are selected according to the system requirements

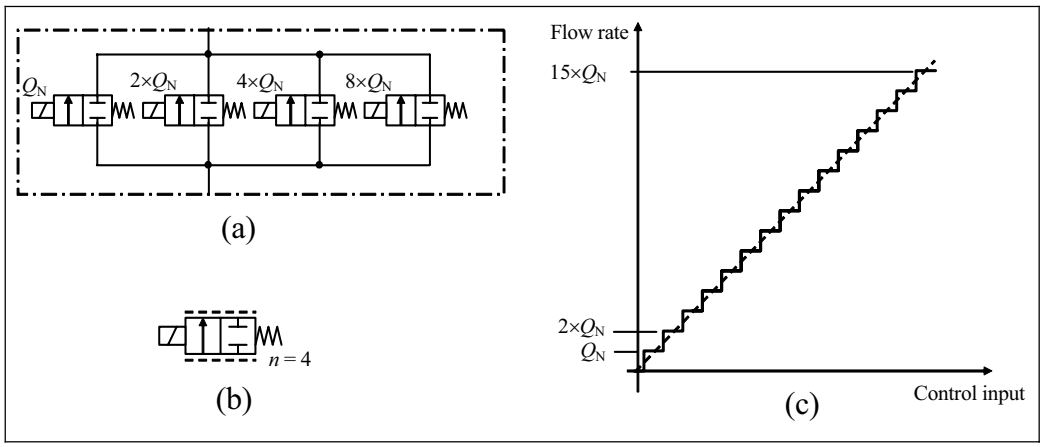

Figure 3. Flow characteristics for binary coded DFCU [2]

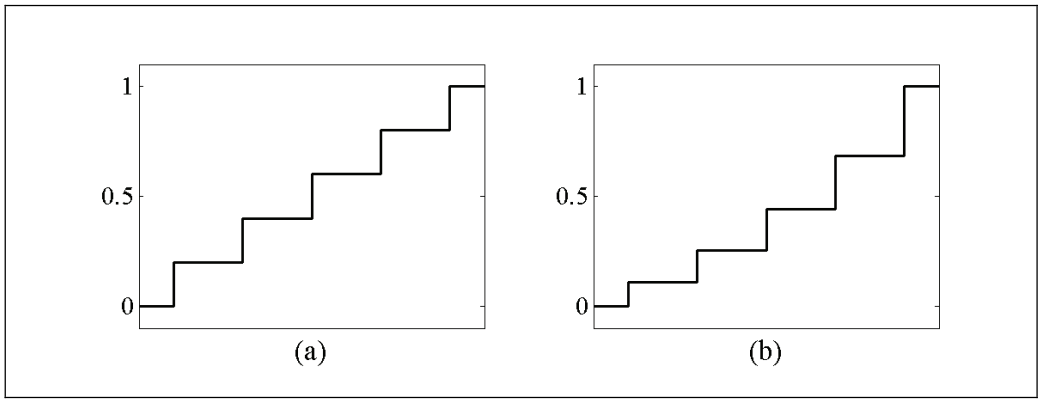

Figure 4. Examples for flow characteristics for PNM (a) and progressive PNM (b) coded systems

3 TEST SYSTEM

3.1 Test Bench

Measurements for traditional servo valve operated system were done with a commercially available punching machine. The punching machine was equipped with Bosch-Rexroth 3WRCE32V servo valve which had slightly modified main stage spool to suit the characteristics of the punching machine.

Test bench build for the measurements with DFCU mimics the real punching machine in respect of hydraulic system and is equipped with similar kind of pump and cylinder used in actual machine. Simplified diagram of the test system is shown in Figure 5. Test system was not equipped with cutting tools and therefore only free movement of the piston was studied.

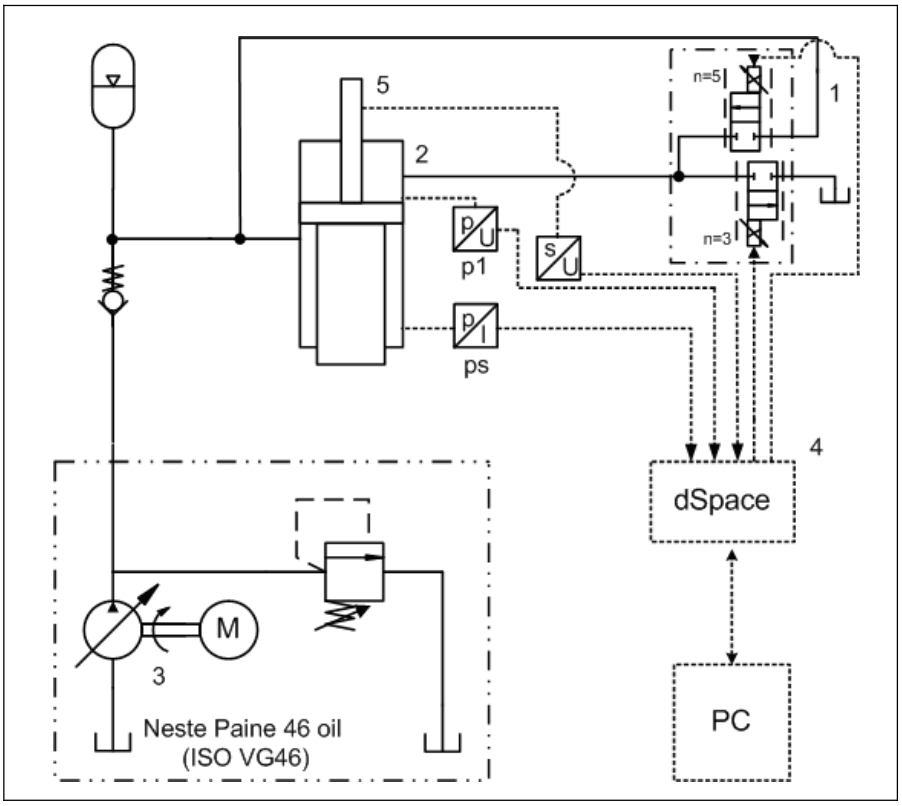

Figure 5. Simplified hydraulic diagram for DFCU operated system

1 Five DFplus in parallel connection as pressure side DFCU and three DFplus in parallel connection as tank-side DFCU.
2 Cylinder
3 Bosch-Rexroth A10VS-71 cm^3 hydraulic pump coupled with 30 kW electric motor
4 dSpace DS1005
5 LVDT sensor

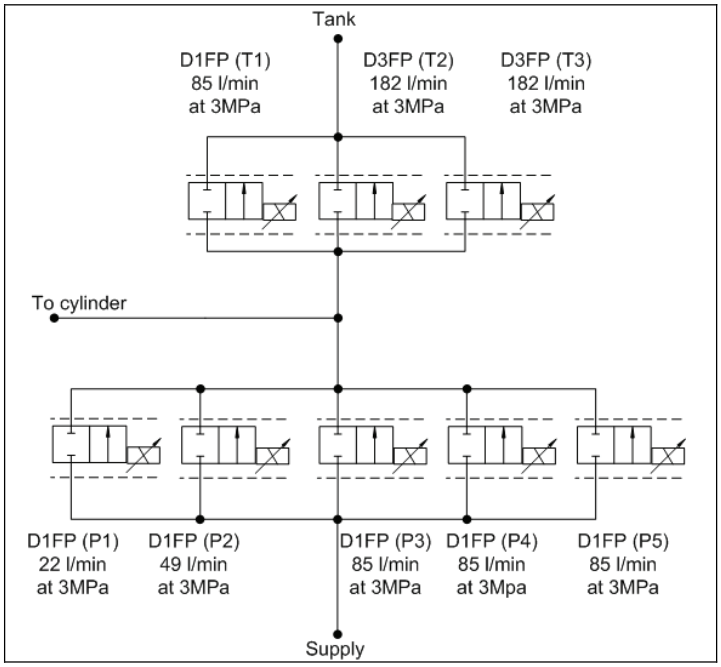

Figure 6. Detailed diagram for DFCU (1 in figure 5.)

3.2 Valves

The servo valve, Bosch-Rexroth 3WRCE32V, with modified main stage spool was used in comparison measurements. Performance characteristics [6] of the servo valve from the manufacturer are shown in Table 1.

Table 1. Performance characteristics for servo valve

Nominal size	NS 32
Nominal size for pilot valve	NG 6
Max. operating pressure	31.5 MPa
Nominal flow(Δp = 0.5 MPa)	180 l/min
Step response (Δp = 40 bar) (0-100%)	22 ms
Step response (Δp = 140 bar) (0-100%)	11 ms
Step response (Δp = 315 bar) (0-100%)	8 ms

Many direct operated on/off valves were studied but at the moment there were not fast enough on/off valves commercially available for this research. The only valves found with satisfying flow rate and switching time was Parker DFplus series valves which are proportional direct operated 3/2 directional control valve. It was decided to run DFplus with on/off like control to mimic real on/off valve.

Two sizes of DFplus are used in this study and both were measured for their performance characteristics. Valve characteristics provided by the manufacturer are shown in Table 2 and are corresponding to the measurements done with the valves.

Table 2. Performance characteristics for DFplus [7]

Characteristics D1FP, D3FP			
		D1FP	D3FP
Size		NS6	NS10
Nominal flow	[l/min]	up to 40 at 3.5MPa (metering edge)	up to 100 at 3.5MPa (metering edge)
Step response 0-100%	[ms]	<3.5	<6
Hysteresis	[%]	<0.05	<0.05
Frequency response at 5% signal (-3dB / -90° Phase)	[Hz]	350/350	200/200

4 EXPERIMENTAL RESULTS

4.1 Work Cycle

Traditional work cycle for punching machine consists of the punch and the time delay needed for the moving of the sheet metal. Sheet is pierced with cutting tool attached to the end of the piston rod. Work cycle without sheet is represented in Figure 7.

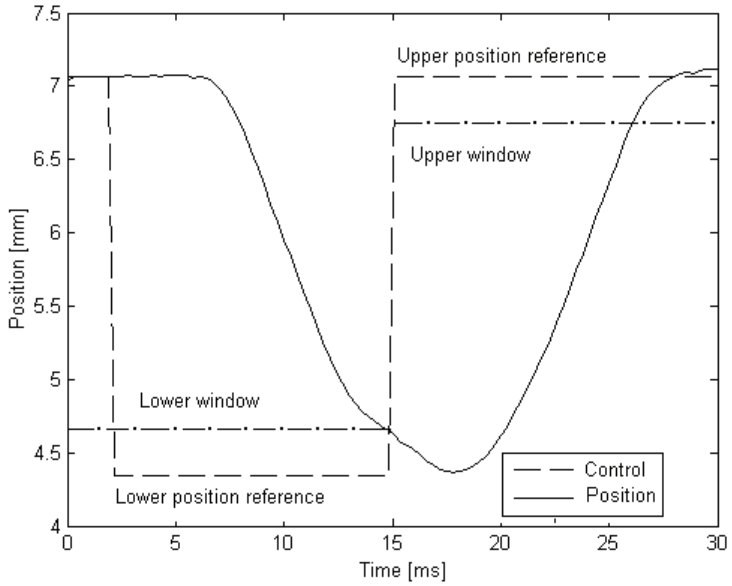

Figure 7. Work cycle for punching machine without sheet

Punch starts when the sheet metal has been positioned. Control signal to valve for return stroke is given when the lower window is reached. Moving of the sheet starts when the tool has passed preset position on the return stroke called upper window. Next punch can be commissioned when the sheet has been repositioned. For the maximum performance the control of the work cycle has to be predicted and the control signals are given in advance to compensate delays. The high accuracy is demanded only on the punch direction and the return stroke can be made as fast as possible with the cost of accuracy.

4.2 On/Off Like Control of DFplus

On/off valves are the backbones of digital hydraulics and for that reason the selected proportional valves are controlled as on/off valves. Opening for each valve is preset according to the selected coding method. Some ramping of the control signal is needed to reduce the overshooting of the valve. Overshoot is a problem mainly in the D3FP and the valve does not have good response for standard rate limiter type ramping. Therefore the control signal is modified with rate limiter and mathematic function tanh(x). Results are shown in Figure 8. The smaller valve, D1FP, behaves better and needs only slight ramp for the control signal on the pressure side DFCU. D1FP on the tank side was driven without any ramps with standard square-type control signal.

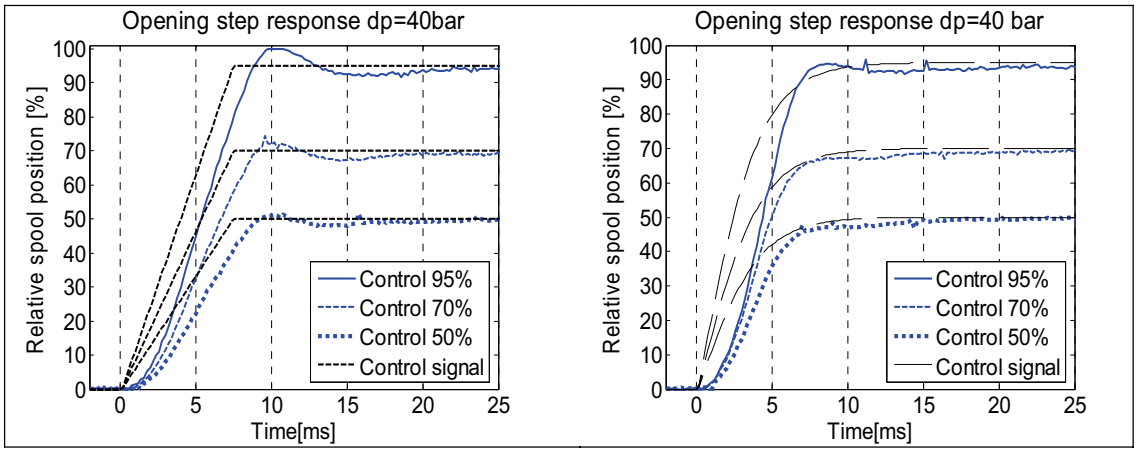

Figure 8. Control signal ramping for DFplus

To compensate flow forces and to double the nominal flow over the valve, both control edges are used. This is done by connecting ports P & B and T & A (Fig. 9).

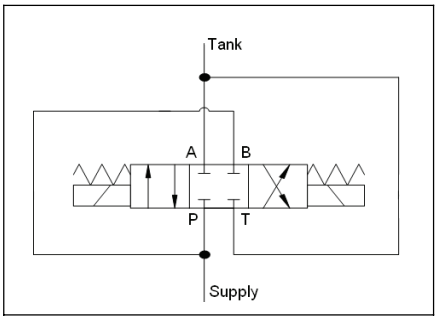

Figure 9. Double flow configuration

4.3 Controller

Principle of the used P-controller is shown in Figure 10. Variables used to control the closing points of the valves are the slope of the control line (P_2) and the closing offset (P_1) for the smallest valve. Variables are tuned according to the stroke lengths and the flow rates versus position for DFCU are as shown in Figure 11.

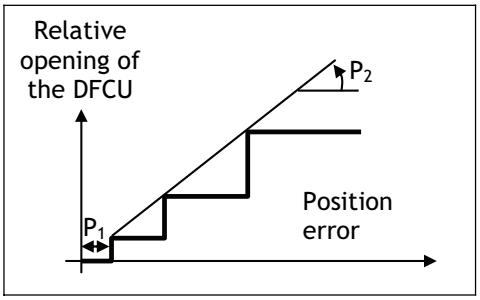

Figure 10. Principles of used P-controller

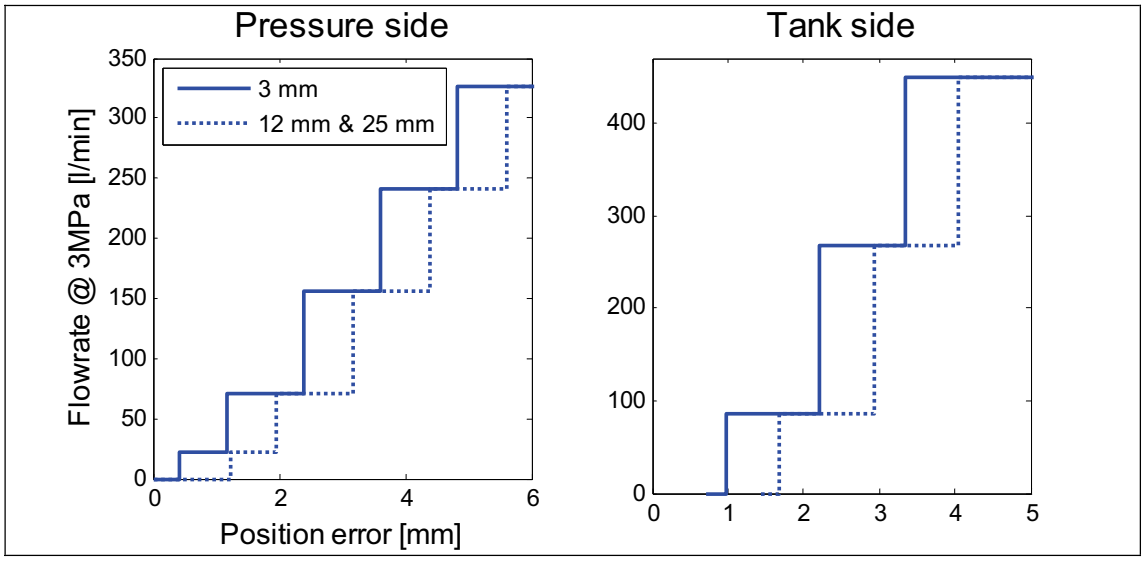

Figure 11. Nominal flow rate versus position error for DFCU at different stroke lengths

4.4 Results with Traditional Servo Valve

Measurements with traditional servo valve operated system were done with actual punching machine [1]. The measurements were done without sheet. The results with different stroke lengths can be seen in Figure 12. In all measurements the control signal for outward stroke is given when time is 0 ms. Piston movement delay from the control signal is low, approximately 3 ms. Five sample α-trimmed mean filter was used to clarify measurements where needed.

4.5 Results with Digital Hydraulic Valve System

The measurements for digital hydraulic operated test bench are shown in figure 13. Measurements show that there is some delay on the start of the punch but repeatability of the system is good and therefore this kind of constant delay can easily be compensated on real machine. Because the possible opening for DFCU is discrete, some additional pressure transients arise when compared to the conventional servo system.

Position responses from both test systems are compared in figure 14. Digital hydraulic operated system has clear upper hand when changing the direction of the piston but the start of the punch is somewhat slow which could be improved with faster valves. Also the maximum speed is somewhat slower in both directions but that could be easily improved by adding one more valve for both DFCU.

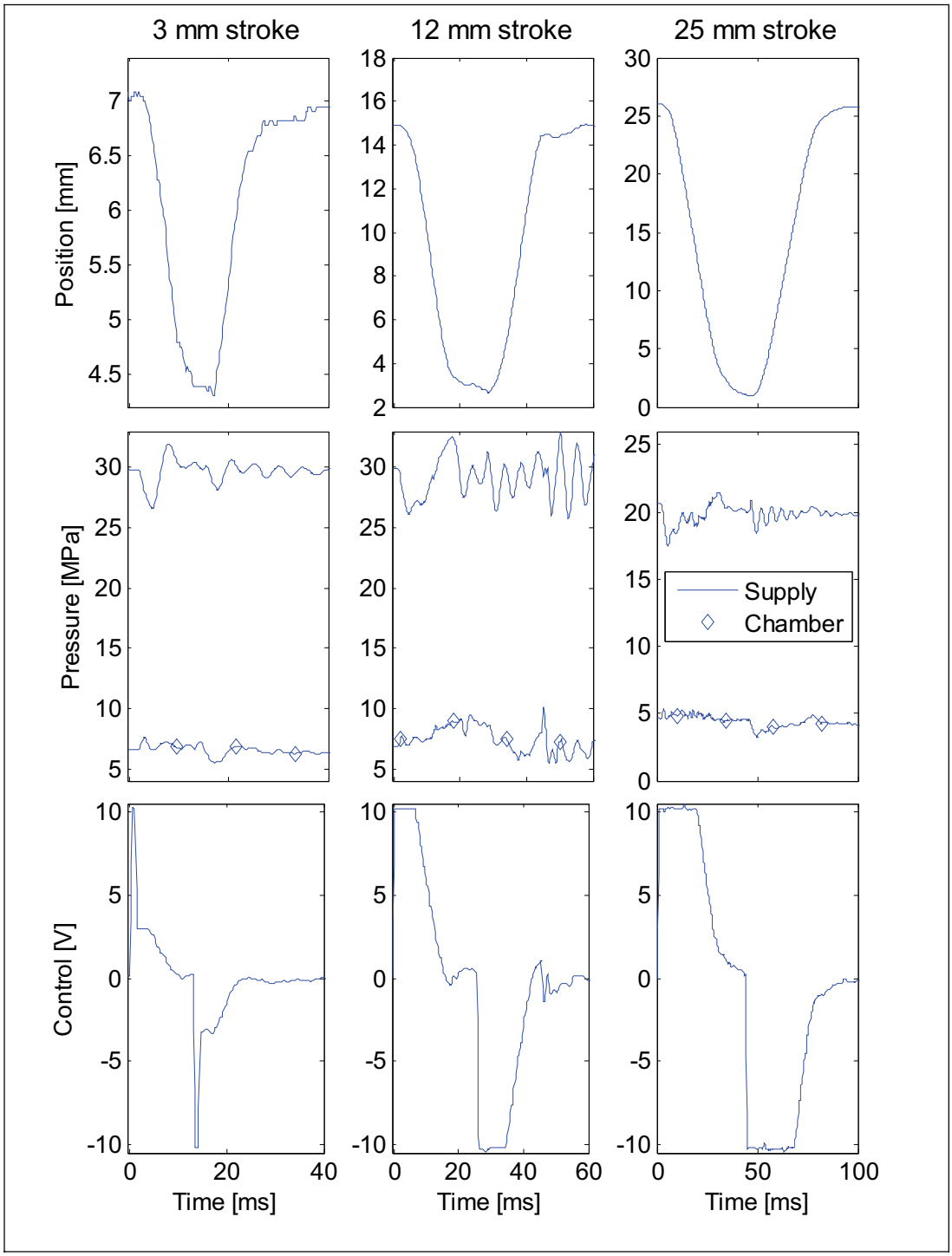

Figure 12. Measurements for servo valve operated system

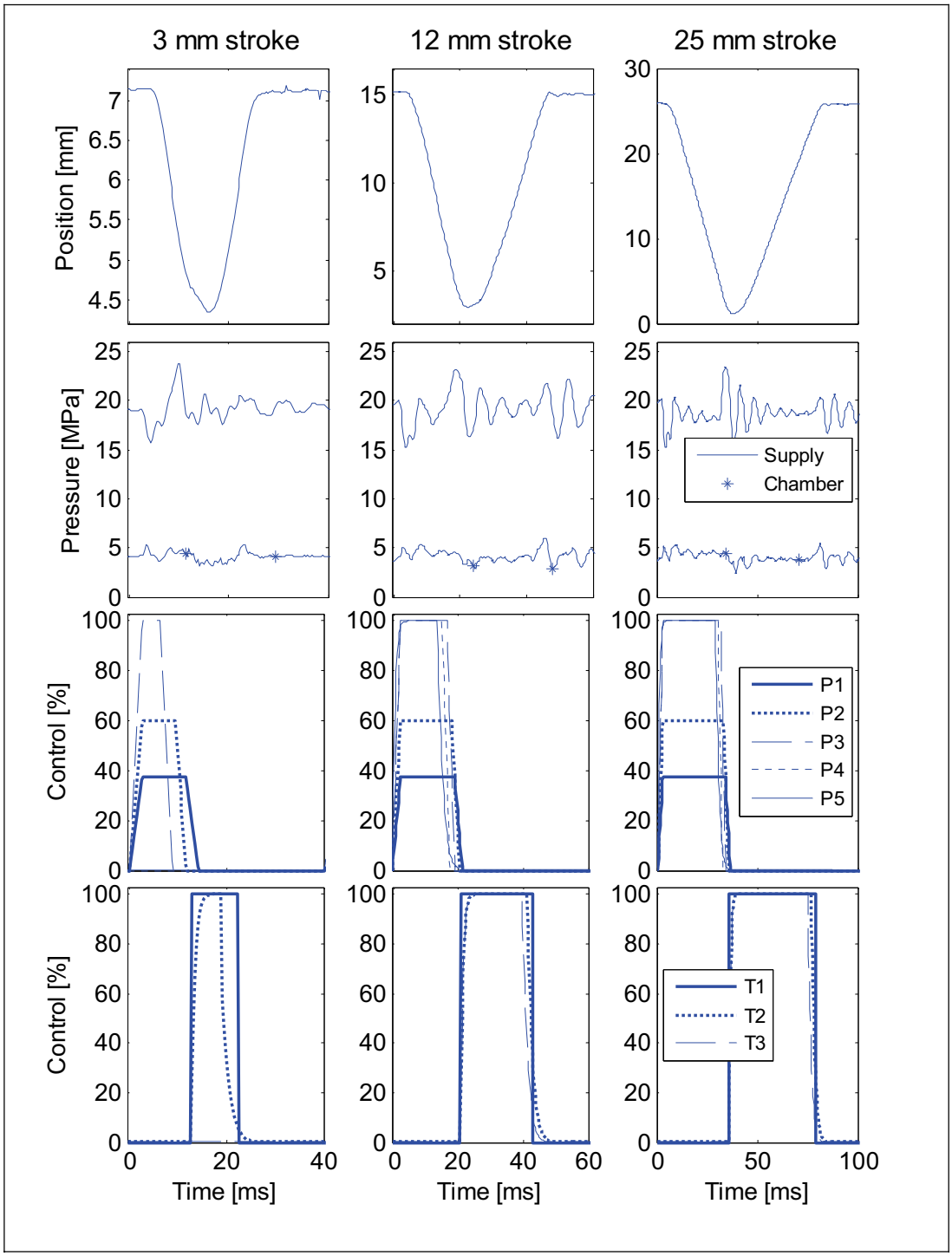

Figure 13. Measurements for digital hydraulic operated system

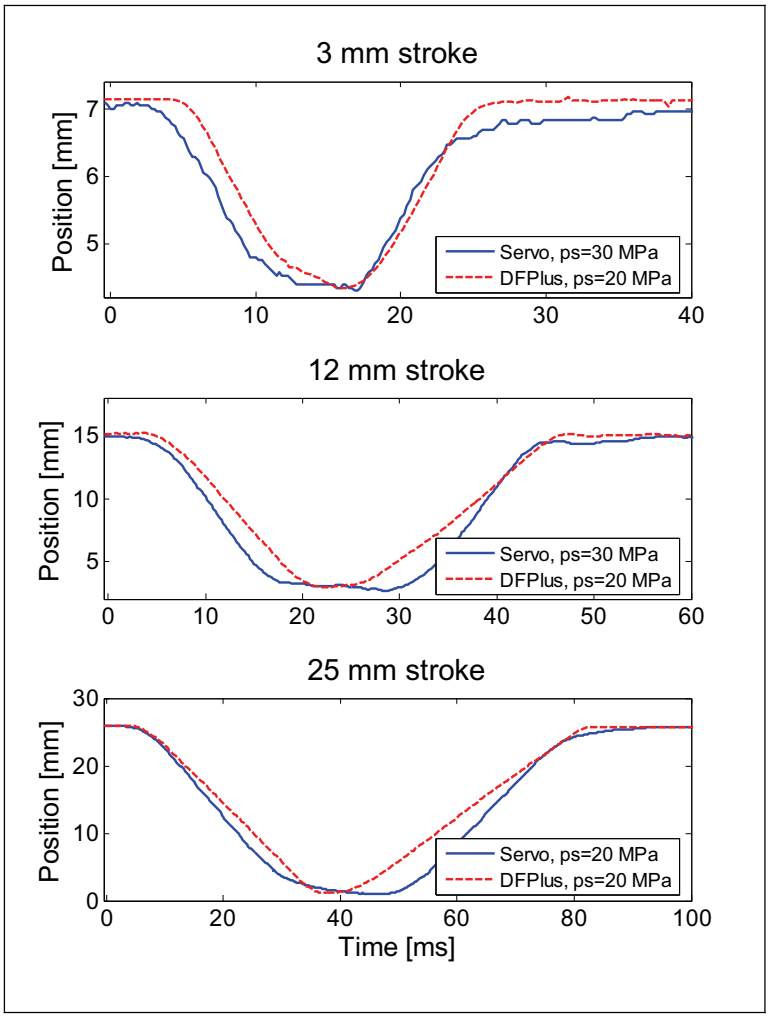

Figure 14. Comparison of position responses for digital hydraulic operated and servo valve operated system.

5 CONCLUSIONS

The results, with digital hydraulic operated system, are promising even though the used valves are relatively slow (~5 ms) when compared to the length of the work cycle. The performance of the system could be improved by faster valves and bigger flow rates. At the moment there are no realistic on/off valves commercially available, with required characteristics.

ACKNOWLEDGEMENTS

The research was supported by the Academy of Finland (Grant no. 80411) and the Finnish Funding Agency for Technology and Innovation (Grant no. 40334/04)

REFERENCES

1 Haikio, S., Huhtala, K., Vilenius, M. & Mäkitalo, J. 2006. Improving efficiency in a linear cyclic motion. In: Johnston, D.N. & Edge, K.A. (eds.)Power Transmission and Motion Control, (PTMC 2006), University of Bath, UK,13-15 September 2006 pp. 15-29.

2 Linjama, M; Laamanen, A.; Vilenius, M. 2003. Is it time for Digital Hydraulics? Proceedings of the Eight Scandinavian International Conference on Fluid Power (SICFP'03), May 7-9 2003, Tampere, Finland.pp.347-366.

3 Siivonen, L., Linjama, M. & Vilenius, M. 2005. Analysis of fault tolerance of digital hydraulic valve system. In: Johnston, D.N., Burrows, C.R. & Edge, K.A. (eds.). Bath Workshop on Power Transmission and Motion Control (PTMC 2005), 7-9 September 2005 pp. 133-146.

4 Laamanen, A., Siivonen, L., Linjama, M. & Vilenius, M. 2004. Digital flow control unit-an alternative for a proportional valve?. Bath Workshop on Power Transmission and Motion Control (PTMC 2004) pp. 297-308.

5 Laamanen, A.; Linjama, M.; Vilenius, M. 2005. Pressure Peak Phenomenon in Digital Hydraulic Systems – a Theoretical Study. Bath Workshop on Power Transmission and Motion Control (PTMC 2005). September 7-9. 2005, Bath, UK. pp.91-104

6 Lallukka, J. 2005. Hydraulisylinterin iskuliikkeen tutkiminen nopeuden muuttuessa. M.Sc.thesis, 2005 Tampere University of Technology (In finnish). 76 pages.

7 Parker Hannifin GmbH, Hydraulic Controls Division. Bulletin HY11-3280/UK, 01/05. http://www.parker.com/euro_hcd/new_web_page/pdf_folder/3280uk.pdf (visited 19.12007)

SYSTEM ANALYSIS AND OPTIMIZATION FOR TRACEABILITY IN DESIGN

Petter Krus
Linköping University
Department of Management and Engineering
SE-58183 Linköping, Sweden
E-mail: petter.krus@liu.se

ABSTRACT

The tendency to integrate different technologies such as mechanical, electrical and fluid subsystems and embedded software, leads to complex systems. More of the engineering effort is therefore placed on system architecture and system integration. It also becomes more important to find and to express requirements more exactly in order to be able to emphasize the right ones, as well as being able to quickly assess the consequences of changing requirements.

In this paper the different representations for design analysis of complex actuation systems are discussed. Sensitivity analysis is a useful tool for trade studies, and to achieve an overview of the importance of different aspects of the design. The introduction of an aggregated design sensitivity matrix greatly improves the ability to handle large systems. In addition an uncertainty influence matrix is used to see the influence of uncertainties in the design and to spot areas where more modelling effort is needed.

Furthermore, there is a functional interaction matrix, derived from the sensitivity analysis, where interaction between function can be studied to disclose conflicting requirements. This is extremely useful in requirement negotiation. Finally, formal ways to establish objective function for optimization is discussed. These tools are demonstrated on a hydraulic system design example..

KEYWORDS: system analysis, optimization, sensitivity analysis, QFD, functional correlation

1. INTRODUCTION

In P Krus, J-O Palmberg [1.] simulation based optimisation was used for component selection and sizing of actuation systems. Although optimisation as such is very useful, it is even more useful when combined with design analysis. The objective of design analysis is to obtain information about the nature of the design solution, and how it can be changed in order to fulfill the requirements, and how requirements can be negotiated

to best fulfill the stakeholder's requirements. Here different matrix methods are useful, since they can be used to display the mapping of relations between system parameters and system characteristics.

The figure below shows the concept development and system level design. This paper focus on the parts indicated as computational design methods. These involve design optimization (quantitative refinement), analysis and evaluation and sensitivity analysis and trade-off analysis.

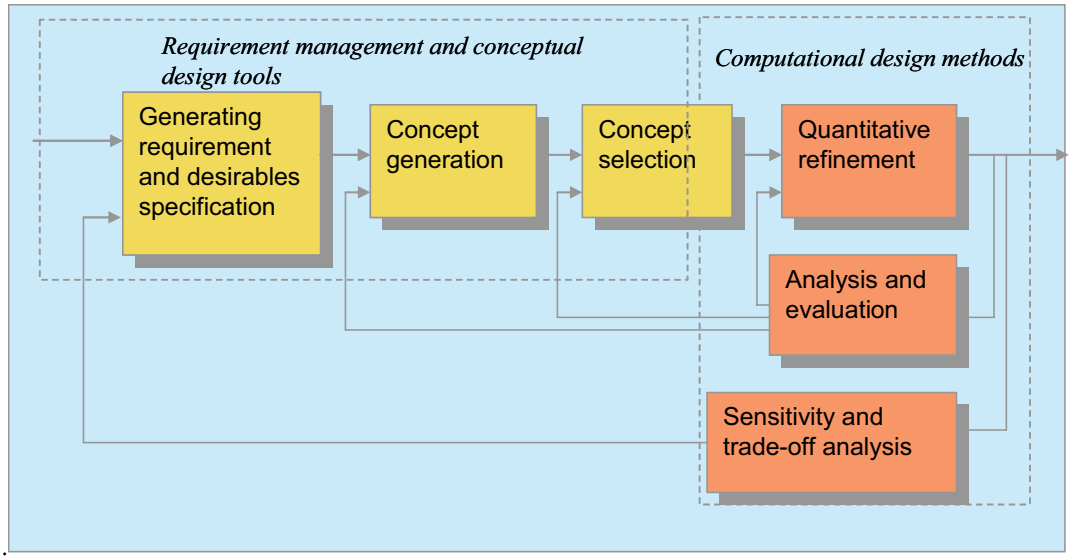

Figure 1. Conceptual design and system level design.

1.1 Requirement specification

Formal methods for establishing the requirements and the desirables of a design are needed in order to ensure the traceability between requirements, desirables and the design. This also involves initial analysis of the value of fulfilling certain customer requirements vs. the cost to do so. This also connects to the post-optimal analysis.

1.2 Concept optimization and selection

Based on computational models, optimisation of different configurations can be carried out. Optimisation has proven to be an extremely useful tool when connected to evaluation models. These can for instance be dynamic simulation models. The advantage with this approach is that it allows the designer to optimize complex non-linear systems in a convenient way, directing the designer's effort to the requirements and system objectives rather than to the actual computation of system parameters.

1.3 Computational models

In order to evaluate different concepts, models at an adequate level of details have to be established. This is a very important task since the design becomes no more accurate than the underlying models. One of the most important shifts in paradigm occurring in engineering system design may well be the adoption of common system models as a foundation for system design. Efficient models for complete aircraft systems simulation

can be established using newly developed tools, where complete systems can be simulated more or less in real time. This allows for a much more effective product development process since a system can be tested in all stages of design.

1.4 Sensitivity analysis for traceability in design

These techniques are very closely tied to the requirement specification and they involve the estimation of sensitivities between design parameters and the functional characteristics. This can also be generalised to estimate the influence of aggregates of parameters, such as whole subsystem on requirements. This can be presented as an aggregated design impact matrix. Sensitivities can also be generalised to involve higher order functions, such as quadratic, which means that approximate analytical expression for the relations between design parameters and functional characteristics. This is a valuable tool for studying parameter variations around a design point when the actual underlying models are computer intensive. It is this activity that really ties the top-level requirements and desirables to the low-level detail design.

2. TOOLS

2.1 House of quality

The house of quality is a matrix method for mapping customer needs to system requirements See Hauser, and Clausing [2.]. It was originally proposed by Taguchi as part of total quality deployment TQM. In Andersson et al [3.] this was applied for formalizing the establishment of objective functions of a hydraulic landing gear system. It can of course be used to map any domains against each other but traditionally it is directed towards customer needs. In this paper the house of quality is used to provide trace-ability in a quantitative way between individual design decisions/design parameters and customer requirements.

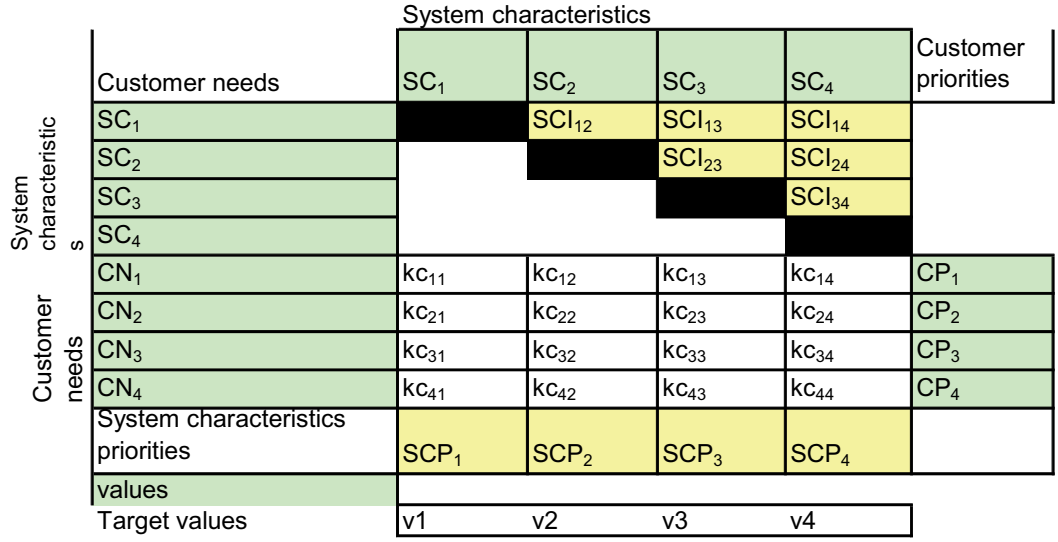

Figure 2. The "House of quality" (or QFD-matrix). The roof is tilted in order to be able to be presented in a spread sheet.

Table 1. The "House of quality" (or QFD-matrix). The roof is tilted in order to be able to be presented in a spread sheet.

Here the system requirements priorities can are calculated as:

$$SCP_i = \sum ks_{ij} CP_j \tag{1.1}$$

which can also be written as:

$$\mathbf{scp} = \mathbf{Ks}^{\mathbf{T}}\mathbf{cp} \tag{1.2}$$

The roof of the house-of-quality displays the interaction between system characteristics. The quantitative evaluation of these from is showed later in this paper.

2.1 Design matrices

In design, matrices can be used to describe the relationship between some design parameters that are to be determined and some aspects of the system behaviour. The notation design parameters are used by Nam P Suh, [4.]. Here the term design parameters are used for the parameters that can be manipulated, while the term system characteristics are used for all parameters that describe the product. The behaviour of the system is called functional requirements, FR, by Suh. Here the notation system characteristics is used. This is a little broader since it covers all aspects of behaviour and properties of the product. There might be cases where there might be some ambiguity to what is a design parameter and a system characteristics, but here it is simply a function of what is the input and what is output from a system analysis.

The relationship between input variables and output variables can be written as:

$$\mathbf{y} = \mathbf{Ax} \tag{1.3}$$

where A is a matrix and x is a vector that is mapped into y through A. This does of course assume linear relationships to be true.

This can be displayed in a table form derived from the QFD-matrix where the system characteristics are used for y and system parameters are used for x .

	System components/parameters				
System characteristics	X_1	X_2	X_3	X_4	System characteristics priorities
SC_1	k_{11}	k_{12}	k_{13}	k_{14}	SCP_1
SC_2	k_{21}	k_{22}	k_{23}	k_{24}	SCP_2
SC_3	k_{31}	k_{32}	k_{33}	k_{34}	SCP_3
SC_4	k_{41}	k_{42}	k_{43}	k_{44}	$SRCP_4$
Component priorities	XP_1	XP_2	XP_3	XP_4	

Figure 3. The sensitivity matrix, with calculation of component priorities.

Here component priorities can be calculated as:

$$\mathbf{xp} = \mathbf{K}^{T}\mathbf{scp} \tag{1.4}$$

Here K is really the sensitivity matrix (defined later in the next section). This representation can also be seen as another representation of the design matrix since

$$\mathbf{sc} = \mathbf{Kx} \tag{1.5}$$

if the system is linear. As an example the QFD-matrix of a pressure controlled hydraulic pump is shown.

Design Analysis

QFD Matrix

2007-03-13
10:55:10

System characteristics

Customer requirements	Max flow	Max pressure	Energy loss	Noise	Stability	Max static pressure error	Max dynamic pressure error	Settling time	Weight	Cost	Customer req. priorities
High power	9	9									1.00
Fast response					9		3	9			1.00
Accurate					3	9					0.75
Reliable		3		3	9		3				1.25
Economical			9						1	9	1.00
Sign	1	1	-1	-1	1	-1	-1	-1	-1	-1	
Demand or whish	1	1	0	0	0	0	0	0	0	0	
Units	m3/s	Pa				Pa	Pa	s	kg	Euro	
Target values	0.00	5.00E+07	100.00	1.00	0.10	1.00E+05	5.00E+06	1.12	15.00	1500.00	
System char. priorities	9.00	12.75	9.00	3.75	22.50	6.75	6.75	9.00	1.00	9.00	

Figure 4. QFD matrix for pressure controlled hydraulic pump.

2.2 Sensitivity analysis

Sensitivity analysis is an excellent tool to study relationships between system parameters and system characteristics. It can quickly give an overview over what parts of the design that is important of the desired behaviour. Furthermore it can be used to study the influence of disturbances and uncertainties in parameters and constants. Sensitivity analysis is the primary tool for studying the degree of robustness in a system. Assuming the system:

$$\mathbf{y} = \mathbf{f(x)} \tag{6}$$

where f is a nonlinear function. However, using linearization around a nominal point, this can be written as

$$\mathbf{y_0} + \mathbf{\Delta y} = \mathbf{f(x_0)} + \mathbf{J\Delta x} \tag{7}$$

where J is the Jacobian, where

$$J_{ij} = \frac{\partial f_i(x)}{\partial y_j} \tag{8}$$

hence

$$\mathbf{\Delta y} = \mathbf{J\Delta x} \tag{9}$$

here the Jacobian J is also identical to the sensitivity matrix k The elements in the sensitivity matrix can also be expressed as:

$$k_{ij} = \frac{\partial y_i}{\partial x_j} \tag{10}$$

Example, pressure controlled pump

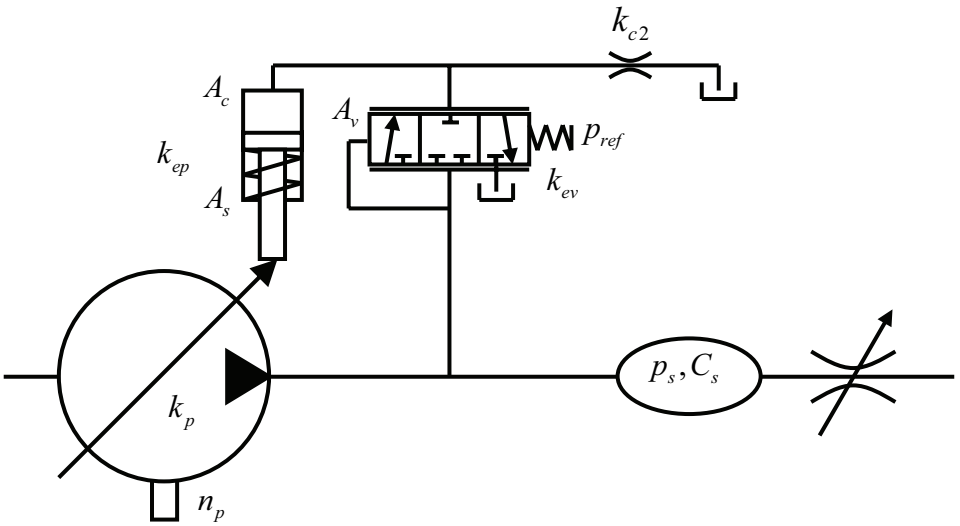

Figure 5. Pressure controlled pump.

As an illustrative example a simple model of a pressure controlled pump is analysed. The model derivation for this system can be found in for example Palmberg et al The model is made in Excel where analytical expressions are used to estimate various characteristics, but it can also use modules located on other computers through web-service technology through the Modelith model integration network, see Johansson, Jouannet and Krus [5.], which could be a combination of simulation models and other models. The relevant system parameters (parameters that are of interest to vary) are organized hierarchically on one worksheet.

System group	System group	System group	System parameter	Value	Unit	Type	Comment
PcPump	pump	pump	Dp	5.00E-05	m3/rev	DP	Displacement
PcPump	pump	pump	Np	7	m		Number of pistons
PcPump	pump	pump	Kcp	8.00E-13	m	UP	Leakage
PcPump	pump	pump	Vext	0.002013906		DP	External volume
PcPump	pump	pump	rhomean	5.00E+03	kg/m3	UP	Pump mean density
PcPump	pump	pump	Pmean	300000	Pa	UP	Structural Mean pressure
PcPump	pump						
PcPump	*pump*						
PcPump	regulator	valve	dv	4.00E-03	m	DP	Spool diameter
PcPump	regulator	valve	xvmax	0.018919557		DP	Spool stroke
PcPump	regulator	valve	wv	2.76E-04		DP	Area gradient
PcPump	regulator	valve	Cq	6.70E-01		UP	
PcPump	regulator	valve	Kev	3.93E+04	N/m	DP	Spring constant
PcPump	regulator	valve	thauv	5.00E-02	s	UP	time constant
PcPump	regulator	valve	Kc1	0.00E+00	m5/Ns	DP	Regulator leakage
PcPump	regulator	valve					
PcPump	regulator	actuator	dc	0.028184383	m	DP	
PcPump	regulator	actuator	fracdr	0.72	m	DP	Regulator piston area
PcPump	regulator	actuator	Kep	1.00E+03	N/m	DP	Regulator leakage
PcPump	regulator	actuator	Kc2	1.10E-12	m5/Ns	DP	Regulator leakage
PcPump	regulator	actuator	Kp	3.26E-03	m2/rev	DP	Regulator gain
PcPump	regulator	actuator					
PcPump	regulator	regulator	Ps	2.00E+07		UP	
PcPump	*regulator*						
PcPump			n	25	rev/s	UP	Pump speed
PcPump							
System	System	System	Vs	0.001	m3	UP	Volume
System	System	System	betha	1.00E+09	Pa	UP	Compressib
System	System	System	rho	855	kg/m3	UP	Mission
System							
Load	Load	Load	KcL	1E-12	m5/Ns	UP	Valve
Load	Load	Load	PL	5.00E+06	Pa	UP	Load pressure
Load							

Table 1. Worksheet with relevant system parameters.

The system characteristics are displayed on another worksheet where the results from the different model modules are linked.

System characteristics	Target values	Formula	Unit	Relative model uncertainty	Direction	D (1) or W (0)
Max flow	1.25E-03	0.00125	m3/s	0.10	1	D
Max pressure	5.00E+07	1.21E+07	Pa	0.10	1	D
Energy loss	100.00	548.096		0.10	-1	W
Noise	1.00	1.687592818		0.10	-1	W
Stability	0.10	0.501708565		0.10	1	W
Max static pressure error	100000.00	125.8611073	Pa	0.10	-1	W
Max dynamic pressure error	5000000.00	23943062.21	Pa	0.10	-1	W
Settling time	1.12	0.099077254	s	0.10	-1	W
Weight	15.00	10.0695277	kg	0.10	-1	W
Cost	1500.00	1006.95277	Euro	0.10	-1	W

Table 2. Table of system characteristics with links to models. Here the relative model uncertainty can be provided for use in robustness analysis.

Normalised sensitivities

If the system is complex and the sensitivity matrix large, it may be difficult to get an overview of the system since the different parameters may have values of different orders of magnitude. The system characteristics are normally also of different orders of

magnitude. In order to make it easier to get an overview of the sensitivities, some kind of normalised dimensionless sensitivities is needed. The first approach to normalise the sensitivities is to employ the following definition

$$k_{ij}^{0} = \frac{x_{s,j}}{y_{s,i}} \frac{\partial y_{s,i}}{\partial x_{s,j}} \tag{11}$$

In this way a non-dimensional value is obtained, that indicates how many percent a certain system characteristic is changed when a system parameter is changed one percent. In this way it is much easier to assess the relative importance of the different system parameters. Using this approach the following table is obtained.

Aggregated normalized sensitivity matrix

It is obvious that if the number of parameters is increased substantially as a design becomes more detailed, the overview is quickly lost. However, since normalised sensitivities are used, it is possible to aggregate all parameters associated with one component by simply adding them together. This has, however the drawback that different sign in sensitivities may cancel each other out. Therefore it is better to add the absolute values of all sensitivities instead. This will at least give a value to the relative importance and hence the magnitude of impact from design changes in a component or subsystem to the different system characteristics.

				PcPump	PcPump	PcPump	PcPump	PcPump	PcPump	PcPump	PcPump	PcPump	PcPump
				pump	regulator	regulator	regulator	regulator	regulator	regulator	regulator	regulator	
					valve	valve	valve	valve	valve	valve	actuator		
					dv	xvmax	wv	Kev	Kc1				
System characteristics	Unit	Target value	Actual value		0.00	0.02	0.00	39300.00	0.00				
Max flow	m3/s	0.00	0.00	**1.00**	0.00	0.00	0.00	0.00	0.00	**0.00**	**0.00**	**0.00**	**1.00**
Max pressure	Pa	5000000.00	12083433.25	**2.10**	0.00	0.00	0.00	0.00	0.00	**0.00**	**0.00**	**0.00**	**2.10**
Energy loss		100.00	548.10	**0.00**	0.00	0.00	0.00	0.00	0.00	**0.00**	**0.87**	**0.87**	**0.87**
Noise		1.00	1.69	**0.00**	0.00	0.00	0.00	0.00	0.00	**0.00**	**0.53**	**0.53**	**0.53**
Stability		0.10	0.50	**0.00**	0.91	0.00	0.47	-0.48	0.00	**1.86**	**2.87**	**4.73**	**4.73**
Max static pressure error	Pa	593917.00	125.86	**1.00**	-2.08	0.00	-1.11	1.00	0.00	**4.18**	**7.74**	**11.92**	**12.92**
Max dynamic pressure error	Pa	117250715.00	23943062.21	**1.00**	-0.70	0.00	-0.36	0.36	0.00	**1.42**	**3.19**	**4.61**	**5.61**
Settling time	s	1.12	0.10	**0.00**	-1.98	0.00	-1.06	0.95	0.00	**3.99**	**0.80**	**4.79**	**4.79**
Weight	kg	15.00	10.07	**1.00**	0.00	0.00	0.00	0.00	0.00	**0.00**	**0.00**	**0.00**	**1.00**
Cost	Euro	1500.00	1006.95	**1.00**	0.00	0.00	0.00	0.00	0.00	**0.00**	**0.00**	**0.00**	**1.00**

Figure 6. Aggregated normalized sensitivity matrix. The matrix is expanded for the regulator parameters. The sum of the absolute values is presented in a column to the right of the subsystem values.

This suggests that the aggregated sensitivities of components and subsystems is a good measurement of the design impact of that component/subsystem and is rather independent of the degrees of details, and degrees of freedoms in the model. The aggregated normalized sensitivity matrix therefore seems to be an excellent tool to ensure that the design efforts are properly balanced in the ensuing design steps, by identifying critical areas at an early stage of the design. The matrix can also be updated and maintained throughout the design process as the degrees of details in the design are increasing and the underlying models get more detailed. Furthermore, the same simple structure can be used at the top level even for the finished products, while more detailed information can be found at lower levels.

Influence of disturbances

The influence of disturbances can be studied in a couple of ways. First, it is possible to study the sensitivities in the same way as from design variables. The other way is to study the influence of removing the uncertainty of one uncertainty variable. The uncertainty of a system characteristic can be calculated as:

$$s_{y,i} = \sqrt{k_{u,i,1}^2 s_{x,u,1}^2 + k_{u,i,2}^2 s_{x,u,2}^2 .... + k_{u,i,3}^2 s_{x,u,3}^2} \tag{12}$$

where s is the standard deviation. The normalized influence of the uncertainties is calculated

$$\Delta s_{0,y,ij} = \frac{s_{y,u,i}}{y_i}\left(1 - \sqrt{\frac{s_{y,u,i}^2 - k_{u,i,1}^2 s_{x,u,ij}^2}{s_{y,i}^2}}\right) \tag{13}$$

This matrix indicates the effect of totally removing the uncertainty of an uncertainty variable on specific system characteristics. This is extremely useful to balance the fidelity of models for different areas of a design. Due to the nature of these expressions, small uncertainties are quickly shadowed by larger uncertainties. This means that it is meaningful only to reduce the dominating uncertainties. In the example shown in Table 7, the influence on range from the properties of the wing is totally shadowed by the uncertainties in airframe (weight calculations) , the propulsion, and the model uncertainty. This provides a valuable tool for allocating resource in the right areas, in order to reduce uncertainty in the system characteristics. Without this kind of tool it is a high risk that the department with the highest status and prestige will be able to argue most successfully for resources.

				Kcp	rhomean	Pmean	Cq	thauv	Ps	n	Vs	betha	rho	KcL	PL	Model uncertainty
System characteristics	Units	Deviation	Normalized deviation	0.00	0.10	0.10	0.30	0.10	0.50	0.20	0.70	0.70	0.10	0.00	1.00	
Max flow	m3/s	0.00	0.22	0.07	0.07	0.07	0.07	0.07	0.07	0.15	0.07	0.07	0.07	0.07	0.07	0.10
Max pressure	Pa	1708855.52	0.14	0.00	0.00	0.04	0.00	0.00	0.00	0.00	0.00	0.00	0.00	0.00	0.00	0.10
Energy loss		687.31	1.25	0.00	0.00	0.00	0.00	0.00	1.15	0.00	0.00	0.00	0.00	0.00	0.00	0.10
Noise		0.86	0.51	0.00	0.00	0.00	0.00	0.00	0.41	0.00	0.00	0.00	0.00	0.00	0.00	0.10
Stability		0.22	0.44	0.00	0.00	0.00	0.02	0.00	0.01	0.01	0.07	0.12	0.00	0.00	0.00	0.10
Max static pressure error	Pa	39.58	0.31	0.00	0.00	0.00	0.10	0.00	0.06	0.00	0.00	0.00	0.00	0.00	0.00	0.10
Max dynamic pressure error	Pa	14069588.43	0.59	0.00	0.00	0.00	0.01	0.00	0.00	0.00	0.07	0.27	0.00	0.00	0.00	0.10
Settling time	s	0.09	0.87	0.00	0.00	0.00	0.03	0.00	0.02	0.00	0.35	0.10	0.00	0.00	0.00	0.10
Weight	kg	1.42	0.14	0.00	0.04	0.00	0.00	0.00	0.00	0.00	0.00	0.00	0.00	0.00	0.00	0.10
Cost	Euro	142.40	0.14	0.00	0.04	0.00	0.00	0.00	0.00	0.00	0.00	0.00	0.00	0.00	0.00	0.10

Figure 7. Hierarchical robustness matrix indicating the the influence of uncertainties on system characteristics from uncertainties in system parameters and models.

Dependencies between system characteristics

In a design the different system characteristics may be conflicting or more or less pulling in the same direction. Information about this is very useful when setting up the requirements for a design since it can show what areas that can be improved without scarifying to much in other areas, or to see what areas that might be worth sacrificing in order to improve others. A simple measure of this is the systems characteristics dependency matrix, SCD. The elements are here defined as:

$$SCD_{ik} = \sum_{j=1}^{m} k_{ij}^0 k_{kj}^0 \tag{14}$$

SCD is always a symmetric matrix. The diagonal element represents a measure of how sensitive, or "controllable", a system characteristic is with respect to the design parameters.

System Characteristics		Max flow	Max pressure	Energy loss	Noise	Stability	Max static pressure error	Max dynamic pressure error	Settling time	Weight	Cost
		1.25E-03	1.21E+07	5.48E+02	1.69E+00	5.02E-01	1.26E+02	2.39E+07	9.91E-02	1.01E+01	1.01E+03
Max flow	1.25E-03	1.00	-1.10	0.00	0.00	0.00	1.00	1.00	0.00	0.00	0.00
Max pressure	1.21E+07	-1.10	2.21	0.00	0.00	0.00	-1.10	-1.10	0.00	1.00	1.00
Energy loss	5.48E+02	0.00	0.00	0.76	-0.46	1.18	2.98	1.00	-0.69	0.00	0.00
Noise	1.69E+00	0.00	0.00	-0.46	0.28	-0.73	-1.83	-0.61	0.43	0.00	0.00
Stability	5.02E-01	0.00	0.00	1.18	-0.73	4.40	0.03	2.29	-3.85	0.00	0.00
Max static pressure error	1.26E+02	1.00	-1.10	2.98	-1.83	0.03	26.54	4.77	3.50	0.00	0.00
Max dynamic pressure error	2.39E+07	1.00	-1.10	1.00	-0.61	2.29	4.77	5.37	1.19	0.00	0.00
Settling time	9.91E-02	0.00	0.00	-0.69	0.43	-3.85	3.50	1.19	6.60	0.00	0.00
Weight	1.01E+01	0.00	1.00	0.00	0.00	0.00	0.00	0.00	0.00	1.00	1.00
Cost	1.01E+03	0.00	1.00	0.00	0.00	0.00	0.00	0.00	0.00	1.00	1.00

Figure 8. System characteristics interaction, SCD.

There is also the adjusted system characteristics which are where the elements in a row are normalized with respect to the diagonal elements. Furthermore, they are multiplied with the sign φ of the desired direction for a system characteristic, so that if a large value is desirable, or required, the $\varphi = 1$ and if a small value is desirable, or required, $\varphi = -1$.

$$ASCD_{ik} = \varphi_i \varphi_k SCD_{ik} / SCD_{ii} \tag{15}$$

This is an asymmetric matrix. Here the influence of system characteristics in the columns on the system characteristics in the rows is displayed. It can also be coloured so that highly negative interaction is marked with red, and positive interactions are green.

System Characteristics		Max flow	Max pressure	Energy loss	Noise	Stability	Max static pressure error	Max dynamic pressure error	Settling time	Weight	Cost
		1.25E-03	1.21E+07	5.48E+02	1.69E+00	5.02E-01	1.26E+02	2.39E+07	9.91E-02	1.01E+01	1.01E+03
Max flow	1.25E-03	1.00	-1.10	0.00	0.00	0.00	-1.00	-1.00	0.00	0.00	0.00
Max pressure	1.21E+07	-0.50	1.00	0.00	0.00	0.00	0.50	0.50	0.00	-0.45	-0.45
Energy loss	5.48E+02	0.00	0.00	1.00	-0.61	-1.57	3.95	1.32	-0.92	0.00	0.00
Noise	1.69E+00	0.00	0.00	-1.63	1.00	2.56	-6.44	-2.16	1.50	0.00	0.00
Stability	5.02E-01	0.00	0.00	-0.27	0.16	1.00	-0.01	-0.52	0.88	0.00	0.00
Max static pressure error	1.26E+02	-0.04	0.04	0.11	-0.07	0.00	1.00	0.18	0.13	0.00	0.00
Max dynamic pressure error	2.39E+07	-0.19	0.20	0.19	-0.11	-0.43	0.89	1.00	0.22	0.00	0.00
Settling time	9.91E-02	0.00	0.00	-0.11	0.06	0.58	0.53	0.18	1.00	0.00	0.00
Weight	1.01E+01	0.00	-1.00	0.00	0.00	0.00	0.00	0.00	0.00	1.00	1.00
Cost	1.01E+03	0.00	-1.00	0.00	0.00	0.00	0.00	0.00	0.00	1.00	1.00

Figure 9. Adjusted system characteristics dependencies, ASCD.

From this matrix it is possible to see conflicting requirements and what properties that are coherent. For instance, the efficiency and stability are conflicting requirements. This comes from the simple fact that energy losses also allows oscillative energy dissipate. Furthermore, it can be seen that low noise and stability are coherent requirements.

The system characteristics dependencies matrix can also be seen as a quantified "roof" to the QFD-matrix in Table 1. Together they form the well known "house of quality".

Note that there really should be a full matrix rather than just a triangle since the ASCD matrix is asymmetric.
Of course, it could also be possible to use the correlation-coefficient instead, but that is limited to the interval [-1,1], and it is symmetric, so there is no information regarding the dominant direction of dependency.

$$SCC_{ik} = \frac{\frac{1}{n}\sum_{j=1}^{n} k_{ij}^{0} k_{kj}^{0}}{s_i s_k} \tag{16}$$

and an adjusted correlation

$$ASCC_{ik} = \varphi_i \varphi_k \frac{\frac{1}{n}\sum_{j=1}^{n} k_{ij}^{0} k_{kj}^{0}}{s_i s_k} \tag{17}$$

Here the standard deviations in the sensitivities are:

$$s_i = \sqrt{\frac{1}{n}\sum_{j=1}^{n} (k_{ij}^{0})^2} \tag{18}$$

System Characteristics		Max flow	Max pressure	Energy loss	Noise	Stability	Max static pressure error	Max dynamic pressure error	Settling time	Weight	Cost
		1.25E-03	1.21E+07	5.48E+02	1.69E+00	5.02E-01	1.26E+02	2.39E+07	9.91E-02	1.01E+01	1.01E+03
Max flow	0.00	1.00	-0.74	0.00	0.00	0.00	-0.19	-0.43	0.00	0.00	0.00
Max pressure	12083433.25	-0.74	1.00	0.00	0.00	0.00	0.14	0.32	0.00	-0.67	-0.67
Energy loss	548.10	0.00	0.00	1.00	-1.00	-0.65	0.67	0.50	-0.31	0.00	0.00
Noise	1.69	0.00	0.00	-1.00	1.00	0.65	-0.67	-0.50	0.31	0.00	0.00
Stability	0.50	0.00	0.00	-0.65	0.65	1.00	0.00	-0.47	0.71	0.00	0.00
Max static pressure error	125.86	-0.19	0.14	0.67	-0.67	0.00	1.00	0.40	0.26	0.00	0.00
Max dynamic pressure error	23943062.21	-0.43	0.32	0.50	-0.50	-0.47	0.40	1.00	0.20	0.00	0.00
Settling time	0.10	0.00	0.00	-0.31	0.31	0.71	0.26	0.20	1.00	0.00	0.00
Weight	10.07	0.00	-0.67	0.00	0.00	0.00	0.00	0.00	0.00	1.00	1.00
Cost	1006.95	0.00	-0.67	0.00	0.00	0.00	0.00	0.00	0.00	1.00	1.00

Figure 10. Adjusted system characteristics correlation matrix, ASCC.

VIII. Conclusion

In this paper a range of linked design analysis tools are presented that are useful in the design process, this range from a quantized house of quality, to system characteristics correlation. This means that there is a transparent coupling between customer requirements down to design parameters. In particular, the aggregated normalized sensitivity matrix is an excellent tool to represent design dependencies in a complex design by introducing hierarchy and enable traceability between top level requirements down to component parameters. The system characteristics dependencies matrix is also a very useful tool when negotiating requirements. Furthermore, it is shown how it is possible to manage the model fidelity and data uncertainty in such a way that the proper resources are allocated where they have the greatest effect on reducing design uncertainty. All the methods described in this paper are implemented as a plug-in (DAtools) to Excel.

References

[1.] Krus P, A Jansson, J-O Palmberg, 'Optimization Using Simulation for Aircraft Hydraulic System Design', Procedings of IMECH International Conference on Aircraft Hydraulics and Systems, London, UK, 1993
[2.] Hauser, J. R. and D. Clausing "The House of Quality," The Harvard Business Review, May-June, No. 3, pp. 63-73. 1988.
[3.] Andersson J, Pohl J, Krus P: “Design of Objective Functions for Optimization of Multidomain Systems”, ASME Annual Winter meeting, November 15-20, Anaheim, USA. 1998.
[4.] Suh.N P “The Principles of Design”, Oxford University Press 1990.
[5.] Johansson B., Jouannet C. and Krus P. "Distributed Aircraft Simulation and Optimization Using Web Service Technology", Aviation Congress and Exposition, SAE-ACE, Montreal, Canada, 2003, also in SAE 2003 Transactions Journal of Aerospace.
[6.] Palmberg J-O, P. Krus, D, Kangzhi, “Dynamic Response characteristics of pressure control pumps. International Conference on Fluid power, Hangzhou, China, 1985

THE EFFECT OF PUMP EFFICIENCY ON DISPLACEMENT-CONTROLLED ACTUATOR SYSTEMS

Christopher Williamson
Monika Ivantysynova
Purdue University
Dept. of Agricultural and Biological Engineering
225 S. University Street
West Lafayette, IN 47907-2093
Phone +1 765 742 1213, Fax +1 765 742 1217
E-mail: williaca@purdue.edu, mivantys@purdue.edu

ABSTRACT

One of the continuing trends in mobile hydraulic systems is the pursuit of higher energy efficiency. Displacement-controlled actuation reduces fuel consumption by eliminating throttling losses and allowing energy recovery. This paper examines the relationship between the efficiency of the pump and the entire hydraulic system using a pump-controlled skid-steer loader as a sample application. Detailed empirical loss models for two different axial piston pumps were used in dynamic simulations of typical loader duty cycles. The effect of the pump loss characteristics on the total energy consumption of the hydraulic system was quantified. Differences in pump efficiency were found to have a significant impact on total energy consumption, particularly at low displacements and pressures.

KEYWORDS: pump efficiency, displacement control, pump-controlled actuation

1 INTRODUCTION

1.1 Throttleless Actuation Systems

A great deal of research has been conducted in recent years to improve the efficiency of hydraulic components and systems, resulting in significant reductions in energy consumption. One topic of interest for mobile applications is the development of resistance-free or "throttleless" circuits, in which control valves are eliminated along with the power losses that are inherent to resistance control. Multiple concepts have been developed, as shown in the tree in Fig. 1. These include circuits based on variable displacement pumps and motors (displacement control), fixed displacement, speed-controlled pumps (known as electrohydraulic actuator systems or EHA) and hydraulic transformers.

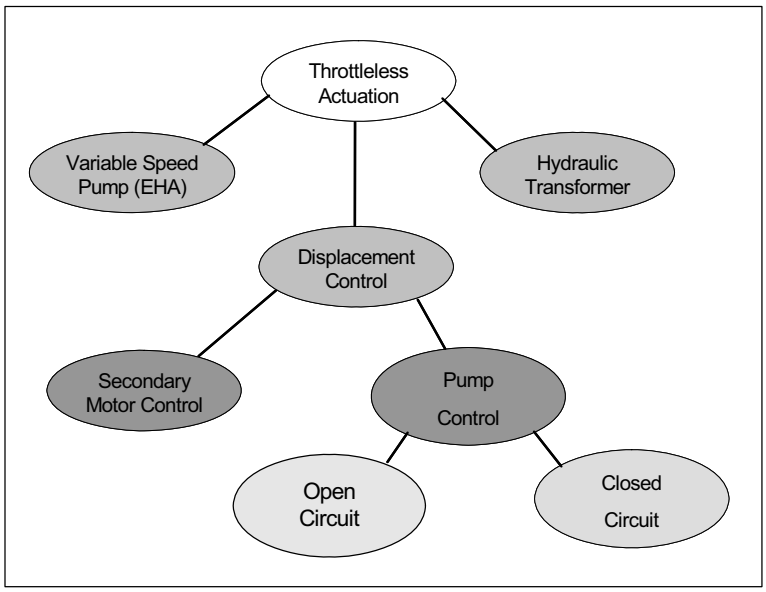

Fig. 1: Throttleless actuator control concepts

For mobile applications, displacement control has been demonstrated to be a promising alternative to traditional valve-controlled systems. A displacement controlled circuit was developed by Rahmfeld and Ivantysynova [1,2] utilizing pilot-operated check valves and a low pressure charge line to compensate for the differential volumetric flow across a single rod cylinder (shown in Fig. 2).

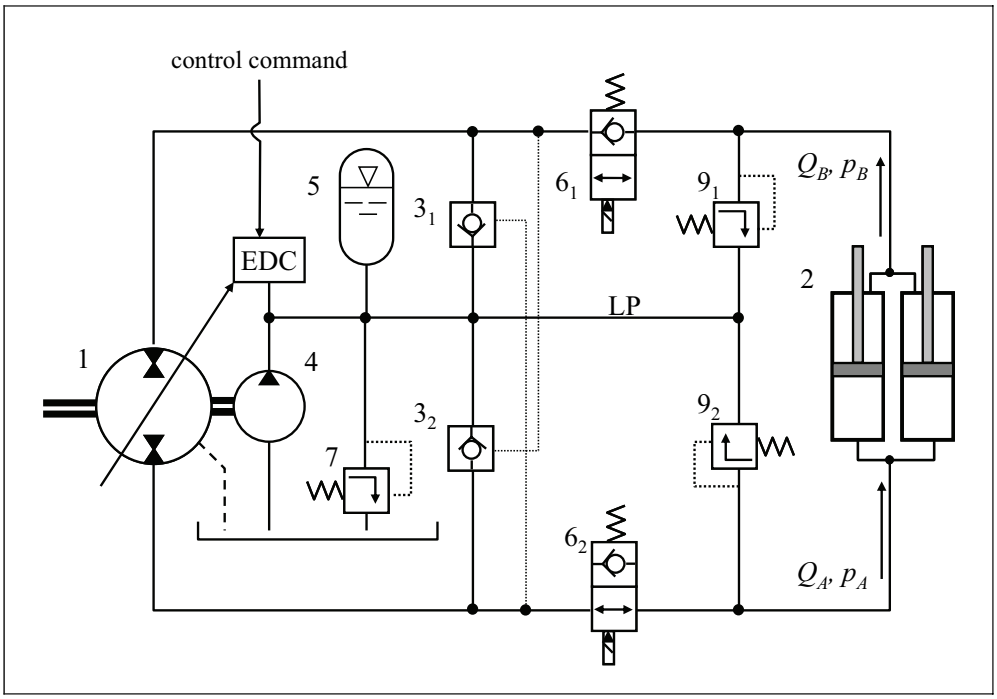

Fig. 2: Closed-circuit displacement control schematic

This circuit has the advantages of eliminating throttling losses as well as recovering energy from aiding load cases by allowing the pump to operate in motoring mode. A recent related concept has been presented by Heybroek et al. which allows for pump-controlled actuation based on an open hydraulic circuit [3].

This paper focuses on systems based on the closed-circuit displacement control concept. While the aims of this work could be satisfied using other throttleless concepts, closed-circuit displacement control has been successfully proven in several prototype

applications and lends itself well to a discussion of energy efficiency with respect to components and systems. In the remainder of this work, the terms "displacement control" and "pump-controlled" are used interchangeably to refer to fluid power systems based on closed circuit displacement control.

1.2 Pump-Controlled Wheel Loader

Past research projects have focused on developing pump-controlled actuation for wheel loaders. One prototype demonstrated energy savings of 15% for a typical duty cycle when compared to a standard loader with LS hydraulics [4]. The pump-controlled prototype also matched or beat the standard machine with respect to speed, accuracy, and operator feel.

Fig. 3: Pump-controlled wheel loader based on O&K 15.5

While the evolution in mobile fluid power systems from valve control to pump control is a significant step forward, there is still much progress to be made in improving energy efficiency. The next logical step for pump-controlled systems is to focus on reducing losses from the pump itself. The purpose of this paper is to examine the effect that improvements in pump efficiency have on the efficiency and energy consumption of the entire system. This is accomplished by comparing two pumps that are of similar size and specifications but have different loss characteristics. Detailed models of these sample pumps were created and used to simulate typical working cycles of a mobile machine. The simulated energy consumption of the mobile system with each pump is then compared quantitatively. It is hoped that these results will serve to motivate and justify efforts to improve the efficiency of hydraulic pumps and motors for mobile applications.

2 PUMP EFFICIENCY CHARACTERISTICS

2.1 Measuring Pump Losses

The physical effects related to frictional and volumetric losses in hydrostatic pumps are quite complex, necessitating an empirical approach for accurately representing loss characteristics without a great deal of computational effort. Consequently, experimental loss data was obtained and used to create a mathematical model for use in simulation.

The international standard for measuring losses and steady-state performance for hydrostatic pumps and motors are given by ISO 4409. The standard calls for careful control and measurement of speed, pressure, oil temperature, and volumetric flow rates. The derived displacement volume V_i of the pump is calculated from these measurements and used to calculate volumetric and torque losses based on measured values. The standard procedure for calculating the derived displacement volume is specified by ISO 8426, in which V_i is calculated for constant pressure. However, the Toet method (in which V_i is calculated for constant speed) has been shown to be more accurate for estimating the displacement volume [5-7]. The Toet method was used for the calculations in this work.

For this study, the steady-state performance characteristics of two axial piston type, variable displacement pumps were measured. They will be referred to simply as Pump A and Pump B, and have maximum displacements of 46 and 42 cc/revolution respectively. Measurements were made across the performance range for each combination of displacement, speed and pressure. Table 1 lists these measurement points, indicating that a total of 336 separate operating points were measured for Pump A and 462 points for Pump B.

Table 1: Steady-state measurement points

	Parameter	Symbol	Unit	Values
Pump A, Pumping mode	Displacement	β	[%]	0, 20, 40, 60, 80, 100
	Pressure	Δp	[bar]	25, 50, 100, 150, 200, 250, 300, 350
	Speed	n	[rpm]	50, 500, 1000, 1500, 2000, 2400, 2800
Pump B, Pumping mode	Displacement	β	[%]	0, 20, 40, 60, 80, 100
	Pressure	Δp	[bar]	20, 50, 100, 200, 300, 400, 450
	Speed	n	[rpm]	200, 500, 1000, 2000, 3000, 4000
Pump B, Motoring mode	Displacement	β	[%]	0, 20, 40, 60, 80, 100
	Pressure	Δp	[bar]	20, 50, 100, 200, 300, 400, 450
	Speed	n	[rpm]	500, 1000, 2000, 3000, 4000

Since motoring mode data was not available for Pump A, the performance in pumping mode was assumed to be the same as motoring. This assumption did not introduce significant errors into the simulation results, as will be explained later in more detail.

2.2 Modeling Pump Losses

Once the pump performance was measured, a mathematical model was created based on polynomial interpolation of the measured data points. Coefficients K_M and K_Q describe the torque and volumetric losses as functions of displacement, speed and pressure. These coefficients are obtained by fitting a least-squares surface to the measured data. Pump losses for any point in the measurement range can then be obtained using Eq. 1 and 2, where i_1, i_2, and i_3 represent positive integer exponents. The process of computing a best-fit polynomial from the measurement data was performed by the POLYMOD program, as described by Mikeska in [8].

$$M_S\left(V_i, n, \Delta p\right)_{T=\text{constant}} = \sum_{i_1=0}^{I_1}\sum_{i_2=0}^{I_2}\sum_{i_3=0}^{I_3} K_M\left(i_1, i_2, i_3\right)\cdot V_i^{i_1}\cdot n^{i_2}\cdot \Delta p^{i_3} \qquad (1)$$

$$Q_S\left(V_\mathrm{i}, n, \Delta p\right)_{\mathrm{T=constant}} = \sum_{i_1=0}^{I_1}\sum_{i_2=0}^{I_2}\sum_{i_3=0}^{I_3} K_\mathrm{Q}\left(i_1, i_2, i_3\right) \cdot V_\mathrm{i}^{i_1} \cdot n^{i_2} \cdot \Delta p^{i_3} \tag{2}$$

One of POLYMOD's useful features is surface visualization using 3D plots. Since the pump losses and efficiency are functions of three variables (namely n, β, and Δp), the interpolating polynomial describes a four-dimensional surface. Thus, 3D plots can only be generated by fixing one of the parameters. For many mobile applications, including wheel loaders, the engine speed (and consequently pump speed) stays relatively constant during operation. Speed n is held constant for the plots given here. Fig. 4 through Fig. 8 allow the two sample pumps to be compared with respect to losses and total efficiency. In these plots, the points represent actual measurement values, while the surface describes the best-fit polynomial. It can be seen that the volumetric losses for Pump A are approximately twice those of Pump B, resulting in power losses that are more than 50% higher for Pump A. In terms of efficiency, the total efficiency of Pump A reaches a maximum at about 85%, while Pump B is up to 90% efficient for the given conditions. The two-dimensional plots in Fig. 8 represent the same information as in Fig. 7, but in a form that more easily allows a quantitative comparison. It is apparent from these figures that the total efficiency of Pump A is approximately 5% less than Pump B across most of the operating range, dropping off a somewhat sooner than Pump B for low pressures and displacements.

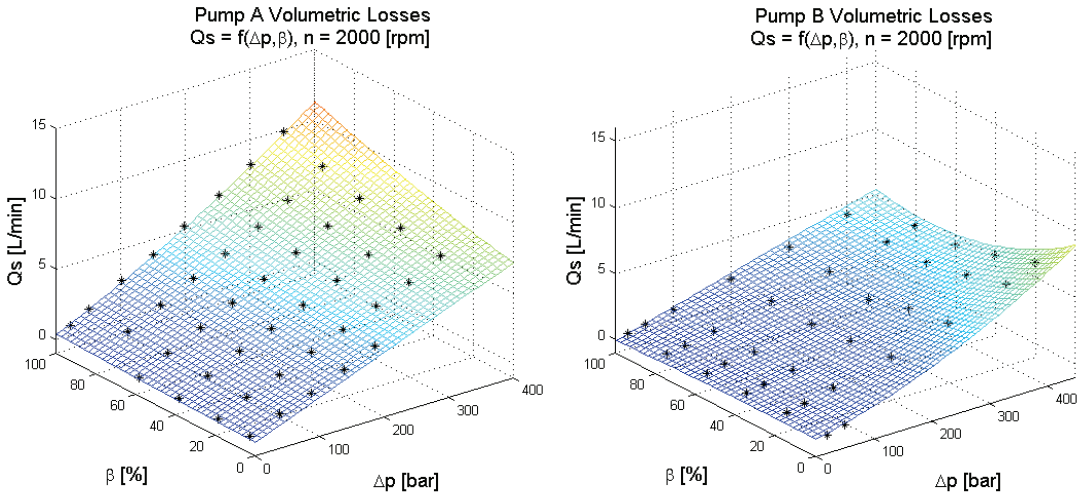

Fig. 4: Comparison of volumetric losses

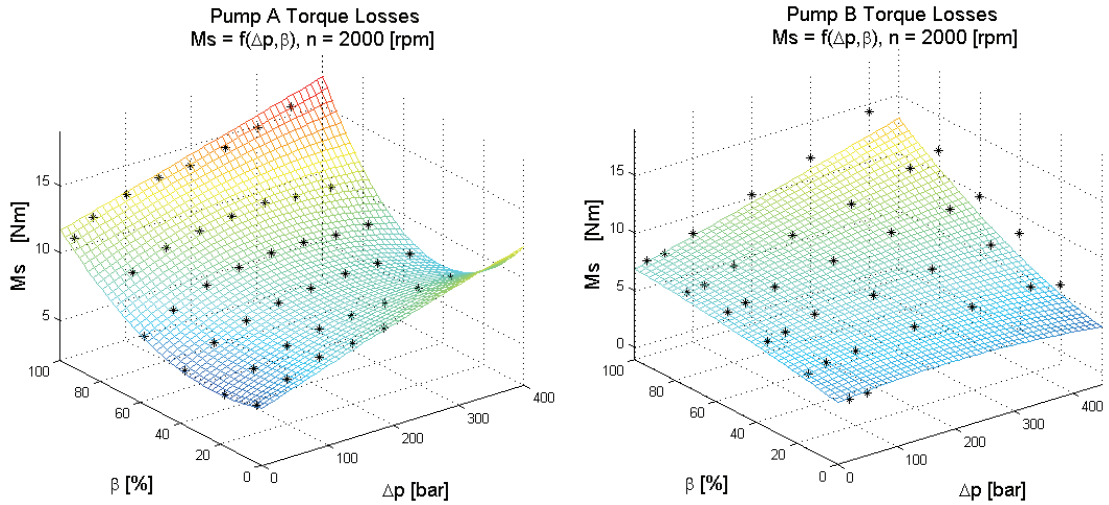

Fig. 5: Comparison of Torque Losses

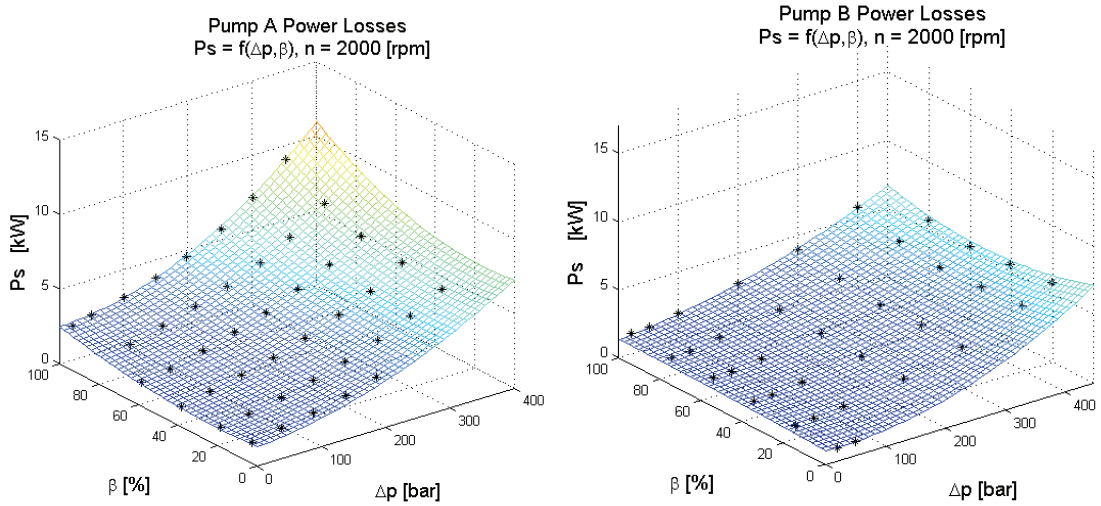

Fig. 6: Comparison of Power Losses

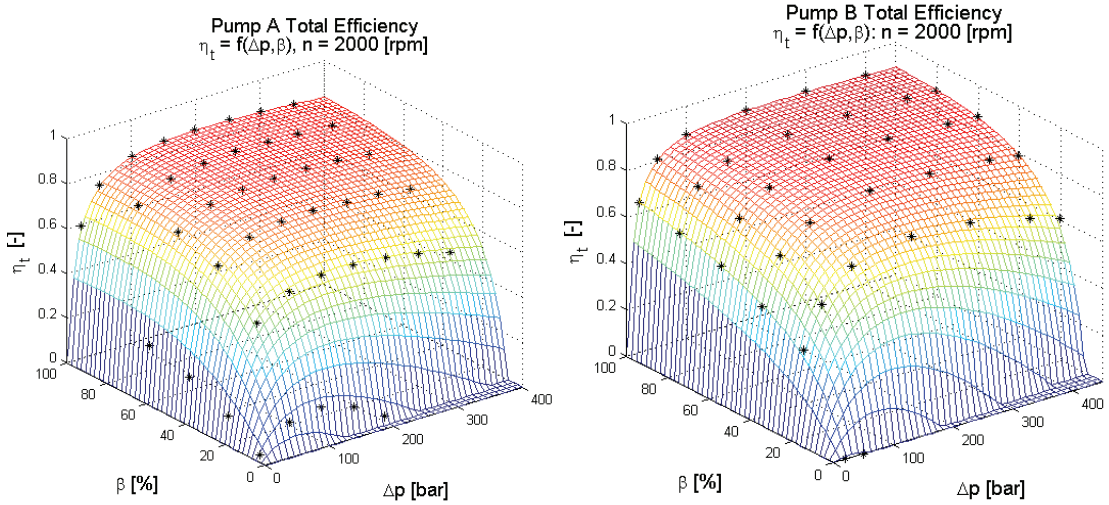

Fig. 7: Comparison of total pump efficiency, surface plots

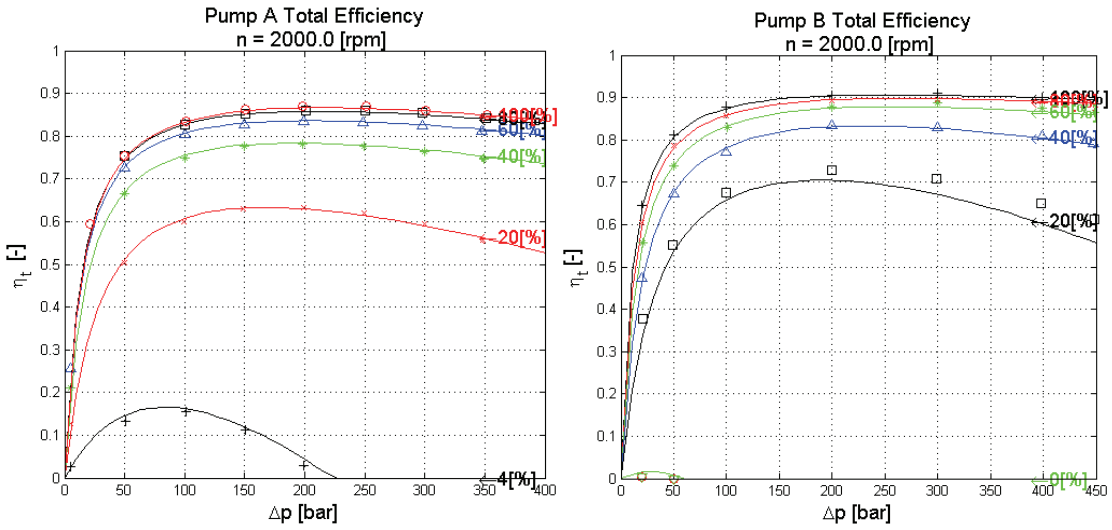

Fig. 8: Comparison of total pump efficiency, 2D plots

Total efficiency in motoring mode for Pump B is described by Fig. 9. Notice that the motoring performance is almost identical to pumping mode, with a slightly higher (~2%) maximum efficiency. While each pump/motor model has different characteristics, these measurements support the assumption of identical pumping and motoring performance made for Pump A.

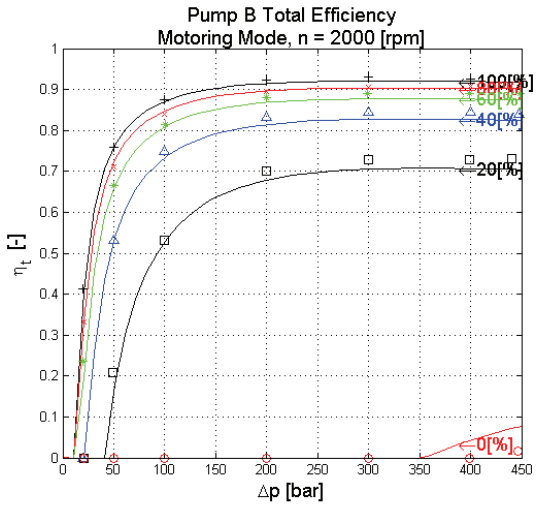

Fig. 9: Pump B total efficiency in motoring mode

The next step in modeling the pump losses was the creation of a four quadrant model. Pumps used for actuator displacement control typically operate overcenter and in both pumping and motoring modes. Assuming that the direction of shaft rotation does not change (that is, $n > 0$), there are four quadrants of operation as defined in Fig. 10. Δp is defined as

$$\Delta p = p_A - p_B \tag{3}$$

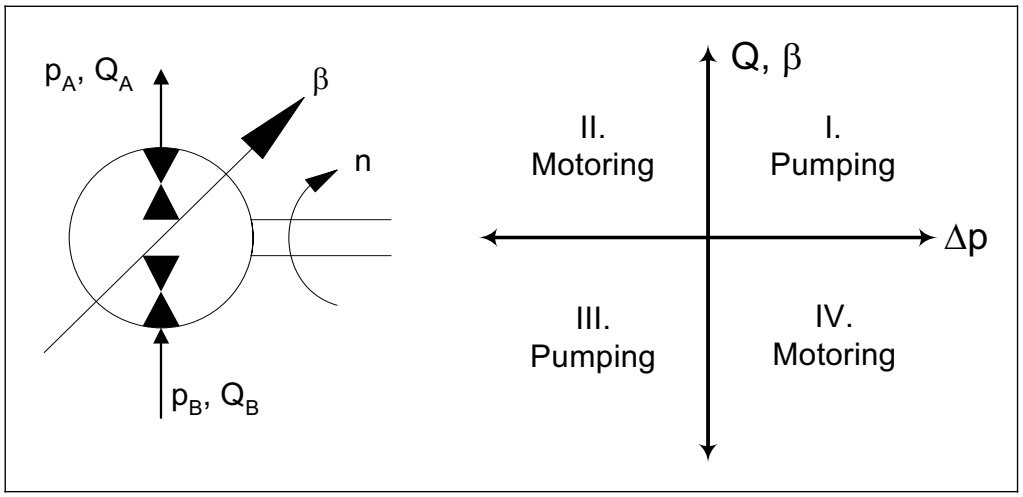

Fig. 10: Definition of four-quadrant operation

For Pump B, the data measured in quadrants I. and II. were copied to III. and IV. to complete the four-quadrant model. The measurements of Pump A in I. were copied to the other three quadrants. The four-quadrant models were then represented in C-code as a Simulink S-function, allowing them to be used in dynamic simulations in the Matlab/Simulink environment.

3 MATHEMATICAL MODEL OF PUMP-CONTROLLED SYSTEM

Essential loader dynamics were modeled mathematically in order to simulate working cycles and calculated energy consumption and distribution. This section describes the development of that model, along with descriptive equations and assumptions. It should be noted that the development of a dynamic model of a pump-controlled actuation system is not intended to be an original contribution of this paper. The work presented here follows the development of similar system models created in the past [9,10] and is included in this paper for the sake of completeness. What is new is the use of this model to compare system performance for components with different loss behaviors, a topic which has not been studied previously.

Mathematical models for the static and dynamic behavior of the hydraulic system are described in Section 3.1. The multi-body mechanical model of the loader structure is covered in Section 3.2, followed by the power/energy model in Section 3.3. Mathematical modeling is limited to the loader's working functions, i.e. the lifting and tilting cylinders and associated mechanical and hydraulic components. The hydrostatic drive is not included in the system model. Although the drivetrain is a significant energy consumer, the aims of this paper could be satisfied without the additional complexity of a more complete model of the loader hydraulics. Engine speed is assumed to be constant, so engine power and efficiency characteristics were also neglected. Perhaps a more complicated model of all energy consumers (working functions, drive, cooling fan, accessories, etc) as well as engine characteristics will be developed in future work.

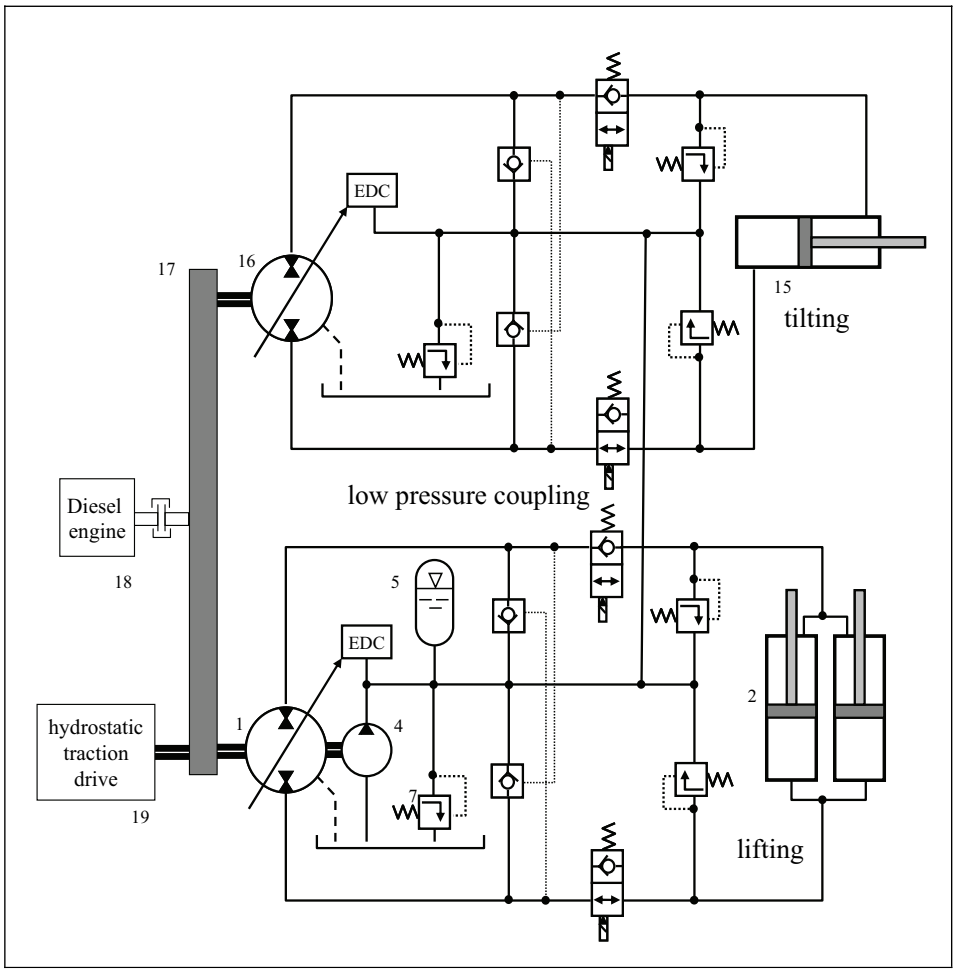

Fig. 11: Schematic of loader working hydraulics

3.1 Hydraulic System Dynamics

3.1.1 Pump Dynamics

A detailed description of the steady-state pump characteristics has been presented previously. Pump dynamic performance is determined primarily by the electrohydraulic displacement control, abbreviated EDC in Fig. 11. The EDC consists of a valve and cylinder which control the pump displacement by adjusting the angular position of the swash plate. This system is represented schematically in Fig. 12.

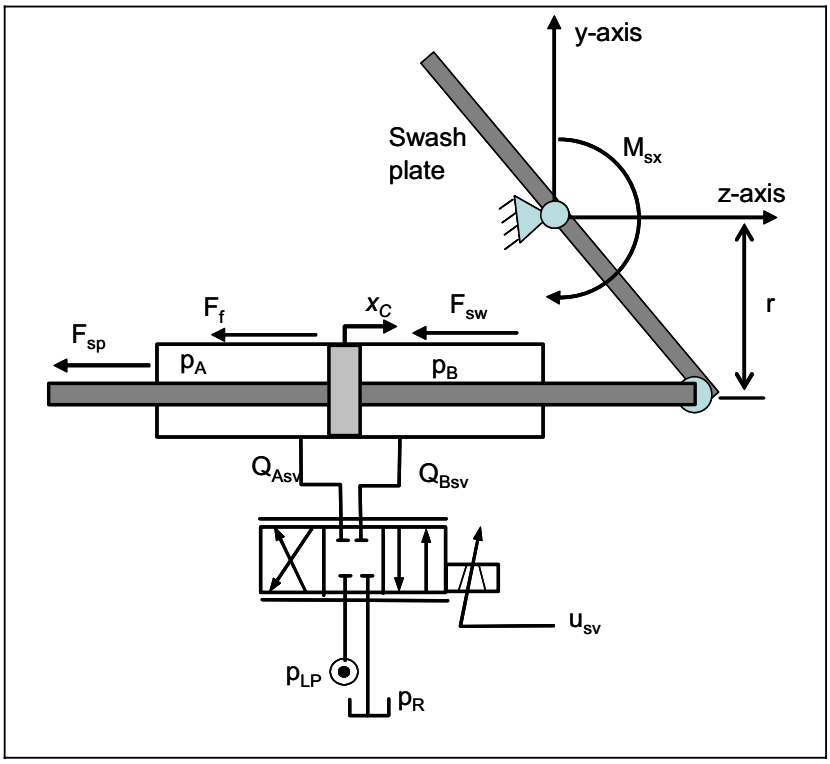

Fig. 12: Schematic diagram of pump control system

A simple linear model of the servo valve dynamics was used in order to reduce the computational effort required for simulation. The valve dynamics are represented by a 2nd order linear system, as in Eq. 4. The volumetric flow rate through the servo valve is calculated with the static flow gain C_y. In both equations, y represents the position of the valve spool.

$$\ddot{y} + 2d_{sv}\omega_{sv}\dot{y} + \omega_{sv}^{\ 2} y = k_{sv}\omega_{sv}^{\ 2} u_{sv} \tag{4}$$

$$Q_{SV} = C_y \cdot y \tag{5}$$

More detailed and accurate models have been derived by the authors in previous works [11]. However, the simplifications involved in using the linear model do not have a significant effect on the overall energy consumption of the system and thus the linear model is adequate for the present work.

The pump control cylinder is a double-rod cylinder with a centering spring. The pressure build-up in the A and B volumes of the cylinder are represented in Eq. 6 and 7. Here K represents the bulk modulus of the fluid and A_C is the annular area of the piston (piston area minus rod area). The internal leakage across the piston seal is represented by Q_{Li}, and external leakage is neglected.

$$\dot{p}_{AC} = \frac{K}{V_{AC}}\left(Q_{Asv} - A_C\dot{x}_C - Q_{Li}\right) \tag{6}$$

$$\dot{p}_{BC} = \frac{K}{V_{BC}}\left(-Q_{Bsv} + A_C\dot{x}_C + Q_{Li}\right) \tag{7}$$

The cylinder position x_C is measured from the center position x_H. Volumes A and B can then be calculated as

$$V_{AC} = V_{\text{line,C}} + A_{\text{C}}(x_{\text{H}} + x_C) \tag{8}$$

$$V_{BC} = V_{\text{line,C}} + A_{\text{C}}(x_{\text{H}} - x_C) \tag{9}$$

Summing forces on the cylinder piston and rod gives

$$m_{eq,c}\ddot{x}_C = (p_{AC} - p_{BC})A_C - F_F - F_{sp} \tag{10}$$

where F_F and F_{sp} refer to the frictional and spring forces, respectively. There are also several simplifying assumptions in this expression. The linkage connecting the control cylinder to the swash plate has been ignored, and the rotational inertia and swash plate moment have been lumped into a single equivalent mass $m_{eq,c}$. Again, this is not the most precise model available, but is sufficiently accurate for the present.

3.1.2 Linear Actuators

Modeling equations for the working actuators are derived in a similar way. Although the lifting and tilting cylinders have different dimensions (e.g. stroke length H, rod area A_r and piston area A_p), the equations describing them are identical. The cylinder geometry is presented generically in Fig. 13 and the equations are written without distinction to working function.

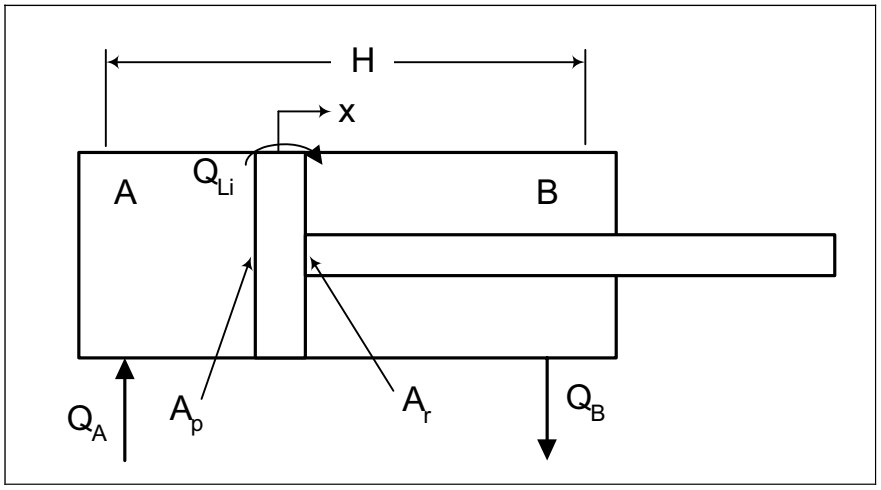

Fig. 13: Single-rod cylinder for lifting or tilting

The pressure build-up equations are expressed as

$$\dot{p}_A = \frac{1}{C_{H_A}}\left[Q_A - A_p\dot{x} - k_{Li}(p_A - p_B)\right] \tag{11}$$

$$\dot{p}_B = \frac{1}{C_{H_B}}\left[-Q_B + \alpha A_p\dot{x} + k_{Li}(p_A - p_B)\right] \tag{12}$$

The differential area due to the single-rod design is accounted for by the cylinder area ratio α, which is defined as

$$\alpha = \frac{A_p - A_r}{A_p} \tag{13}$$

The hydraulic capacitance associated with each cylinder volume is a function of the cylinder position, as shown in the following equations.

$$C_{HA} = \frac{V_A}{K} \text{ and } C_{HB} = \frac{V_B}{K} \tag{14}$$

$$V_A = V_{\text{line}} + A_p x \tag{15}$$

$$V_B = V_{\text{line}} + \alpha A_p \left(H - x\right) \tag{16}$$

The cylinder mechanics were modeled along with the other mechanical parts of the loader (boom, bucket, etc) using commercial multi-body dynamics software. This is explained in greater detail in Section 3.2. The loader mechanics and hydraulics are coupled by the force on the working cylinders. The net force for each linear actuator is modeled by Eq. 17, where c_v is the coefficient of viscous friction.

$$F_{net} = A_p(p_A - \alpha p_B) - c_v \dot{x} \tag{17}$$

3.1.3 Low Pressure Charge System

Because of the differential area across the piston of a single-rod cylinder, there is a difference in the volumetric flow rate through the cylinder as it extends or retracts. The primary purpose of the low pressure charge line for pump-controlled actuation is to compensate for this differential cylinder flow by supplying or accepting the required volume of oil at the required rate of flow. The low pressure line also supplies pressure to the servo valves that control the pump displacement as well as replenishing volumetric losses in the hydrostatic transmission.

The charge pump (labeled #4 in Fig. 11) is a 10 cc/rev gerotor type. Since it operates at constant speed (3000 rpm) over a narrow pressure range (15-30 bar), constant efficiencies were assumed. Efficiency characteristics were taken from the manufacturer's catalog and are listed in Table 2. It is important to choose the smallest possible charge pump required by the system since the entire power consumed by the charge pump represents a power loss.

Table 2: Charge pump loss characteristics

Parameter	Symbol	Value
Volumetric efficiency	η_v	0.91
Mechanical efficiency	η_m	0.81
Total efficiency	η_t	0.74

The low pressure accumulator serves to store oil and reduce the flow rate required from the charge pump by supplying additional volumetric flow for short intervals of time. It should be emphasized that the LP accumulator is not intended to store energy. Due to the small size and maximum pressure of the LP accumulator, only a negligible amount of energy can be stored compared to the energy consumption of the entire system.

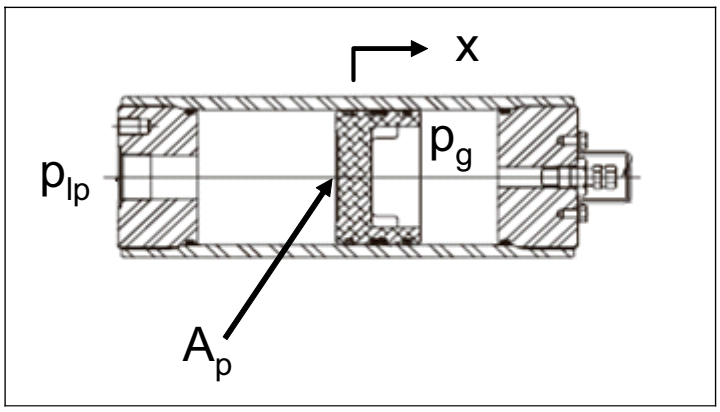

Fig. 14: Low pressure accumulator

As is evident from the figure, the LP accumulator is of the hydro-pneumatic piston type. Its dynamics can be described by summing the forces on the piston, as in Eq. 18.

$$A_p(p_{lp} - p_g) - F_f - m_p\ddot{x}_p = 0 \tag{18}$$

In this equation, p_{lp} refers to the LP oil pressure, p_g is the gas pressure, and F_f is the frictional force on the piston seal. An expression for the gas pressure as a function of the piston position is derived from the ideal gas law using the gas pre-charge pressure p_0 and volume V_0.

$$p_g(x) = p_0\left(\frac{V_0}{V_0 - A_p x_p}\right)^N \tag{19}$$

The polytropic exponent N has a value of 1.4 for an adiabatic process and 1.0 for an isothermal process. A value of N = 1.25 was used for the current work as an approximation of the real thermal characteristics of the accumulator. Combining equations 18 and 19 gives

$$\ddot{x}_p = \frac{A_p}{m_p}\left[p_{lp} - p_0\left(\frac{V_0}{V_0 - A_p x_p}\right)^N\right] - F_f \tag{20}$$

which can be integrated to obtain the piston position (and thus the pressure and gas volume) of the LP accumulator.

The pilot-operated check valves connect the LP charge line to the lifting and tilting circuits (see Fig. 11). These valves are essential for switching successfully between the four quadrants of pump operation. Since the mass of the moving parts (spool and poppet) is very small, the valve dynamics are much faster than the rest of the hydraulic system and can be neglected. Static relationships based on balanced pressure and spring forces were used to determine the position of the valve poppet, eliminating the need to

explicitly consider mass and friction. In simulation, the maximum poppet velocity was limited to prevent chatter.

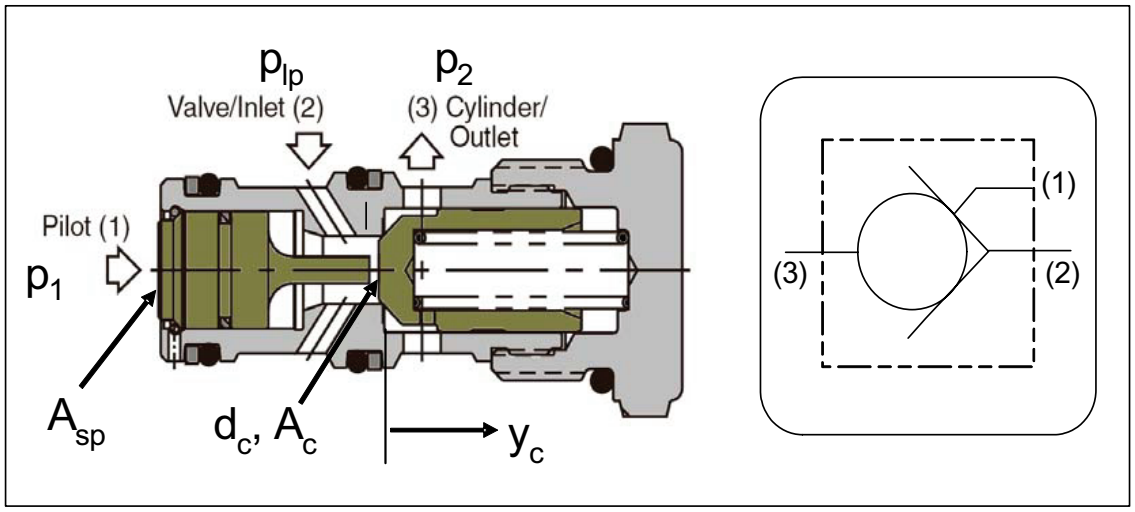

Fig. 15: Pilot-operated check valve

For the normal flow direction, that is, from (2) to (3), poppet position y_c is given by

$$A_c\left(p_{lp}-p_2\right)-\left(F_{k0}+ky_c\right)=0 \tag{21}$$

$$y_c=\frac{1}{k}\left[A_c\left(p_{lp}-p_2\right)-F_{k0}\right] \tag{22}$$

In Eq. 21 and 22, k represents the rate of the spring holding the poppet to its seat and F_{k0} is the spring pre-compression force corresponding to cracking pressure F_{k0}/A_c.

For the opposite flow direction, from (3) to (2), pilot pressure on the spool must also be considered.

$$A_{sp}\left(p_1-p_{lp}\right)+A_c\left(p_{lp}-p_2\right)-\left(F_{k0}+ky_c\right)=0 \tag{23}$$

$$y_c=\frac{1}{k}\left[A_{sp}\left(p_1-p_{lp}\right)+A_c\left(p_{lp}-p_2\right)-F_{k0}\right] \tag{24}$$

Once the poppet position is known, the flow rate through the PO check valve can be calculated with the well-known orifice equation:

$$Q_c=\alpha_{Dc}\left(\pi d_c y_c\right)\cdot\operatorname{sign}\left(\Delta p\right)\sqrt{\frac{2}{\rho}\left|\Delta p\right|} \tag{25}$$

where Δp is defined as

$$\Delta p=p_{lp}-p_2-\frac{F_{k0}}{A_c} \quad \text{(normal flow direction)} \tag{26}$$

$$\Delta p=p_2-p_{lp} \quad \text{(opposite flow direction)} \tag{27}$$

The instantaneous pressure in the LP line can be determined by integrating the pressure build-up equation, which sums the flows entering and leaving the LP control volume.

$$\dot{p}_{LP} = \frac{1}{C_{HLP}}\left(Q_{cp} + Q_{accu} - \Sigma Q_{sv} - \Sigma Q_{PO}\right) \tag{28}$$

The hydraulic capacitance of the LP line is dominated by the capacitance of the accumulator, calculated as

$$C_{HLP} = \frac{V_{LP}}{K} + C_{Haccu} = \frac{V_{LP}}{K} + \frac{V_0 \cdot p_0^{\frac{1}{N}}}{N \cdot p_{lp}^{\frac{N+1}{N}}} \tag{29}$$

3.1.4 Line Losses

Pressure losses due to resistance in the transmission lines are modeled in the traditional manner using lumped resistances. "Major" losses due to frictional drag are given by

$$\Delta p = \lambda\left(\frac{l}{d}\right)\left(\frac{\rho}{2}\right)v^2 = \lambda\left(\frac{l}{d}\right)\left(\frac{8\rho}{\pi^2 d^4}\right)Q^2 \tag{30}$$

$$\lambda = \frac{64}{\mathrm{Re}} \quad \text{(laminar flow)} \tag{31}$$

$$\lambda = \frac{0.316}{\sqrt[4]{\mathrm{Re}}} \quad \text{(turbulent flow)} \tag{32}$$

"Minor" losses due to turbulent flow through fittings, bends and tees are calculated with

$$\Delta p = \alpha_D\left(\frac{\rho}{2}\right)v^2 = \alpha_D\left(\frac{8\rho}{\pi^2 d^4}\right)Q^2 \tag{33}$$

where α_D is the loss coefficient associated with each component. Pressure drop due to hydraulic inductance is not a significant source of losses for the system in question and has been neglected.

3.2 Loader Multi-body Dynamics

There are a number of commercial motion simulation programs available for simulating the dynamics of mechanical systems. Since the hydraulic equations were modeled in MATLAB/Simulink, the SimMechanics toolbox was chosen for convenience. This program allows the geometry and inertia of mechanical bodies to be modeled along with the joints and other constraints that define how these bodies interact with each other and their environment. Sensor and actuator blocks were used to couple the mechanical model to the hydraulics and controls, allowing a simultaneous co-simulation of both the hydraulic system and the loader motion. Information regarding part geometry and

inertia was taken from CAD models provided by the vehicle manufacturer, ensuring a high-fidelity simulation of the loader's physical behavior.

3.3 Power Transmission and Dissipation

Generally speaking, the purpose of fluid power systems is to transmit power from a prime mover to one or more actuators which perform useful work. A portion of the work done by the actuators may be stored in the load being moved as potential or kinetic energy. Pump-controlled systems can recover part of this energy and share the recovered power between the different actuators. If the amount of recovered power exceeds the power demands of the working hydraulics (along with their associated losses), the extra recovered power is transmitted to other power consumers in the vehicle such as the drivetrain and accessories. In this way, the pump-controlled system is able to reduce the total energy consumption of the vehicle by sharing recovered power in real time, rather than by storing the recovered energy and using it later. This power flow is presented graphically in Fig. 16. To calculate the total amounts of energy entering and leaving the system, the power flows are simply integrated over the duration of the duty cycle.

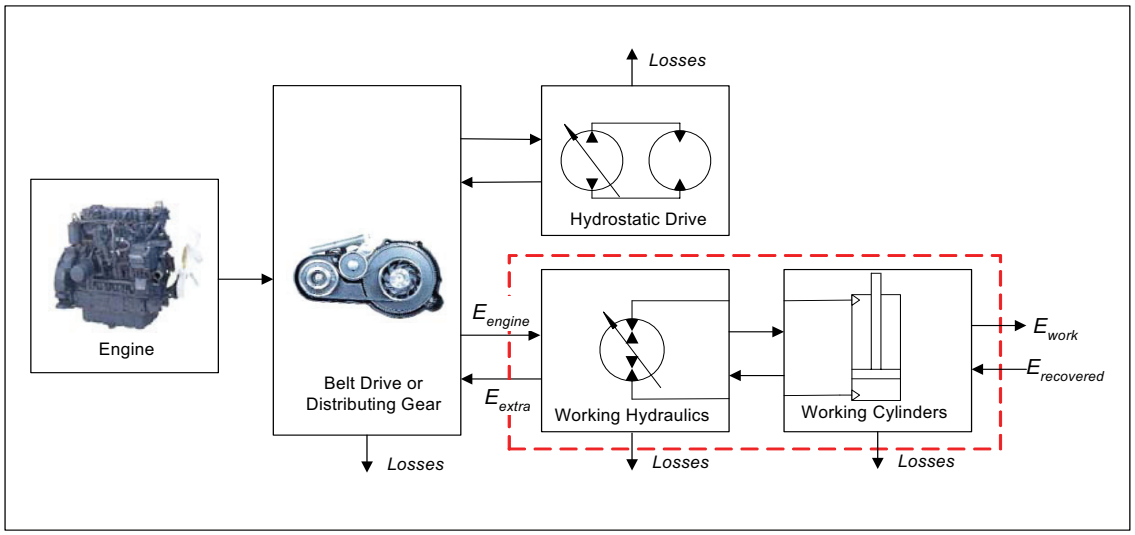

Fig. 16: Power flow diagram for loader hydraulic system

Consider the section of Fig. 16 enclosed by the dashed line, which represents the part of the loader system which was mathematically modeled and simulated. Applying conservation of energy to this "control volume", we obtain

$$E_{\text{in}} - E_{\text{out}} = E_{\text{stored}} \tag{34}$$

Neglecting the small amount of energy stored in the low pressure accumulator, the energy balance reduces to

$$E_{\text{in}} = E_{\text{out}} \tag{35}$$

which is the total energy consumed by the system. Referring again to the power flow diagram, the total energy can be expressed as

$$E_{total} = E_{\text{engine}} - E_{\text{extra}} = E_{\text{work}} + E_{\text{losses}} - E_{\text{recovered}} \tag{36}$$

Although elementary, this derivation is presented to clarify how energy is distributed in the simulated system and the sign convention used for calculating the total energy consumption. It is clear that the total energy can be calculated equivalently by integrating either the power at the pump shafts or the power at the actuators and sundry loss sources. The former approach was used for the sake of simplicity.

3.3.1 Pump Power Model

Power entering and leaving the system at the pump shaft is simply the product of the shaft speed and effective torque.

$$P_{pump} = \omega M_e = \frac{n\pi}{30} M_e \tag{37}$$

Pump losses were obtained from the POLYMOD steady-state loss model, as explained in Section 2.2. The equations used by the program to calculate these losses from experimental measurements are presented here.

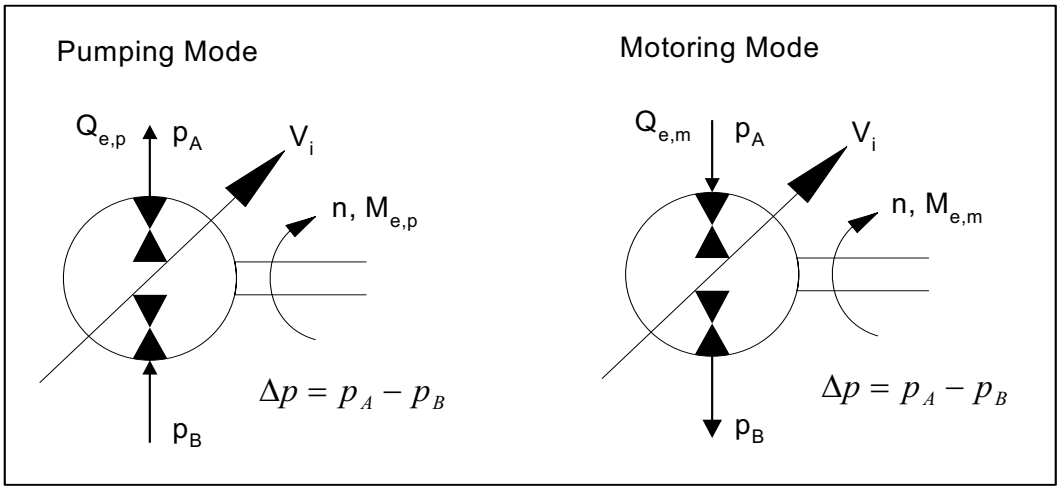

Fig. 17: Parameter definition for calculation of pump power losses

In pumping mode, the volumetric, torque (mechanical) and power losses are given by

$$Q_{s_p} = nV_i - Q_{e_p} \tag{38}$$

$$M_{s_p} = M_{e_p} - \frac{V_i \Delta p}{2\pi} \tag{39}$$

$$P_{s_p} = M_{e_p} \cdot \omega - \Delta p \cdot Q_{e_p} \tag{40}$$

Losses in motoring mode are

$$Q_{s_m} = Q_{e_m} - nV_i \tag{41}$$

$$M_{s_m} = \frac{V_i \Delta p}{2\pi} - M_{e_m} \tag{42}$$

$$P_{s_m} = Q_{e_m} \cdot \Delta p - M_{e_m} \cdot \omega \tag{43}$$

3.3.2 Actuator Power Model

Power entering and leaving the system at the actuators is the product of cylinder force and velocity. Work done *by* the system is

$$P_{cyl} = F_{net}\dot{x} = A_p(p_A - \alpha p_B)\dot{x} - c_v\dot{x}^2 \tag{44}$$

and work done *on* the system (recovered power) is

$$P_{cyl} = A_p(p_A - \alpha p_B)\dot{x} \tag{45}$$

Thus, recovered power reduces the total energy consumption by covering losses, even if the amount of power is insufficient to drive the pump in motoring mode and put power back on the pump shaft.

3.3.3 Valve Power Model

Power losses for the pilot-operated check valves, pump control servo valves and relief valves are simply calculated as the product of pressure drop and flow rate for each valve.

4 SIMULATION OF SAMPLE SYSTEM

A skid-steer loader with pump-controlled lift and tilt functions was selected as a sample system for simulation. The choice of which particular application to simulate is essentially arbitrary, since the system behavior is similar for wheel loaders, skid-steer loaders, and other vehicles of the same type. Two typical duty cycles were simulated. Each cycle was simulated first using Pump A loss models for the lift and tilt pumps and then Pump B loss models for both pumps. All other components remained the same. The total energy consumption based on A pumps and B pumps is then compared to show what effect the difference in pump efficiency characteristics had on the total energy consumption for the same duty cycle.

4.1 Skid-Steer Loader Duty Cycles

Two typical working cycles were selected for simulation. In the first cycle, the loader moves soil or some other granular bulk material from one pile to another. The plot on the left in Fig. 18 shows the motion of the lifting and tilting cylinders as well as the load on the bucket as the loader fills the bucket from pile 1, drives to pile 2, lifts the boom enough to dump the contents of the bucket, and returns for another load.

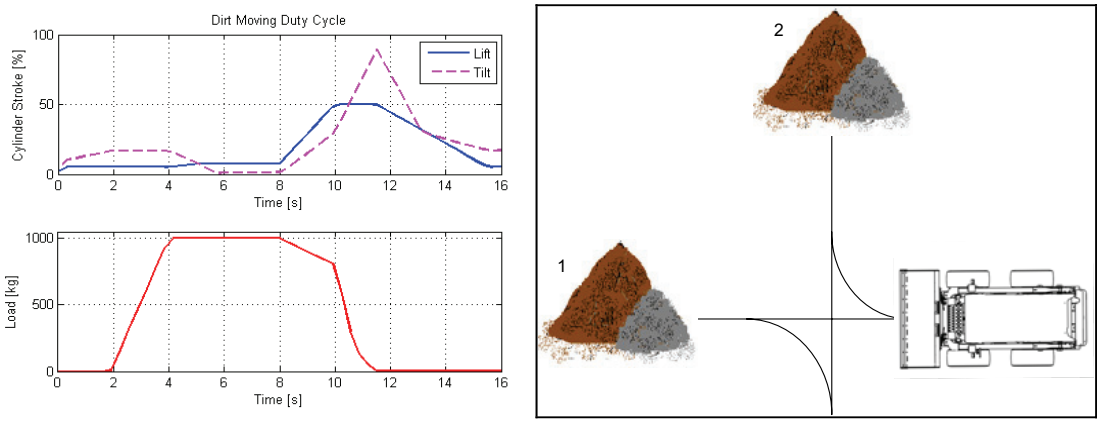

Fig. 18: Dirt moving cycle

The second cycle is almost identical to the first with the exception that the soil is loaded into a truck. This requires that the boom be raised to its maximum height before dumping the bucket, as shown in Fig. 19.

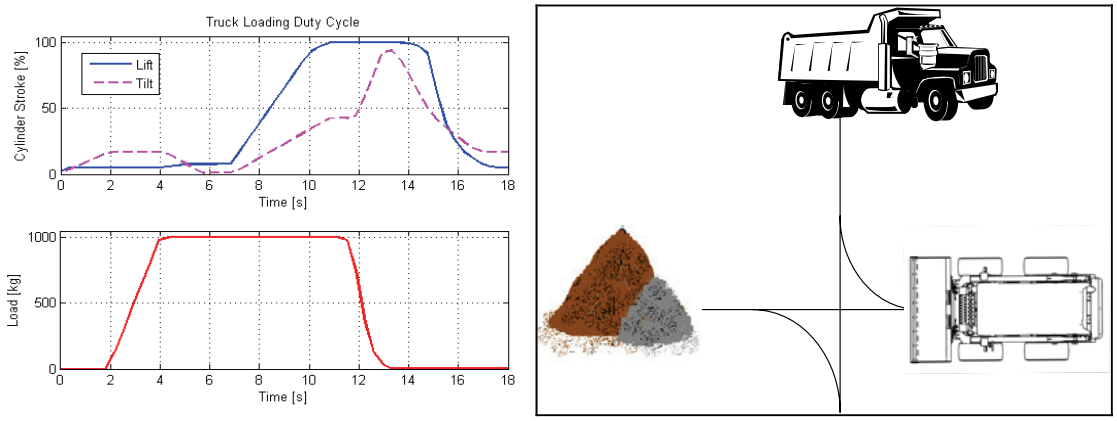

Fig. 19: Truck loading cycle

Both cycles include opportunities for recovering potential energy while both sets of actuators are working simultaneously.

4.2 Simulation Results

4.2.1 Dirt Moving Cycle

Instantaneous power consumption for the dirt moving cycle is plotted in Fig. 20 and Fig. 21. In these plots, the dashed lines represent power flow to each of the three pumps. The solid line is the total power being used by the hydraulic system at a particular instant. The total energy consumption is simply the area under the total power curve. In these plots, negative pump shaft power indicates that the pump is running in motoring mode and supplying energy to the other pumps. The potential for energy recovery in this cycle is fairly low, since the bucket is empty when the boom is lowered. However, the low value of the lift pump power toward the end of the cycle indicates that some energy is being recovered and is reducing losses, but not enough to run the pump as a motor and share power with the other pumps.

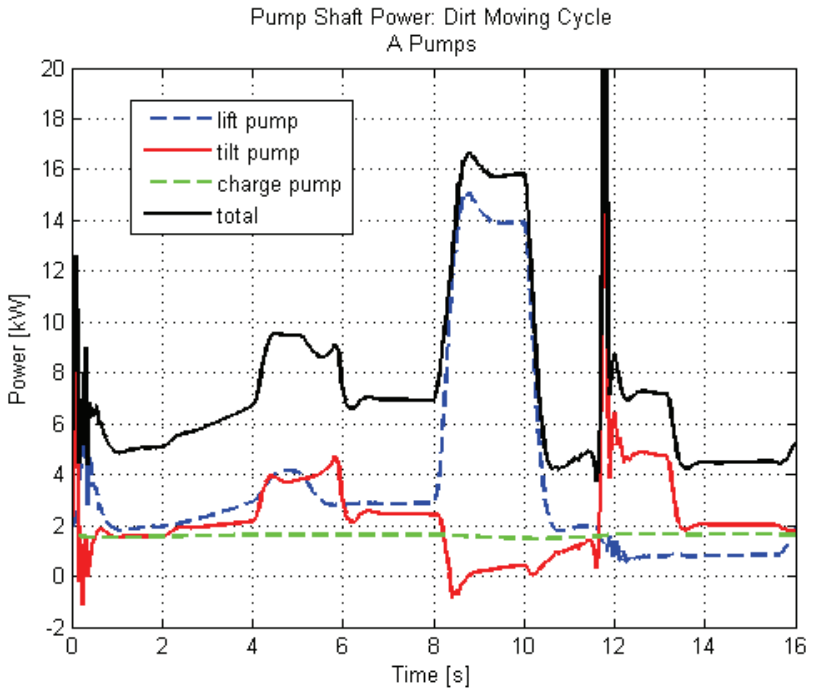

Fig. 20: Power consumption and distribution for dirt moving cycle, A pumps

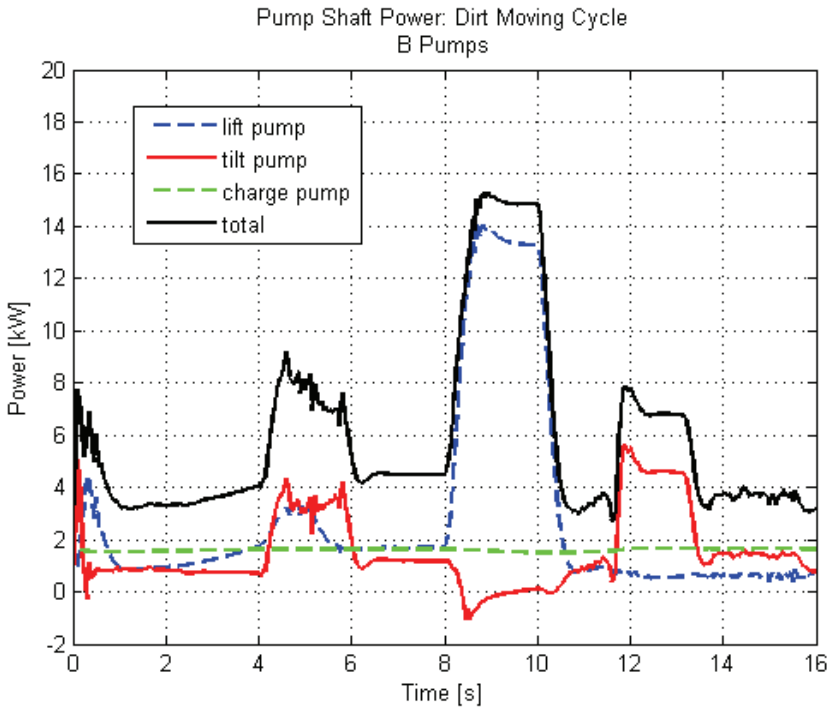

Fig. 21: Power consumption and distribution for dirt moving cycle, B pumps

Upon comparing these figures, it is clear that the A pumps consume noticeably more power than the B pumps. The difference is particularly evident when the pump power curves are summed and integrated to obtain the total energy consumption for the cycle.

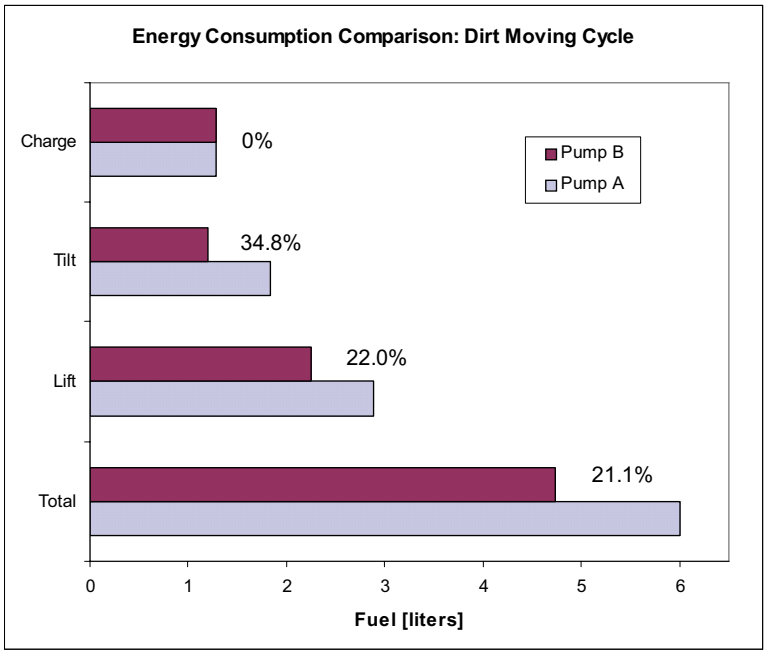

Fig. 22: Energy consumption for dirt moving cycle

Fig. 22 compares the simulated energy consumption for pump losses based on Pump A and Pump B. The values have been scaled assuming that the duty cycle is repeated continuously for 8 hours. A lower heating value of 43,000 kJ/kg and a density of 0.832 kg/l were assumed for diesel fuel in order to convert the energy consumption from kJ to fuel in liters. The ratios of energy consumption (expressed as percentages) remain the same as for a single cycle.

4.2.2 Truck Loading Cycle

Power and energy consumption for the truck loading cycle are given in Fig. 23 through Fig. 25. The simulation results for this cycle were very similar to the previous duty cycle, and the same comments apply. As before, the total energy consumption using B pumps is roughly 20% lower than the A pumps for the same duty cycle.

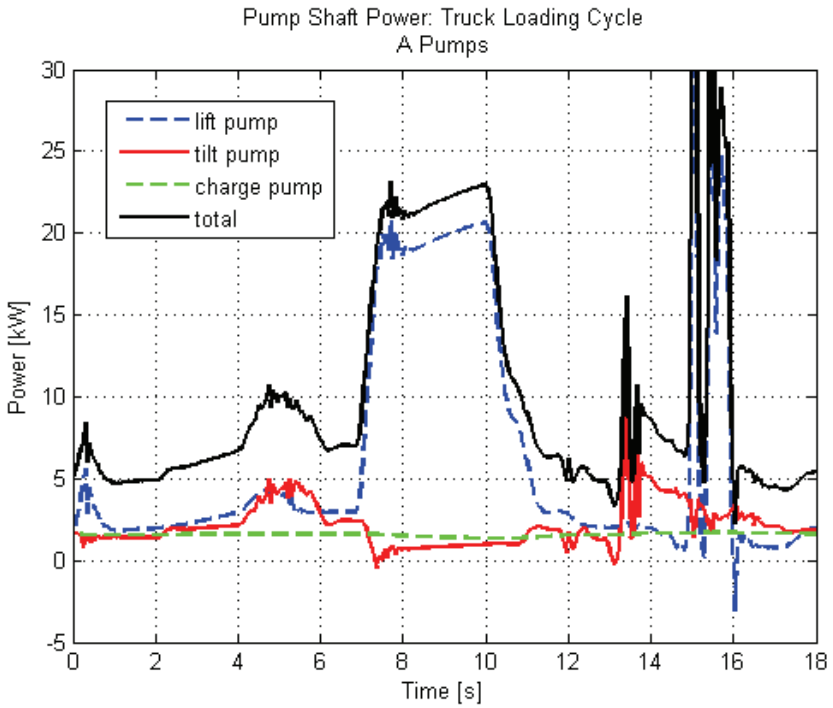

Fig. 23: Power consumption and distribution for truck loading cycle, A pumps

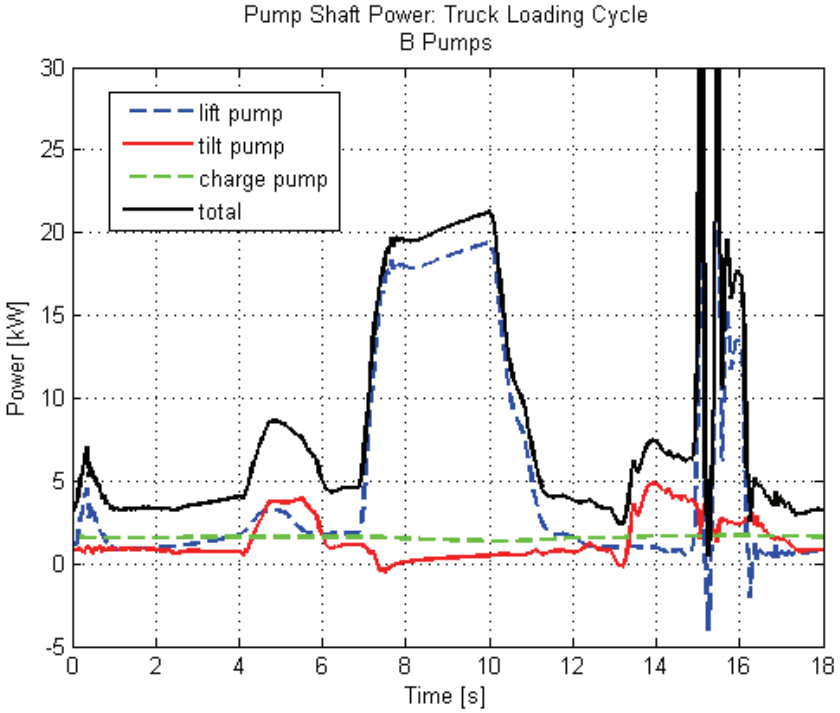

Fig. 24: Power consumption and distribution for truck loading cycle, B pumps

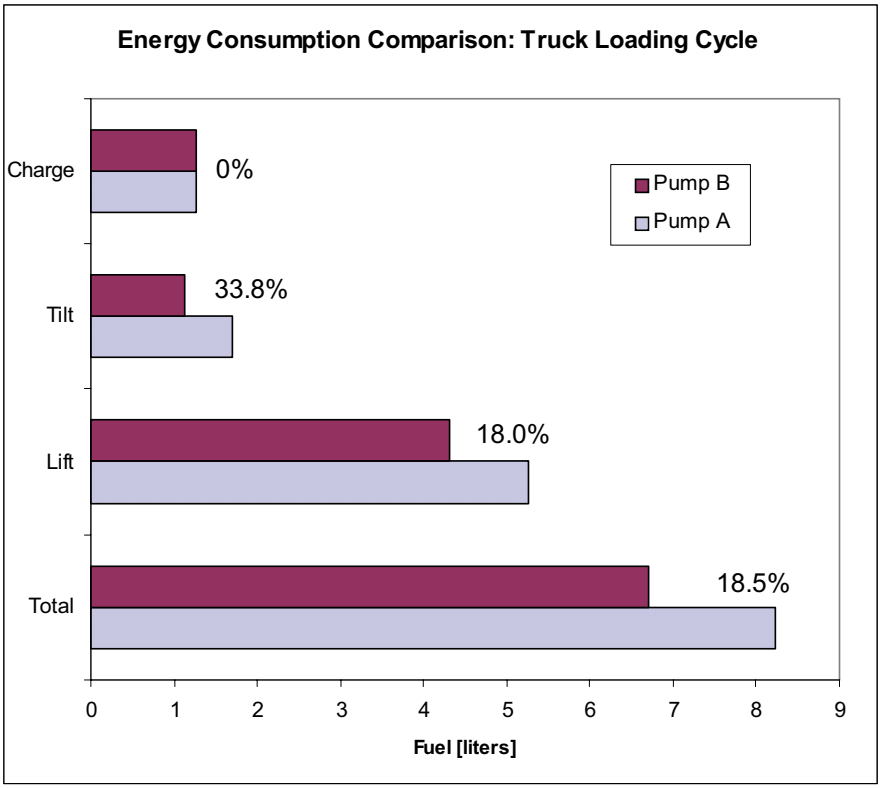

Fig. 25: Energy consumption for truck loading cycle

4.2.3 Discussion of Simulation Results

These results beg the question: To what can the large difference in total energy consumption be attributed? Pump B is not 20% more efficient than Pump A. The answer can be found by examining in which segments of the duty cycles there is the greatest difference in power consumption between the two pumps. The A pumps always require more power than the B pumps, but the difference is more pronounced when the cylinders are stationary or moving slowly. In these cycle segments, the pumps are operating at less than 20% displacement where the total efficiency is quite low. Fig. 7 confirms that the difference in efficiency between the two pump loss models is more significant at low displacements. When integrated over a period of time, the discrepancy adds up to a significant difference in fuel consumption.

It is always difficult to make generalizations about energy savings because actual fuel consumption depends on many variables and is highly cycle dependent. The purpose of this work is not to assert that improving a pump's efficiency map by X% will result in a system energy savings of Y%. The vehicle, pump loss models and duty cycles simulated here are intended to be typical but are certainly not representative of all possible configurations. Rather, the aim of this work is to demonstrate that the impact of pump efficiency on the total efficiency of pump-controlled actuator systems is significant. This effect is particularly noticeable at partial actuator speeds and loads, where mobile machines operate most of the time.

5 CONCLUSION

This paper examines the effect that improvements in pump efficiency have on the energy consumption of a pump-controlled actuation system. Two variable displacement, axial piston pumps were compared. Their maximum displacements were 46 and 42 cc/rev. Steady-state measurements of pump performance were made across the range of operating parameters and used to create best-fit polynomial loss models for each pump. The maximum total efficiency of Pump A was measured to be about 5% less than that of Pump B.

A dynamic model of a pump-controlled skid-steer loader was created which included the pump loss models, multi-body mechanics of the loader structure, and dynamic models of pressure and flow in the hydraulic system. The simulation model included the loader working functions (lifting and tilting) without the hydrostatic drive. Two typical loader duty cycles were simulated using the different pump loss models and the total energy consumption was compared. The pump controlled actuator system based on Pump B losses consumed approximately 20% less energy in both simulated cycles than the pumps with Pump A loss characteristics.

The conclusion of this study is that the effect of pump efficiency on the total energy consumption of a pump-controlled actuator system is considerable. This phenomenon is particularly evident at low pump displacements and pressures.

5 NOMENCLATURE

Symbol	Quantity	Unit
α	cylinder area ratio	[-]
α_D	hydraulic loss coefficient	[-]
β	pump displacement	[%]
η	efficiency	[-]
λ	frictional loss coefficient	[-]
ρ	fluid density	[kg/m^3]
ω	pump shaft speed	[rad/s]
ω_{SV}	servo valve eigenfrequency	[rad/s]
A	area	[m^2]
C_H	hydraulic capacitance	[m/N]
C_y	flow gain	[m²/s]
E	energy	[J]
F	force	[N]
F_f	friction force	[N]
F_{SP}	spring force	[N]
H	cylinder stroke	[m]
K	oil bulk modulus	[Pa]
M_s	torque losses	[Nm]
N	polytropic exponent for ideal gas	[-]
P	power	[W]
P_s	power losses	[W]
Q	volumetric flow rate	[m³/s]
Q_{Le}	external leakage	[m³/s]
Q_{Li}	internal leakage	[m³/s]
Q_s	volumetric loss	[m³/s]
Re	Reynolds number	[-]
V	volume	[m^3]
V_0	accumulator gas volume	[m^3]
V_{AC}	fluid volume of pump control cylinder, A side	[m^3]
V_{BC}	fluid volume of pump control cylinder, B side	[m^3]
c_v	coefficient of viscous friction	[kg/s]
d_{SV}	servo valve damping	[-]
k	spring rate	[N/m]
k_{Li}	coefficient of internal leakage	[m³/s/Pa]
n	pump shaft speed	[1/min]
p	fluid pressure	[Pa]
p_0	accumulator gas pre-charge pressure	[Pa]
v	fluid velocity	[m/s]
x	piston position of lifting or tilting cylinder	[m]
x_C	piston position of pump adjustment cylinder	[m]
x_H	neutral (centred) position of pump adjustment cylinder	[m]
y	spool position of the pump control valve	[m]
y_c	poppet position of pilot-operated check valve	[m]

7 REFERENCES

[1] Ivantysynova, M. 2000. Displacement Controlled Linear and Rotary Drives for Mobile Machines with Automatic Motion Control. *2000 SAE International Off-Highway & Powerplant Congress*, Milwaukee, Wisconsin, USA. SAE Technical Papers 2000-01-2562.

[2] Rahmfeld, R. et al. 2004. Displacement Controlled Wheel Loader – a simple and clever solution. *Proceedings of the 4th International Fluid Power Conference (4.IFK)*, Dresden, Germany, Vol. 2, pp. 183-196.

[3] Heybroek, K.; Larsson, J.; and Palmberg, J.O. 2006. Open circuit solution for pump controlled actuators. *Proceedings of 4th FPNI-PhD Symposium*. Sarasota, FL, USA, 2006, pp. 27-40.

[4] Rahmfeld, R. 2002. *Development and Control of Energy Saving Hydraulic Servo Drives for Mobile Systems*. Dissertation, Technical University of Hamburg-Harburg, Germany. Fortschritt-Berichte VDI, Reihe 12 No. 527, VDI Verlag, Dusseldorf, Germany.

[5] Ivantysynova, M. 1999. Ways for Efficiency Improvements of Modern Displacement Machines. *Proc. 6th Scandinavian International Conference on Fluid Power*, Tampere, Finland, pp. 77-92**.**

[6] Ivantysynova, M. 2001. Energy Losses of Modern Displacement Machines - a New Approach of Modelling. *Proc. 7th Scandinavian International Conference on Fluid Power*, Linköping, Sweden, 2001, Vol. 1, pp. 377 – 395.

[7] Lenord, O. 1998. *Development of mathematical loss models for servo pumps*. MS Thesis (in German). University of Duisburg, Germany.

[8] Mikeska, D. 2002. A precise steady-state model of displacement machines for the application in virtual prototyping of power-split drives. *2nd FPNI-PhD Symposium Modena 2002*, University of Modena, Italy.

[9] Eggers, B. 2004. *Extended control concepts and energetic aspects for active oscillation damping with displacement controlled linear actuators.* Thesis, Technical University of Hamburg-Harburg, Germany.

[10] Rahmfeld, R. and Ivantysynova, M. and Eggers, B. 2004. Active Vibration Damping for Off-Road Vehicles Using Valveless Linear Actuators. *Proceedings of the SAE Commercial Vehicle Engineering Congress & Exhibition.* Chicago, IL, USA. *SAE Technical Paper 2004-01-2655.*

[11] Grabbel, J. and Ivantysynova, M. 2005. An investigation of swash plate control concepts for displacement controlled actuators. *International Journal of Fluid Power,* Vol. 6 (2005), No. 2, pp.19- 36.

FULLY INTEGRATED ELECTRIC-HYDROSTATIC DRIVE BASED ON A GEAR PUMP AND A SWITCHED RELUCTANCE MOTOR

W. Wustmann, S. Helduser
Technische Universität Dresden
Institute of Fluid Power
01062 Dresden, Germany
Phone +49 351 463 33559, Fax +49 351 463 32136
E-mail: mailbox@ifd.mw.tu-dresden.de

U. Schuffenhauer, H. Kuß, N. Michalke
Centre of Applied Research and Development (ZAFT)
at the University of Applied Sciences Dresden
01060 Dresden, Germany
Phone +49 351 462 2861, Fax +49 351 462 2193
E-mail: michalke@et.htw-dresden.de

ABSTRACT

In accordance with the current state of the art, drive and pump are interconnected as individual components for the operation of a hydrostatic drive unit.
This article presents a drive concept in which the components of the hydraulic pump and the electric drive are functionally integrated. Using an external gear pump and a switched reluctance motor, a compact pressure supply has been developed. The integration level of the electric motor and the hydraulic pump is higher than ever as essential functional components of the motor (rotor) are at the same time functional parts of the pump (gear wheels).

KEYWORDS: 'switched reluctance pump', functionally integrated motor-pump, electromagnetic and hydrostatic devices combined

1 INTRODUCTION

A decisive aspect in the optimisation and improvement of electric-hydrostatic drive systems is the integration of modules. The conventional design of hydraulic power supplies is resolved, i.e., it comprises an electric motor, a hydraulic pump, a coupling and a pumping support. So far, efforts to develop compact aggregates focussed on the structural integration of the assembly groups electric motor and hydraulic pump.

However, the functionally resolved arrangement of the individual parts principally remains untouched [1]. A higher level of integration can only be achieved if motor and pump share essential groups. The concept of a 'reluctance pump' may serve as an example of functional integration. It is realised by combining an external gear pump with a switched reluctance motor.

A reluctance drive (**Figure 1** left) is a variation of a synchronous motor in which the rotor has neither winding nor permanent magnets. The constraint-current operation on the windings of certain stator poles generates a magnetic field so that the rotor teeth align in the generated magnetic field. By the subsequent application of current to individual windings of the stator the magnetic field is advanced as desired and the soft magnetic rotor starts moving. The stator teeth with the windings, to which electric current was applied, each attract the nearest rotor teeth. The term *reluctance* defines the magnetic resistance of such a rotor against the electromagnetic field. Revolution speed and torque can be controlled by varying the current flow and the magnetic field with an inverter.

External gear pumps (**Figure 1** right) are among the most popular displacement units in fluid power. In addition to their comparatively simple design, their volumetric and hydraulic-mechanical efficiency is high. They can be used both in low and high-pressure applications. In the external gear pump, two gear wheels with involute gear teeth mesh thus displacing the fluid from the inter-tooth volumes on the pressure side.

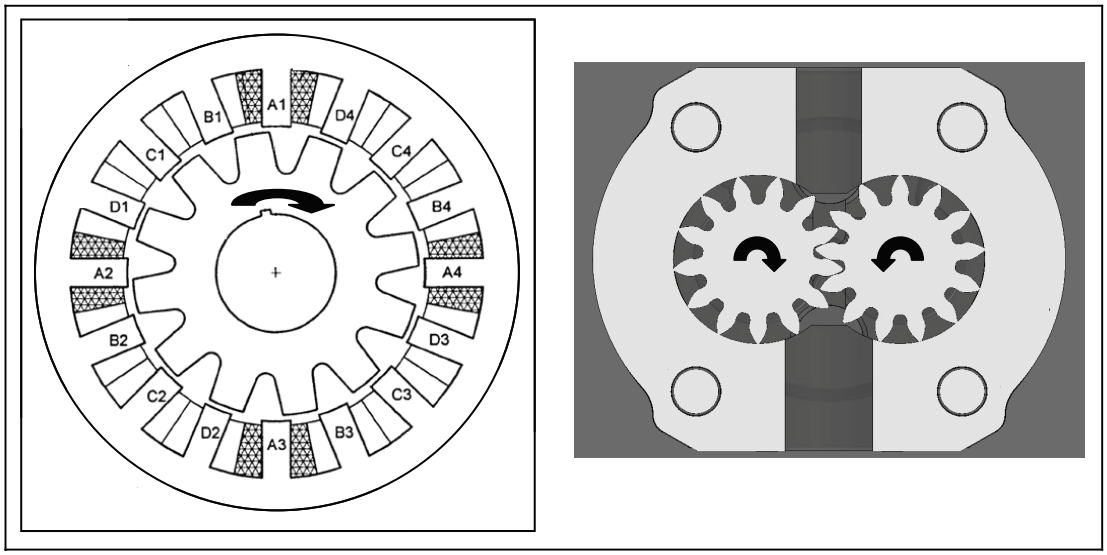

Fig. 1: Typical switched reluctance drive [2] (left) and gear pump (right)

The principle of the 'reluctance pump' combines the function of the teeth for oil displacement with the pole formation for the magnetic circle. Two engaging gear wheels concurrently form distinct poles. The stator, which is extending over 360° in reluctance drives, is cut and two stators of 180° are apportioned among the two gear wheels (**Figure 2**). As a result, both gear wheels have a motor which jointly drives the system gear pump. The pump casing serves also to house the stator package of the electric motor. Since the functional principle of the switched reluctance drive demands an electrically and magnetically insulating gap between the rotor and the stator teeth, the radial hydraulic seal for pump operation is spatially decoupled from the area of motor operation.

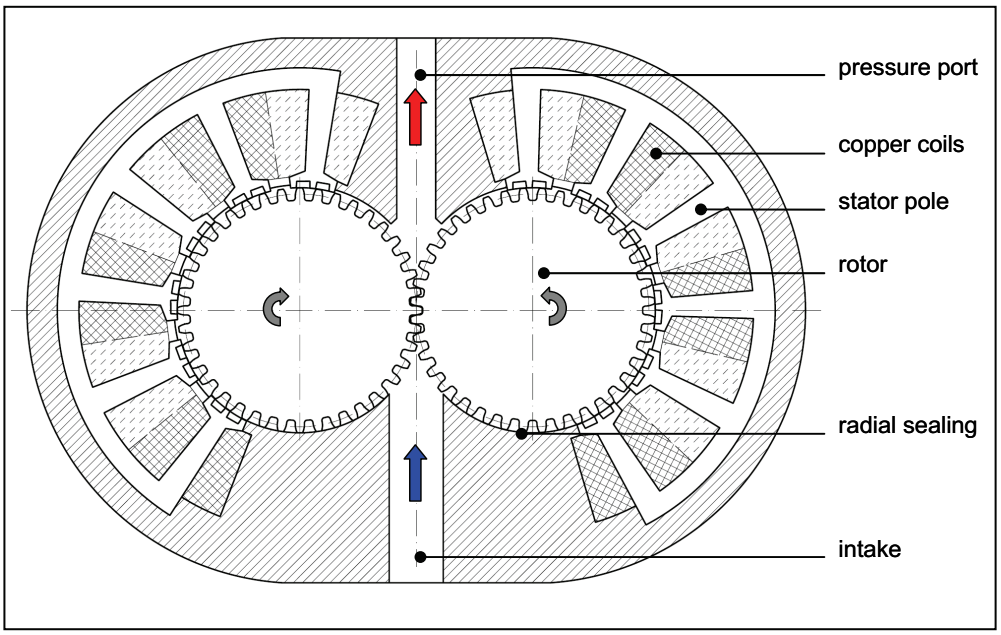

Fig. 2: Design of the 'switched reluctance pump'

The chapters below describe the physical background for the design of the electromechanical system and the dimensioning of the rotor and the stator in accordance with electromagnetic and hydrostatic criteria.

2 DESIGN SPACE

Developing an integrated 'reluctance pump' demands the interdisciplinary co-operation of engineers of both fields – fluid power and electrical engineering as the physical fundamentals of both disciplines cannot be treated separately. The design starts with defining the principal dimensions which result from the torque and power balances. The power output of the switched reluctance drive and the power input of the gear pump P are calculated like this:

$$P = C \cdot d_a^{\,2} \cdot l_i \cdot n = M \cdot \omega = \Delta p \cdot V \cdot n = \Delta p \cdot Q \,. \qquad (1)$$

It holds for the torque M:

$$M = \frac{C \cdot d_a^{\,2} \cdot l_i}{2\pi} = \frac{P}{\omega} = \frac{V \cdot \Delta p}{2\pi} \,. \qquad (2)$$

The utilisation factor C describes the electromagnetic exploitation. It is a motor-specific constant. The typical values of the utilisation factor fall between 50 and 300 kNm/m^3. The machine length l_i describes the axial dimension of rotor and stator. It is identical with the width b of the gear wheel (**Figure 3**). The displacement volume V of an external gear pump is calculated with the module of gear m, the teeth number of gear z, the teeth depth of gear h and the gear set width b:

$$V = m \cdot z \cdot \pi \cdot h \cdot b \,. \qquad (3)$$

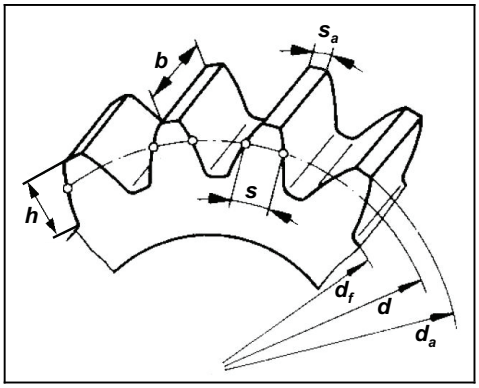

Fig. 3: Geometrical parameters of the gear tooth system

The tooth depth can be given approximately as a double module thereby neglecting the tip clearance factor and the tip modification coefficient:

$$h = 2 \cdot m \,. \tag{4}$$

The displacement volume of the external gear pump is thus approximately:

$$V = 2 \cdot m^2 \cdot z \cdot \pi \cdot b \,. \tag{5}$$

Hence the hydraulically required torque is calculated as:

$$M_{hy} = \frac{V \cdot \Delta p}{2 \cdot \pi} = m^2 \cdot z \cdot b \cdot \Delta p \,. \tag{6}$$

When the gear pump is functionally integrated into the electric motor, mechanical equations of both systems must hold. For the operation of the integrated drive holds:

$$\frac{M_{el}}{M_{hy}} = 1 = \frac{\frac{C \cdot {d_a}^2 \cdot b}{2\pi}}{m^2 \cdot z \cdot b \cdot \Delta p} \approx \frac{C \cdot z}{2\pi \cdot \Delta p} \,. \tag{7}$$

In Equation 7, a sufficiently accurate simplification has been made for adequately large diameters and small tooth depths in so far as the external diameter d_a is set approximately equal to the pitch circle diameter of gear d. Thus, the ratio of electromagnetically producible and hydraulically necessary torque is only a function of tooth number and pressure level.
The relation between the hydrostatic pressure level and the tooth number is linear:

$$\Delta p = \frac{C}{2\pi} \cdot z \,. \tag{8}$$

Due to the limited performance density of the electric motor, a functionally integrated electric-hydrostatic drive on the basis of an external gear pump and a switched reluctance motor demands a large number of rotor teeth z_R to produce a sufficiently high pressure level (**Figure 4**). The gearing module has no effect on the achievable pressure level although its growth, like the increasing number of teeth, results in larger diameters:

$$d = m \cdot z \,. \tag{9}$$

The torque generated by the motor rises quadratically. However, it contributes only to the increase of the flow rate at a constant pressure level because of the quadratic increase of the displacement volume of the pump. If, however, the diameter increases due to more teeth, the rise of the displacement volume is linear, but the electromagnetically generable torque rises quadratically. Since the electromagnetically generated and hydraulically needed torque is proportional to the gear set width *b*, its increase can only enlarge the flow rate while the pressure level remains constant.

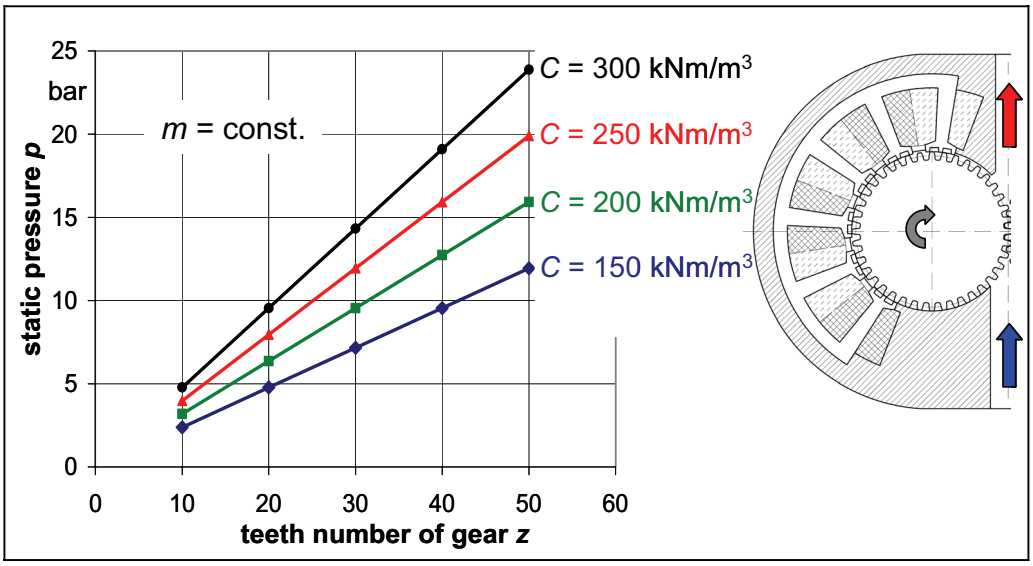

Fig. 4: Achievable static pressure as a function of the teeth number of the gear

The 'reluctance pump' with the same active length for hydraulic pump and electric motor can only be used in low-pressure applications according to Figure 4. Compared with conventional external gear pumps, the 'reluctance pump' can be designed with a relatively large diameter (**Figure 5**). Thanks to the low pressure level, the resulting pressure forces acting on the rotors are limited and thus controllable.

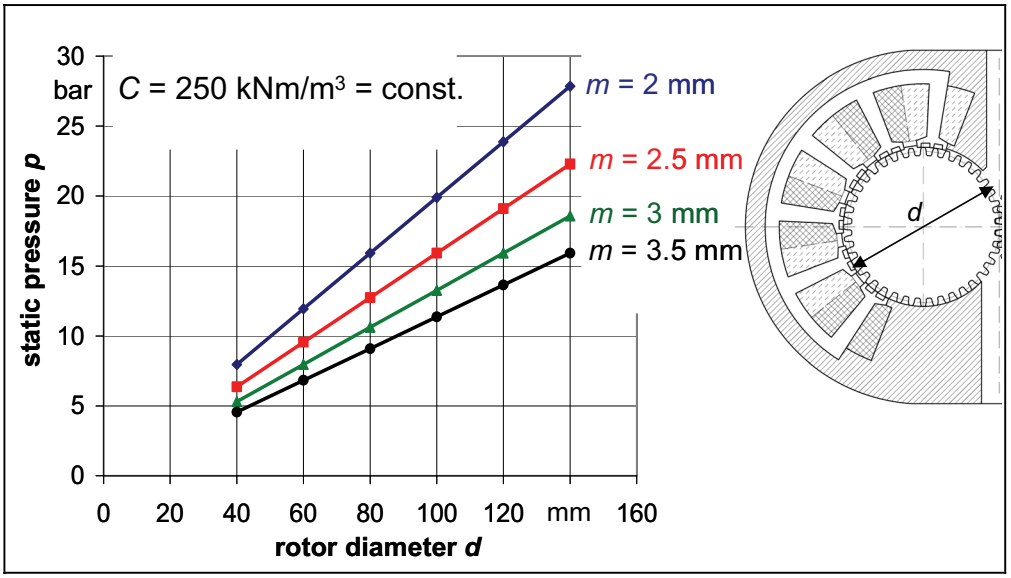

Fig. 5: Achievable static pressure as a function of the rotor diameter

The chosen number of teeth for stator and rotor substantially determines the motor properties. To avoid stationary cogging torques, this number must be different for stator and rotor. Increasing the number of teeth makes the course of the electromagnetically generated torque smoother.
Contrary to conventional external gear pumps, in which the tooth gearing is designed primarily according to hydraulic criteria, such as the degree of non-uniformity [3], the gearing of a 'reluctance pump' shall be designed according to the electromagnetic requirements first of all. Conventional gear pumps with standard angles of pressure > 20° and small negative addendum modification coefficients x with typical tooth numbers between 10 and 15 result in pointed addendum circles. Contrary to this, the tooth thickness on the addendum circle s_a of a 'reluctance pump' shall be designed as large as possible to maximise the magnetic flow Φ which determines the torque. Owing to the involute form of the toothing, the thickness of the teeth decreases towards the addendum circle. Thus the saturation of the tooth tips is larger and the magnetic flow is smaller when compared with rotor teeth of constant thickness. The optimum tooth thicknesses are the resulting compromise between involute geometry, usable magnetic flow, inductance and magnetic leakage fluxes. The teeth thickness shall be the same for the rotor and the stator, basically. To ensure sufficiently large differences of the magnetic conductance between the aligned position of rotor and stator teeth (d position) and the unaligned position (q position), the depth of the rotor teeth shall be approximately 20 times the amount of the gap length between tooth tip diameter and internal stator diameter. This clearance shall be as small as possible to increase the achievable torque and to limit the module size. Typical values of the 'air' gap δ are 0.25 mm $\leq \delta \leq$ 0.6 mm.

The different requirements made on the electromagnetic and the hydrostatic design result in the geometrical data of a pilot sample (**Table 1**).

Table 1: Geometrical data of the pilot sample

b	gear set width	20 mm
d	pitch circle diameter of gear	110 mm
h	teeth depth of gear	5.96 mm
m	module of gear	2.75 mm
s_a	tooth thickness on addendum circle	2.45 mm
x	profile shift factor	-0.4
z	teeth number of gear	40
α	angle of standard gear	20°

3 MOTOR DESIGN WITH FEM CALCULATION

Owing to the occasionally high saturation and the specific character of the field distribution, the torque generated by the switched reluctance drive can be exactly determined only with numerical calculation methods. To increase the static pressure level, the electromagnetic motor design focuses on an optimised motor with maximum torque. Essential boundary conditions for the numerical calculation are given by:

- the radial separation of the motor into decoupled stator halves and separate rotors
- the involute toothing
- and additional mechanical requirements made on the magnet material.

Contrary to the conventional reluctance machine (**Figure 6**), the radial separation of the 'reluctance pump' results in strong demands on the motor separation in terms of the winding distribution and the dimensioning of the magnetic yoke. A magnetic coupling of the two rotors must be avoided where the teeth mesh since the magnetic flux may cause compensating currents. These currents are one of the destruction sources of the teeth surfaces.

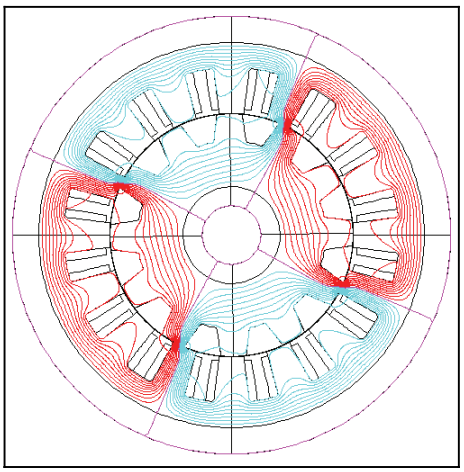

Fig. 6: Magnetic flux lines of a conventional switched reluctance drive according to Fig. 1

The electromagnetic torque is directly proportional to the static pressure level. As could be shown, the interrelatedness of the fields electromagnetics and fluid power engineering demands a large number of teeth. However, the maximum teeth number is limited by the worsening ratio of the magnetic resistance between the aligned teeth position of stator and rotor (d position) and the unaligned position (q position). Moreover, narrow distances between the poles increase the leakage flux. Therefore, a multiple-teeth-per-pole configuration is recommended [4] to increase the power density by adding more teeth. **Figure 7** shows the four-pole separated stator, which has been developed for the 'reluctance pump', with magnetic flux curves. Three stator teeth are combined in one pole. This allows to arrange the windings in the broader pole gaps. Thus a large magnetomotive force θ can be generated for acceptable current densities. The leakage flux remains small thanks to the large pole distance.

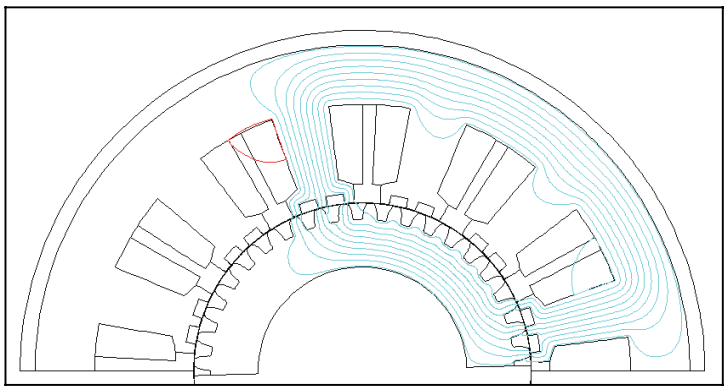

Fig. 7: Field pattern of the divided reluctance motor

The involute of the gear wheel reduces the degrees of freedom of the electromagnetic design, however, it is not in contradiction with the trapezoidal teeth of certain reluctance

machines. In addition to the tooth width, the tooth shape as well influences the torque characteristic and maximum. Tooth shapes tapering toward the 'air' gap increase the inductance ratio between the aligned and unaligned position. As can be seen in **Figure 8**, in such conditions very high magnetic inductions B can be attained in the tooth tips and in the 'air' gap.

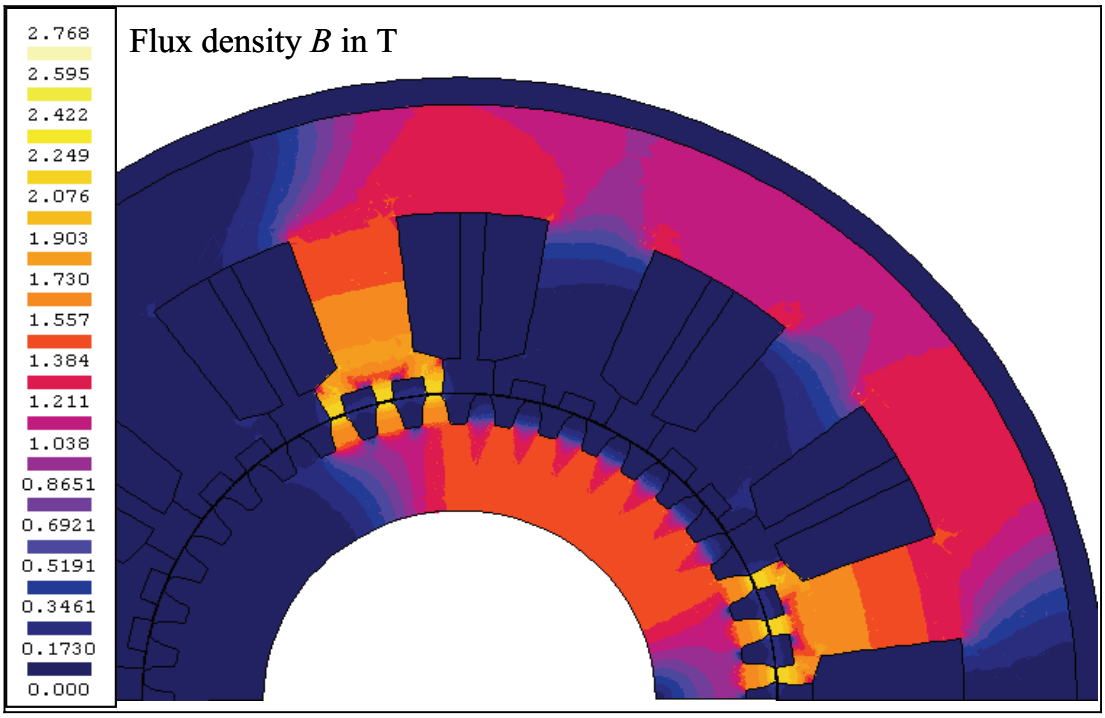

Fig. 8: Magnetic flux density distribution in stator and rotor in aligned position (d position)

In the multi-pole concept, the switching frequencies f_S also increase for large tooth numbers in rotor z_R. In connection with the revolution speed n the frequencies give:

$$f_S = n \cdot z_R \qquad (10)$$

This frequency is substantial for the iron losses and the degree of the core losses in the stator. Additionally, the demands made on the inverter become larger because of a higher switching frequency. For this reason, the chance to increase the power density by speeding up as in other electric machines is restricted. To limit the switching frequency, a rated speed of $n = 1{,}000\ \text{min}^{-1}$ as a maximum has proved most useful for the chosen number of teeth.

The functional integration implies very high demands on the mechanical and magnetic properties of the rotor. First, its mechanical strength and surface hardness shall be sufficiently high and second, it is expected to have soft magnetic properties. Soft magnetic materials are ferromagnetic substances that can be easily magnetised in a magnetic field and whose hysteresis losses during remagnetisation are therefore small. The total loss performance is made up of the interaction between hysteresis and eddy current losses.

A compact massive material cannot be considered at all for stator and rotor because of the eddy currents. To reduce the eddy current share, the rotors can be built from sheet layers each with a maximum thickness of 0.35 mm. Low-loss sheet iron (e.g.: M250-35)

and iron-cobalt alloys of the type Vacoflux or Vacodur by Vacuumschmelze can fulfil this task. To meet the hydrostatic demands in the laminated design, a suitable gluing technique is necessary. By now, there is no experience in glued hydrostatic drives. Alternatively, the rotors can be made of a soft magnetic composite core, such as Somaloy TM500 by Höganäs. It is mostly used in high-frequency applications with three-dimensional structures [5]. Here, the propagation of the eddy currents is restricted by the grit size. However, the currently available soft magnetic sintered materials have comparatively high hysteresis losses.
The rotor teeth shall fulfil soft magnetic requirements, on the one hand, and must have hardened edge layers, on the other, to take up mechanical stress during tooth engagement, e.g., fatigue and cavitation during the entire lifetime. Yet, surface hardening worsens the soft magnetic properties of the material. Equalising currents on the tooth surfaces can be avoided by insulating ceramic coatings which moreover protect the gearing from tear and fatigue.

The varying magnetisation behaviour of the different materials decisively influences the static motor characteristic (**Figure 9)**.

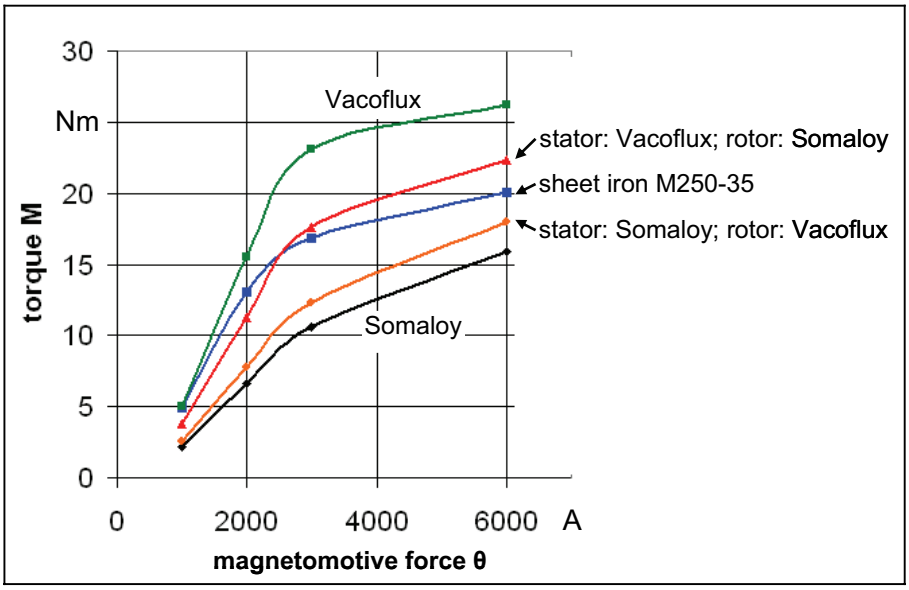

Fig. 9: Torque curves for various material combinations as a function of the magnetomotive force.

Table 2 shows the optimisation results gained by the design of the pilot sample for the material combination sheet iron M250-35 for rotor and stator.

Table 2: Motor and performance data of the pilot sample

maximum torque M	14 Nm (for b = 20 mm)
mean torque $\overline{M}$	10.6 Nm
max. revolution speed n	2,000 min^{-1}
max. power P	2.2 kW
utilisation factor C	299 kNm/m^3
static pressure p	18 bar
max. flow rate Q	75 l/min

4 SEALING CONCEPT

To seal the displacement volumes, the gaps between the side edges of the teeth and the housing (axial gap) and also between the tooth tips and the housing (radial gap) need to be as small as possible. A defined radial 'air' gap between the rotor and the stator teeth is necessary for the principle functioning of the switched reluctance drive, whereas the hydropump needs a sealing contact between the housing and the tooth tips to spatially separate the high pressure range from the suction pressure area.

Three sealing-relevant forces act upon the gear wheels during operation (**Figure 10**): The pressure forces F_p, the tooth forces F_m and the radial forces F_r resulting from the separation of the stator poles into two half spaces.

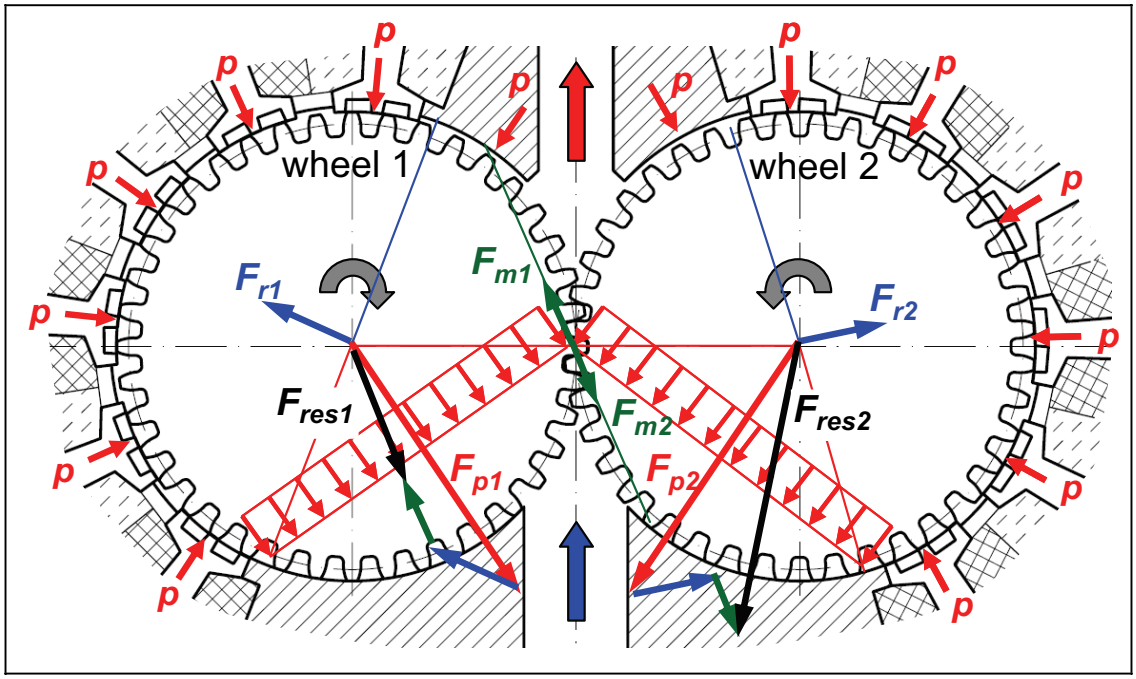

Fig. 10: Current force balance on the rotor shaft of the 'switched reluctance pump'

In conventional external gear pumps, a gear wheel is driven as driver gear by a separate motor unit. The driven gear is carried along by the driver gear. While the pump is being operated, the tooth force acts upon both gear wheels along the line of action. Owing to this force, the flanks of the two gear wheels form a sealing between each other. Contrary to conventional external gear pumps, where one wheel (driver gear) is driven and the other is carried along as driven gear, both gear wheels are driven in the 'reluctance pump'. If current is applied to the stator pole halves uniformly, the total value of the mean torque produced in the two rotors is the same. Conventional external gear pumps are designed with a single flank sealing (**Figure 11** left) with a defined flank clearance between the gear wheels. If this design is applied to the 'reluctance pump', there will be no defined sealing position of the two gear wheels so that the pressure forces cause a permanent leakage current through the flanks. As opposed to the single flank sealing, in a pump with double flank sealing (**Figure 11** right), during the reversing process from the pressure to the suction side the sealing is performed both on the loaded flank and on the non-loaded mating flank of each single tooth. Thus theoretically, there is no flank clearance in this

design variant of the 'reluctance pump' between the two gear wheels so that the sealing position is defined for the whole meshing process.

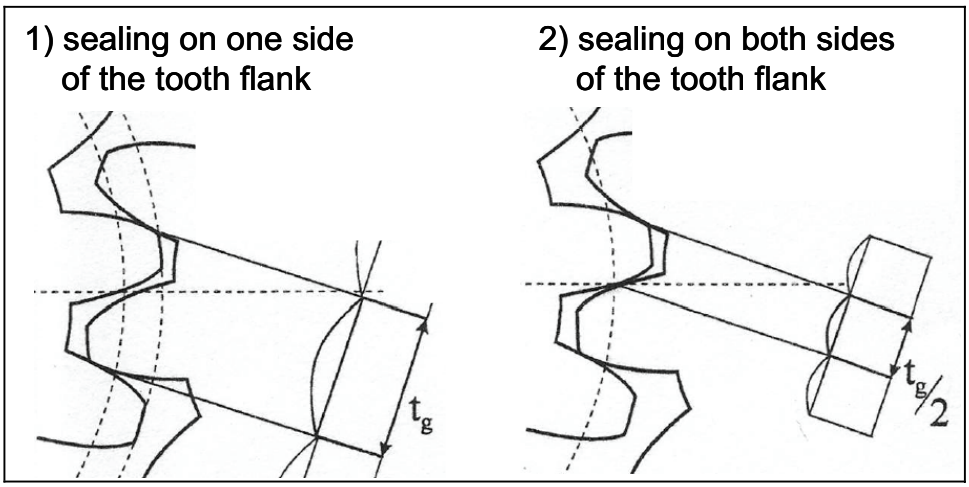

Fig. 11: Single and double contact sealing of the tooth flank [6]

As the design is intended for low-pressure applications only, lateral sealing of the pump gearing with constant axial clearance without movable bearing is sufficient.

5 CONCLUSIONS AND PROSPECTS

Thanks to functional integration, the drive concept of the 'reluctance pump' combines the hydraulic pump with the switched reluctance motor.
Among the benefits of this concept are that it requires no sealings to the outside, especially no shaft sealings, that it is easy to assemble and very compact. Hence this construction promises the highest degree of lifelong proofness. Temperature-sensitive zones in the magnetic field of the electric motor are subject to forced cooling because of the pumped hydraulic oil.
This research, however, shows that functionally integrated drives can only be used in low-pressure applications. The total integration concept presented is mainly restricted by the material. It must not only have soft magnetic properties, but at the same time its mechanical strength and surface hardness shall be very good. As regards the planned lamination of the rotor, long-term testing is necessary. A major drawback of the drive concept is the unused structural space in the core of the machine. The rotor must have large diameter, but its core volume does not contribute to the torque balance. The integration concept may be realised in high-pressure applications by housing the hydraulic pump in the idle core volume of the electric motor. This core integration ideally combines the different requirements of the two drives electric motor and hydraulic pump. An example of such a motor-pump unit is an adjustable-speed reluctance motor with a core-integrated modified internal gear pump (**Figure 12**).

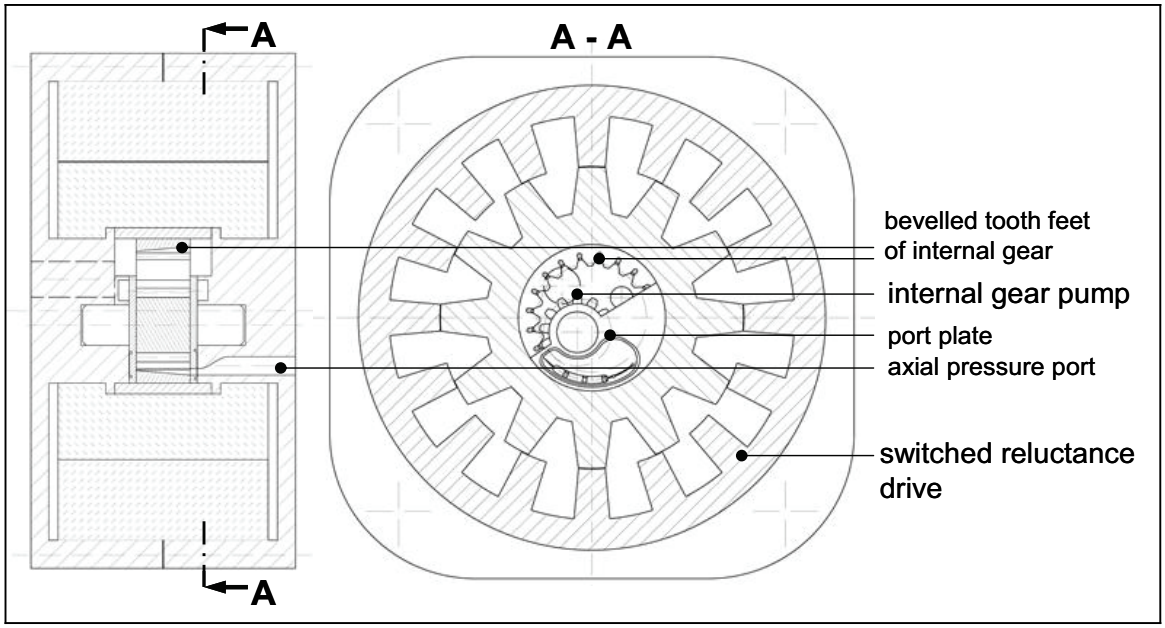

Fig. 12: Design of a motor-pump unit based on a modified internal gear pump for high pressure range

ACKNOWLEDGEMENTS

The German Research Foundation (*Deutsche Forschungsgemeinschaft-DFG*) supports the project 'Development of Integrated Electro-Hydrostatic Drive Systems'. The authors would like to thank the German Research Foundation for their financial support of the research work.

REFERENCES

[1] Motor-Pumpe-Hybridsystem EPAI für Hoch- und Mitteldruckanwendungen Voith Turbo GmbH & Co. KG, product catalogue

[2] Wolff, J.: Drehzahlveränderbarer Industrieantrieb mit Geschaltetem Reluktanzmotor, dissertation, U Karlsruhe, 1999

[3] Gutbrod, W.: Förderstrom von Außen- und Innenzahnradpumpen und seine Ungleichförmigkeit, Ölhydraulik und Pneumatik, 1975, No. 2

[4] Faiz, J.; Finch, J.W.: Design computations and performance characteristics prediction for multiple-tooth switched reluctance motors, International Journal of Computers and Electrical Engineering, Vol. 20, 1994, No. 3, pp. 243-258.

[5] Magnussen, F.; Sadarangani, C.; Svechkarenko, D.; Thelin, P.: Analysis of a PM Machine with Soft Magnetic Composite Core, IEEE Vehicular Power and Propulsion Symposium, Paris, France, 2004

[6] Becher, D.; Rausch, F.: Zweiflankendichtung mindert Volumenstrompulsation an Außenzahnradpumpen, Ölhydraulik und Pneumatik, 1997, No. 2

APPENDIX

Notation

b	gear set width
B	flux density
C	utilization factor
d	pitch circle diameter of gear
d_a	addendum circle diameter of gear
f_S	switching frequency
F_p, F_r, F_m	pressure force, radial force, tooth force
h	teeth depth of gear
l_i	core length
m	module of gear
M	torque
n	revolution speed
Q	flow rate
p	static pressure
P	power
s_a	tooth thickness on addendum circle
V	displacement volume
x	profile shift factor
z	teeth number of gear
α	angle of standard gear
δ	length of 'air' gap
θ	magnetomotive force
Φ	magnetic flux
ω	angular velocity

DESIGN AND IMPLEMENTATION OF ENERGY SAVING DIGITAL HYDRAULIC CONTROL SYSTEM

Matti Linjama[*], Mikko Huova[*], Pontus Boström[**], Arto Laamanen[*], Lauri Siivonen[*], Lionel Morel[***], Marina Waldén[**], Matti Vilenius[*]

[*]Tampere University of Technology, Institute of Hydraulics and Automation
P.O.Box 589, FI-33101 Tampere, Finland
Phone +358 3 3115 2690, Fax +358 3 3115 2240
E-mail: matti.linjama@tut.fi

[**]Åbo Akademi University, Department of Information Technologies,
Turku Center for Computer Science,
Joukahaisenkatu 3-5, FI-20520 Turku, Finland

[***]IRISA – Campus Universitaire de Beaulieu
35042 Rennes Cedex, France

ABSTRACT

Digital Hydraulics is a recently developed alternative for traditional control with servo or proportional valves. The key principle is to use parallel-connected two-way on/off valves together with intelligent control. This paper studies the energy efficiency of a high inertia cylinder drive. A valve manifold with 4×5 two-way screw-in cartridge valves is used to implement digital hydraulic control of the cylinder. A cost function based control solution is used for online minimization of power losses. Different loading conditions are analyzed and it is shown that the differential connection is essential in reduction of power losses. Switching logic between different flow modes is also studied. Implementation of these ideas requires complex control system. In order to ensure that control system functions as intended, modern techniques for software design and validation (Simulink/Stateflow) are used. The main result of the paper is that energy efficient, cavitation free and high-quality motion control is possible with rather slow response on/off valves. Experimental results with different loads demonstrate 36 percent energy saving in lift-and-lower movements, when compared to traditional load-sensing system.

KEYWORDS: Digital hydraulics, energy efficiency, distributed valve systems

1 INTRODUCTION

The main reason for the use of hydraulic actuators is high power to weight ratio. This is why typical applications are in high-power systems, e.g. mobile machines. The total efficiency of typical hydraulically actuated machines is very low, even below 5 percent [1]. This yields of excess fuel consumption, emissions and economical losses. The reason for poor efficiency is not in efficiency of individual components but in poor utilization of hydraulic power [1, 2].

Energy efficiency of hydraulic systems has recently been discussed in general level e.g. in [3, 4]. Peterson [3] mentions poor efficiency as the biggest problem of mobile hydraulics. He states that at least 50 percent reduction in power losses is needed in order to keep hydraulics competitive. Rydberg [4] discusses the use of distributed valves, hydraulic transformers and energy regeneration systems in energy saving. His conclusion is that "hydrostatic systems with valve control and machine control including energy regeneration have possibilities to be a very strong competitor in mobile machinery". This requires proper control strategy and good controllability of components.

Load sensing (LS) is the only widely used energy saving method in hydraulic systems. LS systems have stability problems and efficiency is poor when pressure demands of actuators are not at the same level or when lowering loads. Counterbalance valves cause also parasitic losses. Stability can be improved by using electric load sensing [5], and efficiency can be improved by utilizing pressure compensator spool position measurement [6].

Rather new and widely studied energy saving method is to replace one proportional spool valve with 2–5 independent control valves [7–12]. The approach is known as Programmable Valve, Multifunctional Valve, Separate Meter-In Separate Meter-Out Control, or Distributed Valve. The last name is used in this paper. Figure 1 shows some different distributed valve solutions found in literature. These systems can save energy because parasitic losses can be minimized and because valve system allows the use of different control modes, e.g. differential connection. Basic problems are the need for several high-quality proportional valves as well as complexity of control systems. Typically, a model based controller with closed-loop pressure and flow/velocity controllers are used. Successful pressure control requires high-bandwidth valves, good pressure sensors and accurate dynamic model of the system.

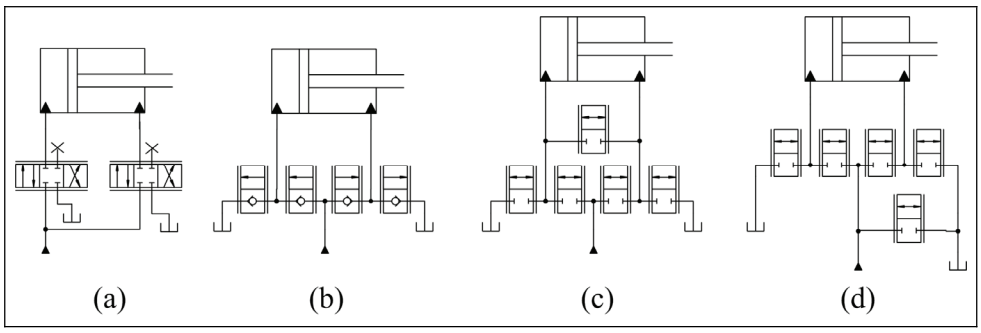

Figure 1. Different distributed valve systems found in literature.

Proper online selection of control mode of distributed valve systems is difficult and more or less unsolved problem. Hu and Zhang [12] controlled only one control edge and selected control mode according to position error. Shenouda and Book [10] used offline optimization in order to find optimal control mode selection scheme for given work cycle. Liu and Yao [9] used adaptive control law together with pressure measurements to select control mode online.

This paper studies so-called digital hydraulic distributed valvesystem [13]. The basic idea is that each flow path is controlled by a parallel-connected on/off valve series – so called digital flow control unit (DFCU), see Fig. 2. The flow capacities of on/off valves are set according to binary sequence, which gives 2^N discrete opening values for each DFCU where N is the number of parallel connected valves. Additional benefits of digital hydraulic solution – when compared to analogue systems – are low cost and robust valves, fault tolerance, exact knowledge of opening without spool position feedback, and faster and amplitude-independent response time [13–15]. The model based control principle has been developed for digital hydraulic valve system in [16, 17]. The controller utilizes the steady-state model of the system, and do not hence require any dynamic model of the system. The core of the control principle is cost function and selection scheme for finding control signals, which minimizes the cost function. Cost function can include terms for power losses and the control approach can therefore be used to reduce power losses. Initial simulation results show that the approach works and similar energy saving can be achieved than with other distributed valve solutions [18]. Objectives of this paper are to verify the results of [18] experimentally and to develop online switching scheme for selection of control mode. Systematic controller development methods described in [19] are utilized in order to achieve correct and reliable control code.

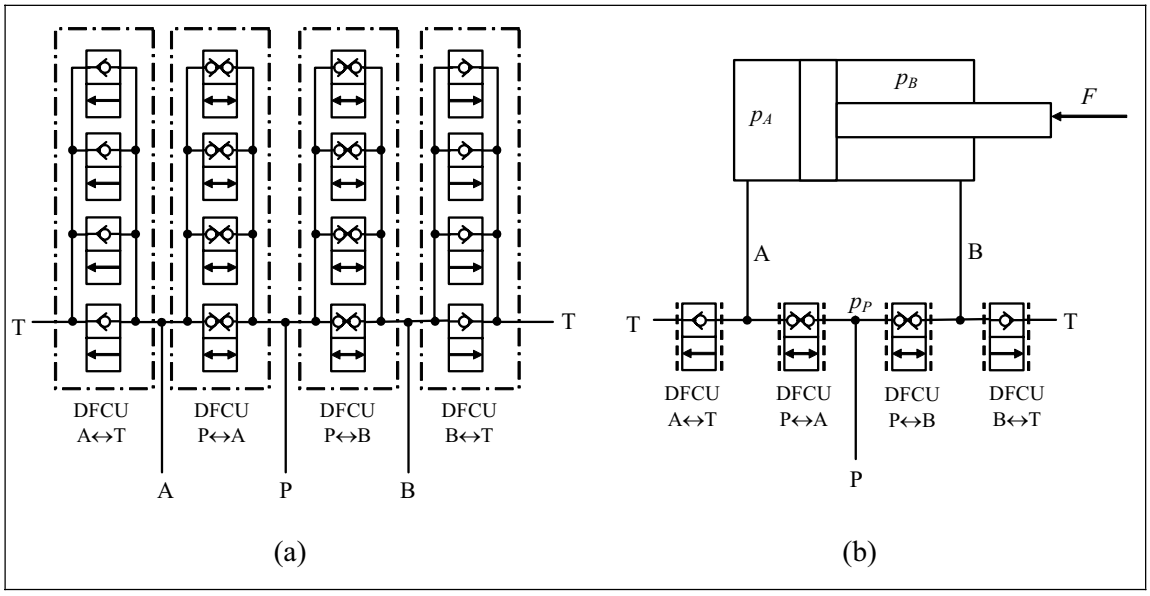

Figure 2. Digital hydraulic distributed valve system. Full circuit diagram with four valves per DFCU (a), and simplified circuit diagram with actuator (b).

2 ENERGY SAVING CONTROL OF DISTRIBUTED VALVE SYSTEMS

This chapter studies energy saving possibilities of distributed valve system of Fig. 1 (b) or 2 (b). Analysis is general and valid for both analogue and digital valve systems. Inputs of the system are external force F, supply pressure p_P and velocity reference v_{ref}. The target is to find rules, which control strategy should be used and how to calculate optimal supply and chamber pressures. Following assumptions are used:

1) Load force F is known e.g. from pressure measurements. By definition, positive load force restricts extending piston movement.
2) Valves set no limits for controllability of chamber pressures.
3) Pressure p_T at T-port is zero.
4) Target values for supply and chamber pressures must be above p_{min} in order to avoid cavitation and to retain stiffness.
5) Target values for supply and chamber pressures must be below p_{max} in order to avoid too high pressure.
6) Pressure differential Δp over active DFCUs should be at value Δp_N if possible and at least Δp_{min} where $\Delta p_{min} < \Delta p_N$.
7) Both sides of actuator must be under active control in order to retain hydraulic spring at both sides.
8) $p_{min} \geq \Delta p_N$
9) $A_A > A_B$

The seventh assumption slightly increases power losses but improves controllability. The target is to retain good controllability of inflow-outflow mode also in differential mode. The third and eighth assumptions are used only to simplify equations. The third and fourth assumptions prevents filling of cylinder chambers from tank.

2.1 Different Control Modes

Distributed valve systems can save energy by two ways. Firstly, opening of each control edge is freely adjustable, which allows minimization of parasitic back pressures. Secondly, valve system can run not only in inflow-outflow mode but also in differential mode. Figure 3 presents some different control modes. Mode 0 is stop mode in which all valves are closed. Modes 1 and 2 are standard inflow-outflow control modes while modes 3a, 3b and 4 are different forms of differential connection. Modes 3a and 3b are similar but load force and supply pressure determines direction of movement. Supply flow is negative in Mode 3b and if this is not allowed, Mode 4 can be used. Mode 4 is not studied in this paper.

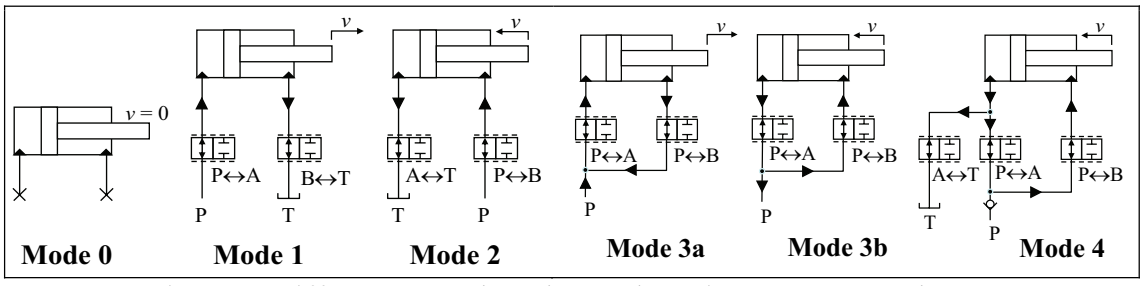

Figure 3. Different control modes. Only active DFCUs are shown.

2.2 Feasibility Ranges of Control Modes

Feasibility of control mode depends on actual load force, actual supply pressure and smallest allowed pressure differential over control valves. Mode is feasible, if chamber pressures p_A and p_B can be selected such that assumptions 1-9 are satisfied. From force balance equation and assumptions, following conditions must hold for Mode 1

$$p_{\min} \le p_A \le p_P - \Delta p \;\;,\;\; p_{\min} \le p_B \le p_{\max} \;\;,\;\; F = p_A A_A - p_B A_B \tag{1}$$

This gives feasibility range for Mode 1

$$\begin{aligned} \text{M1\_feas}(F, p_P, \Delta p) = &\left(p_{\min} A_A - p_{\max} A_B \le F \le (p_{\max} - \Delta p) A_A - p_{\min} A_B\right) \,\&\, \\ &\left(p_P \ge \max\left(p_{\min} + \Delta p \,,\, \frac{p_{\min} A_B + F}{A_A} + \Delta p\right)\right) \end{aligned} \tag{2}$$

The function notation M1_feas(F,p_P,Δp) is used in later derivations. The function returns 1 (TRUE) if mode is feasible and 0 (FALSE) if it is not feasible. The function has three inputs (F, p_P,Δp) and four constant parameters (p_{max}, p_{min}, A_A, A_B). Feasibility of other modes can be derived similarly. Mode 2 is feasible if following holds

$$\begin{aligned} \text{M2\_feas}(F, p_P, \Delta p) = &\left(p_{\min} A_A - (p_{\max} - \Delta p) A_B \le F \le p_{\max} A_A - p_{\min} A_B\right) \,\&\, \\ &\left(p_P \ge \max\left(p_{\min} + \Delta p \,,\, \frac{p_{\min} A_A - F}{A_B} + \Delta p\right)\right) \end{aligned} \tag{3}$$

Supply pressure must be between chamber pressure in modes 3a and 3b. The feasibility ranges are

$$\begin{aligned} \text{M3a\_feas}(F, p_P, \Delta p) = &\left(p_{\min} A_A - p_{\max} A_B \le F \le p_{\max}(A_A - A_B) - 2\Delta p A_A\right) \,\&\, \\ &\left(\max\left(p_{\min} + \Delta p, \frac{F + \Delta p(A_A + A_B)}{A_A - A_B}\right) \le p_P \le p_{\max} - \Delta p\right) \end{aligned} \tag{4}$$

$$\begin{aligned} \text{M3b\_feas}(F, p_P, \Delta p) = &\left(p_{\min}(A_A - A_B) + \Delta p(A_A + A_B) \le F \le p_{\max} A_A - p_{\min} A_B\right) \,\&\, \\ &\left(p_{\min} + \Delta p \le p_P \le \min\left(p_{\max} - \Delta p, \frac{F - \Delta p(A_A + A_B)}{A_A - A_B}\right)\right) \end{aligned} \tag{5}$$

An example system is used to visualize feasibility range of control modes. Numerical parameter values of the example system are: $A_A = \pi \times 0.063^2/2$, $A_B = A_A - \pi \times 0.036^2/2$, p_{max} = 20 MPa, p_{min} = 2 MPa, Δp = 1.5 MPa. Piston areas are same as in experimental test system. Figure 4 depicts feasibility ranges of example system. Note that modes 1 and 2 are feasible also with higher supply pressures than p_{max}.

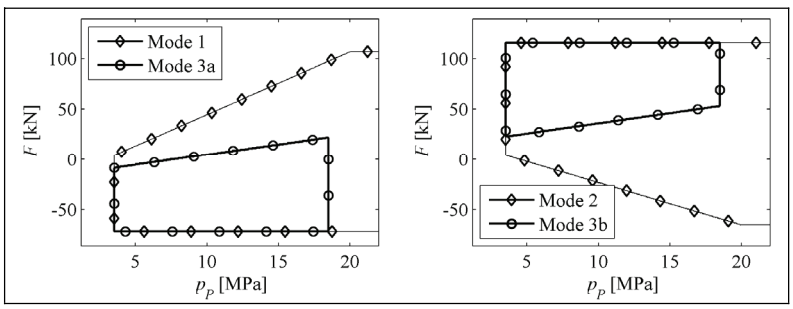

Figure 4. Feasibility ranges of control modes of the example system.

2.3 Calculation of Pressure References

Optimal supply pressure can be calculated from equations 2-5. For optimal energy usage, supply pressure should be as small as possible in modes 1, 2 and 3a, and as high as possible in Mode 3b. This gives

$$\begin{aligned}
p_{P,ref,M1} &= \min\left(p_{\max}, \max\left(p_{\min} + \Delta p_N, \frac{p_{\min} A_B + F}{A_A} + \Delta p_N \right) \right) \\
p_{P,ref,M2} &= \min\left(p_{\max}, \max\left(p_{\min} + \Delta p_N, \frac{p_{\min} A_A - F}{A_B} + \Delta p_N \right) \right) \\
p_{P,ref,M3a} &= \min\left(p_{\max} - \Delta p_N, \max\left(p_{\min} + \Delta p_N, \frac{F + \Delta p_N (A_A + A_B)}{A_A - A_B} \right) \right) \\
p_{P,ref,M3b} &= \max\left(p_{\min} + \Delta p_N, \min\left(p_{\max} - \Delta p_N, \frac{F - \Delta p_N (A_A + A_B)}{A_A - A_B} \right) \right)
\end{aligned} \tag{6}$$

The calculation of target values of chamber pressures is not trivial. In practice, supply pressure is never exactly at target value, which means that pressure differential is not at Δp_N. Simple rule is used in calculation of pressure references: pressure differential over supply-side DFCU should be at Δp_N whenever possible. This together with assumptions of Section 2.1 yield long derivations and final results only are given. Only one pressure reference is given and the other can be solved from force equation $p_A A_A - p_B A_B = F$.

$$p_{A,ref,M1} = \begin{cases} \max\left(p_{\min}, \min\left(\min(p_P - \Delta p_N, p_{\max}), \frac{p_{\max} A_B + F}{A_A} \right) \right) & , \text{ if } \text{M1\_feas}(F, p_P, \Delta p_N) \\ \max\left(p_{\min}, \frac{p_{\min} A_B + F}{A_A} \right) & , \text{ if } \text{M1\_feas}(F, p_P, \Delta p_{\min}) \;\&\; \sim\text{M1\_feas}(F, p_P, \Delta p_N) \end{cases} \tag{7}$$

$$p_{B,ref,M2} = \begin{cases} \max\left(p_{\min}, \min\left(\min(p_P - \Delta p_N, p_{\max}), \frac{p_{\max} A_A - F}{A_B} \right) \right) & , \text{ if } \text{M2\_feas}(F, p_P, \Delta p_N) \\ \max\left(p_{\min}, \frac{p_{\min} A_A - F}{A_B} \right) & , \text{ if } \text{M2\_feas}(F, p_P, \Delta p_{\min}) \;\&\; \sim\text{M2\_feas}(F, p_P, \Delta p_N) \end{cases} \tag{8}$$

$$p_{A,ref,M3a} = \begin{cases} \min\left(p_P - \Delta p_N, \frac{p_{\max} A_B + F}{A_A} \right) & , \text{ if } \text{M3a\_feas}(F, p_P, \Delta p_N) \\ \min\left(\frac{p_{\max} A_B + F}{A_A}, \max\left(p_{\min}, \frac{2 p_P A_B + F}{A_A + A_B} \right) \right) & , \text{if} \begin{cases} \text{M3a\_feas}(F, p_P, \Delta p_{\min}) \\ \;\&\; \sim\text{M3a\_feas}(F, p_P, \Delta p_N) \end{cases} \end{cases} \tag{9}$$

$$p_{B,ref,M3b} = \begin{cases} \min\left(p_P - \Delta p_N, \frac{p_{\max} A_A - F}{A_B} \right) & , \text{ if } \text{M3b\_feas}(F, p_P, \Delta p_N) \\ \min\left(\frac{p_{\max} A_A - F}{A_B}, \max\left(p_{\min}, \frac{2 p_P A_A - F}{A_A + A_B} \right) \right) & , \text{if} \begin{cases} \text{M3b\_feas}(F, p_P, \Delta p_{\min}) \\ \;\&\; \sim\text{M3b\_feas}(F, p_P, \Delta p_N) \end{cases} \end{cases} \tag{10}$$

2.4 Power Losses of Control Modes

If compressibility effects are neglected, input power of control modes can be calculated as a product of supply pressure and flow rate. Input powers of control modes are

$$\begin{aligned} P_{in,M1} &= p_P A_A v \\ P_{in,M2} &= -p_P A_B v \\ P_{in,M3a} &= P_{in,M3b} = p_P (A_A - A_B) v \end{aligned} \tag{11}$$

Note that input power is negative for Mode 3b. Mechanical output power is

$$P_{out} = Fv \tag{12}$$

and power loss is difference between input and output power. Figure 5 depicts input and output powers of Modes when supply pressure is selected according to Eq. 6. The figure shows that Modes 3a and 3b saves energy when compared to Modes 1 and 2.

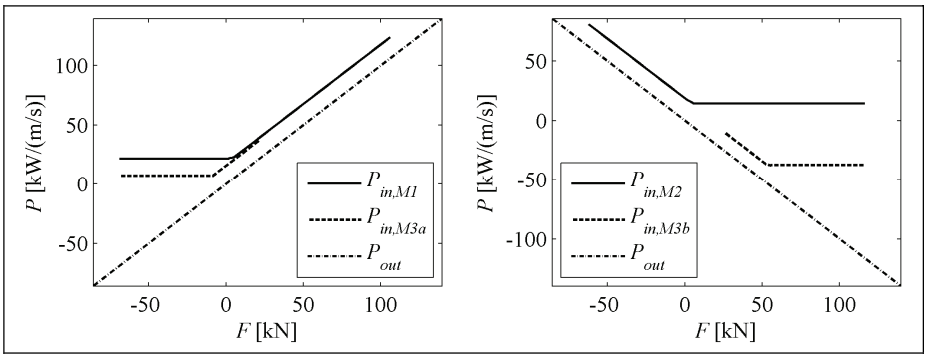

Figure 5. Input and output powers of the example system when optimal supply pressure is used.

2.5 Selection of Control Mode

Several topics must be considered in the selection of control mode. Energy analysis shows that modes 3a and 3b should be favoured over modes 1 and 2. However, mode switching process may cause losses because of finite supply pressure dynamics. For example, switching from Mode 1 to Mode 3a requires increase of supply pressure (while staying in Mode 1) and then switching to Mode 3a. Repetitive switching between different modes – caused by measurement noise and variation in supply pressure and load force – should also be avoided. Hysteresis is a key tool in avoidance of repetitive switching. In this paper, the selection of control mode is based on estimated power saving and switching losses as well as the use of "feas" functions of Equations 2–5. Power saving estimates of modes 3a and 3b can be calculated from Equations 6 and 11

$$\begin{aligned} \hat{P}_{save,M3a} &= p_{P,ref,M1} A_A v_{ref} - p_{P,ref,M3a} (A_A - A_B) v_{ref} \\ \hat{P}_{save,M3b} &= -p_{P,ref,M2} A_B v_{ref} - p_{P,ref,M3b} (A_A - A_B) v_{ref} \end{aligned} \tag{13}$$

where it is assumed that supply pressure is at optimal value and that velocity reference remains constant. Switching losses from Mode 1 to Mode 3a ($W_{sw,M1,M3a}$) and from Mode 2 to Mode 3b ($W_{sw,M2,M3b}$), can be estimated as

$$\hat{W}_{sw,M1,M3a} = \frac{A_A v_{ref} \left(p_{P,ref,M3a} - p_{P,ref,M1} \right)^2}{2 \, \mathrm{d}\, p_P / \mathrm{d}t}$$
$$\hat{W}_{sw,M2,M3b} = -\frac{A_B v_{ref} \left(p_{P,ref,M3b} - p_{P,ref,M2} \right)^2}{2 \, \mathrm{d}\, p_P / \mathrm{d}t} \qquad (14)$$

The equation is based on assumptions of constant velocity reference and linear supply pressure rise with gradient $\mathrm{d}p_P/\mathrm{d}t$. The equation also assumes that required supply pressure is higher in Modes 3a and 3b than in modes 1 and 2. If this is not the case, switching loss is assumed zero.

The approach used in the selection of control mode is to determine mode switching conditions, i.e. when to change from mode to another. Firstly, freely adjustable supply pressure is assumed and the "best possible" Mode (Target Mode) is determined. Then supply pressure reference is set according to Target Mode (Eq. 6), but actual control mode (Actual Mode) is selected according to actual supply pressure. Actual Mode determines control strategy of valves and reference values for chamber pressures. Target Mode and Actual Mode are usually the same except during mode switching period. Selection of Target mode is based on switching conditions given in Table 1. Conditions are given for Modes 1 and 3a only, and conditions for Modes 2 and 3b are analogous.

Table 1. Suggested switching conditions for determination of Target Mode.

From	To	Switching condition
Mode 0	Mode 1	$v_{ref} \geq v_{tres1}$ AND M1_feas(F, p_{max} , Δp_N)
Mode 1	Mode 0	$v_{ref} \leq v_{tres2}$ OR ~M1_feas(F, p_{max} , Δp_{min})
Mode 0	Mode 3a	$v_{ref} \geq v_{tres1}$ AND M3a_feas($F+\Delta F$, $p_{max} - \Delta p_N$, Δp_N) AND $\hat{P}_{save,M3a} \geq P_{tres}$ AND $\hat{P}_{save,M3a} t_{earn} \geq \hat{W}_{sw,M1,M3a}$
Mode 3a	Mode 0	$v_{ref} \leq v_{tres2}$ OR (~M3a_feas(F, $p_{max} - \Delta p_N$, Δp_{min}) AND ~M1_feas(F, p_{max} , Δp_{min}))
Mode 1	Mode 3a	M3a_feas($F+\Delta F$, $p_{max} - \Delta p_N$, Δp_N) AND $\hat{P}_{save,M3a} \geq P_{tres}$ AND $\hat{P}_{save,M3a} t_{earn} \geq \hat{W}_{sw,M1,M3a}$
Mode 3a	Mode 1	~M3a_feas(F, $p_{max} - \Delta p_N$, Δp_{min}) AND M1_feas(F, p_{max} , Δp_N)

Hysteresis is introduced by separating forward and reverse switching conditions. For example, Target Mode is changed from Mode 0 to Mode 1 if velocity reference is bigger than a certain threshold value v_{tres1} and if Mode 1 is feasible with the maximum supply pressure and nominal pressure differential. Reverse switching happens if velocity reference is smaller than another (smaller) threshold value v_{tres2} or if Mode 1 is not feasible with the smallest allowed pressure differential. Mode 3a is used only if it reduces power losses significantly and if switching losses can be earned within time t_{earn}. Switching to Mode 3a requires that it remains feasible even if force increases by ΔF.

Suggested switching conditions for Actual Mode are quite similar and are given in Table 2. There is no Δp hysteresis but all conditions are calculated with minimum pressure differential Δp_{min}. This helps to initiate motion as early as possible but may yield repetitive switchings.

Table 2. Suggested switching conditions for determination of Actual Mode.

From	To	Switching condition
Mode 0	Mode 1	$v_{ref} \geq v_{tres1}$ AND M1_feas(F, p_P , Δp_{min})
Mode 1	Mode 0	$v_{ref} \leq v_{tres2}$ OR ~M1_feas(F, p_P , Δp_{min})
Mode 0	Mode 3a	$v_{ref} \geq v_{tres1}$ AND M3a_feas(F, p_P , Δp_{min}) AND Target Mode = 3a
Mode 3a	Mode 0	$v_{ref} \leq v_{tres2}$ OR (~M3a_feas(F, p_P , Δp_{min}) AND ~M1_feas(F, p_P , Δp_{min}))
Mode 1	Mode 3a	M3a_feas(F, p_P , Δp_{min}) AND Target Mode = 3a
Mode 3a	Mode 1	~M3a_feas(F, p_P , Δp_{min}) AND M1_feas(F, p_P , Δp_{min})

Mode switching is implemented by using Simulink/Stateflow software from Mathworks. Details of the implementation are given in [19].

3 MODEL BASED CONTROLLER

Model based controller for digital hydraulic systems have been developed in [16, 17]. An upgraded version of the controller is used in this paper and operation principle and improvements are briefly presented in this Chapter.

3.1 Steady-State Model and Its Solution

Typical Digital Hydraulic cylinder drive is shown in Fig. 2 (b). Control edges P↔A, A→T, P↔B and B→T are controlled by n_1 parallel connected on/off valves. Control edges are denoted by subscripts PA, AT, PB and BT. On/off valves are modeled as generalized turbulent orifices using equations

$$Q(u, p_{in}, p_{out}) = \begin{cases} u K_v (p_{in} - p_{out})^x & , b\, p_{in} < p_{out} \leq p_{in} \\ u K_v [(1-b) p_{in}]^x & , p_{out} \leq b\, p_{in} \\ -u K_v (p_{out} - p_{in})^x & , b\, p_{out} < p_{in} < p_{out} \\ -u K_v [(1-b) p_{out}]^x & , p_{in} \leq b\, p_{out} \end{cases} \tag{15}$$

where u is 0 if valve is closed and 1 if valve is open. Further, K_v is flow coefficient, p_{in} pressure at inlet port, p_{out} pressure at the outlet port and b critical pressure ratio, which models cavitation choking. The square root model (x=0.5) is usually used in literature but significantly better agreement can be achieved if exponent is not fixed to 0.5. Steady-state model is achieved from the A- and B-side flow balance and force balance

$$\begin{aligned} &\sum_{i=1}^{n_1} [Q_{PAi}(u_{PAi}, p_P, p_A) - Q_{ATi}(u_{ATi}, p_A, p_T)] - A_A v = 0 \\ &\sum_{i=1}^{n_1} [Q_{PBi}(u_{PBi}, p_P, p_B) - Q_{BTi}(u_{BTi}, p_B, p_T)] + A_B v = 0 \\ &A_A p_A - A_B p_B - F = 0 \end{aligned} \tag{16}$$

The steady-state model of Eq. 16 does not have analytical solution but it must be solved numerically. Newton-Raphson iteration is used to solve Eq. 16 for v, p_A and p_B. Fixed number of iterations (n_{iter}) is used and following methods are used to improve robustness and numerical efficiency:

1) Target velocity and pressures are used as initial value
2) Velocity is limited between $-v_{max}$ and v_{max} , and pressures are limited between 0 and $1.25\times p_{max}$ during iterations.
3) Step size is limited to $1/n_{iter}\times 100$ per cent of maximum values of 2). The limitation is implemented such that original search direction is retained.
4) Too small pressure differentials are replaced with small constant value in the calculation of Jacobian in order to avoid infinite elements.
5) Symmetry of flow equations is utilized, which allows the calculation of flow rate and its partial derivative with only one pow-function call.
6) Sparse structure of Jacobian matrix is considered and its inverse is calculated analytically.
7) Solution is accepted only if velocity and force errors are small enough.

3.2 Determination of Search Space

The digital hydraulic system of Fig. 2 (b) has 2^{4n_1} different states because each valve has two states. This means over million states in typical 4×5 valve system. Solving steady-state model of the system is also computationally demanding. New valve model requires computation of one pow-function for each valve while standard square root model would require computation of one square root for each DFCU. It is essential that the number of steady-state solutions is minimized, which calls for careful pre-selection of solution candidates. This determination of search space is made according to [17]. It is assumed that pressures are at target values, and A- and B-side of the system are analysed separately by using following 'direct' cost functions

$$J_A = \left(\frac{1}{A_A} \sum_{i=1}^{n_1} \left[Q_{PAi}\left(u_{PAi}, p_P, p_{A,ref}\right) - Q_{ATi}\left(u_{ATi}, p_{A,ref}, p_T\right) \right] - v_{ref} \right)^2 + \left| v_{ref} \right| W_{pow} \times \left(K_1 \left(\left(p_P - p_{A,ref}\right) \sum_{i=1}^{n_1} Q_{PAi}\left(u_{PAi}, p_P, p_{A,ref}\right) \right)^2 + K_2 \left(\left(p_{A,ref} - p_T\right) \sum_{i=1}^{n_1} Q_{ATi}\left(u_{ATi}, p_{A,ref}, p_T\right) \right)^2 \right) \tag{18a}$$

$$J_B = \left(\frac{1}{A_B} \sum_{i=1}^{n_1} \left[Q_{PBi}\left(u_{PBi}, p_P, p_{B,ref}\right) - Q_{BTi}\left(u_{BTi}, p_{B,ref}, p_T\right) \right] + v_{ref} \right)^2 + \left| v_{ref} \right| W_{pow} \times \left(K_3 \left(\left(p_P - p_{B,ref}\right) \sum_{i=1}^{n_1} Q_{PBi}\left(u_{PBi}, p_P, p_{B,ref}\right) \right)^2 + K_4 \left(\left(p_{B,ref} - p_T\right) \sum_{i=1}^{n_1} Q_{BTi}\left(u_{BTi}, p_{B,ref}, p_T\right) \right)^2 \right) \tag{18b}$$

Cost functions have quadratic term for velocity error and power losses. Power losses are multiplied by v_{ref}, which means that relative importance of power losses reduces at lower velocities. Parameter W_{pow} determines importance of power saving and K coefficients takes into account actual mode according to Table 3.

Table 3. Values of K-coefficients in Eq. 18.

Actual Mode	K_1	K_2	K_3	K_4
Mode 1	0	1	1	0
Mode 2	1	0	0	1
Modes 3a & 3b	0	1	0	1

The search space is determined by calculating J_A for all A-side opening combinations and J_B for all B-side opening combinations. After that, n_{ss} best opening combinations are selected for both sides and their n_{ss}^2 permutations form the search space. Details of this process are given in [17].

3.4 Selection of Optimal Control

Selection of valve control is made by solving steady-state system equations for each element of the search space and selecting the element, which minimizes given cost function. The design of cost function is the most important part of the control design and following cost function is used in this paper

$$
\begin{aligned}
J = {} & \left(v_{ref} - v_{ss}\right)^2 + \left|v_{ref}\right| W_{pres} \left\{\left(p_{A,ref} - p_{A,ss}\right)^2 + \left(p_{B,ref} - p_{B,ss}\right)^2\right\} + \left|v_{ref}\right| W_{pow} \times \\
& \left\{ K_1 \left(\left(p_P - p_{A,ss}\right) \sum_{i=1}^{n_1} Q_{PAi}\left(u_{PAi}, p_P, p_{A,ss}\right) \right)^2 + K_2 \left(\left(p_{A,ss} - p_T\right) \sum_{i=1}^{n_1} Q_{ATi}\left(u_{ATi}, p_{A,ss}, p_T\right) \right)^2 + \right. \\
& \left. K_3 \left(\left(p_P - p_{B,ss}\right) \sum_{i=1}^{n_1} Q_{PBi}\left(u_{PBi}, p_P, p_{B,ss}\right) \right)^2 + K_4 \left(\left(p_{B,ss} - p_T\right) \sum_{i=1}^{n_1} Q_{BTi}\left(u_{BTi}, p_{B,ss}, p_T\right) \right)^2 \right\} + \\
& W_{sw} \sum_{i=1}^{n_1} \left(Q_{N,PAi} \left|\Delta u_{PAi}\right| + Q_{N,ATi} \left|\Delta u_{ATi}\right| + Q_{N,PBi} \left|\Delta u_{PBi}\right| + Q_{N,BTi} \left|\Delta u_{BTi}\right| \right)
\end{aligned}
\tag{19}
$$

where v_{ss} is the calculated steady-state piston velocity, $p_{A,ss}$ and $p_{B,ss}$ are the calculated steady-state pressures in A- and B-chambers, and Δu_{PAi}, Δu_{ATi}, Δu_{PBi} and Δu_{BTi} are changes in control signals of valves when the new control signal is applied. The cost function has four terms. The first one sets penalty difference between target and calculated steady-state velocity. The second term sets penalty for errors between reference and steady-state pressures, and parameter W_{pres} is used to find good compromise between velocity and pressure tracking. The third term sets penalty for power losses similarly as in direct cost functions of Eq. 18. The fourth term is included to reduce activity of valves. The switching of each valve is weighted by its nominal flow rate (calculated at $\Delta p = \Delta p_N$). Activity of valves can be reduced by increasing parameter W_{sw}.

3.5 Block Diagram of Control System

Block diagram of the complete system is shown in Fig. 6. Trajectory generator generates smooth position and velocity references, and feedforward plus P-controller is used to generate closed-loop velocity reference v_ref_C. Steady-state load force is calculated from low-pass filtered pressure signals. Measured supply pressure is also slightly low-pass filtered in order to reduce the effect of measurement noise.

Implementation of the model based controller coupled with energy saving requires a sophisticated controller. To handle the complexity and ensure reliability of the system, adequate controller architectures and development techniques are needed. The controller described in this paper has developed using such techniques. The architecture

used for the controller, as well as techniques for improving the quality of Simulink diagrams are described in [19].

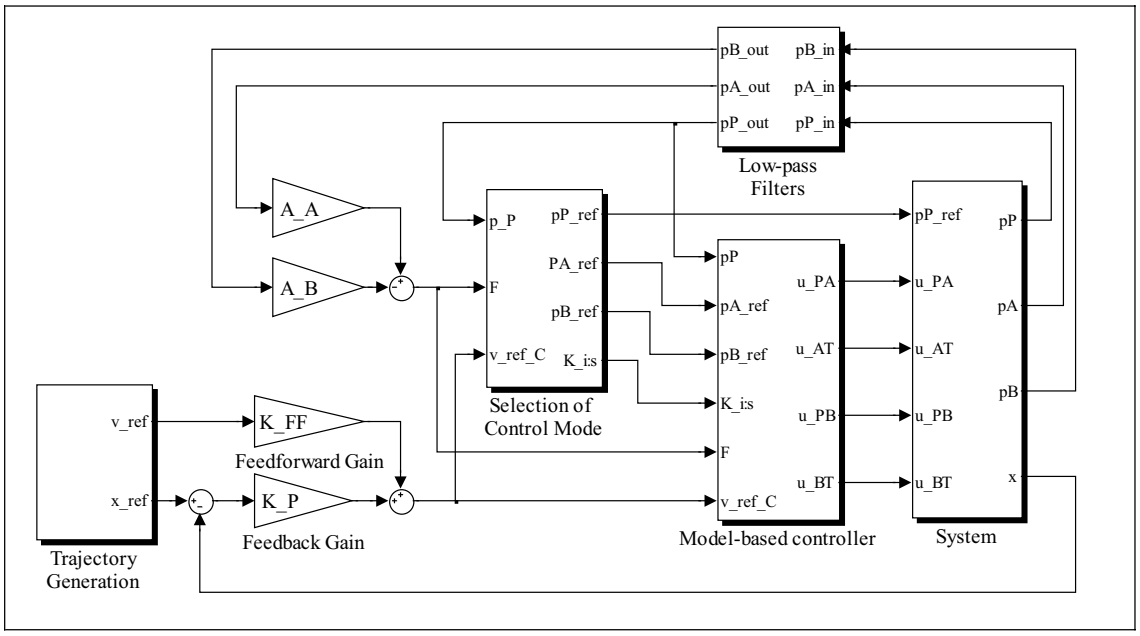

Figure 6. Block Diagram of the control system.

4 TEST SYSTEM

The test system and its hydraulic circuit diagram are shown in Figure 7. The system mimics the dynamics of the joint actuator of a typical medium sized mobile machine boom and its natural frequency is 3–5 Hz with 400 kg load mass. The static and dynamic characteristics of the system are given in [20]. Hydac WS08W-01 screw-in cartridge valves with 12 VDC solenoids are used as digital valves and all four DFCUs are integrated into one manifold. The flow capacities of valves are adjusted by M6 orifices inside the manifold. The biggest valves have also orifices in order to keep pressure differential over valve sufficiently small and to ensure proper functioning of valves. Two biggest valves have same flow capacity in order to maximize flow rate and the others are approximately according to binary sequence. The design is thus "four-and-half bit" and gives in theory resolution of 1:23. In practice, the ratio between maximum and minimum flow of DFCUs is 13–15 because flow rates are not exactly according to binary sequence.

The reference valve is Bosch Rexroth M4-12 mobile proportional valve equipped with ~1 MPa pressure compensator and CAN-bus integrated electronics. A spool with high back pressure (M4-12/10/E045-065N14-17R073057) is used because the system does not have counterbalance valve and because of large force variations. A-port of valve is connected to piston rod side and B-port to piston side of cylinder.

The main pump runs in constant flow mode and supply pressure control is implemented by Bosch Rexroth DBEME 10-5X/200YG24NK31M proportional pressure relief valve. The valve has slightly non-linear control curve, hysteresis and significant overshoot in

step response. Valve characteristics are improved by using closed-loop non-linear PI-controller and by utilizing measured characteristic curve and feedforward from flow rate. The maximum rate of the supply pressure control is about 30 MPa/s, which is relatively low value and causes delay at the beginning of motion.

The control hardware consists of a dSPACE DS1006 controller board with 2.2 GHz AMD Opteron main processor. The valve control electronics is based on H-bridge configuration with Texas Instruments DRV102T high-side PWM driver and International Rectifier IRLR120N low-side FET. Supply voltage is 36 V, pull-on time 10 ms and PWM duty ratio about 30 percent. Flow rate is measured by recording two pulse signals of the sensor via incremental encoder interface.

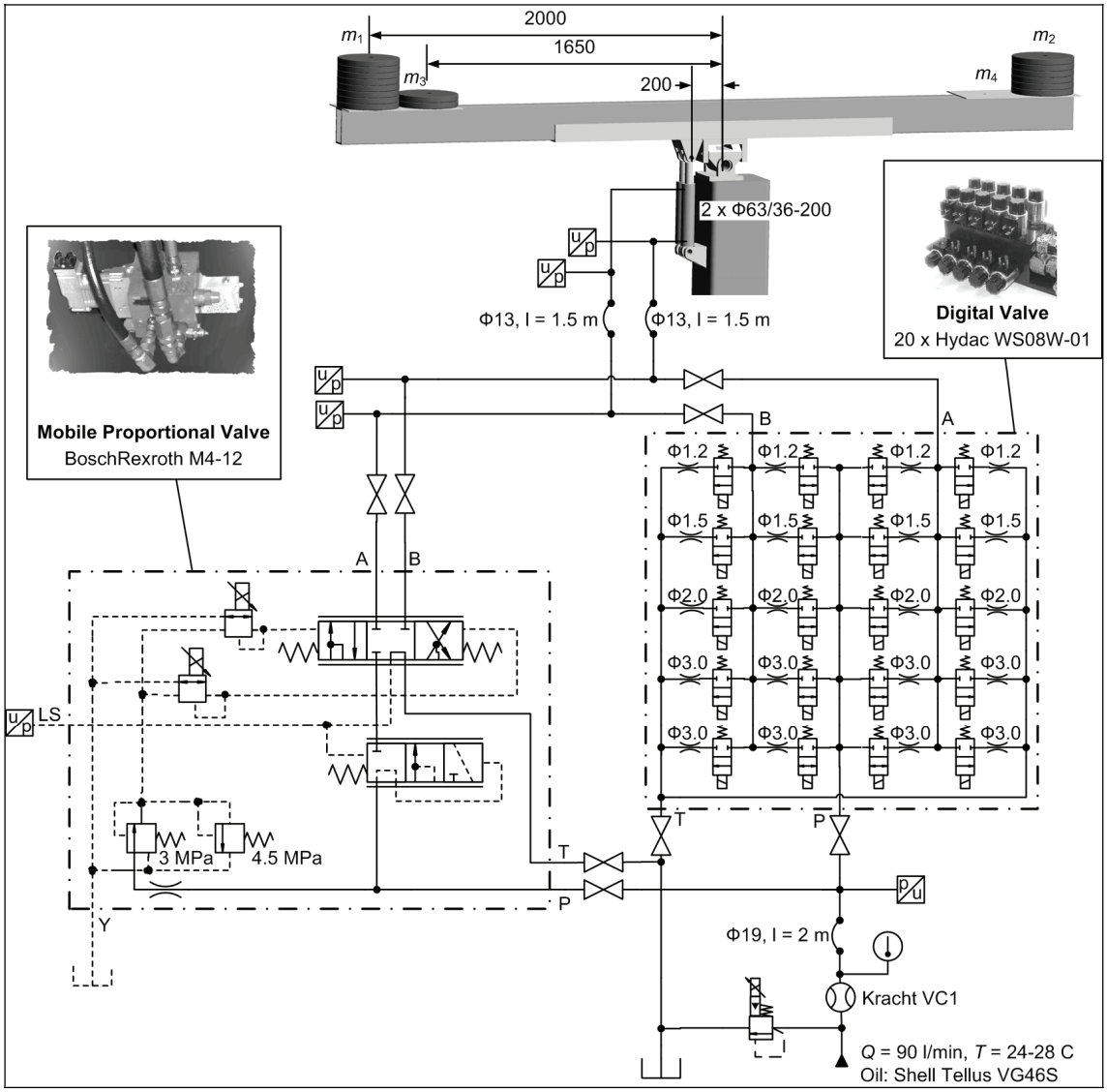

Figure 7. Hydraulic circuit diagram of the system.

5 EXPERIMENTAL RESULTS

5.1 Loading Conditions and Reference Trajectories

Loading conditions are the same as in earlier papers [17, 20] (see Fig. 7 for definition of load masses):

- Loading A: m_1=200 kg, m_2=150 kg, m_3=50 kg, m_4 = 0 kg (almost balanced)
- Loading B: m_1=200 kg, m_2=0 kg, m_3=200 kg, m_4 = 0 kg (restrictive load)
- Loading C: m_1=100 kg, m_2=200 kg, m_3=0 kg, m_4 = 100 kg (overrunning load)

Large and small reference trajectories are used both having two up and down movements. Fifth order polynomials are used as position references and the fastest trajectory is selected such that digital valve system can deliver sufficient flow with 1.5 MPa pressure differential. Movement time is 1.25 s and trajectories studied are:

- Small trajectory: 6 and 12 mm movements. Peak velocities are 9 and 18 mm/s.
- Large trajectory: 35 and 70 mm movements. Peak velocities are 52.5 and 105 mm/s.

5.2 Tuning of Reference Valve System

The directional mobile proportional valve has pressure compensator and pressure differential has only a minor effect on flow characteristics. Piston velocity as a function of control signal is measured in both directions and inverses of these curves are utilized. After that, input can be given as velocity and feedforward plus P-controller of Fig. 6 can be used. Load pressure is measured from the LS channel and target value for supply pressure is LS pressure plus 1 MPa. Smaller pressure differential causes rapidly decreasing control performance. P-controller gain is adjusted to be about 40 percent of critical gain and feedforward gain is adjusted such that there are no heavy overshoots. Tuning values are K_P = 2.5 1/s and K_{FF} = 0.9. LS pressure is filtered with a second order discrete time filter with damping factor of 0.7. It was found that filter is not needed to stabilize the system and break frequency of 200 rad/s was used only to reduce measurement noise.

5.3 Calibration Measurements of Digital Valves

Flow characteristics of each valve of the digital valve system are measured in order to find out parameter values of the valve model. DFCUs PA and PB are measured in both directions with constant 10 MPa inlet pressure and variable outlet pressure while DFCUs AT and BT are measured with small outlet pressure and variable inlet pressure. Parameter values of valve models are given in Table 4. Some exponents differ significantly from 0.5, which means that generalized model of Eq. 15 gives significantly better fit than standard square root model. Critical pressure ratios of tank side valves cannot be determined reliably from measurements and value 0.1 is used for most valves. Delays of valves are estimated from open-loop responses of the test system and opening delays are about 10 ms and closing delays between 10 and 20 ms such that smaller valves closes more slowly.

Table 4. Parameter values of valve models.

	$K_v \times 10^7$	x	b
P→A	[0.65 0.345 0.78 1.05 1.02]	[0.47 0.55 0.52 0.54 0.54]	[0.22 0.34 0.3 0.23 0.19]
A→P	[0.214 0.33 0.8 0.88 0.885]	[0.55 0.55 0.52 0.55 0.55]	[0.2 0.16 0.13 0.1 0.1]
A→T	[0.61 0.835 1.345 0.895 0.91]	[0.48 0.485 0.485 0.555 0.555]	[0.1 0.1 0.1 0.1 0.12]
P→B	[0.48 0.3 1.06 1.07 1.06]	[0.49 0.56 0.5 0.54 0.54]	[0.2 0.36 0.3 0.23 0.23]
B→P	[0.184 0.33 0.61 0.75 0.75]	[0.56 0.55 0.54 0.56 0.56]	[0.19 0.16 0.13 0.1 0.1]
B→T	[0.515 0.945 1.4 1.72 1.245]	[0.485 0.48 0.485 0.515 0.535]	[0.1 0.1 0.1 0.13 0.1]

5.4 Tuning of Digital Valve System

Control system of digital valves has many parameters and tuning is based on extensive simulations. Parameters of steady-state Newton-Raphson solver are found by studying convergence of the solution. Error tolerance is set to 0.5 mm/s for velocity and 200 N for force and four iterations is enough to find solution in most cases. Size of search space is increased until no improvement in control performance is detected, which yields n_{ss}=10. Sampling time is selected to be 24 ms, which is slightly more than biggest delay of valves. Minimum pressure (p_{min}=2 MPa) is selected such that no cavitation occurs and nominal pressure differential (Δp_N=1.5 MPa) such that control performance reduces only moderately. Maximum pressure p_{max} is set to 20 MPa and minimum pressure differential Δp_{min} to 0.5 MPa. Mode switching parameters (v_{tol1}=3.3 mm/s, v_{tol2}=2.4 mm/s, ΔF=5 kN, t_{earn}=0.5 s, P_{tres}=100 W) are selected such that intended switching characteristics is achieved. However, switching conditions of Tables 1 and 2 yield repetitive switchings between modes because of imperfections of supply pressure control. The problem is solved by requiring that negated feasibility conditions (e.g. ~M1_feas) must be true 240 ms before switching occurs. This is formally incorrect because mode can be active even if it is not feasible, which yields short-term violation of input assumptions of pressure references calculation [19]. Weight factors of cost function ($W_{pres}=2\times10^{-16}$, $W_{pow}= 4\times10^{-6}$, W_{sw} = 0.05) are increased one in turn until control performance starts to decrease. Main effort is to minimize power losses (i.e. large W_{pow}) without too big reduction in control performance. Feedforward and P-controller gains are selected similarly as in proportional valve case and values used are K_P = 3.0 1/s, K_{FF} = 0.74. Load force is estimated from filtered pressure signals and filter break frequency has an important effect on characteristics and stability of the system. Rather low break frequency of 8 rad/s is used in order to avoid overshoots. Computation of control code with these parameters takes 6 ms in DS1006.

5.6 Results

Figures 8 and 9 present measured large responses with Loading A. Both valves give rather similar control performance but input energy W_{in} is significantly smaller with digital valve system. Figures 10 and 11 show large responses with Loading B. Cavitation occurs with proportional valve and there are some oscillations in velocity response. Digital valve system utilizes differential Mode 3b (Mode=4) in lowering of load and is able to save energy 44 percent in this response. Controllability remains good in Mode 3b. Figures 12 and 13 present responses with Loading C. Both systems have some oscillations after larger upwards movement. Downwards movement is sluggish with proportional valve and it also cavitates. Digital valve system utilizes differential Mode 3a (Mode=3) in upwards movement and controllability is good also in this Mode.

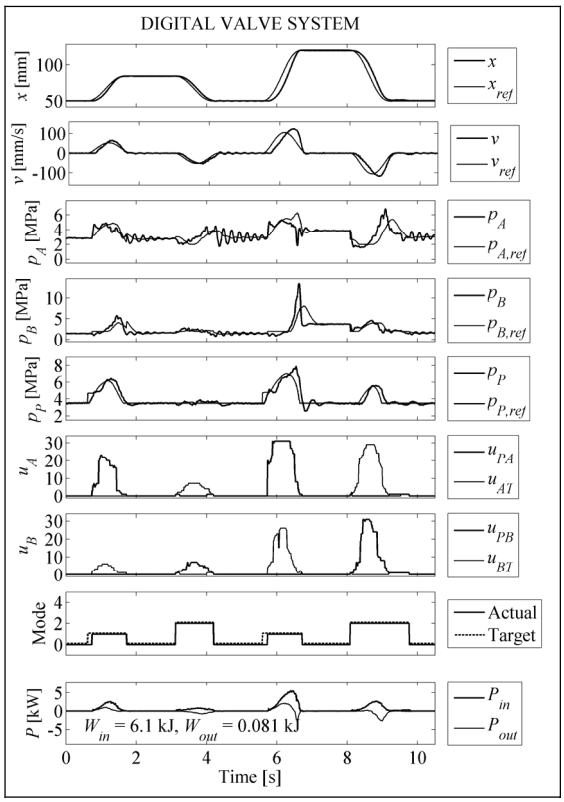

Figure 8. Measured large response with digital valve system and Loading A.

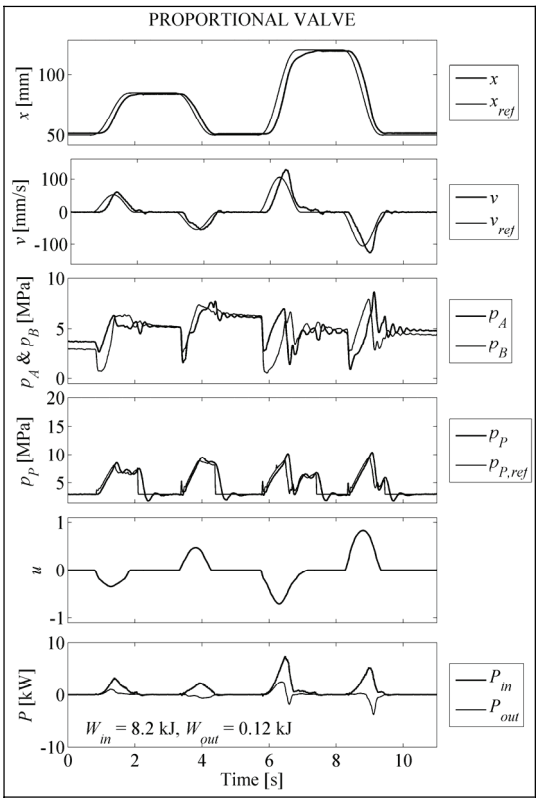

Figure 9. Measured large response with proportional valve and Loading A.

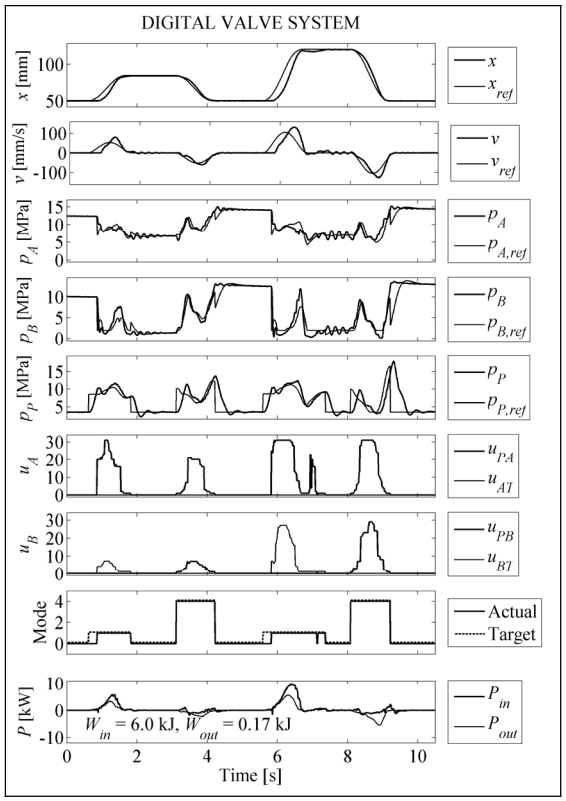

Figure 10. Measured large response with digital valve system and Loading B.

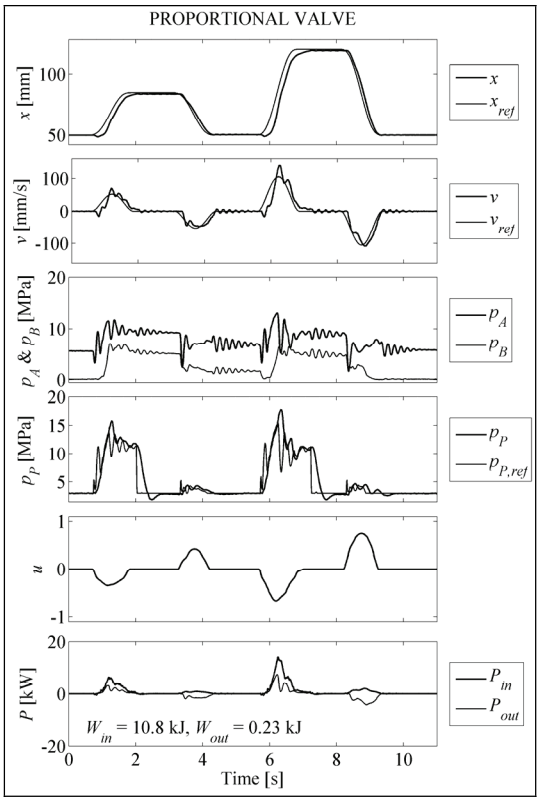

Figure 11. Measured large response with proportional valve and Loading B.

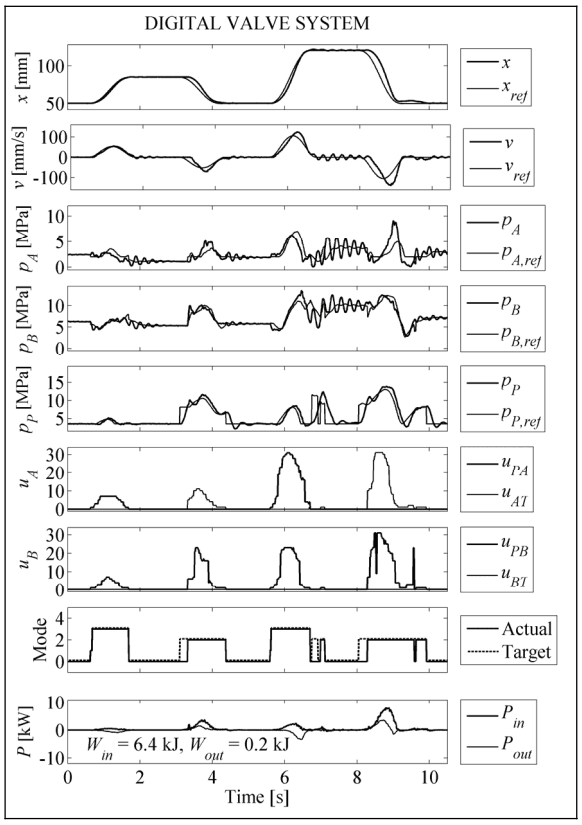

Figure 12. Measured large response with digital valve system and Loading C.

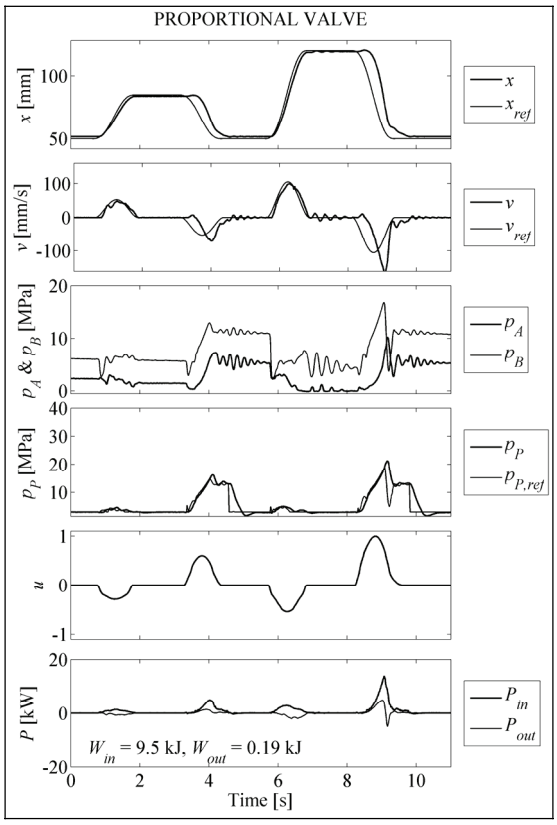

Figure 13. Measured large response with proportional valve and Loading C.

Small trajectory measurements show quite similar controllability in both systems and no cavitation occurs. Input energies of all responses are given in Table 5. Average energy saving with digital valve system is 36 percent.

Table 5. Input energies of all measured responses.

Trajectory	Large			Small			Σ
Loading	A	B	C	A	B	C	
W_{in} with digital valve [kJ]	6.1	6.0	6.4	1.1	0.9	0.8	**21.3**
W_{in} with proportional valve [kJ]	8.2	10.8	9.5	1.3	1.9	1.5	**33.2**

6 CONCLUSIONS

Results show that digital hydraulic distributed valve system can save significantly energy when compared to the traditional proportional load sensing system. Average reduction of 36 percent was achieved in experimental tests but energy saving still increases if cavitation is not allowed in proportional system. At the same time, digital solution improves controllability and removes cavitation. This is possible because pressure level and piston velocity can be controlled independently in distributed valve systems. Important result is also that control performance remains good in differential mode if both control edges are controlled. Results are encouraging but there are still some problems to be solved. The controller is complex, computationally extensive and has many tuning parameters. Mode switching logic presented has also some problems,

such as need for delayed switchings. Proper tools and systematic methods are essential in implementation of this kind of complex control systems. The first experiences with design by contract method [19] are promising.

ACKNOWLEDGEMENT

The research was supported by the Academy of Finland (Grant no. 80411) and the Finnish Funding Agency for Technology and Innovation (Grant no. 40293/05).

REFERENCES

1 Virvalo T. & Vilenius, M. 2000. The Influence of Pumps and Valves on the Efficiency of a Hydraulic Boom. **In:** Garbacik, A. & Stecki, J. (eds.) Developments in Fluid Power Control of Machinery and Manipulators, pp. 183–208 (Fluid Power Net Publication, Cracow, 2000).

2 Backé, W. 1995, Hydraulic Drives with High Efficiency. Fluid Power Systems and Technology, FPST-Vol. 2, ASME 1995, pp. 45–73.

3 Peterson, U. 2005. Fluid Power – the Future in Construction Equipment. Proceedings CD-ROM of the Ninth Scandinavian International Conference on Fluid Power, June 1–3, 2005, Linköping, Sweden, 33 p.

4 Rydberg, K.-E. 2005. Energy Efficient Hydraulic Systems and Regenerative Capabilities. Proceedings CD-ROM of the Ninth Scandinavian International Conference on Fluid Power, June 1–3, 2005, Linköping, Sweden, 12 p.

5 Luomaranta, M. 1999. A Stable Electrohydraulic Load Sensing System Based on a Microcontroller. Proceedings of the Sixth Scandinavian International Conference on Fluid Power, May 26–28, 1999, Tampere, Finland, pp. 419–432.

6 Djurovic, M. & Helduser, S. 2004. New Control Strategies for Electrohydraulic Load-Sensing. **In:** Burrows, C. R., Edge, K. A. & Johnston, D. N. (eds.) Power Transmission and Motion Control, PTMC2004, pp. 201–210 (Professional Engineering Publishing Ltd, 2004).

7 Jansson, A. & Palmberg, J.-O. 1990. Separate Controls of Meter-in and Meter-out Orifices in Mobile Hydraulic Systems. International Off-Highway & Power Plant Congress and Exposition, Milwaukee, WI, USA.

8 Mattila, J. 2000. On Energy Efficient Motion Control of Hydraulic Manipulators. Dissertation, Tampere University of Technology, Publications 312, Tampere.

9 Liu, S. & Yao, B. 2002. Energy-Saving Control of Single-Rod Hydraulic Cylinders with Programmable Valves and Improved Working Mode Selection. The 49th National Conference on Fluid Power, Las Vegas, Nevada, USA, pp. 81–91.

10 Shenouda, A. & Book, W. J. 2005. Selection of Operating Modes of a Multi-Functional Hydraulic Device. 2005 ASME International Mechanical Engineering Congress and Exposition, Nov. 5–11, Orlando, Florida, USA, 11 p.

11 Pfaff, J. 2005. Distributed Electro-Hydraulic Systems for Telehandlers. The 50th National Conference on Fluid Power, March 16-18, 2005, Las Vegas, USA. pp. 779–784.

12 Hu, H. & Zhang, Q. 2002. Realization of Programmable Control Using a Set of Individually Controlled Electrohydraulic Valves. International Journal of Fluid Power, Vol. 3, No 2. pp. 29–34.

13 Linjama, M., Laamanen, A. & Vilenius, M. 2003. Is it time for digital hydraulics? The Eighth Scandinavian International Conference on Fluid Power, May 7–9, Tampere, Finland, pp. 347–366.

14 Siivonen, L., Linjama, M. & Vilenius, M. 2005. Analysis of fault tolerance of digital hydraulic valve system. **In:** Johnston, D. N., Burrows, C. R. & Edge, K. A. (eds.) Power Transmission and Motion Control, PTMC2005, pp. 133–146 (John Wiley & Sons, Ltd., 2005).

15 Laamanen, A., Siivonen, L., Linjama, M. & Vilenius, M. 2004. Digital Flow Control Unit – an Alternative for a Proportional Valve? **In:** Burrows, C. R., Edge, K. A. & Johnston, D. N. (eds.) Power Transmission and Motion Control, PTMC2004, pp. 297–308 (Professional Engineering Publishing Ltd, 2004).

16 Linjama, M. & Vilenius, M. 2005. Improved Digital Hydraulic Tracking Control of Water Hydraulic Cylinder Drive. International Journal of Fluid Power, Vol. 6, No 1, pp. 29–39.

17 Linjama, M. & Vilenius, M. 2005. Digital Hydraulic Tracking Control of Mobile Machine Joint Actuator Mockup. Proceedings CD-ROM of the Ninth Scandinavian International Conference on Fluid Power, June 1–3, 2005, Linköping, Sweden, 16 p.

18 Linjama, M. & Vilenius, M. 2005. Energy-efficient Motion Control of a Digital Hydraulic Joint Actuator. The 6th JFPS International Symposium on Fluid Power, November 7-10, 2005, Tsukuba, Japan, 6 p. (CD-ROM)

19 Boström, P., Linjama, M., Morel, L., Siivonen, L. & Waldén, M. 2007. Design and Validation of Digital Controllers for Hydraulic Systems. Accepted for publication in the Tenth Scandinavian International Conference on Fluid Power, May 21 – 23, 2007, Tampere, Finland.

20 Linjama, M. & Vilenius, M. 2004. Digital Hydraulic Control of a Mobile Machine Joint Actuator Mockup. **In:** Burrows, C. R., Edge, K. A. & Johnston, D. N. (eds.) Power Transmission and Motion Control, PTMC2004, pp. 145–158 (Professional Engineering Publishing Ltd, 2004).

BIOHYDRAULICS – TRUE ALTERNATIVES

Ph.D, R&D Manager Merja Lämsä
AarhusKarlshamn, Technical Products & Feed
Binol BioSafe Oy
Raisionkaari 55
21200 Raisio, Finland
Phone +358 2 443 2746, Fax + 358 2 443 2911
E-mail: merja.lamsa@aak.com

M.Sc, R&D Chemist Kaisa Kosonen
AarhusKarlshamn, Technical Products & Feed
Binol BioSafe Oy
Raisionkaari 55
21200 Raisio, Finland

ABSTRACT

Biohydraulic fluids today have already their third generation raw materials developed. How this huge development has been possible in only two decades is demonstrated. As well the latest laboratory and field test results from longlife, EU Ecolabel approved biohydraulic oils are shown. Also the development work of additives in biolubricants is touched. A testrig solution between laboratory and real life is demonstrated.

KEYWORDS: biolubricants, biohydraulic fluids, vegetable oils, synthetic esters, complex esters

1 INTRODUCTION

Biohydraulic fluids have been on the market over two decades. There has been a huge development during that time in their raw materials and additives. Back in the 1980s the main raw materials were vegetable oils, originally the same as used in the food industry. All the additives were originally meant for mineral oil based lubricants. What has changed since then and how? Still today the basics for biohydraulics´ raw materials are vegetable oils. What has changed is that the chemistry has been taken into the picture: We can synthesize from vegetable oils long-life hydraulic fluids´ raw materials, which are technically superior and at the same time fulfill the environmental and health and safety criteria as well [1, 2, 3, 4].

In the additive side we have today very many possibilities in our hands. In all of them the technical, environmental and health and safety properties have to be tested by standard methods and those results are available for all of us.
We have also today reliable standards and test methods build for environmentally acceptable products. These can be used to categorize different biohydraulics and compare them against the conventional fluids and to show the real properties of the bio fluids in all categories: technical, environmental and health and safety. The latest joined in this family of standards is the EU Eco-label, the flower label, for biolubricants. This is a true guarantee for customers about biolubricants' quality – This standard contains challenging criteria for the technical performance as well for the environmental and health and safety compliance [5].
Forecast for 2007 in Europe for the usage of biolubricants is: 5,5 % in chainsaw oils, concrete release agents 4,5% and hydraulic fluids 85% of the total usage amounts in Europe [6].

Table 1: Usage of lubricants and biolubricants in Nordic countries by volume in 2006 [7]

Product group	Total volumes (tn)	Volumes of biolubes (tn)
Chain oils and conveyor oils	8 000	3000
Hydraulic fluids	43 000	7500
Metal cutting fluids	14 000	1500

Table 2: The market share of biolubricants in Europe geographically in year 2000 and a forecast for 2007 [6]

Year	Germany	France	UK	Benelux	Scandinavia	Switzerland Austria	Italy
2000	4.0	0.1	0.2	2.9	9.0	5.7	1.3
2007	15.5	0.3	0.4	4.9	10.8	8.4	2.0

2 SHORT OVERVIEW TO R&D IN BIOHYDRAULICS

In figure 1 there is a comparison of basic raw material types used in biohydraulics. As mentioned before different vegetable oils were the first raw material choice. When moving on from there, when taking the chemistry first time into picture, of course all the benefits of vegetable oils were utilized: renewability, biodegradability, non-toxicity, non bioaccumulation, high flashpoint, polarity, uniform molecular structure, excellent

lubrication properties, and stability of viscosity in varying temperatures. The poor oxidation stability in higher temperatures and poor low temperature flow properties of vegetable oils were improved.
As can be seen in figure 1, the molecular structures are alike - which means that the nature has given us already rather good tools for building an excellent hydraulic fluid [8, 9, 10, 11].

Figure 1: Examples of different raw materials used in biolubricants

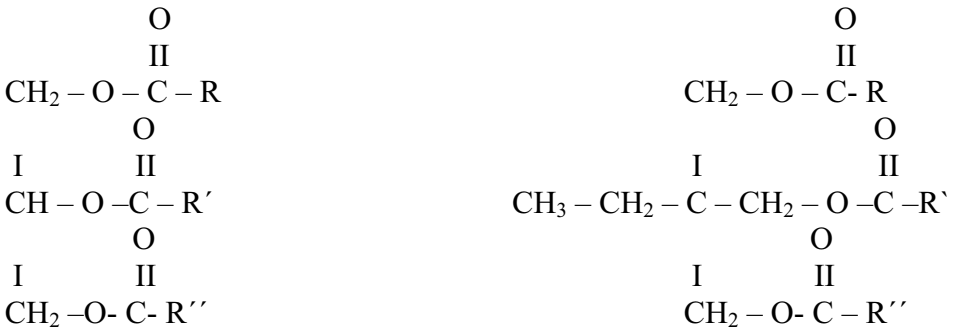

Vegetable oil

TMP –oleate

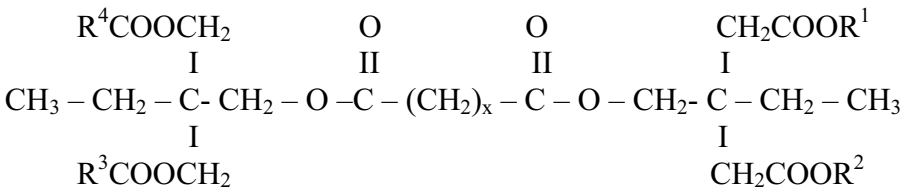

An example of a complex ester type

There is a short summary about the different types of additives used in biofluids in the table 3. Also the environmental properties of these additive types are shown. These additives have to have as low impact as possible on environmental and health and safety aspects, but of course at the same time they have to be as efficient as possible, so that the needed amounts would be as low as possible [12, 13, 14, 15].
The most common additives used in biofluids are the antioxidants, the corrosion inhibitors and the antiwear additives. Sometimes there is a need for antifoam additives and the coldstability improvers.
As can be seen from this table, the total amount of additives in biolubes is very low compared to the conventional fluids. This means that the basic fluid - the basic raw material, the ester - has already the most power in it!

Table 3: A short overview of examples from the additives used in biolubricants

Additive type	Used as	Amount in the product (w-%)	Environ. propert.
Amines	Antioxidant	0.5 – 2.5	WGK 1 OECD 301B>60% OECD201 LC50>100mg/l OECD 203 LC50>100mg/l
Aminephosphate	Antiwear	0.05 -1.00	WGK 1 OECD 301B>20% OECD201 LC50>10mg/l OECD 203 EC50>1mg/l
Aminephosphate	Anticorrosion	0.01-0.5	WGK 1 OECD302B>60% OECD 201 LC50>1mg/l OECD203 EC50>1mg/l
Silicone	Antifoam	0.01-0.5	WGK 1 OECD301B>70% OECD201 LC50>1000mg/l OECD203 EC50>1000mg/l
Metacrylate based Polymer	Pourpoint depressant	0.1 – 5.00	WGK 1 OECD301B>50% OECD201 LC50>2mg/l OECD203 EC50> 1.5mg/l

3 LABORATORY TEST RESULTS FROM LONGLIFE BIOHYDRAULIC FLUIDS

Laboratory test methods in biohydraulics have changed as well during the years. The first laboratory tests were of course the same ones used in the mineral oil based hydraulic fluids. Because the basic chemistry in biohydraulics and in mineral oil based conventional ones is totally different, the test methods need to be different as well and even the tested properties are different ones! Today we have reasonably good laboratory tests, which are designed for ester type of raw materials and finished lubricants. There are as well many reliable standards like ISO 15380, Swedish Standard SIS 155434, German VDMA 24568, Swedish SMR Norm för Hydrauloljor, British BFPA/P57, Caterpillar BF-1, Volvo hydraulic fluid 98610 [16, 17, 18, 19, 20, 21, 22].

Table 4: Chemical and physical properties of different raw material based biohydraulics.

Property	Unit	Method	Hydraulic fluids		
			HF32NE	HF 32SE	HF32XE
Visc./40°C	mm^2/s	ISO 3104	32	32	32
Visc./100°C	mm^2/s		8	7	6
Visc./0°C			200	170	220
Visc./-20°C			900	740	1100
Visc./-30°C			3000	3300	2700
Visc.-30°C/7d			2950 – 3100	3300 – 3400	2700-2750
Visc.index		ASTM D2270	220	205	150
Pourpoint	°C	ISO 3016	-39	-42	-55
Flashpoint	°C	ISO 2592	>300	>300	>300
Oxidation stability					
Baader- test		DIN 51554 teil 3			
Δ in visc./40°C	%		6.2	1.1	0.6
Δ in TAN	mgKOH/g		0.05	0.04	0.03
Oxidation stability					
dry TOST –test		ASTMD 943-81			
Δ TAN 2 mgKOH/g	h		-	672	>5000
Antiwear and friction					
Vickers-test		DIN 51389			
Ring	mm		2.0	2.24	0
Wings	mm		4.1	2.78	0
Hydrolytic stability		ASTM D2619			
Weight of Cu	mg		<0.01	<0.01	<0.01
Outlook of Cu			1b	1b	1b
Δ TAN in H2O	mgKOH/g		12	2.4	0.17
Δ TAN in oil	mgKOH/g		1.2	0.41	0.30
Biodegradability	%	OECD 301F	>80	>80	>80
Toxicity		OECD 201,202,203	non toxic	non toxic	non toxic
Irritation of eyes, skin or Respiratory		OECD 402, 402 404, 405	non irritating	non irritating	non irritating
Bioaccumulation		OECD 305 D	non bioaccum.	non bioaacum.	non bioaccum
Renewability	%		>90	>80	>80

In table 4 there is an overview of different types of biohydraulics and their test results. For example the oxidation stability according to the Baader test (DIN 51554 teil 3) and dry TOST- test (ASTM D 943) has improved significantly moving from vegetable oil based hydraulic fluids to complex ester based ones via synthetic ester based hydraulic oils. It will be shown later (in figure 2) that today´s biohydraulics have even longer lifetimes compared with mineral oil based hydraulic oils. It can be seen in table 4 as well that the properties like antiwear, which has been already a benefit for vegetable oil based hydraulic fluids, have even exceeded when moving from vegetable oils to synthetic esters and is finally superior when ending up complex ester based ones. One important aspect to keep in mind is that these new products are even totally environmentally acceptable and based on renewable raw materials.

In figure 2 test results are shown for different raw material based hydraulic fluids in a special test rig. This test rig was originally designed to satisfy the demands of our customers. There were several customers, who wanted to see more test results, not just the laboratory test results, before entering to field tests or trial marketing with a new product. In figure 3 there is a photo of a test rig and also the operating test parameters. It can be seen from figure 2 that both synthetic ester based and mineral oil based hydraulic fluids tire out more quickly than the new longlife biohydraulic fluid.

Figure 2. ISO VG 46 grade hydraulic oils in a gear pump test rig

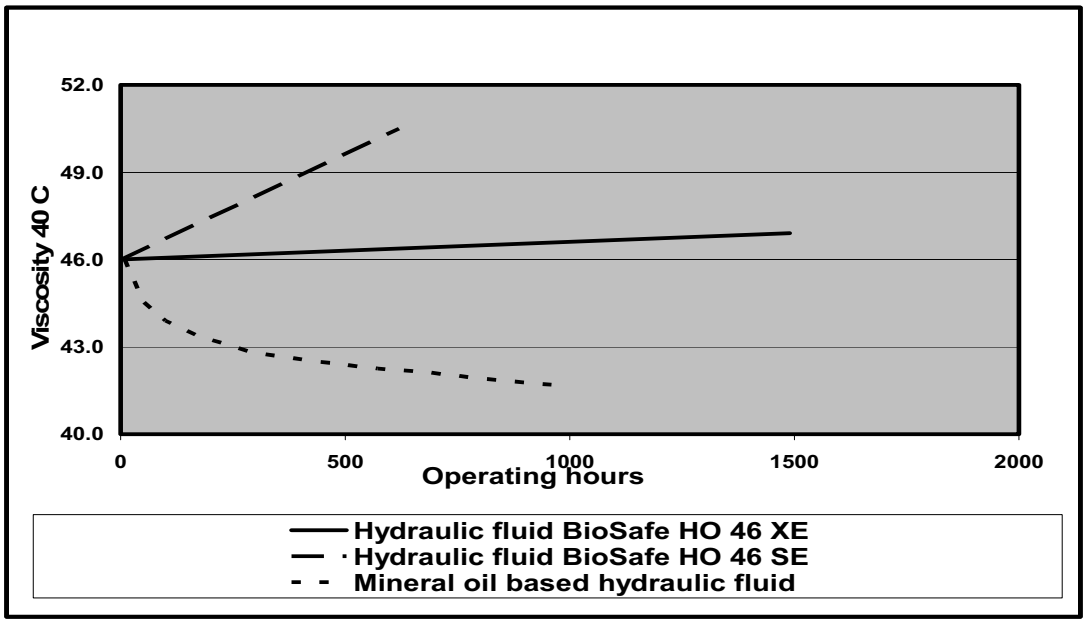

Figure 3. A gear pump test rig

4 FIELDTEST RESULTS FROM LONGLIFE BIOHYDRAULICS

The field tests with longlife hydraulic fluids have been going on for three years now. They are tested in several application areas: in different forest machines, multifunctional tractors, asphalt pavers, excavators, and loaders.

The slight increase in the kinematic viscosity of ISO VG 46 longlife biohydraulic fluid in two mobile hydraulic equipments operating under field conditions is presented in figure 4. The chemical and physical properties of these oils are stable within almost 10 000 working hours.
In figure 5 there is shown the results of a particle count and especially the amount of wear particles of the tested longlife biohydraulic oil. As can be seen the cleanliness level is still in acceptable level for this specific application. From wear and contamination particles, there are hardly any. An explanation is needed for the high zinc content and how it is decreasing in use: The longlife hydraulic fluid does not contain any zinc additives. The initial presence of zinc is due to the hydraulic oil originally used in this machine. Despite the careful flushing procedure, some of the formerly used mineral oil remained in the hydraulic system.
In figure 6 there are results for water content, measured by Karl Fischer- titration. The water content is rather stable and far below the recommended water content for these longlife biohydraulics (0,10 – 0,20 % = 1000 - 2000 ppm). The effect of water, the possible chemical reactions, which means the hydrolytic stability of these tested longlife products were also investigated: No effect of water at all!

Figure 4. Long-life hydraulic fluids in a field trial. A chart of viscosity at 40°C (mm^2/s)

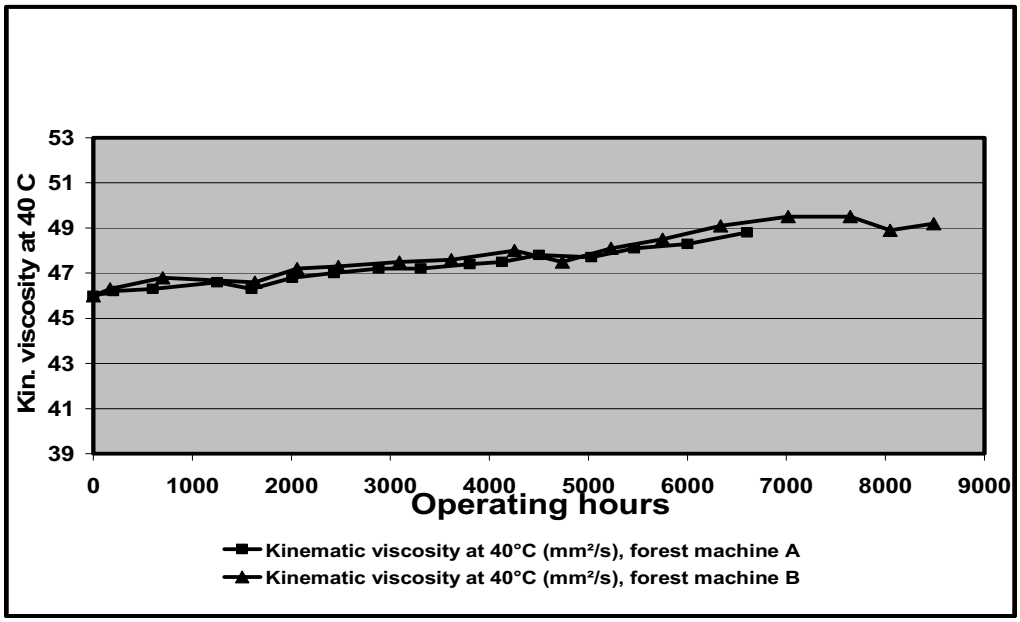

Figure 5. Wear particles and purity classifications of a longlife hydraulic fluid in a field test

		March 2004 ——→ November 2006	
Hours in operation		**0**	**8488**
Kinematic viscosity 40°C (mm^2/s)	ISO 3104	46,0	49,2
Cleanliness level	ISO 4406	16/14	13/11
Contamination and wear metals (ppm):			
Na		<2	<2
Al		<2	<2
V		<1	<1
Cr		<1	<1
Mn		<1	<1
Fe		<1	<1
Ni		<1	<1
Cu		<1	3
Zn		90	72
Mo		<1	<1
Sn		<1	<1
Pb		<1	<1
Ba		<1	<1

Figure 6: Water content of a longlife hydraulic fluid in a field test

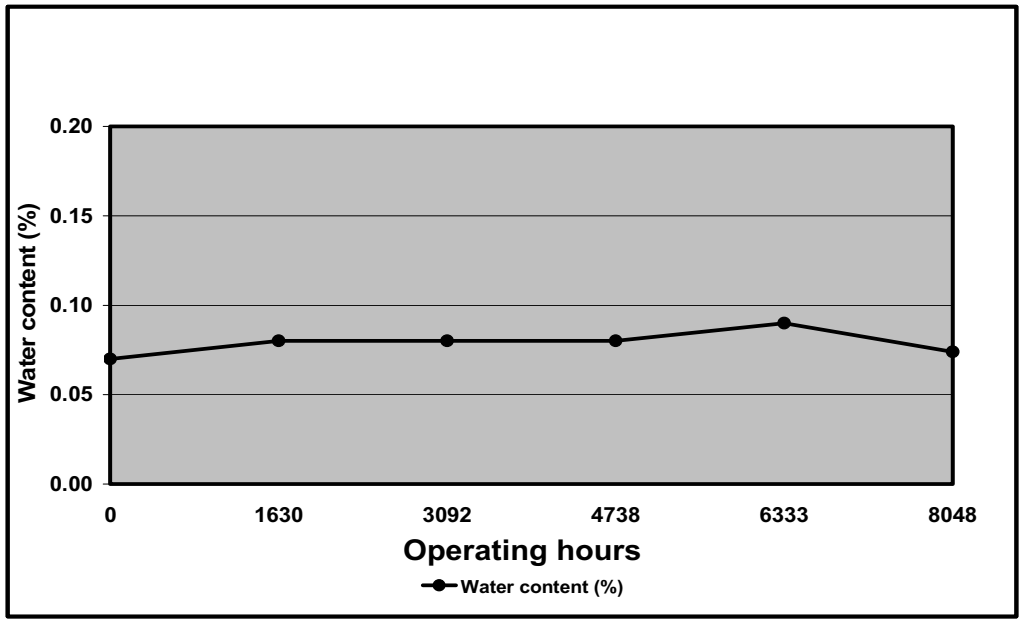

CONCLUSIONS

As the title says biohydraulics are today a real alternative with regard to the technical and environmental aspects [23]. The laboratory and field test results prove that the oxidation stability, the lubrication and coldstability properties and the water tolerance are better than in conventional hydraulic fluids. It can also very clearly be seen that antiwear and anticorrosion behaviour of these new longlife products is much better compared to synthetic hydraulic oils. This means that biohydraulic fluids can compete against and even beat the conventional hydraulic fluids both technically and economically and offer environmentally and occupationally more conscious option. We have come a long way in just two decades!

References:

1. Lämsä, M., Kosonen, K., Latest development in biolubricants raw materials, 15th International Colloquium Tribology - Automotive and Industrial Lubrication, January 2006, Ostfildern, Germany.
2. Lämsä, M., New esters and their test results in bio lubricants, 8th International Tribology Conference of the South African Institute of Tribology, University of Pretoria, 24- 26 March 2004.
3. Lämsä, M., Kosonen, K., Novel esters in biolubricants, the 8th Scandinavian International Conference on Fluid Power, SICF 2003, May 7-9, 2003, Tampere, Finland.
4. Lämsä, M., Environmentally Friendly Products Based On Vegetable Oils, Doctor Thesis, Helsinki University of Technology, Faculty of Process Engineering and Materials Science, technical biochemistry report 2/1995.

5. EU komission päätös, 26. huhtikuuta 2005 ekologisista arviointiperusteista ja niihin liittyvistä arviointi- ja todentamisvaatimuksista yhteisön ympäristömerkin myöntämiseksi voiteluaineille, K (2005) 1372.
6. Frost and Sullivan, market research, 2000.
7. Jörsmo, M., President of AAK/Sweden, President of AAK/Technical Products & Feed, literal information, 2006.
8. Lämsä, M., Ecologically acceptable synthetic hydraulic fluids based on vegetable oils, Proceedings of the 4th International Conference on Fluid Power, September, 1995, Tampere, Finland.
9. Lämsä, M., Environmental safe products based on vegetable oil, 9th Colloquium in Tribology, Technische Akademie Esslingen, 11-13 January 1994, Ostfildern, Germany.
10. Bondioli, P., Della Bella, L., Manglaviti, A., Synthesis of biolubricants with high viscosity and high oxidation stability, OCL 10 (2003) 2, 150-154.
11. Bongardt, F., Properties and use of polyol esters in the lubrication industry, Mineraloeltechnik, 47 (2002) 7, 1-24.
12. MSDS of several chemical companies for additives.
13. Adhvaryu, A., Erhan, S .Z., Perez, J. M., Tribological studies of thermally and chemically modified vegetable oils for use as environmentally friendly lubricants, Wear 257 (2004) 3-4, 359-367.
14. Lay, J., An Introduction to Synthetic Lubrication for Fractional Horsepower Application, Gear Technology, September/October, 2000, 17-26.
15. Duncan, C., Reyes-Gavilan, J., Costantini, D., Oshode, S., Ashless additives and new polyol ester base oils formulated for use in biodegradable hydraulic fluid applications, Lubr. eng. 58 (2002) 9, 18-28.
16. ISO 15380, Lubricants, industrial oils and related products (class L) -Family H (Hydraulic systems)-Specifications for categories HETG, HEPG, HEES and HEPR.
17. Svensk Standard SS 15 54 34, Hydraulvätskor –Krav och provningsmetoder.
18. Verband Deutscher Maschinen- und Anlagenbau e. V. (VDMA) 24568, Biologisch schnell abbaubare Druckflussigkeiten.
19. SMR norm för hydrauloljor-2, Skog Forsk.
20. BFPA/P57, Guidelines to the use of ecologically acceptable hydraulic fluids in hydraulic fluid power systems.
21. Caterpillar Inc, biodegradable hydraulic fluid requirements, BF-1.
22. Volvo Construction Equipment Standard, Hydraulic oil 98610.
23. www.binol.com

FLUID DYNAMICS – COMPARISON AND DISCUSSION ON SYSTEM- RELATED DIFFERENCES

Karjalainen, J-P, Karjalainen, R., Huhtala, K., Vilenius, M.
Tampere University of Technology
P.O.Box 589
33101 Tampere, Finland
Phone +358 3 365 2603, Fax +358 3 365 2240
E-mail: juho-pekka.karjalainen@tut.fi

ABSTRACT

The dynamics of hydraulic fluid is an important factor when dealing with systems demanding increasingly higher accuracy and performance. The most important dynamic fluid parameters are bulk modulus, density and speed of sound in a fluid which can be measured in several reported ways. Usually the main interest is to find out the adiabatic bulk modulus which can be determined along with density by measuring the speed of sound in the fluid.

In this paper the measured dynamic parameters of selected commercial hydraulic fluids are compared. The parameters were measured using two alternative but theoretically similar systems. The systems are also compared to an ISO standardized method, the results of which are to be reported later. The measurements are also compared to simulations. Finally, all the results are concluded for discussing the fluid dynamics in some typical hydraulic systems.

KEYWORDS: adiabatic, bulk modulus, compression, density, dynamics, high-pressure, hydraulic fluid, ISO, isothermal, sound velocity, wave propagation

NOTATION

B	Bulk modulus [Pa]
c	Speed of sound in the fluid [m/s]
p	Pressure [Pa]
p_{atm}	Atmospheric pressure [Pa]
T	Temperature [ºC]
ρ_n	Density at measured pressure and temperature [kg/m^3]
$\rho_{atm,T}$	Density at atmospheric pressure and at temperature T [kg/m^3]

1 INTRODUCTION

When talking about fluid dynamics usually the compression is considered isothermal when the change of state is relatively slow, for example in cylinder compression. The adiabatic compression is related to rapid changes of state and there are several published measuring techniques for adiabatic bulk modulus, e.g. [7, 9, 13, 15, 16]. One thing in common is the theory based on finding out the speed of sound in the fluid. However, there has been some indication that the selection of pressure source might affect the results of measured speed of sound as well as bulk modulus – it might be possible that in some cases the bulk moduli are actually isothermal although expected adiabatic [12]. Therefore the concept of adiabatic process might not be as easy to generalize as stated and the engineer might need further information on the dynamic situation on hand even if the actual fluid parameters would be accurately known. After all, the difference between isothermal and adiabatic parameters might be several percents.

In this paper the results of two different measuring systems for dynamic fluid parameters are compared. Both systems are based on the same theory of finding out the speed of sound in a fluid. The selected and measured commercial hydraulic fluids were exactly the same. The systems are also compared to an ISO standardized method [7] having a lot of similarities both in the theory as well as in the system architecture. The results for the ISO standard are to be reported later. All the systems and the measuring principle are introduced in following chapters. The results are compared also to simulations independent on the systems for finding out whether the results would indicate more isothermal or adiabatic process. Finally, all the results, indicating system related differences, are concluded for discussing the fluid dynamics in some typical hydraulic systems.

2 ISO- STANDARDIZED MEASURING SYSTEM

The ISO 15086-2 standard includes two measuring options for finding out speed of sound in a fluid in a pipe [7]. Basically the idea is identical in both cases but for this paper (and for further studies) the so called three-transducer method (figure 1) was chosen [7, 9].

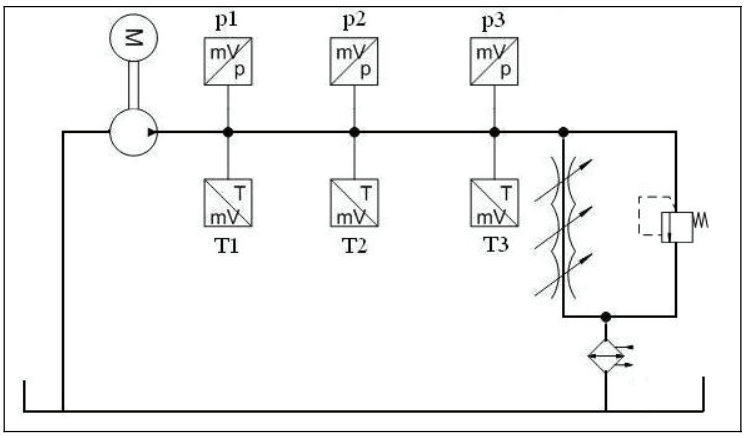

Figure 1. The ISO standardized three-transducer method.

The pressure wave propagation time is measured along a rigid straight pipe using three pressure transducers. Pressure waves are produced with a pressure source such as in this case a radial piston pump and the actual calculations are made according to quite complex transfer function procedures explained in detail in the standard [7]. The pressure level is raised with a loading valve such as a needle valve – in this case due to desired high pressure level a series of throttles were added to avoid cavitation. Also a heat exchanger was added for controlling the measuring temperature. The results of this system are to be reported later.

Once the speed of sound is found out the effective bulk modulus may be calculated from equation (1) [14]. Fluid bulk modulus can be found out by removing system compliances from the effective value. ISO standard requires actual information on measured fluid density which therefore needs to be known beforehand – the same concerns fluid viscosity. Also the pressure wave fluctuation frequency as well as the flow rate need to measured due to the transfer function calculations. The standard itself offers a MATLAB code for performing the iterative calculations. [7]

$$c = \sqrt{\frac{B}{\rho_n}} \tag{1}$$

3 ALTERNATIVE MEASURING SYSTEMS

There are more than one reported measuring systems for finding out the dynamic parameters of fluids. If the adiabatic, or in other words dynamic, bulk modulus is to be measured it can be found out by measuring the speed of sound in the fluid. Cylinder compression of the fluid for example would produce isothermal bulk modulus [1]. The systems introduced here are good examples and the similarity to the ISO standard is quite obvious in both cases, especially in the continuous pumping method. The results of these systems are compared in the following chapters.

3.1 Continuous pumping with two transducers

The continuous pumping method or also known as the cross-correlation method [13, 16] is highly identical in theory to the previously introduced three-transducer method [7], major difference being the number of pressure transducers – two instead of three. The method is also based on measuring the pressure wave propagation time along a rigid straight pipe. Now the propagation time may be found out from the phase shift of the wave between the two transducers. The delay is calculated using a cross-correlation algorithm which then gives the speed of sound since the distance between the transducers is known exactly. Now the bulk modulus as well as the density of the fluid may be iteratively calculated using the previously introduced equation (1) and the equation (2) [4].

$$\rho_n = \rho_{atm,T} e^{\frac{p - p_{atm}}{B_{eff}}} \tag{2}$$

The reported original system was tested with operating pressures up to 300 bar [16]. When the pressure level was raised up to 600 bar the first problem discovered was cavitation due to using only one loading valve – this was solved using a series of throttles [11]. However, the major flaw was pressure wave reflections happening already at lower pressures but becoming clearly apparent at pressures over 300 bar [11]. The problem was solved adding an adjustable damping chamber [2, 5, 8] into the system. After that the system (figure 2) operated very well. Again a heat exchanger was added for controlling the temperature.

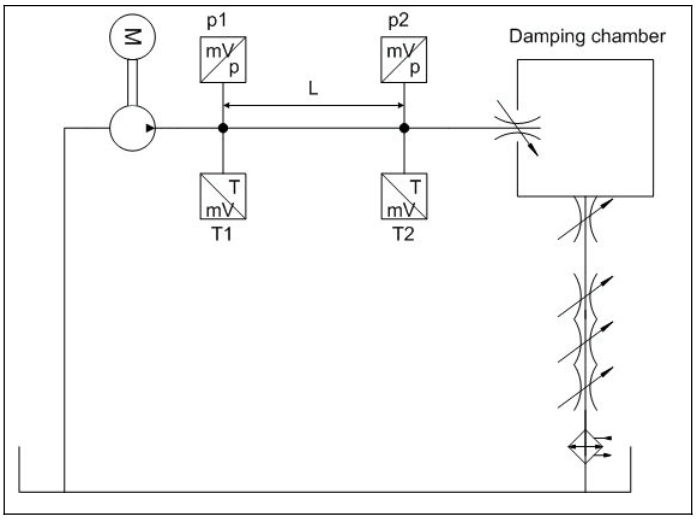

Figure 2. The continuous pumping measuring system.

3.2 Single pressure peak with two transducers

The single pressure peak system [12] (figure 3) is more practical way of measuring fluid dynamics when the desired pressure levels are raised over 1000 bar – it is quite difficult or expensive at least to find a pump for such pressures. Now the static pressure level is raised with an intensifier and one dynamic pressure peak is produced into the measuring pipe by knocking a hydraulic cylinder. Otherwise all the theory and calculations are identical to those of the continuous pumping method. The temperature of the fluid is controlled with a separate control circulation.

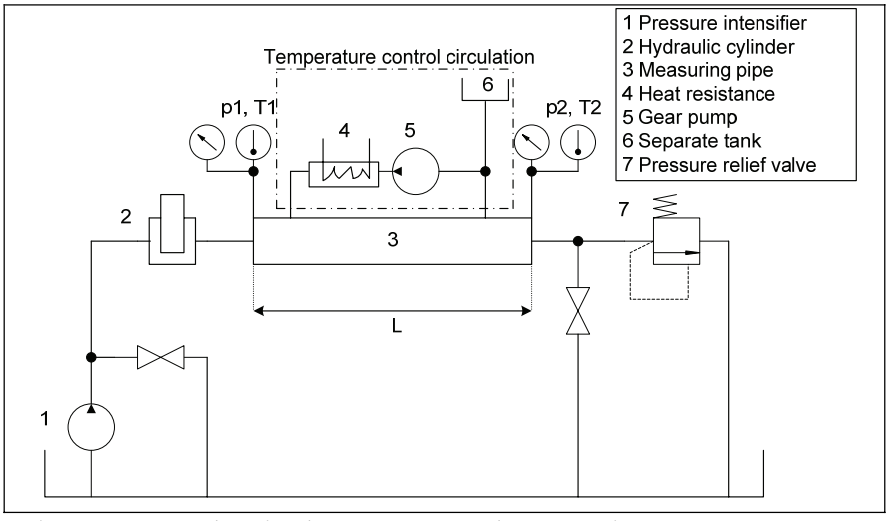

Figure 3. The single pressure peak measuring system.

4 COMPARISON OF THE RESULTS

Dynamic parameters of two commercial hydraulic fluids were measured using the previously introduced continuous pumping method as well as the single peak method. The results for density, speed of sound in a fluid and bulk modulus are presented and compared in the following. The measured fluids were ISO VG 46 mineral hydraulic oil and ISO VG 46 HF-E synthetic ester fluid. The fluid characteristics are listed in table 1. Measuring pressures were up to 600 bars with the continuous pumping method (as well as in ISO three-transducer method to be carried out) – the single pressure peak method was applied at pressures up to 1500 bar. Measuring temperatures were 40 ºC and 70 ºC with all the systems.

Table 1. The measured hydraulic fluids.

Hydraulic fluid	Density, atm.pressure, 15 ºC temperature	Viscosity, 40 ºC temperature	Viscosity, 100 ºC temperature
ISO VG 46 Mineral oil	875 kg/m³	46 cSt	6,9 cSt
ISO VG 46 Synthetic HF-E fluid	928 kg/m³	46 cSt	9,1 cSt

3.1 Density

As mentioned the densities of the fluids were measured using the continuous pumping method and the single pressure peak method. The results of measured fluid densities for both fluids at temperatures of 40 ºC and 70 ºC are presented in figures 4 and 5 respectively. As it can be seen the results were practically identical with both systems as expected. In other words there were no significant system related differences observed. These measured values will be needed in calculating the ISO standard values for speed of sound and bulk modulus, the results of which are to be reported later.

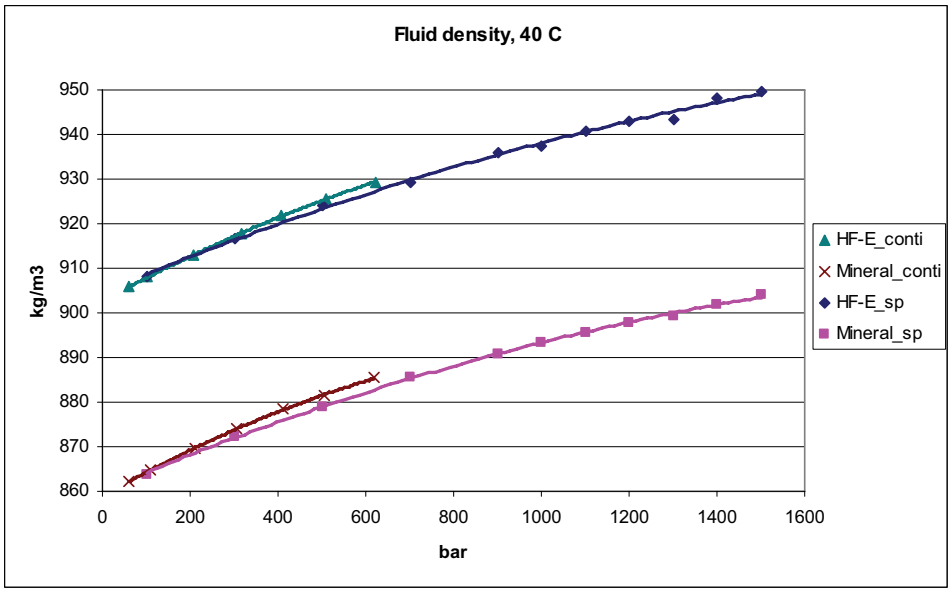

Figure 4. The measured densities of ISO VG 46 Mineral oil and HF-E fluid at 40ºC, with the continuous system (‘conti’) and the single peak system (‘sp’).

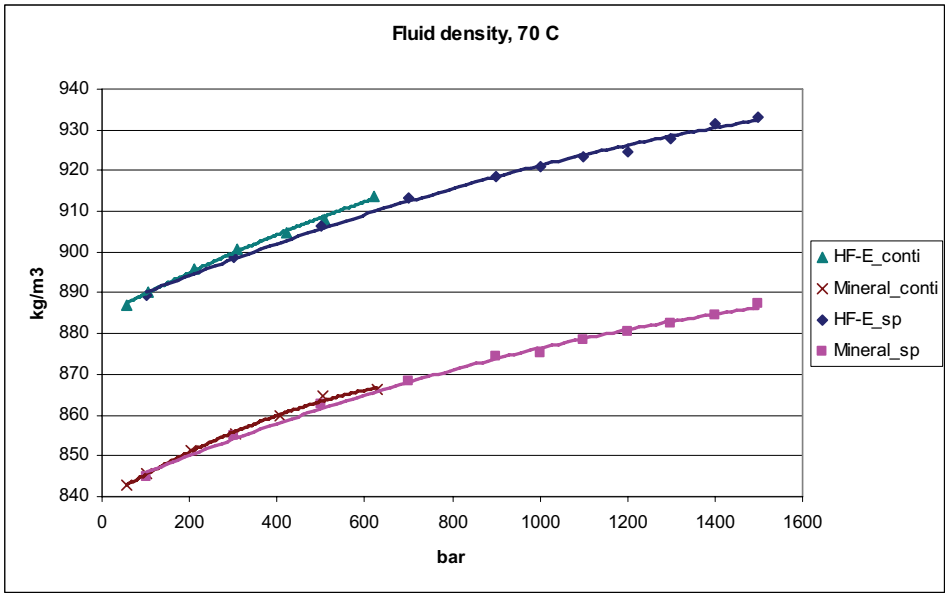

Figure 5. The measured densities of ISO VG 46 Mineral oil and HF-E fluid at 70ºC, with the continuous system ('conti') and the single peak system ('sp').

3.2 Speed of sound

The results for measured speed of sound in the fluids at temperatures of 40 ºC and 70 ºC are presented in figures 6 and 7 respectively. As it can be seen there are no significant differences between the two fluids but the difference between the two systems is clearly distinctive. This is the first indication that the two systems used might not be as equivalent as usually suggested. It will be most interesting to see the results of the ISO method which would at least appear to be highly similar to the continuous pumping method in terms of system architecture. The basic theory behind all the three systems is identical as mentioned earlier.

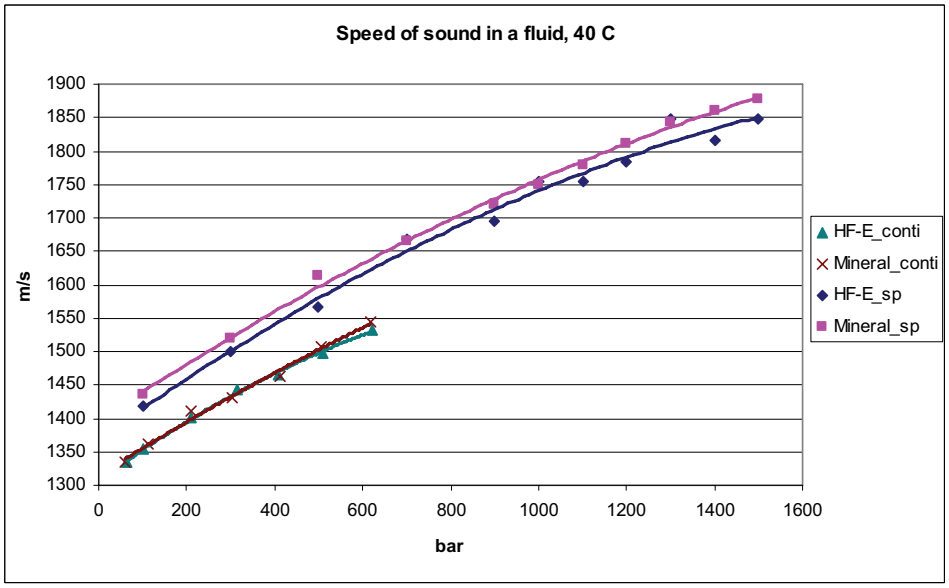

Figure 6. The measured speed of sounds of ISO VG 46 mineral oil and HF-E fluid at 40 ºC, with continuous system ('conti') and single peak system ('sp').

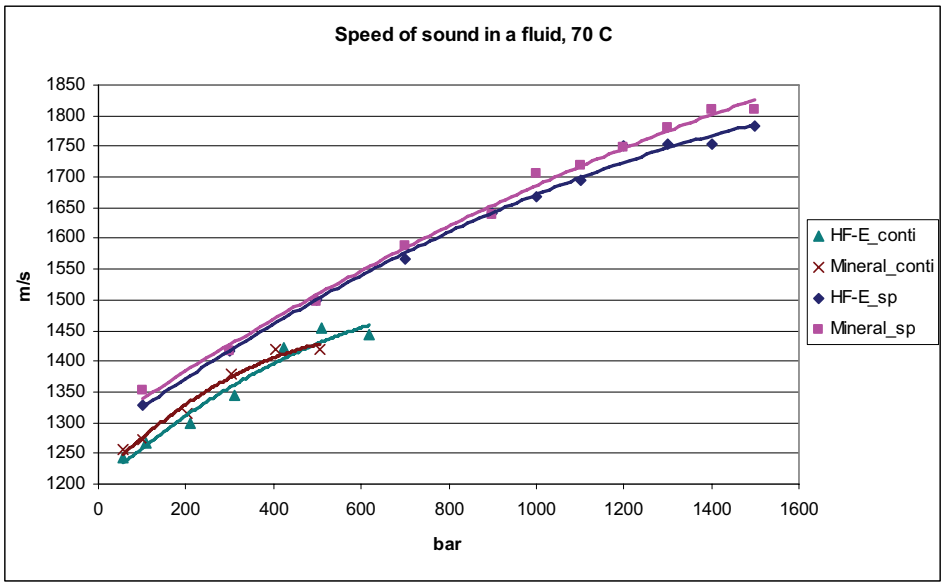

Figure 7. The measured speed of sounds of ISO VG 46 mineral oil anf HF-E fluid at 70 ºC, with continuous system (‘conti’) and single peak system (‘sp’).

3.3 Bulk modulus

The results for measured bulk modulus at temperatures of 40 ºC and 70 ºC are presented in figures 8 and 9 respectively. Now there are differences both between the fluids and between the two systems. The differences between the fluids are quite expected since the selected fluids are chemically different (mineral oil, synthetic ester). But again the differences between two theoretically identical systems are highly unexpected. Having said the measurements with the ISO method might be needed to whether confirm or to question the results. However, the two systems already used are giving different results for fluid dynamics indicating the fluid acting differently in the systems. The reason for this is speculated in the following chapters.

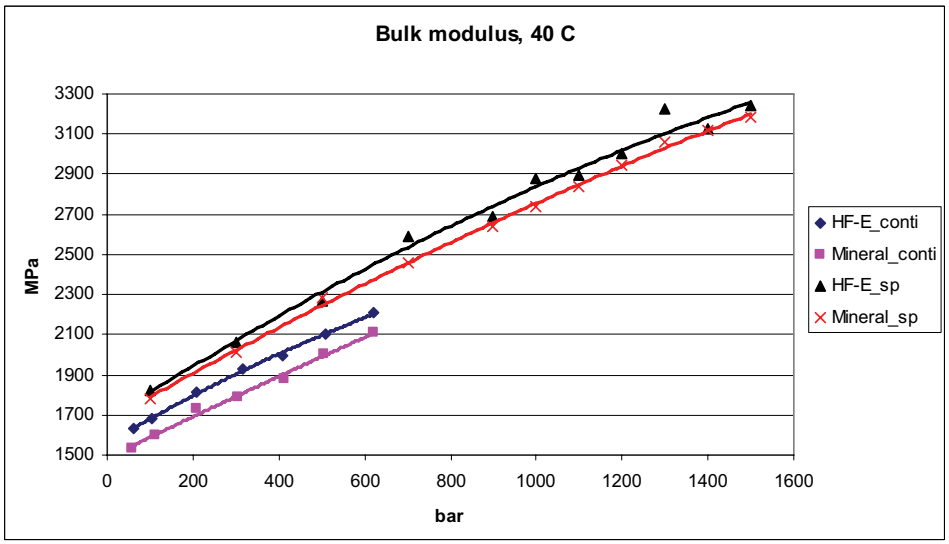

Figure 8. The measured bulk moduli of ISO VG 46 mineral oil and HF-E fluid at 40ºC, with continuous system (‘conti’) and single peak system (‘sp’).

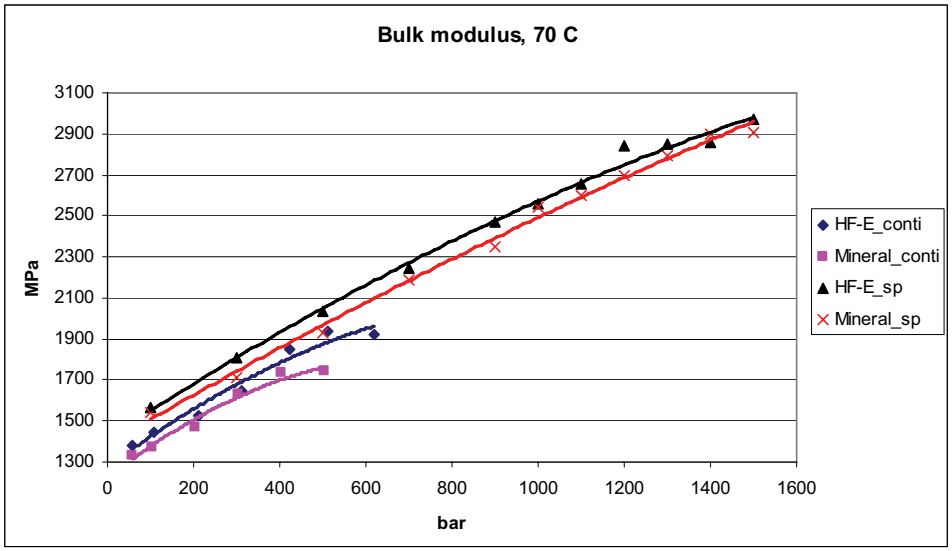

Figure 9. The measured bulk moduli of ISO VG 46 mineral oil and HF-E fluid at 70 ºC, with continuous system (‘conti’) and single peak system (‘sp’).

5 COMPARISON TO SIMULATIONS

The measured bulk moduli and densities were also compared to simulations according to [3] using only the fluid information of table 1. There were no significant differences discovered in correlations between the two fluids or between the two temperatures. Furthermore, the densities correlated very well with the models which is already covered more in detail in [11 ,12]. Thus, only the comparison of measured bulk moduli of ISO VG 46 mineral oil at 40 ºC to simulated values is shown here – the correlation for HF-E fluid was practically identical, as mentioned.

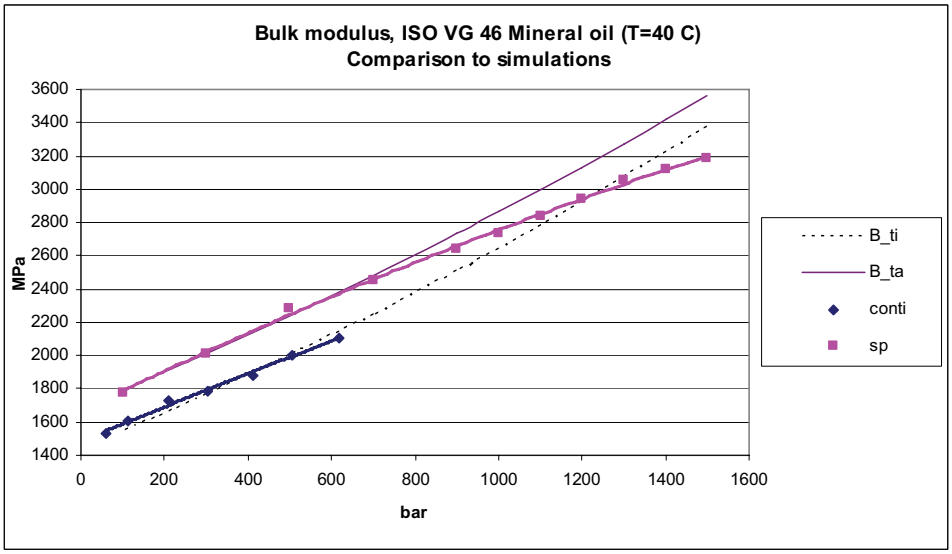

Figure 10. The calculated bulk moduli (isothermal tangent ‘B_ti’, adiabatic tangent ‘B_ta’) compared to the measured values with the two systems (continuous ‘conti’ and single peak ‘sp’).

Figure 10 illustrates the correlation between the calculated tangent values (isothermal and adiabatic) of bulk modulus and the measured values, with the two measuring systems. The calculated secant values are not shown since the measurements clearly correlate with tangent values [11, 12]. It seems clear that the continuous pumping method correlates with isothermal values. The single peak method correlates with adiabatic values, which would have been expected with both the systems.

6 DISCUSSION ON POSSIBLE REASONS FOR SYSTEM- RELATED DIFFERENCES

The measurements with the continuous pumping method and the single peak method clearly revealed system related differences in measured speed of sound in a fluid and bulk modulus. Measuring results with the ISO method [7] (falling into continuous pumping category) may either confirm or question whether there really is a fundamental difference in dynamic fluid behaviour between these types of hydraulic systems – in other words whether the dynamic compression- decompression produced by continuous pumping differs from that of produced by a single rapid pressure peak. As it was mentioned earlier, cylinder compression types of situations are known to be isothermal. Now the results would indicate the continuous pumping to be isothermal situation as well, at least in this particular case. The case with the ISO method is to be reported later.

Having said the measured fluids were exactly the same, even taken from the same barrels. Reflections were a problem with the continuous pumping method, but it was solved and removed from the final system [11]. The systems were built from same high-pressure components (piping, fittings, valves etc.) removing the possibility of incomparable system compliances. Air was removed from both the systems, although air does not even play a big role at such high pressures. Finally the identical results for measured densities practically rule out any errors in the actual measurements. So basically the only possible difference in the results should be due to different dynamic situation in change of state of the fluid. Totally independent simulations correlated very well to be only coincidence. In fact, the same measurements were performed with three other commercial fluids as well and the correlation was exactly the same [11, 12]. Therefore it is at least intriguing to believe in the empirical results.

Isothermal process concerns rather slow changes of state and heat energy transfers between the fluid and surroundings, temperature of the fluid remains constant. Adiabatic process is more rapid and there is no time for heat energy transfer. It is quite clear that the compression in the single peak method is more rapid than in continuous pumping. There are studies (e.g. [10]) discussing that compression processes in hydraulic systems actually might not be as easy to generalize as usually suggested. So it should be possible to think that some systems considered adiabatic might actually be isothermal.

When thinking about possible reasons for differences between continuous pumping and single pressure peak situation one question might be kinetic energy of the fluid. After all, in single peak system the pressurised fluid is static, having in practice zero kinetic energy whereas in continuous pumping the fluid at the same pressure is flowing having also kinetic energy. But should this be of significance in terms of enthalpy or fluid

compression? In the prevailing system the mass of the fluid inside the measuring pipe was about 60g with a velocity of about 3.5 m/s. Therefore the estimated kinetic energy would be less than 0.5 J. Moreover, pumping frequency did not seem to affect the results [11].

Due to energy conservation law kinetic energy is transformed into heat - therefore in single peak system it is also much easier to control the desired temperature. But would this kind of situation itself change the compressive conditions from adiabatic to isothermal? For example, could kinetic energy affect heat energy transfer during the changes of state? In any case, current empirical results would suggest continuous pumping to be isothermal, single pressure peak situation to be adiabatic.

7 CONCLUSIONS

Fluid dynamics may have significant practical difference in terms of system behaviour and design, especially in accurate solutions. Even if the fluid properties are known or can be modelled it is important to be able to choose which values to use. For example the difference of 200 MPa in fluid bulk modulus might be very critical – the error made using adiabatic values instead of isothermal ones.

Measurements using continuous pumping system indicated isothermal behaviour of the fluid change of state. The system itself can be associated to real life systems just as it is. It might be too early to generalize the situation too far before receiving the results of the ISO standardized measurements and before seeing whether those results will also correlate with isothermal simulations. However, it would strongly appear that the changes of state are isothermal at least in some similar cases which are very common in almost any working hydraulic system. The results for ISO method will be reported later.

The single pressure peak method correlated very well with adiabatic simulations and it was the expected result. Pressure peaks in real life systems are easy to associate with this system – whether the pressure peaks are disturbances or coming from e.g. an on-off valve opening or closing. In other words the kind of situations again found in almost any working hydraulic system. This kind of changes of state are usually more rapid compared to continuous pumping and it would appear that such processes are adiabatic.

This paper presented results of measured dynamic parameters of selected commercial hydraulic fluids. The measurements were performed using two different systems, commonly considered equivalent. The results and simulations suggested that there are system related differences between the two methods, correlating those of isothermal and adiabatic processes. Further research is being carried out using the equivalent ISO standardized method for confirmation. The results will be reported later.

REFERENCES

[1] ASTM-D6793-02. 2002. Standard Test Method for Determination of Isothermal Secant and Tangent Bulk Modulus. USA: ASTM. (5 p.)

[2] Bergemann, M. 1993. Systematische Untersuchung des Geräuschverhaltens von Kolbenp. mit gerader und ungerader Kolbenz. DSc thesis. RTWH, Aachen. (pp.27-32)

[3] Borghi, M., et al. 2003. A Numerical Approach to the Hydraulic Fluids Properties Prediction. Proc. 8th SICFP. Tampere University of Tech. (pp.715-729)

[4] Garbacik, A., Stecki, J.S. 2000. Developments in Fluid Power Control of Machinery and Manipulators. Fluid Power Net publication. (pp. 227-257)

[5] Haarhaus, M. 1984. Geräuschentstehung und Geräuschminderung bei Axialkolbenp. in Schrägscheibenbauweise. DSc thesis. RWTH, Aachen. (pp.33-37)

[6] Hodges, P. 1996. Hydraulic Fluids. London: Arnold. (167 p.)

[7] ISO 15086-2:2000. 2000. Hydraulic Fluid Power – Determination of the Fluid-borne Noise Characteristics of Components and Systems – Part 2 (27 p.)

[8] Jarchow, M. 1997. Massnahmen zur Minderung hochdruckseitiger Pulsationen hydrostatischer Schrägscheibeneinheiten. DSc thesis. RTWH, Aachen. (pp. 18-23, 29-31)

[9] Johnston, D., Edge, K. 1991. In-situ Measurement of the Wavespeed and Bulk Modulus in Hydraulic Lines. Proc.I.Mech.E.,Part 1,205.(pp.191-197)

[10] Kajaste, J., et al. 2005. Experimental Validation of Different Models for Effective Bulk Modulus of Hydraulic Fluid. Proc. 9th SICFP, Linköping Sweden. (16 p.)

[11] Karjalainen, J-P., et al. 2005. The Dynamics of Hydraulic Fluids – Significance, Differences and Measuring. Proc. PTMC 2005. University of Bath, UK. (pp. 437-450)

[12] Karjalainen, J-P. et al. 2006. High-pressure Properties of Hydraulic Fluids – Measuring and Differences. Proc. PTMC 2006. University of Bath, UK. (pp. 67-79)

[13] Kojima, E., Yu, J. 2000. Methods for Measuring the Speed of Sound in the Fluid in Fluid Transmission Pipes. Society of Automotive Engineering, Inc. (10 p.)

[14] Merritt, H.E. 1967. Hydraulic Control Systems. USA: John Wiley & Sons Inc.(358 p.)

[15] Smith, jr. L.H., et al. 1960. Hydraulic Fluid Bulk Modulus – Its Effect on System Performance and Techniques for Physical Measurement. NFPA. (19 p.)

[16] Yu, J.,et al. 1994. The Variation of Oil Effective Bulk Modulus with Pressure in Hydraulic Systems. Jour.Dyn.Syst.,Meas.&Contr. vol.116. Trans.ASME.(pp.146-150)

NEW TRENDS REQUIRE NEW HYDRAULIC MEDIA

Dipl. Ing. Gerhard Gaule
Technical Director of
Hermann Bantleon GmbH
Blaubeurerstr. 32
89077 Ulm, Germany
Phone +49 731 3990 19, Fax +49 731 3990 51
E-mail: ggaule@bantleon.de

Abstract

Since 1905 hydraulic oils have been used as transmission media. With about 86 % mineral oil based hydraulic fluids clearly dominate the market. The remaining 14 % are equally divided up into synthetic and hardly inflammable media. Since 1990 the demand for biodegradable oils (so-called bio oils) has been steadily increasing. For this reason the technical guidelines of VDMA 24568/ISO 15380 have been created.

According to these guidelines biodegradable hydraulic media are divided into the categories HEES, HEPR, HEPG and HETG. These technical minimum requirements for "bio-oils" are still valid today. When selecting a "bio-oil" the user has to consider the product characteristics of the medium concerning hydrolysis/oxidation stability, low-temperature behaviour and elastomer compatibility as well as the recommended operating temperature range according to DIN EN ISO 15380 chart 1. Furthermore a holistic view should consider expected reciprocal effects so that in a life cycle balance a positive value can be expected. lt is generally true that eco-labels are not based on a technical norm and do not at all represent a differentiation between "bio" or "not-bio". Rapid biodegradability does not always mean environmental protection, because quick biodegradation can result in a substantial de-oxidation of the environment which may result in serious consequences for plants and small organisms. Media, for which the dismantling rate can be variably defined are on the increase for the medium and long term.

1. New Trends require new hydraulic media

- Aspect Environment
- Aspect Economy / Performance
- Aspect Standards / Test methods

The presentation should show:

- Which reserves of oil-performance should be activated
- The „more“-costs of the fluid/liter is recompensated by its higher performance
- Environmental aspects should not only be reduced to high biodegradability and non toxicity. There is a complete consideration by a life cycle assessment (LCA) study needed !

2. General trends

2.1. General market trends in hydraulic systems

- Higher demands in terms of controllability and servo applications
- Decreased tolerance of modern precision hydraulics
- Decreased leakage
- Decreased maintenance and service requirements
- Extended life expectancy and higher cost effectiveness

2.2. Trends in requirements for hydraulic media

- Improved filtering capability
- Decreased detergent properties up to HLP/HVLP
- Improved air elimination capability, breaking capability
- Shear stability
- Flatter viscosity-temperature characteristic
- Ash-free additives
- More environmentally friendly
- Away from repair-mentality towards integrated ecological compatibility from very start (LCA = life cycle assessment, holistic approach towards environmental performance)

3. Technical background

3.1. New edition of DIN 51524 - 2006

- Filtering test ISO 13357
- Purity class ISO4406, min. 21/19/16
- Concentration of solid contaminants max. 50 mg/kg
- Extension to viscosity classes ISO VG 15/150
- Breaking behaviour
- Shear stability

3.2. Typical gap

		Gap width (µm)
servo valves	control nozzle deflector piston/bushing	130 –150 18 – 63 1 - 4
gear type pump	toothed gear towards plate toothed gear towards casing	0,5 – 5 0,5 – 5
piston pump	piston towards cylinder (radial) valve plate towards cylinder	5 – 40 0,5 – 50
vane pump	tips of the vanes sides of the vanes	0,5 – 2 5 - 13

The gap width between the components is more and more minimized. Thus the requirements on the hydraulic fluids are constantly increasing.

3.3. Comparison of purity classes

new purity classes:

Neue Reinheitsklassen
Reinheitsklasservergleich
*SAE AS 4059:2001 zu ** ISO 4406:1999

SAE AS4059E : 2001 > 4 / > 6 / > 14 µm (c) A / B / C (Size code)	ISO 4406 1999 > 4 µm (c)	ISO 4406 1999 > 6 µm (c)	ISO 4406 1999 > 14 µm (c)
000	8	7	4
00	9	8	5
0	10	9	6
1	11	10	7
2	12	11	8
3	13	12	9
4	14	13	10
5	15	14	11
6	16	15	12
7	17	16	13
8	18	17	14
9	19	18	15
10	20	19	16
11	21	20	17
12	22	21	18

old purity classes:

Alte Reinheitsklassen
Reinheitsklasservergleich
*NAS 1638:1964 zu ** ISO 4406:1991 (alt)

NAS 1638: 1964 2– 5/5– 15/15-25 µm	ISO 4406 1999 (alt) > 2 µm	ISO 4406 1999 (alt) > 5 µm	ISO 4406 1999 (alt) > 15 µm
00	10	8	5
0	11	9	6
1	12	10	7
2	13	11	8
3	14	12	9
4	15	13	10
5	16	14	11
6	17	15	12
7	18	16	13
8	19	17	14
9	20	18	15
10	21	19	16
11	22	20	17
12	23	21	18

Increased requirements concerning purity classes.
Survey of the old and new standardization.

3.4. Comparison of particle sizes

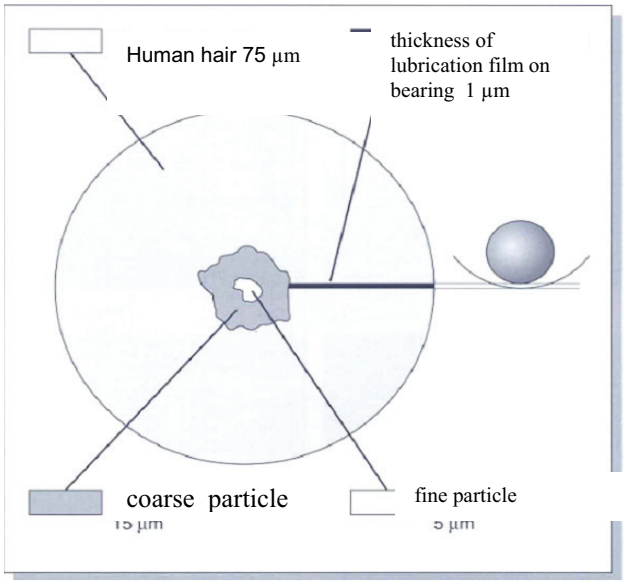

Influencing factor of the particles graphically shown by the example of a human hair.

3.5. Cleanliness requirements

Increased requirements should not be made of new hydraulic media until problem of residual soiling on components is under control.

3.6. Neutralisation number for unalloyed mineral oils with various concentrations of free

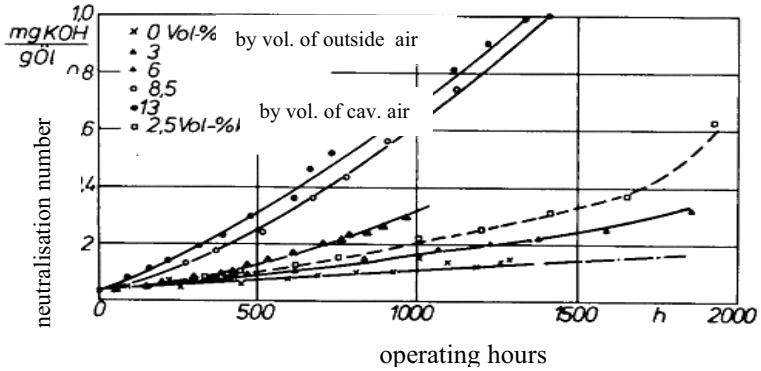

3.7. Main cause of damage in mobile hydraulics

Cavitation is the main cause of damage in mobile hydraulics.

3.8. Region where air separates and dissolves

Air separates and dissolves in front of and behind pump
Influencing factors leading to cavitation.

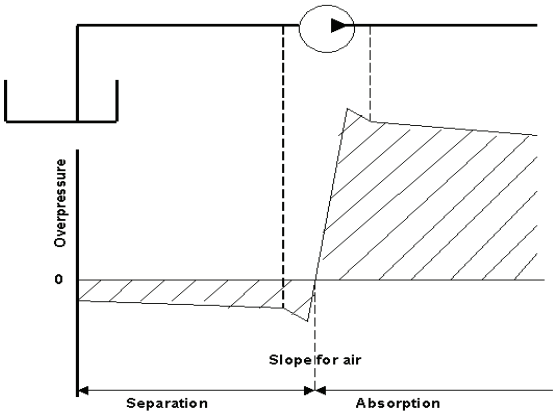

3.9. Cavitation

Cavitation due to hydrodynamic conditions is caused by locally high flow speeds. The consequence is abrasive wear (increased by impurities in medium)

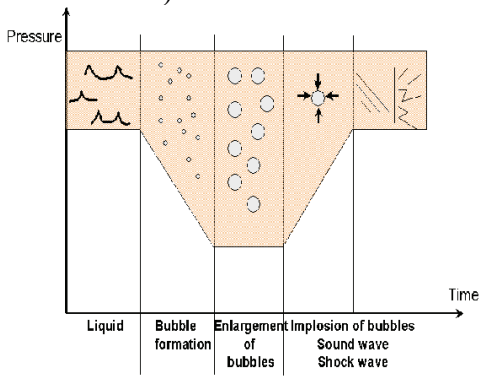

3.10. Erosion

- Due to hydrodynamic conditions

- Cause:
→ Locally high flow speeds

Consequences:
→ Abrasive wear
(increased by impurities in medium)

3.11. Neutralisation number for unalloyed mineral oils with different water content

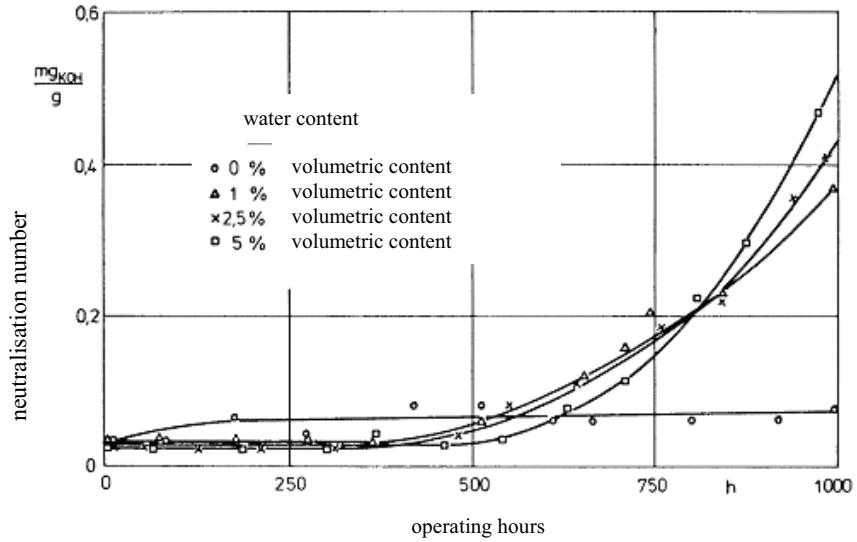

3.12. Moisture content/m³ air

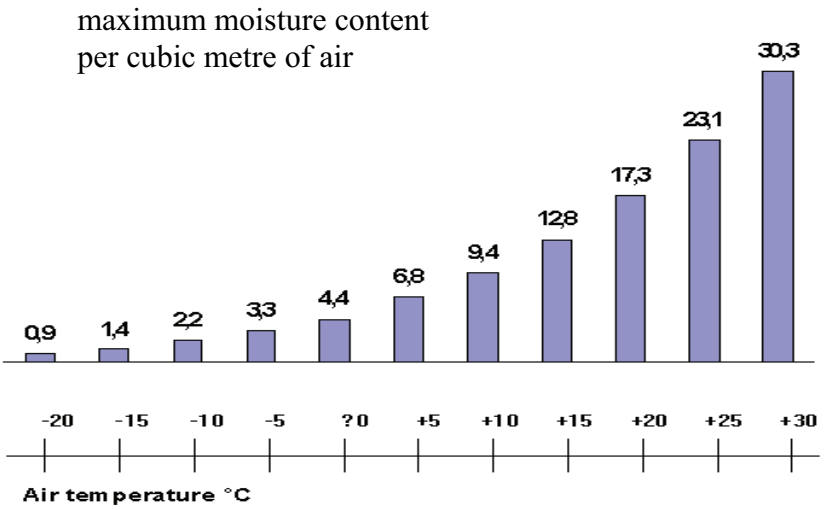

3.13. Comparison of various fluids

Temperature [°C]
- 15 Mineral oil
- 25 Phosphate ester
- 42 Polyisobutylene
- 45 Polyalkylene glycol
- 51 Diester
- 57 Polyolester
- 66 Polyalphaolefine

3.14. High-temperature ranges of various base fluids

Base fluids	Temperature °C
Mineral oil, dimer ester, monoester	110
Diester, aromatic ester, PAOs, polyglycols	110 – 160
Polyolester, PAOs, alkylmethyl silicone oils	160 – 200
Dimethyl and phenylmethyl silicone oils	200 – 260
Fluorinated silicone fluids	260 – 290

3.15. Thermal application range of base fluids

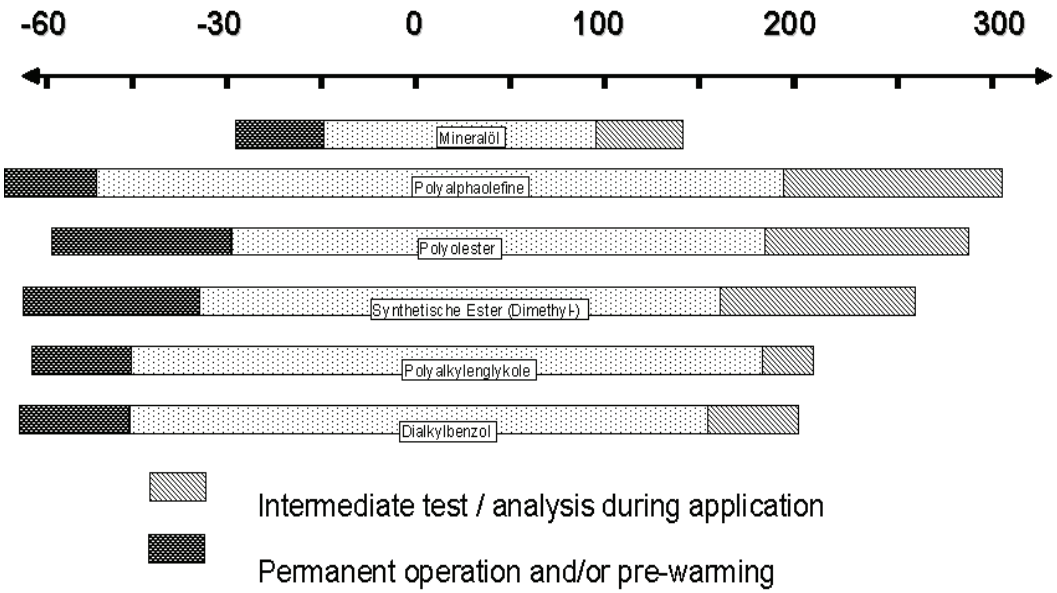

3.16. Comparison of various base fluids

	Mineral	*Di Est.*	*Polyol Ester*	*Dimer Ester*	*Arom. Ester*	*Mono Ester*	*PAO*	*Poly Glyk.*	*Silik.*
VT/M	A	V	V	V	I	V	V	V	E
Low temp.	I	E	V	G	A	E	E	V	E
High temp.	I	G	V	A	G	I	G	G	E
Evaporation	I	E	E	E	E	A	E	G	V
Friction	A	E	V	E	G	G	G	E	I
Degradability	I	E	V	G	I	E	G	A	I
Hydrol. Stab.	E	A	G	A	A	I	E	V	V
Additive sol.	E	V	V	V	V	V	G	A	I
Elastomer	E	I	A	V	I	I	G	V	V
colour/finish	E	I	G	E	I	I	E	I	V
Miscibility (oil)	E	G	G	V	G	G	E	I	I
Cost	E	G	G	V	G	G	V	G	I

I = insufficient A = average G = good V = very good E = excellent

3.17. viscosity index – kinematic viscosity

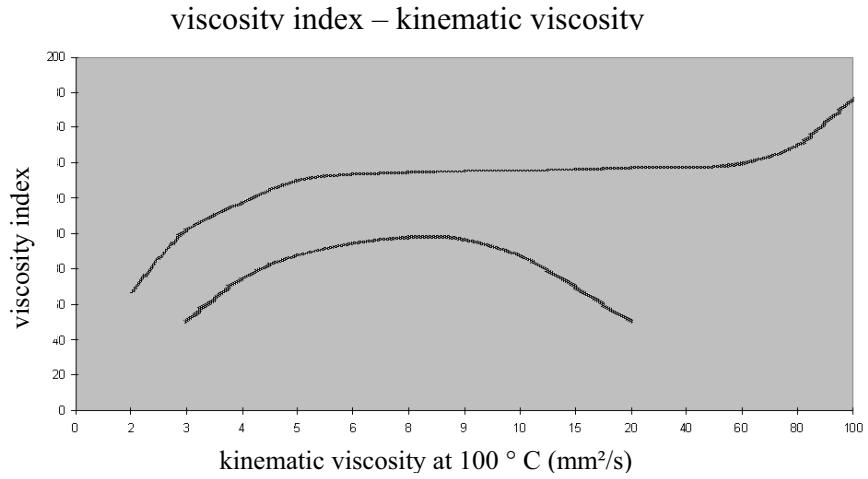

3.18 viscosity comparison

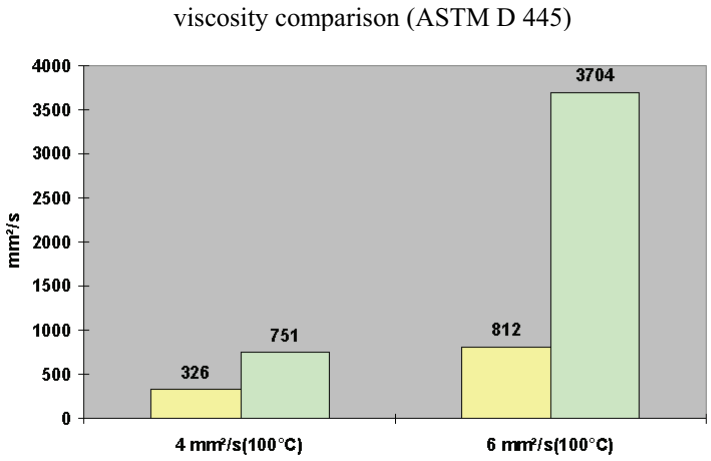

3.19. experiences with PAO

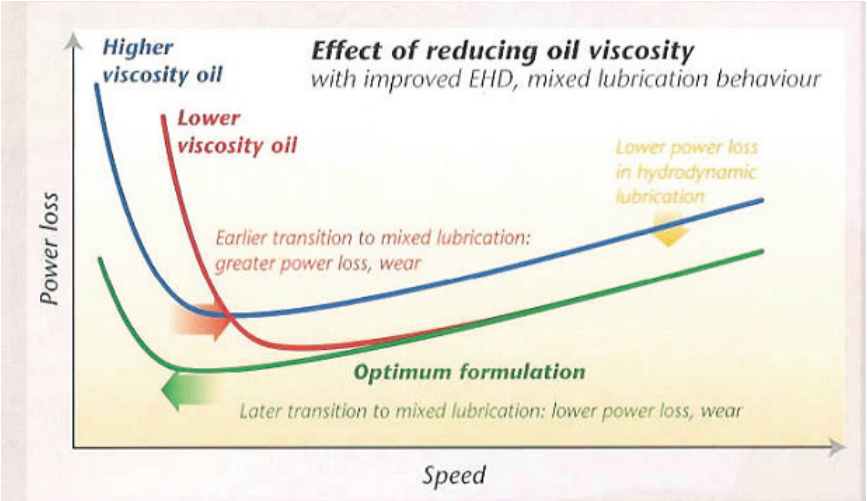

PAO oils behave perfectly concerning performance loss and component security compared to conventional oils. PAO oils show an optimal energy efficiency.

3.20. VT Diagramm

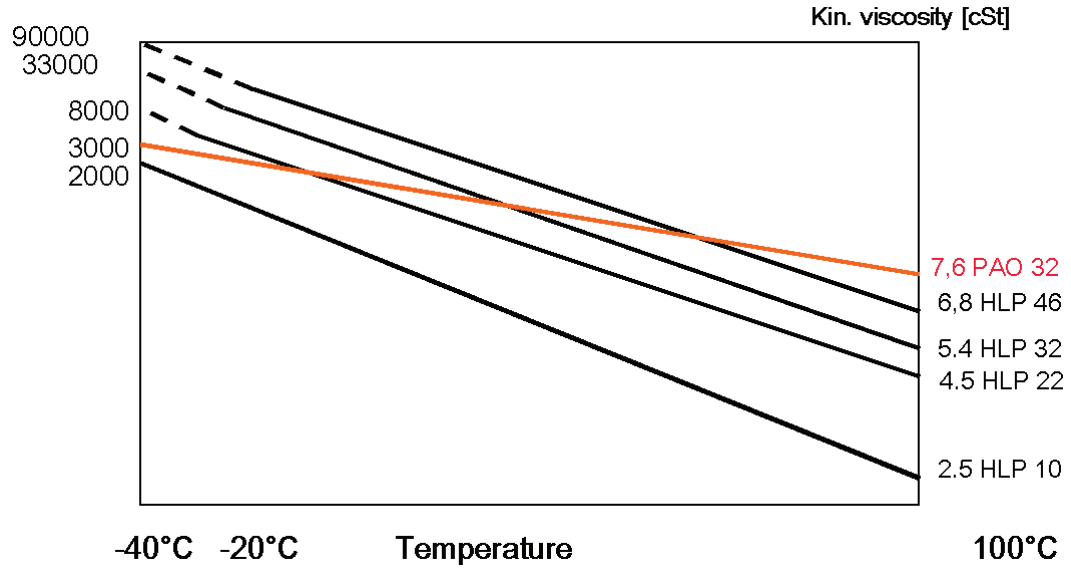

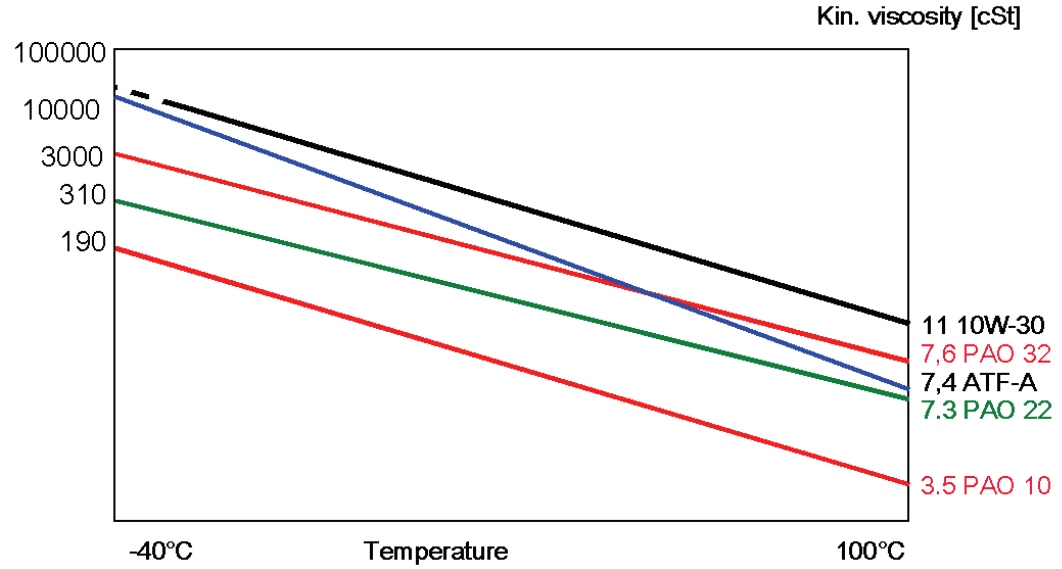

4. Possible advantages in the application of HEPR

A) towards ester-based hydraulic media

1. Miscibility and compatibility with mineral oil based hydraulic oils
2. No loss of fresh oil in case of oil drain amounting to 2 - 4 times of the filling quantity of the hydraulic system because of rinsing necessary due to incompatibility
3. No hydrolytic instability due to water
4. No necessity of water filters in the hydraulic system in order to avoid smallest proportions of water as there is no hydrolytic instability.
5. No aggressiveness towards elastomers/tubes as with esters
6. No special elastomers needed for tubes /seals
7. Lower loss/environmental pollution due to leakage caused by elastomer failure

8. Longer service life due to higher stability and less application risks with the same maintenance and care requirements
9. Better low temperature capability/pumpability even before the pour point is reached due to constant low viscosity even after the influence of low temperatures for a longer period
10. Better air release properties with less air absorption and reduced foaming.

B) towards mineral-oil based hydraulic oils

1. Longer service life of the hydraulic oil medium up to 2 – 3 times towards mineral oil
2. Longer service life of the hydraulic components due to less wear
3. Reduction of cost/working hours due to less need of maintenance and service as well as higher operational safety despite higher oil cost per liter.
4. Saving of rinsing quantity loss of up to 2 – 3 times of filling quantity of hydraulic system with expensive „biological oil“ if HEPR has already been used for first filling, in case of later application in environmental sensitive ranges.
5. Three HLP Hydraulic viscosity categories can be covered with one HEPR hydraulic oil
6. Better low and high temperature capability than mineral oil e.g. broader application temperature range requires less climatic conditioned oil changes.
7. Better cold start performance especially at winter temperatures
8. Better controllability and response time in the hydraulic system especially shortly after cold start.
9. No warming-up phase needed for full serviceability especially at cold start with winter temperatures.
10. Preservation of resources together with less wear of components due to fuel saving and the possibility for smaller dimensioning of pumps and gears
11. No oil-caused efficiency loss especially at low temperatures during the warming- up phase.

5. Total Life cycle costs

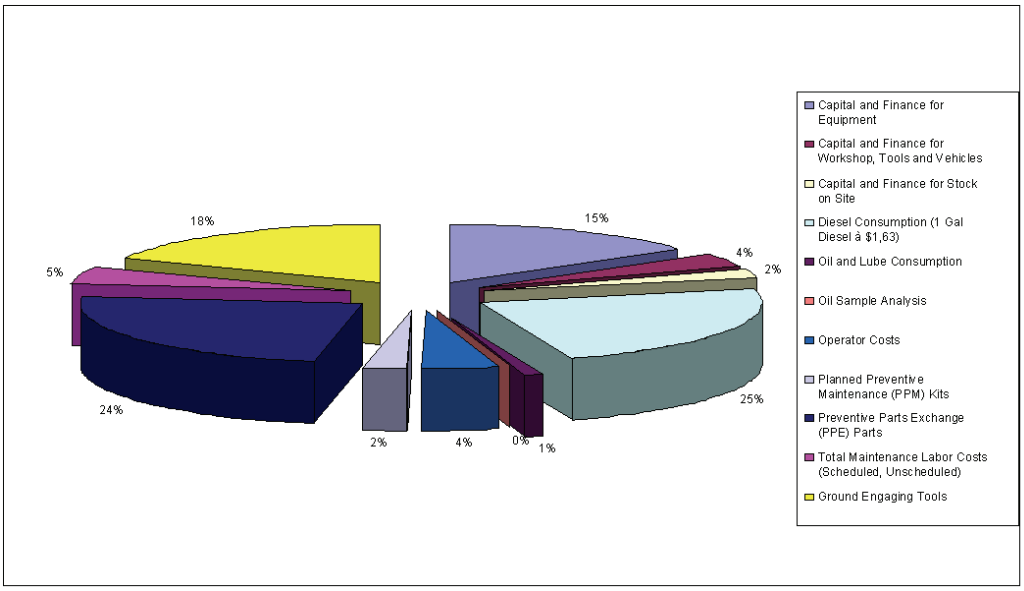

The expenses for lubricants are negligible compared to the investment cost of a construction machine. The added value obtained by the use high quality lubricants is disproportionately high. Very low expenses
lead to a high saving potential.

6. Ecological requirements for hydraulic media and existing standards

6.1. current classifications for hydraulic oils

6.2. distribution of market shares in Germany

6.3. VDMA 24568 / ISO 15380 classifications

- HETG Natural ester / rape seed, soy, sunflower ...
- HEES - synthetic ester / polyolester, TMP, ...
- HEPG Polyalkylene glycol / polyethylene glycol, polyether
- HEPR – Polyalphaolefine (PAO) and related hydrocarbons

6.4. Environmentally friendly thanks to holistic approach

The holistic approach to environmental protection required:

• Expertise in holistic solutions
• "Bio" is intended for the environment and not for profit

→ In the holistic approach, it is essential that business interests are not discredited from the perspective of environmental protection.

A holistic environmental approach illustrates the effective gain for the environment, living conditions and nature.

With ecological measures (e.g., use of "bio-oil"), all accompanying effects are relevant for the environment.

This concerns:
- Resource consumption, energy consumption, CO2 emissions
- Manufacture - use
- Disposal - recycling

6.5. Technical consideration of environmental measures

Before implementing environmental measures, the effects must be subjected to a comprehensive investigation:

With respect to the environmental effects
→ on microbiology, living organisms and plants

With respect to secondary effects on peripheral elements along intended direction of action
→ Improved suitability for longer usage durations
→ Less consumption through longer use of supplies.

6.6. Holistic approach to environmental performance – A comparison…..

Comparison of environmental performance for two different types of hydraulic fluids.

Preliminary studies returned positive findings for AVIA Syntofluid PE-B in comparison with other renowned biodegradable hydraulic fluids.

6.7. Environmental advantages, cost effectiveness of "bio-oils"?

In current "bio-oils", generally the following aspects are considered only:
→ Rapid/easy biodegradability acc. to various applicable test methods
→ Toxicological effect acc. to various applicable test methods

6.8. Environmental advantages, cost effectiveness of "bio-oils"?

Is the use of "renewable" resources in bio-oils truly effective in helping to protect the environment?
This has to be decided on a case-by-case basis!

Since renewable resources can also contain naturally poisonous substances, they are not necessarily always suitable for reducing environmental hazards.
→ The holistic approach to environmental performance also applies to "bio-oils"!

What are the hazards posed to the environment by bio-oils?
→ A lack of knowledge and false information can lead to environmentally hazardous applications using bio-oils.

7. Bulletin on misuse of bio-oils

Bio-oils may be misused due to a lack of training, carelessness, or premeditation. The term "bio-oil" can be misconstrued and encourage inappropriate handling. This bulletin shall serve to protect the environment by counteracting the lack of information available concerning bio-oils. Bio-oils are chiefly used in chainsaw and hydraulic oils as well as in stationary devices. In addition, they are also play a subordinate role in separating agents, greases, gear and metalworking oils.

→ Do not allow bio-oils to enter the environment and never dispose of them there!

This includes water, sewage and soil.
In technical applications, this applies to all lubricants, mineral oils, esters (saturated or non-saturated) in use, as well as to non-technical applications in the food industry sector involving rape seed oils, olive oils, soy oils etc. Even salad oils would have the same effect on the environment as a bio-oil created for a technical application.
As a general rule, one drop of any oil will sufficiently contaminate 1000 litres of drinking water such that the water is no longer of drinkable quality.

→ What to do when oils enter the environment?

Whenever oils penetrate the environment, immediately inform the responsible authorities and ensure that the entire quantity of contaminating oil is fully removed from the environment. Legislators do not differentiate between bio-oils and other types of oil.

When water is contaminated, local fire departments may use oil binding agents to take up oil from the water surface and thus fully remove it from the water, unless of course the oil is water-soluble. It is not possible to remove water-soluble bio-oils and these may cause inadmissible contamination. Oils may only be labelled as "bio-oils" once they have passed various tests with respect to biodegradability and environmental toxicity. The harmful effects on water quality are irreversible even if they are only temporary. In this case, a water-insoluble "bio-oil" is more appropriate since it can be fully removed from water.

If soil is contaminated with oil, the affected area will have to be carried or dredged away as soon as possible regardless of the oil quality. The oil quality can play a role when considering the subsequent problem of how to dispose of the contaminated soil.

8. Rinsing procedure for switchover to "bio-oils"

When switching from mineral-based hydraulic oils to bio-oils,
large quantities of oil are often lost through the rinsing procedure.

9. Environmental advantages, cost effectiveness of "bio-oils"?

Is rapid/easy biodegradability always desirable for bio-oils?

→ Not if quantities in the range of several tens or even hundreds of litres enter the environment!

→ Can lead to oxygen depletion in the vicinity!

Potential consequences:

→ Disruption and killing of micro and other organisms in affected areas of water and earth

Polar elastomers designed for mineral oils may suffer in terms of life expectancy after coming into contact with ester-based media.
If oil leaks from a hydraulic hose and coats the outer surface, this may lead to a chain reaction wherein this oil contacts neighbouring hoses and damages them.

The outer sheathing of hydraulic hoses is much less suitable for contact with hydraulic media than the inner linings.

10. Errors in assessing the technical performance of "bio-oils"

Possible errors in assessing the technical performance of "bio-oils":

The minimum technical requirements for bio-oils are defined in VDMA 24568 / ISO 15380:

→ All test methods and threshold values are based on DIN 51524 for hydraulic fluids. These are not fulfilled by ester-based natural and synthetic fluids.

→ The transferability of test methods and limit values from DIN 51524 to VDMA 24568 /ISO 15380 has not been checked for all cases!

Reason for frequent discrepancy between lack of transferability of test methods to ester-based "bio-oils" is due to different chemical composition of the media:

→ Mineral oils or synthetic mineral oils such as poly-alpha-olefine (PAO)

→ Ester-based oils (saturated, partially saturated or unsaturated) and/or containing renewable resources

11. Which test methods are adapted?

Oxidation test (ageing behaviour):

DIN 51524	→	TOST Test with 2 vol% water (DIN 51587)
VDMA 24568 / ISO 15380	→	dry TOST Test (DIN 51554) w/o water for HETG, HEES

The various oxidation tests (increase of neutralisation number)
can lead to different usage durations!
→ Research is required!

12. Until now, "critical" test methods have not been adapted

→ FZG test with respect to wear in hydraulic pumps

→ Elastomer tests without increased proportion of water are no longer in agreement with actual conditions of current mobile hydraulic systems

13. Assessing the usage quality of "bio-oils"

Additional sources of error in estimating usage quality of "bio-oils"

Low-temperature behaviour estimated from solidifying point or VT characteristic (derived graphically for viscosities at 40°C and 100°C) can lead to optimistic predictions.
If low temperatures prevail for several days, cold-start and/or cavitation problems may result due to increase in viscosity.

Upper temperature limit:
Rape seed oil is limited to max. +60°C (gumming hazard)

(DIN ISO 15380 tolerates a rather generous max. temp. of 80°C
for rape seed oil [HETG])

14. DIN ISO 15380 Table A. 1

Recommended application temperature range for hydraulic oil tanks with environmentally friendly hydraulic oils.

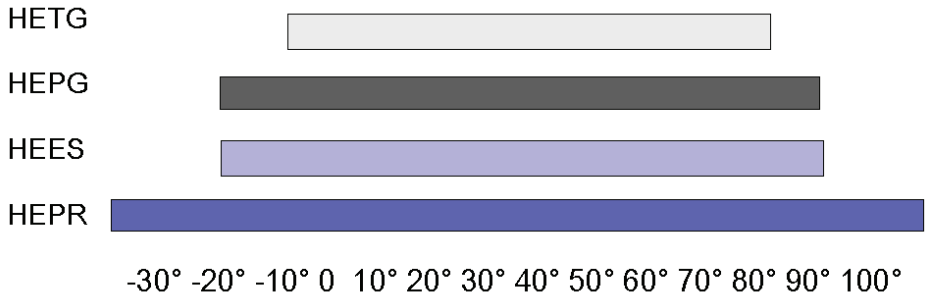

15. Assessing the usage quality of "bio-oils"

The anti-corrosion properties are tested in accordance with the fresh oil inspection standards.

Used oils sometimes behave differently in practice:

→ Hydrolysis may split the ester molecules (HETG/HEES) into alcohol and fatty acids.
→ Free fatty acids may undergo subsequent reactions:

→ Formation of side chains on ester molecules
→ Saponification of metal ions as a result of wear
→ Formation of metallic salts with ions or oxides
→ Corrosion on surfaces possible in vapour area above tank fluid level

16. Corrosion on surfaces

pictures taken in the field

17. Conclusion

→ Current environmental standards often make it difficult to consolidate ecological and economic considerations.
→ The goal of further development of environmental standards is to implement a holistic approach to environmental performance wherein cost effectiveness is to serve as a criterion.
→ A new generation of hydraulic media could fulfil the new targeted standards.
→ These hydraulic media could include:
→ HEPR - AVIA Syntofluid PE-B

Design and Simulation Study of the Measuring Device for Hydraulic Oil Bulk Modulus

Jing Wang，Guofang Gong，Huayong Yang
Institute of Mechatronics and Control Engineering, Zhejiang University

Abstract: In order to get the bulk modulus of hydraulic oil, a bulk-modulus measuring device has been designed according to the definition of the bulk modulus. The measuring is on-line and automatic operation. Some previous problems of the measurement of bulk modulus have been resolved in this design. The simulation study has been carried out using the simulator of AMESim. The results show that the structure parameters of the device and the hydraulic parameters of the testing system are set properly. The measured value of the bulk modulus of hydraulic oil is nearly equal to the theoretical value.
Key words: hydraulic oil；bulk modulus；AMESim

1 Background and introduction

The bulk modulus is a very important physical parameter of hydraulic oil. It affects the natural frequency and damping ratio of the hydraulic components and systems, accordingly it affects the stability and dynamic performance of the hydraulic components and systems. It is very important to use accurate value of the bulk modulus when designing the dynamics of the hydraulic components, the hydraulic transmission systems and the electro-hydraulic servo systems, especially the dynamic simulation. The effective bulk modulus is a function of the bulk modulus of oil and of pipeline, but the former is the main factor. Thus, the study of the compressibility of hydraulic oil is an important subject study in the field of hydraulics. The bulk modulus of hydraulic oil varies with pressure, temperature, air content and molecular structure. In practice, the bulk modulus of hydraulic oil is estimated roughly with the bulk modulus of pure oil, pipeline shape and the rate of the air bubbles. Experiment results show that the estimated value is different with the measured value. Up to now, a reliable and practical measuring device for hydraulic oil bulk modulus is just in academic discussion. Lack of measuring device has become a difficulty in the related practical work. A measuring device for hydraulic oil bulk modulus is very useful in practice. The dynamic simulation analysis will get better calculation precision if the measured value of hydraulic oil bulk modulus can be put into the analytic model. On the other hand, the measured value of hydraulic oil bulk modulus can help researchers and users to evaluate and estimate the effect of the air content to the system performance. In this paper, the design, the operating principle and the simulation analysis of a bulk-modulus measuring device based on the definition of the bulk modulus have been discussed.

2 Design of the bulk-modulus measuring device

The measuring is based on the definition of the bulk modulus.

$$\mathrm{K} = V_0 \frac{\Delta p}{\Delta \mathrm{V}}$$

where，K – the bulk modulus of the hydraulic oil

V_0 – the original volume of the hydraulic oil

Δ V – the variation volume of the hydraulic oil

ΔP – the corresponding variation pressure to the variation volume

There generally exist under mentioned problems when measuring bulk-modulus of hydraulic oil according to the definition formula. The process of forcing on the oil is carried out with hand operation, so it is hard to realize automatic and on-line measurement. The effects of friction and container deformation in the process of forcing on the oil make it hard to assure the measuring precision, for it requires high leak tightness between the relatively slip parts. The measured oil cannot be changed easily, so it is hard to assure the measured results can represent the practical situation.

These problems have been resolved during the process of the bulk-modulus measuring device design.

The basic structure of the bulk-modulus measuring device is shown in **Figure1**. This device mainly includes loading cylinder (1), piston and rod (2), test chamber (3), check valve (4), pressure sensor (5), displacement sensor (6).

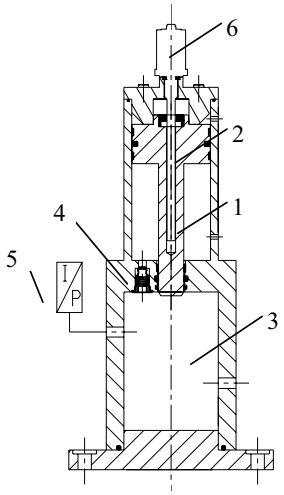

Fig.1 Structure of the bulk-modulus measuring device

Take some of the oil in the hydraulic system as the investigated subject. Force on the hydraulic oil in the test chamber with the loading cylinder. Change the magnitude of the force and get the corresponding variation volume. Then the bulk modulus of hydraulic oil can be computed according to the definition formula of the bulk modulus. The result can be displayed on the secondary instrument or transferred to the computer.

Put the piston rod of the loading cylinder into the test chamber. The rod can move in the test chamber. The load is applied by the loading cylinder, so automatic and on-line measuring can be realized. The material of the test chamber is seamless steel pipe, and the thickness of the pipe is 30mm, so the effect of the deformation of the pipe wall to the measurement of bulk-modulus can be ignored. The magnitude of the force on the hydraulic oil in the test chamber can be measured by the pressure sensor, so the result is independent on the friction of the piston and the piston rod. The oil in the hydraulic system can flow through the test chamber before applying load, so the tested oil in the test chamber is the oil having been cycled.

The oil-in of the check valve is connected with the rod side of the test cylinder, and the oil-out of the check valve is connected with the test chamber. The pressure sensor is installed on the test chamber. The displacement sensor is installed in the piston and rod of the loading cylinder. The rod side and the rodless side of the loading cylinder and the test chamber are connected with the hydraulic system through pipes.

3 Operating principle of the bulk-modulus measuring device

The operating principle of the bulk-modulus measuring device is shown in **Figure2**.

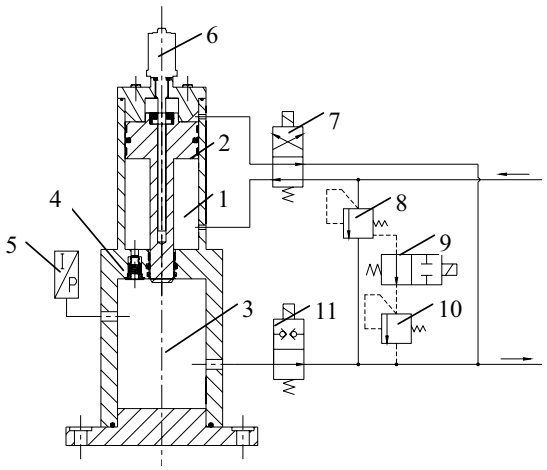

Fig.2 Operating principle of the bulk-modulus measuring device

The measuring process of the device can be divided into the following four steps.

1/ Exchange the tested oil in the test chamber. The electromagnetic controlled directional control valve (9) is power-off. The pressure of the bulk-modulus measuring circuit is 0.7MPa which is determined by the set pressure of the direct-acting pressure relief valve (10) on the pilot control oil circuit of the pilot controlled pressure relief valve (8). The cut-off electromagnetic controlled directional control valve (11) is power-off. The electromagnetic controlled directional control valve (7) is power-off, so the rodless side of the loading cylinder is connected to the tank and the pressure oil enters the rod side of the loading cylinder. When the piston moves to the end of loading cylinder, the pressure of the rod side of the loading cylinder will increase. The pressure oil opens the check valve and enters the test chamber, then flows back to the tank through the cut-off electromagnetic controlled directional control valve (11).

2/ Pre compress. The cut-off electromagnetic controlled directional control valve (11) is power-on, so the rod side of the loading cylinder is connected to the tank and the pressure oil enters the rodless side of the loading cylinder. For the piston area is larger than that of the piston rod, the area ratio is 9.7656:1, the pressure of oil pushes the piston rod downward. The piston rod volume entering into the test chamber increases, so the hydraulic oil in the test chamber is compressed. If the piston rod stops, then record the reading X1 of the displacement sensor (6) and the reading P1of the pressure sensor (5).

3/ Further compress. The electromagnetic controlled directional control valve (9) is power-on. The pressure of the bulk-modulus measuring circuit is 2.0MPa which is determined by the set pressure of the pilot controlled pressure relief valve (8). When the pressure of the loading circuit increases, the pressure of oil continues to push the piston rod downward. So the hydraulic oil in the test chamber is further compressed. If the piston rod stops, then record the reading X2 of the displacement sensor (6) and the reading P2 of the pressure sensor (5). The data is processed by the computer and the value of hydraulic oil bulk modulus is computed according to the definition formula.

4/ Finish compress. The electromagnetic controlled directional control valve (9) is power-off. The pressure of the bulk-modulus measuring circuit is 0.7MPa which is determined by the set pressure of the direct-acting pressure relief valve (10) on the pilot control oil circuit of the pilot controlled pressure relief valve (8). For the pressure of the circuit decreases, the piston rod moves upward. If the piston rod stops, then cut off the electricity supply for the electromagnetic controlled directional control valve (7). So the rodless side of the loading cylinder is connected to the tank and the pressure oil enters the rod side of the loading cylinder. When the piston moves to the end of loading cylinder, cut off the electricity supply for the cut-off electromagnetic

controlled directional control valve (11). The pressure oil opens the check valve and enters to the test chamber, then flows back to the tank through the cut-off electromagnetic controlled directional control valve (11).

Now it comes back to the state of exchanging the tested oil in the test chamber. According to the requirement, the above process can be repeated several times to measure the value of the bulk modulus.

4 Simulation analysis of the bulk-modulus measuring device

Use the visual simulator of AMESim, which is special-purpose software of model building, simulation and dynamic analysis for hydraulic and mechanical system, to carry out simulation study of the bulk-modulus measuring device.

According to the operating principle of the bulk-modulus measuring device shown in **Figure2**, the simulation model which is built with AMESim is shown in **Figure3**.

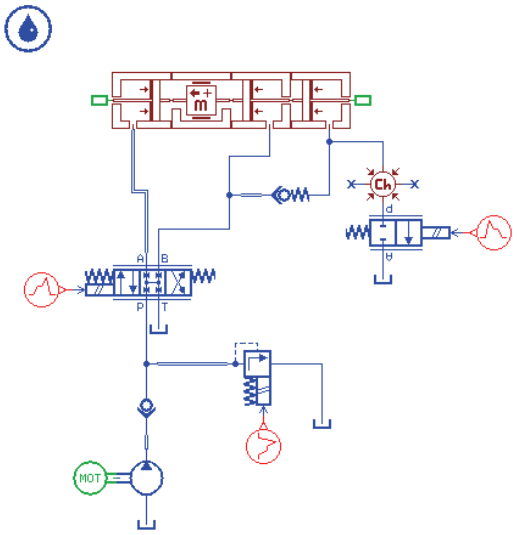

Fig. 3 Simulation model of the bulk-modulus measuring device

Define a work cycle.

No.	Sec.	Pilot relief valve	Three-position four-way valve	Two-position two-way valve
1	0-5s	0.7MPa	Right side	Right side
2	5-6s	0.7MPa	Right side	Left side
3	6-8s	0.7MPa	Left side	Left side
4	8-10s	2.0MPa	Left side	Left side
5	10-12s	0.7MPa	Left side	Left side
6	12-14s	0.7MPa	Right side	Left side
7	14-20s	0.7MPa	Right side	Right side

Set the bulk modulus of hydraulic oil in the simulation model as 1000Mpa.

The displacement, pressure and flow change curve chart in one work cycle is shown in **Figure4-Figure6**.

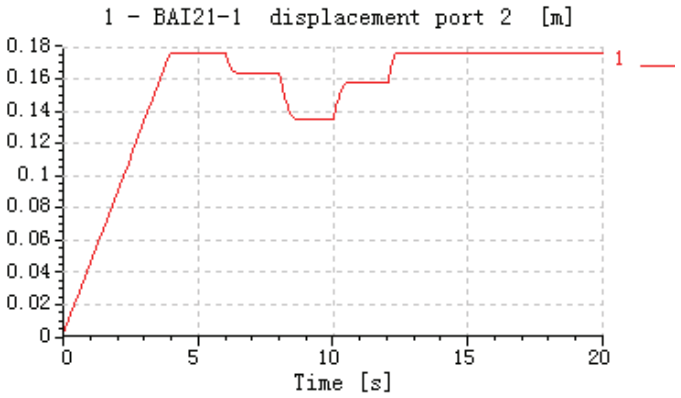

Fig.4 Piston displacement curve

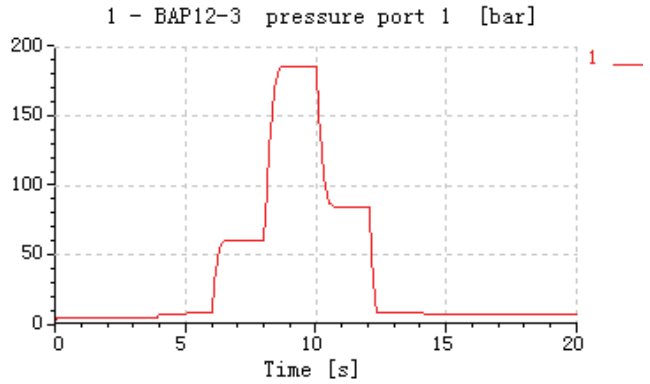

Fig.5 Test chamber pressure curve

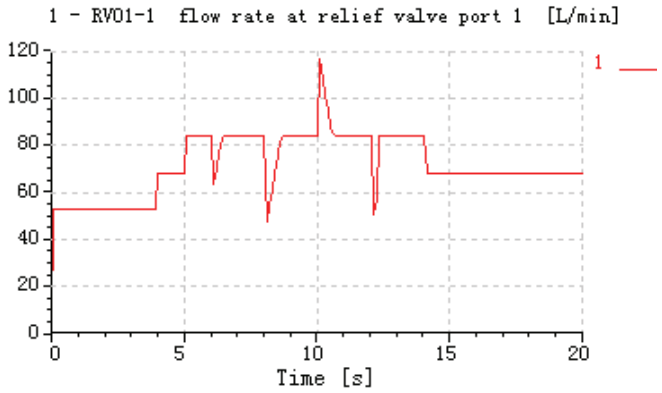

Fig6 Pilot controlled pressure relief valve flow curve

Use the data of above curves to compute the value of hydraulic oil bulk modulus according to the definition of the bulk modulus.

Compute the bulk modulus of hydraulic oil.

$$K = V1 \times \frac{P2 - P1}{V1 - V2} = \left(V0 - \frac{\pi}{4} \times d^2 \times X1 \right) \times \frac{P2 - P1}{\left(V0 - \frac{\pi}{4} \times d^2 \times X1 \right) - \left(V0 - \frac{\pi}{4} \times d^2 \times X2 \right)}$$

$$= 1.9769 \times \frac{18.6526 - 5.957}{1.9769 - 1.9536}$$

$$= 1077.16 Mpa$$

The results show that the measured value of the bulk modulus is nearly equal to the theoretical value. This confirms that the structure parameters of the bulk-modulus measuring device and the hydraulic parameters of the testing system are set properly.

5 Conclusions

1/ The designed measuring device for hydraulic oil bulk modulus can realize automatic and on-line measurement.

2/ Using this device to measure the bulk modulus of hydraulic oil avoid the effect of the friction to the measuring results, so the measuring value of hydraulic oil bulk modulus is accurate and reliable. The process of measuring can be repeated several times.

3/ The tested oil in the test chamber of this device is the oil having been cycled, that assures the result can represent the actual situation of the oil in the hydraulic system.

References

/1/ A.T.J Hayward. How to measure the isothermal compressibility of liquids accurately. J. Phys. D: Appl. Phys., 1971, Vol.4

/2/ Jingchao Sheng. Hydraulic Fluid Mechanics [M]. China Machine Press, 1982.

/3/ Songnian Li. The On-line Measuring Technology of Hydraulic Oil Modulus. Fulid Power Transmission and control symposium, 1987.

CONDITION MONITORING OF PNEUMATIC SYSTEMS USING SELF-ORGANISING MAPS

A. Zachrison and M. Sethson
Department of Management and Engineering
Linköping University
Sweden
E-mail: (anders.zachrison, magnus.sethson)@liu.se

ABSTRACT

Automated monitoring of systems is growing in importance as systems become increasingly autonomous and intelligent control is being used to a growing extent. At the same time, component manufacturers' desire to offer components with embedded condition monitoring systems is also increasing.

This paper discusses one general, adaptive method – the self-organising map, SOM– suitable for such an application. It concerns how to improve interpretation of the fault classification process by using a combination of outputs from the SOM. The simultaneous detection of both known and unknown faults is discussed.

KEYWORDS: Pneumatic; Cylinder; Modelling; Self-Organising Maps; Condition monitoring

1 INTRODUCTION

Condition monitoring of systems and detection of changes in the systems are of integral importance for a fully automated system. Although condition monitoring is already widely used in machinery, the need for it is growing, especially as systems become increasingly autonomous and self-controlled. One of the toughest tasks concerning embedded condition monitoring is to extract the useful information and conclusions from the often large amount of measured data. The converse, drawing conclusions from a minimum of data is also of interest. In this case, interest is at least two-fold: to reduce costs (fewer sensors) and to create redundant monitoring and analysis systems. The use of self-organising maps, SOMs, for embedded condition monitoring may be of interest for the component manufacturer who does not have information about how the component is to be used by the customer, or in what applications and load cases.

Automating monitoring and analysis means not only being able to collect prodigious amounts of measured data, but also being able to interpret the data and transform it into useful information, e.g. conclusions about the state of the system. However, as will be argued in this paper, drawing the conclusions is one thing, being able to interpret the

conclusions is another, not least concerning the credibility of the conclusions drawn. This has proven to be particularly true for simple mechanical systems like pneumatics in the manufacturing industry.

The craft of monitoring complex system is not a trivial task, as condition monitoring is not about a light-bulb on a control panel or a scalar value; it is rather at least a pair of data that must be considered. First, the estimated error or difference from the normal case has to be considered, but this is not enough. Rather, the real value of this measure will depend on how certain we are that it is correct, hence the need for a confidence measure. Such a measure might be the accumulated training of a neuron, compared to the normal or overall amount of training. To further enhance the monitoring process, several measures could also be added and studied simultaneously.

The qualification of the alarm is handled in different ways, depending on what condition monitoring techniques are used. In model based condition monitoring, the variance and mean of the generated residual are normally enough; on the other hand, classical artificial neural network based methods do not give an estimate of the confidence level. Here it is shown that using SOMs for condition monitoring allows the uniqueness of the state to be determined. The uniqueness could be seen as a measure of the confidence of the diagnosis.

The main focuseof the paper is the discussion on how the results and statistics from the SOM could be combined to enhance the interpretation of the decision.

2 TEST SETUP

The test setup consists of a rod-less pneumatic cylinder, controlled by four on/off-valves. See figure 1 for a schematic view of the system.

The piston is controlled in an open-loop fashion, partly due to the fact that open-loop control is quite common in pneumatics, especially in the manufacturing industry. On the other hand, in the industry it is most often a fixed position control and does not use any intermediate positions, as can be found in our sequence, shown in figure 2.

The system is run using six different test cases; these are three different mass loads and (non)leaking exhaust valves. The mass loads are 0, 10 and 20 kg respectively.

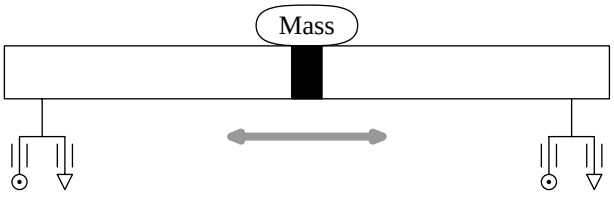

Figure 1: A schematic sketch of the test setup.

3 SELF-ORGANISING MAPS

Self-organising (feature) maps, SOMs, are a special kind of neural network first presented by Kohonen; see for instance [1, 2].

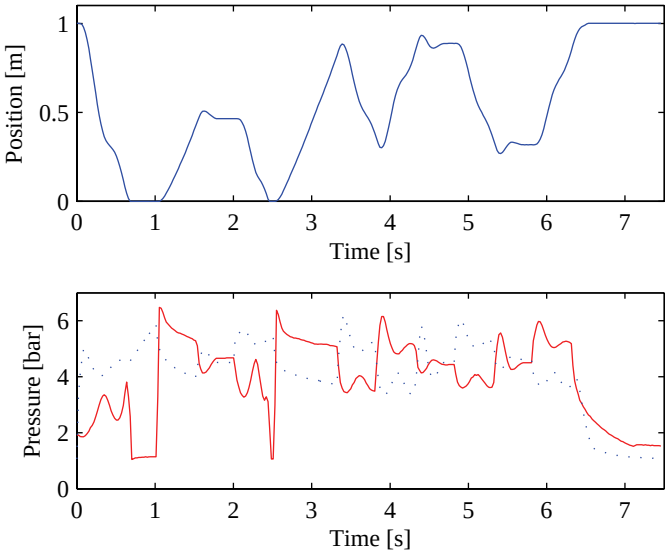

Figure 2: An example of the outcome of the used input sequence. In this example, the mass load is 10 kg and there are no leakages in the exhaust valves. The lower graph shows the two chamber pressures.

The SOM works by approximating the probability distribution of the input vectors by its neurons' weight vectors. As such, it accumulates knowledge during training and this knowledge is distributed in the same areas as the input vectors. This allows the SOM implementation to maintain a record of well-known regions in the input domain, and distinguish these from unknown, novel inputs.

In [3] two ways of using the SOM for condition monitoring are discussed: the quantisation error method, q.e., and classification. In section 4, these two methods are discussed, as well as extensions to them.

3.1 SOM algorithm

The use of the SOM can generally be divided into three phases, of which the last two are used while training the SOM. These three phases (described by Haykin [4]) are: the competitive process, the cooperative process and the adaptive process. The first and last steps are discussed below, and modifications to them are suggested in section 3.2.

3.1.1 Competitive process

The competitive process consists of

$$i(\vec{x}) = \arg\min_j \|\vec{x} - \vec{w}_j\|, \qquad j = 1, 2, \ldots l \tag{1}$$

where $\vec{x}$ is the training vector, $\vec{w}_j$ is the weight vector of neuron j and l is the number of neurons in the lattice.

3.1.2 Adaptive process

The standard learning rule is

$$\vec{w}_j(n+1) = \vec{w}_j(n) + \eta(n) h_{j,i}(n)(\vec{x} - \vec{w}_j(n)) \tag{2}$$

where n is the stimuli iteration, $\eta(n)$ is the time-dependent learning-rate parameter and $h_{j,i}(n)$ is the neighbourhood function, normally chosen as a Gaussian function that shrinks as time passes. This will make the neurons learn fast in the beginning, when the lattice is untrained; at the same time, the neurons closer to the best matching neuron will learn more compared to the rest. The winning neuron, i, will always have $h_{j,i}(n) \equiv 1$.

3.2 Structure of the neurons and the modified competitive process

The study is performed using the following set of features (sensor signals) for stimuli

$$[x_p,\, p_A,\, p_B] \tag{3}$$

i.e. piston position and the two chamber pressures. This set of features has been shown to perform better than the use of either of

$$[x_p, \dot{x}_p, p_A, p_B] \tag{4}$$

$$[p_A, p_B] \tag{5}$$

as has been reported in [5, 6].

The input vector, $\vec{x}$, (and thus also the feature vectors, $\vec{w}_j$) are composed of two parts: an independent part and a dependent part (similar divisions of the input vector can be found in [6–8]). The independent part, $\vec{x}^{ind}$, is formed according to (3). The dependent part, $\vec{x}^{dep}$, consists of two additional features, viz. the mass load, m, and a leak indicator, $leak$. Thus, as an example, (3) becomes

$$\vec{x} = [x_p,\, p_A,\, p_B,\, m,\, leak]^\mathsf{T} \tag{6}$$

Nonetheless, only the original features, (x_p, p_A, and p_B), are used for the competitive process (1). This will enhance the later use of the SOM to evaluate and categorise new measurements. The resulting notation, for the input vector, $\vec{x}$, and the modified competitive process, is as follows:

$$\vec{x} = \left[\vec{x}^{ind\,\mathsf{T}},\, \vec{x}^{dep\,\mathsf{T}}\right]^\mathsf{T} \tag{7}$$

$$i(\vec{x}) = \arg\min_j \|\vec{x}^{ind} - \vec{w}_j^{ind}\|, \qquad j = 1, 2, \ldots, l \tag{8}$$

In order to restrain one of the input dimensions from becoming too dominant, the actual values are scaled such that the normal values are within the interval $[0, 1]$ (outliers and extremes can still be outside this interval). A better scaling might be to translate the features used to build the input vector into a common mean, for instance 0 (with no loss of generality), and thereafter scale the features to a common variance.

4 CONDITION MONITORING

Condition monitoring can be performed using a vast number of methods and measures; the use of SOMs for condition monitoring also gives a large selection of both measures and methods. A broad classification of methods is achieved by looking at whether the primary focus of the method is to detect either previously known or unknown faults.

4.1 Detection of unknown faults/states

In the literature, [1, 3], it is often argued that the best measure to find unknown/new deviations from the normal state, assuming that the SOM is trained using data from only the normal state, is the quantisation error, q.e., which is defined as

$$\text{q.e.} = \|\vec{x}^{ind} - \vec{w}_i^{ind}\| \tag{9}$$

Thus, the q.e. is a measure of the deviation in the feature space and not a physical measure.

4.2 Classification based condition monitoring

That the SOM lends itself to categorisation is a consequence of the organisational property of the SOM algorithm, see [1]. The classification is performed by matching the test vector to the neurons in the lattice, eq. (1), and the class of the test vector is taken from the winning neuron. This, together with the topological ordering of the neurons done in the initial training process, makes the classification results suitable for visualisation (the winning neuron's position in the SOM lattice can easily be shown, see eg.[6, 8]). An example of classification based condition monitoring is [9].

In [6], the usefulness of the q.e. in classification based monitoring is discussed. One benefit of simultaneously using classification and q.e. is that unknown faults/states are handled. Table 1 summarises how the classification and the q.e. interact.

If the visualisation properties are not desired, nor the combined use of classification and q.e., better classification performances can normally be achieved by further training of the SOM through learning vector quantisation, LVQ, see [1, 10]. This will severely reduce the usefulness of the q.e.

Table 1: Combinations of q.e. and fault classification

	Low q.e.	High q.e.
Faulty state	Faulty state	New, resembles faulty
Normal state	Normal state	New, resembles normal

4.3 Accumulated training

To find a measure of the certainty of the knowledge stored in a neuron, the accumulated training, (10), can be used.

$$H_j(N) = \sum_{n=1}^{N} \eta(n) h_{j,i}(n) \tag{10}$$

where $\eta(n)$ is the learning rate as a function of the discrete sample time n, $h_{j,i}(n)$ is the neighbourhood function for neuron j given that i is the best matching neuron in (1). This is the sum of weight from (2) and could also be viewed as the amount of excitation received by the neuron. As $H_j(N)$ increases, the neuron accumulates more and more information and becomes more certain that the stored information is well founded.

A small amount of accumulated training in the winning neuron, H_i, indicates that the system is in an unknown state. This measure, $H_j(N)$, would be at least equally important,

if not more so, in a pure classification based monitoring system. As the position of the best matching neuron in those methods directly implies a fault mode / diagnosis, it is even more important to be sure of the certainty of the decision. Nonetheless, it is necessary to handle this certainty measure with great care, both because the border between low and high levels of excitation depends on the classification (position in the lattice) and the selection of $h_{j,i}(n)$ has some influence upon the accumulation. The latter is especially true in the case of an uneven distribution in the training data between the classes that the SOM should identify.

4.4 Combined classification and accumulated training

The interpretation of the fault mode classification can be further improved by looking at the accumulated training of the winning neuron. As stated in the previous section, a great amount of accumulated training corresponds to a large number of matches between this neuron and the training data. Together with a non-ambiguous classification this translates to a high degree of certainty in the conclusion drawn. A low value for the accumulated training would mean that this is a relatively rare situation, especially if classification is also ambiguous. This is summarised in table 2. Here great care is needed in the interpretation of the high / low levels, as these will depend on the decision area in the SOM lattice (at least when the SOM is trained using non-equal fractions of normal / faulty data).

Table 2: Conditions for Combinations of Fault Classification and Certainty

	Normal state	Faulty state
High excitation	Normal	Faulty
Low excitation	Ambiguous, resembling normal	Ambiguous, resembling faulty

4.5 Combined q.e. and accumulated training

Similar conclusions can be drawn for an unknown fault, in this case using the q.e. together with the accumulated training.

Although the quantisation error is deemed to be one of the best measures for fault detection, [3], (assuming the SOM is trained using only normal states), the interpretation of the results would be further improved by adding a confidence measure. An initial discussion of this combination can be found in [5].

A large q.e. together with a low certainty is a strong indication that something has happened to the system that deviates from its normal state, while a small q.e. and a high certainty mean that the system is operating as normal.

A small degree of certainty indicates that the condition is quite new, no matter what the q.e. is. However, a large q.e. together with a small certainty indicates not only that the system is in a new condition, but also that this condition is non-similar to the old and partially known conditions. A small q.e. would instead imply that although it is a quite new condition, we have probably seen similar ones before (at least we have a closely matching neuron). This is summarised in table 3.

Finally, the combination of a large q.e. and a well trained neuron indicates that the neuron (and the whole SOM) is over-trained, otherwise a neuron receiving a lot of excitation would have the neighbouring neurons' weight vectors closer to its own. Here, the experience of the engineer is needed to recognise what a large accumulated training of the neuron is, as *large* has to be defined in relation to the accumulated level in the rest of the neurons in the lattice, as well as the absolute value.

Table 3: Conditions for Combinations of q.e. and Certainty

	Low q.e.	High q.e.
High excitation	Normal	Over-trained
Low excitation	New, non-unique	New, unique

4.6 Additional use of the accumulated training

Although the main intention of introducing the accumulated training measure was to support the interpretation of the decision as delivered by the SOM, it is nevertheless possible to devise other uses. One possible use is to facilitate and support the alarm generation, as shown in section 4.6.2.

4.6.1 Relative accumulated training

The accumulated training (or excitation) received by each neuron in the SOM lattice during training is defined by (10). When looking at such a measure for the winning neuron of each sample during a working cycle, $H_i(N)$ will vary quite a lot during the cycle. One way to facilitate the handling of this is to look at a normalised accumulated training. One normalisation measure is the accumulated training assuming that the system was non-faulty. This is done by forcing the *leak*-component of the input vector to 0 (normal case), and then calculating the winning neuron, i^0, using the full vector in (11). The forced modified competitive process is as follows:

$$\vec{x}^{forced} = \left[\vec{x}^{ind\,\mathsf{T}},\, leak|_{\text{no leak}}\right]^{\mathsf{T}} \tag{11}$$

$$i^0(\vec{x}) = \arg\min_j \|\vec{x}^{forced} - \vec{w}_j^{forced}\|, \qquad j = 1,2,\ldots,l \tag{12}$$

Thus, using i^0, the following normalisation procedure is achieved:

$$\frac{H_i(N)}{H_i(N)|_{\text{no fault}}} = \frac{H_i(N)}{H_{i^0}(N)} \tag{13}$$

When the system is working in normal conditions, the accumulated training, $H_i(N)$, found while matching the test vector against the whole lattice, will be the same or close to $H_{i^0}(N)$, found while forcing the test vector to match a neuron representing the normal system state. Thus, the fraction will be 1 (or distributed close to 1).

On the other hand, when the system is working in a faulty state, H_i will average to be larger then H_{i^0}, derived using a forced non-faulty state. In this case, i^0 is found in the regions of the lattice that have a low level of accumulated excitation.

Although this fraction will still vary, faulty conditions will become more distinct using the normalised fraction as compared to using $H_i(N)$ directly. The larger the value of the fraction during the fault conditions, the clearer and more distinct the fault classification. A possible application of this is described in the next section.

4.6.2 Alarm generation using $H_i(N)$ and CUSUM

To use the accumulated training measure directly for condition monitoring and not only as an interpretation aid, change detection on the measure is needed (see the previous discussion on the varying $H_i(N)$). One classic algorithm is CUSUM, see eg. [11] for an in-depth description of this and other change detection algorithms.

A test variable, s_t, is created as

$$s_t = \ln \frac{H_i(N)}{H_{i^0}(N)} \tag{14}$$

This variable, s_t, will be distributed around zero in normal conditions and will be positive in faulty conditions. (An illustration showing that this works can be found in figure 6a in section 5.4).

The classical change detection algorithm, CUSUM (15), is applied to the variable s_t. The test statistic, g_t, is then derived as follows:

$$g_t = g_{t-1} + s_t - \nu \tag{15a}$$

$$g_t = 0, \text{ and } \hat{k} = t \text{ if } g_t < 0 \tag{15b}$$

$$g_t = 0, \text{ and } t_a = t \text{ and alarm if } g_t > h > 0 \tag{15c}$$

To prevent a negative drift, the test statistic is reset to 0 each time it becomes negative. A small drift term ν is used to prevent positive drift, that would otherwise yield a false alarm. Once the test statistic becomes greater then the threshold, h, an alarm is raised and the test statistic is reset; a fault will thus result in repeated alarms as long as it is strongly detectable using the test variable s_t. The two time variables, $\hat{k}$ and t_a, represent the estimated change time and the alarm time respectively.

5 RESULTS

The main results of the paper are the exemplification of tables 1 to 3, i.e. the use of combined measures to aid the interpretation, discussed in section 5.2.

5.1 SOM: training and test data

The SOM is trained using a set of training vectors that consists of 100 data sequences (95%) from the normal state (10 kg and no leak) and 5 sequences (5% of the total training set) from test runs with 10 kg mass load and leaking exhaust valves. Each sequence consists of 340 samples, resulting in a total training set of 35,700 training points. Only the features in (3) are used to find the winning neuron, i.e. the additional features m and *leak* are not used in the matching process. The same is true when calculating the q.e.

The SOM is trained by choosing a random training point for each training round. Then the algorithm in section 3.1 is used and the neurons are modified according to (2) (in the modification the full feature vector, (6), is used).

The test (validation) sequence used is a combination of the following test sequences: two new measurements of the normal case (10 kg mass load and no leak), one set with 10 kg and leaking exhaust valves, one set with 20 kg and no leak, and finally one set with 20 kg and leaking exhaust valves. These five sets are combined into one large sequence that isq used for test purposes in the rest of this section.

5.2 Known & unknown faults

The detection capabilities of this configuration of the SOM were primarily discussed in [5] for unknown faults and in [6] for both known and unknown faults.

5.2.1 Quantisation error and fault mode

An overview of the classifications and quantisation errors of the test sequences according to table 1 is shown in figure 3. Here is an easy to understand and interpret graphical representation of the 2-dimensional output from the SOM. The fault mode is represented by the leak indicator on the y-axis, with 0 indicating normal state and 1 leaking exhaust valves. It can be noted that the last set in the test sequence, the combination of both the known and unknown faults is correctly classified as having leakage in the exhaust valves.

The normal working state is clustered in the lower left corner, just as expected. Most of the samples from the faulty state test sequence are found in the upper left corner. However, a number of samples are located with a lower leak classification together with quite small values of the q.e. The reason that some values are classified close to the normal state neurons is that there are quite a few system states in which the state variables (x_p, p_A, and p_B) are almost the same, whether there is leakage or not. The relatively large q.e. that some of the correctly classified neurons shows is due to the low fraction of faulty data in the training set. A further discussion of the high q.e. of some of the samples from the leak conditions shows follows at the end of section 5.2.2. See also[6] for a more thorough discussion.

The similarity between the unknown fault, the added mass load, and the normal state can only be explained by the fact that the system response is close enough in these two cases. Although the system shows more oscillation, no completely new states are introduced, only variations on the already known states. The same is true for the two cases with leakage.

5.2.2 Addition of the accumulated training

A practical example of how illustrations of the tables 2 and 3 might look for real measured data is shown in figure 4. The topmost figures ((a) and (b)) correspond to table 2 and figures (c) to (f) to table 3. An important point to make concerning these figures is that the y-axis shows a normalised excitation level. The excitation level is normalised with the mean excitation level during a working cycle in normal conditions. Thus, the normalised value is expected to be around 1. Hence, no data points in figure 4 represent really new states; the data points that have the lowest normalised excitation level are the points from

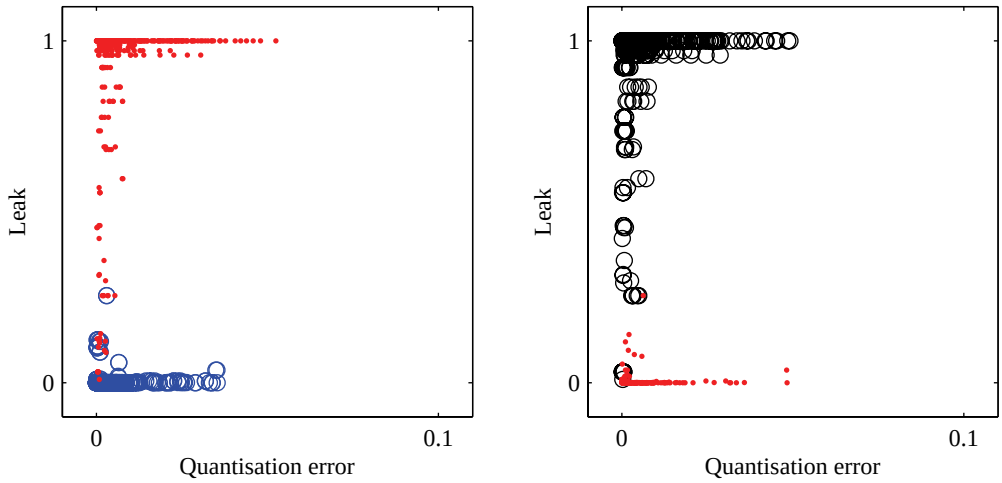

(a) Normal state is shown with circles and the combined fault mode (leakage + added mass) with dots.

(b) Leaking exhaust valves, shown with circles, and the added mass load, shown with dots.

Figure 3: A view of the q.e. versus the fault classification (leak). On the y-axis the leak indicator is shown, with 0 and 1 representing the normal state and leaking exhaust valves, as found in the training data. The same scales are used in both graphs.

the leaking fault mode that fall between the clearly identified fault mode and the normal case.

When comparing the normalised excitation levels, the case of the additional mass load seems to be not too unlike the normal state, which is not that surprising, as it only introduces a more oscillatory behaviour to the system. Just as the combined fault resembles the pure leaking exhaust valves case.

The test case with leaking exhaust valves shows heavy densities of neurons with a high leak coefficient and low to relatively large quantisation errors (figures 4b and 4f respectively). However, as was discussed in [6], there is some dips in the leak coefficient and some peaks in the quantisation error. The spikes in the q.e. are easily attributed to the small portion (5%) of the training set coming from the faulty state, and the dips in the classification to the amount of similarity between the faulty and normal states during certain conditions in the working cycle.

5.3 Mean distance and q.e.

The mean and variance of the q.e., see table 4, still makes it possible to draw conclusions about whether the input conditions are expected to be new or not. However, it is important to know what q.e. to expect in the different regions of the lattice; the mean distance between neurons in the lattice is therefore of great interest. In figure 5, two graphical representations of the mean distance between neighbouring neurons are shown. The area with low x-coordinates primarily denotes the leaking exhaust valves case (especially the border). This is also the area with the largest mean distance. This is to be expected, as a relatively small number of neurons are to model the whole cycle for this case, due to the drastic difference in available training data from the non-faulty and faulty cases.

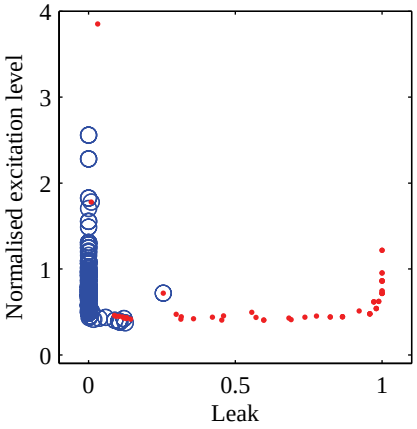

(a) The leak indicator (fault mode) versus the excitation level for the normal case (circles) and the combined case of leaking exhaust valves and additional mass load (dots).

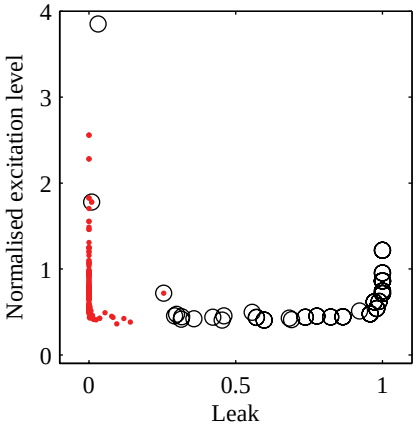

(b) The leak indicator (fault mode) versus the excitation level for the case of leaking exhaust valves (circles) and the added mass load (dots).

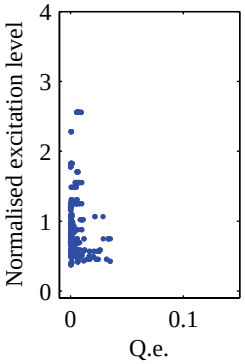

(c) The quantisation error versus the excitation level for the normal case.

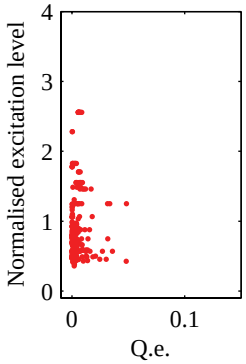

(d) The quantisation error versus the excitation level for the case of the added mass load.

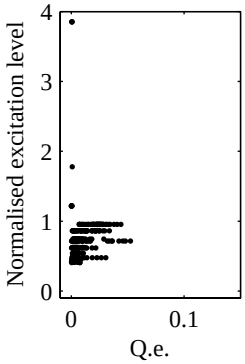

(e) The quantisation error versus the excitation level for the case of leaking exhaust valves.

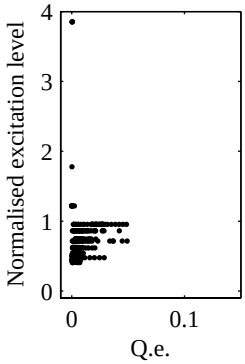

(f) The quantisation error versus the excitation level for the case of both leaking exhaust valves and added mass load.

Figure 4: A view of the interpretation support tables 2 (in (a) and (b)) and 3 in (c) to (f), respectively. The excitation values are normalised with the mean excitation of the winning neurons in the normal working cycle. A normalised excitation level around 1 is therefore to be expected.

Table 4: Mean and variance of the quantisation error.

Test case	Mean q.e.	Variance q.e. $\left(10^{-5}\right)$
Normal state	0.00330	3.43
Leakage	0.00786	9.41
Additional mass	0.00371	4.20
Add. mass + leak	0.00860	10.2

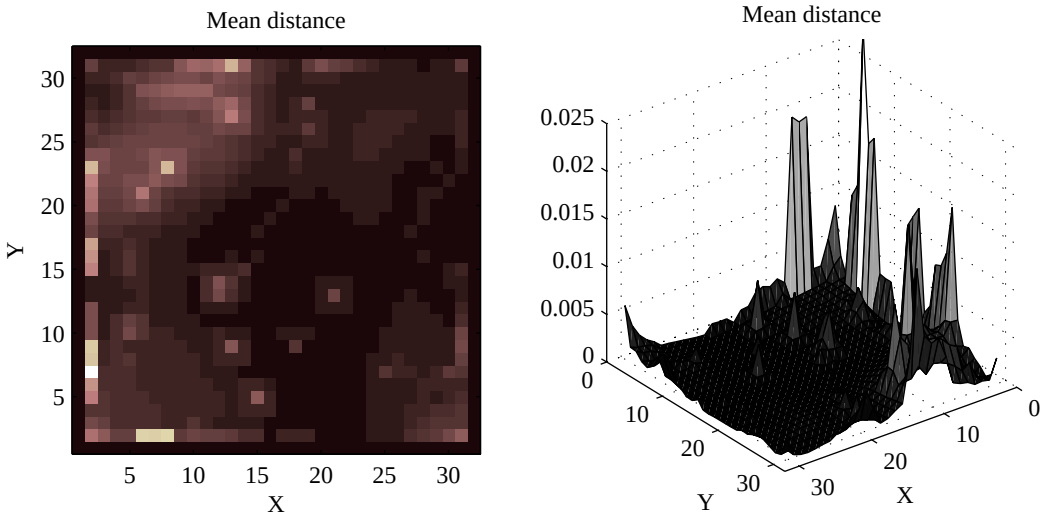

(a) A graph of the mean distance. Darker colours mean a shorter distance.

(b) A 3-d graph of the mean distance.

Figure 5: The mean distance in feature space between neighbouring neurons. As can be seen, over a large part of the lattice, the mean distance is uniform. A larger mean distance is primarily found in the left area of the lattice, which also happens to correspond to the leaking exhaust valves.

5.4 Relative accumulated training and CUSUM

In figure 6 some results from using a test variable based on (14) are shown. Figure 6a shows a running total of (14), while figures 6b and 6c show the test statistic, g_t, in (15) with 10 and 5 respectively, as the threshold parameter, h. The drift parameter $\nu = 0$ in all cases. In these two latter graphs, the alarms raised are also shown, using vertical dash-dotted lines. In both cases, and especially in the last case, the alarms are generated quite soon after the entering the test sequence from the known fault. At the same time, the test statistic, g_t, is quite stable otherwise. An even smaller alarm threshold could therefore easily be used without too many false alarms generated.

6 DISCUSSION

The usefulness of SOMs for condition monitoring has previously been shown in several works, see for instance[1, 3, 5] for a few examples.

All condition monitoring technique requires knowledge and preferably some confidence measure in order to correctly interpret the result. Monitoring techniques using the self-organising map, have often been discussed and used without such a measure. Here, one such measure, the accumulated training,is discussed together with how the interpretations are influenced. The use of the accumulated training as an interpretation aid still requires a knowledgeable operator. Some of the judgement that is needed concerns what amount of excitation is normal and what constitutes a new condition. Nonetheless, it is a measure that provides additional information.

Over-training is always a question when working with neural networks. What would happen in this case is that the average amount of accumulated training during the normal

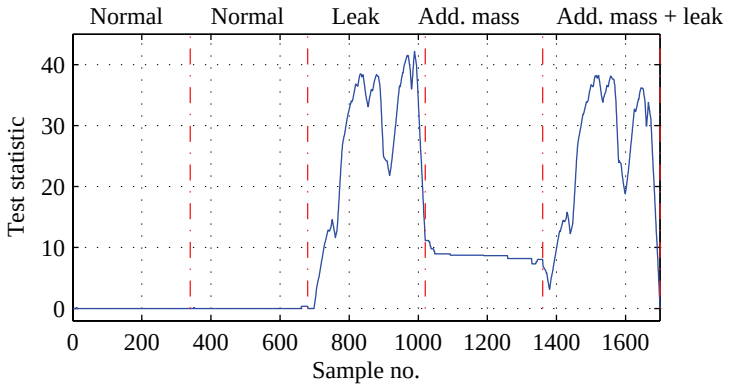

(a) The test statistic used in the CUSUM test. In this figure, the vertical dash-dotted bars show the border between the test sequences (see section 5.1).

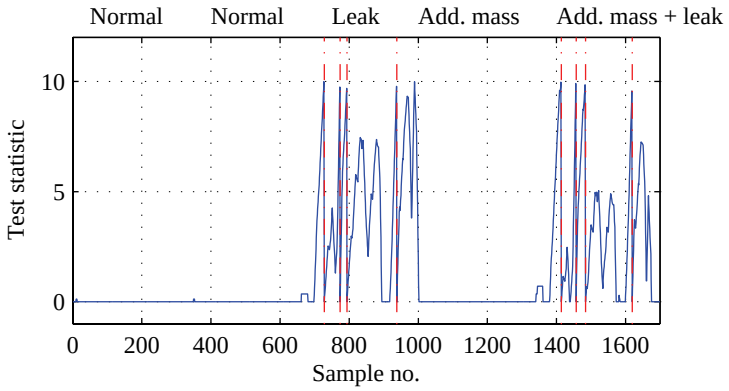

(b) The test statistic used in the CUSUM test and the alarms generated (vertical dash-dotted lines) by a threshold of 10.

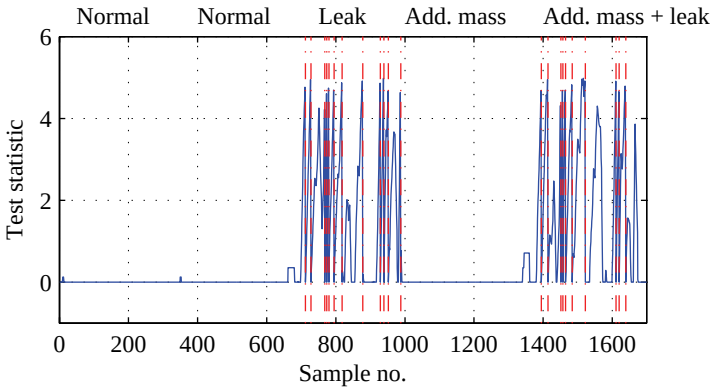

(c) The test statistic used in the CUSUM test and the alarms generated (vertical dash-dotted lines) by a threshold of 5.

Figure 6: The CUSUM test statistic and alarm generation based on the accumulated training measure.

working cycle would be inflated, possibly severely. This would in the long run move the $H_i(N)$ for the normal state further away from the $H_i(N)$ of the faulty state, thus making it seem like all faulty conditions are unknown, at least to the uninitiated eye. However, the difference between normal state and new unknown conditions are quite likely to increase. A normally over-trained SOM could thus actually be advantageous for us when trying to detect unknown faults using a SOM trained to categorise certain faults.

A somewhat simpler interpretation support is found when simultaneously studying the quantisation error and the fault classification as suggested in section 4.2 and with experimental results in 5.2.1. Here it is of the uttermost importance to know what q.e. is to be expected within certain regions of the lattice. In one region a certain q.e. might indicate a new condition, while in another it would be a good match. It is still necessary to note that individual sample could still be misclassified, and therefore it is necessary to look at a number of consecutive samples in order to be able to draw any conclusions with any certainty.

To further facilitate the diagnosis and to more distinctively find the unknown fault, it would be beneficial to add further diversification to the neurons, possibly in the form of the position/time coordinate in the work cycle or to include previous samples in the neurons' weight vector.

The decision to use only 5% training data from the faulty case was made to simulate a real system that has gained its training data from normal operations. Thus, only a small portion of faulty data exists. Obviously, this is not the ultimate situation; it would have been preferable to use equal amounts of faulty and non-faulty data. One way is to have several SOMs; one trained only on normal data to detect deviations and another used for the categorisation the detected deviation/fault.

7 CONCLUSION

Self-organised maps used as a technique for condition monitoring of pneumatic systems were investigated using a pneumatic cylinder as the experimental test bench. One of the main differences between this work and several others using SOMs for condition monitoring is that specific features are often identified and fed to the SOM, while the measurements here are directly and continuously fed to the SOM.

The properties of the SOM that allow identification of known faults and detection of unknown faults/disturbances are also discussed and exemplified. The SOM trained to detect leaking valves also proved to be capable of detecting a changed mass load.

Possible ways to improve the straightforward interpretation of the outcome of the SOM are discussed. As a result, it is argued that the outcome of a condition monitoring system is at least 2-dimensional (decision and excitation measure); three dimensions were used in this work (decision, q.e., and excitation measure). The interpretation support is exemplified using 2-dimensional plots of the outcome.

A discussion of how a kind of confidence measure, accumulated training, can influence the interpretation of the classification decision. Although the result shown using accumulated training as a confidence measure might give the impression that it is not useful, it still provides additional insights. Especially in the case where the SOM is trained to diagnose certain faults, to interpret the meaning of $H_i(N)$ it is necessary to understand how the SOM lattice is structured, e.g. where in the lattice the winning neuron is located and how the mean distances in the lattice are distributed (figure 5). However, the accumulated

training as a confidence measure either needs to be further developed or an alternative confidence measure developed, to allow an easier interpretation for the non-specialist.

REFERENCES

[1] T Kohonen. *Self-Organizing Maps*, volume 30 of *Springer Series in Information Sciences*. Springer-Verlag Berlin Heidelberg New York, 3rd edition, 2001.

[2] T Kohonen. The self-organizing map. *Proceedings of the IEEE*, 78(9):1464–80, September 1990.

[3] M Kasslin, J Kangas, and O Simula. Process state monitoring using self-organizing maps. In I Aleksander and J Taylor, editors, *Artificial Neural Networks 2: Proceedings of the 1992 International Conference (ICANN-92)*, volume 2, pages 1531–4, Brighton, UK, September 1992. Elsevier, Amsterdam, Netherlands.

[4] S Haykin. *Neural Networks: A Comprehensive Foundation (2nd. ed.)*. Prentice Hall, Upper Saddle River, NJ, 1999.

[5] A Zachrison and M Sethson. Detection of system changes for a pneumatic cylinder using self-organizing maps. In *Proc. of 2006 IEEE International Symposium on Computer-Aided Control Systems Design*, pages 2647–52, Munich, Germany, October 2006. IEEE. DOI: 10.1109/CACSD.2006.285524.

[6] A Zachrison and M Sethson. Self-organising maps for monitoring pneumatic systems. In D N Jonhnston and K A Edge, editors, *Power Transmission and Motion Control 2006*, Power Transmission and Motion Control, pages 181–94. University of Bath, Hadleys Ltd, September 2006.

[7] Frank Schütte, Stefan Beineke, Horst Grotstollen, Ulf Witkowski, Ulrich Rückert, and Stefan Rüping. Structure- and parameter identification for a two-mass-system with backlash and friction using a self-organizing map. In *7th European Conference on Power Electronics and Applications, EPE97*, volume 3, pages 3358–3363, Trondheim, Norway, 8 - 10 September 1997.

[8] A Zachrison and M Sethson. Self-organising maps for illustration of friction in a pneumatic cylinder. In *The Ninth Scandinavian International Conference on Fluid Power, SICFP'05*, Linköping, Sweden, June 2005. Linköpings universitet.

[9] V E Lumme. Distributed knowledge in automated remote monitoring. In O P Shrivastav, B Al-Najjar, and R B K N Rao, editors, *Proceedings of COMADEM-2003*, pages 209–18, Växjö, Sweden, August 2003.

[10] H Marzi. Real-time fault detection and isolation in industrial machines using learning vector quantization. *Proceedings of the Institution of Mechanical Engineers, Part B: Journal of Engineering Manufacture*, 218(8):949–59, 2004. ISSN 0954-4054. DOI: 10.1243/0954405041486109.

[11] F Gustafsson. *Adaptive filtering and change detection*. John Wiley & Sons, Ltd, 2000.

THE CONDITION MONITORING OF HYDRAULIC HOSES

[1]Lauri Elo, [1]Esa Mäkinen and [2]Matti Vilenius
Tampere University of Technology
[1]Institute of Hydraulics and Automation (IHA) - Rauma Research Unit[1]
P.O.Box 236
FIN-26101 Rauma, Finland
Fax +358 2 823 4974

[2]Institute of Hydraulics and Automation (IHA)
P.O.Box 589,
FIN-3301 Tampere, Finland

E-mail: lauri.elo@tut.fi

ABSTRACT

Hydraulic hoses are widely used in industrial applications. In many cases hydraulic hoses are the most critical components of hydraulic systems, and they play an important role in reliable operations in industrial processes. Damage of hydraulic hoses can cause large economic losses and, furthermore, danger to the environment.

So far, not enough attention has been paid to the condition monitoring of hydraulic hoses, and the replacement of hoses is mainly based on the calendar, not on the real condition of the hoses. Recent development in sensor and information technology has raised up new possibilities for monitoring tasks. The main goal is the life-cycle determination of hydraulic hoses, so that the replacement can be done just in time, in order to quarantee reliable, safe and economical operation of the hydraulic system.

The purpose of this paper is to present and discuss the on-line continuous condition monitoring methods of hydraulic hoses. The paper first presents a survey of the properties and requirements set for hydraulic hoses, as well as their most common malfunctions. Then the most common fault mechanisms of hydraulic hoses and requirements set to the storage and use of hoses are given. Finally the possibilities for continuous on-line measurements and the most potential properties of hydraulic hoses for condition monitoring are presented and appraised.

KEYWORDS: Hydraulic system, hydraulic hose, condition monitoring, rfid

1 INTRODUCTION

Hydraulic pipes are widely used in industrial applications in hydrostatic transmission systems. However, there is sometimes a need to use hydraulic hoses because they have a flexible structure, giving them some superior properties: they are easy to install, they allow relative movement between the machine parts, they damp vibrations and noise, and reduce the effective bulk modulus and pressure shocks. In many cases hydraulic hoses are the most critical components of hydraulic systems and they play an important role in reliable operations in industrial process.

So far, not enough attention has been paid to the condition monitoring of hydraulic hoses in industry, and this is mainly due to two reasons. First, the direct investment costs of hydraulic hoses are low, and secondly it has been difficult to realize the monitoring in practice. Nowadays, the replacement of hoses is mainly based on the scheduled maintenance, not on the real condition of the hoses. This causes two types of problems. First, too early replacement of hydraulic hoses increases operational costs as well as risks related to the new components and assembly work. Secondly, replacing hydraulic hoses too late increases the risk of failure, which can always cause great personal and material damages.

However, recent development in sensor and information technology has raised up new possibilities for the monitoring tasks. This study is part of a research project in which a prototype of an intelligent hose (IHO) will be developed. The aim of the IHO-project is to realize the monitoring tasks by integrating new sensor- and rfid-technology into hydraulic hoses. The main goal is the life-cycle determination of hydraulic hoses so that the replacement can be done just in time, in order to quarantee reliable, safe and economical operation of the hydraulic system.

In this paper on-line continuous condition monitoring methods of hydraulic hoses are presented and discussed. First a survey of the properties, requirements and most common malfunctions are presented. The survey is based on standards, manufacturer information, and a report done for the IHO-project on common practices and experience of using of hydraulic hoses in a paper mill. Finally the possibilities for continuous on-line measurements and the most potential properties of hydraulic hoses for condition monitoring are presented and appraised.

2 REQUIREMENTS SET FOR HYDRAULIC HOSES

The following section will deal with the demands set on hydraulic hoses, so that the usability and reliability would be as good as possible. Hydraulic hoses comprise three main parts, namely an inner tube, texture reinforcement, and surface material.

The innermost layer is an inner tube, the material of which is usually neoprene rubber, nitrile rubber, thermo plastic material or Teflon. The task of the layer is to keep the fluid to transferable inside the hose.

The following layer from within is texture reinforcement, the material of which is steel thread, synthetic fibre or cotton. There can be one or more layers of texture

reinforcement on top of each other, and it is woven either as a cross-texture or as a spiral texture. The weaving direction of the texture will have a significant effect on the behaviour of the hydraulic hose when the hose is pressurised. Depending on the direction the texture, the hose can either lengthen or shorten due to the effect of pressurisation. The outside diameter of the hose change correspondingly, depending on the direction of the texture. The task of the texture reinforcement is to give the hose the necessary pressure resistance. [1, 2]

The topmost layer is a surface material which sometimes is made from synthetic neoprene rubber, from a thermo plastic material, or in special hoses from a steel texture. The task of the surface material is to protect the texture structure from external stress.

The requirements of hydraulic hoses have been recorded in different hose standards. According to the standard EN ISO 1402 (International Organization for Standardization), the pressure resistance of hydraulic hose must be at least four times bigger than the allowed working pressure. In addition to this, the hose must not contain any leaks before the burst pressure. Also, a test has been determined for the duration of the hose bend. It is determined on the basis of its smallest bend radius. The hose must pass the test without leaks and fractures at -40 °C. In addition to this, demands have been set wear resistance, oil permanence and ozone permanence. [3]

The required operating life for the hydraulic hose has been defined in the SAE standard of hydraulic hoses according to the pressure impulses. One-fiber-braid reinforced hydraulic hose must tolerate at least 150 000 impulses at an overpressure of 25 % in comparison to its ordinary operation pressure. Two-fiber-braid of reinforced hydraulic hose must tolerate at least 200 000 impulses at an overpressure of 33 % in comparison to the normal operating pressure. In this standard, the significant factor is not the age but the pressure tests that have been performed in the laboratory. According to the German DIN 20066:2002 (Deutsches Institut für Normung) standard, the operating life of hydraulic hose is only dependent on the calendar time. The longest operating life of a hose arrangement is six years which may include a period of storage which may not last more than two years. A hose arrangement must not be made from a hose of which the manufacturing day is more than four years. According to this standard the longest operating life possible, since the manufacturing day of the hose, would be ten years. According to a draft version of ISO/TR 17165-2 standards on the products, the operating life of hydraulic hose can be directly determined according to the manufacturing date. Thus the operational time should not exceed 40 quarters of a year, in other words altogether 10 years. However, there is a demand that the hose is stored according to the ISO 2230 standard. [2, 4, 5]

2.1 Demands of standard ISO 2230 for the storage of hydraulic hoses

The hoses have to be stored in a dry and cool warehouse. It is said about the temperature that normal room temperature is suitable, but there is no drawback from colder temperature either. In addition to this, the air of the warehouse should be filtered as well as possible from extra particles.

The hoses have to be protected against direct sunlight, in which case the warehouse should be as dark as possible. Near the hoses there may be no big electric power

supplies or strong magnetic fields. One should also avoid corrosive chemicals, ultraviolet radiation, radioactive radiation and noxious animals. [2, 4]

3 MALFUNCTION MECHANISMS OF THE HYDRAULIC HOSE

The malfunction mechanisms of the hydraulic hose can be divided into three different groups: malfunction caused by external load, malfunction caused by internal pressure, and malfunction caused by internal medium, as shown in Table 1.

Table 1. The malfunction mechanisms of the hydraulic hose

Reason	Failure
The external load	• Chafing of the cover • Corrosion of fiber braids of the reinforcement • Ozone • Buckling of the hose • Clogging of the hose
The internal pressure	• Split time of the hose • Fitting getting loose • Clogging of the fitting
The internal material	• Splitting of the inner tube at high oil temperature • Small holes in the hose

The following section deal with a few malfunction mechanisms which have been found to be problematic. They are dealt with on the basis of the above chart.

The chafing of the outer surface of the hose has mainly resulted from the fact that the hose has been able to move in the adhesions, or the hose has chafed against other hoses. Similar damage is also created when the hose chafes against a sharp corner or support. In the operating situations in which the hose must be able to move over a wide area, the chafing of the hose can be reduced by installing a hose protective sleeve (Figure 1).

Figure 1. Protection sleeve of the hose [1]

If the bend radius set for the hose has not been considered, the hose can buckle and consequently clog. Also, the hose may have been under compression, thus resulting in clogging. Such malfunctions have particularly appeared in repair situations and in situations subsequent to stoppages. [2]

In several studies fittings becoming loose have also been a problem. The reason for the fitting becoming loose can be the wrong compression measure of the connector which, in turn, can be caused by too small or too big a compression. The fact that the sleeve and the fitting must be compatible has also been found to be a problem. The sleeves and fittings of different manufacturers are not always compatible even though they are almost similar. One reason for the loosening of a fitting can be that the hose has been too short to its target in question or the direction of the connective tissue of the hose in relation to the target in question has been wrong. The optimal value of the strand corner of the connective tissue been presented as follows. [6]

$$\tan\alpha = \sqrt{2} \Rightarrow \alpha \approx 54{,}7° \quad (1)$$

In this case the dimensions of the hose do not change when pressure is conducted to the hose. When angle α is being smaller than the nominal angle, the hose shortens and the diameter increases. When the strand angle is over the nominal value, the opposite happens.

4 ON-LINE MEASUREMENTS OF HYDRAULIC SYSTEMS

There are many different quantities that can be measured from hydraulic systems. It is quite common to use on-line measurements to control the condition of hydraulic systems, but, so far, not much attention has been paid on the condition control of hydraulic hoses. However, many hydraulic hoses are very critical components from the malfunction point of view. The malfunction of one hydraulic hose can stop an important

process in a paper mill. Therefore there would be a need to invest more on the condition monitoring of hydraulic hoses in operation than is at done the moment. Temperature, pressure, acceleration and the bend of the hose are the most important features to be measured when we consider the condition monitoring of hydraulic hoses. In addition to these quantities we also need reliable information about the manufacturing date of the hose material, about the manufacturing date of the arrangement, as well as the installation day of the hose.

It is perhaps the easiest to measure the temperature of the hose. The measuring can be done from the surface of the hose with a thermo pair. The measuring accuracy of the temperature does not need to be very exact, and the measuring frequency does not have to be high. However, the sensor requires memory in to which the necessary data can be recorded.

There are several methods to take pressure measurements. In this paper utilization of strain-gages are studied for continuous pressure measurements. The strain-gage can be used to measure the pressure level and the pressure shocks by fastening the strain-gage around the hose. After this the pressure information can be determined about the change in the resistance of the strain-gage. It is not possible to measure static pressure with an acceleration sensor, but it is suitable for the definition of pressure shocks. A accelerations can also be measured with a piezoelectric sensor. In that case the sensor itself will not need a voltage supply, but when a piezoelectric crystal is mechanically loaded by the action of the acceleration power, the crystal will give birth to the electric charge. However, the measurement of pressure shocks and of accelerations requires a counter circle to the sensor in addition to the amplifier.

5 MOST POTENTIAL PROPERTIES OF HYDRAULIC HOSES TO BE USED FOR CONDITION MONITORING

In this section the most potential properties of hydraulic hoses are discussed and their suitability for on-line measurements are appraised. Later, the use of these properties for on-line monitoring purposes will be tested both in a laboratory and in industrial environment.

It is not necessary to measure some properties, like the age of the hose, if this information is already stored on to a database. The use of The Radio Frequency Identification (rfid) technique could be utilized to have this information available continuously and on-line.

This section presents the most potential properties of hydraulic hoses which could be suitable for on-line measurements.

5.1 Utilization of rfid technique for condition monitoring of hydraulic hoses

The previous section presented the requirements set by the standards for hydraulic hoses and results of the report were given on the common practice and experience of using hydraulic hoses in a paper mill. It emphasized that the operating life of the hydraulic

hose is based on the scheduled maintenance. For this reason the manufacturing date, storage history and the use history of the hydraulic hose should be very clear. The report on the hydraulic hoses in a paper mill showed that detailed information of hydraulic hoses is not stored in databases. It is difficult or almost impossible to obtain individual information related to the hydraulics if data is stored on separate databases. The Radio Frequency Identification (rfid) technique could be utilized to clarify the data. Rfid means the identification of parts with the help of radio frequencies. The most general frequencies that have been used are high frequency (hf) and ultra high frequency (uhf). The advantages of uhf are reading distance and speed. The reading distance can vary between 0 and 5 meters. With hf one can reach the maximum distances of half a meter. The rfid-system is composed of an identifier tag, from a reader and a control system. The identifier tag consists correspondingly of an aerial and of a microchip. Figure 2 shows examples of identifier tags. [7, 8]

Figure 2. Different dipole-type UHF tags [7]

The identifier tags can be divided into three different classes. A passive tag does not contain a power supply but the necessary power is obtained from the rf-signal of the reading device. The rf-signal induces an electric current on the tag aerial. A half-active tag has its own power supply which it uses for the functions of the microchip. An active tag in turn uses its own power supply also for the communication. The advantage of the active tag that it allows longer reading distances, and it is possible to record sensor information in to the tag's memory. The weakness of the half active and active tags is that the service life of their battery is limited. The tag which is integrated into the hydraulic hose must serve 6 to 10 years. Instead of a battery, some other existing energy sources, such as pressure and vibration, can be utilized as a power source for the tag. By installing a passive rfid in the hydraulic hose, the hydraulic hoses can be identified from a distance. The id of this hose can be automatically used to pick up the information from the database concerning the hose in question. [7, 8]

The following information can be recorded in the database about the hydraulic hose:

- Technical information of the hydraulic hose including its length and manufacturing date

- Completion time of the arrangement
- Installation time of the hose
- Performance time of the pressure test
- Information about the location of the hose
- Fluid type to be used
- Sensor information to be obtained from condition database

Furthermore, it could be possible to obtain out the recorded information about the operating temperature of oil, the pressure levels and pressure shocks from a general condition database. When using an active rfid-tag, we can directly install a sensor to the hose, the sensor giving the history data of the hose.

5.2 Utilising a strain-gage in the condition monitoring of the hydraulic hose

The previous section dealt with the use of the strain-gage in measuring the pressure of a hydraulic hose and in measuring pressure shocks. Figure 3 shows the change of resistance of different stretch slips as the function of length change.

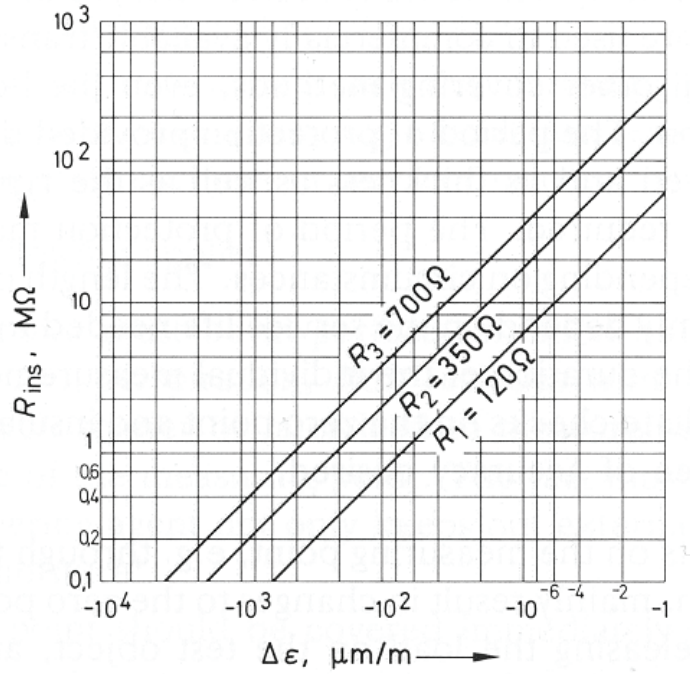

Figure 3. Diagram for determination of the insulation resistance of a strain-gage application. [9]

From Figure 3 one can calculate that on the distance of 120 ohms the change area of the length is 0,1 to 10^{-4} % of the total length. In Figure 4 shows the changes in the diameter and the length of the high pressure hydraulic hose in the laboratory as the function of pressure. The target of the examined hydraulic hose was: “Forester -8 1/2" DN 12 WP 360 bar SHA IC 126/8”. The feed pressure needed in the measuring of Figure 4 was produced with a hand-operated hydraulic pump. The change in the length of the hose was measured with the help of the caliper square. The change in the length of the hose was measured from an unpressurized hose from a 95 mm length. The changes in the

hose diameter were measured with a micrometer screw. The original diameter of the unpressurized hose was about 23 mm.

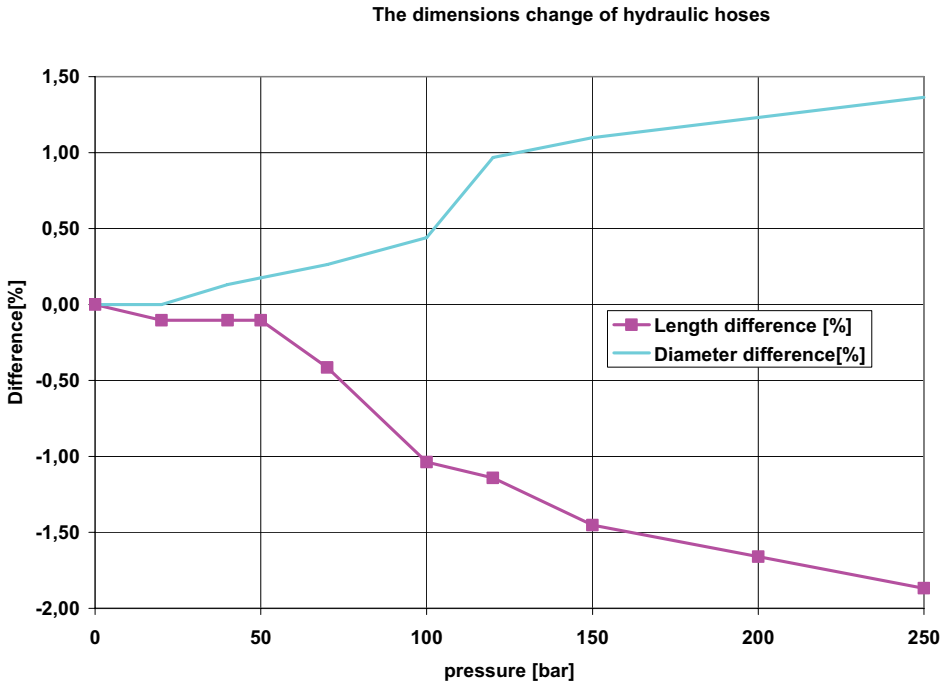

Figure 4. The dimension changes of hydraulic hose.

Figure 4 shows that the change in the diameter of the hydraulic hose is about 1,5 % at its height. Therefore the strain-gage cannot be installed directly to the surface of the hose, because the measured area of the strain-gage is essentially smaller than the necessary distance. The measuring of pressure could be carried out so that a metal collar could be installed around the hose, onto which strain-gage would be fixed.

6 CONCLUSIONS

Great demands are set for the hydraulic hose. The inner tube of the hydraulic hose must tolerate mechanical and chemical stress of many kinds of fluids. The hose must bear high pressure levels, pressure shocks and mechanical stress. The surface material of the hydraulic hose must tolerate external mechanical stress, the effect of chemicals and the effect of sunlight. Furthermore the hydraulic hose must meet all these demands also at large temperature ranges. Even more demands are set on the hose because, according to the new standards, the service life of the hydraulic hose can be, at its best, as long as 10 years. This longest service life can be reached only if the storage of the hydraulic hose has also been done according to the required instructions.

Attention has not yet been paid to the operation-time condition monitoring of hydraulic hoses even though hydraulic hoses may be very critical components indeed, especially from the point of view of the operation of the whole system. It would be possible to monitor the condition of the hydraulic hose by measuring the temperature, the pressure level of the hose, and its accelerations.

This paper has dealt with rfid-technique which can be used in condition monitoring of the hydraulic hose. In the near future the prototype of the intelligent hose will be made, and on to it will be integrated the rfid-tags, pressure sensor and temperature detector. This prototype of the intelligent hose will be tested in a laboratory environment.

7 REFERENCES

[1] Volanen J., 2006. Letkut ja asennus. Fluid Forum 2006, Scancic Tampere 22-23.3.2006. Tampere. 23 p. (in finnish)

[2] Anon. Hose, Fittings and Equipment. Catalogue 4400/UK, 2005. Parker Hannifin UK Ltd. 488 p.

[3] EN ISO 1402. Rubber and plastics hoses and hose assemblies -- Hydrostatic testing. 1994. 5 p.

[4] ISO 2230. Rubber products -- Guidelines for storage. 2002. 11 p.

[5] ISO/TR 17165-2. Hydraulic fluid power -- Hose assemblies -- Part 2: Recommended practices for hydraulic hose assemblies. 2006. 20 p.

[6] Kiviniemi A., Reliability of Hydraulic Hoses. Master of Science Thesis, November 2000, 80 p., (in finnish)

[7] Sydänheimo, L., Studies towards advanced mobile systems in industrial applications. Ph.D. thesis, Tampere 2005, Tampere University of Technology. 68 p.

[8] Ukkonen, L., Development of passive UHF RFID tag antennas for challenging objects and environments. Ph.D. thesis, Tampere 2006, Tampere University of Technology. 112 p.

[9] Hoffmann, K. An Introduction to Measurements using Strain Gages. Darmstadt 1989, Hottinger Baldwin Messtechnik GmbH. 291 p.

Compensation of Variable System Dynamics to Enhance Condition Monitoring for Hydraulic Pumps

Dr.-Ing. Christian Stammen
RWTH Aachen University
Institute of Fluid Power Drives & Controls
Steinbachstr. 53 B
52074 Aachen, Germany
Phone +49 241 8027533, Fax +49 241 8022194
E-mail: christian.stammen@ifas.rwth-aachen.de

ABSTRACT

The paper presents the influences of different hydraulic systems on dynamic pressure signals on an axial piston pump. Due to these influences, pump condition monitoring for a certain application by means of pressure pulsation measurement is not easily applicable to other cases. Focus of the work is the development of a compensation method for variable system dynamics to ease the application of condition monitoring for pumps. The experimental verification was taken out for a variety of operating points. As an outlook, the application of the method on mechanical vibration signal is proposed.

KEYWORDS: Condition Monitoring, axial piston pumps, transfer function, FFT, compensation, system dynamics, fault detection

1 INTRODUCTION

Since the late 80s, a variety of fault diagnosis and condition monitoring methods for hydraulic pumps and motors were developed. Most of the work on Condition Monitoring for hydraulic pumps based on dynamic measurement of pressure or mechanical vibration and a transformation of the signals in the frequency domain. The correlation between changes in frequency peaks and the condition of the displacement unit is done by means of signal based methods, neural networks or expert systems [1] [2] [3] [4]. There are good results under controlled conditions or on laboratory test benches, but significant difficulties occur when the prepared algorithms have to be used for different pumps or for the same pump with a different hydraulic circuit connected to it. The different system dynamics of the connected hydraulic circuit lead to a different shape of the pressure signals. Hence it is important to compensate the influences of the hydraulic system connected to the displacement unit in order to ease the application of frequency-based Condition-Monitoring. This need for "easy to use"-algorithms suitable for a variety of applications with little additional effort already brought out the main points in research on Condition Monitoring for hydraulic linear drives and pneumatic applications [5] [6].

A simulation model of an axial piston pump [7] connected to a variable hydraulic circuit was used to study the influence of system changes on the pressure signals. To generate data for fault diagnosis tests, changes in the pump model simulate different faults. Comparing the frequency spectrum of the pressure signals, differences between a pump in original condition and a faulty pump were examined. Additionally, the frequency spectrum and the effect of system changes depend on pressure level and volume flow.
A new method to compensate the negative effects of variable system dynamics on condition monitoring for hydraulic pumps is proposed [8]. The simulated pressure signals are used during the development of the algorithms. The simple calculations cause low computational effort.
To verify the compensation algorithm, a test rig, allowing for the preset of rotational speed and load pressure and thus simulating a broad variety of conditions, is used. A system of pipes and ball valves simulates different pipe length. The axial piston pump is connected to this system via a hose, a proportional valve imposes various load pressure values.
It can be concluded, that the effect of different hydraulic systems showing off in the frequency spectrum of a pressure signal can be compensated. A Condition Monitoring System which has been set up for a pump in a certain hydraulic is still applicable when the pump is used in any other application. In effect, effort and cost for the application of Condition Monitoring decrease significantly.

2 FLOW AND PRESSURE PULSATION IN AXIAL PISTON PUMPS

The kinematic flow rate of an axial piston pump can be computed from displacement volume and rotational speed [9]. The instantaneous flow rate of a displacement machine is affected by flow pulsation due to the limited number z of displacement chambers. The flow from a single piston is discontinuous, hence the total flow rate of the pump Q as a summation of the piston flows oscillates between a minimum flow rate Q_{min} and a maximum flow rate Q_{max}. **Figure 1** depicts the flow rate of an axial piston pump for a pump with 5 pistons. The pressure buildup in the displacement chambers and the pressure losses at the control plate are neglected. For an odd number z of pistons, the non-uniformity grade of flow δ_Q defined as the quotient of the flow ripple $Q_{max} - Q_{min}$ and the minimum of flow Q_{min} is:

$$\delta_Q = \frac{Q_{max} - Q_{min}}{Q_{min}} = \frac{\pi}{2 \cdot z} \cdot \tan \frac{\pi}{4 \cdot z} \qquad \text{(Eq.1)}$$

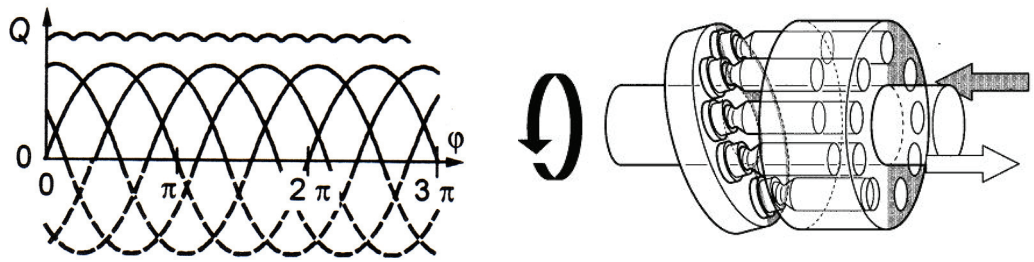

Figure 1: Flow pulsation of an axial piston pump (z = 5) and schematic view (z = 9)

Together with the flow pulsation, pressure pulsation occurs. The dynamic flow rate contains several frequencies f related to the rotational speed n and the number of pistons z as given in Eq. 2. For a rotational speed n of 750 1/min and a 9-piston pump, a frequency f = 112.5 Hz for the first order can be calculated.

$$f = n \cdot z \cdot i \quad i = 1,2,3,... \qquad \text{(Eq.2)}$$

The frequency spectrum shown in **Figure 2** illustrates these dynamics of the pressure pulsation. The pressure peaks are highlighted and connected with lines, as they have the highest significance. The first peak at lower frequencies of about 15 Hz is not affected significantly by a changing rotational speed, it shows resonances of the hydraulic system. This discrete frequency spectrum is used throughout the whole work.

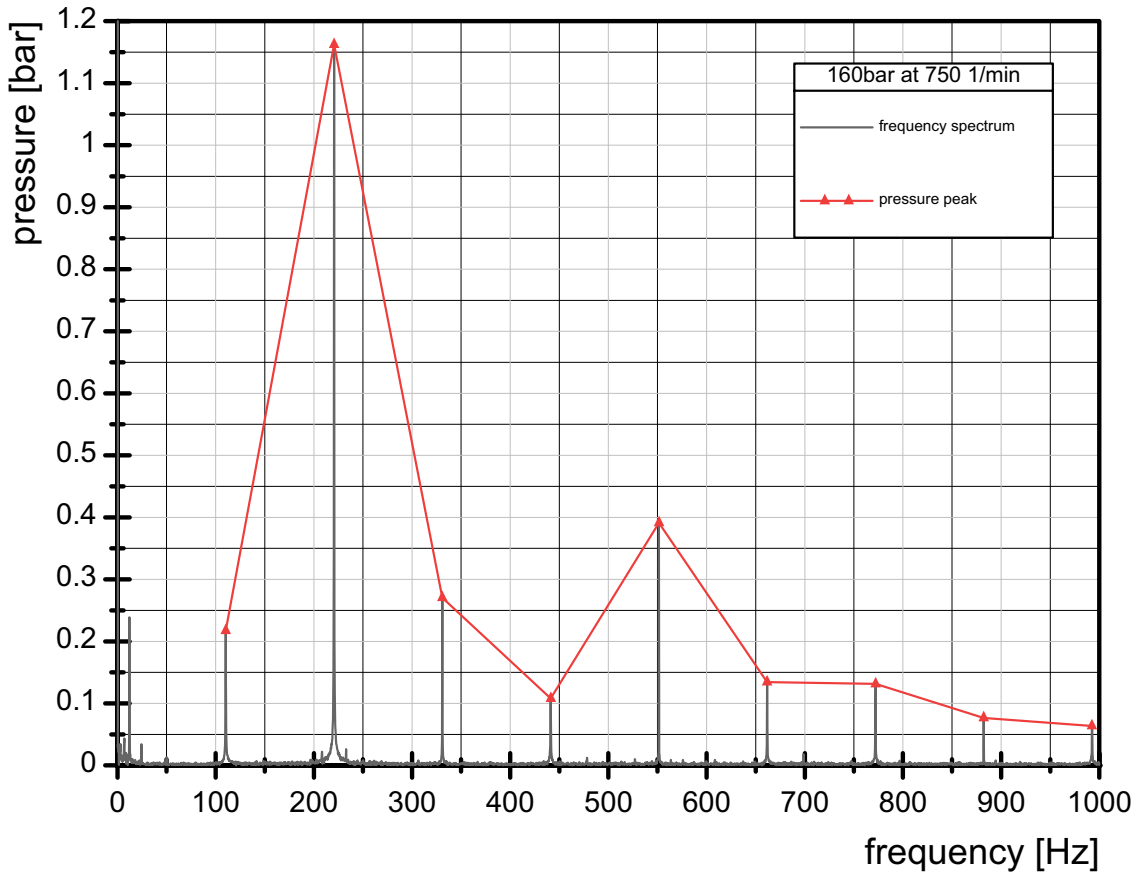

Figure 2: pressure pulsation (frequency spectrum)

To clarify the interrelationship between the hydraulic systems parameters and the pressure pulsation, **Figure 3** shows a simplified hydraulic scheme of the axial piston pump to depict the connection between the displacement chambers and the hydraulic system.

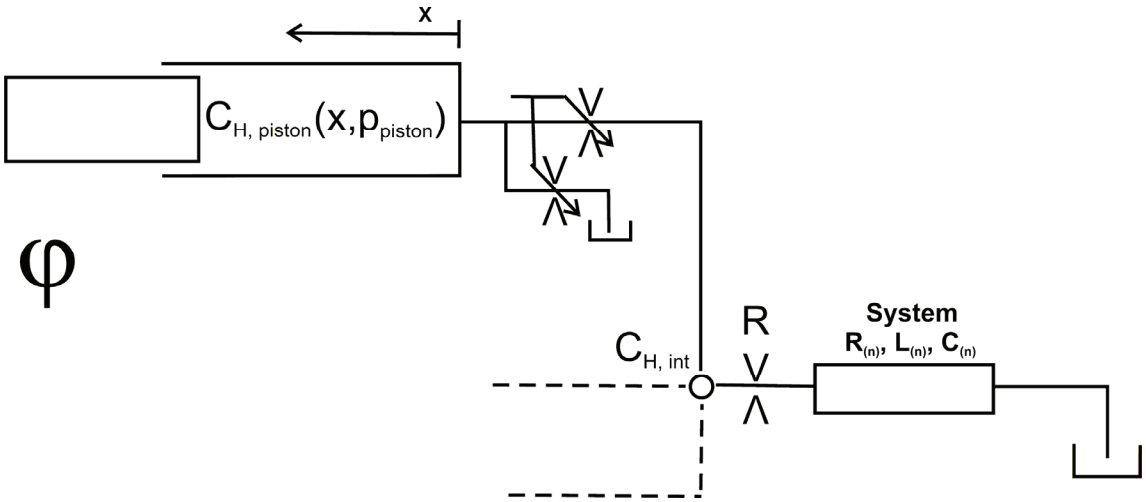

Figure 3: connection of the displacement chambers to the hydraulic system

The static pressure level p_{stat} depends of the load $R + R_{(n)}$ and interacts with the flow pulsation. The dynamic behavior of the connected hydraulic system influences both the pressure pulsation and the flow pulsation. The pressure buildup in each displacement chamber is affected by the hydraulic capacity $C_{H,piston}$. The hydraulic capacity $C_{H,piston}$ is a function of the chamber volume and the bulk modulus of the fluid. It therefore depends on the piston position x and the pressure p_{piston}. The control plate connects the displacement chamber to either the low pressure side or the high pressure side of the pump with a hydraulic capacity $C_{H,int}$ and the resistance R_{int}. As the internal volume remains constant, $C_{H,int}$ is only affected by the pressure level. The hydraulic system itself consists of a combination of multiple resistors $R_{(n)}$, capacities $C_{(n)}$ and inductivities $L_{(n)}$. The whole system has a complex transmission behavior with multiple eigenfrequencies, many of them variable due to load and pressure changes. The nature of these effects was studied using a detailed pump model provided by Deeken [7] for DSHplus.

3 TEST RIG AND PRESSURE PULSATION MEASUREMENTS

To examine the influence of changes in the hydraulic system on the pressure pulsation, a test bench was set up which allows for the variation of pipe length between pressure relief valve and a proportional 4/3-way-valve as a load simulator. The axial piston pump is connected to this system via a hose. A dynamic pressure sensor is applied next to the pump. The test bench is based on a precursor used for oil condition monitoring, hence the tank is very small and there are some other limitations like the unusual cooler position. This limits the maximum flow rate to approximately half of the nominal value to prevent cavitation. The hydraulic circuit is shown in **Figure 4**.

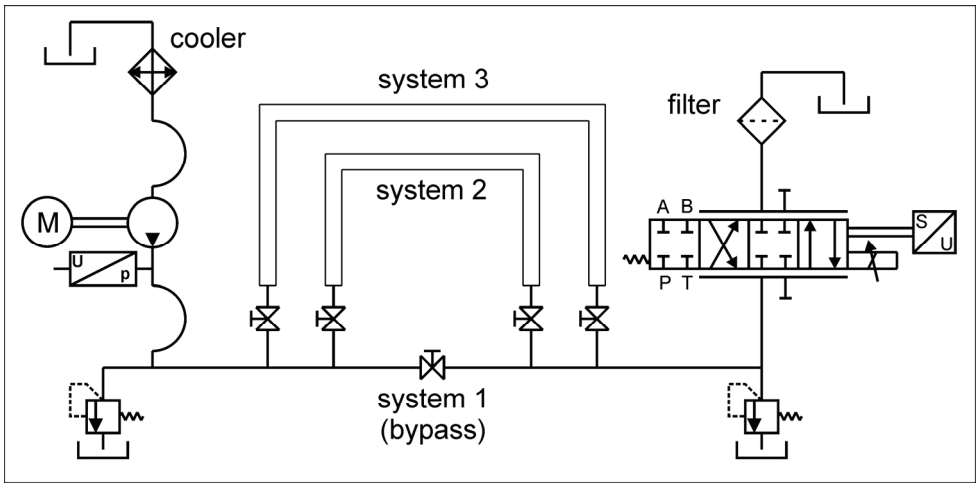

Figure 4: test stand

As an example, **Figure 5** shows the discrete frequency spectra of the pressure pulsation at the 9 lowest pump orders measured with two unmodified axial piston pumps A and B of the same type and size for 3 different hydraulic system configurations. The height of the pressure peaks at a certain frequency in the spectrum of both pumps shows the same particular order, from system 1 to system 3 or vice versa, and there are remarkable similarities in the proportions. In accordance to the hydraulic capacity C_H of the 3 simulated systems rising, the eigen frequencies are lowering from system 1 to system 3. Depending on the system dynamics, different pump orders are amplified or damped.

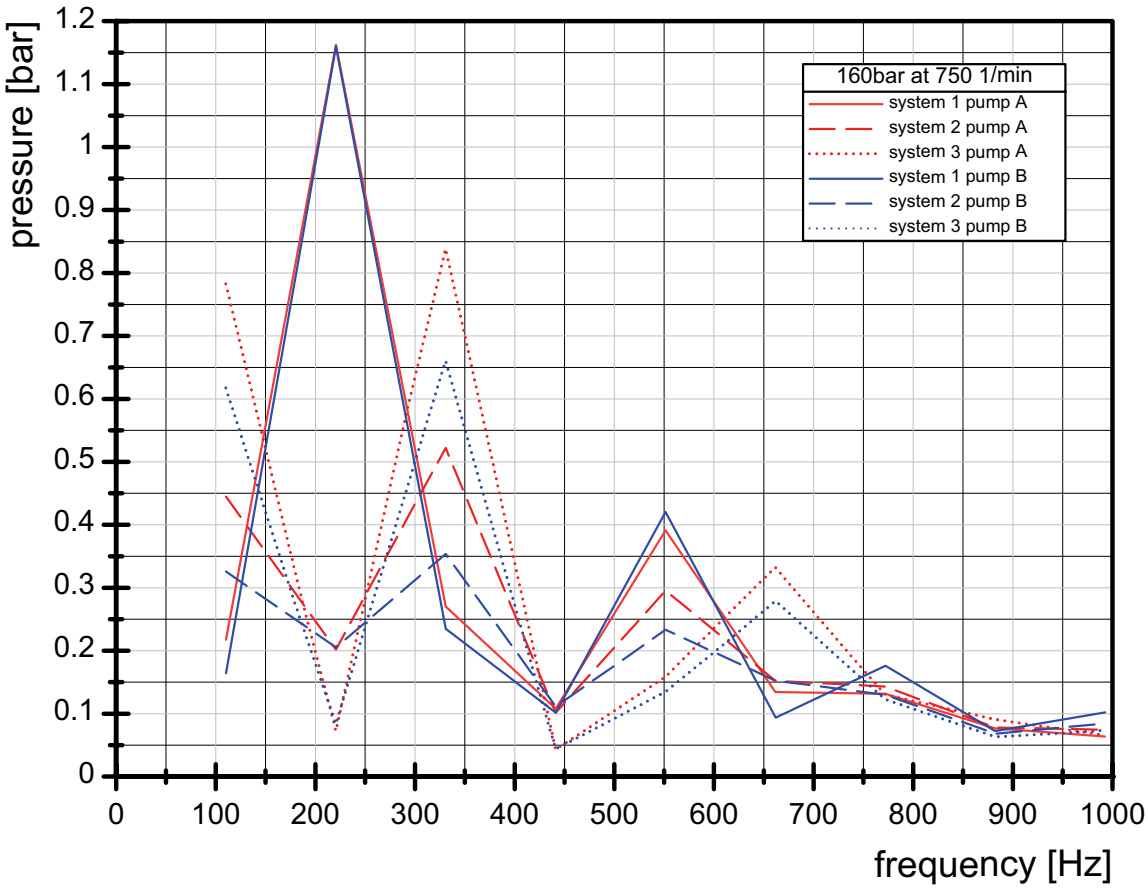

Figure 5: frequency spectra of pump A and B (both unmodified) connected to different systems

Even the both unmodified pumps show a different pressure pulsation, therefore a condition monitoring algorithm prepared for pump A would not be applicable for pump B. Due to these differences, the influence of faults on pressure pulsation was examined comparing measurements with pump A before and after replacing one of the pistons with a worn one.

The modified pump A is referred to as pump D. From the comparison of these measurements shown in **Figure 6** with those in Figure 5, it can be concluded that the measurement does show an existing fault. However, the differences between pump A and D are smaller than those between the two unmodified pumps A and B. The influence of the different hydraulic systems remains, without reference to the introduced fault.

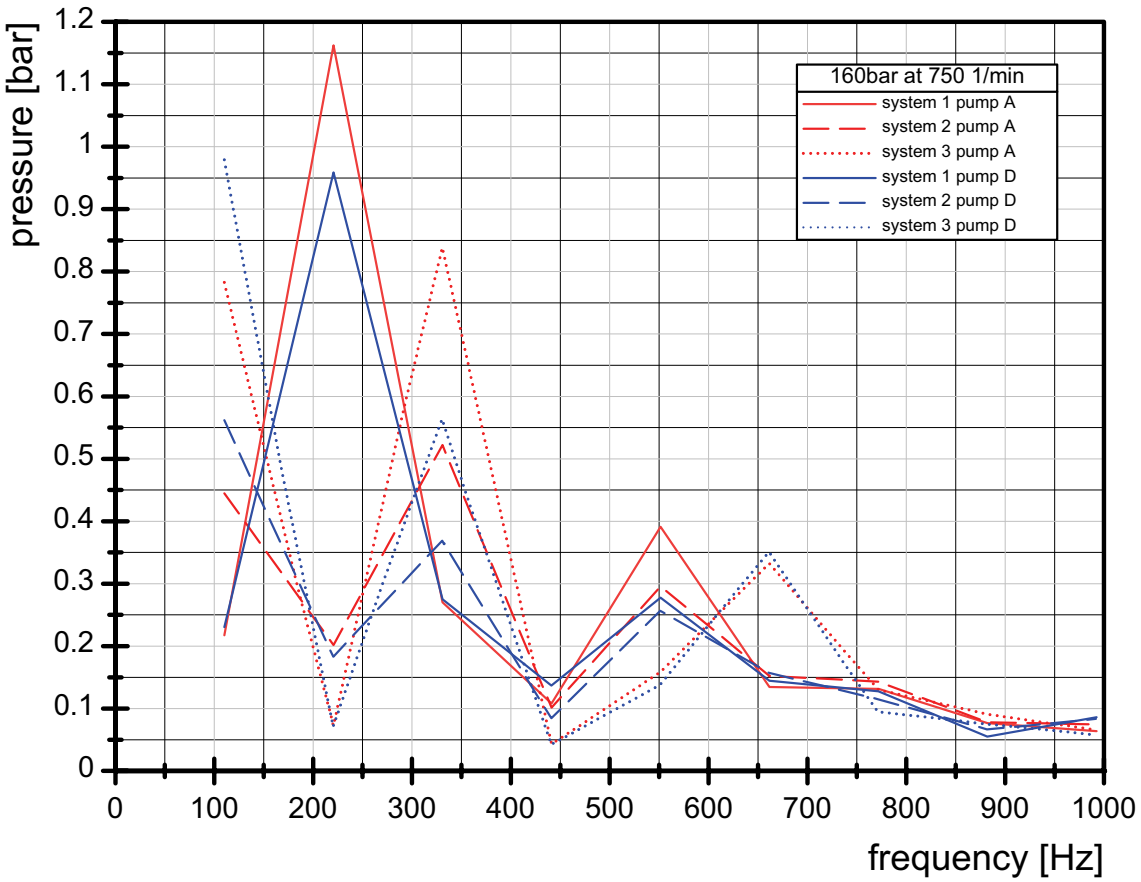

Figure 6: Frequency spectra of pump A and D (A with worn piston) connected to different systems

4 COMPENSATION OF VARIABLE SYSTEM DYNAMICS

The different system dynamics lead to a different shape of the pressure signals and their frequency spectra. As the effect of different hydraulic systems on the height of the pressure peaks is similar for the examined pumps and independent of their state, a compensation of variable system dynamics seems possible. To give a compact representation for the proportions of the pressure peaks in different systems, the frequency spectra of the pressure pulsation measured in a reference system are divided by the frequency spectra measured in any other hydraulic system (**Figure 7**). The result can be regarded as a transfer function representing the relation between the different

systems. To reduce the effort for measurements, the pump test stand used for quality control can be used to gain the necessary reference data.

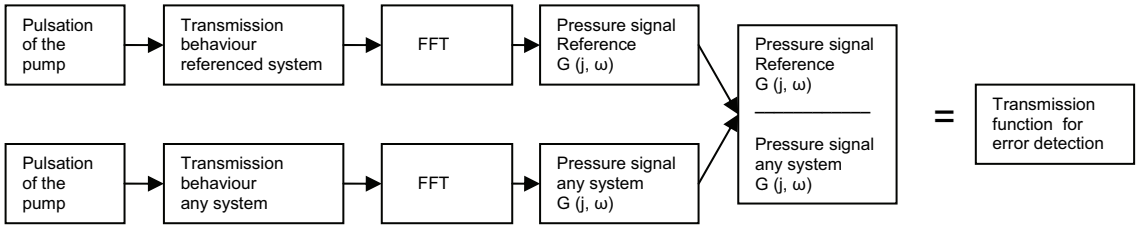

Figure 7: Calculation of the transfer function for system compensation

Based on simulation data, the algorithms were developed and tested under almost ideal conditions. For the application on test stand data, improvements were necessary for robustness against minor inaccuracy of the operation point settings. Using the discrete frequency spectra introduced with Figure 2, a discrete transmission function is introduced, concentrating on the pump order frequencies. The peaks are identified and the values are saved in a vector for the first 9 pump orders, a second vector contains the corresponding frequencies. Afterwards, the pressure peak values are divided to compute the transmission function, the frequency vectors are substracted and the result is used to test the accuracy of the setting of the rotational speed. It turned out that even minor deviation in the operating points shifting the pump orders and the peak frequencies by only a fraction on the frequency scale lead to unemployable transfer functions when dividing the whole spectrum. Thus, applying the discrete transfer function derived from discrete spectra, the algorithm is more robust. Additionally, there are advantages in computational and memory effort.

To compensate the effect of a hydraulic system, the transfer function can be used on the measurements to transform the pressure pulsation spectrum. The transfer function can be computed from the reference measurement taken right after the production and a first measurement after mounting the pump in the application. As **Figure 8** depicts, the frequency spectrum is multiplied with the transfer function, the resulting frequency spectrum is then shaped as if it would have been measured in the reference system.

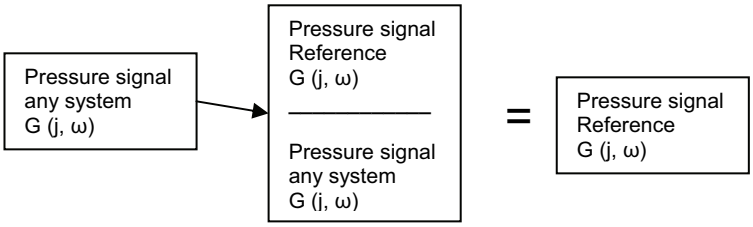

Figure 8: conversion of frequency spectra to compensate system dynamics

The application of the transfer function as a pre-processing step together with frequency-based Condition-Monitoring is illustrated in **Figure 9**. The pressure signal of the faulty pump is multiplied with the transfer function (derived from measurements without fault), the result can be compared to the reference to detect changes.

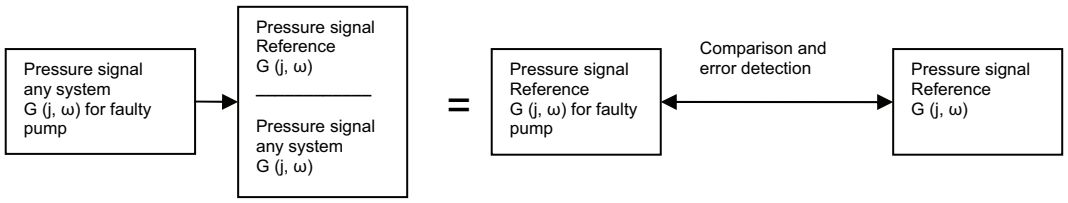

Figure 9: Application of the transfer function for system compensation as a part of a CM-concept

During the explanation it is supposed that the operating point (rotational speed, pressure and flow) of the reference system and any application is the same. A changing operation point, e.g. constant rotational speed and flow, but changing load pressure, requires a set of transmission functions for different pressures, as the dynamics depend on the Capacity C_H which is affected strongly by the actual pressure. For this case, the reduction of memory requirements using a discrete representation of spectra and transfer function provides additional benefit.
It is assumed, that a pump fault does not affect the dynamics of the hydraulic system as long as the pressure level remains, e.g. due to a pressure relief valve. If a major fault occurs that strongly effects the hydraulic system behavior and not only the pulsation generation, the approach described above would not lead to an exact result. Nevertheless, it can be assumed that there is still a deviation in the result to detect those major faults.

5 VERIFICATION

For verification of the approach, measurements were taken out with pump A, B and D for a variety of operating points with pressure levels from 20 bar to 200 bar and rotational speeds in the range from 300 1/min to 750 1/min. As reference system, system 2 was chosen. From measurements in this reference system and in system 3, a transfer function was computed for each operating point. Afterwards, these transfer functions were used to transform signals measured in system 3 to match the conditions of measurements with system 2.
To verify a set of possible applications, the transfer functions to compensate the system effects were computed for pump A and B from measurements taken out for the whole range of operating points and then applied on the modified pump. First, the pressure signal from pump D (the modified pump A) is converted with the transfer function computed from pump A. This is the normal application, as the pressure signal of the faulty pump is multiplied with the transfer function computed from the pump in good condition. The result can be compared to the measurement taken out with the reference system 2 (**Figure 10)**. The measured and the computed curves show only little differences, the changes in the peak heights between pump A and D due to the fault can be detected in the computed curves from measurements in system 3 at the same certain pump orders, as it can be done from the measurements in the reference system.
Additionally, measurements with pump A in system 3 were transformed with a transfer function computed from measurements with pump B, to analyse possible interdependencies of different pumps and different hydraulic systems. Both pumps strongly differ in their pressure pulsation, but it is assumed that the effect of the hydraulic system is independent of the pulsation generation inside of the pump. Figure 10 shows for this case the compensation works as well as it does for the faulty pump A.

It can be concluded that the effect of the pulsation generation on the system dynamics is negligible.

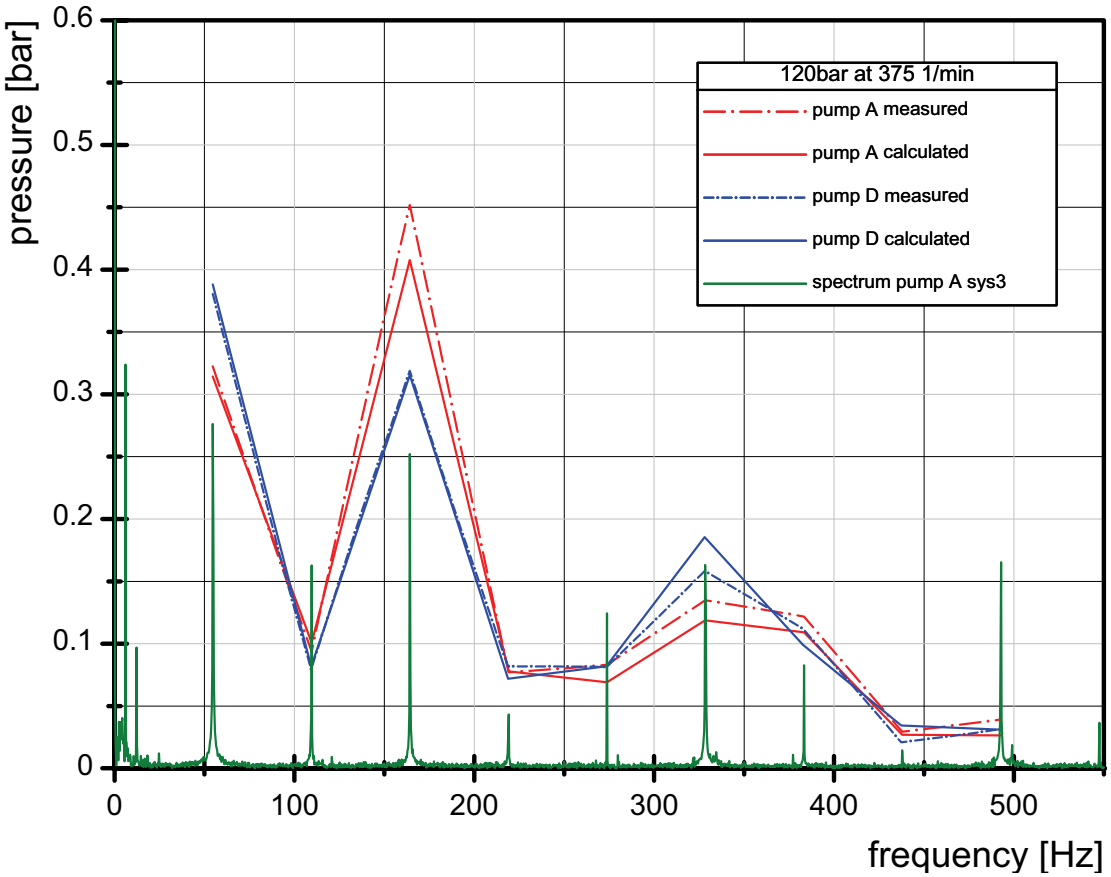

Figure 10: Verification for pump A and D at 375 1/min and 120 bar

The same application is done for a second operation point with higher rotational speed and higher pressure and shown in **Figure 11**. Again, the pressure signal of the faulty pump D is multiplied with the transfer function computed from pump A, and measurements with pump A in system 3 were transformed with a transfer function computed from measurements with pump B. Due to the higher rotational speed, the pump orders are shifted to higher frequencies. The measured and the computed curves show small differences, the changes in the peak heights between pump A and D due to the fault are significant in orders 1 and 3 in both the pressure pulsation spectra transformed from system 3 to the reference system shape and in the measured pressure pulsation spectra of the reference system.
The additional measurements with pump A transformed with the transfer function from pump B, display again the independency of the pulsation generation and the system dynamics.

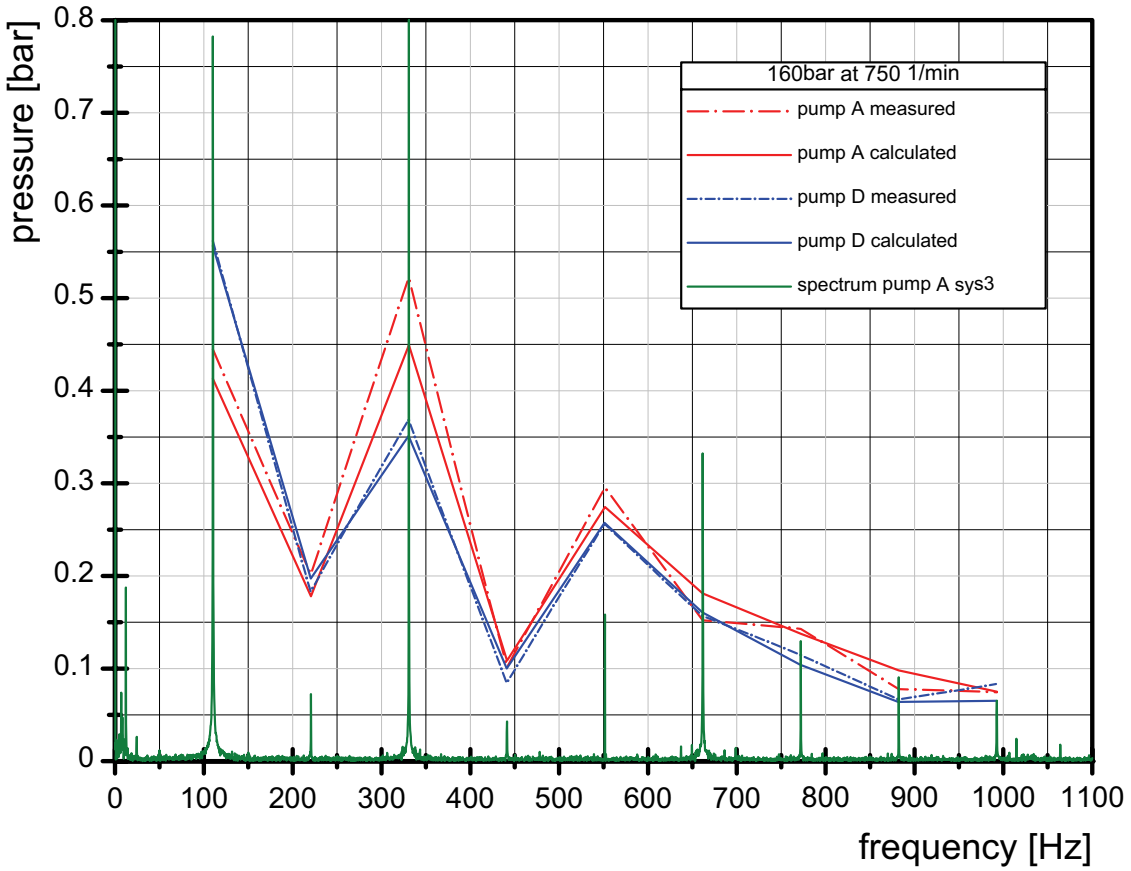

Figure 11: Verification for pump A and D at 750 1/min and 160 bar

For all cases, the system compensation is achieved with good quality. The differences between system 3 and the reference system 2 are reduced to a minimum by the compensation. To illustrate the differences, a continuous pressure pulsation spectrum of pump A in system 3 is inserted in Figure 10 and Figure 11.
The best accuracy is achieved for the 3 to 5 lowest pump orders, depending on the rotational speed. For higher frequencies, there are two negative effects on accuracy. On the one hand, the pressure peaks are smaller for high pump order and the signal to noise ratio is worse than for higher peaks at lower pump orders, on the other hand small deviations in rotational speed lead to a higher deviation in frequency for higher pump orders.

6 CONCLUSION

This paper proposes a new method for the easier setup of Condition Monitoring for hydraulic pumps on different applications. Differences in hydraulic system dynamics leading to a different shape of the pressure signals can be compensated using a transfer function computed from measurements in a reference system and in the application. A discrete transmission function is introduced, concentrating on the pump order frequencies and leading to simple and exact calculations with low computational effort.
The verification of the compensation algorithm was performed at a test rig for a variety of operating points by changing rotational speed and load pressure. A set of pipes was used to affect system dynamics. It can be concluded that the effect of different hydraulic systems showing off in the frequency spectrum of a pressure signal can be

compensated. A Condition Monitoring System which has been set up for a reference system can now still be applied after the pump is used in any other system. Effort and cost for the application of Condition Monitoring decrease.
It is expected that a similar approach could be applied on the signals of accelerometers for vibration analysis to compensate changes in transmission behavior due to different mounting conditions of pump or sensors.

7 REFERENCES

[1] Langen, H. J. "Einsatz der Körperschallmessmethode zur Schadensfrüherkennung an hydraulischen Verdrängereinheiten", Dissertation, RWTH Aachen, 1986

[2] Ramdén, T. "Condition Monitoring and Fault Diagnosis of Fluid Power Systems – Approaches with Neural Networks and Parameter Estimation", Dissertation, Linköping University Schweden, 1998

[3] Schwarz, T. "Schallanalyse zur Diagnose von Schäden an Hydraulikpumpen", Dissertation, RWTH Aachen, 1990

[4] Byington, Carl „Data-Driven Neural Network Methology to Remaining Life Predictions for Aircraft Actuator Components", 2004 IEEE Aerospace Conference Proceedings, S.3581ff

[5] Deeken, M. „Simulation of the reversing effects of axial piston pumps using conventional CAE tools" („Simulation der Umsteuergeometrie von Schrägscheibeneinheiten mit Hilfe gängiger CAE-Tools"), Ölhydraulik und Pneumatik 46 Nr. 6 (2002), english version as non-printable PDF on www.ifas.rwth-aachen.de

[6] Stammen, C.; Schumachers, C. „Kompensation des Systemeinflusses auf Zustandserkennungsverfahren für Axialkolbenpumpen", Proceedings of the 6.AKIDA (Aachener Kolloquium Instandhaltung Diagnose und Anlagenüberwachung) 14.-15.11.2006, Verlag Mainz, Aachen 2006, ISBN-13: 978-3-9810344-3-1

[7] Fritz, S.; Stammen, C. „Dem Verschleiß auf der Spur – Möglichkeiten zur Anlagendiagnose in der Pneumatik" , Ölhydraulik und Pneumatik 7-8 (2006), english version as non-printable PDF on www.ifas.rwth-aachen.de

[8] Stammen, C. „Condition Monitoring für intelligente hydraulische Linearantriebe", Dissertation, RWTH Aachen, 2005

[9] Murrenhoff, H. „Grundlagen der Fluidtechnik, Teil 1: Hydraulik", IFAS Umdruck zur Vorlesung, Aachen 2005

ABOUT CALIBRATION OF LIGHT EXTINCTION AUTOMATIC PARTICLE COUNTERS

C. PEUCHOT[1], Managing Director, N. PETILLON[2], Test Manager
INTERNATIONAL FILTER TESTING SERVICES
BP 292 – 47007 AGEN – France
Phone +33 553 958 394, Fax +33 956 695
[1]christophe.peuchot@ifts-sls.com
[2]nicolas.petillon@ifts-sls.com

ABSTRACT

Light Extension Automatic Particle Counters are the favourite instruments used in independent and industrial laboratories to measure the particulate contamination level of hydraulic fluids, fuels and in some cases, lubricants. As well, they are the only reliable instruments to count particles upstream and downstream filters to measure their instantaneous efficiency at various sizes. These two families of applications are detailed in several international standards.

As all measuring instruments, they have to be regularly calibrated. Because oil has chemical and optical properties different from that of water, the size calibration material cannot be made of latex spheres as recommended in USP 28. ISO 11171 defines SRM 2806 certified by NIST as the APC calibration suspension. It is made of classified silica sand in a standard mineral oil.

The authors describe the way the new batches of SRM 2806b shall be prepared and certified. They make some proposals to make ISO 11171 and ISO 11943 easier to understand and apply for not expert end users. Some results of international round robin tests performed these last years within few ISO expert groups are presented and interpreted from the point of view of APCs calibration.

KEYWORDS

Contamination – Particle – Calibration – Reference Materials – Efficiency – Particle Counter.

1. Introduction

Many mechanical systems use a liquid as a source of energy, e.g. in internal combustion engines, as a mean of energy transfer, e.g. in fluid power systems, or as a mean of lubrication of mooving parts, e.g. in engine lubrication circuits. Their reliability is directly affected by the presence of particulate contaminants in the fluid. Indeed, surfaces may wear what may create leakages. Clearances may be reduced or increased what generates loss of yield. Orifices may clog what creates loss of pressure or flowrate. Many other examples of negative effects of a particulate contamination could be listed.

In other cases, the particulate contamination level of the liquid may alter the quality of the product made with it, e.g. microelectronic components and chips rinsed with ultraclean water, purity of crystals obtained by precipitation of two solvents, medicines and parenteral drugs to which an hill organism may react badly and many others.
In all cases, professionals have adopted means and methods to assess the particulate contamination level, the most common of which is particle counting and sizing with automatic instruments having light extinction sensors.
APCs are privileged instruments to count particles at various sizes in suspension in a liquid upstream and downstream a filter to calculate its filtration efficiency.
Because of economic impacts of both uses, the accuracy and exactness of APCs is of the utmost importance. This is achieved through calibration.
The calibration of APCs to count particles in water based liquids and many chemicals uses monosized plastic spheres as specified in ASTM F 658-87.
When applied to assess cleanliness of oil based liquids, APCs are calibrated with a reference suspension of silica powder in a standard mineral oil as specified in
ISO 11 171.
This article gives some guidance on how to interpret this standard and reports on work on progress and states proposals to make new calibration suspensions more accurately certified.

2. Applications of APCs

2.1 Fluid contamination level measurement

The use of Automatic light extinction Particle Counters to determine the particulate contamination level (at sizes above 1 micron) of various liquids is specified in few standards (1, 2, 3).

Contamination level is often reported by a code or a class obtained by comparing actual particle counts, standardised to a given fluid volume, to that of tables specified in standards (4, 5, 6, 7).
As table 1 shows, one changes of one contamination class by doubling the number of particles in the size range considered. Thus requirements on the accuracy of particle counts for this application are not very high.

		Maximum Contamination Limits (particles/ 100 mL)				
Size Range, Optical Microscope (1) or APC Calibrated per ISO 4402 (2)		5 to 15 µm	15 to 25 µm	25 to 50 µm	50 to 100 µm	> 100 µm
Size Range, APC Calibrated per ISO 11171 or Electron Microscope (3)		6 to 14 µm(c)	14 to 21 µm(c)	21 to 38 µm(c)	38 to 70 µm(c)	> 70 µm(c)
CLASSES	**00**	125	22	4	1	0
	0	250	44	8	2	0
	1	500	89	16	3	1
	2	1 000	178	32	6	1
	3	2 000	356	63	11	2
	4	4 000	712	126	22	4
	5	8 000	1 425	253	45	8
	6	16 000	2 850	506	90	16
	7	32 000	5 700	1 012	180	32
	8	64 000	11 400	2 025	360	64
	9	128 000	22 800	4 050	720	128
	10	256 000	45 600	8 100	1 440	256
	11	512 000	91 200	16 200	2 880	512
	12	1 024 000	182 400	32 400	5 760	1 024

(1) Particle size based on longest dimension
(2) For reference only; ISO 4402 has been withdrawn
(3) Particle size based on projected area equivalent diameter

Table 1 : Maximum Contamination Limits For Differential Particle Counts

The pharmaceutical industry directly reports the number of particles greater than 15 and 25 µm per unit volume of liquid.

2.2 Filter efficiency testing

Several international and an European standard methods specify the use of light extinction particle counters to measure the instantaneous efficiency of the filter (8). Results of international round robins organised to validate recently adopted ISO standards have emphasized the requirement for correct calibration and matching of APCs and their sensors if comparable, repeatable and reproducible results are to be obtained.

2.3 Principle of operation of APCs

Figure 1, recalls the operating principle of light extinction automatic particle counter sensors.

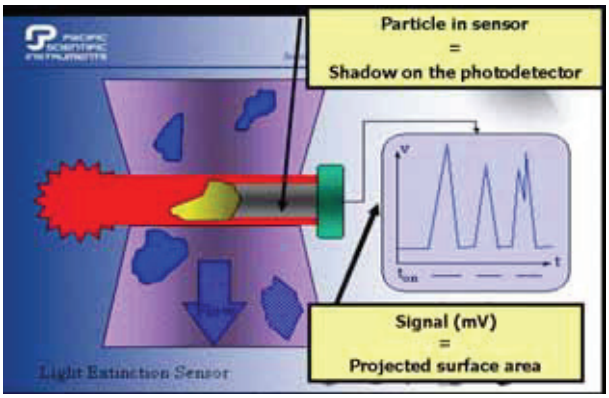

Figure 1 : Principle of operation of light extinction APC sensors

The sensor detects each particle individually and measures electric signal intensity changes which are proportional to the projected area (the shadow) of the particles. The size measured is said to be the diameters of the sphere with the same projected area. Such a detection principle means that one particle with an irregular shape may be seen with different diameter depending on its orientation and that, reciprocally, two identical diameters may correspond to particles with a very different size and/or shape.

The practical limitations of use of optical sensors are interferences (electrical noise, vibration, …), saturation (too many particles do not create a linear response), coincidence (two particles at a time in the sensor are reported as a larger one) and flow conditions.

3. Sizing calibration

3.1 Monosized spheres

The most accurate way of calibrating an APC is to use certified monosized spherical particles (picture 2).

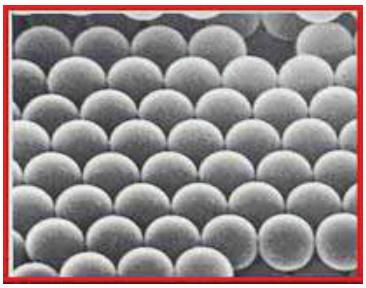

Picture 2 : Certified monosized spherical particles

Such a procedure is described in (1). The size of the reference materials should have been measured using SEM or optical microscope with an image analysis software the parameters of which (magnification, µ/pixel,…) should have been verified with graticules certified to BCR (Community Bureau of References).
Such a reference material has an undisputable and traceable size.
The limit of this method is its cost since several diameters have to be used to draw the full scale of the calibration curve. Another limitation is that since spherical particles in the micron range are only available as latex, e.g. polystyrene spheres in water and surfactant, they cannot be used to calibrate APCs used with mineral oils or fuels.

3.2 Polydispersed particles : ISO 11171

To overcome the problem stated above, the fluid power international community has asked the US organism NIST (National Institute for Standards and Technology) to prepare Reference Material made of one batch of ISO MTD (ISO 12 103, A3), in standard mineral oil DCSEA 415 (NATO H515 or MIL H 5606).
The particle size distribution of the reference suspension, sold as SRM 2806, is certified using a rigorous protocol defined in ISO TR 16 144.
The sizing calibration procedure is described in clause 6 of ISO 11171. In its annexes are specified protocols to determine the limit flowrate, the coincidence error limit, the resolution and the counting accuracy of the APC.

The wording used both in ISO 11 171 and on NIST SRM 2806 bottles create a confusion in many users' minds. A result is that the majority of APCs used by industry today are not really, or at least precisely, calibrated.

4. Vocabulary clarification

The situation could easily be clarified by clarifying the vocabulary and its definitions. Schematics are used to explain the proposal.

4.1 Primary Calibration

This is the calibration of an APC per ISO 11 171 with primary Standard and Reference Materials NIST SRM 2806.

APC 1 + NIST SRM 2806 = REFERENCE APC

The results of a Reference APC count shall never be contested and in no case its thresholds settings shall be changed. Reference APCs should not be used daily but rather to check other instruments.

4.2 Secondary calibration and APC Matching

It consists in calibrating an APC with a secondary suspension. A secondary suspension is a suspension of ISO MTD (but it could be any other suitable silica powder) in DCSEA 415 oil, the particle size distribution of which has been determined with a Reference APC. Such a secondary calibration suspension can be prepared in small quantities in bottles or in larger ones using a close circuit rigorously validated per ISO 11 943. The secondary calibration then consists in setting the secondary APC thresholds so that it counts the particle numbers found with the Reference APC. It should be emphasized that the particle size distribution of a secondary suspension does not require to be and is probably actually never the same as that of NIST SRM 2806.

REFERENCE APC + ISO 11 943 LOOP + APC 2 = SECONDARY APC

A secondary APC can be used daily.
In case of multipass testing of filters, it is possible to use a Reference APC and a secondary APC upstream and downstream. When a test lab has several multipass test stands and thus several pairs of APCs, it has to perform the matching of all APCs stand by stand. The matching is synonymous of a secondary calibration and shall be performed on a loop (e.g. the multipass circuit) validated per ISO 11 943.

Attention is drawn on the fact that SRM 2806 is a suspension of ISO MTD in
MIL H 5606 with a certified particle size distribution but that in no case a suspension of ISO MTD in MIL H 5606 has the particle size distribution of SRM 2806. This confusion is today the source of many errors made in many, if not in nearly all, contamination analysis and filter testing laboratories.

4.3 ISO MTD : A test not a reference powder

Laboratories using their own in-house prepared ISO MTD suspensions make important errors which explain the discrepancies found in ISO round robins.
Indeed :

4.3.1. ISO MTD bought to the monopolistic supplier is an industrially prepared powder. It complies with the table 2 of ISO 12 103-1 (Table 2).
When transformed in particle number limits, the % volume fraction tolerance become significant. This means that two batches of ISO MTD fully complying with ISO 12 103-2 A3 spec may have very different particle size distribution (PSD) by number.

Size µm	Maximum volume fraction, %			
	A1 ultrafine	A2 fine	A3 medium	A4 coarse
1	1 to 3	2,5 to 3,5	1 to 2	0,6 to 1
2	9 to 13	10,5 to 12,5	4,0 to 5,5	2,2 to 3,7
3	21 to 27	18,5 to 22,0	7,5 to 9,5	4,2 to 6,0
4	36 to 44	25,5 to 29,5	10,5 to 13,0	6,2 to 8,2
5	56 to 64	31 to 36	15 to 19	8,0 to 10,5
7	83 to 88	41 to 46	28 to 33	12,0 to 14,5
10	97 to 100	50 to 54	40 to 45	17,0 to 22,0
20	100	70 to 74	65 to 69	32,0 to 36,0
40	—	88 to 91	84 to 88	57,0 to 61,0
80	—	99,5 to 100	99 to 100	87,5 to 89,5
120	—	100	100	97,0 to 98,0
180	—	—	—	99,5 to 100
200	—	—	—	100

Table 2 : Range of ISO MTD particle size distribution

4.3.2. Sampling of few grams of ISO MTD from the jar it is supplied in, is not a trivial procedure and very few contamination analysis and filter testing laboratories are aware, of much less experts, powder sampling. In a lab, two operators will necessarily take samples with different particle size distributions. The difference is higher between labs.

4.3.3. Preparing a suspension of ISO MTD in MILH 5606 requires to accurately measure the mass and the volume to guarantee its concentration in mg/L. Here again, sources of errors are lot and it is sure that no lab will prepare the same as its neighbour. The sum of the three above sources of errors lead to the current situation : labs thinking and claiming to prepare their own secondary suspension all prepare different ones and in no case an SRM 2806. Then by applying to their "home" made "calibration suspension" the numbers of NIST SRM 2806 certificate, they perform a really wrong calibration of their sensors. And they obtain approximate fluid contamination levels and higher approximate filtration efficiencies or β ratios if they test filters.

4.4 Explanation of and improvements to ISO 11 171

A routine application of ISO 11 171 to calibrate particle counters (8 are daily in used on single and multipass filter test stands) and customer ones leads to several proposals to improve the understanding of the standard.

a) In the introduction, it should not be stated that ISO MTD is the calibration material but an industrial powder (specified in ISO 12 103 -1 A3) with reduced tolerances but not a certified particle size distribution.

b) In § 6.4, NIST RM 8631 is a batch of ISO MTD powder rigorously sampled in the same batch as SRM 2806 (4090 C) thus with a very similar particle size distribution. But as stated above there is no chance that two labs purchasing this RM prepare two suspensions with the exactly same PSD as SRM 2806 because the volume in which they will be prepared cannot be exactly the same.

c) In § 6.4, it should be more clearly stated to draw the calibration curve mV = f(x) and the drawing below could explain the text.

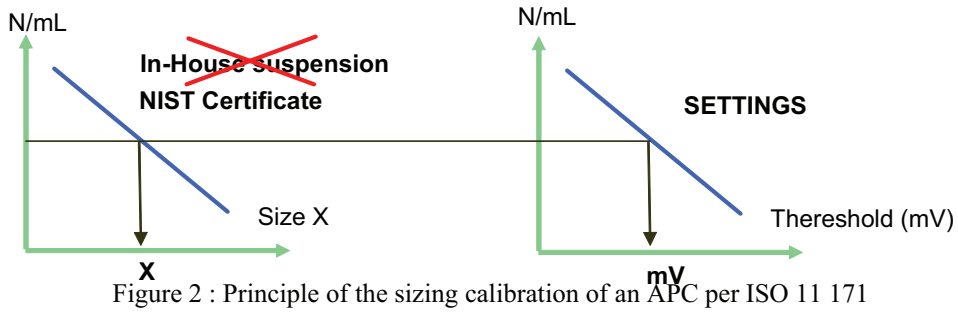

Figure 2 : Principle of the sizing calibration of an APC per ISO 11 171

d) In Table 4, the traceability to the APC primary calibration should be reported. If a secondary suspension is used, quality management requires to be able to trace to NIST SRM 2806.
For clarity, "Initial" should be replaced with "First" and "Final" with "Third" or "Last".

e) In Annex F, (secondary calibration suspensions), a too confusing wording brings users to misunderstand both the scope and the operation to be performed. The tittle should be changed for **"Preparation and verification** of secondary calibration suspensions **in bottles"**. Indeed the verification could be done online on the preparation loop.

As well, annex F2 should refer to ISO 11 943 preparation loop and recommend online counting since a much more accurate and repeatable technique than bottle counting.
In annex F3, the APC calibrated with NIST SRM 2806 should clearly be labelled "Reference APC".
Then a schematic should explain that this clause allows two operations : first check the stability of counts with time, what means the low bottle to bottle particle number dispersion and : second obtain the certification of the secondary suspension particle size distribution in N/mL at various sizes.

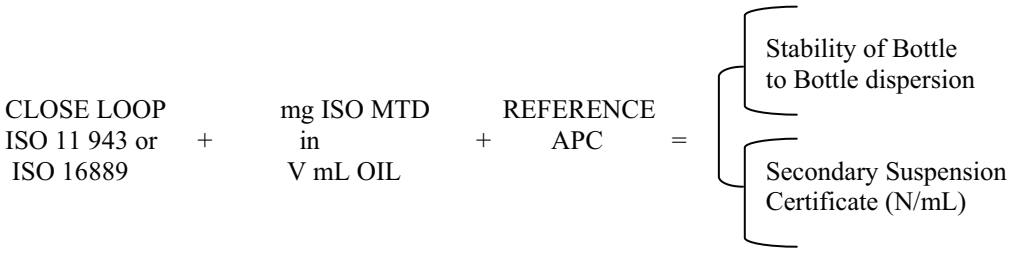

4.5 Proposal of improvements to SRM 2806

The procedure used by NIST to prepare and certify the particle size distribution of SRM 2806 is detailed in ISO TR 16 144 (8). It includes several steps briefly summarised below :

- prepare a large amount of an homogeneous suspension of ISO MTD in MIL H 5606 and fill in a few hundreds of 400 mL bottles,
- sample in several bottles randomly sampled few mL of suspension using a pipette,
- filter its content on a 0.2 µm membrane and ensure an homogeneous deposit of particles on the whole surface area,

- Examine the membrane under a SEM and size particles observed in several fields randomly selected.

The result of the certification process is the table attached to every bottle sold by NIST (Table 3).

Model particle Concentration (1/mL)	Design particle Concentration (1/mL)	Projected area Diameter [a] (µm)	u Sampling (µm)	u Volume (µm)	u Digitization (µm)	u Length (µm)	u Size fractionation (µm)	Uc Combined standard uncertainty (µm)	U Expanded uncertainty [b] (µm)
108400	108960	1	0.004	0,004	0,0006	0,127	0,051	0,137	0,274
27035	28094	2	0,006	0,006	0,00003	0,123	0,049	0,133	0,265
11209	10918	3	0,009	0,010	0,0005	0,122	0,059	0,136	0,272
6095	6506,4	4	0,011	0,013	0,002	0,121	0,094	0,154	0,308
3737	3860,7	5	0,012	0,015	0,004	0,121	0,167	0,207	0,414
2395	2918,8	6	0,016	0,016	0,006	0,131	0,246	0,280	0,560
1573	1814,3	7	0,019	0,017	0,009	0,131	0,236	0,271	0,542
1055	1220,0	8	0,024	0,018	0,013	0,131	0,210	0,250	0,499
725,8	810,21	9	0,031	0,019	0,017	0,131	0,235	0,272	0,544
513,7	570,90	10	0,041	0,021	0,021	0,131	0,289	0,322	0,643
374,6	423,84	11	0,052	0,023	0,025	0,131	0,351	0,380	0,759
281,0	314,86	12	0,065	0,025	0,029	0,131	0,467	0,490	0,981
216,4	238,97	13	0,081	0,027	0,031	0,131	0,616	0,637	1,273
170,4	190,38	14	0,101	0,030	0,033	0,131	0,810	0,828	1,655
136,8	147,12	15	0,123	0,032	0,033	0,131	1,090	1,106	2,211
111,3	119,62	16	0,146	0,034	0,033	0,131	1,190	1,207	2,414
91,33	97,156	17	0,168	0,035	0,033	0,131	1,439	1,455	2,910
75,29	79,509	18	0,187	0,036	0,034	0,131	1,706	1,722	3,444
62,17	65,359	19	0,204	0,036	0,036	0,131	2,036	2,050	4,101
51,35	53,621	20	0,219	0,036	0,041	0,131	2,509	2,522	5,045
42,40	45,411	21	0,235	0,036	0,047	0,131	2,473	2,488	4,976
35,01	37,919	22	0,255	0,036	0,056	0,131	2,738	2,754	5,508
28,95	31,885	23	0,281	0,037	0,068	0,131	2,953	2,970	5,941
23,99	24,973	24	0,314	0,038	0,081	0,131	3,267	3,286	6,573
19,95	20,272	25	0,356	0,039	0,097	0,131	3,450	3,472	6,945
16,66	16,925	26	0,408	0,040	0,115	0,131	3,603	3,631	7,261
13,98	13,817	27	0,468	0,041	0,135	0,131	3,983	4,015	8,030
11,80	11,202	28	0,539	0,043	0,158	0,131	4,144	4,184	8,369
10,02	8,7036	29	0,618	0,045	0,184	0,131	4,247	4,298	8,595
8,568	8,3281	30	0,706	0,047	0,212	0,131	4,914	4,971	9,943

a) The particle diameter was determined for the dust particles in their most mechanically stable orientation and thus the particle area approaches on average the largest possible value. Literature values for the ratio of mean projected diameters for random and for stably oriented quartz particles (common to ISO Medium Test Dust) is approximately 0.8.
b) Each combined standard uncertainty is the square root of the sum-of-the-squares of the standard uncertainty derived or estimated from the measurement process. The expanded uncertainty in the projected area diameters are twice (coverage factor k = 2) the combined standard uncertainties. In cases where all uncertainties are type A (uncertainties evaluated by statistical means), then k = 2 level defines a confidence interval of approximately 95 % [25].

Table 3 : NIST Certificate of particle size distribution of SRM 2806

It shows that the SRM is certified within 30 % of the certified size. This is a much too broad range to consider the material as a reference one.
Despite this certificate, counts performed by qualified laboratories over several months on several bottles have shown much tighter tolerances (figures 3, in Ref. 9)

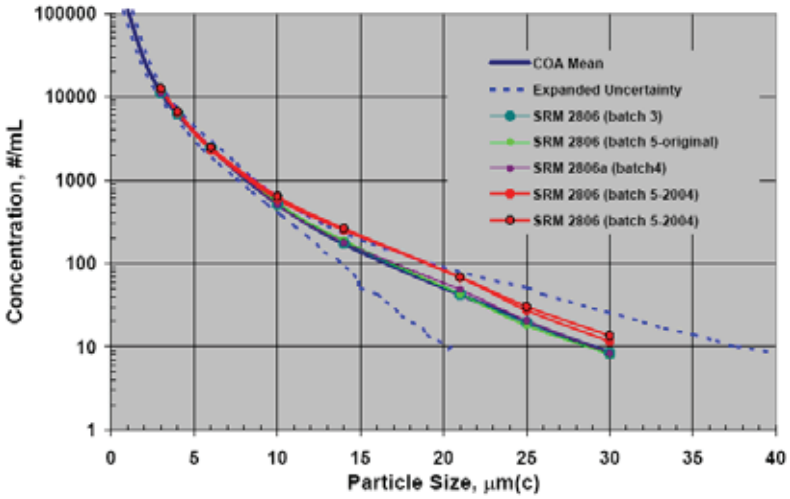

Figure 3 : NIST data on SRM 2806

Efforts are to be made to reduce the differences between two bottles of SRM 2806-b or c under preparation and then to make more accurate the SEM counting process. Ways of success are to increase the volume of fluid sampled in a bottle and to improve the sampling process. This may require to prepare several membranes from the same bottle. Then to increase the number of particles counted and sized. The error on sizing itself can be considered neglectible due to the high accuracy of the SEM at the magnification used.

5. Conclusion

Automatic light extinction Particle Counters are instruments used in many laboratories to either quantify the particulate contamination of various liquids or measure the efficiency of various filters.
When the counted liquid is a mineral oil based one, the calibration of the instrument requires using Standard Reference Materials SRM 2806 and the procedure defined in ISO 11 171.
The wording used in this standard and in ISO 11 943 related to online counting system validation and the labelling of SRM 2806 bottles have created some confusion in laboratories and APC manufacturers performing the calibration.
Improvements could easily be brought to existing tests so as to clearly differentiate primary and secondary calibrations as well as ISO MTD and SRM 2806. Then results of contamination analysis would become more accurate and exact and round robin tests organised to validate ISO hydraulic, lubricant and fuel filter efficiency test methods would have given more reproducible results.

6. Bibliography

6.1 ASTM F 658-87 : Standard Practice for Defining Size Calibration, Resolution, and Counting Accuracy of a Liquid-Borne Particle Counter Using Near-Monodisperse Spherical Particulate Material.

6.2 ISO 11171 : Hydraulic fluid power – Fluids – Calibration of liquid automatic particle counters for liquids.

6.3 European Pharmacopea 2.9.19. : Contamination Particulaire : Particules non visibles (version 5.0) - 2006

6.4 NF E 48-658 : Hyrdaulic fluid power – Fluids – Determination of particulate contamination by automatic counting using light interruption principle.

6.5 ISO 4406 : Hydraulic fluid power – Fluids – Methods for coding level of contamination by solid particles.

6.6 ISO 11218 : Aerospace – Cleanliness classification for hydraulic fluids.

6.7 NF E 48-655 : Hydraulic fluid power – Fluids – Expression of results.

6.8 ISO TR 16144 : Hydraulic fluid power – Fluids – Calibration of liquid automatic particle counters – Procedures used to certify the stand reference material SRM 2806.

6.9 Report regarding SRM 2806 issues, B. VERDEGAN, April 2005, ISO TC 131/SC6/WG1 N 103.

THE TENTH SCANDINAVIAN INTERNATIONAL CONFERENCE ON FLUID POWER

PROCEEDINS OF THE CONFERENCE

Volume 3

MAY 21-23, 2007

TAMPERE, FINLAND

Editors: Jani Vilenius and Kari T. Koskinen

Technical editor: Janne Uusi-Heikkilä

ISBN 978-952-15-1757-0
978-952-15-1758-7 (Vol. 1)
978-952-15-1759-4 (Vol. 2)
978-952-15-1760-0 (Vol. 3)
978-952-15-1761-7 (CD-ROM)
978-952-15-3272-6 (PDF)

ORGANISING COMMITTEE

Professor Matti Vilenius, TUT / IHA, Conference Chairman
Professor Kari T. Koskinen, TUT / IHA, Conference Vice Chairman
Senior Researcher Jani Vilenius, TUT / IHA, Conference Manager
Secretary Virpi Multanen, TUT / IHA, Conference Secretary
Professor, Senior Adviser for Board of Manag. Matti Kleimola, Wärtsilä Corp.
Professor Aarne Halme, TKK / ATL
Manager, Research and Rock Drills R&D Erkki Ahola, Sandvik UGHRM
Director Technology and Engineering Seppo Taatila, Ponsse Oyj
Managing Director Kalle Tuohimaa, Bosch Rexroth Oy
Technical Director Jussi Hanski, Parker Hannifin Oy Lokomec
General Manager Risto Käkelä, Avant Tecno Oy
Vice President R&D Juha Mäkitalo, Finn-Power Corp.
R&D Manager Merja Lämsä, AarhusKarlshamn Ab Technical Products
Vice President Ilari Orpana, Polarteknik PMC Oy Ab / Chairman of FHPA
Section Manager Olli Pohls, Hytar Oy Water Hydraulics
Professor Kalevi Huhtala, TUT / IHA
Professor Petteri Multanen, TUT / IHA
Professor Jari Rinkinen, TUT / IHA
Professor Tapio Virvalo, TUT / IHA

SICFP'07 Secretariat
Chairman Prof. Matti Vilenius

Institute of Hydraulics and Automation (IHA)
Tampere University of Technology (TUT)
P.O.Box 589
FI-33101 Tampere, Finland

Tel. +358 3 3115 2264
Fax +358 3 3115 2240

PREFACE

This year we really have reason to celebrate! This is the *tenth* time SICFP is organized.

The first international conference on fluid power in Tampere was held in 1987. That was the start of the series of Scandinavian fluid power conferences. In 1993 it was decided that the name of the conference is Scandinavian International Conference on Fluid Power. At the same time it was also decided that SICFP will be held every second year alternately in Tampere and Linköping. So we have already a 20 years' tradition, which is also worth of celebration.

This conference is organized by Institute of Hydraulics and Automation (IHA) at Tampere University of Technology (TUT) together with network of Fluid Power Centres in Europe (FPCE).

This tenth anniversary conference includes various traditional themes like mobile hydraulics, water hydraulics and industrial hydraulics. However, in addition this time there are many more new areas included like digital hydraulics, intelligent mobile machines and teleoperation. They are reflecting well the situation, where electronics, modern information and communication technology is integrating with traditional hydraulics and automation.

We received about 125 interesting and high-level proposals. In addition to five invited speakers, about 80 papers were selected for the final programme. We believe that the conference will give the participants fine opportunities to listen interesting presentations, to exchange opinions and strengthen of old contacts and to establish new ones.

This time the conference proceeding will be published as a printed book and also as a cd-rom. We hope that this proceedings will serve you well during the conference but also far in the future as a source of reference.

We would like to express our sincere appreciation to everybody who has contributed to the success of the conference.

Tampere, 4th of April, 2007

Kari T. Koskinen, Professor
Vice-Chairman, SICFP07

Jani Vilenius, Dr. Tech.
Conference Manager, SICFP07

TABLE OF CONTENTS – Volume 3

PLENARY SESSION P3

SESSION A6: Intelligent Mobile Hydraulic Systems

SESSION B6: Simulation and Virtual Reality

SESSION C6: Control of Hydraulic Systems

SESSION A7: Mobile Hydraulic Systems

SESSION B7: Pumps and Systems

SESSION C7: Teleoperation and Actuators

SESSION A8: Condition Control for Monitoring

SESSION B8: Hydraulic Valves

SESSION C8: Water Hydraulic Components and Systems

Development of A Self-energising Electro-Hydraulic Brake (SEHB) for Rail Vehicles

Matthias Liermann, Christian Stammen
RWTH Aachen University
Institute for Fluid Power Drives and Controls (IFAS)
Steinbachstr. 53, 52074 Aachen, Germany
Matthias.Liermann@ifas.rwth-aachen.de, Christian.Stammen@ifas.rwth-aachen.de

Abstract

This paper presents the innovative concept of a Self-energising Electro-Hydraulic Brake (SEHB) which is developed at IFAS for a railway application. Its advantages over conventional air brakes are high dynamics, the possibility to control the actual retarding torque, more compact design, higher braking forces and higher efficiency compared to conventionally used air brakes. Due to the concept of self-energisation only low electric power is required for brake actuation and no central hydraulic power supply is needed, thus significantly reducing design interfaces to the bogie. After introducing the working principle of the innovative SEHB system, some safety features are presented that allow load adaptive braking and braking for long periods. The non-linear system simulation gives insight into potential brake performance and supports the development process of the first brake prototype on the basis of an automotive brake calliper. The paper closes with an outlook on the further development of SEHB, including a full-size prototype for tests on a brake test rig for heavy rail vehicles.

KEYWORDS: Hydraulics, Self-reinforcement, Self-energisation, Brake, Brake coefficient, Simulation, Pressure control, Friction, Friction coefficient, Trains

1 Introduction

Today, pneumatic brake systems clearly dominate in the market for heavy rail vehicle brakes. This is mainly due to the easy handling of "air", the robust safety concept which can be implemented by an end-to-end pneumatic brake line, and the simplicity of pneumatic couplings between waggons. Advantages of hydraulic brakes are short reaction times, much more compact design and higher braking forces. In commuter rail services, where reduced installation space has superior priority, hydraulic brake systems are well established. In fact, low-floor car concepts would not have been possible without switching from pneumatic to hydraulic brakes. Commonly in these trains the hydraulic brakes are connected to a power unit installed in each bogie. Since this carries the danger of loosing all brakes of a bogie in case of hydraulic power supply failure, the direction of actual developments is towards independent actuators with individual power supply, [2].

This paper presents the concept of a new brake called the Self-energising Electro-Hydraulic Brake (SEHB), which is being developed at the Institute for Fluid Power and Controls (IFAS, RWTH Aachen University) within a research project funded by the DFG (German Research Foundation). The SEHB concept was first published in [1]. It offers the advantages of hydraulic brake actuation without the mentioned disadvantages of a centralized bogie power supply. This is possible by the principle of self-energisation. The wheelset's inertia momentum is used by each calliper as the source of power to supply hydraulic pressure for braking. Only low electric power for the operation of a small hydraulic valve, pressure sensors and controller electronics is required to operate the brake as explained in Section 2. Section 3 shows that one of the major advantages of this concept is the possibility to control the actual braking torque, unlike conventional brakes that can only control the perpendicular force due to uncertainty of friction coefficient and brake radius. Inherent safety is very important for brake systems in heavy rail trains. With safety features like hydraulic-mechanical fall-back solutions presented in section 4 it is likely to be possible to meet the high safety standards of today's pneumatic brake systems. SEHB has been successfully studied in simulation with a proportional feedback control. Section 5 discusses the braking dynamics on the basis of an example design. The main aim of the project currently is the verification of the brake principle on a small scale test rig, which will be described in Section 6.

2 Working principle of SEHB

Unlike conventional brakes, where the brake calliper is mounted firmly to the bogie, in the SEHB concept it is movable tangential to the friction contact. A hydraulic supporting cylinder connects the calliper to the bogie structure, thus fixing it between two columns of oil. In case of friction contact one of the oil columns is charged with a certain pressure according to the brake force. This pressurised oil can in turn be used as a hydraulic power source for brake actuation via a control valve, see **Fig. 1**.

For understanding the SEHB working principle it may be helpful to define the difference between a self-reinforcing and a self-energising brake. For any brake principle the brake coefficient C^*, also known as the shoe factor [3], is a measure for the self-reinforcement. It is defined as the quotient of the total circumferential force on the brake area F_{Brake} divided by the tightening force of the brake shoe F_{Clamp}.

$$C^* = \frac{F_{\mathrm{Brake}}}{F_{\mathrm{Clamp}}} \tag{1}$$

For drum brakes the brake coefficient is between 1.5 to 20, [4]. A self-energising brake may now be defined as a brake where the brake coefficient C^* becomes infinite or even turns negative. This means that no tightening force is needed to achieve any desired circumferential force, and even a negative tightening force (lifting force) results in positive friction. The self-reinforcing brake amplifies an external tightening force with a specific ratio, defined by C^*. In these terms it is always a question of design whether a brake is self-reinforcing or self-energising. However, in most cases a self-energisation is not desirable because it leads to an unstable process and self-locking, if not controlled.

Fig. 2 compares two popular self-reinforcing principles, the drum brake and the wedge brake. The braking coefficients C^* depend on the design of the angle α and on the friction

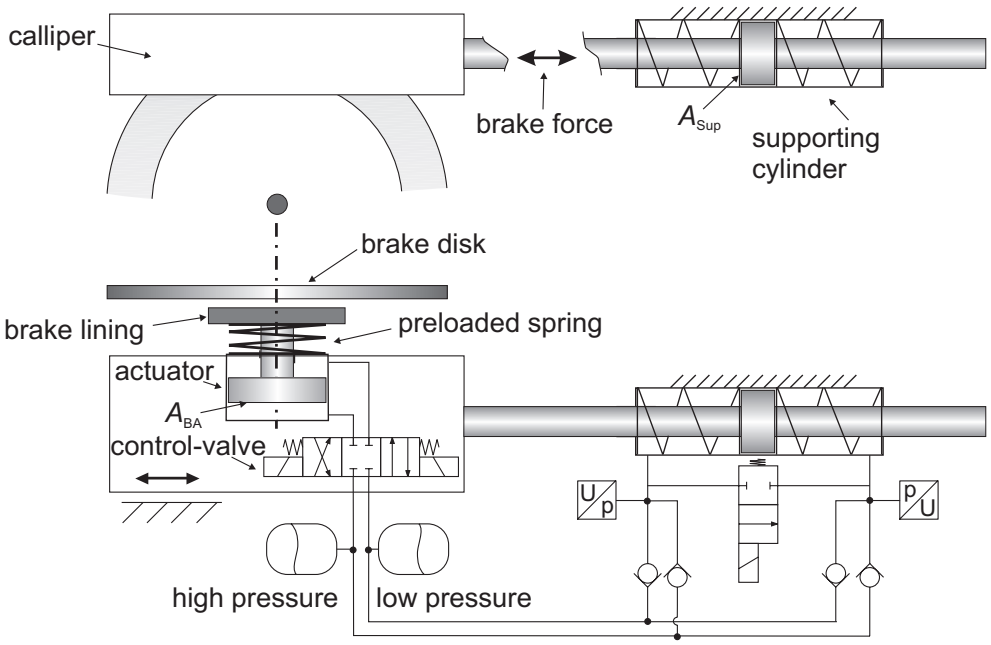

Figure 1: Principle of self-energising electro-hydraulic brake, (SEHB)

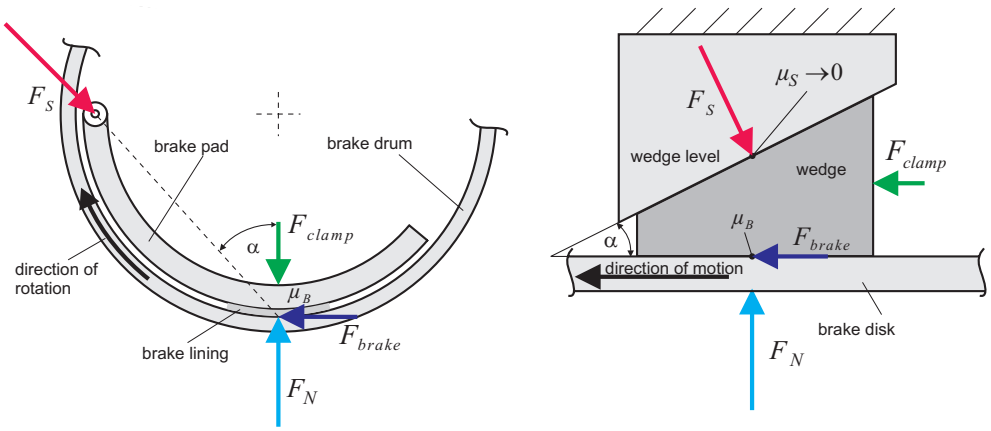

Figure 2: Comparison of the self-reinforcing principles for drum and wedge brake

coefficient μ:

$$C^*_{\text{Drum}} = \frac{\mu \tan\alpha}{\tan\alpha - \mu} \quad , \quad C^*_{\text{Wedge}} = \frac{\mu}{\tan\alpha - \mu} \tag{2}$$

In both cases, designing the brake such, that $\tan\alpha$ becomes smaller than μ, self-energisation is reached and the brake will be self-locking, if not controlled. The idea of the electronic wedge brake, developed by Siemens VDO, is to control the position of the wedge pulled into the self-energising friction contact with electric spindle nut drives. The required power of a tested prototype for auto mobiles is 100W in average during a brake actuation which is fairly low compared to concepts of direct actuation, [5], [6].

Similarly the self-energising electro-hydraulic brake has design parameters that determine whether the brake is self-reinforcing or self-energising. The following considerations apply in the case where the right flow scheme of the proportional brake valve in Fig. 1 is active. Given an actual brake force, the smaller the A_{Sup}, the higher the pressure in the supporting cylinder. Consequently, the bigger the A_{BA}, the higher the perpendicular force

is achieved. The brake coefficient C^* of the self-energising hydraulic brake thus depends on the ratio between the pressurised piston area in the supporting cylinder A_{Sup} and the brake piston area A_{BA}.

$$C^*_{\mathrm{SEHB}} = \frac{i_{\mathrm{L}}\mu}{\frac{i_{\mathrm{L}}A_{\mathrm{Sup}}}{2A_{\mathrm{BA}}} - \mu} \tag{3}$$

If the supporting cylinder is connected to the calliper via a joint lever, an additional gear transmission ratio i_{L} has to be accounted for in Eq. 3. By the factor 2 the fact is considered that the perpendicular force is applied from both sides of the brake disc. For the derivation of the SEHB brake coefficient, F_{clamp} was assumed to be the spring force at the actuator. The precondition for self-energisation follows from Eq. 3 and yields:

$$\frac{i_{\mathrm{L}}A_{\mathrm{Sup}}}{2A_{\mathrm{BA}}} \overset{!}{\leq} \mu \tag{4}$$

The special feature of the SEHB concept is that by activating the left flow scheme of the proportional brake valve in Fig. 1, self-energisation is turned into self-extinction. As simulation shows in section 5, all is needed is a small solenoid to actuate the valve of the size like those used in automotive antilock brake system.

Fig. 1 contains some features that have not been explained yet. Obviously, without further actuation, the brake is not energised during a stand-still or when the brake is not engaged yet. A spring between actuator and brake pad bracket presses the actuator against the brake disk. When opening the proportional brake valve, the spring initiates the braking operation. The energy to lift the brake actuator away from the brake disk and to set a defined clearance must be provided by a high-pressure accumulator that is charged during regular operation. The low-pressure accumulator depicted in Fig. 1 is necessary as an expansion tank because the brake actuator is a differential cylinder. A differential cylinder takes in more volume when it is extended. Without an expansion tank, cavitation would occur. High-pressure and low-pressure sides are separated by check valves that act as a hydraulic rectifier and allow bidirectional braking. The springs in the chambers of the supporting cylinder allow the retraction of the supporting cylinder to its initial mid position when the brake is lifted and the 2-way switching valve is opened.

3 Control strategy of SEHB

The SEHB concept allows the direct control of the actual friction force, independently of friction coefficient changes. Since μ is influenced by speed, brake pressure and temperature, for conventional brakes it is an unknown parameter. Uncertainty about μ consequently means uncertainty about the actual friction force F_{brake} and the retardation torque respectively. The retardation torque, however, is the control variable for vehicle dynamics control systems like the Electronic Stability Programs (ESP). The dynamics of self-reinforcement of SEHB depends on the friction coefficient μ, similar to the drum and wedge brake as can be seen in Eq. 3. But SEHB offers a simple way to measure the actual friction force F_{brake} via pressure transducers connected to the chambers of the supporting cylinder. Therefor the load pressure in the supporting cylinder can be used as control variable for SEHB in a closed loop control.

Proportional-action controllers offer a suitable solution for conventional valve-controlled closed-loop pressure control systems without disturbances in the form of volume flow

values, [7]. The proportional controller was therefore used in simulative examinations of SEHB. It proportionally controls the valve input corresponding to the deviation of the actual friction force from a given set value, see control scheme in Fig. 5. If the deviation is positive (actual brake force is smaller than required brake force) the control valve is acuated to apply high pressure to the piston face (right flow scheme). If the deviation is negative, it connects the piston face to low pressure side. The valve closes completely when the setpoint is achieved. Further investigations are being carried out at IFAS to adapt the friction force control to the varying operating conditions.

4 Safety features of SEHB

A new brake actuator for railways must comply to or exceed the high safety performance of state-of-the-art air brakes. According to the basic safety policy a brake has to be fail-safe, [8]. In any case of failure of control systems or components a brake system must fall back into a fail-safe mode, to stop the train within a predefined maximum distance. Safety requirements for railway brake actuators also include that the power for braking has to be inexhaustible in all possible scenarios. A passive adaptation of brake force respective wagon load as well as wheel slide protection systems (WSP) are essential to keep braking distances within the limits defined by the railway operator. The maximum braking distance should be as small as possible since it has direct influence on the travel interval between successive trains. SEHB depends on closed loop control, therefore special attention has to be given to fail-safe features that work without electric energy. **Fig. 3** shows which safety properties (inexhaustibility, load adaptation, and wheel slide control) have to operate in different braking scenarios. Safety is a property of a brake system as well as of each brake actuator. This section focuses on solutions for a fail safe brake actuator. The safety properties

- inexhaustibility and
- load adaptation

shall be discussed and a solution for SEHB will be presented. Since wheel slide control can be achieved by adapting the friction force set value for the brake, it is not further discussed here.

Inexhaustibility Air brakes have air reservoirs mounted in the wagons supplying power, enough that they are assumed as inexhaustible, considering that air is also delivered from the main brake line. SEHB is inexhaustible by principle since the brake power comes from the train's motion. There are a few exceptions, however, which need a closer look.

1. *Supporting cylinder in end position.* The brake controls must prevent the critical situation, that the supporting cylinder would reach its end position.
2. *Repeated braking and venting during stop.* Activating the brake during stand still (e.g. for test purposes) releases pressure off the high-pressure accumulator to accelerate the brake initiation.

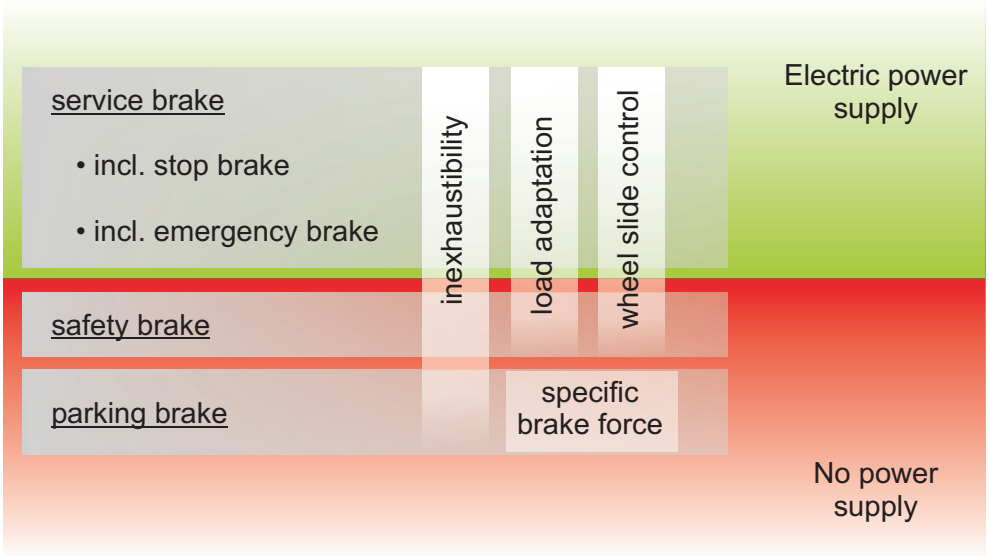

Figure 3: Safety properties of railway brake

3. *Leakage.* Long periods of standing on a slope require the cylinders to be absolutely leak proof especially the supporting cylinder that carries the load

Several design requirements result from these critical points. For example the supporting cylinder stroke should be enough to deliver power for any operating condition. Blending between brakes in one bogie is a method to permit the retraction of one actuator while the others are in service. Through proper accumulator design it has to be ensured that there is always enough pressure left to lift the brake pads from the disk. Leakage has to be minimized in the control valve and prevented, especially at the piston sealing in the supporting cylinder and all external sealings. The parking brake has to maintain its braking pressure for long periods of time up to several years. A separate or separable pressure circuit might be helpful as a proof of safety for the parking brake. Seat valves are widely used as safety relevant components in applications where heavy loads have to be hydraulically held e.g. in jacks, cranes, and elevators. A seat valve like the parking valve shown in **Fig. 4** significantly reduces the number of safety relevant sealings.

For parking, a specified friction force has to be ensured. According to [9] the minimal brake force of the parking brake in a commuter train has to ensure stand still of the empty train in a slope of up to 4%. In case every brake of a train has a parking brake mode, this results in a relatively small braking force for each brake. A pressure reduction valve can be used to load a parking accumulator with a corresponding parking pressure during regular service. This parking pressure is applied on the actuator for parking.

A differential cylinder produces the clamping force

$$F_{\mathrm{clamp}} = p_{\mathrm{A}} A_{\mathrm{area\_of\_rod}} + (p_{\mathrm{A}} - p_{\mathrm{B}}) A_{\mathrm{area\_of\_ring}} \tag{5}$$

With both chambers pressurised it still produces a braking force with the advantage that no leakage can occur between the piston and the cylinder boring. The parking valve depicted in Fig. 4 connects the high-pressure line with both actuator chambers. Thus, the number of safety-critical parts is reduced to the external piston rod sealing and the check valves to high and low-pressure feed lines.

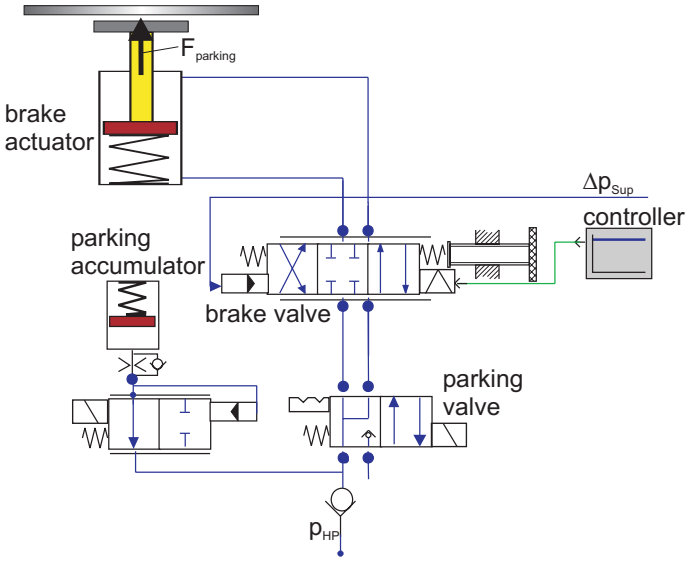

Figure 4: Separate parking circuit through parking valve and brake valve with hydraulic pressure feedback

Load adaptation Since the kinetic energy $E_{\text{kin}} = \frac{1}{2}mv_0^2$ grows proportional to the translatory and rotary inertia m of the train, the retardation torque must be load dependent to satisfy required stopping distances. Air brakes match the brake demand signal with the pressure in the air suspension to achieve the required load adaptation. The SEHB load adaptation could be done by the brake controller in terms of signal processing using pressure transducers. Special care would have to be given on the reliability of the sensors and their energy supply.

The concept of SEHB is capable of incorporating a subsidiary hydraulic–mechanic fall-back solution which also allows a secure load adaptation without sensors. Therefore it provides a fail-safe mode in case of total loss of electric power. As can be seen in Fig. 4, the valve spool is balanced between two springs of which the right one can be offset by an actuator. By creating a leftward offset of the right spring, in case of electricity drop-out the valve would give way for braking. On the opposite side of the valve spool, high pressure from the supporting cylinder is applied, resulting in closing the valve spool when a specified pressure is reached. The offset of the spring could be designed to depend on the air pressure of the air suspension to achieve the load dependency.

5 Simulation of SEHB

A DSH*plus* simulation model served the verification of the SEHB concept. **Fig. 5** illustrates the layout of the model. It is comprised of a hydraulic section with cylinders, accumulators and valves, and a signal section including the state dependent friction coefficient and the closed loop control.

Friction force calculation The parameters of the components represent the current development status of the first prototype. The brake force calculation corresponds to a

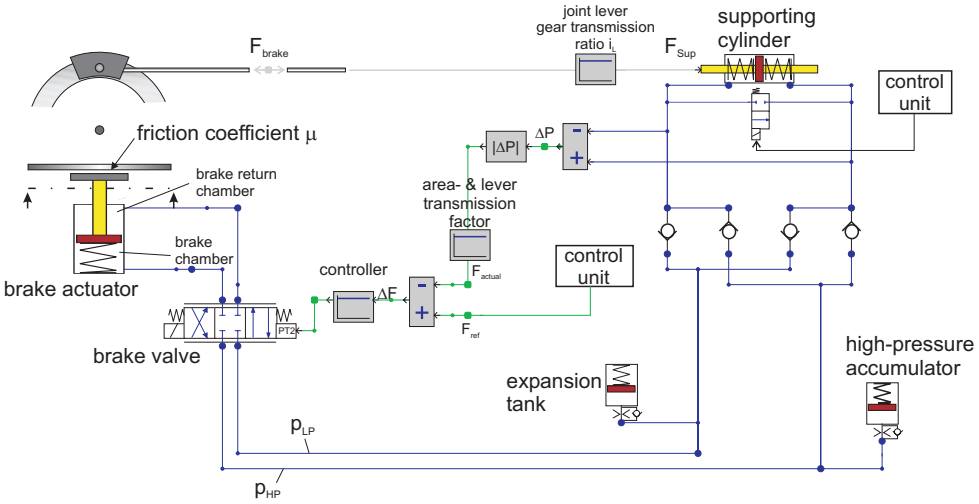

Figure 5: Layout of the brake simulation model

fictive train car design that has been agreed on within the research project “EABM” of the German Research Foundation (DFG).

- Maximum speed: $v_0 = 120\ \frac{\mathrm{km}}{\mathrm{h}}$
- Maximum waggon load: $m = 13.6\ \mathrm{t}$
- Two pairs of individual wheels, four disc brakes
- Diameter of wheel (new / old): $d_{\mathrm{wheel}} = 920\ \mathrm{mm}/840\ \mathrm{mm}$

According to [9], taking a maximum stopping distance of 500 m at maximum velocity and a response time of 0.8 s into account, it makes sense to calculate the brake parameters for a maximum deceleration of $d = 1.2\ \frac{m}{s^2}$. The maximum retardation force F_d is then calculated by multiplying the mass inertia per disc brake times deceleration plus a constant force resulting from slope of $s = 4\ \%$ and acceleration of gravity g. The rotary inertia of wheels and drives is included with a factor $k_r = 1.1$ in the translatory inertia.

$$F_d = \frac{m}{4}(k_r d + sg) = 5822\ \mathrm{N} \tag{6}$$

The maximum friction force F_{brake} acting on a friction radius of $r_\mathrm{f} = 245\ \mathrm{mm}$ then yields:

$$F_{\mathrm{brake}} = F_d \frac{d_{\mathrm{wheel_{new}}}}{2 \cdot r_\mathrm{f}} = 10931\mathrm{N} \tag{7}$$

Brake design parameters The supporting cylinder translates the friction force into pressure via a potential joint lever with gear transmission ratio $i_\mathrm{L} = 1.8$. The supporting cylinder has a piston diameter of $d_{1\mathrm{Sup}} = 32\ \mathrm{mm}$ and a piston rod diameter of $d_{2\mathrm{Sup}} = 20\ \mathrm{mm}$. At maximum brake force it produces a pressure of $p_{max} = 222\ \mathrm{bar}$. Friction of the supporting cylinder is parametrised with $50\ \mathrm{N}$ breakaway force. The size of the actuator follows from the precondition of self-energisation, Eq. 4. The minimum friction coefficient is appointed $\mu > 0.1$. From manufacturer catalogue data an appropriate differential thruster with piston diameter of $d_{1\mathrm{BA}} = 80\ \mathrm{mm}$ and piston rod diameter

of $d_{2\mathrm{BA}} = 60\ \mathrm{mm}$ with $40\ \mathrm{mm}$ stroke is chosen. Friction is parametrised with $200\ \mathrm{N}$ breakaway force. The spring in the actuator initiates the braking, and compensates for all losses due to friction and pressure difference in the system. Its task is twofold. Firstly it overrides friction $F_{f\mathrm{BA}}$ and pressure force $F_{\Delta p} = \frac{\pi}{4}(p_{1\mathrm{BA}} d_{1\mathrm{BA}}^2 - p_{2\mathrm{BA}}(d_{1\mathrm{BA}}^2 - d_{2\mathrm{BA}}^2))$ in the brake actuator. This is to pull out the actuator piston until clearance is zero. The second task is to compensate friction $F_{f\mathrm{Sup}}$ and spring force $F_{\mathrm{Spring_{Sup}}}$ in the supporting cylinder which has a suppressive effect on the self-energisation, once the friction contact is achieved. From this requirement follows Eq. 8 to calculate the spring force F_{Spring}.

$$F_{\mathrm{Spring_{BA}}} = F_{\Delta p} + F_{f\mathrm{BA}} + \frac{F_{f\mathrm{Sup}} + F_{\mathrm{Spring_{Sup}}}}{2\mu^2} \tag{8}$$

For the presented simulation the spring in the actuator applies $1225\ \mathrm{N}$ and has a stiffness of $35\ \frac{\mathrm{N}}{\mathrm{mm}^2}$. The balancing springs in the actuator have a cumulative stiffness of $4\ \frac{\mathrm{N}}{\mathrm{mm}^2}$. The brake valve is parametrised as a zero-overlapped 4/3-way control valve with $2\ \frac{\mathrm{l}}{\mathrm{min}}$ nominal flow at $35\ \mathrm{bar}$ and $30\ \mathrm{Hz}$ natural frequency. The low value is intended to accentuate the fact that robust, reasonably priced components can be used. The high-pressure accumulator has a storage capacity of $8\ \mathrm{ml}$, enough for retracting the actuator for more than $3.5\ \mathrm{mm}$. The expansion tank has a storage capacity of $141\ \mathrm{ml}$. Fully charged it generates a system pressure of around 5 bar on the low-pressure side. The accumulator is fully charged when the brake piston is completely retracted.

The parameters of the fluid simulate the behaviour of HLP 46 hydraulic fluid. Pressure dependency of the bulk modulus and the influence of contained air is accounted for. The bulk modulus has a significant influence on the initiation performance of the brake, as proved by simulation. The simulation results shown below were yielded for an undissolved air content of 0.1%.

The mechanical stiffness of the brake calliper, brake linings and brake disc is estimated to be $25\ \frac{\mathrm{kN}}{\mathrm{mm}}$. At the beginning of a simulation a clearance of $0.5\ \mathrm{mm}$ is parametrised between brake pads and disc.

Friction coefficient model The frictional force is calculated using a characteristic diagram. It was derived in the context of this research project from test data supplied by a manufacturer of brake linings. Based on the conclusion found in various friction related publications [10], that temperature below a critical value of approximately $150\ ^\circ C$ does not have a distinct influence, **Fig. 6** shows the friction coefficient trajectory in relation to velocity and pressure used for the simulation.

The friction model facilitates a more realistic simulation. The friction coefficient rises while the vehicle is decelerating. Therefore the brake controller will act to minimize the resulting brake force deviation. Also for the initiation of the brake it gives valuable insight. For very low braking pressures, as they occur in the initiation phase, the friction coefficient and the self-energisation respectively is lower than for higher pressure. This leads to more realistic evaluation of the rise time of the brake.

Simulation results The simulation results provide evidence of the dynamic efficiency of the brake. The dynamic performance essentially depends on whether the high-pressure accumulator has been charged by a previous braking operation or not. It also gives insight

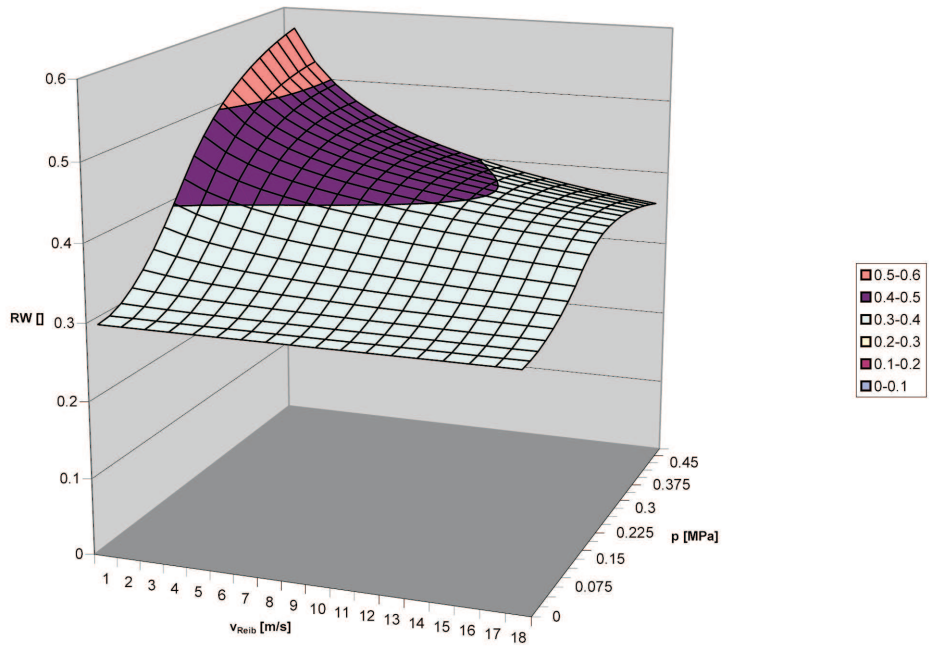

Figure 6: Characteristic diagram of friction coefficient over velocity and pressure

into the system's dead time. This can be defined as the period between brake demand and $10\ \%$ achievement of the set value.

The response of the brake can be demonstrated particularly well with reference to a sudden change in the reference input variable. This is not intended to be the simulation of a typical rail vehicle braking operation, which, of course, is not sudden for reasons related to passenger comfort and safety. The achievable brake dynamics plays an important role for wheel slide protection performance and constitutes one of the main advantages of hydraulic systems over pneumatic brakes. Three simulations with sudden changes in the reference input variable give information about the expected dynamic performance of the brake:

1. Initiating braking with maximum braking force $F_{\mathrm{brake}} = 10931\ \mathrm{N}$ with high-pressure accumulator completely discharged, Fig. 7
2. Venting the brake and setting the air clearance, Fig. 8
3. Initiating braking with maximum force with preloaded high-pressure accumulator, Fig. 9

Under worst-case conditions, the high-pressure accumulator is completely empty and cannot make any contribution towards overcoming the air clearance. **Fig. 7** shows the result of the above specified simulation for the case when the brake is initiating without pressure in the high-pressure accumulator.

Because of the relatively strong spring in the actuator the clearance is overridden in only $150\ \mathrm{ms}$. After that for a time of about a second nothing much seems to happen. The only significant change takes place in the movement of the supporting cylinder. It moves

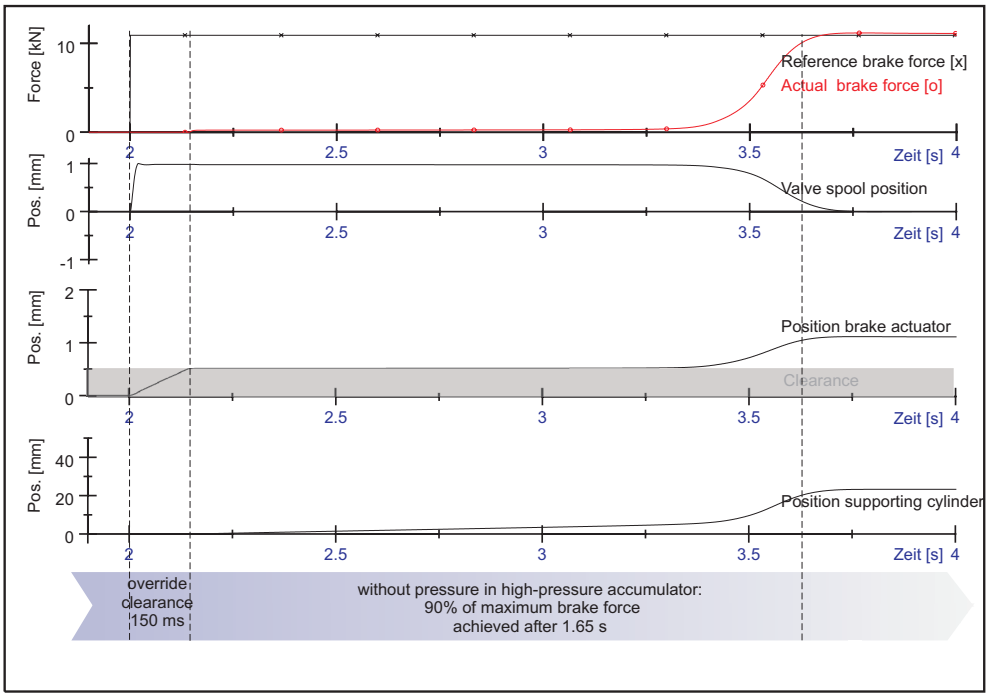

Figure 7: Simulation of braking initiating with maximum braking force $F_{\text{brake}} = 10931$ N with high-pressure accumulator completely discharged

4.4 mm while the braking actuator only moves 8 μm without any changes in the high-pressure accumulator. The reason why the self-energisation starts so slowly is because of the compressibility of the fluid which, at low pressures with small contents of unsolved air, is comparatively low. The orifices and friction forces in the system slow down the initiation process. Therefore, in the development of SEHB, special care has to be given on friction and compressibility. A previous plan to use silicon oil as alternative braking fluid was cancelled for the sake of its lower bulk modulus compared to mineral oil. The rise time for 10 % of the maximum force of 10931 N is 1.41 s, the rise time for 90 % is 1.65s, which is too slow for a future implementation. Reducing the dead time is very important for reducing stopping distance and has to be further studied.

If the braking force set value suddenly changes to 0 kN the servo-valve opens in the other direction and relaxes the compressed fluid of the brake piston to the expansion tank. The brake actuator releases, as shown in **Fig. 8**.

During venting the brake the high-pressure line is connected to the surface of the brake actuator piston ring, increasing the relaxing effect. The surface of the brake actuator piston ring is small compared with the surface of the piston face, which means that considerably less volume flow is required for the return stroke. The fluid stored in the high-pressure accumulator is sufficient to lift the brake, as is shown by the fact that the supporting piston does not give way any further. It even moves backward slightly as the previously highly compressed fluid relaxes. The proportional-action controller is not capable of cancelling out the brake force completely. The spring power in the brake actuator acts as a disturbance and, where a proportional-action controller is used, the principle is such that a permanent system deviation remains. The final static value is reached after around 0.5 s with 125 N supporting force. At this moment ($t = 5.3$ s), a control pulse opens the servo-valve negatively again for controlled lifting of the actuator away from the brake disk and to set a predetermined air clearance.

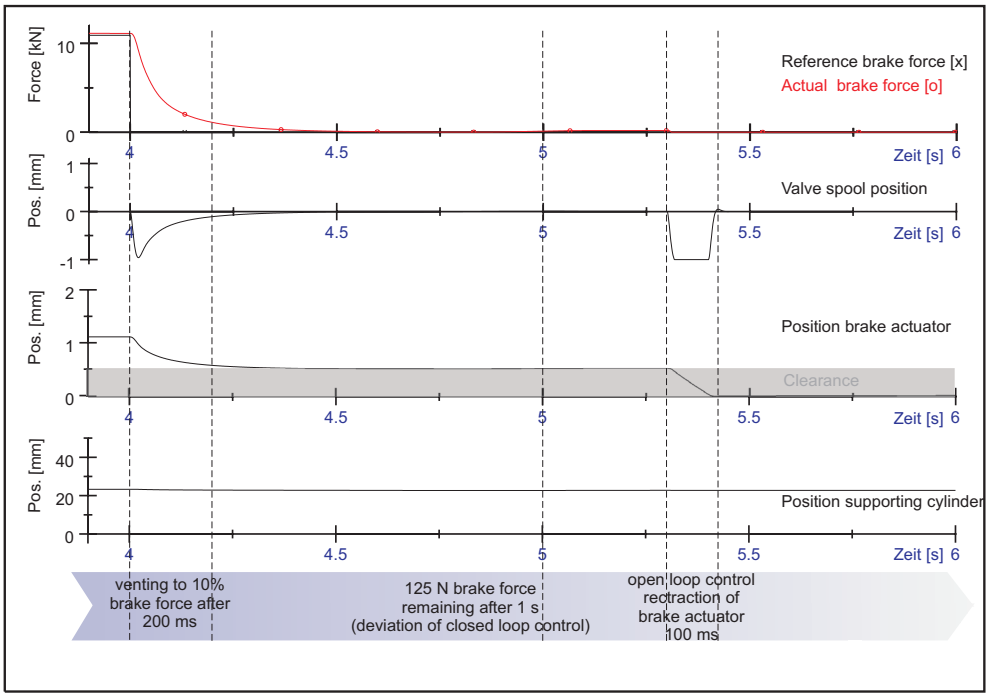

Figure 8: Simulation of venting the brake and setting the air clearance

Under normal operating conditions, it may be assumed that the high-pressure accumulator is still preloaded from a previous braking operation. **Fig. 9** shows the way in which the response time improves when the high-pressure accumulator is preloaded.

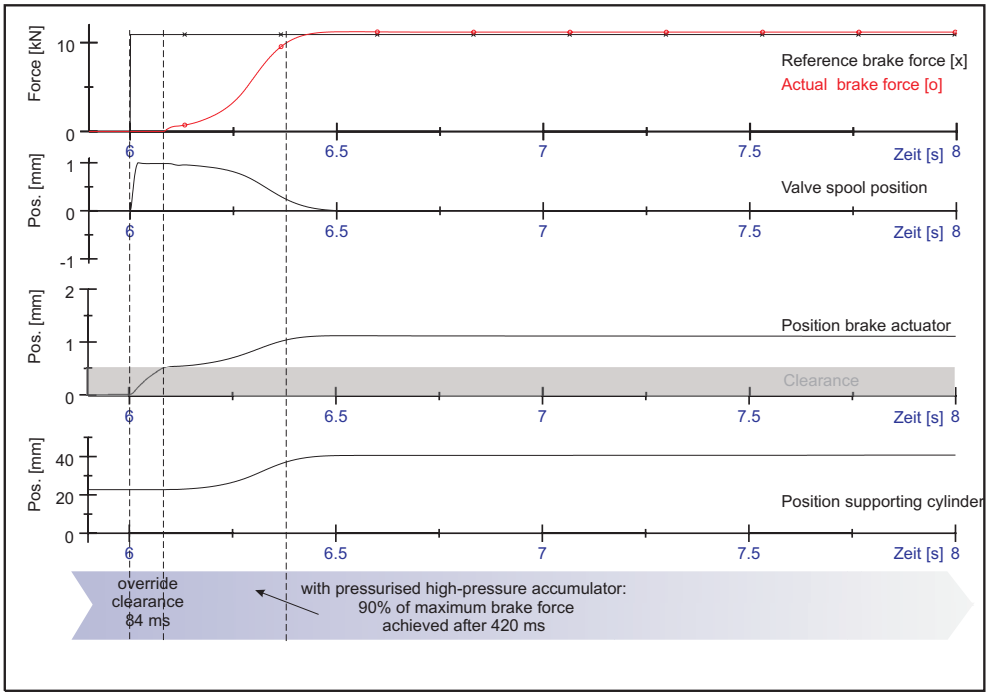

Figure 9: Simulation of braking initiation with maximum force with preloaded high-pressure accumulator

The application spring in the brake actuator is now assisted by the high-pressure accumulator, so that the brake linings are already being pressed against the brake disk after $84\ \mathrm{ms}$.

Compared with the characteristic shown in Fig. 7, the self-energizing process ignites with a much steeper initial gradient. It has reached $10\ \%$ of the target value of $10.931\ \mathrm{kN}$ already after $165\ \mathrm{ms}$ and $90\ \%$ after $336\ \mathrm{ms}$. The total period, including the dead time required to overcome the air clearance, amounts to $420\ \mathrm{ms}$. This means that the time for reaching $10\ \%$ of the target value has been reduced by $88\ \%$ and for $90\ \%$ target value by $74\ \%$.

6 Prototype design

Current efforts focus on the implementation of the self-energising electro-hydraulic brake. After having analysed the principle and its dynamics in simulation it is a vital matter to verify the theoretic results by laboratory tests. For this purpose a down-scaled prototype is being designed on the basis of a automotive brake disc driven by a hydrostatic velocity controlled drive in connection with a flywheel. The goal is to prove the hydraulic design which is independent of the size of the brake disc. With the experience gained from experiments with the first prototype which are scheduled for April 2007, a second prototype will be designed for testing on a railway roller dynamometer. **Fig. 10** shows the assembly of the first SEHB prototype.

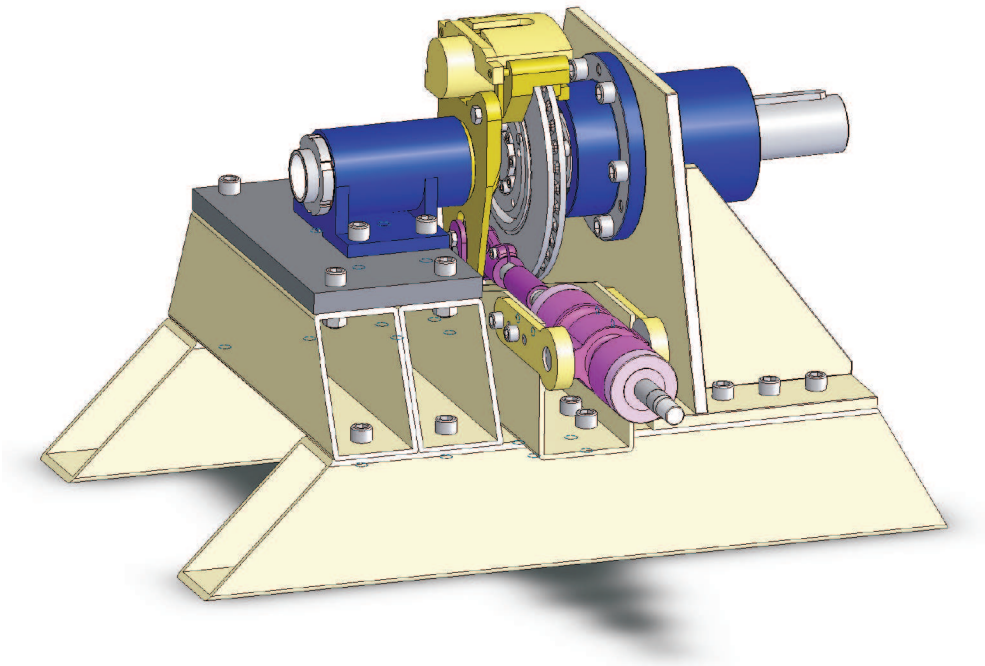

Figure 10: Design of the first testing prototype of self-energising electro-hydraulic brake

The brake and the brake disk are mounted on two separate aligning shafts. The supporting cylinder is connected to the brake calliper via a lever with a slotted hole that allows adjustment of the transmission ratio. The brake calliper is from an original car brake since the SEHB principle does not necessarily need a double acting differential thruster as brake actuator. **Fig. 11** shows a sectional view cut through the calliper.

A special feature of this arrangement is that the shaft which the brake is mounted on

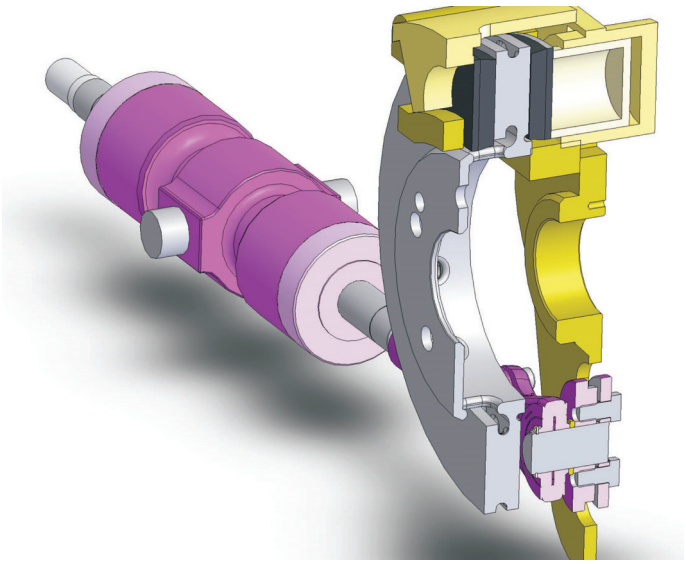

Figure 11: Sectional view of SEHB

experiences twice the braking force, because both brake calliper and supporting cylinder, conduct the same force into the lever if the transmission ratio i_{L} is 1. This setup was chosen because it causes only few flexural stresses and yet is very compact. Efforts to put the supporting cylinder in tangential alignment to the friction radius result in a bigger design. It is also important to note that to connect the supporting cylinder on a radius larger than the friction radius ($i_{\mathrm{L}} > 1$) necessitates a smaller supporting cylinder or a larger brake actuator respectively, as can be seen from Eq. 4. Since the piston area of the automotive brake could not be arbitrarily changed, it was important in this case to reach $i_{\mathrm{L}} = 1$.

7 Conclusion and Outlook

The principle of a Self-energising Electro-Hydraulic Brake for a railway application was introduced and discussed concerning some specific railway related safety issues. A more comprehensive safety concept will be addressed in future work. The control concept has been explained. Currently, only a proportional-acting controller has been applied in simulative studies. Further studies are being done to analyse the dynamic interaction in theory and enhance the closed-loop performance using an adaptive controller. We will also pursue a control using switching valves in analogy to ESP and ABS systems. The dynamic performance has been shown in simulation. In the actual simulation phase the brake shows good performance during braking, anticipating good braking performace in applications using wheel slide control, but also shows shortcomings in reaction times for the case when the brake has to override clearance. A better choice of spring stiffness for the springs in the cylinders, friction force minimization, and optimization of accumulators will be further investigated. The assembly of the first prototype design has been presented. The results from measurements scheduled April 2007 will be used to improve the simulation model and thus serve for a deeper understanding of the system. On this basis a second prototype will be designed for testing on a railway roller dynamometer. The authors want to express their thank for the support by the German Research foundation

(DFG).

References

[1] Matthias Liermann, Christian Stammen *Selbstverstärkende hydraulische Bremse für Schienenfahrzeuge - Intelligentes, Integriertes Einzelrad-Antriebs-Brems-Modul*, O+P 10/2006, 500-507

[2] Johannes Carsten Kipp *Elektrohydraulische Bremssysteme für schienengebundene Nahverkehrsfahrzeuge*, ZEV+DET Glasers Annalen, Vol 119 , 518–524, 1995.

[3] William c. Orthwein *Clutches and Brakes - Design and Selection, (2^{nd} Edition)*, Marcel Dekker, 2004

[4] Bert Breuer, Karlheinz H. Bill (Publisher) *Bremsenhandbuch - Grundlagen, Komponenten, Systeme, Fahrdynamik [Brake Handbook - basic principles, components, systems, dynamic of vehicle movement], (2^{nd} Edition)*, Vieweg Verlag, 2004

[5] Bernd Gombert, Philipp Gutenberg *Die elektronische Keilbremse – Meilenstein auf dem Weg zum elektrischen Radantrieb*, ATZ 11/2006, Vol. 108, 904-913

[6] Toni Lewin *Second chance for by-wire brakes*, Automotive News Europe, 12/06/2006, p. 13

[7] Hubertus Murrenhoff *Servohydraulik [Servo-Hydraulics], 2^{nd} Edition*, Shaker Verlag, 2002

[8] UIC 540 *Brakes - Air Brakes for freight trains and passenger trains, 5^{th} Edition*, International Union of Railways, Railway Technical Publications, Nov. 2006

[9] DIN EN 13452-1 *Railway applications – Braking – Mass transit brake systems - Part 1: Performance requirements*, 2005

[10] Nikolaj Krieg *Modellierung und Simulation eines zustandsabhängigen Reibkontaktes und Temperaturentwicklung am Beispiel einer Schienenfahrzeugscheibenbremse*, student research project at IFAS, RWTH Aachen, 2006

INTELLIGENT OIL FLOW MANAGEMENT WITH EFM: THE POTENTIALS OF ELECTROHYDRAULIC FLOW MATCHING IN TRACTOR HYDRAULICS

Dipl.-Ing. K. Mettälä, Dipl.-Ing. M. Djurovic, Dr.-Ing. G. Keuper, Dr.-Ing. P. Stachnik
Bosch Rexroth AG
BRH-STF2
Postfach 30 02 40
70442 Stuttgart, Germany
Phone +49 711 811 49032, Fax +49 711 811 518 49032
E-mail: kari.mettala@boschrexroth.de

ABSTRACT

Electrohydraulic flow matching (EFM) is a new concept for the implement hydraulics in mobile working machines. From a large variety of alternatives, some solutions were selected for practical testing in a tractor. The system is based on commercially available components from the mobile hydraulics components program of Rexroth. The first test results confirm the suitability of the concept in practice. It shows especially good dynamic behavior as well as low energy consumption. The commands from the operator are transferred directly and without delay into working movements in the machine. Therefore, the operator is less stressed and the operation of the machine becomes easier.

KEYWORDS: control systems, robustness, dynamic, energy consumption

1. INTRODUCTION

The hydromechanically controlled hydraulic systems are widely used today in different kinds of working machines in the middle and the upper power classes. The trend in research during the last years, however, has gone more and more into the direction of electrohydraulic systems, in which the hydraulic processing of the signals is replaced by an electric control system. The main goal of these activities is the improvement of the static and dynamic behavior of the systems as well as an increase in flexibility. Hence, the machines are able to cope with increasingly complex tasks.

The electrohydraulic flow matching (EFM) is one of these new concepts. The large variety of its solutions makes it interesting for mobile working machines. In this study, an EFM-system was tailored to the tractor application.

2 EFM IN A TRACTOR APPLICATION

2.1 Load-Sensing – the conventional solution

The tractors in the middle and the high power classes set high demands for the implement hydraulics systems:

- low energy consumption
- stable functions
- load-compensated oil supply to the consumers
- high level of robustness and reliability
- easy handling
- low purchase and maintenance costs

Load-sensing-systems (LS) fulfill most of these requirements very well and are therefore widely used. The conventional LS-system is shown in figure 2.1. The hydromechanic LS-controller controls the pump so that the pressure in the pressure line is always kept at a fixed level higher than the highest load pressure in the system. The set pressure difference over the system guarantees the adequate supply to the consumers. The individual pressure compensators are located before the control edges in the mobile valve and are used for avoiding the interaction of the parallel connected consumers.

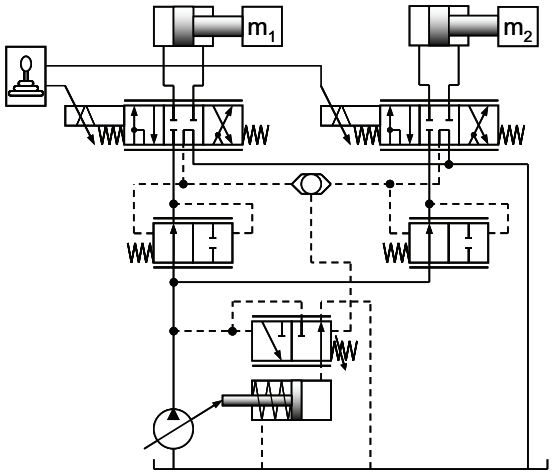

Figure 2.1: Conventional LS-circuit used in tractor hydraulics

LS-systems are well established on the market. Nevertheless, the hydraulic processing of the signals in the system limits the flexibility of the system layout as well as the system control. In some cases, this can lead to problems regarding the tuning of the sys-

tems. The electric signal processing offers the possibility to decrease these problems and to improve the performance of the system.

2.2 The principle of the EFM system

In an EFM-system the variable pump is controlled electrically. The target is to supply a user-dependent oil flow, i.e. a flow from the pump which is exactly matched to the demand of the consumers in the system. The solution is to control the variable pump according to the commands of the operator [4, 5, 6]. In this case a pure flow control is used. Figure 2.2 shows such a system.

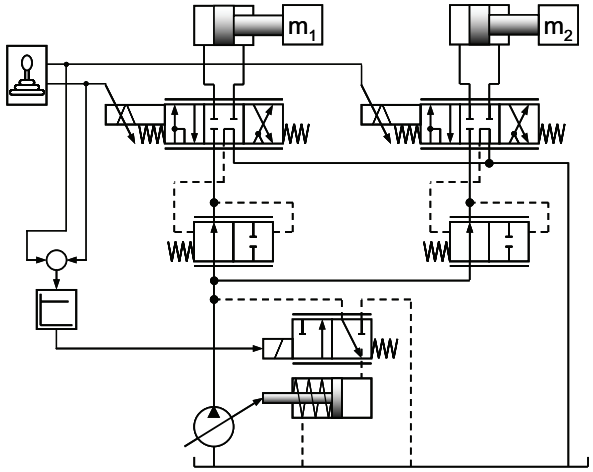

Figure 2.2: Principal circuit of an open loop EFM-system

The basic system and the function of the valve control is similar to LS-systems. The major difference is in the pump control. The LS-line from the valves to the pump is missing. In order to be able to control this kind of EFM-system, the swivel angle of the pump must be controlled proportionally according to the control signal. Thanks to the electric pump control the system reacts almost without delay to the operator's commands. This means a good response of the system and a better controllability of the working movements.

The static accuracy of an open loop EFM-system depends on the linearity of the pump controller and the volumetric efficiency of the pump. In order to electrically compensate these errors depending on the working-point, several sensors as well as a sophisticated pump control is needed.

A simple and more cost efficient alternative is to use a 3-way pressure compensator in the inlet element of the valve block (figure 2.3). If the pump is supplying too much flow, the excess flow is led over the pressure compensator back to the tank. The control strategy of the system is based on a small, pre-defined overshoot of the pump flow, either by directly measuring the excess-flow after the pressure compensator or indirectly by measuring the position of the spool of the pressure compensator. The second solution is preferred because of the higher robustness as well as the good availability of position sensors.

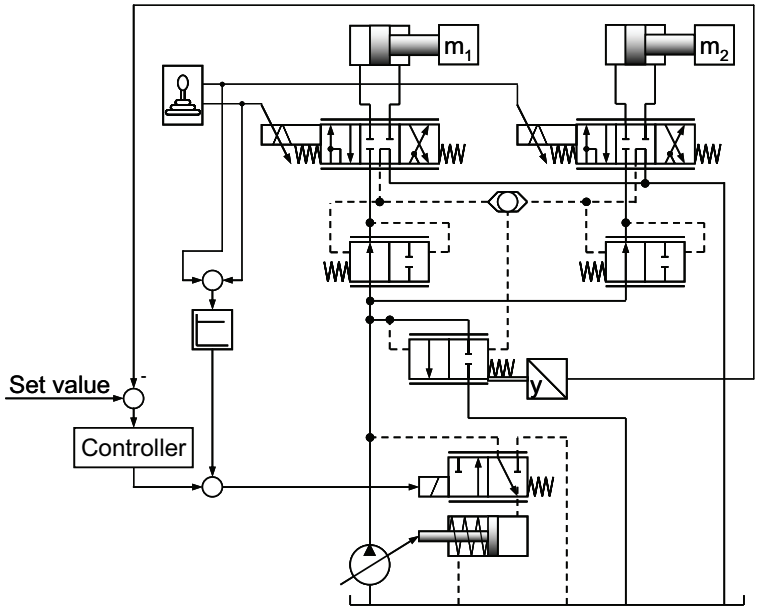

Figure 2.3: Principal circuit an EFM-system with 3-way pressure compensator

The position-control of the pressure compensator is responsible for compensating the relatively low flow error of the open loop EFM-system. In order to save energy, the excess flow over the pressure compensator should be kept as low as possible. However, the excess flow also provides a flow reserve, wich, in some cases, can enhance the system's reactiveness. The electric signal processing enables a flexible commanding of the position control of the pressure compensator and the adaptation to different demands. The consumers with a constant flow can be operated with a very small excess flow, when – for example in case of changing movements – an adequate flow-reserve can be served.

2.3 Testing in a tractor

The represented EFM-system was tested in middle-power class tractor. The electronic control was realized with a development environment of MATLAB/Simulink/dSPACE. The main components in the new system were a variable pump A10VO63EK1DS [7] and a mobile control block SB23LS-EHS [8] from the standard mobile hydraulics program of Rexroth. The changes in comparison to the standard installation of the system were small. In order to have the possibility to make comparisons, the conventional LS-system remained in the tractor and could also be used. The LS-pressure difference was set to 2.5 MPa in order to guarantee the maximum pump flow in the system.

Several standard working-cycles were developed for the practical testing of the system in the tractor. In the figure 2.4. shows a selection of two of these cycles. The cycle "mowing the shoulder" with the rotational cutter function as a constant, continuous consumer is ideal for energy measurements. The cycle "loading a trailer with a front loader" was used for the dynamic tests. All measurements were carried out with a ma-

chine in standstill, although the driving time was taken into account in the cycles.
.

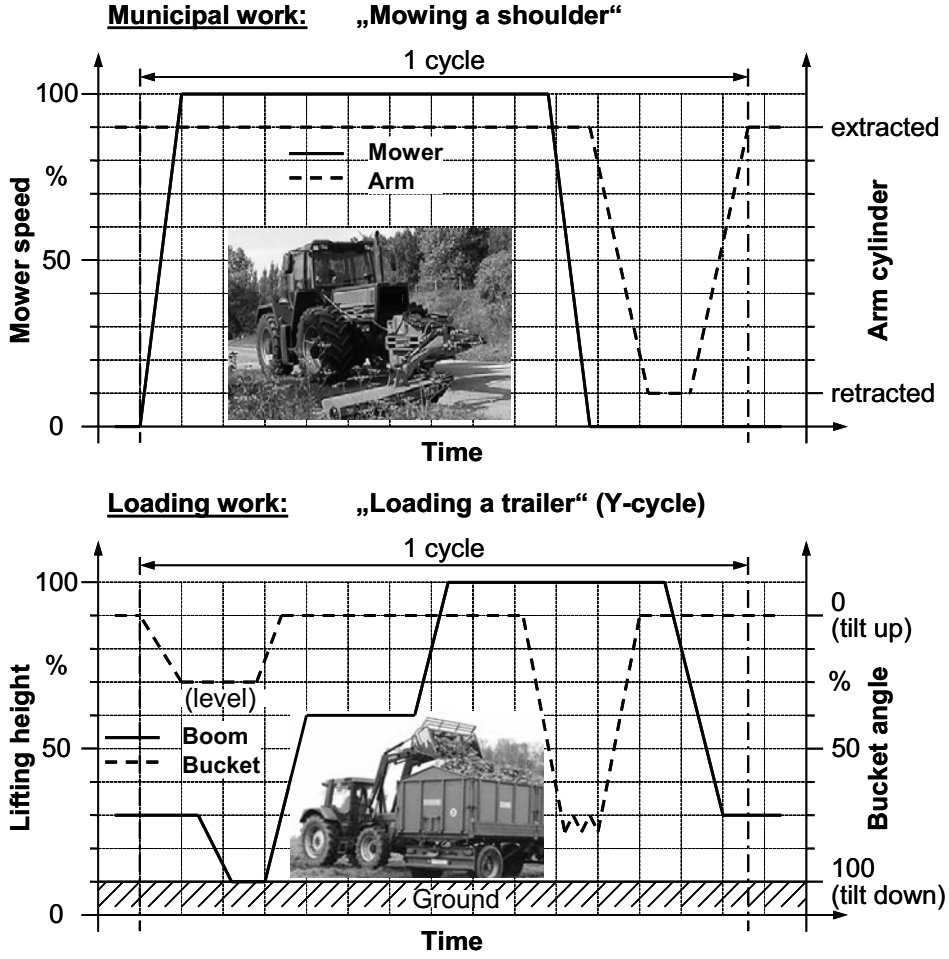

Figure 2.4: Standard cycles for the study of the machine

As shown in figure 2.5 the energy-loss using the EFM-system is significantly lower compared to an LS-system. This corresponds to an improvement of about 5% of the efficiency related to the hydraulic energy supplied by the pump. This improvement depends largely on the working cycle of the machine. Actually, the energetic advantage of the EFM-system is in principle always reached while the pressure overshoot is automatically adjusted according to the flow requirement of the system. Especially during partial loading, the EFM-system offers its advantages. A further improvement of efficiency can be achieved through sophisticated control strategies. One possibility is to detect the consumer with the highest load and open its valve completely, whereas the pump control remains unchanged. For the chosen cycle, a further improvement of 9% was achieved. However, this strategy works only with the open-loop pump control and therefore possibly with reduced flow accuracy.

Another advantage in comparison to an LS-system is the dynamic behavior of the EFM-system. Figure 2.6 shows the run of the swivel angle as well as the speed of the movement while operating a front loader. In comparison to the hydraulic control of the pump, the changes in the load pressure have almost no influence on the EFM-control, because it is extensively separated from the control loops of the pressure compensators. The swivel angle is running smoothly and without oscillations, and the cross-influences with

the speed of the load are minimal. The machine behaves more stable and the stress to the operator is lower.

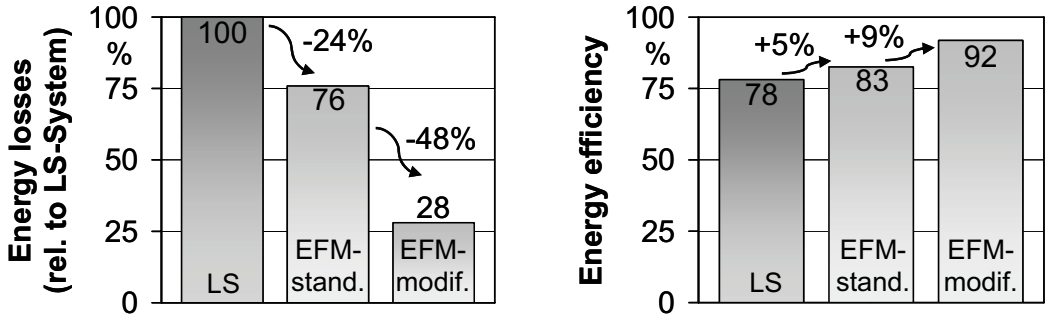

Figure 2.5: Comparison LS – EFM: the usage of energy during mowing

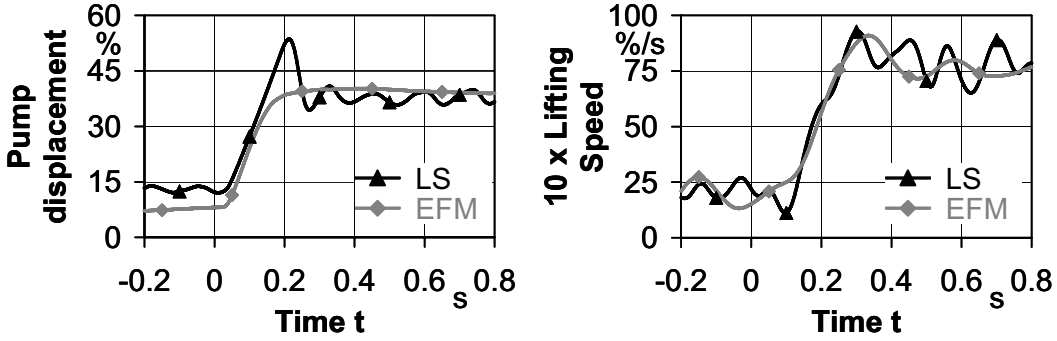

Figure 2.6: Comparison LS – EFM: dynamical behavior at front loader work

2.4 EFM for the Power Beyond operation

Many tractors have a Power Beyond connection (PB) for supplying oil to the externally connected consumers, like attachments equipped with own control valves. The PB-consumer represents a disturbance in the hydraulic system because its flow-demand is usually not known. Therefore, especially under saturated conditions, an uncontrolled behavior of one or several consumers can occur. Often the control pressure of the main hydraulic valve and the valves in the PB-circuit may vary from each other. In some cases, also a prioritization of certain functions is desired. Therefore, some adaptations of the system are necessary.

Figure 2.7 shows a simplified diagram of the EFM-circuit for a prioritized connection of the PB-user, with a simultaneous lifting of the pressure when PB is operated. Therefore, instead of the conventional open center pressure compensator, a 3/3-pressure compensator is used in the pressure line of the valve block of the implement hydraulics. If no user is activated, the pump swivels back and the pressure compensator closes (position 0). When the working hydraulic circuit is activated, the pressure compensator takes on position 1 with a low control pressure difference. Once a a PB-user is activated, the pump

is controlled in such a manner that the pressure compensator switches to position 2. A small excess flow of the pressure compensator is in this case allowed, which can be selected according to the same criteria as with the EFM-system in figure 2.3. The increase in pressure in position 2 of the pressure compensator can either be achieved automatically by means of a suitable spring set or through an active adjustment of the spring. As long as the system is not saturated, all users are supplied according to the demand. In case of saturation the prioritization of the PB-user is hydraulically secured. The command signals can be integrated as before in the electronic control system.

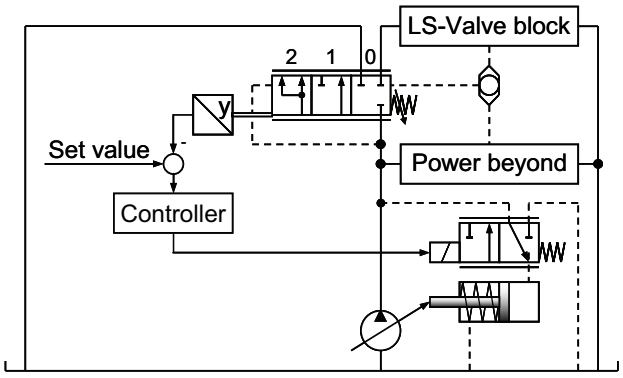

Figure 2.7: Principal circuit of the EFM-system for the Power Beyond operation

The pressure compensator represents an additional hydraulic resistance in the system, which should be as small as possible. As seen in figure 2.8, already with the first compensator prototype better results were measured than with an LS-system. The efficiency can be increased by further optimization of the flow properties of the compensator. The sophisticated control described above is also applicable to the present solution, offering a further increase in efficiency.

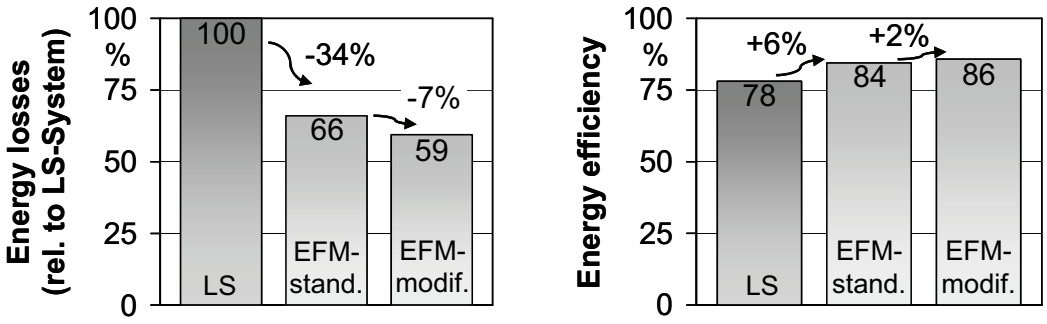

Figure 2.8: Comparison LS – EFM with a 3/3-pressure compensator: Usage of energy during mowing

When the PB-user is active, the improvement in the efficiency is marginal in comparison to a LS-system. However, the behavior of the system during dynamical changes in the working conditions is very interesting. In Figure 2.9 shows the reaction of the EFM-

system to a step-wise connecting of the PB-user. At the point of time t = 0 the PB-valve is opened, the PB-user is served with a higher priority. The user in the working hydraulic circuit is undersupplied for a short time. The duration of this stage depends on the flow relations as well as on the settings of the EFM-controller. The swiveling time of the pump also causes a limiting factor to the response time of the system.

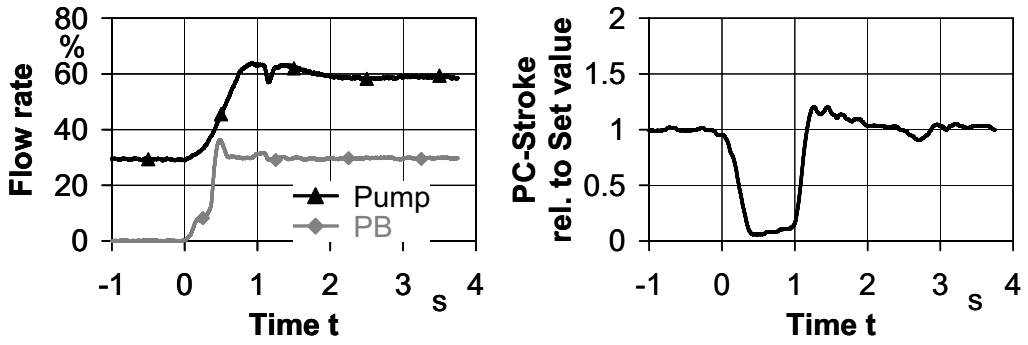

Figure 2.9: The step response of the EFM-system with a 3/3-pressure compensator in PB-operation

3 SUMMARY

Electrohydraulic flow matching combines the cost-advantages and the robustness of the conventional load sensing systems with higher controllability and flexibility of electrohydraulic systems. Relatively small changes to the system are required when implementing EFM. The principle of the direct impressing of the hydraulic flow makes it interesting for mobile applications. The first results of the practical tests in a tractor confirmed the benefits compared to the conventional concept. Better controllability, smoother dynamic behaviour as well as lower energy consumption were achieved. The system can also be adapted to special demands as f.ex. to Power Beyond use. Therefore, this new concept offers an interesting alternative to the implement hydraulic systems in mobile working machines.

4 REFERENCE

[1] US 6640163 B1. United States Patent, 2003 (Husco International, Inc.).

[2] DE 10340993 A1. Deutsches Patentamt, 2005 (Wessel-Hydraulik, Völkel Mikroelektronik).

[3] Fedde, T., Harms, H.-H., An adaptive hydraulic system for mobile applications. 5. International Fluid Power Conference, Aachen, 2006, Vol. 3, pp. 95-106

[4] Djurovic, M., Helduser, S., Elektrohydraulisches Load-Sensing – Neue Lö-sun¬gen für mobile Arbeitsmaschinen. O+P Ölhydraulik und Pneumatik 48 (2004) Nr. 10, S. 635-640, Nr. 11-12, S. 712-716

[5] Zähe, B., Energiesparende Schaltungen hydraulischer Antriebe mit veränderlichem Versorgungsdruck und ihre Regelung. Dissertation, RWTH Aachen, 1993

[6] Harms, H.-H., Entwicklungstendenzen in der Mobilhydraulik. 11. Aachener fluidtechnisches Kolloquium, 1994, Band 2, S. 19-54

[7] Bosch Rexroth AG, Verstellpumpe A10VO Baureihe 53, RD92703/11.05, Elektroproportionale Schwenkwinkelregelung, RD92708/04.05
[8] Bosch Rexroth AG, Wegeventile SB23LS, 1987760513/03.98

PORTABLE REMOTE CONTROL FOR TELEOPERATED HYDRAULIC MOBILE MACHINE

Jarno Uusisalo, Jani Vilenius, Antti Vuohijoki, Sanna-Maria Hirvonen, Otso Karhu, and Kalevi Huhtala
Tampere University of Technology
Institute of Hydraulics and Automation
P.O.Box 589
33101 Tampere, Finland
Phone +358 3 3115 4485, Fax +358 3 3115 2240
E-mail: jarno.uusisalo@tut.fi

ABSTRACT

A portable remote control for short-range teleoperation is developed at the Institute of Hydraulics and Automation in the Tampere University of Technology. The remote control is based on a commercial game controller. Electronics of the game controller is redesigned and the wireless communication between the remote control and the machine is carried out with lightweight low-cost radio modems. Implementation of the portable remote control is introduced in this paper. Also, other alternative solutions to implement teleoperation of the machine are discussed.

KEYWORDS: Remote control, Teleoperation, Mobile machine

1 INTRODUCTION

Hydraulic mobile machines often work under dangerous or uncomfortable circumstances. Protecting the operator of the machine against the environment may be difficult or expensive. In some cases, using teleoperation of the machine is an easier, better and more cost effective way to carry out the task. Moreover, in some tasks controlling the machine is easier for the operator when he can have a different view of the situation, not only a view from the machine.

In this paper the term teleoperation is used as a synonym for the term remote control. It means that control commands between the master (operator) and the slave (machine) are transferred wirelessly. A motion of the slave is not the same as the motion of the master in all cases and a mental transformation from the operator is needed. For instance, in one solution the turning of the machine is controlled with a steering wheel even though

the machine is skid-steered, and in the other solution the machine is controlled with small joysticks. However, mental transformation (i.e. rotation, translation, and scaling), which is needed, is low level transformation and test experiences have shown that it does not distract the operator who has used similar controls earlier.

Teleoperation can be divided into two concepts according to distance. Long-range teleoperation is based on a camera view and controlling of the machine usually takes place in the control room. Short-range teleoperation is based on a visual perception (eye contact) and cameras are not needed.

2 TELEOPERATED HYDRAULIC MOBILE MACHINE

The mobile machine studied is a small skid-steered wheel loader with mass of approximately 720 kg. Some changes to the hydraulics and electronics of the machine have been done to make the teleoperation of the machine possible. The body of the machine has not been modified. [1]

Various attachments, such as different kinds of buckets, brooms, and excavators are available for the basic machine. This research is focused on controlling the machine with a bucket and an excavator. Teleoperation, however, also works with other attachments. [1]

2.1 Hydraulics

In the original machine all valves were mechanically controlled on/off valves. To make the teleoperation of the machine possible, all valves were replaced with electronically controlled ones. In the modified machine the control valves are proportional valves which are designed for mobile purpose [2]. The characteristic of those valves make controlling of the machine challenging. In addition to proportional valves, electronically controlled on/off valves were installed to carry out some simple tasks. On/off valves are used as lock valves for the boom and the bucket for safety reason and also to save energy. One on/off valve is used to select either one pump or two pumps. A pressure relief valve was installed to enable load sensing system.

Other hydraulic components are original ones. There are two constant displacement pumps in the machine. Either one or two can be used. The telescope boom and the bucket of the machine are moved by means of hydraulic cylinders. Hydrostatic transmission is carried out with four hydraulic motors. Front and rear motors of each side are in series. The machine is skid-steered which makes controlling challenging especially on the surfaces where the friction is high, like tarmac for instance. The hydraulic diagram of the machine after modifications is shown in figure 1.

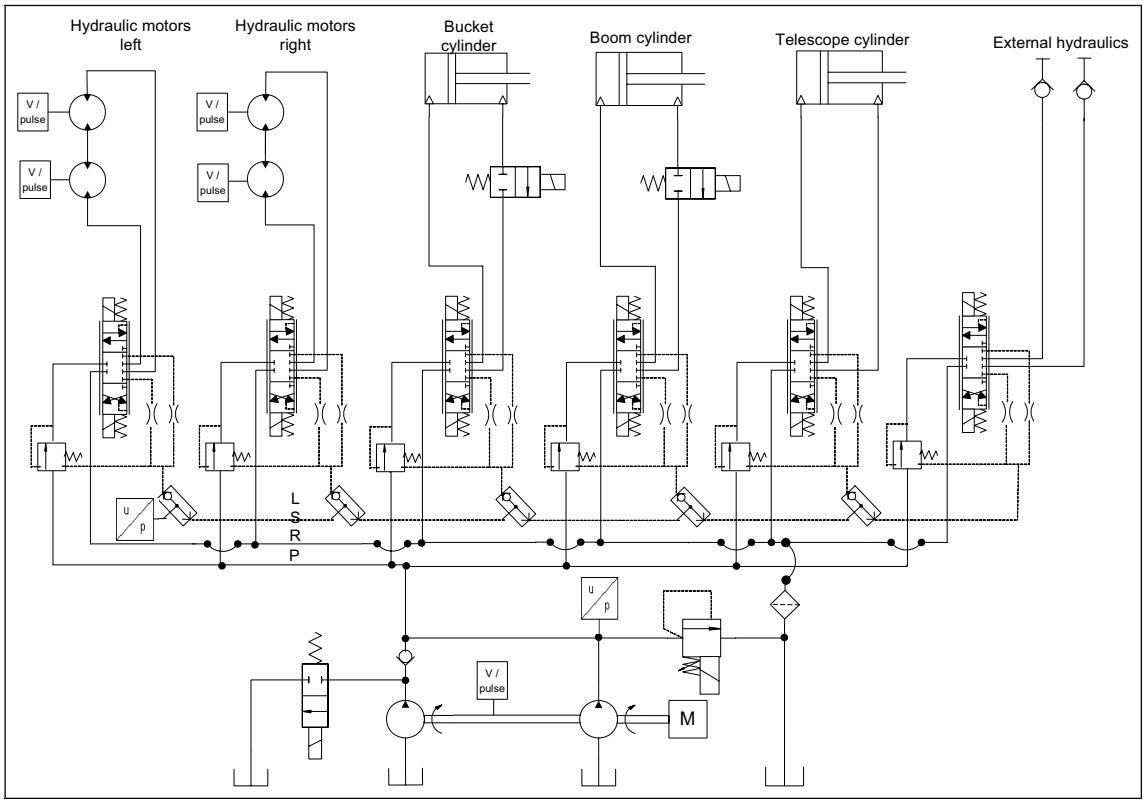

Figure 1. *Hydraulic diagram of the studied machine.*

2.2 Electronics

The electronics of the machine consists of a display module, I/O modules, a radio modem, an electric gas, controls, and sensors. All electronic components are robust and selected for mobile use. The most important components are marked in figure 2.

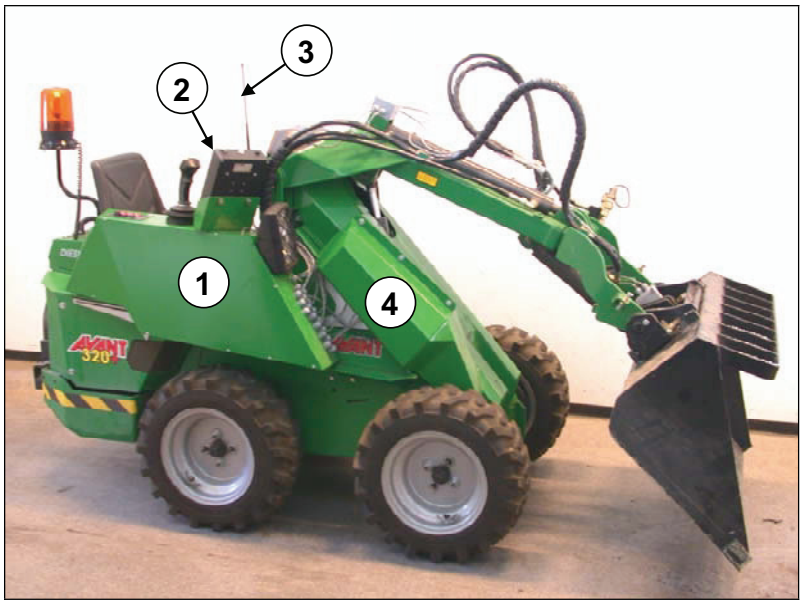

Figure 2. *The most important components of the studied machine. Numbered items in the figure: (1) I/O modules, (2) display module, (3) radio modem, (4) proportional valve.*

The display module DM586 is the master module of the system. It carries out all high level control tasks of the system. The display module is also a user interface for the operator while the machine is operated manually. Multipurpose I/O modules control the valves and the electric gas. As input, the modules read values from the sensors. The display module and I/O modules communicate via CAN bus. [3, 4]

The wireless link between the machine and the operator is carried out with commercial radio modems. Radio modems are cost-effective, robust (temperature range, supply voltage etc.), and free to use (license free frequency band). Delays of the data transmission are also predictable and with intelligent software possible data losses can be compensated. Two different types of radio modems are used. Serial transmission (RS-232/RS-422) is used in both cases. In the machine the radio modem is connected to the serial port of the display module.

Simplified block diagram of the connections between the modules, sensors, valves, and control devices in the machine is shown in figure 3. Direction of the arrows in figure 3 describes the direction of the signals. Lines without arrows are busses. Power feed lines have not been drawn.

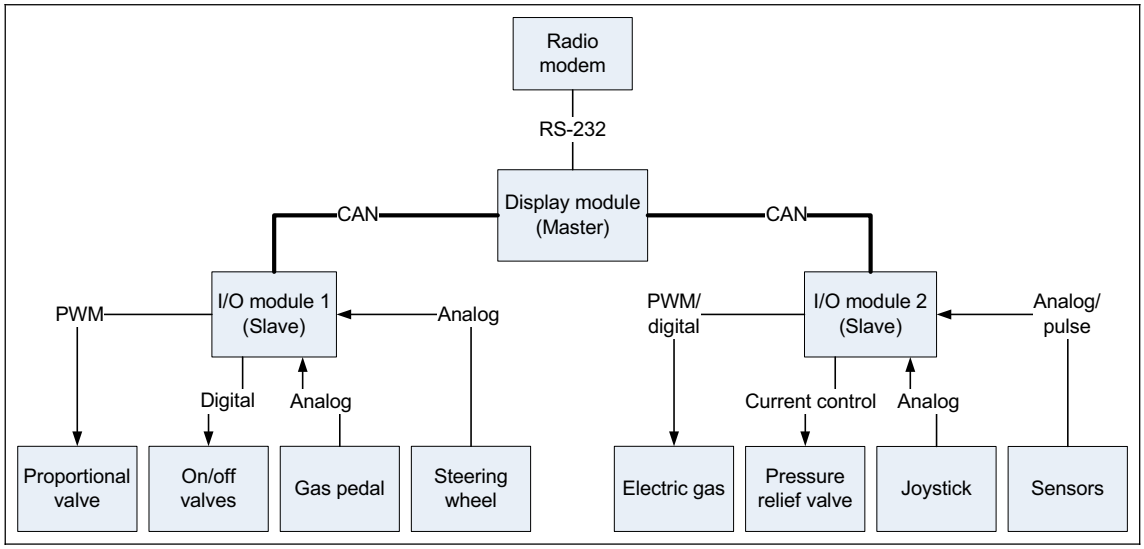

Figure 3. *Block diagram of the electronics in the machine.*

3 DIFFERENT TYPES OF USER INTERFACES FOR TELEOPERATION

The user interface of the teleoperation can be divided in two categories on ground of the distance between the machine and the operator. In both cases, short-range and long-range teleoperation, the wireless point-to-point link is carried out with radio modems. Also, the data transmission protocol is identical in both cases. The user interface (controls) is, however, different.

Different kinds of tasks require various user interfaces to achieve the best possible work efficiency and ergonomics. Four different user interfaces are designed and implemented for different requirements for the studied machine. The main characteristic, including benefits and disadvantages of the user interfaces are represented in this chapter.

3.1 Long-range teleoperation

Visual feedback from the machine in long-range teleoperation is based on a camera view. In this research project, a test hall is used as a test environment. Three video cameras are installed in the test hall and one wireless video camera is mounted in the machine. Two cameras are mounted in the corners of the hall and one PTZ-camera (Pan-Tilt-Zoom camera) is ceiling mounted. Camera views from the hall cameras are transferred for the operator via cables. A commercial wireless transmitter is used for the wireless camera. Other feedback information, such as pressure values, velocity of the machine, and motor speed (rpm), from the machine is transferred via radio modems.

3.1.1 Control room

A control room is built near the test hall. The user interface in the control room consists of two LCD televisions, a laptop, and control devices (steering wheel, pedals, and joystick). The radio modem for the wireless link is mounted on the wall of the test hall. SATELLINE-3AS(d) radio modem is used because of high output power (from 10 to 1000 mW) [5]. The modem is relatively large and weights 250 g. Size or weight, however, does not bother since the operator does not have to carry the modem all the time. Another advantage is that the modem supports RS-422 serial protocol for long distances. A twisted pair and RS-422 protocol are used between the control room and the test hall. The view from the control room can be seen in figure 4.

Figure 4. *The view from the control room is shown on the left side. The view from the test hall can be seen on the right side.*

The control room is a suitable solution (user interface) for cases where the worksite is long-lasting and the operator can be located near the worksite. The ergonomics of the control devices is good and with laptop, various feedback parameters from the machine can be provided for the operator. Disadvantages of this solution are a requisite. Cameras have to be installed on the worksite. A laptop and televisions are also needed. Building up the control room takes time and it is not a possible choice for temporary, short-term cases.

3.1.2 Controlling via internet

In some cases the operator can not be located near the worksite. In that case, only a server is needed in the vicinity of the worksite. The control room itself can be located elsewhere. Communication between the control room and the server of the worksite is carried out via internet. The biggest benefit of this solution is that the same control room can be used for several worksites and one operator can control several machines on separated worksites. Only a server and cameras for each worksite are needed.

3.2 Short-range teleoperation

In the short-range teleoperation cameras are not needed because the operator is near the machine and the visual feedback is based on an eye contact. Two different kinds of user interfaces are designed and implemented for short-range teleoperation in this research project. Also, two different radio modems are used.

3.2.1 Teleoperation trolley

A similar user interface as in the control room is constructed on a trolley (see figure 5). The radio modem for the wireless link is also similar. The trolley is relatively easy to move to the worksite. The teleoperation trolley user interface is relatively ergonomic. The biggest benefit compared to driving the machine manually is that the operator is not exposed to the vibration of the machine which increases comfort. However, noise and temperature, for instance, still affects to the operator since he has to see the machine all the time.

Figure 5. *Teleoperation trolley.*

The teleoperation trolley is a good solution when the operator does not want to drive the machine manually because of vibration of the machine or dangerous nature of the task and changing the angle of view during work task is not necessary. On the other hand working environment itself must not be dangerous.

3.2.2 Portable remote control

A portable user interface is developed for cases when the machine is sometimes driven manually and sometimes by teleoperation. It is also a good solution if the operator wants to change the angle of view during a working task. For example, let us consider the case when the operator is using the excavator [6]. The operator can drive the machine manually to the right position and then control the excavator from the place where he can see the target better.

The user interface differs from previously presented solutions. Instead of steering wheel and gas pedal, small joysticks are used. Display has not been used because of weight and size of the portable remote control. On that account, feedback information from the machine is limited. A smaller and lighter radio modem is used, since in this case the operator has to carry also the modem all the time. The smaller radio modem is also more cost effective, which is a notable matter since the portable remote control is designed for part-time use. Output power of this radio modem is smaller that of the other modem. Portable remote control is, however, designed for cases where the operator is close to the machine and long range is not needed. [7]

4 IMPLEMENTATION OF PORTABLE REMOTE CONTROL

A few goals for the portable remote control were set at the beginning of the design project. The remote control should be wireless, light, and easy to use. All functions of the machine have to be controllable with the remote control. Essential feedback information from the machine has to be provided for the operator. Secondary information, however, can be ignored.

4.1 Electromechanics and encapsulation

To achieve good usability, it was decided to utilize existing solutions concerning control units. A game controller was chosen as a starting point for design. A cordless game controller for Playstation 2, manufactured by Logitech, was used, since it has a sufficient number of analog (joysticks) and digital (buttons) input devices. The controller also enables providing essential feedback with a few LEDs. Since the original controller was cordless, the mounting for batteries, which are needed, already exists. Another advantage of the game controller is that it is commonly used and many operators are adjusted to use corresponding devices. [8]

Only enclosure, joysticks, and buttons were used from the original controller. Two eccentric electric motors, which were used for enabling vibration in game mode, were removed to minimize weight. The radio modem was fastened to the body of the

controller. A main power switch was also added. The circuit board was totally redesigned.

4.2 Hardware

A digital signal processor DSP56F803 is used as a CPU of the remote control. The processor provides enough digital interfaces for buttons and LEDs. The joysticks of the original remote control are based on two potentiometers per each joystick. An inclinometer is added to measure the angle of the controller. This information is used while controlling the machine by turning the remote control. Voltage values of the joysticks and inclinometer are read by means of the internal A/D converter of the processor. All digital and analog signals are filtered with passive low pass filters. The radio modem is connected to the serial port of the processor. [9]

The enclosure defines the shape of the circuit board. In addition, locations and sizes of the mounting holes have to be taken into account. These features make designing the circuit board challenging and compromises were made during the layout design. The critical signal routes, however, have been designed and implemented as well as possible. A double-sided printed board is used. Both sides of the printed board assembly are shown in figure 6.

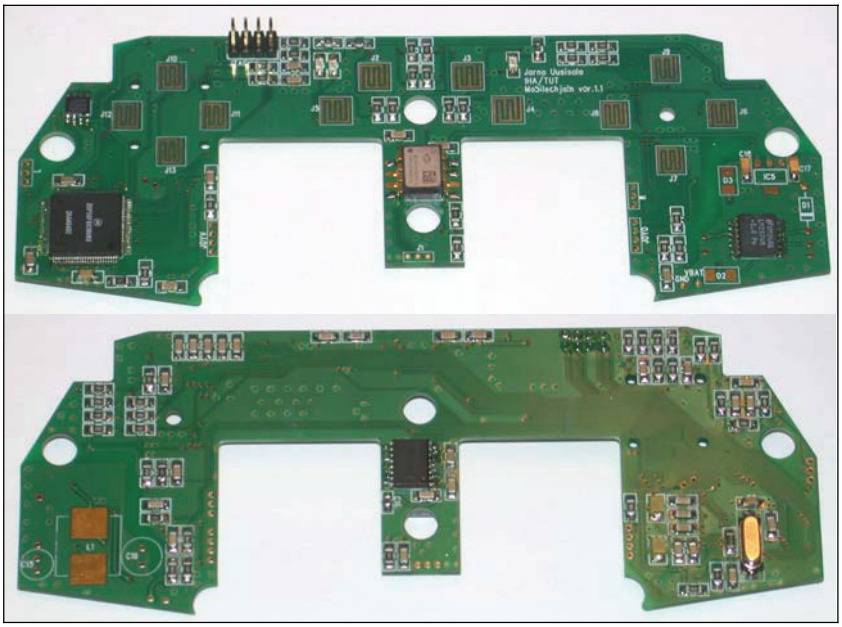

Figure 6. *Printed board assembly of the implemented remote control. Top side of the board is shown in the upper part and bottom side in the lower part of the figure.*

4.3 Software

Some filtering for digital signals are implemented by software in addition to hardware filtering. Scaling for the joystick values are carried out with software. For the serial data transmission a CRC (Cyclic Redundancy Check) algorithm is used to discover and ignore possible incorrect data packets [10]. Flowchart of the program is introduced in figure 7.

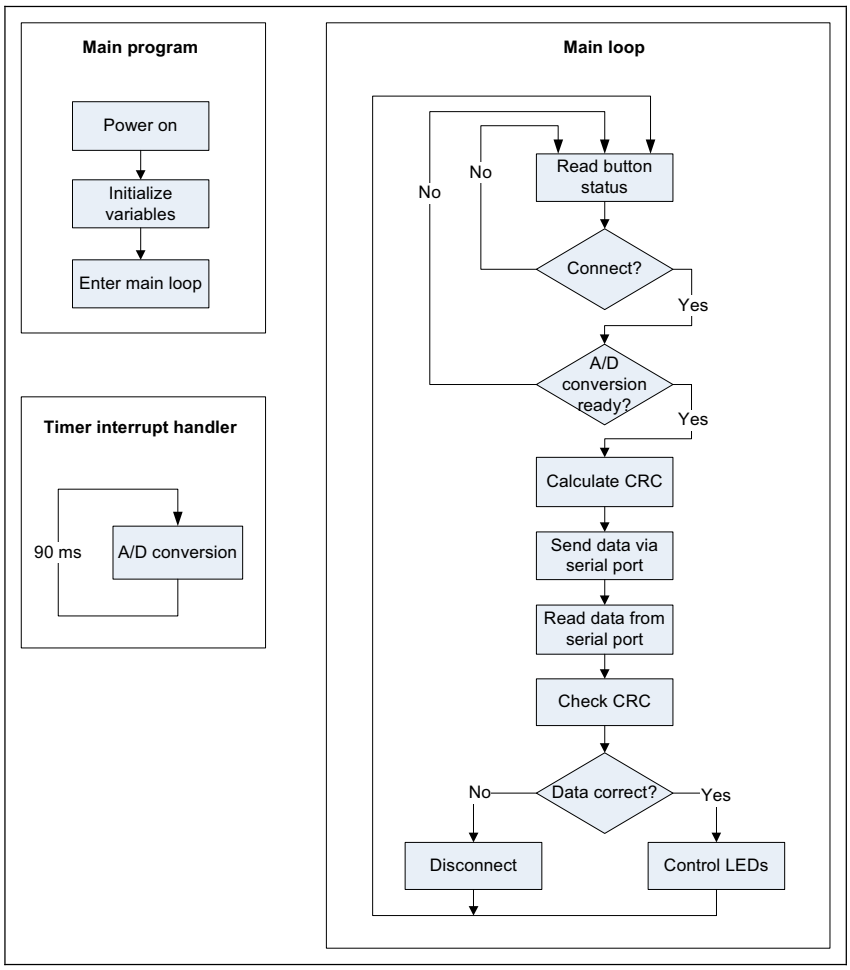

Figure 7. *Flowchart of the program.*

4.4 Functions of the remote control

A front view of the implemented portable remote control is shown in figure 8. The devices used (joysticks, buttons and LEDs) are marked with numbers in figure 8. Corresponding functions are described in table 1. Some devices have several functions depending on the mode used. These optional functions are explained after table 1.

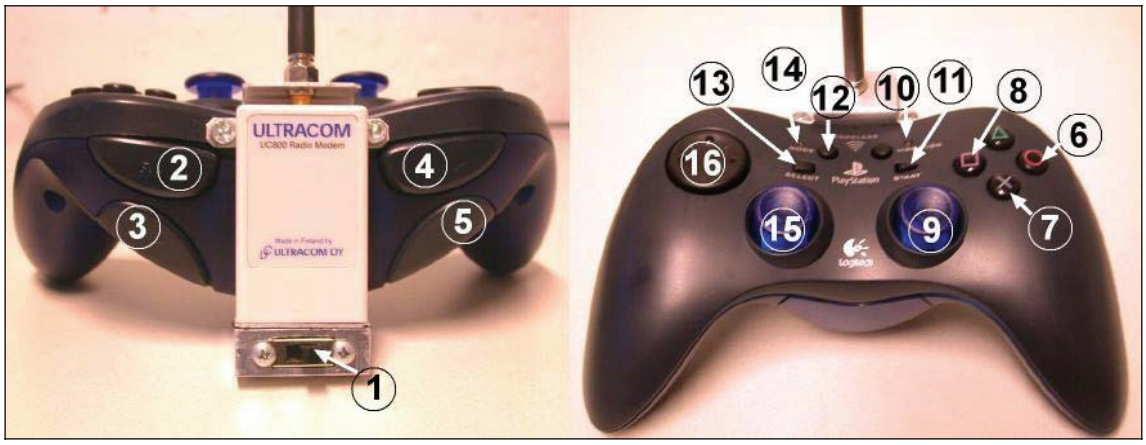

Figure 8. *The front view of the portable remote control on the left and the top view on the right.*

Table 1. *Functions of the portable remote control.*

Number in figure 8	Device	Function
1	Switch	Main power on/off
2	Button	Enable/disable double pump
3	Button	Enable inclinometer [1]
4	Button	Telescope out
5	Button	Telescope in
6	Button	Headlights on/off
7	Button	Horn
8	Button	Brake
9	Joystick	Gas/Direction/Steering
10	LED	1 pump/2 pumps
11	Button	Start/stall engine
12	Button	Enable excavator mode [2]
13	Button	Remote/manual
14	LED	Battery level / remote/manual [3]
15	Joystick	Boom and bucket control
16	Button	External hydraulics control

[1] If the inclinometer mode is enabled, steering of the machine is controlled by turning the remote control. Horizontal direction of the joystick 9 does not have an effect in this mode.

[2] While the excavator mode is enabled, both joysticks and buttons 4 and 5 (Telescope control) are used for controlling the excavator. Driving the machine is not possible in this mode.

[3] The LED 14 is blinking. It shows in turns the battery level of the remote control and the state of the remote/manual mode. If the battery level is too low, the LED is red all the time.

CONCLUSION

Teleoperation is often considered to be a solution for dangerous work tasks where an operator can not be present. When the user interface of the teleoperation is selected soundly, teleoperation can, however, be used to improve convenience of the work task as well. Diverse user interfaces should be used for different kinds of tasks. In this paper, various user interfaces are represented and the suitability of those solutions for different cases is discussed.

For long-lasting, dangerous, or extremely uncomfortable worksites, a control room is the most suitable user interface. Disadvantages are the requisite, cameras for example. Building up the control room is also a time-consuming task. Teleoperation via internet enables the same operator to control several machines on various worksites. A teleoperation trolley is easier to build than a control room and fewer requisites are needed. Visual feedback is based on eye contact. Otherwise the same feedback

information can be provided for the operator as within the control room solution. Convenience, however, can be worse than in the previous case.

A portable remote control is lightweight and easy to carry. All work movements of the machine can be controlled with the remote control. Feedback information, such as pressure values, is limited. In most cases, however, the operator does not need that secondary information. The portable remote control is a good solution when the machine is sometimes driven manually and sometimes by teleoperation.

The portable remote control is implemented by exploiting the body of the game controller. Electromechanics and encapsulation of the original game controller is used. Electronics is totally redesigned by taking into account the shape of the enclosure. Software is also implemented for this application. Then wireless link between the machine and the remote control is carried out with a commercial radio modem.

REFERENCES

[1] Avant 300 series, 500 series. Ylöjärvi, Finland 2005, Avant Tecno Oy.

[2] PVG 32 Proportional Valves, Technical Information. Lincolnshire, IL, USA 2006, Sauer-Danfoss Inc. 80 p.

[3] Display module DM586, Technical Datasheet. Tampere, Finland 2003, Axiomatic Technologies Inc.

[4] Multipurpose I/O module MVMIO24, User Manual. Tampere, Finland 2002, Axiomatic Technologies Inc.

[5] Satelline-3AS(d) radio modem, User Guide. Salo, Finland 2005, Satel Oy.

[6] Karhu O., Vilenius J., Uusisalo J., Moya Cid J., and Huhtala K. "Intelligent Excavator for Hydraulic Mobile Machine", 22nd International Symposium on Automation and Robotics in Construction, Ferrara, Italy 2005.

[7] Ultracom UC800 radio modem, Brochure. Kempele, Finland 2004, Ultracom Oy.

[8] Logitech Cordless Action Controller for Sony Playstation 2. http://www.logitech.com. (7.12.2006)

[9] DSP56F803, Datasheet. Austin, TX, USA 200, Freescale Semiconductor Inc. 52 p.

[10] CRC algorithm. http://www.ciphersbyritter.com. (8.12.2006)

A REVIEW OF ACTIVITIES FOR AUTOMATION IN MOBILE MACHINES

Dr.-Ing. Thorsten Lang,
Dipl.-Ing. Thomas Fedde,
Prof. Dr.-Ing. Dr. h.c. H.-H. Harms
Technical University of Braunschweig
Institute of Agricultural Machinery and Fluid Power
Langer Kamp 19a
33106 Braunschweig, Germany
Phone +49 531 391 2670, Fax +49 531 391 5951
E-mail: T.Lang@tu-bs.de

ABSTRACT

In recent years the use of electronics in mobile hydraulics has grown significantly. Electronics are the key for the implementation of automated functions in mobile hydraulics to improve the efficiency of the operating processes and to ease the handling of the machine.
Especially at the working hydraulics closed loop controls are in the centre of interest. The control of several motion drives is a challenge in mobile hydraulics because of the varying load conditions at mobile machines and the dynamic behaviour of the commonly used Load-Sensing systems.

The following paper deals with an review of previous and actual activities for the introduction of automations in mobile hydraulics at the Institute of Agricultural Machinery and Fluid Power. The presentation gives the results of several projects at the institute and picks up newly launched industrial products.

KEYWORDS: Automation, Hydraulic Systems, Actuators, Sensors

1 GENERAL DEVELOPMENTS

Since a couple of years, the Institute of Agricultural Machinery and Fluid Power at the Technical University of Braunschweig, Germany, is researching on the field of automated processes and optimizing the power systems (which means the hydraulic system) for theses automated functionality on mobile machines. In 1997, an industrial powered project started with the intension to modify the power lift system (also called "Three-Point-Hitch") on agricultural tractors. The degrees of freedom and the potential of automation should be enlarged, but still meet the standards of dimensions and other common technical properties for using older attachments. For this, some mechanical fixed assemblies were disconnected and eliminated. Instead of this, three length controlled hydraulic cylinders were installed. The worldwide first prototypes of fully integrated length sensors were developed with another industrial partner and used for this project. The result, shown in figure 1, was a flexible power lift system with a lot of new functional benefits, for example the parallel or steep lift function, teach-in memorized motions or automated repositioning. The system was presented at several conferences, e.g. in Linköping 2001 [1].

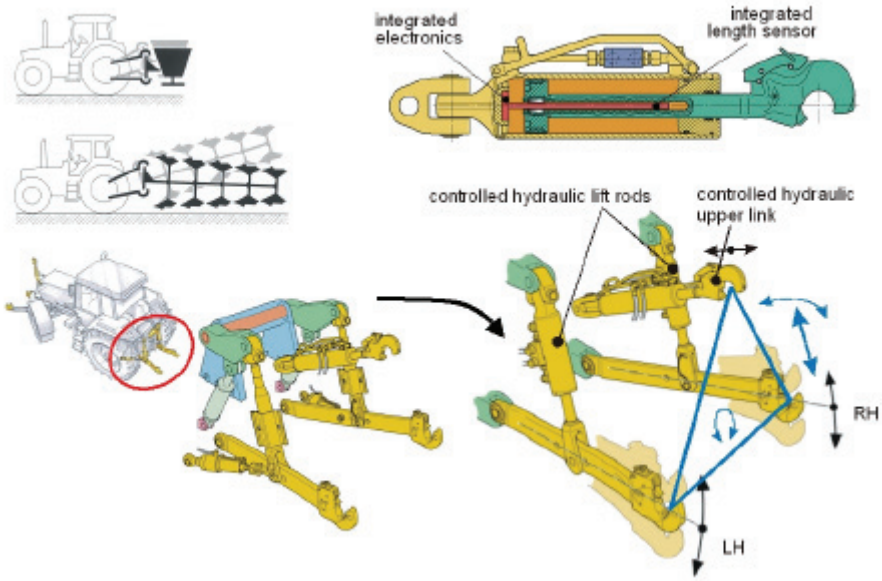

Figure 1: The modified power lift system of agricultural tractors

Beside the user-orientated functional benefits, the realized system established a basis to further extensive control developments, for example a strategy named "attachment controls tractor". These kind of systems demands an essential new technical philosophy, the mechatronical way of thinking with commonly well known substantially three aspects:

- The **integration of components** characterizes the design of compact, easily plug-able units with integrated sensors, actuators, electronics, processors and et al.
- The **integration of functionality** describes the displacement of functions from an outer, higher level into the local system or, otherwise expressed, the increasing of distributed intelligence
- The **adjustability by software** means, that the functionality of a subsystem should be depending as much as possible on software, not on the construction design. Otherwise expressed: The objective is to build universally applicable subsystems.

Applied on mobile hydraulics, it is possible to define three basic systematic areas of subsystems to modify and redesign (e.g. presented in Tampere 2003 [2]:

- **Intelligent actuators**, with integrated sensors for position, speed and pressure.
- **Intelligent controls** (valves) with disintegrated control edges and a possibility to switch between open and closed center behavior by software:
- **Intelligent power supply** with the main task to ensure enough clean and cool hydraulic energy for high dynamic motions simultaneously with an acceptable efficiency.

Considering the experiences in automated systems on mobile machines, in the following the activities and the state of art in the above named fields are described.

2 HYDRAULIC SYSTEMS

Actually several new solutions for the working hydraulics in mobile machines are discussed. The basic approach is the usage of the information of the flow demands for the adjustment of the pump displacement in contrast to the Load-Sensing system, where the pump control is only realized as a closed loop pressure control. Current hydraulic systems of modern mobile machines are predominantly equipped with electronically actuated proportional valves, so that the information of the demanded flow can be calculated by the valve opening and the flow characteristic of the valve. Several publications show interesting results, e.g. the optimization of the system efficiency and the dynamic behaviour ([2], [3], [4], [5]).

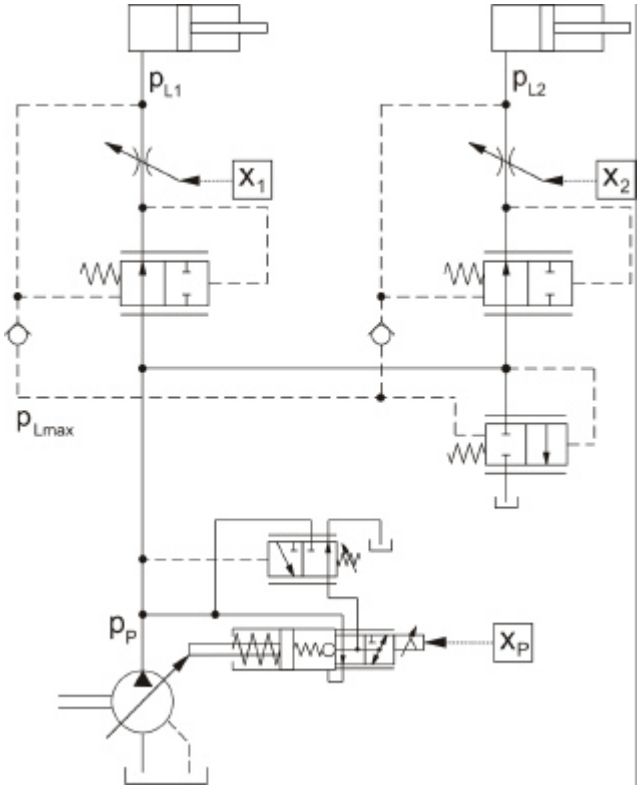

Figure 2: Flow demand system with an additional bypass valve

At the Institute of Agricultural Machinery and Fluid Power a system, based only on the information of the flow demands was investigated for the use in tractors. Figure 2 shows

the functional hydraulic circuit of the system, where the pump displacement is adjusted by the flow demands in open loop control. An additional pressure control of the pump is necessary to protect the system against overrunning pump pressure. This can be done by a pressure control according to the Load-Sensing system. One possibility is to attach an hydraulic-mechanic pressure compensator as bypass, shown in figure 2. The bypass cuts off the excessive pump flow. If a relevant overhead flow is added to the demand pump flow an increased dynamic behaviour is achievable.

2.1 DYNAMIC BEHAVIOUR

Figure 3 shows step responses of the hydraulic consumer while increasing the pump flow and contains the cylinder velocities of the boom cylinder of a front-end loader at lifting.

The measured step response of the Load-Sensing is shown for comparison. The measure of the Load-Sensing step response has been carried out under the same initial conditions, with the same components.

The step responses of the Flow-Demand system are characterized by higher dynamics than those of the Load-Sensing system. The acceleration of the consumer is higher compared to the Load-Sensing in general and the acceleration of the actuator increases with the pump flow overhead. In the range of –3 l/min to 0 l/min pump flow overhead the system shows a lower acceleration and a 3% lack of the actuator velocity after ending of the transient effects. In the range of 0 l/min to +3 l/min the step response is optimal, here the cylinder achieves the desired speed of 60 mm/s around 100 ms earlier than in Load-Sensing mode with a smaller overshoot. With a pump flow overhead above + 10 l/min the overshoot and the oscillations increase together with the acceleration. The acceleration phase is mainly influenced by the pump flow overhead. This is optimal usable in a flow overhead range of – 5 % up to 20 % of the nominal valve flow .

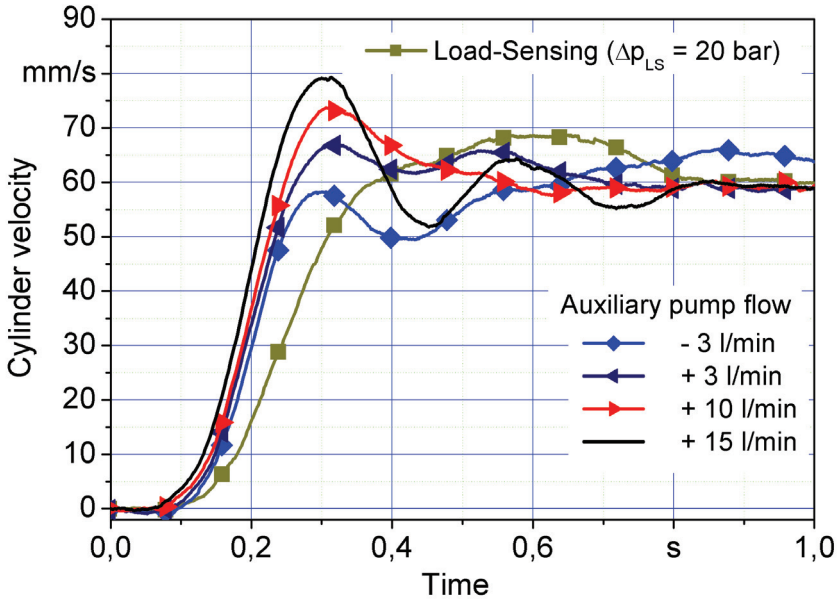

Figure 3: Measured step responses of the OC-Flow-Demand system and the Load-Sensing system

2.2 SYSTEM EFFICIENCY

If the pump flow of the Flow Demand system is adjusted minimal below the demanded flow of the valves, the pressure difference at the individual pressure compensators decreases. The pressure compensator of the valve with the highest load pressure opens corresponding to the reduced flow at the metering edge of the valve. This causes a lower pressure drop at the valve. The bypass closes because of the decreased difference between pump and load pressure. If a single valve is activated, a significant increase of the system efficiency around 10% in the main working range is possible.

The so called EFM concept (Electrohydraulic flow matching) from Bosch Rexroth is build up on the same hydraulic circuit with an additional sensor for the detection of the position of the bypass valve. The position is given by the pressure difference between load and pump pressure, so the position is a measure for the accuracy of the effective pump flow. The system is able to compensate for flow losses at pilot stages and other not known hydraulic actuators and leakage. A disadvantage of the bypass is the loss of flow at itself, so it decreases the efficiency of the hydraulic system [3].

3 VALVES

A problematic situation at LS-systems occurs in case of negative loads (pulling loads, the direction of load and motion is equal). Current LS-valves combine the flow control by four mechanical connected metering edges (lifting-lowering/inflow-outflow) at one spool. In the normal operation mode with pushing loads (see figure 4), the cylinder velocity is proportional to the spool displacement due to the controlled constant pressure drop of LS-systems. The outflow metering edge features a higher flow coefficient for low pressure losses. In case of pulling loads the flow is controlled by the outflow metering edge and thus the cylinder velocity is extremely depending on the actual load pressure. At high pulling loads the outflow will be clearly higher than the inflow. The result is, that the enlarging cylinder volume is not completely filled with fluid, which means that the piston is no longer clamped. This effect will be enforced using differential cylinders (depending also on the installation position) and by different flow coefficients of the metering edges.

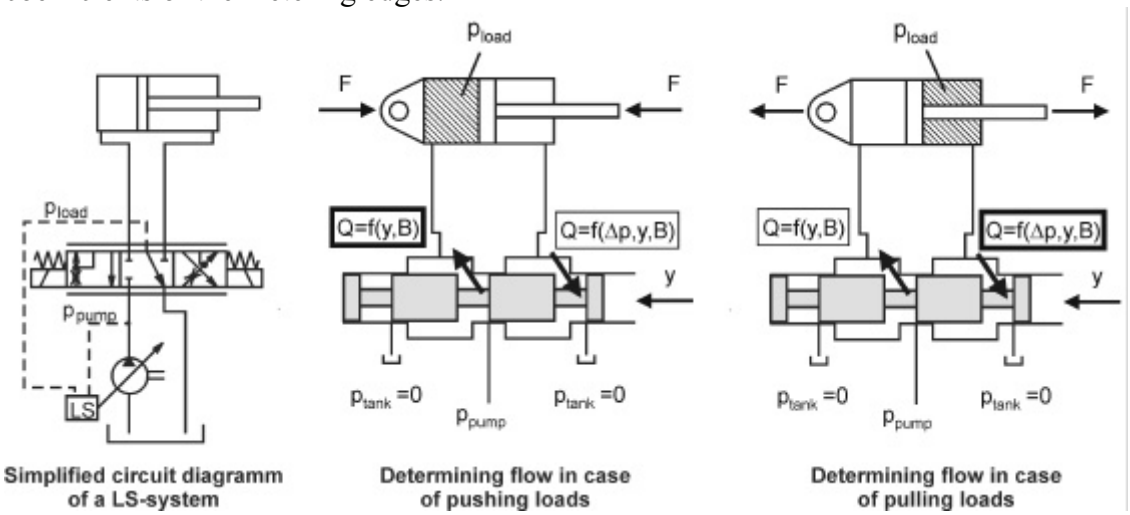

Figure 4: Determining metering edge of Load-Sensing System at pushing and pulling loads [2]

New valve concepts with separated metering edges and the necessary control concepts were discussed the last years (e.g.: [6], [7], [8]). Actual the first systems with separate metering valves are offered at the market ([9], [10]). The valves are based on spool or poppet valve technology and it requires a sophisticated control to achieve a load independent controllability of the consumer. For the investigation of the functionality of the new concepts a test bench with a special arrangement of the load was realized. Figure 5 shows the principle of the load mechanism. In expanded state the cylinder has to lift up the smaller load mass m. While retracting the seesaw begins to pick up the second load mass M, whereby the load condition at the cylinders is inverted. The flexibility of the mechanical structure is responsible for the characteristic of the change of the load. In practical a soft change is necessary to protect the hardware. Figure 6 shows a measure of the system. The motion starts at retracted position with a pulling load while expanding the cylinder. At 4,5 s the load change starts with a mechanical impact of the load mass M on the ground. This can be observed by the rapid change of the load pressures A and B and the following oscillations. After that the valve has to fill up the necessary flow for the compression volume. This effects a temporary reduced cylinder velocity and requires a period of around 1 s until the load pressures achieve stationary levels. The mechanical flexibility also requires a stroke of the cylinder. The present velocity deviations give motivation for optimizations but compared to conventional Load-Sensing valves an essential improvement of the controllability of pulling loads is realized.

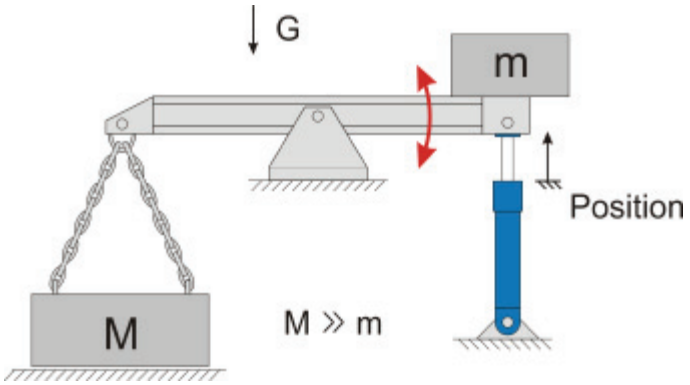

Figure 5: Lab arrangement for measurements with over-running load

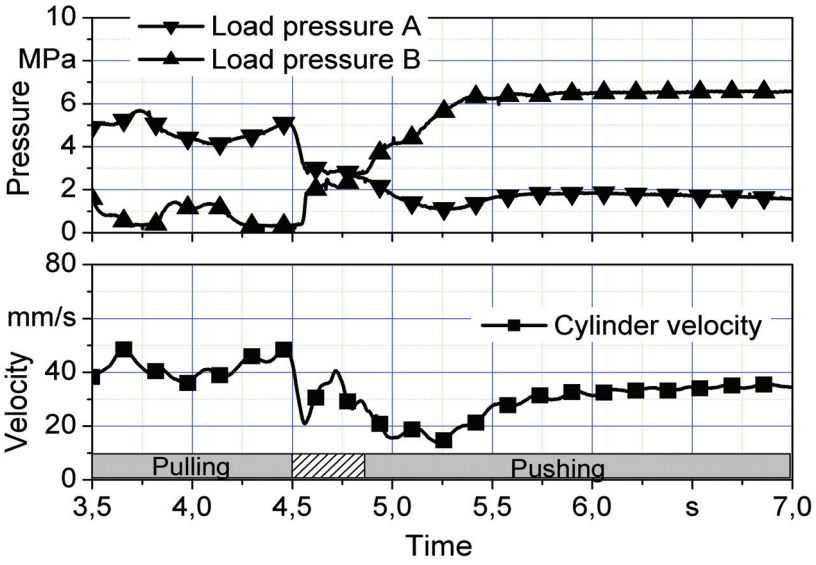

Figure 6: Measured velocity of a double acting hydraulic cylinder with over-running load conditions with Eaton Ultronics Twin Spool valve

4 SENSORS

In recent years the use of electronically activated components in mobile hydraulics has grown significantly. This initiates an accelerated development of controlled hydraulic drives in mobile machines.
An important challenge is to determine the motion states of the operated devices with appropriate sensors. The determination of the current position and velocity of hydraulic cylinders allows to build closed loop-controls for several synchronized hydraulic axes.
Compared to industrial applications in mobile hydraulics special requirements have to be met. On one side these are special resistivities concerning temperature, contamination, voltage fluctuation, impact and vibration loads etc. On the other side lower requirements of precision can sometimes allow a simplification of the sensor and consequently the reduction of costs.

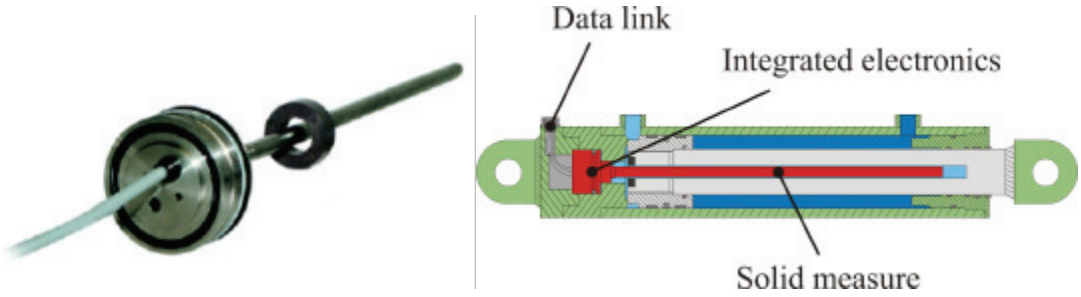

Figure 7: Integrable position sensor for differential cylinders

As generally known, a main problem of differentiating signals from position sensors to generate velocity signals is the influence of white noise and, by digital differentiation, the influence of quantisation noise. Normally, this effect leads to special filtering actions afterwards, which entails unavoidable phase shifts of the signals and a destabilization of the closed loop control.
The integration of the differentiation-process into the housing of the position sensor is investigated in order to avoid this problem. For measuring the rod displacement of a differential cylinder a conventional MTS Temposonic position sensor as shown in Figure 7 is used. The non-contact measurement is based on the principle of magnetostriction ([11]). With this system the delay of outgoing and incoming pulses, which are reflected at the magnetic field of the position magnet, is used to determine the position of the moveable position magnet. The electronic device produces an analogue voltage signal and is integrated serially into the housing at the head of the sensor.

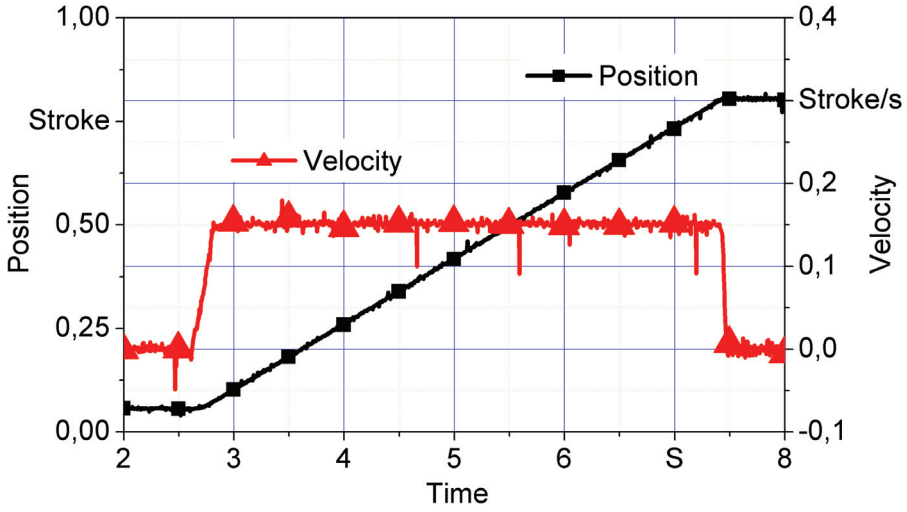

Figure 8: Position and velocity measurement of a movement cycle, unfiltered.

The sensors have been tested under several conditions. Figure 8 shows the signals of a position switch at open loop control without other filtering actions. The velocity analysis is normalized to 1 stroke per second, equivalent 500 mm/sec. The actual measured piston speed is about 0,14 stroke/sec or 70 mm/sec.
The dynamic behaviour and the noise of the velocity signal are important for closed loop velocity controls. It is clear, that the integrated velocity analysis is less problematic with regard to the noise influence at the signal lines and its effects on the quantisation and differentiation process.

4 SUMMARY

The realization of automated systems on mobile machines requires some modifications of components and respectively subsystems. The main objectives are the increasing of dynamic behavior, finding the best efficiency depending on the actual working process, considering of changing loads (especially pulling loads), adapting the system characteristics depending on the actual process and further developments of several integrated sensors. In the last 10 years, a lot of developments and researches have been carried out, so that a high technical level is achieved today, but further optimizations are feasible.

References

[1] Lang T., Harms, H.-H., Coenen, H.: A new Concept for using Position-Controlled Hydraulic Cylinders for the Three-Point-Hitch on Agricultural Tractors. The Seventh Scandinavian International Conference on Fluid Power, 30. Mai-1. Juni 2001, Linköping, Schweden, Vol. 3, p. 3 – 10, ISBN 91-7373-056-4..

[2] Lang T., Harms, H.-H.: Concepts of Mechatronics and Distributed Intelligence in Mobile Hydraulics. The Eight Scandinavian International Conference on Fluid Power, 7.-9. Mai 2003, Tampere, Finnland, Bd. 2, p. 1155 – 1160.

[3] Djurovic M., Keuper, G., Stachnik, P.: Intelligentes Ölmanagement mit elektrohydraulischem Flow Matching. In proceedings 4. Kolloquium Mobilhydraulik, Braunschweig 2006 pp. 1 – 10.

[4] Joengebloed H., van Büren D., Völkel U., Jabs, C.: Energy-Saving Valve System for Mobile Hydaulic Applications – Load Control System (LCS). 4th International Fluid Power Conference, Dresden 2004, p. 117 – 128.

[5] Fedde, T., Harms, H.-H.: An adaptive hydraulic system for mobile applications. In proceedings Internationales Fluidtechnisches Kolloquium 2006, Aachen, Vol. 3, pp. 95 – 106.

[6] Bin, Z., Bing, X., Xiaoping, O., Huayong, Y.: Research on performance of the common pressure rail adopting new hydraulic transformer to drive loads. In: Proceedings SICFP 2005 Linköping. pp.20-21.

[7] Erikson, B., Larsson, J., Palmberg, J.-O.: Study on individual pressure control in energy efficient cylinder drives. In: Proceedings FPNI-PhD Symposium 2006, Sarasota. pp. 77-99.

[8] Münzer, M. E.: Control of mobile hydraulic cranes. In: Proceedings 1st FPNI-PhD Symposium 2000 Hamburg. pp. 475-483.

[9] Jinks, A.: Twin spool digital hydraulic systems for Mobile equipment. In proceedings 4. Kolloquium Mobilhydraulik, Braunschweig 2006 pp. 93 – 102.

[10] Pfaff, J. L.: Distributed Electro-Hydraulic Systems for Telehandlers. In proceedings 50th National Conference on Fluid Power 2005, Las Vegas, pp. 779 – 784.

[11] MTS Sensors Group: Physical basics about magnetostriction product brochure, 2002.

Thermal Simulation As A Part Of A Life-Time Simulation Of Hydraulic Oils

Prof. Dr.-Ing. Hubertus Murrenhoff
Dipl.-Ing. Oliver-Carlos Göhler
RWTH Aachen University
Institute of Fluid Power Drives & Controls
Steinbachstr. 53 B
52074 Aachen, Germany
Phone +49 241 8027533, Fax +49 241 8022194
E-mail: carlos.goehler@ifas.rwth-aachen.de

ABSTRACT

The paper focuses on the thermal simulation embedded in the simulation concept for life-time of hydraulic fluids. It describes the set up of a thermal simulation model for a test rig as an example for a hydraulic circuit. As simulation tool a system simulation extended by thermal properties is used. A method to determine the necessary parameters of the model is proposed. The simulation results of the model are verified by measurements of the temperature distribution.

KEYWORDS: thermal simulation, oil ageing

1 INTRODUCTION

The collaborative research centre 442 "Environmentally compatible tribosystems by means of suitable composites and precursor materials, using the machine tool as an example" was established at RWTH Aachen University in 1997. The involved institutes, with disciplines ranging from chemistry and medicines to mechanical engineering and material science, enable a new approach to redesign ecologically compatible tribosystems. The applications for these tribosystems range from power transfer to forming processes. They not only contribute towards functional performance, but also exert a significant influence on the economic and ecological balance of the technical systems. These are affected to a particular extent by the high eco-toxicological risk potential of the mineral-oil-based precursor materials containing additives. This is because the precursor materials may leak into the environment and give rise to contamination problems. The lubricants used for the new designed tribosystems should be unrefined and unfortified, wherever possible. The functions performed by the

additives in conventional contacts are transferred to newly developed coating systems on the surfaces of the friction contact pairs [MUR].

One subtask within the field of "Materials and Material Behaviour" of the Collaborative Research Center 442, established at RWTH Aachen University, Germany, focuses on the ageing behaviour of environmentally compatible lubricants. The investigation of ageing mechanisms [ZHA], the development of appropriate test methods and testing of the ageing stability of new developed lubricants [SCH] are topics of the conducted research. The chemical synthesis of new environmentally compatible fluids is accompanied by both laboratory and test rig methods. The influences of the applications on the ageing are investigated. Ageing of lubricants and especially hydraulic fluids due to time and load means a change of properties which lead to changing properties of the hydraulic system. To optimize the performance of the system a change of the oil due to its deterioration is necessary. These changes can be done in experience based fixed intervals or determined by condition monitoring methods. With a life-time simulation the intervals can be calculated and the influence of changes to the set up of the system on the life-time can be evaluated.

2. CONCEPT FOR A LIFE-TIME SIMULATION

A neural network is to be used to predict the lifetime of the fluid in a hydraulic circuit in the same way as for the simulation of ageing on laboratory scale [SCH]. This should simulate the ageing characteristics of the fluid and the associated reaction to the complex of loads acting on it. The simple structure of the load acting on the fluid in the laboratory is at odds with the much more complex load structure in a hydraulic circuit. The constant temperature load in the rotary bomb test becomes an uneven distribution of heat in the system when leaving the laboratory scale. Temperature distributions in hydraulic systems are described by [KEM] for example. The oxidation test does not simulate shearing loads of the type that occur in areas where there are considerable differences in flow rate, as is the case when fluid flows through orifice plates, for example, or the catalytic materials that accelerate ageing like those used in pumps and motors. Furthermore, the large number of possible hydraulic circuits, ranging from simple pump-motor combinations right through to more bifurcated systems with numerous consumers, give rise to a number of differences. This means that, compared with the simulation of ageing on laboratory scale, there are many additional variables that describe the structure of the hydraulic circuit and the load acting on the fluid and these must also be taken into consideration.

The simulation structure shown in Fig. 1 is used in order to be able to use the ageing simulation for these variable requirements. A distinction must first be made between the necessary training of the neural network shown above and the actual simulation application shown below. The simulation is divided into two possible paths: one of these beginning from an existing circuit diagram and the other beginning from an existing system. The velocity k of chemical reactions is a function of temperature T, activation energy E_A , universal gas constant R and the pre-exponential factor A in accordance with the Arrhenius equation (Eq. 1).

$$k = Ae^{-E_A / RT} \qquad \text{Eq. (1)}$$

Compared with other factors a dominance of the thermal influence on ageing is evident in many previous studies [KEM, WER, SCH; ZHA]. It is therefore important to know the way in which heat is distributed throughout the system and this is determined by means of a thermal simulation or by measuring the heat in the various partial volumes V_i within the system. The pressure values p_i for the partial volumes can also be determined at the same time. As the size and number of partial volumes generally vary from one hydraulic circuit to another and a neural network always requires a constant number of input variables, the temperature and pressure distribution values obtained by simulation or measurement must be processed in an appropriate manner. This is done by generating suitable characteristic values, which combine the temperature distribution values and constitute characteristic variables for the structure of the circuit. These characteristic values are therefore the input variables for a neural network, which calculates the lifetime prediction as a function of the complex of loads acting on the fluid. While the load acting on the fluid is described in the characteristic values irrespective of the fluid's properties, the neural network implicitly contains the oil-specific ageing properties.

Training is necessary in order to optimise the initially unknown weighting factors for the neural network. This is shown in the upper part of Fig. 1. Different hydraulic circuits are selectively simulated on suitable test rigs for this and the distribution of temperature and pressure are measured. Characteristic values are generated from this data and specified as the input variables for the neural network. The lifetime of the fluid is determined experimentally for each configuration by means of ageing tests. The measured lifetime serves as the specified output variable for the neural network. These output variables can then be combined with the appropriate input variables, enabling the use of algorithms to optimise the weighting factors.

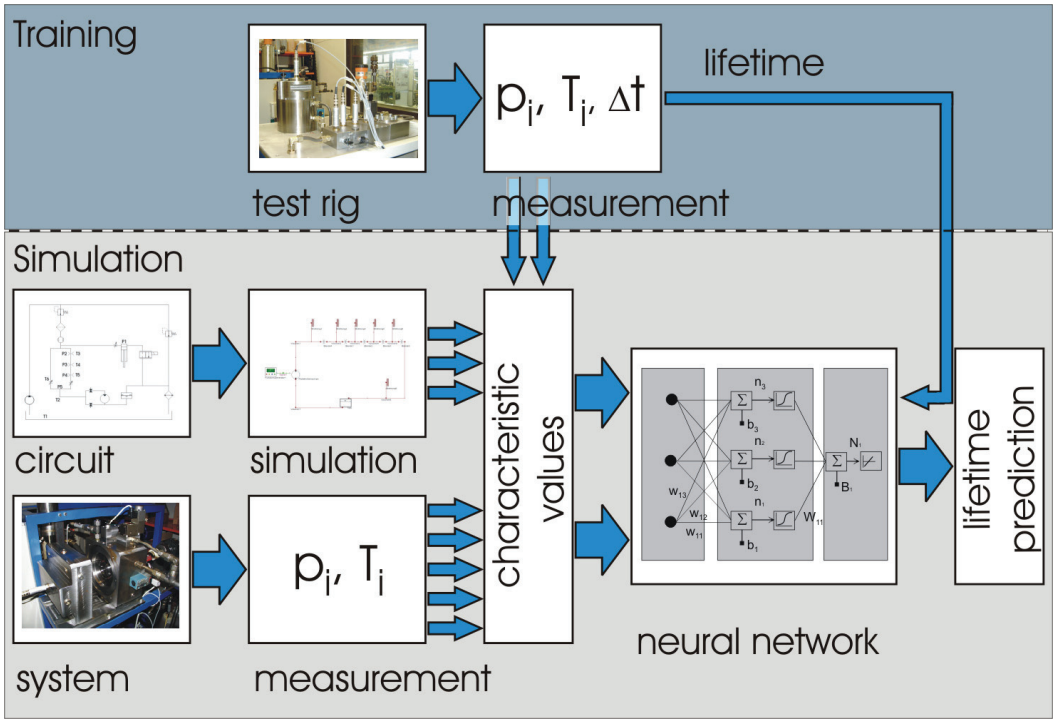

Figure 1: Ageing simulation structure [GOE]

3. SIMULATION TOOL

Digital simulation tools are a common part in the development of hydraulic systems. Computational fluid dynamics (CFD) enable the analysis of fluid flow in hydraulic components for example valves in order to optimize the flow characteristics. These tools are able to calculate heat flow as well as volume flow and can be used for a combined hydraulic and thermal analysis of a hydraulic component. Due to the efforts necessary to model each volume with a grid of finite elements common CFD programs are only capable to simulate components instead of complete hydraulic systems. For the purpose of a life-time simulation of oil, the knowledge of the temperature distribution throughout the system is necessary. Therefore CFD simulation tools are not suitable in this context.

The dynamic behavior is of interest in the design process of many hydraulic drives. To gain knowledge concerning the dynamics of a system without cost intensive prototypes digital system simulation programs are used. The system is divided into components and for each component a flow function is used to describe its flow characteristic. When defining volumes between each component the pressure build up can be calculated, Fig. 2.

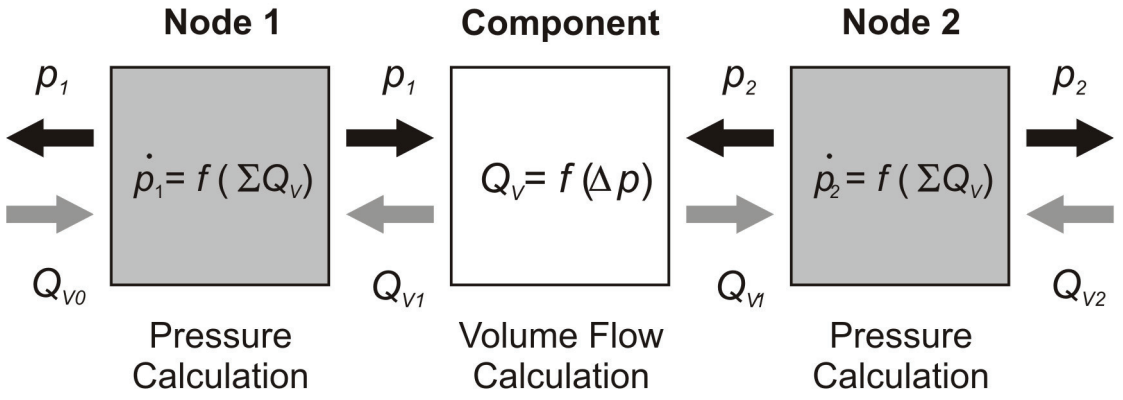

Figure 2: Approach of system simulation

The used software DSHplus [NN] offers libraries which contain common components with their specific flow characteristics $Q_v = f(\Delta p)$. Due to the simplification of each component to a mathematical description, the modeling of complete systems including tanks, pumps, valves and motors is possible. The components can be arranged graphically and linked together by nodes.

Analogous to the balance of the volume flows Q_V and the calculation of the pressure build up a balance of heat transfer $\dot{Q}_H$ and the change in temperature is computed in the nodes, if thermo hydraulic components are used, Fig. 3. Each thermo hydraulic component is either a heat source, for example an orifice where hydraulic power is converted in heat, or a heat sink. Because of this real physical components have to be modeled with two components. The thermo hydraulic behavior of a valve for example will be calculated by a valve component which describes the volume flow pressure dependency and forms the heat source. The heat transfer of the housing of the valve is modeled by a “HeatEmission” component with the parameters heat transfer

coefficient α, surface of heat exchange *A* and a heating delay time after which a change in fluid temperature becomes apparent at the wall surface.

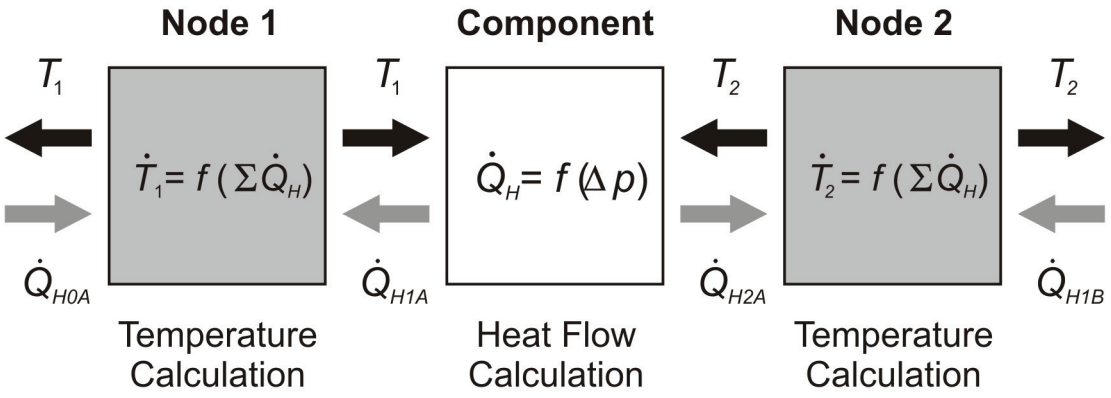

Figure 3: Temperature calculation

The heating delay time is necessary due to the definition of the control volume. The balance of heat is formed on the boundary of the fluid. The heat capacity of the surrounding hardware component, for example the housing of a valve, is not taken into consideration. The heating delay time enables a coupling of the volume of the fluid and the surface of the component. This is correct in steady state conditions, but causes to high fluid temperatures during the unsteady heating up. The heating delay time is used to parameterize a PT_1 element which only delays the transport of heat. Heat originating from hydraulic power losses with in a component is not used to heat up the cold component in this simulation approach. Therefore the fluid temperature down stream of the component is calculated to high during the heating up.

The heat transfer coefficient can be either estimated, which can lead to simulation results far from reality, or calculated by use of thermodynamic and heat transfer theorems.

4. THERMODYNAMICS

The first law of thermodynamics for steady flow processes as given in eq. 2 is an energy balance for a mass flow $\dot{m}$ between the states 1 and 2. The left side of the equation describes the power output across the balancing boundary consists of a thermal $\dot{Q}_{H12}$ and mechanical P_{12} part. The right side of the equation contains the energy of the mass flow with the enthalpy *h*, the kinetic energy, described by the flow velocity *c*, and the potential energy, described by the acceleration of gravity *g* and the height *z*. If the changes in kinetic energy and the change in the potential energy are neglected, eq. 2 can be simplified to eq. 3.

$$\dot{Q}_{H12} + P_{12} = \dot{m}\left[h_2 - h_1 + \frac{1}{2}\left(c_2^2 - c_1^2\right) + g\left(z_2 - z_1\right)\right] \qquad \text{Eq. (2)}$$

$$\dot{Q}_{H12} + P_{12} = \dot{m}\left(h_2 - h_1\right) \qquad \text{Eq. (3)}$$

Equation 3 allows the calculation of temperature in state 1 and 2 if the exchanged heat and power is known. The differential equation, which is solved by DSHplus, is based upon eq. 3. It can be used to calculate the necessary heat exchange coefficient, if the states 1 and 2 are measured exactly. The disadvantage of this approach is the high effort of temperature, pressure and power sensors on the one hand and the difficulty of transferring the findings from one system to the next on the other hand. Thus a method based on the heat transfer theorems is necessary.

Heat transfer can be divided into the principles of heat conduction, convection and radiation. Heat conduction takes place in the housing of each component to transfer the heat from the flow to the surface of the component. The term convection means a heat transfer by a flow of gas or liquid. The air flow on the outside of the component is an example for a heat transfer by convection. Radiation describes the heat exchange between two surfaces by photon radiation without regarding the temperature of the medium between the surfaces.

If the air flow surrounding the component where convection takes place is laminar, the heat flow $\dot{Q}_{HC}$ can be calculated by Newtons approach:

$$\dot{Q}_{HC} = \alpha A(\vartheta_S - \vartheta_\infty) \qquad \text{Eq. (4)}$$

In eq. 4 α is the average heat transfer coefficient, A the size of the surface, ϑ_S the average temperature of the surface and ϑ_∞ the air temperature in distance to the surface. The average heat transfer coefficient α depends on velocity and temperature distribution around the surface. The temperature distribution can be described by the nondimensional Nußelt number *Nu*, with the heat transfer coefficient α, a characteristic length L and thermal conductivity λ, eq. 5.

$$Nu = \frac{\alpha L}{\lambda} \qquad \text{Eq. (5)}$$

For each convection problem the Nußelt number *Nu* can be described as a function of nondimensional coordinates on the surface *x y*, the Grashof number *Gr* and the Prandtl number *Pr*.

$$Nu = f(x^*, y_S^*, Gr, \mathrm{Pr})$$
$$Gr = \frac{g\beta(\vartheta_S - \vartheta_\infty)L^3}{\upsilon^2} \qquad \text{Eq. (6)}$$
$$\mathrm{Pr} = \frac{\eta}{\lambda / c_P}$$

The Grashof number contains the acceleration of gravity g, expansion coefficient β, the surface temperature und temperature in a distance, the characteristic length L and the dynamic viscosity υ. The Prandtl number is a material specific number formed by the cinematic viscosity η, the thermal conductivity λ and the specific heat c_p. For air as cooling fluid the Prandtl number can be derived from tables.

The function of the Nußelt number can be determined in experiments with model shapes. For a number of model shapes such as discs, cylinders, spheres or cubes

functions are available[FUJ] The function for a horizontal disc with a laminar flow the Nußelt number can be calculated by eq. 7 [REN]:

$$Nu = 0.54(Gr * \Pr)^{0.25} \qquad \text{Eq. (7)}$$

The shapes of the components of the hydraulic system have to be reduced to simple shapes with known functions for the Nußelt number. Then surface temperatures can be measured and the Grashof and Prandtl numbers can be calculated. Based on these numbers and the function of the shape model the Nußelt has to be computed. By use of eq. 5 the desired heat transfer coefficient α for convection can be calculated.

In addition to convection, radiation has an effect on the heat flow balance of each component. A part from the ideal blackbody, which absorbs all radiation on its surface, the radiation behavior of an existing grey body is determined by the grade of transmission, reflection and absorption depending on the wavelength of the radiation. The exchange of energy between two surfaces by radiation depends on the temperatures of the surfaces, their character and their orientation towards each other. All surfaces visible from the emitting surface have to be taken into a balance of radiation. The complex geometry of existing systems and their surrounding makes this balance impossible. A simplified radiation model for a surface completely surrounded by a second one is used to estimate the influence of radiation on the heat transfer coefficient. Figure 4 illustrates the assumption. Each of the surfaces is described by its size *A*, the grade of emission ε and the grade of reflection ρ.

According to [CEB] the flow of radiation $\Phi_{N,12}$ for this model is given by eq. 8, with the surface temperature of the component T_1 and the distance temperature T_2.

$$\Phi_{N,12} = C_{12} A_1 \left[\left(\frac{T_1}{100} \right)^4 - \left(\frac{T_2}{100} \right)^4 \right] \qquad \text{Eq. (8)}$$

[VDI] recommends C_{12}= 4.7 W/m²K^4 for technically grey surfaces.

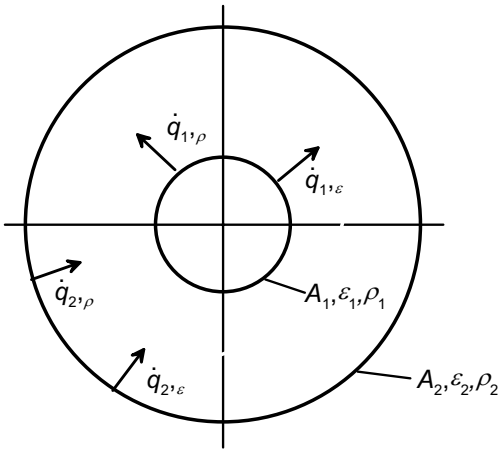

Figure 4: Surrounding surfaces

Based on the flow of radiation and the same temperature difference for convection and radiation an apparent heat transfer coefficient for radiation can be defined [CEB],eq. 9.

$$\alpha_r = \frac{C_{12}\left[\left(\frac{T_S}{100}\right)^4 - \left(\frac{T_\infty}{100}\right)^4\right]}{\vartheta_S - \vartheta_\infty} \qquad \text{Eq. (9)}$$

The sum of the heat transfer coefficient for convection and the apparent heat transfer coefficient for radiation is the desired total heat transfer coefficient to parameterize the heat exchange component of DSHplus.

The calculation shall be illustrated by an example in the following. For a fitting and a tube as given in figure 5, the heat transfer coefficient will be computed. Similar to this, all components of the hydraulic system have to be evaluated.

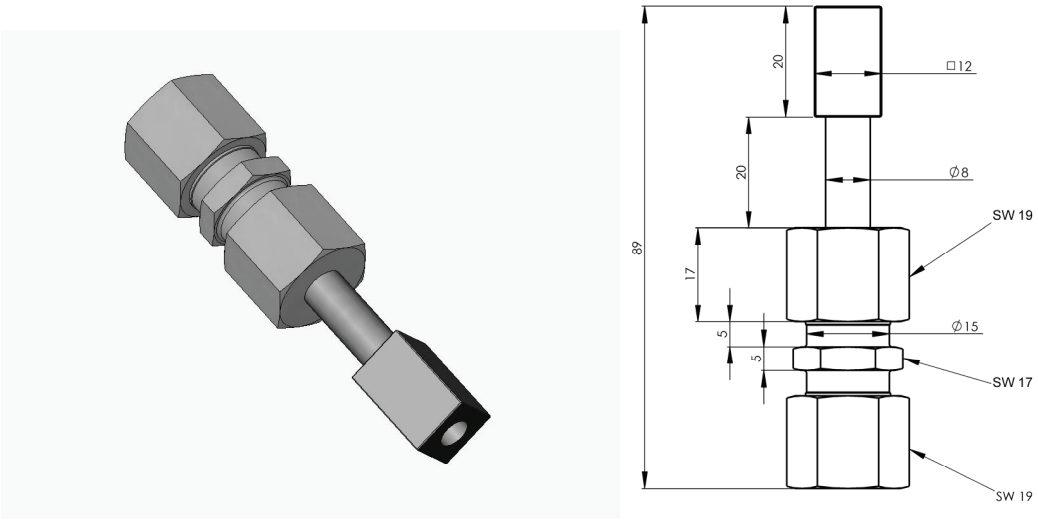

Figure 5: Component example

The component example consists of different parts of different diameter and length. The components will be modeled as a single vertical cylinder. Therefore a reduced diameter is necessary. The weighted average of the hydraulic diameter $d_{hyd} = 4A/U$ with the length as weight is used. Equation 10 gives the weighted average of the diameters of the components. The example component is thus simplified by a singlevertical cylinder with the length L = 89 mm and the diameter d = 14,93 mm.

$$d_m = \frac{1}{L}\sum d_i l \ = 14{,}93mm \qquad \text{Eq. (10)}$$

The Nußelt number for a vertical cylinder according to [FUJ, VDI] is equal to the Nußelt number of a vertical disc with the same height and the term $0.87 * L/d_m$. Combined with the Nußelt number for a vertical disc [VDI]equation 11 results.

$$Nu = \left[0.825 + 0.387\left(Gr * \mathrm{Pr} * \left(1 + \left(\frac{0.492}{\mathrm{Pr}}\right)^{9/16}\right)^{-16/9}\right)^{1/6}\right]^2 + 0.87\frac{L}{d_m} \qquad \text{Eq. (11)}$$

With the Grashof number and Prandtl number according to eq. 6 and a surface temperature $\vartheta_S = 90°C$, a distance temperature $\vartheta_\infty = 20°C$, an expansion coefficient of 1/293 K, a cinematic viscosity of $18.63*10^{-6}$ m²/s and a Prandtl number of 0.7095 the Nußelt number is 28.21. With equation 5, the heat transfer coefficient for convection can be calculated to 8.94 W/m²K.

The apparent heat transfer coefficient for radiation can be calculated according to eq. 9. Additionally to the values above the surface of the model cylinder with $A = \pi d_m L = 41.74$ cm² is used to compute $\alpha_r = 6{,}72$ W/m²K.

The sum of both calculated heat transfer coefficient 15,66 W/m²K is than used to parameterize a DSHplus component.

5. RESULTS

Special ageing test rigs have been set up at the IFAS in order to provide a sufficient high volume of data for network training. The flexible connection facilities of these test rigs offer a means of mapping a large number of different circuits and examining their respective ageing characteristics. Figure 6 shows the hydraulic circuit diagram for the test rigs. The so-called resistor unit can be seen on the left-hand side, comprising three screw-in orifices and a variable restrictor connected in parallel. Various hydraulic circuits can be simulated by varying the orifices and the throughput characteristics of the restrictor. There is a tribometer on the right-hand side. It consists of one static and one rotating disc, which are pressed together with a defined load. Both discs contain grooves in their contact surfaces which allow the hydraulic fluid to enter the tribological contact and to interact with the surface materials. The cylinder is used to press the two discs together and one of these is driven by the fluid motor. The fluid flowing back into the motor is used to lubricate the mating surfaces of the two test specimens. Different characteristic tribosystems with their respective ageing influence can be introduced into the system by varying the test specimen, the surface pressure and the relative velocity. The test rig has been designed in such a way as to enable the measurement of pressure and temperature distribution

The set up of the test rig is build up in the simulation program successively in several steps of increasing detail starting with pump, tank and pressure relief valve in order to avoid errors. This basic system was enlarged step by step by more components up to complete system by measuring the surface temperatures at a steady state of operation and calculating the heat transfer coefficient according to chapter 4.

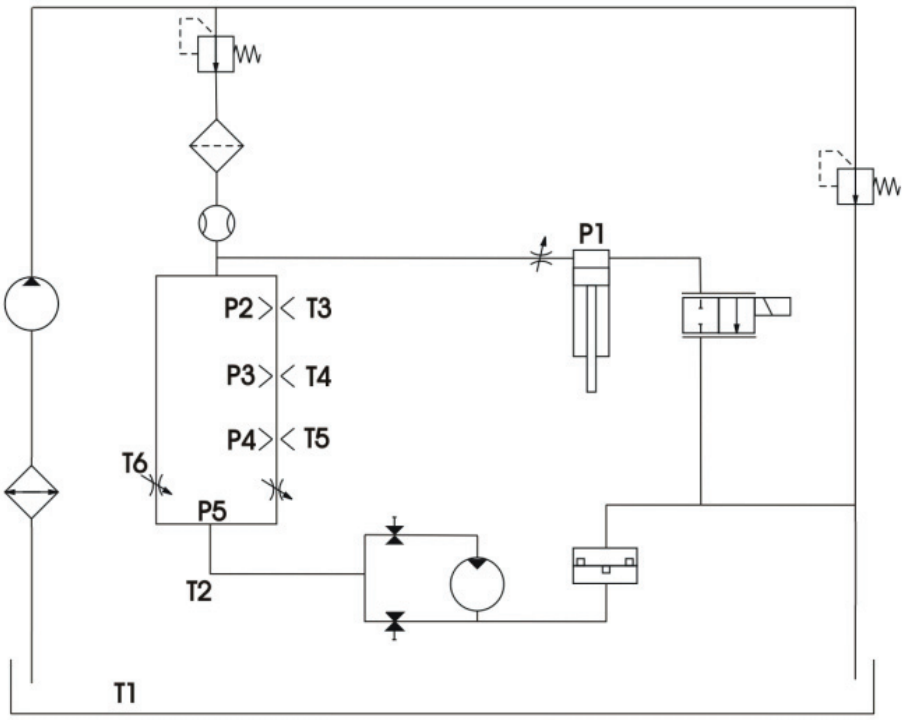

Figure 6: Test rig lay out

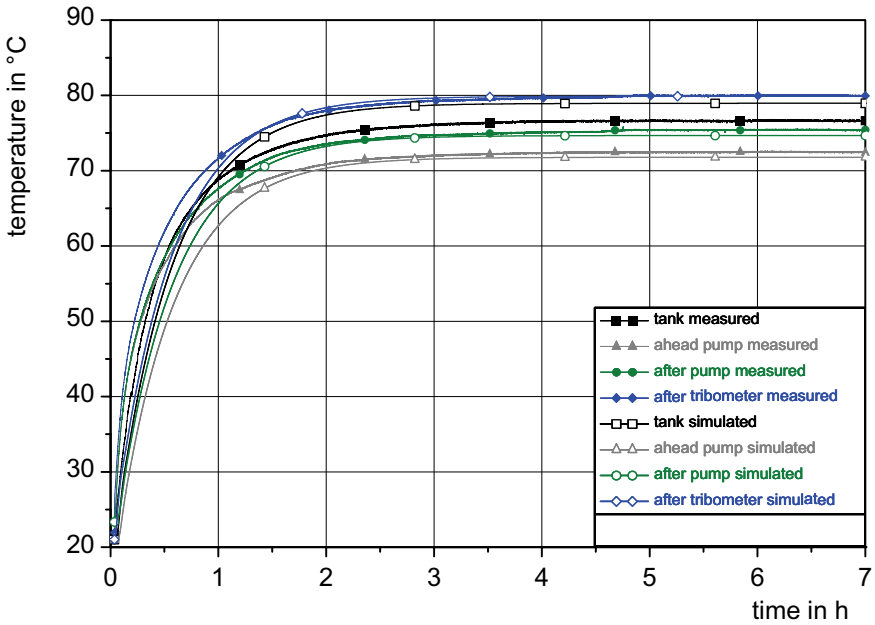

Figure 7: Comparison of the simulated and measured temperatures

A simulation concerning the temperature distribution within the test rig has been conducted. The set up contained the tank, the heat exchanger, the pump, the filter

element, the volume flow sensor, the orifices and the tribometer in passive mode. This means, that the hydraulic motor is bypassed and not rotating. Thus no friction was applied to the tribo contact within the tribometer. Figure 7 shows a comparison of the simulated and measured temperatures. Due to the simplifications of the radiation, the apparent heat transfer coefficient is slightly to high. This can be concluded from the temperature difference between measured and simulated temperature in figure 7. The measured temperature is always higher. The maximum difference occurs at the tank volume with a 3 °C higher measured temperature.

6. CONCLUSION

To conduct a life-time simulation for hydraulic fluids, knowledge concerning the temperature distribution in the hydraulic system is necessary. To simulate the temperature distribution a method to parameterize thermohydraulic components was suggested. Based on heat transfer theorems models for each component can be derived in order to calculate a heat transfer coefficient. Due to the complex processes of heat transfer, measurements in advance of the simulation are necessary to derive the input parameters to heat transfer models. With the developed temperature simulation model the temperature distribution can be simulated with an error of 3 K. In the future work this simulation tool will be embedded in the simulation concept for the life-time of hydraulic fluids.

7. ACKNOWLEDGEMENT

The work described in this article makes up part of sub-project A3 of the research project concerning "environmentally compatible tribosystems by means of suitable composites and precursor materials, using the machine tool as an example" conducted by collaborative research centre 442 at the Institute of Fluid Power Drives and Controls (IFAS) at RWTH Aachen University. This collaborative research centre is sponsored by the German Research Committee (DFG) and the authors would like to thank the DFG for its financial support.

Thanks to Mr. Dipl.-Ing. Andreas Laakmann who made many improvements of the simulation possible.

8. REFERENCES

[CEB] Cerbe, Günter; Hoffmann, Hans-Joachim, 1996, Einführung in die Thermodynamik, 11. Auflage

[FUJ] Fujii, Tetsu; Uehara, Haruo, 1970, Laminar natural-convective heat transfer from the outer surface of a vertical cylinder, Int. Journal Heat and Mass Transfer 13

[GOE] Göhler, O.-C., 2006, Approach to the simulation of ageing of environmentally compatible fluids in hydraulic systems, International Journal of Fluid Power 7, No 2

[KEM] Kempermann, C. 1999. Ausgewählte Maßnahmen zur Verbesserung der Einsatzbedingungen umweltschonender Druckübertragungsmedien [Selected measures to improve the operating conditions of environmentally compatible hydraulic media], Dissertation, RWTH Aachen University

[MUR] Murrenhoff, H. 2004. Einführung zum Symposium des SFB 442, Umweltverträgliche Tribosysteme [Introduction to the Symposium of the Collaborative Research Center 442 'Environmetally Friendly Tribo Systems'] Proceedings of "Reibung und Verschleiß", march 9th to 12th 2004, Fürth, Germany

[NN] N.N. ,2006, User Manual DSHplus 3.5, Fluidon GmbH, Aachen, Germany

[REN] Renz, U. 1988: Grundlagen der Wärmeübertragung, lecture notes, RWTH-Aachen

[SCH] Schmidt, M. 2003. Untersuchung und Ansätze zur modellhaften Beschreibung der Alterung auf Estern basierender Zwischenstoffe für den Einsatz in umweltverträglichen Tribosystemen [Study and approach for modelling of the ageing behaviour of ester-based precursor materials for use in environmentally compatible tribosystems], Dissertation, RWTH Aachen University

[VDI] N.N., 2002, VDI-Wärmeatlas, 7.Auflage, Verein Deutscher Ingenieure

[ZHA] Zhang, X. 2004. Alterungsmechanismen ökologisch verträglicher Druckflüssigkeiten [Ageing mechanisms of ecologically compatible hydraulic fluids], Dissertation, RWTH Aachen University

Learning environment for training the forest machine mechanics

Palonen, T., Leino, T., Koskinen, K.T.
Tampere University of Technology
Institute of Hydraulics and Automation

Ranta, P., Punki, J., Mäkelä, T.
Tampere University of Technology
Hypermedia Laboratory

P.O.Box 589
33101 Tampere, Finland
Phone +358 3 365 2177, Fax +358 3 365 2240
E-mail: tuija.palonen@tut.fi

ABSTRACT

In this paper we describe the theoretical framework and technological solutions of the development of virtual and intelligent learning environment project (ForMecVir). Objective of project is to develop efficiency, quality of instruction and learning and attractiveness to the field of forest machine mechanics. Project will be realized in co-ordination with North Karelia Municipal Education and Training Consortium.

The pedagogical framework presented in this paper supports the development of appropriate learning environment for vocational education of the forest machine hydraulics for mechanics.

The physical modelling of the forest machine boom consists of three cylinders. The proportionally working directional valves controlling the flow to the cylinders include the Load Sensing function that is applied by the use of the variable displacement pump. Three-dimensional dynamic graphics of the hydraulic system will provide essential help for students in understanding functions of the hydraulic system.

KEYWORDS: Mechanics training, virtual learning environment, intelligent learning environment, Real-time simulation, 3D-graphics

1 INTRODUCTION

Operating systems of the mobile work machines have been developed during last years and the change will continue rapidly due to digitalization and automatisation. The understanding of digital management, control and measurement system requires new kinds of diagnostic skills, measurement, troubleshooting and assembling. How these skills could be educated efficiently? This means also challenges especially to the competence requirements of professional assemblers and mechanics. How we are able to support complex troubleshooting skills, deep understanding of whole system, combining theory and practice to reasoned actions? Nowadays vocational education is front of this challenge. This means also challenges for manufactures, who are implementing new generation technologies, because there are demanding requirements of utilization rate. There is the significant need for know-how of a skillful mechanic. There is also a lack of students who are interested in to become a mechanic especially in the Nordic countries. Also a huge amount of experienced mechanics will be retired during following years, when there are also fears that a huge amount of tacit knowledge will disappear. These challenges are identified in many branches especially in forest machine mechanic education.

Virtual learning environments are one solution to tackle challenges, because possibilities of educational technology have been developed to the appropriate level due to the PC, software and network technologies. This gives possibilities to enhance education with interactive, real time and dynamic simulations, 3D virtual reality illustrations, web-based interfaces, adaptive hypermedia, learning material repositories and intelligent tutoring systems. These technologies make possible to develop new kind of tools for instructors to develop didactical methods to match needs of education, new generation students and requirements of industrial branches. There are many new educational approaches, which give reasoned framework to develop learning environments appropriate way. The implementation of educational technology does not solve all educational challenges. Lehtinen stress the use of educational technology is essential part of a broad comprehensive training development program [1].

Diagnostic systems of forest machines have been developed significantly during last years. Those systems are able to limit the failure into certain area, but the actual problem solving and the causality is far more difficult. There are a lack of learning environments, instructional methods and training materials.

1.1 ForMecVir – Project

ForMecVir learning environment contain tools for students and teachers. Main tools are 3D dynamic visualization of the system and circuit diagram with the visualization of the process. It is possible to measure for example pressures, flows and temperatures. Student can control and observe movements of machine. He or she can also adjust and repair components of hydraulic system. Tutor and adaptive learning materials offer support and guidance for fault diagnosis and inference. An instructor is able to do task description, plan the learning process, publish the task, guide, arrange debriefing and evaluate the result with help of the tools of virtual learning environment. Principle of result evaluation is based on framework for the instructional assessment [2].

In ForMecVir project several organizations work in cooperation. These organizations are Tampere University of Technology (Institute of Hydraulics and Automation and Hypermedia Laboratory), eLearning Network –elTRIO, North Karelia College Valtimo, Ponsse Oyj, Komatsu Forest Oy, John Deere Forestry Oy, Witraktor CAT and Parker Hannifin Corp. Project is supported by Finnish Ministry of Education and forest machine colleges. Project will continue to year 2009.

2 PEDAGOGICAL FRAMEWORK

Pedagogical framework of ForMecVir -project is ground to the idea that the virtual learning environment should have the added values to forest mechanic education and it offers tools for instructors to develop quality of learning. It should be suitable for varied pedagogical approaches and methods, because it is very demanding to define one optimal "grand theory of learning" for every context. There are more than 50 different theories of learning [http://tip.psychology.org/theories.html]. It is also hard to try combine different frameworks into one model because educational decisions are very often compromises. Main idea of the virtual learning environment is to make possible to utilize student centered, shared knowledge construction and problem based approaches interlinked with collaboration and traditional methods.

The traditional problem of the vocational education is how to combine theory and practice in the development of deep understanding. The development of deep understanding and assembling skills of modern control and management systems is very challenging, if the whole is insufficiently managed. The question is how we are able to develop both conceptual, declarative knowledge (what and why) and operational, procedural skills (how) interlinked with instructional methods and possibilities of learning environment? Another question is how we are able to support decision making, meaningful knowledge construction and reflection in or on action in these dimensions [3]? Our idea is that with tools of virtual learning environment it is possible to achieve varied and meaningful views and knowledge of the scope of a subject. This interlinks theoretical and practical dimension together. One example is that a student is able to study tasks in same scope of a subject with hydraulic diagram, animated interactive process diagram, cutaway view of the moving machine, measurement and illustration tools of dynamic features and video of real machine.

The learners are not acting impulsively or haphazardly in the learning environment, but are able to take cognitive responsibility of their own learning process. It is possible to reach deeper understanding by taking the cognitive responsibility and reflecting on what is to be expected [1]. Education is always oriented with the goals. These goals are shared with students and instructors. However, one cannot guarantee that every learner takes the cognitive responsibility even if the methods and tools are "optimal".

According to Jonassen et al. traditionally technologies have been used in schools to "teach" students, much the same as teachers "teach" students. When technologies teach information is stored in the technology, which presents the information to the students, who try to understand and remember it. Jonassen et al. also argues that technologies should be used as knowledge construction tools that amplify abilities of the learner to construct knowledge for themselves, rather than be "taught" by preprogrammed lessons

[4]. In the design of virtual learning environment several points of view should be taken into account. Pohjolainen et al. emphasis strong forms of interaction in learning environment by designing the assignments, the content, the feedback, the collaborative and cognitive tools to operate together in supporting the learning towards the objectives [5]. Youngblut stress also appropriate feedback and meaningful interactivity [6].

Transfer of learning is basic concepts of education. The learning processes and outcomes should be transfer to the real environment. Transfer of learning is the application of skills and knowledge learned in one context being applied in another context [7]. De Corte defines transfer as the broad, productive, and supported use of acquired knowledge, skills, and motivations in new contexts and learning tasks [8]. Features of virtual learning environment should support transfer of learning so that students can construct mental model and mind tools, which can support action in new contexts [9]. The concept "infer" has very narrow meaning of this idea. According to Ranta support of decision making is important part of learning in simulator-based learning environment [10, 11].

Authentic problems and cases are important. Grabinger and Dunlap emphases that learners should be presented with complex environments that represent interesting and motivating tasks, rather than contrived sterile problems [12]. In the context of education of mechanic the appropriate approach should be defined by professional instructors. Without knowledge and experience of domain, it is not possible to develop appropriate solutions.

Huhtamäki et al. suggests that there is also need for a system, which will capture the recording of the action in a way that it can be reflected. The user is more likely to learn when his progress is tracked and meaningful information is delivered to him as he is experiencing problems. In the simulator domain the debriefing is a very important part of the learning and teaching process. If we can move a part of the debriefing to system using intelligent tutoring systems, it is possible to evaluate the recorded action according to a set of appropriate themes. [2]. Idea is connected with the explicit and tacit knowledge of experienced doer. This knowledge can be used as a reference model to assess tutoring needs, define intelligent rules of support and in debriefing.

Tacit and explicit knowledge have been expressed in terms of knowing-how respectively. They have also been viewed as embodied knowledge and theoretical knowledge, respectively. Knowing-how, or embodied knowledge, is characteristic of the expert who makes judgment or decisions without explicitly going through a set of rules. By contrast, knowing that, or theoretical knowledge, is when person learning a skill articulates available knowledge using explicit instruction, rules, principles, or procedures [13]. Tacit knowledge is primarily heuristic (rules of thumb), mind-sets, and unconscious values. The downside is that is occasionally wrong and hard to change [14].

A troubleshooting and problem solving in very complex environment is demanding, so there is need to support and scaffold these processes. Discussion with experienced mechanics, instructors and maintenance heads shows that mechanics have quite similar thinking process. It has plenty of analogies with thinking of engineers. A mechanic should have a broad and deep understanding in conceptual and pragmatic levels.

1. Focus and limit a fault(s) with reasoning, heuristics, experience, tests, diagnostic tools, and guides.
2. Make hypothesis of a reason of fault(s).
3. Plan reparation solutions based on the hypothesis with temporary or final operations.
4. Repair the fault
5. Plan and do the test.
6. Reflect on the consequence of this problem solving and reparation. Make documentation.
7. If needed, start from the beginning or previous states.

It seems meaningful to use this kind of metaphor in instructional tasks. Also narrative of troubleshooting in real like working context with experienced virtual tutors and product support of machine manufacture gives motivational analogy to study.

We can use also cognitive tools to support learning. According to Jonassen cognitive tools refer to learning with technology (as opposed to learning through technology). These help learners with complex cognitive learning activities and critical thinking. Jonassen stress technologies afford the most meaningful thinking when used as tools [9]. Cognitive tools are learner controlled in the sense that they construct their knowledge themselves using the tools rather than memorizing knowledge. Traditional computer based cognitive tools are memos, concept maps, knowledge visualisations, debriefing solutions and simulation.

Lehtinen compiles pedagogical guidelines for designing computer-based learning environment for complex learning [1]:

1. Facing complexity from the beginning of the study process.
2. Appropriate integration of expert guidance and spontaneous exploration.
3. Integration of authentic problems and abstract reasoning.
4. Improving task-related social interaction.
5. Providing multiple representations.

Design of ForMecVir -learning environment requires multidisciplinary group, where professionals of domain, computer science, educational planners, instructors, technology developers, usability experts, administrators and also users are in collaboration. ForMecVir - project has this kind of research and development group.

3 SIMULATION OF HYDRAULICS

Simulation model will be developed so that the typical faults appearing in this king of hydraulic systems in forest machines can be modelled and the signals of the system state can be sent to the user interface. The requirement that the system simulation must run as a real-time mode makes special demands on the modelling. The exact physical description of the real system may not be used in real time, but the details of the component structures must be simplified, while preserving the models ability to express the fault in the component. The current plan is to use two parallel models – an accurate, highly detailed model that is not used in the real-time mode, and a simplified real-time

model, which is verified against the detailed model. The model structure must be such that the phenomena detected by the mechanic in the general fault diagnostics can be found. The model gives also many other quantities that are not possible to measure in the real system. Despite that they can not be used in teaching of the fault detection, they are valuable to the student when trying to understand the operation of the hydraulics system.

The hydraulic system to be modelled is composed of the parts typical of a general forest machine. In the first phase of the project, the parts are from a loader boom of the forwarder. In practice, the actuators moving the loader are applied using the Load Sensing functions in the modern forwarders. In this case, the main parts of the hydraulic system are three cylinders making the motions of the lifting, luffing and extension booms. Three similar load sensing valves are used with the variable displacement pump. The valves and the pump are from the same manufacturer and are designed to work together so that the pressure between the pump and the valves follows the maximum pressure needed in the actuators. The simplified hydraulic diagram without the additional valves is presented in Figure 1.

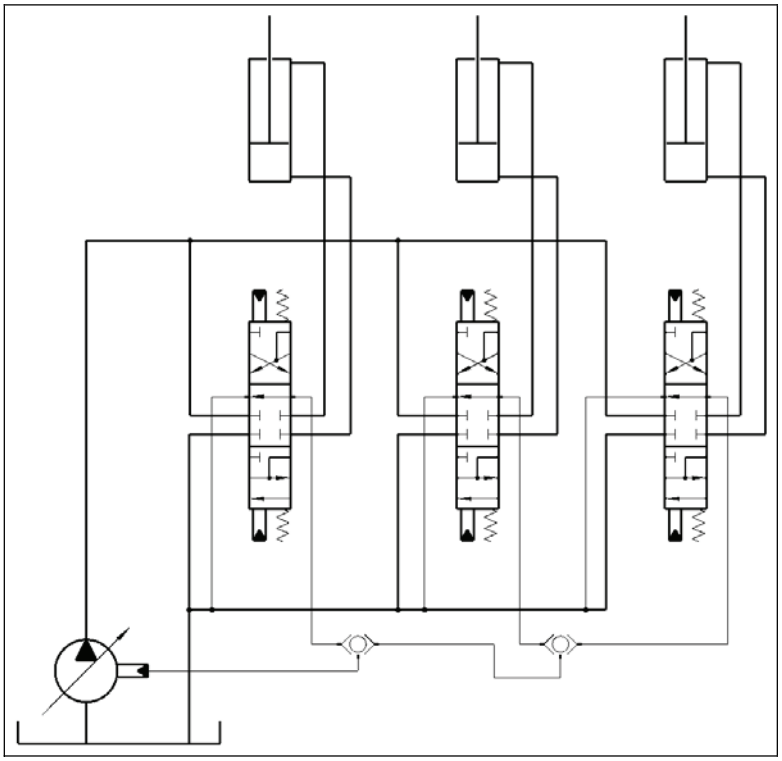

Figure 1. Simplified hydraulic diagram.

The real hydraulic system of the forwarder includes also much more than the actuators, valves and the pump. However, the present system is focused to analyse faults in these components and in their operation together. Only these components will therefore be modelled in detail. The connection to the other parts of the hydraulic system will be made as simplified or will be left off, if operation of the other system part has no influence to load sensing system and there is no intension to model faults that are transferred from that part of the system. In some cases, it is still possible to allow for the influence of the outer system. These are, for instance, the faults in the braking system

that are causing the load sensing pressure to behave abnormally or similar faults in the auxiliary actuators.

The directional valve having the load sensing function contains several separate valves and there are many alternatives for the complete configuration of the valve. Figure 2 introduces the parts inside the load sensing valve. All the parts will not be in use in all three valves in the system.

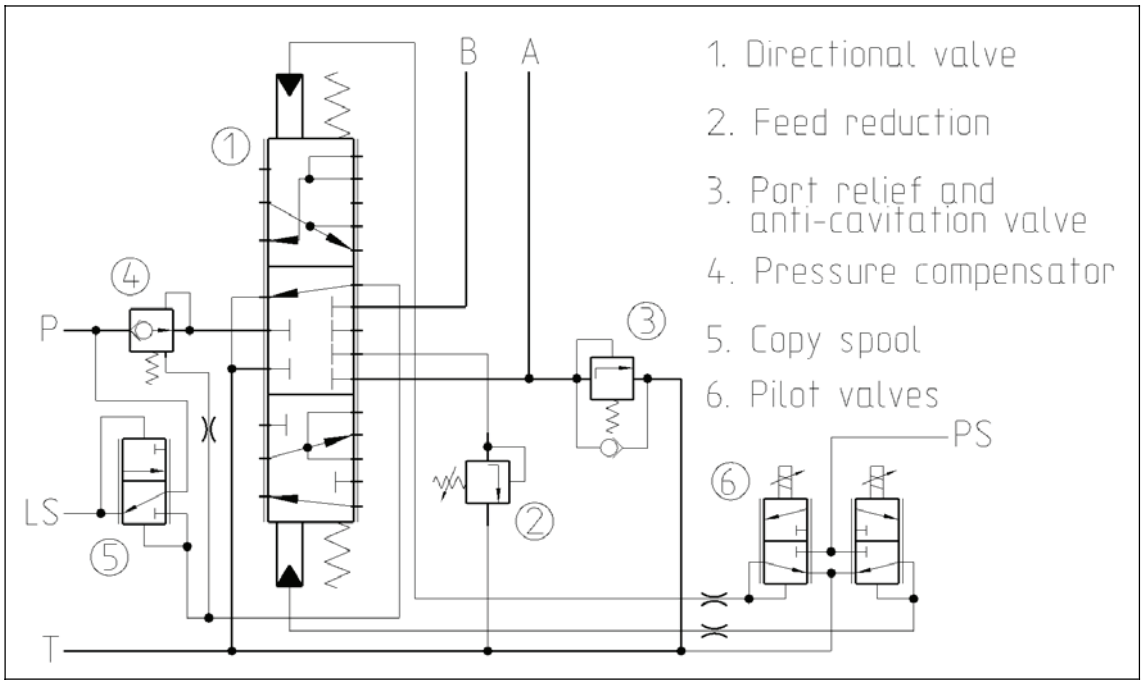

Figure 2. Load sensing valve with additional valves.

Typical faults in the valve are caused by contamination of dirt restraining the motion of the mechanical parts or blocking the flow in orifices. Potential places for the blockage are the orifices in the pilot valves. The other type of faults is leakage, which may be caused by damage or wear in the seal. The contamination can also cause leakage. One example of this is if there is installed the valve for copying internal load sensing pressure from the pressure line to the pump load sensing line, but it is not enabled. In this kind of case the dirt may bunch to the valve and cause a leak. Clear faults, like mentioned above, are simple to add into the simulation model by just modifying the size of the orifice or adding new orifice to describe the leakage. The blockage or leakage can also be different in the other direction than the other. In such a case, the fault is modelled as a combination of the orifice and the check valve.

The simulation will be realised in Matlab Simulink model. The end use of the simulation will run in an Embedded Matlab xPC machine that makes larger model possible to run in real-time, because any additional operating system is not needed in the computer. This configuration prevents the use of the sophisticated variable step solvers. The use of them is still possible in the detailed model and thus the verification of the solver influence can be made.
Few questions in piloting were focused to the simulation and how it should be seen and adjustable by the end users. Most of the participants had an opinion that the real-time effect is important to the learning environment. The opposite alternative in the question

was the analysing of the information given by the simulation. Another question was about the openness of the model i.e. how much the end user is allowed to adjust the parameters in the model. The public opinion was that the teacher is absolutely necessary to get modify the model so that he/she can create new fault situation. It these situations, the system internal tutoring can not follow the students problem solution process. It was also seen important, that the student can change parameters like pipe lengths, orifice sizes etc. to learn how the system works.

4 LEARNING ENVIRONMENT

The structure of the ForMecVir -learning environment is operationalised and designed based on the pedagogical framework. This virtual learning environment has several similar features as training simulators and simulated learning environment. According to Lehtinen effective simulated learning environment should fulfill some basic criteria [1].

1. Simulated cases or problem situations have to be presented authentically. This means that students have to be able to believe that exactly similar problems can be faced in professional practice.
2. There must be enough representational support available for students, which make them possible to cope with the complex problem without too demanding cognitive load.
3. There should be flexible opportunities for students to move between concrete cases and systematic theoretical models.
4. There should be a feedback system in the environment which encourages students to reflect their own solution making processes.
5. The learning environment should facilitate student-to-student and student-to-teacher interaction.
6. The computer-based environment should be an integrated part of the whole instructional context.

Previous list concentrate on the scope of learning processes. It is also necessary to support the work of instructors, so that their resources could be allocate as much as possible to support planning and managing of instruction, learning processes, interaction with students, collaboration, feedback, debriefing and evaluation. Virtual tools and adaptive hypermedia give a plenty of possibilities to support routines of instruction e.g. task description, learning content management, integration with eLearning systems, tailoring, publishing, course management, managing profiency exams, monitoring and assessment, selection of virtual features and parameters and re-use. These kinds of issues raise also needs to develop teachers' competence, organizational factors and instructional methods.

Virtual reality learning environments as training simulators has many added values e.g. repeatability, secure environment, economy, possibilities to control and plan practice, but also limitations [15, 16, and 17]. Ranta [18, 10, 11], van Emmerik [19] and Nählinder [20] find out possibilities e.g. to use pedagogical augmented virtual reality methods in virtual learning environment, which means that a trainee has a chance to get meaningful illustrations to learning, which cannot be used in real learning

environments. In this way an expert or a teacher can analyse operation and they are able to make appropriate guiding decisions. This gives also possibility to create easier learning environments (context) for newcomers and several possibilities to support learning, scaffolding learning, debriefing and reflection in and on action.

4.1 Structure of the learning environment

Based on the pedagogical framework, appropriate pedagogical features of virtual learning environment, ideas of domain professional structure of learning environment seems to consist of following seven subparts.

1. Main course forum
2. Virtual hydraulics learning laboratory (VHLL)
    - Real-time dynamic simulation of hydraulic system,
    - Interactive hydraulic diagram
    - Illustration tools including 3D visualization
    - Measurement and operation facilities
    - Intelligent tutoring system
    - Time manipulation tools
    - Operating models of experienced mechanics
    - Cognitive tools
3. Task management tools
    - Task description
    - Task management of features in VHLL
    - Briefing- studying -debriefing -process management
    - Task library
    - Collaboration tools
4. Assessment reports and debriefing tools
    - Recording
    - Learning process analysis
    - Assessment tools
    - Illustrations
    - Time manipulation tools
    - Assessment library
5. User and role management
6. Learning content repository and adaptive learning material

One important part of the design of virtual learning environment is usability. Use of tools, views and navigation should be designed as user-centered methods. Difficult use and huge amount of information can affect cognitive load so learning process will disturb or even interrupt.

5 TECHNOLOGICAL POSSIBILITIES

Prototype of ForMecVir learning environment is implemented as distributed system. Hydraulic simulation unit is connected via network to end users visualization and control unit. System is designed to be used in class room environment with standard

PCs. There will be also a server for digital learning material and task library which is accessed via Internet. Open document formats like XML is used for learning material. Domain vocabulary can be used to automate the material management [2].

Piloting as part of software development process is a powerful method to test and research new concepts. It also helps keeping the direction of development towards end users real needs [21]. The first piloting event was held to education and industry experts of forest machinery domain. In the event participants used prototypes of learning environment. Used research methods were survey, video recording and discussions about possible features of system. Results that were analyzed and summarized will be taken account in next development step. Main result included that there is a need for this kind of system and hope for easy and practical tool. Results also showed that the current direction of approach is right. The future piloting event will be held to forest machine mechanic students, which are the main target group of system.

5.1 Intelligent tutoring

Eliot & Woolf [22] describes intelligent tutoring as a guidance that adapts suitable for every student during tutoring process. Halff [23] defines three characteristics for intelligent tutoring system. Tutor represents instructional knowledge and appropriate materials of the subject matter. Tutor must be able to respond to student questions about the subject matter. Tutor must be able to determine when students need help and what sort of help is needed.

Intelligent tutoring system (ITS) like any educational program needs same kind of knowledge that is used by teachers: knowledge about students, domain area, teaching and interacting with students [24]. The basic model structure of ITS divides knowledge to student, expert and tutor modules. ITS uses rule engine as a tool for reasoning. Rules are realizations of domain knowledge. Theoretical background of reasoning is mathematical logic.

Tutoring in ForMecVir is divided in tracking of troubleshooting and actual tutoring process. Tracking is used for following and inferencing the situation of troubleshooting process and how the student is proceeding. Tracking uses three sources for information which are user actions, simulation data and externalization of user reasoning. Externalization is needed because ITS can not read users thoughts. Tutoring process is used for giving feedback and advice about current situation to support troubleshooting and learning processes. In ForMecVir user interface of tutoring will be implemented with dialog type interaction.

Results of piloting event regarded to tutoring included some important notices. In prototype target system of troubleshooting was too simple to get good result about how tutor affect on learning and understanding the hydraulic system. Technical support was considered the best metaphor for tutor. Supporting students in troubleshooting is more important than evaluation of the results of exercise. It’s important to teach and encourage students to use some organized troubleshooting method. Both using tutor and working with small groups is hoped to be possible in the learning environment without losing the student models.

5.2 Graphics

In the first stage of the project simulated system will be forest machine boom with three cylinders. Main goal of graphics is to help understanding of LS-system operation. This requires graphical models of the LS-system and boom. Simplified, general 3D-models of boom parts and cylinders will be used in illustrating boom movements. 3D-models of the LS-system components will be created from production drawings for authenticity. Software for the graphics generation will be DirectX-based.

3D-models alone will not give additional information compared to real LS-system. Different kind of additional features create better understating of the LS-system. Using 3D-models allows cutaways and see-through coverings for providing view to inside the component. Inside view means view to the hydraulic fluid. Hydraulic fluid movement can be presented with moving lines and pressure in fluid with colours (Figure 3). Free floating camera allows different views of the system components. Free floating camera will be bounded to movements of mouse. Moving parts of components will get their exact translations and rotations from the simulation model output.

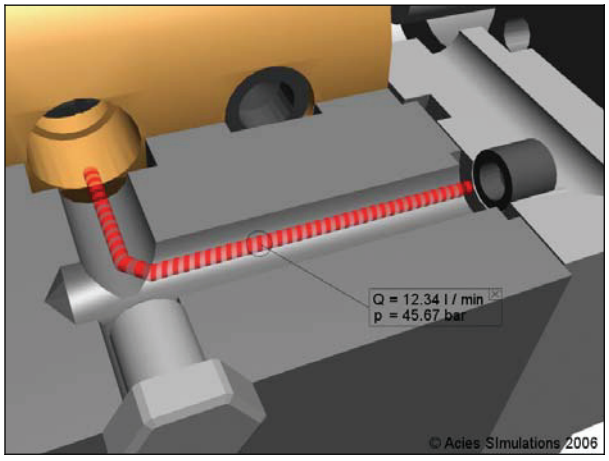

Figure 3. Presentation of fluid movement and pressure [25].

5.2.1 Piloting result for the graphics

In first piloting event, 3D-modelled hydraulic system with moving camera view and simple user interface was presented to audience. Hydraulic system presented had no presentation for hydraulic fluid, only dynamic arrows to present the direction and amount of volume flow. Hydraulic system is seen on Figure 4. Hydraulic system used real-time simulation model to create movement of cylinder piston and valve stem. Simulation model produced also numerical data for measurement curves. The piloting event gave new ideas for creating of the graphical models and changed priority of the additional features.

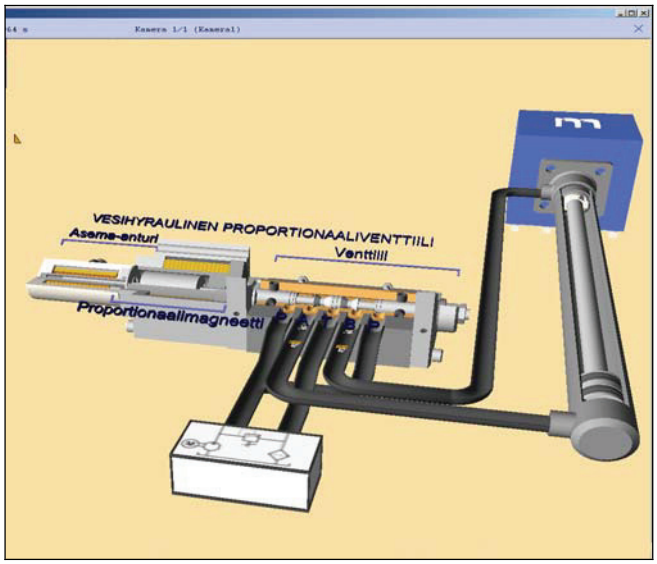

Figure 4. Hydraulic system model used in piloting [26].

Few main points for creating 3D-graphics were presented by piloting audience. Smaller value in answers means better suitability to the learning environment graphical presentation.

Graphical model for the hydraulic fluid presentation was seen important to the learning process. As seen in Figure 5, seven respondents out of ten saw the fluid presentation crucial and three respondents as rather important.

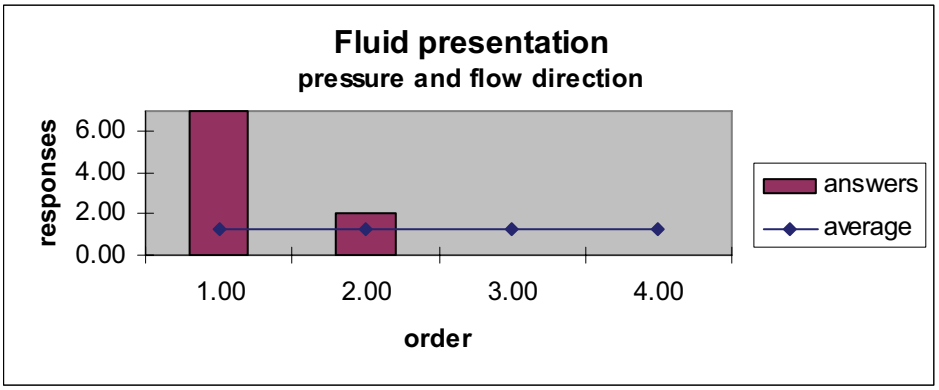

Figure 5. Responses for the fluid presentation importance.

In piloting, freely floating camera was discovered too difficult to handle. Either fixed camera with free target selection or better controlling algorithm was presented by the audience. Pre-saved camera angles were seen important, but teachers in audience also wanted the possibility to save camera angles by themselves. Forced camera angles could prove useful in attracting attention to certain parts of the hydraulic system.

User interface needs to be simple enough that user can learn to use it without instruction. Choice boxes for different functions were seen best way to present functions (pre-saved camera angles, open measurements, etc.) in use.

Presentation way for measured variables and realization of measurement were the conversation pieces. Measurement presentation way should be made seen as real as possible. The variables measured by oscilloscope should be presented as curve and others with numerical value or analog meter. Measurement windows should not disturb the 3D-graphical image, so the solid location was preferred. Realization of measurement should be done with measurement points like in real hydraulic system. Because of that, names (supply pressure, tank flow, etc.) for measured variables will not be used.

In graphical presentation 3D-models of system components can be moved by user. This makes disassembling of the hydraulic system possible. It was noted in piloting that assembling should happen in predetermined order or teacher could determine disassembling order.

While cut-a-ways and see-through covering provide better view inside component, teachers want to select themselves which parts should be modified. This will realized by offering extensive selection of cut-a-ways and translucent parts.

6 FUTURE DEVELOPMENT

Learning environment project for forest machine mechanics training has had positive reception among to vocational schools that train heavy-duty mechanics. There are also shared consensus of the general pedagogical approach and the features of ForMecVir - virtual learning environment. The integration of different technologies is challenging, but there are possibilities to develop application, where interoperability, expandability, updating, reuse, usability and generic solutions are taken into account.

The actual work of the hydraulic simulation is starting until now. The impending difficulties are related to the load of the real-time simulation and the solving of that problem, for instance by creating approximations for the physically accurate detailed models, will require a significant investment of time. The partners in the project have had desires for adding also other parts of the forest machines in the simulation. Those have been the harvester head and the hydrostatic drive transmission, for instance. It is undoubtedly feasible, because one of the essential aims in the project is to make the system as generalisable to the other areas of the machine mechanics training that makes the changes of the hydraulic system possible anyway.

In 3D-graphics, editing of valve production drawings has been started. After simplification of the drawings, software development for displaying of the graphics will be started. Software development has to be synchronized with simulation model development, because UDP-interface between simulation and graphical part is crucial part of the learning environment.

7 REFERENCES

[1] Lehtinen E. (2000) Pedagogical guidelines for designing computer-based learning environment for complex learning. PEG 2001. eds. Ruokamo H. et al.

[2] Huhtamäki, J., Ranta, P. & Pohjolainen, S. 2005. On the modelling-based framework for the instructional as-sessment of dynamic processes. In: Méndez-Vilas, A. et al. (eds.). Proceedings of the 3rd International Conference on Multimedia and Information & Communication Technologies in Education (m-ICTE 2005),) Cáceres, Spain on June 7-10th, 2005. pp. 1293-1298.

[3] Schön, D.A. 1983. The Reflective Practioner: How professionals think in action. Cambridge, MA: Basic Books.

[4] Jonassen, D.H., Peck K.L & Wilson B.G. (1999). Learning with technology. A constructivist Perspective.

[5] Youngblut, Christine. 1997. Educational Uses of Virtual Reality Technology. IDA Document Report Number D-2128. Available as a WWW resource: [Online reference, http://www.hitl.washington.edu/scivw/youngblut-edvr/D2128.pdf; referred 9th January 2006].

[6] Pohjolainen, S., Hautakangas, S., Ranta, P., Levasma J. & Pesonen. K. 2001. A Learning Experiment in Mathematics using A&O-Learning Environment. PEG 2001. eds. Ruokamo H. et al.

[7] Cormier & JD Hagman. 1987. Transfer of Learning.

[8] de Corte, E. 2003. Transfer as the productive use of acquired knowledge, skills, and motivations. Current Directions in Psychological Science Volume 12 Issue 4 Page 142.

[9] Jonassen, David. H. (1994), Technology as Cognitive Tools: Learners as Designers, ITForum.

[10] Ranta, P. 2005. Operators´ tacit knowledge supports forestry machine simulator based education. p. 39-48.in Ranta P. 2005. ed. Proceedings of the International Seminar on Simulator-Based Training of Forest Machine Operators. Tampere University of Technology. Digital Media Institute. Hypermedia Laboratory. Report 1/2005.

[11] Ranta P. (2006). Pedagogical aspects of simulator training. SIMSEM 2006 in London on 26.-28.9.2006. [Online reference http://www.norsim.org; referred 9th January 2006]

[12] Grabinger, R.S. & Dunlap, J.C. 1995. Rich environments for active learning: a definition, Association for learning a Technology journal 2, 5-34.

[13] Sveiby, K-E. (1997) Tacit knowledge. [Online reference, see http://www.sveiby.com/articles/polanyi.html ; referred 25th January 2005]

[14] Awad, E.M. & Ghaziri, H.M. (2001). Knowledge Management. International Edition. Pearson Education International.

[15] Vartiainen, M. (1985). Simulaatio työtaidon kehittäjänä. TKK.

[16] Reed, M.P. & Green, P.A. (1999). Comparison of driving performance on-road and in a low cost simulator using a concurrent telephone dialing task, Ergonomics, 42(8) 1015-1037.

[17] Ranta,P. 2003. Virtuaalitodellisuus opiskeluympäristönä. eTampere tietoyhteiskuntaohjelma. [Online reference, seehttp://www.uta.fi/laitokset/ISI/julkaisut/ Virtuaalitodellisuus_opiskeluymp_loppuraportti.pdf; referred 25th January 2005]

[18] Ranta, P. 2003. Possibilities to develop forest machine simulator based studying. Proceedings of PEG 2003. Powerful ICT Tools for Teaching and Learning

[19] van Emmerik, M.L., van Rooij, J. (1999). Efficient Simulator Training: Beyond Fidelity, Proceedings of the 10th International Training & Education Conference.

[20] Nählinder, S. (2006). Training of fighter pilots in the Swedish Air force. SIMSEM 2006 in London on 26.-28.9.2006. [Online reference http://www.norsim.org; referred 9th January 2006]

[21] Preece, J., Rogers, Y., Sharp, H., Benyon, D., Holland, S. & Carey, T. 1994. *Human-Computer Interaction*. Wokingham, UK: Addison-Wesley. 775 p.

[22] Eliot, C. & Woolf, B. 1995. An Adaptive Student Centered Curriculum for an Intelligent Training System. User Modeling and User-Adapted Interaction 5. pp. 67-86.

[23] Halff, H. 1988. Curriculum and Instruction in Automated Tutors. In: Polson , M.C. & Richardson, J.J. (eds.) Foundations of Intelligent Tutoring Systems. Lawrence Erlbaum Associates, Hillsdale. pp. 79-108.

[24] Suutarinen, I. 1996. Älykäs opastus opetusohjelmissa. Licentiate thesis. Department of Mathematics, University of Jyväskylä.

[25] Erkkilä, Riku. Acies Simulation 2006.

[26] Erkkilä, Riku. Institute of Hydraulics and Automation. 2005.

INFLUENCE OF THE EXPERIMENTAL PROCEDURE ON THE RESULTING MASS FLOW RATE CHARACTERISTIC OF A SINGLE PNEUMATIC COMPONENT

Rosario de Giorgi, Sylvie Sesmat and Eric Bideaux
Laboratoire Ampère, UMR CNRS 5005, INSA-Lyon, F-69621, France
25 avenue Jean Capelle, F-69621 Villeurbanne
rosario.degiorgi, sylvie.sesmat and eric.bideaux@insa-lyon.fr

ABSTRACT

The presented work investigates the existing approaches applied for characterizing the mass flow rate within a pneumatic component and tries to discuss the adequacy of the measurement procedures and of the models for accurate simulation purposes. First is given a summary of the theoretical and empirical formulations of the mass flow rate in an orifice in order to analyze the relevancy of the orifice model according to the measurement and the simulated circuits. Second, due to technological constraints, the circuit to be implemented for the charge or discharge methods is constituted by the cascade of several orifices. Some care is then required to determine properly the characteristic of the tested orifice or component.

KEYWORDS: Pneumatic systems, orifice modelling, flow characteristic, cascade of orifices, experimental procedures.

NOMENCLATURE

γ	: ratio of specific heat		q_m	: mass flow rate	[kg/s]
ρ	: density	[kg/m^3]	q_{mN}	: normalised mass flow rate	[kg/s/Pa]
a	: cracking ratio		Q	: heat	[J]
A	: flow area	[m^2]	R	: gas constant	[J/(kg.K)]
b	: critical pressure ratio		t	: time	[s]
C	: sonic conductance	[s.m^4/kg]	T	: static temperature	[K]
C_m	: flow parameter	[K$^{0.5}$.s/m]	T_t	: total temperature	[K]
C_q	: flow coefficient		v	: air velocity	[m/s]
m	: subsonic index				
p	: static pressure	[Pa]			
p_t	: total pressure	[Pa]			

Indices

0	: reference conditions
1	: upstream
2	: downstream
c	: critical
d	: downstream
g	: global
i	: intermediary
out	: from the tank
th	: throttle
v	: tank

1 INTRODUCTION

Information concerning the flow rate of pneumatic components is essential for both selecting the right component at the design stage and validating different performances of a circuit. Although the flow rate characteristic has to be as accurate as possible for modelling purposes, only a reference associated to a specific procedure has to be defined in order to compare several components and to make a selection for first level design purposes. The difficulty in the case of the pneumatic technology relies on the lack of theoretical models allowing a simple and accurate characterization of flow rate to be used for both modelling purposes and specifying component performances.

Models based on the convergent-divergent throttle [1] including Mach condition of the flow [2] were developed very early, but these formulations show inaccuracy in most of real applications as this specific geometry of orifices is generally not verified. Even if parameters [3] can be introduced in order to take into account the deviation of the geometry from the ideal case, experimental identifications remain up to now the best way to characterize the mass flow rate through an orifice.
In order to proceed to the mass flow rate characterization, the ISO6358 standard [4] defines the experimental conditions and the bench assembly in the case of a constant section orifice. It proposes a mathematical approximation of the mass flow rate through the characterized orifice. Although the utilization of this standard is restricted to the characterization of single orifices, it offers an approach that enables both modelling purposes and specifications of component performances. However, the need of expensive equipments and the time required to achieve the measurement using the ISO6358 standard is an important drawback for its extension in an industrial context. Moreover, as the rig configuration is usually far from the topology of real circuits, the obtained characteristics can only be used for simulation purposes under specific conditions.
Recently, some other procedures, based on the measurement of the transient response for the charge or the discharge of a tank, have been proposed. Kagawa et al. [5, 6] and Oneyama [7] have proposed such a method [8] to identify the sonic conductance C and the critical pressure ratio b, the mass flow rate being obtained from the pressure response using the state equation of gas. Although other approaches are acceptable but requires more detailed models, the isothermal chamber technique introduced by Kagawa and Kawashima [9] is an interesting (but costly) solution for solving the heat transfer problem. These last procedures are corresponding to an inverse approach for identifying the mass flow rate in a component. Although it allows the experimental procedure to be shortened, the accuracy of the results are strongly related to the sizing of the experimental rig and influenced by the off-line data processing methods.

Illustrations of these difficulties are given in this paper. First is given a summary of the theoretical and empirical formulations of the mass flow rate in an orifice, then the paper focuses on the comparison of the results obtained from both experimental procedures. This will finally point out the requirements in order to stay independent from the measurement layout and method.

2 FLOW IN A PNEUMATIC ORIFICE ACCORDING TO FLUID MECHANICS

Inside a pneumatic component for fluid power applications, the circuit of the fluid is composed of several contractions and expansions that form a network of orifices of different shapes. The flow can be of different nature, but in most of the cases, it is turbulent due to the high velocities and low viscosity. The fluid behaviour is generally considered as compressible but it can be not compressible in some particular cases.

2.1 Flow in an ideal convergent nozzle

However, in most cases, the considered reference law is the stationary adiabatic release of a moving fluid through an ideal convergent nozzle without any mechanical work. The classical hypotheses are the following ones:

- air is a perfect gas, not viscous,
- the flow is one-dimensional,
- the thermodynamic transformation is isentropic (adiabatic and reversible).

Using the energy conservation law between an upstream point on a section of area A_1 and a downstream point corresponding to the throttle of the convergent nozzle of area A_{th} and the properties of the perfect gas, the mass flow rate at the nozzle throttle has the following form:

$$qm = A_{th} \frac{p_1}{\sqrt{T_1}} Cm\left(\frac{p_{th}}{p_1}, \frac{A_{th}}{A_1}\right) \tag{1}$$

where Cm is the flow parameter [2]

- Cm is equal to C_{m_c} in sonic flow $\left(\frac{p_{th}}{p_1} \le \frac{p_{th_c}}{p_1}\right)$,

C_{m_c} being defined by an implicit relation only depending on the area ratio $\frac{A_{th}}{A_1}$:

$$\frac{R(\gamma-1)}{2\gamma}\left(\frac{A_{th}}{A_1}\right)^2 \left(C_{m_c}\right)^2 - \frac{\gamma+1}{2}\left(\frac{R}{\gamma}\right)^{\frac{\gamma-1}{\gamma+1}} \left(C_{m_c}\right)^{2\left(\frac{\gamma-1}{\gamma+1}\right)} + 1 = 0 \tag{2}$$

- and Cm is given by formula (3) in subsonic flow: $\frac{p_{th}}{p_1} > \frac{p_{th_c}}{p_1}$

$$C_m\left(\frac{p_{th}}{p_1},\frac{A_{th}}{A_1}\right)=\frac{\sqrt{\frac{2\gamma}{R(\gamma-1)}\left\{\left(\frac{p_{th}}{p_1}\right)^{\frac{2}{\gamma}}-\left(\frac{p_{th}}{p_1}\right)^{\frac{\gamma+1}{\gamma}}\right\}}}{\sqrt{1-\left(\frac{A_{th}}{A_1}\right)^2\left(\frac{p_{th}}{p_1}\right)^{\frac{2}{\gamma}}}} \tag{3}$$

The critical pressure ratio can be defined as a function of the critical flow parameter C_{m_c} and it is thus depending on the area ratio:

$$\left(\frac{p_{th_c}}{p_1}\right)=\left(C_{m_c}\sqrt{\frac{R}{\gamma}}\right)^{\frac{2\gamma}{\gamma+1}} \tag{4}$$

Figure 1 shows, for several area ratios, the normalised flow parameter variation according to the pressures ratio by reference to the one obtained with an infinite upstream section (null upstream velocity). It points out that the upstream velocity begins to have a significant influence on the mass flow rate as soon as the upstream area is less than twice the throttle area. For example, the maximum flow parameter is increased by 10% if the upstream area is only 1.5 times larger than the throttle area.

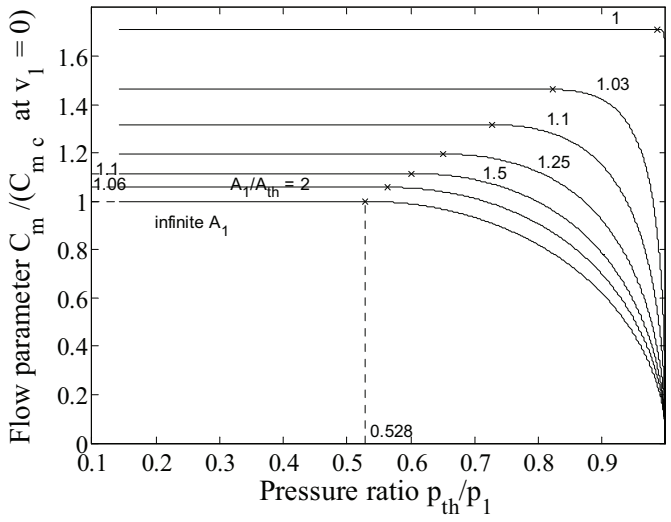

Figure 1 Change of the flow parameter according to the area ratio (i.e. upstream velocity).

In other equivalent formulations, the upstream velocity can be taken into account using either the upstream Mach number [10], or the downstream and upstream velocities ratio, or also the upstream total pressure and the upstream total temperature [1, 11]. In this last case, using total pressures and temperatures, the mass flow rate expressions are:

- in subsonic flow, $\frac{p_{th}}{p_{t1}}>\frac{p_{th_c}}{p_{t1}}$ with $\frac{p_{th_c}}{p_{t1}}=\left(\frac{2}{\gamma+1}\right)^{\frac{\gamma}{\gamma-1}}$,

$$q_m = A_{th} P_{t1} \sqrt{\frac{2\gamma}{\gamma - 1} \frac{1}{RT_{t1}} \left[\left(\frac{p_{th}}{p_{t1}} \right)^{\frac{2}{\gamma}} - \left(\frac{p_{th}}{p_{t1}} \right)^{\frac{\gamma+1}{\gamma}} \right]} \tag{5}$$

- in sonic flow, $\frac{p_{th}}{p_{t1}} \leq \frac{p_{th_c}}{p_{t1}}$, $\qquad q_{m_C} = A_{th} \frac{p_{t1}}{\sqrt{RT_{t1}}} \sqrt{\gamma \left(\frac{2}{\gamma + 1} \right)^{\frac{1+\gamma}{\gamma-1}}}$ (6)

2.2 Flow through a real orifice

In practice, real orifices show differences with ideal convergent nozzles, mainly on the following points:

- there is a local loss in total pressure at the inlet of the real orifice [12],
- there is a contraction of the fluid lines (vena contracta) leading to a real area smaller than the geometrical one,
- friction losses are not always negligible [1],
- according to the rate of the kinetic energy recovering, the pressure is higher downstream than at the throttle.

In order to take into account these differences, the expression of the mass flow rate in a real orifice is derived from the formulation obtained in the ideal case. Considering in formula (1) an ideal convergent nozzle of the same geometrical area, a corrective parameter, the flow coefficient C_q , is included and the throttle pressure is substituted by the downstream pressure. The mass flow rate is thus given by equation (7), where the flow parameter is then a function of the ratios of the downstream and upstream areas and pressures:

$$q_{m_c} = A_2 \frac{p_1}{\sqrt{T_1}} C_q \, C_m \left(\frac{p_2}{p_1}, \frac{A_2}{A_1} \right) \tag{7}$$

The flow coefficient C_q must generally be determined experimentally. However it can be set constant or chosen as a function, which depends on the pressures ratio, like those determined by Perry [3, 11].

In most cases, the upstream velocity is considered as negligible, considering that there is an upstream tank with a large diameter (its area being almost twice the downstream area according to Figure 1). The flow parameter is then just a function of the pressure ratio:

$$q_{m_c} = A_2 \frac{p_1}{\sqrt{T_1}} C_q \, C_m \left(\frac{p_2}{p_1} \right) \tag{8}$$

Even with this last simplification, the theoretical expressions of the mass flow rate given by (7) and (8) have the drawback to require a precise knowledge of the geometrical characteristics of the restriction and their use is limited to simple restrictions. It can hardly be used for components. Therefore, mathematical approximations have been proposed enabling to characterise the mass flow rate in an orifice or a component with only a few parameters.

3 MATHEMATICAL APPROXIMATIONS

3.1 ISO 6358 : 1989 standard [4]

Based on the previous results obtained from fluid mechanics in the case of a negligible upstream velocity (8), Sanville [13] and Wartelle [2] have proposed two equivalent mathematical approximations, which have been adopted for the ISO 6358 standard. These models represent the subsonic flow by a quarter of ellipse, and consider that the mass flow rate is directly proportional to the upstream pressure in sonic conditions. These approximations have the advantage to define the mass flow rate characteristic of an orifice with only two parameters. The mostly used parameters are the sonic conductance C, corresponding to the sonic flow, and the critical pressure ratio b delimiting the two flow conditions.

- in subsonic flow: for $\frac{p2}{p1} > b$,
$$q_m = C p_1 \rho_0 \sqrt{\frac{T_0}{T_1}} \sqrt{1 - \left(\frac{p_2 / p_1 - b}{1 - b} \right)^2} \qquad (9)$$

- in sonic flow: for $\frac{p2}{p1} \leq b$, $q_{mc} = C p_1 \rho_0 \sqrt{\frac{T_0}{T_1}}$ (10)

Although the ISO6358:1989 mathematical model stems from an approximation of the theoretical law corresponding to an ideal convergent nozzle, this approximation is widely used in industry. It provides good results for many types of real components with a constant throttle area such as restrictor valves, solenoid valves (at maximal opening) and blow nozzles, when these components are used in such conditions that the upstream velocity can be considered as negligible. Furthermore, the accuracy of this approximation is still acceptable if theoretically the flow coefficient C_q is a function of the pressure ratio, since this formulation enables the critical pressure ratio b to be changed from its theoretical value (equal to 0.528).

3.2 New approximation from the Japanese Industrial Standard [8]

Pneumatic circuits include however many other types of components such as silencers, tubes, valve manifold, pressure regulators, servovalves or other combination of complex components for which the use of the ISO 6358 : 1989 is no more possible. Kagawa et al. [8, 14] have proposed the use of two additional parameters to extend the range of the ISO 6358:1989 standard. These parameters are: the subsonic index m, and the cracking ratio a (respectively equal to 0.5 and to 1 in the ISO 6358:1989 standard) and according to equation (11), they provide an extension of the elliptic function used as the mass flow rate characteristic approximation:

- in subsonic flow: $\frac{p_2}{p_1} > b$,
$$q_m = C p_1 \rho_0 \sqrt{\frac{T_0}{T_1}} \left(1 - \left(\frac{p_2 / p_1 - b}{a - b} \right)^2 \right)^m \qquad (11)$$

- in sonic flow: $\frac{p_2}{p_1} \leq b$, $q_{m_c} = C p_1 \rho_0 \sqrt{\frac{T_0}{T_1}}$ (12)

This new form of the approximation is all the more relevant that it overcomes several limitations of the ISO6358:1989 standard that are not only related to component type but also to the condition of use of these components. For example, Figure 2 points out that even for an ideal convergent nozzle, if the upstream velocity is not negligible $A_1 = 1.1A_{th}\left(<2A_{th}\right)$, the ISO 6358:1989 is unable to give a correct approximation of the mass flow whereas this new formulation with the parameter *m* equal to 0.37 leads to a more acceptable approximation.

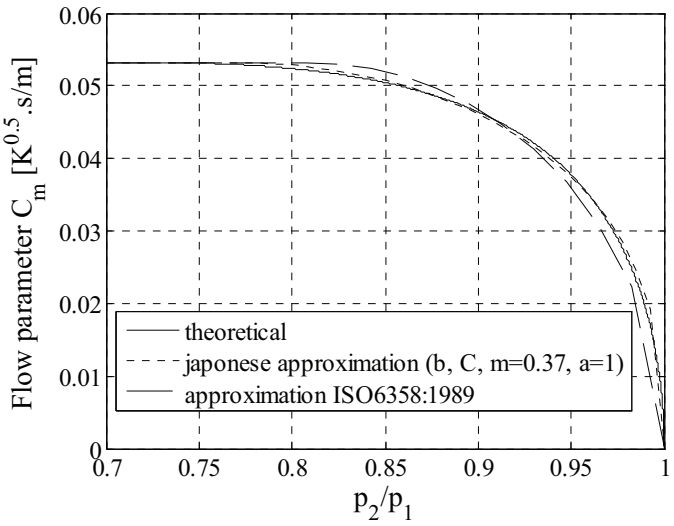

Figure 2 : Comparison between the theoretical flow parameter and its approximations (e.g. for an area ratio equal to 1.1).

4 EXPERIMENTAL CHARACTERISATIONS

The ISO 6358:1989 standard proposes a stationary characterisation procedure to determine the characteristic parameters. This method has however the drawback to be mainly applicable to small components due to air consumption and time cost. For these reasons, new procedures have been proposed. These approaches are based on transient responses obtained from the discharge or the charge of a tank, isothermal or not [5, 15, 16, 17]. The mass flow rate is then identified using an inverse model. The use of an isothermal tank leads obviously to a very simple expression of the mass flow rate according to the pressure rate of change during the tank charge or discharge. The procedure is still applicable otherwise, but the use of standard tanks requires naturally an adequate thermal model to represent the heat transfers [18].

Although these last procedures could have been thought as straightforward, they can lead to erroneous results without special attention on the characterisation bench layout. As an illustration of this, let us consider the flow characterisation of a 5 mm diameter double barbed 135° fitting. This type of fitting has the specificity to connect pipes with an internal diameter close to the internal diameter of the fitting (generally, the pipe diameter is 1 mm greater than the fitting one). In some industrial applications (for example in braking circuits), these connectors may have a significant influence on the dynamic performances of the full pneumatic circuit. Their flow characterisation is therefore necessary for simulation purposes.

4.1 Test bench

In order to compare the stationary flow characterisation from the ISO 6358 standard with the transient characterisation obtained from the discharge of a tank, the same bench (Figure 3) is used. Apart from the tank pressure sensor, all the pressure transducers are mini-sensors implemented flushing in specific flanges on the pipes.

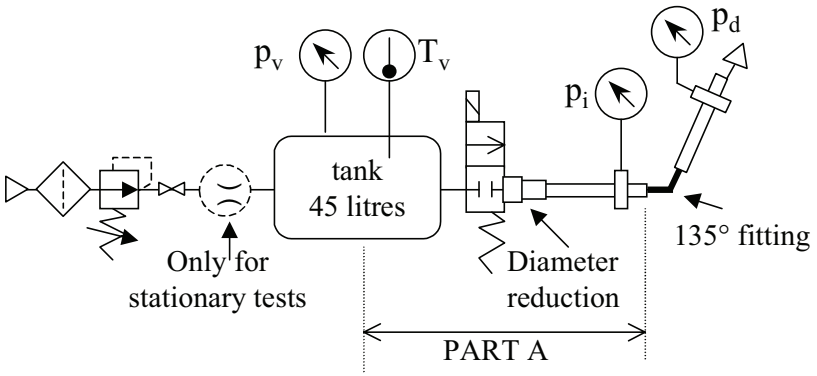

Figure 3: Test bench layout for transient or stationary characterisations.

Stationary tests have been carried out according to the ISO 6358 procedure. In this case, the pressure regulator is used to set the upstream pressure during the measurements and the mass flow meter is placed upstream the tank. In the second case for the measurement of the tank discharge, the initial pressure is fixed using the pressure regulator, and then a valve closes the upstream circuit. This layout presents the advantage here to keep unchanged the downstream circuit in the two experimental procedures.
For the stationary or the transient characterisations, with either an isothermal tank or a standard tank, the obtained mass flow rate characteristics correspond to the same downstream circuit: the outlet tank orifice, the shut-off valve, the component to be characterised and all the connection pipes. Naturally, in order to characterise properly the component, the outlet tank orifice and the shut-off valve characteristics must be chosen so that their influences on the measurements are as low as possible. Therefore, their sonic conductances have to be much larger than the one of the characterized component.
In spite of this caution, this layout induces necessarily a reduction to connect the component to the shut-off valve, which constitutes actually a new non-negligible restriction compared to the fitting one, as it will be pointed out in the next sections.
According to these remarks, the downstream circuit is constituted of an upstream equivalent orifice and of the component to be characterised. In the first place, the characterisation of the upstream orifice is carried out, and then the difficulties to obtain the flow characteristic of the component are underlined. It will justify our approach, and the characterisation of the complete downstream circuit will be discussed as a cascade of two restrictions.

4.2 Characterisation of the upstream restriction alone

The first part of the circuit is preliminary studied in order to check the flow limitation introduced by this part of the test bench. This restriction is an arrangement of standard fittings corresponding to a diameter reduction from 14mm to 6mm.

For the mass flow rate characterisation, the test bench is consequently reduced to the part A of the circuit (Figure 3): the component, which constitutes the real element to be characterized, is disconnected.
The stationary tests, done according to the ISO 6358:1989, show a relatively good agreement with the fluid mechanics hypotheses. Since the upstream pressure and temperature are measured on the tank with a large diameter, the flow is turbulent and the upstream velocity can be considered as negligible. Figure 4a shows that the mathematical approximation with m=0.5 and a=1 in equations (11) and (12), corresponding to the 1989 standard, leads to a good approximation of the experimental data.

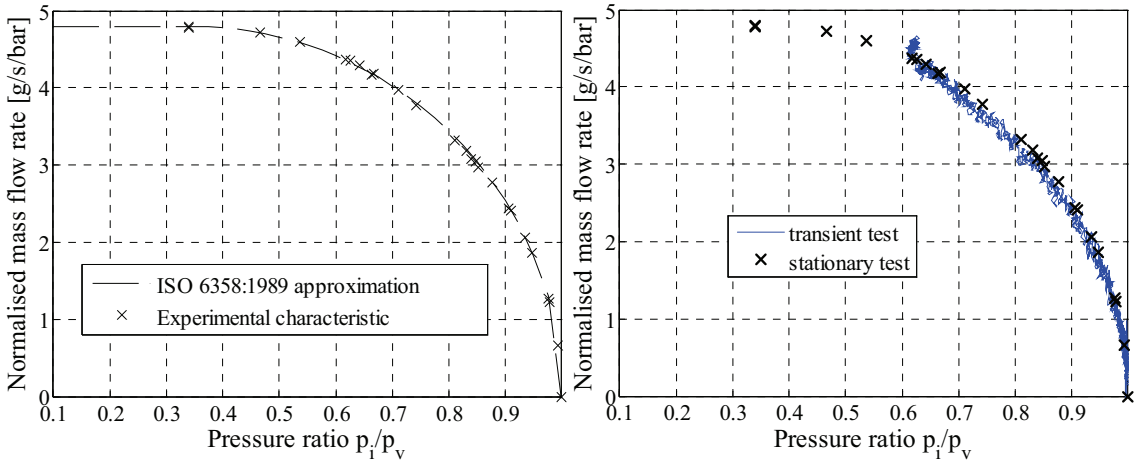

a - Stationary characteristic. b – Stationary and transient results

Figure 4: Experimental characterisation of the upstream restriction.

For the procedure based on transient responses, in the case of a standard tank discharge, the equations governing the tank pressure and temperature are [17]:

$$\begin{cases} \dfrac{dP_v}{dt} = -\dfrac{r\gamma T_v}{V} q_{m_{out}} + \dfrac{\gamma - 1}{V} \cdot \left(\dfrac{\delta Q}{dt} \right)_{gas} \\ \dfrac{dTv}{dt} = \dfrac{(\gamma - 1) T_v}{P_v V} \left[-r T_v q_{m_{out}} + \left(\dfrac{\delta Q}{dt} \right)_{gas} \right] \end{cases} \quad (13)$$

With the knowledge of the tank temperature and of the transient pressure measurements, model (13) inversion enables the instantaneous mass flow rate (14) to be calculated. The heat transfer can simultaneously be computed but this information is here not necessary.

$$q_{m_{out}} = \frac{V}{RTv} \left(-\frac{dpv}{dt} + \frac{pv}{Tv} \frac{dTv}{dt} \right) \quad (14)$$

In regard with this approach, it has to be underlined that the data acquisition and data processing are crucial since the pressure, temperature and their derivatives are required to compute the transient mass flow rate. Whereas the pressure can easily be measured in transient condition, this is still inaccessible for temperature. The tank temperature was then indirectly measured using the ‘stop method’ described by Kawashima et al. [6]. This procedure consists in several partial discharges, always starting from the same initial conditions [17], which enable the reconstruction of the transient temperatures during the tank discharge.

The comparison of the normalised flow characteristics obtained respectively in stationary conditions and in transient conditions (Figure 4b) shows a good agreement. Note that the noise on the characteristic obtained in transient conditions is a consequence of the signal differentiation. Low-pass filters can lower it, although this can hide some unexpected phenomena.

4.3 Characterisation of the fitting

For the characterisation of the fitting, the complete test bench of Figure 3 is used. According to the ISO 6358:1989, stationary conditions are reached for different upstream pressures and the mass flow rate in the circuit is measured.
In transient conditions, it was assumed that, at any time, the mass flow rate in the tested component (fitting) is the same as the tank outgoing flow. The effects of the pipe and valve on the flow gradient are here considered as negligible since the volume and the length of the first part of the circuit are small. The instantaneous mass flow rate is then obtained using the procedure described in section 4.2 and using equation (14).
It is important to note that the obtained mass flow rate characteristics and the model parameters (b, C) in equations (9) and (10), or (b, C, a, m) in equations (11) and (12) do not correspond to a single component but to the part of the circuit located in between the upstream and the downstream pressure sensors. These characteristics are thus depending on the characterization circuit itself, i.e. mainly on the size and shape of the upstream pressure and temperature tubes. Two questions arise then. “Is the air velocity really negligible in the upstream measurement tube?” since the area ratio is equal to 1.4, and is thus less than to 2 (Figure 1). “What is the upstream temperature?”
In the next sections, we are going to point out these difficulties by building three different flow characteristics for the fitting.

4.3.1 First approach

The first approach consists in the computation of the mass flow rate characteristic of the fitting assuming that the upstream velocity is negligible. In this case, the upstream pressure is the pressure p_i measured upstream to the fitting, and the upstream temperature is the tank temperature T_V (the tank being considered as the upstream temperature tube of the ISO 6358 standard). In this case, from equations (9) and (10) or (11) and (12), the normalised mass flow rate, noted $q_{m_{N1}}$, is finally equal to:

$$q_{m_{N1}} = \frac{q_{m_{out}}}{p_i}\sqrt{\frac{T_V}{T_0}} \tag{15}$$

4.3.2 Second Approach

The second approach relies on the use of the static pressure p_i and of the static temperature T_i measured upstream to the fitting assuming that the velocity v_i is not

negligible. According to equation (7), the corresponding normalised mass flow rate, noted q_{mN2} , is:

$$q_{m_{N2}} = \frac{q_{m_{out}}}{p_i}\sqrt{\frac{T_i}{T_0}} \tag{16}$$

If the velocity v_i is not negligible in the circuit, the upstream static temperature T_i is different from the temperature of the air inside the tank Tv. This last one can however be considered as a total temperature. Assuming that the flow is adiabatic between the tank and the fitting, the upstream temperature is deduced from:

$$T_i = T_v - \frac{\gamma - 1}{R\gamma}\frac{v_i^2}{2} \tag{17}$$

where the upstream velocity can be expressed as function of the mass flow rate:

$$v_i = \frac{q_{m_{out}}}{A_i}\frac{RT_i}{p_i} \tag{18}$$

With equations (17) and (18), the intermediary static temperature becomes:

$$T_i = \frac{-1 + \sqrt{1 + 4T_v \frac{(\gamma-1)R}{\gamma}\left(\frac{q_{m_{out}}}{A_i\, p_i}\right)^2}}{2\frac{(\gamma-1)R}{\gamma}\left(\frac{q_{m_{out}}}{A_i\, p_i}\right)^2} \tag{19}$$

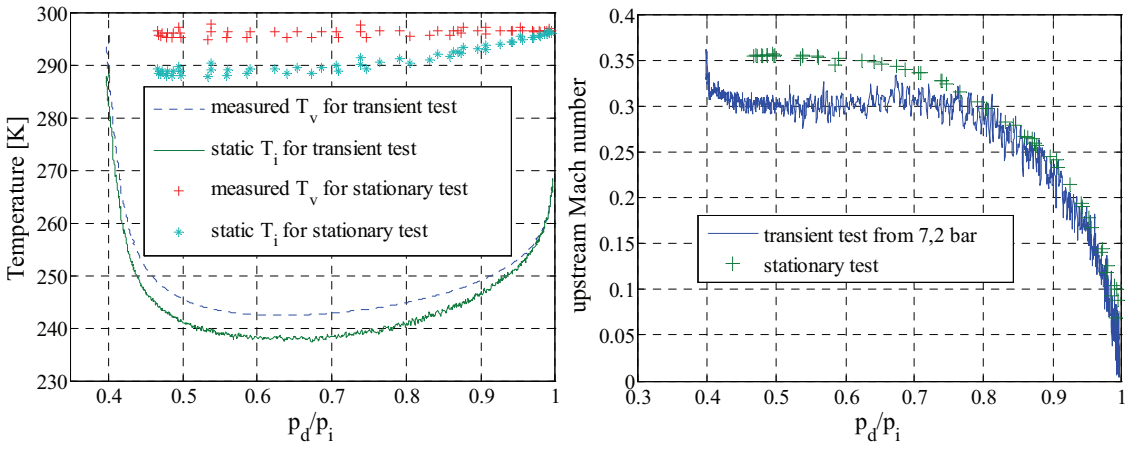

a – Static and total temperatures b – (Upstream) Mach numbers

Figure 5: Static and total temperatures and (upstream) Mach numbers in the intermediary chamber in both characterisation procedures.

Figure 5 shows that, assuming adiabatic conditions, the upstream velocity induces a static upstream temperature about 10K inferior to the tank one (total temperature). In order to verify the influence of the upstream velocity on the flow characteristic, we can compare the normalised mass flow rate characteristic q_{mN2} taking into account the velocity, with the normalised mass flow rate considering the upstream conditions at null

velocity, i.e. the tank pressure and temperature equivalent to the total pressure and temperature. According to (8) this normalised mass flow rate noted $q_{m_{Ng}}$ is defined by:

$$q_{m_{Ng}} = \frac{q_{m_{out}}}{p_V}\sqrt{\frac{T_V}{T_0}} \tag{20}$$

On Figure 7, since the computed mass flow rate $q_{m_{N2}}$ is greater than $q_{m_{Ng}}$, it shows that the influence of the upstream velocity is in agreement with figure 1 (area ratio equal to 1.4). This means that the adiabatic assumption seems to be valid. Figure 7 shows also that the normalised mass flow rate characteristics $q_{m_{N1}}$ and $q_{m_{N2}}$ are very similar. It can be concluded that in our case, the tank temperature Tv could be used instead of the calculated static temperature T_i for computing the fitting flow characteristics, as proposed in paragraph 4.3.1.

4.3.3 Third approach

In the third approach, the influence of the upstream velocity is also taken into account but using now the upstream total pressure and total temperature. According to (5) and (6), the normalised mass flow rate is then:

$$q_{m_{N3}} = \frac{q_{m_{out}}}{p_{t_i}}\sqrt{\frac{T_{t_i}}{T_0}} \tag{21}$$

Considering the adiabatic hypothesis, the total temperature corresponds to the tank temperature, and considering an isentropic flow between the tank and the fitting, the total pressure is equal theoretically to the tank pressure:

$$\begin{cases} T_{t_i} = T_v \\ p_{t_i} = p_v \end{cases} \tag{22}$$

From the upstream static pressure p_i, the total temperature $T_{ti}=T_v$ and the mass flow rate, in the isentropic conditions, the upstream total pressure [1, 11] can be calculated according to:

$$p_{t_i} = p_i\left[\frac{1}{2} + \sqrt{\frac{\gamma-1}{2\gamma}RT_{t_i}\left(\frac{q_{m_{out}}}{p_i A_i}\right)^2 + \frac{1}{4}}\right]^{\frac{\gamma}{\gamma-1}} \tag{23}$$

Figure 6 shows the comparison between the measured tank pressure p_v and the upstream total pressure p_{ti} obtained from (23). The difference between the two pressures shows that the isentropic hypothesis is not correct. There is naturally a potential energy loss in the first part of the circuit.
Figure 7 shows that either in stationary conditions or in transient conditions, taking into account total pressures and temperatures gives a different result for the mass flow rate

characteristics. The isentropic assumption seems not verified, and consequently, this approach has to be avoided for computing the characteristic parameters.

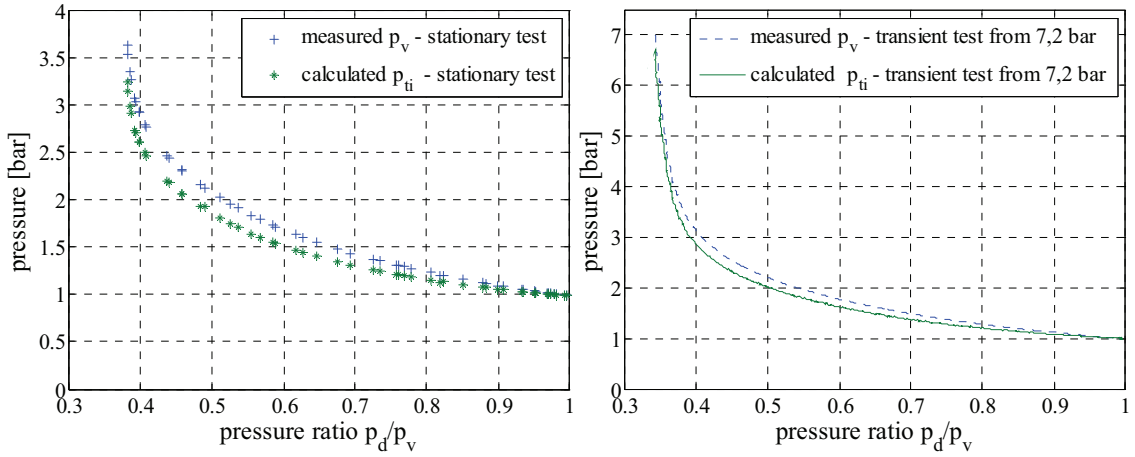

a – Stationary tests b - Transient tests

Figure 6: Comparison of the tank pressures and corresponding total upstream pressures.

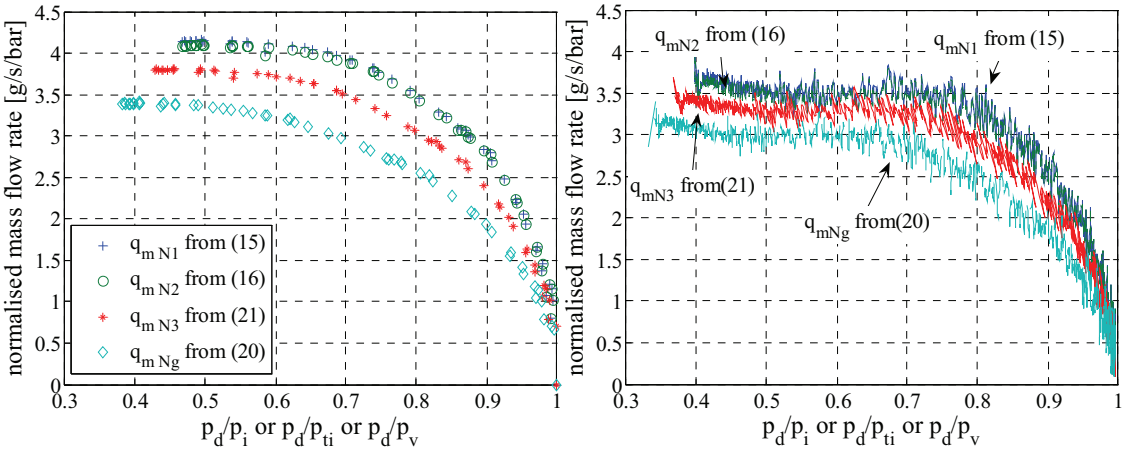

a – Stationary characteristics b – Transient characteristics

Figure 7: Different normalised mass flow rate characteristics of the fitting.

4.3.4 Analysis of the different approaches and conclusions

This study of the fitting flow rate characteristic points out that the main problem relies on the knowledge of the thermodynamic conditions in the first part of the circuit, which have an influence on the intermediary static temperature. This information is however necessary because this temperature cannot be measured easily.

Finally, figure 8 points out the large difference between stationary and transient characteristics, mainly in the sonic part of the characteristic, and this, whatever is the assumption used to obtain the characteristics (considering upstream static pressure and temperature according to (16) or considering upstream total pressure and temperature according to (21)). It means that, for this bench layout at a given pressure ratio, the flow within the fitting is not the same in stationary conditions as in transient conditions.

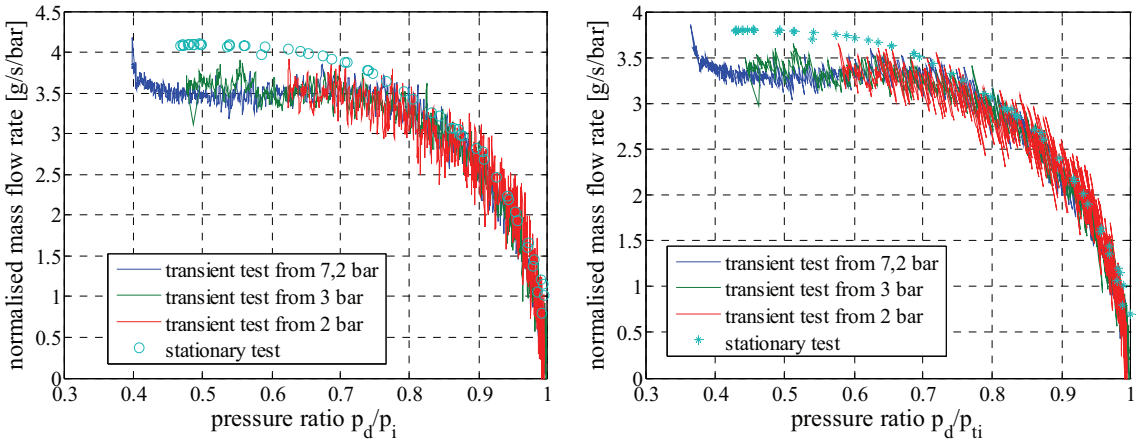

a – with upstream static pressures and temperatures (16)

b – with upstream total pressures and temperatures (21)

Figure 8: Comparison of the stationary and transient mass flow rate characteristics of the fitting.

4.4 Global characterisation

The mass flow rate characteristics of the part A of the circuit (paragraphs 4.2) and those of the fitting (paragraph 4.3) can be compared in the stationary case (Figure 9a). It shows that the part A of the circuit and the fitting have in fact very similar characteristics. This means that the complete test bench has to be considered as a cascade of two equivalent restrictions and it confirms that the velocity upstream the characterised fitting cannot be neglected.

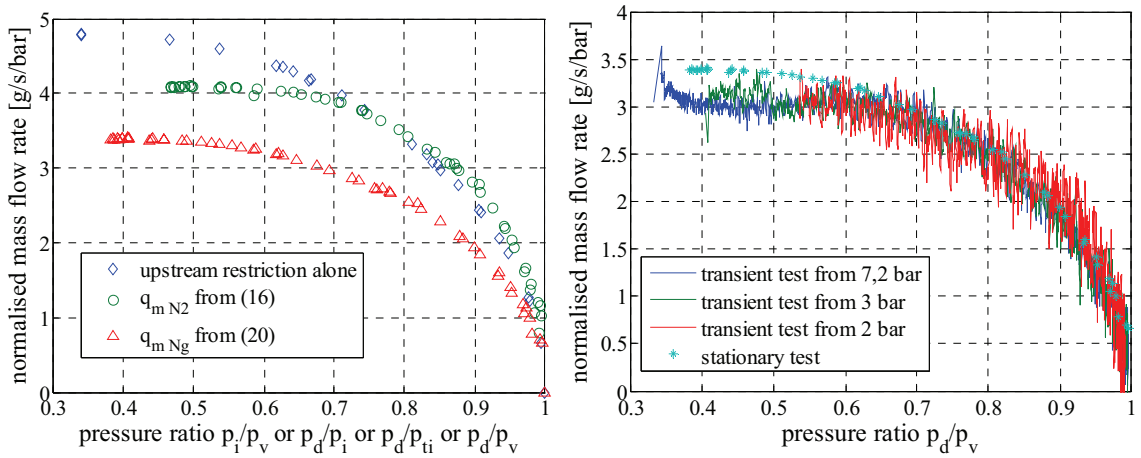

a – Individual stationary characteristics

b – Global characteristics $q_{m_{Ng}}$

Figure 9: Individual and global characteristics of the downstream circuit.

The normalised global mass flow rate $q_{m_{Ng}}$ defined by (20) is obtained from the mass flow rate measured or computed with the complete test bench (Figure 4) using the tank pressure and temperature as upstream values: it corresponds therefore to the global characteristics of the whole circuit downstream the tank. In this case, as the tank has a very large diameter, the tank pressure and temperature can be undoubtedly considered as

total values. Figure 9b shows that there are again differences between the stationary and the transient mass flow rate characteristics, especially in sonic conditions. This last comparison confirms that the full pneumatic circuit downstream the tank does not have the same flow behaviour in stationary and in transient conditions. This leads to the conclusion that the classical assumption, in which the transient flow in the circuit is neglected, is certainly not valid.

In order to confirm that the main problem results from the coupling of the two parts of the circuit, i.e. the part A and the characterised orifice, it is possible to build the mass flow rate characteristic of the upstream restriction. Considering now the intermediary pressure as the downstream pressure and using equation (24) for the normalised flow rate, it appears that the stationary and the transient characteristics are now in good agreement (Figure 10) and corresponds to the results obtained when this part of the circuit is isolated (Figure 4, paragraph 4.2). However, only the subsonic part of the characteristic can be compared here. Because the difference between the stationary and the transient procedure mainly appears in sonic conditions on the global characteristic (Figure 9), it is therefore difficult to conclude definitively from this last results.

$$q_{mN} = \frac{q_{m_{out}}}{p_v}\sqrt{\frac{T_V}{T_0}} \qquad (24)$$

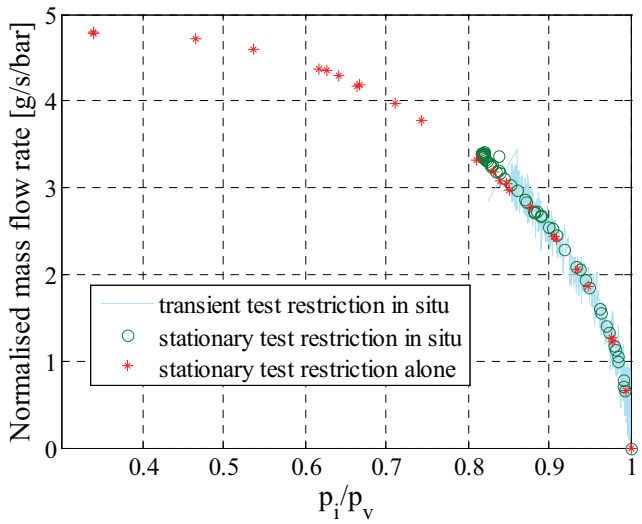

Figure 10: Comparison of the upstream restriction characteristics measured alone or with the complete bench (in situ).

5 CONCLUSIONS

In comparison with the formulations coming from the fluid dynamic theory, the mathematical approximations deduced from experimental characterisations are of a simpler use, especially for components with complex internal circuit. Since 1989, the ISO 6358 was based on stationary characterisations, but transient characterisations are yet available and the independency to the experimental procedure has to be proven. This paper has shown with the characterisation of one particular fitting that some important difficulties can arise when these new experimental procedures are used.

We showed that our test bench presents a cascade of two restrictions nearly equivalent. This particularity comes from the necessity in the transient procedure, to have a shut-off valve connected to the characterised component and therefore a circuit composed of two parts with a diameter reduction.
As a first result, it appears that when a single restriction is characterised (the upstream one alone), the stationary and transient results are in perfect agreement. However, it is no more the case if the cascade of the two restrictions is considered. This is a consequence of the structure of the circuit, which is corresponding, in this case, to two restrictions in cascade separated by an "intermediary chamber". The difference between the stationary and the transient measurements can be related to the influence of this "intermediary chamber", perhaps not small enough to validate the hypothesis that the flow is the same at any point in the circuit.
Considering the flow characteristic of the second restriction (the fitting in our case), this work underlines also the difficulties to determine properly the upstream pressures and temperatures, which have to be used because the upstream velocity can not be neglected anymore in the mass flow rate formulations. It has been shown that the classical fluid dynamics hypotheses have to be carefully verified for each circuit. The adiabatic behaviour of the flow, which is necessary to calculate the static temperature, seems to be valid. But it is not the case with the isentropic hypothesis, needed for the calculus of the total pressure upstream to the fitting.
The aim of this paper was to point out the problems induced by introducing a cascade of restrictions in the circuit when the transient procedure is applied to characterise a component. The solutions that have to be investigated should not be limited to an improvement of the test bench in order to decrease the influence of the first part of the circuit. It seems also important to know how to characterise cascade of orifices because it is the most often observed configuration for real pneumatic circuits or complex components. These characterisations must enable not only to compare different components but also to simulate their behaviour in stationary flow conditions as well as in transient flow conditions.

To go further, the next step of this work is obviously to try to understand what is really happening in the intermediary chamber. This can be done using the Computational Fluid Dynamic analysis [19] but our final goal, will be the development of a dynamic model of this kind of intermediary chamber taking into account the thermal effects and the kinetic energy of the fluid.

6 REFERENCES

[1] B.W. Andersen The analysis and design of pneumatic systems. New-York : John Wiley and Sons, 1967, 302p.

[2] C. Wartelle. Caractéristiques de débit des appareils à fluides compressibles considérés isolément ou montés en série. In : Les mémoires techniques du CETIM, volume 209(13), pages 1–54. Sept. 1972.

[3] J.A. Perry. Critical flow through sharp edged orifices. Transaction of ASME, 71:757–764, October 1949.

[4] International Standard ISO 6358. Pneumatic Fluid Power Components using Compressible Fluids – Determination of Flow-rate Characteristics, 1989. 15p.

[5] T. Kagawa, K. Kawashima, and T. Fujita. Effective area measurement method using isothermal chamber. Hydraulics and Pneumatics, Vol. 26(1):pp. 76–78, 1995.

[6] K. Kawashima, T. Kagawa, and T. Fujita. Instantaneous flow rate measurement of ideal gases. Transaction of the ASME Journal of Dynamic Systems, Measurement and Control, vol. 1222:174–178, march 2000.

[7] N. Oneyama. Flow-rate characteristics of pneumatic components. Fluid Power, vol. 15(4):7–11, 2001.

[8] JIS B 8390. Pneumatic Fluid Power Components using Compressible Fluids - Determination of Flow-rate Characteristics, 2000.

[9] K. Kawashima, Y. Ishii, T. Funaki, and T. Kagawa. Determination of flow-rate characteristics of pneumatic solenoid valves using an isothermal chamber. Transaction of the ASME Journal of fluids Engineering vol. 126, March 2004.

[10] J.P.T. Mo. Analysis of compressed air flow through a spool valve. In: Proceedings of the Institution of Mechanical Engineers, 1989, vol. 203, n°2, p. 121-131

[11] D. Mc Cloy D. and H.R. Martin. Control of Fluid Power: Analysis and Design. Chichester (England), Ellis Horwood, 1980. 510p.

[12] L.A. Zalmanzon Components for pneumatic control instruments. Oxford : Pergamon press, 1965, 320 p.

[13] F.-E. Sanville. New method of specifying the flow capacity of pneumatic fluid power valves. Hudraulic and pneumatic power, n°195, vol. 17, mars 1971.

[14] T. Kagawa, M. Cal, K. Kawashima, T. Wang, T. Nagaki, T. Hasegawa, and N. Oneyama. Extended representation of flow-rate characteristics for pneumatic components and its measurement using isothermal discharge method. In Power Tansmission and Motion Control, PTMC'04, pages 271–282, Sept. 2004.

[15] S. Ben Chabane, M. Bonis, J.P. Lecerf Economic measurement of iso pneumatic coefficients. In 11th AachenerFluidtechnisches Kolloquium, Vol.3, p 131-141,1994.

[16] K. Kuroshita, Y. Sekiguchi, K. Oshiki, N. Oneyama Development of new test method for flow-rate characteristics of pneumatic components, In Power Tansmission and Motion Control, PTMC'04, pages 243–256, Sept. 2004.

[17] R. de Giorgi, E. Eric Bideaux, and S. Sesmat. Using inverse models for determining orifices mass flow rate characteristics. In The 6th JFPS Japan International Symposium on Fluid Power, Tsukuba, Japan, November 7-10, 2005.

[18] R. De Giorgi, E. Bideaux, S. Sesmat Dynamic thermal model of a discharging process of a pneumatic chamber, 4th FPNI PHD Symposium, Sarasota, 2006.

[19] E. Bideaux, J.Y. Champagne, and S. Scavarda. Pneumatic orifices characterization using a computational fluid dynamics approach. In Fourth International Symposium on Fluid Power Transmission and Control, SIFPC'03, Wuhan, China, April 2003.

Vehicle Active Suspension System Control Using Neural Network

Professor Jyh-Chyang Renn and Graduate Student Tsung-Han Wu
Department of Mechanical Engineering,
National Yunlin University of Science and Technology,
640 Douliu, Yunlin, Taiwan
E-mail: rennjc@yuntech.edu.tw

ABSTRACT

Nowadays, the active suspension is the key technology for vehicles to achieve both ride comfort and control performance. In this paper, a new 1/4T servo-hydraulic vehicle active suspension system is developed and two control schemes are utilized. The first one is a conventional PID controller obtained from Ziegler-Nichols method and the second one is the neural network controller. Neural network, which is a network system interlinked by Neuros, possesses the ability of on-line learning and identification. The neural network controller proposed in this paper is able to adjust the weight via error back propagation algorithm and minimize the error between the actual output and the desired output of the suspension system. In addition, the utilization of MATLAB/Simulink software enables the dynamic simulation of the control system. From both simulation and experimental results, it is shown that two proposed control schemes can restrain significantly the vibration and acceleration of vehicle body. However, the performance of neural network controller is somewhat better than that obtained from the PID controller.

KEYWORDS: Servo-hydraulics, Active Suspension, Neural Network Controller, PID Controller.

1 Introduction

As shown in Fig. 1, the suspension system is classified as a passive, semi-active, and active suspension system, according to its ability to add or extract energy. Among these three systems, the passive suspension is perhaps the most commonly used one and may be found in most vehicles. However, the passive suspension has no means of adding external energy to a system because it contains only passive elements such as a damper and a spring. For the semi-active suspension, though it is possible to continuously vary the rate of energy dissipation using a controllable damper, it provides only moderate performance. By contrast, the active suspension can supply energy from an external source and generate force to achieve the optimal desired performance. For these reasons, the active suspension is investigated in this study.

Surveying some previous reports, it is found that the active suspension control have been attracting undoubtedly the attention of many engineers and researchers. Typical studies are summarized as follows: Sunwoo et al. [1] used the sky-hook damping model reference adaptive control to improve the ride performance for a quarter car model. Kuo & Li [2] applied the PI and PD fuzzy controllers to the active suspension system, and the optimum parameters of fuzzy controller were obtained by genetic-algorithm (GA).
Chantranuwathana & Peng [3] strived to improve the performance of the active suspension system by compensating a dynamic system of hydraulic actuator using a robust controller. Rao & Prahlad [4] proposed a tunable fuzzy logic controller for a quarter-car active suspension model to reduce the vertical acceleration for better ride comfort. Thompson [5] as well as Kashani and Kiriczi [6] applied the optimal control theory to the design of an active vehicle suspension system, but they needed accurate system parameters and road variation information. Lin and Kanellakopoulos [7] employed nonlinear back-stepping design for the control of active suspension systems, which improved the inherent trade-off between ride quality and suspension level. Kim and Ro [8] used sliding mode control scheme to ensure robustness for a wide range of operating conditions for vehicle active suspension system. Jang and Kim [9] utilized the gain-scheduled control for an active suspension system to improve the ride comfort. Wu and Lee [10] used a neural-network-based fuzzy controller for half-car active suspension systems. However, most of them were based only on computer simulations. In other words, very few experimental results were discussed in these reports.

In this paper, the design concepts as well as the modeling, simulation and experimental studies of a newly developed 1/4T servo-hydraulic active suspension test rig will be discussed. In addition, two controller schemes will be utilized. The first one is the conventional PID controller and the second one is the neural network controller. In the following, the structure of the vehicle active suspension system will firstly be outlined.

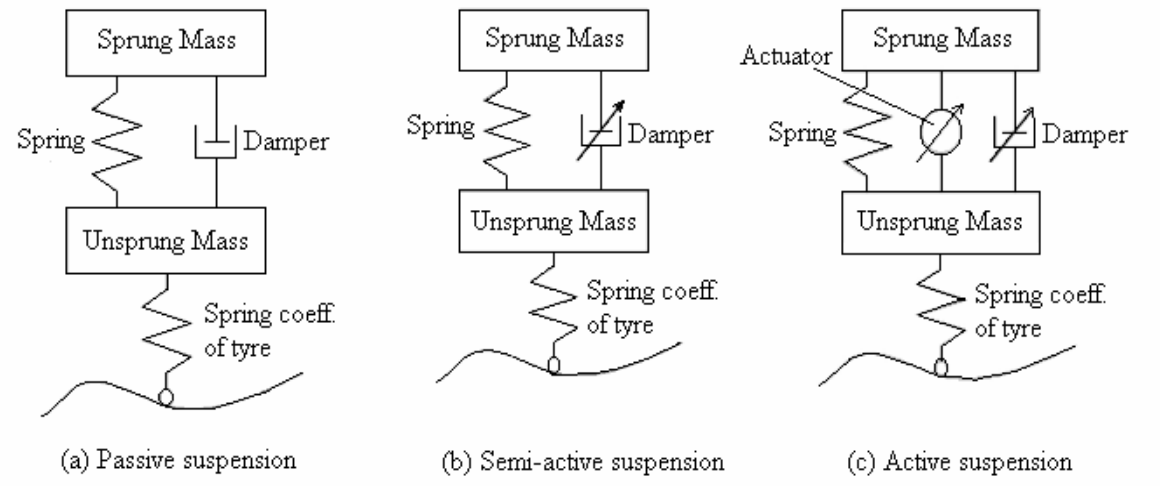

Figure 1. Classification of vehicle suspension system

2 Active Suspension System

The introduction of active suspension system is expected to improve efficiently the control performance and the ride comfort for passengers in a vehicle. Generally speaking, a high-quality active suspension system can separate the vehicle chassis from the vibration arising from road surface. It further ensures the contact between the wheels and road surface for a better ride comfort and safety. A 1/4T vehicle model using a so-called

sky-hook damper is shown in Fig. 2. The sky-hook damper refers to a damper attached between the top and ceiling of vehicle. This damper is found to have excellent suppression effect against the vibration of vehicle body [1]. The b_{sky} denotes the damping coefficient of the sky-hook damper.

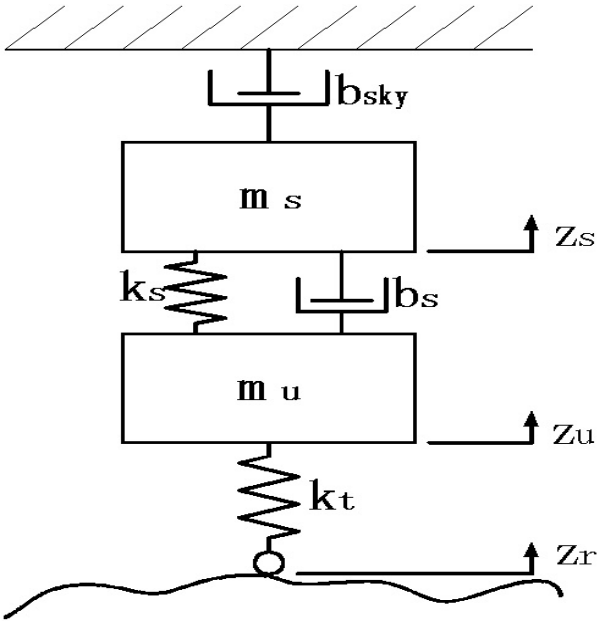

Figure 2. Sky-Hook Suspension System

Since it is difficult to practically implement the sky-hook suspension system, this study adopts a feedback control structure instead of the sky-hook suspension and designs a servo-hydraulic active suspension system as shown in Fig. 3. The basic principle is described as follows: a hydraulic actuator is mounted between the vehicle and wheels, such that the controllable output force of the hydraulic cylinder is used to replace the virtual damping force provided by the sky-hook damper. This helps to realize the same damping effect of sky-hook damper. The parameter F_a denotes the output force provided by the hydraulic cylinder.

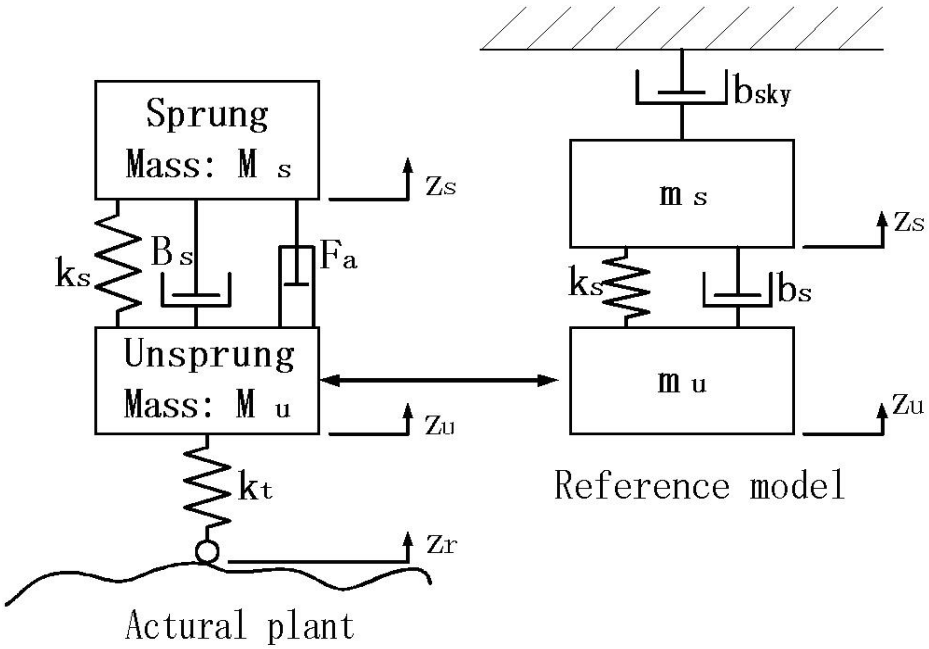

Figure 3. Active suspension system of sky-hook reference model

The dynamic equations for the active suspension system are

$$m_s \ddot{z}_s = k_s\left(z_u - z_s\right) + b_s\left(\dot{z}_u - \dot{z}_s\right) + F_a, \tag{1}$$

$$m_u \ddot{z}_u = -k_s\left(z_u - z_s\right) - b_s\left(\dot{z}_u - \dot{z}_s\right) + k_t\left(z_r - z_u\right) - F_a. \tag{2}$$

Where m_s : sprung mass (303 kg),
m_u : unsprung mass (65 kg),
k_s : spring constant (16812 N/m),
k_t : spring constant of tyre (190000 N/m),
b_s : damper coefficient (10000 Ns/m) ,
Z_s : displacement of vehicle chassis relative to plain ground,
Z_u : displacement of wheel relative to plain ground,
Z_r : uneven road surface relative to plain ground,
F_a : output force provided by the servo-hydraulic cylinder.

As shown in Fig. 4, the servo-hydraulic actuator consists of a servo valve (or proportional valve) and a hydraulic cylinder. The output actuating force F_a is calculated by

$$F_a = AP_L \ . \tag{3}$$

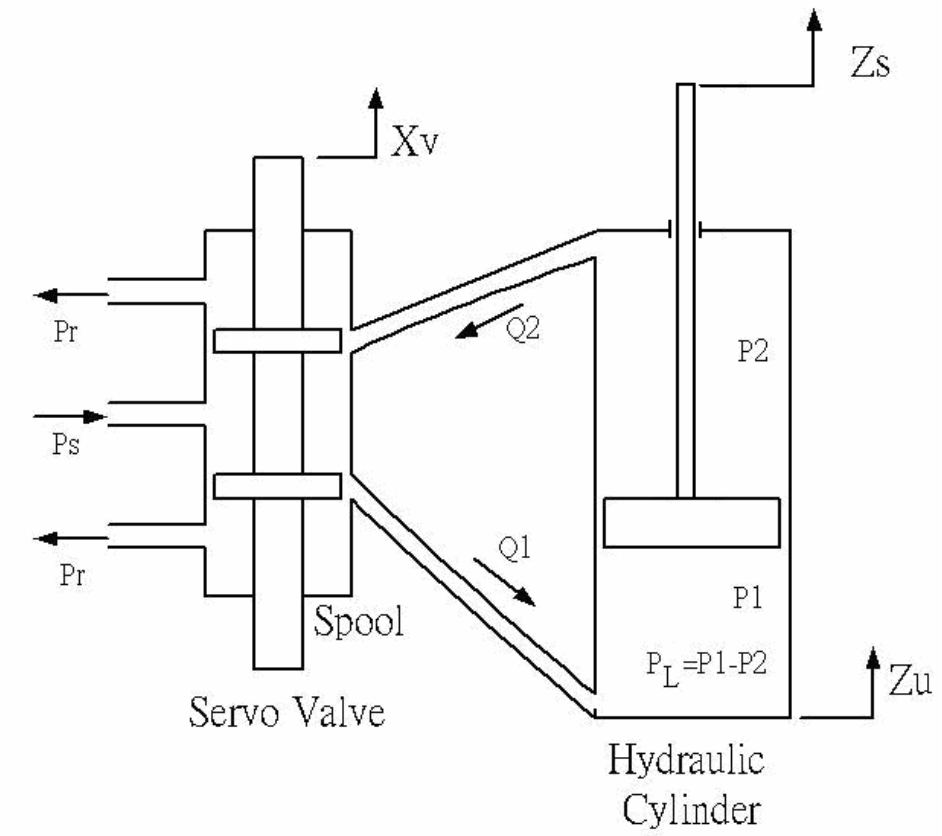

Figure 4. The servo-hydraulic actuator

From the continuity equation [11], Eq. (4) can be derived.

$$\frac{V_t}{4\beta_e}\dot{P}_L = Q_L - C_t P_L - A\left(\dot{z}_s - \dot{z}_u\right). \tag{4}$$

From the Bernoulli's equation [11], assuming that the rod diameter is negligible, we have

$$Q_L = C_d w x_v \sqrt{\frac{1}{\rho}(P_S - P_L)}\,. \tag{5}$$

Where A : effective cross-sectional area of hydraulic cylinder (903 mm^2),
P_L : load pressure,
V_t : effective volume of hydraulic cylinder,
β_e : bulk modulus of oil,
C_t : leakage coefficient of hydraulic cylinder,
Q_L : load flow,
C_d : discharge coefficient,
w: area gradient of servo valve,
x_v : spool displacement of servo valve,
ρ: oil density,
P_s: supply pressure (110 bar).

In addition, the spool displacement of servo valve, x_v, is controlled by an input current, u. The corresponding dynamic relation can be simplified as a first-order differential equation.

$$\dot{x}_v = \frac{1}{\tau}(-x_v + k_a u)\,. \tag{6}$$

From Eqs. (1) to (6), if the state variables are selected as: $x_1 = z_s - z_u$, $x_2 = \dot{z}_s$, $x_3 = z_u - z_r$, $x_4 = \dot{z}_u$, $x_5 = P_L$ and $x_6 = x_v$, the state equations for the active suspension system may be written as

$$\begin{aligned}
&\dot{x}_1 = x_2\,,\\
&\dot{x}_2 = \frac{1}{m_s}[-k_s(x_1 - x_3) - b_s(x_2 - x_4) - Ax_5]\,,\\
&\dot{x}_3 = x_4\,,\\
&\dot{x}_4 = \frac{1}{m_u}[k_s(x_1 - x_3) + b_s(x_2 - x_4) + k_t(Z_r - x_3) - Ax_5]\,,\\
&\dot{x}_5 = -\beta x_5 - \alpha A(x_2 - x_4) + \gamma x_6\sqrt{P_S - \mathrm{sgn}(x_6)x_5}\ \ ,\\
&\dot{x}_6 = \frac{1}{\tau}(-x_6 + k_a u)\,,\\
&y = Ax_5\,.
\end{aligned} \tag{7}$$

Where $\alpha = \frac{4\beta_e}{V_t}$, $\beta = \alpha C_t$, $\gamma = \alpha C_d w\sqrt{\frac{1}{\rho}}$.

3 PID and Neural Network Control Theory

In this study, the first utilized control scheme is the PID controller, in which the optimal gains are determined by the criterion proposed by Ziegler and Nichols [12]. The discrete-time PID-controller can be formulated as

$$u(k) = u(k-1) + \Delta u(k)\,, \tag{8}$$

$$\Delta u(k) = K_P[e(k) - e(k-1)] + K_I e(k) + K_D[e(k) - 2e(k-1) + e(k-2)], \quad (9)$$

where $u(k)$: actuating signal,

$\Delta u(k)$: actuating signal change,

$e(k)$: error signal,

K_P : gain of the proportional controller,

K_I : gain of the integral controller,

K_D : gain of the derivative controller.

The second control scheme proposed in this paper is the neural network controller. On the one hand, the neural network possesses the structure of Multilayer Perception (MLP) and utilizes the algorithm of Error Back Propagation (EBP). The combination of MLP and EBP is called the BP Neural Network or simply BPN, which is the most frequently used neural network controller for engineering applications. On the other hand, the main framework of the BPN consists of the multilayer feedforward structure as well as the supervised learning architecture. It features a higher level of nonlinear mapping and rapid learning. Therefore, the BPN can be used to replace the conventional nonlinear equations and the corresponding complex calculations [13].

Figure 5 shows the schematic BPN controller proposed in this paper. It is observable that the controller consists of three layers. They are input, hidden and output layer respectively. This structure is called the multilayer feedforward network, which can be used to solve complex nonlinear model. The input and output layer represents the input and output value respectively. The number of Neuros in input or output layer is determined simply according to the number of utilized input or output variables in the model. In addition, the necessary number of Neuros in hidden layer depends chiefly on the complexity of the control system. Generally speaking, more Neuros result in better learning ability. By contrast, the learning efficiency decreases because more time is required for computation. Therefore, trial-and-error method is generally used to determine the optimal number of Neuros in hidden layer. Besides, the number of hidden layer can be increased from one layer to several layers depending also upon the complexity of the system. In this paper, however, only one hidden layer with three Neuros is employed. In addition, both the input and output layer consists of a single Neuro respectively. The Neuros in various layers are interlinked by different weight. The input pattern is directly transferred to the hidden layer through the input layer. After some calculations including weighting, summation and activation, a set of output values in hidden layer is obtained. Similarly, the actual output values in output layer can also be derived. Figure 6 shows the simplified control block diagram of the active suspension system using neural network controller. The desired input, Z_{sd}, is set to be zero in order to maintain zero displacement of vehicle body (i.e. sprung mass) regardless of the disturbance, Z_r, caused by uneven road profile. Obviously, the only one input value to the input layer is the minus vehicle body displacement, $-Z_s$. Some details of the BPN will be depicted in the following paragraphs.

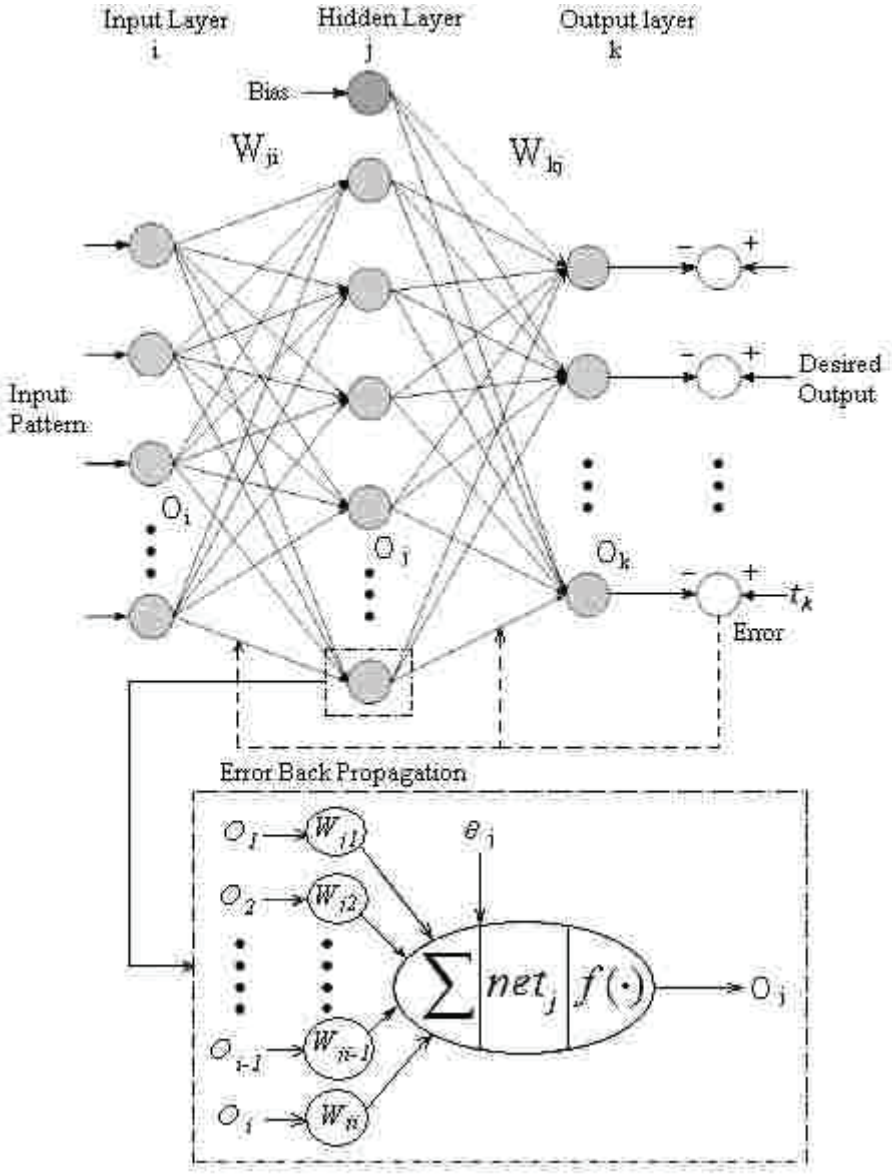

Figure 5. BP Neural Network controller

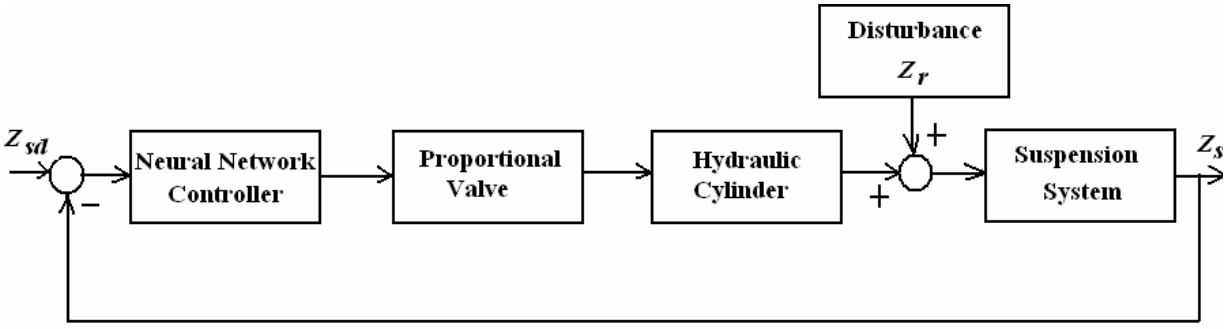

Figure 6. Simplified block diagram of the active suspension system using neural network controller

The most essential element of neural network is the neural cell, which is called Neuro in this study. Figure 7 illustrates the model of a Neuro, in which the symbol $f(\cdot)$ denotes the activation function. In this paper, the Sigmoid activation function is utilized because it is continuously differentiable. The mathematical equations for the Neuro are [13]

$$net_j = \sum \left(W_{ji} \cdot O_i \right) + \theta_j \,, \tag{10}$$

and

$$O_j = \frac{1}{1 + \exp\left(- net_j \right)} . \tag{11}$$

Where W_{ji} : weight from Neuro i in input layer to Neuro j in hidden layer,
θ_j : bias or threshold at Neuro j,
O_i : input value from Neuro i in input layer,
O_j : output value of Neuro j in hidden layer.

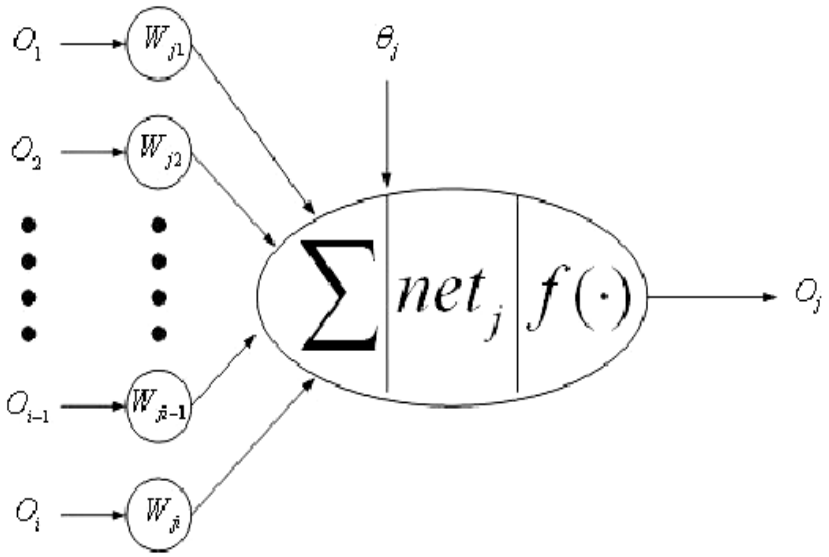

Figure 7. The model of a Neuro

Figure 8 shows the network of EBP, which is proved to be the most effective supervised learning architecture. The basic principle is the utilization of Gradient Steepest Descent Method (GSDM) [13]. First, an error function is defined using GSDM. Thus, it is possible to adjust the weight and/or bias during the learning process if this error function is minimized. The error function, E, is defined as

$$E = \frac{1}{2} \sum \left(t_k - O_k \right)^2 . \tag{12}$$

Where t_k : desired output value of Neuro k in output layer,
O_k : actual network output value of Neuro k in output layer.

The output value, O_k, in output layer can be obtained through

$$O_k = f_k(net_k) = \frac{1}{1 + \exp(-net_k)} , \tag{13}$$

$$net_k = \sum \left(W_{kj} \cdot O_j \right) + \theta_k . \tag{14}$$

Where W_{kj} : weight from Neuro j in hidden layer to Neuro k in output layer,
O_j : output value of Neuro j in hidden layer,
θ_k : bias or threshold at Neuro k.

To minimize the error function, E, the following equation is utilized.

$$\Delta W = -\eta \frac{\partial E}{\partial W} . \tag{15}$$

Where ΔW is the weight change and η denotes the learning rate, which is the proportional gain between the weight change and the partial differential error function. Thus, the weight can be adjusted or updated by

$$W(k)=W(k-1)+\Delta W. \tag{16}$$

This iteration process stops if the error function, E, converges within a preset bound.

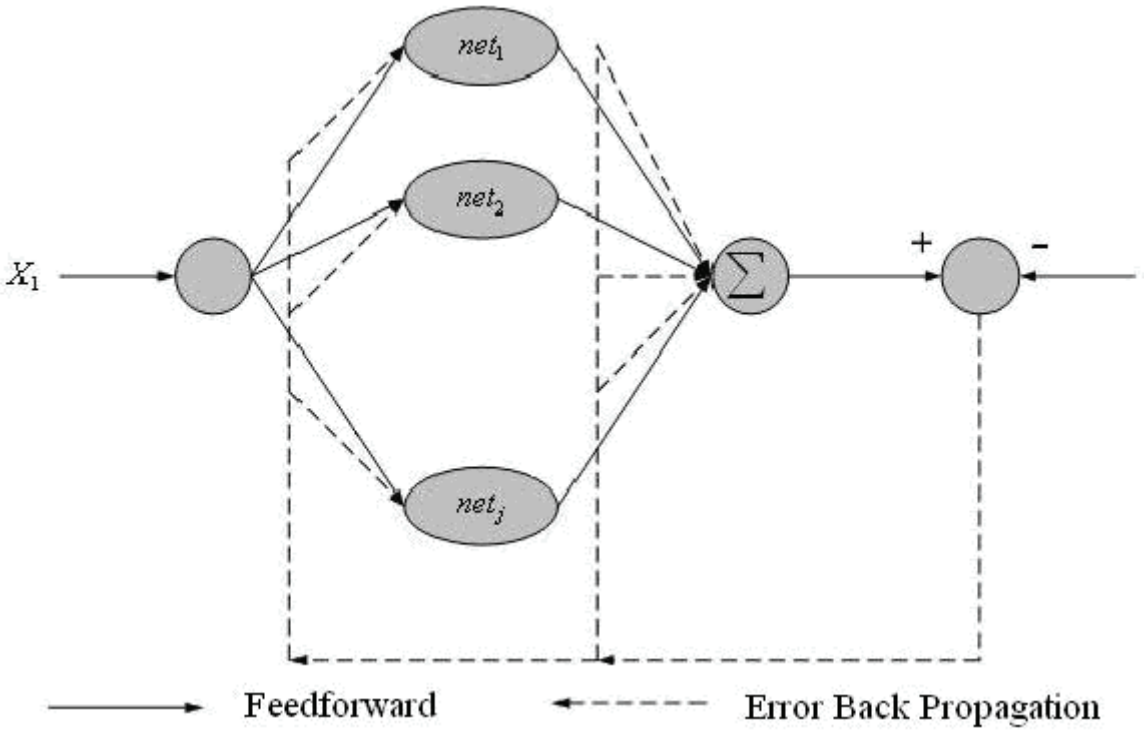

Figure 8. The network of EBP

4 Experimental Test Rig

Figure 9 shows the schematic layout of the test rig. The functional block diagram is shown in Fig. 10. There are two closed-loop hydraulic control units installed in the test rig. One is the road profile simulator unit used to simulate different road excitation. The other is the closed-loop controlled servo-hydraulic active suspension system to attenuate the road disturbance. The road actuator is basically a single-acting hydraulic cylinder with a maximal stroke of 150 mm. To precisely control the displacement of the road actuator, a linear potentiometer and a high-speed proportional valve (Parker-D1FH series) are employed. The system pressure is fixed at 70 bar. Thus, different road excitations can be generated in the laboratory.

As for the active suspension system, the controllable output force of the single-acting hydraulic cylinder is used to maintain the zero displacement of the sprung mass. To achieve this, a linear potentiometer as well as a high-speed proportional valve

(Parker-D1FH series) is also utilized. The suspension hydraulic cylinder (component No. 5 in Fig. 9) has an effective cross-sectional area of 903 mm^2 and a maximal stroke of 150 mm. For evaluating the ride comfort, an accelerometer is installed on the sprung mass to measure the vertical acceleration. The system pressure is fixed at 110 bar. Finally, the control of this test rig as well as the acquisition and processing of measured data are all integrated in a PC-based control unit with a multi-functional peripheral interface card.

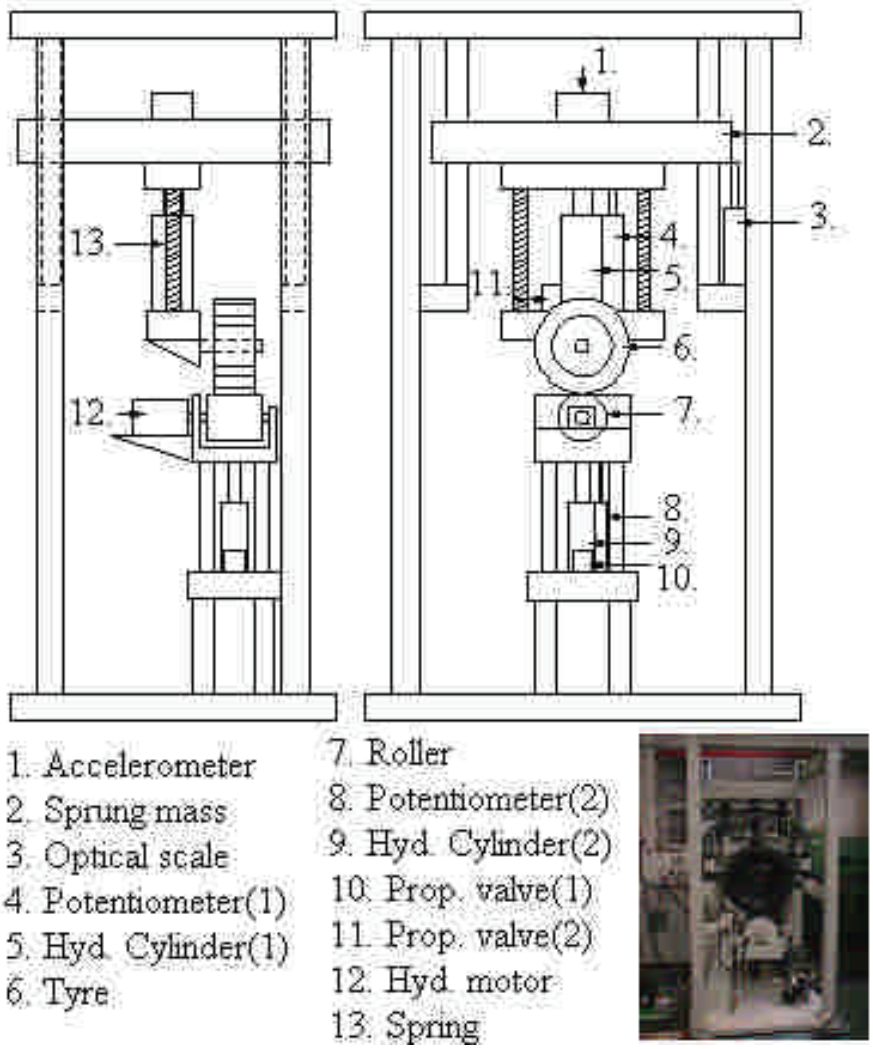

Figure 9. 1/4T test rig for active suspension system

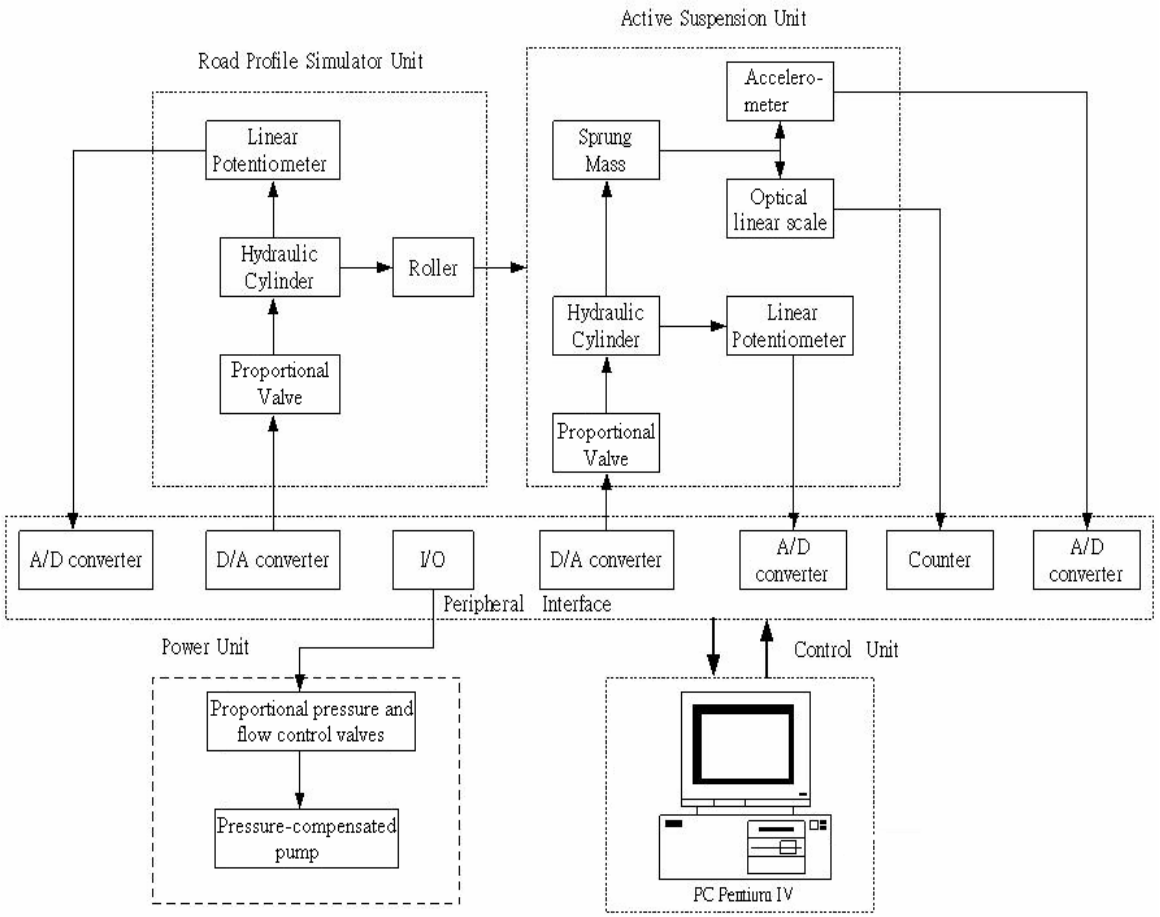

Figure 10. Functional block diagram of the test rig

5 Simulation and Experimental Results

For vehicles, the most critical road affecting the ride comfort is the random and uneven road profile. In the laboratory, however, simplification of the real road profile is necessary. The road profile test input chosen in this study is a flat road surface with a sinusoidal concave bump followed by a sinusoidal convex bump, which is generated by the closed-loop controlled road profile simulator (component No. 9 in Fig. 9). Figure 11 shows the simulation results using the state equations (7) as well as the MATLAB/Simulink software. The experimental results are shown in Fig. 12. The displacement signal is measured by the optical linear scale (component No. 3 in Fig. 9) attached to the chassis (i.e. sprung mass) of the vehicle. It is observed that the amplitude of oscillation of the vehicle body after passing the bumps with active suspension using neural network controller is somewhat smaller than that using the PID controller. That is, the control performance is improved.

On the other hand, Fig. 13 and Fig.14 show the corresponding simulation and measured acceleration signals. In addition to two main acceleration signals of vehicle body obtained from PID and neural network controller respectively, the acceleration of the road profile generated by the servo-hydraulic road simulator is also shown in the figures for references. Although the measured acceleration signals are oscillatory, the acceleration of the vehicle body using neural network controller is smaller. In other words, the ride comfort is improved. Table 1 shows the quantitative comparisons between the performances using PID and neural network controller. From either the maximal absolute value of body

acceleration or displacement, it can be concluded that the proposed neural network controller is somewhat better than the conventional PID controller.

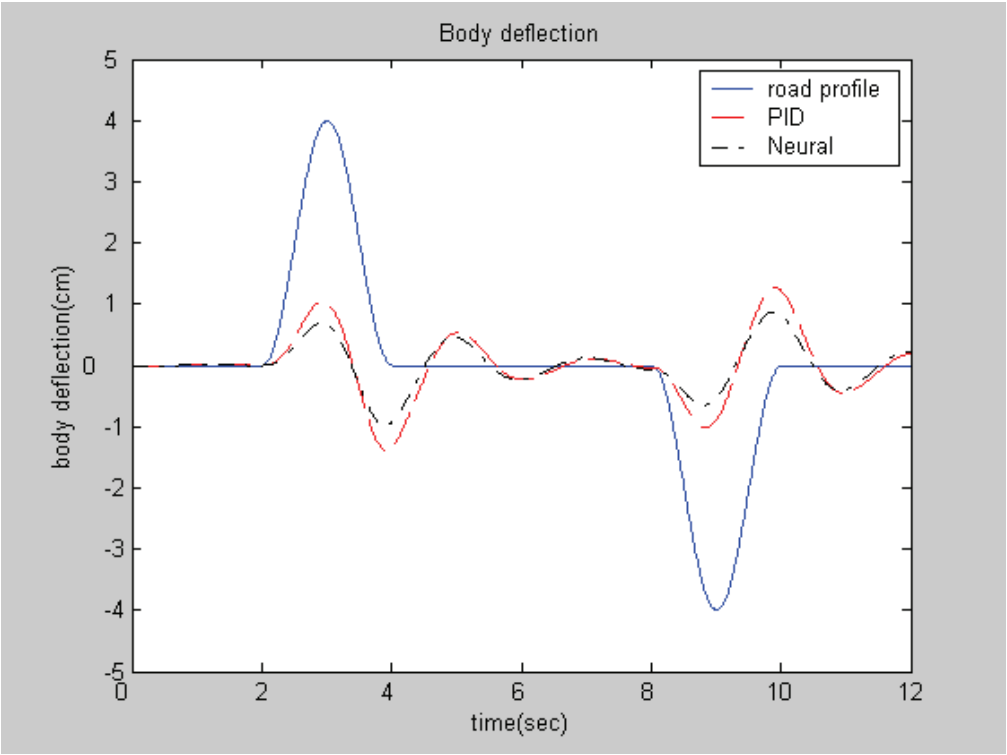

Figure 11. Simulation results showing the displacement of vehicle body subjected to 4 cm convex and concave bumps

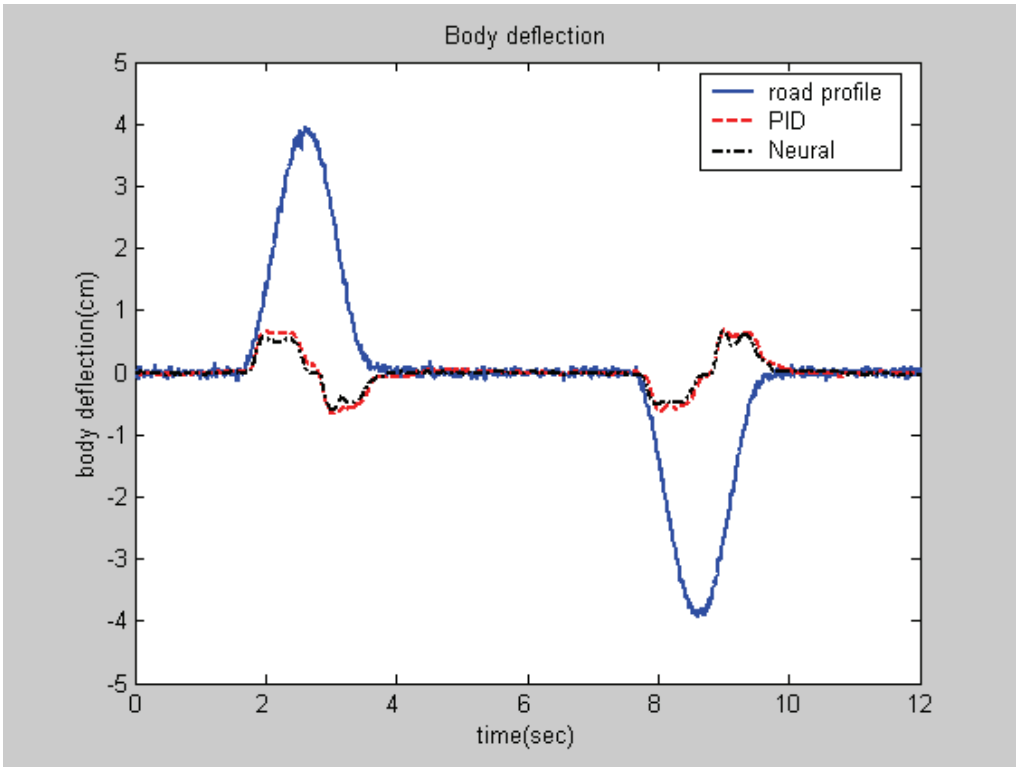

Figure 12. Experimental results showing the displacement of vehicle body subjected to 4 cm convex and concave bumps

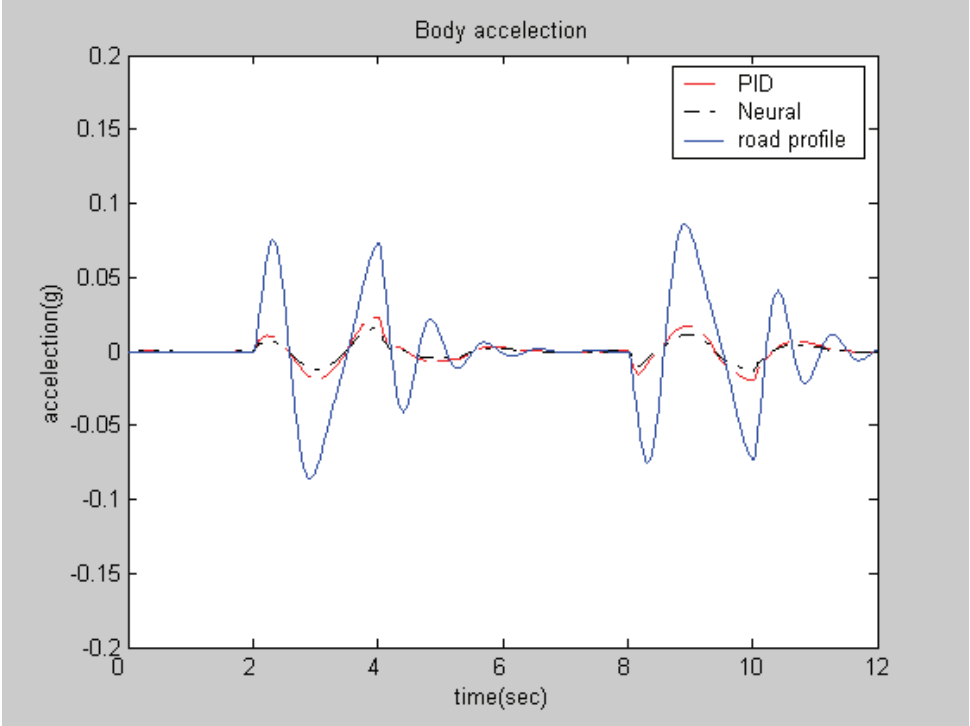

Figure 13. Simulation results showing the acceleration of vehicle body subjected to 4 cm convex and concave bumps

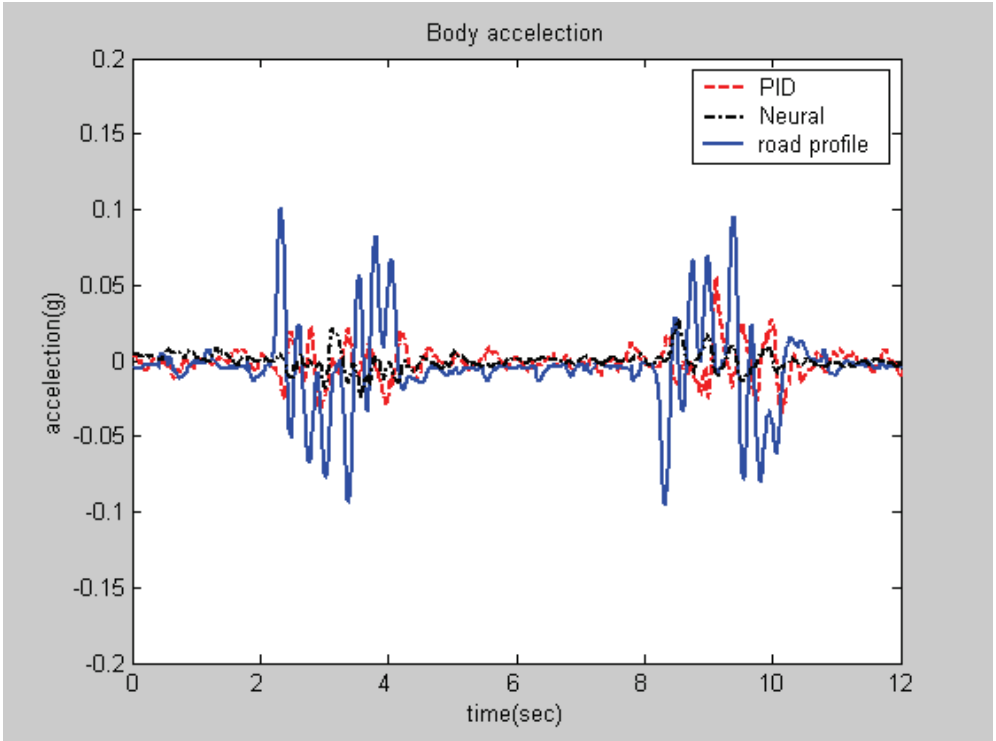

Figure 14. Experimental results showing the acceleration of vehicle body subjected to 4 cm convex and concave bumps

Table 1. Quantitative comparisons between PID and neural network controller

		Maximal absolute acceleration [g]	Maximal body absolute displacement [cm]
PID	*Simulation*	0.03	1
	Experiment	0.04	0.8
Neural Network	*Simulation*	0.02	0.7
	Experiment	0.03	0.7

6 Conclusion

In this paper, a test rig of servo-hydraulic active suspension system for vehicles is successfully developed. From simulation and experimental results, it is proved that both two control schemes can restrain the vibration and acceleration of vehicle body significantly. However, four remarks may be given as follows.

(1) For application in vehicles, the active suspension system is the key technology for vehicles to achieve both ride comfort and control performance.
(2) For the real application in vehicles, the proposed active suspension structure faces inevitably some challenges including the cost, the required space in vehicle and the difficulty to acquire the displacement of wheel, Z_u. In the developed test rig, the displacement of wheel was easily measures by the installed potentiometer (component No. 8 in Fig. 9). In a real vehicle, however, the install of such a potentiometer is practically impossible. One possible solution is the utilization of an accelerometer to acquire first the acceleration of the wheel. And then, the numerical integration may be used to calculate the required position signal.
(3) The developed PC-based controller can actually not be implemented in a real vehicle application because of the bulky dimension. One feasible solution is the introduction of DSP control system.
(4) Since the servo-hydraulic system is highly nonlinear and time-varying, it is reasonable to have the result that the proposed neural network controller is able to suppress the vibration amplitude and subsequent acceleration of the vehicle body in a more efficient manner than the conventional PID controller. For the real application, however, PID controller is still the best choice because of its simplicity and easy implementation.

7 Acknowledgement

The financial support of the National Science Council of ROC under grant number NSC-95-2212-E-224-032 is greatly appreciated.

8 References

[1] M. Sunwoo, K. C. Cheok and N. J. Huang, 1991, “Model Reference Adaptive Control for Vehicle Active Suspension Systems,” IEEE Trans. on Industrial Electronics, Vol.38, No.3, pp.217-222.

[2] Y. P. Kuo, T. Hseng and S. Li, 1999, “GA-Based Fuzzy PI/PD Controller for Automotive Active Suspension System,” IEEE Transactions on Industrial Electronics, Vol.46, No.6, pp. 1051-1056.

[3] S. Chantranuwathana and H. Peng, 1999, “Adaptive Robust Control for Active Suspensions,” Proc. of the 1999 American Control Conference, pp.1702-1706.

[4] M.V.C Rao and V. Prahlad, 1997, “A Tunable Fuzzy Logic Controller for Vehicle-active Suspension System,” Fuzzy Sets and Systems, Vol. 85, pp. 11-21.

[5] A. G. Thompson, 1984, “Optimal and Suboptimal Linear Active Suspensions for Road Vehicles,” Veh. Syst. Dynamics, Vol. 13, pp. 61-72.

[6] S. B. Kiriczi and R. Kashani, 1992, “Robust stability analysis of LQG-controlled active suspension with model uncertainty using structure singular value, μ, method,” Veh. Syst. Dynamics, Vol. 21, pp. 361-384.

[7] J. S. Lin and I. Kanellakopoulos, 1997, “Nonlinear Design of Active Suspensions,” IEEE Control System, June, pp. 45-59.

[8] C. Kim and P. I. Ro, 1998, “A Sliding Mode Controller for Vehicle Active Suspension Systems with Nonlinearities,” Proc. Instn. Mech. Engrs., Vol. 212 Part D, pp. 79-92.

[9] Y. J. Jang and S. W. Kim, 2002, “Gain-Scheduled Control for an Active Suspension System with an Asymmetric Hydraulic Actuator,” IEICE Trans. Fundamentals, Vol. E85-A, No. 4, pp. 903-908.

[10] S. J. Wu, C. T. Wu and T. T. Lee, “Neural-Network-Based optimal Fuzzy Control Design for Half-Car Active Suspension Systems,” *Proceedings, Intelligent Vehicle Symposium*, Las Vegas, June (2005).

[11] H. E. Merritt, 1967, Hydraulic control system, John Wiley & Sons, Inc.

[12] J. G. Ziegler and N. B. Nichols, 1942, “Optimum Settings for Automatic Controllers,” Trans. of ASME 64, pp. 759-768.

[13] T. Fukuda and T. Shibata, 1992, “Theory and Application of Neural Networks for Industrial Control System,” IEEE Transaction on Industrial Electronics, pp.472-489.

MOTION CONTROL FOR OVERCONSTRAINED PARALLEL SERVOHYDRAULIC MECHANISMS

Professor Andrew R Plummer
Centre for Power Transmission and Motion Control
University of Bath
Bath BA2 7AY
UK
Phone +44 1225 386140, Fax +44 1225 386928
E-mail: A.R.Plummer@bath.ac.uk

ABSTRACT

A practical position control method is presented for parallel servohydraulic mechanisms in which the payload behaves as a rigid mass. The ability of this method to decouple the control axes is demonstrated. A modal control approach is used – i.e. the modes of vibration of the table are controlled individually. These modes are dependent on the inertial properties of the table with specimen and the compliance of the actuators due to oil compressibility. In some parallel servohydraulic mechanisms there are more actuators than degrees-of-freedom: i.e. they are overconstrained. It is shown how the proposed control method can be extended to such overconstrained systems. Simulation results are presented based on a validated model of an overconstrained earthquake simulation table.

KEYWORDS: motion systems, electrohydraulic servosystems, redundant actuators, vibration testing, multi-axis control, parallel kinematic mechanisms

1 INTRODUCTION

Parallel servohydraulic mechanisms (PSHMs) are used where the motion of an object must be controlled in two or more directions simultaneously, and both the forces and speed of response required are high. Servohydraulic actuators provide high force and bandwidth with relatively low mass and size; a parallel kinematic arrangement provides greater stiffness than a serial connection of actuators, and hence the potential for higher bandwidth.

This paper is concerned with high performance motion control for PSHMs, and includes the case of overconstraint, i.e. where the number of actuators exceeds the number of rigid-body degrees of freedom. The work has been motivated by the need to improve

control for multi-axis vibration test rigs. These are normally PSHMs which need to accurately control motion at high frequencies, sometimes up to several hundred hertz. They normally have a fairly small range of motion, so that the geometry-related non-linearities do not have a very significant influence on the dynamic properties, and so can be neglected. Larger systems, particularly shaking tables for earthquake simulation, have more actuators than degrees of freedom. This enables the forces to be distributed more evenly on the table structure.

Figure 1 shows a typical arrangement for a 6 degree-of-freedom (DOF) multi-axis vibration table with a payload capacity of a few hundred kilograms. Larger tables are required for seismic testing of model buildings; these can typically accommodate payloads of at least several tonnes. The recently commissioned Japanese E-defense facility can handle payloads up to 1200 tonnes – large enough for the testing of four-storey buildings at full scale [1]. Figures 2 and 3 show examples of earthquake simulation tables.

In this paper, a practical position control method is presented for parallel servohydraulic mechanisms in which the payload behaves as a rigid mass. The ability of this method to decouple the control axes is demonstrated. A modal control approach is used – i.e. the modes of vibration of the table are controlled individually. These modes are dependent on the inertial properties of the table with specimen and the compliance of the actuators due to oil compressibility. It is shown how the method can be extended to overconstrained systems. Simulation results are presented based on a validated model of an overconstrained shaking table.

A modal decoupling approach for PSHMs was first described in [2]. The issue of overconstrained systems was not addressed. Simulation results were presented using a very simple (proportional plus lag) closed-loop compensator. Little has been published on the multi-axis control of vibration tables, although a number of uni-axial studies have been performed (e.g. [3-5]).

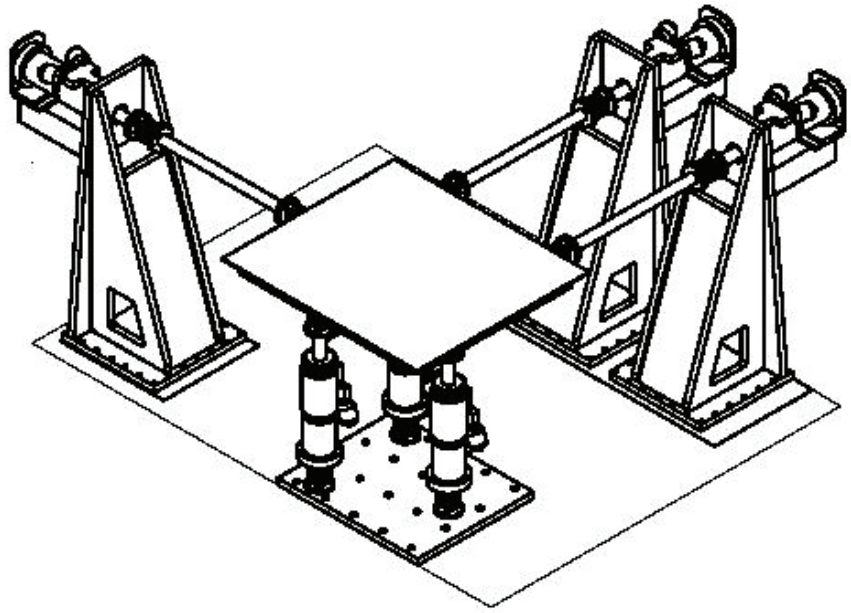

Fig 1: A 6 DOF multi-axis vibration table (6 actuators): 0.5 tonne capacity

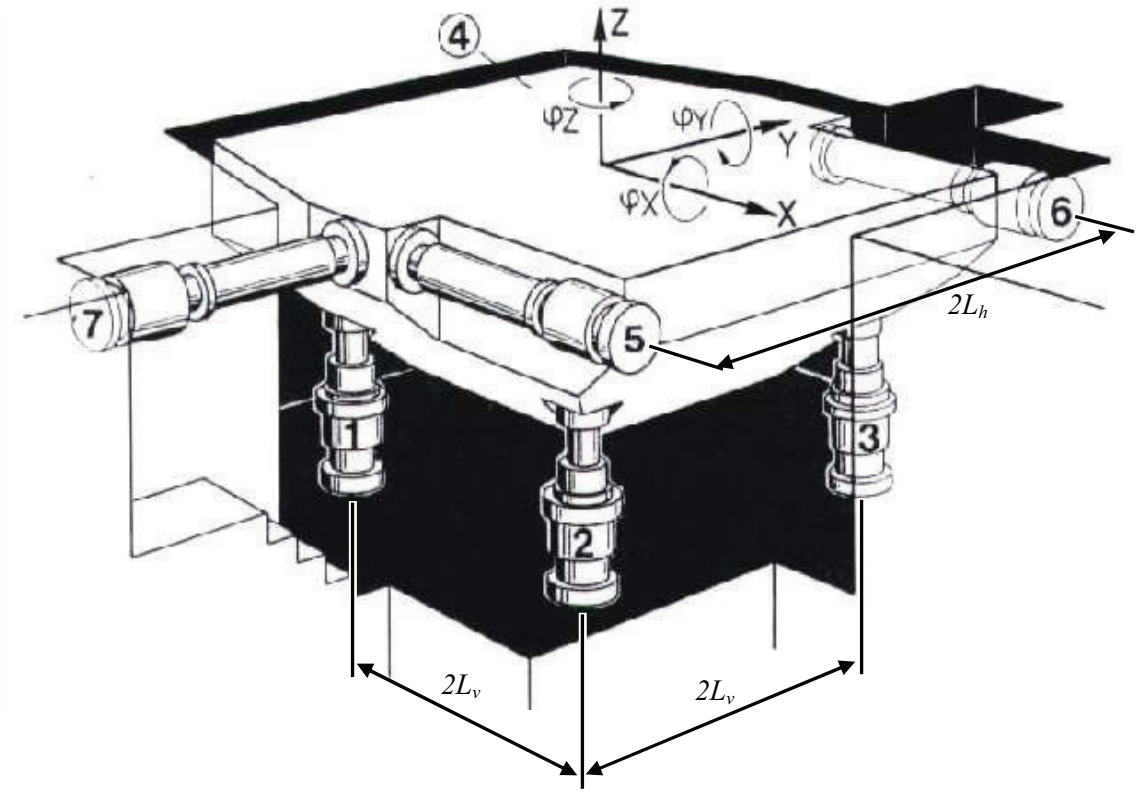

Fig 2: 6 DOF seismic table (7 actuators): 20 tonne capacity

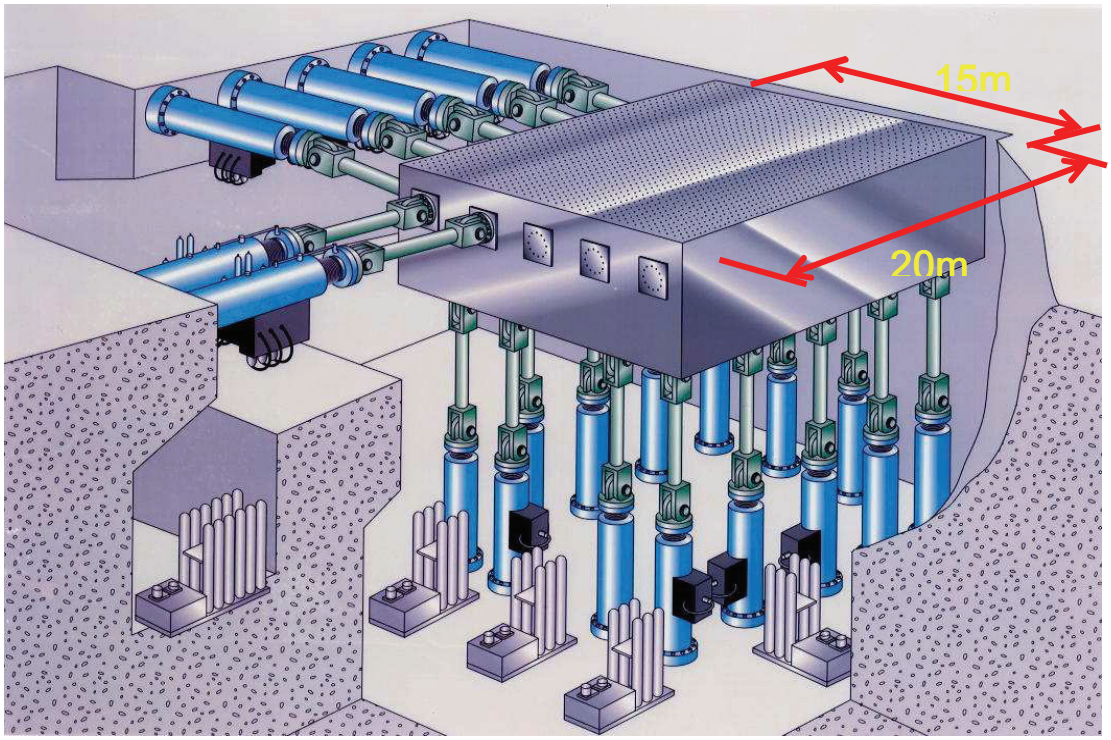

Fig 3：6 DOF seismic table (24 actuators): 1200 tonne capacity

2 SINGLE AXIS MODELLING AND CONTROL

A conventional linear model of the position response of a hydraulic actuator driving an inertial load has the form:

$$y_i = \frac{hk}{s(ms^2 + cs + k)} v_i \tag{1}$$

where y_i is the piston position, v_i is the valve spool position, m is the mass driven by the actuator, c is the effective damping, k is the hydraulic stiffness and h is the steady state gain of actuator velocity over spool position. Such a model can be derived from a small perturbation analysis of the non-linear equations describing valve and cylinder behaviour [6]. It is assumed that the hydraulic resonant frequency given by equation (1) is the same order of magnitude as the valve bandwidth, so the valve dynamics cannot be ignored. The response of the valve spool position to control signal u_i can be approximated by a second order transfer function plus delay [7]:

$$v_i = V(s)u_i \tag{2}$$

where

$$V(s) = \frac{\omega_{nv}^2 e^{-sD}}{s^2 + 2\zeta\omega_{nv}s + \omega_{nv}^2}$$

Figure 4 shows an example plant frequency response; this is actually the Y-direction response of the shaking table shown in Figure 2. A best-fit model is shown for comparison. In this case the parameters are: h = 53, m = 23 000kg, c = 1.20×10^6 Ns/m, k = 484×10^6 N/m, D = 0.002s, ω_{nv} =754 rad/s, ζ = 0.70

A variety of methods can be used to design a controller for this type of system [8]. This paper is primarily concerned with multi-axis systems, rather than controller design for single axes. However, as an example, the controller shown in Figure 5 can be used, and this gives the closed-loop frequency response of Figure 6. This controller incorporates command feedforward, and an inverse model to compensate for actuator dynamics; the approach is described in more detail in [9].

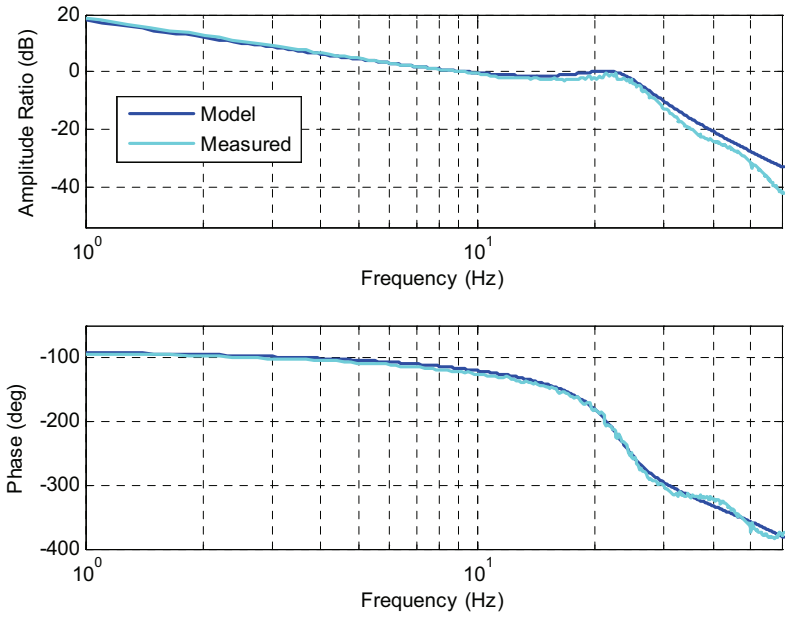

Fig 4. Example plant frequency response

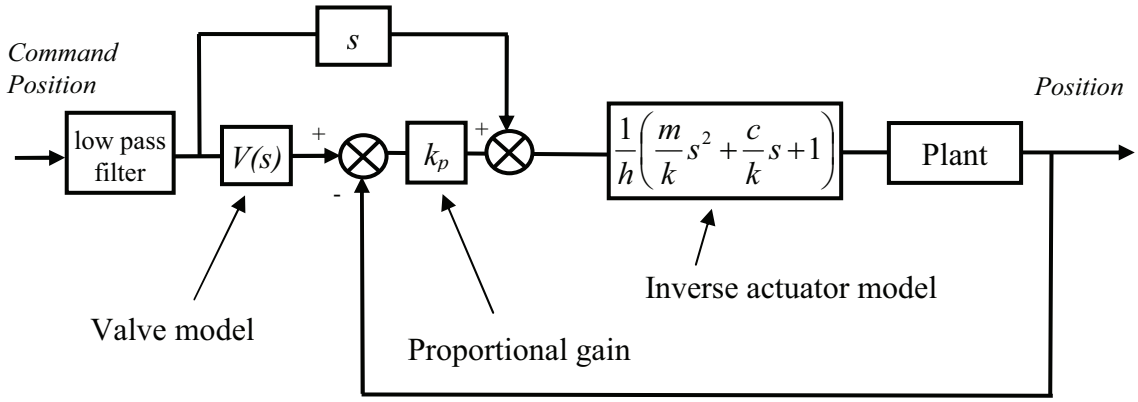

Fig. 5. Electrohydraulic position control system (single axis)

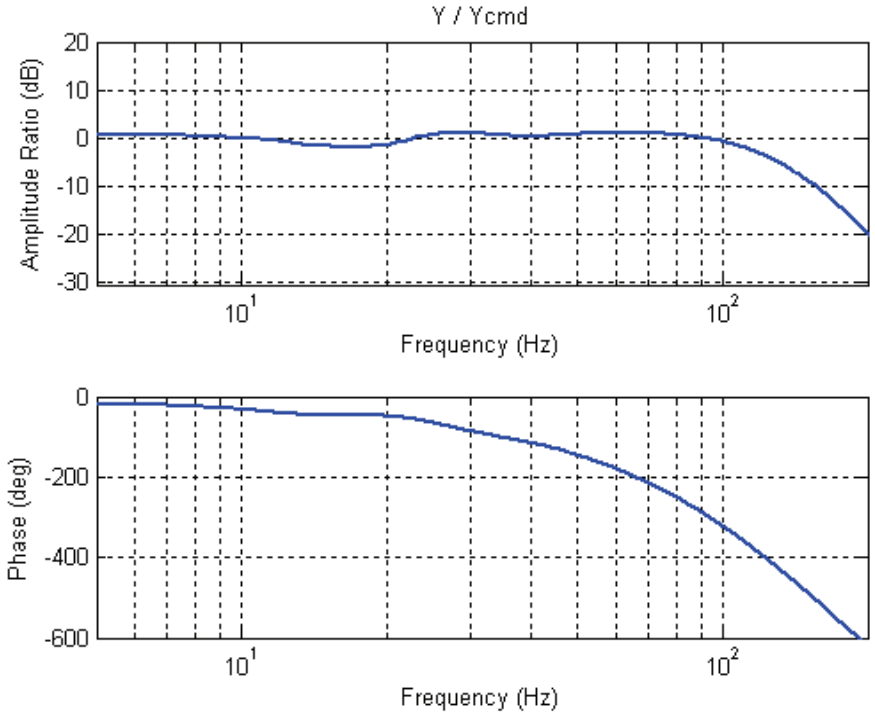

Fig. 6 Closed-loop position frequency response

3 MODAL CONTROL: 6 ACTUATOR SYSTEM

3.1 Linear model and decoupling control

A linear multi-axis model can be derived as an extension of the single axis model. First, reconsider equation (1). Defining x_i to be the 'no load' actuator position:

$$x_i = \frac{h}{s} v_i \tag{3}$$

Then neglecting the small damping term:

$$y_i = \frac{k}{ms^2 + k} x_i \tag{4}$$

or

$$ms^2 y_i + k(y_i - x_i) = 0 \tag{5}$$

For a 6 DOF, 6 actuator table, a *6*x*6* mass matrix **M** can be derived relating small perturbations in table acceleration to table force, and the *6*x*6* hydraulic stiffness matrix **K** can be derived relating small perturbations in table postion to table force. Table motion and forces are defined in terms of three orthogonal linear axes (x,y,z) and three orthogonal rotary axes (roll, pitch and yaw Euler angles) of a table-fixed frame {C}relative to a world frame (see Figure 7). The calculation of **M** and **K** are described in section 3.2. If these are found for the mid-position of the table, then the multi-axis model linearized about this mid-position is:

$$\mathbf{M}s^2 \boldsymbol{y}_c + \mathbf{K}(\boldsymbol{y}_c - \boldsymbol{x}_c) = 0 \tag{6}$$

$$s^2 \boldsymbol{y}_c + \mathbf{M}^{-1}\mathbf{K}(\boldsymbol{y}_c - \boldsymbol{x}_c) = 0 \tag{7}$$

where $\boldsymbol{y}_c$ is the vector of *6* table displacements (linear and angular) of frame {C}, and $\boldsymbol{x}_c$ is the equivalent vector of *6* no load displacements.

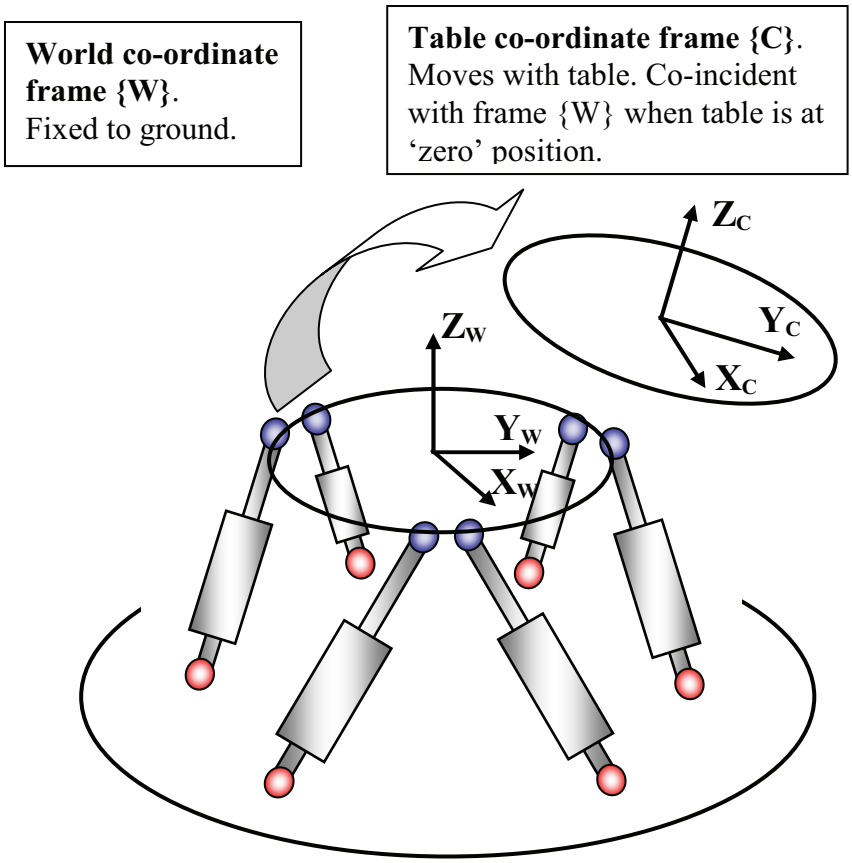

Fig. 7 Co-ordinate frames

The *6* axes in this model will only be decoupled if $\mathbf{M^{-1}K}$ is diagonal, which in general is not the case. However transforming the displacements into some other co-ordinate system provides an opportunity to diagonalize $\mathbf{M^{-1}K}$. A linear transformation into 'modal displacements' $\boldsymbol{y_m}$ is given by:

$$\boldsymbol{y_m} = \mathbf{P}^{-1}\boldsymbol{y_c} \qquad \boldsymbol{x_m} = \mathbf{P}^{-1}\boldsymbol{x_c} \tag{8}$$

Giving:

$$s^2\boldsymbol{y_m} + \mathbf{P}^{-1}\mathbf{M}^{-1}\mathbf{K}\mathbf{P}(\boldsymbol{y_m} - \boldsymbol{x_m}) = 0 \tag{9}$$

Matrix $\mathbf{P}$ should be chosen to diagonalize $\mathbf{P^{-1}M^{-1}KP}$. For example, if $\mathbf{P}$ has as its columns the eigenvectors of $\mathbf{M^{-1}K}$, and the eigenvectors are linearly independent so that $\mathbf{P}$ is non-singular, then this diagonalization is achieved, and:

$$\mathbf{P}^{-1}\mathbf{M}^{-1}\mathbf{K}\mathbf{P} = \mathbf{\Omega} \tag{10}$$

where:

$$\mathbf{\Omega} = \begin{bmatrix} \omega_1^2 & & & 0 \\ & \omega_2^2 & & \\ & & \ddots & \\ 0 & & & \omega_N^2 \end{bmatrix} \tag{11}$$

Each ω_i^2 term is the square of the natural frequency of one mode; these are the eigenvalues of $\mathbf{M^{-1}K}$. If no two of the natural frequencies are the same then this guarantees that the eigenvectors will be linearly independent.

Define a matrix $\mathbf{Q}$ which transforms the frame {C} table displacements into individual actuator displacements:

$$\boldsymbol{y} = \mathbf{Q}\boldsymbol{y_c} \tag{12}$$

where $\boldsymbol{y}$ is the vector of 6 actuator displacements y_i. Thus referring to equation (8):

$$\boldsymbol{y} = \mathbf{R}\boldsymbol{y_m} \tag{13}$$

where

$$\mathbf{R} = \mathbf{Q}\mathbf{P} \tag{14}$$

Completing the system model, the valve dynamics are assumed to be the same for each actuator, so:

$$\boldsymbol{v} = V(s)\boldsymbol{u} \tag{15}$$

where $\boldsymbol{u}$ is the vector of valve drive signals, $\boldsymbol{v}$ is the vector of spool positions, and *V(s)* is the scalar transfer function of equation (2) representing valve dynamics. This gives:

$$\boldsymbol{x} = \frac{hV(s)}{s}\boldsymbol{u} \tag{16}$$

$$\boldsymbol{x_m} = \frac{hV(s)}{s}\boldsymbol{u_m} \tag{17}$$

where

$$\boldsymbol{u_m} = \mathbf{P}^{-1}\boldsymbol{u_c} \tag{18}$$

From equations (9), (10) and (17), the complete model is:

$$s^2\boldsymbol{y_m} + \mathbf{\Omega}(\boldsymbol{y_m} - \frac{hV(s)}{s}\boldsymbol{u_m}) = 0$$

or

$$s(s^2\mathbf{I} + \mathbf{\Omega})\boldsymbol{y_m} = hV(s)\mathbf{\Omega}\boldsymbol{u_m} \tag{19}$$

This is diagonal, so each control loop can be designed independently based on scalar plant models of the form:

$$y_{mi} = \frac{h\omega_i^{\,2}}{s(s^2 + d_i s + \omega_i^{\,2})} V(s) u_{mi} \tag{20}$$

Note that a damping term has been re-introduced: as damping is small it can be approximated by de-coupled terms. The complete multi-axis controller is shown in Figure 8, in which D is the diagonal damping matrix containing elements d_i.

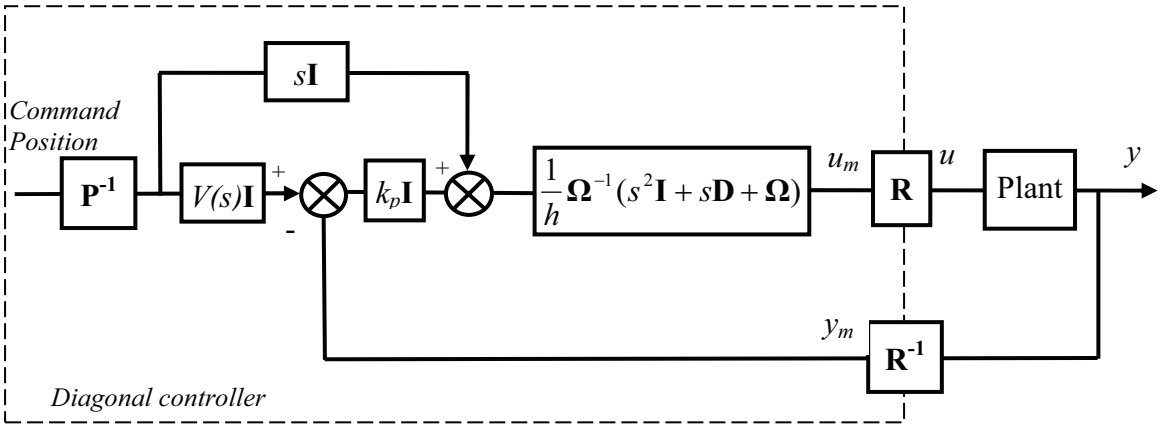

Fig. 8 Diagonal multi-axis controller

3.2 Mass and stiffness matrices

The linearised equation of motion for the combined table and payload is:

$$^{c}\boldsymbol{f}_t = \mathbf{M}\ ^{c}\boldsymbol{a}_t \tag{21}$$

where $^{c}\boldsymbol{f}_t$ is the vector of three orthogonal forces and three orthogonal moments acting on the table at frame {C}, $^{c}\boldsymbol{a}_t$ is the vector of three orthogonal linear accelerations and three orthogonal angular accelerations of frame {C}.

Define the mass matrix about the table/payload centre of gravity as:

$$\mathbf{M}_{cg} = \begin{bmatrix} m_t \mathbf{I}_3 & 0 \\ 0 & \mathbf{I_t} \end{bmatrix} \tag{22}$$

where m_t is the table plus payload mass, $\mathbf{I}_3$ is the 3x3 identity matrix, and $\mathbf{I_t}$ is the 3x3 matrix of moments and products of inertia. This needs to be transformed to frame {C}, and also the mass contributions from actuators and/or pushrods needs to be added:

$$\mathbf{M} = \mathbf{M}_c + \sum_{i=1}^{N} \mathbf{J_i}^{-\mathrm{T}} \mathbf{M_{ai}} \mathbf{J_i}^{-1} \tag{23}$$

where $\mathrm{M_c}$ is the transformed table/payload mass matrix, and the Jacobean matrices $\mathbf{J_i}$ relate actuator velocities to table velocities, and $\mathbf{M_{ai}}$ are the actuator mass matrices.

The hydraulic stiffnesses referred to frame {C} are given by:

$$\mathbf{K} = k\mathbf{Q}^{\mathrm{T}}\mathbf{Q} \tag{24}$$

where the parameter k is the individual actuator stiffness, assumed to be the same for each actuator

4 MODAL CONTROL: OVERCONSTRAINED SYSTEMS

The principles described above can be extended for overconstrained tables, i.e. those with more than 6 actuators. Most seismic testing tables come into this category. There are extra control axes to be considered, in addition to the 6 modally decoupled axes described above. For example, where there are four vertical actuators as in Figure 2, there is the ability to structurally deform the table in twist, a motion which is additional to the six rigid body motions. A formal definition of the additional deformation axes of an overconstrained table is given below.

For an *N*-axis table, equation (13) can be augmented as follows:

$$\begin{bmatrix}\mathbf{QP} & \mathbf{A}\end{bmatrix}\begin{bmatrix}\boldsymbol{y}_m \\ \boldsymbol{y}_a\end{bmatrix} = \boldsymbol{y} \tag{25}$$

where **P** is the 6x6 decoupling matrix as before, **Q** is now an *N*x6 matrix, and **A** is a new *N*x(*N*-6) partition. The *N*-6 length vector $\boldsymbol{y}_a$ contains the deformation displacements

The rigid body displacements $\boldsymbol{y}_m$ should fit (in some sense) the actuator displacements as closely as possible. Adopting a least squares fit, then:

$$\boldsymbol{y}_m = \mathbf{P}^{-1}(\mathbf{Q}^{\mathrm{T}}\mathbf{Q})^{-1}\mathbf{Q}^{\mathrm{T}}\boldsymbol{y} \tag{26}$$

This is the pseudoinverse of **QP**.

Multiplying equation (25) through by $\mathbf{Q}^{\mathrm{T}}$:

$$\mathbf{Q}^{\mathrm{T}}\mathbf{QP}\boldsymbol{y}_m + \mathbf{Q}^{\mathrm{T}}\mathbf{A}\boldsymbol{y}_a = \mathbf{Q}^{\mathrm{T}}\boldsymbol{y} \tag{27}$$

and substituting using equation (26) gives:

$$\mathbf{Q}^{\mathrm{T}}\mathbf{A}\boldsymbol{y}_a = 0 \tag{28}$$

As this is true for all $\boldsymbol{y}_a$, then:

$$\mathbf{Q}^{\mathrm{T}}\mathbf{A} = 0 \tag{29}$$

Thus the columns of **A** are the vectors which form the orthonormal basis of the null space of matrix $\mathbf{Q}^{\mathrm{T}}$ (found, for example, using the Matlab *null* function). For the tables with four vertical actuators in a square formation, a column of **A** will turn out to define one deformation displacement as moving one diagonal pair of actuators up while moving the other diagonal pair down, i.e. twist.

The block diagram of Figure 6 is still applicable in this case. It is now an *NxN* multivariable controller, with:

$$\mathbf{R} = \begin{bmatrix}\mathbf{QP} & \mathbf{A}\end{bmatrix} \tag{30}$$

The deformation control loops would normally be commanded to zero. In practice, there would be an advantage in controlling deformation force rather than deformation position, as for a stiff table small errors in position measurement could lead to large deformation forces. A force controller for the deformation axes is shown in Figure 9. As described in [10], the hydraulic actuator force when driving into a stiffness-dominated load can usually be well controlled by a simple proportional (or proportional plus integral) controller.

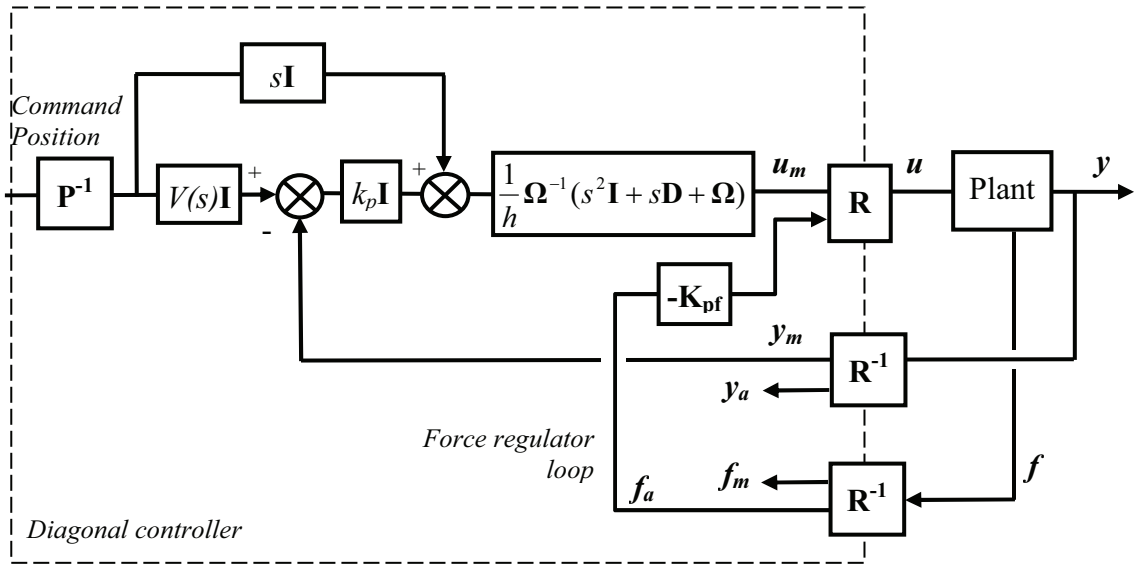

Fig. 9 Multi-axis controller for overconstrained system

5 EXAMPLE

The 7-actuator table of Figure 2 is used here as an example. By choosing the frame {C} as shown in the Figure, with its origin at the intersection of the lines of symmetry between the actuators in all three planes, then the matrix Q which relates table to actuator displacements (equation (12)) is given by:

$$\mathbf{Q} = \begin{bmatrix} 0 & 0 & 1 & -L_v & L_v & 0 \\ 0 & 0 & 1 & -L_v & -L_v & 0 \\ 0 & 0 & 1 & L_v & -L_v & 0 \\ 0 & 0 & 1 & L_v & L_v & 0 \\ -1 & 0 & 0 & 0 & 0 & -L_h \\ -1 & 0 & 0 & 0 & 0 & L_h \\ 0 & 1 & 0 & 0 & 0 & 0 \end{bmatrix}$$

From equation (29), this yields:

$$\mathbf{A} = \begin{bmatrix} 0.5 & -0.5 & 0.5 & -0.5 & 0 & 0 & 0 \end{bmatrix}^T$$

which defines the deformation axis. There is only one deformation axis as there is one degree of over-constraint. In this simple case the deformation axis is twist of the table as expected.

The combined table and payload mass, m_t, is 43 000kg, and the moments of inertia are I_x = 134 000kgm^2, I_y = 114 000kgm^2 and I_z = 102 000kgm^2. The centre of gravity is vertically above the origin of frame {C}, at a height of h = 0.93m. The inertial

contribution from the attached actuators/pushrods is small in this case and can be neglected; the products of inertia are also small. This gives a mass matrix of the form:

$$\mathbf{M} = \begin{bmatrix} m_t & 0 & 0 & 0 & m_t h & 0 \\ 0 & m_t & 0 & -m_t h & 0 & 0 \\ 0 & 0 & m_t & 0 & 0 & 0 \\ 0 & -m_t h & 0 & I_x + m_t h^2 & 0 & 0 \\ m_t h & 0 & 0 & 0 & I_y + m_t h^2 & 0 \\ 0 & 0 & 0 & 0 & 0 & I_z \end{bmatrix}$$

The frame {C} origin happens to be at the 'centre of stiffness' in this case, i.e. at a point where there is no cross-axis stiffness interaction. So the stiffness matrix **K** is diagonal:

$$\mathbf{K} = \begin{bmatrix} 4.50x10^8 & 0 & 0 & 0 & 0 & 0 \\ 0 & 3.80x10^8 & 0 & 0 & 0 & 0 \\ 0 & 0 & 1.19x10^8 & 0 & 0 & 0 \\ 0 & 0 & 0 & 3.64x10^9 & 0 & 0 \\ 0 & 0 & 0 & 0 & 3.64x10^9 & 0 \\ 0 & 0 & 0 & 0 & 0 & 3.53x10^9 \end{bmatrix}$$

From equation (10), this gives:

$$\mathbf{P} = \begin{bmatrix} 1 & 0 & 0 & 0 & -1.30 & 0 \\ 0 & 1 & 0 & 1.30 & 0 & 0 \\ 0 & 0 & 1 & 0 & 0 & 0 \\ 0 & -0.135 & 0 & 1 & 0 & 0 \\ 0.160 & 0 & 0 & 0 & 1 & 0 \\ 0 & 0 & 0 & 0 & 0 & 1 \end{bmatrix}$$

The decoupling matrix **R** can now be derived as in equation (14). Implementing the control scheme shown in Figure 9 gives the step responses for three of the degrees of freedom shown in Figure 10. The corresponding regulation of the twist force f_a is also shown. These results are generated from a detailed and validated non-linear simulation of the multi-axis table. The position sensors are modelled with a realistic linearity error which causes a disturbance in the twist force loop when the table moves.

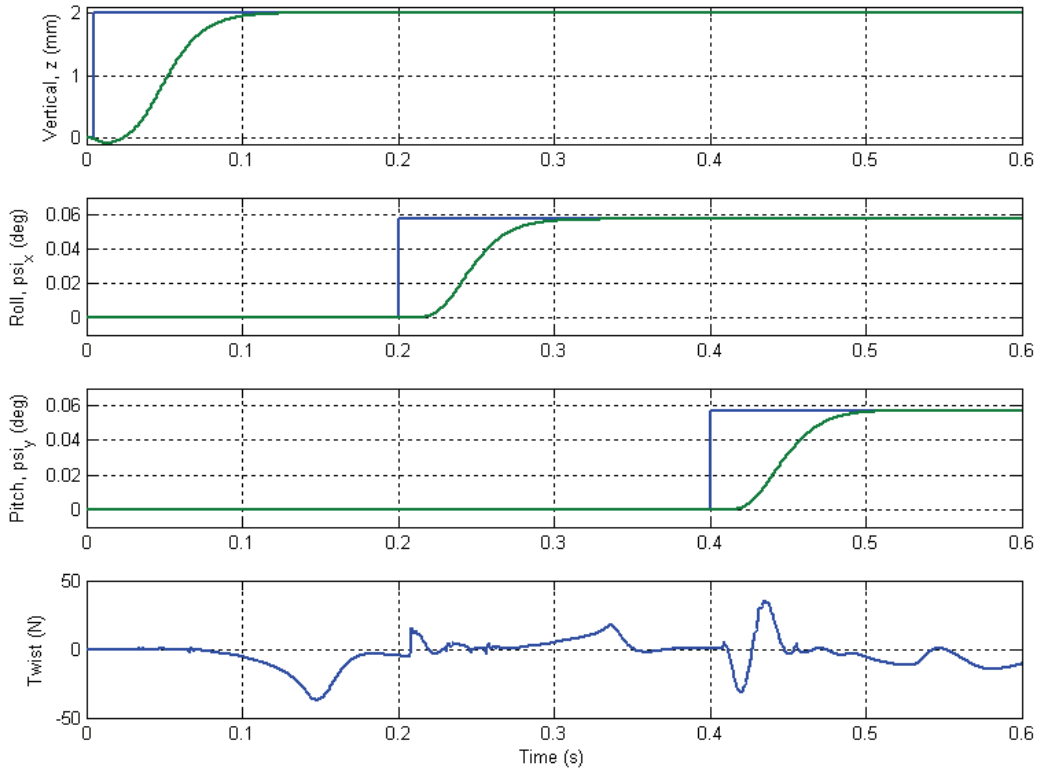

Fig. 10. Step responses (simulation)

6 CONCLUSIONS AND DISCUSSION

A decoupling modal control approach has been described for an overconstrained multi-axis vibration table with a simple inertial load. Although the approach is based on a linearised analysis, it is shown to work well around the mid-position. The displacement range of this type of table is normally quite small, and so the linear approach is expected to be reasonably accurate throughout the working range.

For systems with overconstraint, the additional deformation axes that the method determines would be commanded to zero to prevent actuators 'fighting' one another and damaging the table. It is argued that, where possible, force control for these additional axes is preferable, as in position control substantial deformation forces may still be applied to the table due to errors in position measurement. In the 7-actuator system used as an example, the additional twist axis determined by the method could have been arrived at intuitively. However, for a more complex configuration, such as the 24-actuator table of Figure 3, there the optimal definition of the 18 deformation axes could not be arrived at heuristically.

For PSHMs with a larger displacement range, such is flight simulator motion systems, the linear analysis used here may not be applicable. However, the calculation speed of

modern real-time computer systems is such that it would be feasible to calculate the decoupling matrix on-line, and to use a linearised controller appropriate to the current local operating point.

REFERENCES

[1] Ogawa, N., Ohtani, K, Katayama, T., Shibata, H. "Construction of a three-dimensional, large scale shaking table and development of core technology". Phil Trans R Soc Lond A, 359, pp. 1725-1751 (2001)

[2] Plummer, A. R., "Modal control for a class of multi-axis vibration table" *Control 2004*, Bath, UK, Sept 2004.

[3] Iwasaki, M, Ito, K, Kawafuku, M, Hirai, H, Dozono, Y, Kuosaki, K. "Disturbance observer based practical control of shaking tables with non-linear specimen" *16th IFAC World Congress*, Prague, July 2005.

[4] Kakegawa, T, Suzuki, T, Sato, E, Kajiwara, K, Tagawa, Y. "Linear model derivation and three-variable control (TVC) of the world's largest 3-D full-scale shaking table" *Trans of the Japan Society of Mechanical Engineers, Part C*, 69(2), 343-348 (in Japanese)

[5] Kuehn, J., Epp, D., Patten, W.N. "High-fidelity control of a seismic shake table" *Earthquake Engng. Struct. Dyn*. 28, 1999, 1235-1254.

[6] D. McCloy, H R Martin, "Control of Fluid Power: Analysis and Design". Ellis Horwood, Chichester (1980).

[7] Plummer, A R A new acceleration feedback design method for electrohydraulic motion control systems. *PTMC 2006*, Bath, September 2006.

[8] Edge, K.A., "On the control of electrohydraulic systems – some recent research contributions." *The Eighth International Conference on Fluid Power, SICFP'03,* Tampere, Finland, May 2003.

[9] Plummer, A.R. "Closed-loop velocity control for an electrohydraulic impact test system" PTMC 2005 Bath, September 2005, 75-90.

[10] Plummer, A.R. [2007] "Control techniques for structural testing: a review" *Proc. Instn. Mech. Engrs, Part I, Journal of Systems and Control Engineering,* Accepted. (Due March 07)

VIBRATION DAMPING OF THE CRANE

Heikki Paavilainen, Jari Savolainen, Jyrki Kullaa
Helsinki Polytechnic
Department of Mechanical and Production Engineering
P.O.Box 4021
00099 City of Helsinki
Phone +358 9 31083552, Fax +358 9 31083500
E-mail: heikki.paavilainen@stadia.fi

1. ABSTRACT

At the modern hydraulic cranes the combination of relative slim boom structure, high load and the use of load sensing hydraulic system make them sensitive for oscillations. There's not always an expertise driver available for damping the vibrations and it's also exhausting for him/her to do it all the day. The modern embedded control systems offers calculating capacity witch is not often fully exploited. This paper presents two practical damping methods which can be used together with embedded control system and some pressure sensors for reducing the lowest natural frequency vibrations of the crane. They are developed at the final form using literature sources, simulations and experimental test with the laboratory crane. The used vibration damping algorithms are based on the Electric Load Sense (ELS) and on the Pressure Feedback. They are developed to be easily programmable even to very simple micro controllers. The ELS is able to stabilize the load pressure oscillations during the drive. With the pressure feedback the vibrations during drive and also the end-effect vibrations can be damped. Motivation for the project was the increasing use of computer technology and field buses at the working machines.

KEYWORDS: Pressure feedback, Active damping, Electric load sensing

2. INTRODUCTION

The use of durable materials and optimized structures enables the use of high payloads at the hydraulic cranes. When the booms are long and relatively flexible the deflections are rather high too. LS-systems (Load Sensing) are widely used due to better efficiency and control properties. However they are also more sensitive for oscillations. All these facts set high demands for the control system, especially when the demands for the overall efficiency, productivity and also conveniences have been increased.
Traditional hydro mechanical solutions have had an important role due to demands of environment conditions and high reliability in operation. In most of the cases the mobile valves have to be specified according to the application. Unique specifications and

solving the problems with hydro mechanical components make the valves easily rather complex and expensive.
There is a clear trend toward increased use of computer technology in working machines and this will offer new approaches. Even the electronic components are relatively cheap; the sensors are still quite expensive. The increased use and competition at the market will also lower the price of sensors. At some applications the use of computer technology and the field buses are already a standard.

This paper is targeting to damp the lowest natural frequency vibrations of lift and slewing functions. Those vibrations can be damped using relatively slow mobile valves, which are already belonging to the system. In most of the cases the low frequency vibrations are also most harmful for the driver.
This study is a part of the Intelligent Machine Project. The project consists of three main parts: Improving the controllability of the hydraulic crane, condition monitoring of the mechanical structure and developing methods for programming and developing the control software. The final result will be the software frame which includes the developed methods. In addition of the vibration control the other areas in this project included in to the controllability are coordinate control, load handling with separate restrictors, volume flow distribution, power and saturation handling. The results of those studies are also included to the control software frame.

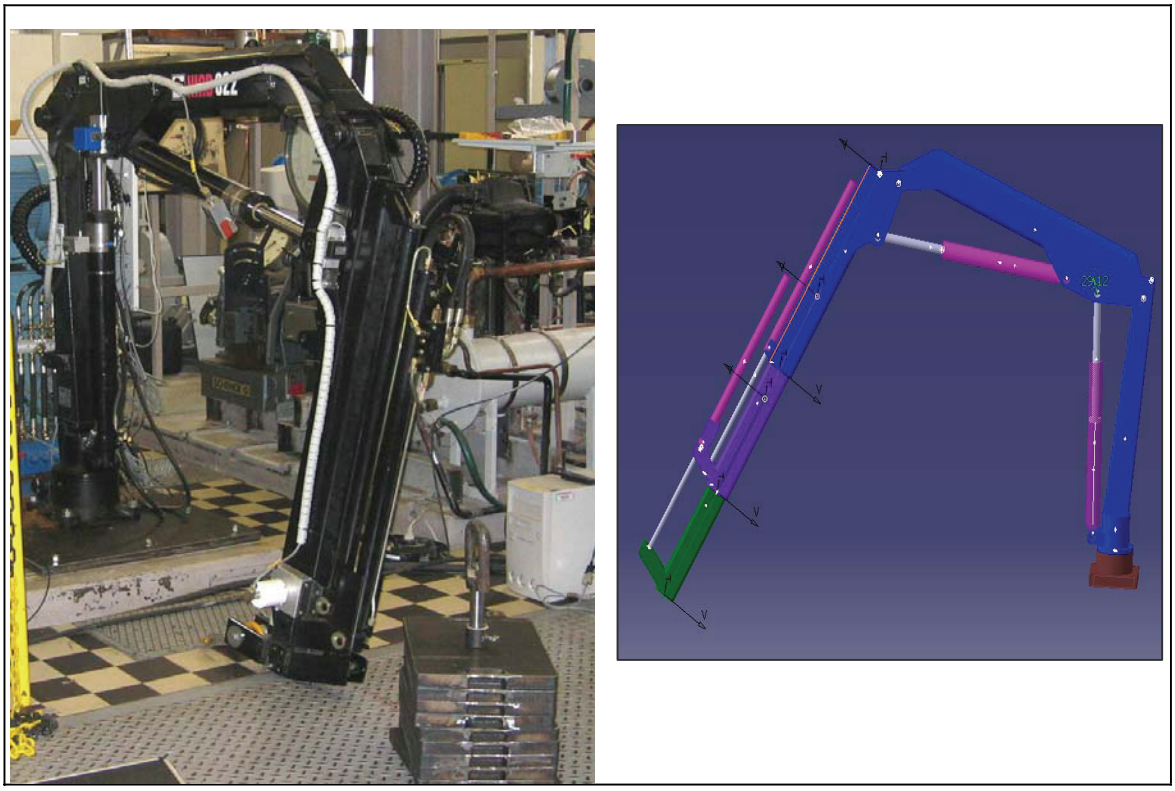

FIGURE 1: Test Crane and Virtual Model

Simulations and experimental tests with the laboratory crane have been used in developing the damping methods. The mechanics of the test crane has been modeled using MSC.Adams Software. All booms and arms in the simulation model have been ridged. The hydraulic system has been modeled using Adams Hydraulics. The model has been verified according the laboratory crane. The control system for the simulation model has been programmed with C/C++ and connected to work with the Adams model. The reason for using C/C++ was that the results are easy to transfer to the test

crane. The control system used at the test crane has also been developed at the Intelligent Machine Control Project [1].

Figure 2 shows typical oscillations, which may appear, when the lift boom gets a stepwise control signal. The results are measured from the test crane. Those oscillations don't mean instability, only sensitivity for oscillations. Oscillations during the drive are typical for LS-systems due to the load pressure feedback. There exist also vibrations when the actuator is halted caused by the load inertia (end-effect vibrations). A skilful driver can damp them by using the joystick on the right way. However, the manual damping 8 hours per day might be stressful. The reasons for instability of the Load Sensing systems have been studied by Peter Krus at the reference [2].
Vibrations during the drive can be avoided by using ELS or the pressure feedback. Vibrations during interception can be suppressed by using pressure feedback. In addition the feed forward method [3], which shapes the control curve, has been successfully tested, but those results are not included.
At this study the pressure feedback had been applied electrically. At some valves the pressure feedback has been adapted hydro-mechanically using a special pin type spools or on auxiliary restrictors.

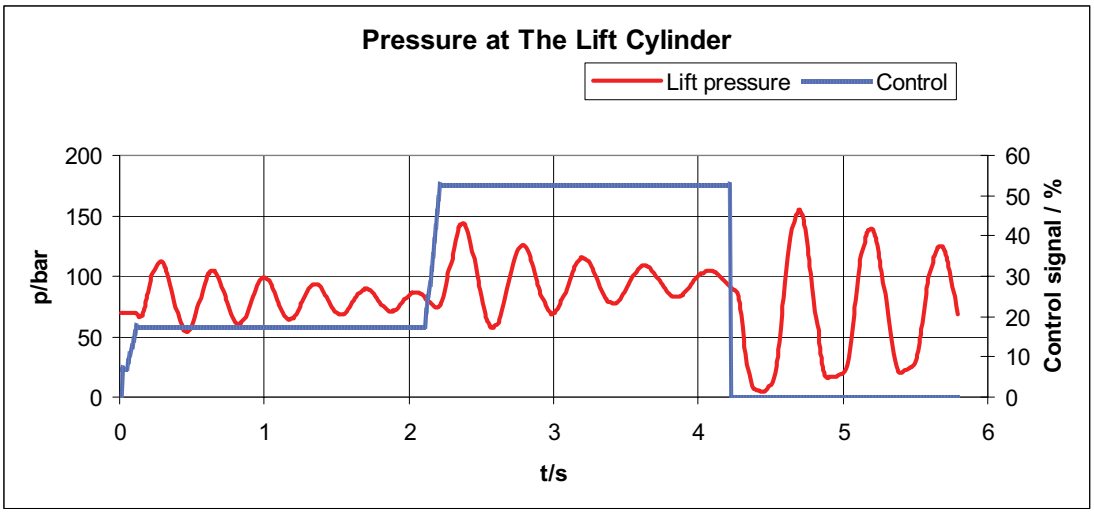

FIGURE 2: Lift Function at The Undamped Hydraulic Crane (measured)

The damping effort of the pressure feedback spool at the test crane is visualized in the figure 3. Spools with pressure feedback are mostly used with lift and slewing functions. They can damp only the vibrations during the drive. The use of pressure feedback spools reduces also the maximum volume flow. Therefore a one size bigger spool might be needed.
The control system at the test crane was developed at the Intelligent Machine Control Project [1]. The control system based on the open source developing tools and operation systems. Linux was used for offering stable, fast and standard interface. Low price is an advantage too. CANopen communication protocol was utilized. Programming has been carried out with C++ and UML (Unified Modeling Language). User interface for modifying the control system with other applications have been utilized using Domain Specific Modeling (DSM). Due to that interface there's no need for special programming skills. The user interface enables to apply those methods developed in the project easily to the control software. Configuration of CAN-buses as well as a hydraulic systems and sensors can be done by using this tool. Picture 4 visualizes the system configuration tool.

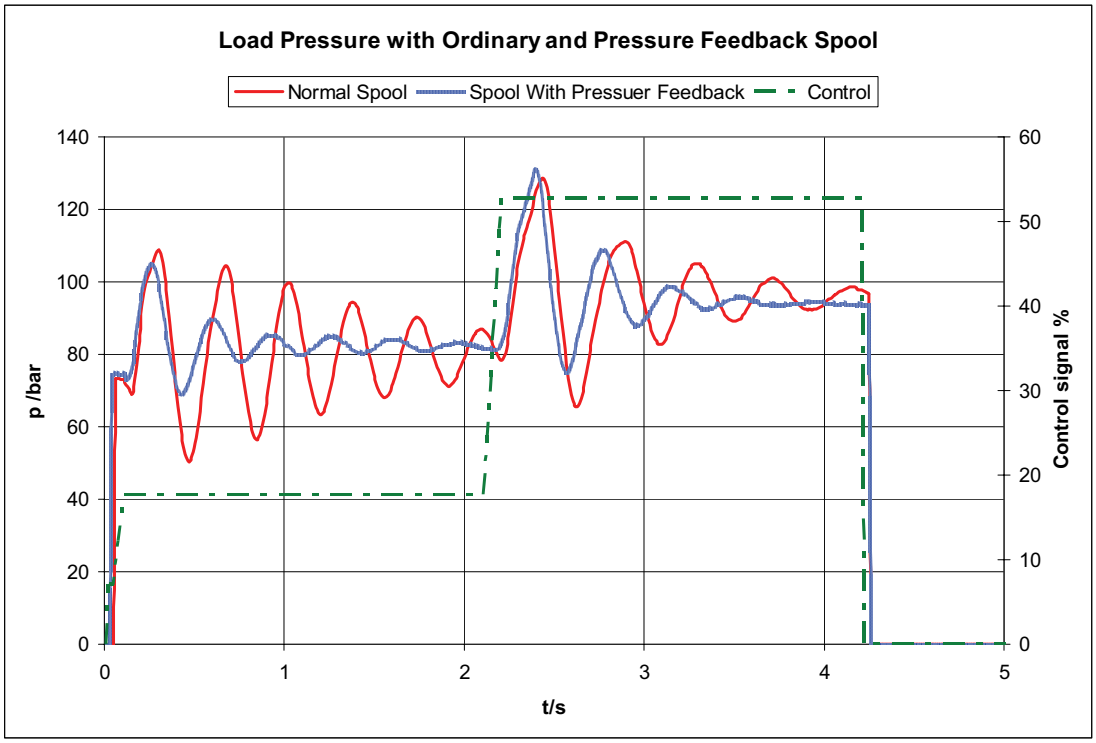

FIGURE 3: Load Pressure with Ordinary Spool and Spool with The Pressure Feedback (measured)

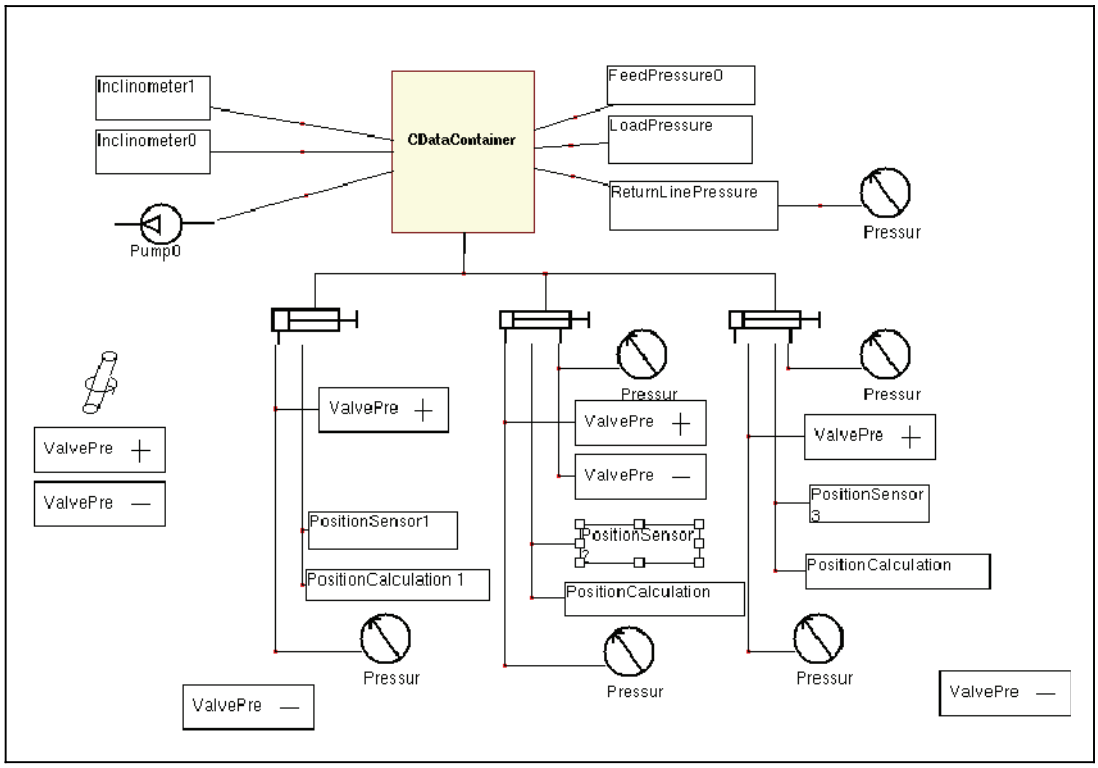

FIGURE 4: Object Model of Boom

The framework for hydraulic boom contains functionality for vibration control, electronic load compensation, counter balance control of cylinder and x-y-coordination drive.

The lowest natural frequency of the crane needs to be defined when the ELS or the pressure feedback are used. The Recursive Least Square method (RLS) [4] can be used for that. It's also possible to define the natural frequencies in advance in function of

load and cylinder positions [5]. In this paper a method based on measuring the wavelength of the vibration was used.

3. ELECTRIC LOAD SENSE, ELS

At the ordinary LS-system the load pressure is received from the main valve and it is delivered to the pump through the pipe. The pump-load interaction and long pipelines make the systems sensitive for oscillations. Restrictors at the LS-line are often used for suppressing the oscillations. Effective damping with restrictors will increase the response time and make the system sensitive for temperature changes. The size of the restrictor must also be rather small.
The LS-line can be replaced with the pressure sensor and the micro controller. This type of system is called Electric Load Sensing (ELS). In the references [6], [7] and [8] ELS-systems are studied. The measured load pressure needs to be filtered on a reasonable way for having the stable feed pressure. Furthermore the electrically controlled pump will be needed. The use of the supply pressure sensor will be recommended for establishing a certain pressure-setting value table or if the closed loop control will be used as in reference [8]. In this paper a pump with electric pressure regulator was used. The ELS-pump can have the integrated proportional pressure control valve as in the figure 5 (left). Also a traditional LS-pump can be equipped with external control valve according to figure 5 (right).

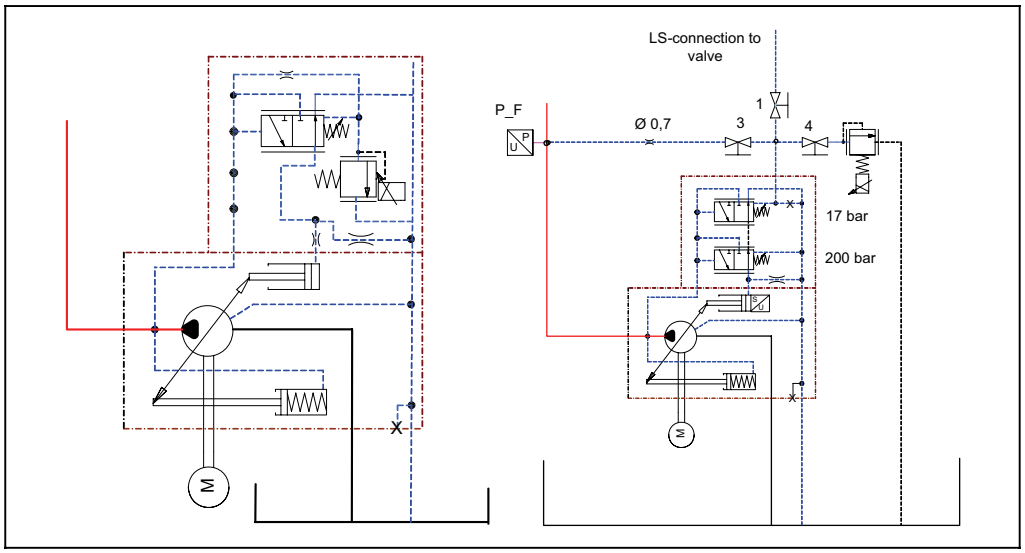

FIGURE 5: The Pump with Integrated Electric Pressure Regulator (left) and The Pump with External Pressure Regulator (right).

It's also possible to use pump with the direct electric displacement control as in reference [8] but in this case the pump as in figure 5 (right) was used. That type of pump apples to compare both the LS and ELS systems to each other. Taps 1, 3 and 4 are meant for choosing the system type.
LS-pressure can be measured from the LS-port of the main valve or from each supply ports. If supply ports are used more sensors will be needed but them can serve also other applications. At the test crane each supply ports were equipped with external pressure sensors. Final load pressure is the highest pressure at the active supply.
The ELS-control was included to the control system. Control signals given by the joysticks are available for recognizing the active ports. The drawback in measuring the LS-pressure from the LS-connection is the response time of the spool. There will be a

small delay before the LS-pressure appears but it can be removed by boosting the pump with man-made signal during the delay time. Boosting is needed only when the movements are activated. With individual sensors on the each supply port the load pressure will be available immediately when the control signal appears and the boosting is not necessary.
The proportional pressure control valve, which was included to the pump, produces the pressure signal for the pump. The control curve of the proportional valve might not be linear. The pressure setting of the pump was done in this case with the certain pressure-setting table.
When the pump will be started for the first time the setting value table will be established. The table will be measured with certain software loop, where the pump setting value is slowly increasing. After each one bar change the setting value is stored to a variable *u[p]*, where the feed pressure *p* is the pointer. When the maximum pressure level is reached the table will include all the setting values with one bar resolution up to the maximum pressure. The resolution of one bar is enough to offer smooth control. The results are also saved to a file from which they can be read every time when the system is started.
The measurement is easy to automate. In practice the measurement will be done with zero volume flow. During operation with the higher volume flow there might be a noticeable pressure drop at the supply line. That lowers the supply pressure level at the valve end.
The pressure drop is easy to take into a count by calculations or by measurements. The final fsupply pressure p_f equals to the sum of Δp, the measured load pressure p_L and the pressure drop Δp_h at supply line, e.g.

$$p_f = p_L + \Delta p + \Delta p_h \qquad (1)$$

The stable feed pressures based on the low pass filtering of measured load pressure. The special demands for filtering have been treated more at the references [6] and [7].

3.1 Pressure signal filtering and defining the lowest natural frequency

The lowest pressure oscillation frequency can be below 1 Hz, depending of the load and extension of the crane. Proper filtering with low frequencies leads to a slow response time, especially when average filtering, as here, is used. For fastening the response time the variable filtering length was used. At the steady state situations the arithmetic medium value of the load pressure is presented in (2).

$$\bar{p}_L = (p_1 + \ldots p_n)/n = \frac{1}{n}\sum_{i=1}^{i=n} p_i \qquad (2)$$

In equation (2) p_1 to p_n are measured load pressures and n explains how many pressure samples from the pass were taken into account. For having the right medium value there must be samples during one wavelength. The length of the pressure wave can be measured as a distance of zero points of the derived load pressure signal. Therefore the actual pressure signal needs to be numerically derived (3).

$$\dot{p} = \frac{\sum_{i=1}^{i=m} p_i - \sum_{i=1+k}^{i=m+k} p_i}{m \cdot k \cdot t_n} \qquad (3)$$

Parameter m defines how many samples were included to the medium value and parameter k how many samples are between those two medium values. Parameters m and k depends on the quality of the measured pressure signal and on the sample time. At this case they were chosen experimentally. Pre-filtering of pressure signals will be recommended for preventing higher frequencies to disturb results. The pressure signals at the simulation model doesn't include any noise. Therefore a quite small values for m and k can be used. High values of m and k can increase the phase shift. Phase shift is not so dangerous during nominal frequency definition, but it must be taken into account when the time dependency of results is important. In practice it's better to check the derivation results before choosing final value for m and k.

The amount of sample values n used in the filtering at the equation 2 is defined by calculating how many times the sample time t_n fits between the zero points of derived signal, equation 4. Time t_w is the half wavelength.

$$n = \frac{t_w}{t_n} \cdot 2 \qquad (4)$$

A filtering length of one wavelength is normally used but at the transient situations for fastening the response time, the change of joystick signal is taken into account as in the figure 6. When the derived joystick signal exceeds the certain limit the filtering length drops to value 1 (= no filtering). Filtering length returns back to full length using ramp when the derived joystick signal is degreasing. The ramp time is a parameter and can be chosen experimentally.

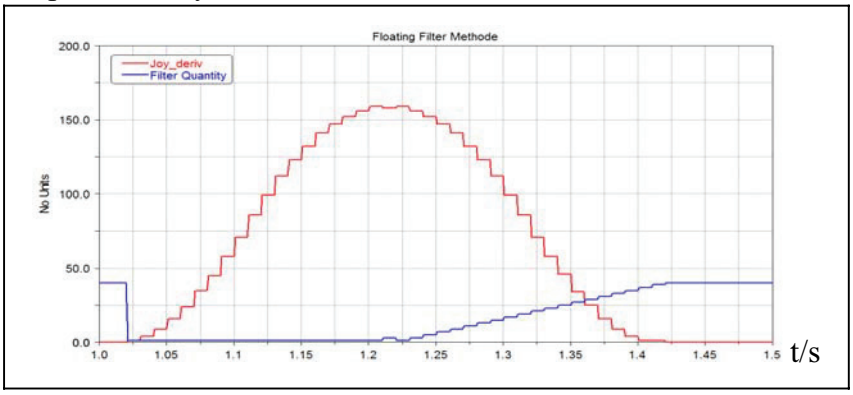

FIGURE 6: Filtering Length in Function of Derived Joystick Signal (simulation)

Disadvantage of measuring the wavelength is that other frequencies are not possible to separate, especially if they are high enough to inflict the change of sign at the derived pressure signal. More accurately the lowest nominal frequency can be defined by using Recursive Least Square method (RLS) [4]. As a comparison the figure 7 shows the results of wavelength by using both methods at the test crane application. Results are quite near each other.

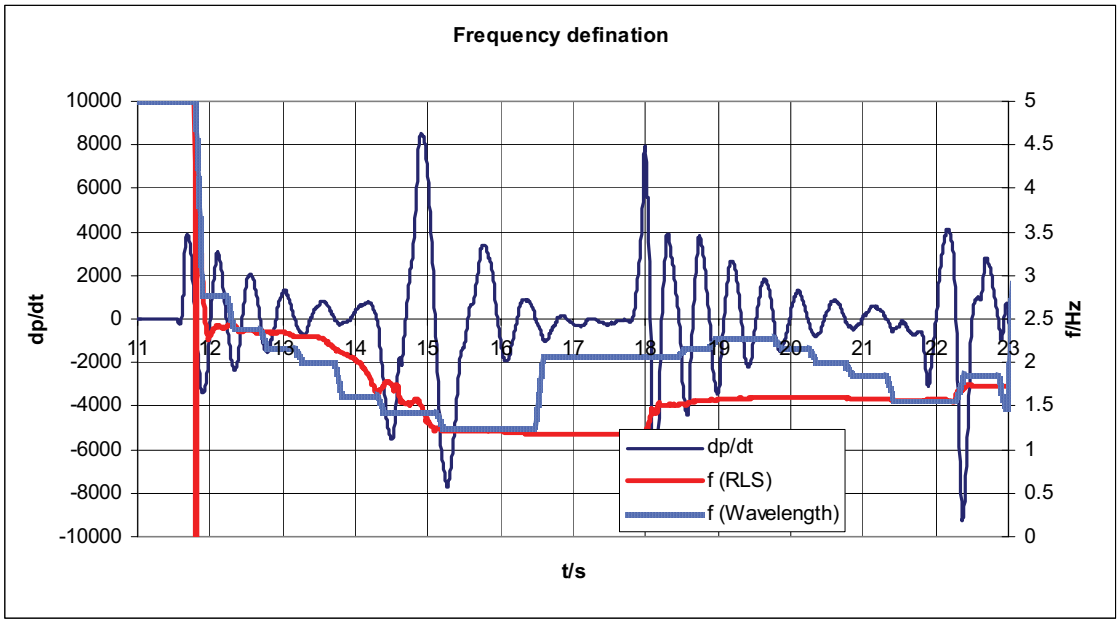

FIGURE 7: Comparison of the Nominal Frequency Definition (measured)

3.2 Results using ELS

The ELS enables a stable supply pressure over the highest load pressure level. The stable supply pressure offers the same advantage as the constant pressure systems. Varying pressure difference over the spool tries to stabilize also the load pressure. Figure 8 shows some simulated results when ELS- and LS-systems are compared with the same control signal. However the results are not always that good. Pressure compensators are often used with the mobile valves to offer the load independent velocity. Ideally acting pressure compensator tries to maintain the pressure difference over the spool constant. Thus the pressure compensator isolates the supply pressure and the load pressure from each other and the damping effect of ELS is not so effective. At figure 9, LS- and ELS-systems are compared both with the pressure compensators. Results are measured from the test crane. Even the ELS system has rather stable supply pressure the load pressures at the both systems are almost equal. At the figure 10 there's a different kind of valve and the crane. In this case the ELS was able to damp the load pressure vibrations even there was the pressure compensator included.
Better damping was possible with higher speeds (spools more open). According the simulations the increased leakage of the pressure compensator improves the damping more effectively. Also replacing the pressure compensator with the check valve, figure 11, improves clearly the damping. That was tested with the laboratory crane.
In addition the better stability with the faster response time is possible when the ELS is used. According the measurements with the test crane the feed pressure started to rise in average about 40 ms faster when the ELS was used, picture 12. Similar results are also presented in reference [7] when the opening delay of the spool was avoided.

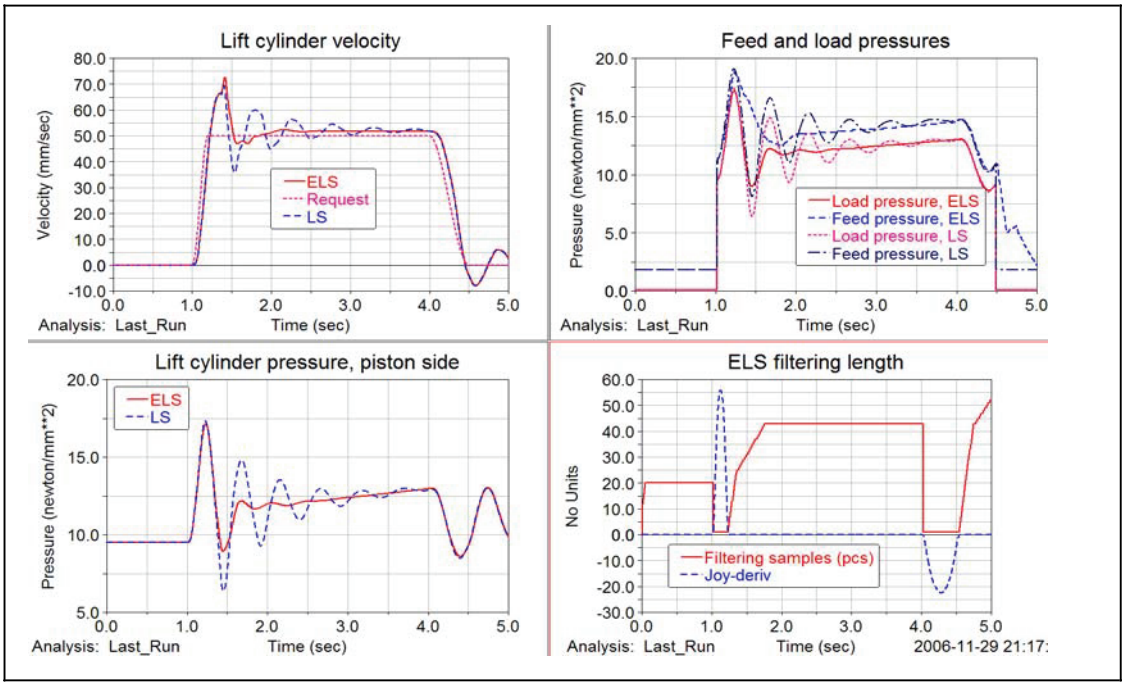

FIGURE 8: Feed- and Load Pressure at the LS- and ELS-Systems (simulation)

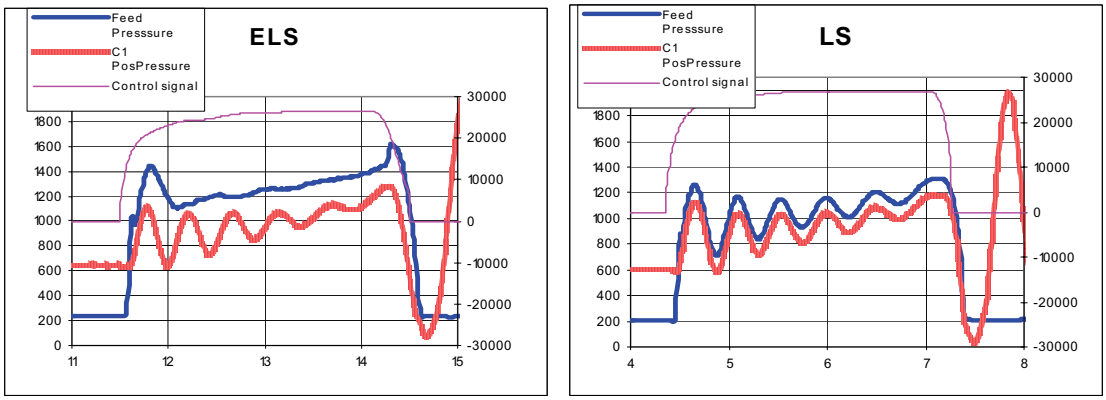

FIGURE 9: Supply- and Load Pressures at the LS- and ELS-Systems (measured)

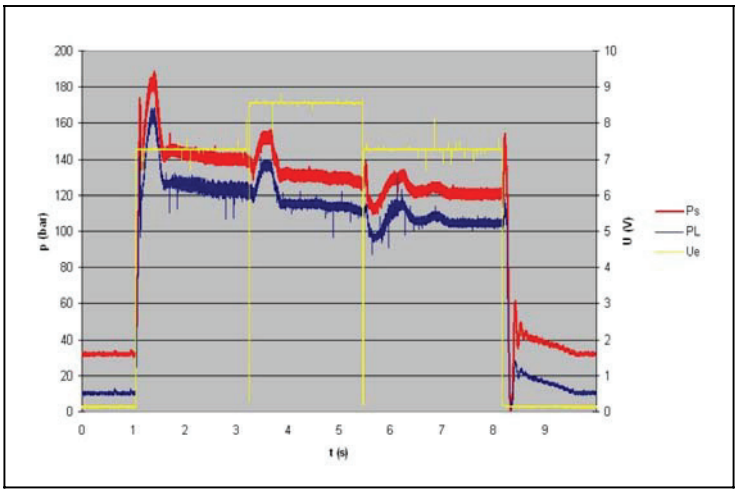

FIGURE 10: Stable Load Pressure with ELS and Pressure Compensator (measured)

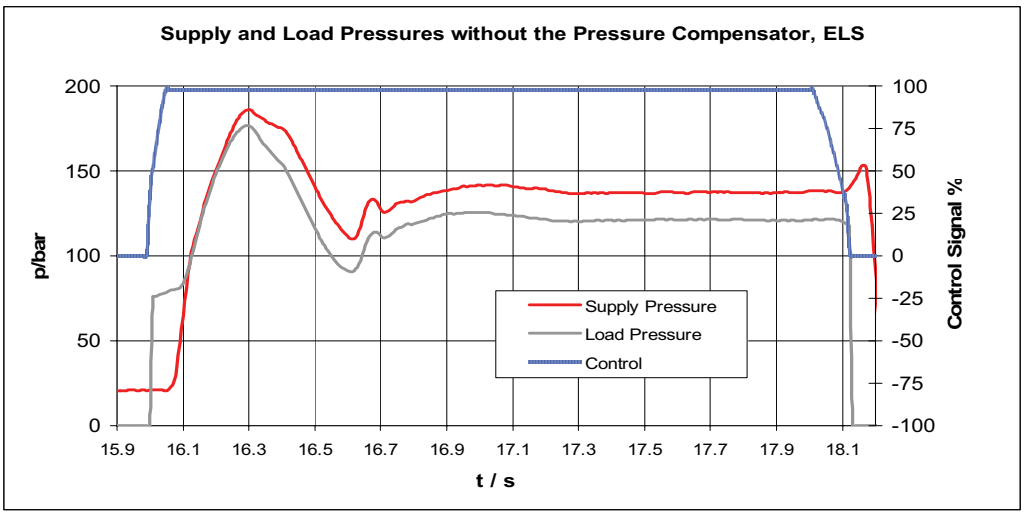

FIGURE 11: ELS-System without Pressure Compensation (measured)

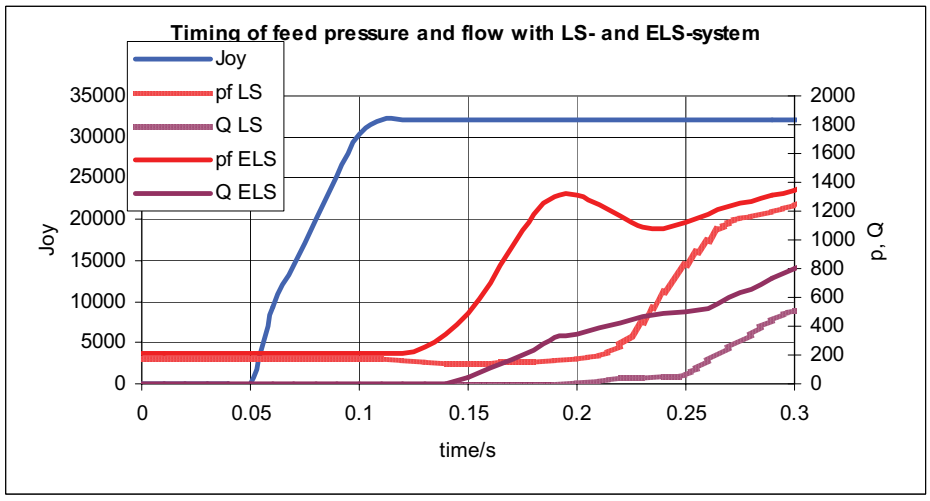

FIGURE 12: Step Response of Supply Pressure and Pump Displacement (measured)

After halting the actuator the ELS-system is not able to suppress vibration anymore due to the main valve is closed. Therefore other methods will be needed for after-effect damping.

4. ACTIVE DAMPING WITH PRESSURE FEEDBACK

During halting the movement oscillation occurs because of the load inertia. Experienced driver can damp the vibrations by giving the compensating control signal. Even the damping is at least a half automatic procedure for experienced driver, might it become exhausting during the day. The pressure feedback [2], [5] and [9], is rather well known method to increase damping. It's easy to apply and that's why it was chosen as one of the damping methods to the software frame. On the modern cranes the needed components for the damping are often available (pressure sensors, electrically controlled valve and micro controller).

As mentioned earlier those vibrations damped with ELS can be damped also with pressure feedback. Because the crane is typical multi body structure all movements are influencing with other actuators. If allowed the pressure feedback reacts to all disturbances and sometimes some unwanted phenomena might appear.

4.1 Pressure feedback application

The simplified situation of the lift cylinder is presented in figure 13. Variable y(t) describes the motion caused by the incoming volume flow. Dynamic function of the cylinder is described in equation 5.

$$m\ddot{x} + c(\dot{x} - \dot{y}) + k_r(x - y) = 0 \qquad (5)$$

Where: $z = x - y$, from which

$\dot{z} = \dot{x} - \dot{y}$

$\ddot{x} = \ddot{z} + \ddot{y}$

Equation 5 can be written into a form 6 and 7.

$$\ddot{z} + \frac{c}{m}\dot{z} + \frac{k_r}{m}z = -\ddot{y} \qquad (6)$$

$$\ddot{z} + 2\varsigma\omega_n\dot{z} + \omega_n^2 z = -\ddot{y} \qquad (7)$$

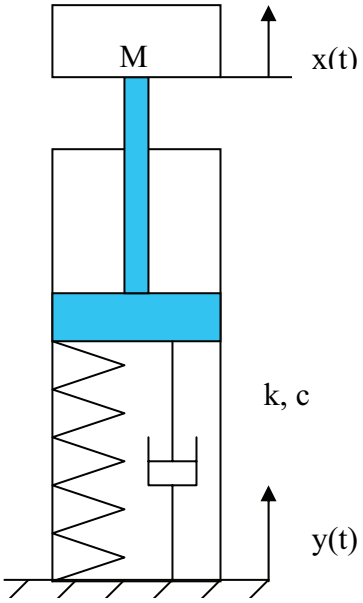

FIGURE 13: Simplified Figure from the Lift Cylinder

The feedback is marked $\dot{y} = Kz$ and $\ddot{y} = K\dot{z}$ is inserted to the equation 7. Result is the equation 8.

$$\ddot{z} + (2\varsigma\omega_n + K)\dot{z} + \omega_n^2 z = 0 \qquad (8)$$

The new damping factor can be solved: $2\varsigma\omega_n + K = 2\varsigma_{new}\omega_n$. Where the new damping factor is chosen to be $\zeta_{new} \approx 0.7$. The original damping factor was $\zeta \approx 0.02$ (based on the measurements). After that the damping gain can be solved (9).

$$K = 2\omega_n(\varsigma_{new} - \varsigma) \qquad (9)$$

The feedback can be solved (equation 10) assuming that kz is proportional to the pressure change Δp in the cylinder when the damping factor ζ is small. Quantity $\dot{y}$ describes the excitation and G is the gain.

$$\dot{y} = Kz = G\Delta p \qquad (10)$$

The new damping gain is solved in equation 11.

$$G = \frac{2\omega_n(\varsigma_{new} - \varsigma)A}{k} \qquad (11)$$

Assuming that the pipe volumes are negligible and inserting the cylinder spring constant k into the equation 11, the damping gain for double action cylinder can be written to form (12) and for singe action cylinder to form (13). The stroke of the cylinder is L and the position of the piston is s. The cylinder area ratio $\lambda = A_2/A_1$.

$$G = \frac{2\omega_n(\varsigma_{val} - \varsigma)}{B\left(\frac{1}{s} + \frac{\lambda}{L-s}\right)} \qquad (12)$$

$$G = \frac{2\omega_n(\varsigma_{new} - \varsigma)s}{B} \qquad (13)$$

The Δp in equitation 10 is determined by the measurements. The static part of the cylinder pressure can be separated by high pass filtering but in this case it has been done by subtracting the medium pressure from the actual pressure. The medium pressure can be calculated according the equation 2. The value $\dot{y}$ can be used as the input signal for the valve when the setting value – volume flow (velocity) characteristics are known. In this case that is determinate according the measurements so that the curve $Q=AU^2+BU+C$ (second-order polynomial) has been fitted to the measurements. When the velocity $\dot{y}$ (= Q/A_{cyl}) is known the setting value U can be solved and give to the valve. The dynamic behavior of the valve has not been taken into account.

The block diagram at the figure 14 explains how the pressure feedback is used at this study for the lift cylinder. Measured pressure signal is derived for finding the vibration frequency as explained in the chapter 3.1.1. The medium pressure p_m is calculated according to equation (2). The wavelength value defines the filtering length (how many samples will be taken into account). Even the basic gain changes adaptively, additional gains K+ and K- can be used for tuning the damping more accurately to the application. Also during the drive a separate gain can be used. The change to the end damping gains takes place when the control signal is 20…30 % of the maximum level. The duration time for the end damping can also be tuned according the application. The feedback signal is added to the original control signal.

The lowest nominal frequencies are meant be damped. Because the vibration frequency estimation is not able to define different frequencies, it will interpret all vibrations together, especially if the higher frequencies are big enough. Therefore the resulting frequency might be too high. Still in most of the cases this method gives rather useful results. Errors can be avoided by using limits for the realistic frequencies. The errors occur mostly during damping or when the oscillations are small. In both cases errors can be avoided by keeping the old wavelength value under those circumstances.

The pressure feedback application of the lift cylinder can also be activated during driving the second boom because they both have the same lowest nominal frequency. However the result might not always be satisfactory if the both booms are driven simultaneously and high excitations are used. In this study the damping will be kept off when actuator is not any more controlled and the end-effect vibrations have been damped.

The use of volume flow-setting value characteristics as a valve gain offers efficient dead band compensation but leads also a high spool excitation during damping, as visible at the figure 15.

At the equations 12 and 13 the position of the piston needs to be known. In practice that's not always possible. The test crane was equipped with the single acting cylinder. A fixed cylinder length was used ($s \approx L/2$) during the tests and results were relative good at the normal working range.

Commonly used valve gain includes two fixed gain values (separate for dead band area and normal flow control area). However on that way it's more difficult to use equation 10 and the tuning of the additional gains must be done experimentally.

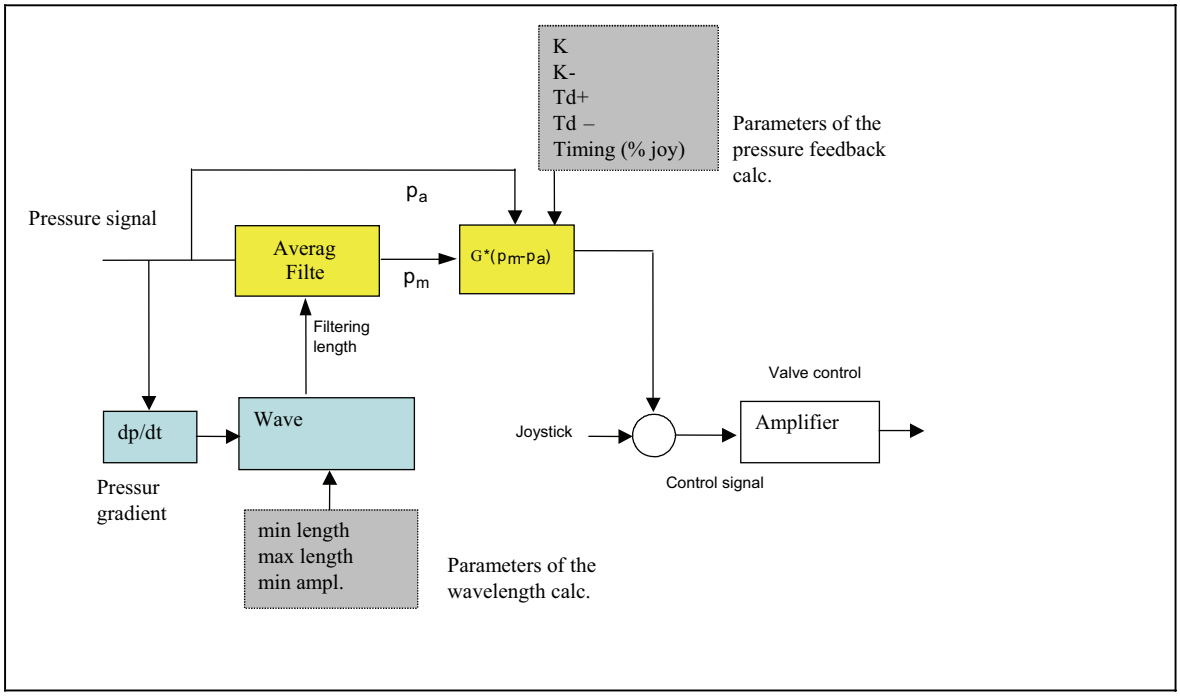

FIGURE 14: Block Diagram of Pressure Feedback Application

Figure 15 shows how the use of pressure feedback shapes the joystick signal. The differences can be seen in the end of the signal. Also the valve gain shapes the valve signal. Large discontinuous in the final signal are visible. It's possible to get more continuously changing movement for spool if the dead band compensation can be avoided. That will also help to avoid the jerks during compensation. On the other hand the tuning of the feedback gain will be more difficult.

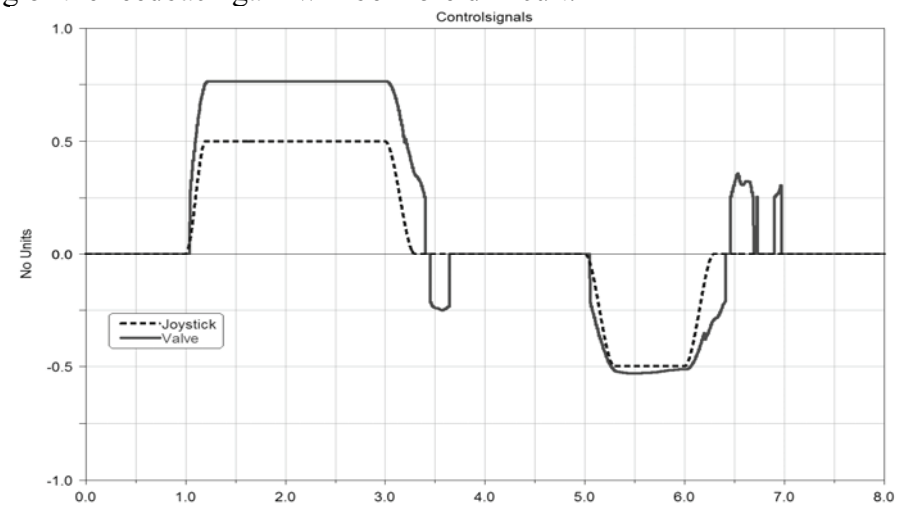

FIGURE 15: Original and the Shaped Control Signal (simulation)

4.2 Results with pressure feedback

At figure16 the pressure feedback was used to damp the slewing function. Similar results can also be obtained with lift function. At the simulation model a gear rack and a hydraulic cylinder was used to generate the slewing function. That part of the model was not verified properly due to the test crane was equipped with hydraulic motor

instead of cylinder. When the slewing function is halted a high vibrations will follow if the control signal is not gently enough. The pressure feedback was used to damp both the after-effect vibrations as well as the vibrations during the drive. The ELS gives a sufficient damping during the drive too. Figures 17 and 18 shows the results when pressure feedback is implemented to the lift function of the test crane. At the figure 17 there's no pressure feedback used. Pressure oscillations after halting the movement are high.

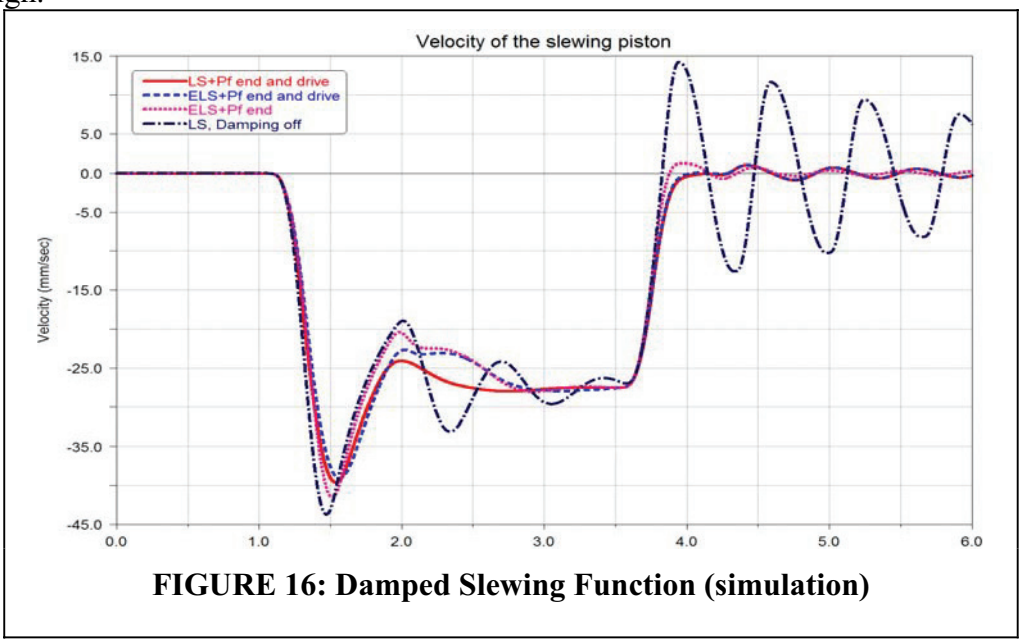

FIGURE 16: Damped Slewing Function (simulation)

At the figure 18 the pressure feedback was on. The vibrations were smaller in this case even not as good as with simulations. There were some higher frequency vibrations after damping the lift-up function. That's typical if the damping gain is too high. Because the pump is often slower than the valve it might reduce the damping effect with higher frequencies.

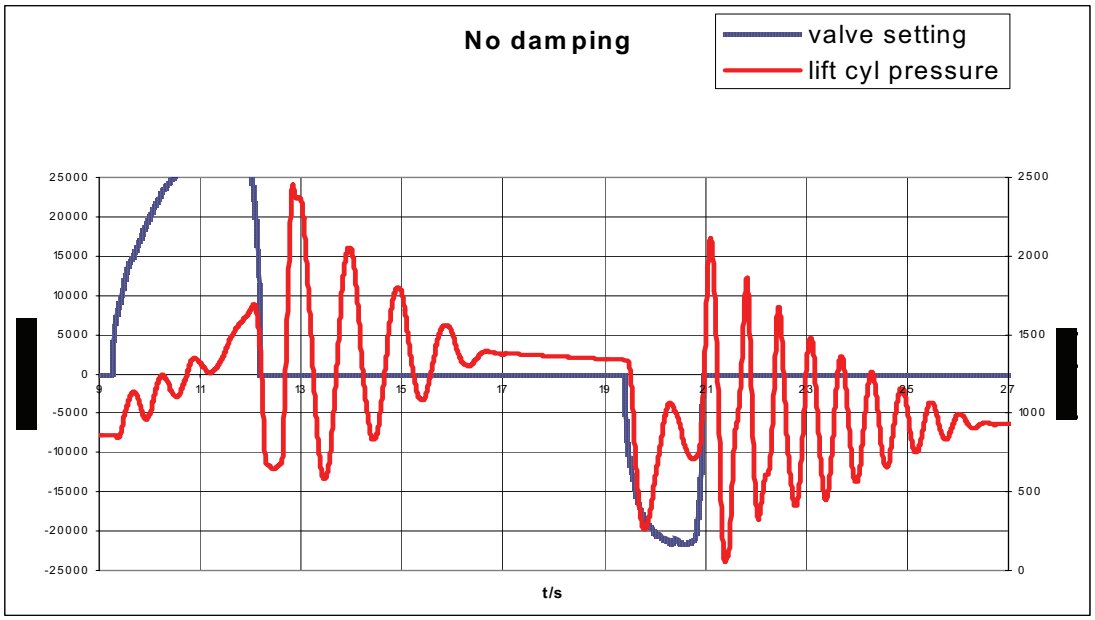

Figure 17: Lift Function of the Test Crane without Pressure Feedback (measured)

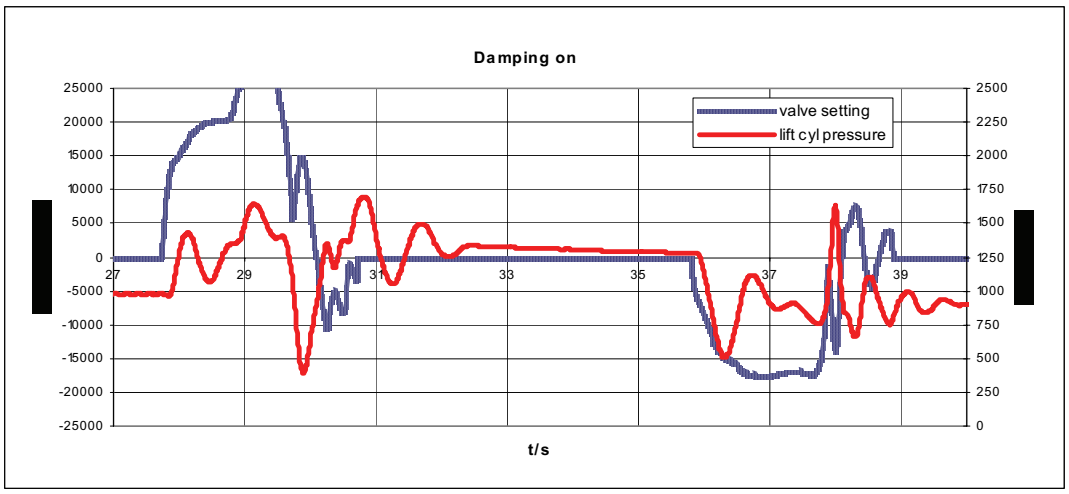

FIGURE 18: Pressure Feedback Implemented to the Lift Function (measured)

5. CONCLUSIONS

In this paper the ELS and pressure feedback was used to damp the vibrations. The pressure feedback is an active damping method. The pressure feedback has been tested with the lift, transfer and the slewing functions (slewing only by simulations). The feedback according equation 10 and 13 (gain) offers rather good damping at the all conditions in the test crane even the cylinder position was replaced with fixed value (L/2). The gain of the valve based on the measured volume flow – setting value characteristics. The use of additional gains (experimental tuning) for different directions improves the damping. The gain according equation 13 seems to give a bit too high gain with small boom extension (higher frequencies).

The determination of the nominal frequency is important. In the simulations the nominal frequency was measured using wavelength method. At the test crane the nominal frequency was determinate by RLS-method. In some cases both of them might give wrong values. A method based on the FFT (Fast Fourier Transform) will be further tested.

According the practical tests the pressure feedback applied to the lift cylinder, was able to reduce vibrations both in the lift and transfer cylinders. The feedback was active also during drive and no any disadvantages even with simultaneously drive was noticed using reasonable control signals. Still more tests will be needed.

The response time of the pump is normally higher than with valves. That's why the response time of the pump might be critical. Anyway at the test crane with nominal frequencies 1…4 Hz both the valves and pump were fast enough for damping purposes.

The sampling rate should be sufficient fast. In this case 10 ms was used. The use of the feed forward [3] might be useful because it shapes the control signal in advance. That method divides the control signal into the two steps. The second step appears after half wavelength. As a result it reduces oscillations both during the drive and during the end effect. According to the tests it seems to be more practical with the higher frequencies. With low frequency the response time might be too long. In the test crane both the pressure feedback and feed forward was used simultaneously with good results.

In this study a load holding valves were not included. Because the counterbalance valves are very commonly used, further studies with them will be needed. The pressure sensors must anyway in those cases be located between the actuator and the load holding valve.

The ELS is passive method for suppressing the vibrations during the movements. Final damping effect is depending on the characteristic of used pressure compensator. Ideally functioning pressure compensator can reduce the damping effect. Adding some leak to the pressure compensator in the simulation model, improves the damping effect. Both the good and poor results were got using the ELS with separate valves and situations. The reason was supposed to be depending of the characteristic of the pressure compensator. At the moment it's not possible to give more accurate instructions. Anyway adding some leak increase the damping effect. The ELS offers also faster response time and there are no disadvantages of the long LS-line. One advantage of the ELS is the possibility to use smaller pressure difference over the spool, which offers a slightly better efficiency. The ELS is a passive damping method and therefore there is no danger to increase vibrations. Both methods are easy to apply even to small micro controllers without floating number capabilities.

ACKNOWLEDGEMENT

This research was performed in the MASINA Technology Program of the Finnish Funding Agency for Technology and Innovation (TEKES).

REFERENCES

1. Jari Savolainen, Object Oriented and Open Development Environment for the Controller of Hydraulic Booms. Conference presentation ICC 2006.

2. Krus P. 1988. On Load Sensing Fluid Power System With Special Reference to Dynamic Properties and Control Aspects. PhD thesis, Lindköping Studies in Science and Technology. Dissertations No. 198.

3. William E. Singhouse, Trajectory Planning for flexible Robots, Robotics and Automation Handbook, Chapter 9.

4. P Krus, S Gunnarsson, 'Adaptive Control of a Hydraulic Crane Using On-line Identification'. Proceedings of the Third Scandinavian International Conference on Fluid Power, Linköping, Sweden, 1993.

5. Janne Kovanen, Improving dynamic characteristics of open-loop controlled log crane, Acta Universitatis Lappeenrantaensis 163, 2003

6. Markku Luomaranta, A stable electro hydraulic load sensing system based on a micro controller, Conference presentation SICFPO'99, 1999.

7. Heikki Paavilainen, Hydraulisen puomin värähtelyjen vaimennus sähköisen kuorman takaisinkytkennän avulla. Lisensiaattityö, Tampereen Teknillinen korkeakoulu, 1998.

8. Esders, H.: Elekrtohydraulisches Load-Sensing fur mobile Anwendungen. Dissertation, TU Brunshweig, 1995.

9. Michael Rygaard Hansen, Torben Ole Andersen, Improved Functionality and Performance of Mobile Cranes Using Pressure Feedback, Drives and controls / power electronics conference

HYDROSTATIC TRANSMISSION AS A PART OF CLOSED LOOP CONTROL

Researcher Mika Ijas *, Manager of Research Unit Esa Mäkinen *, Professor Matti Vilenius**, Chief Designer Hydraulic Systems Pertti Ijäs ***

*Tampere University of Technology
Institute of Hydraulics and Automation
P.O.Box 236
26101 Rauma, Finland
Phone +358 2 823 4970, Fax +358 2 823 4974
E-mail: mika.ijas@tut.fi
E-mail: esa.makinen@tut.fi

**Tampere University of Technology
Institute of Hydraulics and Automation
P.O.Box 589
33101 Tampere, Finland
Phone +358 3 3115 2267, Fax +358 3 365 2240
E-mail: matti.vilenius@tut.fi

***Rolls-Royce Oy Ab
Deck Machinery
P.O.Box 220
26101 Rauma, Finland
Phone +358 2 83 791, Fax +358 2 8379 4913
E-mail: pertti.ijas@rolls-royce.com

ABSTRACT

The control of a hydrostatic transmission (HST) is usually open loop control. There are lots of studies in which different control strategies of HST are considered. Usually, the aims of these studies are the total efficiency of the HST or the total efficiency of a machine. In this paper the feasibility of the HST as a part of a closed loop position control of a winch is studied.

The studied hydraulic Self-Contained Winch of Rolls-Royce Oy Ab. The Self-Contained Winch is a new type intelligent winch drive system equipped with the HST and an electronic controller. The winch with the HST is especially suitable for mooring and anchoring use. The new electronic controller makes it possible to develop and utilized different sophisticated rope control strategies. It is possible to control a rope force by using working pressure as a controlled parameter (force control or autotension). It is also possible to control a rope speed or a rope position using the closed loop control. In this study the closed loop position control was experimental studied using a winch bench. The Self-Contained Winch was installed to the test bench, which was connected a vertical moving mass with a rope. The mass used of the test bench was 6800kg.

1 INTRODUCTION

1.1 Hydraulic Self-Contained Winch for Merchant vessels

There are several winches in a large vessel. These winches are using to mooring operation and to anchorage. There can be even 12 winches in a big vessel. When winches are traditional hydraulic type winches with central hydraulic units they need massive pipe systems. Long hydraulic pipe lines need lot of space in the vessel and the installation of pipe systems is time-consuming and expensive.

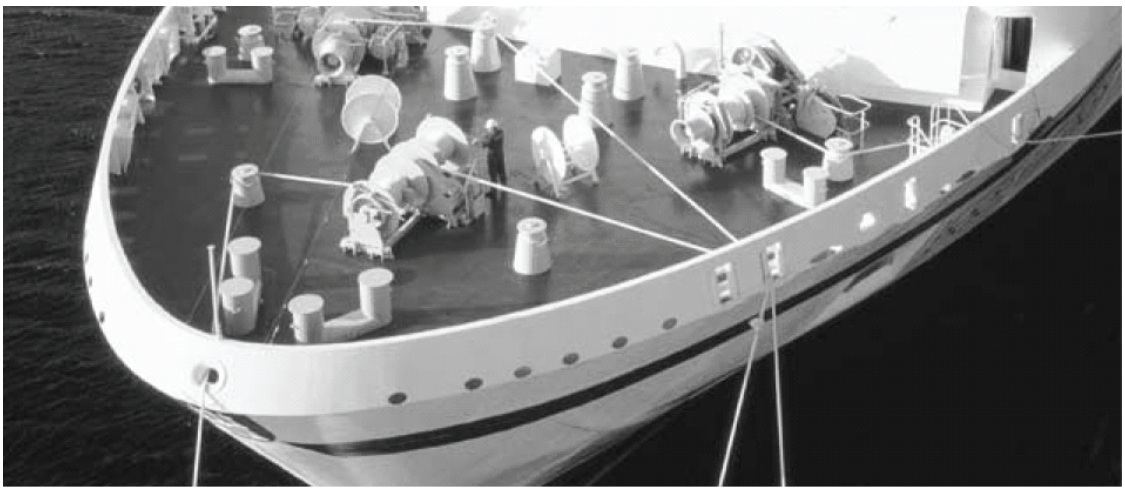

Fig 1. Winches on the vessel deck.

In hydraulic self contained system the hydraulic pump, the hydraulic motor (hydrostatic transmission system), hydraulic tank, hydraulic control valve and the electric motor are integrated into same, compact unit. Hydraulic self-contained drive system is developed to keep in mind safety, independent and environmentally friendly operation as well as easy and fast installation at shipyards.

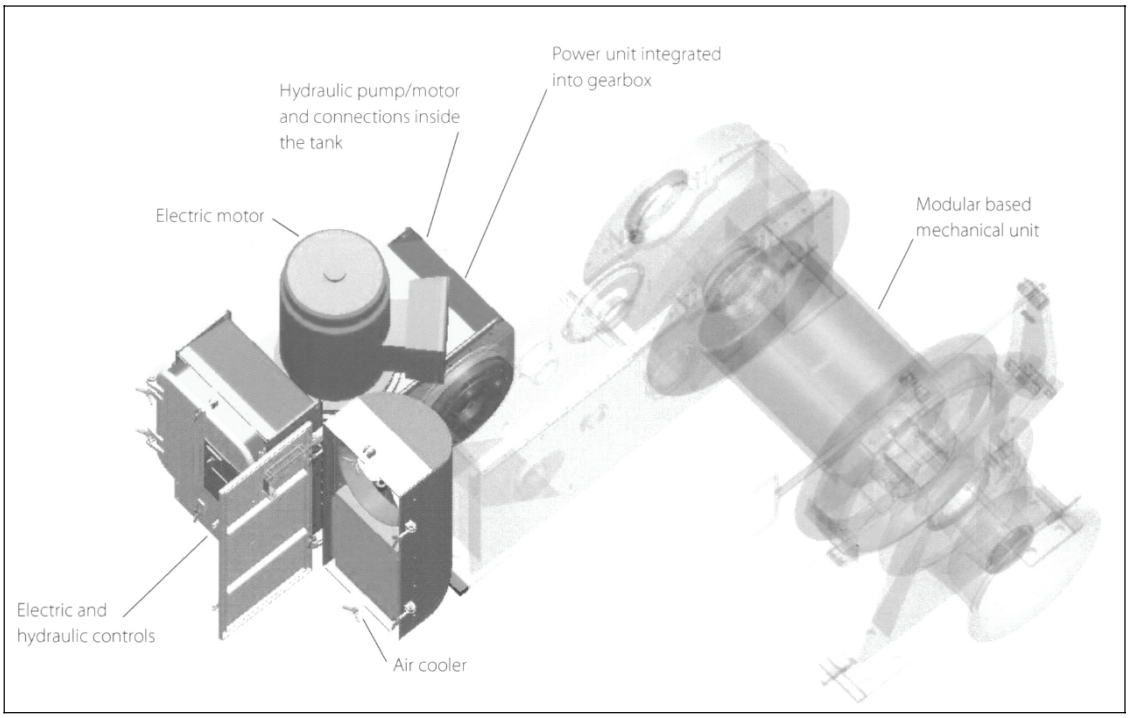

Fig 2. Self-Contained winch and the mechanical unit [2].

The control of the Self-Contained Winch can be realized by an electronic controller and then the result is a safe and operation friendly winch. It is possible to control the rope force by working pressure of the HST (pressure cutting). It is possible to control the velocity of the rope or the position of the rope or to use constant power control to maximize the speed of the rope or the anchor chain. Two winch units can be connected together and both units can be control by one joystick.

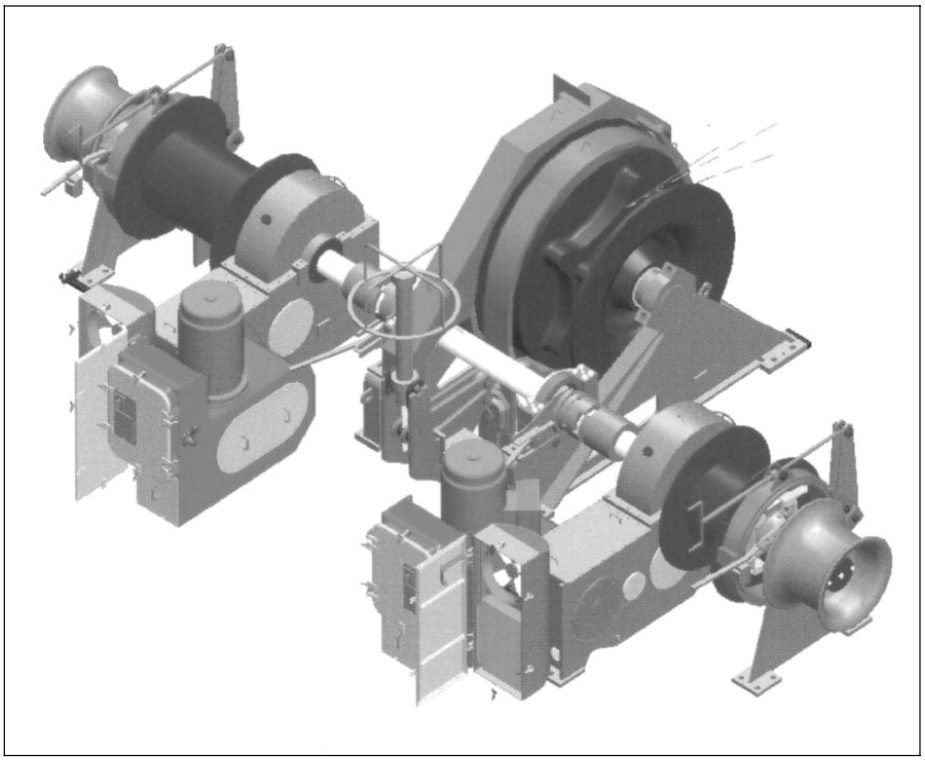

Fig 3. High capacity anchor windlass driven by two self contained mooring winches [2].

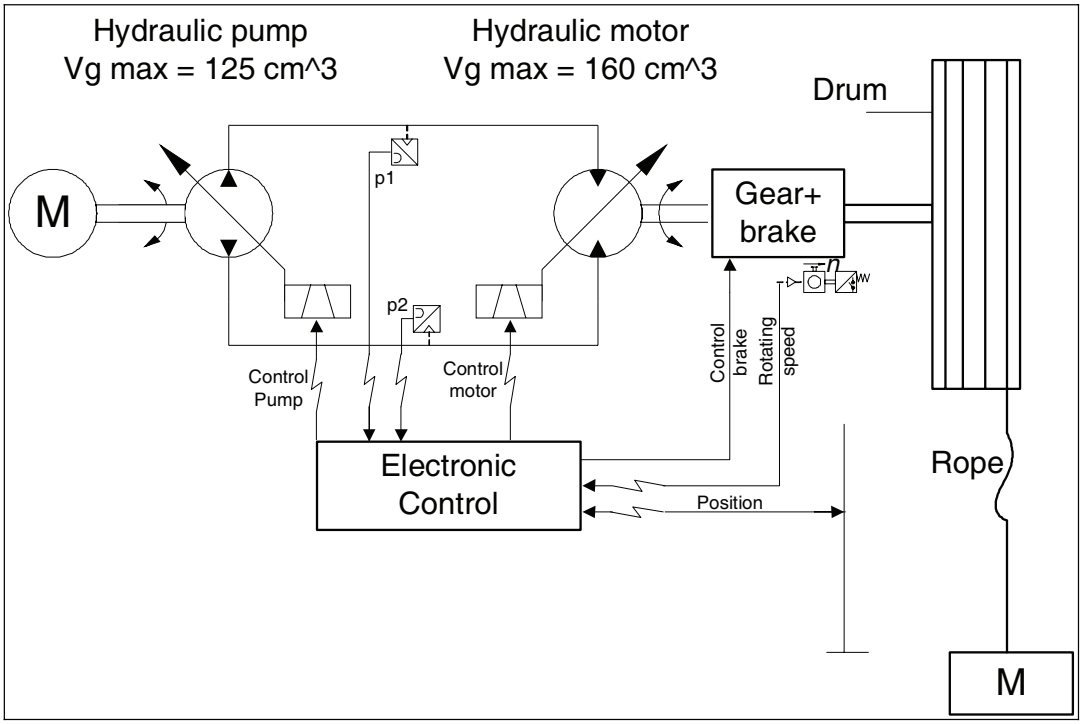

Fig 4. Schematic picture of Self-Contained winch.

The heart of the Self-Contained winch is a traditional hydrostatic transmission system (HST). The pump is driven with an electric motor. Because of a hanging load the gear is equipped with a disc brake.

The electronic control-unit controls the system by control the angle of the hydraulic pump and by control the angle of the hydraulic motor. In this paper the high level control was realized by Matlab Simulink dSpace –system. The position sensor used for feedback of the position controller was UniMeasure Cable Transducer HX-P510 (0-12.5m). Other measurement signals are for monitoring purpose only (pressures and rotating speed of the hydraulic motor).

1.2 Test bench

In the fluid power laboratory of TUT IHA – Rauma Research Unit is a test bench for a winch system. The test bench is designed for a testing winch up to 20t load. The length of the rope is 28 m and the stroke length is 8 m (Fig 5). It is possible to study properties of the winches experimentally in laboratory conditions. The position sensor is installed to the moving mass.

Fig 5. The bundle rack, height about 9 metres.

2 POSITION CONTROL USING HYDROSTATIC TRANSMISSION

Figure 6 shows the principle of the position control of the HST, which was used in this study. The dead bands of the controllers of hydraulic pump and motor were compensated in dSpace control system. The mass used was 6800 kg and the brake of the gear was connected off in tests.

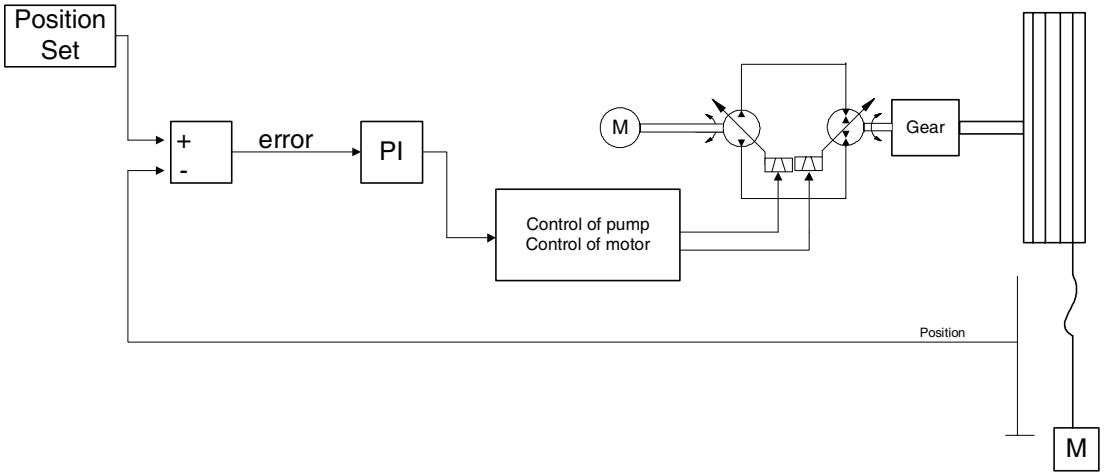

Fig 6. The position control with PI-controller.

The control of HST (pump and motor) operates as a traditional HST-control [1]. The volumetric displacement of the hydraulic pump is first increased from zero to 1 (the volumetric displacement of the hydraulic motor is at value one). If there is a need to increase the speed of the hydraulic motor, the volumetric displacement of the motor has to be reduced from one to its minimum value (in this paper to 1/3 from maximum value).

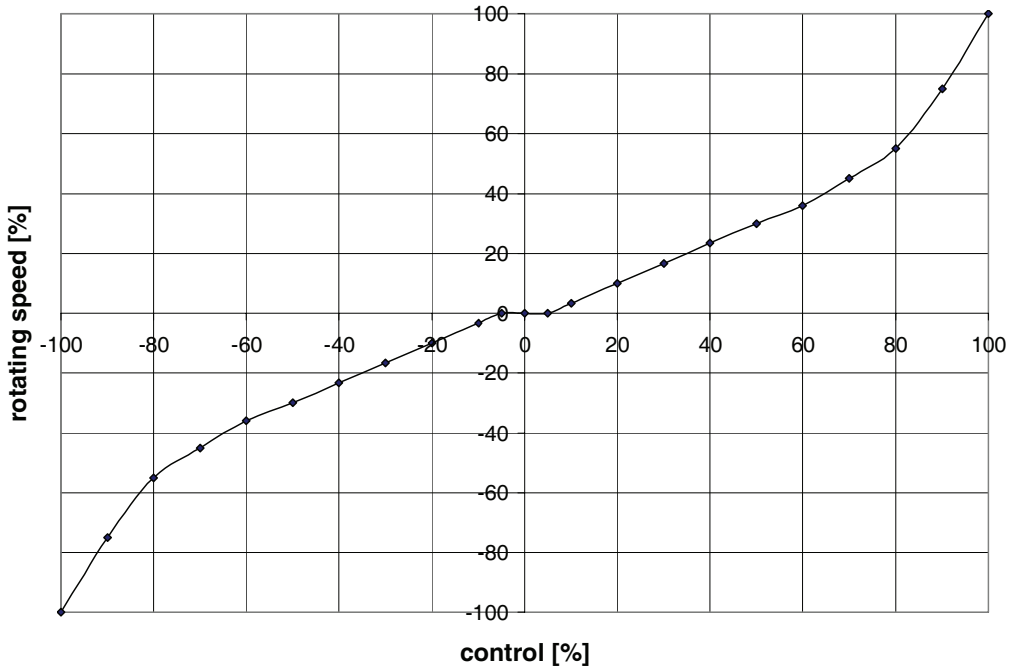

Fig 7. Control of HST.

In this study 50% control corresponds to about 33% rotating speed (Figure 7). The dead band around the zero control was compensated using dSpace control system.

The position control loop was tuned experimentally. First the control was only P-control. The gain was raised so that the oscillation was woken. Then the gain was decreased that the system was clearly stable. The integrator term was brought into use because it decreased continues position error. However, the value of integrator should be quite minor. The control starts oscillates easily with integrator term.

3. TEST RESULTS

The position controlled Self-Contained Winch was tested in the laboratory conditions. Installation was as mentioned in chapter 2. The speed of the winch was limited because the risk of an accident.

The result is quite good (Figures 8 and 9) when it is taken into consideration that the moving mass is big and the motion is a vertical direction. The final position error is about 10cm and the response time is downward direction 9s and upward direction 12s.The maximum instantaneous rotating speed of the hydraulic motor is about 3000 rpm, which is quite high value. However the mass is under control during the test run.

The control system keeps position without brake. The hanging load needs about 150 bar pressure in the work pipe that position stay at a constant (for example at time 18 s in Figure 9).

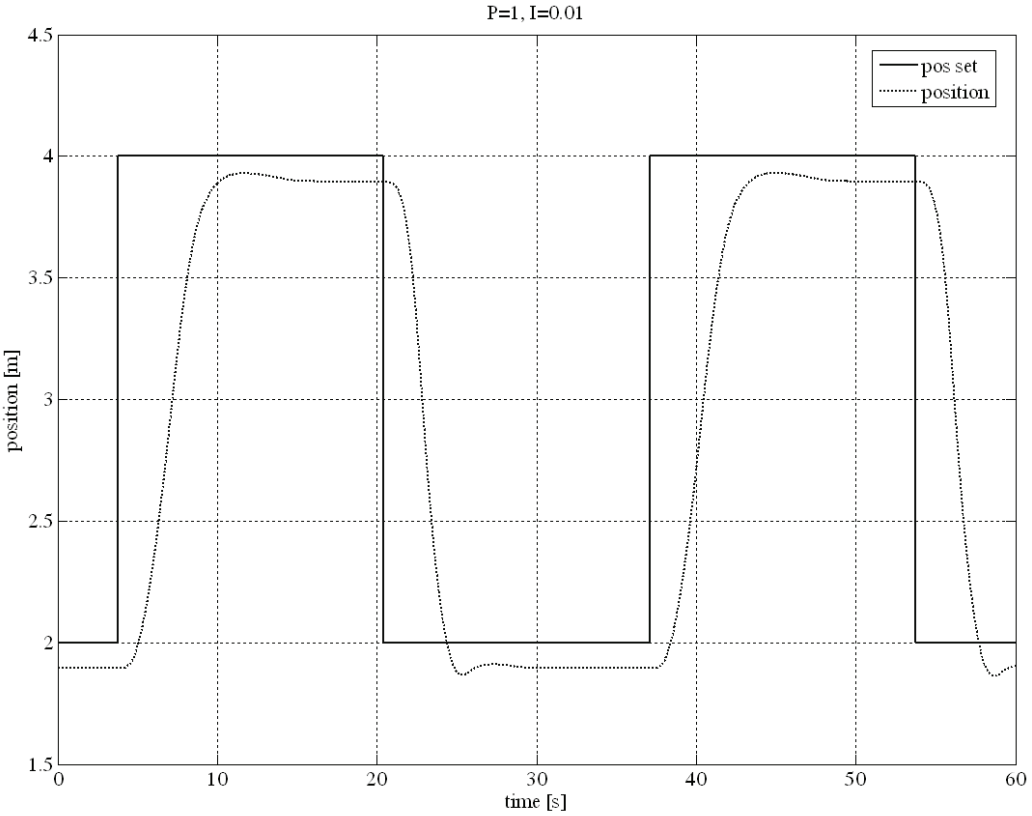

Fig 8. Step response of the position controlled winch ($K_p = 1$ and $K_I = 0.01$).

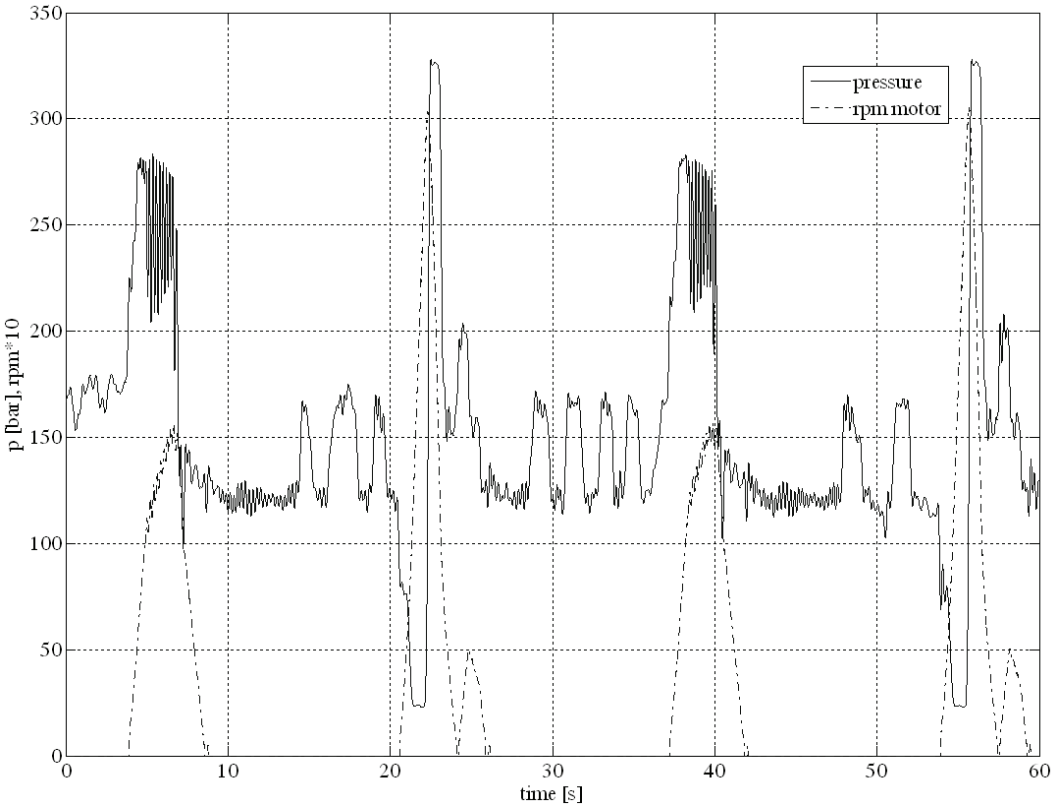

Fig 9. Pressure and rotating speed of motor during test step.

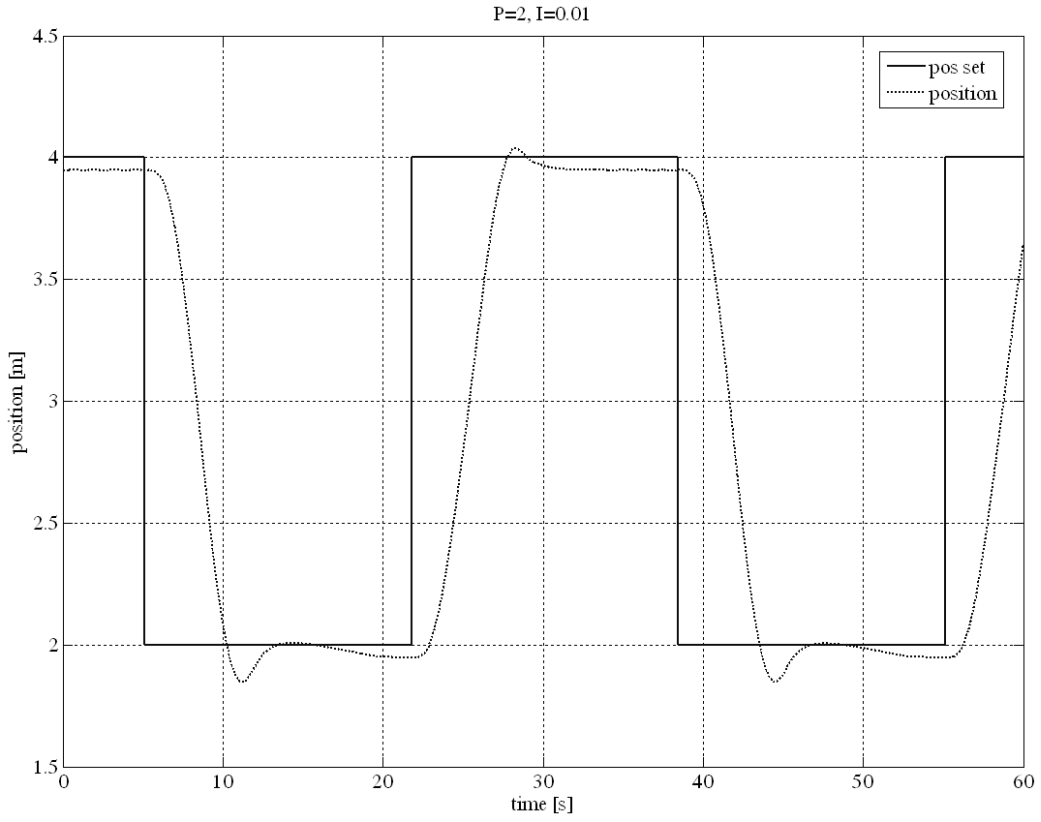

Fig10. Step response of the position controlled winch ($K_p = 2$ and $K_I = 0.01$).

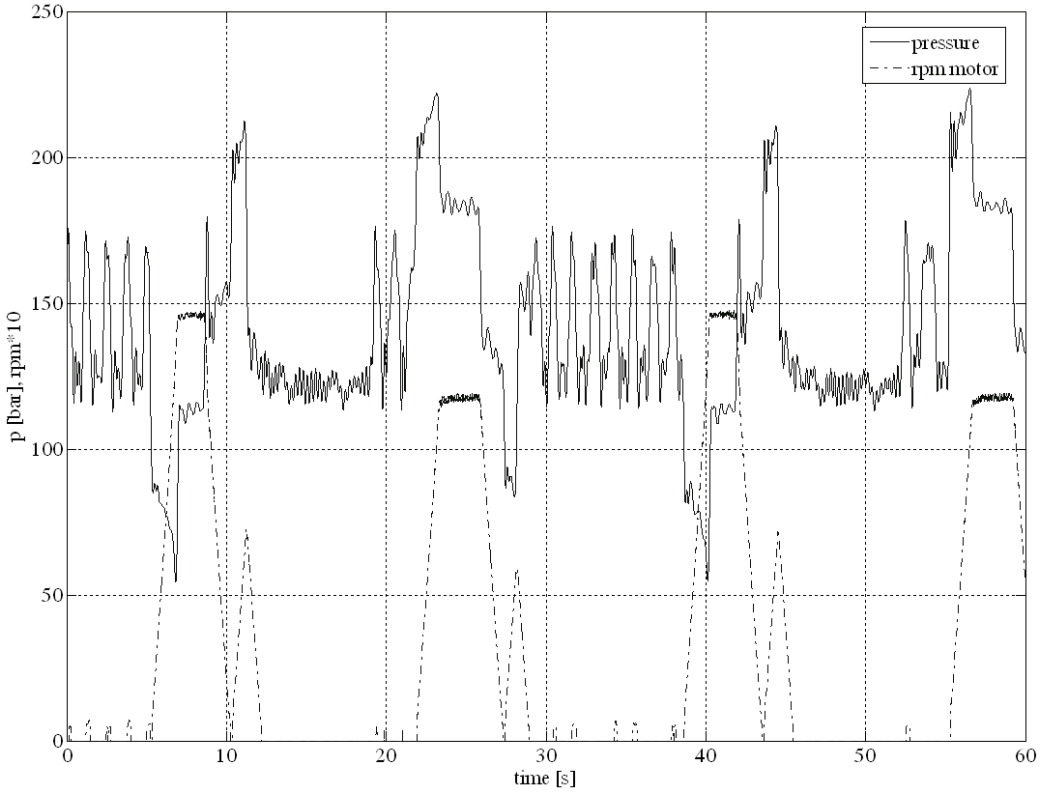

Fig 11. Pressure and rotating speed of motor during test step.

Next the gain was raised from 1 to 2 and same test run was replaced. The final position error is about 5cm and the response time is 8 s in both directions. There can been seen little overshoot in the position in both directions. The response is quite good and acceptable in many applications. Pressure or the rotating speed doesn't rise too high and the movement is evenly. Probably better result could be found with changing the gain and the integration time but now this result satisfies.

4 DISCUSSIONS

The Self-Contained winch with PI-controlled position control was tested in the laboratory. HST operates as a part of closed loop control as opposed to normally use.

According to tests the PI-controlled winch works in promising. When the mass moves to vertical directions there are two challenges to solve:

- because the leakage of hydraulic the mass strive to move downwards all the time
- responses are different at different directions because the gravity

The system kept the position without the brake. The mass didn't sink down much. There wasn't high pressure oscillation during keeping the position.

Although the responses are different at different directions the system was quite easy to tune. These tests were preliminary tests and the results could be better with extra-tests.

The main results of the study can be concluded in the following statements:

- When the mass was 6800 kg the position error was below 5 cm.
- The system kept positions without the brake
- Control parameters were easy to tune
- The temperature didn't rise much in the keeping situation

5 REFERENCES

[1] Fonselius, J. 2001. Comparing Different Control Strategies of Hydrostatic Transmission System. Acta Polytechnica Scandinavica, Mechanical Engineering Series No. 151, Espoo, Finland. 83p.

[2] Rauma Brattwaag. Electro Hydraulic Self-Contained Anchoring and Mooring Systems for Merchant Vessels. Fact Sheet, Rolls-Royce Marine AS, Dept. Deck Machinery

The Tenth Scandinavian International Conference on Fluid Power, SICFP'07, May 21-23, 2007, Tamerforss, Finland

ROBUST DESIGN OF A POWER STEERING SYSTEM WITH EMPHASIS ON CHATTERING PHENOMENA

M. Rösth and J-O. Palmberg
Department of Mechanical Engineering,
Linköping University, Sweden
E-mail: marro@ikp.liu.se

ABSTRACT

This paper investigates the chattering effect occurring in power steering systems. Chattering is experienced as noise and vibration in steering systems and occurs when the steering system is activated by the driver or driven by the load, aligning torque. Chattering is a problem, which is a result of poor system layout with regards to system stability. The problem can reduce the performance of the system but is mainly a quality problem from the user's point-of-view. In this paper, the phenomena is investigated with the help of a linear model of the system where the stability margin is analyzed for different characteristics of the valve.

KEYWORDS: Power Steering, Chattering, Linear Model

1 INTRODUCTION

A traditional hydraulic power steering system consists of a flow controlled pump, lines, an open-center valve unit and a hydraulic cylinder. Coupled to the hydraulic system are the steered wheels and the steering wheel. Together it is a multiple spring mass system with a hydraulic force amplifier in the middle, where the amplification is dependent on the torque applied to the steering wheel. From a handling point-of-view, the layout of the system is an intricate manipulation of the wheel suspension and the characteristic of the hydraulic system, [1] [2]. In this design, the hydraulic system is seen as a static system with a fix characteristic concerning the relationship between amplification and applied torque. Normally, this is visualized with the so-called boost curve, where the system pressure or load pressure is plotted against the applied steering wheel torque. Since the hydraulic system is a closed-loop system, an "uncareful" system layout can lead to instability problems. Instability results in oscillation in the system, and noise is emitted. In power steering systems, this phenomena is called chattering or hydraulic grunt.

In this paper, the chattering phenomena is studied and analyzed in order to establish the condition of instability. Both non-linear and linear models are used to explain the phenomena and how to avoid it. The models used are validated with measurements. Chattering is classified as noise, vibration, and harshness (NVH) problem, which has been a field of study regarding power steering systems. NVH problems are often related to the pump unit. However, in this case, the NVH problem is related to vibration caused by closed-loop limit cycling. This phenomena is called chattering but is also mentioned as shuttering, shuddering or hydraulic grunt and has been studied by among others, G.R Ferries et al. J.M. Smith et al. and T. Wong, [3], [4] and [5]. In this paper, the chattering phenomena is studied with regards to tolerance outcomes of the valve unit. Bad valve layout plays an important role in the chattering problem.

2 SYSTEM DESCRIPTION

In order to simplify reality, the real system has to be separated into pure mechanical components and hydraulic components. From a mechanical point-of-view, the system consists of masses, which are connected to each other with the help of the springs. The motion of some masses may be pure rotational movement; whereas, some may be linear motion. In order to handle this, the system is transformed to consist of only linear motion, where inertias and torsional stiffness are recalculated into equivalent masses and spring stiffness. Gear ration has to be considered during the transformation; in this paper, all the motion is related to the movement of the hydraulic piston. This makes it possible to rearrange the masses as displayed in Figure 1. In this figure, the masses from the steering wheel, m_{sw}, down to the wheels, m_s, can be identified together with the connecting springs; the viscous friction is also added.

$$m_{ekv} = \frac{I}{r^2} \tag{1}$$

In this work, both linear and non-linear models have been used, but with different purposes. The non-linear model has mostly been used to validate the system parameters and

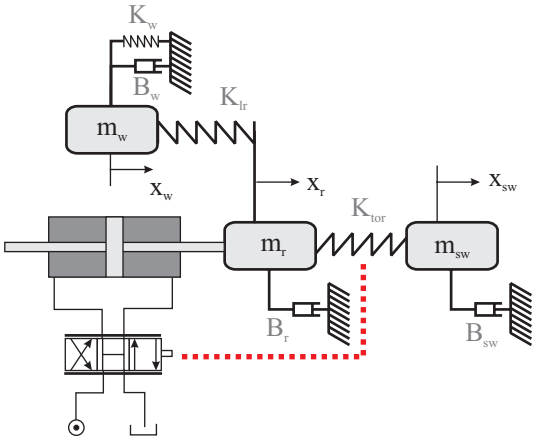

Figure 1: Schematic description of the system.

has been tuned to fit the real system. With this model, it is possible to regenerate the chattering problem and study it in the time domain. The problem studied has a stability problem, which is not suitable to studies in the time domain and why a linear model is used to study and analyze the system.

2.1 Linear model

$$\begin{bmatrix} \dot{x}_w \\ \ddot{x}_w \\ \dot{x}_r \\ \ddot{x}_r \\ \dot{x}_{sw} \\ \ddot{x}_{sw} \\ \dot{p}_L \end{bmatrix} = A \begin{bmatrix} x_w \\ \dot{x}_w \\ x_r \\ \dot{x}_r \\ x_{sw} \\ \dot{x}_{sw} \\ p_L \end{bmatrix} + Bx_v$$

$$A = \begin{bmatrix} 0 & 1 & 0 & 0 & 0 & 0 & 0 \\ \frac{-K_w - K_{lr}}{m_w} & \frac{-B_w}{m_w} & \frac{K_{lr}}{m_w} & 0 & 0 & 0 & 0 \\ 0 & 0 & 0 & 1 & 0 & 0 & 0 \\ \frac{K_{lr}}{m_r} & 0 & \frac{-K_{lr} - K_{tor}}{mr} & \frac{-B_r}{m_r} & \frac{K_{tor}}{m_r} & \frac{B_{sw}}{m_r} & \frac{A_p}{m_r} \\ 0 & 0 & 0 & 0 & 0 & 1 & 0 \\ 0 & 0 & \frac{K_{tor}}{m_{sw}} & \frac{B_{sw}}{m_{sw}} & \frac{-K_{tor}}{m_{sw}} & \frac{-B_{sw}}{m_{sw}} & 0 \\ 0 & 0 & 0 & \frac{-A_p}{C} & 0 & 0 & \frac{-K_c}{C} \end{bmatrix} \quad (2)$$

$$B^T = \begin{bmatrix} 0 & 0 & 0 & 0 & 0 & 0 & \frac{Kq}{C} \end{bmatrix}$$

Hydraulic coefficients

In the model, the mechanical coefficients are static and will not vary with time or working point. However, the hydraulic coefficients are strongly coupled to the working point. The working point depends on the displacement of the valve and the load flow, which defines the pressure balance in the valve. There is also dependency regarding the position of the

steering rack, due to the volume change in the piston chambers. However, this is neglected in the work presented in this paper. The model of the hydraulic part is also based on the geometry of the valve, where the area functions are essential. These can be measured from the geometry of the valve, which is time consuming. The method used in this work is based on the static measurements of the valve. The boost curve is used in an optimization routine, where the area coefficients are identified. The area functions are assigned as a 3rd degree function with four unknown coefficients. One of these coefficients can be resolved from the boost curve, where the pressure drop of the valve is seen. The rest of the coefficients are decided by the optimization routine. In the real valve, the upper limit of the area opening is limited by the inlet of the valve body; this is not taken care of in this model but simulation shows small deviation in results, due to the fact that the metering orifice is clearly dominant in this situation. In this section, the hydraulic dependent coefficients, K_c, K_q and C, used in Equation 2, will be derived.

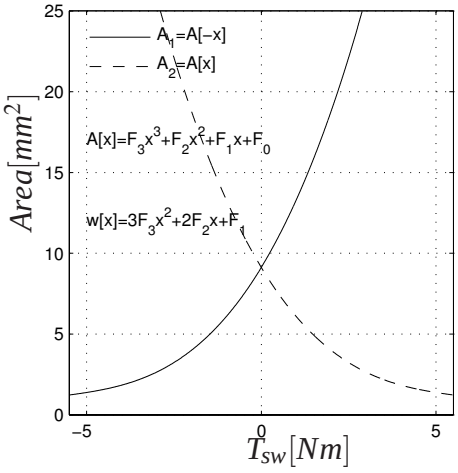

Figure 2: Area function of the valve openings related to the areas shown in Figure 3

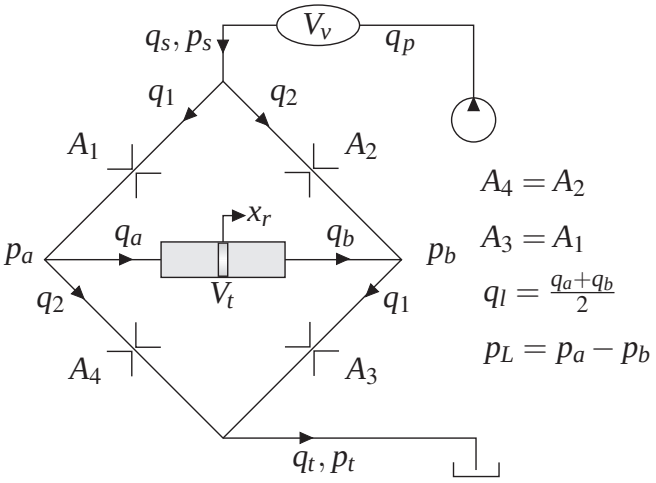

Figure 3: Lumped model of the valve unit in Wheatstone configuration.

In Figure 3, a schematic sketch of the the valve and ingoing hydraulic components are shown. According to Merritt, [6], the system flow and the load flow can be described as in Equations 3 and 4 if the area in the valve is symmetrical ($A_1 = A_3$, $A_2 = A_4$) and matched ($A_1[x] = A_2[-x]$), see Figure 2. This is true for this valve except for when the valve opening is greater than the inlet orifices of the valve. However, this can be neglected, due to the fact that the metering orifices are dominant during these conditions.

$$q_s = C_q A[-x]\sqrt{\frac{p_S - p_L}{\rho}} + C_q A[x]\sqrt{\frac{p_S + p_L}{\rho}} \tag{3}$$

$$q_L = C_q A[-x]\sqrt{\frac{p_S - p_L}{\rho}} - C_q A[x]\sqrt{\frac{p_S + p_L}{\rho}} \tag{4}$$

In addition, the continuity equations consider the compressibility effects in the system. These equations include the compressibility within the hydraulic cylinder, Equation 5, and in the supply line between the pump and the valve unit, Equation 6.

$$q_L = A_p s x_p + \frac{V_0}{2\beta_e} s p_L \tag{5}$$

$$q_p - q_s = \frac{V_v}{\beta_e} s p_S \tag{6}$$

Linearizing Equations 3-6 gives the following equations:

$$Q_L = K_{q1} X_v + K_{c2} P_S - K_{c1} P_L \tag{7}$$

$$Q_S = -K_{q2} X_v + K_{c1} P_S - K_{c2} P_L \tag{8}$$

$$Q_L = A_p s X_p + \frac{V_0}{2\beta_e} s P_L \tag{9}$$

$$Q_p - Q_s = \frac{V_v}{\beta_e} s P_S \tag{10}$$

With the help of Equations 7-10, the load pressure can be resolved as a function of the valve displacement, pump flow and cylinder velocity, Equation 11. This equation consists of an additional dynamic, which can be reduced. The first dynamic consists of a first order filter in the nominator and the second order dynamic in the denominator can be reduced to a first order low pass filter. This is due to the fact that the second order dynamic is over dampened and can be separated into two first order filters, see Equations 12 and 13. The flow gain dynamic, Equation 11, is out of range and much higher than the rest of the system; therefore, it is neglected. The dynamic concerning the delivery flow from the pump is also neglected when these flow variations are neglected in further investigation of the system dynamic.

$$P_L = \underbrace{\frac{K_{c1}}{K_{c1}^2 - K_{c2}^2}}_{=1/K_c} \frac{\overbrace{\left(1 + \frac{V_V}{K_{c1}\beta_e} s\right)}^{\approx \frac{1}{1+\frac{s}{\omega_n}}}}{\left\{1 + 2\frac{\delta_0}{\omega_0} s + \frac{s^2}{\omega_0^2}\right\}} \cdot \left\{ \underbrace{\frac{\left(1 + \frac{V_V s}{\left(K_{c1} + \frac{K_{q2}}{K_{q1}} K_{c2}\right)\beta_e}\right)}{1 + \frac{V_V}{K_{c1}\beta_e} s}}_{\approx 1} \underbrace{K_{q1}\left(1 + \frac{K_{c2}K_{q2}}{K_{c1}K_{q2}}\right)}_{=K_q} X_v \right.$$

$$\left. - \frac{K_{c2}}{K_{c1}} \frac{1}{1 + \frac{V_V}{K_{c1}\beta_e} s} Q_p - A_p s X_p \right\} \tag{11}$$

$$\omega_0 = \sqrt{\frac{2\left(K_{c1}^2 - K_{c2}^2\right)}{V_0 V_V}} \beta_e$$

$$\delta_0 = \frac{1}{\sqrt{2}} \frac{K_{c1}}{\sqrt{K_{c1}^2 - K_{c2}^2}} \frac{\frac{V_0}{2} + V_V}{\sqrt{V_0 V_V}}$$

$$2\delta_0\omega_0 = \frac{2K_{c1}\left(\frac{V_0}{2} + V_v\right)\beta_e}{V_0 V_V} \approx \frac{K_{c1}\beta_e}{V_V} = \omega_t \tag{12}$$

$$\frac{\omega_0}{2\delta_0} = \frac{K_{c1}^2 - K_{c2}^2}{K_{c1}} \frac{\beta_e}{\frac{V_0}{2} + V_v} = K_c \frac{\beta_e}{\frac{V_0}{2} + V_v} = \omega_n \tag{13}$$

The flow gain and the pressure depending flow gain have to be established in order to perform any dynamic analysis of the system. From Equations 3 and 4 the derivatives K_{c1}, K_{c2}, K_{q1} and K_{q2}, can be calculated. The results can be seen in Equations 14-17.

$$K_{q1} = -C_q\sqrt{\frac{p_S - p_L}{\rho}}w[-x] - C_q\sqrt{\frac{p_S + p_L}{\rho}}w[x] \tag{14}$$

$$K_{q2} = C_q\sqrt{\frac{p_S - p_L}{\rho}}w[-x] - C_q\sqrt{\frac{p_S + p_L}{\rho}}w[x] \tag{15}$$

$$K_{c1} = \frac{C_q A[-x]}{2\sqrt{(p_S - p_L)\rho}} + \frac{C_q A[x]}{2\sqrt{(p_S + p_L)\rho}} \tag{16}$$

$$K_{c2} = \frac{C_q A[-x]}{2\sqrt{(p_S - p_L)\rho}} - \frac{C_q A[x]}{2\sqrt{(p_S + p_L)\rho}} \tag{17}$$

From Equations 3 and 4, Equations 18 and 19 can be established and used to eliminate the pressure dependency in the flow coefficients. To further simplify, the normalized load flow is introduced, Equation 20.

$$p_S - p_L = \frac{\rho}{4}\left(\frac{q_s}{C_q A[-x]}\right)^2\left(1 + \frac{q_L}{q_s}\right)^2 \tag{18}$$

$$p_S + p_L = \frac{\rho}{4}\left(\frac{q_s}{C_q A[x]}\right)^2\left(1 - \frac{q_L}{q_s}\right)^2 \tag{19}$$

$$q = \frac{q_L}{q_S} \tag{20}$$

The result is flow coefficients that are dependent on the valve displacement system flow and load flow as input variables.

$$K_{q1} = -\frac{q_s}{2}\left((1+q)\frac{w[-x]}{A[-x]} + (1-q)\frac{w[x]}{A[x]}\right) \tag{21}$$

$$K_{q2} = \frac{q_s}{2}\left((1+q)\frac{w[-x]}{A[-x]} - (1-q)\frac{w[x]}{A[x]}\right) \tag{22}$$

$$K_{c1} = \frac{C_q^2}{q_s\rho}\left(\frac{A[-x]^2}{(1+q)} + \frac{A[x]^2}{(1-q)}\right) \tag{23}$$

$$K_{c2} = \frac{C_q^2}{q_s\rho}\left(\frac{A[-x]^2}{(1+q)} - \frac{A[x]^2}{(1-q)}\right) \tag{24}$$

The coefficients given in Equation 11 are lumped together to form global flow coefficient values and are defined by Equation 25 and 26.

$$K_c = \frac{K_{c1}^2 - K_{c2}^2}{K_{c1}} \tag{25}$$

$$K_q = K_{q1}\left(1 + \frac{K_{c2}K_{q2}}{K_{c1}K_{q1}}\right) \tag{26}$$

$$C = \frac{\frac{V_0}{2} + V_v}{\beta_e} \tag{27}$$

The state concerning the hydraulics in the state space model, Equation2), is the reduced to Equation 11. Equation 28 is a simplified representation with capacitance, Equation 27, calculated from Equation 13. In order to use the linear model, the coefficients have to be calculated for each studied working point, where the stability can be studied locally.

$$\dot{P}_L = -\frac{K_c}{C}P_L + \frac{K_q}{C}X_v - \frac{A_p}{C}\dot{X}_p \tag{28}$$

2.2 Stability analysis

The basic idea of the system is to generate assistance to the driver. In reality, the system is similar to a classic position follower servo. This view is used when studying the stability of the system, regarding position control. The open-loop system is defined by the transfer function $G_o(s) = \frac{\Delta X_p}{\Delta X_v}$. In Figure 4, the transfer function for the system is displayed. The system regarded is related to the boost curve in Figure 5. With the help of the linear model, it is possible to establish the stability margin for the system during different working points. This model is used later in the paper to analyze the system and explain the chattering phenomena.

3 CHATTERING PROBLEM

Chattering is a result of bad system layout with regards to system stability. The problem can reduce the performance of the system but is mainly a quality problem from the users point-of-view. Figure 6 shows measurements from a chattering scenario. In this case, the steering unit is driven by an external load, not the driver; he/she merely controls the movement by adding breaking torque to the steering wheel. This is compared with a vehicle exiting a cornering manoeuver, the aligning torque generates a force to center the steering wheels. In this scenario, the steering wheel torque acts in the opposite direction of steering unit motion, cylinder. This will increase the amplification in the loop and result in vibration in the steering unit, due to instability in the closed-loop system.

4 WHY IS THE SYSTEM INSTABLE?

The reason for instability in the steering system can be divided into two separate problems that co-exist. The first problem is the pumping motion of hydraulic cylinder, which affects

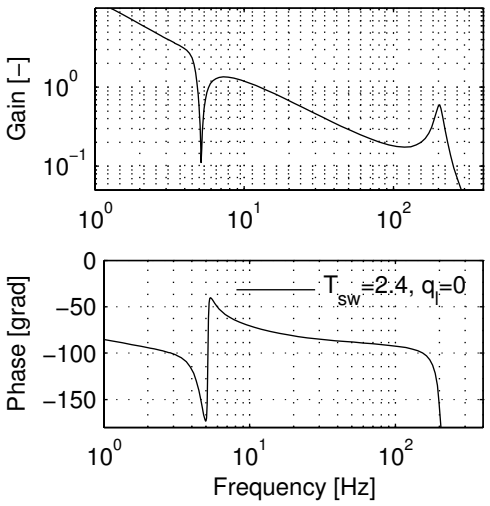

Figure 4: Bode plot of the open loop system the working point, Steering wheel torque and load flow, is given in the figure

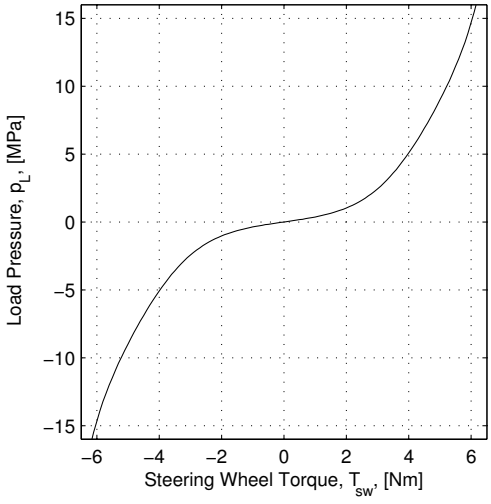

Figure 5: Boost curve of the studied system.

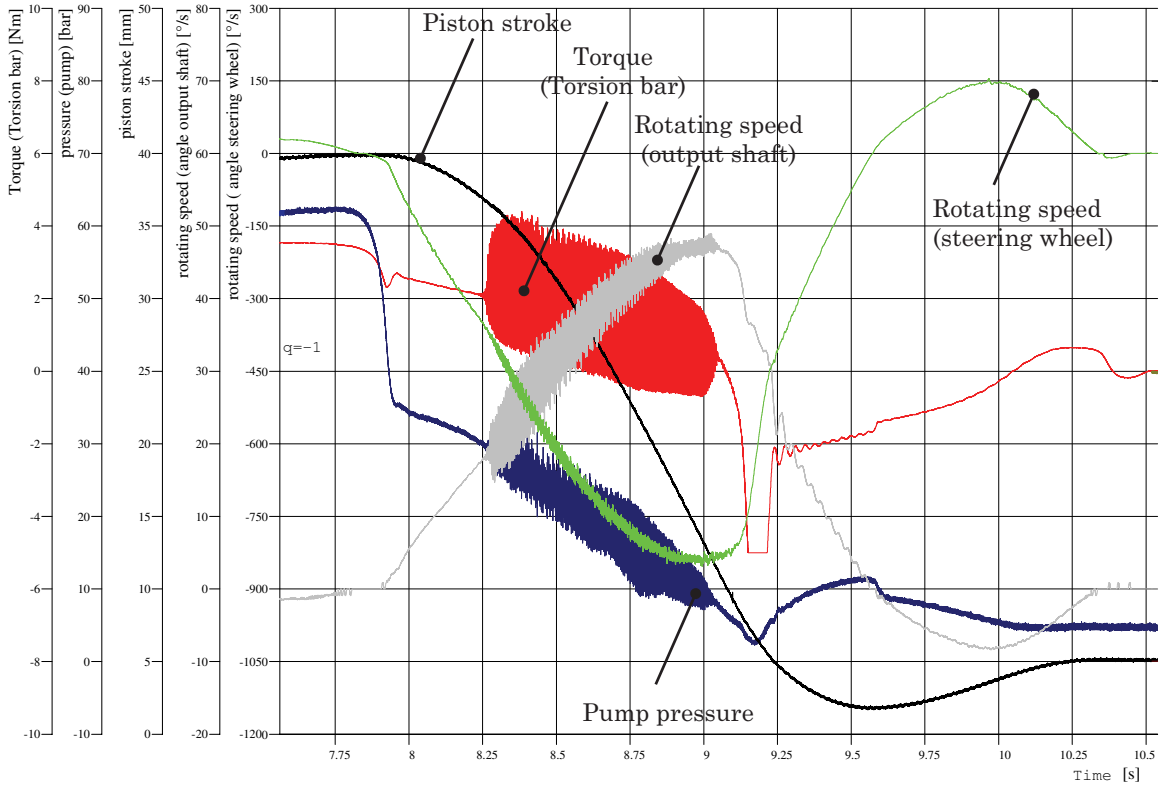

Figure 6: Measurements from a chattering scenario where the system is driven by the load, steering wheel torque and steering rack velocity in opposite directions.

the system gain. The pumping motion decreases or increases the system gain. The second problem is the imperfect valve geometry. The characteristic of the valve varies, due to tolerances in the production process. In this section, these two problems will be discussed along with their affects on the stability of the system.

4.1 Variation in the load flow

The static characteristic of the valve changes with the load flow, Equation 29. This can be visualized in the static characteristic of the valve. If the pressure modulation is in the same direction as the motion of the cylinder, the system gain is reduced. If the cylinder generates an equal load flow to the input flow from the pump, the system will not be able to produce any assisting force, also known as catch-up effect. This a common phenomena that is taken care of in the design of the steering unit, and basically gives the maximal speed of the steering wheel [7].

$$p_L = \frac{\rho q_s^2}{8C_q^2}\left(\left(\frac{1-q}{A[x]}\right)^2 - \left(\frac{1+q}{A[-x]}\right)^2\right) \tag{29}$$

If the motion of the cylinder is opposite to the generated assisting pressure, the gain in the system increases. This scenario occurs when the steered wheels are driven by the aligning torque, exiting a corner. In cars, this torque will not generate a high speed on the steering rack, and therefore, not introduce any problems. In trucks, the aligning torque is higher and induces a higher velocity on the steering rack, which produces a negative load flow. In Figure 7, the change in the boost curve is plotted with both negative and positive load flow. In the figure, the inner curve represents a load flow of q=-0.8 and the outer q=0.8. A load flow of q=1 means that the load flow and the pump flow are equal, and no assisting is possible.

The change in characteristic affects the static gain of the system, and therefore, the stability margin. As seen in Figure 8, the amplitude margin of the system is significantly reduced when the load flow is negative, but will not lead to instability problems.

4.2 Variation in tolerances of the valve

In the manufacturing of the valve unit, the outcome is affected by the production process, which in turn gives the valve a static characteristic with certain tolerances. These are often given by the producer as the expected outcome. However, these tolerances have different affects on the dynamic characteristic of the valve. In Figure 9, typical tolerances are visualized in the static boost curve, where the span of the characteristic can be seen.

In Figure 10, the bode plot of the system is plotted at the worst case scenario. As seen in the plot, this chosen working point results in an unstable system due to negative amplitude margin and chattering. In Figure 11, the scenario displayed in Figure 6 is plotted. The plot shows the amplitude margin as a contour of a function of the given torque and load flow. The trajectory of the scenario is plotted with time stamps. Notice that the trajectory enters the instable area with a negative amplitude margin after 8.1 seconds and exits at 8.9 seconds,

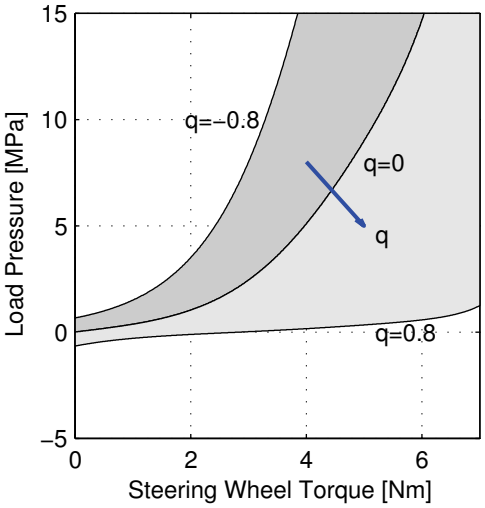

Figure 7: Change in the static characteristic due to change in load flow.

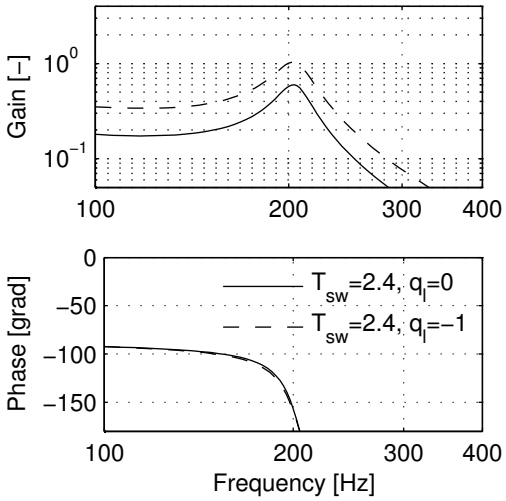

Figure 8: Reduction of the amplitude margin due to negative load flow.

compare with Figure 6. The system studied has a valve characteristic close to the inner limits in the tolerance specification, which gives the system an unstable behavior. In contrast to this plot, Figure 12 displays the stability margin for a normal valve characteristic. As can be seen in this contour plot, the system is in an area where the amplitude margin shows a stable behavior. *Note that in the graphs, the numbers on the amplitude margin are negative, negative amplitude margin stable positive unstable unit dB.*

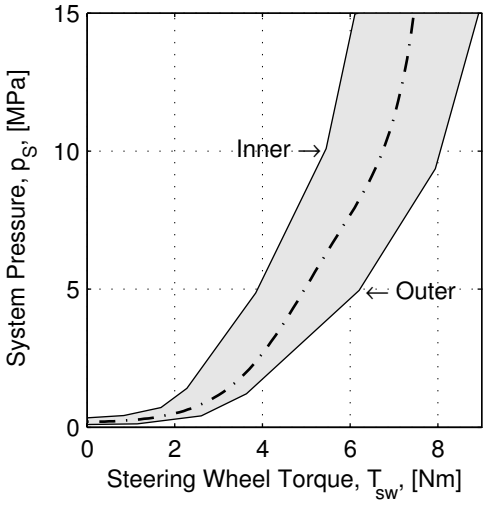

Figure 9: Change in the static characteristic due to tolerances in the production of the valve.

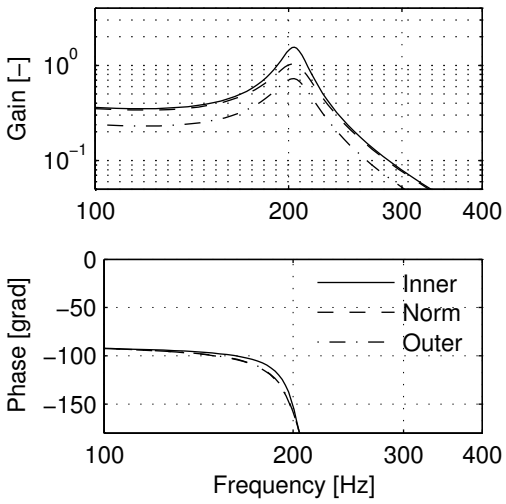

Figure 10: Reduction of the amplitude margin due to negative load flow and changes in the valve characteristic based on tolerances.

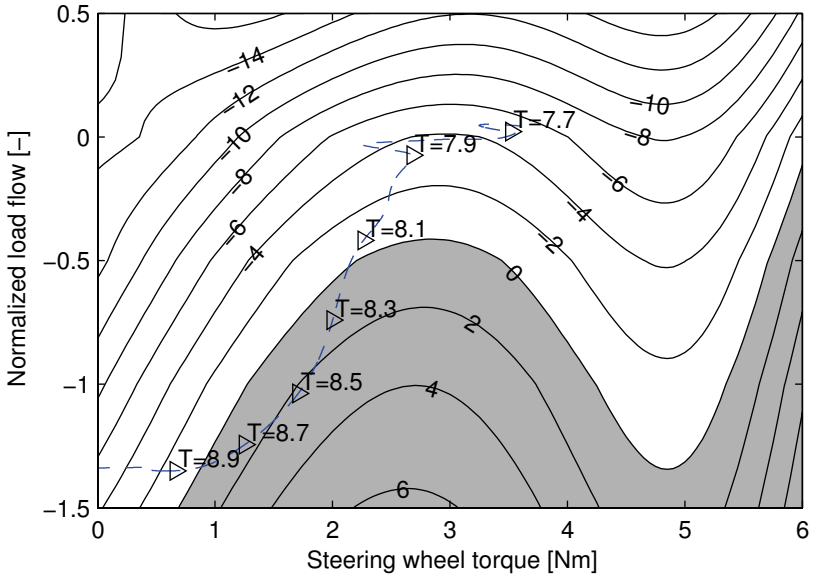

Figure 11: Amplitude margin of the system depending on the applied steering wheel torque and normalized load flow. The trajectory of the rack motion is on top, based on Figure 6. Valve characteristic representing inner curve in Figure 9. Gray area represent negative amplitude margin, Amplitude margin in [dB].

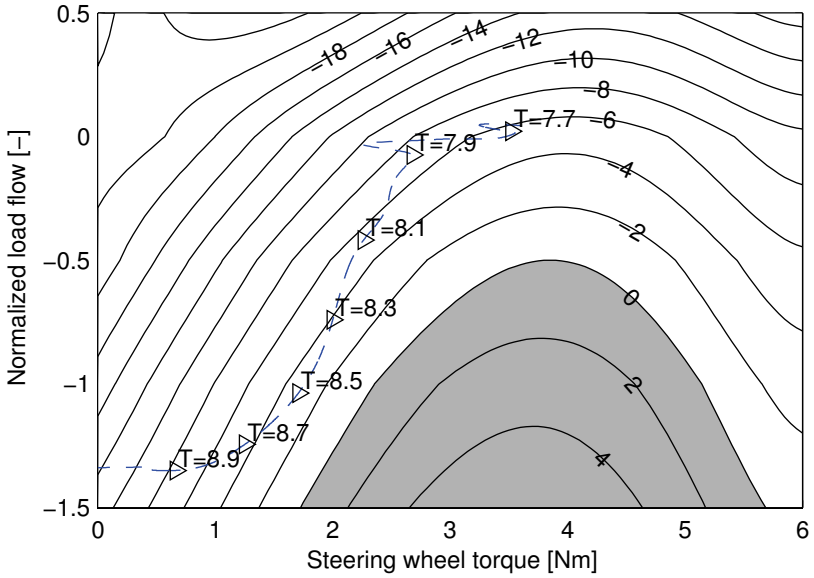

Figure 12: Amplitude margin of the system depending on the applied steering wheel torque and normalized load flow. The trajectory of the rack motion is on top, based on Figure 6. Valve characteristic representing normal curve in between inner and outer in Figure 9. Gray area represent negative amplitude margin, Amplitude margin in [dB].

5 ROBUST DESIGN IN A DYNAMIC PERSPECTIVE

Based on the stability analysis performed in this paper, the outcome of the tolerances is the major cause of instability. This means that the problem may not be visible in the early testing of the the new vehicle, but rather late in production. This makes the problem hard to predict without reliable models. With the model presented in this paper, it is possible to predict the dynamic behavior of the system when it comes to stability, thereby ensuring or defining the tolerances such that a robust design is achieved. Robust design gives the product an insensitive functionality due to variation in tolerances. This means that the system should work correctly even if the ingoing components do not conform according the norm values.

The nominal characteristic of the system is, as mentioned early, determined by the desired handling characteristic of the vehicle. Based on this characteristic, the outer limit of the tolerance outcome can be calculated in order to ensure a stable system. This would lead to a robust design in a dynamic perspective and reduce the risk of chattering phenomena in the production vehicle.

6 CONCLUSION AND DISCUSSION

In this paper a linear model of a power steering system has been presented. This model has been used to study and explain the chattering phenomena that can occur in hydraulic power steering units with poor layout of the valve characteristic in terms of stability. In order to secure a stable system independent of the outcome of tolerances, a model has to be used. The linear model presented can be used in the early design process to avoid stability problems by establishing the inner limit of the static boost curve. The method presented is based on establishing the amplitude margin as a measure of stability, which varies with other factors except for the valve characteristic. Different layouts and system geometry affect the system stability. Different bussing affects the friction and the spring coefficients in the system and changes the parameters in the models. However, the valve characteristic is the factor that has the greatest impact on the stability margin.

7 NOMENCLATURE

β_e	Bulk modulus of the oil	$[Pa]$
ρ	Density of the oil	$[kg/m^3]$
$A_{1,2}$	Metering orifice area with in the valve	$[m^2]$
A_p	Cylinder area	$[m^2]$
B_{sw}	Viscous friction steering wheel	$[Ns/m]$
B_r	Viscous friction rack	$[Ns/m]$
B_w	Viscous friction wheel	$[Ns/m]$
C	Hydraulic capacitance	$[m^5/N]$
c_q	Flow coefficient	$[--]$
F_i	Coefficient in area function	$[-]$
I	Inertia	$[kgm^2]$
K_{lr}	Spring coefficient link-rod	$[N/m]$
K_{tor}	Spring coefficient torsion bar	$[N/m]$
K_c	Linearized flow–pressure coefficient	$[m^5/Ns]$
K_q	Flow gain	$[m^2/s]$
K_w	Spring coefficient wheel	$[N/m]$
m_{ekv}	Equivalent mass	$[kg]$
m_{sw}	Mass steering wheel	$[kg]$
m_r	Mass rack	$[kg]$
m_w	Mass wheel	$[kg]$
p_L	Load pressure	$[Pa]$
p_s	System pressure	$[Pa]$
q	Normalized load flow	$[--]$
q_l	Load flow	$[m^3/s]$
q_p	Pump flow	$[m^3/s]$
q_s	System flow	$[m^3/s]$
r	Radius	$[m]$
T_{sw}	Steering wheel torque	$[Nm]$
w	Area gradient	$[m]$
V_t	Total volume in cylinder	$[m^3]$
V_v	System Volume	$[m^3]$
x_{sw}	Steering wheel position	$[m]$
x_r	Rack position	$[m]$
x_v	Valve displacement	$[m]$
x_w	Wheel position	$[m]$

REFERENCES

[1] Adams, F. J., 1983. "Power steering 'road feel'.". In SAE Technical Paper Series, no. 830998.

[2] Norman, K. D., 1984. "Object evaluation of on-centre handling preformance". In SAE International Congress and Exhibition, no. 840069.

[3] Ferries, G. R., and Arbanas, R. L., 1997. "Control/structure interaction in hydraulic power steering systems". In American Control Conference, AACC, pp. 1146–1151.

[4] Smith, J. M., Ferrues, G., and Arbanas, R., 1995. "An analytical control systems approach to steering shudder". In SAE Noice and Vibration Conference, no. 951254.

[5] Wong, T., 2001. "Hydraulic power steering system design and optimization simulation". In SAE World Congress, Steering and Suspension Technology Symposium, no. 2001-01-0479 in SAE Technical Paper.

[6] Merritt, H. E., 1967. *Hydraulic Control Systems*. No. ISBN 0–471–59617–5. John Wiley & Sons, New York.

[7] Rösth, M., and Palmberg, J.-O., 2005. "Modeling and validation of power steering system with emphasis on catch-up effect". In The Ninth Scandinavian International Conference on Fluid Power, SICFP´05.

PAYLOAD ESTIMATION IN FOUR WHEEL DRIVE LOADERS

Jahmy Hindman
Deere & Company
Construction and Forestry Division
P.O. Box 538
Dubuque, Iowa USA 52001
Phone 001 563 589 6194, Fax 001 563 589 5601
E-mail: hindmanjahmy@johndeere.com

Richard Burton & Greg Schoenau
University of Saskatchewan
Department of Mechanical Engineering
Saskatoon, SK Canada S7N 0J5
Phone 001 306 966 5373
E-mail richard.burton@usask.ca
greg.schoenau@usask.ca

ABSTRACT

Dynamic payload estimation in hydraulically actuated linkages is a diffucult task compounded by friction, compressibility, manufacturing variation, and linkage nonlinearity among other things. This problem is made even more difficult when the linkage is mobile as is often the case with off-highway equipment such as four-wheel-drive loaders, cranes, and excavators. The rigid body motion of this type of equipment affects the gravitational loads seen in the linkage and impact the payload estimate. The commercially available state-of-the-art load estimation solutions rely on the mobile machine becoming pseudo-static in order to maintain accuracy. This requirement increases the time required to move the material and decreases the productivity of the machine. A novel solution to this problem that enables the machine to remain dynamic and still accurately estimate the payload is discussed in this paper. Development and implementation on an actual four-wheel-drive loader is shown.

KEYWORDS: Dynamic, Load, Estimation, Mobile, Hydraulic, Neural Network

1. INTRODUCTION

2.1 Background

Hydraulic technology utilized in mobile hydraulic equipment such as four-wheel-drive loaders, excavators, cranes, forest machines, etc has advanced significantly in the last

twenty years. This time period has seen increased system efficiency from technology changes such as fixed versus variable displacement pumps, closed center versus open center control valves and hydrostatic transmissions among other technologies. All of these changes have been aimed at reducing the energy consumed by the equipment. The driving economic principle behind these advances stemmed from reducing energy consumed and thus reducing the amount of fuel consumed by the machine. The stark reality of the present day fossil fuel prices dictates that further technological advances be made in this area. Dynamic estimation of payload to reduce starts and stops in the work process is one such energy saving approach that is considered in this paper.

Towards that end, it is useful to briefly describe the current state of the art for mobile machine weighing systems. These systems are typically used to weigh the amount of material being moved from an excavation to a truck. The truck in turn will move the material to another location on the job-site or to another work area. It is critical to know the weight of material in the truck because of various governmental regulations in both Europe and North America that constrain the weight of hauling trucks to increase road surface durability. The state of the art for a typical four-wheel-drive loader weighing system today requires the loader to come to a pseudo-static equilibrium before an accurate measurement can be taken. This requires the machine operator to decelerate the machine and then accelerate again to reach the truck. This disruption in the work cycle uses energy that could be eliminated if an accurate dynamic measurement was possible. Additionally, if the weight of the material being carried by the mobile equipment is too much to complete a truckload under the legal limit, the operator must dispose of some material and re-weigh. The re-weigh operation, while possibly not being eliminated, should require the minimum amount of consumed energy in order to be fuel efficient. A typical truck loading cycle for a wheel loader may take 40 seconds with five seconds being used to weigh the material. If the five seconds could be eliminated, the cycle time could be improved by 12.5% and the energy consumed reduced.

The thrust of this research work was to develop a weighing system/algorithm that delivers current state-of-the-art accuracy (+/-1% full scale) while the machine is operating in its normal dynamic cycle. The economic motivation behind this work is reducing the energy consumed by the vehicle and thus reducing the input fuel costs. The machine chosen for this research work is a Deere 644J 4WD loader as shown in Figure 1.

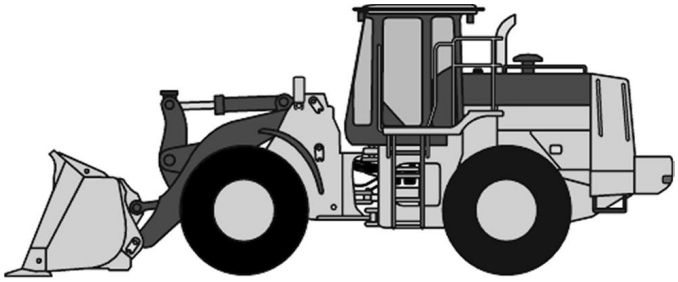

Figure 1: Deere 644J 4WD Loader

2.2 Literature Review

The topic of dynamic payload estimation and related work has created a small, but pertinent volume of research. Some of this research is involved with estimating kinematic parameters for linkages and actuators in preparation for developing a model-based payload estimation algorithm or for control purposes. Tafazoli et al [1] describe a method for estimating gravitational linkage parameters for an excavator and then use these estimated parameters in conjunction with load pins (i.e. instrumented joint pins capable of measuring joint forces) that the payload in the excavator bucket can be estimated to within 5% full scale. Similar work towards estimating gravitational and friction parameters in mobile linkages may also be found in [2][3].

Additionally, the topic of dynamic payload estimation has been researched significantly in applicable industries. Kyrtsos et al in [4] describe a method of estimating payload in a four-wheel-drive loader utilizing the lift cylinder pressures and linkage position. The method described relies on fitting a polynomial to the pressure information in order to smooth it out and provide a consistent payload estimate. This methodology is further refined in [5] and [6] with [6] describing the algorithm in entirety, presumably as implemented on wheel loaders described in the patent. The final algorithm adds correction factors for the velocity at which the lift was accomplished but is otherwise similar to the algorithm described in [4]. It should be noted that [6] claims that the algorithm can be utilized while the machine is moving, but this simply means while the lift is occurring, not rigid body motion of the entire vehicle.

2. METHODOLOGY

2.1 Description

A typical four-wheel-drive loader linkage can be seen in Figure 2. This linkage is referred to in the industry as a z-bar linkage due to the geometry of the bucket linkage (bucket cylinder, bell crank, and bucket link).

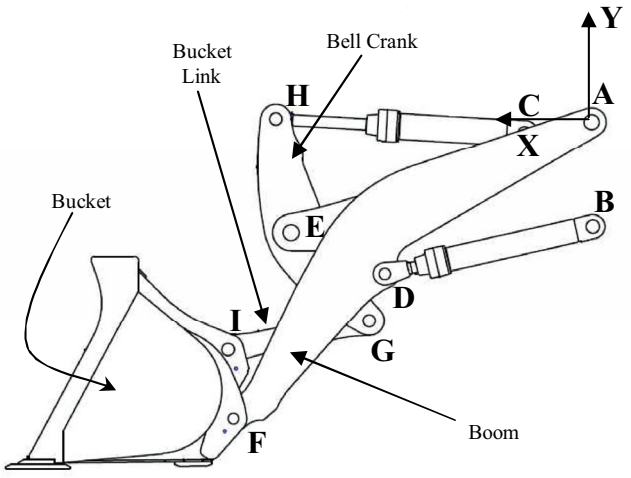

Figure 2: Four-Wheel-Drive Loader Linkage

While the research discussed here was performed specifically on the z-bar linkage, the methodology may be generalized for other hydraulically manipulated kinematic linkages.

In general, a payload weighing algorithm for a four-wheel-drive loader is focused on determining the weight of material that has been excavated and is resident in the bucket of the loader. This problem becomes difficult in practicality due to several influencing factors including volume and mass variations in material being moved, hydraulic cylinder and pin joint friction forces that vary with temperature and velocity, acceleration of the complete loader vehicle, acceleration of the loader linkage and inclination of the complete machine with respect to the gravitational force. These influencing factors make the problem a difficult one and nevertheless, the owner of a four-wheel-drive loader expects an error with the algorithm of less than +/-1% full scale. For the John Deere 644J loader shown in Figure 1, the full scale load is approximately 6,750 kg. 1% accuracy therefore means the scale needs to be within +/-67.5 kg. Additionally, the owner of a four-wheel-drive loader equipped with a scale today is required to bring the machine to a pseudo-static state during the boom lifting operation in order to achieve the accuracy described. This requirement interrupts the work cycle and introduces inefficiencies in time, fuel, and ultimately, money spent. It is this problem, estimating within 1% under dynamic conditions so as not to cause a disruption to the work cycle that this research is focused.

2.2 Algorithm Development

As a benchmark for algorithm development, a two-dimensional kinematic model of the linkage in Figure 2 was developed. This kinematic model was then utilized to calculate the linkage joint positions and linkage component (boom, bucket, bell crank, bucket link) center of gravity for any boom or bucket cylinder length. Using this information and neglecting friction terms, a simple summation of torques about joint "A" can be accomplished to solve for the remaining unknown of payload mass. This calculation assumes a known payload center of gravity which is assumed from knowledge of the bucket geometry. The resulting equation for calculating the payload weight is:

$$W_{Payload} = \frac{\begin{pmatrix} -M_{Boom}X_{CGBoom} - M_{BellCrank}X_{CGBellCrank} - M_{BucketLink}X_{CGBucketLink} \\ -M_{Bucket}X_{CGBucket} - \dfrac{\left(Fx_{BoomCyl}Y_D + Fy_{BoomCyl}X_D\right)}{9.8} \end{pmatrix}}{X_{CGPayload}} \quad (1)$$

where:

$W_{Payload}$	=	Weight of payload (kg)
M_{Boom}	=	Mass of boom (kg)
X_{CGBoom}	=	"X" coordinate of boom center of gravity (m)
$M_{BellCrank}$	=	Mass of bell crank (kg)
$X_{CGBellCrank}$	=	"X" coordinate of bell crank center of gravity (m)
$M_{BucketLink}$	=	Mass of bucket link (kg)
$X_{CGBucketLink}$	=	"X" coordinate of bucket link center of gravity (m)
M_{Bucket}	=	Mass of bucket (kg)
$X_{CGBucket}$	=	"X" coordinate of bucket center of gravity (m)
$Fx_{BoomCyl}$	=	"X" component of boom cylinder force (N)
Y_D	=	"Y" coordinate of joint "D" (m)
$Fy_{BoomCyl}$	=	"Y" component of boom cylinder force (N)
X_D	=	"X" coordinate of joint "D" (m)
$X_{CGPayload}$	=	"X" coordinate of payload center of gravity (m)

A set of data was collected from a John Deere 644J four-wheel-drive loader. This data included: bucket cylinder stroke, boom cylinder stroke, bucket cylinder rod-end pressure, bucket cylinder head-end pressure, boom cylinder rod-end pressure and boom cylinder head-end pressure. Data was collected on these four sensors at 40Hz sampling frequency using a 3hz low-pass filter. Utilizing equation [1] and the data set collected, the payload was estimated for a variety of machine conditions using the inputs of $Fx_{BoomCyl}$, $Y_{D,}$, $Fy_{BoomCyl}$, X_D. The mean error in the payload estimate is for these various machine conditions is seen in Figure 3.

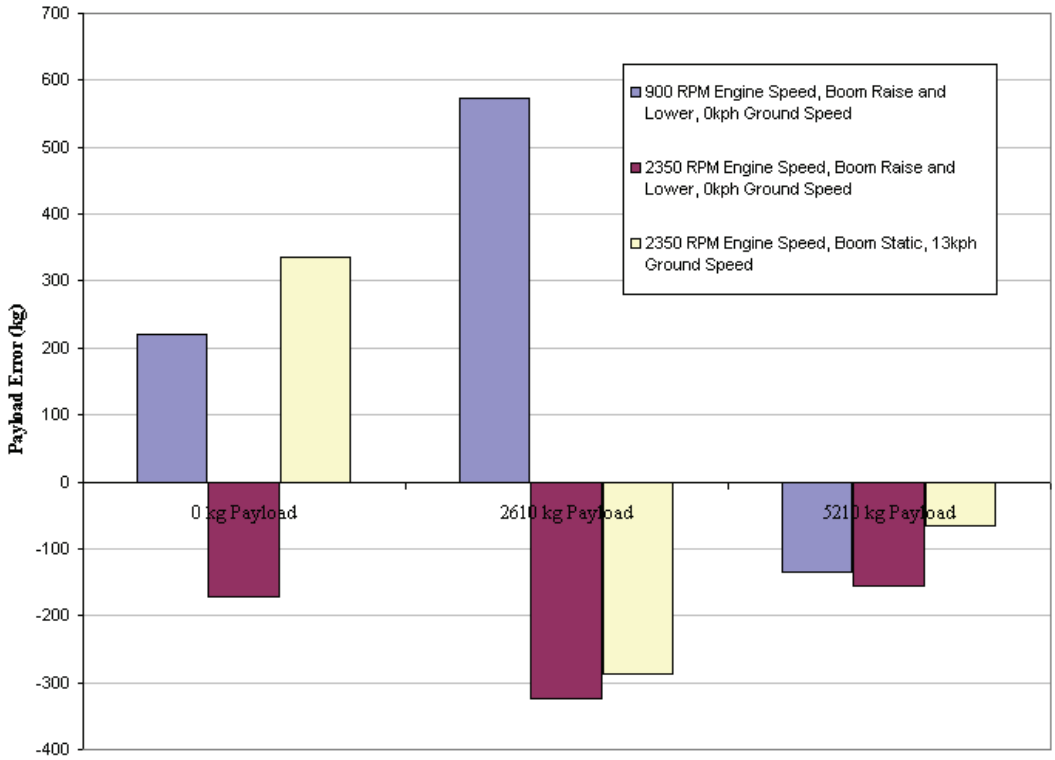

Figure 3: Payload Estimate Error from Kinematic Model

It can be seen in Figure 3 that the payload estimate is significantly higher than the desired +/-67.5 kg. Additionally, the variance in the estimate is high with a standard deviation of 306.8 kg. It is obvious from these results that this method falls short of meeting the requirements.

A second method was attempted. This method makes use of the data set collected for the kinematic model. Instead of using the boom and bucket cylinder lengths and pressures for the kinematic model, this data was utilized to train a feed-forward artificial neural network. A four-layer artificial neural network (ANN) with 5 neurons in the first layer, 10 in the second, 10 in the third and one in the output layer was trained with half of the collected data set. This training was accomplished with the Levenberg-Marquardt back-propogation algorithm [9] and implemented with Matlab®. The inputs to this network was the pressure differential across the boom cylinder (proportional to lift force) and both cylinder lengths for a total of three inputs. The network was trained for 25 epochs of the input training set until the mean squared error was less than .0005 kg. The

network was then subjected to a new set of input data obtained from the same wheel loader with 3436 kg of payload. The results of this effort are shown in Figure 4.

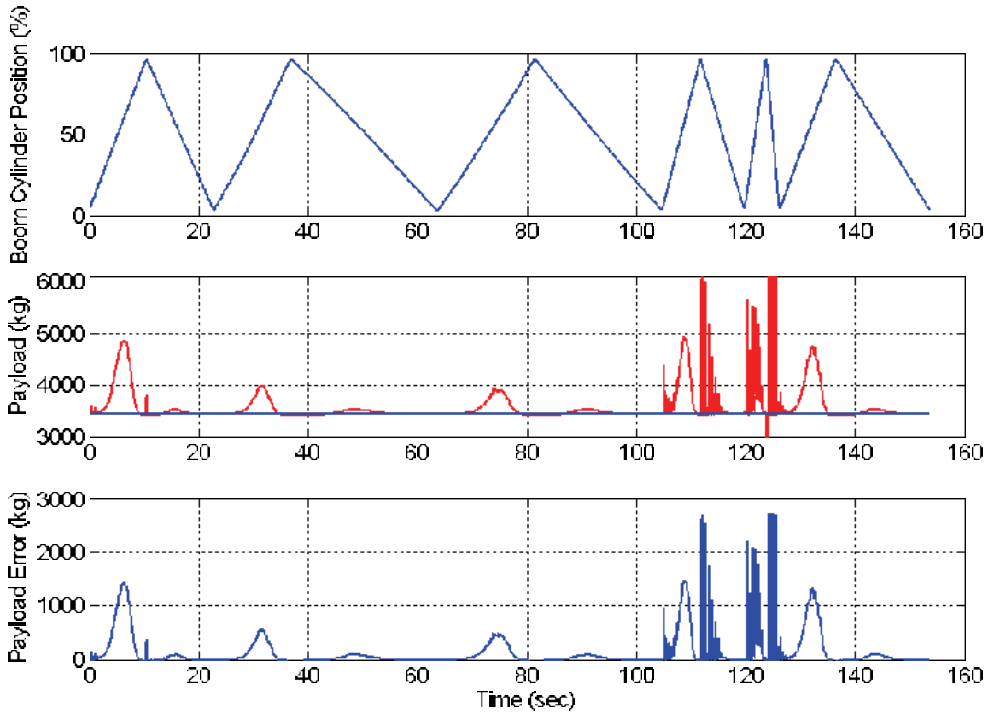

Figure 4: Neural Network Payload Estimate

In Figure 4, the data shown from time zero until 105 seconds consists of boom raise and lower events with the engine at 900 rpm and the machine in a static (not propelling) condition. From 105 seconds to 155 seconds, the machine is being driven at 15kph across rough ground while raising and lowering the boom. It can be seen that during the static boom raise and lower portion of the data, the payload estimate is well behaved with a mean error of 91.12 kg and a standard deviation of 236.3 kg. This performance is only slightly better than utilizing the kinematic model directly. In the dynamic portion of the data, the payload estimate is not well behaved with a mean error of 255.0 kg and a standard deviation of 552.7 kg. This is significantly worse performance than the kinematic model directly.

In an attempt to improve the fidelity of the payload estimate, some changes were made to the ANN. These changes consisted of adding a calculated boom velocity and the kinematic model output as inputs to the ANN. In total, the new topology consisted of five inputs: differential pressure across the boom cylinder, boom cylinder length, bucket cylinder length, boom cylinder velocity, and kinematic model payload estimate. The line of reasoning for attempting this network topology was first to improve the fidelity of the payload estimate with the additional inputs and secondly to determine if the network size could be reduced to reduce the computational burden of the algorithm. The same network utilized previously was trained with the data set containing the additional inputs of boom cylinder velocity and kinematic model payload estimate for 25 epochs of data. The results of this network when simulated using the same data obtained from the wheel loader with 3436 kg payload are shown in Figure 5.

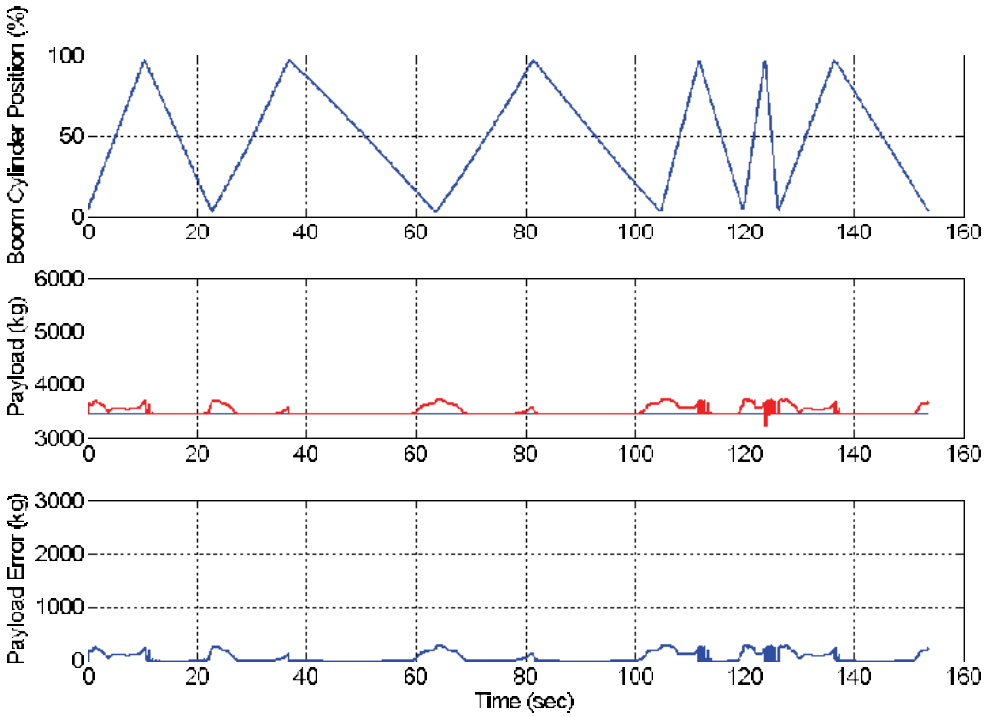

Figure 5: Neural Network Payload Estimate with Velocity and Kinematic Inputs

It can be seen visually, that the results of the ANN trained with the additional inputs is significantly better than the results in Figure 4 without the additional inputs. It can be seen that during the static boom raise and lower portion of the data, the payload estimate is well behaved with a mean error of 74.72 kg and a standard deviation of 77.4 kg. This performance is significantly better than utilizing the kinematic model directly or the ANN without the additional inputs. In the dynamic portion of the data, the payload estimate is nearly as well behaved with a mean error of 75.6 kg and a standard deviation of 80.7 kg. This is also significantly better performance than the kinematic model directly or the ANN without the additional inputs. The worst case error represented in Figure 5 for a 95% confidence interval is 75.6kg +/-158.7kg. More explicitly, the 95% confidence interval is -83kg to +234.3. This represents an accuracy of 3.47% full scale. This error is not less than the 1% full scale required by the industry and thus the algorithm as show, while presenting a significant improvement over the previous algorithms, would not be acceptable. Additional error will be seen as the application moves from being simulated in a floating point, 32-bit microprocessor to the more common fixed point, 16-bit processors of on-board mobile electronics. It is towards the topic of algorithm implementation that the next section is presented.

2.3 Algorithm Implementation

It is important to briefly discuss the computational overhead required to implement the algorithms described above. This discussion is important because any algorithm developed must not only provide 1% full scale accuracy, but also is required to run on the computational resources available on-board the mobile machine. In lieu of delving into the nuances of fixed versus floating point operations and 16 bit versus 32 bit

computations, a general metric of the time to perform the required computations when compiled from C code on a Pentium IV 2.0GHz microprocessor was used.

The kinematic model was developed through a straightforward kinematic chain analysis using a rectangular coordinate system and solving for the algebraic unknowns. This model required .002007 seconds of computation time for each sampled data point on the Pentium IV 2.0GHz processor. The 5x10x10x1 ANN with three inputs required .000006731 seconds of processor time and the 5x10x10x1 ANN with five inputs required .000008558 seconds of processor time. In the case of the ANN with five inputs however, since one of the inputs was the output of the kinematic model, the time required to run this network was the sum of both the kinematic model run time (.002007 seconds) and the five input ANN run time (.000008558 seconds) for a total of .002015558 seconds.

The C code was then compiled for the five input ANN with the kinematic model using a tasking C compiler and run on the 40MHz microprocessor utilized in the on-board microcontroller. The run time for this algorithm as implemented was .126 seconds. It should be noted that this experiment does not include any other computational overhead (i.e. other machine control) that needs to be accomplished at the same time as the calculation and thus would affect processor load. It can be said however that the minimum transport delay between measurement of required data and payload estimate output would be on the order to 126 milliseconds with the five input ANN and kinematic model algorithm. This delay is well within the more typical 500 millisecond update of critical machine performance operation (temperatures, speeds, etc) and deemed acceptable.

3. FUTURE WORK

Future work will focus on improving the payload estimate accuracy through improving the fidelity of the kinematic model with the addition of hydraulic cylinder and pin joint friction models. Additionally, improvements in filtering the pressure and position information will be pursued. Additional work may also focus in determining discrete operating points at which the operator is warned that the estimate may no longer be accurate to reduce the operational requirements of an implemented system. Additionally, the algorithm will continue to be implemented on the actual hardware utilized on the John Deere 644J four-wheel-drive loader to determine real-world accuracy and performance in a variety of conditions.

4. ACKNOWLEDGEMENTS

The authors would like to thank Deere & Company for providing the test vehicle and data with which to develop the algorithm. Specific appreciation is should be given to Cory Brant and Kevin Campbell for collecting the data used in this study.

5. REFERENCES

[1] Tafazoli S., Lawrence, P.D., Salcudean S.E., Chan D., Bachmann S., and de Silva C.W., *Parameter Estimation and Actuator Friction Analysis for a Mini Excavator*, Proceedings of IEEE International Conference on Robotics and Automation. pp. 329-334. April 1996.

[2] Zweiri Y.H., Seneviratne L.D., and Althoefer K. *Parameter Estimation for Excavator Arm Using Generalized Newton Method*, IEEE Transactions on Robotics. Vol. 20, No. 4. pp. 762-767. August 2004.

[3] Tafazoli S., Lawrence P., and Salcudean S., *Identification of Inertial and Friction Parameters for Excavator Arms*, IEEE Transactions on Robotics and Automation. Vol. 15, No. 5. pp. 966-971. October 1999.

[4] Kyrtsos C., and Worrell D., *Dynamic Payload Monitor*, United States Patent 4,919,222. April 24, 1990.

[5] Kyrtsos C., and Worrell D., *Dynamic Payload Monitor*, United States Patent 5,070,953. Dec 10, 1991.

[6] Kyrtsos C., *Dynamic Payload Monitor*, United States Patent 5,105,896. April 21, 1992.

[7] Kyrtsos C., and Gudat A., *Dynamic Payload Monitor*, United States Patent 5,182,712. January 26, 1993.

[8] Karumanchi A., *Dynamic Payload Monitor*, United States Patent 5,509,293. April 23, 1996.

[9] Hagan, M.T. & Menhaj, M. *Training Feed Forward Networks with the Marquardt Algorithm*. IEEE Transactions on Neural Networks. Vol. 5(6). pp. 989993.

PUSHING THE LIMITS

How to Improve Lifetime and Performance of Machines Running Above the Extreme

Ronnie Werndin
Parker Hannifin AB
Pump and Motor Division

SE-461 82 Trollhättan, Sweden
Phone +46 520 404584, Fax +46 520 37105
E-mail: ronnie.werndin@parker.com

ABSTRACT

Today, the lifetime expectance of hydraulic machines can in most cases be fulfilled, mainly due to reasonable system designs and operating conditions within the operation boundaries of the machine. However, in a few applications the operating conditions are pushed beyond the unit specifications. In these cases, the systems are seldom adapted to simplify the life of the machine working under these demanding conditions. One typical example of such an application is the harvesting head saw motor in forestry machines. Requirements on increased productivity and reduced bucking splits, put high demands on fast cuts and have increased the motor speed far beyond the normal operating speed for such a motor. Furthermore, the rapid load changes combined with a non-forgiving system allow even higher speed peaks, hazardous to the motor. Under these conditions, lifetime of the motor decreases due to cavitation and wear.

In order to increase the lifetime of a motor, working under these conditions, speed peaks have to be limited to certain levels and systems has to be adapted to fulfil the need of the motor. As a consequence of speed rise when loosing load the flow needed at the motor will exceed the instantaneous pump flow, with cavitation as a result. Also the shut off method of cutting the flow to the motor, leaves the unit with unsatisfactory inlet conditions with severe cavitation. Furthermore, high inertia forces of the rotating parts at these high speeds will cause wear.

In this paper an overview of the life of a saw motor will be given. Based on this application a new solution for saw motors will be presented, adapted for the demanding life on the edge, fulfilling a reasonable lifetime expectance.

KEYWORDS: fluid power, hydraulic motor, forest machines

INTRODUCTION

In modern timber processing, usage of single-grip harvesters, figure 1, with the cut to length method is pre dominating in Europe and steadily increasing in other regions. The harvester fells, de-limbs and cuts the tree to selected lengths in an ongoing sequence. Forest industry has for a long time increased the productivity. This has put higher demands on the complete timber processing function, where the saw function is a critical part, affecting both productivity and timber quality.

Excellent saw performance is necessary for achieving fine timber quality. Fast cuts minimises the risk of bucking splits, especially if cutting speed can be kept high at the end of the cut, which is most sensitive for bucking splits [2].

When trying to avoid bucking splits and improve the productivity, motor and chain speeds has been increased up to and even above the recommendations from motor and chain manufacturers, this results in degrading the life time expectance of the motor and increases the risk of chain shoot [4].

Today, open loop control of the saw function is most commonly used, which means that motor speed is set by limiting the flow delivered to the motor and the force of the saw bar is set by a static pressure level. Traditionally, these values are set by best practice, trying to keep the speed and pressure drop over the motor as constant as possible throughout the cut. As there is no feedback, the tuning will only be optimal for a small variety of tree species, tree diameters and environmental conditions. This means that re-tuning of the system is needed to avoid reduction in performance, as the properties of the forest changes. Tuning is done manually on the on board computer, is time consuming and affects productivity.

Another interesting question is how the saw function is tuned? What are the criteria for good? Is the sound right? Does it feel right? Every harvester operator has a feeling about what is good or bad, based on experience, but the question is how the “good” corresponds to the highest possible saw performance?

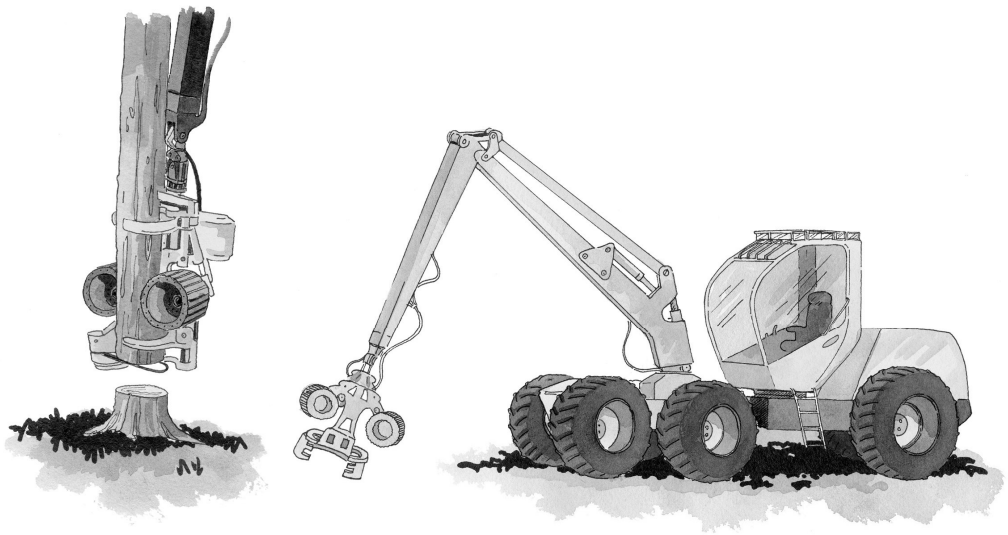

Figure 1. Single-grip harvester.

DEMANDING APPLICATION

The saw motor application in harvester heads is a highly demanding application. The need of fast cuts to avoid bucking splits and to have high productivity has increased the power output of the motor close to the limits of the operating envelope. Traditionally, the increased power has been realized by a higher rotational speed, often high above the specifications of the motor. The systems of today have no function of limiting speed over shoots when going through the log at full system pressure, where the load on the motor disappears. As a consequence the flow needed at the motor will exceed the instantaneous pump flow, with cavitation as a result, figure 2. These speed peaks can in worst case be as high as above 50% on top of the already high rotational speed, where the high inertia forces of the rotating parts will cause wear, figure 3. Finally, the shut off method of most systems of today, where the flow to the motor is stopped, leaves the unit with unsatisfactory inlet conditions and severe cavitation, unless a high return pressure can be maintained during the deceleration of the motor, allowing the anti cavitation function to work properly, figure 2. Working under these conditions, the lifetime of the saw motor is reduced due to cavitation and wear, unless these areas can be avoided.

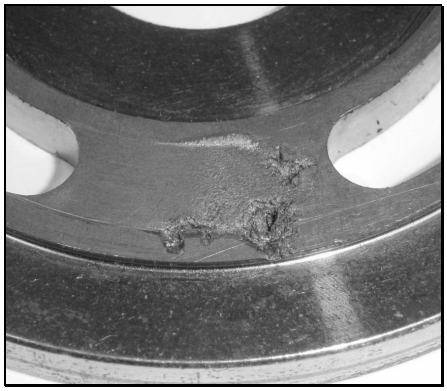

Figure 2. Valve plate with cavitation wear due to bad operation conditions.

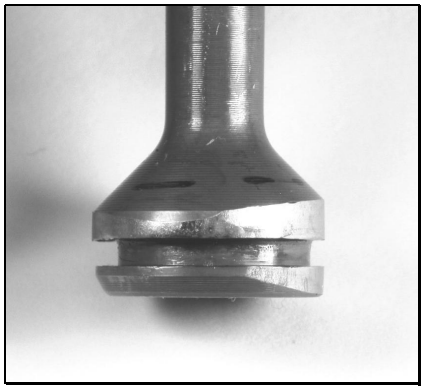

Figure 3. Piston with severe high speed damages.

DEDICATED SAW MOTOR

In order to guarantee satisfying operation conditions for the saw motor working close to the extremes in the demanding harvester application, a dedicated motor adapted for the application is needed. During the development of the new, Parker F11-19 iP, saw motor, figure 4, two major areas has been focused on, lifetime and performance. To maintain a reasonable lifetime in such a demanding application, full control of the operating conditions has to be fulfilled. The unit has to guarantee that no over speeding and no cavitation occurs during operation, which both have impact on the lifetime.

As high performance is of great importance for the cutting function, resulting in high timber quality and high productivity, a coordinated control of motor speed and saw bar feed rate has to be realized. To coordinate the control of chain speed and saw bar feed rate, means maintaining a controlled chain speed throughout the cut independent of tree species and environmental conditions. It also means adapting automatically to available pressure level, using highest possible power to the cut [1], resulting in high cut performance and minimising the risk of bucking splits.

To further enhance the productivity, the patented Power Boost™ solution is integrated in the design, minimising the internal losses and thereby increasing the efficiency at high rotational speeds, giving an extra 3-5kW output power.

Including the solution in the motor is beneficial in many aspects and a necessity regarding the ability to avoid speed overshoots. If the intelligence is integrated in the motor, it comes as a complete package ready to install, no further intelligence in the surrounding system is needed. The control is independent of changes in the base machine system, resulting in a robust function without additional tuning.

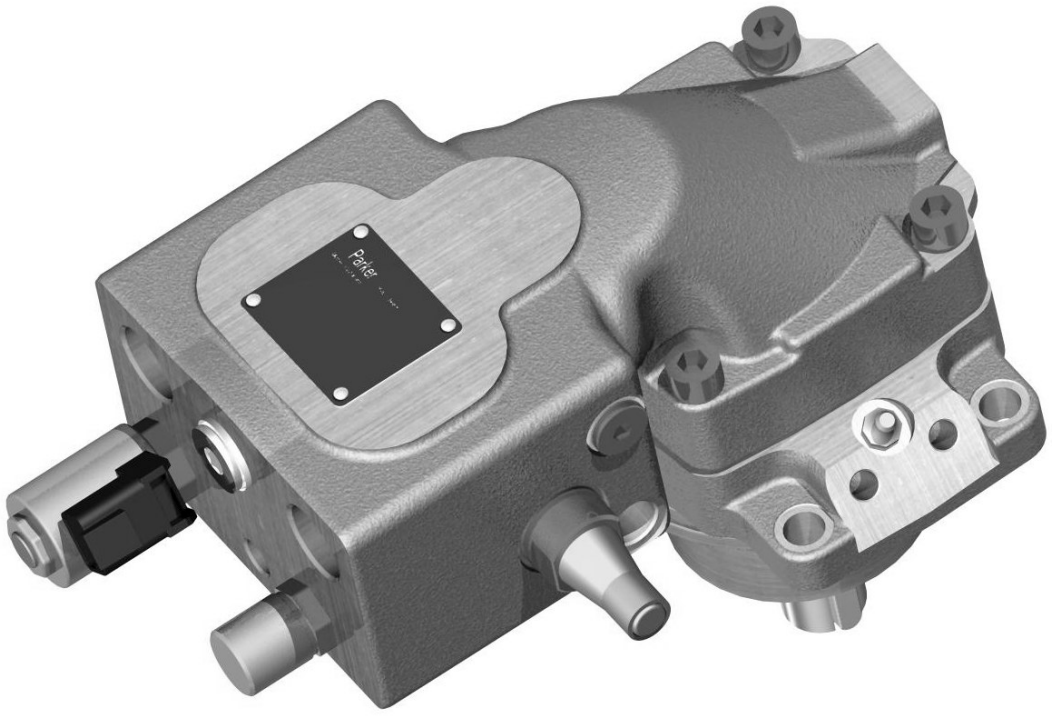

Figure 4. Parker F11-19 iP, dedicated saw motor.

PRINCIPLE

The speed control system is designed to keep rotational speed constant and below a maximum set value. During cutting, feed rate of the saw bar is dynamically controlled to meet the reference speed of the motor, utilizing all available system pressure. When going through the log, a meter-out compensator will activate and avoid speed over shoots. The same compensator is also used to start and stop the unit by bypassing the controller. Thereby, the critical areas of over-speeding and cavitation are avoided.

As the system has an active control of the saw bar, based on the rotational speed, it will adopt regardless of species of tree, diameter, weather, etc. and keep the highest possible torque on the motor by increasing or decreasing the feed rate dynamically to maintain the wanted motor speed. Consequently, feed rate will also increase at the end of the cut as the effective area of the log becomes smaller, increasing the cutting speed and minimising the risk of bucking splits [2].

The choice of a pure hydraulic control with the exception of an electrical on/off control is natural. The high acceleration have the potential of realising 50% speed overshoots in less than 20ms, putting high demands on response time of the system. This can be realized by a hydraulic control. Finally, the hydraulic control gives a robust and reliable solution in the harsh environment of the harvester head.

Furthermore, when operating at high rotational speeds, churning losses due to the oil filled housing becomes important. By adding the Power Boost™ solution, which reduces the viscous friction inside the housing, these losses can be minimised, adding an extra 3-5kW output power, figure 5.

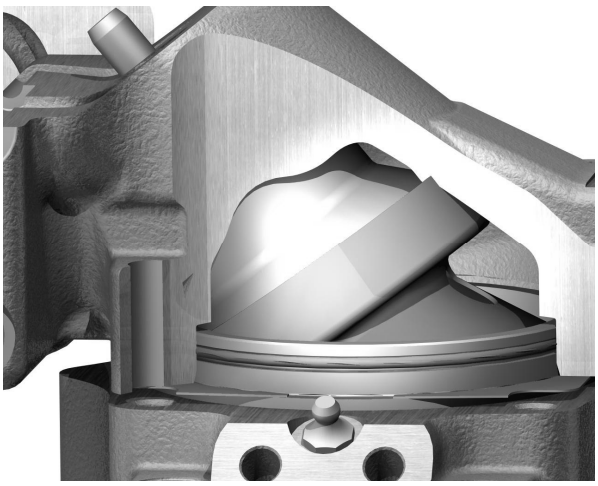

Figure 5. Power Boost™ insert.

RESULTS

During the development, several tests in laboratory have been performed. These tests have shown good results, both regarding increased productivity and avoidance of cavitation and over speed damages. In the life test, the saw motor was cycled in a process simulation where the unit was accelerated, loaded and decelerated repeatedly for 3.9 Million cycles before it was decided to be stopped, this without any signs of either cavitation or over speed damages, figure 6-8.

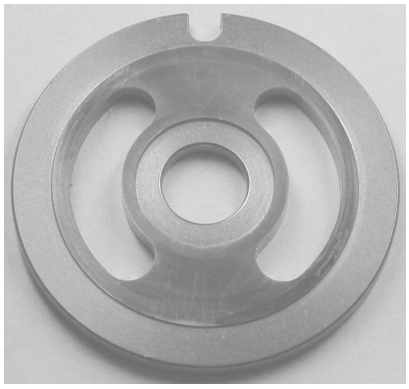

Figure 6. Valve plate after 3.9 million cycles.

Figure 7. Piston after 3.9 million cycles.

Figure 8. Cylinder barrel after 3.9 million cycles.

Results from different field tests have proved that no tuning is needed; best performance is achieved regardless of tree species, if it is frozen/non frozen etc. Furthermore, an increased productivity has been realized due to the coordinated speed/saw bar feed control, which adapts the feed force dynamically to achieve a controlled chain speed throughout the cut, figure 9. This is done using all available system pressure at the same time, figure 10, allowing all available power in to the chain, making a cut as quick as possible.

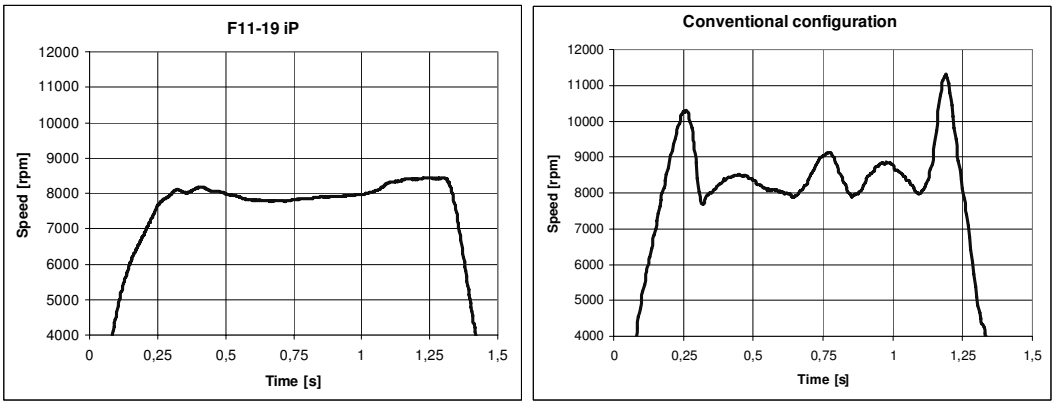

Figure 9. Comparison of motor speed during a cut sequence (field measurements). Left; Parker F11-19 iP, right; Conventional saw motor system.

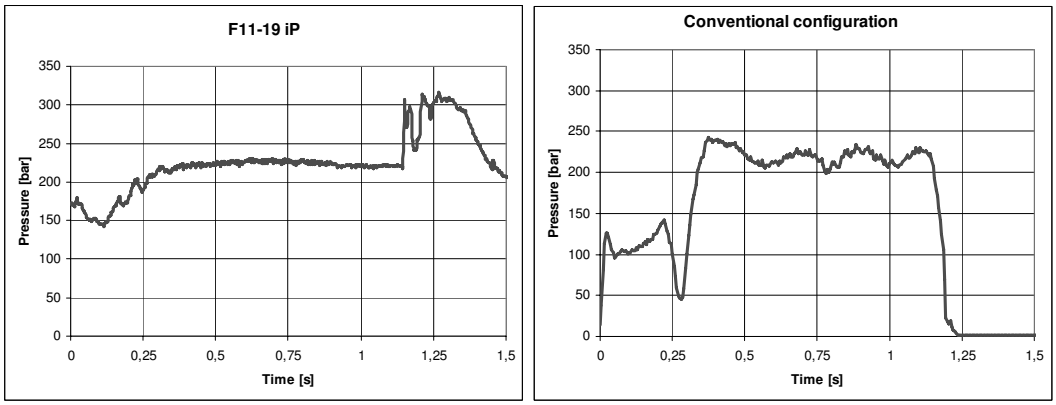

Figure 10. Pressure level during cut sequence (field measurement). Left; Parker F11-19 iP, right; Conventional saw motor system.

Field measurements have shown improvement up to 45% regarding the cutting performance, measured as cross-sectional surface of cut per second [cm^2/s], compared to conventional systems at same chain speed reference (40 m/s). Even compared to conventional system at higher chain speed (56 m/s), improvement is still as high as 17%. Adding the Power Boost™ increases the possible output power by an extra 3-5kW which improves the cutting performance even more, increasing the values above to 60% and 30% respectively, figure 11 and 12.

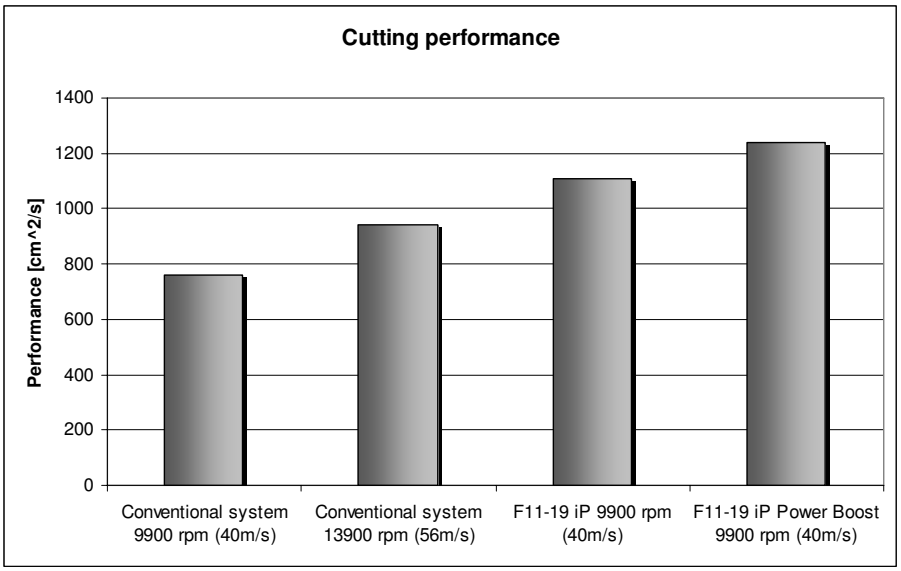

Figure 11. Comparison of cutting performance, from left to right: conventional system at normal speed, conventional system at over speed, F11-19 iP at normal speed without Power Boost™ and F11-19 iP at normal speed with Power Boost™.

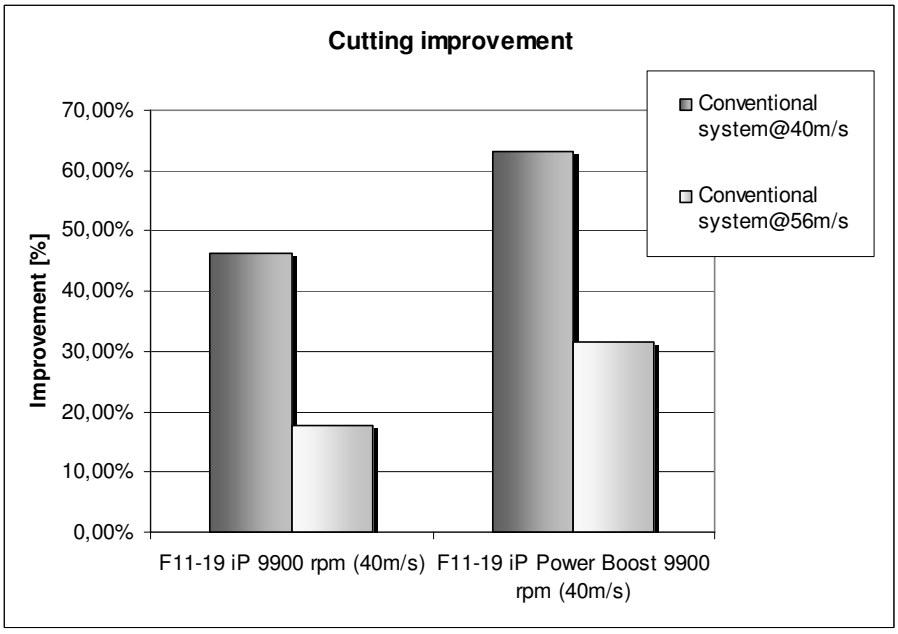

Figure 12. Comparison of improved cutting performance. Form left to right: F11-19 iP without Power Boost™, compared with conventional system at normal speed and over speed, F11-19 iP with Power Boost™ compared with conventional system at normal speed and over speed.

REFERENCES

[1] Patterson, M. J., *"OREGON® 16H & 18H SAW CHAIN Performance and application"*, Technical report, August, 1998.

[2] Hallonborg, U. & Granlund, P. *"Färre kapsprickor med rätt teknik"*. Skogforsk Resultat Nr. 19/1999. 4 p. (in Swedish).

[3] Inberg J., "The Problems of timber cutting in forest machines", Proc. Of 1st FPHNI-PhD Symposium, pp. 23-32, Hamburg, 2000.

[4] Oregon, "Mechanical Timberharvesting Handbook", March 15, 2004.

MODE SWITCHING AND ENERGY RECUPERATION IN OPEN-CIRCUIT PUMP CONTROL

Kim Heybroek, Jonas Larsson and Jan-Ove Palmberg
kimhe@ikp.liu.se, jonla@ikp.liu.se, janpa@ikp.liu.se
Fluid- and Mechanical Engineering Systems
Department of Mechanical Engineering
Linköpings Universitet, S-581 83 Sweden

ABSTRACT

Today's mobile machines most often contain hydraulic valve controlled drives in an open loop circuit. For the purpose of saving energy, the constant pressure pumps have in the past frequently been replaced by load-sensing pumps and load-sensing valves. However, considering applications where the load is helped by the gravitational force, even these hydraulic systems often suffer from poor efficiency. In this article, a novel pump-controlled hydraulic system is studied where energy recuperation from lowering motions is possible. The pumps are fully displaceable in both directions, working as motors when lowering loads. The amount of recuperated energy is highly dependent on the chosen control strategy, the hydromechanical properties as well as the target application. Furthermore, the article describes how valve design becomes an important feature in an attempt to reach high efficiency and machine operability.

KEYWORDS: pump control, open circuit, energy efficiency, energy recuperation

1 INTRODUCTION

In mobile applications load-sensing solutions have significantly reduced energy consumption. However, in applications with unequal drive pressure levels the load sensing systems still result in energy losses, referred to as metering losses. In addition to these losses, most hydraulic systems today do not include the possibility to recuperate the potential energy stored in elevated loads, when these are lowered. Previously, several authors have shown that so called pump control or displacement control is a strong competitor in the energy efficiency debate because of its comparatively few loss elements and versatility in control [1–4]. However, in few of these articles is the utilization of energy recuperation is examined to any great extent, if even mentioned.

The main purpose of this study is to describe how well the open-circuit solution, previously presented by the author [5], can recuperate energy in lowering motions, depending on the chosen control strategy, and how the recuperated energy can be utilized by the application in hand. Furthermore, a theoretical linear analysis and non-linear simulations demonstrate the challenges in the an energy efficient load lowering mode, referred to as the differential mode.

2 OPEN-CIRCUIT SOLUTION

In this paper the author has studied a hydraulic system configuration where each actuator/-supply system comprises a variable displacement pump/motor working in an open-circuit together with four separate valves, see Figure 1 . The four valves render a concept versatile in control, as the cylinder chambers can be connected to pump and/or tank as well as be closed at any time. The concept effectively eliminates the metering losses; it has the potential of energy recuperation and enables a four quadrant load actuation.

In either operation quadrant the load speed is controlled directly by the relative pump displacement. The pump controller is capable of switching between displacement control and pressure control in case of excessive pressures. The valve configuration allows loads to be lowered in several different ways. Similar to conventional load-sensing systems, flow-control via the meter out orifice to tank (A-T) is possible. This manner of lowering a load is what we try to avoid in this study, as all potential load energy will be converted to heat in the orifice, thus accounted for as an energy loss. In contrast to this, the author of this study looks upon the advantages of letting lowering flow go through the pump (A-P), controlling the load speed by adjusting the relative pump/motor displacement. This can be achieved either by letting all flow from the piston chamber go to the pump, referred to as "normal lowering"; alternatively, the flow can be divided into one part going to the pump and the other to the piston rod chamber (P-B). This approach is referred to as "differential lowering" and can be seen as a pressure-flow transformation resulting in a decreased amount of pump flow needed to achieve the same piston speed. Since a pump/motor has a limited flow capability at a certain engine speed, the differential mode will make it possible to lower loads faster without increasing the pump size. On the other hand, the pressure level will increase at the same rate, making the load capability lower. An apparent advantage of the differential mode is that the cavitation issue in "normal lowering" is intrinsically solved as flow is taken directly from the piston chamber.

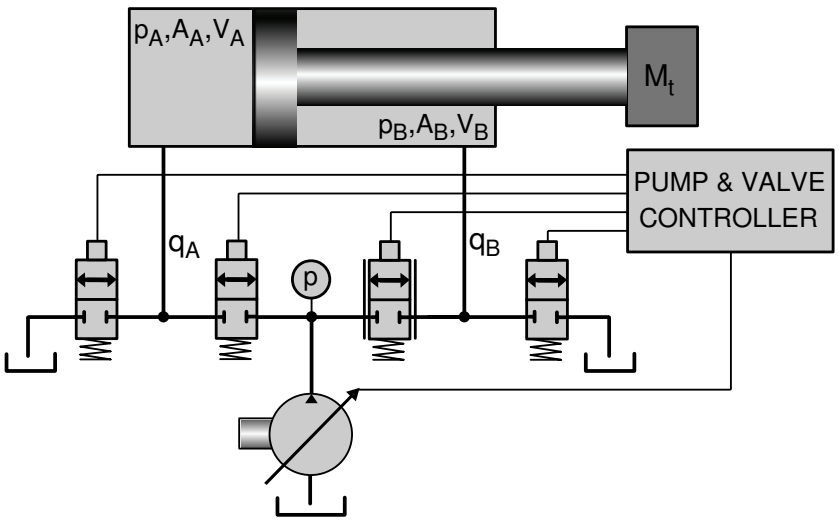

Figure 1: Pump controlled open-circuit solution

2.1 Valve Configuration

For good functionality of the open circuit solution the valves that are used for mode switching in the change of operation quadrant, must meet certain requirements. They must have a relatively high bandwidth, provide a "soft closing" in addition to producing low pressure losses at high flows. The valve configuration must also incorporate anti-cavitational capabilities for the load side. To meet these demands, four seat valves of the valvistor type have been chosen for each working cylinder. The valvistor is shown in Figure 2(a). In the main poppet there is an inner orifice that consists of a small rectangular slot with a total area that equals the pilot valve maximum orifice area. When the pilot valve opens, x_{pilot}, the pressure, p_c, will decrease and the poppet force equilibrium yields a poppet displacement upwards, x_{pop}, until the slot orifice area equals the pilot orifice area. Hence, the valvistor is a follower servo. More details on the functionality of the valvistor are presented by Eriksson, B. [6]. In this study the standard valvistor, originally presented by Andersson, B. [7], has been modified to allow flow control in both directions, see Figure 2(b). This modification is necessary to achieve the desired recuperative lowering motions, when flow from the load cylinder is taken back via the pump/motor.

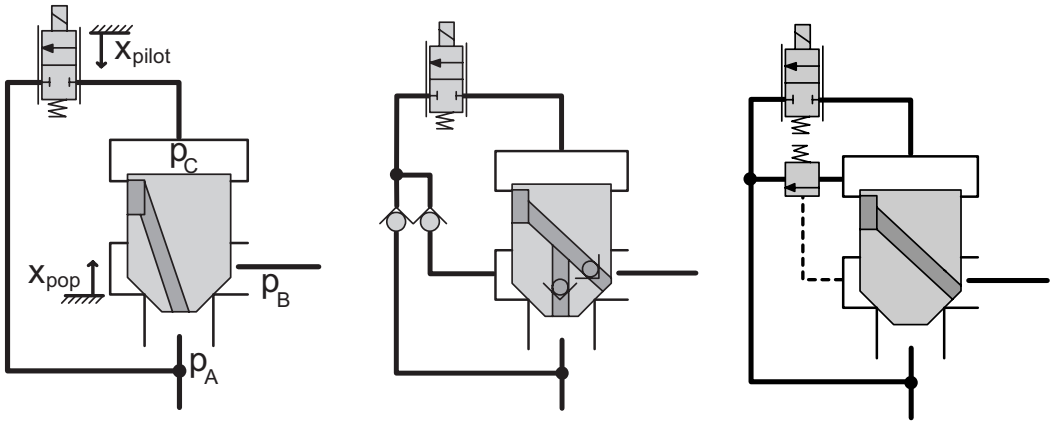

(a) A-type valvistor (b) Bi-directional valvistor (c) Pressure limited valvistor

Figure 2: Different valvistor configurations

There are several reasons why the valvistor has been chosen for this concept. First, the dynamics of a valvistor is generally described as a first order system, which in this case brings out the advantageous property of soft valve closing which is good as the valve is used for fast mode-switching. Furthermore, the valvistor is suitable as a load holding valve because of its inherently great stiffness against pressure disturbances as well as low leakage properties in closed condition. Moreover, the valvistor pilot circuit can in a simple manner be complemented with a pressure relief function, see Figure 2(c). The valvistor yields cost efficient and compact solutions since the pilots are relatively small due to the high flow gain from pilot stage to main stage. The open-circuit solution with valvistors inserted to it is illustrated in Figure 3.

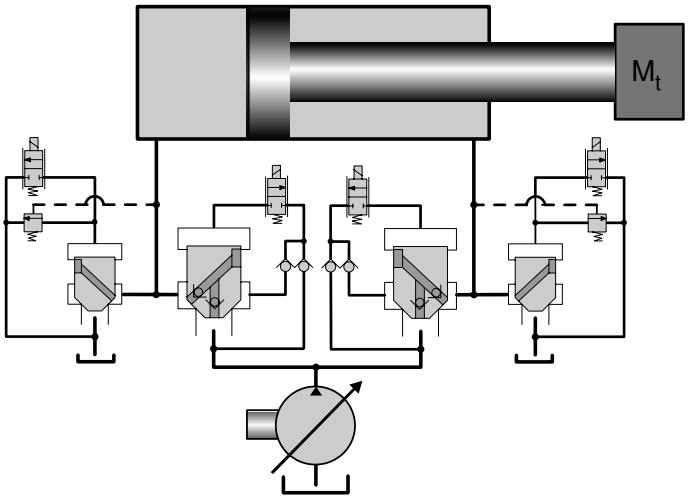

Figure 3: Open-circuit solution with four valvistors implemented

2.2 Energy Management

The open-circuit has no hydraulic accumulators or other chargeable devices, which means that all potential energy must be consumed while it is recuperated. The load energy is transferred via the pump/motor shaft, through a power take-out (PTO) to all other energy consuming functions as well as back to the primary power source. Consequently, other energy consumers must be present, otherwise the power loss, which usually takes place in a meter out orifice, has merely been replaced with a power loss in engine friction.

In the following fictive example the open-circuit solution is implemented in a wheel loader. Concerning the hydraulics, the lowering power generated by the load could be used to help all other hydraulic pumps attached to the PTO to power their functions respectively, see Figure 4. For example, bucket lowering and the steering function, or tilting, are often used simultaneously, [8]. Another interesting possibility is to transfer recuperated power to the vehicle drivetrain via the combustion engine. Furthermore, the speed of the cooling fan motor could be increased when recuperated power is available. By doing so the fan could work at lower speed during the rest of the working cycle, consuming less energy.

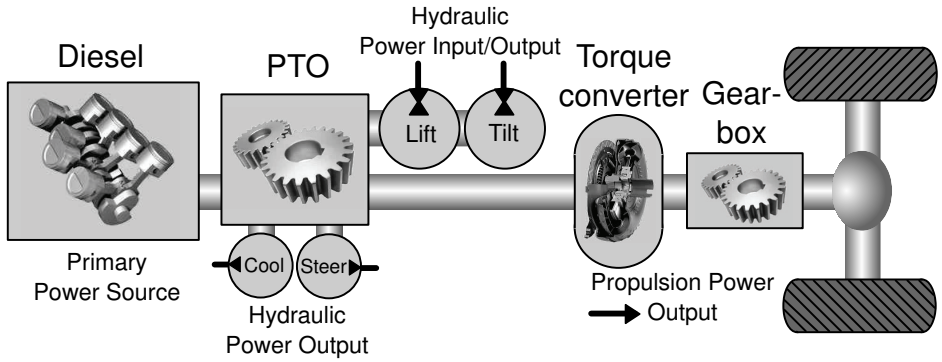

Figure 4: Energy distribution of recuperated energy in a wheel loader application

One must note that the most energy efficient operator driving characteristics for a conventional hydraulic system are not the same as for the system presented here. In the open-circuit solution, the operator can affect the energy efficiency, to a much greater ex-

tent, for example by letting the load lowering drive the vehicle backwards when reversing out from a truck. Figure 5 illustrates the potential load energy versus the required energy while lowering a load in a typical loading cycle of a wheel loader with load-sensing hydraulics. The black area in Figures 5(a) and 5(b) represents the sum of the energy required by the steering, propulsion and cooling for the lifting and tilting functions respectively. The grey area is the ideally recuperable energy for each function. While lowering the bucket, cooling is a relatively small energy consumer compared to the energy required for vehicle propulsion backwards as well as for steering. When the bucket is tilted out, there is not much other activity to consume the potential load energy; this operation consequently requires either a change in control strategy or increased engine rpm. However, in using the potentially recuperable energy in the present solution the total hydraulic energy consumption for this loading cycle will be reduced by 5-10%. In a future solution the surplus power can be transferred to a hydraulic or electric buffer, which would save approximately another 5%.

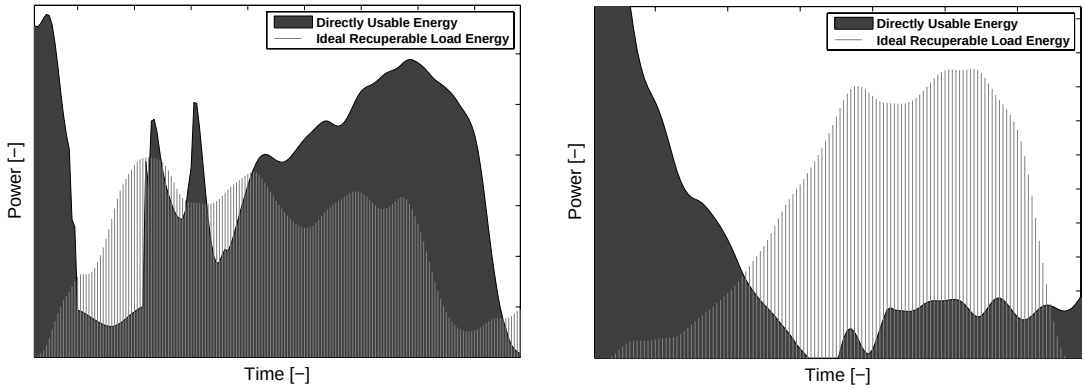

(a) Recuperation potential in lift function (b) Recuperation potential in tilt function

Figure 5: Recuperable energy in a typical loading cycle of a wheel loader

To choose the most energy optimal control strategy for the working hydraulics, the system controller must be capable of estimating the total available power online as well as the total required energy. One way to implement this is to supervise the diesel engine, and compute what power it generates. Also, the total power take out must be estimated online. In practice these actions often require extra transducers installed on certain components. In case of recuperative motions, the control system must also define where recuperated power can be consumed, i.e. by other working hydraulic functions or by the powertrain.

3 RECUPERATION EFFICIENCY

Figure 6 illustrates the working range for various lowering modes. The axis pointing upward is the recuperation efficiency, η. Here a cylinder area ratio, κ=2/3, is used together with a pump of typical size for a medium sized construction machine. For simplicity the desired maximum lowering speed is set to three times the maximum lifting speed. As seen in Figure 6(a) full energy recuperation can only be achieved up to a third of the desired lowering speed because of the limited pump capacity. In Figure 6(b) the cylinder area ratio makes it possible to lower at the desired speed, but because of the pressure increase,

only a third of the desired loading capability can be obtained. The figures show that the overall potential in energy recuperation is the same in both cases, but depending on the most common point of operation one of the solutions is better than the other. In applications where lowering with high speeds and low loads is the most common, the differential mode is the most advantageous. When it is more common to lower heavy loads at low speeds, the normal mode is to be preferred. For example, if the application is a wheel loader loading gravel, the bucket is usually lowered empty at high speed; hence would the differential mode be more appropriate. However, where switching between these two modes is possible, higher recuperation efficiency could be obtained over a greater working range, illustrated in Figure 6(c).

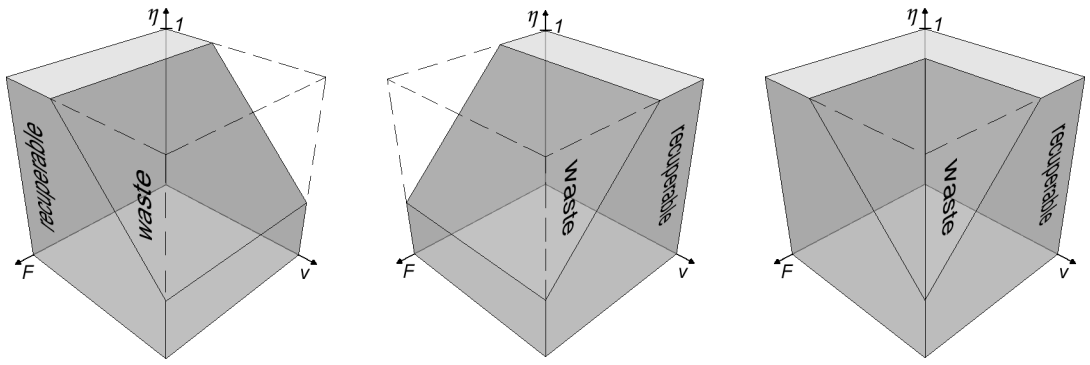

(a) Normal lowering mode (b) Differential lowering mode (c) Differential/normal lowering mode

Figure 6: Ideal efficiency regarding maximum system pressure and pump flow

In order to realize the normal lowering over the whole working range one must control flow to tank over an orifice to reach speeds exceeding the maximum pump capacity, thus decreasing the recuperation efficiency. In the differential case, one must instead restrict "the degree of" differential mode at higher loads to avoid the maximum pressure level. In practice, this can be achieved by using a valve, that senses the pressure level in the piston chamber, which for a given maximum pressure level, starts closing the connection between the cylinder chambers (Figure 7(a) in Section 3.1), converting all power related to the pressure exceeding the pre-defined maximum level to heat. If this valve closes completely, normal mode is achieved, and flow to the piston-rod chamber must instead be taken from tank (T-B). See Section 3.1-3.3 for further analysis in this subject. However, the most obvious difference between these two solutions is that the differential mode requires pressure control of an orifice while the normal mode requires flow control over an orifice. The most energy efficient strategy is determined according to the application and under what working conditions the machine usually operates. Given that point of operation, one can decide which solutions is the most suitable. In case a mode switching solution is selected there are of course important changes in system properties to consider. For example in case of going from normal mode to differential mode not only the pressure level will change but also the dynamic load properties, such as hydraulic hydraulic damping and eigenfrequency.

3.1 Static Calculations

To demonstrate the basic functionality of the system, operating in the differential mode, a static model was constructed on the basis of the system shown in Figure 7(a). Here the control valve, which is a normally open pressure limiter, is mounted directly in the main circuit to simplify the calculations. The flow through the valve is given by the orifice equation, Eq.1

$$q_B = K_s \cdot (x_{max} - x_v) \cdot \sqrt{p_A - p_B)} \tag{1}$$

where K_s is the orifice coefficient and x_v is the valve closure. The static force equilibrium is given by Eq. 3

$$-p_A \cdot A_{red} + k_s \cdot l_s + k_s \cdot x_v = 0 \tag{2}$$

In this model the fluid compressibility and the valve dynamics have been ignored. Neither has cavitational effects been taken into account. This yields a piston speed, v_p, directly proportional to the pump flow, independent of the valve closure.

$$v_p = \frac{q_p}{A_A} \cdot \frac{1}{1-\kappa} \tag{3}$$

The input variables to the calculation are pump flow, q_p, and load force, F_L. In Figure 7(b) the pump flow is kept constant and the load force is ramped up from zero (right axis). When the pressure level (left axis) has reached the pre-defined cracking pressure (25 MPa in the figure), the pressure in the piston chamber, p_A, is kept at a fairly constant level and the other pressure, p_B, is closing up to zero as the load force increases further.

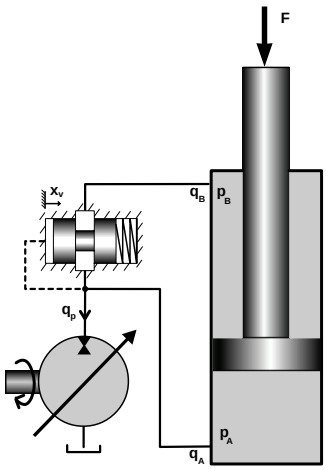

(a) Simplified system, base for static calculations

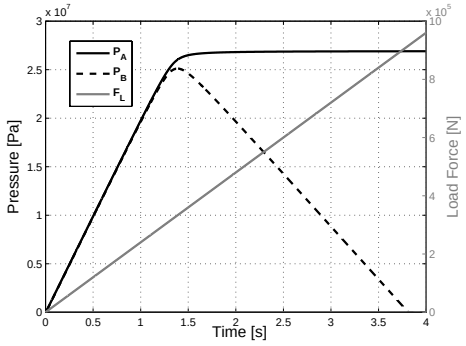

(b) Static pressure response to applied load pressure

Figure 7: Static behavior of system pressure limiter

3.2 Linearized Model

The static calculations in Section 3.1 are good to describe the conceptual idea of the pressure limiter, but to get a better understanding of the dynamic system behavior a linearized model is derived.

A realistic linear model can be concieved from the physical equations described in Section 3.1 along with equations for the load dynamics. After linearization and Laplace transformation of these equations, Eq. 5–9 are obtained.

$$\Delta Q_A = \Delta Q_B \tag{4}$$

$$\Delta Q_B = K_q \cdot \Delta X_v + K_c \cdot (\Delta P_A - \Delta P_B) \tag{5}$$

$$\Delta P_A = (-\Delta Q_A + s \cdot \Delta X_p \cdot A_A) \cdot \frac{\beta_e}{V_A \cdot s} \tag{6}$$

$$\Delta P_B = (\Delta Q_B - s \cdot \Delta X_p \cdot A_B) \cdot \frac{\beta_e}{V_B \cdot s} \tag{7}$$

$$\Delta X_p = \frac{\Delta P_B \cdot A_B - \Delta P_A \cdot A_A + \Delta F_L}{M_t \cdot s^2 + B_p \cdot s} \tag{8}$$

To further consider the valve dynamics, the pressure limiting valve is looked upon according to Figure 8. After linearization and Laplace transformation the valve closure ΔXv is given by Eq.9.

$$\Delta Xv = -\Delta P_A \cdot \frac{C}{1 + T_r \cdot s} \tag{9}$$

, where the constant C is related to the spring coefficient, k_s, and pressurized area, A_{red}, within the valve pressure-sense port.

$$C = \frac{A_{sen}}{k_s} \tag{10}$$

and T_r is a time constant, determined by properties related to the spring as well as the sense-channel volume and orifice.

$$T_r = \frac{k_s V_{sen} + \beta_e A_{sen}^2}{k_s \beta_e K_{c,sen}} \tag{11}$$

Interesting for further analysis is the transfer function from external load disturbance, ΔF_L, to the change of pressure in the piston chamber, Δp_A. The algebraic solution to this closed loop circuit, computed in a typical operating condition for a construction machine, yields a fourth order transfer function.

$$G_{sys} = \frac{\Delta P_A}{\Delta F_L} = \frac{(s+\omega_1)(s+\omega_2)}{(s+\omega_3)(s+\omega_4)(\frac{s^2}{\omega_5^2} + \frac{2\delta_h s}{\omega_5} + 1)} \tag{12}$$

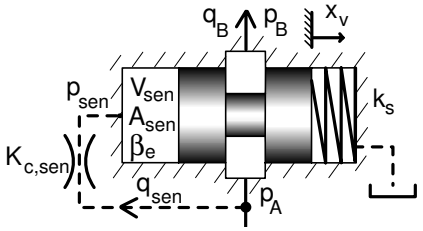

Figure 8: Assumed valve functionality

3.3 Stability of the Linear Model

The C-value is determined by what pressure level, p_{max}, beyond the cracking pressure level, p_{crack}, is acceptable before the pressure limiter should be completely closed.

$$x_{max} = (p_{max} - p_{crack}) \cdot \frac{A_{red}}{k_s} \tag{13}$$

which along with Eq10 yields the C-value

$$C = \frac{x_{max}}{(p_{max} - p_{crack})} \tag{14}$$

Furthermore, there are physical restrictions on the valve properties, such as the choice of a realistic spring coefficient as well as size of the pressurized area in the sense port, see Eq. 10. Also the minimum diameter of the valve orifice is critical as cavitation on the piston rod chamber must not occur at full lowering speed. For example, in a 350 bar system the cracking pressure is set to, say 250 bar, then at 350 bar the valve should be completely closed. In this case $C = 1 \cdot 10^{-9}$ is a suitable value in order to get an appropriate valve size and closure.

If the cracking pressure is set closer to the maximum this yields a higher C-value. Looking at the poles of the transfer function in Eq. 12, an increase in C-value eventually leads to system instability. How the other system parameters, such as cylinder area ratio, working volumes and inertia load affects the limit for instability is rather complex. However, for a given application, these properties are known, only leaving out the properties of the pressure limiting valve as design parameters. Except for the C-value, the adjustable parameters are; the valve time constant, T_r, described by Eq. 11 and the geometric characteristics of the valve, described within K_q and K_c in Eq 5. In practice, an increased value of T_r corresponds to a slower valve response to pressure increase. This would intuitively mitigate the risk of instability as the dynamic pressure build-up, will not be as remarkable as the valve will react slowly, adopting its closure only to static changes in pressure. In Figure 9 the system damping is shown for a set of realistic C and T_r values, linearized close to the valve cracking pressure.

The black plane illustrates where the system damping is zero, thus marginally stable. Seen in Figure 9(b) high C-values can be chosen either by using a very fast valve or quite a slow valve. Note that without the pressure limiting valve, the system damping is zero as

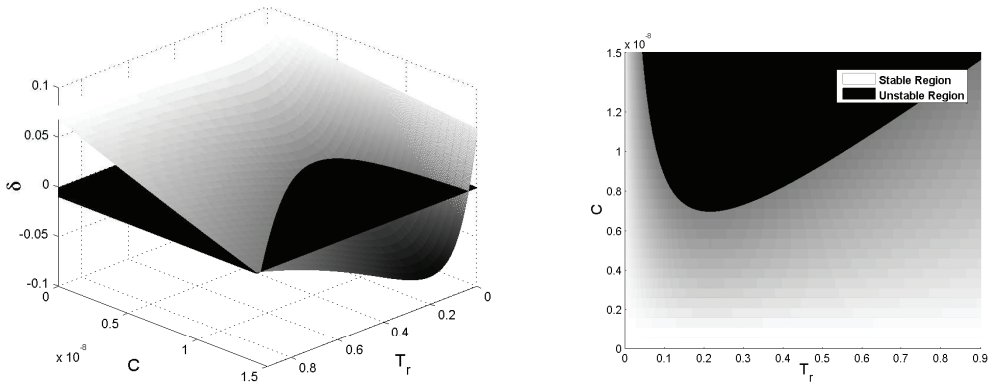

(a) Hydraulic damping in respect to T_r and C

(b) Stable region in respect to T_r and C

Figure 9: System damping and stability when linearizing at valve cracking pressure

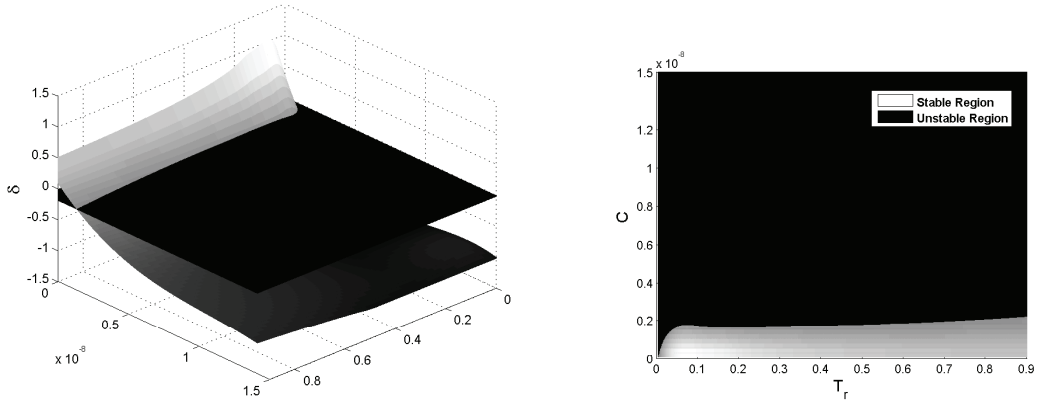

(a) Hydraulic damping in respect to T_r and C

(b) Stable region in respect to T_r and C

Figure 10: System damping and stability region when linearizing

this is an ideal pump controlled system. This stable region will be greater in case further system damping is introduced, such as friction and leakage. However, as G_{sys} in Eq.12 will change with a different point of linearization, the stability region will also change. Figure 10(b) illustrates the stability region when the valve opening is chosen closer to zero. The stable region is now substantially smaller and will become even smaller as the valve closes further. Here, it still helps to use a higher value in T_r but eventually no realistic value is good enough to maintain stability.

3.4 Non-linear Model

To proceed with the analysis and to get a better understanding of the instability issue, described in Section 3.3, the system was modelled in Modelica. Complementing the static system of equations, in Section 3.1, with the missing dynamic equations for the load and the valve, a dynamic and non-linear model is conceived. Moreover, the main orifice and the sense-channel orifice are both modelled as turbulent restrictors, seen in Figure 11.

The load case parameters are the same as for the linearized model in previous section. The C-value is still described by Eq 10, but T_r is now determined by the properties of the sense-channel turbulent restrictor and will hence vary with valve closure. However,

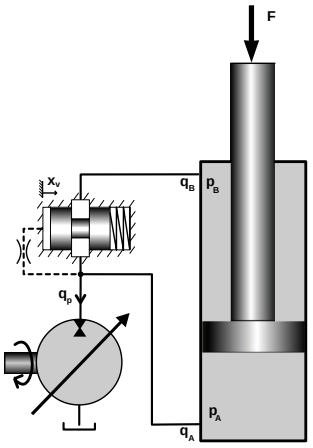

Figure 11: Base for non-linear model

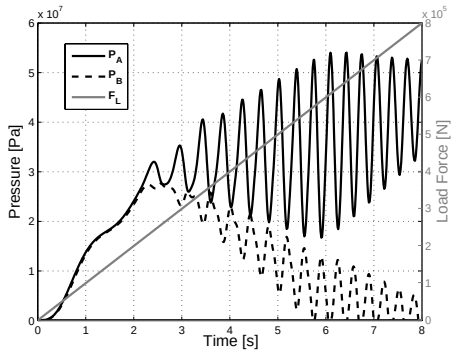

(a) Dynamic pressure response to applied load pressure, low T_r-value

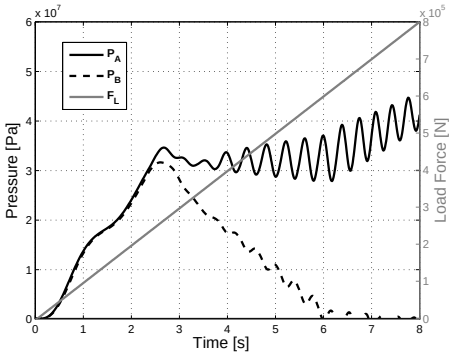

(b) Dynamic pressure response to applied load pressure, high T_r-value

Figure 12: Non-linear, dynamic pressure response of system pressure limiter

making the restrictor area smaller will of course still increase the Tr-value, given the same pressure level. Furthermore, a higher T_r value will dynamically increase the cracking pressure which is statically given only by the C-value. In Figure 12(a) the instability issue is obvious. In this figure, a very fast valve has been used, low T_r-value. In Figure 12(b) a higher T_r-value is used, thus a more stable behavior is shown even though instability is a fact as the valve opening approaches zero.

4 FUTURE WORK

The open-circuit solution will be implemented in a full scale wheel loader, where it will be evaluated in respect to energy efficiency and operability. Different ways of recuperating energy from the lowering motions will be evaluated, especially the strengths and weaknesses of the differential mode. The hydraulic solution of the differential mode presented in this article, will be further investigated. This solution and its instability issues are familiar from previous investigations on the dynamic properties of the over-center valve, by Persson, T. [9]. His work will be an inspiration for further research. An alternative solution to the differential mode is to accommodate electro-hydraulic pressure control of an orifice, thus making the control strategy more flexible. Concerning implementation, the pressure limiting valve will be implemented in the valvistor valve configuration.

5 CONCLUSIONS

The chosen valve configuration for the open-circuit carries out a flexible solution that allows the working hydraulics to lift and lower loads in several different modes of operation. In a wheel loader application the energy recuperated from load lowering can in many cases be used immediately by for instance vehicle propulsion and/or other hydraulic functions. Furthermore, the advantages with normal lowering mode versus differential lowering mode have been investigated. Which mode is the most suitable depends on what the operator is trying to do. To achieve an energy efficient load lowering the choice of mode depends on the requested speed, the magnitude of the load as well as pump/motor efficiency at that given operating condition. Moreover the possibility to switch between

normal mode and differential mode is an interesting aspect regarding increased efficiency. In this study a hydraulic solution to the differential mode is suggested and analyzed. The suggested pressure limiting valve demonstrates an unstable behavior when its valve closure approached zero. This behavior is explained by the dynamic pressure build-up, present in the up-stream volume due to the increased valve closure, amplifying the load pressure which further closes the valve.

6 LIST OF NOTATIONS

Quantity	Description	Unity
A_A, A_B	Effective area, piston chamber, piston rod chamber	m^2
A_{red}	Pressurized area in pressure limiter sense port	m^2
B_p	Viscous cylinder friction coefficient	$\frac{Ns}{m^2}$
C	Valve closure coefficient, $\frac{A_{red}}{k_s}$	$\frac{m^3}{N}$
F_L	Load disturbance force	N
G_{sys}	Transfer function from ΔF_L to ΔP_A	$\frac{1}{m^2}$
β_e	Bulk modulus	Pa
κ	Cylinder area ratio	$-$
δ_h	Hydraulic damping at the hydraulic resonance frequency	$-$
ΔF_L	Linearized load disturbance force	N
ΔP_A, ΔP_B	Linearized pressure acting on A_A, A_B	Pa
ΔQ_A, ΔQ_B	Linearized flow from/to the cylinder chambers	$\frac{m^3}{s}$
ΔX_p	Linearized piston displacement (stroke)	m
ΔX_v	Linearized valve displacement	m
ω_i	Resonance frequency for the i:th pole of G_{sys}	$\frac{rad}{s}$
K_c	Flow-pressure coefficient	$\frac{m^3}{sPa}$
k_s	Spring coefficient	$\frac{N}{m}$
K_s	Valve coefficient, $C_q w \sqrt{\frac{2}{\rho}}$	$\frac{s}{m}\sqrt{N}$
K_q	Flow gain coefficient	$\frac{m^2}{s}$
l_s	Spring pre-contraction	m
M_t	Inertia mass load	kg
p_A, p_B	Pressure acting on A_A, A_B	Pa
p_c	Pressure in volume between valvistor poppet and pilot	Pa
p_{crack}	Pressure when pressure limiting valve starts to close	Pa
p_{max}	Maximum allowable system pressure	Pa
q_A, q_B	Flow from/to the cylinder chambers	$\frac{m^3}{s}$
q_p	Flow to/from pump	$\frac{m^3}{s}$
s	Laplace operator	$-$
T_r	Time constant of pressure limiting valve	s
V_A, V_B	Volume of piston chamber, piston rod chamber	m^3
v_p	Piston velocity	$\frac{m}{s}$
x_v	Valve displacement	m
x_{max}	Maximum valve displacement	m
x_{pilot}	Valvistor pilot valve displacement	m
x_{pop}	Valvistor main poppet displacement	m

REFERENCES

[1] S. Habibi and G. Singh. Derivation of design requirements of optimization of a high performance hydrostatic actuation system. *International Journal of Fluid Power*, 1(2):11–23, 2000.

[2] R. Rahmfeld and M. Ivantysynova. Displacement controlled linear actuator with differential cylinder - a way to save primary energy in mobile machines. *5th International Conference on Fluid Power Transmission and Control (ICFP'2001)*, pages 296–301, 2001.

[3] Dantlgraber D. Spath O. Wilke Feuser, A. Servopumpenantriebe für differentialzylinder. *Ölhydraulik und Pneumatik 39 Nr. 7*, pages 540–544, 2002. Mainz, Germany.

[4] G. Wendel. Hydraulic system configurations for improved efficiency. *Proceedings of the 49th National Conference on Fluid Power*, pages 567–573, March 2002.

[5] K. Heybroek, J-O. Palmberg, and J. Larsson. Open circuit solution for pump controlled actuators. *Proceedings of the 4th FPNI-PhD Symposium*, 2006. Sarasota, Florida, USA.

[6] B. Eriksson, B.R. Andersson, and J-O. Palmberg. The dynamic properties of a poppet type hydraulic flow amplifier. *The Tenth Scandinavian International Conference on Fluid Power, SICFP'07*, 2007. Tampere, Finland.

[7] Bo R. Andersson. *On the Valvistor, a proportionally controlled seat valve*. PhD thesis, LiTH, 1984. ISBN 91-7372-748-2.

[8] R. Filla. *Operator and Machine Models for Dynamic Simulation of Construction Machinery*. IKP Linköpings Universitet, 1 edition, April 22 2005. ISBN 91-85457-14-0.

[9] T. Persson, P. Krus, and J-O. Palmberg. The dynamic properties of over-center valves in mobile systems. *Second International Conference in Fluid Power Transmission and Control*, 1989.

THE RESEARCH OF THE PUMP AND MOTOR OF THE SAME WIDTH AND WITH SINGLE-ROLLOR AND DOUBLE-STATORS

Professor Wen Desheng
Yanshan University
College of Mechanical Engineering
066004 Qinhuangdao, China
Phone +86 335 8074 068
E-mail:wendesheng@ysu.edn.cn

Wen Jia
Yanshan University
College of Information Science and Engineering
066004 Qinhuangdao, China
Phone +86 335 8074 068
E-mail:wjyanyuan@yahoo.com.cn

ABSTRACT

In view of the questions that only one pump cannot control many hydraulic actuators which have different diameter and different output volume to realize synchronization, and that only one pump cannot act as oil resource of many defferent pressure system without pressure valve etc, a new type of hydraulic pump (motor) is invented. This especial hydraulic pump (motor) includes one rotor and two stators, which has obtained Chinese Inventive Patent (Patent NO: 02144406.4). It realizes the function that there are two pumps in one pump body. Many more functions can be realized by changing the structure of the pump. This type of pump not only has many advantages to solve many present difficult problems, but also adds a new type of theory in the field of hydraulic pump (motor). It will become a new series pump and motor, and in virtue of its advantages, it will be applied to middle or low pressure hydraulic system widely.

KEYWORDS: same width double-stators pump motor

1 INTRODUCTION

Recently, the hydraulic transmission application is widespread, and the hydraulic equipments and the elements are developed extremely rapidly. The hydraulic pump is the power source and core component of hydraulic system, so the criterion of its pressure, noise, efficiency, service life, anti- impact, specific power, control mode etc. is more and more high.

Many researchers are researching the material, sealing, lubrication etc. to enhance the performance index of the pumps or motors only on the base of present principle of pumps and motors. Few researchers change the working principle of pumps or motors to improve their service life or apply them to special industry.
The same width pump (motor) with double-stators is a new type of hydraulic pump (motor) which has obtained Chinese Inventive Patent (Patent NO: 02144406.4), and it is a breakthrough in hydraulic pump principle and structure.Just as gear pump, vane pump, piston pump, it will become a new type of principle series in the field of hydraulic pump. If such a pump is successfully completed, it will be able to take place of a series of middle-pressure or low-pressure pumps or motors. At the same time, this type of pump can be extensively used to the fields, such as agricultural machinery, manufacturing machinery, heavy machinery, light industry machinery, marine machinery, chemical machinery, mining machinery, traffic machinery, forestry machinery, aeronautical machinery etc..

2 DESIGN FEATURE

2.1 The same width single-action variable displacement pumps and motors with double-stators

Fig.1 is the principle abridged drawing of the same width, single-action, double-output, variable displacement pump and motor with double-stators and single-roller. The followings are main characteristics of this type of pump:
2.1.1 There are one rotor and two stators (outer stator and inner stator) in this pump body. On the one hand, rotor and outer stator, roller, valve devices and side plate compose an outer pump. on the other hand, rotor and inner stator, roller, valve devices and side plate make up an inner pump.

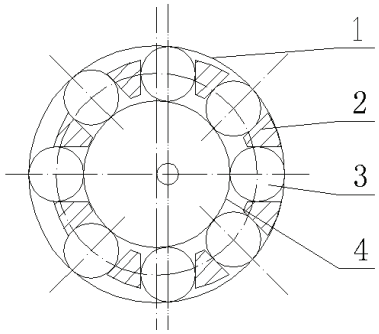

Fig.1 The principle abridged drawing of the same width, single-action, double-output, variable displacement pump and motor with double-stators and single-roller
1-outer stator 2-rotor 3-roller 4-inner stator

2.1.2 There is rolling friction between roller, inner stator and outer stator. Each pairing element is in wholly lubrication when pump works.
2.1.3 The outer curve of inner stator and the inner curve of outer stator are similar, and the distance between the two curves is constant, that is to say, there is no relative movement between the function roller and the stator curves in the radial direction. So backward spring and other elements are not needed, which brings great advantages to the device to work as hydraulic motor.
2.1.4 There is an eccentricity between the centerline of the rotor and the centerline of the stators. When the eccentricity changes, the pump will become a variable

displacement pump. When it is used as motor, it is equal to two constant proportional variable motors, and it can also be used as a multi-speed variable displacement motor.
2.1.5 If the structure and form of the same width, single-action, double-output, variable displacement pump and motor with double-stators and single-roller are changed, many same width, single-action pumps with double-stators can be obtained. The respective figures are as follows.

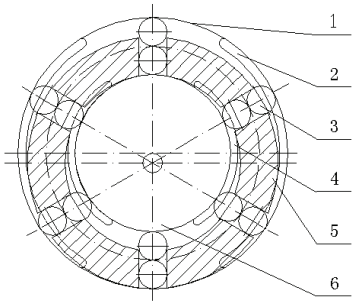

Fig.2 The principle abridged drawing of the same width, single-action, double-output, variable displacement pump and motor with double-stators and double-rollers
1-outer stator 2-the variable volume of outer pump 3-roller 4-the variable volume of inner pump 5-rotor 6-inner stator

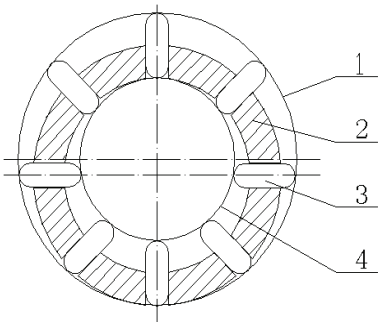

Fig.3 The principle abridged drawing of the same width, single-action, double-output, variable displacement pump and motor with double-stators and sliders
1-outer stator 2-rotor 3-slider 4-inner stator

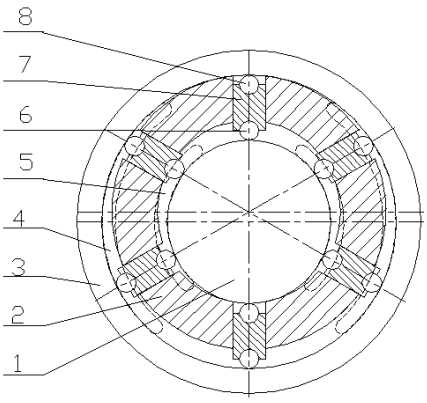

Fig.4 The principle abridged drawing of the same width, single-action, double-output, variable displacement pump and motor with double-stators and connecting rods
1-inner stator 2-rotor 3-outer stator 4-the variable volume of outer pump 5-the variable volume of inner pump 6-inner roller 7- connecting rod 8-outer roller

2.2 The same width, double-action pumps and motors with double-stators

Fig.5 is the principle abridged drawing of the same width, double-action, four-output pump and motor with double-stators and single-roller. The followings are main characteristics of this type of pump:

2.2.1 The structural difference between this type of pump (motor) and the same width, single-action, double-output, variable displacement pump (motor) with double-stators and single-roller is the curves of the two stators.

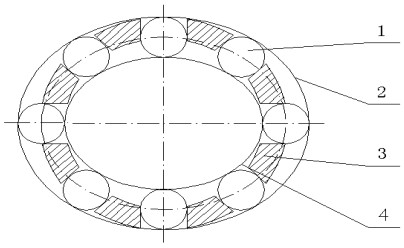

Fig.5 The principle abridged drawing of the same width, double-action, four-output pump and motor with double-stators and single-roller

1-roller 2-outer stator 3-rotor 4-inner stator

2.2.2 With the similar truth, change the structure and form of the same width, double-action, four-output pump and motor with double-stators and single-roller, many same width, double-action pumps with double-stators also can be obtained. Some of them can be showed as follows.

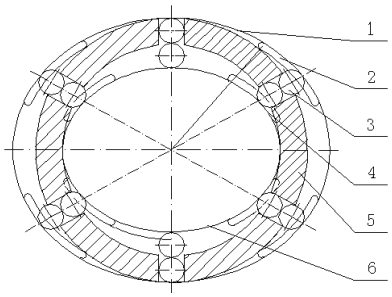

Fig.6 The principle abridged drawing of the same width, double-action, four-output pump and motor with double-stators and double-rollers

1-outer stator 2- the variable volume of outer pump 3-roller 4- the variable volume of inner pump 5-rotor 6- inner roller

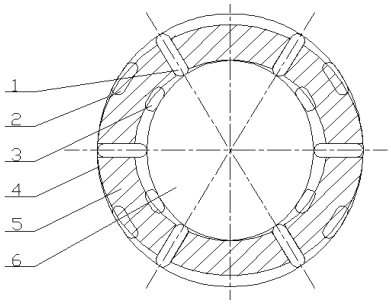

Fig.7 The principle abridged drawing of the same width, double-action, four-output pump and motor with double-stators and sliders

1-slider 2- the variable volume of outer pump 3- the variable volume of inner pump 4- outer stator 5-rotor 6- inner roller

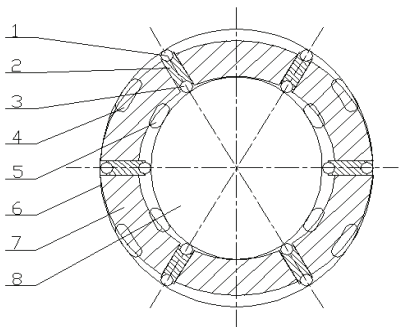

Fig.8 The principle abridged drawing of the same width, double-action, four-output pump and motor with double-stators and connecting rods

1-outer roller 2-connecting rod 3-inner roller 4- the variable volume of outer pump 5- the variable volume of inner pump 6- outer stator 7- rotor 8- inner stator

2.3 The same width, multi-action pumps and motors with double-stators

In this type of pumps (motors) there are many more suction chambers and delivery chambers than the same width, single-action pumps (motors) with double-stators. In addition, if they are used as motors, they can be regarded as many constant proportional motors, and just as double-action pumps mentioned above, they can be used as muli-speed motors. Some of their structural figures are as follows

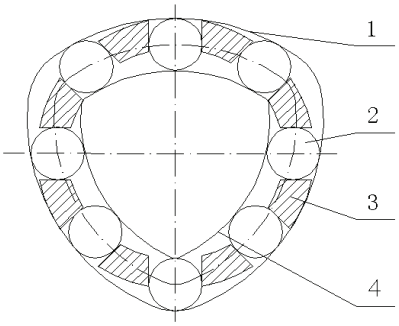

Fig.9 the same width, three-action, six-output pumps and motors with double-stators and single-roller

1-outer stator 2-roller 3-rotor 4-inner stator

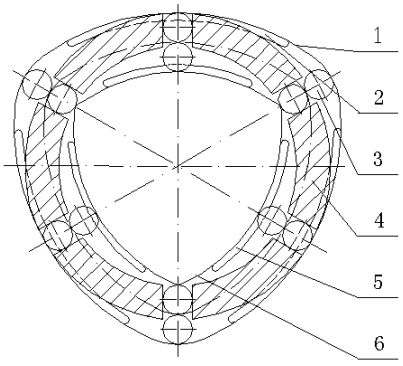

Fig.10 the same width, three-action, six-output pumps and motors with double-stators and double-roller

1-outer stator 2- the variable volume of outer pump 3-roller 4-rotor 5- the variable volume of inner pump 6- inner stator

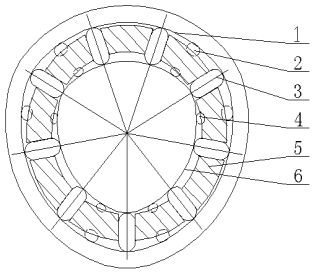

Fig.11 the same width, three-action, six-output pumps and motors with double-stators and sliders
1-outer stator 2- the variable volume of outer pump 3-slider 4- the variable volume of inner pump 5-rotor 6- inner stator

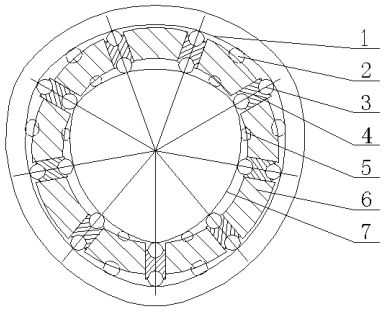

Fig.12 the same width, three-action, six-output pumps and motors with double-stators and connecting rods
1-outer stator 2- the variable volume of outer pump 3-roller 4-connecting rod 5-the variable volume of inner pump 6-rotor 7- inner stator

3 PRINCIPLE OF OPERATION

This paper introduced twelve double-stators pumps(motors) with different structures, but their basic principles of operation are similar. Here only take the same width, single-action, double-output, variable displacement pump and motor with double-stators and single-roller as an example to analyze the principle of operation, because its structure is the simplest among the twelve pumps and it is easy to understand.

As Fig.1 has shown to us, when the rotor is rotating, the double-stators pump then creates two pumps inside its body. One is the outer pump, which is composed of rotor, outer stator, roller, valve devices and sided plate, and the other is called inner pump, built up by rotor, inner stator, roller, valve devices and sided plate. With the rotor's rotating, some fluid is pushed into the outer pump, at the same time, some fluid is ejected into the outlet port of the inner pump. But when fluid is pushed into the inner pump, some is ejected into the outlet port of the outer pump. Hence, the double-stators pump builds two pumps which work at the same time and output in the equal rate. There are two inlet ports and two outlet ports in the body of pump. The two outlet ports can be either used as two outlet ports respectively, or just as one uniform outlet port. For the former, the amount of the two flows are of a certain ratio, so it can be used as the equal-ratio output dual-pump. When this design is used as a motor, it can work as a multi-speed motor.

Once the eccentricity between rotor and stators is changed, this design will become two equal-ratio and variable-displacement pumps. If it is used as a motor, this design will become two equal-ratio and variable-displacement motors, or become a multi-speed and variable-displacement motors. However, for the double-action and three-action pumps

and motors shown by Fig.5~12, there is no eccentricity between the centerline of the rotor and the centerline of the stators, so they cannot realize variable displacement.

4 KINEMATIC ANALYSE

Here also take the same width, single-action, double-output, variable displacement pump and motor with double-stators and single-roller as an example. Its principle figure is Fig.1. The main moving parts are rotor and rollers of the pump. The rotate speed of rotor is equal to that of driving motor which is close to a constant. So, here mainly analyze the movement situation of the roller.

The absolute motion of roller is the rolling of roller along the stator curves. It is composed of the convected motion, the relative motion and the rotation of roller. The convected motion is the rotation of roller along rotor. The relative movement is between roller and rotor. The rotation of roller is the movement of roller circling its own spool thread. The convected velocity is expressed by ω_{e1} which is equal to the rotate speed of rotor, and the rotate speed of rotor is expressed by ω. The above velocity and acceleration are all relational with polar radius which is expressed by ρ. So the polar radius should be deduced, then velocity and acceleration are counted.

As Fig.13 shows, the polar coordinate is established and expressed by OrX, and the polar radius and the polar angle (θ) are expressed by OrA and $\angle$AOrX respectively.

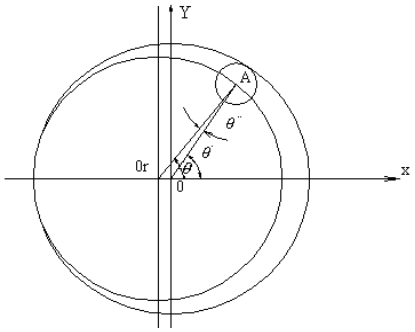

Fig,13 The drawing of polar coordinate

In the triangle AOrO, the following equation can be deduced according to Sine Law or Cosine Theorem.

$$\rho = (R_1 - r)(1 + \varepsilon\cos\theta - 0.5\varepsilon^2\sin^2\theta) \quad (1)$$

Where R1——The inner circle radius of stator

r ——The radius of roller

e ——The eccentricity between stator and rotor

ε ——The eccentric rate

$$\varepsilon = e/(R1-r) \quad (2)$$

4.1 The velocity analyse of roller

The relative velocity between roller and rotor is expressed by symbol Vr1, and the following equation can be obtained.

$$V_{r1} = \frac{d\rho}{dt} = -\varepsilon(R_1 - r)\omega(\sin\theta + 0.5\varepsilon\sin 2\theta) \quad (3)$$

The convected velocity expressed by symbol Ve1 is as follows:

$$V_{e1} = \rho\omega = \omega(R_1 - r)(1 + \varepsilon\cos\theta - 0.5\varepsilon^2\sin^2\theta) \quad (4)$$

The absolute velocity of roller along inner curve of stator expressed by symbol Va1 can be deduced as following equation:

$$V_{a1} = \sqrt{V_{e1}^2 + V_{r1}^2} \tag{5}$$

The rotate speed of roller circling its own spool thread expressed by symbol ωr can be accounted by the follows:

$$\omega_r = \frac{V_{a1}}{r} \tag{6}$$

4.2 The acceleration analyse of roller

The absolute acceleration of roller denoted by symbol aa1 is composed of the convected acceleration denoted by symbol ae1 , the relative acceleration denoted by symbol ar1 and the Coriolis acceleration denoted by symbol ak1. So the following equation can be obtained.

aa1=ar1+ae1+ak1 (7)

Where ar1, ae1, ak1 can be expressed by follows:

$$a_{r1} = \frac{d^2\rho}{dt^2} = -\varepsilon\omega^2(R_1 - r)(\cos\theta + \varepsilon\cos 2\theta) \tag{8}$$

$$a_{e1} = \omega^2\rho = \omega^2(R_1 - r)(1 + \varepsilon\cos\theta - 0.5\varepsilon^2\sin^2\theta) \tag{9}$$

$$a_{k1} = 2\omega V_{r1} = 2\varepsilon(R_1 - r)\omega^2(\sin\theta + 0.5\sin 2\theta) \tag{10}$$

$$a_{a1} = \sqrt{(a_{e1} - a_{r1})^2 + a_{k1}^2} \tag{11}$$

4.3 The kinematic curves of roller

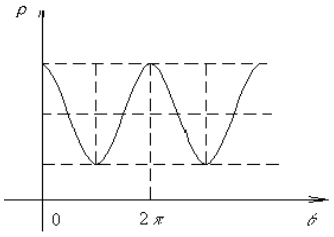

Fig.14 The change rule curve of polar radius ρ

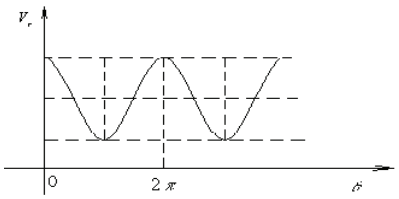

Fig.15 The change rule curve of relative velocity Vr1

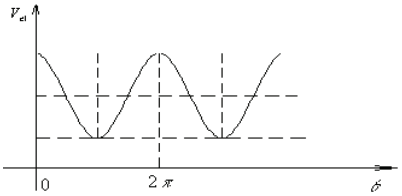

Fig16 The change rule curve of convected velocity Ve1

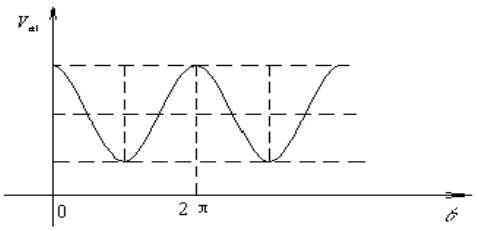

Fig.17 The change rule curve of absolute velocity Va1

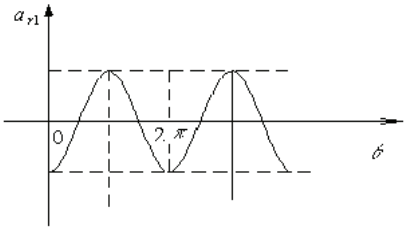

Fig.18 The change rule curve of relative acceleration ar1

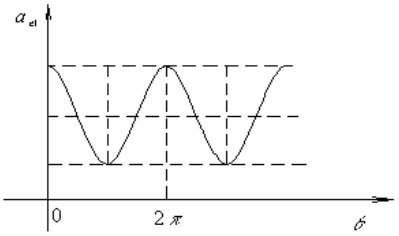

Fig.19 The change rule curve of convected acceleration ae1

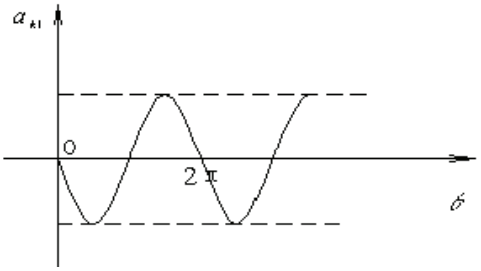

Fig.20 The change rule curve of Coriolis acceleration ak1

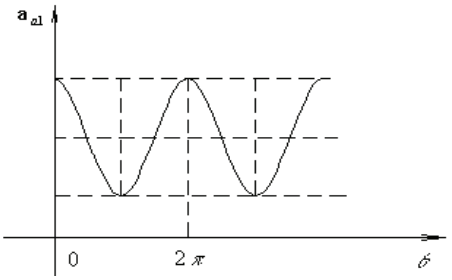

Fig.21 The change rule curve of absolute acceleration aa1

5 EXPERIMENTAL RESEARCH

Many samples of this type of pumps with different structure have been manufactured successfully. The follows are the test.

5.1 The parameters of the tested sample

rotate speed: 1500 n/min

Power of motor: 30KW；5KW
System pressure: 20Mpa
Separation between two stators: 30mm
Eccentricity of the single-action pump: 5mm
Roller length (Slider thick)： 45mm
Roller diameter of single-roller pump: ϕ30mm
Slider length of pump with sliders: 30mm
Roller diameter of double-roller pump: ϕ15mm
Roller diameter of double-roller pump with connecting rods: ϕ10mm
Slider width: 15mm

5.2 The pictures of typical prototype structure of the tested sample

The main situation of the pump on testing spot is showed in Fig.22~24.

Fig.22 Installation situation of the pump

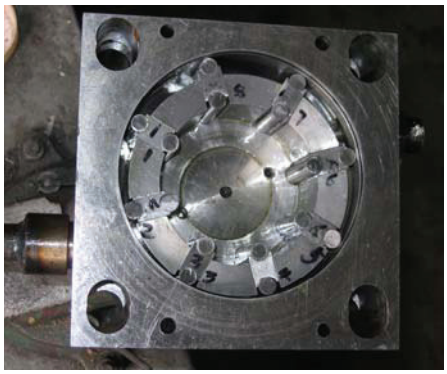

Fig. 23 The structure drawing of the same width, double-action, four-output pump and motor with double-stators and connecting rods

Fig. 24 The working situation of pump on the testing spot

5.3 The test result

In the principle test, flowrate measurement result of this type of pumps is compared with the flowrate of the single-stator pumps under the same weight or the same volume. The output flowrate is improved by 20%~40%.

6 CONCLUSIONS

Through the principle research and the practical test, the following conclusions can be obtained.

(1) In this new type of pump, the control chamber is composed of one rotor, two stators, two side plates and a group of rollers. The process of pushing and ejecting fluid controlled by the valve device. There are several pumps in one pump body, and it is rolling friction between roller and stators. So, mechanical efficiency, the specific power and service life are increased greatly.

(2) If suction times is equal to displacing times as rotator revolves one turn, double-stators pump has more suction chambers and displacing chambers than single-stator pump. There is a kind of proportional relation between output flowrate of two displacing chambers.

(3) This type of pumps have multi-inlet and multi-outlet, they can be used respectively, and also can be combined optionally according to actual situation. So, only one this type of pump can control many hydraulic actuators which have different diameter and different output volume to realize synchronization, and can act as oil resource of many defferent pressure systems without pressure valve etc..

(4) Instantaneous delivery of double-stators pump is uniform, and flow wave character is small.

(5) For this kind of pump, with the equal distance between two stators and the special structure, when working as a motor, there is no problem with the drawback process, and the simple components, and easy operating, the operational life span and security are greatly improved, so that the large-lot production is easily realized.

7 References

[1] Lei Tianjue. Fluid Power Engineering Hand Book.Beijing: China Machine Press,1990,2183(In Chinese)

[2] Wen Desheng. The same width curve pump with double-stators and roller. Patent No: 02144406.4,2002(In Chinese)

[3]Wen Desheng. The couple motor (pump) with double stators. Patent No: 02144407.2,2002(In Chinese)

[4] Wen Desheng. Research on a new type of axial piston pump: an open channel axial piston pump. Chi Hsieh Kung Ch'eng Hsueh Pao/Chinese Journal of Mechanical Engineering. 1987,v 23, n 2, Jun, p 74-77(In Chinese)

[5] Wen, Desheng etc. Comparison of self-cooling of CY pump and SPB pump. Jixie Gongcheng Xuebao/Chinese Journal of Mechanical Engineering. 2002, v 38, n 9, p 150-154(In Chinese)

LOW RIPPLE SOLUTION: VANE-IN-GROOVE PUMP WITH PRECOMPRESSION

A. Stroganov, L. Sheshin, Y. Volkov, S. Ryadnov, A. Nikiforov
Lumex JSC, St. Petersburg, Russia,
Phone +7 812 251 6989, Fax +7 812 251 6989
E-mail: strog@lumex.ru

ABSTRACT

Paper presents new approach to pressure ripple and acoustic noise reduction in a vane pump with working chamber located in annular groove of a rotor face (Vane-In-Groove pump) by means of working fluid precompression.

Vane-In-Groove pumps with adaptive rotor comprise means for variation of the volume of working fluid transferred portions and pressure in them. This feature as well as lengthy enough transfer zone makes possible precompressing the transferred portions so that to balance working fluid pressure in them with the output pressure. Thus the origin of decompression impacts eliminates completely.

Two main methods for adjusting the degree of the working fluid precompression are described. The first method works with adjusting the amplitude of the transferred portions volume variation depending on operational pressure and is preferable for reduction of remaining kinematical ripple down to 0.2% and lower. The second method works with adjusting the total transfer angle and is preferable cost wise. One embodiment of the second method was tested and described in details.
The tests equipment, schematic diagram and procedure for output pressure ripple measurement are presented as well as the tests results for 28 cm^3 pump. The test results illustrate low levels of output pressure ripple at 500 – 2000 RPM and 10 – 30 MPa.

KEYWORDS: low pressure ripple, quiet operation, vane pump/motor, Vane-In-Groove, decompression flow, working fluid precompression

1. INTRODUCTION

The origin of pressure ripple in the Vane-In-Groove pumps comes from a common shortcoming of all existing positive displacement pumps that have high volumetric efficiency. The point is that when a closed transferred volume of a working fluid moves from the suction to the pumping cavity the pressure in it does not reach the outlet pressure by the moment of merging with the pumping cavity. At that moment, due to compressibility of a working fluid, a counter flow (*decompression flow*) of the working fluid from the pumping cavity to the transferred volume arises. The decompression flow

equalizes the transferred fluid pressure and the pressure in the pumping cavity and gives rise to the delivery pulsations as well as the pressure ripple in an outlet line. This in it's turn lead to power losses, vibrations and noise and can cause destruction of outlet line elements and a pump itself.

2. VANE-IN-GROOVE PUMP WITH WORKING FLUID PRECOMPRESSION

Known methods of reducing a decompression impact can be divided in two types. The first one use a counter flow (actually leakage) created between a transferred volume and an outlet cavity before they merge. This allows fluid pressure in a transferred volume to approach the outlet pressure thus reducing the pressure drop that generates a decompression flow. There are many implementations of this method in all types of positive displacement pumps. This method can be called passive from the point of view that no actions are taken on a transferred volume while it travels between a suction and a pumping cavities. Two major disadvantages of this method are obvious. Firstly, some useful power dissipates in mentioned counter flow heating a working fluid and a pump. Secondly, the method can be only optimized for a certain combination of parameters: fluid compressibility and viscosity, rotation speed, delivery and outlet pressure.

Real solution of the decompression problem can be achieved by the active pulsation suppression system based on the working fluid precompression provided in transferred volumes while they are separated from both a suction and a pumping cavities.

This solution can be referred to the second type of known methods. Usually [8] precomrpession is provided in inter-vane cavities of radial-vane pumps due to special shape of a cam ring. However this implementation of the precomrpession method has the same disadvantage [7], namely it can be only optimized for a certain combination of working parameters. Another disadvantage is it's inapplicability for variable displacement pumps.

Vane-In-Groove pump with Adaptive Rotor (see [9]) offers easy implementation of the working fluid precompression based on the ability of the supporting part of the adaptive rotor to move relative to its working part. In particular, the supporting part (1) of the rotor can be tilted at a small angle g around the axis perpendicular to the axis of rotation of the working part (2) of the rotor, as is shown in Fig. 1. Since the rotor parts are hydraulically connected to each other via the force chambers of variable length (3) and each force chamber is a part of the corresponding transferred volume (4), when it's length is changed the corresponding transferred volume is changed as well. If the tilt axis of the supporting part of the rotor lies parallel to the line connecting the middle points of the forward and backward transfer areas, the volume of the force chambers will cyclically vary according to the sine law thus providing sine variation of the transferred volumes.

Detailed description of the active pulsation suppression system and it's mathematical model is given in [5]. The system provides several methods of regulation of the transferred volumes variation needed for adjusting the system to outlet pressure and delivery changes. Paper [5] describes one of these method, namely the amplitude regulation of the transferred volumes variation. The other methods as well as their embodiments in a Vane-In-Groove pump/motor are described in details in patent application [6].

Present paper discloses simple and cost wise preferable method – phase (or total angle) regulation of the transferred volumes variation. The essence of this method is regulating the total angle φ_{total} i.e. the angle of the rotor rotation between the angle of detaching the transferred volume from the inlet cavity φ_{detach} to the angle of it's merging the outlet cavity $\varphi_{merg.}0$. Thus the total angle is the angle range within which the transferred volume is separated from both the inlet and outlet cavities. Total amplitude of the transferred volumes variation at this method of regulation is chosen corresponding to the maximum pressure drop between the inlet and outlet ports and maximum pump displacement. The corresponding variation of the transferred volumes and pressure of the working fluid in it are shown in Fig. 2 (curves 1a, 1b). All graphs are traced against the angular travel of the transferred volume within the range from φ_{detach} to $\varphi_{merg.}0$.

Method of the phase regulation can be implemented as follows (Fig. 1): the total angle is changed by connecting the transferred volume (4) with the outlet cavity (5) ahead of time, at the moment when the pressure in the transferred volume becomes equal to the outlet pressure. This type of implementation is called the regulation of the angle of merger. As a result of the ahead of time connection further change of pressure of the working fluid in the transferred volume stops (curves 2b, 3b in Fig. 2). This ahead of time connection of the transferred volume with the outlet cavity can be done by shifting the vane (6) that is currently separating the mentioned transferred volume from the outlet cavity or by connecting the transferred volume with the outlet cavity through a normally closed bypass duct (7). In the latter case starting from the moment of unlocking bypass duct a part of fluid is displaced out of the transferred volume via the bypass duct to the outlet cavity (curves 2c,d, 3c,d in Fig. 2) (for a hydromotor – out of the outlet cavity to the transferred volume). Bypass duct can be unlocked, for example, by back-pressure valve (8) that is opened when the sign of the pressure difference between the ends of the bypass duct is changed. The shape of vanes used in Vane-In-Groove pumps is chosen so that to provide hydrostatic pressing of a vane to forward transfer limiter (9) where the pressure of a working fluid ahead of a vane is higher than behind it. This allows to use a vane itself as a back-pressure valve and no external bypass duct is needed.

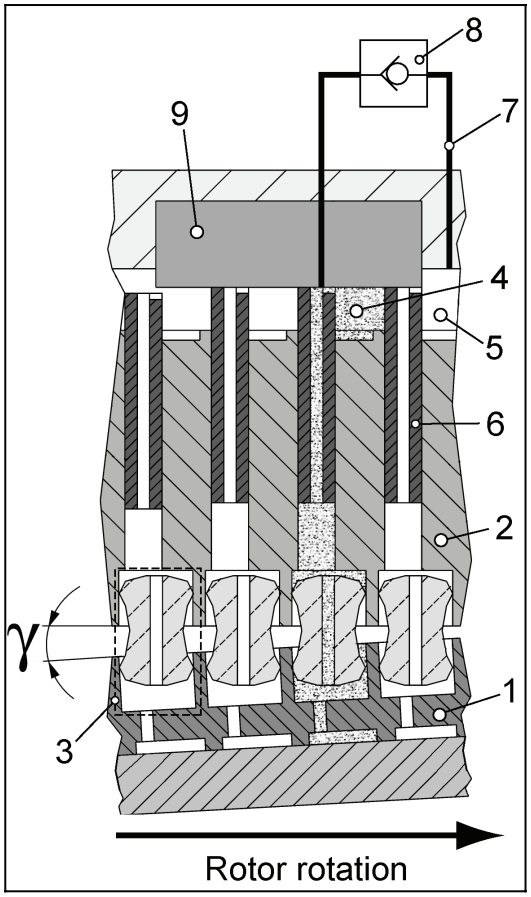

Figure 1: Schematic representation of the phase regulation method implemented in a form of regulating the angle of merger $f_{merg.}$

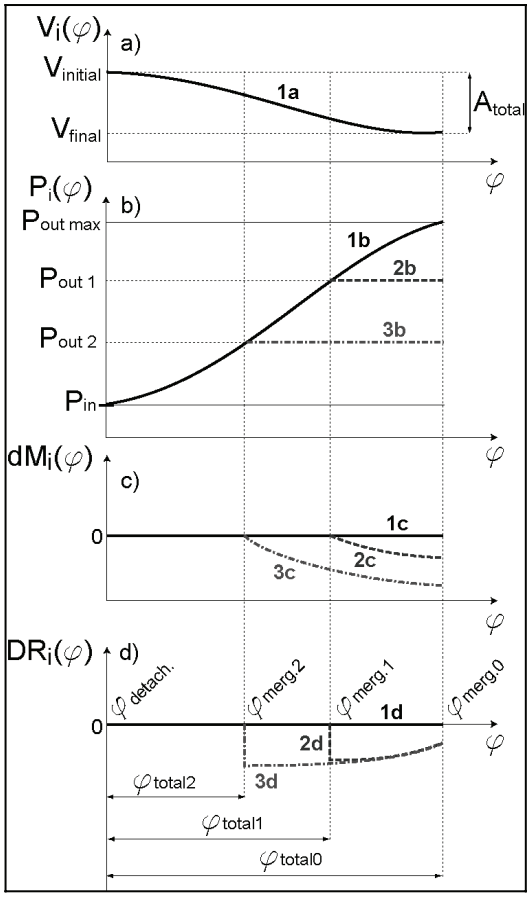

Figure 2: Variation of the transferred volume (a), change of mass (c) and pressure of the working fluid in it (b) and fluid flow rate between the transferred volume and outlet cavity (d)

Obvious advantage of the phase regulation method is it's simplicity. The major disadvantage of this method is secondary flow pulsations appearing at the outlet pressure lower than maximal operational pressure. Since the total amplitude of the transferred volumes variation is adjusted for the maximal outlet pressure the fluid pressure in the transferred volume reaches the outlet pressure at the moment before their merger. Since that moment the transferred volume is no longer separated from the outlet cavity and some part of the fluid is displaced from the transferred volume to the outlet cavity generating additional delivery. This process repeats for each transferred volume producing secondary flow pulsations. The good thing is that these flow pulsations don't have high frequency components because sharp decompression impact has been completely eliminated.

To verify the active pulsation suppression system in real-life prototypes with phase regulation of the transferred volumes variation (namely regulation of the angle of merger by vane shifting) have been designed assembled and tested on our internal testing stand. All they have shown functionality and good performance. One of the Vane-In-Groove pump prototypes with fixed displacement of 28 cm? was put to the comparative test for outlet pressure ripple in two modifications: with the active pulsation suppression system adjusted for 20 MPa and without it. Required adjustment is done by choosing corresponding tilt angle (equal to 0.9 degree) of the rotation axis of the supporting part of the rotor.

3. TEST INSTALLATION AND PROCEDURE

Figure 3 presents schematic of the internal testing stand. The test circuit is closed type without backup. Industrial oil similar to HLP 46 was used as a working fluid. The water cooling system (11) working on counter-current flow principle kept up the fluid temperature within the limits of 30±5 °C. Adjustable orifice (9) was used as a load. Maximal drive power provided by the electromotor was 30 KW. Outlet pressure and pressure ripple oscillogram, oil temperature and pump housing temperature were recorded.

The purpose of this test was to compare the outlet pressure ripple amplitudes produced by "regular" Vane-In-Groove pump and the same pump provided with the active pulsation suppression system adjusted for 20 MPa. This will give an idea on how the fluid born component of the pump noise changes when the active pulsation suppression system is used.

The test matrix was defined as follows:
- operating pressure: 10, 20 and 30 Mpa, i.e. the pressure lower, equal and higher than 20 MPa that the active pulsation suppression system was adjusted for.
- rotation speed: 1500 revolutions per minute

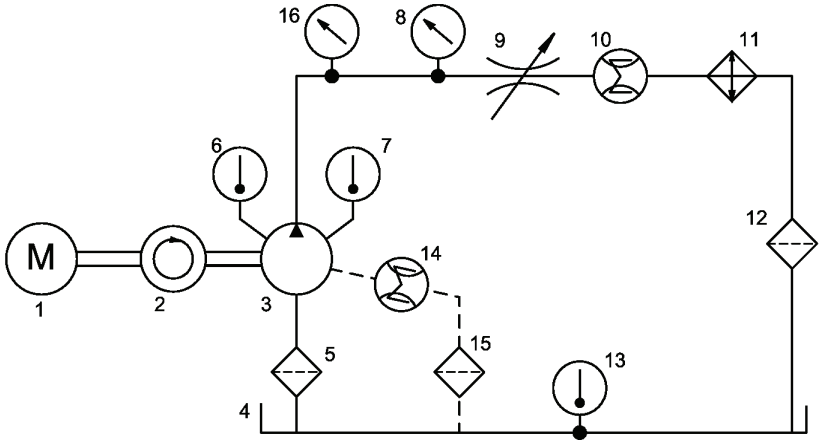

Figure 3: Scheme of the internal testing stand (auxiliary and safety equipment is not shown) 1– electromotor, 2 – tachometer, 3 – tested pump, 4 – tank, 5, 12, 15 – filters, 6, 7, 13 – thermometers, 8 – dynamic pressure sensor, 9 – adjustable load throttle, 10, 14 – flow meter, 11 – counter-current flow cooler, 16 – pressure gauge

4. TEST RESULTS

The outlet pressure ripple amplitude was measured by dynamic pressure sensor, at stationary working points of the test matrix and the results are presented as oscillograms in Fig. 6, Fig. 7, Fig. 8, Fig. 9. High frequency oscillations (about 1450 Hz) are the result of wave reflections in the outlet line between the outlet cavity and the load. For comparison Figure 10 is given that presents theoretically calculated outlet pressure ripple for "ideal" model (with no leakages) of the tested pump at 40 MPa (solid curve).

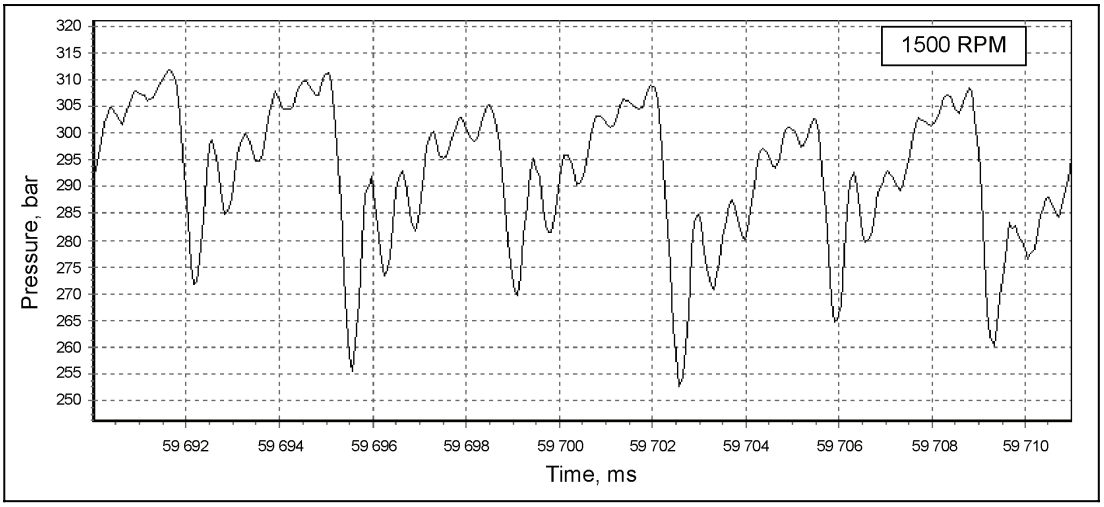

Figure 6: Amplitude of the outlet pressure ripple at 30 MPa (300 bar) and 1500 RPM against time for the pump **without** the active pulsation suppression system

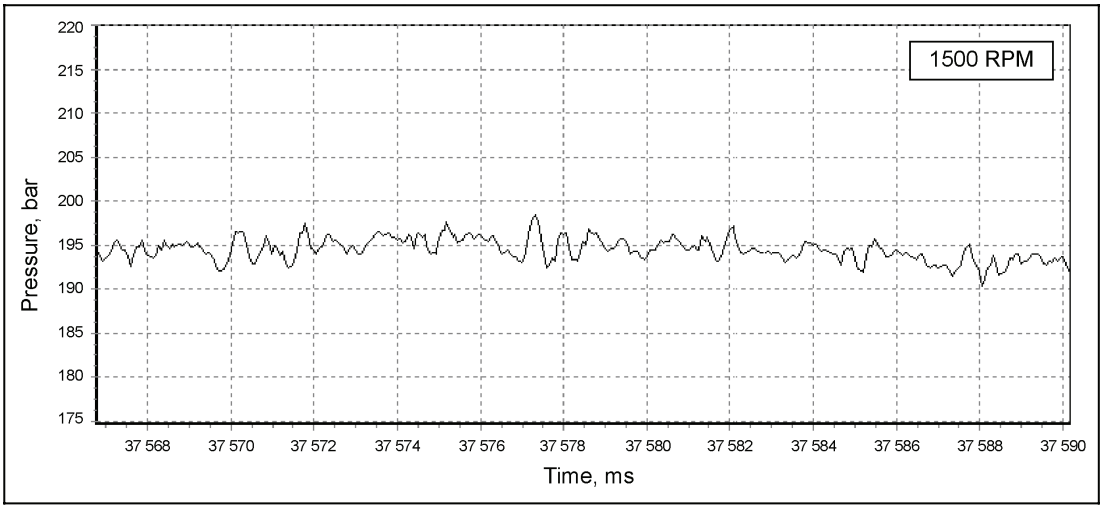

Figure 7: Amplitude of the outlet pressure ripple at 20 MPa (200 bar) and 1500 RPM against time for the pump **with** the active pulsation suppression system adjusted for 20 MPa (200 bar).

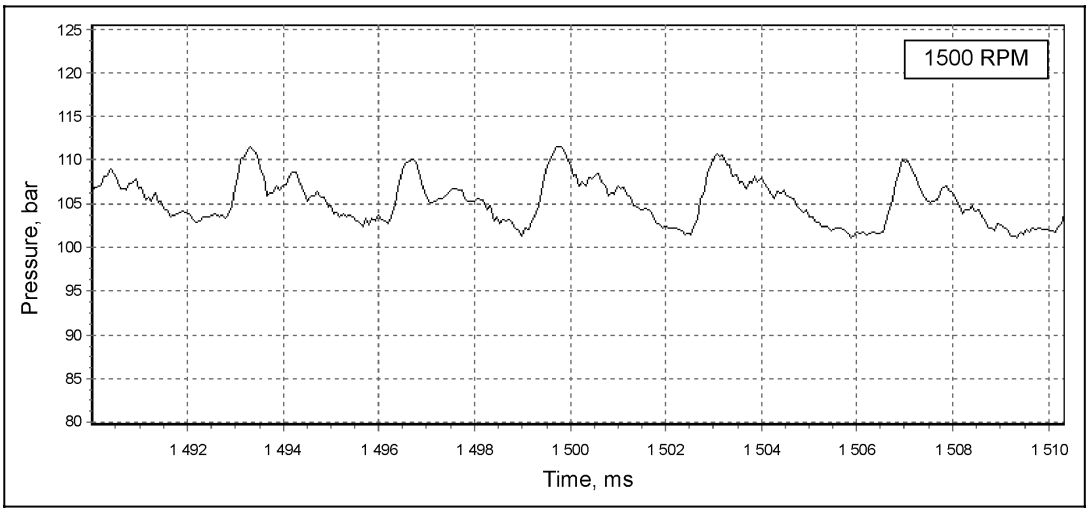

Figure 8: Amplitude of the outlet pressure ripple at 10 MPa (100 bar) and 1500 RPM against time for the pump **with** the active pulsation suppression system adjusted for 20 MPa (200 bar).

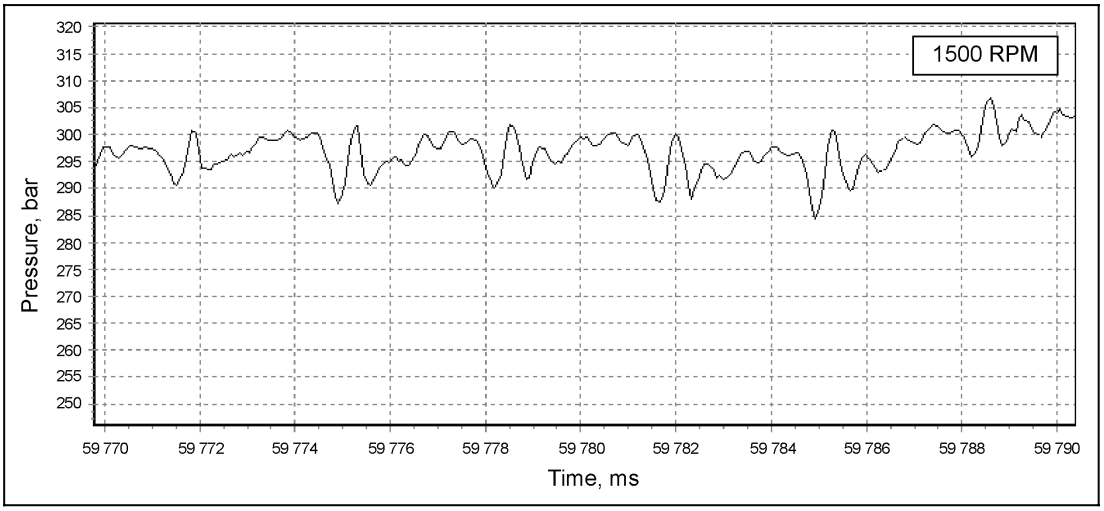

Figure 9: Amplitude of the outlet pressure ripple at 30 MPa (300 bar) and 1500 RPM against time for the pump **with** the active pulsation suppression system adjusted for 20 MPa (200 bar).

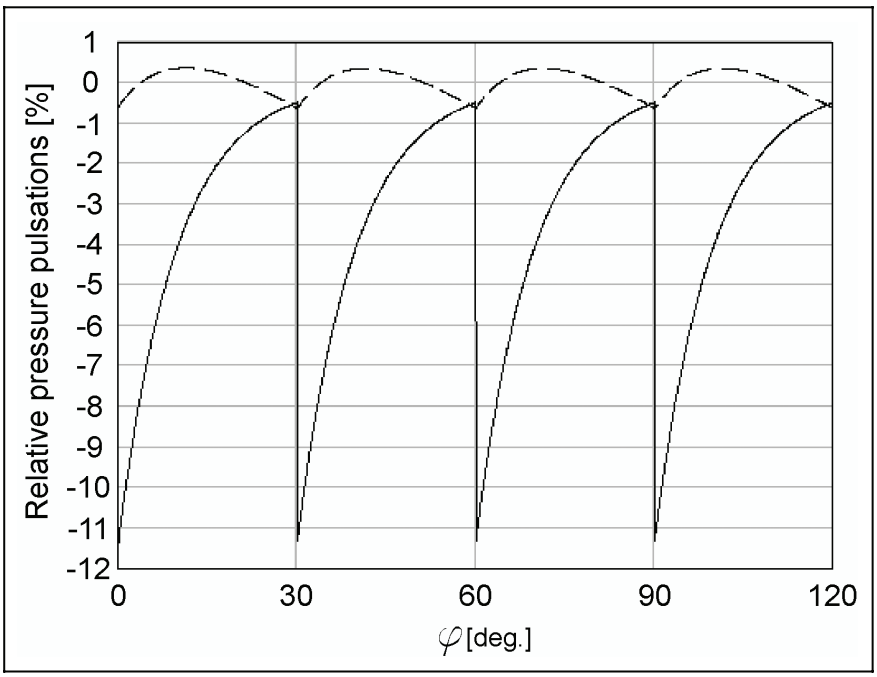

Figure 10: Outlet pressure behavior (average level and ripple) against the angle of the rotor rotation for "ideal" pump at 40 MPa (400 bar):
without (solid line) and with the active pulsation suppression system (dash line)

Figures 7 show significant reduction of the outlet pressure ripple amplitude especially at the vane's frequency when using the active pulsation suppression system. So, at 1500 RPM the pressure ripple amplitude drops down from 17% to 1,2% of the average outlet pressure. This corresponds to the theoretical calculations (Fig. 10) if high frequency ringing of the measuring tract is smoothed in Fig. 6 – Fig. 9.

Figure 8 shows reduction of the outlet pressure ripple amplitude in case of excess precompression (outlet pressure is lower than calculated for complete elimination of decompression). Since the fluid pressure in the transferred volume reaches the outlet pressure before it merges the outlet cavity the vanes in the forward transfer area unlock corresponding the transferred volumes ahead of time producing positive outlet pressure peaks (rather than negative). These peaks amplitude is defined by the pressure drop required to unlock the vanes. Some pump complication namely mentioned back-pressure valve installed in a bypass duct can reduce the amplitude of these positive peaks.

Figure 9 shows reduction of the outlet pressure ripple amplitude in case of insufficient precompression (outlet pressure is higher than calculated for complete elimination of decompression). Since the fluid pressure in the transferred volume never reaches the outlet pressure some decompression flow occurs when current transferred volume merges the outlet cavity. Residual decompression flow generates negative outlet pressure peaks. These peaks amplitude is defined by residual pressure drop at the moment of merging the transferred volumes with the outlet cavity. Even in this case the pressure ripple amplitude drops down from 17% (without the active pulsation suppression system) to 4% (with the active pulsation suppression system) of the average outlet pressure.

CONCLUSION

Data presented in 4 show significant reduction of the outlet pressure ripple and fluid born component of acoustic noise when using the active pulsation suppression system based on the precompression method. This system transforms sharp decompression pressure pulsations to relatively small secondary cinematic nonuniformity of displacement which can be readily surmounted in a pressure line and useful load by volumetric capacity. Additional positive effect of this system implementation is recycling some part of energy otherwise being wasted on decompression.

REFERENCES

1. Stroganov, A.A., and Volkov, Y.M., “New Adaptive Rotor in the Vane-In-Groove Pumps: Significant Reduction of the Mechanical Losses,” Proceedings of the 50th National Conference on Fluid Power, March 16-18, 2005, Las Vegas, Nevada USA, pp 531-540
2. Stroganov, A., Volkov, Y., Zimnikov, A., and Drouzhinin, A., “New Type of Reversible, Invertible, Variable Hydraulic Pump/Motor,” Proceedings of the 49th National Conference on Fluid Power, March 19-21, 2002, Las Vegas, Nevada USA, pp 123-128
3. Stroganov, A.A., Volkov, Y.M., and Zimnikov, A.N., “New Type of Reversible, Invertible, Variable Hydraulic Pump/Motor,” Proceedings of the Eighth Scandinavian International Conference on Fluid Power, May 7-9, 2003, Tampere, Finland, Vol. 1, pp 239-251
4. Stroganov, A.A., and Zimnikov, A.N., “Rotary Machine,” Patent No.: US 6,547,546 B1, Apr. 15, 2003
5. Stroganov, A.A., Volkov, Y.M., Ryadnov, S.A., “Active and Adaptive Annihilation of the Pressure Pulsations in the Vane-In-Groove Pumps,” Proceedings of the 50th

National Conference on Fluid Power, March 16-18, 2005, Las Vegas, Nevada USA, pp 541-559
6. Ryadnov S.A, Stroganov, A.A., Volkov, Y.M., “Method of generation of a surgeless flow of the working fluid and a device for its implementation”, International Application No.: PCT/RU2006/000163
7. Hattori Katushiko, “Hydraulic vane pump”, Patent No.: US 4,738,603, October 27, 1986
8. Agner, “Vane pump precompression chamber”, Patent No.: US 5,975,868, November 2, 1999
9. A. Stroganov, L. Sheshin, Y. Volkov, S. Ryadnov, A. Nikiforov, “High Efficiency at 100 – 2000 RPM and 10 – 35 MPa: Vane-In-Groove Pumps With Adaptive Rotor”, Proceedings of the Tenth Scandinavian International Conference on Fluid Power, May 21-23, 2007, Tampere, Finland

CHANGING THE PARADIGM

Peter A.J. Achten
Innas BV
Nikkelstr. 15
4823AE Breda, Netherlands
Phone +31 76 542 4080, Fax +31 76 542 4090
E-mail: pachten@innas.com

ABSTRACT

The stronghold of the hydraulic industry is the cylinder. Nothing beats a hydraulic cylinder if it comes to compactness, durability, stiffness, or costs. In the field of rotational power however, hydrostatic drives have a strong competition from mechanical and electrical transmissions. Whereas hydrostatic transmissions are favoured for their power density and variable transmission ratios, the lower efficiency (especially at part load and break away conditions), higher noise levels and higher costs offset these strengths. As a result the mobile hydraulic industry is locked in the (albeit large) market niche of excavators, loaders and other off-road machines where hydraulic cylinders are a must.

The floating cup principle for hydrostatic pumps, motors and transformers can change this situation. Its high efficiency and starting torque, the low pressure and torque variations, the high power density and the low cost design enable the realization of a full hydrostatic drive train with in-wheel hydraulic hub units in all wheels. The floating cup principle also allows the realization of the Innas Hydraulic Transformer. Finally, the combination of in-wheel hydrostatic motors and hydraulic transformers creates the opportunity for making a 'hydrid': a hydrostatic hybrid vehicle having all the advantages of hybrid electric vehicles but without the cost increase of these vehicles.

KEYWORDS: Floating cup principle, hydraulic hybrid vehicle

1 THE UGLY DUCKLING

The fluid power industry has a rock-solid reputation. Hydraulic components and systems are able to deliver robust, reliable and compact solutions where mechanical and electromechanical transmissions even can't get close. The diversity of the applications is enormous as is the variety of hydraulic components. However, the fluid power industry also has a rock-solid reputation if it comes to component cost, noise and (lack of) efficiency. The specific production cost (in €/kg) of hydraulic pumps and motors can

be up to an order of a magnitude higher than of automotive manual transmissions. The cost increases further if insulation or dampers have to be applied for noise attenuation. Also the poor efficiency causes higher investment and running cost. Although hydraulic systems have the inherent advantage of energy losses being carried away by the oil, a larger installed cooler capacity increases the system cost. Moreover, friction results in higher torque losses. Especially at start-up conditions this can result in a strong reduction of the breakaway torque of hydrostatic motors. As a result, larger and more expensive motors have to be installed, often in combination with an expensive 2-speed option.

On the other hand, the overall efficiency of hydrostatic transmissions is not necessarily worse than of electric motors, automatic gear transmissions or CVT's. Especially if the hypoid and differential gear can be avoided, and with that, the losses of these transmissions, hydrostatic transmissions might have a good chance for application in hybrid vehicles, even in passenger cars. After all, the most efficient and cost effective differential is the hydraulic T-joint. In case of a 4-wheel drive the advantage would even be doubled due to the complex mechanical configuration having three differentials (see figure 1). The limited energy capacity of hydraulic-pneumatic accumulators is not much of a concern either, since the size of the energy storage is largely determined by the power demand at low temperatures, at which conditions especially electrochemical batteries have a poor performance.

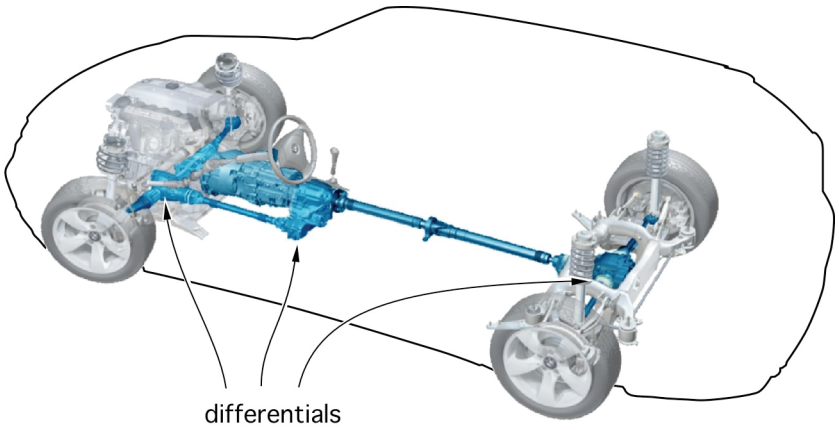

Figure 1: All-wheel-drive vehicle

This raises the question whether there is a chance for full hydrostatic transmissions in the automotive market? And what would be needed to improve the feasibility of these transmissions? This paper attempts to address these questions. The approach taken differs from several previous projects in which the hydrostatic system is considered to be an add-on in a parallel hybrid configuration such as in the system developed by Permo-Drive [1] or the hydraulic launch assist (HLA) from Eaton [2]. It also differs from the recent HHV-development of the Environmental Protection Agency (EPA) in the USA [3] or the latest generation of Cumulo systems developed by Volvo Hydraulics in Sweden [4]. These designs are serial hybrid systems with a hydrostatic unit connected to the differential gear of the rear axle.

This paper discusses the opportunity to completely eliminate the mechanical transmission, including the differential gear and the driving shafts. In this configuration, wheels are directly driven by means of hydraulic hub motors and all power distribution

is achieved by means of hydraulic lines. The recuperation of energy during deceleration of the vehicle is considered to be an option: even without the use of energy storage the hydrostatic transmission has to be competitive with the mechanical driveline.

2. FLOATING CUP PRINCIPLE

The floating cup principle (figure 2, [5-12]) is considered to be a breakthrough technology for such an automotive hydrostatic transmission. The floating cup is a rather new axial piston principle featuring a large number of pistons and a low-friction behaviour. The principle can be applied in hydrostatic pumps and motors, both constant and variable, as well as in hydraulic transformers [5, 15].

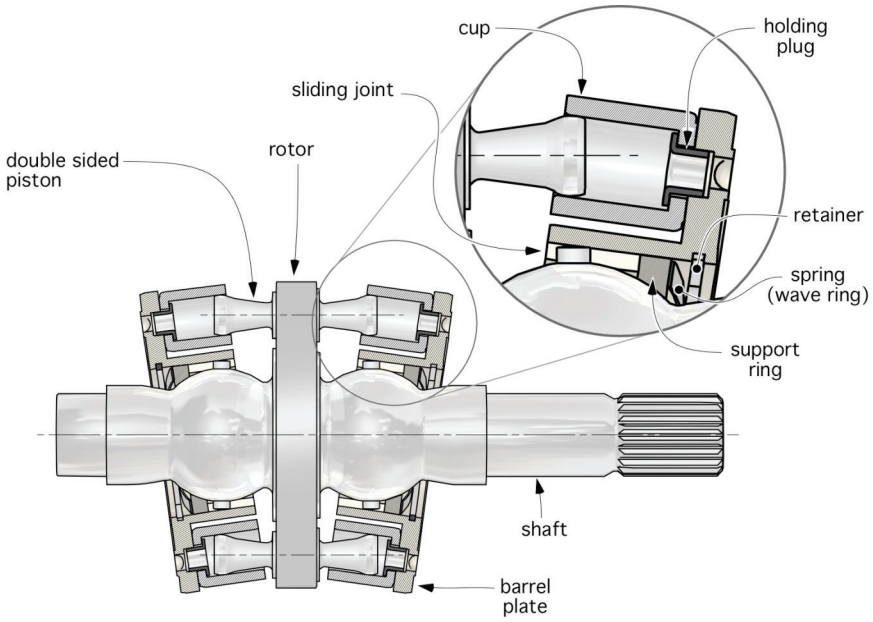

Figure 2: Rotating parts floating cup principle

The high number of pistons (about 3 times as much as in conventional axial piston pumps and motors) strongly reduces the torque variations. Combined with the low-friction behaviour this results in a high start-up torque.

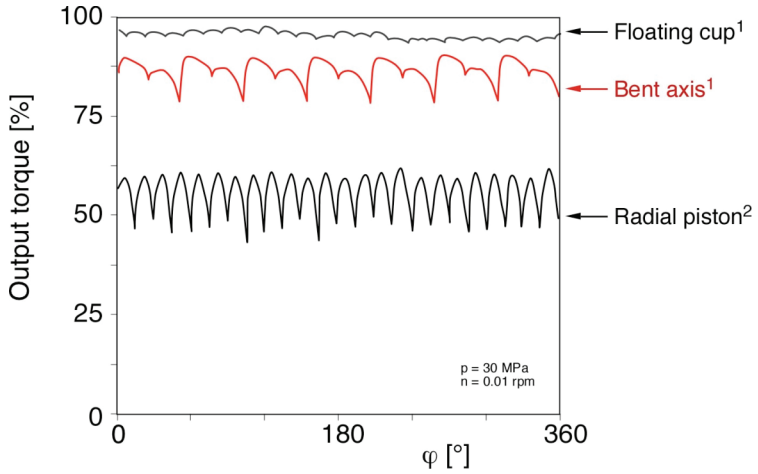

Figure 3: Start-up torque efficiency for 3 different constant displacement motors
[1]measurements IFAS Aachen [11] [2]measurements Parker

Figure 3 shows a comparison of the breakaway torque efficiency relative to the maximum theoretical torque for a floating cup motor, a bent axis machine and a radial piston motor. The floating cup motor has by far the smallest torque variation and the highest starting torque.

An important characteristic of the floating cup principle is the small tilt angle of the barrel, being around 10°, which is much smaller than the 45° angle of some bent axis units. Despite the small barrel angle the floating cup principle is extremely compact and low-weight. For a range of displacement volumes figure 4 presents the weight of a series of floating cup machines compared to state-of-the-art bent axis and slipper type machines. The comparison has been made for the same rated pressures and speeds and assuming cast iron as the material for the housing. A more extensive analysis of the power density of the floating cup principle can be found in the literature [10].

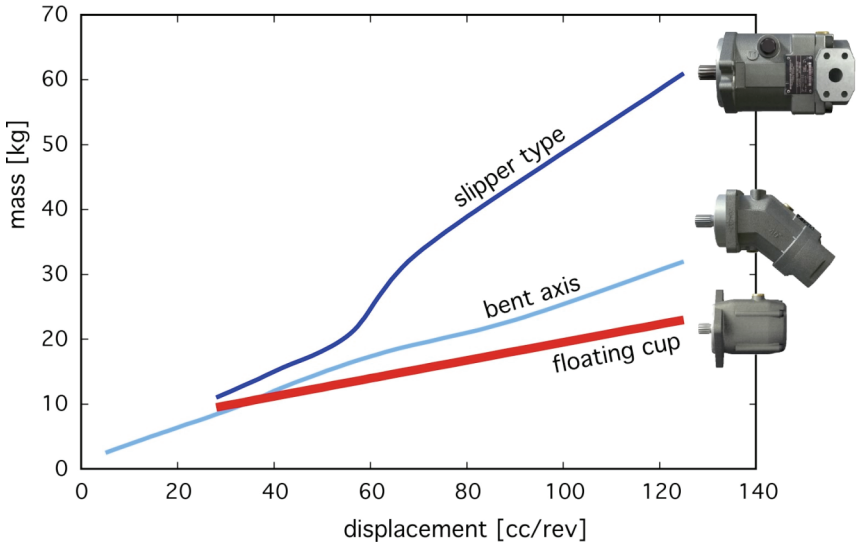

Figure 4: Weight comparison of constant displacement axial piston motors at equal pressure and speed rating

The comparison clearly shows the high power density of the floating cup principle. Furthermore the floating cup machines are shorter than the slipper type and bent axis machines, which is favourable for mounting the unit in the wheel hub.

The higher power density, the high start-up torque and the high efficiency of the floating cup machine all contribute to cost reduction. But above all the design of the floating cup principle is designed for low manufacturing cost. Although the principle is a multi-piston design having many components, the only critical tolerance is between each piston and cup. Because these are separate components, the cups and pistons can be sorted. This has the advantage that the production of the components itself does not need to be precise. Instead the sorting and matching process achieves the required tolerance, similar to the way that bearings, hydraulic lash adjusters and many other (automotive) components are manufactured. Furthermore, the components of the floating cup machines are designed as such that they can be produced by means of modern cost effective production technologies like deep drawing, stamping, fine blanking and sintering. These technologies have been applied for decades in the automotive industry, also for the production of automotive *hydraulic* components like chain tensioners, or variable camshaft driving systems.

3. THE ‘HYDRID’ VEHICLE

There are many reasons for eliminating the mechanical transmission in automobiles (and other road vehicles). Mechanical transmissions are characterized foremost by being inflexible in terms of transmission ratios, energy storage, power management and vehicular design. The design of the car is rather influenced by the position of the mechanical drive train components, especially if all wheels have to be driven. The manual gear transmission offers only a limited number of gear transmission ratios, whereas the continuously variable transmission or CVT suffers from a lower efficiency. New demands, like increased safety or reduced carbon dioxide emissions will put further pressure on the pure mechanical transmission.

To overcome the limitations of the mechanical transmission, in some vehicles the drive train has been expanded with the addition of electro-mechanical transmissions, electrical converters and electro-chemical batteries. All sorts of hybrid transmissions have been designed, ranging from micro-hybrid, like the GM Saturn Aura, to full or strong hybrid solutions like the Toyota Prius. In theory the mechanical transmission could be eliminated completely, thereby avoiding ‘double trouble’. The limited power and torque density as well as the high costs of current electric motors, inverters and batteries however does not allow for a direct drive of the wheels. Instead a compromise is made utilizing the electric drive for urban stop-and-go operation and the stronger internal combustion engine for driving on highways and interstates.

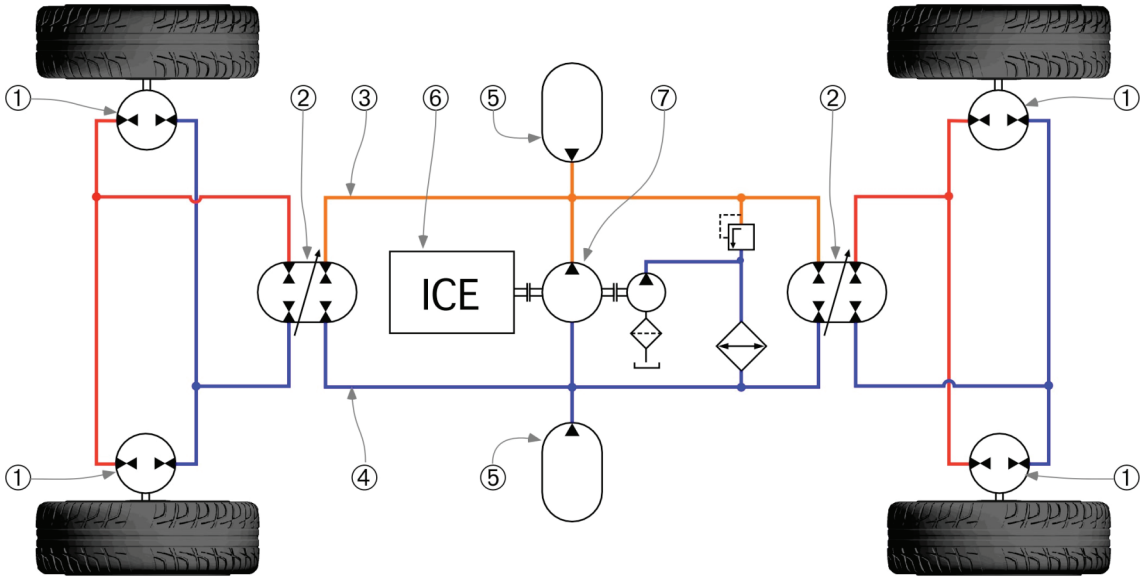

① constant displacement hydrostatic pump/motor
② hydraulic transformer
③ common pressure rail: high pressure
④ common pressure rail: low pressure
⑤ hydraulic accumulator
⑥ internal combustion engine
⑦ supply pump

Figure 5: Lay-out of a ‘hydrid’ vehicle having a full hydrostatic automotive transmission

As an alternative, a full hydrostatic transmission is proposed (figure 5), completely avoiding the clutch, the mechanical transmission, the final gear and the differential gears as well as any shafts and constant velocity universal joints. In this hydraulic hybrid or 'hydrid' concept, each wheel has its own hydrostatic hub unit, having a hydraulic differential for the front and one for the rear 'axis'. The torque delivered by the hub units would be linearly dependent on the pressure level at the high pressure site, which in turn would be controlled by means of a hydraulic transformer.

The hydraulic transformer is coupled to a common pressure rail or CPR, similar to the voltage rail of an electrical grid. Hydraulic-pneumatic accumulators can be connected to the CPR-system creating the possibility for power management of the internal combustion engine and recuperation of the kinetic energy of the vehicle during braking. The CPR is the backbone of the system to which other hydrostatic loads can easily be connected. It also offers the opportunity for a closed centre steering system, thereby eliminating most of the high power and energy consumption of current hydraulic power steering systems. It would even be possible to connect a battery to the CPR by means of a small electro-hydraulic unit, creating the possibility for a larger amount of energy storage.

The application of hydraulic transformers has a number of advantages:

- The engine operation is separated from the load. In the hydrid system the engine has the function of a power station, supplying energy and power to the common pressure rail, whereas the hydraulic transformers control the wheel torque, fulfilling the function of a CVT. With that, the engine can become smaller and can be operated better in or near its optimum or 'sweet' point.

- One transformer can control two or even all four wheel motors. In the latter case the second transformer has to be replaced by a valve, which allows for the coupling or decoupling of the second axis. The hydraulic differential eliminates the need for an active load control for the left and the right wheel. It also offers a simple solution for creating a differential lock between the left and right wheel.

- The wheel motors can be simple constant displacement units. Although the hydraulic transformer creates some extra losses, this is compensated by the higher efficiency of the constant displacement units. The constant displacement units are also much smaller and lighter than secondary controlled variable displacement units. Furthermore, constant displacement units can be better optimized for low noise and pulsation levels than variable displacement machines.

- The transformer can also amplify the pressure [15], creating the ability of having a high break-away torque with relatively small wheel motors.

- The transformers allow for four-quadrant operation, creating the opportunity for recovery of the kinetic energy of the vehicle.

It has already been shown that a transformer can be built on the basis of a constant displacement principle [15]. This Innas Hydraulic Transformer or IHT has the transmission characteristic of a DC motor, being able to deliver high loads at low rotational speeds and high flows at low loads. In order to reduce the pressure pulsations

and improve the low speed characteristics the number of pistons has to be maximized. The floating cup principle meets this demand.

The application of hydrostatic units being mounted in the wheel hub sets strict demands for the size, dimensions, weight and costs of these units. As already mentioned, the application of hydraulic transformers creates the opportunity for having simple, small and light constant displacement units. The application of a hydrostatic unit in all wheels further decreases the size and the weight of the units. This creates the opportunity for combining the need for high traction at low speeds, having all four motors in operation, and reduced oil flows at high vehicular speeds, thereby putting one of the hydraulic transformers in the neutral position. The all-wheel-drive (AWD) configuration has a much better traction distribution and traction control than a standard 2-wheel drive, but contrary to a mechanical AWD-configuration the two transformers give the ability of a full variable control of the torque distribution between the front and the rear axis. Different from most hybrid electric vehicles, the hydrostatic AWD-configuration also has the advantage of having energy recovery at all 4 wheels. Finally the elimination of the mechanical axis and constant-velocity joints also eliminates any turning angle restriction created by the mechanical wheel drive and gives the opportunity for a smaller turning angle of the vehicle, eventually allowing steering action on all four wheels.

4. HYBRID ELECTRIC VEHICLES

Hybrid vehicles, or better to say, hybrid electric vehicles (HEV's) have become a hype in the past 10 years, especially driven by the US-market. In 2006 more than 250.000 HEV's were sold in the USA, representing 1.5% of all light duty vehicles sold in the US in that year. Toyota is leading the market, having a market share of more than 75%. Many other car manufacturers have followed Toyota and have also introduced or are working on the development of hybrid vehicles. Without any exception these are all hybrid electric vehicles. Also in the heavy-duty truck market, almost all developments point in the direction of electric versions of hybrid drive trains. An exception is the project of the US environmental protection agency (EPA), Eaton and UPC in which a hydraulic hybrid delivery truck has been developed [3].

The driving factor behind the hybrid vehicle is to reduce fuel consumption and exhaust gas emissions, especially carbon dioxide. Most of the time, automotive internal combustion engines are driven in part load conditions. This has a detrimental effect on the efficiency of the internal combustion engine, in particular in the case of gasoline engines. According to German (in [16]) the fuel efficiency can be improved by 5 to 15% by means of engine optimization or downsizing. Furthermore a considerable part of the fuel is burned during idle operation. Some hybrid systems only try to eliminate or reduce the idle fuel consumption, resulting in an efficiency gain of 5 to 8%. Other, larger sized hybrid systems also try to improve the engine efficiency by assisting the engine in delivering extra power and traction at low speed conditions. In these so called strong or full hybrid systems, the engine size is reduced and the engine is operated more near the point of optimum efficiency. In full hybrid electric vehicles (like the Toyota Prius, see figure 7) the battery capacity has to be expanded in order to facilitate sufficient electric power. The larger batteries also have the advantage that part of the kinetic energy can be recuperated during braking. The fuel efficiency of the vehicle could then be increased further by another 5-20%. According to Green et al [17] the fuel economy of passenger cars can be improved up to 40% if a full hybrid system is

implemented. Borgmann and Klüting [18] however expect a reduction of the fuel consumption of only 17-20%.

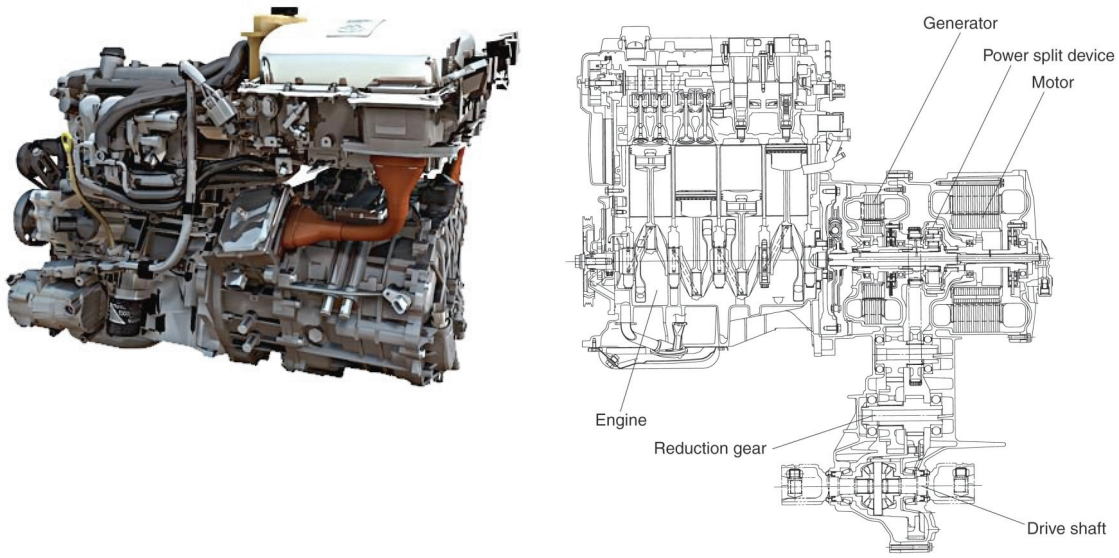

Figure 7: Engine and transmission of the Toyota Prius II. The photo on the left also includes the power control unit on top of the transmission. The batteries are not shown.

Finally the batteries can also be charged by means of the electricity grid (the plug-in hybrid electric vehicle or PHEV-concept). Although this does not improve the efficiency of the vehicle as such, the target of the PHEV is to reduce oil dependency of vehicles. For that the battery capacity has to be expanded considerably. Plug-in HEV's are therefore much more expensive than non-plug-in vehicles [19].

In recent years detailed studies [20-25] have been performed investigating the pros en cons of HEV's. Many reports show a significant reduction of the specific fuel consumption compared to standard gasoline cars, although in most studies the fuel consumption proved to be considerably higher than what was claimed by the manufacturers. Non-hybrid vehicles driven by an efficient diesel engine can achieve about the same mileage as gasoline HEV's, however with a much smaller cost penalty. The incremental costs of the additional electrical system are considered to be the most limiting factor for hybrid electric vehicles. Currently the Toyota Prius II costs US$ 7.600 more than a comparable conventional Corolla [26]. In Germany and France the cost difference is around €8.750. Even at large scale production the incremental manufacturing cost for a full hybrid electric vehicle are estimated to be between $1800 and $4600, depending on the size of the vehicle [27]:

Table 1: Incremental manufacturing cost for full hybrid vehicles at large scale production (US$ year 2000)

compact	2908
mid-size	1826
large pick-up	4603
mini-van	3492
SUV	4001

For the retail price of the vehicle this means a cost increase of around 20%. Full hybrid electric vehicles are also in the long run expected to be around 85 kg heavier than comparable non-hybrid vehicles [28]. The relatively low weight of the Toyota Prius is mainly achieved by applying lightweight body parts. There is also more energy needed for the production of hybrid electric vehicles. According to Toyota [29] it costs about 45% more energy to manufacture the Prius than a comparable gasoline car. A study performed by Weiss, et al [30] showed a similar result if only virgin materials were to be used.

In order to reduce the cost of hybrid electric vehicles, the manufacturing cost of electric motors, inverters and controllers, and batteries have to be reduced strongly, whereas at the same time the durability, abuse safety and efficiency have to be increased. According a recent industry forecast study [31] mild-hybrid vehicles will predominate the HEV-market in the future, offering launch assist and avoiding engine idling, but having limited or no capacity for energy recuperation during braking. Other studies claim a further reduction of costs for batteries, inverters and electric motors and generators [25, 27, 32]. On the battery site most developments focus on the Lithium-ion (Li-ion) battery, which has a higher power and energy density than NiMH-batteries as well as a higher efficiency. Another development is the development and application of super- or ultracapacitors [33]. The characteristics of these storage devices are very similar to hydraulic accumulators, having a poor energy density but a much higher power density than NiMH, Li-ion or other chemical batteries. Other advantages of the supercapacitors are the high efficiency and good lifetime (> 100.000 cycles).

5. ABANDONING THE MECHANICAL TRANSMISSION

A more radical approach in the design of (hybrid) electric vehicles is visible in some concept cars like the Toyota Fine (figure 7) or the Mitsubishi MIEV in which the mechanical drive train is completely eliminated.

Figure 7: Toyota Fine-X concept car having 4 in-wheel electric hub motors

In these concepts, all 4 wheels are driven by each an electric in-wheel hub motor. Siemens VDO (eCorner) and Michelin (Hy-Light) have announced concepts in which not only an electric wheel motor replaces the mechanical drive but also the suspension and brake functions are made electrical. The advantages of these all wheel drive concepts are obvious [34]:

- increased climbing performance
- increased traction performance
- improved moving-off traction
- more precise handling
- increased pay-load and trailer load
- improved crash resistance due to energy absorption by the whole power train
- identical roll steer effect under different weather conditions

In fact, these are the same advantages as for any other mechanical all-wheel drivetrain. But having a separate motor in each of the wheels would give additional controllability advantages, as well as improved maneuverability.

Current automotive transmissions are however hart to beat. Especially manual transmissions are rather efficient and low-cost. According to Lechner [34] a manual transmission has an average efficiency of 92-97%. Kluger [35] measured an average efficiency of 96.2%. (Locked) automatic transmissions and continuously variable transmissions have a lower efficiency, showing average efficiencies of around 85% [35]. All these values are excluding the final gear, differential and auxiliaries like power steering. Especially bevel gears can introduce substantial extra torque losses, having a maximum efficiency of around 92% [34]. This is especially of importance for four-wheel and all-wheel mechanical drive trains in which three differentials are being used to split the power across the wheels. The efficiency of manual gear transmissions is not much influenced by the gear chosen. According to Kluger [35] the efficiency varies between 92% (second gear) and 97% (forth gear). In automatic transmissions the gear influence is larger, having an efficiency of 89% in the fifth gear and only 70% in the first gear. Summarized, the total average drive-train efficiency between clutch and wheel varies between 78% for an all-wheel driven vehicle with automatic gearshift, to 90% for a simple manual transmission.

Figure 8 shows the influence of the gear on the total efficiency of the vehicle, including the efficiency of the engine. The low efficiency at low gear is especially due to the part load efficiency of the internal combustion engine. By means of adding an extra power source to the vehicle, the engine size can be reduced and the engine can be driven more near the point of highest efficiency.

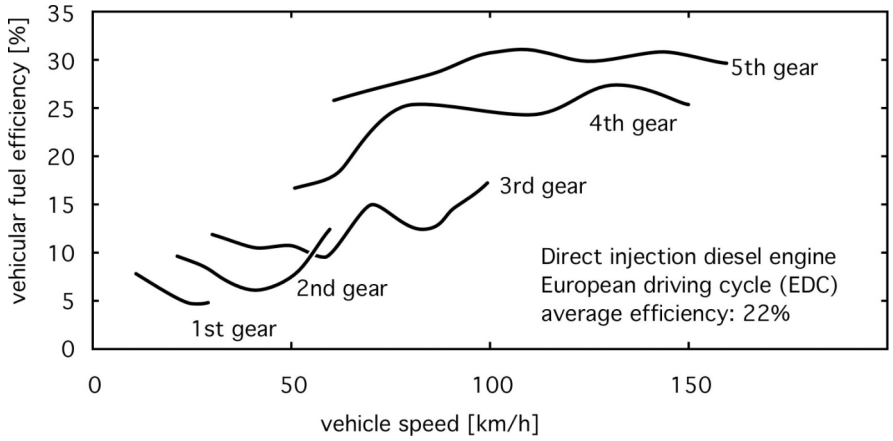

Figure 8: Fuel efficiency of a passenger car (Lenz TU Wien in [36])

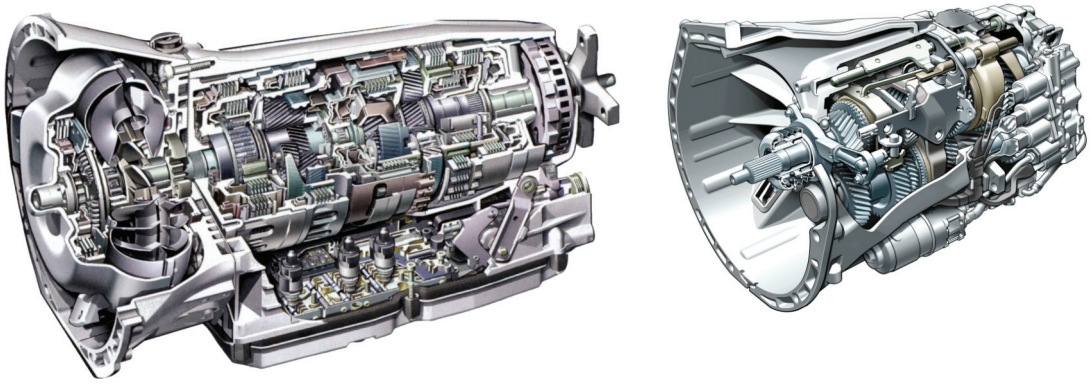

automatic gear transmission manual gear transmission

Figure 9: Automotive gear transmission

The costs of transmissions are strongly related to the type of transmission, the maximum torque requirement and the number of gear steps [34]. In a recent study the US Environmental Protection Agency and FEV [3] have given specific manufacturing costs of automotive components. Due to their complexity, automatic transmissions are per unit of weight 21% more expensive than manual transmissions [34]. This than results in the following weight specific manufacturing costs for automotive transmissions:

Table 2: manufacturing cost in US$ (year 2000) per kg

Engine:	9.11 $/kg
Automatic transmission:	10.45 $/kg
Manual transmission:	8.63 $/kg

In another study [37] an average value of 10 €/kg has been used.

In an elaborate study [38] of Porche and the ULSAB (UltraLight Steel Auto Body, a consortium of 35 sheet steel producers from 18 countries) a detailed analysis of the weight structure of a Ford Focus is made. Combining the data from the ULSAB-study with information from the automotive industry results in the following weights and costs of automotive drive train components, assuming a specific cost of 10 €/kg:

Table 3: Drive train component mass and manufacturing cost (at 10 €/kg)

Component	Mass [kg]	manufacturing cost [€]
Gasoline engine (1.4 L, 55 kW)	148	1480
Diesel engine	184	1840
Manual transmission	64	640
Automatic transmission	92	920
All-wheel-drive manual transmission	156	1560
All-wheel-drive automatic transmission	184	1840

Any competitive alternative for the mechanical transmission should stay within the above constraints. The alternative should not weight more than around 60-180 kg, and the average efficiency should be at least 90% if compared to a manual gear transmission.

6. THE HYDRAULIC ALTERNATIVE

The hydraulic hybrid transmission shown in figure 5 complies with these requirements. For a mid-size vehicle, having an empty weight of 1300 kg, a maximum vehicle speed of 190 km/h, and a dynamic wheel radius of 0,31 m, the main components have the following dimensions:

Table 4: component size and characteristics of the hydrid drive train:

Component	max. power	size	max. pressure	max. speed
Internal combustion engine	55 kW			6000 rpm
Pump		17 cc/rev	350 bar	6000 rpm
Hydraulic transformers		36 cc/rev[1]	500 bar	3500 rpm
Hydraulic motors		30 cc/rev	500 bar	1620 rpm (@ 190 km/h):

[1] defined in pump equivalents

The size of the internal combustion is chosen to be able to deliver the same maximum power at maximum vehicular speed as for the original mechanical transmission. It is estimated that the engine size can be reduced from 84 kW for the mechanical transmission to 55 kW for the 'hydrid' configuration. In the hydrid transmission, the torque curve of the engine no longer determines the torque delivered at start-up (see figure 10). Instead the hydraulic motors deliver the maximum torque almost independent of the vehicular speed, up to a point where the hydraulic transformer demands the maximum power of the internal combustion engine. The smooth torque delivered by the floating cup motors also allow for smooth vehicle behaviour even at very low vehicular speeds.

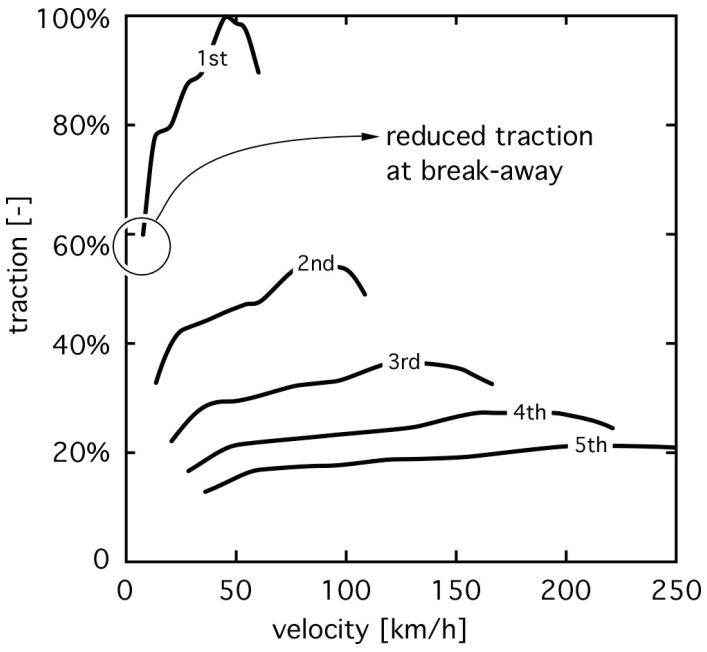

Figure 10: Traction curves of a mid-sized car at different gears, showing the reduced traction at starting or break-away conditions [34]

Each hydraulic in-wheel motor has a mass of about 9 kg. The weight can further be reduced if the hydrostatic units are integrated in the bearing structure of the wheel. Excluding the housing and the bearings, the rotating group of the wheel motor would only weight 3.5 kg. The hydraulic transformers are the heaviest components, having each an estimated weight of about 19 kg. The pump does not need to supply the full flow required by the four in-wheel motors at high vehicular speeds. The reduced torque requirement at high vehicle speeds will be met by the control of the hydraulic transformers, thereby reducing the supply flow to the transformers. If, for instance the motors only require a flow of 100 L/min at a pressure level of 100 bar, the pump only needs to deliver 33 L/min at 300 bar. This strongly reduces the size of the pump, resulting in a maximum displacement of 17 cc/rev, having an estimated weight of only 6 kg.

Constant displacement floating cup machines have a peak efficiency of 98%, hydraulic transformers of 96%. Idle losses will be avoided completely since the internal combustion engine only runs if needed for maintaining the pressure level in the high-pressure accumulator. As an option the accumulators could be enlarged to allow (at least for a part) for recuperation of the kinetic energy of the vehicle during deceleration. Accumulators can have an efficiency of 98% [39], much higher than the NiMH-batteries of current hybrid electric vehicles having an efficiency of 70-85% [25]. Like super-capacitors, the hydraulic accumulators are excellent devices for handling high power levels and have an almost unlimited cycle life-time.

7 BRINGING TWO WORLDS TOGETHER

The total weight of the full hydraulic transmission for a mid-size vehicle will be around 150 kg. Taking into account the lower weight of the smaller internal combustion engine and the weight of the replaced mechanical transmission, the net weight increase will be on par with current mechanical 2-wheel drive trains. For that the vehicle will obtain:

- an all wheel drive
- in-wheel motors in all 4 wheels
- high starting torque at break away conditions
- separate continuously variable transmissions for the front and the rear axes
- hybrid vehicle fuel economy benefits, without the high costs of electric systems
- including an option for energy recuperation on all 4 wheels
- full integration of other hydraulic actuators, like (close centre) power steering and active suspension systems

Unlike many electric components, hydraulic components and systems have an outstanding reputation if it comes to reliability, being able to resist high loads, large G-forces, humidity and dirt. Moreover they can operate in a wide operating temperature range. On the other hand the hydraulic industry has to learn from the automotive industry how to lower manufacturing cost by means of introducing mass production technologies into the design of hydrostatic components. Up till now the mobile machinery market has been separated from the automotive market. It is time to bring the two together.

REFERENCES

[1] www.permo-drive.com/

[2] "Eaton and Peterbilt to Produce Hydraulic Hybrids", Green Car Congress, 20 October 2004, www.greencarcongress.com/2004/10/eaton_and_peter.html

[3] J. Alson et al (2004), Progress report on clean and efficient automotive technologies under development at EPA – Interim Technical Report, www.epa.gov/otaq/technology.htm

[4] C. Hugosson (1995) Cumulo Hydrostatic Drive – a Vehicle Drive with Secondary Control, The Third Scandinavian Int. Conference on Fluid Power, Linköping, Sweden, May 25-26, 1995, vol. 2, pp 475-494

[5] P.A.J. Achten (2002) "Dedicated design of the Hydraulic Transformer", Proc. IFK.3, Vol. 2, IFAS Aachen, pp. 233-248

[7] P.A.J. Achten, T.L Van den Brink, T. Paardenkooper, T. Platzer, H.W. Potma, M.P.A. Schellekens and G.E.M. Vael (2003), "Design and testing of an axial piston pump based on the floating cup principle", Proc. SICFP'03, Vol. 2, Tampere University of Technology, pp. 805-820

[8] P.A.J. Achten (2003), "Designing the impossible pump", Proc. Hydraulikdagar 2003, Linköping University

[9] T. Platzer, R.A.H. van Malsen and P.A.J. Achten (2004), "Floating Cup - Ein neues Konstruktionsprinzip für hydrostatische Maschinen", Ölhydraulik und Pneumatik, (5)

[10] P.A.J. Achten (2004), Power Density of the Floating Cup Axial Piston Principle, IMECE2004-59006, 2004 ASME Int. Mech. Eng. Congress and Exposition, Novem¬ber 13-20, 2004, Anaheim, California USA

[11] P.A.J. Achten, Schellekens, M., Murrenhoff, H., Deeken, M., 2004, Efficiency and Low Speed Behavior of the Floating Cup Pump, SAE 2004-01-2653

[12] P.A.J. Achten, T. van den Brink, M. Schellekens, (2005) Design of a variable displacement floating cup pump, Proc. 9th Scandinavian Int. Conf. on Fluid Power, SICFP'05, Linköping, Sweden.

[13] P.A.J. Achten (2005) Volumetric Losses of a Multi Piston Floating Cup Pump, NFPA/IFPE 2005, Las Vegas, March 16-18, 2005

[14] W. Post (2004), Determination of steady-state performance of Innas Floating Cup type of axial piston pumps (ISO 4409), DCT-report 2004-127, Eindhoven Technical University

[15] P.A.J. Achten, Zhao Fu, G.E.M. Vael, Transforming future hydraulics: a new design of a hydraulic transformer, Proc. SICFP '97, Part 3, IKP, Linköping University, 1997

[16] J. Alson, B. Ellies, D. Ganss (2005) Interim report: New powertrain technologies and their projected costs, Transportation and Climate Division, Office of Transportation and Air Quality U.S. EPA

[17] D.L. Greene, K.G. Duleep, W. McManus (2004) Future potential of hybrid and diesel powertrains in the U.S. light-duty vehicle market, Oak Ridge National Laboratory.

[18] K. Borgmann, M. Klüting (2006) Effiziente Dynamik – Langfristige Entwicklungstrends bei BMW-Antrieben, MTZ Extra – Antriebe mit Zukunft

[19] T. Markel, A. Brooker, J. Gonder, M. O'Keefe, A. Simpson, M. Thornton (2006) Plug-In hybrid vehicle analysis, National Renewable Energy Laboratory (NREL), NREL/MP-540-40609

[20] R. Winkel, E. van denTillaart, E., J. Eelkema, R. Smokers (2002) Comparative assessment of fuel consumption for conventional and hybrid vehicles, Proceedings 19th International Battery, Hybrid and Fuel Cell Electric Vehicle Symposium (EVS 19), Busan, Korea, October 19 - 23, 2002 (TNO-paper VM 0208)

[21] S. Plotkin et al (2001) Hybrid electric vehicle technology assessment methodology, analytical issues, and interim results, Argonne National Laboratory report ANL/ESD/02-2

[22] M.R. Cuddy, K.B. Wipke (1997) Analysis of the fuel economy benefit of drivetrain hybridization, SAE 970289

[23] G.Y. Liao, T.R. Weber, D.P. Pfaff (2004) Modelling and analysis of powertrain hybridization on all-wheel-drive sport utility vehicles, Proc. Instn. Mech. Engrs Vol 218 Part D: J. Automobile Engineering, p. 1125-1134

[24] Karner (2005) US Department of Energy hybrid electric vehicle battery and fuel economy testing, 11th Asian Battery Conference Ho Chi Minh City, Vietnam - 6th-10th September 2005

[25] P. Christides, et al (2005) Hybrids for road transport –status and prospects of hybrid technology and the regeneration of energy in road vehicles, European Commission Technical Report EUR 21743 EN

[26] R. Smokers et al (2006) Review and analysis of the reduction potential and costs of technological and other measures to reduce CO2-emissions from passenger cars, Final Reort, TNO, The Netherlands

[27] T.E. Lipman, M.A. Delucchi (2003), Hybrid-Electric vehicle design retail and lifecycle cost analysis – final report, UCD-ITS-RR-03-01, Institute of Transportation Studies, University of California

[28] P. ten Brink et al (2005) Service contract to carry out economic analysis and business impact assessment of CO2 emissions reduction measures in the automotive sector – final report, Institute for European Environmental Policy

[29] Prius Green Report, Toyota

[30] M.A. Weiss, J.B. Heywood, E.M. Drake, A. Schafer, F. AuYeung (2000) On the road in 2020 – a life-cycle analysis of new automobile technologies, Energy Laboratory MIT Cambridge, Energy Laboratory Report MIT EL 00-003

[31] The Freedonia Group (2006) World Hybrid-Electric Vehicles to 2010

[32] R.M. Cuenca, L.L. Gaines, A.D. Vyas (1999), Evaluation of electric vehicle production and operating costs, Argonne National Laboratory, report ANL/ESD-41

[33] Kötz (2005) Supercaps -Eigenschaften und Fahrzeuganwendungen, VDI-Berichte Nr. 1874, 2005 p. 175-188

[34] G. Lechner, H. Naunheimer (1999) Automotive transmissions – fundamentals, selection, design and application, Springer Verlag ISBN 3-540-65903-X

[35] M.A. Kluger, D.M. Long (1999) An overview of current automatic, manual and continuously variable transmission efficiencies and their projected future improvements, SAE 1999-01-1259

[36] M.Pulfer (2006) Konzept 2004-2007, Technologiebereich Verkehr & Technologiebereich Akkumulatoren – Effizient bewegen & wirksam speichern! Bundesambt für Energie BFE, Switserland

[37] E. Wijn (2005) Feasibility study for an ultra-compact hybrid driveline, Eindhoven University of Technology, Report DCT 2005.113

[38] ULSAB-AVC (2001), PES Engineering Report, Chapter 2, Program Targets

[39] G.R. Wendel, T.W. Jackson (2006), Balance of power – hydraulic-powered components add to vehicle efficiency, reduce emissions, Technology Today, Fall 2006, p. 2-5.

THE USE OF VIRTUAL PROTOTYPING AND SIMULATION IN ITER CMM/SCEE-MOVER CONTROL SYSTEM DEVELOPMENT

Salvador Esqué[1], Jouni Mattila[1], Hannu Saarinen[1], Liisa Aha[1], Mikko Tolonen [1], Ali Muhammad[1], Tapio Virvalo[1], Arto Timperi[2], Jorma Jarvenpää[2], Mikko Siuko[3], Jim Palmer[3], Mike Irving[3], Matti Vilenius[1]

[1)] Tampere University of Technology,
Institute of Hydraulics and Automation
PO Box 589, 33101 Tampere, Finland
Phone +358 3 3115 2213, Fax +358 3 3115 2240
E-mail: salvador.esque@tut.fi
[2)] VTT Industrial Systems, PO Box 1300, 33101 Tampere, Finland
[3)] EFDA-CSU Garching, Boltzmannstrasse 2, 85748 Garching, Germany

ABSTRACT

The ITER maintenance concept relies in the removal and installation of relatively large and modular systems from the lower part of the vessel reaction chamber. These operations are carried out by a mover mechanical device. The mover has five degrees of freedom and it is actuated by water-hydraulics servo cylinders. Due to the compactness of the overall ITER reactor, high position accuracy of the mover joints is required. This paper describes how virtual prototyping techniques have been used to develop the controllers of the actuators as well as the control software and user interfaces required to operate the mover remotely. By means of virtual prototyping tools, an advanced level of development has already been achieved. This rapid development will facilitate the implementation of the control system in the upcoming DTP2 physical full-scale divertor test platform.

KEYWORDS: Remote handling, water hydraulics, ITER divertor, simulation, virtual prototyping

LIST OF ACRONYMS

CMM	Cassette Multi-functional Mover
CTM	Cassette Toroidal Mover
DTP	Divertor Test Platform
HMI	Human-Machine Interface
JET	Joint European Torus
MACS	Moog Axis Control Software
MSC	Moog Servo Controller
MVM	Multi-axis Virtual Model

OPC	OLE for Process Control, OLE = Object Linking and Embedding
RH	Remote Handling
SAM	Single Axis Model
SCEE	Second Cassette End-Effector

1 INTRODUCTION

ITER is an international project for the design and construction of a Tokamak fusion reactor. ITER – "the way" in Latin – will be the next major step in an experimental Tokamak facility after some leading fusion experiments carried out over the past decades. In 1991, controlled fusion reactions were achieved for the first time, releasing a power of 1.7 MW on the Tokamak JET (Joint European Torus) located near Oxford. In 1994, the Tokamak TFTR in USA produced 10 MW of fusion power. In 1996, JT-60 (Japan) produced an equivalent fusion power amplification (ratio between the generated fusion power and the power injected into the plasma) above unity. In 1997, JET produced the largest amount of fusion power so far, 16 MW, although the power amplification factor was below one. The previous experiments have provided the expertise, in fusion physics and technology, and confidence which are required to design and build the next Tokamak project, called ITER. It aims at generating 500 MW of fusion power during a one-hour pulse, and with a power amplification factor larger than 10. ITER will operate under power plant conditions and it will be integrated with the technologies to make fusion a viable energy source.

1.1 Fusion

The easiest known fusion reaction involves two hydrogen isotopes: deuterium and tritium. In order to fuse, sufficient kinetic energy has to be inputted to the atomic nuclei to overcome the mutual electrostatic repulsion occurring during collision. Kinetic energy is provided by heating the deuterium-tritium fuel up to 100-150 million degrees. At these temperatures fuel is completely ionized, and plasma is formed. At this high temperature range, the plasma cannot come into contact with the walls of the reaction container, since its surface layer would evaporate and the plasma would be polluted and cooled.

The Tokamak, invented in the 1950's by Russian scientists, is a device consisting of a toroidal chamber which is able to produce and confine a large volume of high temperature plasma by means of a strong magnetic field, known as "magnetic confinement". The magnetic confinement is generated through external coils and by an induced current flowing in the plasma, holding the plasma in the toroidal vessel and keeping it away from the walls. Up to date, the Tokamak has become the most advanced magnetic confinement fusion approach in the world.

The deuterium-tritium fusion reaction produces a helium nucleus and a neutron. The helium nucleus carries about 20% of the released fusion energy in the form of kinetic energy. These particles slow down in the plasma and transfer their energy to the bulk of the deuterium-tritium fuel. This "self-heating" process makes the temperature required for fusion being obtained mostly from the reaction. On the other hand, the neutron obtained from the fusion reaction carries about 80% of the generated fusion energy. Neutrons are not confined in the magnetic field and find the way into blankets covering the walls of the torus. A circulating coolant in the blankets absorbs the neutrons energy.

The coolant is then brought to heat exchangers, where steam is produced and used to drive turbines for the generation of electricity.

Fusion can be considered a safe and environmentally friendly technology for the production of electricity. The main advantages are listed below:

- Practically inexhaustible fuel supply. The amount of fuel needed in a fusion power reactor in relatively small: 10 grams of deuterium and 15 grams of tritium would be enough to provide the entire lifetime energy needed by a citizen living in a developed world. Deuterium is obtained inexpensively from water (35 grams of deuterium in every cubic meter). Tritium is extremely rare in nature but it can be produced artificially from lithium, a very abundant metal on the earth.
- No transportation of radioactive material. Tritium is the radioactive fuel component. However, tritium will be produced within the reactor itself in a lithium containing blanket surrounding the plasma. Neutrons released by the fusion reaction will react with the lithium in the blanket, transforming it into tritium.
- Waste. The fusion reaction does not generate a radioactive product. However, neutrons produced in the fusion reaction activate the metal structures surrounding the plasma. Low-activation structural materials are being specially developed so that radioactivity decays rapidly to levels where re-use can be possible in about 100 years.
- Fusion reaction is inherently safe. The difficulty involved in maintaining the plasma conditions, makes the nuclear fusion a passively safe process. Fusion reaction occurs in pulses and can be interrupted in a few seconds time by simply stopping the fuel injection to the plasma or by deactivating the magnetic field.

1.2 ITER Divertor Maintenance

Figure 1 shows a cross-section of the ITER design. The fusion reaction takes place in the Tokamak vessel, which has a toroidal D-shape profile. The in-vessel components are degraded due to the erosion occurring during the plasma-wall interaction. Components may also need to be replaced due to unexpected failure. During the plasma operation, the in-vessel components will be activated by neutrons and contaminated with tritium and beryllium dust. Because of this, special remote handling techniques are required for the repair, inspection and maintenance of ITER in-vessel components.

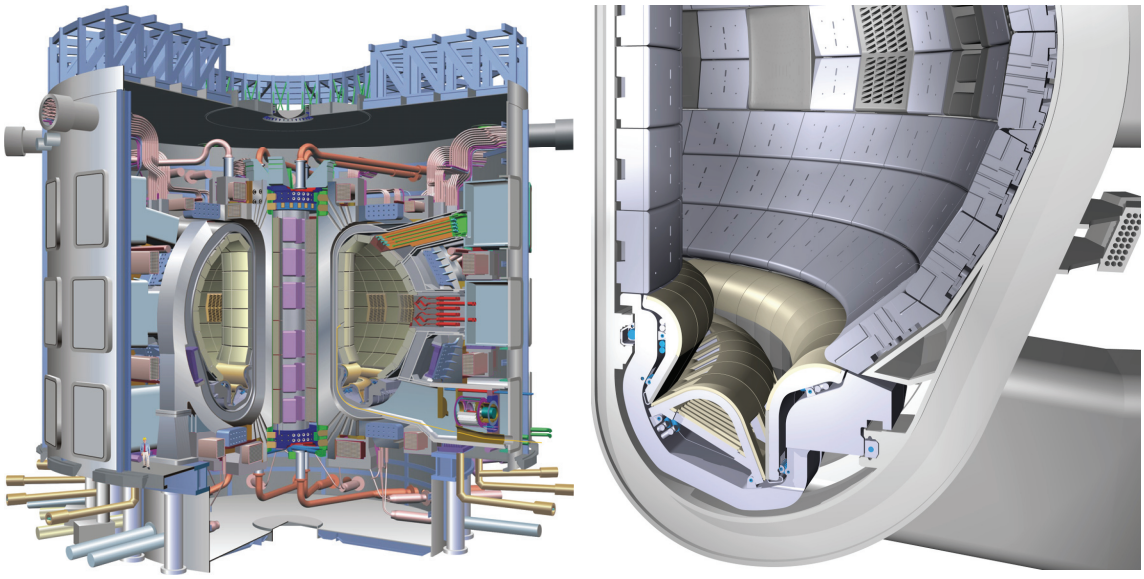

Figure 1. Cross section of ITER reactor (left). Cross section of divertor area and cassettes (right)

The ITER reactor chamber contains thousands of in-vessel components, from which the divertor region constitutes the largest system. The divertor occupies the lower part of the plasma chamber and it is segmented into 54 independent modular cassettes. Divertor cassettes are mounted on two concentric in-vessel toroidal rails. The main function of the divertor system is to exhaust the major part of the alpha particle power, helium and impurities from the plasma. The divertor is the main interface component between the plasma and material surfaces and it is still an experimental device. This makes the divertor to be replaced and upgraded several times during the life of ITER. The removal and installation of such divertor cassettes constitute the major challenge in the ITER maintenance. Each of the divertor cassettes has an estimated mass of 10 tonnes and an external size of 3.5 x 2 x 0.8 meters (length x height x width).

Three equi-spaced remote handling (RH) ports allow the radial transport of the cassettes in and out from the vacuum vessel, using radial rails (see Figure 2). Cassettes are remotely handled by the cassette multi-functional mover (CMM), which transports the cassettes through the RH port. A cassette toroidal mover (CTM) is used to perform in-vessel toroidal cassette handling operations, collecting cassettes positioned at some distance from the RH port. The CMM is equipped with a hydraulic manipulator arm [1] that can lock/assemble primary close plates of the RH ports, central cassettes (in front of RH ports), second cassettes (located at left-hand side of central cassettes), and CTM.

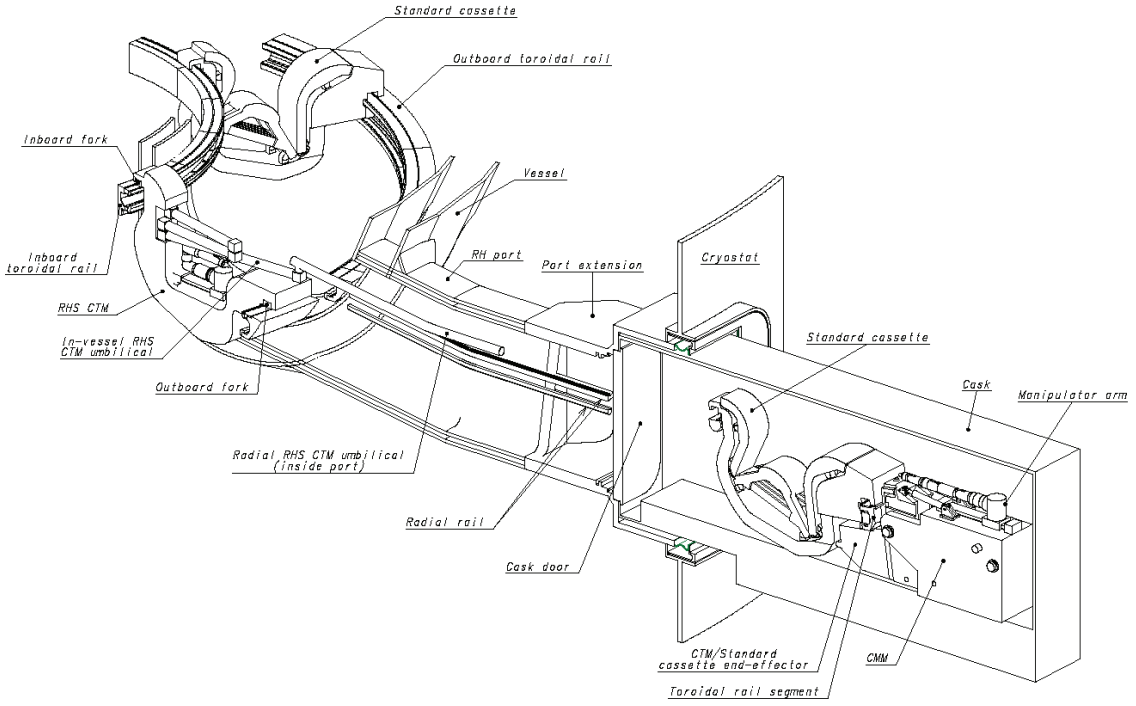

Figure 2. Divertor and remote handling port

Divertor cassettes are transported to a hot cell facility, which provides space and handling facilities for the reception, dispatch, decontamination, storage, repair, refurbishment and testing of divertor cassettes and other in-vessel components. Because of their contamination, divertor cassettes, movers and diagnostics equipment are transported between the vessel and the hot cell inside a transport cask. Transport casks are remotely guided by an air-cushioning platform and they are equipped with a double door to dock at the RH and hot cell ports. An extended description of the divertor maintenance operations can be found in [2].

1.3 Divertor Test Platform

Divertor repair and replacement is a major remote handling operation for the ITER machine. It is therefore required that its duration is minimised and its feasibility shown before construction. During the period 1995-2002 the main EU activity regarding the divertor maintenance was focused on the development of a Divertor Test Platform (DTP) for the ITER'98 design. The DTP is a full-scale remote handling facility developed to study the cassette removal and insertion process under remote construction. The facility was constructed at the ENEA research centre in Brasimore (Italy). The facility comprised:

- A 72 degree sector of the lower region of the vacuum vessel with four divertor ports
- Divertor cassette mock-ups.
- In-vessel environment, including the toroidal and radial vacuum vessel rails.
- Cassette mover prototypes
- Auxiliary remote handling equipment
- A control room with control and data acquisition systems

The DTP showed that cassettes could be manoeuvred and positioned with the required accuracy and repeatability. It also confirmed the right choice of materials and identified the weak points of the prototype performance.

The latest ITER 2001 design is a more compact machine where much of the divertor handling equipment has significantly changed. In the new design the gaps between the cassette and the vacuum vessel have been reduced, and the position of the toroidal rails has been raised. The trolley case for transporting the cassettes through the RH port has been replaced for the more complex cassette multi-functional mover CMM, since the vertical position of the cassette during its radial transportation through the RH port must be continuously adjusted in order to fit within a more complex shape of the port.

As a consequence of the above design changes, a new Divertor Test Platform (DTP2) has been planned. In the autumn of 2004, EFDA-CSU (European Fusion Development Agreement – Close Support Unit), VTT Industrial Systems and Tampere University of Technology (TUT) agreed the joint effort to build the new DTP2 facility in Tampere, Finland [3]. Finland has been participating actively in the European FUSION program since 1994. From the beginning, the Institute of Hydraulics and Automation (IHA) at TUT has been active in robotics and in virtual reality tools. IHA participated in the mechanical design of the CMM by providing its expertise in virtual reality and dynamic simulation models. Current activities of IHA concerning the divertor maintenance are focused on the implementation of the control system and control software of the CMM and in the development of a 6 degree-of-freedom water hydraulic manipulator arm assisting the CMM.

This paper shows the development of the control system and software required to guide the cassette mover in the installation/removal of divertor cassettes between vacuum vessel and the transport casks. The design and development have been carried out prior the construction of a full-scale test platform, and therefore virtual prototyping tools and specially built mock-ups are being used.

2 SINGLE AXIS CONTROL WITH THE SAM MOCK-UP

2.1 Divertor maintenance tasks with CMM and Second Cassette

The purpose of the cassette multi-functional mover (CMM) is the radial transport of equipment (mainly divertor cassettes) through the RH port (Figure 4). CMM consists of a main body and an articulated two-link mechanism, which provides lifting and tilting motions. When coupled with the Second Cassette End-effector (SCEE), the CMM is added with two extra rotational joints, cantilever and hook plate joints. These joints allow the installation/removal of cassettes located in the vicinity of the RH port (Figure 5). Lift, tilt, cantilever and hook plate rotational joints are driven by hydraulic cylinders, using high pressure water, and they are controlled by Moog 30-417 servovalves attached to the body of the CMM. Figure 3 displays the CMM/SCEE group and its joints. The radial drive of the CMM is achieved by means of two electrical servomotors driving two sets of rack-and-pinion systems. The resolver integrated in the radial drive housing in the CMM body can determine its position with an accuracy of 2 mm. Multi-speed pancake resolvers used in hydraulic cylinders have an accuracy of 25 arc-seconds.

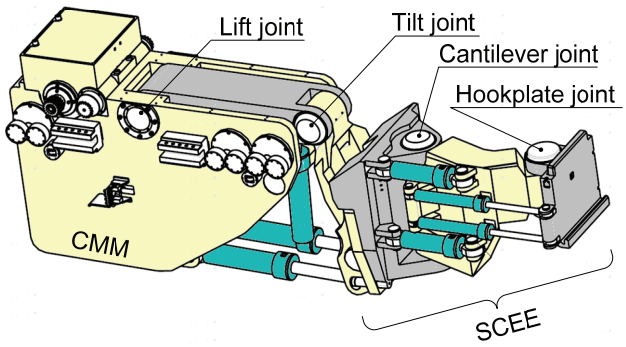

Figure 3. Cassette multi-functional mover (CMM) and second cassette end-effector (SCEE)

The control of CMM/SCEE joint positions faces two main challenges:

- The radial transportation of divertor cassettes through the RH port (see Figure 4). In this operation, lifting and tilting cylinders need to be adjusted continuously in order to avoid the collision of the divertor cassette with the upper and lower part of the RH port. According to the current design, and with the use of simulation, the minimum vertical gaps between the divertor cassette and the RH part are about 23 mm.

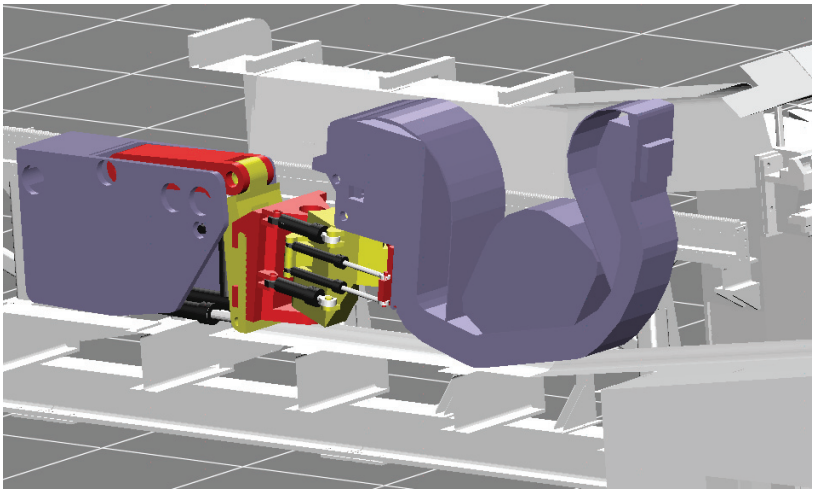

Figure 4. Transportation of divertor cassette through the RH port

- The installation of second cassette (see Figures 5 and 1). This operation consists of moving the second cassette toroidally by actuating the cantilever and hook plate joints. Position of tilt and lifting joints must be also controlled in order to keep the vertical gap between the inner/outer rails and the divertor cassette. The gap has been measured in graphical simulations and its value is in the order of 10 to 20 mm. A radial gap between inner/outer cassette and vessel attachment points must also be controlled.

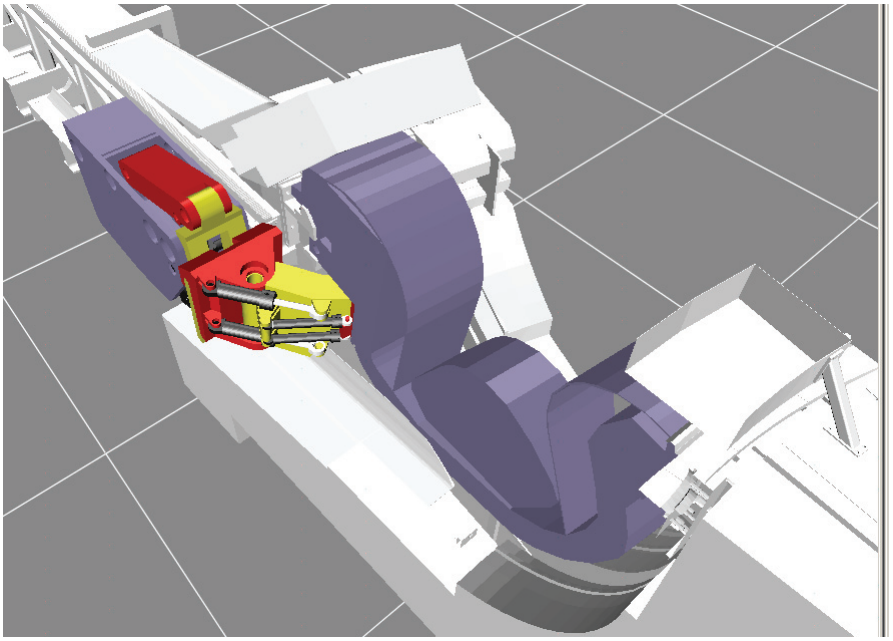

Figure 5. Installation of second cassette in the divertor

A high performance motion control system [4], from Moog M3000, has been chosen as the hardware to implement the controllers of the hydraulic servovalves and the electric servo. The Moog Servo Controller (MSC) is a programmable multi-axis controller that facilitates rapid and precise control of process variables such as position, velocity and power. It is suitable to be used in many type of actuating systems such as electric and hydraulic drives. MSC uses standard programming languages and libraries. Controllers can be developed in PC software using a graphical and object oriented approach. The M3000 module can also communicate with other system devices via CAN-bus and Ethernet. It also comes with 2 sensor interfaces for encoders, 8 digital I/O interfaces, 2 analog outputs and 8 analog inputs.

2.2 Single Axis Model (SAM) mock-up

Prior to the construction of DTP2 facility, the control system, software and User Interfaces to operate the CMM/SCEE are being designed and developed at IHA. In order to have an understanding of the dynamics of the CMM/SCEE a relatively small physical mock-up, named SAM (Single Axis Model), has been built [5]. Figure 6 shows the main components of the device. It consists of a horizontal boom structure rotating, in its midpoint, over a fixed base. The boom structure is driven by a hydraulic cylinder, which is attached to a pair of movable fastening forks. Additional masses can be placed at both ends of the boom.

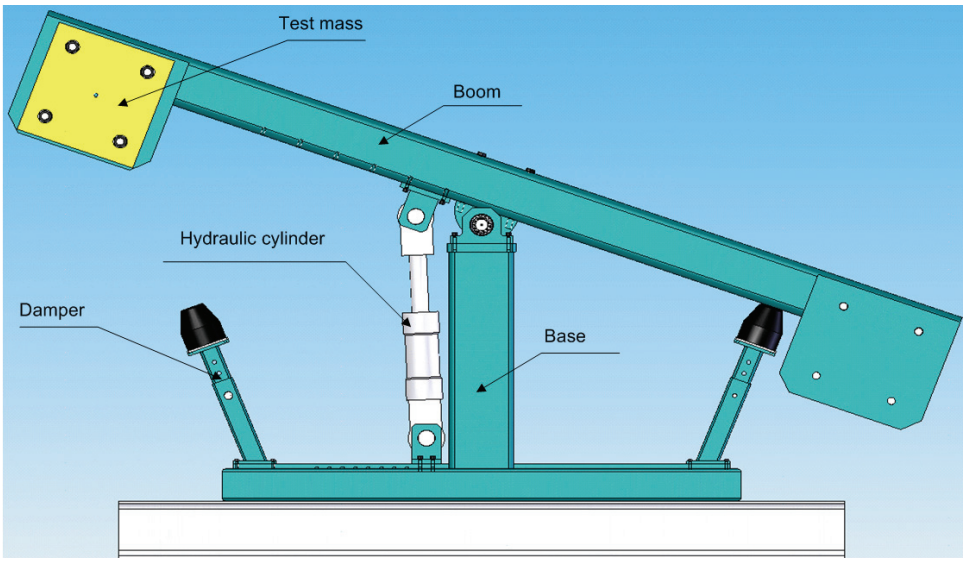

Figure 6. The Single Axis Model (SAM) mock-up

The purpose of SAM is basically to reproduce the dynamic characteristics of each of the hydraulic actuators in the CMM/SCEE. By adjusting the side masses and the torque arm of the hydraulic actuator (by moving the fastening forks), the dynamics of the SAM can match the same natural frequencies, one at a time, seen by the actuators in the full-scale CMM/SCEE. A 125/80-230 water hydraulic cylinder and extra masses at one side of the boom are used to simulate the gravity load of the lifting and tilting axes. A smaller 32/25-230 cylinder with masses at both ends of the boom is used to simulate the high inertias during cantilever and hookplate operations. A Moog servo controller M3000 is used to control the joint position of the SAM. A complete list of all components attached to the SAM device is following (refer to Figure 7 for a diagram of the connections):

- M3000 Moog servo controller, reference signal ± 10 mA
- Moog 30-417 servovalve, reference signal ± 10 mA
- ROD 426 encoder, 5000 pulses/rev
- Heindenhaim IBV 102 signal converter
- Druck PTX pressure sensors (250 bar), sensor signal 4...20 mA
- 24VDC and 5 VDC power supply units
- HMI (Human-Machine Interface) PC
- Host PC

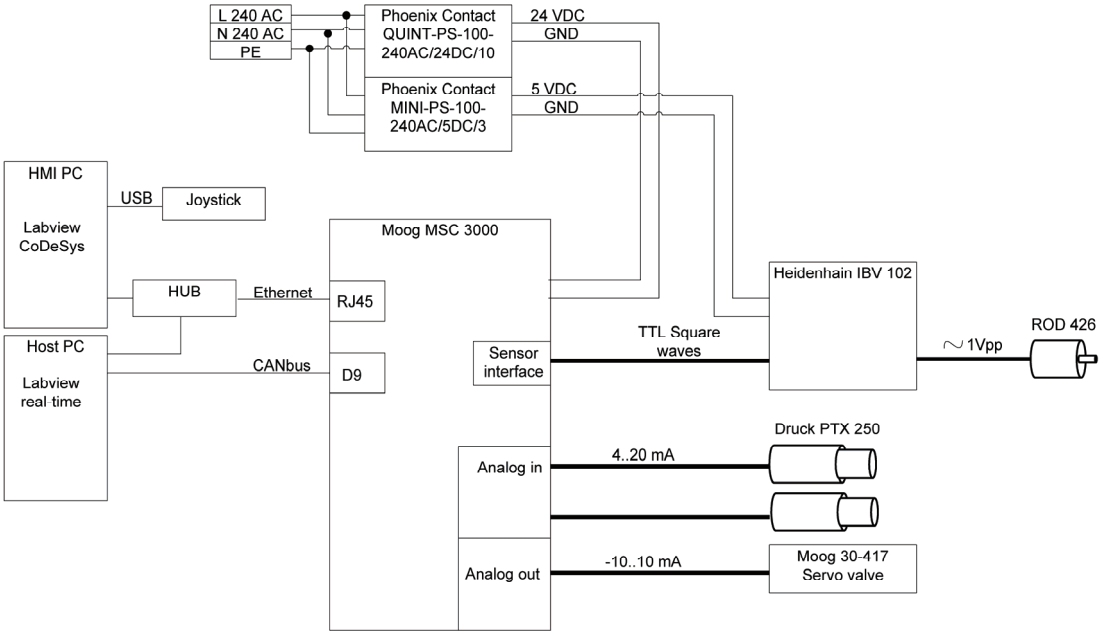

Figure 7. Schematic of the electrical connections to SAM

The **HMI PC** computer performs the following functions:

- Programming of the MSC. HMI PC hosts the Moog Axis Control Software (MACS) development environment. The MACS software is needed to create an executable program for the M3000 controller. Within MACS, in-the-loop tasks to be performed by the controller are set, like definition of the controller, reading CAN-bus data from Host PC, writing of CAN-bus data received from sensor and analog I/O interfaces.
- Provides a user interface for setting the controller gains of the SAM joint. The graphical user interface capabilities of Labview are employed to provide a set of visual tools to perform this operation. OPC (OLE for Process Control, OLE = Object Linking and Embedding) is used to bind parameters in Labview to parameters in the MSC.
- Main User Interface. This is an application panel built in Labview Virtual Instruments. From this panel the user can receive information concerning states, variables and performance of the system. The panel also allows the user to send commands and instructions to the motion controller. A screenshot of a user interface similar to the SAM is displayed in Figure 9. Among others, the main features of the user interface are:
    - Generating reference signals. Joint reference signals to the M3000 controller can be created either from existing ASCII files containing trajectories or from joystick teleoperation. The User Interface displays the content of a library with existing trajectory files. These can be selected and piled in a queue in order to be executed sequentially.
    - Displaying the status of the operations and connections.
    - Graphical and numerical display of actual joint position (measured from the encoder), reference joint values, and errors.

The **Host PC** is running the processes which are considered to be time-critical for the optimal performance of the controller. These processes are executed under Labview real-time software, which runs on a real-time operating system. The main functions appointed to the Host PC are listed below:

- Execution of the Trajectory Generator module in order to transform an ASCII file containing few control points in Cartesian coordinates into a continuous trajectory of points in joint coordinates throughout the time.
- Storage, in a shared library, of the generated trajectories (reference signals), which are sent in real-time to the M3000 through the CANbus.
- Real-time data acquisition from the M3000 via CANbus (reference joint angle, and actual joint angle)

2.3 Controller and preliminary results

For the position controller of the rotational joint in the SAM device, it was thought that a P-controller would provide a good enough accuracy, due to the relatively slow velocity of the load (less than 2 deg/s). After a careful tuning of the servovalve offset, very good steady state positioning accuracies of the joint angle were achieved. However, the tests showed that the P-controller approach was too sensitive to zero point drift of the servovalve and, due to the low damping of the system, also to force and feedback disturbances.

A state controller is currently being tested as a position controller of the SAM device. The state controller uses position, speed and acceleration feedback, and speed feed forward. Its realization can be made with the use of a single high accuracy position sensor. Velocity and accelerations are then obtained by placing the so-called observers in the feedback of the state controller. The state controller has been tested on the SAM with different types of follow-up reference signals: sinusoidal waves, third order polynomials and with a real cantilever joint trajectory path.

Although the tuning and testing of the state controller is still being under development, some conclusions can already be stated. The state controller has increased the effective damping of the system, and the overall stability has been remarkably improved when compared to the P-controller approach. Concerning the position accuracy, in general terms, the state controller is currently providing a tracking accuracy of 0.01 degrees @ 0.2deg/s angular velocity, being about ten times more accurate than the previous P-controller.

3 MULTI-AXIS CONTROL WITH THE MVM VIRTUAL MODEL

The main limitation of the SAM device is that only a single axis can be controlled at a time. This implies that the driven axis is isolated from the rest of the structure and therefore force/torque contributions of other moving elements are ignored. The Multi-axis Virtual Model (MVM) attempts to solve the above issue by means of a virtual prototype enclosing the entire CMM/SCEE and divertor cassette [6]. The MVM consists of two main components: a dynamic simulation model running in real-time and a 3D virtual model. The layout is shown in Figure 8.

The **dynamic simulation model** contains:
- Multi-body system dynamics of CMM, SCEE and divertor cassette: The mathematical model is comprised of rigid bodies and idealized joints. Body masses, location of centres of gravity, and body tensor inertias have extracted from existing 3D CAD designs. The model is built using the object-oriented approach found in the MathWorks SimMechanics software package. SimMechanics is integrated with

Mathworks Simulink and with code generated products. This enables the integration of the mechanical structure, controllers and fluid power components in the same Simulink environment. The entire system can then be compiled, as a whole, and deployed into a xPC Target computer.

- Hydraulic circuit and components: As a result of IHA expertise in water hydraulics and in fluid power modelling and simulation, accurate and efficient mathematical models of fluid power components have been built. The fluid is modelled as two-regime flow and its compressibility is also taken into account.
- Controllers of the servovalves: State controllers are now implemented as software within the dynamic simulation model.

The **3D virtual model** main goal is to provide a video feedback to the operator. This is achieved by means of a 3D virtual environment modelling software developed at IHA. IHA3D software is programmed in C++ and uses Microsoft Foundation Classes and OpenGL. Graphical models can be imported to IHA3D from existing CAD designs. Within IHA3D, *Device* entities can be defined. A device consists of a kinematic chain of parts linked with idealized joints, such as prismatic and revolute, and with parent-child relationships. Devices can then be moved and positioned in the virtual environment by simply defining the current values of their joint positions. Two of the main utilities of the software are:

- The capability of reading joint position data from an external source – establishing a UDP/IP connection through Ethernet – and refreshing the graphical rendering of the virtual model in real-time. In our application, the simulated joint positions are acquired by the Real-time PC, and this forwards them to the IHA3D. AS a result, the user can visualize, in real-time, the position of the device. Several windows and cameras can be set up simultaneously in the virtual environment in order to keep visual track of the most critical operations.
- Collision detection. Collisions occurring between different parts of the graphical model are detected automatically by the software. Colliding parts are easily detectable as they are highlighted differently during two phases: when collision is imminent and when collision occurs. IHA3D calculates the instantaneous collision distance and the direction of the contact force vector. The software is able to send this contact information in real-time through UDP to the xPC Target computer (running the dynamic simulation model of the MVM). This collision information is then used, within the dynamic model, to calculate the contact forces between the colliding parts.

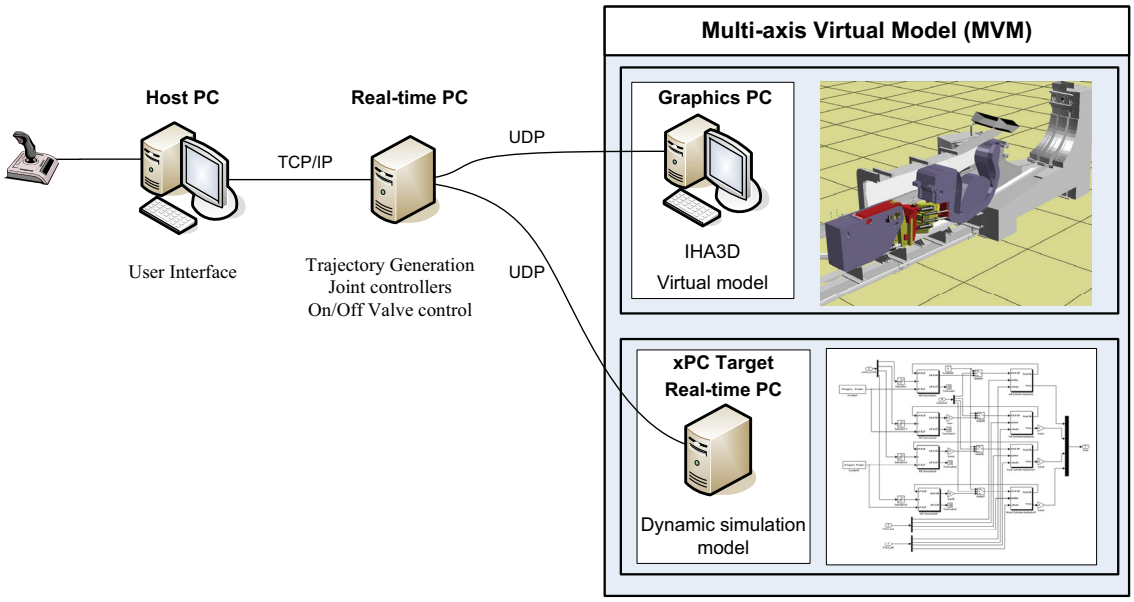

Figure 8. Multi-axis Virtual Model setup

The CMM/SCEE can be moved both in teleoperated and in automatic modes. Commands and instructions to operate the MVM are sent from the Host PC to the Real-time PC (as shown in Figure 8). The latter processes the instructions provided by the user and sends, in real-time, the joint reference signals to the virtual model. The MVM needs to be provided constantly with a stream of trajectory points during the simulation. At every step of the dynamic simulation, a set of reference joint values have to be available for the servo controllers. The task responsible of creating a stream of trajectory points is called *trajectory generator*. This software module is executed and managed in the Real-time PC.

From the User Interface (Figure 9), running in the Host PC, the user can choose among three different driving modes for commanding the MVM. These modes are explained below:

- **Joystick joint mode**. In this mode, joint angles are directly commanded by joystick devices. The operator selects, in the User Interface, the joints to be commanded and also sets the position of the On/Off valves. Joint reference signals are transferred to Labview real-time, running in the Real-time PC, which sends the reference signal values to the servo controllers modelled in the MVM xPC Target computer.
- **Automatic mode**. In automatic mode, the CMM/SCEE follows a set of given control points. Control points are expressed in Cartesian coordinates and they have the origin in the centre of the toroidal Tokamak chamber. Control points are usually placed on the exterior surfaces of the divertor cassette with a potential risk of collision during the transportation through the RH port, and during its installation on the rails in the toroidal chamber. Control points have been located using 3D CAD models of the divertor maintenance elements. Envision and IHA3D software are used to place the graphical models in a virtual environment, measure collision gaps and extract Cartesian coordinates of such critical points. A control point consists of XYZ Cartesian coordinates, RPY (Roll-Pitch-Yaw) angles and its speed. A set of control points defines therefore a trajectory. Sets of control points are stored in data files and they are accessible through a database displayed in the User Interface.
  Before the simulation execution starts, the Trajectory Generator software module converts the discrete set of Cartesian control points into a continuous stream of Cartesian positions indexed with simulation time tag. Therefore, at every simulation integration step, a reference position is available to be fed to the servo controllers.

This interpolation between the control points is made taking into account some conditions specified in the User Interface. These conditions are maximum speed, acceleration and jerk values of the control points. In the next step, the continuous stream of Cartesian positions is converted into joint coordinates (joint angles). The *inverse kinematic* equations of the CMM/SCEE device must be provided in order to perform this operation. The obtained stream of joint coordinates is then verified and stored in the memory in order to be accessible during the simulation.

- **Joystick controlled automatic mode**. This mode performs in the same way as the Automatic mode, but the trajectory execution speed is controlled with a joystick device.

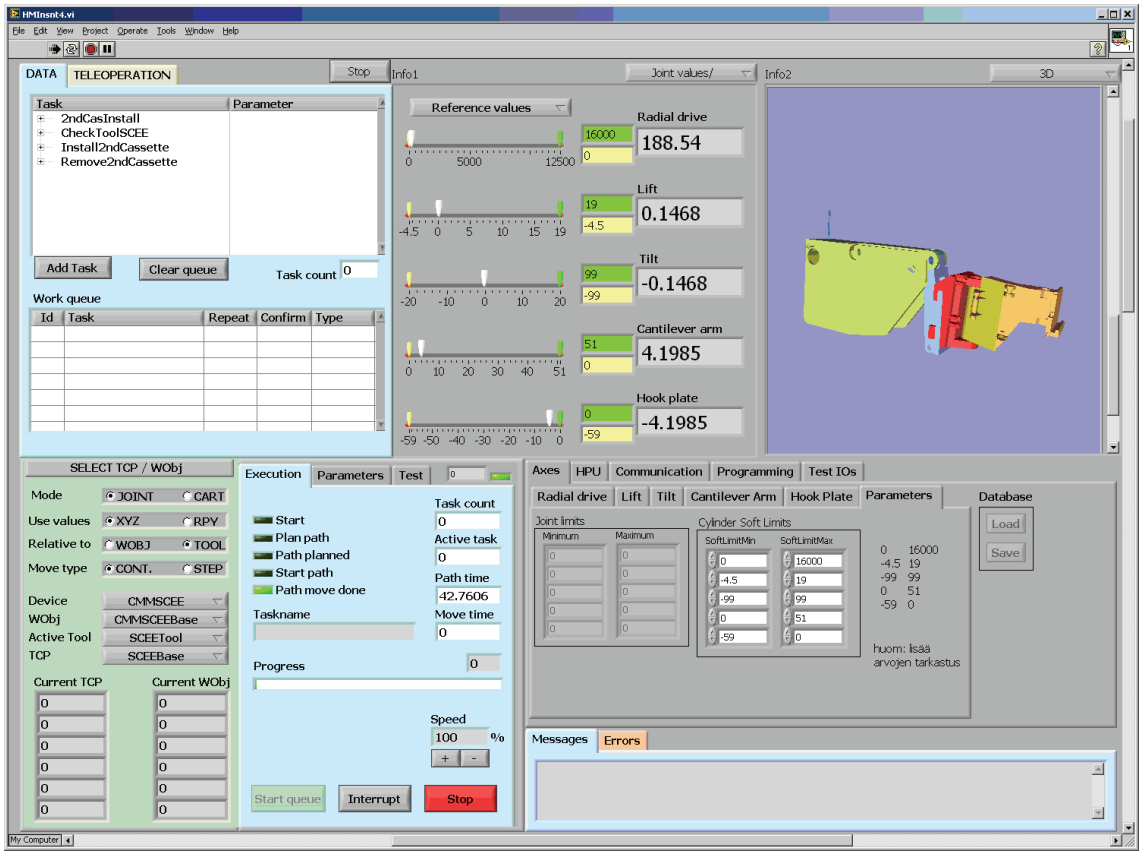

Figure 9. User Interface of the MVM

4 CONCLUSIONS

Controllers, control software and User Interface to be implemented in the upcoming DTP2 test platform have been developed using virtual prototyping techniques and a small scale mock-up. State servo-controllers have shown promising results in terms of stability and joint position accuracy in different follow-up experiments. Further improving and validation of the controllers is currently being developed by using simultaneously virtual prototyping tools (MVM) and physical mock-up (SAM).

ACKNOWLEDGMENT

This work, supported by the European Communities under the contract of Association between EURATOM / TEKES, was carried out within the framework of the European

Fusion Development Agreement. The views and opinions expressed herein do not necessarily reflect those of the European Commission.

REFERENCES

[1] Muhammad, A., 2007, “Water Hydraulic Teleoperation System”, Proceedings of the Tenth Scandinavian International Conference on Fluid Power, Tampere, Finland

[2] Palmer, J., 2004, “Remote Maintenance of the ITER Divertor”, 10th Robotics & Remote Systems Mtg. Proceedings, Gainesville, Florida (2004), pp. 29-34

[3] Timperi, A., 2006, “DTP2 Laboratory Situation in Tampere, Finland”, Symposium on Fusion Technology SOFT’06, Warsaw, Poland.

[4] Almqvist, A., 2003, “New approach for high performance motion control”, Proceedings of the Eighth Scandinavian International Conference on Fluid Power, Tampere, Finland, pp. 367-381

[5] Mäkinen, H., 2006, “Fuusioreaktorin huoltorobotin testausjärjestelmän suunnittelu”, Master of Science Thesis, Tampere, Finland

[6] Raneda, A., 2002, ”Utilization of virtual prototyping in development of CMM”, Proceedings of the 22nd SOFT, Helsinki, Finland, 2002, Fusion Engineering and Design 69 (2003), pp.183-186

Water Hydraulic Teleoperation System for ITER

Ali MUHAMMAD, Salvador ESQUE, Mikko TOLONEN, Jouni MATTILA,
Peetu NIEMINEN, Olli LINNA, Matti VILENIUS
Tampere University of Technology
Institute of Hydraulics and Automation
P.O. Box 589
33101 Tampere, Finland
Phone +358 3 365 2177, Fax +358 3 365 2240
E-mail: ali.muhammad@tut.fi

ABSTRACT

In hostile industrial environments where human access could be a health risk, a reliable and flexible teleoperation system is an eminent need. ITER is such an example where a dexterous teleoperation system is required for remote handling tasks in a nuclear environment. The compactness of space, high load capacity and reliability makes hydraulic manipulator an obvious choice. However, possible oil leakage from traditional hydraulic systems and the characteristics of water (fire and environmentally safe, chemically neutral, not activated, not affected by radiation) makes the use of water hydraulics the only choice. This paper describes the development of a teleoperation system for ITER consisting of a water hydraulic manipulator as a slave, a commercial haptic device as a master, a human machine interface to assist the operator and a graphical system providing a virtual 3D view of the environment. Virtual prototyping has been used extensively during the development of this teleoperation system resulting in reduction of development time and cost. Although the system has been developed to carry out remote handling operations in ITER, the modular design and flexibility makes its use possible in many industrial applications.

KEYWORDS: Teleoperation, Remote Handling, Water Hydraulic

ACRONYMS

DOF	:	Degrees Of Freedom
FBIC	:	Force-Based Impedance Control
EFDA	:	European Fusion Development Agreement
GUI	:	Graphical User Interface
ITER	:	International Thermonuclear Experimental Reactor
PBIC	:	Position-Based Impedance Control
RH	:	Remote Handling
WHMAN	:	Water Hydraulic Manipulator

1 INTRODUCTION

One major characteristic which makes the use of robotic manipulators most advantageous is their capability to execute tasks in the hazardous and the most hostile environments. Fume packed chemical plants, nuclear environments with high radioactivity, vacuum conditions of space and high pressure areas like ocean depths are the main examples of such environments. The presence of humans in such places could be life threatening or the cost to equip them to survive in these environments can be too high. Operations within these environments bring up not only the need of manipulators but also the need of controlling, manipulating and operating them from remote locations. The operator sits in a room, distant and safe from the dangers of the site, while he can fully perform the operations and control the robot at the site. ITER is an example of such an environment where a dexterous teleoperation system is a required for remote handling tasks.

Using hydraulics is always a choice of interest in industrial applications where high forces are required with compact size actuators. Simple construction and high reliability are added advantages of hydraulics. It has been proving its worth in applications like automobiles, excavators and airplanes with a high degree of reliability and low maintenance. With the developments in water hydraulics (water is used as a pressure medium rather than oil), the scope of hydraulic applications has widened further. The characteristic advantages of hydraulics together with the water as the pressure medium (fire and environmentally safe, chemically neutral, not activated, not affected by radiation) are highlighted in critical applications such as remote handling operations in ITER [1].

Virtual prototyping technology has become a very valued tool in the early phases of the product design. The time frame of the development process can be shortened by using the advantages and possibilities of the virtual technologies. The use of virtual technologies is of special interest in the development of the ITER maintenance devices, mainly due to the large costs, sizes and complexity of physical prototypes. Virtual prototyping has been used extensively during the development of this teleoperation system, resulting in reduction of development time and cost.

The use of force reflective (haptic) devices or so called “touch displays” can fairly increase the reliability of remote operations. It has been reported that haptic-augmented interactive systems seem to give about a two-fold performance improvement compared to purely graphical interactive systems [2]. Today a wide variety of haptic devices are available in the commercial market. With controls and software tools provided by the manufacturers, these devices can be employed as a master manipulator in a wide variety of schemes. In addition, the use of a commercial force reflecting device makes the system more modular, adaptable and economical.

The video feedback to the operator can be enhanced with the use of calibrated virtual 3D model of the remote environment. In most cases, not all the objects in the environment are significant for the task completion. Therefore these models can be simplified to accommodate only the objects of interest from the remote environment. This fact is actually advantageous as virtual models may only offer an improvised view of the environment but it helps the operator to focus on the relevant objects [3]. The use of virtual 3D models also results in the improved reliability of the teleoperation system.

The fact is evident in [4] where task completion was possible by using the virtual model despite the loss of live video feedback. Another advantage of computer generated models is predictive display. This feature is helpful for the planning, practicing and simulating the task in virtual environment before the operator performs the task in the actual environment. In this way a great number of errors and unpredictable situations can be avoided during the performance of the task.

Much research has been conducted in the past on teleoperating hydraulic manipulators in many industrial applications. However, most of these teleoperation schemes were developed for custom made manipulators with specific teleoperation capabilities. No off the shelf techniques or general solutions are available. With the development of ITER, once again, the need of investigation for such a system has become evident. In the ITER environment, the teleoperation system requirements can be summarized as:

1. The slave manipulator should be compact with high load capacity and should be radioactive tolerant.
2. The teleoperation system should be highly reliable as it should be recoverable from unforeseen situations and in case of failures.
3. The teleoperation system should be highly flexible as:
   - The remote handling tasks cannot be completely defined.
   - The fact that ITER is an experimental platform, remote handling requirements are most likely to change in the future.

The following sections describe the development of a teleoperation system at IHA/TUT. The system consists of a water hydraulic manipulator as slave, a commercial haptic device as master, a human machine interface to assist the operator and a graphical system providing a virtual 3D view of the environment. In section 2 the general architecture of the teleoperation system is presented. Section 3 discusses the development of the water hydraulic manipulator, its instrumentation and control. The master manipulator and its graphical user interface will be introduced in section 4 and 5 respectively. The 3D modeling software IHA3D developed at IHA/TUT will be detailed in section 6. The last section concludes a brief summary of the development work.

2 ARCHITECTURE OF THE TELEOPERATION SYSTEM

The Ethernet has been chosen as the communication medium because of its wide availability and long familiarity in the industrial world [5]. The deterministic and nondeterministic data is exchanged between the system components by using UDP (User Datagram Protocol). Software tools have been implemented at application layer to tackle the unreliable and nondeterministic behavior of UDP. The general architecture of the teleoperation system is shown in figure 1.

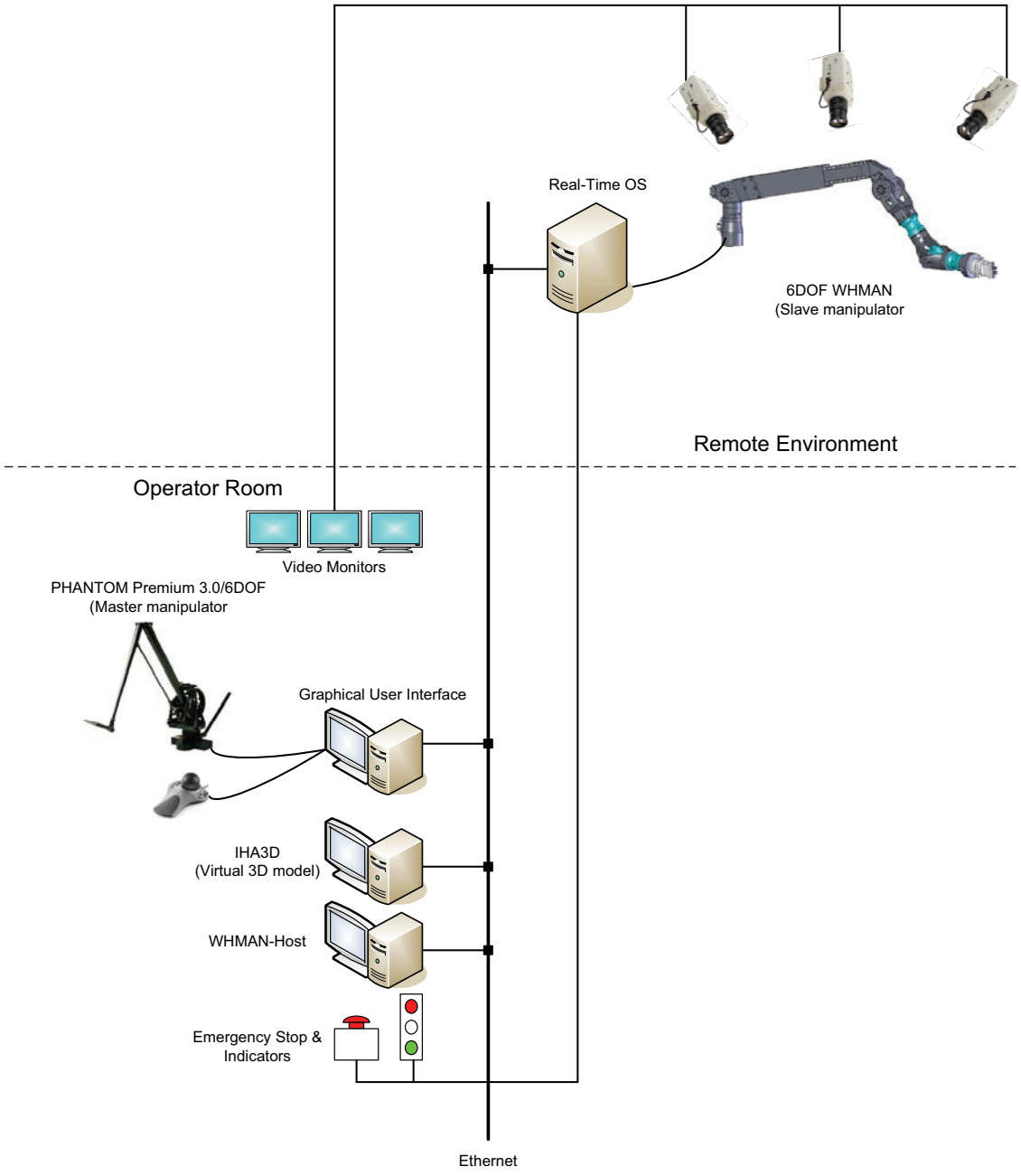

Figure 1: Teleoperation system architecture

The WHMAN is employed as the slave manipulator to carry out the tasks in the remote environment. A real time operating system running on a computer performs the low level control and measurement operations for WHMAN. The detail instrumentation and control features of this manipulator will be discussed in the next section. Several cameras are located at the remote site to provide live video feedback of the environment and the task to the operator.

The operator site is equipped with computers, video monitors, a haptic device, a joystick, light indicators and an emergency stop switch. The operator control stations provide many levels of control for slave manipulator and several aids to perform remote handling tasks. The operator of the WHMAN-host controls and monitors the online status of WHMAN and has the highest authority. In case of an unforeseen situation the

operator can either shut down the slave manipulator with the emergency switch or can take over the control of the manipulator.

One or two operators can use the GUI (Graphical User Interface) and Phantom Premium 3.0/6DOF master manipulator. Operator/s can control the slave manipulator from this station in several possible modes, provided the permission is granted by the WHMAN-host operator. These control modes will be explained in more detail in section 5.

The live video feedback from the environment is provided using a vision system. The vision system comprises of several cameras (with pan, tilt and zoom) located at remote site and video monitors in operators room. The pan tilt and zoom of cameras can be controlled by the operator to suite requirement. In addition to live video feedback, the operators have the visual access to the virtual 3D model of the task and environment on a station called IHA3D. This model is helpful not only during the task execution but also for the task planning, practicing and simulating. Further features of IHA3D will be discussed in section 6.

3 SLAVE WATER HYDRAULIC MANIPULATOR

A 6-DOF WHMAN is under development at IHA/TUT. The arm of the manipulator is composed of three rotational and one linear joint. The rotational joints provide a spherical workspace while linear joint provides the telescopic motion of the arm. A spherical wrist is attached at the end of the arm resulting in improved dexterity and reachability of the arm. A 3D model of the arm is shown in figure 2.

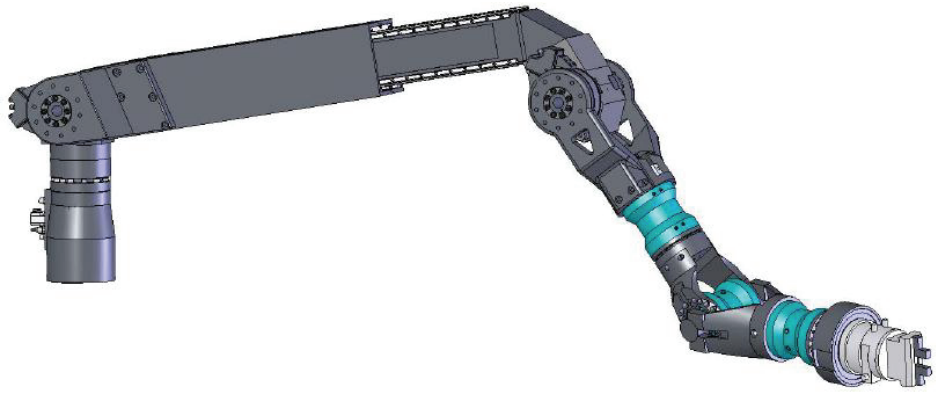

Figure 2: 3D model of 6-DOF WHMAN

The development of 6-DOF WHMAN is based on the experience acquired from the earlier prototypes like 5-DOF WHMAN. 5-DOF WHMAN is a step towards more advanced and sophisticated water hydraulic manipulators such as 6-DOF WHMAN. The purpose of 5-DOF WHMAN is to gain the insight knowledge about water hydraulic components and to develop and investigate control strategies. Currently, the 5-DOF WHMAN (Water Hydraulic Manipulator) pictured in figure 3 is employed as the slave manipulator.

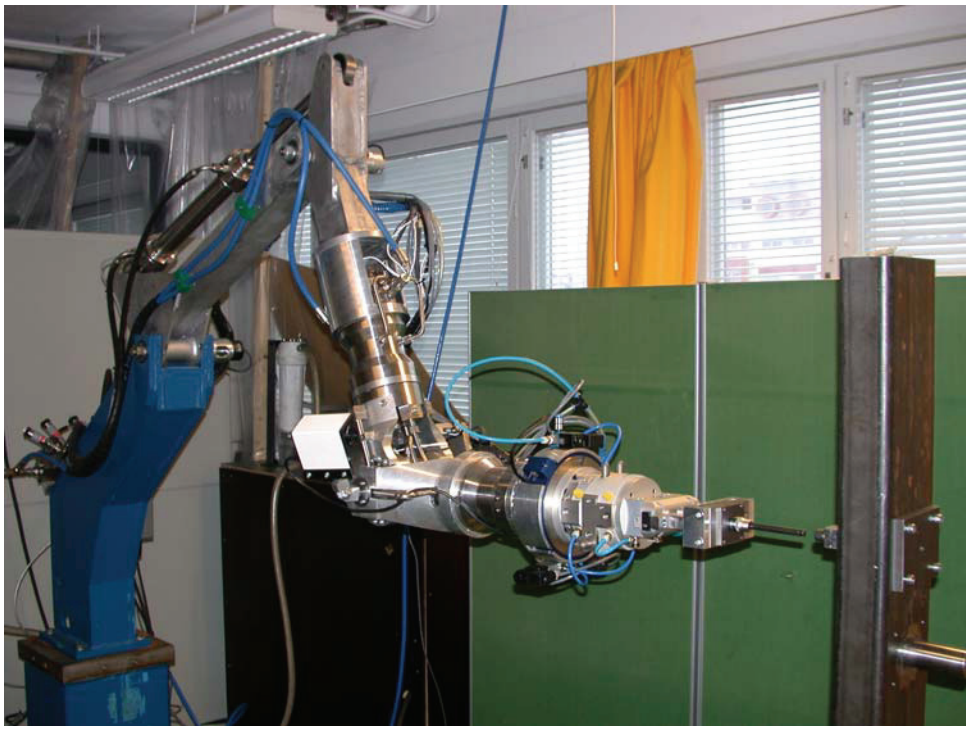

Figure 3: 5 DOF WHMAN with a wrench tool

The manipulator consists of a 2-link planar arm with shoulder and elbow rotational joints, powered by water hydraulic cylinder actuators. The end of the planar arm is fitted with a robotic wrist, with three rotational joints powered by water hydraulic vane actuators custom designed and developed at IHA/TUT. A tool changer is installed at the flange of the manipulator to which various electrical, pneumatic and water hydraulic tools can be attached, such as for the operations required in ITER: cutting lip-seals, gripping and handling plates, bending cooling pipes, and inserting and removing hydraulic jacks and pins. A 6-DOF force sensor is attached at the wrist of the manipulator to directly measure the contact forces. In following paragraphs we will consider the development and control strategies for WHMAN.

3.1 Virtual prototyping

Virtual prototyping technology has become a very valued tool in the early phases of product design. The use of virtual technologies is of special interest in the development of the ITER maintenance devices, mainly due to the large costs, sizes and complexity of physical prototypes. Virtual prototypes are built and implemented using simulation tools.

Although the 6-DOF WHMAN is still under construction, virtual models can be used to design, implement and test the teleoperation and the controllability of the remote manipulator. The virtual manipulator consists of its full dynamic simulation model and a 3D graphical representation of the device and its environment. In order to obtain a realistic and accurate simulation model, not only the kinematics of the manipulator has been considered but also the dynamics of the multi-body mechanism and the dynamic equations governing the hydraulics. The simulation model has been built using Matlab/Simulink programming language, and when compiled, it is able to run in real-

time from an xPC real-time kernel. The use of an accurate dynamic model of the manipulator has been of a great help for the preliminary design of a control and teleoperation architecture. Controllability, environment interaction and force feedback have been tested under different conditions by means of a virtual platform.

3.2 Control system

3.2.1 Position control

Although several control strategies have been experimented and are planned to be experimented, currently the experimentation with state feedback controllers is underway. State feedback controllers are based on the pole placement design, which results in improved damping of the system and higher values of the gains can be chosen. The choice is made on the basis of stability and steady state position accuracy of the manipulator. The dynamic characteristics of joints actuators were experimentally determined and then used to find out the tuning of parameters for the controller. The parameters were later fine tuned to obtain the cartesian tracking and positioning accuracy of ±1 millimeter.

3.2.2 Force Control

In remote handling cases where the end-effecter of manipulator comes in contact with the environment, task-space force control of manipulator becomes essential. Two major approaches have been widely adopted for the force control of manipulators: hybrid force/position control and impedance control. In hybrid force/position control, the task-space is divided into degrees of freedom in which either position or force is controlled. In impedance control, the relationship between position and force at the end-effecter of the manipulator is controlled rather than only position or force.

The objective of an impedance controller is to establish a desired dynamic relationship between the endpoint position and the environment contact forces. The feedback loops at the manipulator joints are closed in a way that the manipulator appears as specified impedance to its environment, which, in turn, behaves as admittance to the manipulator. Two types of impedance control have been researched and implemented since its introduction by Hogan [6] in 1985: Position-Based Impedance Control (PBIC) and Force-Based Impedance Control (FBIC.) The PBIC consists of an inner position feedback loop with an outer force feedback loop. In effect, PBIC softens a stiff position source. The FBIC consists of an inner force feedback loop with an outer position feedback loop. In effect, FBIC stiffens a soft force source. Since hydraulic actuators are essentially position/velocity sources, where actuator velocity is proportional to input valve voltage, the PBIC becomes the obvious choice.

3.3 Teleoperation architecture

A 4-channel teleoperation scheme has been opted for the system to achieve transparency between master and slave stations. A simplified model of this scheme is presented in

figure 4 below. As the name of the scheme suggests, all of the four channels are utilized to exchange information. Forces as well as positions of both master and slave are bilaterally exchanged. Thus the operator not only feels the contact forces from the environment but also can apply controlled forces on the environment for the execution of sophisticated tasks such as tightening of a bolt. Several other control parameters and signals are exchanged between the master and slave system such as control modes, error flags, etc.

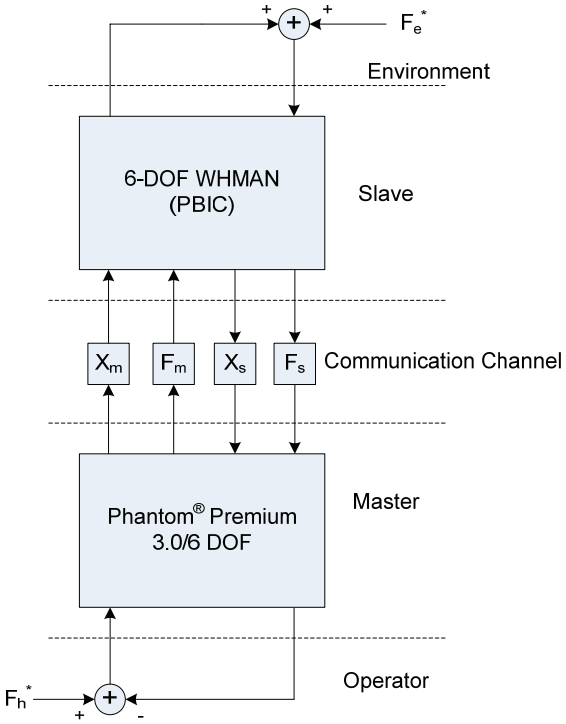

Figure 4: 4-channel Teleoperation Scheme

4 MASTER MANIPULATOR (HAPTIC DEVICE)

The PHANTOM Premium 3.0/6DOF which is a commercial haptic device is used as the master manipulator. The device provides force feedback in three translational degrees of freedom and torque feedback in three rotational degrees of freedom. Hence the operator can feel not only the cartesian contact forces from the environment but also the rotation torques. This feature is helpful for performing sophisticated force control tasks in the environment such as bolting or unbolting a screw. The Phantom premium has proved beneficial for a number of reasons:

- The use of commercial haptic device as a master manipulator has made the system more economical and faster to develop.
- The kinematic similarity between Phantom premium and WHMAN results in the ease of control for the operator.
- With controls and software tools provided by the manufacturer, the device can be implemented as master in a number of fashions. This feature has been particularly helpful during the experimentation and development phase of the teleoperation system.

PHANTOM Premium 3.0/6DOF connects to a computer via a parallel port. The servo loop runs in a scheduler at a frequency of 1 kHz to ensure the stable position and force feedback to the operator's hand. A single push button is available on the handle of Phantom Premium for reindexing. When the button is pressed, the master manipulator disengages from slave and can be repositioned independently. The release of the push button engages the master again with slave and the operator can start controlling the motion. Table 1 summarizes some of the main characteristics of the Phantom Premium. Figure 5 shows a picture of Phantom Premium.

Figure 5: Phantom Premium 3.0/6DOF

Table 1: PHANTOM Premium 3.0/6DOF Technical Specifications

Workspace	X, Y, Z	900 × 900 × 300 mm
	Yaw, Pitch, Roll	297 × 260 × 335 degrees
Resolution	X, Y, Z	~ 0.02 mm
	Yaw, Pitch	0.0023 degrees
	Roll	0.0080 degrees
Force feedback	X, Y, Z	22 N
	Yaw, Pitch	515 mNm
	Roll	170 mNm

5 GRAPHICAL USER INTERFACE

The Graphical User Interface (GUI) has been designed to be used with Windows XP operating system. The software has been developed using C++ and Microsoft Foundation Classes (MFC). Object oriented approach has been followed for the development of this software, and application is divided into classes. These classes permit future modifications, reliability and maintenance of the system. The package diagram of figure 6 shows the general architecture of the control software. The GUI can be started in a regular fashion as any other Windows® program by double clicking the icon or a shortcut to the program. In a similar way any user familiar with Windows® user controls can learn to use the GUI within no time.

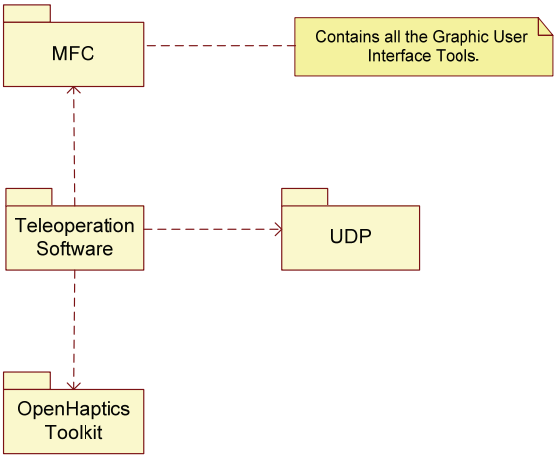

Figure 6: Package diagram

GUI has been designed as a tool for the operator to interact with the master and slave manipulators. With the aid of provided functionalities, the operator can manipulate the WHMAN independently in a number of possible modes or engage the master-slave mode to manipulate WHMAN using Phantom. A screenshot of figure 7 shows a Phantom control mode (bilateral teleoperation control mode) out of several control modes. A brief description of these control modes have been provided in following subsections. All the modes are synchronized in a way that when WHMAN is in motion, the control modes cannot be switched from one to another. At the moment, together with the controls provided on WHMAN-host, the teleoperation system provides good functionality and flexibility. However, the GUI is planned to provide more control modes in the future, such as the joint control mode with Phantom or joystick, etc.

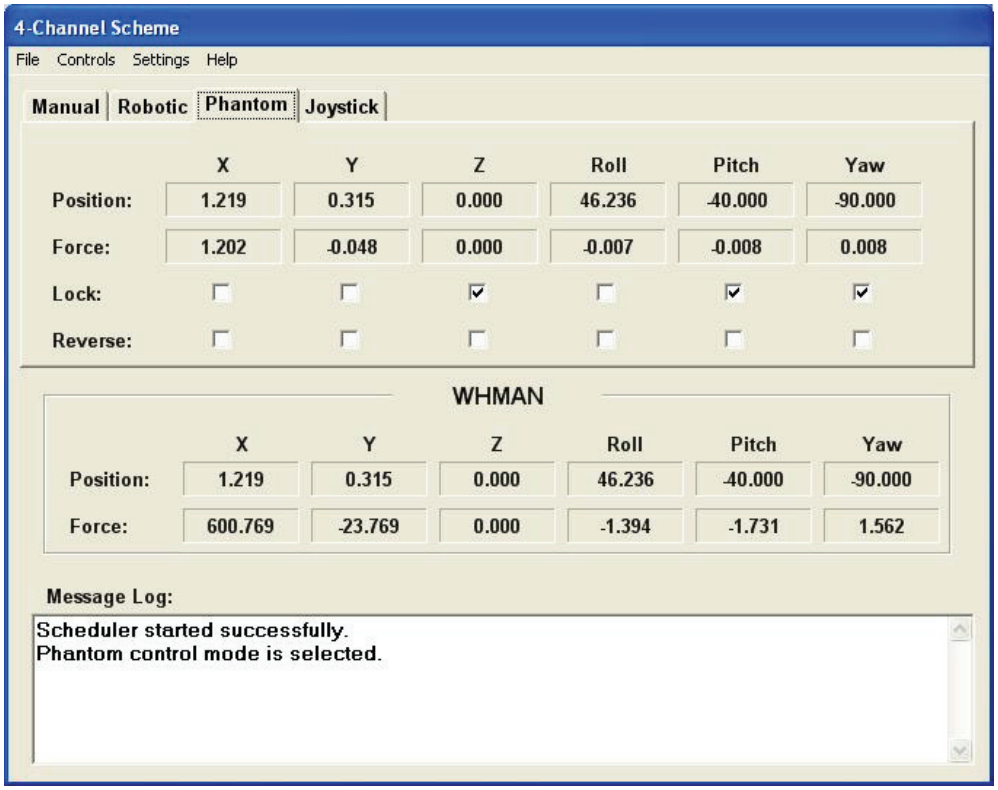

Figure 7: GUI of the remote control software

5.1 Manual mode

The mode is used for the point-to-point manipulation following a trajectory. The operator can input a set of target position and orientation values and command the WHMAN to reach the target point. The mode is helpful during the task planning.

5.2 Robotic mode

A set of predefined points (trajectory file) including start and end points can be loaded and WHMAN can be ordered to follow this trajectory. This mode can be used to execute certain robotic motions under user supervision such as ‘move to near tool’ and ‘move near to target’.

5.3 Phantom mode

This is the master-slave mode, in which, the WHMAN is engaged with the Phantom and follows its motion as the operator moves it around. The forces from the environment are felt by WHMAN and fed back to the Phantom where they are reflected on the operator’s hand. Thus the operator can control the forces applied on the objects in the environment. The added functionalities to enhance the usability of this mode can be summarized as follows:

- Any number of motion or orientation axes can be locked/frozen to provide the operator an easier control of manipulator. When a certain axis is locked, the WHMAN only follows the motion of Phantom along the unlocked axis. The feature can be extremely helpful in tasks such as tightening or loosening a bolt. Once the operator has engaged the tool with the bolt, the operator can freeze the motion of the manipulator in all the axes by locking them except for the final rotation to bolt or unbolt the screw.
- A single push button is available on the handle of Phantom Premium for reindexing. When the button is pressed, the master manipulator disengages from slave and can be repositioned independently. The release of the push button engages the master again with slave and operator can start controlling the motion.
- If a heavy tool is attached to the manipulator or if the operator is manipulating a heavy object in the environment, the gravity forces can be compensated to make the object feel weightless. The functionality is useful to avoid operator’s fatigue during long operations.
- Forces felt from the environment by the operator can be scaled up or down to fit the operator’s preference.
- The maximum velocity of the master can be adjusted in a way that fast motions of master by the operator are neglected. The feature not only improves the controllability but also adds a safety feature in case the master operator is suddenly released from the operator’s hand.

5.4 Joystick Mode

The motion of WHMAN can be controlled through a joystick connected to the system. A virtual joystick is also provided on the screen in the form of push buttons which can be used to control the motion of WHMAN in each axis and orientation.

6 IHA3D

The video feedback to the operator can be enhanced with the use of a virtual 3D model of the remote environment. IHA3D is a modeling software, developed at IHA/TUT, using MFC and OpenGL (Open Graphic Library) to run under the Windows® platform. Figure 8 demonstrates the implemented virtual model. The software communicates with the rest of the system over the Ethernet. The objects developed in the CAD software can be loaded by IHA3D to create the virtual environment. A frame is attached to each object to define its position and orientation in the environment with respect to one global frame.

Another purpose of IHA3D is to provide a simulated virtual environment. This feature is helpful for planning, practicing and simulating a task in the virtual environment before the operator performs the task in the actual environment. In this way a great number of errors and unpredictable situations can be avoided during the performance of the task. Trajectory points can be defined by the operator and can be tested beforehand. The operator can move and rotate his/her point of view to monitor the operation closely in a way providing access to innumerable cameras. These trajectory points can be stored in a file for later use with WHMAN during the task execution.

IHA3D provides information about the collisions of the object in the environment in the following ways:

- By changing the color of colliding objects on the screen.
- 0/1 digital online information over the Ethernet.
- IHA3D also provides the online location of the objects in the environment. Together with the collision information, this data can later be plotted to locate the exact collision points.
- By providing an online force vector depending on the depth of collisions which can be used to regenerate forces on Phantom during practicing a task.

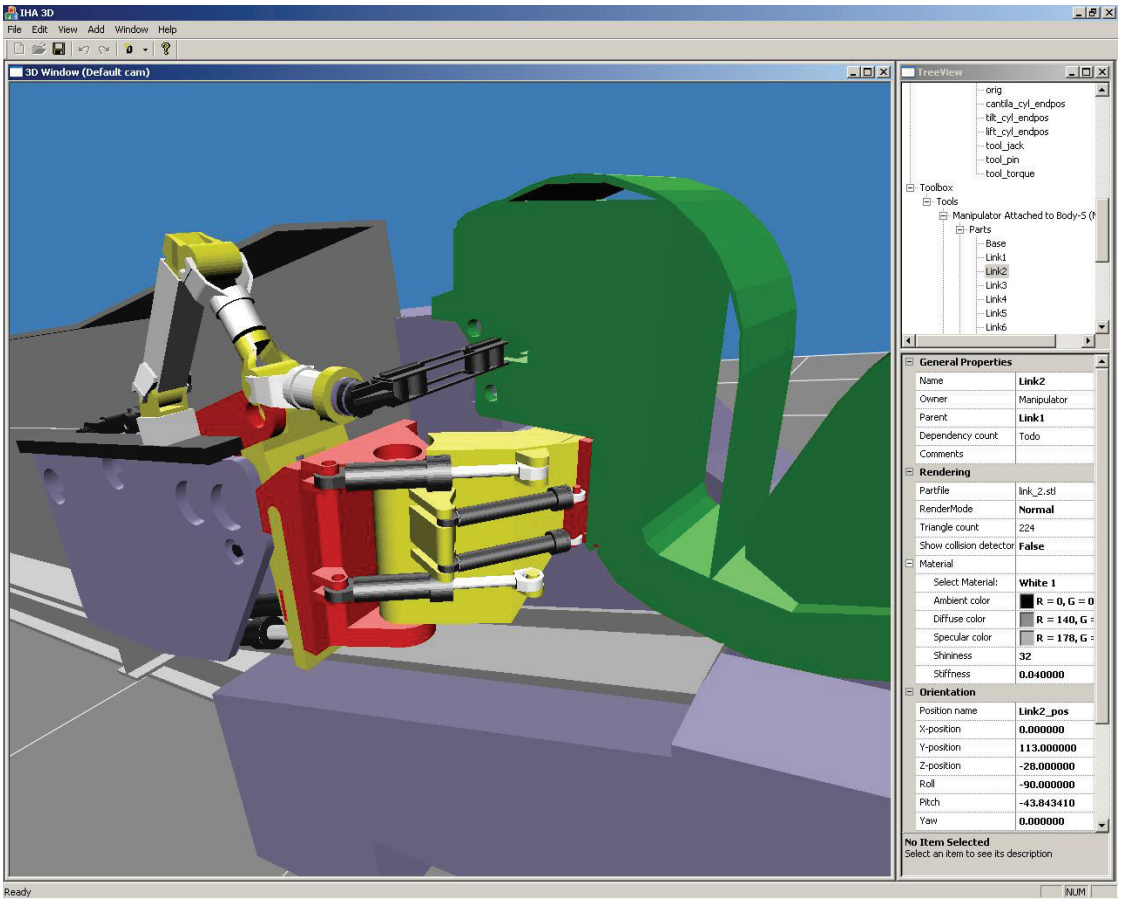

Figure 8: Virtual model of 5DOF WHMAN

8 CONCLUSIONS

A dexterous teleoperation system is required for remote handling tasks in a nuclear environment such as in ITER. A teleoperation system is under development at IHA/TUT, consisting of a water hydraulic manipulator as slave, a commercial haptic device as master, a human machine interface to assist the operator, a vision system comprising of cameras and video monitors and a graphical system providing a virtual 3D view of the environment. Virtual prototyping has been used extensively during the course of the development of this teleoperation system, resulting in reduction of development cost. Although the system has been developed for carrying out remote handling operations in ITER, the modular design and flexibility makes its use possible in many industrial applications.

ACKNOWLEDGEMENTS

This work, supported by the European Communities under the contract of Association between EURATOM/TEKES, was carried out within the framework of the European Fusion Development Agreement. The views and opinions expressed herein do not necessarily reflect those of the European Commission.

REFERENCES

1. Siuko, M., Pitkäaho, M., Raneda, A., J. Poutanen, J., Tammisto, J., Palmer, J. and Vilenius, M., “Water hydraulic actuators for ITER maintenance devices”, Fusion Engineering and Design 69 (2003) pp. 141-145.

2. Frederick P. Brooks, Ming Ouh-Uoung, James J. Batter and P. Jerome Kilpatrick, Project GROPE, “Haptic Displays for Scientific Visualization”, ACM Computer Graphics, 24(4):177-185, 1990.

3. Rovetta A., Cosmi F., Molinari Tosatti L., Termite L., **“**Evaluation of human control in telerobotics by means of EMG**”,** Intelligent Robots and Systems '94. 'Advanced Robotic Systems and the Real World', IROS '94. Proceedings of the IEEE/RSJ/GI International Conference on Volume 1, 12-16 Sept. 1994 Page(s):268 – 272

4. Lane J., Carignan C., Akin D., “Advanced operator interface design for complex space telerobots”, Proc. Of the IEEE International Conference on Robotics and Automation, 2000, California, USA.

5. Moss, B., “Real-Time Control on Ethernet”, Dedicated System Magazine–2000 Q2©, Page(s): 53 – 60

6. Hogan N., “Impedance control: an approach to manipulation: Parts I, II, III”, Journal of Dynamic Systems, Measurement and Control, Vol. 107, pp. 1–24, 1985.

THE DESIGN AND DEVELOPMENT OF ITER DIVERTOR RH EQUIPMENT @ DTP2 FACILITY

J. Mattila[1], J.Poutanen[1], H.Saarinen[1], T.Kekäläinen[1], M.Siuko[2], J.Palmer[2], M.Irving[2], A.Timperi[3],
[1)] Tampere University of Technology, Institute of Hydraulics and Automation
PO Box 589, 33101 Tampere, Finland
Phone +358 3 3115 4441, Fax +358 3 3115 2240
E-mail: jouni.mattila@tut.fi
[2)] EFDA-CSU Garching, Boltzmannstrasse 2, 85748 Garching, Germany
[3)] VTT Industrial Systems, PO Box 1300, 33101 Tampere, Finland

ABSTRACT

A key ITER maintenance activity is the exchange of the divertor cassette, which is scheduled to be performed after every 3-4 years of plasma operations. ITER divertor maintenance is classified as an RH Class 1 activity and as such, detailed design of the associated RH equipment and verification of its operation before ITER construction by way of prototypes and mock-ups, is considered an essential activity. Throughout the course of the ITER design activities one of the major focuses of the EU RH programme has been the study and development of remote handling equipment necessary for divertor exchange. The current major step in this programme involves the construction of a full scale physical test facility in which to demonstrate and refine RH equipment designs with prototypes closely replicating those proposed for ITER. This paper reports on the latest prototype designs and outlines the current building status and planning for the test facility.

Keywords: Remote Handling, water hydraulics, DTP2, ITER

LIST OF ACRONYMS

CMM	Cassette Multi-functional Mover
CTM	Cassette Toroidal Mover
DTP2	Divertor Test Platform 2
EFDA	European Fusion Development Agreement
ITER	International Thermonuclear Experimental Reactor
MC	Motion Controller
RH	Remote Handling
SCEE	Second Cassette End-Effector
WHMAN	Water Hydraulic Manipulator

1 INTRODUCTION

ITER (International Thermonuclear Experimental Reactor) is a large international scientific project aiming to prove that it is possible to harness the nuclear fusion reaction into energy production purposes. The ITER test reactor construction in Gadarache France has recently started and is estimated to be completed within 9 years, costing about 2500 MEur.

Due to the erosion of the plasma facing components inside the reactor and possible need for improving the design of critical items, maintenance is an important issue for assuring a smooth operation of the machine. A key ITER maintenance activity is the maintenance procedure of the divertor cassette, located at the bottom of the D-shaped toroidal reactor vessel (Tokamak). The divertor system comprises a set 54 cassettes supported on the inner and outer vacuum vessel walls by a pair of toroidal rails. Each cassette is expected to weight 8-9 tonnes and their external dimensions are approximately 3.5m long x 2.1m high x 0.8m wide. Figure 1 shows the ITER reactor design and the divertor cassettes.

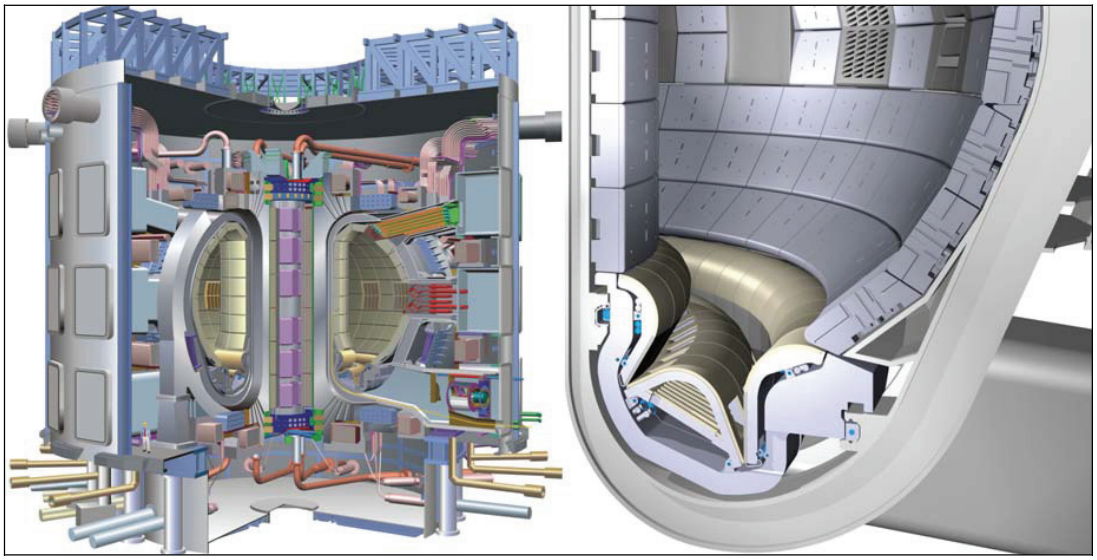

Figure 1. Cross section of ITER reactor and zoomed view of the divertor area and cassettes

The divertor maintenance is scheduled to be performed after every 3-4 years of plasma operations. For the maintenance operations, the divertor cassettes must be removed from the reactor vacuum vessel and carried to separate service area called Hot Cell. The cassettes will be sequentially removed from the reactor in batches covering one sixth of the divertor region through 3 maintenance ports using remotely operated devices known as “cassette movers”. There are two types of movers designed for this procedure; one that travels along radial rails to remove cassettes positioned directly in front of the Remote Handling (RH) port, known as the “Cassette Multi-functional Mover” or CMM (See Figure 2), and one that travels toroidally around the vessel to deliver / collect cassettes positioned at some distance from the RH port, known as the “Cassette Toroidal Mover” or CTM. The CMM, fitted with a variety of alternative end-effectors, is also used to handle the port closure plate and different diagnostic assemblies housed within the RH port. [1]

During the maintenance, also multi-purpose manipulators will be used for various assisting work such as bolting/unbolting, pipe cutting and welding etc.

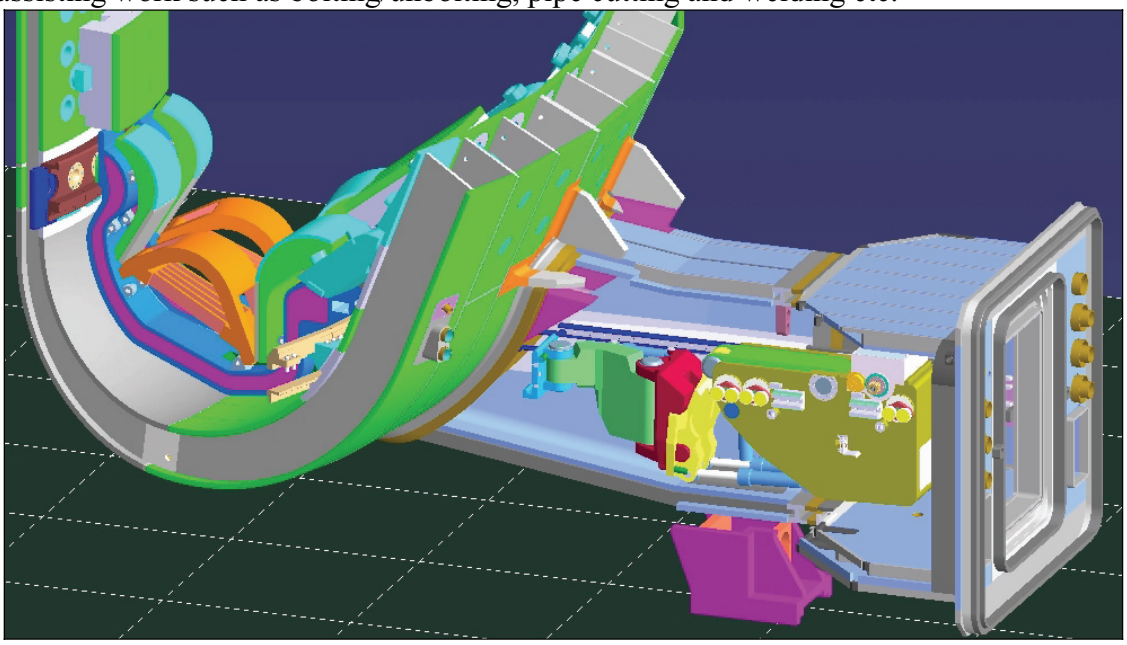

Figure 2. Virtual model of CMM traveling through the RH maintenance port (UUSI)

ITER construction by way of prototypes and mock-ups, is considered an essential activity. Therefore, since late 2003 the EU Participant Team has been continuously engaged in the detailed design of the ITER divertor handling equipment and more recently begun to construct a new full-scale RH mock-up test facility, called "Divertor Test Platform 2" (or DTP2) where ITER divertor replacement operations are studied, developed and demonstrated. In the autumn of 2004, EFDA-CSU (European Fusion Development Agreement – Close Support Unit), VTT Industrial Systems and Tampere University of Technology (TUT) agreed the joint effort to build the new DTP2 facility in Tampere, Finland [2].

Divertor maintenance tasks are expected mostly to be teleoperated due to radioactive environment, which prevents human presence inside the reactor vessel. In addition, most of the maintenance tasks require force feedback (human-in-the-loop) due to complex tasks and limited viewing system. High requirements for accuracy, reachability and controllability, as well as typically very high payloads, are the main reasons for choosing hydraulics as the operating principle for the maintenance equipment because of its compactness (high power-to-size ratio) and reliability. However, instead of oil, hydraulic systems will use water as a pressure media to eliminate the risk of contaminating the reactor elements. Water is also not activated or effected by the radiation of the environment.

During years from 1994 to 2006 IHA has participated in several projects in the field of ITER divertor maintenance, mostly on CMM design, documentation and virtual modelling, water hydraulic manipulator (WHMAN) development, and water hydraulic components development.

This paper presents the current situation of the DTP2 facility, main components (CMM, CTM and manipulators), and relevant development work that has been carried out during the last years.

2 THE DTP2 FACILITY

The development of the DTP2 facility will progress in two stages. The first phase will concentrate on testing radial movement of cassettes along the divertor level RH ducts and the installation / removal of cassettes through the maintenance port (see Figure 3). These operations will be trialled with the handling of so-called second cassettes (located immediately on either side of the access port) using a prototype CMM and Second Cassette End-Effector (SCEE).

Figure 3. DRM including the maintenance tunnel and reactor section under construction in VTT

DTP2 structure is designed to be modular; therefore it can be extended toroidally to study transferring of cassettes from locations at some toroidal distance from the RH ports. These tests will be made using a prototype CTM. Also other additional upgrades are possible. In the future, these upgrades will provide the necessary mock-up structures to carry out RH trials on the cutting and re-welding of cassette radial cooling pipes and handling trials with a central cassette.

The DTP2 facility is hosted and operated by the Finnish Fusion Association Tekes and is located at the premises of VTT Systems Engineering in Tampere. Reference designs for the major DTP2 elements; Divertor Region Mock-up (or DRM), cassette mock-up and the prototype CMM plus SCEE (including control hardware) were developed jointly by EFDA-CSU, IHA and VTT. Based on these reference designs, four separate procurement contracts were placed for the detailed design, manufacture and installation of these main DTP2 sub-systems (see Figure 4). For better understanding of the full maintenance process, it was decided to not to use commercial control softwares for any of the subsystems, therefore all components will be delivered without software. All control etc. software will be developed on site by IHA, so that possible compatibility problems are avoided. This centralized software development also means that the operators will have to use only one software instead of several different ones, which helps training, and simplifies the operation.

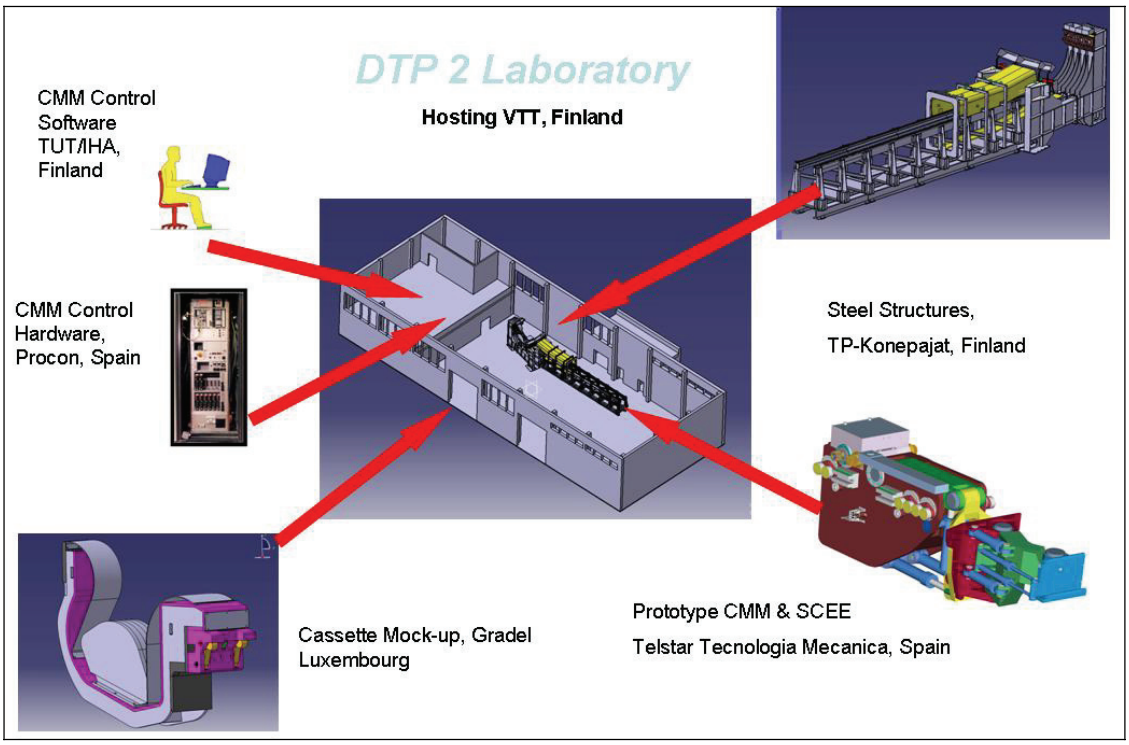

Figure 4. Major subsystems of the DTP2 facility

The design of the mock-up structures (divertor region and cassette) has been done by concentrating only on geometrical and physical features which impact directly on the design of the RH equipment and/or execution of RH tasks. For example detailed modelling (in terms of geometry and material) of the cassette locking systems and their toroidal rail interfaces, and use of reactor relevant AISI 660 material for the radial rail hard cover plates and racks.

The current stage of the facility includes the divertor region and RH port steel structures. Full integration and commissioning of the other components and subsystems is estimated to happen during spring 2007, thus allowing RH trials to begin in summer 2007.

3 PROTOTYPE CMM AND SCEE DESIGN

For cassette refurbishment, the divertor cassette is picked up from the reactor, and transported to maintenance area. In co-operation with EFDA, IHA defined the cassette replacement procedure. The whole divertor replacement cycle involving all CMM tasks was studied buy means of virtual prototyping, and based on these studies the second cassette handling was determined as the most demanding task. The task is demanding, since it includes moving the cassette toroidally (by actuating the cantilever and hook plate joints), while position of tilt and lifting joints must be also controlled precisely in order to keep the vertical gap between the inner and lower rails and the divertor cassette. Therefore IHA has concentrated on the CMM and the second cassette end effector design and development.

The reference design geometry for the CMM and SCEE, together with the type, location and range of their degrees of motion, was created using state-of-the-art virtual reality

techniques. Virtual prototyping software tools like CATIA V5®, Envision®, ADAMS® and MATLAB/Simulink® have been used extensively to verify motion trajectories, check clearances and interferences during the cassette installation/removal processes and to understand the dynamic behaviour of the equipment before manufacturing any physical prototypes.

The design and development work of CMM started from defining divertor cassette replacing task, based on preliminary study by Framatome, and will gradually proceed towards testing cassette replacement scenario with real applications in DTP2 facility. The development has progressed in following order:

1. Studying the CMM tasks, and specify the design requirements.
2. Designing CMM basic mechanical structure and hydraulic system, and selecting preliminary electrical components.
3. Providing design changes for the CMM and the SCEE meeting the latest design of the ITER reactor design. Updating the documents and drawings and re-analyzing mover strength, due to the changes.
4. Updating 3D virtual models of the CMM, SCEE and the reactor environment.
5. Providing a reference design plus technical assistance and expertise to EFDA for call-for tenders of the CMM mock up.
6. Testing the general applicability of an commercial motion controller to a large water-hydraulics actuator, and confirming that such a system can achieve the positional accuracy and speed required for the CMM under a number of realistic load conditions.
7. Producing the low-level software required for driving the CMM hydraulic axes well before the CMM system is available.
8. Developing the high level software, which, interfacing with the low level software, will enable the real CMM/SCEE prototype to carry out its required overall functions.
9. Finally, when the CMM prototype is delivered (summer 2007), start testing the cassette replacement scenarios with full-size prototype.

The CMM/SCEE incorporates a total 5 axes of motion: one electrical (radial drive), and 4 powered by water hydraulic cylinders (Lift, Tilt, Cantilever Arm Rotation and Hook Plate Rotation). The CMM to SCEE mechanical interface is equipped with an integral electrical and hydraulic connector to allow the SCEE to be easily detachable from the main CMM under remote conditions. The hook plate itself is a mechanical interface capable of remote attachment to the cassette. Figure 5 presents the CMM design.

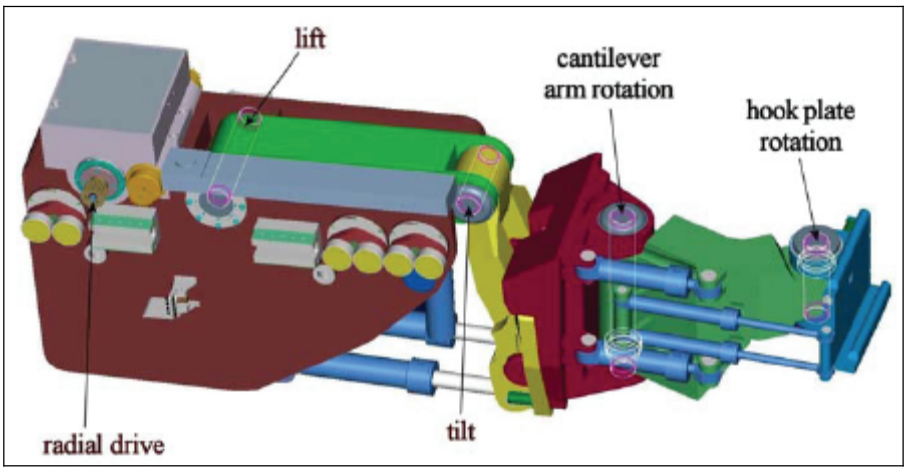

Figure 5. CMM design

The radial drive is powered by two brushed servomotors operating in parallel and driving pinions on each side of the CMM which engage with racks mounted along the length of the radial rails. Both motors are equipped with a 24V DC brake and analogue tachometer. The radial position of the CMM will be determined with an accuracy of ± 1-2 mm by a single-turn geared resolver integrated to the radial drive housing.

Each of the 4 hydraulic axes consists of one (or two) water-hydraulic cylinders, which are controlled with servovalves located in the body of the CMM. Water hydraulic supply pressure (and return) is brought to the CMM via two separate umbilical drag chains (left and right) which also carry all the electrical wiring from the control system. All hydraulic axes incorporate a multispeed pancake resolver with accuracy to ±25 arc seconds mounted directly on the joint axis. Both CMM to SCEE, and SCEE to cassette interfaces are equipped with electrically operated locking devices, as well as microswitches confirming that the interface has been locked correctly. Each axis also incorporates microswitches warning of joint overtravel.

An important aspect of this latest prototyping exercise is to work within certain design constraints specific to operation in a fusion device like ITER, namely:

- Use of stainless construction materials for elements which can come in contact with the in-vessel region
- Double containment of organic lubricants or use of vacuum compatible (dry) lubricants were this is not possible
- Selection of components (e.g. motors, sensors, cables etc) which have an adequate level of radiation tolerance for the ITER environment

Radiation issues

The radiation tolerance issue was a major factor in selecting of resolvers and microswitches to control joint position since both have demonstrated good reliability under radiation testing and require no on-board electronics. Also pressure sensors have been selected so, that they do not contain integrated electronics.

Radiation tolerance of water hydraulic cylinders seals was recently studied by a testing programme [3]. During the tests, first a number of commercially available seal options were evaluated and their performance was tested under CMM relevant operating conditions. The seals were radiated with different doses, and the post-radiation

performance was tested. The tests indicated reliable operation of the seals up to an integrated dose of 1 MGy. Since the operational radiation exposure for the CMM is estimated to be at around 300kGy during a typical divertor exchange, the seal radiation tolerance appears to be sufficient. Bushed DC motors were selected for the radial drive (rather than more modern brushless alternatives) because possible recovery situations are easy to perform simply using a DC power supply.

4 CMM CONTROL SYSTEM DESIGN AND DEVELOPMENT

The control system architecture for the DTP2 prototype movers is based on the design principles suggested for RH equipment outlined in Irving [4]. This architecture is based on commercially available modern Motion Controllers (MC) which incorporate a large amount of motion control software, including management of the servo loops at high refresh rates and comprehensive safety provisions.

Following a thorough selection process, the Moog Servo Controller, part of the Moog M3000 Control System range, was chosen as the best overall candidate MC for the prototype CMM/SCEE application. Therefore the control hardware design is based around this system. The main reason for choosing Moog Servo Controller was the easy and flexible software development characteristics. A major advantage of the architecture being utilized here is that with proper attention to modularity in the design, updates can be incorporated with minimum impact on the remainder of the system.

A second major element of the CMM/SCEE controller is the Host computer. Industrial PC's were selected for that purpose, since they have sufficient power, and versatility. Communication with the MC's will be by a serial based communications system (CANbus), and so in principle an alternative host could always be substituted if there are reasons to do so at a later date.

In order to maintain a full understanding of the development process of the DTP2 exercise, it was decided to not to use any commercial control software, but to develop the application based software (tuning of the MCs, Host and HMI programming) on site (by IHA). Significant steps have already been made well in advance before the delivery of any DTP2 hardware by developing physical and virtual models of the CMM and/or SCEE mechanics and hydraulics linked to the CMM controller. An example of these CMM related virtual models is presented in [5]. Figure 6 presents the CMM high level controller prototype user interface developed by IHA.

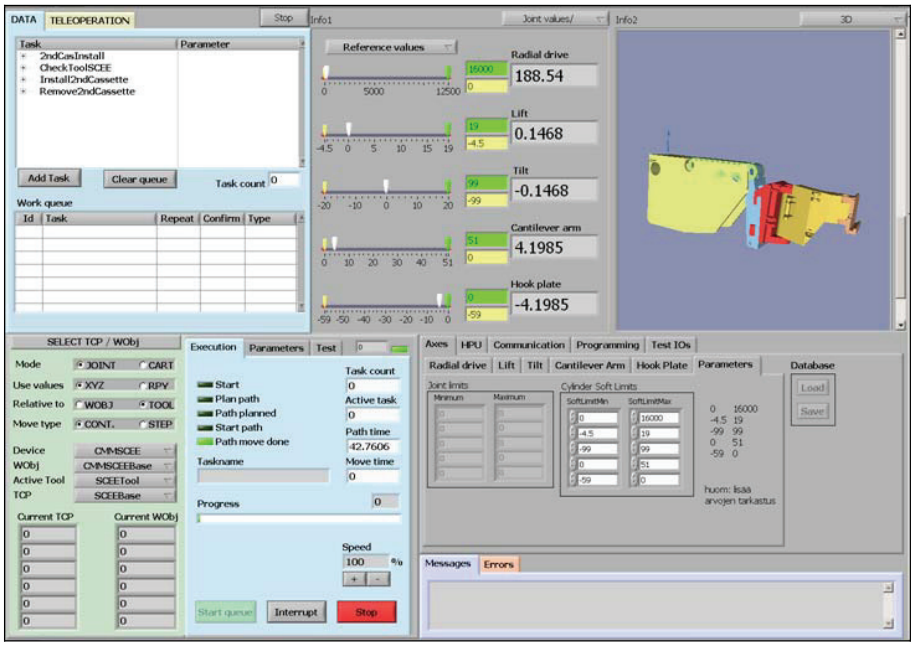

Figure 6. Graphical user interface of the CMM High Level Controller

5 PROTOTYPE CTM DESIGN [6]

The basic function of the Cassette Toroidal Mover (CTM) is travelling toroidally around the reactor vessel, collecting cassettes positioned at some distance from the RH port, and delivering them to the RH port, where CMM can pick them up. In addition to the basic cassette transporting operation, the CTM performs the final radial and toroidal positioning, the locking & unlocking of the supports and the inspection of the standard divertor cassettes. Both right-hand side and left-hand side CTM are required to perform the cassette replacement sequence.

The CTM is equipped with the following main components:
- the chassis forming the main structural body of the CTM
- the drives to move the CTM on the divertor rails
- the locking mechanism to position and to fix the CTM to the divertor rails
- the gripping, lifting and moving mechanism for the divertor cassettes
- the CTM WHMAN for the handling of service tools
- the hydraulic supply unit for the hydraulic equipments
- the umbilical guides

An overview of the CTM design, developed by Framatome ANP GmbH, is presented in Figure 7. The figure also incorporates a manipulator, designed by IHA, located on top of the CTM.

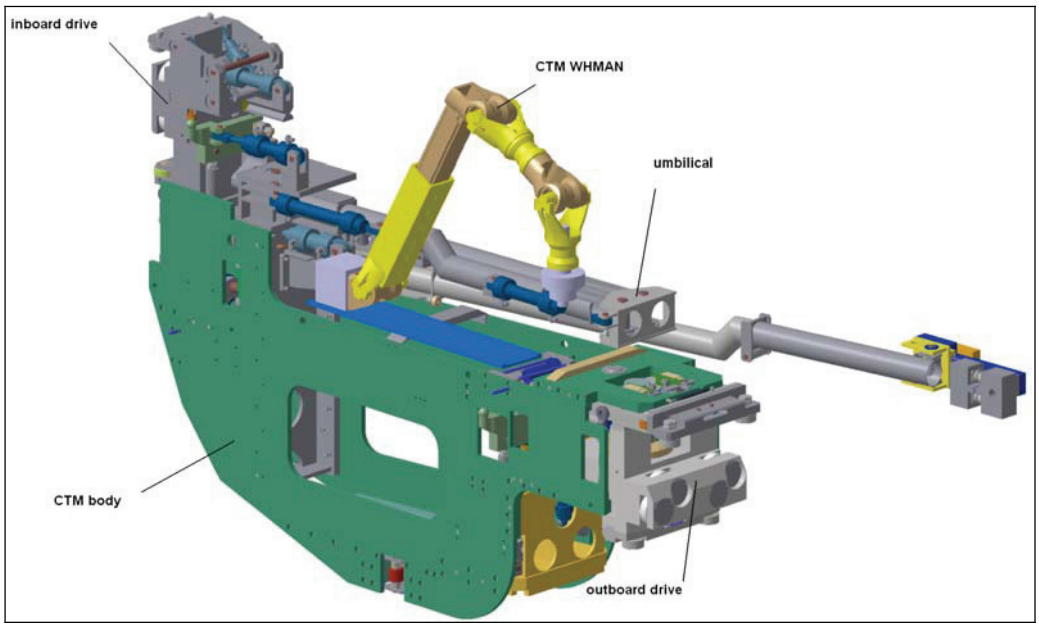

Figure 7. CTM design and main components

The CTM operation is based on cantilevered lifting concept. Due to the geometry of the divertor rails and the locking system the cassette must be moved also in radial direction during lifting, which would be impossible with a simple fork concept. With the proposed hook system concept the lifting and the radial movement can be performed at the same time; one cylinder lifts the hook, another cylinder tilts the hook for the radial movement and a third cylinder retracts the hook in the park position inside the CTM.

The inboard and outboard divertor rails guide the CTM. A rack system for the drive of the CTM is integrated into the rails. Due to possible tolerances the inboard and outboard drive of the CTM have to be independent, and the drives are connected to the chassis by joints. Also, in order to compensate tolerances from the inboard to the outboard rail in radial direction one drive has to be connected to the chassis by a linear guiding. Since the connecting CTM platform tolerates the independent movement of both drives, each drive is guided by rollers and by the rail in all relevant directions.

This type of connection constrains the vertical displacement of the chassis, but allows rotation around vertical axis and horizontal displacement. Nevertheless, each joint has 3 DOF (rotation, radial displacement and tangential displacement) which means that the chassis position is not defined. This is not desired, since the location of the CTM should be defined if the tangential position of the drives is known. To solve that, some of the DOF must be constrained.

• The displacements of the outer drive is constrained so that only rotation is free. This effect is obtained adding a bearing joint.

• The tangential displacement of the Inner drive is constrained, but the rotation and the radial displacement remain free. This effect is obtained with adding a pin with a socket hole.

At the end, the chassis has only 3 DOF. The position and orientation of the CTM are defined, but a relative displacement between drives is allowed. Figure 8 shows schematically the relative displacement philosophy.

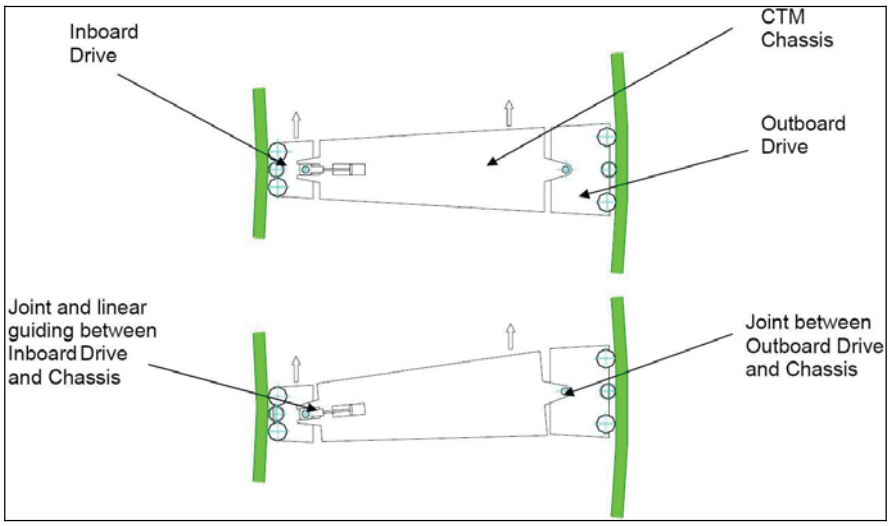

Figure 8. CTM kinematics

6 MANIPULATOR DEVELOPMENT

In addition to large task-specific maintenance devices, such as CMM and CTM, also multi-purpose 6DOF manipulators are required in ITER divertor maintenance for various supportive tasks. Such tasks are for example pipe cutting, welding, bolting/unbolting and operating cassette locking mechanisms. Water hydraulics is chosen as the operation principle of the manipulators due to high force requirements, limited space, and radiation tolerance issues.

6.1 CMM manipulator

IHA has been developing a water hydraulic manipulator concept (WHMAN), including sophisticated force-feedback teleoperation control systems by using Phantom desktop 6DOF force/torque feedback master arm [7]. The work has so far concentrated mainly on a WHMAN located on top of CMM, whose operation relates closely to the divertor cassette refurbishment cycle, which will be one of the first studies at DTP2.

The development process started from defining the manipulator tasks and gradually proceed towards creating a prototype manipulator for DTP2-platform, where ITER divertor replacement operations are studied, developed and demonstrated. The development has progressed is logical steps:

1. Defining manipulator tasks.
2. Creation of preliminary manipulator mechanism design, and testing it in virtual environment.
3. Designing and building a general purpose simplified (3 DOF) teleoperated prototype Water Hydraulic Manipulator and study teleoperation with it.
4. Proceeding towards a more complex manipulator design by adding degrees of freedom (6 DOF) to the prototype.

5. Continuing on the path towards creating a prototype manipulator suitable for ITER relevant operational scenarios and environment.
6. Studying and developing control methods, remote handling and force feedback operation.

Figure 9 presents the latest 6 DOF manipulator design, which is currently under manufacturing. The 3DOF wrist shown in the figure is currently installed to 5DOF arm mock-up and teleoperation studies are made at IHA [7].

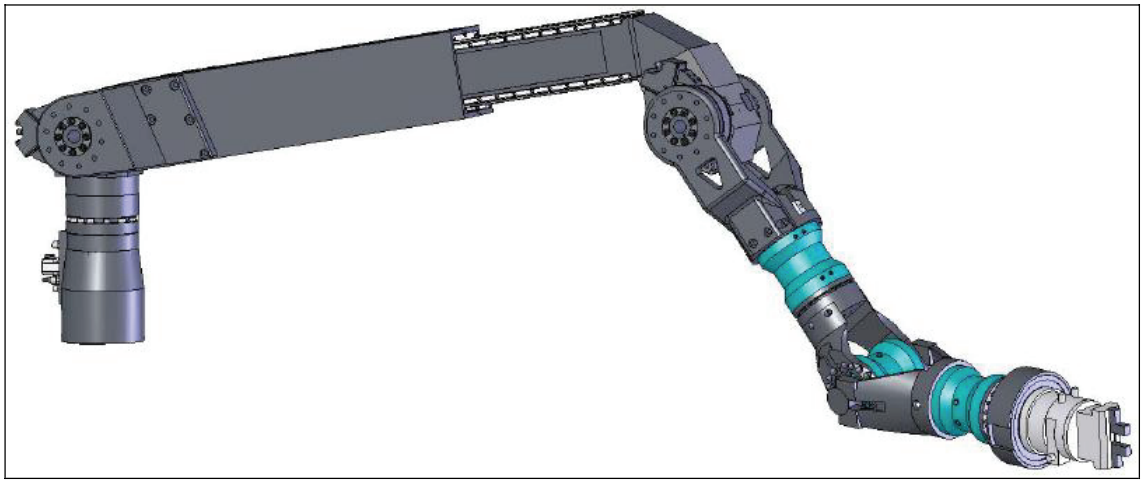

Figure 9. The latest 6 DOF WHMAN design

In parallel with the manipulator design, a development of robust designs for water hydraulic rotary joints has been carried out to support the overall manipulator development. Vane actuator has superior performance when light and compact in volume but still high torque actuator is needed to drive a robotic joint at wide (>120 deg) motion ranges. The downside of the vane actuator is difficulty in finding an optimal balance between actuator seal leakage and seal friction. In order to proceed towards prototype manipulator, a new vane actuator design has been developed at IHA.

6.2 CTM manipulator

A brief initial feasibility study of suitability of IHA developed CMM WHMAN has been carried out, since the CTM will be equipped with a 6DOF manipulator very similar to CMM WHMAN. The CTM WHMAN uses tool gripper to manipulate the tools needed for different operations. Its main operations are cassette locking/unlocking and the cassette cooling pipe maintenance, including pipe cutting/welding. Standard cassette locking/unlocking are the same operations as with first and second cassette. Only difference is that they are made with CTM WHMAN and that the CTM brings the cassettes to the RH port for CMM to pick them to the transfer cask. Pipe cutting/welding are also similar and the only thing that changes is the location of the cooling pipes.

For CTM WHMAN the most difficult part in the procedures is the pipe cutting and welding of furthest of standard cassette cooling pipes where one of the pipes is on the way of the manipulator and the second one is on the other side of the cassette (see Figure 10). Preliminary studies indicate that the manipulator needs a linear actuator and slide on top of the CTM to reach to the furthest cooling pipes of the cassettes, otherwise

the first two links of the CTM WHMAN would have to be inconveniently long. More research is needed for the placement of the linear slide and its design. The CTM umbilical and its guiding system design reserves most of the space on top of the CTM and therefore there is not much space for the WHMAN and its tools.

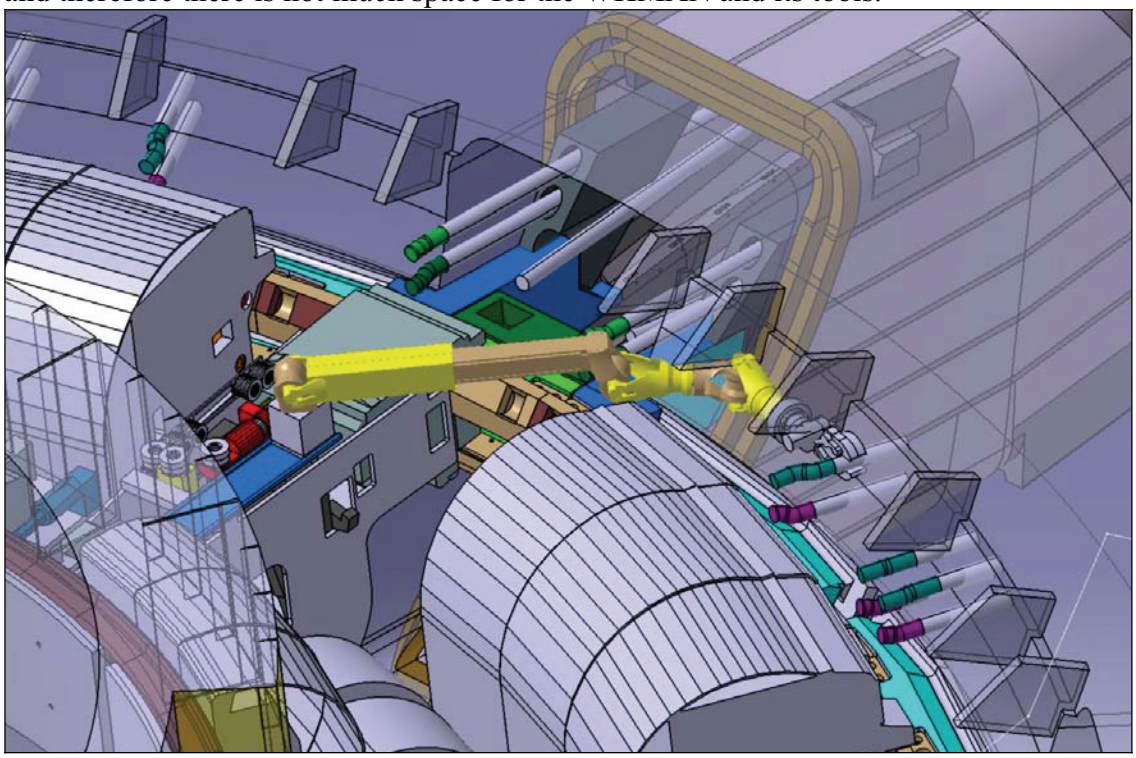

Figure 10. CTM WHMAN operating standard cassette cooling pipes

Preliminary studies at IHA indicates that a similar manipulator as the IHA CMM WHMAN (chapter 6.1) can be used as CTM WHMAN, due to its modular and dextrous design, because it can do all the needed operations, fit to the small spaces behind the cassettes quite easily and standard cassette locking/unlocking is possible

7 DTP2 OPERATION

The basic idea of the DTP2 facility is to prove that the divertor maintenance procedure is possible with the designed RH prototype devices and, in the future, work as a training facility for the maintenance personnel. In order to fully accomplish this target, the whole cassette collecting/installing cycle should be possible to perform at the test platform.

The total divertor replacement procedure is complex task and requires many phases:
1. The maintenance procedure begins with opening of the RH port: CMM is transported to the port (in a transport cask), and it opens the RH port door with the aid of manipulator. Door is unbolted, lip seal welds are cut, and then the door is picked up by CMM and carried away in the cask.
2. Next step is the diagnostic rack removal. Again CMM, equipped with suitable end effector and with the aid of the manipulator, unbolts the rack, picks it up and carries it away in the cask.
3. After the diagnostic rack is out of the way, the CMM picks the central cassette up, using a special end effector, and carries it away

4. Next step is to remove the right- and left-hand side second cassettes, which are estimated to be the most demanding tasks of the cycle, because of the cantilevered toroidal motion is required.
5. The CTM is brought to its place on toroidal rails, and its umbilical is connected.
6. CTM travels toroidally to the next cassette, unlocks it (with the aid of its manipulator), picks it up carries it to the RH port, where the CMM can pick it up.

Each task (door opening, rack removal, first and second cassette handling, etc.) requires its own end effector, so between each of these tasks the CMM has to go to tool exchange pit, and change the correct end effector.

In the real application all this is done remote operated with only limited viewing system, due to hostile radioactive environment. In addition to these challenges, the equipment must have adequate radiation tolerance, they must able to recover from failure or emergency stop, possible small distortion or damages of the cassettes must not affect the operation, and the equipment should be as maintenance-free as possible and stay operational for several years. Payloads are very high and clearances are small, yet collision with the reactor wall etc. are not allowed. So overall, the divertor cassette maintenance is a very challenging task, and the requirements for the equipment are exceptionally hard. The DTP2 facility should give valuable information about the maintenance operation, point out possible weak points, and enable new ideas for improving the maintenance procedure or equipment. Also centralized control software development for the maintenance applications is a very important issue, which highlights IHA's role as one of the DTP2 hosts.

8 CONCLUSIONS

Effective and efficient remote replacement of the ITER divertor is essential to the successful execution of the ITER project. With this in mind, significant European effort is being focused on the creation of a new RH mock-up facility to allow for the thorough testing full-scale RH equipment prototypes and careful examination the proposed divertor replacement processes. The most important target of the DTP2 project is to ensure that the cassette movers supplied to ITER during its construction will be based on well matured 'second generation' designs which have benefited from the experience and lessons learnt from the building and operation of the first generation prototypes.

ACKNOWLEDGMENT

This work, supported by the European Communities under the contract of Association between EURATOM / TEKES, was carried out within the framework of the European Fusion Development Agreement. The views and opinions expressed herein do not necessarily reflect those of the European Commission.

REFERENCES

[1] Palmer, J., 2006, "The Design And Development of Divertor RH Equipment for ITER", Proceedings of the 24th Symposium on Fusion Technology (SOFT)'06, Warsaw, Poland

[2] Timperi, A., 2006, "DTP2 Laboratory Situation in Tampere, Finland", Proceedings of the 24th Symposium on Fusion Technology (SOFT)'06, Warsaw, Poland.

[3] Irving M., 2006, "Post-irradiation performance tests on seals for water hydraulic applications", Proceedings of the 24th Symposium on Fusion Technology (SOFT) '06, Warsaw

[4] Irving M., 2004, "Generic control system design for the cassette multifunctional mover and other ITER remote handling equipment", Proceedings of the 23rd Symposium on Fusion Technology (SOFT) '04, Venice, Italy

[5] Esqué S., 2007, "The Use of Virtual Prototyping And Simulation in ITER Maintenance Device Development", Proceedings of the Tenth Scandinavian International Conference on Fluid Power, Tampere, Finland

[6] Gottfried R., 2004 , "ITER CTM Design Development, Framework Contract - EFDA Order No. 93/851 IN, Final Report", Framatome ANP GmbH IBERTEF

[7] Muhammad, A., 2007, "Water Hydraulic Teleoperation System", Proceedings of the Tenth Scandinavian International Conference on Fluid Power, Tampere, Finland

DIAGNOSTICS AND VISUALIZATION IN HYDRAULIC PRESS

Sami Stormi
Raute Oyj
P.O.Box 69
FIN-15551 Nastola, Finland
Phone +358 40 822 8779
E-mail: sami.stormi@raute.com

Professor Jari Rinkinen
Tampere University of Technology
Institute of Hydraulics and Automation
P.O. Box 589
FIN-33101 Tampere, Finland
Phone +358 3 3115 2263
E-mail: jari.rinkinen@tut.fi

ABSTRACT

Troubleshooting and adjusting of hydraulic system of plywood press lines has been problematic in plywood mills according to service reports of Raute Oyj. The knowhow of operators and service personnel has significant role in this. In this article different ways that were tested in improving the current situation are discussed. User interface of press line was used to visualize the actuation of the hydraulic system of press line and also diagnostics was developed. In the development of diagnostics the idea has been to exploit already existing information that electrical control of press lines provides.

KEYWORDS: Diagnostics, hydraulic press, visualization

1 INTRODUCTION

Service reports of Raute Oyj show that it is common that the operators of press lines and service personnel in plywood mills have insufficient knowledge of the hydraulics used in press lines. This leads to a situation where troubleshooting time is lengthened unnecessarily, in the case of faults, and the hydraulic actuations of press lines are not adjusted in the best possible way. Poor adjustments cause loss of production and increase faults. Because oil hydraulics are widely exploited in the plywood press lines it is very important to find ways to improve the current situation of the troubleshooting and adjustments.

To improve the current situation the actuation of the hydraulic system of press line was visualized in the user interface of press line. The main objective of visualization was increasing the knowledge of operators and service personnel. Visualization means graphs and graphical representations that aid the operators and service personnel to understand the actuation of the hydraulic system.

Diagnostics ease troubleshooting directly and in some cases faults can be diagnosed in beforehand. Due to the possibilities that diagnostics provide some new diagnostics methods were implemented in the hydraulics system of press line. The electrical control of press line provides a lot of already existing data that can be used in diagnostics. This data is for example control signals of proportional valves and signals from sensors and switches. Data can be logged for later analyzing but it can also be used for instance to calculate actuation times and movement velocities. In the hydraulic system of press line new sensors will probably be utilized in oil condition monitoring.

The implementation of the new diagnostics methods and visualization means in the hydraulic system of press line was performed during the Master of Science Thesis of Sami Stormi. The examiner of the Thesis was professor Jari Rinkinen.

2 KNOWHOW OF OPERATORS AND SERVICE PERSONNEL

Suzuki [1] says, “Front-line operators closest to the equipment must be willing and able to look after it themselves. Meanwhile, maintenance personnel must acquire the requisite technology and skills to act as its professional custodians.” This should be the ideal case but unfortunately the reality is sometimes very far away. The operators often don’t understand functions of equipment and technology that makes the functions happen. As a result of this the operators are unable to react in the case of faults and unusual situations and they are also unaware of capabilities and full capacity of their equipment. This leads to a situation where the operators are satisfied with the current performance of equipment although it could be possible to increase the productivity of equipment.

Even 34 years ago Bradbury [2] said, “Modern machines are becoming more and more complex because machines have to be faster and more efficient to meet the growing needs of competitiveness”. This is true also today. Increasing complexity sets higher requirements to service personnel. There are often situations when the service personnel is not skilled enough and this results in lack of maintenance and problems when finding remedy after fault. The service personnel is also sometimes unable to adjust the machines although the operators know that the performance could be boosted or matched with the current production.

2.1 Knowhow of Hydraulic Systems

Oil hydraulic systems have been widely used in industrial machinery for decades but still operators and service personnel often have inadequate skills and knowledge of hydraulics that is used in machines that they work with. Operator skills have significant effect on faults in hydraulic systems. One operator can have several component breakdowns or machine malfunctions while another operator has none [3].

It is very important that at least service personnel, but also operators, know how to adjust hydraulic systems. Wrong adjustments can increase faults and reduce production. Machines usually last longer if they are used below their maximum capacity. Due to

this, the machines should always be tuned to match the current rate of production. It is very rarely that every machine in a mill should work at its maximum capacity and there is no need for a machine to complete its duties faster if this results only in lengthened idle time. On the other hand there are sometimes also situations where a machine is the bottleneck in a mill although its production could be boosted just simply by adjusting it. If a machine is adjusted very poorly, its actuations can be too sudden or too fast, which causes mechanical faults and pressure peaks that reduce the lifetime of hydraulic components. The knowhow of operators and service personnel has the key role in troubleshooting hydraulic systems

2.2 Improving Current Situation

According to service reports of Raute Oyj, operators and service personnel often lack knowledge about adjusting and troubleshooting hydraulic systems. In a mill usually exists only one or two persons, or sometimes no one, who knows how to adjust their machines properly.

There are different ways to increase the knowhow of hydraulic systems in plywood mills. Personnel can be given training about hydraulic systems. The training should be customized and it should discuss different topics such as normal use, maintenance, troubleshooting and adjusting of hydraulic systems. Documentation that is provided with machine deliveries is as well very important in increasing knowhow.

Built-in diagnostics and real-time information about the actuation of the hydraulic system can also be used in increasing the knowhow. If operators and service personnel know what is currently happening in the hydraulic system they can react faster in the case of faults.

3 PRESS LINE

In plywood manufacturing laid up veneers are pressed to panels in press line (Figure 1). A typical plywood press line comprises different machinery such as lift platforms, charging and discharging lift, charging device, back-stop and the actual press. Main actuations are effected with oil hydraulics. Hydraulic cylinders and motors are used as actuators.

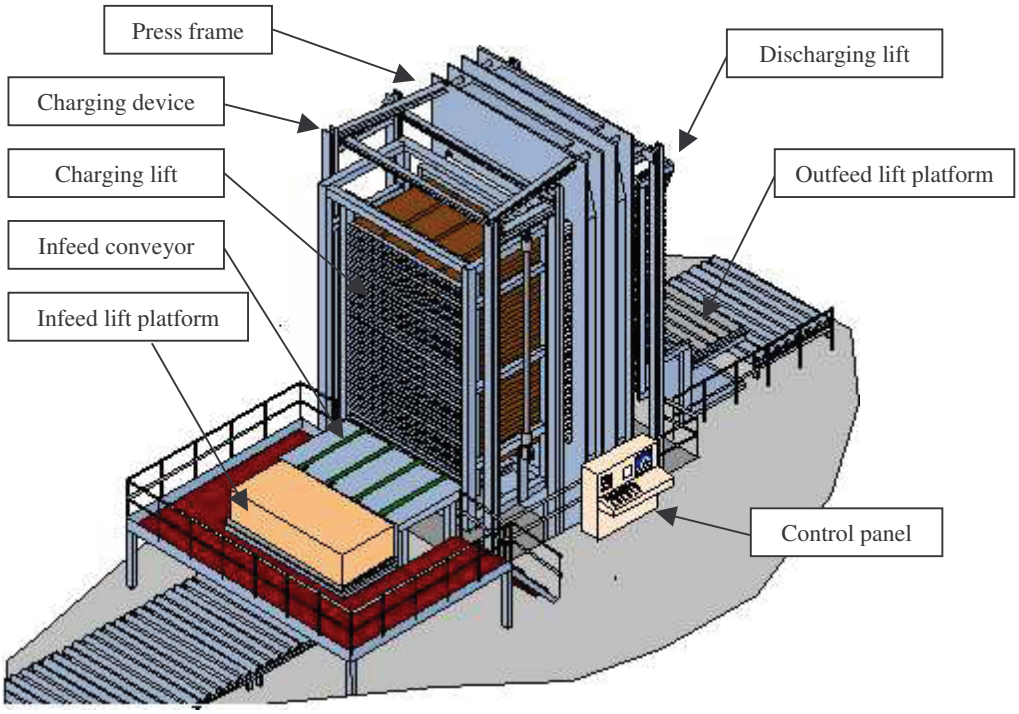

Figure 1. Main parts of press line.

For hydraulic actuations press line has one hydraulic power unit. Typically the hydraulic system includes four main pump units. Both on/off and proportional valves are used and the system is equipped with sensors for oil level and temperature and filter clogging. For PLC control the system has several pressure transducers, limit switches and position measurement sensors.

3.1 User Interface and Control Logic

All the line operations are controlled by a control logic. Information gathered from different parts of the system (sensors, switches, feedbacks, etc.) is processed by the control logic. The system state is presented to the operators via an user interface. The operators can also use the user interface to set pressing parameters and to control the line operations via the logic.

The press line user interface is a windows based application. The operators can set pressing variables such as size and amount of pressed panels, pressing pressure and pressing time. Different alarms are presented to the operators on the user interface windows. For example a clogged filter, too high oil temperature, unwanted actuator movements and sensor faults are presented as alarms in the user interface. The user interface provides many possibilities for presenting diagnostics data and actuation of the hydraulic system to the operators.

4 PRESENTING PRESS ACTUATION

Understanding the actuation of hydraulic system of press line is vital for both the operators and service personnel. If the knowhow of operators and service personnel is increased, the press line can be operated more effectively, troubleshooting time is decreased and also number of accidents is reduced. In this chapter new ways to present the press actuation in the user interface are presented. These new ways were developed and implemented as a part of Master's Thesis project.

The user interface of press line provides many possibilities to present the line actuation in real-time, i.e. to visualize the actuation. These presentations can be for example graphs or graphical representations. There has especially been a need to give a clear and simple presentation of the actuation of the hydraulic system.

Relatively simple representations can help the operators and service personnel. A simplified hydraulic diagram (Figure 2) gives an outlook of the main components in the hydraulic system.

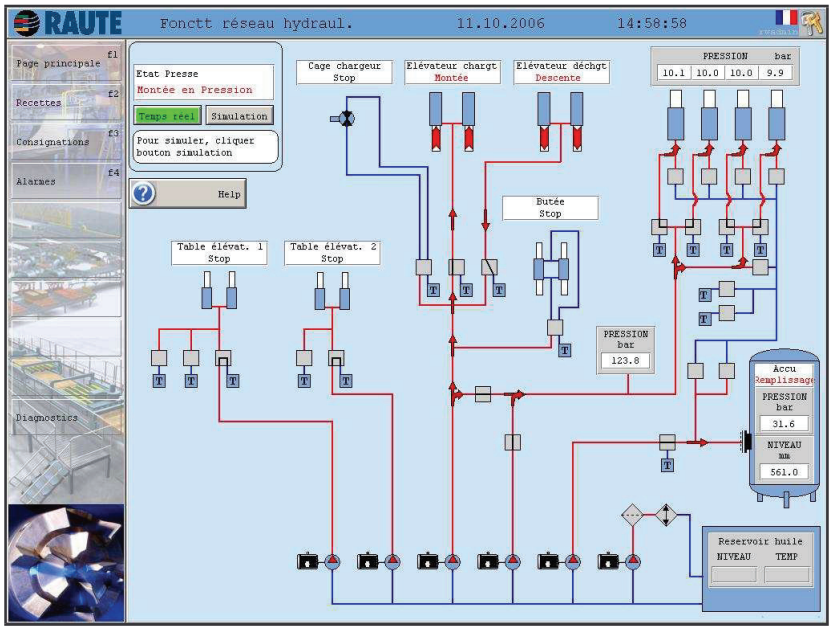

Figure 2. Window presenting the operation of the hydraulic system.

The simplified hydraulic diagram shows which actuations and components are active and which are not. From the diagram it can also be seen which actuations are connected in parallel and can affect each other. There has also been need to present the inputs and outputs of the PLC in the user interface. These inputs and outputs are control signals of valves and states of sensors and switches.

4.1 Presenting Control Signals of Valves and States of Sensors and Switches

The control signals of valve solenoids from PLC can easily be presented in the user interface. In figure 3 a window presenting the control signals of valves is shown. In the window solenoids are grouped based on their functions in the hydraulic system. The lines that connect the solenoids and other components tell which solenoids and

actuations affect each other. This information is very useful in troubleshooting: fault is not always in the action that appears abnormal. Actions that act or are connected in parallel can affect each other and understanding the effects of these parallel connections is very important.

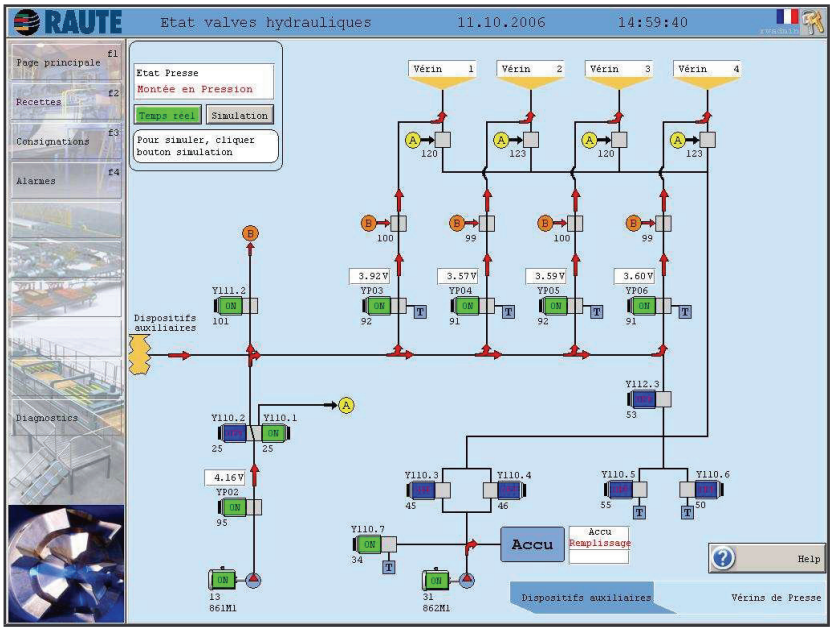

Figure 3. Window presenting the states of solenoids.

In the case of proportional valves it is reasonable to present the control signals of solenoids also as graphs (Figure 4). These graphs can be used in investigating for example sequences of different actuations, adjustments or faults in the connection between the solenoids and the PLC.

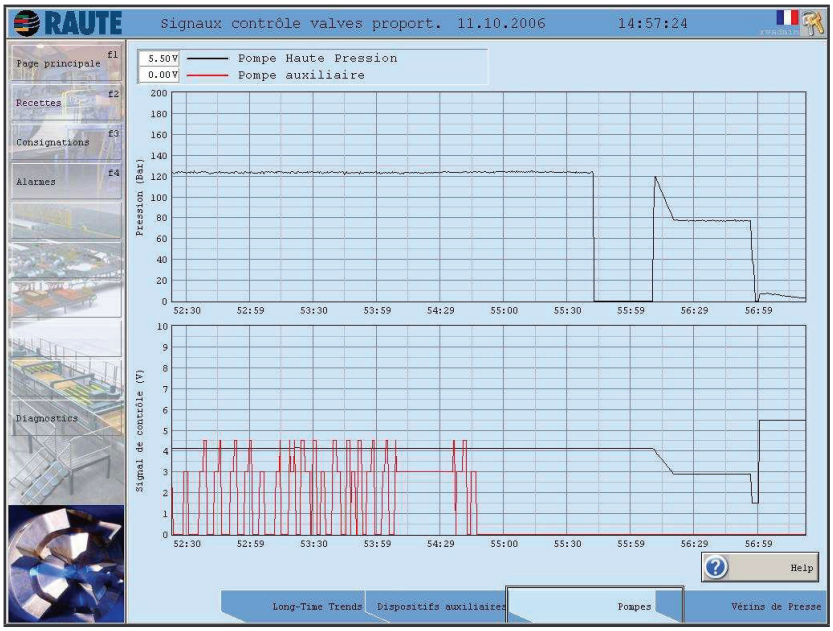

Figure 4. Pump pressure and control signals of proportional pressure control valves.

To obtain a comprehensive image of the actuation of the hydraulic system of press line it is necessary to know also the states of sensors and switches. A window presenting

these states was also developed. If states of sensors and switches are known operators can easily look for causes for line stops. For example dirt in front of a photocell can cause line to stop. The operator can see from the window if the photocell in question is in abnormal state.

Presenting states of sensors and switches in the user interface is useful in the condition monitoring as well. If change in the sensor or switch state is not visible in the window either the component or the connection between the component and the PLC is not functioning properly

5 DEVELOPING DIAGNOSTICS OF HYDRAULIC SYSTEM

Meaning of diagnostics is increasing all the time. Machines need to be more reliable and this makes information about true condition of machines valuable. Modern technology provides many possibilities, but also challenges, for diagnostics. In this chapter new diagnostics methods that were implemented in the hydraulic system of press line are presented.

Diagnostics can be used to measure condition of a component and in the unwanted case of breakdowns diagnostics can be used in troubleshooting. Maintenance services business plays an increasing role in Raute Oyj and built-in diagnostics can be used to provide better quality maintenance services to the customers.

The electrical control of the press line provides many possibilities for diagnostics without changes or additions in the hardware. The computing power for showing and analyzing diagnostics data real-time is also readily available in the press line. Diagnostics can be advantageous in adjusting the press line and as well in troubleshooting. Diagnostics data can be shown real-time or logged for later analysis.

In Raute Oyj the development of diagnostics was started with utilizing already existing information that the electrical control provides. In the development the emphasis was put on logging inputs and outputs of PLC, measuring actuation times and velocities and long term trending of control signals of proportional valves. New sensors and diagnostic components will be added when suitable components are found. At first it seems that new sensors will be used in oil condition monitoring.

5.1 Logging of PLC Data

Logging the inputs and outputs of PLC is extremely useful in finding causes of abnormal actuations that happen only occasionally. Logged data can also be used in investigating wether sequences of different actuations are correct or not. Raute Oyj supplies press lines worldwide and, in the ideal case, by investigating logged data specialists can analyze problems before traveling on site.

In the press line data logging is be performed on the PC that runs the user interface. PLC inputs and outputs are transferred to PC and stored on the hard drive. Most interesting data on the PLC are the measured pressure values from pressure transducers

and the control signals of proportional valves. To obtain a comprehensive image of the press actuation many on/off values are also logged. These include sensor, switch and solenoid states.

Logged data is worthless if there is no way to interpret and analyze it. For the data logging a simple and easy to use tool for presenting and analyzing logged data was developed. The analyzing tool was created with Microsoft Excel. Excel is used because it is widely in use in different parts of the world and people have the knowledge of its basics. Excel is also efficient enough for handling large quantities of data. The purpose of the analyzing tool is to get easily an overall picture of the functions of press during a time span. Also viewing trends of different values is convenient.

With the analyzing tool logged data can automatically be viewed as graphs and diagrams describing the press line. Graphs are the best way to show trends over periods of time and in analyzing tool for instance pressures and proportional valve control signals are presented as graphs (Figure 5). The analyzing tool contains built in tools for zooming and scaling selected graphs. Convenient and swift editing of graphs is essential when finding abnormalities in the trends over different periods of time.

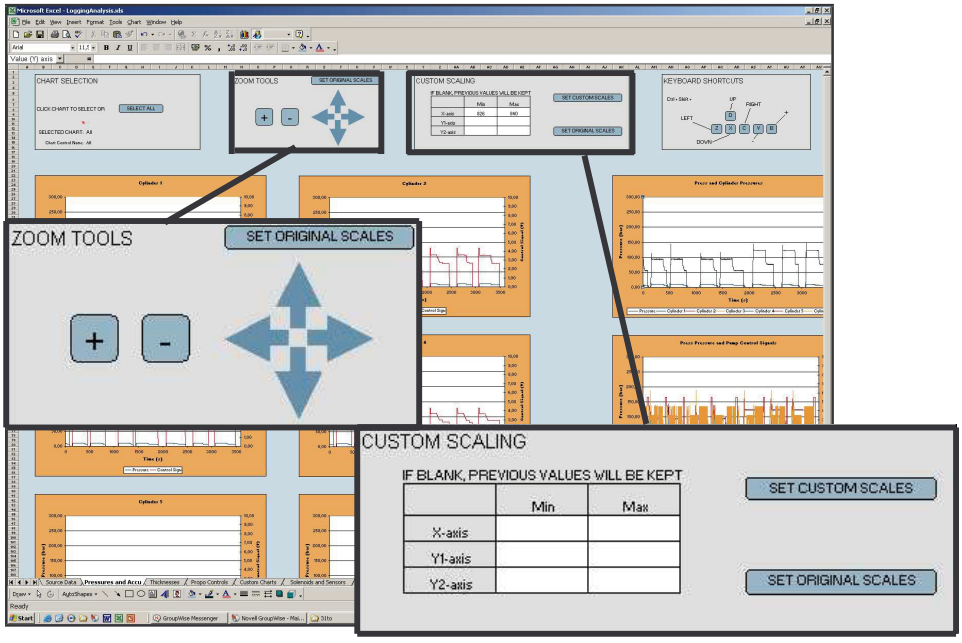

Figure 5. Graph window of analyzing tool.

The solenoid, sensor and switch values are presented in a general level diagram and an overall figure of the press (Figure 6). These values are on/off values and due to this graphs are not suitable for presenting these values.

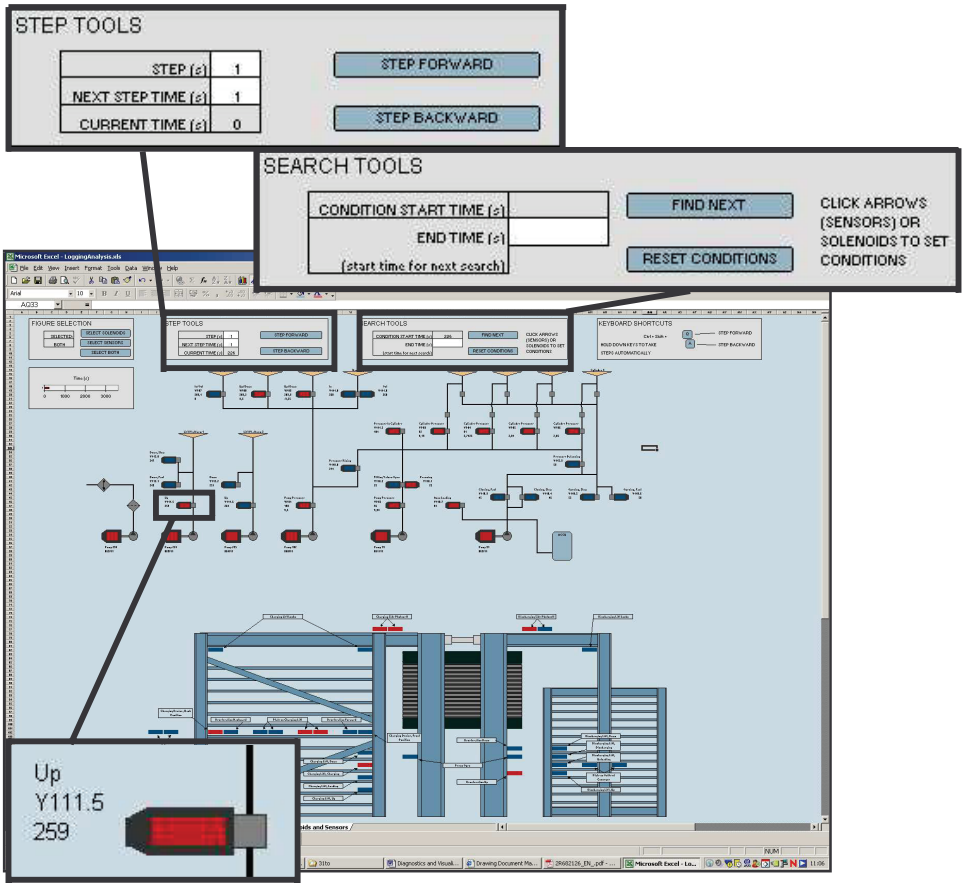

Figure 6. Window of analyzing tool presenting the states of solenoids, sensors and switches.

The states of solenoids are presented in a diagram that describes the hydraulic system of press at a general level. The diagram is similar to the diagram in the user interface. The solenoids are placed in a logical order and grouped by functions. Color of a solenoid indicates the solenoid state.

The states of sensors and switches are presented in a simplified figure that describes the press. In the figure the sensors and switches are positioned in their physical locations. Also in this figure color indicates the state of component.

The states of solenoids, sensors and switches on a specific time are shown simultaneously. This makes it very easy to get a comprehensive outlook on what was happening in the press at a chosen moment. This is very useful when finding causes for abnormal actions. The analyzing tool contains tools for presenting states on chosen time and tools for instance for taking specified steps back and forth on time line and a search tool that can be used in finding a time when specified conditions were met.

5.2 Measuring Actuation Times and Velocities

Measuring actuation times and velocities gives information on adjustments of different functions. The actuation times indicate also condition of components, e.g. pumps. If a

movement time of a function increases, that is a clear signal that either the adjustments have changed or a component might be breaking down.

In press line the PLC uses information from different limit switches in controlling the actuations of the press line. This limit switch information can also be used to calculate the actuation times and velocities of the press line actuations. The actuation times and velocities are calculated during the normal operation of the user interface and calculated values are shown in the user interface.

In the press line start-up optimal times for different actuations are set in the user interface. The operators can compare the calculated values with the optimal values and if these values differ greatly, adjustments can be done or investigation for possible future breakdowns can be started. Operators don't necessarily notice slowly happening changes in actuation times, but automatic calculation of actuation times makes tracking of changes easier.

5.3 Long Term Trending of Control Signals

Long term trending of for example valve control signals can be very useful in valve condition monitoring. Rinkinen [4] describes an example where monitoring valve control currents in long term can be used to predict failures.

In the press long term trending of control signals of proportional pressure control valves of pressing cylinders is very interesting (Figure 7). Even though the pressures vary between pressings of different kind of veneers there is always a constant pressure phase in the beginning of each pressing when the pressure is kept close to the maximum pressure. During this constant pressure phase the control logic gets the cylinder pressures from the pressure transducers and based on these pressure values the logic adjusts the control signals of the proportional pressure control valves. If the cylinder pressure is below the wanted pressure, the PLC increases the control signal of the valve in question.

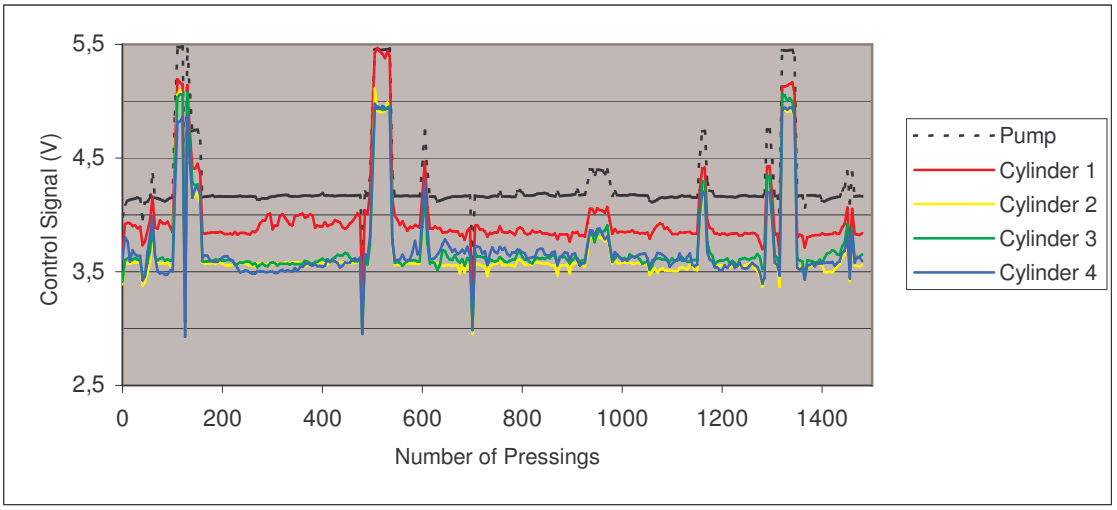

Figure 7. Long term trends of control signals of proportional pressure control valves.

Especially interesting with long term trending of these control signals is that they can be compared with each other. The set pressures during the constant pressure phase are the same in each cylinder. If trends show that the control signal of one valve starts differing from the values of the other valves, it indicates that something has changed. Differing values don't show what exactly causes the values to differ, but at least these trends act as a signal for further investigation and hopefully this investigation can be done before a breakdown that causes the press line to stop.

The control signal values in figure 7 have been logged during a period of 1500 pressings, i.e. approximately one month. Trends show that the control signal of proportional pressure control valve of cylinder one is slightly higher than the control signals of valves of other cylinders. This indicates that the characteristics of the proportional pressure control valve of cylinder one differ from the characteristics of other valves. The control signal of the proportional pressure control valve of pump is the highest because the pump pressure is kept higher than the cylinder pressures. Based on the logged trends in figure 7 it can be said that the valves are acting normally but at least the valve of cylinder one should be given special attention.

5.4 Oil Condition Monitoring

Dirt in oil and oil quality have significant effects on performance of hydraulic systems and component durability. Particles in oil can cause jamming of valves and increase wear. The oil quality deteriorates over time and this leads to insufficient lubrication and protection against, for example, corrosion. Nowadays there are many components in the markets that can be used to monitor the oil condition continuously during the normal operation of system.

For oil condition monitoring HYDACLab sensor from HYDAC was tested at Raute Oyj to find out its suitability for Raute's products. Properties of HYDACLab seemed very interesting. The sensor measures temperature, relative moisture content and relative change in viscosity and dielectric constant. Values that HYDACLab measures should rather reliably indicate if the condition of fluid has changed greatly and actions need to be taken.

There are tools, such as portable display units for viewing the measured values, but at least with new press line deliveries values can be shown conveniently in the user interface. The user interface window that was created for testing the HYDACLab sensor is presented in figure 8. For continuous oil condition monitoring it is essential that measured values can be accessed easily. In the user interface the values can be stored and trends can be showed over long periods of time. What comes to modernizations of already existing press lines portable display units might be in question.

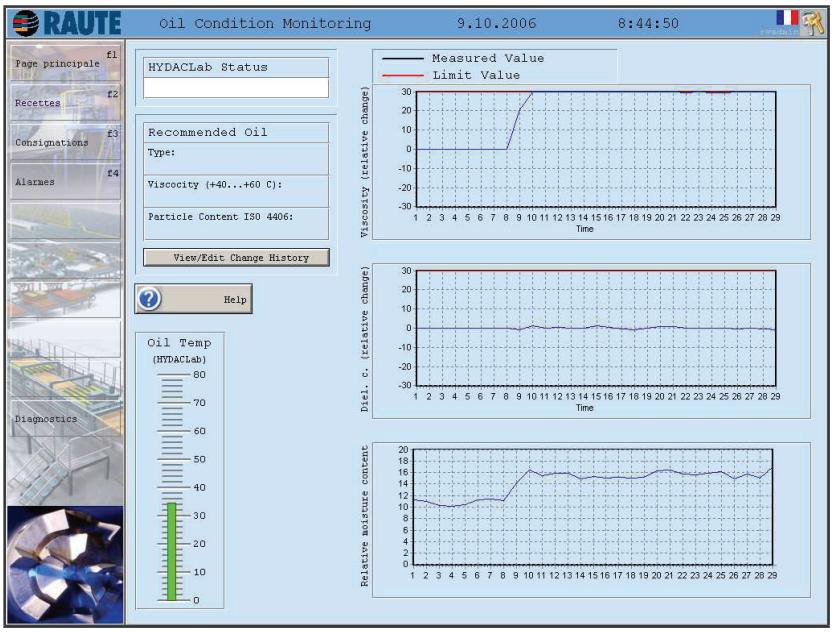

Figure 8. Window for oil condition monitoring.

Measuring the condition of oil continuously makes it possible to react instantly if the condition changes dramatically. Adding oil condition monitoring sensor to the hydraulic system of press line can bring extra value to the customers of Raute Oyj. The characteristics of HYDACLab were satisfying during the testing but selecting the best possible sensor or sensor combinations requires more testing.

6 CONCLUSIONS

Service reports of Raute Oyj show clearly that there is need to ease troubleshooting and adjusting of hydraulic system of plywood press lines. To improve the situation the knowhow of operators and service personnel has to be increased. In increasing the knowhow training and documentation can be used but the user interface of the press line provides possibilities for also other interesting means. The actuation of the press line can be visualized in the user interface. Visualization means graphs and graphical representations that help the operators and service personnel to understand what makes the different actuations happen.

Diagnostics ease troubleshooting and adjusting directly. In developing diagnostics for the hydraulic system of the press line different methods have been utilized. The idea has been to exploit already existing data that the electrical control provides. This information is for example control signals of valves and signals from sensors and switches. The user interface provides computing power and convenient tools for presenting the diagnostics information. At first, a way to log and analyze PLC data was developed. Emphasis has been put also on measuring actuation times and velocities of different actuations and long term trending of control signals of proportional valves. New sensors will probably be utilized in oil condition monitoring. In further development of the diagnostics it is important to follow what new diagnostics components and possibilities manufactures of hydraulic components will develop.

Decreasing troubleshooting time and keeping the press lines better adjusted will bring extra value to customers of Raute Oyj. Development and evaluation of visualization tools and diagnostics methods will continue in future.

REFERENCES

[1] Suzuki, T. 1994. TPM in Process Industries. Portland: Productivity Press. 391 p.

[2] Bradbury, F. 1972. Hydraulic Systems and Maintenance. London: Iliffe. 377 p.

[3] Rinkinen, J., Rusanen, H. & Koivula, T. 2005b. Hydraulijärjestelmien vikaantumisen päätekijöitä. Kunnossapito (4). pp. 28-32.

[4] Rinkinen, J., Koivula, T. 2005a. Experiences and Proposals for Condition Monitoring Methods of Hydraulic Valves. Second International Seminar on Maintenance, Condition Monitoring and Diagnostics, Oulu. Sept. pp. 28.-29., 2005. Oulu, University of Oulu and POHTO - The Institute for Management and Technological Training. pp. 117-131.

Setting Control Limits for Water Contamination In Hydraulic and Lubrication Systems.

Mike Day, MSc. Pall Europe Ltd.,
Havant Street, Portsmouth, PO1 3PD, UK
Tel: +44 (0) 2392 302353
Fax: +44 (0) 2392 302507
e-mail: mike_day@europe.pall .com

Mika Vesala,
Oy Colly Company AB
Laboratory Services
Iso-Heikkiläntie 8
20200 Turku
Finland
Tel: +358 (0)2 469 0025
Fax: +358 (0)2 469 0026
E-mail mika.vesala@colly.fi

Abstract

This paper explains the harmful effects that water has on both the oil based lubricant and hydraulic fluid and its consequential effect on the life and reliability of oil wetted systems. It introduces a new method of measuring the water state of the oil directly in-line, so that the measurement is continuously available and corrective actions can be implemented quickly if there is an "out of limit" situation. This way damage to both the components and the lubricant is minimised. The paper also shows how water specifications can be derived to either provide basic protection to systems or to enhance bearing life.

Keyword: Water contamination, Oil systems, Measurement, Control limits.

1 Introduction

It has long been recognised that the presence of dirt in hydraulic or lubricating oil can be responsible for about 50 to 60% of failures to oil wetted systems [1, 2]. In the '80s & 90s, these studies prompted a review of the design, build and operational procedures with the intention of reducing the incidence of dirt related failures. As a result, particulate contamination levels have fallen substantially [3] and system performance and reliability have improved as a result. The emphasis has moved from controlling contamination to maintaining cleanliness. More and more companies are taking a holistic approach and are applying "Total Cleanliness Control" over their fluid systems and processes as they see that this route can realise both immediate and long term improvements in efficiency and profitability [4].

The work by Rabinowicz [1] showed that corrosion, caused mainly by the presence of water in the lubricant or hydraulic fluid, accounted for 20% of failures to the equipment he studied. As systems have become progressively cleaner and more reliable as a result, water has now become proportionately more important as a source of unreliability [5]. Thus, the control of water in the oil must be addressed if the life and reliability now demanded by users is to be achieved.

Measurement is the basis of control and instruments are now available that measure the water state directly in-line so that the result is continuously available and corrective actions can be implemented if there is an "out of control" situation. As this can be done with the minimum of delay, the damage to both the components and lubricant is minimised. The water data has to be compared to a specification and this is where substantial improvements have to be made. This paper explains the effects of water on both components and the lubricant, briefly details the methods of measuring the levels of water in oils and presents the latest in-line device. It then explains how to set control limits based upon individual requirements rather than 'third party' recommendations.

2 Water in Oil

Water can be present in the oil in three states:-

a) Dissolved

Small quantities of water will always be bound up in oil at the molecular level and the oil usually has a 'clear' appearance, provided that it is not too oxidised. The point at which the oil cannot hold any more water is called the ***saturation point***, and it is temperature dependent. The amount of water that can dissolve in the oil will depend upon the type of base stock used, its additive package, the oils condition, and the temperature. For instance, new, highly refined parafinic circulation oils with few additives will hold little water before becoming saturated, say 100 parts per million (PPM) at 20º C. At the other extreme, oils that are used in certain ship-board hydraulic systems or in rolling mill applications can have saturation levels of 4,000 ppm at 20º C. This is because they have to keep relatively large amounts of water in suspension before allowing free water to form. Also, some synthetic oils, because of their chemistry, have a 'natural' tendency to hold water and so have high saturation levels (say 4,000 to 8,000

PPM at 20º C) depending on the type. Figure 1 shows a typical effect of temperature on the saturation characteristics of an oil. If the oil has a fixed amount of water, say 100 PPM at 60° C, all of the water will be dissolved in the oil's structure and is said to be dissolved in it. If the temperature reduces and the amount of water remains constant, free water will form at about 50° C.

Figure 1 Effect of Temperature on Oil's Saturation Characteristics

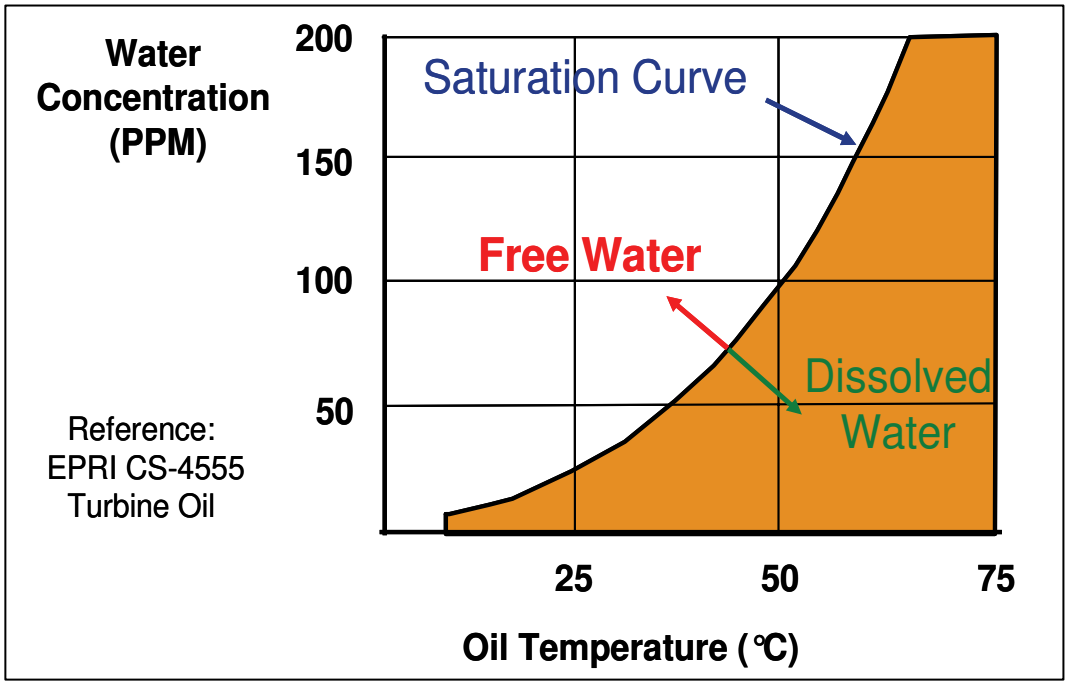

b) Free Water

Free water occurs when the oil can no longer hold any more water and it comes out of solution to form microscopic droplets. The oil becomes hazy at this stage. Any further increase in water content or decrease in temperature will cause more water to come out of solution and these droplets can coalesce together to form larger droplets. If the relative density (S.G.) of the oil is <1.0 and the oil is stationary, the water will fall under gravity, perhaps into 'dead' areas such as reservoirs, gear casings etc. In the case of some synthetic oils where the S.G. of the oil is >1.0, these will gradually rise to the free surface provided that there is little disturbance.

c) Emulsified

When free water is present and the oil is subjected to shearing action, as occurs in pumps, gears and control valves etc., the water is broken down into small relatively stable droplets and these can be held in suspension. Oils used in applications where water abounds are formulated to promote emulsification rather than separation. In this state, the water will affect the properties of the oil and hence the wear rates will increase but the water will not have a significant affect on the system corrosion rates.

3 Effects of Water in Oils

The presence of water in the oil can have wide ranging effects and these are summarised below:

- Reduced lube film thickness
- Loss of lubricity
- Increased compressibility
- Fluid Oxidation
- Additive depletion
- Accelerated surface fatigue
- Corrosion of component surfaces
- Icing at low temperatures
- Bacterial growth

Loss of fluid properties hence increased wear to components

Some of these are major and some are minor, but it is the authors' opinion that the greatest effect of water on the oil is to reduce the properties of the oil particularly its ability to lubricate and protect the component. This damages the component surfaces through increased wear, and the effects are triple edged:

- The presence of water accelerates the oil's decomposition rate through oxidisation, especially when particles are present. The presence of reactive particles like iron and copper in combination with water greatly increases the degradation rate [5].
- Water in the oil reduces the lubrication film and exposes the moving surfaces to increased wear through abrasion, adhesion and fatigue.
- The presence of free water increases the compressibility of the oil in the contact zone of bearing surfaces which further increases the rate of fatigue wear and leads to a regenerative wear situation.

A factor that is often overlooked is that acidic products in the oil are usually polar and have a high affinity for water. They readily dissociate from the oil to the water phase making the water more acidic and thus greatly accelerate system corrosion rates.

Another serious effect is on the fatigue life of rolling element bearings. This was studied by Cantley in 1977 [6] who investigated the effect of dissolved water on the fatigue life of bearings. Most of his work was done with an SAE 20 mineral oil containing rust and oxidation inhibitors (oil #3) at 65.5ºC (150° F), a stress level of 2.03 GPa, and a speed of 2,700 RPM. Water concentrations of 25, 100 & 400 PPM were used and the life of 32 bearings was evaluated at each condition. From this data, the $L_{15.9}$ Weibull life was calculated. Cantley then looked at the influence of water content on the life of bearings relative to that at 100 PPM, and this is presented in Figure 2.

Cantley performed a least squares analysis to obtain the much used relative bearing life factor L,

$L = (100/X)^{0.6}$ where L= Relative life to 100 PPM, X= water concentration in PPM.

A less well known part of Cantley's work was the investigation into the saturation characteristics of various oils. Unfortunately, the saturation tests were performed at 38° C not at the bearing test temperature of 65.5° C so there is no direct relationship

between bearing life and to the % Relative Humidity or the % of Saturation (% RH or % Sat). To investigate this, the saturation level at 65.5°C is required.

Figure 2 Effect of Water Content on Bearing Life –R E Cantley

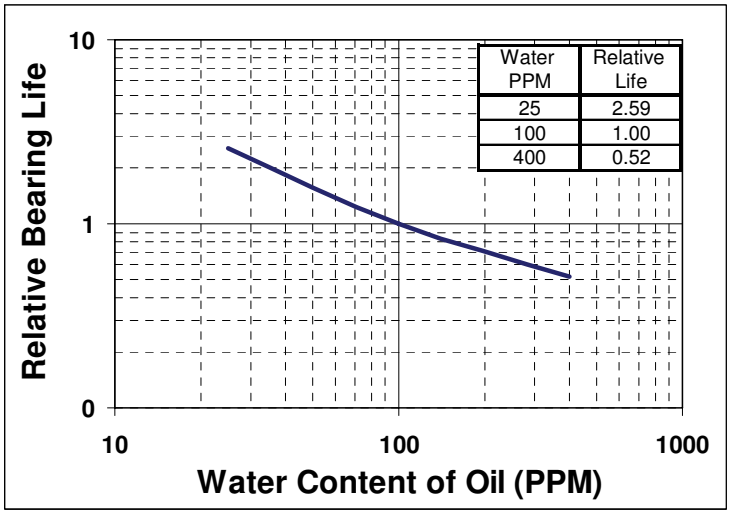

The attempt to determine this value was not successful, which is not surprisingly after such a long time. The next option was to match the characteristics of the test oil with oil and use this saturation level. The closest match using data to hand was also a highly refined circulating oil with rust, oxidation inhibitors and has a saturation value at 65.5 °C of 440 PPM. The equation derived by Cantley can be used to study the relationship between the water state (% RH or % Sat) and the relative bearing life. To do this, values of L have been calculated over a range of PPM values and the %RH values calculated on the basis of the assumed saturation value at 65.5°C of 440 PPM. The relative life values have also been recalculated based upon the unit life at 100% saturation. The results are seen in Figure 3 and show some surprising results.

Figure 3 Effect of Water State on Bearing Life

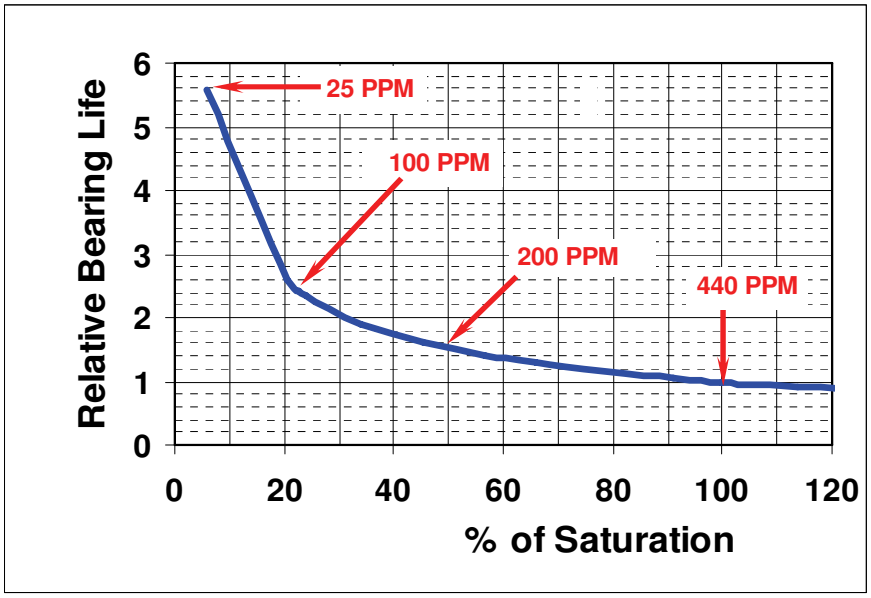

The data indicates that if free water is present then only a relatively small increase in bearing life can be expected even though a significant reduction in water content is made. It is only when the water state becomes dissolved and dry are substantial improvements in life achieved. Furthermore, the data indicates that it is not until the RH is below about 20 % RH that significant improvement in bearing life can be achieved. For instance, if the bearings function with dry oil (say 20% RH) then the life of the bearing can be increased by about 2.7 times compared to operation at and around the 100% level.

This trend is somewhat surprising as it was the authors' understanding that the reduction in bearing life caused by water in oil was due to a combination of reduced lubricity and hydrogen embrittlement in the fatigue cracks. It is therefore logical that greater increases in life should result when proportionate reductions in the levels of free water are made compared to similar reductions in dissolved level. As this discussion is beyond the scope of this paper, no further discussions are made. It does indicate the need for further research.

4 Measurement of Water Content

There is a wide variety of methods for determining the water content of oil and it is beyond the scope of this paper to discuss these as the choice of which method to use depends upon the purpose for monitoring as much as the speed and accuracy required. Also, most techniques are laboratory based so there is obviously a delay between taking the sample and receiving the results. Two methods are discussed, the Karl Fischer Titration [7] method as this has become the most widely used "off-line" method and the recently introduced capacitive water sensor that measures the water content directly in the system flow line.

a) Karl Fischer Titration Method

The ease of use, generally short analysis time (about 2 minutes for the direct injection method), ability to analyse a wide range of water content (typically 2 to 25,000 PPM or 2.5%) and good accuracy of repeatability (< 2% depending on water concentration) has made this the most widely used method. The instrument can be used both in the laboratory and on- site.

Despite its considerable advantages, current experience indicates that the reading is affected by certain additives contained within the oil, principally those that are zinc based, but also those additives that bind the water molecules to the oil's structure. These usually increase the water content readings. This is overcome by either changing the reagent or by boiling off the water in an evaporator and injecting the vapour into the cell using dried nitrogen. This increases the analysis time and also the variability in measurement, especially with dry oils.

A view of a typical instrument is seen in Figure 4. It works on the Coulometric (electrochemical) Titration principle, where the water in the oil is converted proportionally into iodine and the amount of iodine is measured by the instrument. The oil sample is injected into the cell after its volume or weight has been measured. The instrument gives the PPM by weight or volume.

Figure 4 View of Coulometric Titration Equipment

b) Capacitive Water Sensor

This instrument is a development of the successful air moisture sensor. It consists of a capacitive cell formed by sandwiching a dielectric polymer between gold electrodes. The lower electrode is deposited upon a carrier substrate which is impervious to moisture whilst the upper capacitor plate allows the transmission of water molecules, but not other materials e.g. additives. Water molecules migrate into or out of this layer depending on the humidity of the polymer relative to the oil. This alters its dielectric constant and thus the capacitance of the capacitor. This change in capacitance is then converted into a signal proportionate to relative humidity of the oil. The instrument can display "% Sat" directly and PPM if calibrated on the oil being used.

The instrument is designed for in-line analysis where the probe is inserted directly in a major flow line.

Figure 5 Capacitive Water Sensor

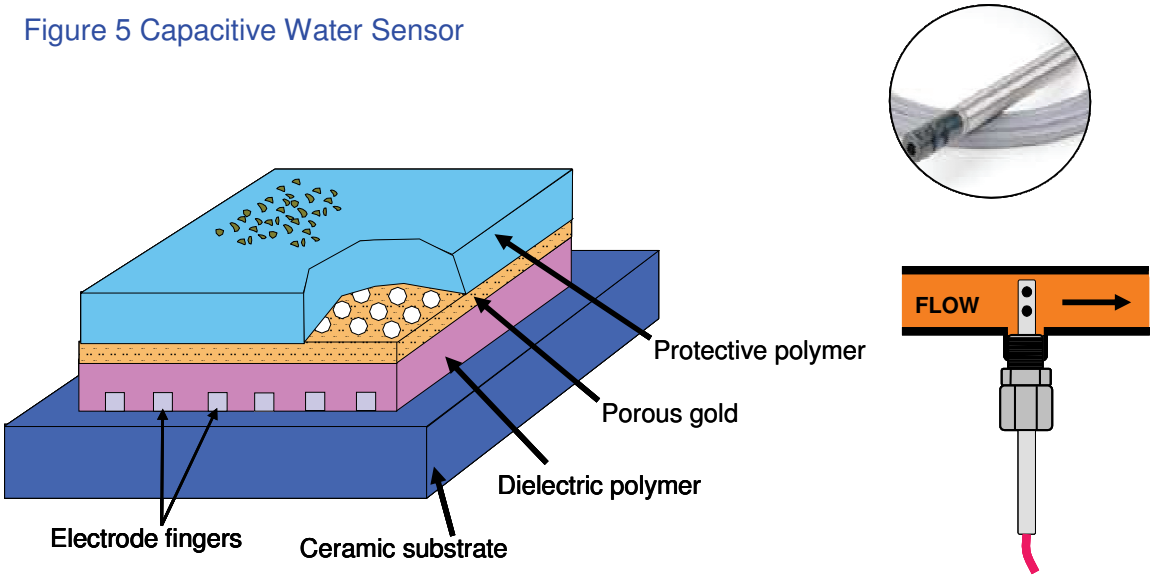

This instrument provides data that is immediately available both visually on a local display and in a control room or remote terminal via Ethernet, Bus or wireless data transmission protocols. Thus corrective actions can be taken long before an "out of

limit" situation occurs and becomes a problem. Maintenance moves from a reactive regime to a proactive one and this ensures that the plant operates at its optimum efficiency. Perhaps of greater importance for the operator is that wear rates will be minimised, corrosion should be eliminated and reliability enhanced.

5 How to Select Maximum Water Levels

It is the authors' opinion that this aspect is perhaps reminiscent of the 'dark ages', as there does not appear to be a documented method to enable operators to select the level that is appropriate for their system and requirements. All too often, certainly in bearing systems, we hear "200 PPM" being stated as the optimum level without any technical basis for it. From section 3 we see that 200 PPM may be adequate for some systems but not give the life and reliability that others require. So, how should water levels be selected?

As we see it there are two ways of selecting these levels depending upon the level of control required. In this paper these are termed the "Protection Level" and the "Life Extension Level".

a) Protection Level

Here the philosophy is to avoid the formulation of free water as this will eliminate both system corrosion and many of the factors identified in Section 2. For this, the user needs to know two factors: firstly, the lowest temperature that the system will be exposed to, which is nearly always experienced when the system is stationary, and account is taken of the chilling effects of cold draughts. Secondly, the saturation / temperature characteristic of the oil is required and a typical one is seen in Figure 6a.

Figure 6 Saturation Characteristics of a Paper Machine Oil

a) Protection b) Life Extension

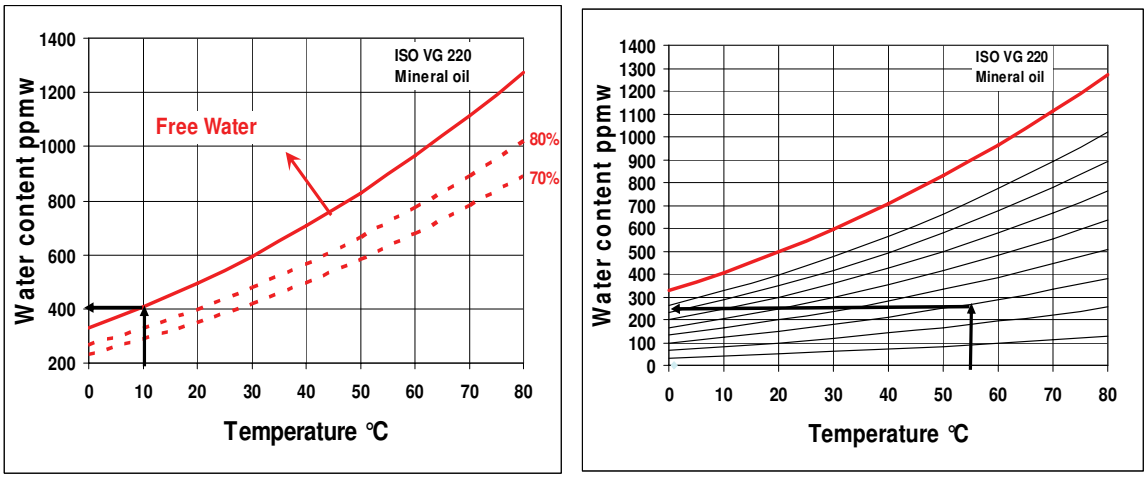

Using Figure 6a, the user selects the minimum temperature and interpolates the absolute water content (PPM) to give saturation point at this temperature. For instance, if the minimum temperature of the system (and oil) is 10° C then the saturation point is 400 PPM. The user then decides on a factor of safety; say 80% or even 70% of this value

and this gives the control limit. For the 70 & 80 % levels the control limits become 280 & 320 PPM respectively.

If a water sensor is used, then an output of PPM is the most convenient for comparing the output to the specification, but also displaying the % RH has the advantage that the approach of the saturation point (free water being formed) can be seen and more readily understood. It is worth pointing out at this stage that the saturation point of oils can both increase and decrease with time (adding different oils, aging of the oil etc) so reliance solely on PPM values can be problematic.

b) Life Extension Level

This is an extension of the above process and is designed for bearing systems where a greater level of reliability and longer life is required. Here the data derived from the work by Cantley and Figure 3 is used to obtain the %RH value to give a certain life extension. For instance, if a life extension of 2 times is required the %RH value from Figure 3 is 30%. The user then uses an extended saturation curve like the one in Figure 6b to obtain the PPM value to give this %RH value at the operating temperature. If the operating temperature is 55° C, for this example the control limit at 30% RH is 260 PPM.

Although this paper has concentrated on the life of rolling element bearings, the life of journal bearings can be significantly reduced by running with a wet lubricant. Research has shown that the wear rate of a journal bearing running on oil with 1% water can be nearly 10 times that with dry lubricant [8}. However, journal bearings differ from rolling element bearings in that sulphurous products from oil and perhaps the process tend to dissociate to the water phase and have a greater effect on white and Babbitt metal bearings compared to the rolling element type

6 Conclusions

The demands on operators of fluid systems to improve efficiency by reducing failures and extending life have focused attention on reducing contamination levels. As particulate contamination is now under control (or should be!!) attention is being directed to water contamination. Water can have equally serious consequences on the life and reliability as it affects the properties of the lubricant, which in turn affects the wear rates of the system. Hence, like dirt levels, the control limits for water must be made of a system to system basis.

To successfully control water levels two factors are required, a specification or the maximum permissible water content for the oil being used and a means of rapidly monitoring the moisture content so that prompt corrective actions can be implemented to limit the damage should an “over limit” situation occur.

There does not appear to be a rational method for selecting oil moisture levels based upon individual system and user requirements and the methods proposed in this paper were developed for that purpose.

The introduction of the capacitive water sensor is a significant advance in the maintenance and management of systems as data on the moisture content is now immediately available. Thus corrective actions can be taken long before an “out of

limits" situation occurs thereby minimising the damage to the system and the lubricant. Maintenance can then move from a reactive mode to a proactive one and this will ensure that the plant is operated at its optimum efficiency and best use is made of maintenance staff.

7 References

1 E. Rabinowicz Lecture presented to the American Society of Lubricating Engineers, Bearing Workshop, USA, 1981.

2 UK DTI "Contamination control in fluid power systems, Vol. 1 Field Studies", Dept. Trade and Industry, N.E.L., East Kilbride, Glasgow, UK, 1984.

3 M. J. Day, "Developments in cleanliness control in fluid systems", Presented at "Workshop on Total Contamination Control", Monash University, Australia, August 1999.

4 M. J. Day "Increasing profitability through a policy of total cleanliness control", Presented at I Mech. E seminar on "Cleanliness Control in Fluid Systems", I Mech. E, London, November 1997

5 M. Weinschelbaum, "A study of the invisible but measurable particulate contaminants in hydraulic systems," Proceedings of National Conference on Fluid Power, Volume XXIII, pp. 265-277, 1969

6 R. E. Cantley, "The effect of water in lubricating oil on bearing fatigue life", ASLE Transactions, American Society of Lubrication Engineers, Volume 20, No. 3, pp. 244-248, 1977, from a presentation at the 31st Annual ASLE Meeting, Philadelphia, PA.

7 ISO 12937 "Petroleum products-Determination of water-Coulometric Karl Fisher titration method.", International Standards Organisation, Geneva, Switzerland, 2000.

8 J. Fitch et al "Moisture, the second most destructive lubricant contaminant and is effect on bearing life", P/PM Technology, pp 50-53, 1994.

Condition Monitoring for Hydraulic and Lubricating Fluids

Dr. Horst Mannebach
HYDAC ELECTRONIC GMBH
Hauptstrasse 27
66128 Saarbrücken, Germany
Phone +49 681 7099 291, Fax +49 681 7099 189
E-mail: dr.horst.mannebach@hydac.com

ABSTRACT

Friction, wear, leakage and excessive temperatures all leave their impact on hydraulic and lubricating fluids. This impact can manifest itself in the form of particulate or fluid contamination or fluid degradation as a result of thermal oxidation. In this sense the fluid constitutes a fingerprint of the condition of the complete system. Consequently, the on-line monitoring of fluid parameters presents an efficient way to predict component failure, achieve longer fluid service life and to implement condition-based or predictive maintenance procedures. Today, robust and cost effective on-line sensors to measure various fluid properties are available. This paper summarizes sensor principles and technologies and provides suggestions for sensor installation in hydraulic and lubricating systems.

KEYWORDS: condition monitoring, sensors, hydraulic fluids, lubricating fluids

1 INTRODUCTION

Objectives such as higher system availability, planned maintenance intervals and condition-based servicing require cost-effective and rugged monitoring sensors to monitor and sense the state of machines on-line. The on-line monitoring of the state of hydraulic and lubricating fluids plays a decisive role in general on-line condition monitoring of the entire system and individual applications. Monitoring of these fluids is of critical importance as they serve the vital functions of the transmission of power, lubrication, dissipation of heat and corrosion protection.
Friction, wear, leakage and excessive temperatures all leave their impact on these fluids the form of, for example, particles and water. Apart from this, the fluids themselves are subject to the aging processes, which also can result in corrosion and equipment failures. In this manner, the oil condition is so-to-speak a fingerprint of the condition of the complete system. Consequently, the cost-efficient and reliable determination of

particle and water content, as well as other oil properties that are possible today constitute an efficient yet simple methods for condition monitoring of hydraulic and lubricating systems.
Employment of these methods provides reliable information on impending damage, for example, of slipping and rolling bearings or hydraulic components that can be detected in due course and allow for maintenance work to be carried out based on the detected system condition. The following paper summarizes sensor principles and technologies and provides suggestions for sensor installation in hydraulic and lubrication systems.

2 SENSOR PRINCIPLES

2.1 Measurement of cleanliness classes / particle count

Particle contamination has often been recognized as one of the main causes of failures of hydraulic and lubricating systems. The online measurement of cleanliness classes therefore plays an important role in the detection of wear and serves as preventive diagnosis of impending damage. A further significant advantage in this regard can be provided by the continuous recording of contaminant levels as compared against off-line analysis of oil samples. This is because the on-line monitoring not only provides a random snapshot but the full development of the oil condition over a longer period of time. For example, in gearbox applications, the monitoring and detection especially of small particles has been found particularly helpful in that it has led to the early detection of micropitting and gray spots, which, in turn, has allowed for early detection of the impending bearing damage even before it was indicated by vibration analysis.
Figure 1 shows the comparison between the on-line particle counts and the results of vibration analysis as tools for early detection of mechanical failures.

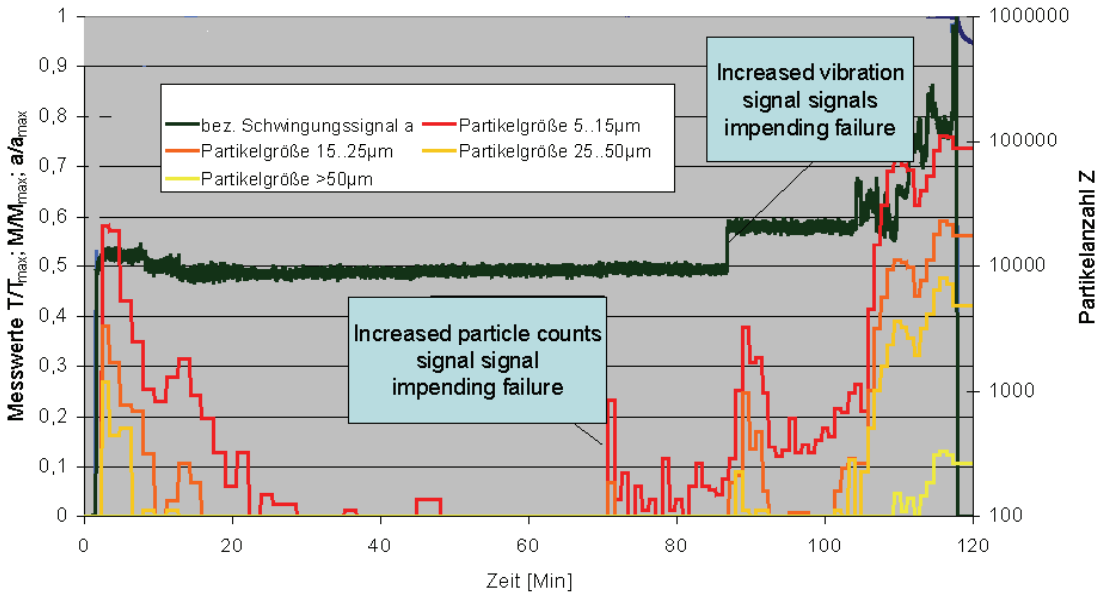

Our HYDAC particle counters are optical extinction particle counters. The number and size of particles is determined by the shadow that particles project on a light detector. Figure 2 shows the measuring principle of the particle counter:

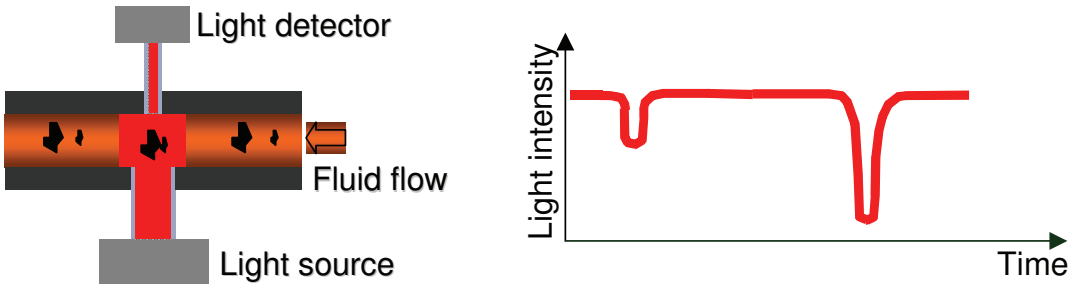

The advantages of these measuring instruments include their wide measuring range, measuring accuracy, self-monitoring capability, as well as traceability to recognized calibration standards, such as the ISO 11943 for on-line measurements. Moreover, their susceptibility to oil turbidity caused by contamination can be compensated by readjusting the intensity of the light source. In accordance with the ISO 4406 (1999) standard, the cleanliness levels are assessed on the basis of the determination of the number of particles in three different size ranges (>4 µm(c), >6 µm(c), >14 µm(c)). According to this standard, an increase or a reduction of the cleanliness class by one corresponds to doubling or halving the number of particles in the given size range.
In the field of optical particle counters, the technological development has led from the portable particle counters designed for use as a service tool, to sensors for stationary installations, e.g. on test benches, and finally to small, rugged and cost-effective sensors for installation in almost any lubricating or hydraulic system.
Thanks to the features such as compliance to the IP 69K standard, vibration resistance, load dump and high level of EMC compatibility, our CS 1000 sensor is an ideal device for mobile and stationary applications. The device is available with various analog or digital interfaces and with or without the digital display. It can operate in pressures of up to 100 bar. As an additional feature, it monitors oil temperature via the integrated oil temperature sensor. Figure 3 shows the online particle counter CS 1000

.

2.2 Water Sensors

In practice, water represents one of the greatest threats to hydraulic and lubricating oils. This is because water reduces the load carrying capacity of the lubricant film and acts as a catalyst in the aging and degradation processes. This is especially true in regard to the bio-degradable fluids which are extremely vulnerable to water. Water can appear in three forms in hydraulic and lubricating oils:

- Dissolved, invisible to the naked eye (single phase fluid)
- Emulsified, visible in the form of water droplets finely dispersed in the oil
- Free, clearly visible as a separated phase

A sensor technology that has lent itself particularly well for the purpose of monitoring water content in the industrial hydraulic and lubricating fluids is capacitance. This is because the capacitor sensing elements typically employed for these applications are inexpensive and robust which makes them suitable for operation in a wide variety of different fluid types and system conditions.

Capacitance based sensors respond to changes in relative humidity in the surrounding environment. This translates into percent saturation in hydraulic and lubricating oils or fluids. Oil or a fluid is said to be 100% saturated when it holds the maximum amount of water under existent temperature and pressure conditions. In addition to being dependent on the temperature and pressure conditions, the solubility of water in different fluids also depends on the chemical compatibility between water and the solvent fluid. Consequently, the saturation levels can vary considerably among fluids of different base stocks and different formulations of additive packages. As a result, the relative humidity readings cannot be directly correlated to water content in weight percent or parts per million by weight usually obtained through the wet-chemical techniques, such as Karl Fischer analysis. Thus, although the saturation or relative humidity values are independent of the fluid type, the sensors need to be additionally calibrated for different fluids, or classes of fluids, if the information about the water content by weight is desired or required. However, because in most cases the relationship between percent saturation and water content exhibits a linear behavior at fixed temperature, this calibration can be readily accomplished. A sensor that provides information about both percent saturation and water content by weight then becomes a really powerful diagnostic tool because on the one hand it provides direct information about the possible onset of free water formation and phase separation while on the other it alerts about the absolute changes in water content that occur as a result of ingression due to leakage or depletion due to treatment such as dehydration.

A new development in this field is the Aqua Sensor AS 1000. This sensor is intended for use by OEMs in new machines and systems. Reduced to the size of a pressure sensor, it allows for continuous determination of humidity with an optimum price/performance ratio. The sensor can be installed in hydraulic and lubrication lines up to 250 bar. Apart from humidity, the sensor also measures the temperature of the fluid. The capacitance measurement technique can also be applied for measurement of free water content above the saturation level. This technique relies on the large difference in electrical permitivity between water and oil and derives water content from measuring the capacitance of a fluid-filled tubular capacitor. In this manner, our AS 8000 sensor allows for continuous monitoring of free water content above 0.5 vol%.

Figure 4 shows an AS 1000 and an AS 8000 sensor.

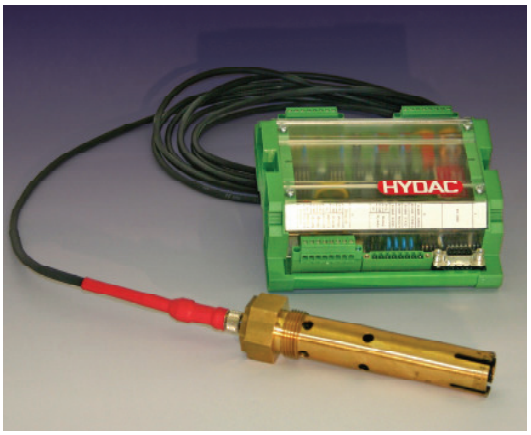

2.3 Oil condition sensor

An entirely new sensor category is exemplified by our HYDACLab oil condition monitoring sensor. Oil aging is a complex chemical process, in which the base fluid becomes oxidized in a series of chain reactions under the influence of elevated temperatures and air. In addition, metal particles and water often act as catalysts to accelerate the aging process. In the course of these oxidation reactions, carboxylic acids and higher molecular weight chemical species are formed. Due to their chemical nature, carboxylic acids contribute to corrosion of system components, whereas the higher molecular weight products impair the system functionality by clogging fluid passages and causing stiction of components. HYDACLab is a multi-component sensor for monitoring several critical fluid parameters through the measurement of relative changes in viscosity and permitivity as well as the relative humidity and temperature. Figure 5 shows the HYDACLab and it's multi-sensor measurement element.

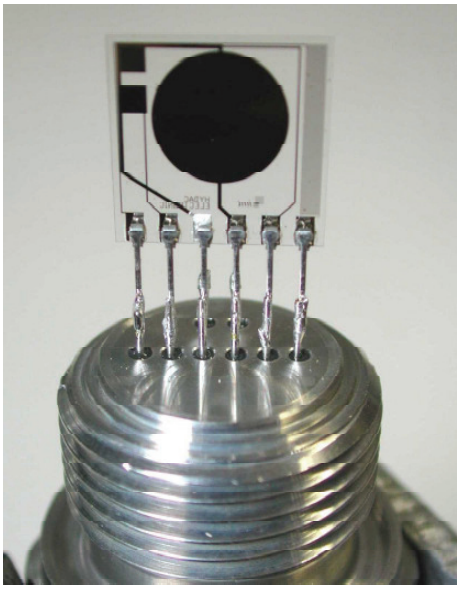

2.3.1 Viscosity measurement

HYDACLab measures viscosity with the quartz crystal microbalance or QCM. When a QCM is immersed in a fluid, its resonant frequency is reduced as a result of an effectively coupled interfacial layer that forms between the surface of the crystal and the fluid film. One of the issues of concern when employing QCMs in high pressure applications is the distribution of stress induced on the quartz oscillator by the system pressure. This is because if the stress induced on the QCM by the system pressure is applied only to one side of the QCM, it can result in dramatic changes in the QCM resonant frequency. The changes in the resonant frequency induced by an uneven stress distribution could easily exceed the ±10% range of viscosity limits typically of interest in industrial applications and thus lead to erroneous viscosity readings. In order to overcome this limitation, we adapted the QCM sensing element in our sensor such that it remains in constant contact with the fluid on both sides of the quartz which cancels out the stresses induced by the system pressure.
In addition to the stress distribution due to the system pressure, it is also necessary to consider the effects stemming from the relatively high viscosities of hydraulic and lubricating fluids. Because our aim was to make the sensor compatible with the broadest possible range of fluids and applications, we likewise found it necessary to take the widest range of viscosities into consideration. In this regard, when dealing with high viscosity fluids, such as gearbox lubricating oils (viscosities on the order of 460 cSt), it is important to remember that these viscosities will severely dampen the oscillation of the quartz in the QCM. This viscosity damping effect is particularly severe with QCMs that employ relatively small quartz crystals. Because of these considerations we found it necessary to employ a larger quartz element and sustain its oscillation with a comparatively sophisticated electronic circuitry.
The measurement of the viscosity is carried out through evaluation of the extent of dampening of the quartz resonant frequency by the surrounding fluid. However, in contrast to laboratory methods, this measurement does not return the value of absolute viscosity. Therefore we developed an algorithm which starts off with the evaluation of quartz frequency in the new fluid at various system operating temperatures. Subsequently, the algorithm exploits this initial relationship between the quartz frequency and fluid viscosity and issues a flag when the change in viscosity exceeds a preset limit. The diagram in Figure 6 shows laboratory data obtained for a polyolester oil.

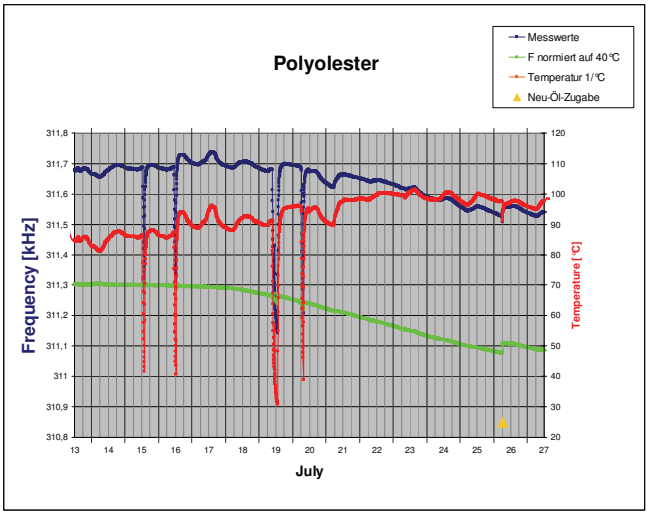

The onset of oil aging after an initial incubation period is clearly visible as a kink in the resonance frequency curve in the left diagram. The temperature normalized frequency begins to fall which corresponds to the increase in viscosity.
The diagram in Figure 7 shows data from a construction machine and displays the temperature compensated viscosity change and the temperature versus time. The quality of the temperature compensation is excellent and the shown increase in viscosity was validated with lab measurements as indicated in the diagram.

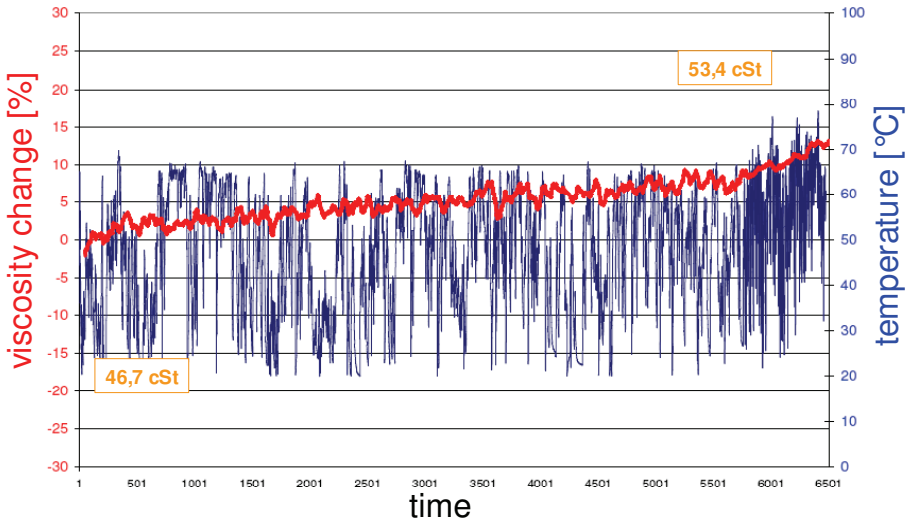

2.3.2 Permittivity measurement

The monitoring of the chemical changes in hydraulic and lubricating fluids presents a particular challenge because of the difficulty of adapting typical laboratory techniques for in/on-line industrial applications. The aging of the fluids and the degradation of the additive package components is typically associated with changes in the molecular structure of the chemical species in question. These changes in chemical composition are often accompanied by changes in the electrical properties (such as polarizability) and therefore the dielectric constant or electrical permitivity of the fluid is a parameter that indicates changing fluid conditions quite well. The measurements of the dielectric constant are normally carried out with inter-digital capacitors. However, these devices suffer from the limitation of a shallow penetration depth due to their relatively small structure where the individual elements are typically separated by distances on the order of 10 to 50 µm. Consequently, they are able to access only a thin surface layer of the fluid. In addition, they are very sensitive to surface contamination and varnish formation. In order to overcome these limitations we have turned to rectangular structures that are more than one millimeter apart and located on the same quartz substrate as the QCM device. This construction then allows for probing deep into the fluid and exhibits greater stability towards contaminants and varnishing. The diagram in Figure 8 shows the laboratory data for the permittivity obtained for the polyolester in the same experiment as Figure 6.

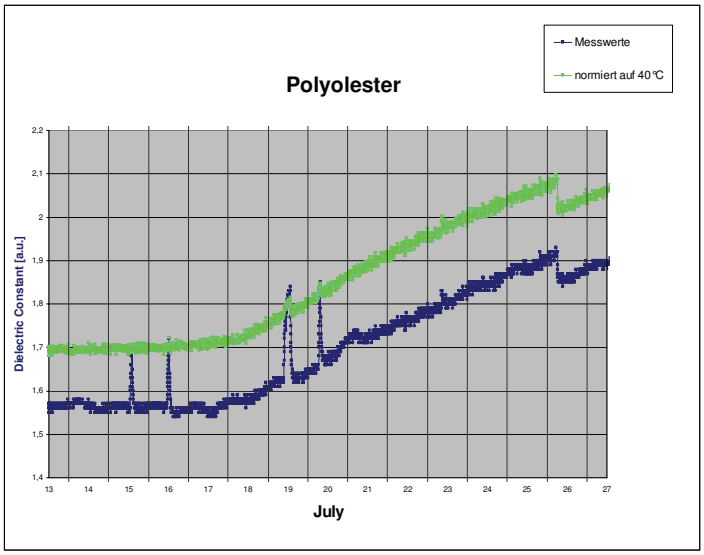

The diagram in Figure 9 shows the temperature compensated permittivity change and temperature versus time for the construction machine. The increase in permittivity can be attributed to a small TAN increase.

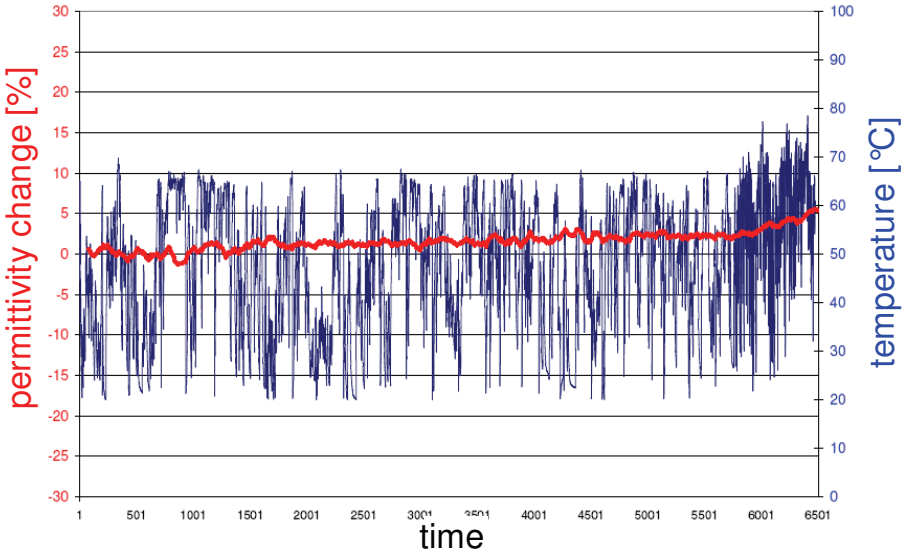

2.3.2 Humidity and temperature measurement

Humidity measurements are carried out with the same sensing element as in the AS 1000 sensor and the temperature is measured with a resistance element located near the QCM device.

2.4 Clogging indicator

The filter clogging or differential pressure indicators also undergo continuous further development. While simple, optical or electromechanical pressure switches were used in the past, today, the extent of filter clogging can be measured continuously with the help of electronic indicators. The latest HYDAC product in this area is the DirtController GW. This sensor measures the system or inlet pressure as well as the differential pressure across the filter by means of two electronic pressure sensors that are integrated in the housing. Figure 10 shows a DirtController GW and a sectional drawing..

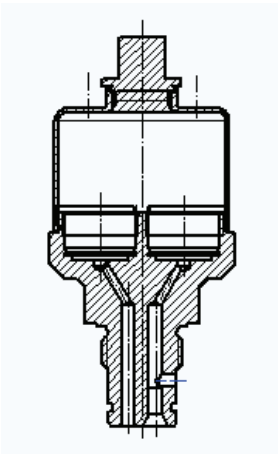

Two 4 – 20 mA outputs offer freedom to set various triggers and allow for monitoring, for example, of the by-pass cracking pressure or whether a filter element is installed in the housing. The DirtController GW is therefore a condition monitoring sensor for monitoring filters and systems and can provide valuable information about long-term contaminant level changes in the complete system.

3 APPLICATIONS

The field of application of the discussed condition monitoring tools encompasses a whole range of mobile and industrial hydraulic and lubrication systems. A prominent example is the condition monitoring in wind turbines. Figure 11 shows the schematics of AGMA 6006 Standard for Design and Specification of Gearboxes for Wind Turbines.

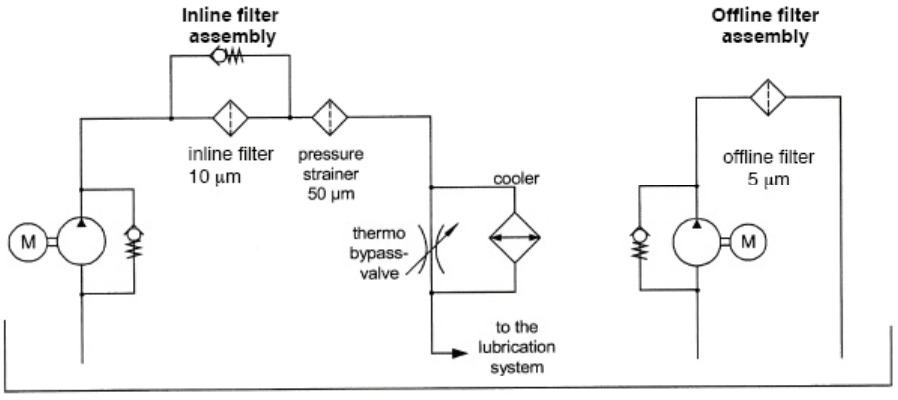

The above system design readily allows for incorporation of online condition monitoring sensors. In order to overcome certain operational difficulties, we have designed the HYDAC Contamination Sensor Module CSM 2000 to eliminate the common interference problem which air bubbles cause in optical particle counters. The unit in Figure 12 shows the system equipped with a CS 1000 and a HYDACLab.

3 CONCLUSION

Condition monitoring allows equipment manufactures and plant operators to increase availability, extend service life and offer condition-related instead of time-related servicing. Due to the amount of information available, hydraulic and lubricating fluids are in a way the fingerprint of the whole system. Hence they are ideal for online monitoring and diagnosis. As a result of ongoing sensor innovation presented in this paper, condition monitoring can be implemented in a timely and cost-effective manner.

STRUCTURAL HEALTH MONITORING OF A VEHICLE CRANE

Jyrki Kullaa, Timo Heine, Tero Olsamo
Helsinki Polytechnic Stadia
Department of Mechanical and Production Engineering
P.O. Box 4021, FIN-00099 City of Helsinki, Finland
Tel. +358 9 310 83 531, Fax +358 9 310 83 500
E-mail: jyrki.kullaa@stadia.fi

ABSTRACT

Structural damage can be detected from changes in the monitored damage-sensitive features. The influences of environmental or operational variations, however, can make vibration-based health monitoring difficult and unreliable due to false identifications of damage. A novel method is proposed to eliminate these influences. It is based on the factor analysis, the main advantage of which is that the measurement of underlying variables is not needed. Damage detection capability was first investigated with a finite element model of a vehicle crane having four latent variables and using the modal parameters of the structure and power spectra as the damage-sensitive features. All damage stages could be detected, whereas without factor analysis damage detection was not possible. Vibration-based monitoring experiments for a vehicle crane were also performed in the laboratory. The features were extracted from the response data of the crane vibrating around a slightly varying static equilibrium. All damage scenarios could be detected from the accelerations using the proposed method, whereas without the elimination of the operational effects damage detection was not possible. The pressure data were not as sensitive to indicate the structural changes.

KEYWORDS: Structural health monitoring, Operational effects, Factor analysis, Vibration measurements

1 INTRODUCTION

Structural health monitoring of machines and structures often utilizes information extracted from vibration measurements. Changes in the selected features extracted from the measurements compared with those of the healthy structure can be interpreted as an indication of damage. However, the normal variation in environmental or operational

conditions may also influence the same features and thus cause false indications of damage [1–12].

Structural health monitoring of rotating machinery is already a widely accepted practice, whereas that of fixed structures is still under a research stage. The research is active especially for civil structures like bridges and high-rise buildings, or aerospace structures. However, less attention has been focused on manipulators such as mobile hydraulic cranes (Figure 1). It is the purpose of this paper to study the possibility to apply vibration-based structural health monitoring to such structures.

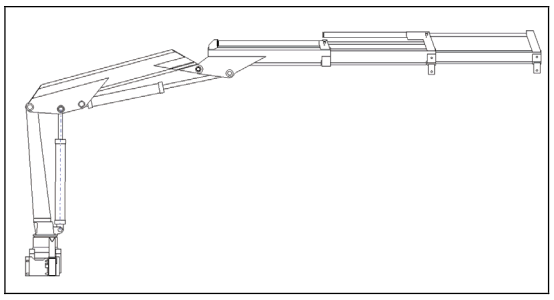

Figure 1: Vehicle crane HIAB-022-2L.

Compared to fixed structures, manipulators exhibit a highly non-linear behaviour. The configuration of the manipulator and consequently also the dynamic properties vary constantly during operation and results in difficulties in the feature extraction from the time history data. One possible solution is to monitor the crane under its slightly varying static equilibrium. The structural behaviour is linear, but the prevailing configuration influences the measured properties. In the vehicle crane the joint positions, load, friction, or the viscosity of the hydraulic oil can vary during normal operation. These effects also influence the dynamics of the structure making damage detection difficult. These influences must therefore be eliminated from the data, which can be performed using latent variable models. Latent variable models have several advantages: the operational variables need not be measured, or the underlying physical phenomena need not even be known, and several effects can be present simultaneously. No mathematical model of the structure is needed. Similarly to other damage detection problems, training data is first collected from the healthy structure. A statistically significant change in the features is an indication of damage.

Structural health monitoring is applied to a vehicle crane using both numerical and experimental data. With the numerical model, tedious collection of monitoring data can be effectively accelerated and different damage scenarios (stiffness degradation) can be easily simulated without actually damaging the structure. Also, different features can be investigated without identification procedures that usually increase complexity to the health monitoring system. In addition, arbitrary sensor arrangements can be included. Different operational variations can also be simulated. It is important to include noise in the simulation results in order to assess the damage detection capability, because in real systems noise is always present.

An experimental study gives invaluable additional information unavailable in the numerical model. For example, unmodelled effects can exist in experiments, such as joint friction or viscosity variation. Also excitation has to be considered and noise is always present in the measurements. In addition, identification must be performed to extract the features from the data, which results in a further source of uncertainty. Usually realistic damage scenarios (e.g. fatigue cracks) are difficult to generate artificially, or sometimes damaging the structure is not allowed. Due to these facts, added point masses are used in this study to represent damage, or the change in the dynamic properties of the structure.

2 FACTOR ANALYSIS

Factor analysis is a mathematical model that attempts to explain the correlation between a large set of variables in terms of a small number of underlying factors. A major assumption of factor analysis is that these factors are not observed directly. The variables depend upon the factors but are also subject to random errors. The underlying model is sketched in Figure 2. Mathematically it can be written as [13]:

$$\mathbf{x} = \mathbf{\Lambda}\boldsymbol{\xi} + \boldsymbol{\varepsilon} \tag{1}$$

where $\mathbf{x}$ is a $p\times1$ vector of the measured variables, $\mathbf{\Lambda}$ is a $p\times m$ matrix of *factor loadings,* $\boldsymbol{\xi}$ is an $m\times1$ vector of unobservable factors, and $\boldsymbol{\varepsilon}$ is a $p\times1$ vector of *unique factors.*

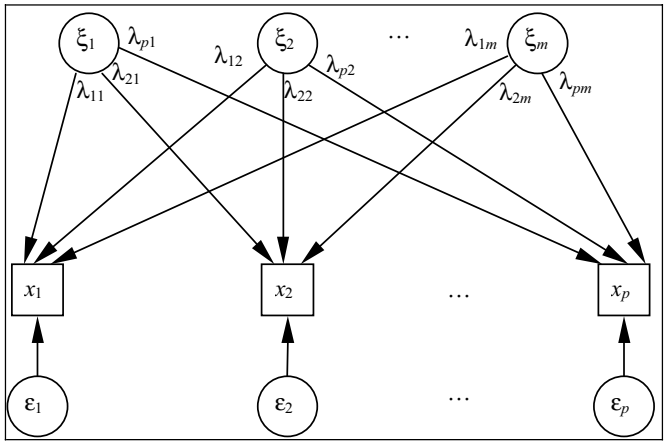

Figure 2: Factor model. x_i are measured variables, ξ_i are common factors, ε_i are unique factors, and λ_{ij} are factor loadings.

In structural health monitoring the measured variables $\mathbf{x}$ can be for example the lowest natural frequencies of the structure; the factors $\boldsymbol{\xi}$ are the latent variables affecting those natural frequencies, e.g. joint positions. Originally the objective of factor analysis is to search or identify the underlying latent factors. In structural health monitoring, however, we are usually not interested in the quantitative values of the factors, but merely in their effects on the measured variables, which makes the analysis much easier and possible to automate.

The steps in the factor analysis include selecting the training data (features), preparing the correlation matrix, extracting a set of factors from the correlation matrix, determining the number of factors, and finally computing the unique factors $\boldsymbol{\varepsilon}$, which should be independent variables and insensitive to the operational conditions. These unique factors are then used for damage detection. If the structure deteriorates so that the measured variables change, the previously trained factor model cannot explain their changes. These changes would therefore remain in $\boldsymbol{\varepsilon}$ causing an alarm signal in the health monitoring system. The learning phase should contain a full range of operational conditions. It should also be emphasized that the model is solely based on measurement data; no structural model is needed.

It is assumed that the factors are mutually independent, normally distributed with zero mean and unit variance: $\boldsymbol{\xi} \sim N(\mathbf{0},\mathbf{I})$. The vector of unique factors $\boldsymbol{\varepsilon}$ is normally distributed with zero means and a diagonal covariance matrix $\boldsymbol{\Psi}$: $\boldsymbol{\varepsilon} \sim N(\mathbf{0},\boldsymbol{\Psi})$. The diagonality of $\boldsymbol{\Psi}$ is one of the key assumptions in factor analysis. According to the model (1), $\mathbf{x}$ is therefore distributed with zero mean

$$\begin{aligned} E(\mathbf{x}) &= E\left[(\boldsymbol{\Lambda}\boldsymbol{\xi}+\boldsymbol{\varepsilon})\right] \\ &= \boldsymbol{\Lambda}E(\boldsymbol{\xi})+E(\boldsymbol{\varepsilon}) \\ &= \mathbf{0} \end{aligned} \tag{2}$$

and covariance matrix, $\mathbf{R}$:

$$\begin{aligned} \mathbf{R} &= E(\mathbf{x}\mathbf{x}^T) \\ &= E\left[(\boldsymbol{\Lambda}\boldsymbol{\xi}+\boldsymbol{\varepsilon})(\boldsymbol{\Lambda}\boldsymbol{\xi}+\boldsymbol{\varepsilon})^T\right] \\ &= E\left[(\boldsymbol{\Lambda}\boldsymbol{\xi}+\boldsymbol{\varepsilon})(\boldsymbol{\xi}^T\boldsymbol{\Lambda}^T+\boldsymbol{\varepsilon}^T)\right] \\ &= E(\boldsymbol{\Lambda}\boldsymbol{\xi}\boldsymbol{\xi}^T\boldsymbol{\Lambda}^T)+E(\boldsymbol{\varepsilon}\boldsymbol{\varepsilon}^T) \\ &= \boldsymbol{\Lambda}\boldsymbol{\Lambda}^T+\boldsymbol{\Psi} \end{aligned} \tag{3}$$

The measured variables are then also normally distributed: $\mathbf{x} \sim N(\mathbf{0}, \boldsymbol{\Lambda}\boldsymbol{\Lambda}^T + \boldsymbol{\Psi})$.

The objective of factor analysis is to estimate the parameter matrices $\boldsymbol{\Lambda}$ and $\boldsymbol{\Psi}$ that best model the covariance structure of $\mathbf{x}$. This can be done using e.g. the principal factor analysis [13]. The method is iterative regardless of the linearity assumption. The factors are assumed uncorrelated, and Equation 3 can be written as

$$\boldsymbol{\Lambda}\boldsymbol{\Lambda}^T = \mathbf{R} - \boldsymbol{\Psi} \tag{4}$$

The right hand side of the equation gives the correlation matrix with the *communalities* in the diagonal. Communalities are estimates of the common variance among the variables. Estimates of the factor loadings, $\boldsymbol{\Lambda}$, are obtained by computing the eigenstructure of the $\mathbf{R}$–$\boldsymbol{\Psi}$ matrix. However, because the estimate of $\boldsymbol{\Psi}$ is not known, an iterative procedure is needed to estimate the communalities. The correlation matrix is subjected to the principal component analysis (PCA) and the communalities are estimated. These communalities are substituted in the diagonal of the correlation matrix. The modified correlation matrix is subjected to another PCA. The procedure is repeated until the estimates of communality converge.

Given $\mathbf{\Lambda}$ and $\mathbf{\Psi}$, the estimate of the *factor scores* $\hat{\boldsymbol{\xi}}$ can be obtained using e.g. the following formula.

$$\hat{\boldsymbol{\xi}} = \mathbf{\Lambda}^T \mathbf{R}^{-1} \mathbf{x} \tag{5}$$

Finally the unique factors $\boldsymbol{\varepsilon}$ can be computed from Equation 1 once the factor scores $\boldsymbol{\xi}$ have been estimated:

$$\hat{\boldsymbol{\varepsilon}} = \mathbf{x} - \mathbf{\Lambda}\hat{\boldsymbol{\xi}} \tag{6}$$

The dimensionality of the feature vector (unique factor scores) is not affected by the factor analysis. Therefore, it is usually necessary to perform a dimensionality reduction before using statistical methods to assess damage. Principal component analysis [13] is one of the most used data reduction techniques and is used also in this study. Moreover, if the multivariate Hotelling T statistic is used in damage detection, the linear factor analysis alone is not sufficient, because the Hotelling T statistic of the original variables $\mathbf{x}$ and the unique factor score estimates $\hat{\boldsymbol{\varepsilon}}$ are identical [14].

3 CRANE MODEL

Structural health monitoring was applied to the finite element model of a vehicle crane (Figure 1). The simulation corresponded to monitoring the crane vibrating around its static equilibrium. The configuration, however, was different each time resulting in a variation of the extracted features. The attempt was to study and then eliminate the effects of the varying configuration on the damage-sensitive features.

The structure was modelled with planar beam and plane stress elements. The hydraulic cylinders were modelled with spring and dashpot elements. A point mass represented the load at the tip. The bottom of the fixed link was clamped and constraint equations were used for the prismatic links.

The natural frequencies and complex mode shapes were first chosen as the damage-sensitive features. They were influenced by four latent variables corresponding to the configuration: three cylinder strokes and the load at the tip, which were assumed unknown. In the simulations they varied randomly in a limited range. Figure 3 shows the limit configurations. The load varied randomly between 0 and 50 kg. In addition, the relationship between the cylinder stiffness and stroke was non-linear.

Damage was modelled as a stiffness reduction in the bottom beam element of the fixed link. Different sizes of damage were studied, ranging from 1 to 10 percent of the original stiffness. The undamaged structure was first monitored with 2000 measurements. Then, damage was gradually increased, and each case was monitored with 250 measurements. Different amount of noise was added to all features, the standard deviation ranging from 0.5 to 10 percent.

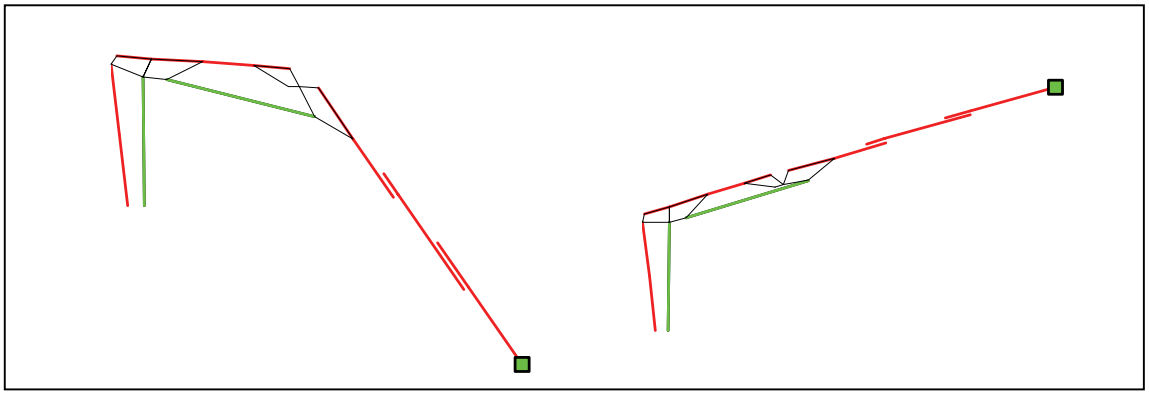

Figure 3: Finite element models of the crane in the limit configurations.

The complex mode shapes were recorded at four different positions of the structure in the transverse direction of each link. Five lowest modes were used for damage detection (Figure 4). Because of the normalization of the mode shapes, the final number of features was 35. The five lowest natural frequencies from each simulation are shown in Figure 5 without additional noise. The change in the frequencies due to damage is not visible in the figure.

The first 700 observations were used to train the factor model. Next 700 observations were used as the in-control samples to compute the control limits for the control chart. After the factor analysis, the largest principal value of the multivariate feature vector was used for damage detection using the Shewhart control chart [15]. The control chart without the factor analysis is shown in Figure 6. Even if no noise was added, damage detection was not possible due to the large normal variation of the features. The point of initiation of each damage level is also shown.

Control charts after the factor analysis and the subsequent principal component analysis are shown in Figure 7 with different amount of added noise. The effect of the noise on damage detection can be seen. Because the noise was uncorrelated, it could not be eliminated from the features. Increasing the noise level made structural health monitoring less sensitive to damage. However, all sizes of damage could be clearly observed.

The number of factors was determined to account for at least 99.9% of the variance in the data [10], resulting in 15 factors for data with 10% noise and 11 factors for all other amounts of noise.

Factor analysis clearly eliminated the operational effects. All damage levels were detected and only occasional false indications of damage were present, suggesting that at least two successive out-of-control samples should be present before alarm signal is generated. It is interesting to notice that the linear factor analysis worked perfectly also for the non-linear data.

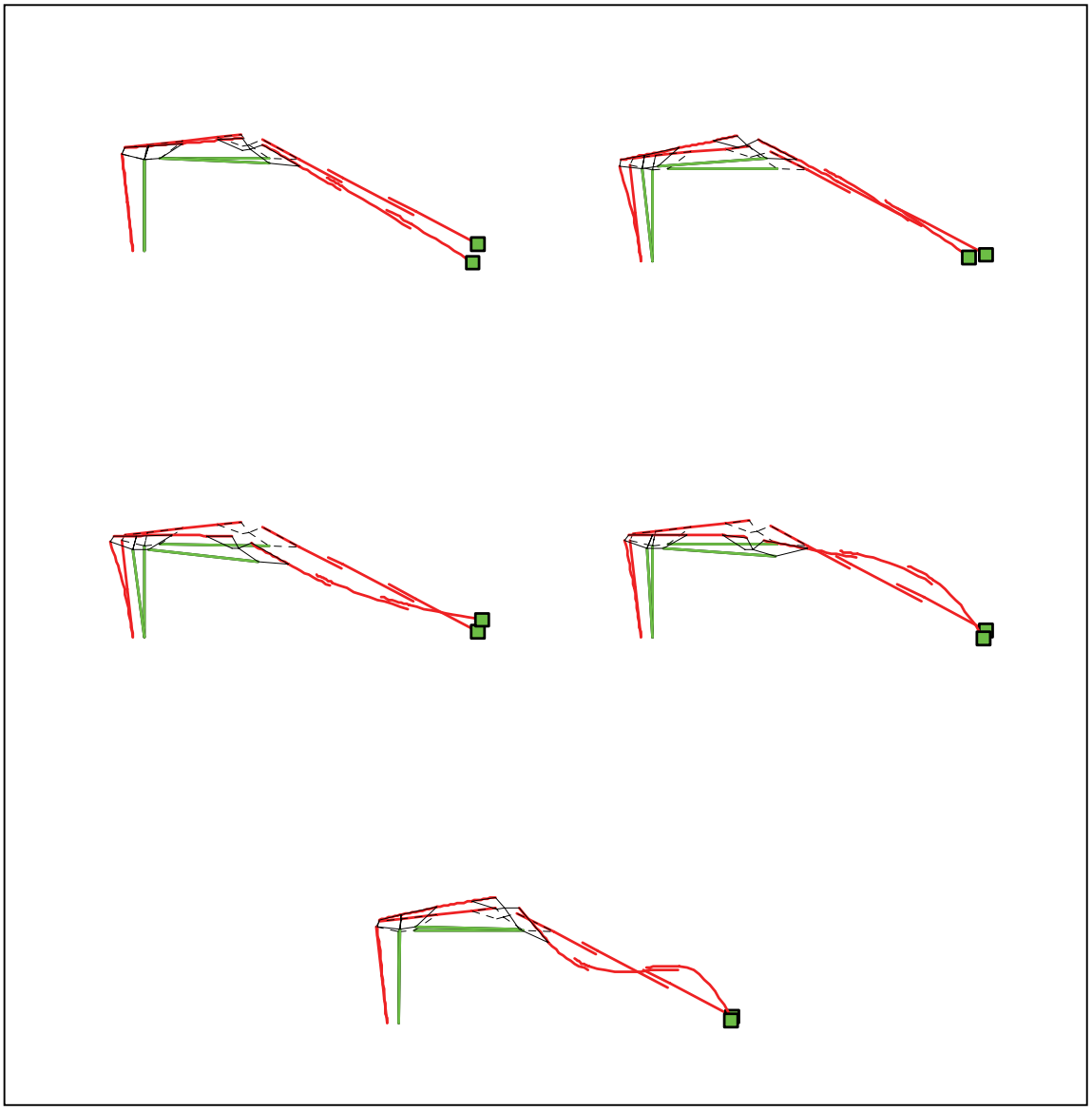

Figure 4: Five lowest modes of the crane in an intermediate configuration.

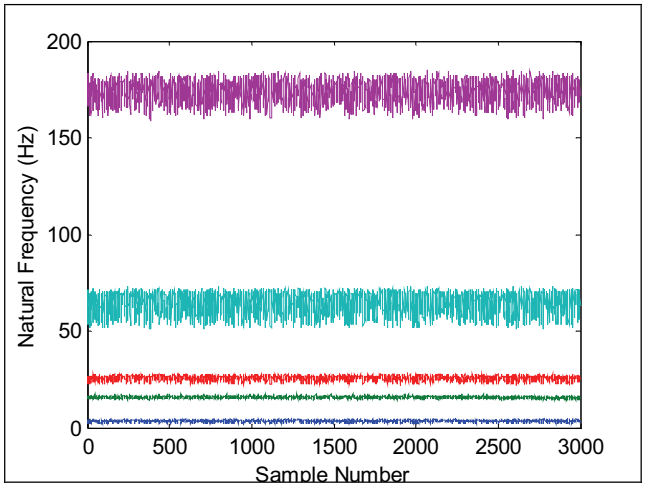

Figure 5: Variation of the natural frequencies without added noise.

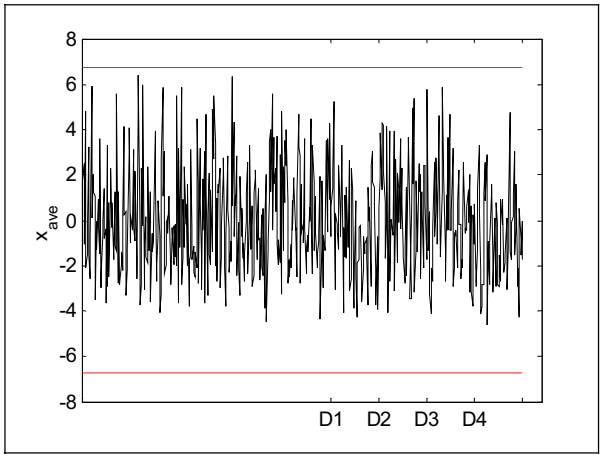

Figure 6: Control chart for original features without added noise.

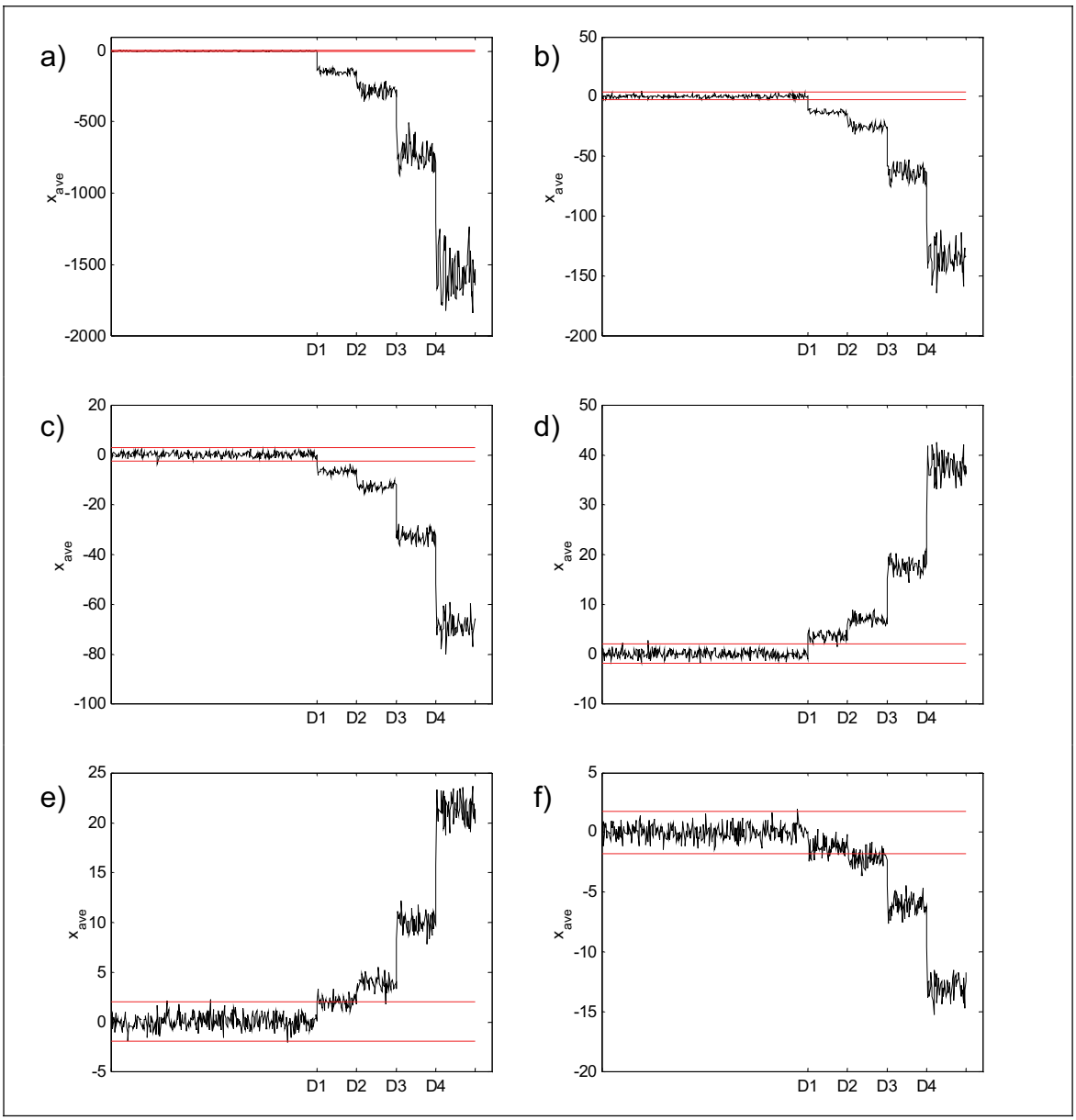

Figure 7: Control charts with different amount of added noise: a) 0%, b) 0.5%, c) 1%, d) 2%, e) 5%, and f) 10%.

To study the damage-sensitivity of different features, control charts separately for natural frequencies and mode shapes were plotted in Figure 8. It can be seen that both features were affected by damage, but the mode shapes were clearly more sensitive than the natural frequencies. This result has also been observed with civil engineering structures.

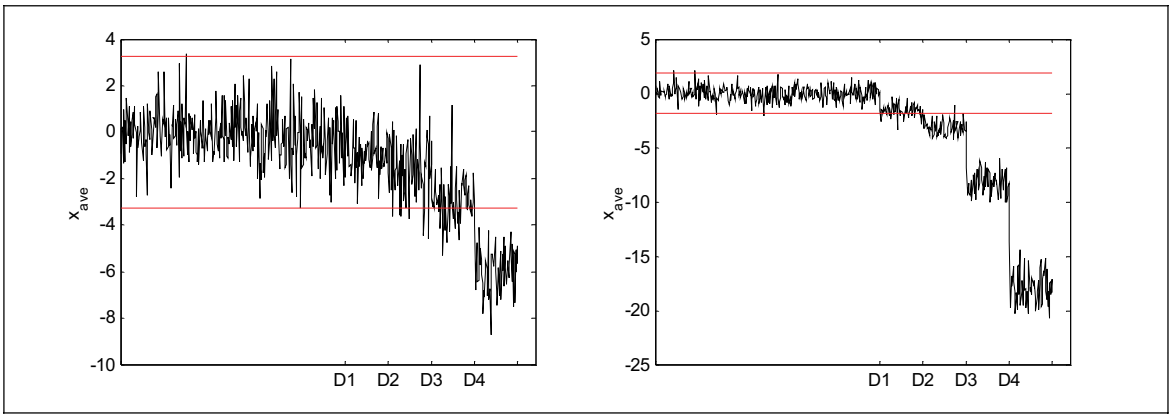

Figure 8: Control charts for natural frequencies (left) or mode shapes (right) with 5% noise.

Another simulation was performed using the power spectra as the damage-sensitive features. The configuration of the crane varied as in the previous example. The structure was excited at the tip in the lateral direction with respect to the link with a signal having a flat spectrum. Velocity was recorded at four locations. The velocity power spectra were computed from 0.5 to 50 Hz with the frequency resolution of 0.5 Hz. The number of variables was therefore 400. In order to decrease the dimension, the frequency range from 0.5 to 30 Hz was chosen for damage detection resulting in 240 features. The resulted spectra are shown augmented in Figure 9. The variation can be clearly seen. Because spectrum is a squared variable, logarithm was first applied to the spectra. Noise with standard deviation of 10 percent was then added to the features.

The first 4000 samples were recorded from the healthy structure. Damage was then introduced similarly to the previous case with 250 samples from each damage level. The first 1500 samples were used to train the factor model. The following 1500 samples were then used as the in-control data to build the control charts. The control chart of the first principal component is shown in Figure 10 left. No indication of damage can be observed from the chart. Factor analysis resulted in 113 factors. The control chart for the first principal component of the estimated unique factors is shown in Figure 10 right. The drastic improvement can be noticed. All damage levels are clearly visible. The results show that spectral data can also be used as damage-sensitive features.

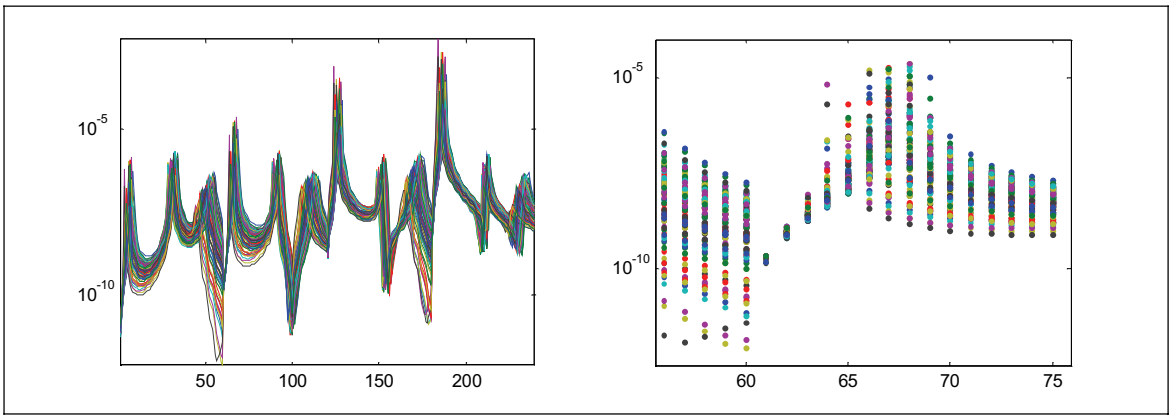

Figure 9: Augmented power spectra at 100 different crane configurations. A detail is shown on the right.

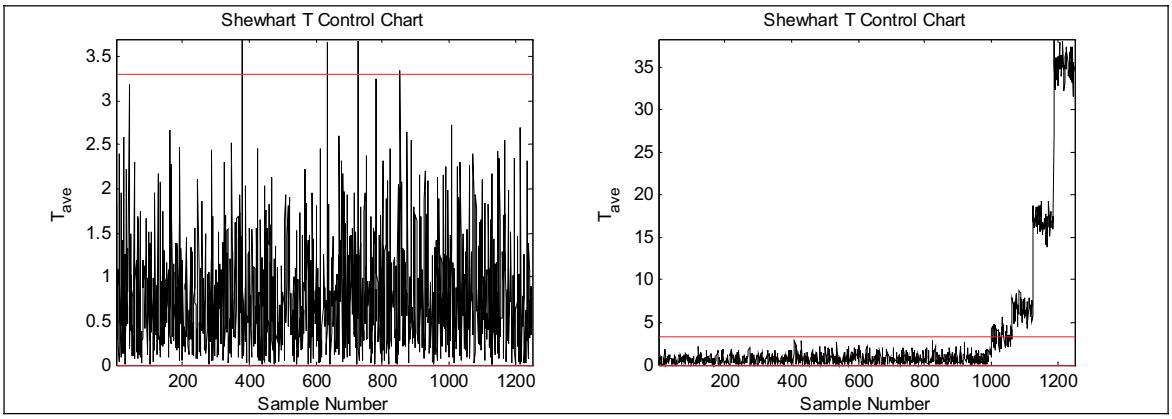

Figure 10: Control charts for spectral data without factor analysis (left) and using factor analysis (right).

4 EXPERIMENTAL STUDY

Vibration-based monitoring tests for a vehicle crane HIAB022-2L (Figure 11) were performed in the laboratory. The features were extracted from the measurements on the crane vibrating around a slightly varying static equilibrium. The crane was excited with a random excitation using its own hydraulic lift cylinder. Four accelerations (positions and directions shown in Figure 11) and two cylinder pressures were measured. First 400 measurements were recorded from the undamaged structure. Fifteen different structural changes were then made using additional masses of five different sizes at three locations. The magnitudes of the additional masses for each damage scenario were 1.4, 3.4, 5.4, 7.4, and 9.4 kg, and their locations are shown in Figure 11. Each damage scenario was monitored with 50 measurements. The time period of each measurement was 60 seconds with a sampling frequency of 550 Hz.

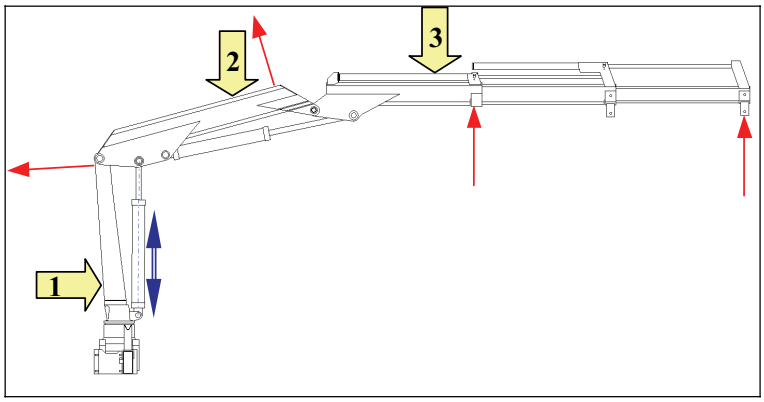

Figure 11. Vehicle crane HIAB-022-2L. The numbered arrows indicate the damage locations, the double arrow is the excitation, and the single arrows are the response positions.

Ten AR coefficients were extracted from each time record. The 40 coefficients from the four acceleration signals are plotted in Figure 12 including the undamaged structure and damage position 1. The first 200 observations were used as training data to estimate the mean and covariance matrix. The same observations were used as the in-control samples to compute the control limits for the control chart.

After 128 measurements from the undamaged structure, a static pressure in the transfer cylinder was introduced in order to control the descending of the boom. This action, however, resulted in a change of features as can clearly be seen in Figure 12. Fortunately, because the training data consisted of the first 200 samples, it was possible to eliminate the effect using the proposed method without losing any data.

The factor analysis was applied to the features resulting in the residual, a new feature that was then used for damage detection. The number of features still remained unchanged, which was too many for a reliable statistical analysis. Therefore, a dimensionality reduction was performed using the principal value analysis (PCA) and choosing the largest principal value for damage detection. Damage detection was performed using control charts shown in Figure 12. Each statistic is the average of four successive features and the damage is therefore introduced at sample number 100. It can be seen that all damage cases could be detected without too frequent false indications of damage.

It is interesting that the level of damage (size of the added mass) was not indicated in the control charts. It was anticipated that with a higher mass the statistics would have fallen further away from the control limits.

The 20 AR coefficients from the two pressure signals are plotted in Figure 13 including the undamaged structure and damage scenario 1. The effect of the pressure increase can again clearly be observed, but could be eliminated using the proposed method. The control charts for the first principal component of the residuals from the factor analysis are also shown in Figure 13. It can be seen that damage could not be detected from the pressure data.

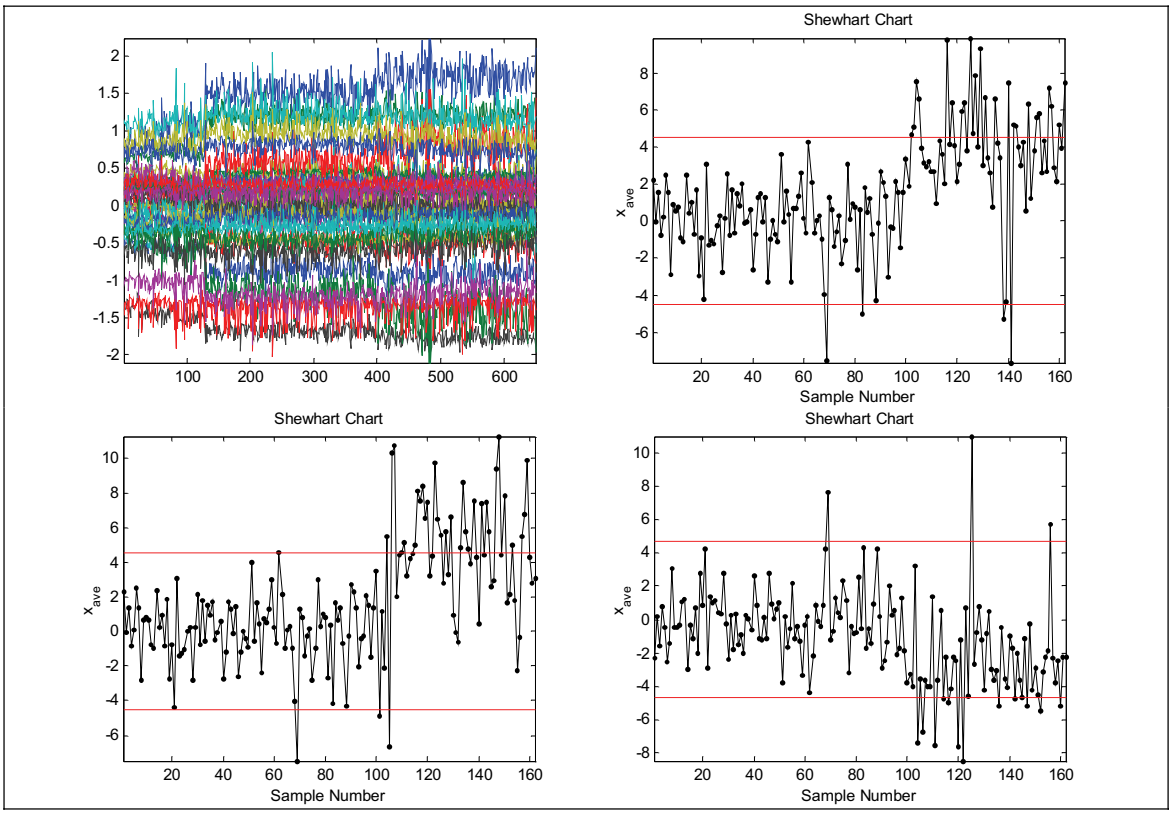

Figure 12. AR coefficients from the acceleration measurements. Control charts for damage 1, 2, and 3.

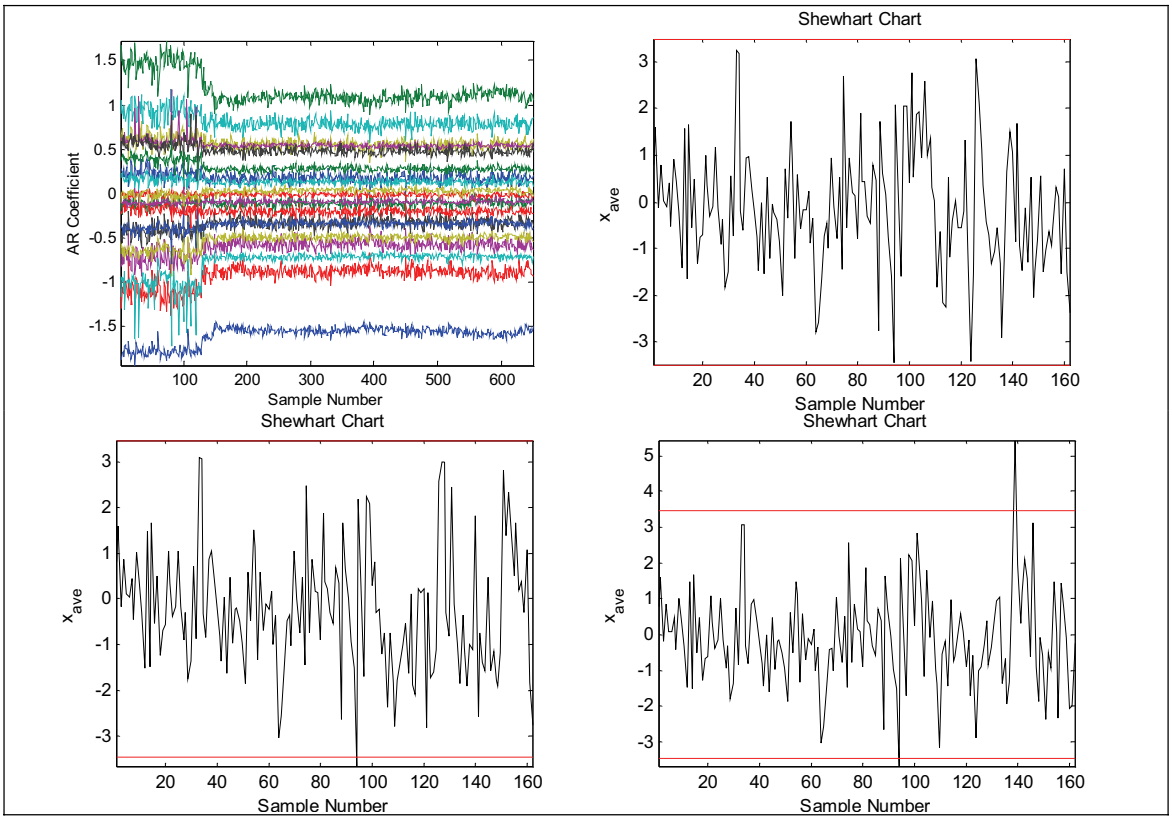

Figure 13. AR coefficients from cylinder pressure measurements. Control charts for damage 1, 2, and 3.

5 CONCLUSION

The condition of a vehicle crane structure can be monitored using multichannel vibration measurements. No mathematical model of the structure is needed. The objective is to detect possible damage in the crane. Damage detection is based on features extracted from the vibration measurements. Training data is first collected from the healthy structure. A statistically significant change in the features is an indication of damage.

Factor analysis was successfully applied to eliminate operational effects from a structural health monitoring data. It offers many advantages compared to other techniques. The underlying quantities need not be measured, they need not be even known, and there can be several factors acting simultaneously.

Structural health monitoring was applied to a vehicle crane using both numerical and experimental data. With the numerical model, the dynamic properties of the structure were used as damage-sensitive features and damage was introduced to the fixed link as a stiffness degradation. Also noise was added to the features. Different operational parameters were varied. All damage levels could be detected, whereas without factor analysis damage detection was not possible.

In the experimental study, the crane was shaken with a random excitation using the lift cylinder. The response was recorded with four accelerometers and two pressure sensors. Ten AR parameters from each record were identified for damage detection. Damage was introduced with additional masses attached to different locations of the structure. All damage scenarios were detected from the acceleration measurements, whereas the pressure measurements were less sensitive to the increased mass.

The main restriction of the factor analysis is its linearity assumption. Development and application of non-linear latent variable models is a subject for further studies, as the influence of the operational parameters is often non-linear. In addition, it would be important to find new features for damage detection having the following global properties: they must be automatically and reliably extracted from the measured time histories and be sensitive to damage of unknown type or location.

ACKNOWLEDGEMENT

This research was performed in a MASINA technology program of the Finnish Funding Agency for Technology and Innovation (TEKES). The first author is also a partner in the S3HM project (www.s3hm.be) under the coordination of the ESF EUROCORES S3T program.

REFERENCES

1. Wahab, M.A. and De Roeck, G. 1997. Effect of temperature on dynamic system parameters of a highway bridge. Structural Engineering International, No. 4, 266–270.
2. Farrar, C.R., Doebling, S.W. Cornwell, P.J. & Straser E.G. 1997. Variability of modal parameters measured on the Alamosa Canyon Bridge. Proceedings of IMAC-XV: A Conference on Structural Dynamics, Orlando, Florida, USA, February 1997. Society for Experimental Mechanics, Bethel, Connecticut, 257–263.
3. Alampalli, S. 1998. Influence of in-service environment on modal parameters. Proceedings of the 16th International Modal Analysis Conference, Santa Barbara, California, February 2–5, 1998. Society for Experimental Mechanics, 111–116.
4. Cornwell, P., Farrar, C.R., Doebling, S.W. and Sohn, H. 1999. Structural testing series: Part 4. Environmental variability of modal properties. Experimental Techniques, Vol. 23, No. 6, 45–48.
5. Peeters, B., De Roeck, G. 2000. One year monitoring of the Z24 bridge: Environmental influences versus damage effects. Proceedings of IMAC-XVIII: A Conference on Structural Dynamics, San Antonio, Texas, USA, February 7–10, 2000. Society for Experimental Mechanics, Bethel, Connecticut, 1570–1576.
6. Rohrmann, R.G., Baessler, M., Said, S., Schmid, W. and Ruecker, W.F. 2000. Structural causes of temperature affected modal data of civil structures obtained by long time monitoring. Proceedings of IMAC-XVIII: A Conference on Structural Dynamics, San Antonio, Texas, USA, February 7–10, 2000. Society for Experimental Mechanics, Bethel, Connecticut, 1–7.
7. Sohn, H., Farrar, C.R. & Hunter, N.F. 2001. Data normalization issue for vibration-based structural health monitoring. Proceedings of IMAC-XVIII: A Conference on Structural Dynamics, Orlando, Florida, USA, February 2001. Society for Experimental Mechanics, Bethel, Connecticut, 432–437.
8. Sohn, H., Farrar, C.R., Hunter, N.F. and Worden, K. 2001. Structural health monitoring using statistical pattern recognition techniques. Journal of dynamic systems, measurement, and control, Vol. 123, 706–711.
9. Manson, G. 2002. Identifying damage sensitive, environment insensitive features for damage detection. Proceedings of the Third International Conference on Identification in Engineering Systems, Swansea, April 15–17, 2002. Institute of Physics Publishing. 187–197.
10. Kullaa, J. 2002. Elimination of environmental influences from damage-sensitive features in a structural health monitoring system. First European Workshop on Structural Health Monitoring, Paris, July 10–12, 2002. Onera. DEStech Publications. 742–749.
11. Sohn, H., Worden, K., and Farrar, C.R. 2003. Statistical damage classification under changing environmental and operational conditions. Journal of Intelligent Material Systems and Structures, Vol. 13, No. 9, 561–574.
12. Kullaa, J. 2003. Is temperature measurement essential in structural health monitoring? Proceedings of the 4th International Workshop on Structural Health Monitoring. Stanford, CA. September 15–17, 2003. Stanford University. DEStech. 717–724.
13. Sharma, S. 1996. Applied multivariate techniques. New York. John Wiley & Sons. 493 p.

14. Fukunaga, K. 1990. Introduction to Statistical Pattern Recognition. 2nd edition. Boston. Academic Press. 591 p.
15. Montgomery, D.C. 1997. Introduction to statistical quality control. 3rd edition. New York. John Wiley & Sons. 728 p.

IMPROVING CHARACTERISTICS OF ON/OFF SOLENOID VALVES

Jaakko Mikkola, Ville Ahola, Timo Lauttamus, Markku Luomaranta, Matti Linjama, Matti Vilenius
Tampere University of Technology
Institute of Hydraulics and Automation
P.O. Box 589
33101 Tampere, Finland
Phone: +358 3 3115 2344, Fax: +358 3 3115 2240
E-Mail: jaakko.mikkola@tut.fi

ABSTRACT

This paper studies simple measures to reduce response times of commercial directly operated solenoid valves. Two directly operated spool type solenoid valves, nominal sizes 6 and 4, and one seat type screw-in cartridge valve are studied. The main issue is that due to the time constant of typical coil, the current rises slowly with the nominal voltage and causes delay in valve opening. This can be overcome by using a short pulse of higher voltage to the coil. This is achieved by using a booster circuit. Also the structure of the valves is modified by eliminating the springs in the valve and by using 4/3 valves as 2/2 valves in double flow configuration. The seat type screw-in cartridge valve is used only with the booster circuit. Experimental results show an improvement of 50-70 percent in response times. Also the energy consumption in average use reduces and maximum flow capacity improves in the spool valves. With the seat type screw-in cartridge valve mainly the response time improves because the structure of the valve remains original.

KEYWORDS: Solenoid valves, On/off valves, Booster circuit, Response time

1 INTRODUCTION

The biggest problem with commercially available on/off valves is slow and varying response time. Typical response times are 20-50 ms but they can vary even tens of percents. In digital hydraulics applications this may cause pressure peaks, and vibrations [1,2]. The problems in commercial valves are mainly caused by the solenoid – spring return working principle but improving properties of these valves is possible with simple modifications.

Commercial on/off valves are usually opened against the force of the closing spring and require a constant current to keep the valve open. This requires the solenoid to be

designed to last constant current at its nominal voltage. This results in large solenoids with large time constant, which causes the force of the solenoid to develop slowly when voltage is connected to the coil. In addition, the solenoid has to move the spool against the spring force, which causes the opening of the valve to take long time and significant variations in opening time can occur. If the opening of the valve can be hastened, the variations also diminish and application of these valves in digital hydraulics becomes easier.

Related work is presented in [3,4]. Mäkinen et al. [3] studied the effects of different booster circuits on the performance of solenoid operated pneumatic valve. R.Van Ham et al. [4] used a speed up circuitry and removed the springs to speed up pneumatic on/off valves. Similar methods are used in this study to improve the performance of hydraulic solenoid valves. Valves studied are two 4/3 spool valves and one 2/2 seat valve. The two spool valves used are a Moog WE43P06E03PC0BN NS6 with 24 V and 12 V solenoids and a Bosch Rexroth 4WE420/EG24N9K4 NS4 with 24 V solenoids. The seat valve used is a Hydac WS08-01 with a 12 V solenoid.

2 METHODS USED TO IMPROVE PERFORMANCE OF THE VALVES

2.1 Spool valves

The spool valves are mechanically modified by removing the return springs and shortening the stroke of the spool. The modifications made to the NS4 valve are shown in Figure 1 and the NS6 in Figure 2. Removing the springs reduces opening delay because the solenoid does not have to work against the force of the spring. To close the valve without the springs the solenoid in the other end of the valve has to be used. In order to improve the force of the solenoid closing the valve, the spool (3) is shortened in the NS6 valve and the solenoids pushrod (5) is shortened in the NS4 valve. This is done because the solenoid produces the more force the closer it is to the end of its travel. The stroke of the spool is shortened by removing the other end position by adding a positive stop (1) to the other end of the spool. A special washer (2) is required in the other end in place of the spring. The springs may be retained to preload the washers as in Figure 2. The 4/3 valves are also connected in double flow configuration as shown in Figure 3. This way the flow capacity of the valve can be doubled. These modifications make a 4/3 valve essentially a 2/2 valve.

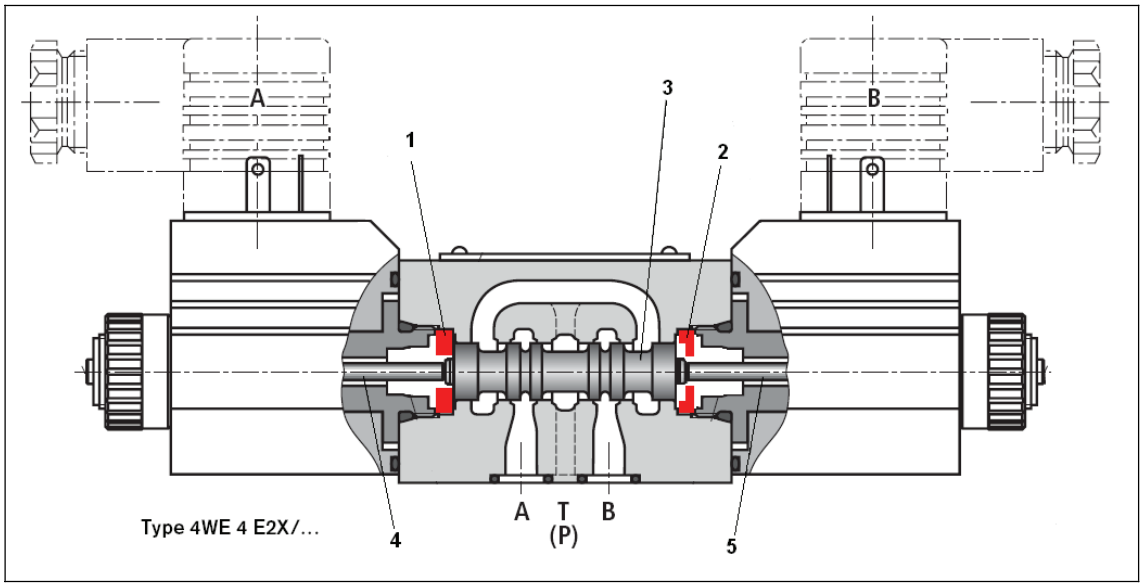

Figure 1. Mechanical modifications to the NS4 valve (original picture from [5] by courtesy of Bosch Rexroth Oy).

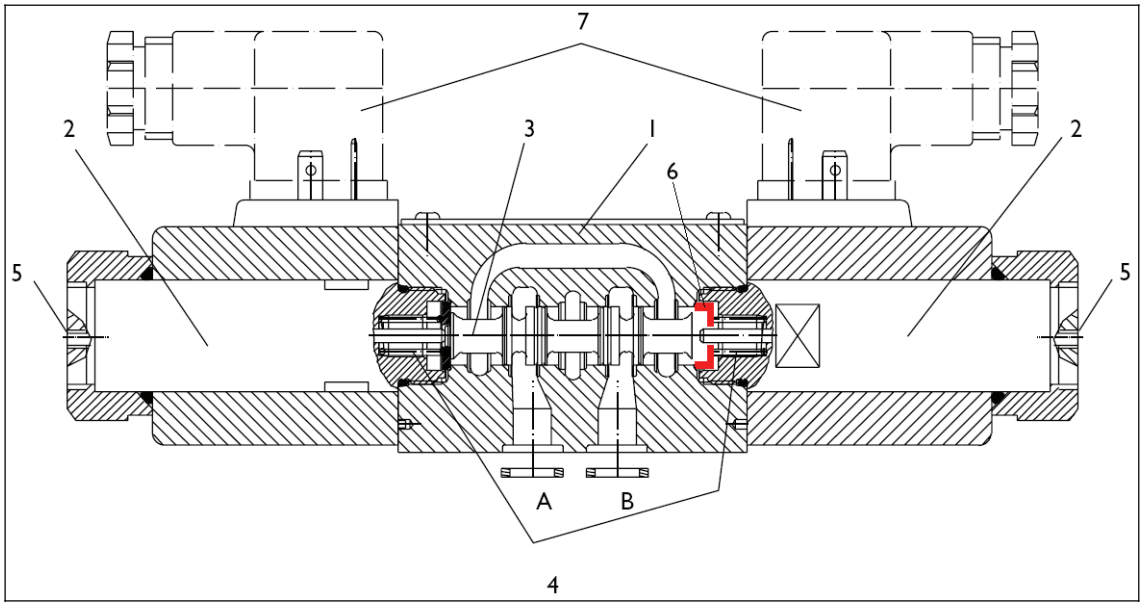

Figure 2. Mechanical modifications to the NS6 valve (original picture from [6] by courtesy of Moog Oy).

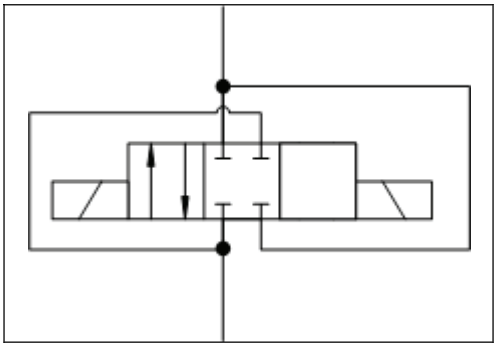

Figure 3. The double flow configuration used.

A booster circuit is used to raise the current in the solenoids coil faster and thus decreasing the time it takes the solenoid to develop sufficient force to move the spool and reducing the switching time of the valve. This is achieved by connecting a short pulse of overvoltage to the solenoid to raise the current faster to the desired level. After the opening pulse current is stabilized to the nominal level of the coil with pulse width modulation (PWM) control. The closing response of the solenoid can also boosted by allowing negative voltage difference over the coil which damps the current. This can be realized directly with filed effect transistor (FET) or with diode as presented in Figure 4. The studied booster circuit was implemented with 10 ms opening boost and 50 VDC clamp diode. The booster circuit has only one channel so the tests with the spool valves are made so that closing and opening responses are measured on separate occasions and changing the coil that the booster controls in between. The other coil is controlled in normal fashion with its nominal voltage and IPS0151 Smart Power MOSFET.

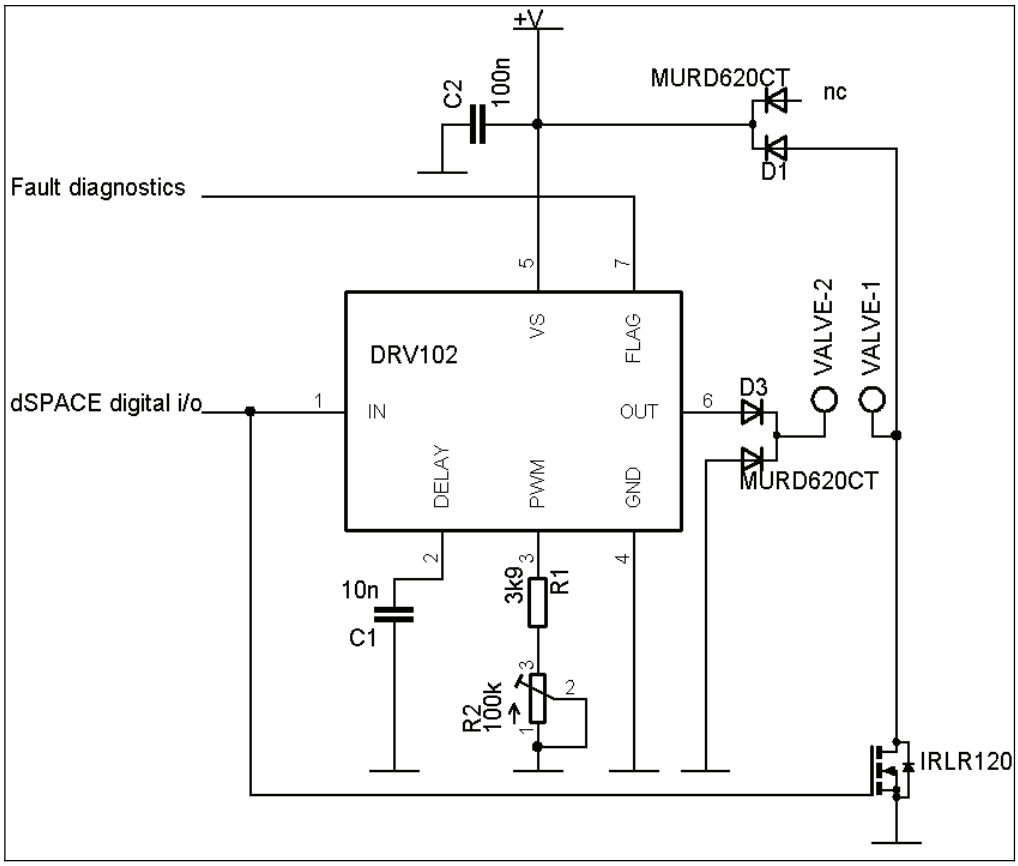

*Figure 4.*The wiring diagram of the booster.

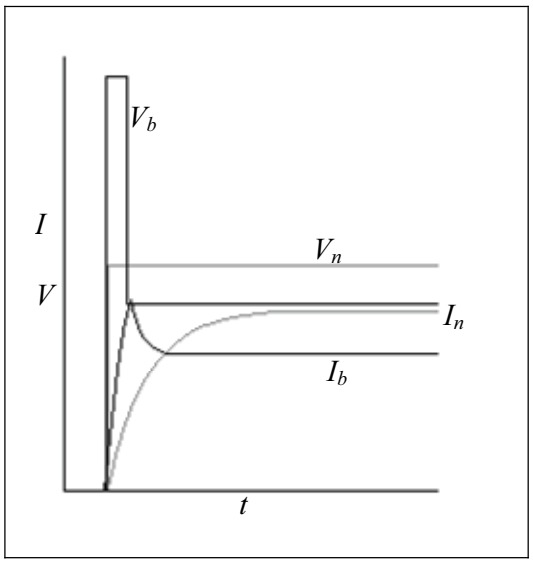

Figure 5. Voltage and current of the solenoid when opening the valve with booster.

2.2 Seat valve

With the seat valve only the booster circuit is used with no mechanical modifications. The booster used with the seat valve is a different specimen than used with the spool valves but of the same desing. This booster limits the used overvoltage to 40,1 V.

3 MEASUREMENTS AND RESULTS

3.1 Measuring system and methods

The schematics of the measurement system is presented in figure 6. The inlet side consists of a pressure filter, pressure relief valve and a 10 liter pressure accumulator in the supply line before the valve. The pressure relief valve is used to set the supply pressure to the desired level and the 10 liter accumulator is used to level off the pressure pulsation. Pressure difference over the valve is measured with two pressure transducers connected directly to the valve block. Flow through the valve is measured with a Volutronic VC5 mounted as close to the valve block as possible. Downstream side has a 20 liter pressure accumulator and a adjustable orifice. The accumulator is used to level the pressure after the valve during the step response measurements and the pressure is set with the adjustable orifice.

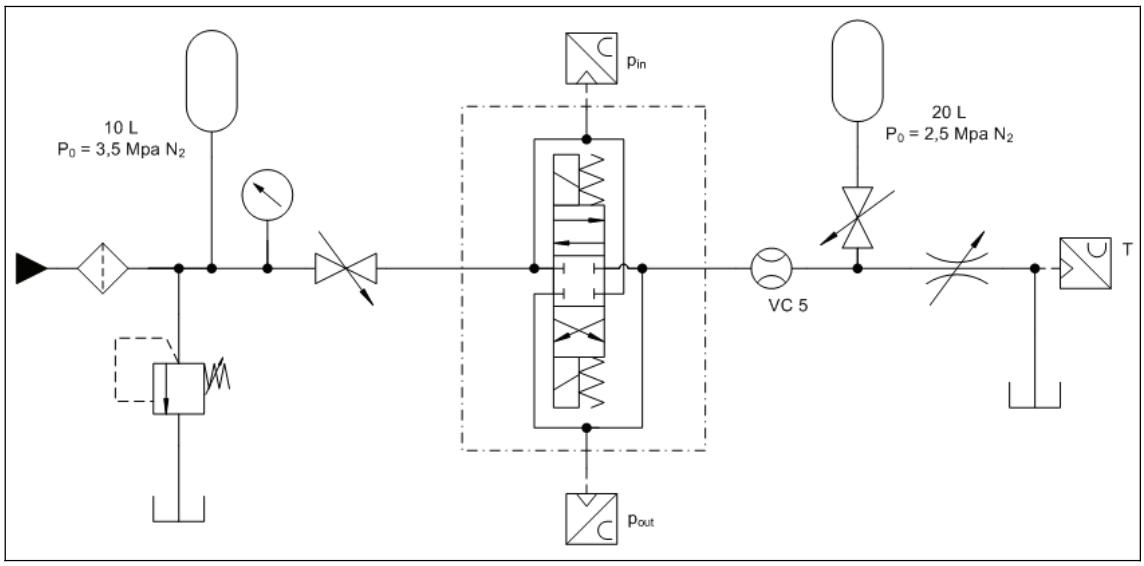

Figure 6. Schematics of the system used to measure the valves.

Response times are measured from pressure response because spool position cannot be measured. Response time is calculated from the change of the control u to the point where the pressure difference changes more than its normal fluctuation as presented in Figure 7. All measurements are made with 10 MPa supply pressure. The response times of the NS4 valve are calculated with Matlab from the time conrol signal changes to the time pressure signal has changed ± 0.3 MPa from the value on the time of the control change. The response times of the other valves are calculated manually from the pressure signal in the same fashion.

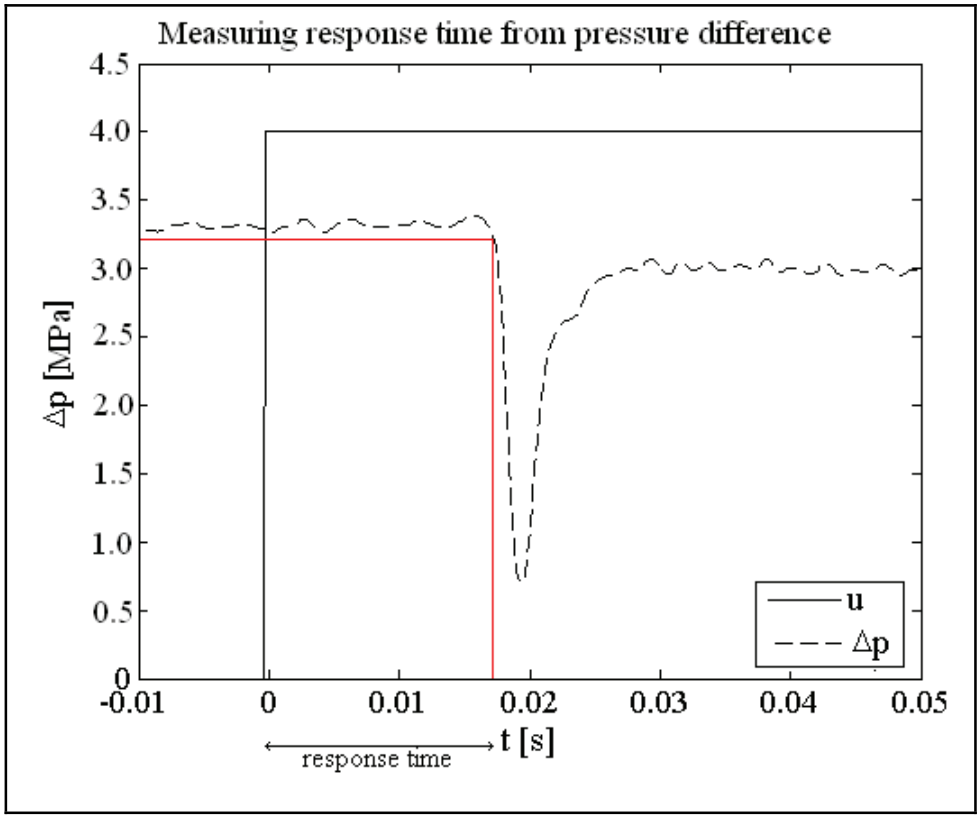

Figure 7. The method of measuring response time from pressure difference.

3.2 Results

3.2.1 Bosch Rexroth 4WE (NS4)

Bosch 4WE420/EG24N9K4 NS4 is modified by removing the springs, limiting stroke of the spool as described in figure 1, shortening the solenoid pushrod and using a booster circuit to drive up the current in the solenoid faster. Different length pushrods are tested in order to find optimum length so that response time is as short as possible and the valve still fully opens.

At first the effect of using one coil to open and another to close the valve was measured. The springs were in their original places. The valve remained otherwise original in this test. Using two coils expanded the operation limit of the valve to 85 l/min compared to 75 l/min of the original valve in double flow configuration.

Next the valve is modified mechanically to shorten the response times. Springs are removed and stroke of the spool is limited to 1.9 mm so that only the other end position remains. This is done by adding stops to the ends of the spool and shortening the solenoid pushrods. The original solenoid pushrods are 28.5mm long. The pushrod in the coil closing the valve can be shortened so that the coil does not try to push to spool to the other end position but only to the closed middle position. This is achieved with a 26.8 mm pushrod. Reducing the length of the pushrods even more in both coils produced faster response times because the force the coil produces at the start of the spool movement is greater. To this end a 26.3 mm pushrod in the closing coil and a 27.8 mm pushrod in the opening coil are tested. Response times with different pushrods are presented in table 1. The holding current is set to the nominal current of 0.7 A.

Table 1. Response times of Bosch Rexroth 4WE valve with different length solenoid pushrods.

	Opening delay [ms]		Closing delay [ms]	
Testing of different length pushrods	Δp 3MPa	Δp 1MPa	Δp 3MPa	Δp 1MPa
26.8mm closing, 28.5mm opening	20.8	21.9	30.8	20.1
26.3mm closing, 28.5mm opening	18.4	19.5	25.4	20.2
26.3mm closing, 27.8mm opening	18.1	18.6	22.5	19.3

The best combination of pushrods is selected as the basis for the rest of the measurements. Next a booster is added to hasten the rise of current in the coil. It is clearly visible that response time of the valve is mainly dependent on speed of the current rise in the coil because 69 V supply voltage produced faster response than 49 V supply voltage. Results of all modifications are presented in table 2. The original valve is measured in double flow configuration using 24 V supply and IPS0151 Smart Power MOSFET.

Table 2. Response times of Bosch Rexroth 4WE valve.

	Opening delay [ms]		Closing delay [ms]	
Method of improving	Δp 3MPa	Δp 1MPa	Δp 3MPa	Δp 1MPa
Original valve	21.9	18.5	20.1	16.3
Original valve using 2 coils	24.2	28.5	26.7	19.0
Springs removed, using 2 coils	18.1	18.6	22.5	19.3
Added booster (49V supply voltage)	9.9	11.8	not	measured
Added booster (69V supply voltage)	8.6	9.7	8.2	8.1

The mechanical modifications caused the response times to increase as is evident in table 2. This is particularly visible with using two coils with no other changes. This is probably caused by the inductance of the coils which upholds the current and causes a residual force in the coil after the voltage is disconnected. This force has to be overcome by the other coil trying to change the state of the valve and this slows down the response of the valve. The operation limit of the valve was not measured after removing the springs but it is likely to have increased as with the NS 6 valve. With all the modifications the opening response is improved 47 % compared with the original (18.5 ms) as described in figure 8 and closing response is improved 50 % compared to the original (16.3 ms). Adding the booster circuit has the biggest effect on valve performance.

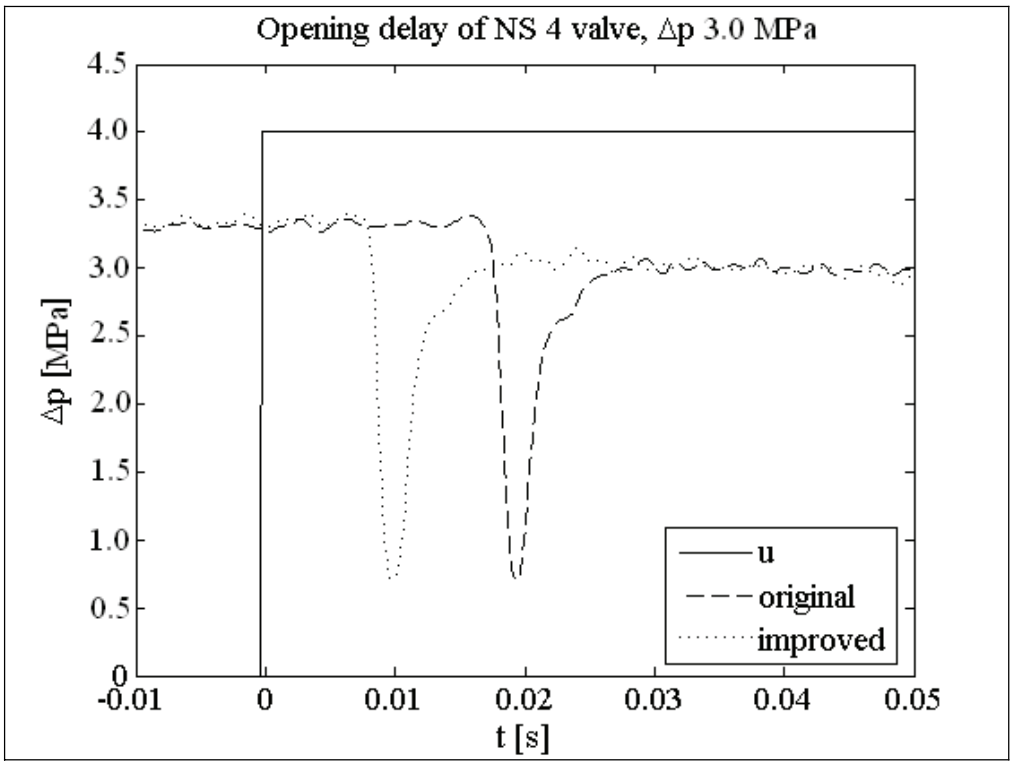

Figure 8. The improvement of opening delay of Bosch Rexroth 4 WE valve.

3.2.2 Moog WE43 (NS6)

Moog WE43P06E03PC0BN NS6 valve is modified by shortening the stroke of the spool as described in figure 2, connecting the valve in double flow configuration and using the booster with 50 V overvoltage. The stroke is shortened by cutting the other end of the spool shorter because the Moog valve does not have separate pushrods in the

coils. This also prevents testing with different pushrod lengths to improve the initial force of the coil. The valve is available with 24 V or 12 V coils and both coil are tested. As expected the 12 V coils are faster due to lower inductance and greater relative overvoltage. The original valve is measured in double flow configuration using 24 V supply and IPS0151 Smart Power MOSFET.

Table 3. Response times of Moog WE43 valve.

	Opening delay [ms]		Closing delay [ms]	
Method of improving	Δp 4MPa	Δp 1MPa	Δp 4MPa	Δp 1MPa
Original valve with 24V coil	38	31	29	16
Springs removed and using 2 coils	24	26.5	26	20.5
Added booster (50V supply voltage)	17	18	10	11
24V coils substituted with 12 V coils	12	11	8	8

The results show that opening of the valve was quickened 68 % at best and closing 72 %. Substituting the 24 V coil with 12 V coils had particularly strong effect because the boosters overvoltage is relatively greater than with the 24 V coils. All the performed modifications had the expected effect. The operation limit of the original valve was 220 l/min in double flow configuration. The modified valve worked properly up to the maximum flow rate of the test system (260 l/min).

3.2.3 Hydac WS08-01

Hydac WS08-01 is a cartridge type seat valve. Because of this, the only modification made was the use of the booster. Measurements are made in same fashion as with the other valves. This time the booster used was different with the only difference being its lower maximum voltage that was 40.1 V. The results are presented in table 4 below. The response times are in pairs so that the first number is the response time with 12 V supply and IPS0151 Smart Power MOSFET and second with the booster and 40.1 V supply voltage. The operation limit of the original valve was 35 l/min in 2 to 1 direction and over 80 l/min in 1 to 2 direction (up to maximum pressure of the manifold). The operation limit was not measured after adding the booster but it is at least the same since same hold current is used.

Table 4. Response times of Hydac WS08-01.

Opening [ms]			Closing [ms]		
	1 to 2	2 to 1		1 to 2	2 to 1
dp 1.5 Mpa	18.1 / 5.3	16.2 / 5.2	dp 1.5 MPa	8.6 / 7.8	8.4 / 7.9
dp 3.0 Mpa	18.5 / 5.3	15.5 / 5.2	dp 3.0 MPa	7.1 / 7.6	7.8 / 6.7

These results show that at best the opening of the valve is improved 70 % and the closing of the valve 9 %. The closing is not improved radically because the valve is still closed with the closing spring and that IPS0151 Smart Power MOSFET used with the 12 V supply voltage kills the residual current as quickly as the booster circuit.

4 CONCLUSIONS

This study shows that the characteristics of commercially available solenoid valves can be improved significantly with simple mechanical modifications and improved control electronics. The developed methods enable commercial solenoid valves to be used in digital hydraulics and promote applying digital hydraulics to production systems. Response times of the valves were reduced up to 70 % depending of the valve used. All valves responded positively to the tested modifications with the booster circuit usually having the biggest effect. The response times could probably be further improved by using a two channel booster and lowering the current after the opening pulse below the nominal current of the coil.

ACKNOWLEDGEMENTS

The research was supported by Academy of Finland (Grant no. 80411) and the Finnish Funding Agency for Technology and Innovation (Sykli project, grant no. 40334/04)

REFERENCES

1. Linjama, M.; Laamanen, A.; Vilenius, M. 2003. Is it time for Digital Hydraulics? Proceedings of the Eight Scandinavian International Conference on Fluid Power (SICFP´03), May 7–9 2003, Tampere, Finland. pp. 347-366.

2. Laamanen, A.; Linjama, M.; Vilenius, M. 2005. Pressure Peak Phenomenon in Digital Hydraulic Systems – a Theoretical Study. Bath Workshop on Power Transmission and Motion Control (PTMC 2005). September 7-9. 2005, Bath, UK. pp. 91-104.

3. Mäkinen E.;Virvalo T.; Tuominen P.; Mattila J.1994. The Comparison of Different Booster Circuits used to Improve Characteristics of On/Off-valves. Proceedings of Tampere International Conference on Machine Automation, February 15-18 1994, Tampere, Finland. pp. 599-610.

4. Van Ham, R.; Daerden, F.; Verrelst, B.; Lefeber, D.; Vandenhoudt, J. 2002. Control of Pneumatic Artificial Muscles with Enhanced Speed Up Circuitry. 5 th International Conference on Climbing and Walking Robots (CLAWAR 2002), September 2002, Paris France. pp. 195-202.

5. Bosch Rexroth AG, Industrial Hydraulics. 4/3-, 4/2- and 3/2-way directional valves with wet pin DC solenoids Type WE 4. http://www.boschrexroth.com/Rexroth-IHD/Home.cfm?Page=RDSearch&Filter=23161 2004. (visited 3.1.2007)

6. Moog Inc., Industrial Controls Division. WE Series Directional Control Valves ISO4401 Size 03. http://www.moog.com/Media/1/weseries.pdf (visited 10.1.2007)

A NOVEL VALVE CONCEPT INCLUDING THE VALVISTOR POPPET VALVE

Björn ERIKSSON, Jonas LARSSON and Jan-Ove PALMBERG
Division of Fluid and Mechanical Engineering Systems
Department of Mechanical Engineering
Linköping University
58183 Linköping
SWEDEN
Email: bjorn.eriksson@liu.se

ABSTRACT

These days, energy efficient mobile fluid power systems are of great interest. A mobile system containing several different cylinder drives supplied with a single load sensing pump (LS-pump) has a number of advantages as well as disadvantages.

One of the main advantages is the need only one system pump. This makes the fluid power system compact and cost-effective. A challenge is to keep the hydraulic losses at a low level, especially losses at smaller loads.

This paper introduces a fail-safe proportional valve element that is based on the Valvistor poppet valve. Due to the demands of flexibility the poppet valve is bi-directional. The valve has an innovative hydro-mechanical layout that makes it fail-safe, unwanted lowering loads, for example, never occur.

The new valve includes simple sensors that are suitable for identification of mode switches, e.g. between normal, differential and regenerative modes. It is also possible to manoeuvre the system with maintained velocity control in the case of sensor failure.

In a less complex system the concept has benefits as well. For example in systems where fail-safe bi-directional on/off valve are needed, then without mode sensing capabilities.

KEYWORDS: fluid power, poppet valve, Valvistor, bi-directional, fail-safe

NOMENCLATURE

The quantities and subindexes used in this paper are listed in tables 1 and 2.

Table 1: Quantities

Quantity	Description	Unity
q	Flow	$\frac{\mathrm{m}^3}{\mathrm{s}}$
p	Pressure	Pa
C_q	Flow coefficient	–
w	Area gradient	m
ρ	Density	$\frac{\mathrm{kg}}{\mathrm{m}^3}$
F	Force	N
κ	Area ratio	–
A	Area	m^2
α	Angle	$^\circ$
ω_b	Break frequency	$\frac{\mathrm{rad}}{\mathrm{s}}$
g	Flow gain	–
K_C	Flow pressure coefficient	$\frac{\mathrm{m}^5}{\mathrm{Ns}}$

Table 2: Subindexes

Subindex	Description
m	Main stage
$m1$	Between compensator and pilot valve number 1
$m2$	Between compensator and pilot valve number 2
A	A-side of the Valvistor
B	B-side of the Valvistor
C	Chamber above the poppet in the Valvistor
p	Pilot
s	Slot in the poppet of the Valvistor
tot	Total
0	Initial
P	Pressure pin in the compensator
c	Compensator
$ideal$	Ideally

1 INTRODUCTION

These days, energy efficient mobile fluid power systems are of great interest. A mobile system containing several different cylinder drives supplied with a single LS-pump has a number of advantages as well as disadvantages.

One of the main advantages is the need for only one system pump. This makes the fluid power system compact and cost-effective. A challenge is to keep the hydraulic losses at a low level, especially losses at smaller loads.

Currently there are two main options to avoid these kinds of losses. Those are either supplying each cylinder from different dedicated pumps, or using hydraulic transformers with each cylinder together with one system pump. Both solutions entail undesired increased cost and more usage of space.

Another way to reduce the losses at small loads is to allow the cylinders to operate in differential and regenerative mode when possible. This solution implies a need for more flexible valves. The mechanical link between meter-in and meter-out has to be broken.

This paper proposes a valve, based on the Valvistor seat valve [1], that meets the flexible properties mentioned above. The proposed valve can be sized for a wide flow range that suits most mobile applications.

In a less complex system the concept has benefits as well. For example in systems where fail-safe bi-directional on/off valve are needed, then without mode sensing capabilities, see [2].

2 AIMS

The aim of this paper is to propose a design of a flexible, robust and fail-safe proportional bi-directional poppet valve. The valve has to be robust and fail-safe. Critical functions such as pressure compensation and load holding can not rely on sensors. Nonetheless, the valve must have good metering properties such as pressure-flow characteristics. It is desirable to have some sensors to be able to determine the operational conditions, especially pressure drop direction.

To make a valve system like this possible to produce, at a reasonable cost, it has to be modular. For instance, opportunities must exists to use the same pilot components for all or most valve sizes. The need for actuation force should be kept at a low level to minimize cost.

3 RELATED RESEARCH

There are several ongoing projects around the world in the area of split spool valves, for example Eatons Ultronics™ valve [3], and Huscos INCOVA® [4]. The Ultronics design uses fast high performance pilot operated spool valves. INCOVA consists of poppet valves.

The difference between these concepts lies mainly in the hardware layout. The Eatons Ultronics™ concept uses two three-way spool valves, that connect each cylinder chamber to pump line and tank. Huscos INCOVA® concept uses four independent two way poppet valves that connect each cylinder chamber to pump line and tank independently.

4 FAIL-SAFE

Mobile fluid power applications usually handle a large amount of energy. If something in such a system goes wrong, it will presumably cause considerable damage. This is one reason why a robust and fail-safe components are needed. When gaining flexibility through making valves bi-directional, there is a risk that new failure modes will be introduced, for

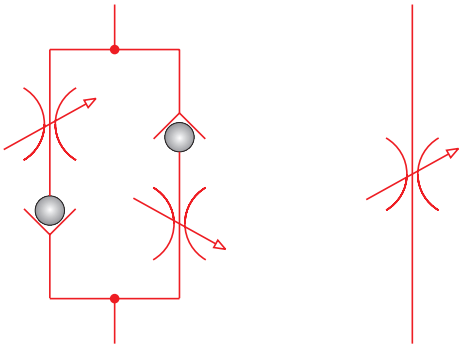

(a) The double pilot concept (b) A single valve concept

Figure 1: Schematic sketch of the Fail-safe properties of the valvistor valve

instance flow in an unwanted direction.

In order to produce a valve that never opens up for flow in the wrong direction, the one proposed here is equipped with two parallel pilot circuits, schematically shown in figure 1(a). If the aim is to achieve a flow from the B-side to the A-side in figure 2, then the right-hand pilot in figure 2 valve is used. However, if the pressure P_A is higher than the pressure P_B the result will be that the valve remains closed. This is important as a fail-safe feature.

In a mobile application, a telehandler for example, it is important to prevent falling loads. The schematic valve arrangements in figure 1 are assumed to be meter-in valves, flows upward in the figure. Suppose that the load will be lifted, flow upward in the figure. The left-hand valve in figure 1(a) is used. If the pressure drop is positive in the upward direction a flow will be obtained, otherwise the check valve will prevent a flow. The valve in figure 1(b) would have behaved in the same manner. But if the pressure drop had acted in the other direction, the load would have fallen to the ground. The valve in figure 1(b) is often used together with two pressure sensors to determine the pressure drop and thereby also the possible flow direction. The problem is that if some of the sensors fail, the application can be unpredictable. The demand for pressure sensor accuracy is considerably high. This is because of the wide range of operation. The sensors need to be able to measure pressures in the range of zero up to full system pressure; several mega pascals at the same time as the interesting pressure drop is just a few bars. This means that accuracy has to be extremely high, only a few fractions of a percent.

5 PILOT CIRCUIT

In most applications of a valve like this it would be of interest to have pressure compensation. Since the Valvistor valve amplifies the pilot flow it is favorably to pressure compensate the pilot valve. Through this arrangement the compensator can be kept small. One reason for keeping the compensation feature in the hardware is robustness. When using pressure sensors for pressure compensation the sensors need to be extremely accurate. This is because the system has to be able to measure a small pressure difference with two sensors that can manage a large pressure range, see section 4.

In this proposed valve, compensators are used instead of pressure sensors.

6 THE BI-DIRECTIONAL VALVISTOR

The Valvistor valve would be a suitable choice in a split spool concept. One of the benefits of the Valvistor valve is the high flow gain that can be obtained. To meet the flexibility requirement however the Valvistor valve needs to be bi-directional.

The traditional Valvistor concept is a proportional poppet valve in one direction and acts like a check valve in the other direction [1]. By modifying the original Valvistor concept according to figure 2, it becomes bi-directional and fail-safe, patent pending.

The modified Valvistor consists of a combination of the properties from an A-type and a B-type Valvistor. In an A-type Valvistor the slot in the main poppet connects the A-side with the chamber above the main poppet, in a B-type Valvistor the slot connects the B-side with the chamber above the main poppet; see [1] for more on A- and B-type Valvistor. To make this work it is necessary to add a shuttle valve, or two check valves, inside the main poppet that chooses the highest pressure of P_A and P_B.

If $P_B > P_A$ and the left pilot valve is operated in figure 2, nothing will happen. The valve then acts as a check valve and closes in the direction from A-side to B-side. On the other hand, if the right-hand pilot valve is actuated, flow will start from the B-side to the A-side. It works analogously in the other direction when $P_A > P_B$. This valve is an A-type and a B-type Valvistor at the same time. In one direction it is an A-type Valvistor and in the other direction a B-type.

Used in a system, this valve is not critically dependent on sensors, for instance drifting pressure sensors, to determine flow direction. This is due to the fact that the Valvistor valve is a proportional valve, but acts as a check-valve in the upstream direction. This avoids falling loads. The idea is to use sensors to add intelligence and performance but not reduce robustness and fail-safe properties. The fundamental, critical, function is not allowed to depend on sensors in this valve.

Using this modified Valvistor in a system means a considerable number of elements, in particular pilot valves. One aim of this paper is therefore to find a valve solution where the pilot actuators are independent of the flow capacity of valve. If the same pilot valve elements can be used in almost every size of the valve, it is possible to reduce the manufacturing costs the more that are produced.

To keep the basic functionality independent of sensors, the proposed valve solution must contain a hydraulic pressure compensation in the pilot circuit.

7 STATIC BEHAVIOR

The valve has almost the same properties in both flow directions. The difference is the leakage when the valve is closed. In the B-side to A-side flow direction it is leakage-free, a B-type Valvistor. In the A-side to the B-side flow direction there is a small leakage, an A-type Valvistor. There is one possible leakage path in the Valvistor valve, the clearance around the poppet.

When it comes to leakage the difference between the A- and B-type Valvistor is that in the A-type there is a pressure difference between the outlet, B-side, and the chamber above the poppet, and a leakage will occur in the clearance around the poppet. In the B-type case it is different; there is no pressure difference between the inlet, B-side, and the chamber above the poppet, and no leakage flow will be present in the clearance around the poppet.

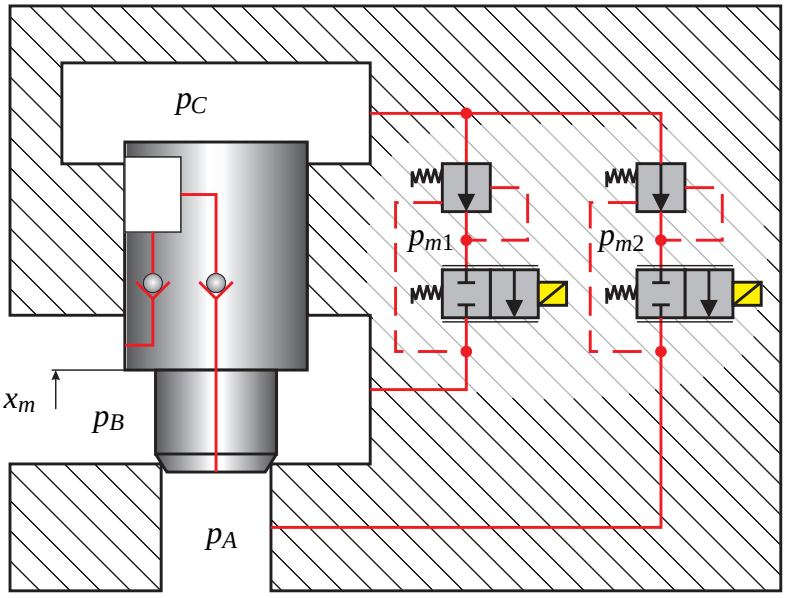

Figure 2: The modified bi-directional Valvistor valve

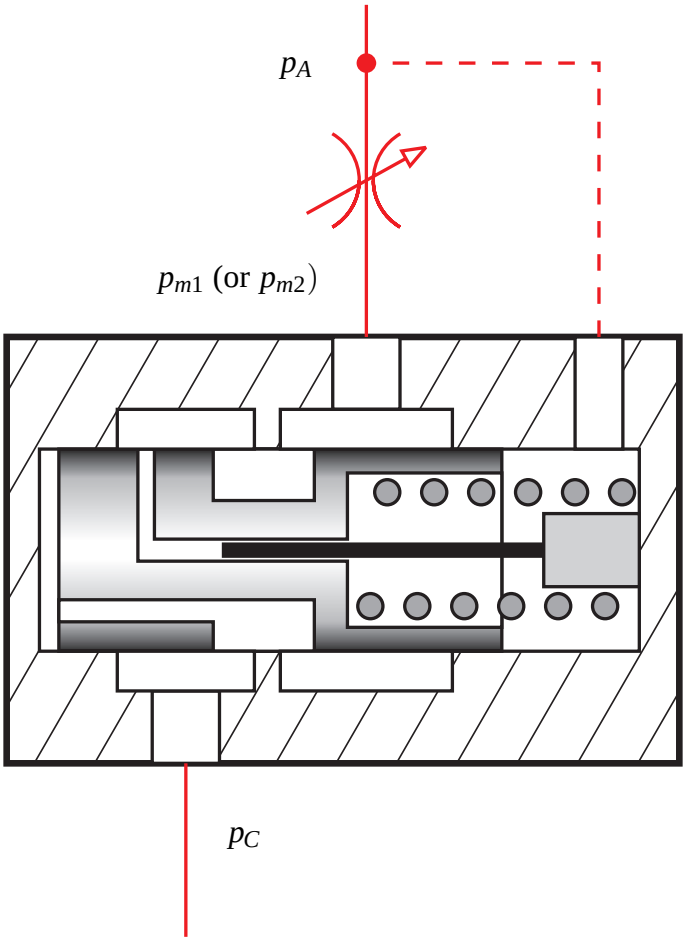

Figure 3: The compensator used in the pilot circuit. (observe the pin in the spool)

The static behavior of the valve is described by the equations below. The derivation of the equations used is shown in [5]. It is assumed that the pressure $p_B > p_A$. The right-hand pilot in figure 2 is used. The spring constant in the compensator is ignored.

$$q_m = C_q w_m x_m \sqrt{\frac{2}{\rho}(p_B - p_A)} \tag{1}$$

$$q_p = C_q w_p x_p \sqrt{\frac{2}{\rho}(p_{m2} - p_A)} \tag{2}$$

$$q_s = C_q w_s (x_m + x_{m0}) \sqrt{\frac{2}{\rho}(p_B - p_C)} \tag{3}$$

$$q_s = q_p \tag{4}$$

$$q_{tot} = q_p + q_m \tag{5}$$

$$A_m p_C + F_s = \kappa A_m p_B + (1-\kappa) A_m p_A \tag{6}$$

$$F_s = 2 C_q w_m x_m (p_B - p_A) \cos\alpha \tag{7}$$

$$A_C p_{m2} - p_C A_P - p_A (A_C - A_P) - F_0 = 0 \tag{8}$$

If the underlap, x_{m0}, and the flow force, F_s, are ignored the ideal flow gain is

$$g_{ideal} = \frac{q_{tot}}{q_p} = 1 + \frac{\frac{w_m}{w_s}}{\sqrt{1-\kappa}} \tag{9}$$

otherwise the gain is

$$\begin{aligned} g = \frac{q_{tot}}{q_p} &= 1 + \frac{\frac{w_m}{w_s}}{\sqrt{1-\kappa+\frac{F_s}{A_m(p_B-p_A)}}} - \frac{C_q w_m x_{m0}\sqrt{\frac{2}{\rho}(p_B-p_A)}}{q_p} \\ &\approx 1 + \frac{\frac{w_m}{w_s}}{\sqrt{1-\kappa}} - \frac{C_q w_m x_{m0}\sqrt{\frac{2}{\rho}(p_B-p_A)}}{q_p} \end{aligned} \tag{10}$$

The flow force can often be ignored, and the gain will thereby decrease when the pressure drop increases due to the underlap, the last term in equation (10).

Solving equations (1) to (8) gives the diagrams in figure 4. The underlap influences the flow gain in the valve, see equations (9) and (10). The flow pressure coefficient, $K_C = \frac{dq_{tot}}{d(p_B - p_A)}$, of the valve becomes negative when the pilot is ideally compensated and an underlap is present. Figure 4(c) shows the negative flow pressure coefficient, K_C, in the area where the compensator is active. It is possible to affect the flow characteristics using the pilot circuit. A compensated valve when an underlap is present can be archived by adding a pin that disturbs the pressure balance in the pilot compensator, see figures 3 and 4(a). The slope of the flow pressure characteristics in the pilot circuit is increased. The pin can be sized so that the K_C-value is always positive.

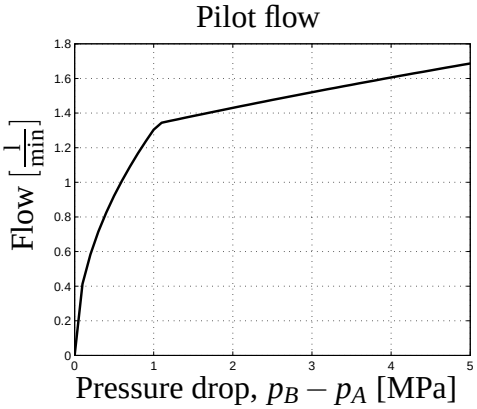

(a) Compensated pilot flow where pilot opening is held constant

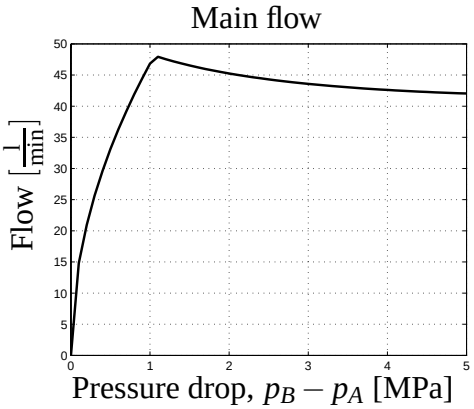

(b) Total flow, q_{tot}, through the valve with the pilot flow from figure 4(a)

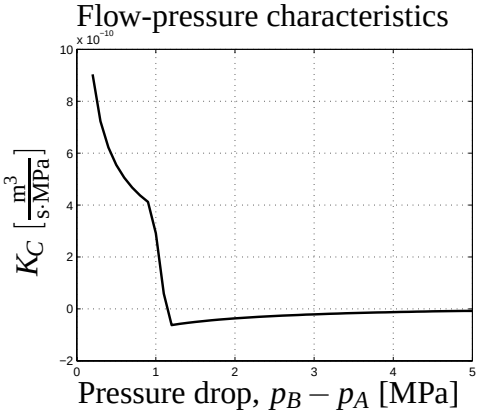

(c) Flow pressure coefficient for the complete valve

Figure 4: Flows and flow pressure coefficient as function of pressure drop

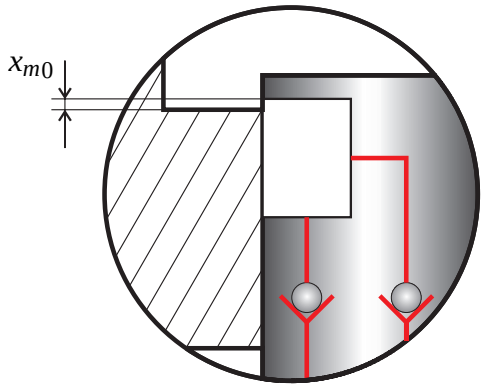

Figure 5: Underlap in the poppet

The main design parameters in the poppet concern the slot, primarily the width, which determines the flow gain, see section 7, and the underlap, which over-compensates the valve, see figures 5 and 4.

There are both dynamic and static aspects to consider when designing the slot in the poppet.

Statically

Flow gain The poppet design determines the flow gain of the valve, see equation (9).

Leakage properties When the pilot is closed the main poppet is also closed. A leakage in the pilot will be amplified and an unwanted valve opening will occur. An underlap prevents the main poppet from opening at small pilot flows, such as leakage.

Dynamically

Dynamic opening At a pressure increase and with no underlap the main poppet will dynamically open and compress the chamber volume above the main poppet. With an underlap the main poppet will stay closed since the chamber pressure will follow the changing pressure.

The mass of the poppet can be ignored dynamically due to the high actuation forces on the poppet. The area ratio (κ) of the poppet should be $\frac{1}{2}$, otherwise the properties become different in the two flow directions.

The slot in the poppet determines the flow gain of the valve, see equation (9), as well as the bandwidth of the valve. The bandwidth is proportional to the slot width, w_s, see equation (11). The influence of flow forces is ignored. [6]

$$\omega_b = \frac{C_q w_s}{A_m} \sqrt{\frac{2}{\rho} (1 - \kappa) (p_B - p_A)} \tag{11}$$

Consequently, the design of the slot is a trade-off between flow gain, bandwidth and dynamic properties in closed position.

When designing this kind of valve, there are often demands on both bandwidth and flow capacity at a desired pressure drop. The flow capacity demand determines the size of the main poppet area gradient, w_m. Together, the bandwidth demand and the chosen w_m determine the slot width from the flow gain equation (9). The pilot circuit can now be sized to match the slot orifice since the orifices ideally, ignoring flow forces, have the same pressure drop and the same flow.

Most applications are constituted such that the bandwidth demand decreases when the flow demand increases. This fact fits the valve design. It is a fact that low inertia loads demand high bandwidth. This is often the case for partial loads in a mobile system, not the highest load in the system. The pressure drop is then high and the bandwidth thus also high, see equation (11).

9 CONCLUSIONS

This paper proposes an alternative bi-directional design of an existing valve, the Valvistor valve. The valve can be used in a flexible complex system in a fail-safe manner because of the arrangement of the double check valves inside the poppet and the double pilot circuits. It can be designed for a high range of flows due to high flow gain capabilities.

The valve seems to have good metering properties which can be adjusted by modifying the unbalance pin in the compensators.

The fundamental properties of the valve, such as flow gain and bandwidth, allow the same pilot valves to be used in a wide range of flow capacities of the main valve.

Actuation forces of the pilot valve can be kept small because of the pressure compensator in the pilot circuit and the fact that the valve allows a high flow gain and therefore a relatively small pilot flow due to the total flow.

REFERENCES

[1] Bo R. Andersson. *On the Valvistor, a proportionally controlled seat valve*. PhD thesis, LiTH, 1984. ISBN 91-7372-748-2.

[2] K. Heybroek, J. Larsson, and J-O. Palmberg. Mode switching and energy recuperation in open-circuit pump control. In *The Tenth Scandinavian International Conference on Fluid Power*, 2007.

[3] Stephen Brian Turner and David Franz Lakin. Electrohydraulic proportional control valve assemblies. European Patent, 1997. EP 0 809 737.

[4] Keith A. Tabor. A novel method of controlling a hydraulic actuator with four independent metering using load feedback. SAE, 2005.

[5] Herbert E. Merritt. *Hydraulic Control Systems*. John Wiley & Sons, New York, 1967. ISBN 0-471-59617-5.

[6] B. Eriksson, B. Andersson, and J-O. Palmberg. The dynamic properties of a poppet type hydraulic flow amplifier. In *The Tenth Scandinavian International Conference on Fluid Power*, 2007.

EFFECTS OF TEMPERATURE ON PROPORTIONAL VALVE DYNAMICS AND RELIABILITY

Henri Hänninen, Heikki Kauranne and Matti Pietola
Helsinki University of Technology
Faculty of Mechanical Engineering
Department of Machine Design
P.O. Box 4400
FIN-02015 TKK
FINLAND
Phone +358 9 451 2860, Fax +358 9 451 3986
E-mail Henri.Hanninen@tkk.fi

ABSTRACT

In this article, two proportional pressure control valves are studied in terms of temperature dependencies in their performance and reliability. The valves used in this study are both directly operated, spool type proportional valves of nominal size 6. These mechanically almost identical valves differ from each other by their electronics. One of the valves is equipped with traditional analogical electronics and the other with digital electronics. Both of the valves can be controlled with analogical signals and in addition the one with digital electronics can be controlled, set up and monitored with dedicated software via CAN interface. The valves are tested under different ambient temperatures and results from measurements are analyzed. In addition to finding out their behavior in high temperatures the results of these tests were hoped to show some pre fault indicator for the valves.

Both of the valves were found to exhibit negligible change in dynamics under thermal load. They were also found to be extremely reliable even in high temperatures: neither of the valves was permanently damaged during the tests. Even though the highest test temperatures were higher than in the real system, the duration of the tests however was relatively short compared to the time span in which the valves have been found to break. This means that the mechanism that leads to failure is most likely not so dependant of maximum temperature than long exposures to relatively high temperatures.

KEYWORDS: Proportional valve, electronics, temperature, performance, reliability

1 INTRODUCTION

Striving for higher levels of machine performance and economic efficiency necessitates better controllability, reliability and operation predictability of machines. This in turn calls for a system that monitors the machine and its subsystems and components and either simply reports the machine operator the changes in the behavior of the machine or in addition to this produces information to be used in the control of the machine in order to maintain the demanded quality of end-product. At least in latter case the monitoring should be continuous and done on-line.

This type of system, a condition monitoring system, presumes that the monitored systems or components are equipped with appropriate monitoring instruments capable to detect the changes in monitored quantities within the scale and resolution that are essential for keeping up the quality of operation. The monitored quantity should be selected to be the one that best represents the systems or components operation or output although this is not always possible and some other quantity or group of quantities must be used.

Besides monitoring the general operation of components or systems the condition monitoring data can be used for identifying the type of fault and predicting the remaining operating life of a component. However this calls for knowledge of at least the most common faults or damages and their propagation mechanisms and access to models depicting the characteristics of these. The model can simply be based on empirical knowledge of time dependency of fault propagation under certain operational conditions or in more advanced cases the model is actually able to depict the propagation of fault, e.g., the abrasive effect of fluid on valve spool.

Basic requirement in achieving all this is that the components to be monitored are equipped with relevant monitoring instruments or transducers that supervise the essential quantities. In fluid power this is being promoted by the tendency of integrating the control and support electronics into components which also enables easy integrating of different transducers into them. These are typically used for control purposes but can also be used for condition monitoring. This possibility is even more encouraged by introduction of digital electronics and its signal processing capabilities.

Incorporating electronics into components makes them more convenient to use since no additional housing for the electronics needs more to be provided. However this comes with drawbacks because the electronics is exposed to the same environment as the fluid power component. Electronics has to be placed into a closed housing in order to protect it from dirt and spillage which eliminates the possibility to accurately control the temperature of the electronics. In some applications the temperature may rise to levels that can be harmful and in industry long time exposure to high operating temperatures has been reported to cause altered characteristics of electronics or even malfunctions incurring costly downtime of machines.

Most of the studies concerning valve faults or condition monitoring have been directed to investigating the effects of fluid impurities on the mechanical parts of the valves [1-3]. If the valve is operated in environment where the impurity concentration of the fluid is kept low, but the other environmental loading is not controlled the most common failure mechanism is not necessarily mechanic. In this study the focus is set on finding out the effects of environment temperature on onboard electronics of valves.

2 MEASUREMENT SYSTEM AND METHODS

The measurements were done in a test bench that is schematically presented in Fig. 1. The studied valve is marked with number (1), pump and motor with (2), pressure relief valve which is used to set the pressure level for the P-port of the studied valve with number (3) and throttle valve with (4)

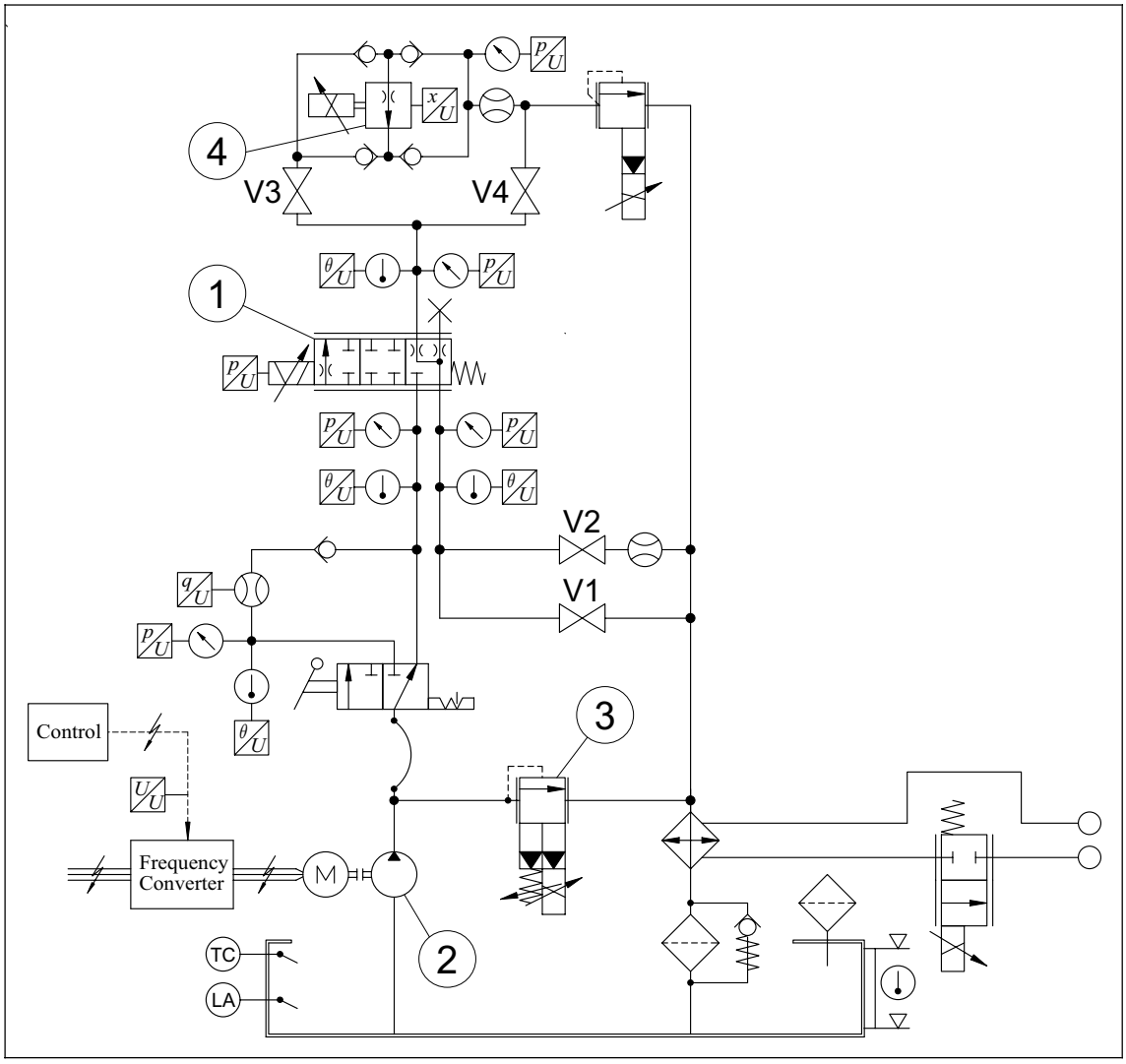

Figure 1. The fluid power circuit used in the measurements; 1) studied valve, (2) pump and motor, (3) throttle valve and (4) pressure relief valve

The studied valves are both directly operated, spool type proportional pressure control valves of nominal size 6. Basic properties of these valves are presented in Table 1. The main difference between these valves is the type of their amplifying and control electronics. D635, which is fitted with analog electronics, has only a few adjustable parameters (adjustment is made with potentiometers). In D638, however, almost every possible parameter can be adjusted. This is done via CAN-interface with designated software.

Table 1. Basic properties of studied valves [4,5]

	Moog D635	Moog D638
Valve type	Pressure control	Pressure control, flow control
Pressure range [bar]	0 - 105	0 - 110
Amplifying and control electronics	Analog	Digital
Interfaces	7-pin connector	7-pin connector, CAN
Transducers	Pressure	Pressure, LVDT
Maximum operating temperature [° C]	60	60

The measurements were made with NI PCI-6031E measurement board utilizing DASYLab-measurement software which was also used for timing and controlling the function generator that was used for control signal generation.

For the measurement of ambient temperatures of the electronics, three temperature sensors were installed in the electronics boxes of the valves. In addition one sensor was attached just outside the boxes for measuring the outside temperature of the valves. The placement of the sensors for both valves is presented in Fig. 2.

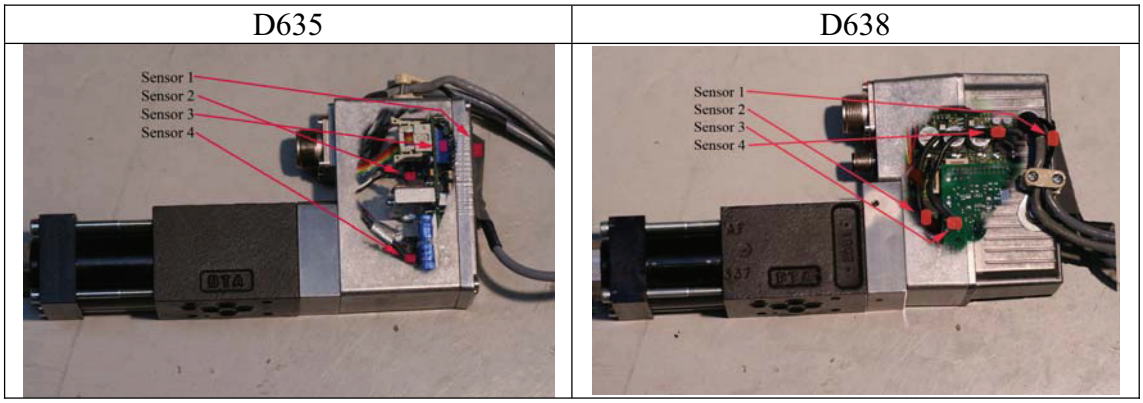

Figure 2. Temperature sensor placement for valves D635 and D638

Dynamic performance tests consisted of step and frequency response tests. The step response tests were conducted using three step sizes which are presented in Table 2.

Table 2. Pressure command signals for dynamic tests

	Pressure commands	
	Step response	Frequency response
Signal type	Rectangular wave	Sine sweep
Command: Test 1	2,5 - 97,5 -2,5	2,5 - 97,5
Command: Test 2	2,5 - 50 - 2,5	77,5 - 82,5
Command: Test 3	2,5 - 25 - 2,5	47,5 - 52,5

In frequency response tests the control input to valve was linear sine sweep. The sweep ranged from 0 to 40 Hz for valve D635 and from 0 to 60 Hz for D638. The larger frequency range for D638 was needed because of the better performance of valve D638. For both of the sweep ranges, duration of sweeps was set to 60 seconds.

The tests were conducted in seven different ambient temperatures of the valve electronics. The lowest temperature was made in room temperature, that is, no additional heating of the valves was used. Without additional heating the temperature of electronics rose approximately to 50 °C. The higher test temperatures were in increments of 10 °C, highest being 110 °C.

The measured signals were found to be superimposed by significant interference noise stemming from frequency converter controlling the motor which drives the pump of the test system and also switching power supply that was used as valves power source. To reduce this noise all of converters cables were changed to ones with better electrical insulations. This operation reduced the noise amplitude vice to a third compared to the previous cabling. In addition small capacitors were connected to ground in parallel to signal lines of pressure command and measured pressure. Their capacitances were selected so that they would filter high frequency noise as much as possible, still leaving real signal unaltered.

In addition to the electrical interference also the inherent properties of the hydraulic circuit induced in some cases oscillations in to the system. The effect of these was especially noticeable in frequency response measurements. The vibrations were found to be very sensitive to the settings of throttle valve (Fig. 1, number 4). In order to maintain the consistensy throughout the measurements only extremely small alterations of its settings were allovable. In most cases this was still enough to remove the oscillations.

To further combat these issues and increase the reliability of the results, all of the measurements were repeated ten times. The final responses to be analysed were calculated as averages of these. The total number of measurements in both step and frequency responses is hence 210 (3*7*10) per valve.

For measuring electrical power consumption of the studied valves, a small auxiliary circuit was build. The state of the valve that is the pressure setting of the valve was found to be observable via consumption of power but only if the ratio of change in pressure value was not too fast. This was because the power consumption signal needed to some extent averaging due to fast fluctuation of valves input current. Power consumption averages were measured during all performance tests.

3 RESULTS OF STEP AND FREQUENCY RESPONSE TESTS

In this chapter are presented the results of dynamic performance tests in seven different ambient temperatures of the valve electronics box. In addition, electrical power consumption averages for all measurement types are also presented.

3.1 Step Response

Measured step responses are presented for valve D635 in Fig. 3. The step response graphs are divided into graphs of rising and falling edges. It should be noticed that in Fig. 3 f) the time axis differs from the other falling edge subfigures. This is due to overshooting and long settling time of the measured signals.

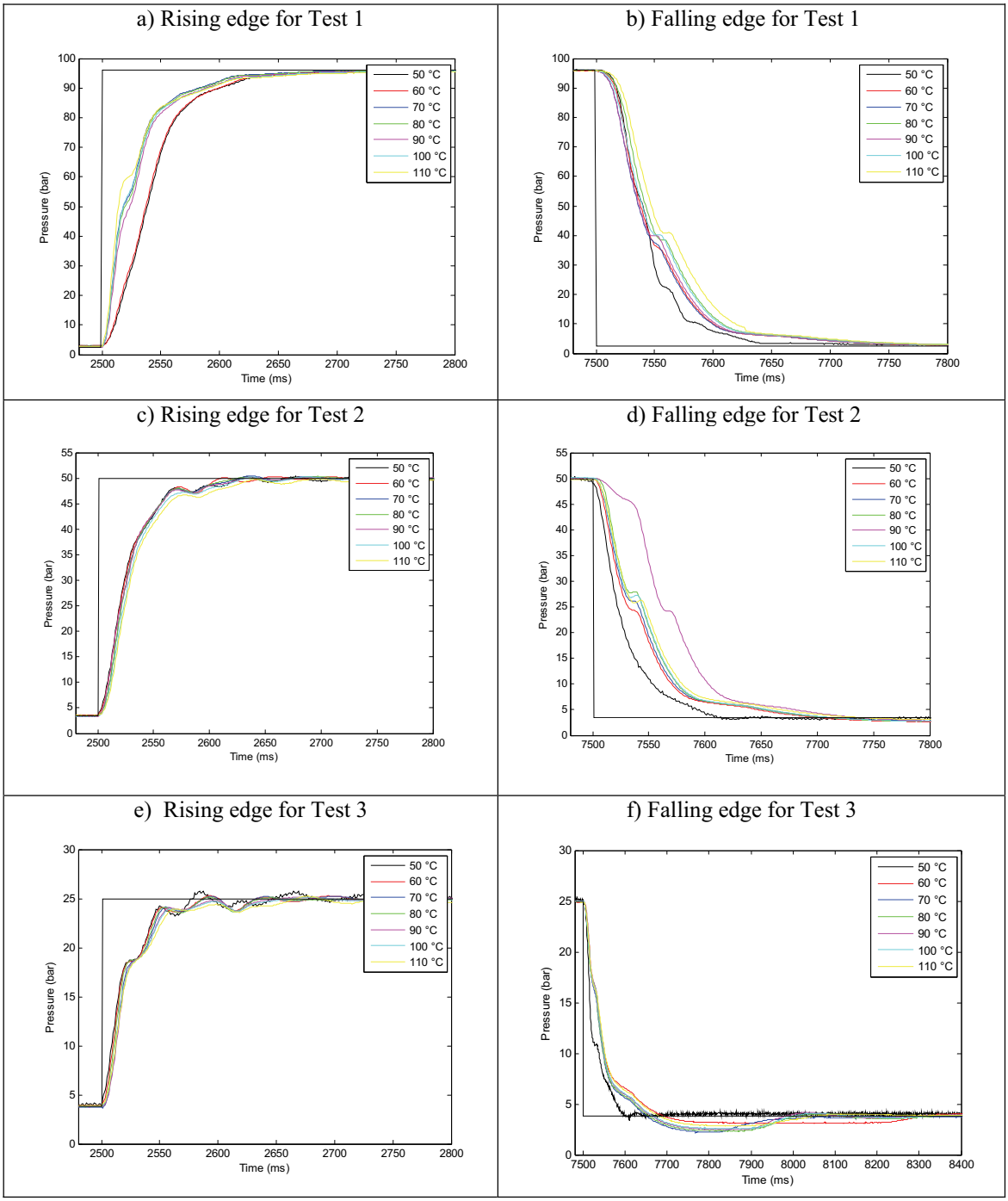

Figure 3. Step response graphs for valve D635

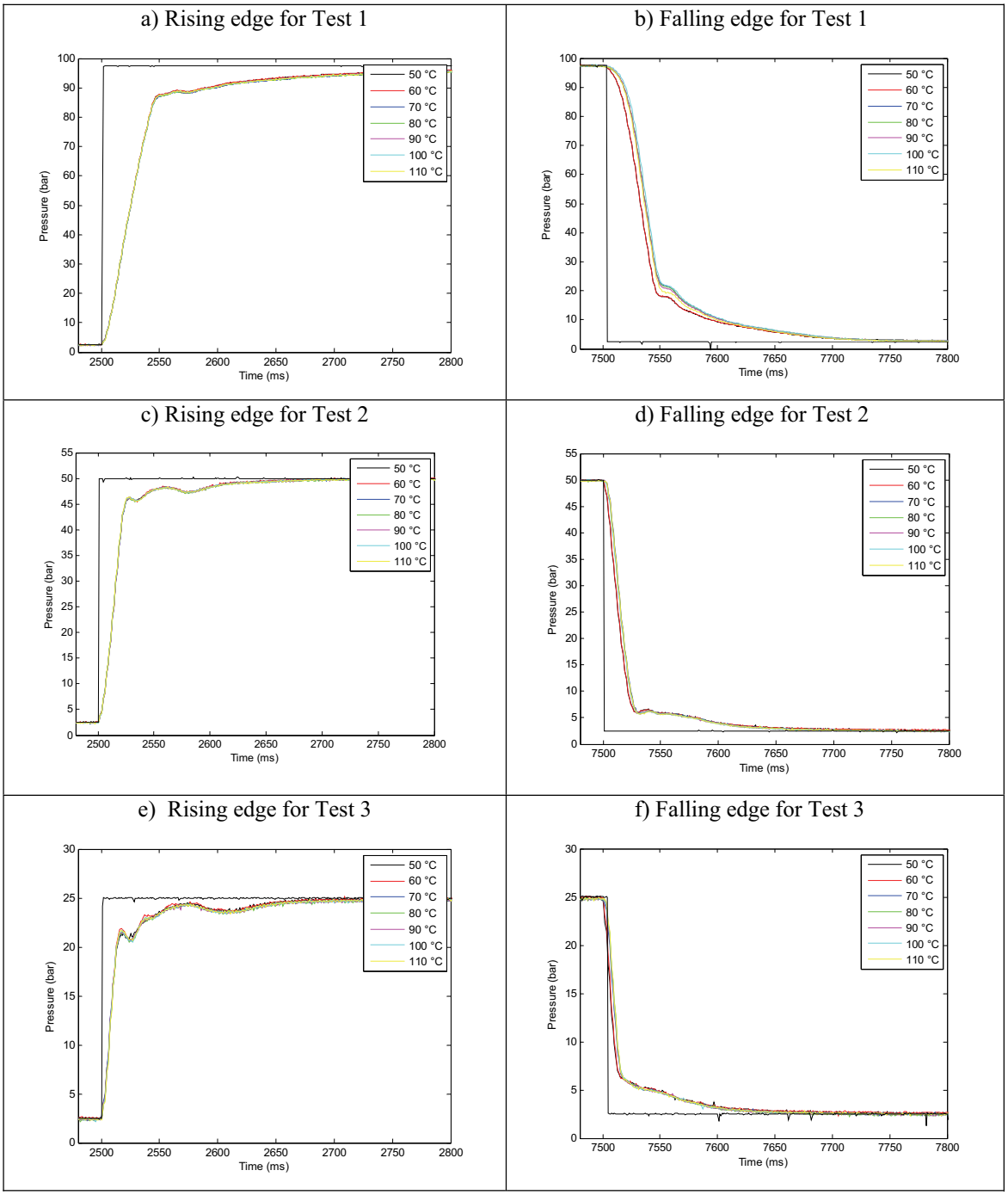

Figure 4. Step response graphs for valve D638

Figure 4 presents the corresponding responses for valve D638. This valve seems to be faster and less prone to vibration. Also the tendency for overshooting which was observed for D635 in some cases is nonexistent for D638.

3.2 Frequency Response

Measured frequency responses are presented for valves D635 and D638 in Figs. 5 and 6 respectively.

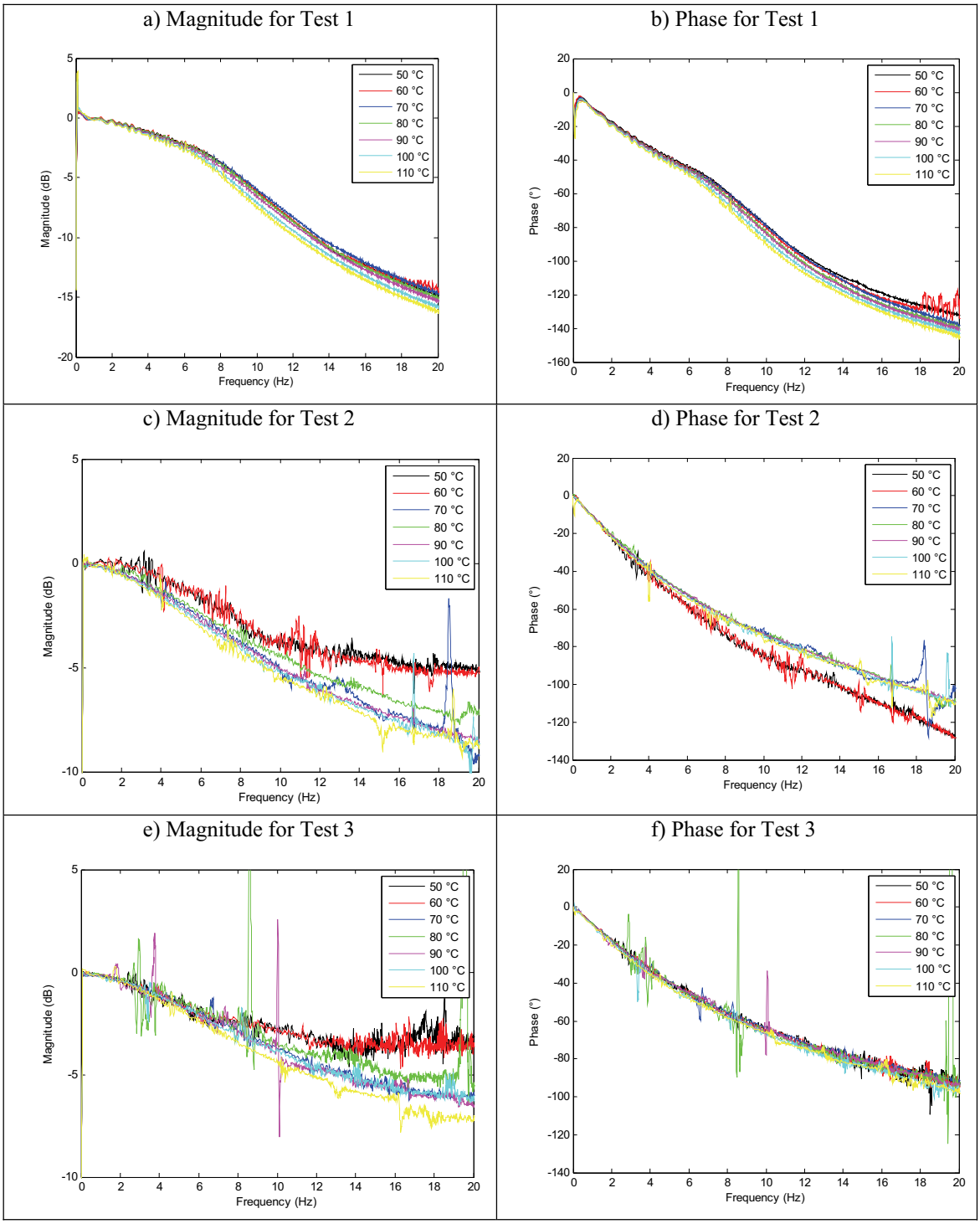

Figure 5. Frequency response graphs for valve D635

In the frequency response graphs with smaller amplitude input signal (tests 2 and 3) the electrical interference of the measurement system is clearly visible due to higher signal to noise ratio than in test 1.

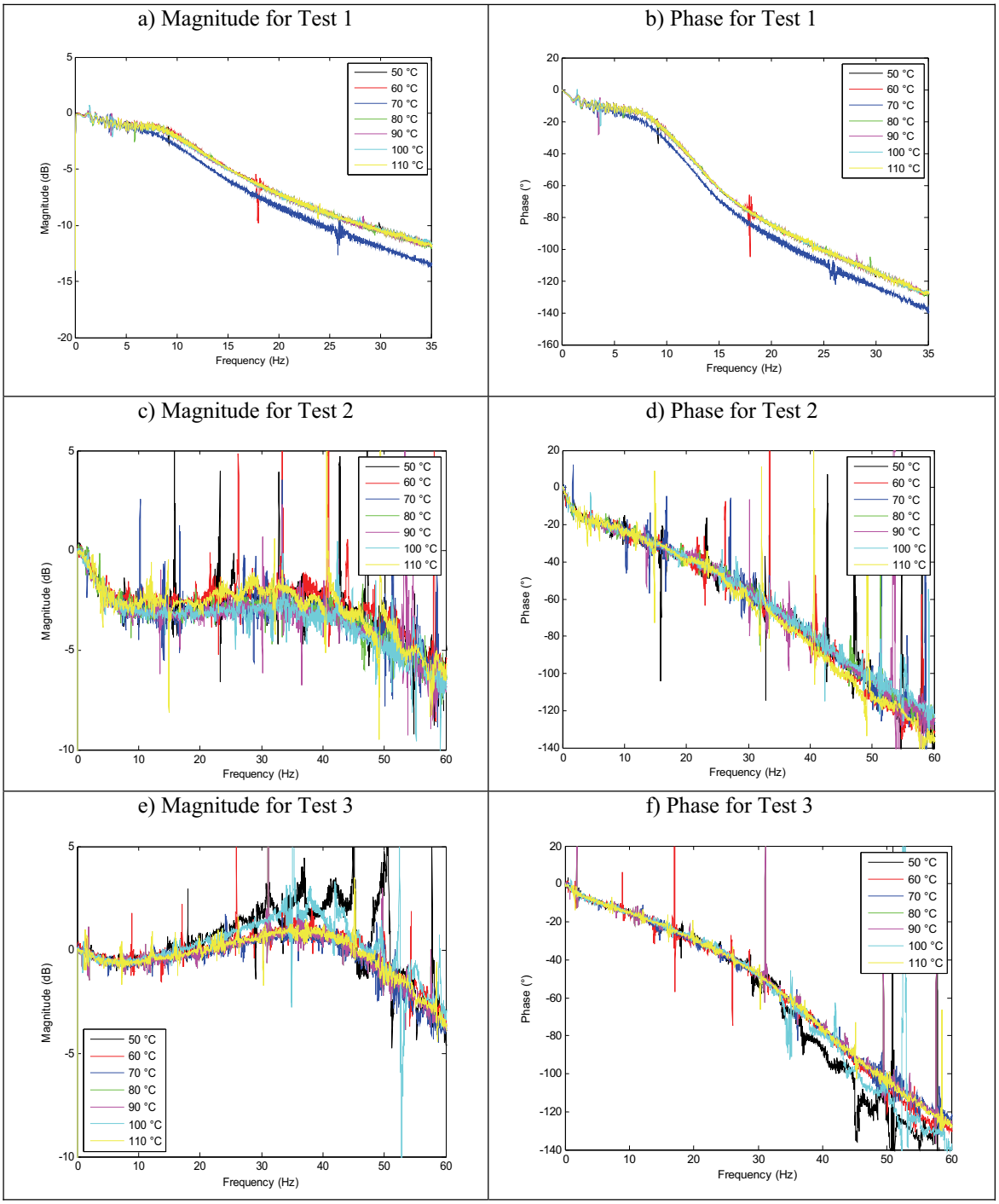

Figure 6. Frequency response graphs for valve D638

3.3 Power Consumption

Averages of electrical power consumption of the valves during performance tests are presented in Figs. 7 and 8.

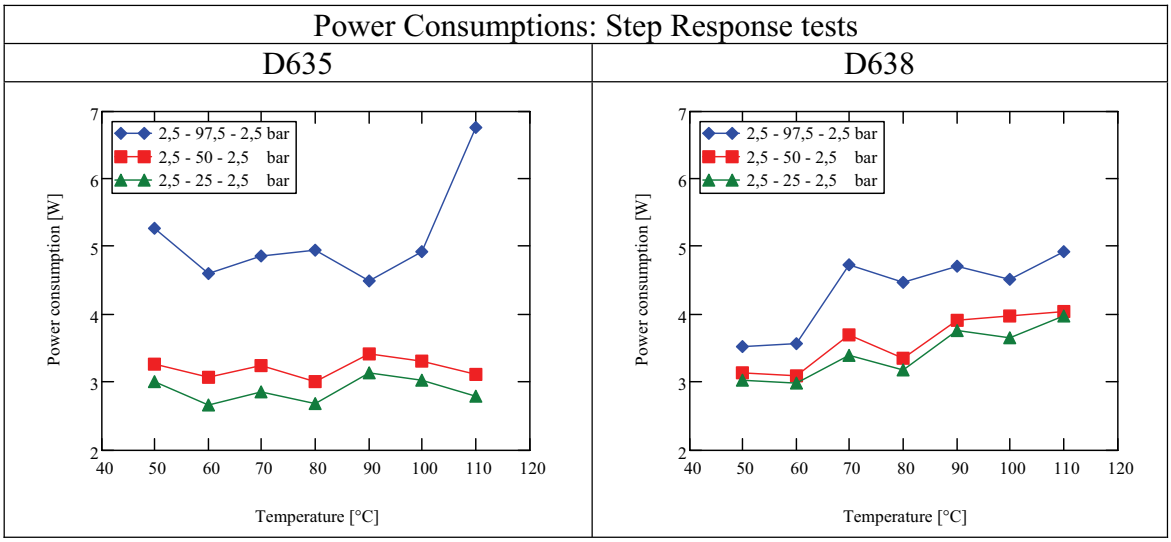

Figure 7. Power consumption averages for valves D635 and D638 in step response tests

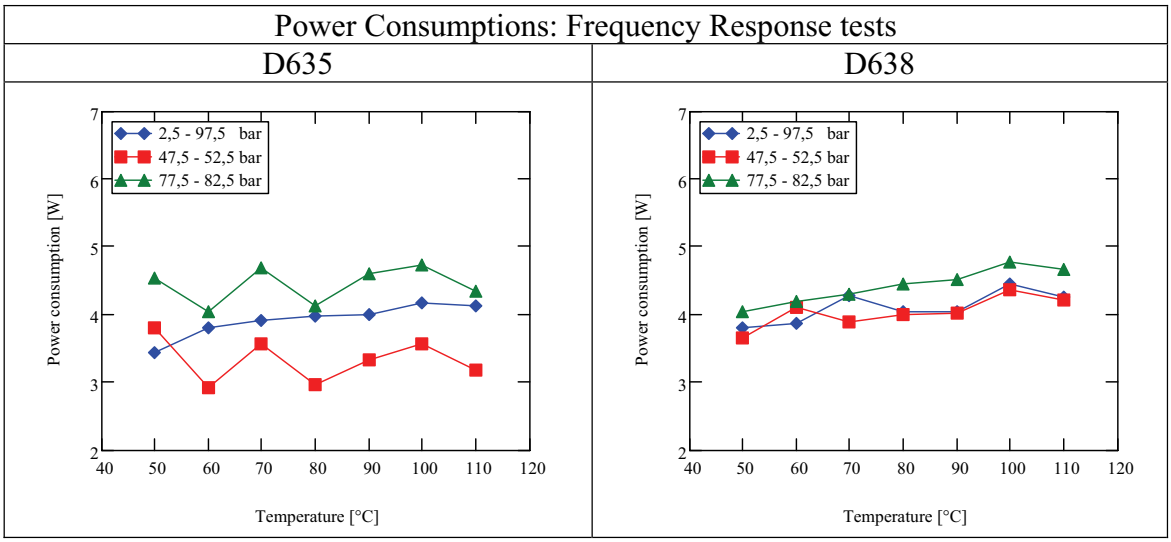

Figure 8. Power consumption averages for valves D635 and D638 in frequency response tests

4 DISCUSSION

In general the measurements demonstrated that the valve dynamics had only minor or nonexistent correlation with ambient temperature. In step responses (Figs. 3 and 4) the largest variations in characteristics between different temperatures appear with valve equipped with analog electronics (D635) while the valve with digital electronics (D638) seems to be insensitive to temperature. The variations of step characteristics with D635

are however not largely coherent with temperature but it seems that at the lowest measured temperature (50 °C) the valve is slightly faster although the difference between this and the results of other temperatures is minor and at higher temperatures the responses are practically identical.

The frequency responses (Figs. 5 and 6) demonstrated quite similar results as step responses. The most significant differences are again occurring with valve equipped with analog electronics (D635) while the valve equipped with digital electronics (D638) is again virtually insensitive to ambient temperature. At smaller signal amplitudes the disturbances of power electronics on measured signals become significant but the main line of valve behavior is still interpretable. The dynamic characteristics of D635 appear to somewhat deteriorate with rising ambient temperature the change in -3 dB boundary frequency being of magnitude of 1–3 Hz depending on the command amplitude.

Even though the differences between the dynamic characteristics of the valves are minor, some are still notable. The dependence on ambient temperature is smaller with the valve equipped with digital electronics (D638) and the dynamic performance of this valve is far better over the valve equipped with analog electronics. The reasons for these are probably better implemented temperature compensation of electronics and the possibility to easily adjust the values of operating parameters to optimal. In addition, from the condition monitoring point of view the digital electronics and communication via CAN bus enables ease transmission of monitoring data from the valve to a monitoring unit. So far the valves resources are somewhat limited in control monitoring sense stemming from the fact that the aspect of condition monitoring has not been taken into account in the overall design of the valve. This includes for example the types of integrated transducers and less condition monitoring friendly software. These features should be easy to add/enhance in future.

On contrast to the better dynamic characteristics the power consumption of the valve equipped with digital electronics (D638) proved to be somewhat higher and more temperature sensitive compared with its analogical counterpart (D635). The D635 seems to be insensitive to ambient temperature and only at highest amplitude of frequency tests there exists minor but clear dependency between power consumption and ambient temperature. The D638 instead shows clear temperature dependency at every step and frequency response. In step responses the power consumption is also clearly dependent on the step magnitude while in frequency responses the power consumption is more or less inversely dependent on amplitude size.

Our assumption is that major part of the noted power consumption behavior of the valves is due to the method of implementation of temperature compensation. In the valve equipped with analog electronics (D635), the compensation is probably realized using NTC-resistors. This would explain the fact that the power consumption is not temperature dependent. On the other hand in the valve equipped with digital electronics (D638) the compensation is probably implemented using integrated temperature sensor which explains the slight increase in power consumption.

The measurement of the power consumption of valves was found to be efficient for detecting states that the valves were unable to reach. These include for example the jamming of valve spool or unexpectedly high flow need (leakage) on the controlled side.
The tests made demonstrated that the ambient temperature had no clear immediate effect on valve electronics and operation in cases where the operational electronics was

exposed to short-timed high temperatures even though the highest temperatures exceeded the maximum values recommended by valve manufacturer by 80 %. Nor did the valves exhibit any faults or failures during the tests. So the findings of this study did not correspond to the findings made in industry. Had the exposure times been longer, e.g., months instead of a week, it is possible or even probable that the differences in dynamic responses between different ambient temperatures would have been greater. It is also possible that thermal load is not the only reason for malfunction of electronics but that the reason is combined thermal and mechanical loading, i.e. vibration. Outlining this would however have required much longer test times and greater quantity of test valves which was not possible at this time.

The general trend in electronics, e.g. in mobile phones and entertainment electronics, is to reduce component sizes and increase packing density. This has created a growing need to study the effect of temperature on electronic components [6] and their failure mechanisms [7]. However, the results of these studies are usually application specific and can not be generalized to point out the most failure prone components. Yet, some typical components susceptible to temperature originating failures are electrolytic capacitors and IC components. It must be noted that decreasing component sizes makes them also more prone to contributory factors for failure such as vibration and electrostatic discharge (ESD).

5 CONCLUSIONS

The ambient temperature was found to have little effects on the performance of the valves in general and even more so for valve with digital amplifying and control electronics (D638). The valve with analog electronics exhibited some minor variations in performance but they were inconsistent, that is variations in one test were not present in another. The overall performance of D638 was well above the performance of D635 regardless the temperature.

The power consumption of D638 was found to be slightly higher than its analog counterpart D635. This feature was also found to be more temperature sensitive with D638, while the D635 seemed to be insensitive to ambient temperature and only at highest amplitude of frequency tests there existed minor but clear dependency between power consumption and ambient temperature.

The valves did not exhibit any fault or failures during the tests even though the highest ambient test temperatures well exceeded the highest recommended operating temperatures. This implies that the observed electronic failures are driven by a fault mechanism that is not so dependant of extremely high temperatures than longer exposures to relatively high temperatures.

ACKNOWLEDGEMENTS

This article was made in the research project that was funded by the National Technology Agency of Finland and Finnish industry.

REFERENCES

1. *Laitinen Lauri. Hydraulitekniikan kunnonvalvonnan State of the Art. Venttiilit ja epäpuhtaudet. Espoo: Teknillisen korkeakoulun Koneensuunnittelun julkaisuja, 2003. 42 s. [Condition monitoring in Fluid Power – State of the Art, In Finnish]*

2. *Laitinen Lauri. Effect of Contamination on Wear of Proportional Control Valves. The Ninth Scandinavian International Conference on Fluid Power, SICFP ´05, June 1-3, 2005 Linköping, Sweden*

3. *Laitinen Lauri. Aging-dependent characteristic changes of a pressure control valve for a model-based condition monitoring in fluid power. Bath Workshop on Power Transmission & Control, PTMC 2004, 1-3 September 2004. p. 285-295.*

4. *Moog Pressure Control Valve With Integrated Electronics Cetop 3 Series D 635. Datasheet. Böblingen: Moog GmbH, 1999. 8 s.*

5. *D 636/D 638 Series. Direct Drive Servo-Proportional Valves with Integrated Digital Electronics and CAN BusInterface. Operating Instructions. Böblingen: Moog GmbH, 2002. 65 s.*

6. *Lenkeri Jaakko, Majamaa Tero, Jaakola Tuomo, Karppinen Mikko, Kololuoma Tero. Tulevaisuuden elektroniikan pakkaus- ja komponenttitekniikat. VTT tiedotteita 2213. Espoo, Oulu:VTT,2003. 86 s.*

7. *Lall Pradeep, Pecht Michael, Hakim Edward. Influence of Temperature on Microelectronics and System Reliability:A Physics of Failure Approach. New York: CRC Press, 1997.307 s.*

MINIATURIZED BISTABLE SEAT VALVE

Jukka-Pekka Uusitalo*, Timo Lauttamus**, Matti Linjama**, Lasse Söderlund*, Matti Vilenius**, Lauri Kettunen*

*Institute of Electromagnetics
Tampere University of Technology
P.O.Box 692, FI-33101 Tampere, Finland
Tel: +358 3 3115 11, Fax: +358 3 3115 2160

**Institute of Hydraulics and Automation
Tampere University of Technology
P.O.Box 589, FI-33101 Tampere, Finland
Tel: +358 3 3115 11, Fax: +358 3 3115 2240

ABSTRACT

To make digital hydraulic systems competitive the volume of existing solenoid valves should be reduced to about a half. Thus, the development of a small, fast and low power on/off valve is one of the key issues in modern digital hydraulics. So far, digital hydraulic systems have been implemented using traditional solenoid valves which are in general big and slow. A particular problem with seat valves has been the spontaneous closing due to pressure difference over the opened valve. In this work, a new seat valve design using several restrictions and bistable electromagnetic actuator is described. Hydraulic and electromagnetic parts have been designed together in order to minimize the size of the valve. The electromagnetic actuator uses permanent magnets to achieve bistable properties, which means work is needed only to change valve state. The valve as a whole is designed using results from both hydraulic and electromagnetic computations. The valve actuator is modelled using CEM and the hydraulic part of the valve is modelled using CFD. Experimental results include the properties of the actuator and the valve. Results show significant reduction in volume and response times.

KEYWORDS: fast valve, small valve, electromagnetic actuator

1 INTRODUCTION

The traditionally used on/off solenoid valves are big, slow and they consume a lot of power. Therefore, there is a need for a smaller, faster and power saving application.

An on/off valve means a binary controlled valve in this context. One of the biggest problems with the traditional solenoids is the need for a constant current to maintain one of the two positions. This is due to both the hydraulic properties of the traditional seat valve and the monostable properties of the traditional solenoid-spring combination. The problem with the hydraulic properties, the spontaneous closing in high flow rates, has been lately solved using several restrictions in the hydraulic part [1]. Another problem with the traditional on/off seat valves has been the unoptimized use of space. The hydraulic and electromagnetic parts are distinct leading to a non-integrated device.

The aim of this study is to develop a fast, energy saving and small on/off seat valve using the several restrictions method. About 50% reduction in volume would make digital hydraulic valve packages small enough to be implemented to commercial solutions [2]. Permanent magnets provide bistable properties and high energy density which among the several restrictions method help in achieving the goals. Bistable systems have been implemented among others in mechanics, hydraulics and electromagnetics. A microhinge [3] and an elastic beam [4] are examples of mechanical bistability. In hydraulics, the bistability of the system depends often on the flow rate. Electromagnetic bistability has been implemented widely. The following papers [5], [6], [7] include electromagnetic actuators and/or digital latches that are examples of bistable electromagnetic systems using permanent magnets. In Sturman digital latching valve [8] both electromagnetic and hydraulic parts are optimized and highly integrated.

2 BASICS OF MAGNETIC FORCES

Magnetic forces are about interactions between macroscopic and microscopic currents. The current of a coil is of macroscopic nature, and the atomic scale currents which cause the magnetic properties of the iron parts of a valve are about microscopic ones. Whatever currents are in case, the elementary idea is that the biggest forces are observed when the magnetic flux density B is perpendicular to the currents.

Now, in case of a valve actuator the goal is to generate as large force to the armature as possible. For this one needs a "source" B-field, which in our case is generated by permanent magnets. The permanent magnets cause the armature to stay either in opened or closed position. To move the armature to the other position, the actuator has also a coil which generates another component to the B-field. The remaining task is to find a design with minimal volume such that the forces generated are big enough to make the armature to move between the open and close position.

In this process the basic idea of having B perpendicular to current density J is crucial. That is, if the magnetic properties of the permanent magnet are represented by so called equivalent magnetization currents, then all one needs to do is to find a shape for the magnetic circuit which optimizes the perpendicularity between B and J. The rest of the design relies on standard techniques. Once the underlying second order boundary value problem is numerically solved, forces can be rather easily evaluated e.g. by integrating the so called Maxwell stress tensor (MST) over the armature.

3 TECHNICAL DESIGN

The actuator of a valve needs to produce a certain amount of force for a certain amount of time to create enough linear momentum to get the flow channel of the valve opened. In the case of an electromagnetic actuator, the force is directly proportional to the magnetomotive force of the coil and it is defined as the number rounds in the coil (N) times the current of the coil (I). Among the maximum force an electromagnetic actuator can provide, another important question is how fast the force can be provided. The basic rule in coils is: the bigger the slower. Also, the smaller the coil is, the bigger are the currents and the temperatures inside the coil. Therefore, if a smaller rms-current can be applied it leads to power saving and smaller and faster coil.

Monostable systems need external energy in order to maintain one of the two positions. In the case of an on/off solenoid valve, a spring holds the armature in one position and the electromagnetic force using constant power holds it in the other one. If the system spends a lot of time in the latter position, it consumes a lot of power.

Bistable electromagnetic actuators need to produce the same maximum force as the monostable actuators, but the force is needed only transiently, that is, as long as the armature of the valve is changing its position. Therefore, bistable actuators need less rms-power resulting to smaller and faster coils, at least in low-frequency range.

The idea of the valve design is to reduce power consumption and decrease volume by using bistable behaviour and integrated design of the valve. Bistability is achieved with permanent magnets with the help of the method of several restrictions. If there is a pressure difference over the valve, the use of the several restrictions method causes the armature to have a closing hydraulic force when placed in closed position and an opening hydraulic force in opened position. The volume of the valve is also minimized by placing the electromagnetic and hydraulic parts within each other resulting in an integrated device.

The permanent magnets can be placed in many ways to the body of the valve. If an armature made of ferromagnetic material is used, the permanent magnets can be placed in two different positions according to figure 1. If the permanent magnet is attached to the armature, there are fewer components in the valve and the used volume decreases. The actuator uses two coils for further optimization of the volume and force. The two coils push and pull the permanent magnet in turns during the displacement procedure depending on the direction of the movement. Using two coils the magnetized circuit will be best optimized. In the outer part of the magnetic circuit the magnetic flux is driven through two paths instead of just one as in traditional solenoids. This means that the outer magnetic circuit needs 50% less material. The two possibilities with the permanent magnet attached to the armature are shown in figure 2.

When designing the electromagnetic actuator, one must take the requirements of the hydraulic parts into account. Using the several restrictions method requires to make a hole through the permanent magnet of the actuator. This kind of hole will cause a small loss in the force exerted on the magnet. The force that an external magnetic field exerts on the permanent magnet can be understood as an interaction between a magnetic field and an equivalent current density as explained in section 2.

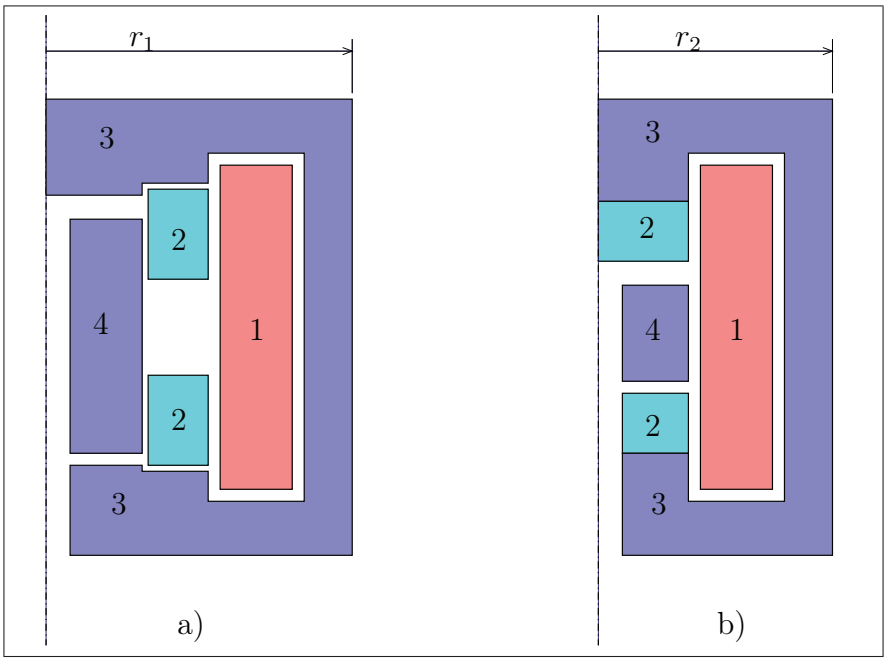

Figure 1: The valve actuator using ferromagnetic armature. Pictures a) and b) represent optimized concepts for maximization of force and minimization of volume ($r_1 > r_2$). Actuator components 1. Coil, 2. Permanent magnet(s), 3. Magnetic circuit, 4. Ferromagnetic armature.

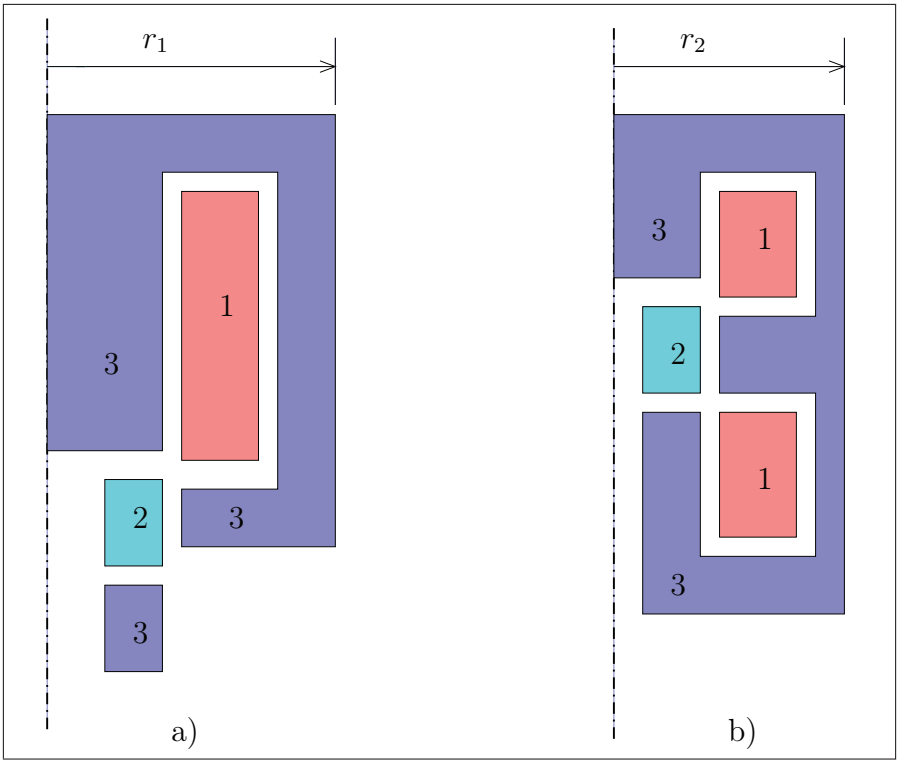

Figure 2: The valve actuator using permanent magnet attached to the armature. In figure a) one coil and in b) two coils is used ($r_1 > r_2$). Actuator components: 1. Coil(s), 2. Permanent magnet (Armature), 3. Magnetic circuit.

If the permanent magnet has a homogeneous magnetization the equivalent current density will be a surface current density and a force is exerted to the magnet by an external magnetic field if the magnetization and the magnetic field are not parallel. The force exerted on an axially symmetric permanent magnet is described in figure 3. On the left of the figure a case of zero force is presented. An external magnetic field traverses through the permanent magnet orthogonal to the magnetization causing the net force exerted on the magnet to be zero. On the right a case of maximum force is presented. An external magnetic field enters the magnet from the outer edge and leaves from up causing the axial net force exerted on the magnet to be maximized.

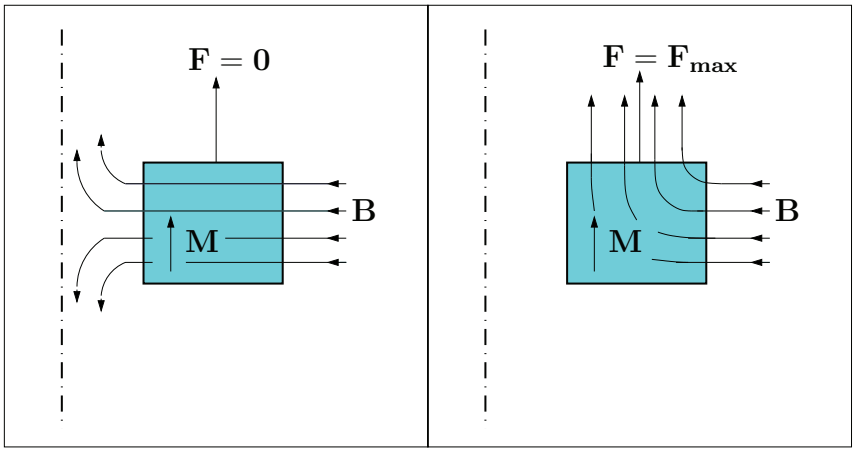

Figure 3: Force exerted on an axially symmetric permanent magnet. On the left a case of zero force and on the right a case of maximum force.

Inside the actuator a thin pressure vessel (pv) is used to separate the coils from the hydraulic fluid. The pv is made of magnetic circuit material and therefore causes a small magnetic flux that passes the permanent magnet causing a small reduction to the force exerted on the permanent magnet. This loss is so small compared to the advantage gained in much simpler construction of the valve, that it is acceptable. The pv is made too thin to hold the maximum pressure by itself. The coil formers and the magnetic circuit are used to complete the pv in order to hold the maximum pressure of 210 bar inside the pv. The coil formers and the pv are presented in figure 4.

To make the valve small, it was also designed to differ from a typical concept of a side in - nose out screw-in valve. The shape of the prototype is cylindrical and it is to be attached to the valve block with a cover plate. The inflow and outflow channels are placed in bottom of the valve so that inflow channels are in outer circle and the outflow channel is in the middle. The flow channels are separated by O-ring ring. This is also taken into account in the actual block, which has corresponding features.

The permanent magnet used in the actuator is a NdFeB-magnet of type N30. It's dimensions are: inner radius $2,5$ mm, outer radius $6,9$ mm, height 6 mm. The coils are winded with a copper wire with a diameter of $0,4$ mm copper which makes a total of 210 rounds divided to the coils and a resistance of $2,0\ \Omega$ in room temperature and $2,7\ \Omega$ in 120 Celsius degrees. This results in a minimum peak current of $8,4$ A with an operating voltage of $23,0$ V in maximum working temperature. Operating voltage can be easily converted to 24 V using different coil winding. A cut picture of the valve with named parts is presented in figure 4. The dimensions of the valve are presented in figure 5.

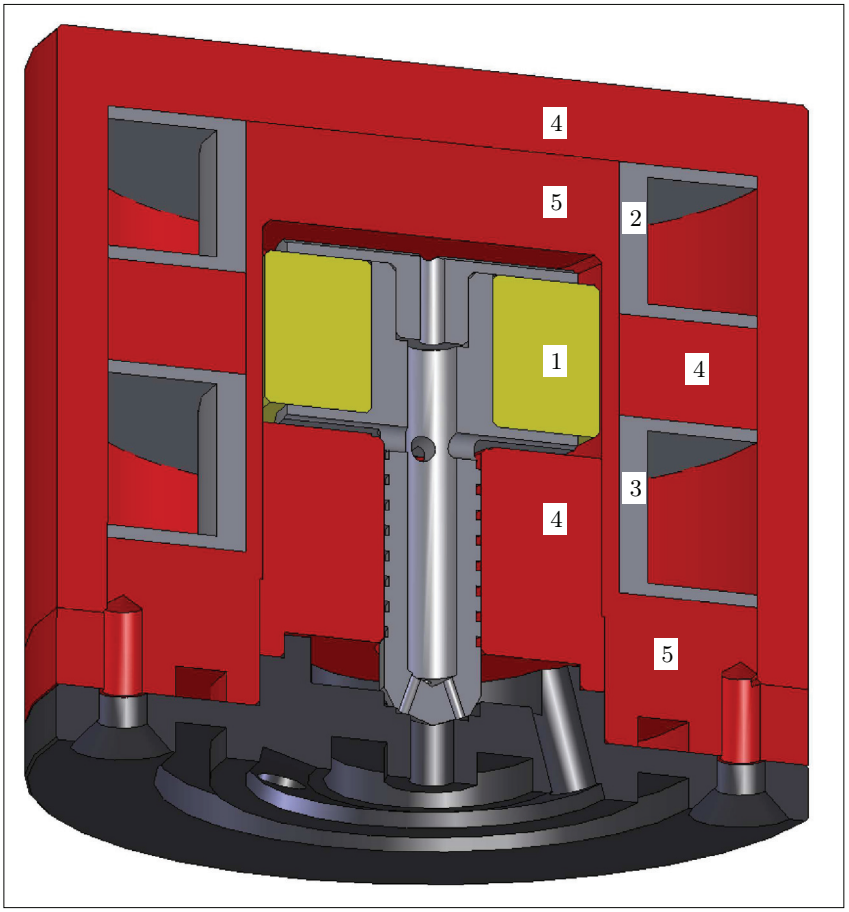

Figure 4: Cut picture and parts of the designed valve. 1. Permanent magnet, 2. Upper coil former, 3. Lower coil former, 4. Magnetic circuit, 5. Pressure vessel (pv).

4 MEASUREMENT METHODS

The valve is designed and analyzed theoretically using the mechanical model with lumped parameters. In the model, the force on the armature consists of three parts: static electromagnetic force, pressure force and friction force. The electromagnetic force is calculated solving second order boundary value problems using VF opera electromagnetic modelling program and MST. The pressure forces can be found from [1]. In friction forces, only steady state flow friction of oil by-pass the armature is modelled.

The computational response times are predicted to be smaller than actual response times, because mechanical friction and dynamic effects (so called back EMF) in the electromagnetic actuator are ignored in the lumped parameter model.

The force measurements on the electromagnetic actuator were done on a test bench with a digital scale. The actuator was pushed against the scale in different modes of utilization.

To study the hydraulic properties of the prototype valve, response time and flow rate were measured. These characteristics were studied with a test circuit shown in figure 6. The circuit was fed by a power unit with a pressure controlled variable displacement

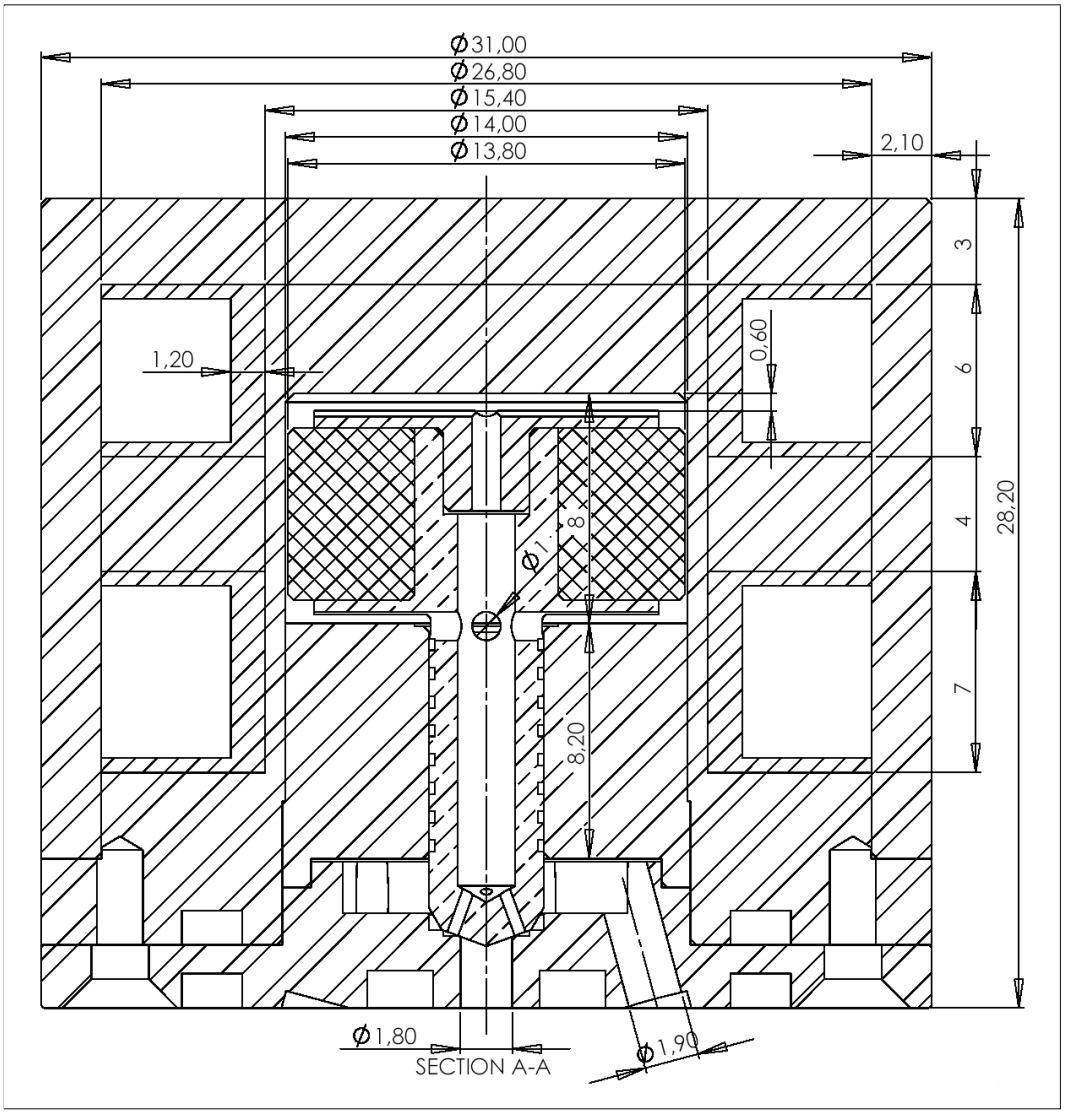

Figure 5: Dimensions of the valve.

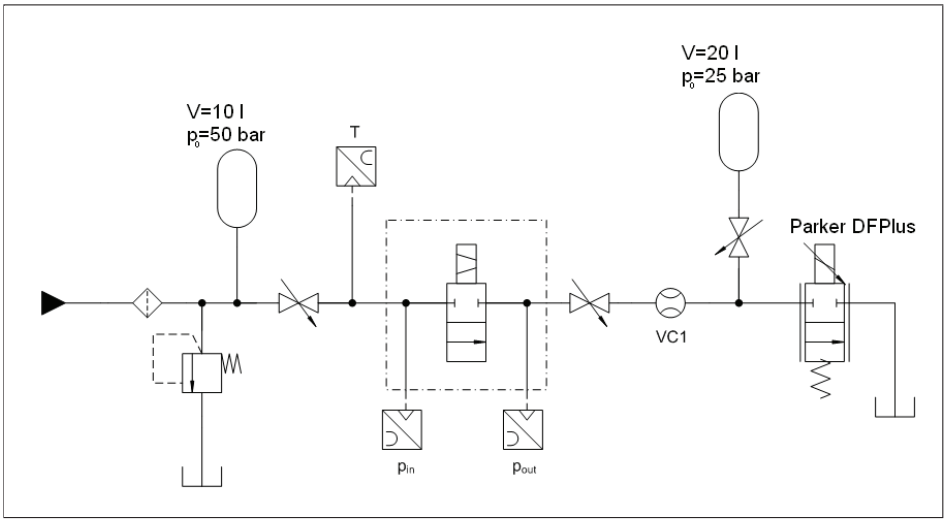

Figure 6: Hydraulic diagram of the test circuit.

Figure 7: The prototype valve.

pump and necessary auxiliary devices. The actual circuit included a pressure filter, a pressure relief valve, two accumulators, two Kistler RAG25A500BV1H pressure transducers, a Kracht VC1 volume flow transducer, an oil temperature transducer, a high quality proportional valve used as a variable orifice and the actual poppet valve prototype. The valve is shown in figure 7 compared to a typical 9 V battery. Accumulators were used to dampen the vibrations in supply pressure and to control the outflow pressure in response time test. Pressure and temperature transducers were installed within a few centimeters from the valve to minimize the effect of compression of oil and to get the accurate temperature of inflow.

Measured data was recorded by a PC and a dSPACE DS1102 controller with sample rate of 5 kHz. Recorded signals include supply pressure, output pressure, inflow temperature, volume flow and control signal and control current for the valve. Data was analysed with Matlab. Measurements were conducted with warm oil with nominal temperature of 40 C to keep the viscosity of the fluid within normal boundaries. The fluid in system was Shell Tellus T 46 with nominal viscosity of 46 mm^2/s and viscosity index of 150.

The first of two tests was the flow rate test, which was done as a continuous test, rather than separate measurement points. Pressure in supply line of the valve was set by the pressure relief valve to 210 bar. Flow through the opened prototype valve was controlled by the proportional valve. Flow was set at first to zero and then gently increased until it was totally saturated. After the saturation point flow was again degreased to zero. After the test volume flow was plotted as function of pressure differentials. Pressure and flow signals were filtered off line with five sample α-trimmed mean filter.

After the flow rate had been measured, two response time tests were done. In these tests, the second accumulator was connected to the system in order to dampen pressure peaks caused by cyclic valve operation. The valve was controlled with 3 Hz signal and 5 ms control pulses. The supply voltage for the valve was 24 VDC, which resulted in peak current of 9,8 A. Tests were conducted with two supply pressures (140 bar and 210 bar) and with several pressure differentials, at least three times per operation point. In these points, pressure differential was set to be an average of value of the point. Response time with maximum pressure differential was measured without the second accumulator, because it ran empty during the cycle and therefore could not prevent the water hammer effect anyway. The response time of the valve was calculated to be the

time from change of control signal to undisputed change in signal of pressure differential. Result of response time is calculated as an average of at least four switchings. Again the only signal filtering used was the α-trimmed mean filter.

5 RESULTS

The computational and measured forces of the valve are presented in table 1. Hold forces are in room temperature (20-23 degrees Celsius). In the measured opening and closing forces, the smaller coil had a surface temperature of 70-75 degrees Celsius. In computational opening and closing forces the modeling temperature is 80 degrees Celsius.

Situation	Computational value	Measured value
Hold force in closed position	$7,0$ N	$9,4$ N
Hold force in opened position	$14,3$ N	$16,0$ N
Opening force	$63,9$ N	$64,9$ N
Closing force	$53,9$ N	$52,6$ N

Table 1: Comparison of measured and computational values of actuator forces.

The computational response times of the valve are $2,5$ ms for opening and $1,2$ ms for closing. The measured response times are $1,6$ ms and $3,2$ ms respectively. Computational values are obtained using 80 degrees Celsius as the modeling temperature. In both cases a pressure of 210 bar's is used as input pressure and 100 bar as the pressure difference.

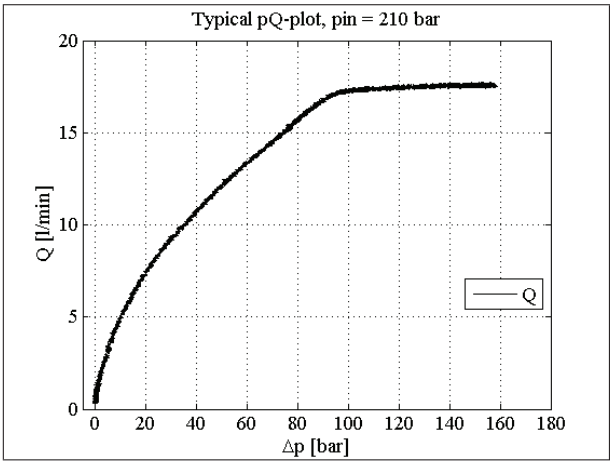

Figure 8: Flow rate and temperature graph with supply pressure of 210 bar. The temperature of the oil was 45 ± 1 degrees Celsius.

A typical graph of measured flow rate is shown in figure 8. It is clearly seen that the valve is prone to cavitation which chokes the flow as the pressure differential is more than 45 % of supply pressure. The test shows that the nominal flow rate for the prototype valve is 4,4 l/min with a pressure differential of 10 bar.

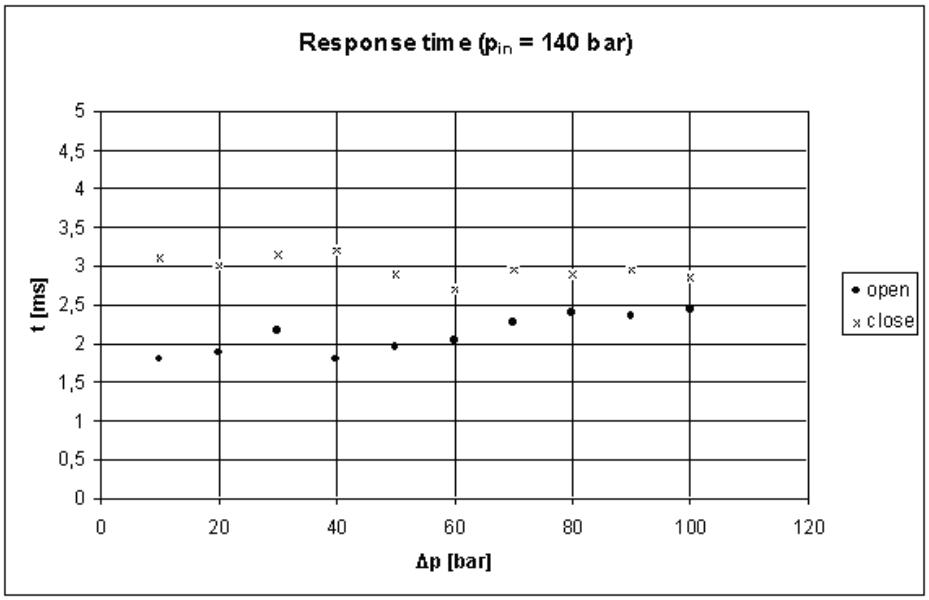

Figure 9: Response time with supply pressure of 140 bar.

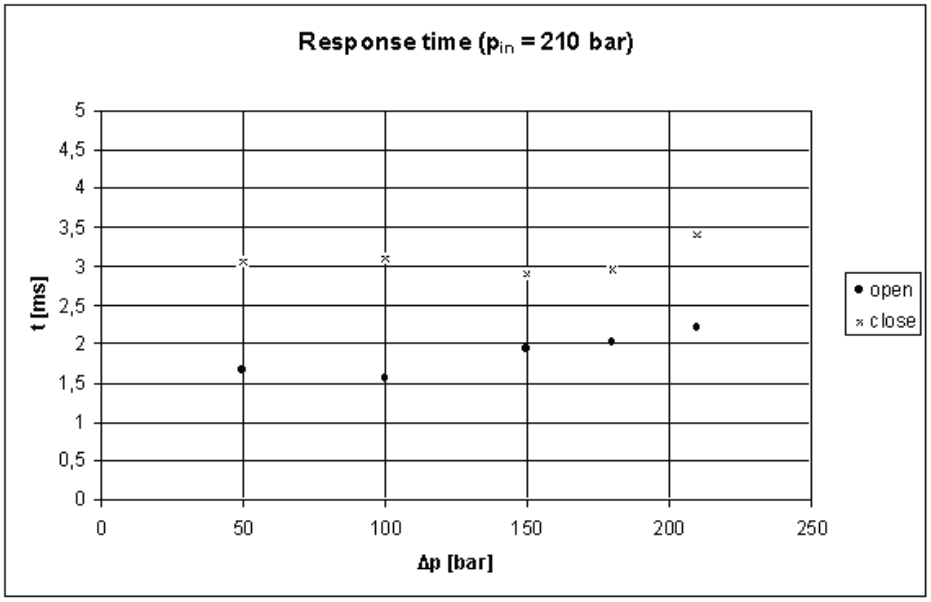

Figure 10: Response time with supply pressure of 210 bar.

The step response test showed that development of the prototype valve is a success. Response time for the valve is from 1,5 ms to 3,5 ms depending mainly on switching direction as pressure differential has only slight impact. The results are shown in figures 9 and 10.

Accuracy of results was calculated in following way. First accuracy of measurement instruments was charted. For Kistler RAG25A500BV1H pressure transducer absolute accuracy is ±0,25 % FSO, which corresponds ±1,25 bar with maximum value of 500 bar. For Kracht Volutronic VC1 flow meter absolute accuracy is ±0,3 % of measured value. Measured maximum flow was 18 l/min, which leads to total accuracy of ±0,054l/min. All measured quantities have total accuracy of correspondent sensor, but accuracy of

pressure differential has to be calculated as sum of accuracies of supply pressure and outflow pressure. This gives ±2,5 bar. All measured quantities but pressure differential are relatively accurate, but one has to keep in mind that this method gives a pessimistic result for accuracy.

Property	Designed valve	Flo-control	Lee valve	Moog NG6	Sturman	Hydac
Switching time (ms)	$< 3,5$	$7 - 15$	< 30	> 20	$0,45$	> 20
Operating frequency (Hz)	30	?	20	5	?	?
Nominal flow rate (l/min) @ $\Delta p = 10$ bar	$4,4$	$0,8$	$0,5$	100	$17,3$	17
Maximum pressure differential (bar)	210	210	?	45	?	40
Theoretical maximum flow (l/min)	20	$3,7$	?	212	?	34
Volume (cm^3)	$21,3$	~ 58	$\sim 18,5$	~ 400	~ 40	~ 80
Nominal flow density $(\frac{l/min}{cm^3})$	$0,21$	$0,014$	$0,027$	$0,25$	$0,43$	$0,21$
Maximum flow density $(\frac{l/min}{cm^3})$	$0,94$	$0,064$	?	$0,53$	?	$0,43$

Table 2: Comparison of the designed valve and the best in-market valves.

Comparison between Flocontrol valve [9], Lee valve (number SDBB3322013A) [10], Moog NG6, Sturman digital latching valve [8], Hydac WS08W-01 and the designed valve is presented in table 2. The information on Moog and Hydac valves are based on measurements on individual valves at IHA. The designed valve, Flocontrol valve and Lee valve are seat valves, the Moog valve and Sturman valve are spool valves and the Hydac valve is a seat valve with a dynamic seal. In the table 2 the switching times have all been measured without any booster circuits and the operating frequency means the maximum continuous operating frequency. For the volume of the valve only the volumes of electromagnetic actuator and active hydraulic parts are considered (excluding all pipes and terminals). The flow density is defined as $\frac{Nominal\ flow\ rate}{Volume}$. If the valve has to work with a pressure difference of 210 bar, which is often the case in digital hydraulics, some of the valves will not work anymore. Their maximum operating pressure differentials are too low and the usage of them requires an extra restriction in series with the valve. Therefore, maximum flow rates and maximum flow densities (defined as $\frac{Theoretical\ maximum\ flow}{Volume}$) are calculated in order to find out the maximal level of performance for each valve.

6 CONCLUSIONS AND DISCUSSION

In this work the design of a bistable miniaturized valve using the several restrictions method and permanent magnets is described. A table of characteristics of the designed valve is presented in table 3. The designed valve shows a significant reduction in

switching times and volume compared to best in-market commercial valves. When comparing the maximum flow density values (theoretical maximum flow divided by the volume of the valve), the designed valve has about two times bigger value then the best in-market spool valves or seat valves with a dynamic seal. In this sense, the goal of reducing the volume of the valve to about a half is achieved. Therefore, the designed valve benefits many systems using digital hydraulics.

Property	Value
Volume	$21,3\ cm^3$
Operating voltage	23,0 V
Switching time	$< 3,5$ ms
Maximum operating frequency	45 Hz
Maximum continuous operating frequency	30 Hz
Maximum opening	0,6 mm
Opening force	64,9 N
Nominal flow rate	4,4 l/min @ $\Delta p = 10$ bar 10,0 l/min @ $\Delta p = 35$ bar
Maximum volume flow rate	18 l/min
Maximum pressure differential	210 bar
Maximum operating pressure	210 bar
Maximum rms power	29 W
Nominal flow density $= \frac{Nominal\ flow\ rate}{Volume}$	$0,21\ \frac{l/min}{cm^3}$
Maximum flow density $= \frac{Theoretical\ maximum\ flow}{Volume}$	$0,94\ \frac{l/min}{cm^3}$

Table 3: Valve characteristics. Volume includes electromagnetic and hydraulic parts but no manifold. Maximum operating frequency means the maximum frequency rate at which the valve can be opened and closed continuously.

ACKNOWLEDGEMENT

The research was supported by the Academy of Finland (Grant no. 80411) and the Finnish Funding Agency for Technology and Innovation (Grant no. 40334/04).

REFERENCES

[1] T. Lauttamus, M. Linjama, M. Nurmia, and M. Vilenius. A novel seat valve with reduced axial forces. In *Proc. of Bath Workshop on Power Transmission and Motion Control, PTMC'06*, pages 426–438, Bath, UK, September 13-15 2006.

[2] Matti Linjama, Arto Laamanen, and Matti Vilenius. Is it time for digital hydraulics? In *Proc. of The Ninth Scandinavian International Conference on Fluid Power, SICFP'03*, pages 347 – 366, Tampere, Finland, May 7-9 2003.

[3] J. Tsay, H-A. Chang, and C-K. Sung. Design and experiments of fully compliant bistable micromechanisms. *Elsevier, Mechanism and Machine Theory*, 40:17–31, August 2004.

[4] M. Garstenauer and R. Scheidl. High-speed switching valves actuated by parametrically excited structures. In C. R. Burrows and K. A. Edge, editors, *Power Transmission and Motion Control, PTMC'99*, pages 137–150, Bath, UK, September 8-10 1999.

[5] Standard Telephones and Cables Limited. *Bistable electromagnetic actuator*. The Patent office, London, Patent No. 18467/61, Connaught House, 63 Aldwych, London, W.C.2, England, 1961.

[6] A. M. Pawlak and C. H. Leung. *Magnetically latching solenoid apparatus*. United States Patent, Patent Number: 5,883,557, General Motors Corporation, Detroit, Mich., 1999.

[7] E. Kallenbach, H. Kube, V. Zoeppig, K. Feindt, R. Hermann, and F. Beyer. New polarized electromagnetic actuators as integrated mechatronic components - design and application. *Mechatronics*, 9(7):769 – 784, Oct 1999.

[8] B. Johnson, S. Massey, and O. Sturman. Sturman digital latching valve. In J.-O. Palmberg, editor, *Proc. of The Seventh Scandinavian International Conference on Fluid Power, SICFP'01*, volume 3, pages 299 – 314, Linköping University, Linköping, Sweden, 2001.

[9] Matti Linjama, Pekka Tamminen, Bo Andersson, and Matti Vilenius. Performance of the valvistor with digital hydraulic pilot control. In *Proc. of The Ninth Scandinavian International Conference on Fluid Power, SICFP'05*, pages 14 on CD–ROM, Linköping, Sweden, June 1-3 2005.

[10] The Lee Company. *Technical Hydraulic Handbook, Release 10.3*. 2003.

WATER MIST FIRE FIGHTING – HIGH-PRESSURE WATER MIST NOZZLES

Max Lakkonen
FOGTEC Fire Protection
Schanzenstrasse 19a
D-51063 Köln, Germany
Phone +49 221 96 223 0, Fax +49 221 96 223 30
E-mail: max.lakkonen@fogtec.com

ABSTRACT

The use of water mist for fire fighting has increased rapidly. The effectiveness of water mist has been known since beginning of the last century. Commercially it has been applied in fire protection since early thirties. However, the latest boost to the development of the water mist technology has been a ban of halon systems in fire extinguishing. During the long history of water mist system the core of water mist systems has been the nozzle, which does the atomization of water to small droplets. Nozzle principles have not changed a lot since the beginning of the technology. Still the most often used atomization mechanisms are jetting and swirling flow nozzles. Both of them have benefits and drawbacks. In this paper is presented shortly the principle of high-pressure water mist fire fighting, focusing to the nozzle design. The general theory of nozzles is explained, additionally a new water mist nozzle concept is introduced. This nozzle design is a combination of two most popular water mist nozzle types, swirling and jet flow nozzles. Also the first test results with the new nozzle are discussed.

KEYWORDS: Water mist, fire protection, nozzle, high pressure

1 INTRODUCTION

1.1 History of water mist fire fighting

The effectiveness of water mist has been known since beginning of the last century, but it starting of commercial applying in larger scale was as late as in 1990's. Some first commercial efforts of marketing water mist fire fighting have been reported in 1930's [5]. The US Navy used fog fire fighting nozzles during World War II, later adopting the technology for fixed installations during the 1950s. In the 1980's high-pressure water mist systems were introduced and developed for land-based systems, especially in Sweden and Norway. The 1990's was the decade of commercializing water mist fire fighting in larger scale. Especially, marine segment invested a lot to "new" technology that provided certain benefits compared to old systems. One of the main driving forces for water mist industry was the rejection of halon-based systems in fire extinguishing [1]. Water mist fire fighting has continued in expanding new applications and markets, thanks to superior fire fighting properties of water mist compared to traditional systems.

The focus has changed from marine to land based applications. An example of water mist industry development can be seen in the number of member companies of IWMA (*International Water Mist Association*). There were 5 member companies in IWMA in year 2000. Nowadays there are 48 member companies who present main manufacturers, test institutes, leading approval authorities [7].

Since water mist often is considered as new technology, a full scale fire tests has to be carried out in order to prove the effectiveness of technology compared conventional technologies. One of the latest new markets to water mist technology is road tunnel protection. In past tunnels were not protected at all, but as a result of continuously happening serious accidents, tunnel society has looked to active fire fighting system in tunnels and the benefits of water mist technology have been superior compared other technology. The following picture presents fully developed fire in a test tunnel with fire load that simulates truck (HGV, heavy good vehicle) [2]. High-pressure water mist system controls the fire and makes the survivability of people possible already 5-20 meter distance from the fire.

Picture 1. Full scale fire tests in test tunnel *(www.solit.info)*

1.2 Water mist systems vs. water hydraulics

Water mist fire fighting, especially high-pressure systems, can be considered as one special part of water hydraulics. This is quite often neglected since fire fighting system mean open hydraulic circuits; water is taken from tank, pumped, controlled with valves to right location and sprayed with nozzles. Often water hydraulics is considered to consist only of industrial water hydraulics that presents more oil hydraulic kind of closed circuits where same pressure medium is being circulated continuously. Due to properties of oil, similar kind of open hydraulic circuits are not very common. An

exception is probably diesel fuel injection systems where exactly same as in water mist systems are being done.

1.3 Water mist systems fire fighting

The superior effectiveness of water mist in fire fighting relies on the fact that water mist is able to fight fire against every element that is needed to combustion. The combustion process needs always three elements, which are heat, oxygen and fuel.

A. Cooling
The most important property of water as a suppressant is the cooling capacity. Water can absorb energy at a rate of over 2MJ/kg in vaporization, which is superior to any other known suppressant. Water mist systems use much less water compared conventional sprinkler systems, because the heat absorbation abilities are so much higher. The average droplets of high-pressure water mist yield a total surface area at least 100 times greater than conventional sprinkler droplets for the same volume of water.

B. Oxygen depletion
The vaporization of water inerts locally the atmosphere as the volume of water expands to over 1700 times of the original volume in vaporization process. The inerting effect is very local and happens in places where the heat is highest. This naturally means the flames and direct surrounding area of fire. It is essential that water mist penetrates to the fire effectively and often high-pressure is needed to enough high momentum for droplets to carry out this.

C. Blocking Radiant Heat
Water mist also works as a heat barrier against radiant heat fire source to atmosphere. The surrounding water mist cools the atmosphere an prevents fire spread and also allows both people to escape and fire fighters to approach the fire more safely.

2 HIGH-PRESSURE WATER MIST NOZZLES

The nozzles are the core of water mist systems, because the atomizing of water of water takes place in them. Normally, this process needs quite lot energy if very fine droplets are produced with high flow rates. Therefore, it is common to use high-pressure level in order to ensure this process will have good results. According water mist standards high-pressure is defined to start from 35 bar [3], but the practice has shown that much higher pressure is needed if fine droplets are wanted to be produced with sufficient flow rates for fire fighting. All leading manufactures today use pressure level of 70-200 bar in their water mist systems. This pressure level is a common technology in other fields of water hydraulics and it can be considered to be even only medium pressure because of many water hydraulic application apply much higher pressure levels [4].

2.1 Water mist quality

The basic definition for the water mist systems is naturally the quality of the spray, which has to be “mist”. The existing standards define water mist with the droplet size

which has to be smaller than 1000 µm in 99% of all droplets [3][8]. This definition covers quite high droplet sizes. The practice is that the most of the commercial high-pressure water mist systems have much smaller droplet size. The range varies normally between 50-250µm depending on protected application.

2.1 Water mist nozzle principles

As mentioned before, nozzles in the end define the water mist quality and quantity. Nozzles can be divided to three main categories according to function principle, which are explained below. However, the following picture shows the fire fighting water mist nozzle from 1930's and 2010's [5][6]. Same principles were used already then, only nozzle size, materials and manufacturing quality has changed since those days.

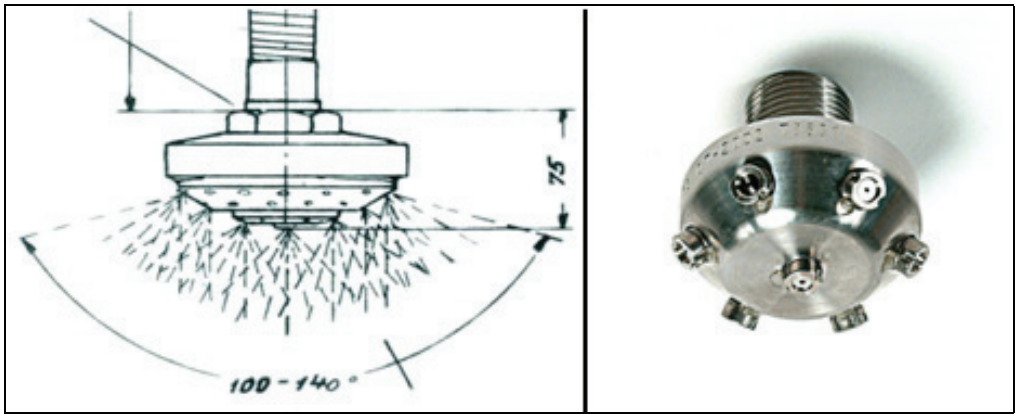

Picture 2. Water mist spray heads from 1937 (Lechler Gmbh) and 2007 (FOGTEC)

There are several different principles how water can be atomized in water mist nozzles to small droplet size sprays. However, the main mechanisms used in water mist fire fighting are A. Creating very turbulent and cavitating jet flow, B. Colliding water jets and C. Swirling the spray. The short explanation of these is explained in following. Sometimes nozzle can be divided to sub-cateogires according to the shape of spray pattern. The main categories in this case are hollow cone, full cone, stream/jet and flat fan sprays. However, it is more practical to use the nozzle function as categories when discussing water mist nozzles.

A. Jet flow nozzles

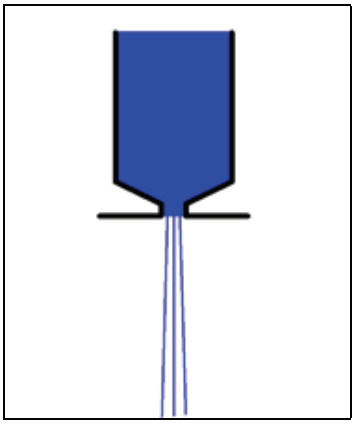

Picture 3. Jet nozzle

The principle of jet flow nozzle is that flow stream is accelerated to high velocity in the nozzle. The jet will brake to small droplets in a certain length after the nozzle due to the turbulence and cavitation effects. The average velocity of streaming jet might be 150 m/s in high pressure water mist nozzles. Due to the high kinetic energy jet nozzles have good abilities to penetrate to the fire. The nozzle design is also very simple compared to other atomizing principles. The main disadvantage is the energy density of the jet, which is very centralized spray does not open as effectively than with other nozzles.

B. Colliding jet nozzles

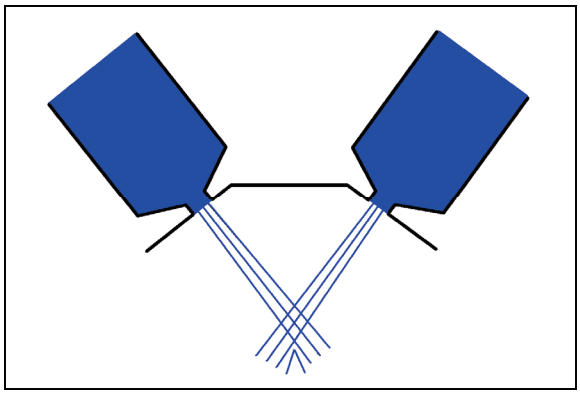

Picture 4. Example of colliding jet nozzles

The principle of colliding jet nozzles is to create at least two separate jets that will collide after coming out of the nozzle orifices. The colliding makes the atomization normally much better than with normal jet nozzles.

C. Swirling flow nozzles.

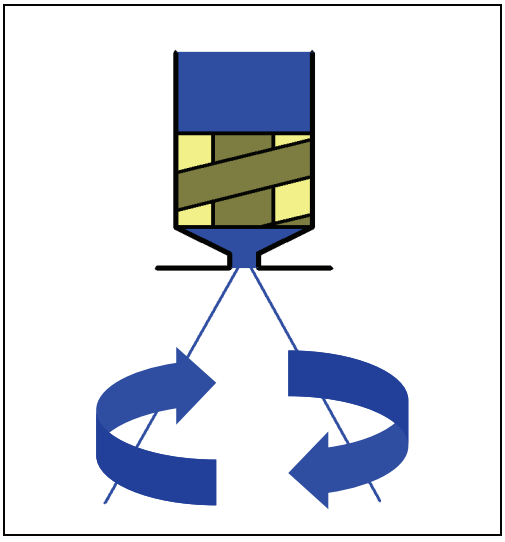

Picture 5. Example of swirling flow nozzle

Swirling the flow is normally done by using a separate mechanical swirling device to force the stream to swirl. This is normally done in a chamber before the actual orifice boring. The swirling flow nozzles are the most used atomization mechanism in high-

pressure water mist extinguishing systems. The benefit of swirling flow nozzle compared to simpler jet nozzles is that spray opens immediately after passing the orifice boring. This gives additional benefit for spreading to the droplets to protected volume more effectively.

Normally water mist spray heads consist of several (micro)nozzles that are spraying in different directions as it is important to deliver mist to the whole volume. The following picture shows an example of spray head that consist of six swirling flow nozzles.

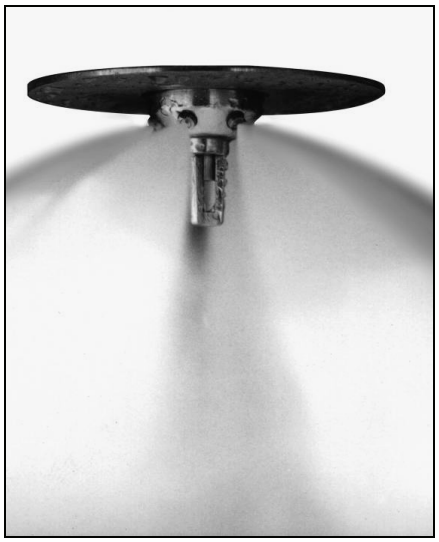

Picture 6. Example of high-pressure swirling flow spray head [6]

3 NOZZLE DESIGN PARAMETERS AND THEORY

The standardization of water mist system does not specify very accurately the design parameters of water mist nozzles. Only the testing procedures, filtration, material and other functional/lifetime related test procedures are specified [8]. Parameters like droplet distribution, maximum power density of stream/jet in certain distance from the nozzle, pressure level etc. are up to nozzle manufacturers own experience. Because of this reason there are many different high-pressure nozzle types and principles available in the market. Standardization of water mist systems gives full freedom to water mist fire fighting nozzle manufacturers to do their own nozzle design basically without any real limitations. The effectiveness of nozzles will be in the end tested with the fire tests which show the functionality of nozzles in real application.

The main design parameters of high-pressure water mist nozzles from fire extinguishing point of view are naturally flow rate, droplet distribution and axial/tangential momentum of droplets. In following is explained these nozzle design parameters in more detail using the jet simplest nozzle type, round shape jet flow nozzle as an example.

3.1 Flow Rate

Flow rate through the orifice is the most important parameter of the nozzle, because it **indicates water quantity that can be leaded through the nozzle to the protected**

space. The flow rate of nozzles is normally specified in fire protection by using K-factor. K-factor indicates the flow rate of individual nozzle type in very simple way. The nozzle manufacturer has to specify K-factors for every nozzle type and spray head. Normally, this is done with experimental tests. The definition of K-factor is shown in following.

$$Q = K \cdot \sqrt{p} \tag{1.}$$

K = K – factor (l/min/√bar)
Q = Flow rate (l/min)
p = Pressure (bar)

However, it is very important to know where K-factor comes from theoretical point of view and what actually happens in the nozzle. The starting point of theoretical study is Bernoulli equation, which states that energy is constant for stationary flow with incompressible liquid.

$$h + \frac{p}{\rho} + \frac{v^2}{2 \cdot g} = C_{const} \tag{2.}$$

h = Height (m)
p = Pressure (Pa)
ρ = Density of water (kg/m^3)
g = Gravity (m/s^2)
v = Flow velocity (m/s)
C_{const} = Constant (-)

The following geometry for the nozzle geometry can be created in order to study the flow and energy through different levels.

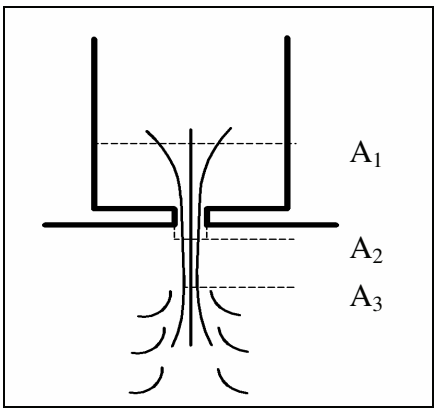

Picture 7. Flow through orifice in jet nozzle

For nozzle geometry the Bernoulli equation can be written for levels A_1 and A_0.

$$h_1 + \frac{p_1}{\rho \cdot g} + \frac{v^2{}_1}{2 \cdot g} = h_2 + \frac{p_2}{\rho \cdot g} + \frac{v^2{}_2}{2 \cdot g} \tag{3.}$$

The stationary height difference (h_1 and h_0) is insignificant in this case and can be discarded. The energy in the nozzle will change from the pressure to the kinetic energy. The area A_1 in the nozzles is much larger than the area of nozzle boring A_2. Therefore, the velocity energy in level A_1 can be neglected and energy balance written as follows.

$$\frac{p_1}{\rho}+\frac{v^2{}_1}{2}=\frac{p_2}{\rho}+\frac{v^2{}_2}{2} \tag{4.}$$

On the other hand because of continuity of the flow it can be written that the flow is equal in all cross-sectional areas of the flow.

$$A_1 \cdot v_1 = A_2 \cdot v_2 \tag{5.}$$

If equations are combined the velocity in are A_2 can be written as follows. Now the velocity in orifice can be written.

$$v_2 = \frac{1}{\sqrt{1-\left(\frac{A_2}{A_1}\right)^2}} \cdot \sqrt{\frac{2\cdot(p_2-p_1)}{\rho}} \tag{6.}$$

Following the flow rate through the area A_2 can calculated as follows.

$$Q = A_2 \cdot v_2 \tag{7.}$$

If equations are combined, flow rate through the nozzle can be written by using energy balance and continuity as follows.

$$Q = \frac{A_2}{\sqrt{1-\left(\frac{A_2}{A_1}\right)^2}} \cdot \sqrt{\frac{2\cdot(p_2-p_1)}{\rho}} \tag{8.}$$

Normally the area the nozzle body is much larger than the nozzle boring $A_2 << A_1$ and equation 8. can be written.

$$Q = A_2 \cdot \sqrt{\frac{2\cdot(p_2-p_1)}{\rho}} \tag{9.}$$

The energy equation assumes that all energy can be changed from one to the other form without any losses. This is not true in practice and therefore the equation 9 has to be changed. The common way to do is to use one factor that includes all limiting factors. This factor is often called as *discharge coefficient* C_d and flow through a turbulent orifice is calculated as follows by using it.

$$Q = C_d \cdot A_2 \cdot \sqrt{\frac{2\cdot(p_2-p_1)}{\rho}} \tag{10.}$$

If this equation is compared to commonly used K-factor, it can be seen that K-factor actually combines all other terms in this, except the pressure. All these terms can be considered constants so this can be done in order to make the definition of flow rate through the nozzle as simple as possible.

If the origin of discharge coefficient is wanted to be defined in detail, more attention has to be paid towards the flow geometry shown in picture 7. The first stage of flow is the distance between areas A_1 and A_2. Between these points pressure energy changes to kinetic/velocity energy and flow particles are accelerated a jet velocity. Sometimes this stage is also called as laminar stage due to the very symmetric and uni-directional flow geometry. If the flow geometry is studied in detail it can be seen that the smallest cross sectional area is not in the nozzle boring A_2 but shortly after it in downstream. The reason for this is the inertia of fluid particles which keeps them to continue moving in a curved path at the orifice opening. This point along the jet where the jet are becomes a

minimum is called *vena contracta* and it can be seen as A_3 in picture 7. If the right flow rate through the nozzle wanted to be calculated only the area of the vena contracta should be used. The ratio of cross sectional flow areas between orifice A_2 and vena contracta A_3 is called the *contraction coefficient*.

$$A_3 = C_c \cdot A_2 \tag{11.}$$

Due to the viscosity friction the energy of the moving flow is not same between points A_1 and A_3 where the flow is really accelerated to the maximum value. This effect can be taken account by using an empirical factor called the *velocity coefficient* C_v. The velocity factor can be included to the equation which is already corrected to take account the cross sectional area of vena contracta A_3 instead of area of boring A_2.

$$v_2 = \frac{C_v}{\sqrt{1-\left(\frac{A_3}{A_1}\right)^2}} \cdot \sqrt{\frac{2 \cdot (p_2 - p_1)}{\rho}} \tag{12.}$$

Correspondingly, the equation for flow rate can be written as follows.

$$Q = \frac{C_v \cdot A_3}{\sqrt{1-\left(\frac{A_3}{A_1}\right)^2}} \cdot \sqrt{\frac{2 \cdot (p_2 - p_1)}{\rho}} \tag{13.}$$

Normally, it is much more convenient to use orifice area A_2 instead of vena contracta A_3 since it is known .

$$Q = \frac{C_v \cdot C_c \cdot A_2}{\sqrt{1-C_c^2 \cdot \left(\frac{A_2}{A_1}\right)^2}} \cdot \sqrt{\frac{2 \cdot (p_2 - p_1)}{\rho}} \tag{14.}$$

If equations 10 and 14 are compared, the discharge coefficient C_d can be defined as follows.

$$C_d = \frac{C_v \cdot C_c}{\sqrt{1-C_c^2 \cdot \left(\frac{A_2}{A_1}\right)^2}} \tag{15.}$$

As earlier stated the area of nozzle body is much larger normally in water mist nozzles than the nozzle boring $A_2 << A_1$ so the discharge coefficient can be written.

$$C_d = C_v \cdot C_c \tag{16.}$$

The literature of fluid dynamics gives values for the different nozzle geometries. Both contraction and velocity coefficients are dependent on the shape of the nozzle and properties of the liquid. Generally, it can be said that the velocity coefficient is close to 1 in most of the cases. This means that the contraction coefficient is mainly defining the discharge coefficient of the nozzle.

The definition of the velocity and contraction coefficient is really hard to do by calculating, because of complexity and small dimensions of the nozzles in high pressure water mist. More practical way is to use modeling with CFD *(Computational Fluid Dynamics)*. However, the best and normally the easiest way is to use experimental methods. This shows accurately the discharge coefficient for the studied geometry. Though, the separation between contraction and velocity is impossible to do with

experimental methods. The following equation can be used for measuring the discharge coefficient of water mist nozzle experimentally. The pressure in downstream can be considered to be zero, because spraying happens to atmospheric pressure. On the other hand the pressure level of water mist system is normally high compared to differences to atmospheric pressure that it can be neglected.

$$C_d = \frac{Q}{A_2 \cdot \sqrt{\frac{2 \cdot (p_2 - p_1)}{\rho}}} \tag{17.}$$

3.2 Droplet size

Droplet size is the design parameter which **indicates the effectiveness of water mist against fire**. The droplet size is not the absolute indicator of fire fighting abilities, but a good indicator anyway. As explained in introduction chapter, smaller droplets mean better filling of protected volume and more surface area for vaporization/cooling.

Water spray coming out of the nozzle is always combination of different size droplets. Therefore the common way is to use mean value or distribution as unit for droplet quality of spray. In following picture is shown an example droplet distribution plot of some high-pressure water mist nozzle.

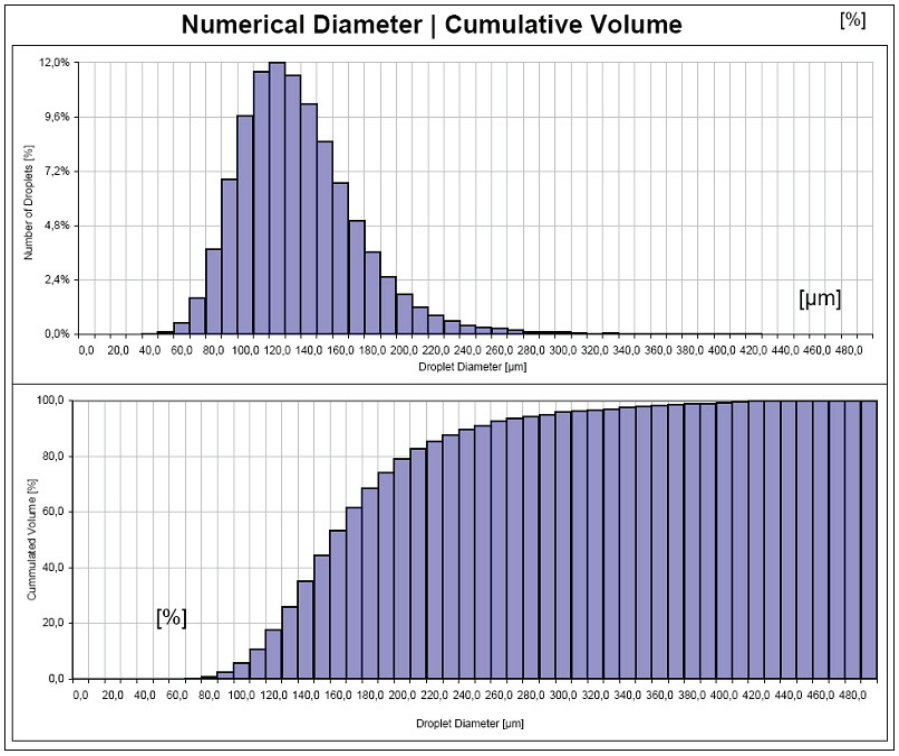

Picture 8. Example of water mist nozzle droplet size distribution [5]

Water mist quality or droplet sizes in other words can be evaluated with following ways using x_i as number of droplets and d_i as diameter of droplet.

a. Linear mean diameter

$$d_0 = \frac{\sum x_i \cdot d_i}{\sum x_i} \tag{18.}$$

b. Surface area mean diameter

$$d_1 = \left(\frac{\sum x_i \cdot d_i^2}{\sum x_i} \right)^{1/2} \quad (19.)$$

c. Volume mean diameter

$$d_2 = \left(\frac{\sum x_i \cdot d_i^3}{\sum x_i} \right)^{1/3} \quad (20.)$$

d. Volume/surface mean diameter (SMD, Sauter mean diameter)

$$d_{21} = \frac{\sum x_i \cdot d_i^3}{\sum x_i \cdot d_i^2} = \frac{d_2^3}{d_1^2} \quad (21.)$$

Sometimes it is also practical to use the distribution of droplets for example Gauss distribution is practical to show the general characteristics of droplet distribution. It is also very important to measure the droplet sizes from right places of the spray, because measurement position has an influence to the results. For example CEN-water mist standard *(draft)* defines the places for measurement and this should be used in order to get comparable results between different nozzles and nozzle manufactures [9]. The atomization capabilities of nozzles vary a lot depending on the used nozzle type. In former studies has been noticed that the increase of pressure will decrease the droplet size independently of the used nozzle type. Especially, the distribution of droplets becomes narrower and the most of the droplets are close to average diameter.

The theory of atomization is quite complex. First of all there is not any universal model that would explain all of the atomization principles comprehensively. Secondly, the most of the existing models include at least one experimental based factor, which means that experimental tests have to be carried out in order to get modeling realistic for the new flow geometry.

The atomization of liquid jet can be basically be divided to two types, primary atomization near the nozzle and secondary atomization, which is the break-up of drops in downstream. Furthermore the atomization happening in the second stage can be divided to few main types which are presented in picture 9.

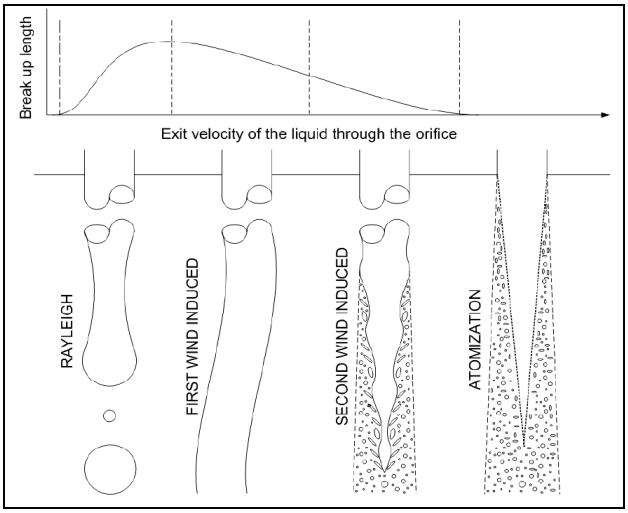

Picture 9. Atomization of round shape liquid jet

Rayleigh break-up area presents the situation when the droplets are still larger than the orifice diameter [11]. The droplets are formed far after the orifice in down stream. Normally mean velocity is less than 2 m/s.

First wind induced break-up area presents the situation when droplets have similar diameter than the orifice. The droplets are formed far after the orifice in down stream. Normally the mean velocity is less than 10m/s.

Second wind induced break-up area presents the situation when droplets have smaller diameter than the orifice. The droplets are formed slightly after the orifice in down stream. Normally the mean velocity is less than 30m/s.

Atomization area presents the situation when droplets have greatly smaller diameter than the orifice. The droplets are formed just after the orifice in down stream. Normally the mean velocity is less than 100m/s.

The main acting stresses on the liquid during break-up are inertial, viscous and surface tension which definitions are shown below.

$$\text{Intertia} = \rho \cdot v^2 \tag{22.}$$

$$\text{Viscous} = \frac{\mu \cdot v}{L} \tag{23.}$$

$$\text{Surface Tension} = \frac{\sigma}{L} \tag{24.}$$

ρ = Density of water (kg/m^3)
μ = Viscosity (Ns/m^2)
v = Flow velocity (m/s)
σ = Surface tension (N/m)
L = Length scale

The importance of these effects can be characterized by using two main indicators, Reynolds and Weber number [10] [13]. Reynolds number presents the ratio of inertial forces / inertial forces and Weber number inertial forces / surface tension forces. This can be written as follows.

$$\text{Re} = \frac{\rho \cdot v \cdot L}{\mu} \tag{25.}$$

$$\text{We} = \frac{\rho \cdot v \cdot L}{\sigma} \tag{26.}$$

Reynolds and Weber numbers can also be combined together as one parameter, which is the viscosity group, ratio of viscous and surface tension forces. This parameter is often called also as Ohnesorge-number.

$$\text{O} = \frac{\mu}{\sqrt{\rho \cdot \sigma \cdot L}} \tag{25.}$$

The Ohnesohne and Reynolds number can be used for characterizing the round shape jet flow and different atomization stages in it. The different stages of the jet flow are

presented in the following picture by using the orifice diameter as length scale for the case.

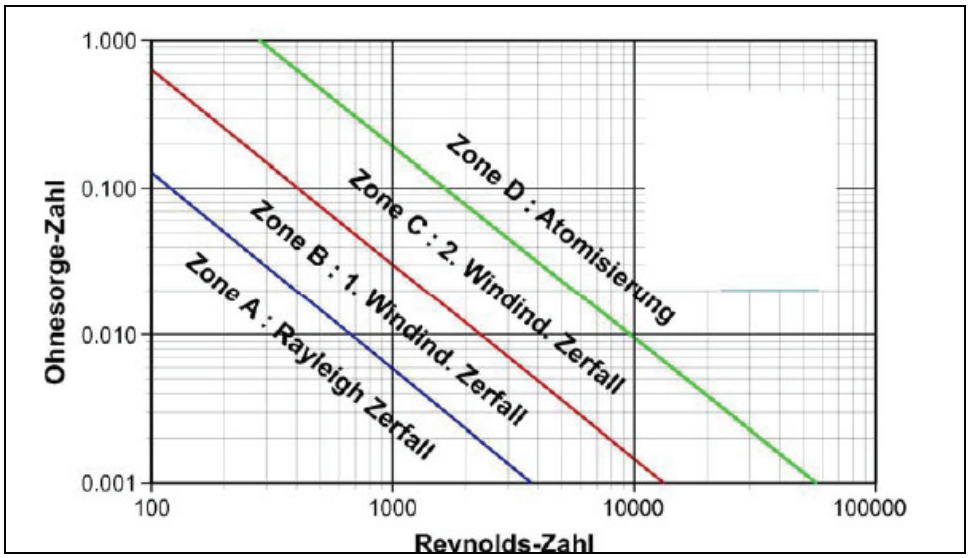

Picture 10. Different atomization stages in jet flow [12]

The characterizing of other atomizing methods like colliding jets or swirling flow nozzle is more complicated numerically and need normally experimental tests anyway. Therefore it can be stated that experimental methods are always quite easy and reliable approach to study the atomization abilities of nozzles.

C. Momentum

Momentum as design parameter refers to the kinetic energy which droplets have after coming out from nozzle orifice. The momentum can be divided to two directions, axial- and rotational. The momentum works as an **indicator for ability to penetrate into the fire and protected space**. If the axial momentum is high, it means that droplets have a high velocity and they reach to the far distance out from the nozzle.

Momentum is highly dependent on the used nozzle type. The velocity in vena contracta can be calculated in order to understand the momentum that stream has in the initial stage. The velocity can be calculated if the pressure difference over the nozzle, nozzle diameter and flow rate is known.

$$v_3 = \frac{Q}{A_3} = \frac{Q}{C_d \cdot A_2} \tag{26.}$$

In high pressure nozzle the maximum mean velocity might be over 150m/s. One single droplet with all possible velocity directions is shown in following figure. The directions differ depending on the nozzle for example jet nozzles mainly have momentum in axial direction downstream from the nozzle. The drag forces, turbulence, cavitation, friction etc. causes slight change to movement also to other directions, but the main stream is going to initial direction. Swirling flow nozzle instead has already high rotational momentum in the initial stage of the atomization. This means that velocity happens strongly “side” direction towards directions v_x and v_z. Furthermore droplets are moving also other directions and spray opens.

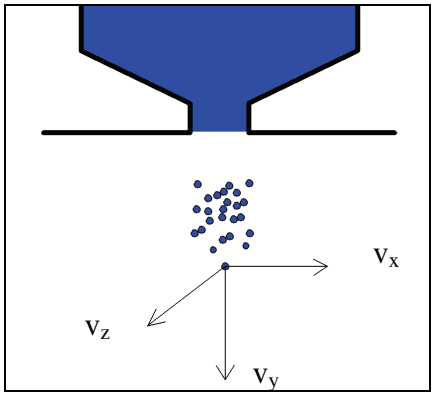

Picture 11. Possible droplet directions

The earlier studies have shown that the deceleration of droplets happens really fast, especially if droplet size is small. However, deceleration takes more time with larger droplets. The studies have shown that with droplet sizes of 500 µm the velocity might be reduced only from 100m/s 50-60 m/s after distance of 0.75 meter from the nozzle [13]. Correspondingly, with 100µm small droplet sizes the values are 10 m/s after distance of 0.35 meter from the nozzle. This is the generally problem of jet type nozzle, because the droplet atomization is not so effective than with other types. On the other hand the droplets mainly have momentum only one direction, downwards from the nozzle and droplets are spread to rather narrow area. This makes the energy density of the spray area high, especially if high pressure is used which can give initial velocity of 150 m/s to droplets.

4. NEW HIGH-PRESSURE NOZZLE

FOGTEC fire protection has developed a new kind of water mist nozzle which is a combination of swirling flow and jet flow nozzle. The new nozzle concept is designed in a way that only changing one boring in the nozzle structure the atomization principle can be changed from one to the other. Nozzle can have either jetting or swirling atomization mechanism, but most important is that nozzle can be a combination of these two mechanisms. By doing this the good features of both nozzle can be achieved, which makes it very competitive compared old nozzle types.

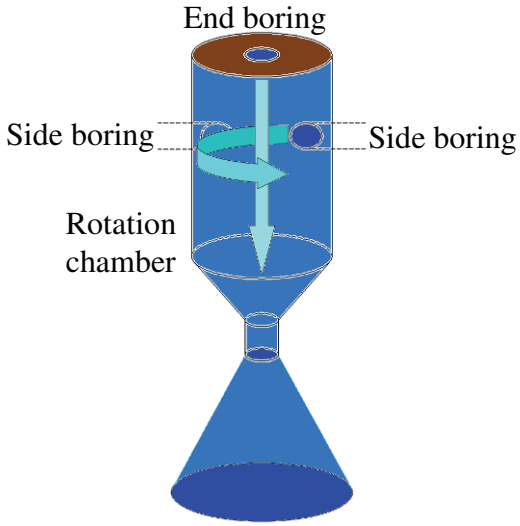

Picture 12. New high-pressure water mist nozzle concept

The nozzle has an internal rotation chamber before the nozzle orifice. On the side wall of rotation camber there is one to four borings which are not in the center line of the nozzle but coming tangentially to the chamber. This structure gives a rotation effect for the nozzle which magnitude can be adjusted by choosing different side boring diameter compared to the orifice boring. However, the general problem of swirling nozzles is that the axial momentum of the spray pattern might be quite weak. Because of this reason there is a third boring called as end boring in the end of rotation chamber. The end boring is axially on same line than the orifice boring. By choosing different end boring sizes the character of the nozzle can be changed significantly. An example of this is shown in next picture.

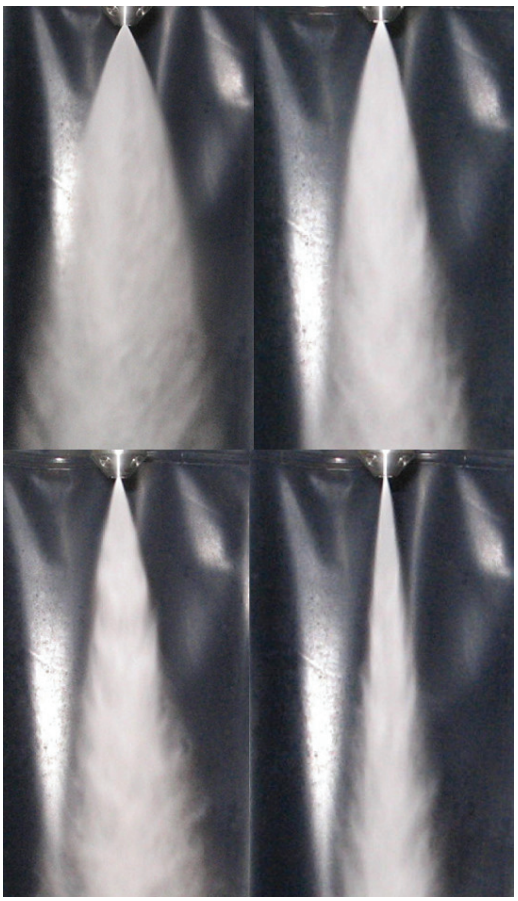

Picture 13. Same nozzle with different end boring sizes

5 TEST RESULTS

The preliminary tests with new nozzle structure have shown that nozzle principle works well in practice. By varying the end boring totally different flow geometries can be achieved. In picture 14 is shown the perceptual change of spray angle as function of parameter, which is called ratio of side and end boring diameter. Parameter can be defined as presented in following. The center and side boring sizes were 0.8mm in the nozzle used in tests presented in this paper.

$$\text{Ratio} = \frac{d_{\text{end boring}}}{d_{\text{side boring}}} \tag{26.}$$

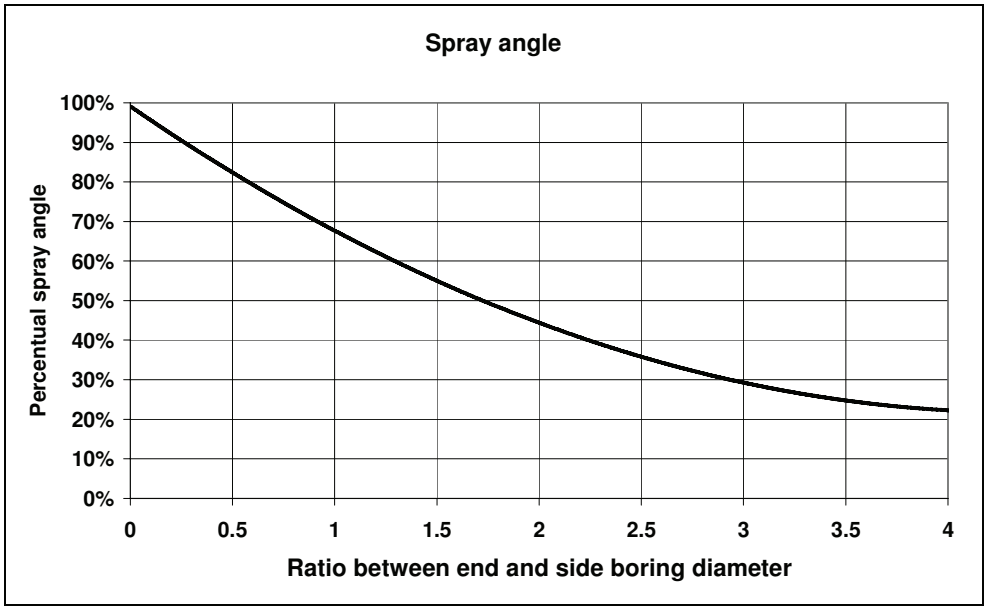

Picture 14. Percentual change of flow angle as function of end / side boring diameter

Results show that if end boring size is increased from 0 to 4 times of side boring diameter, the spray angle can be focused only to approximately 20% of original initial area. The angle is measured from nozzle to 0.40 meter level to downstream. If the effect of momentum is considered, it is better to change the angle to effective area. This basically means round shape level located horizontally 0.40 meter directly below the nozzle. This can be considered as cross-sectional spray pattern are as well, which the most of the droplets pass through. If this effective spray area is compared with different boring sizes the difference can be seen better only comparing spray angles.

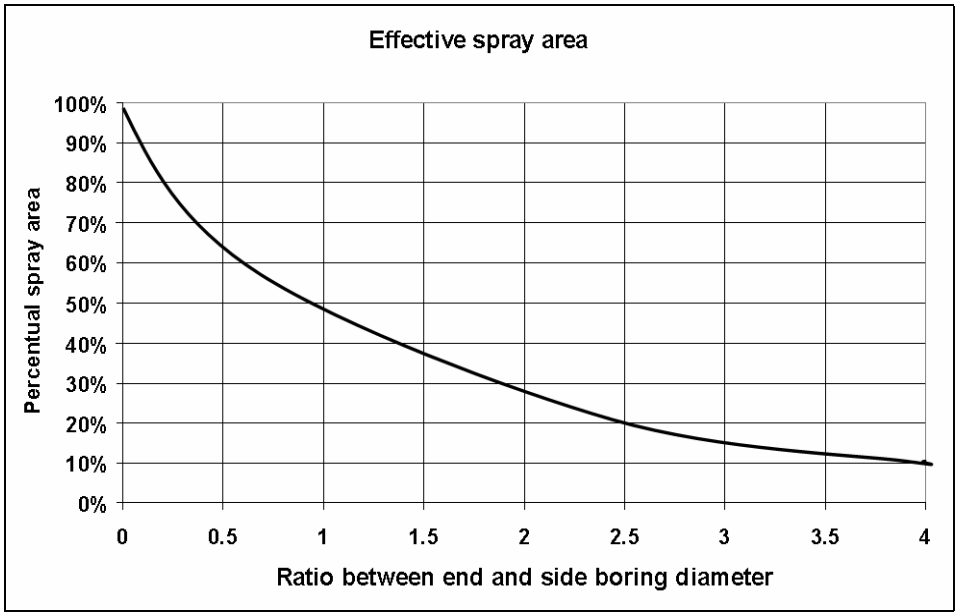

Picture 15. Percentual change of cross-sectional spray area as function of end / side boring diameter

As it can be seen the droplets will be sprayed much larger area if there is lot of rotation momentum in the spray. This means that the size of end boring is significantly smaller than the side borings. However, if the diameter of end boring is increased, the spray area

decreases a lot and nozzle works like normal jet nozzles. The effective area can easily be less than on tenth of the area it is with high swirling.

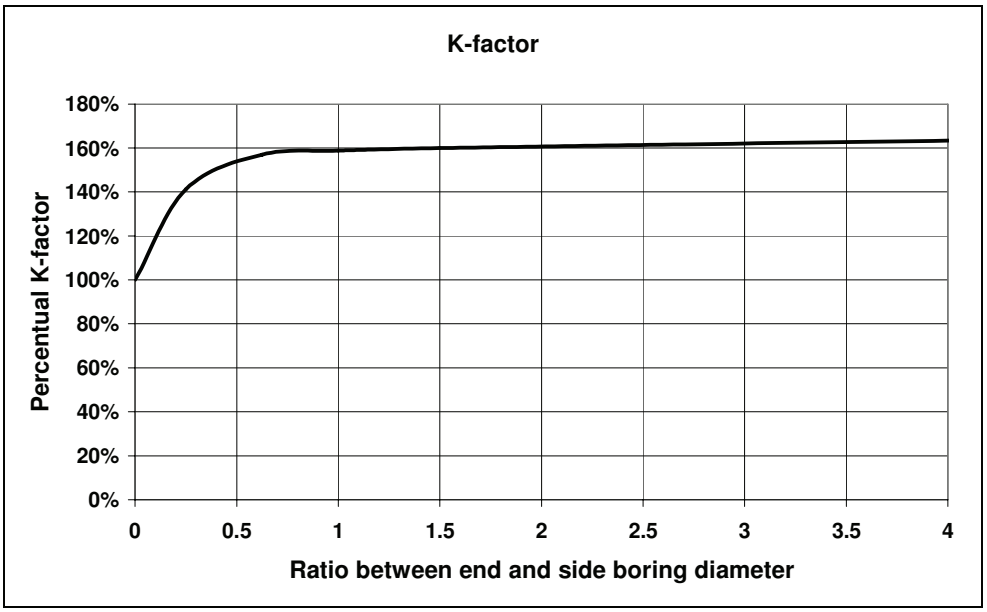

Picture16. Percentual change of K-factor as function of end / side boring diameter

The effect of different end and side boring ratio to the K-factor of the nozzle can be seen in picture 16. It can be seen that there is relatively big difference. The K-factor is significantly lower if the end boring is less than 20% of the diameter of side boring.. Explanation for this is the strong swirling effect with small end boring size which causes additional resistance through the orifice boring..

After the ratio between the end and side boring diameter is more than 20%, the difference in K-factor is relatively small and it had saturated to constant value.

6 CONCLUSIONS AND FUTURE WORK

High-pressure water mist systems have superior benefits compared to conventional fire extinguishing and suppression technologies. The core of water mist systems is the nozzle that does the atomization of water to small droplet sprays. Flow rate (K-factor), droplet size and momentum of the droplets are the main measures if nozzles are evaluated. The theory behind these elements is relatively complicated and includes often experimental based information. However, these can be calculated even analytically if the flow situation is simple like in jet nozzle. However, the better tool is CFD computational fluid dynamics to model the behavior of different nozzle types.

The new nozzle concept can combine the positive features of two main nozzle types in the market, jet nozzles and swirling flow nozzles. The design allows that the character of the nozzle can be changed only by changing the diameter of one boring. Preliminary test results have been promising both in theoretical point of view and also in practical tests.

More development will be done in future. The main objective is to find an analytical model, which would help the designer to calculate right design parameters. The nozzle

will be modeled by using CFD as well. One of the most important objectives is to define the boundaries for different design parameters.

REFENCES

[1] Vaari, J., Water Mist for Healthcare, Business Briefing: Hospital engineering & facilities management, USA, January 2003.

[2] Safety of Lifes in Tunnels – Research program, www.solit.info 2006.

[3] NFPA750, Standard on Water Mist Fire Protection, US National Fire Protection Agency 2000.

[4] Lakkonen, M., Water Mist Systems and Industrial Water Hydraulics – Similarities and Differences from Technical and Design Point of View, IWMA *(International Water Mist Association)* Conference, Berlin, Germany October 2005.

[5] Lechler Archieves.

[6] FOGTEC Archieves.

[7] IWMA, International Water Mist Association, www.iwma.net 2007.

[8] FM Global Technologies, Approvals Standard for Water Mist Systems, Class 5560, 2005.

[9] CEN/TC 191, Fixed Fire Fighting Systems – Water mist systems – Design and installation (draft) prEN14972, 2004.

[10] Lefebvre, A., Atomization and Sprays, Taylor&Francis, USA 1989.

[11] Nasr, G.G, Yule, A.J. and Bendig, L., Industrial Sprays and Atomization – Design Analysis and Applications, Springer-Verlag, UK 2002.

[12] Schneider, B.M., Experimentelle Untersuchnungen zur Spraystruktur in transienten, verdampfenden und nicht verdampfenden Brennstroffstrahlen under Hochdruck, Dissertation, Nr.15004, ETH, Zürich 2004.

[13] Paulsen Husted, B., Holmstedt, G. and Hertzberg, T., The Physics Behind Water Mist Systems, IWMA *(International Water Mist Associsation)* Conference, Rome, Italy October 2004.

PROPORTIONAL TECHNOLOGY WITH ELECTRONICS ON BOARD

Dipl.-Ing. Marc Emmaneel
Tiefenbach Wasserhydraulik GmbH
Nierenhoferstraße 68
45257 Essen, Germany
Phone +49 201 8483 170, Fax +49 201 8483 10
E-mail: marc.emmaneel@tiefenbach-wasserhydraulik.eu

ABSTRACT

Continuously increasing economic requirements have made it necessary to develop new parts for proportional valve technology. The same economic pressures have resulted in shorter delivery times and less time allowed for the installation of new equipment. The time for replacement, fitting, configuration and commissioning of components, and in this particular case of proportional valves, is now at a critical minimum. It was therefore necessary to look at improving certain individual design aspects of these valves in order to simplify and accelerate this procedure. The result is a new proportional valve technology incorporating on board electronics, a feature requested for some time now by our industrial clients.

A second issue, especially evident in recent years, is the continued rise in system operating pressures, leading automatically to higher flow rates. To avoid the wear problems unavoidably associated with these higher flow rates, the use of new materials for water-hydraulic systems and valves has been indispensable. In this regard Tiefenbach Wasserhydraulik GmbH tests any relevant new materials almost as soon as they become available to the engineering industry. Great importance is placed on achieving a compromise between the properties of these new materials, their cost and their practicality in the harsh environment of water hydraulics. With this article we also hope to show our experience with some of these materials.

KEYWORDS: new materials, on-board electronics, proportional valves, water hydraulics

1 PROPORTIONAL TECHNOLOGY WITH ELECTRONICS ON BOARD

1.1 Motivation

Proportional control technology in water-hydraulics has up to now required the use of a proportional control valve with a separate control card. Operating circumstances at many sites pose difficulties simply because of the large distances between the valve its control card. In cooperation with our customer Thyssen Krupp, Hoesch Hohenlimburg, Germany, we have worked towards a solution to this problem, one which both shortens this distance and reduces installation time. At Hoesch Hohenlimburg these valves are installed in the roll-bend circuit of a hot rolling mill. To improve strip quality a slight bend is applied to the rollers on the reversing millstands. The hydraulics controlling this cicuit are pressure regulated using proportional valves. A further point of note is that in the past the control signals transferred between the proportional valve and the control card has been subject to outside interference. So the permissible length of this connection has been reduced to a critical minimum. It should be mentioned at this point that this development has been made easier as a result of the support of personnel at the Hoesch Hohenlimburg plant.

Figure 1: Hot rolling mill TyssenKrupp Hoesch Hohenlimburg

By using the classical proportional technique the inlet and outlet valve as well as the measuring unit are to be connected with the control card.

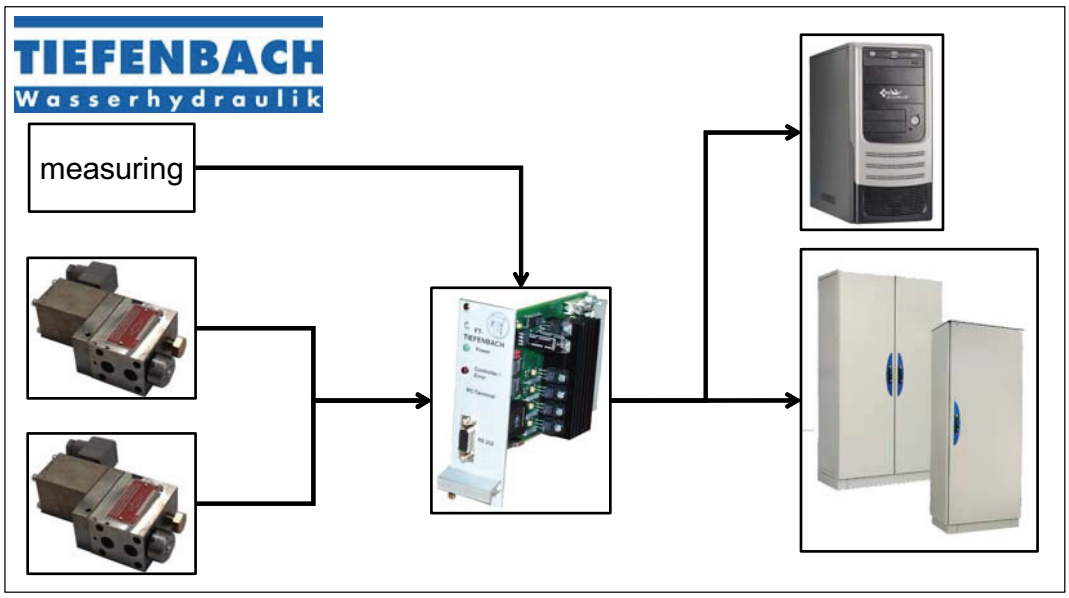

Figure 2: Classic proportional technique

The following were the requirements for a new design approach to proportional control:

- monitoring capability
- elimination a remote, external control card
- easy maintenance and trouble shooting
- simple installation
- contactless configuration capability (infra-red or similar)

1.2 The proportional technique with electronics on board

The control card is integrated in the proportional valve solenoid.

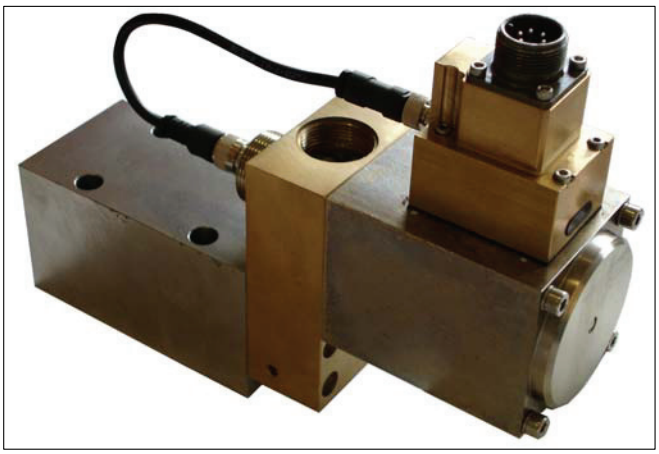

Figure 3: Proportional technique with electronics on board

Apart from the valve itself the solenoid is no different to that of the classic proportional valve. So many years of experience can be applied to the new proportional valve with on board electronics.

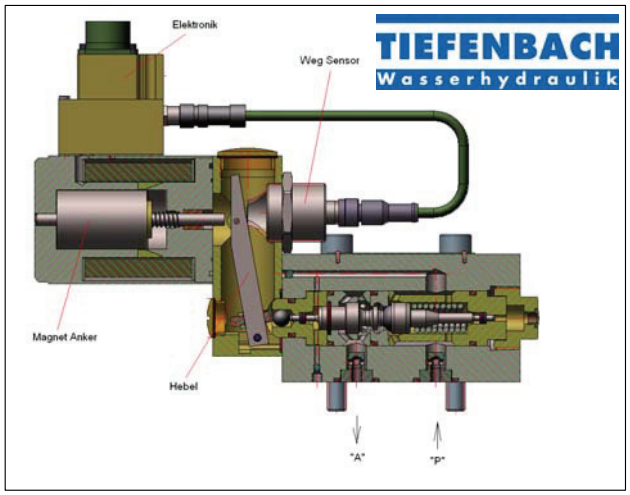

Figure 4: Sectional drawing of the proportional valve

The integration of an infrared interface makes it possible to configure the valve contact-less by using a notebook. The valve with the integrated control card and the infrared interface is called “Master Valve”.

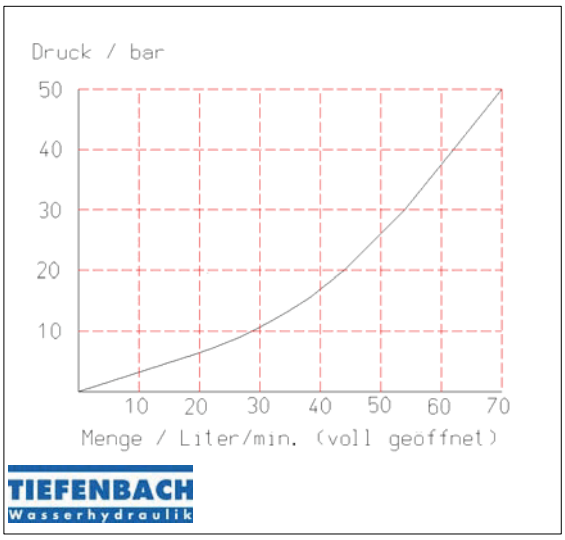

Figure 5: Pressure / flow diagram

The measuring unit is directly connected with the master-valve.
With either pressure or position control a second proportional valve is necessary. This valve has neither an infrared interface nor an integrated control card and is designated the slave valve. It is hard-wired to the master valve as shown in figure 6.

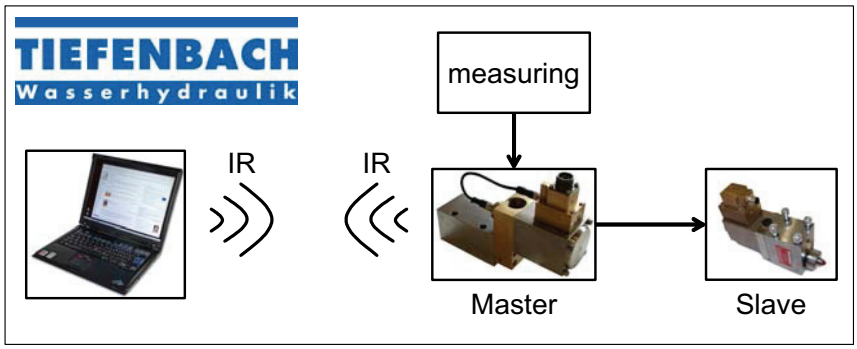

Figure 6: Proportional technique with electronics on board

The new design makes it possible to send the feedback value to the control unit continually. The set-up software used with the proportional valve permits valve diagnosis in real time via the infrared interface. In short, a valve has been developed, which satisfies almost all of today's requirements as regards monitoring.

The error output, integrated directly into the valve plug, sends error messages to the control unit. Valve malfunctions and connection problems are reported immediately. Because there is less cable with fewer connections the probability of transmission problems occurring due to cable faults are reduced anyway
The valves can be controlled by the voltage, which has values between 0 und 10 V or by 0 – 20mA signal.

1.3 Configuration of the proportional valve

It is not enough to have a soundly developed valve in order to guarantee simple maintenance and short downtimes. You must also have intelligent software; software which makes it possible to calibrate the valve and the controller quickly and accurately.

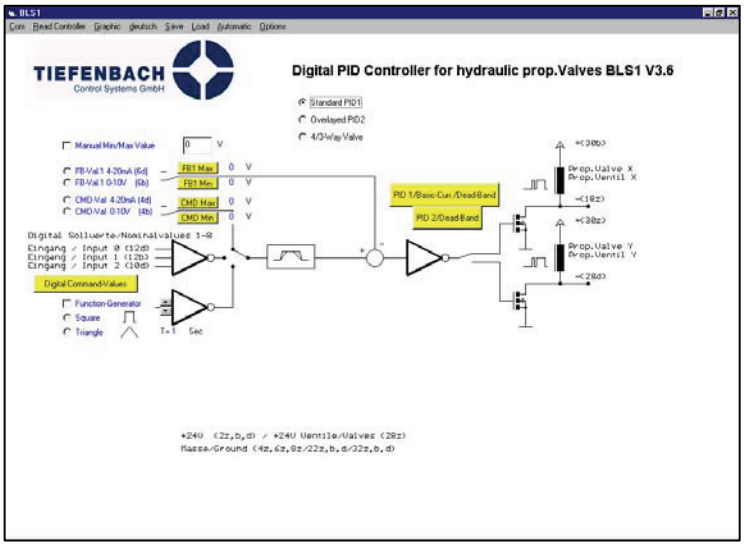

Figure 7: Control card software

The software written especially for this valve permits automatic calibration and configuration of the valve. The base currents for the inlet and outlet solenoids X and Y and the P, I and D values, all of which are significant factors in good valve performance, are identified and set by the automatic calibration routine. Here the P-value is the proportional gain of the command-feedback error, the I-value the gain of the integral of the command-feedback error and the D-value the gain of the differential of the command-feedback error. The values identified can be saved and in the event of a valve change can be reloaded and transferred to the new valve.
Using the integrated function generator fine tuning of the P, I and D-values can be performed once the automatic setup is completed.

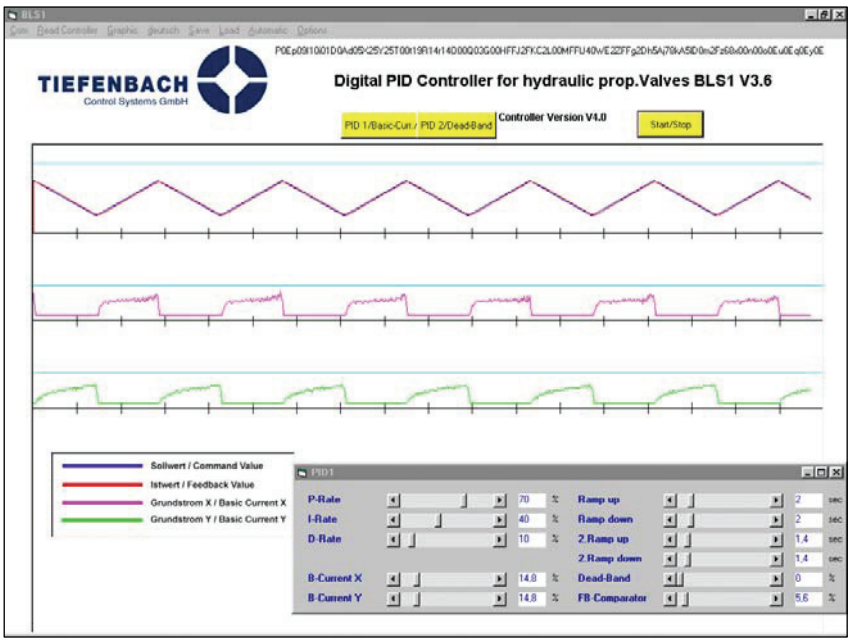

Figure 8: Function generator

1.4 Operating Experiences

The application of new proportional technology with on board electronics has achieved the hoped-for reduction in installation time, and reduced both maintenance and down-

time. In fact customers using this technology have measured change-out times in minutes rather than hours as was previously the case. This includes the time for configuration of the new valve.

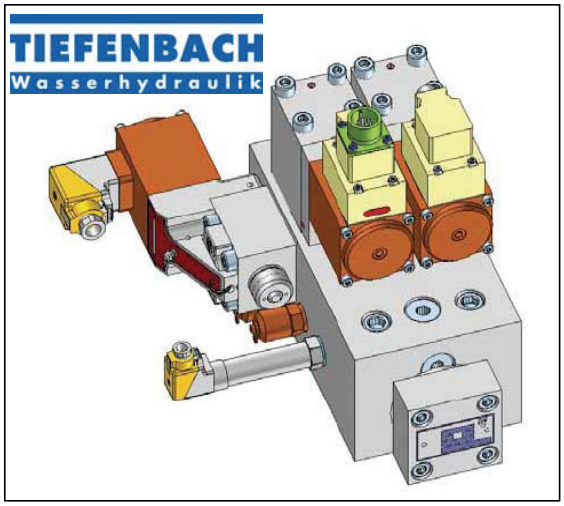

Figure 9: Control unit with new proportional technology

One reason is that we intentionally designed the valve with only four screws, which have to be loosened to change the valve. Another is that the control unit is centralized with no long distances to the control unit, making it easier to pinpoint errors. Checking the integrity of the connections and valves can be performed in seconds at one single location.
The modular design viz. Master-valve, Slave-valve, control unit and a 2/2 directional control valve as an isolating device for even faster valve replacement has motivated a number of users to adopt this the new proportional technology.
Long-term tests show that the lifetime of the new technology is as long as that of the classic proportional design. We are currently developing a bus solution for the Master-valve, to allow us to use the same approach for applications with multiple parallel inlet and outlet valves, as required as pilots for larger proportional valves.

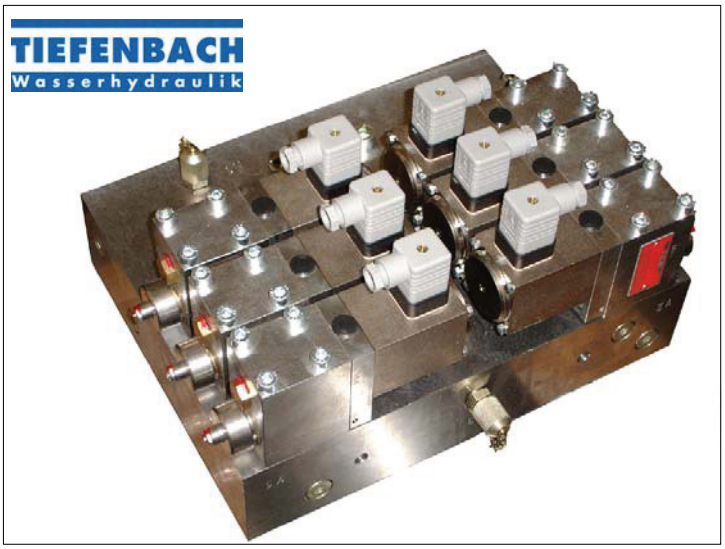

Figure 10: Pilot-control unit with classic proportional technology

In the future one master-valve will control a number of slave valves, significantly decreasing the price for pilot control units.

2 MATERIALS USED FOR WATER-HYDRAULICS

In the past the most manifolds and valve housings have been manufactured out of 1.4104 material. Experience with this material has been and remains positive. However, the tendency to higher pressure requirements and higher flow rates makes it necessary to think about using other materials. Nowadays many machines are running with pressures higher than 320 bar, much higher than in the past, requiring the more frequent use of materials such as 1.4313, particularly if manifold block height and width exceed 400 mm.

Figure 11: Manifold

1.4313 is a martensitic stainless steel with good stiffness properties. In particular it is more resistant to erosional damage at higher pressures. The disadvantage is the somewhat longer machining time, resulting in higher manufacturing costs and ultimately affecting the market price of the component.

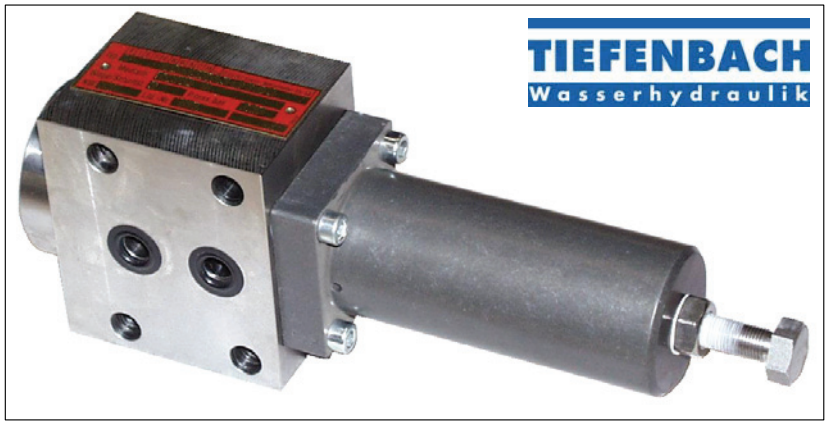

Figure 12: Pressure reduce valve

In particular pressure reducing valves are exposed to high demands because of continuous flow through some parts of the valve. Conventional steels are not sufficiently wear resistant, which is the reason for looking closely at manufacturing parts such as the valve seat and piston out of powder steel M390 PM for example. When using this material the parts are vacuum hardened as a second step. The advantage of this material is excellent machining performance before hardening of the material. One disadvantage is

the high price of the material, so that it only makes sense to manufacture the most stressed parts of the valve out of powder steel.
If valves have to meet special requirements such as very low weight or very good corrosion resistance the use of the material titanium is advised.

Figure 13: Seawater valve

Especially valves for the navy or civil shipbuilding industry are of titanium.

3 SUMMARY

It has been shown that the development of a new proportional control technology with on board electronics is important when competing with oil hydraulic and so is important for the future of water hydraulics. Testing new materials will enable us to use water-hydraulics at ever higher pressures and flow rates.

4 REFRENCES

[1] **Nikolaus Fecht**. *Stillstandzeiten minimieren.* Fluid 3/2006, Verlag Moderne Industrie

COMPARATIVE TRIBOLOGICAL INVESTIGATIONS OF CONTINUOUS CONTROL VALVES FOR WATER HYDRAULICS

Franc Majdič, Jožef Pezdirnik, Mitjan Kalin
Centre for Tribology, Technical Diagnostics and Hydraulics
Faculty of Mechanical Engineering
University of Ljubljana, Slovenia
Aškerčeva 6
1000 Ljubljana, Slovenia
Phone +386 1 477 1413, Fax +386 1 477 1469
E-mail: franc.majdic@fs.uni-lj.si

ABSTRACT

Reduction of oil usage and its almost daily increasing price is directing world development in the field of hydraulic fluids towards alternative sources. One possible alternative source is water, which is environmentally blameless, low-cost and nonflammable.

Taking into consideration the body accessible information about water power-control hydraulics (PCH), we constructed a simple hydraulic test rig to investigate the basic tribological and hydraulic behaviour of such systems under pressures up to 150 bar and flows up to 30 L/min. With that aim we designed and constructed a proportional 4/3 directional continuous acting spool type sliding valve, a simplified model but still with the shape and working parameters resembling real valves. Tribological properties and static as well as dynamic behaviour can be investigated on this model by employing components of different materials. All other applied components of this test rig were taken from normal serial production, meaning that these components are available on the market. In this work, a design of the test rig and testing schemes are presented, while the real-scale preparation and testing procedures are on-going.

However, in order to ensure a satisfactory useful life time of the proportional 4/3 directional control valve, an optimal tribological pair is required in the valve. With this aim in mind, we carried out preliminary tribological tests of different material-pairs lubricated with additive-free distilled water. The tested materials were stainless steel, PI, PEEK and Al_2O_3. The results of the preliminary tribological tests of different material pairs are described in this paper. The best material pair considering low wear and a low coefficient of friction was obtained with graphite-modified PEEK composite against Al_2O_3.

KEYWORDS: high pressure water systems, power-control hydraulics, distilled water, proportional directional control sliding type valve, tribological properties, pin-on-disk, stainless steel, PI, PEEK, Al_2O_3

1 INTRODUCTION

A great number of countries are making considerable efforts to protect their environment. In the past in Slovenia we have investigated bio-degradable fluids [1 - 4] and their application in power-control hydraulics [5], especially for machines working in environmentally sensitive areas. Yet additives must be added to such fluids, and they are not environmentally blameless. But the use of tap water as a hydraulic fluid has no adverse effects on the environment. That is the reason for our decision to investigate tap water as a hydraulic fluid for power-control hydraulics (PCH). Several components for acceptable high pressures using this fluid have already been developed and are available on the market [6, 7, 8, and 9]. In the field of hydraulic valves the ball- or poppet-seat type of valves are usually available on the market at designer's or customer's disposal [6 and 7]. But this type of valve is badly suited for continuous regulation functions, especially for continuous and fine flow regulation. Other weak points of such valves are their large dimensions and quite complicated construction [7].

Using water instead of mineral oil as the pressure medium entails significant changes in the physical parameters [10]. Compared to mineral oil water differs, in the following physical parameters which are important for PCH: about 30- times lower viscosity (at 20°C) and thus poorer lubrication, a more than 12 million-times higher vapour pressure (at 50°C), and 33 to 60 % higher bulk modulus (at 20°C). Water also provokes corrosion of parts that are not corrosion resistant.

In designing spool sliding valves for water power-control hydraulics we have to consider that the very low viscosity of water, compared to that of mineral oil, plays a dominant role. Assuming a lower viscosity, *Trostmann* et all [10] found that in order to ensure the same amount of leakage using water instead of mineral oil as the pressure medium, a one-third reduction in the radial space gap is required, holding other parameters as constant. This suggests that the tolerances and dimensional characteristics are much more strict and demanding in water than oil. This further imply more severe contact conditions and poorer performance under the same conditions is anticipated.

The higher energy *density of the pressure fluid flow* in water hydraulics and the higher vapour pressure of water compared to that of mineral hydraulic oil may cause serious problems of erosion (via cavitation) and abrasion, higher leakage flows and problems in valve functioning [10]. A lower viscosity also means a lower lubricating film, which can increase friction and wear, unless we use suitable material-pairs [11].

Furthermore, the dynamic behaviour of water power-control hydraulic systems (PCHS) differs significantly from that of mineral oil PCHS, especially in pressure amplitudes and oscillating periods in the case of underdamped oscillatory motions. The bulk modulus of water is about 70 % higher than that of mineral oil. The results of a mathematical model [12 and 13] suggest about 24 % higher pressure amplitudes in water PCHS compared to those of mineral oil PCHS, other system parameters being the same for both systems.

However, the actual dynamic performance, tribological properties, and resistance to motion must be – in addition to theoretical predictions- verified in tribological and real-scale testers. Accordingly, in this work we present a newly developed dedicated

hydraulic test rig for testing the water-based hydraulic systems, which can use testing components from different materials. For comparison, conventional "oil-test" can also be performed In addition, a preliminary model tribological tests with different material combinations consisting from ceramics, plastics and stainless steel are presented. Present data suggest that the most promising material pair resulting in a low wear and a low coefficient of friction was obtained with graphite-modified PEEK composite against Al_2O_3.

2. CONSTRUCTION OF TEST RIG

2.1. Project requirements

The water power-control hydraulic (PCH) testing rig should be simple, controllable, and it should represent an almost real hydraulic system. It should enable to:

- Measure pressure, flow and temperature before and after the testing specimen – namely, a proportional directional control valve.
- Assure a constant flow through the proportional directional control valve independently of a possible decrease in pump volumetric efficiency.
- Simulate loading and control its response.
- Assure variation of loading.
- Assure controlled temperature value of the fluid (via cooling).
- Assure a full automatic life-cycling test.
- Assure measurement of the dynamic response of the system.
- Assure measurement of the dynamic response of the specimen – the proportional directional control valve.
- Assure simple measurement of the leakage of the specimen – the proportional directional control valve.

2.2 Construction of water hydraulic test rig

We constructed a water PCH test rig which satisfies all the project demands. Figure 1 shows the hydraulic circuit of our test rig. It contains a standard Danfoss axial piston pump, type PAH 25 (Fig. 1, pos. 4.0), with a flow rate of near by 35 L/min [6] at 1450 r./min and a volumetric efficiency of 97%. This pump delivers water through a pressure-compensated flow control valve (Fig. 1, pos. 19), which ensures a constant flow of 30 L/min through the specimen – the proportional directional control valve (Fig. 1, pos. 20). This proportional directional control valve is controlled from a PC in a closed loop. On connection A of the proportional valve, we have a flexible hose of 2 m, a pressure transmitter, and a double-acting through-rod hydraulic cylinder (Fig. 1, pos. 22). The second branch from connection B to the hydraulic cylinder is equal to the first, already described. On the end of the cylinder's rod a translator-moving mass (Fig. 1, pos. 24.1) with minimum friction coefficient is connected. This linear oscillating mass is used for short-term dynamic tests. For life time cycle tests of the proportional directional control valve, another double-acting through-rod hydraulic cylinder (Fig. 1, pos. 124.1) is used instead of the moving mass.

With this hydraulic cylinder we simulate a load through the double throttle (Fig. 1, pos. 127) and four check valves (Fig. 1, pos. 126). The hydraulic medium in this hydraulic cycle is mineral oil. This oil-hydraulic cycle has its own pump (Fig. 1, pos. 101), which

delivers oil to the hydraulic cylinder (Fig. 1, pos. 124.1) with the residual flow through an air cooler and filter. The main aim of this pump is to provide an oil flow for cooling and filtering. Its second aim is not driving or powering the hydraulic cylinder, but just assurance of inlet flow. Return flow from the cylinder is taken through an air cooler and oil filter. This solution assures near constant temperature conditions of the oil hydraulic cycle which simulates load.

The assemblage of pipe valve and double T-pipe-connectors (Fig. 1, pos. 14.i and 15.i) give us an opportunity for periodical control of flow and temperature at different positions. The water relief valve (Fig. 1, pos. 6) is set to 160 bar. We used a dynamic centrifugal water pump (Fig. 1, pos. 13) to maintain constant temperature (air cooler) and to enable off-line filtering.

Control of the proportional magnets (Fig. 1, pos. 26.1 and 28.1), data acquisition and control of the electro-motors is provided by and automated through a PC.

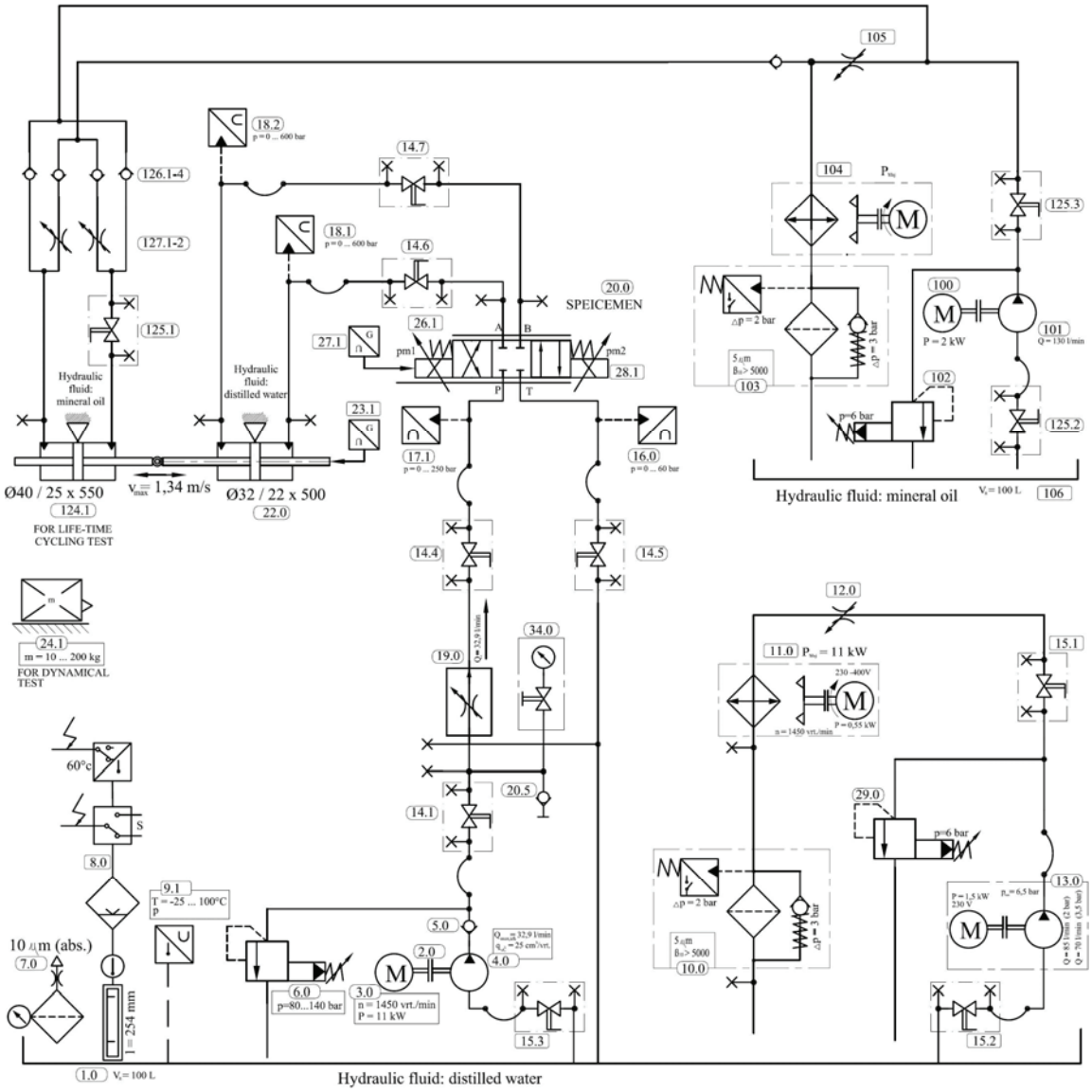

Figure 1: Hydraulic circuit of water PCH test rig

2.3 Construction of proportional 4/3 directional control valve

As the seat type of valve, either poppet or ball-type, is not convenient for use as a continuous valve, we designed and constructed a proportional 4/3 directional control sliding valve. It is used in our water hydraulic test rig for motion control of the water double acting hydraulic cylinder with double-ended rod.

In order to study the tribological performance using different materials, a simple, well-controlled and easily replaceable testing samples need to be used. Also, their size and shape should enable fast and easy surface analyses. For this purpose, we designed and manufactured functional prototype of water proportional 4/3 directional sliding control valve as shown in three-dimensional model in figure 2.

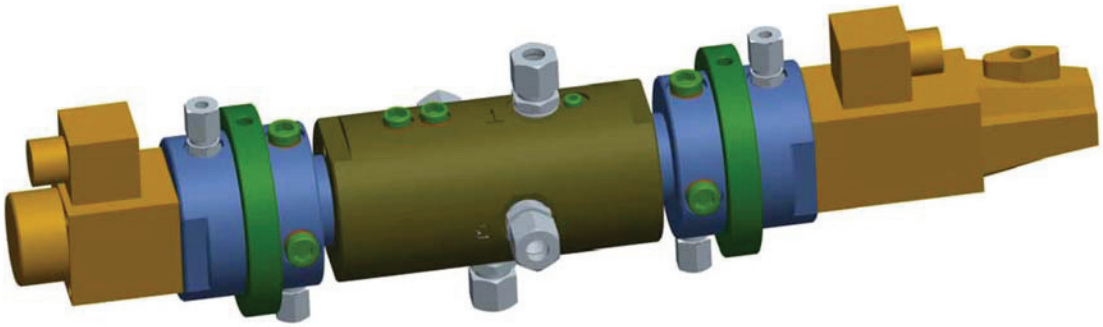

Figure 2: 3D model of a functional prototype of a proportional 4/3 directional sliding control valve

Main parts of the functional prototype of a proportional 4/3 directional sliding control valve are (figure 3): sliding spool, housing sleeve, outer housing, adaptors for proportional solenoid, and two proportional solenoids, one of them with inductive transducer.

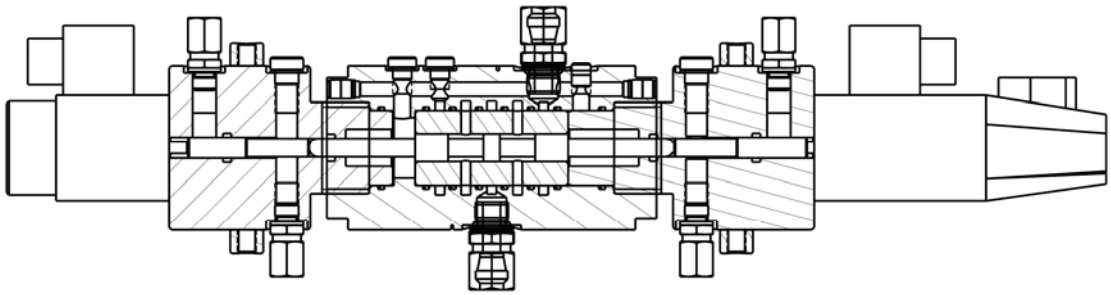

Figure 3: Cross section of the functional prototype of a proportional 4/3 directional sliding control valve

In the main part of our specimen – functional prototype of proportional 4/3 directional control valve sleeve and spool are simple in geometry and can thus be indeed easily changed (Fig. 4). We can manufacture these key-parts rather easily and in inexpensive way and thus test different materials, also those more expensive and those difficult to produce in more complex shapes, for example ceramics.

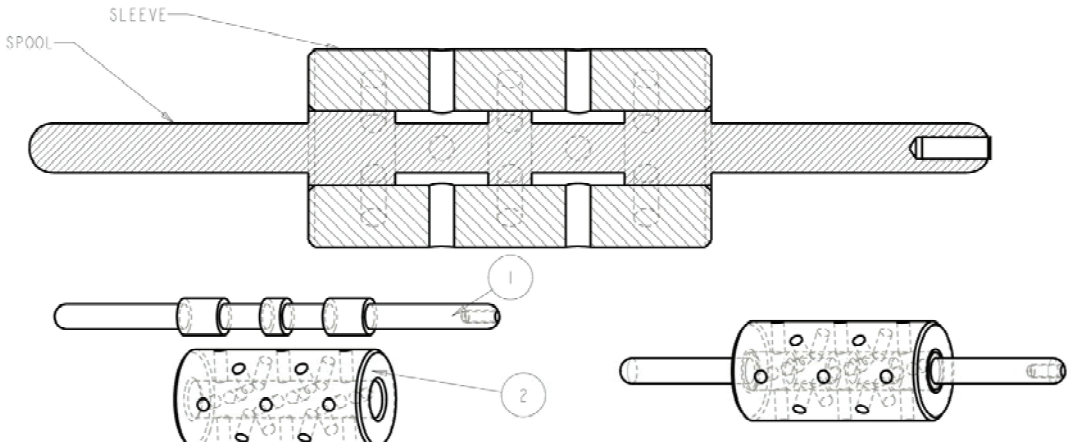

Figure 4: Main parts of the specimen: 1) spool and 2) sleeve

2.4 Testing procedure

In the real-scale life tests, loading cycles can be varied with pressure and flow to achieve different working regimes. The pressure can be changed up to 150 bar and flow up to 30l/min. As mentioned before, materials of studied parts can also be changed, both, the spool and the sleeve. Fluid temperature and fluid flow through specimen and spool stroke can be controlled; being varied or constant, depending on the testing parameters. Figure 5 briefly introduces the testing parameters and time cycle procedure for the selected system with the proportional 4/3 directional control sliding valve.

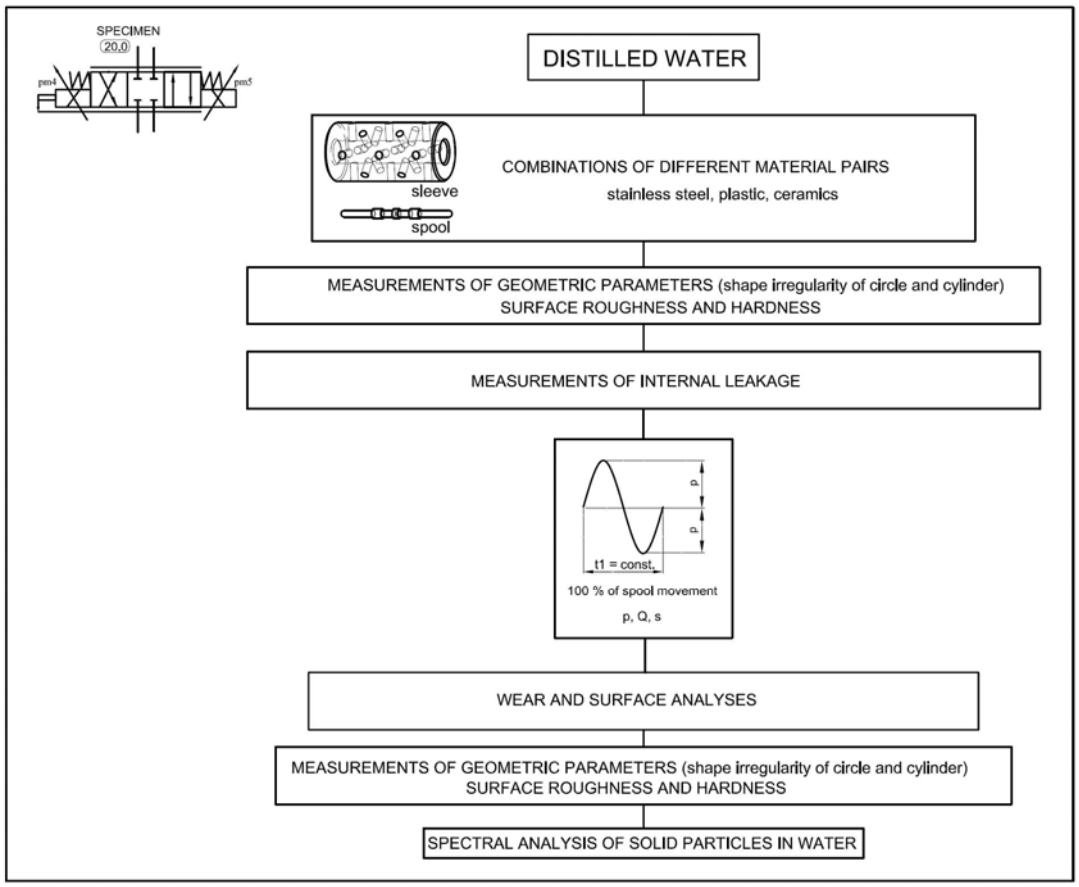

Figure 5: Course of life-time measurement on the main test rig

Before and after tests the geometric parameters of the spool and sleeve (shape irregularity of circle and cylinder) need to be measured and analyzed. Also, measurements of surface roughness and surface hardness are made. After the tests, the parts are dismounted and checked for wear loss, as well as the surfaces need to be analyzed to determine the wear mechanisms, Sometimes, the amount of solid particles in the system – or produced by the system - can alos be of interest and this can be done on-line or after the test is finished.

Internal leakage can also be measured. The directional control valve is set in the neutral position (all ports blocked) and a pressure is assured by alternating on each port (P, A and B). After pressurizing each single port, the leakage is measured on the other three ports and sum them together.

The test rig was designed in way, to allow runs of different types of tests. They can be long-term tests to study the performance during longer periods and consequences of wear of the parts, primarily investigating the wear mechanisms by subsequent surface analyses, leakage, formation of wear debris, etc. However, short-term experiments can also be performed. Primarily, the dynamic response and effects of different geometrical and fluid characteristics is anticipated for these type of test runs. Namely, the majority of hydraulic systems are subjected to fast dynamic changes of flow and consequently pressure. The pressure responses of the test rig during gradual changes of hydraulic fluid flow can be measured. In this case we can use a known mass (Fig. 1, pos. 24.1) instead of the double acting through-rod hydraulic cylinder (Fig. 1, pos. 124.1). Comparison of the pressure / flow response of the specimen (proportional 4/3 directional control valve) at outlet port A and B (Fig. 1, pos. 20) with change of spool position and change of electrical current on the proportional solenoids (Fig. 1, pos. 26.1 and 28.1) can be performed.

3. TRIBOLOGICAL TESTS OF VARIOUS MATERIAL PAIRS

3.1 Experimental

In order to investigate the change in hydraulic parameters, in particular wear resistance and useful life in selected hydraulic tests for different possible material combinations, model tribological tests were performed to make an initial or preliminary selection. Generally, stainless steel (SS) is the most typical and in-expensive material already used in several hydraulic parts and was thus reasonably the first-choice material. Other potential groups of materials include ceramics and polymers. Since ceramic materials are very costly and also have a low fracture toughness, they were not considered as the most suitable materials for the real-scale tests through which we would like to compare materials in the later stages of this research. Therefore, they were not included as the "studied" material (disk) in the first screening tribological tests; however, a ceramic was used at least as a counter-material, i.e. pin, which should also give us some indication of the tribological properties of the selected couples. Different commercially available polymeric materials were also considered. We selected those that can be used in water for a longer time-span [14 - 16] and gave some promising tribological results in the past, and which are also easily commercially available and suggested by world-wide known producers. Thus, we selected two different types of materials from two groups of polymeric materials, i.e. polyetheretherketone (PEEK) and polyimide (PI). A

commercially available PEEK (Victrex Europa GmbH, Germany) containing 30 % of carbon (CA30) and 30 % of glass (GL) fibers were used. Polyimides (Vespel) from DupontTM without any addition (SP1) and containing 15% of graphite fibres were also tested. Pin materials were SS (X105CrMo17), obtained from Aubert&Duval and hardened to 55 Hrc, and alumina ceramic balls (99.7 % purity, 10 mm diameter) from Hightech Ceram. In total, 4 types of polymeric materials and stainless steel were selected as disc materials, while pins were of the same stainless steel and alumina ceramics. Table 1 presents the selected combinations.

Table 1: Material pairs used in preliminary tribological tests

Disc material	Pin 1	Pin 2
PEEK 30% glass (GL30)	Stainless steel (SS)	Alumina (Al_2O_3)
PEEK 30% graphite (CA30)	Stainless steel (SS)	Alumina (Al_2O_3)
PI no addition (SP1)	Stainless steel (SS)	Alumina (Al_2O_3)
PI 15% graphite (SP21)	Stainless steel (SS)	Alumina (Al_2O_3)
Stainless steel (SS)	Stainless steel (SS)	Alumina (Al_2O_3)

Tests were performed in a pin-on-disc apparatus (CSEM, Switzerland) with uni-directional sliding between the disc and the pin, see Figure 6. The relative sliding velocity was 0.1 m/s and a load of 1N was applied (Fig. 7), which corresponded to 40-70 MPa of initial contact pressure, depending on the material pair. In the open literature [14 - 16], data are available for some selected polymeric materials at lower pressures, but our goal was to investigate the higher-end load-region of those materials. Tests were run for 370 m of total sliding distance. All the tests were performed in a cup with distilled water at around 21^{o}C, i.e. at room temperature conditions. These conditions correspond to a boundary lubrication regime, where hydrodynamic effects are negligible and the tribological performance depends primarily on surface and interface phenomena. Friction was monitored during the test and wear loss of the disc materials was subsequently calculated. The first empirical friction and wear results are presented in Figures 8 and 9, respectively. At present, detailed surface analyses, which would allow determination of wear and friction mechanisms and confident interpretation of the results, are still in progress.

Figure 6: Pin-on-Disc wear tester (CSEM)

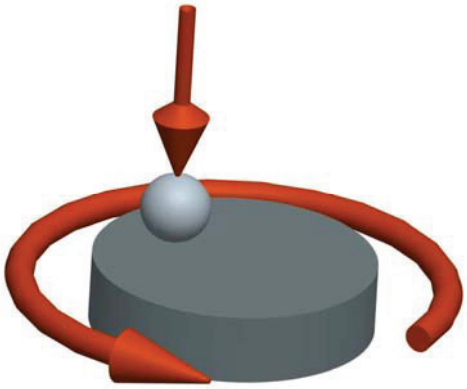

Figure 7: Functional principle of tribological pin-on-disk tests, lubricant: distilled water

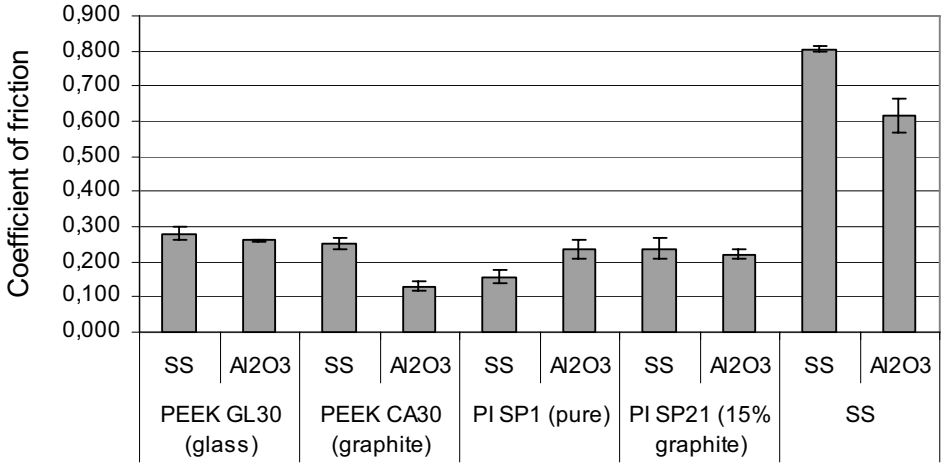

Figure 8: Coefficient of friction for selected material pairs (disc against two pin materials is shown)

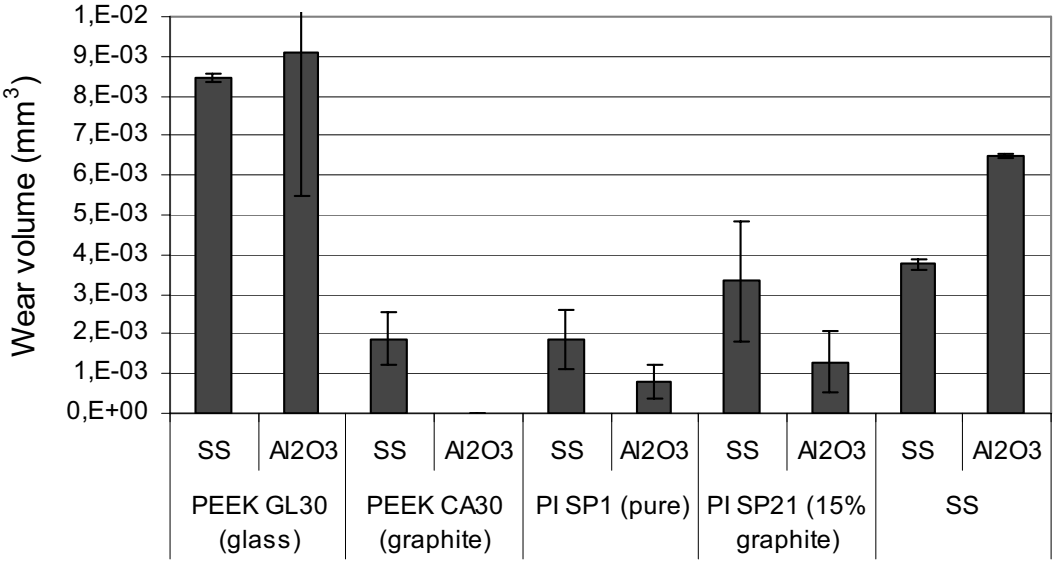

Figure 9: Wear loss for selected material pairs (disc against two pin materials is shown)

Compared to polymeric materials, significantly higher friction values were measured in contacts with SS discs, which were in the range of 0.6-0.8. Other friction data show friction values between 0.13 and 0.28, which is 2-3 times less than with SS discs. With

the exception of pure polyimide (SP1), with all other polymer discs, contacts with alumina pins resulted in lower friction than against SS pins. However, these differences were not very high. Nevertheless, it is to be noticed that friction in the polyimide SP1 / SS contact resulted in the second lowest friction – about 0.16. This is important, because the polymeric material contain no additional components and is thus simpler and cheaper. Moreover, the SS pin is also the most preferred counter-material from a practical point of view. The lowest friction in this study was, however, obtained with the PEEK CA30/Al2O3 combination, where friction was about 0.13.

In accordance with friction the data, the wear of PEEK CA30 in contact with an alumina pin was so low that was not possible to measure it with the techniques we used (stylus tip measurement with a resolution of around 50 nm in the z-axis). Therefore, this contact combination seems to be clearly the most promising of all those tested in this study. Low wear against alumina pins was also measured in the SP1 and SP21 polyimide samples. PEEK CA30, PI SP1 and PI SP21 also provided reasonably low values of wear in contacts against stainless steel pins. On the other hand, discs of SS and PEEK GL30 always resulted in higher wear losses. This was particularly pronounced against alumina pins, which is the opposite behaviour compared to PEEK CA30, PI SP1 and PI SP21.

4. RECAPITULATION AND CONCLUSIONS

- A simple test rig for investigation of the tribological and hydraulic behaviour of a water hydraulics system was designed. The conditions, materials and geometry can be well-defined and controlled. The test rig allows for testing of several hydraulic, operational, dynamic and tribological properties of selected systems.
- We also made preliminary model tribological tests to investigate the adequacy of different material pairs for use in a proportional 4/3 directional (sliding type) control valve.
- The lowest friction was obtained for the PEEK CA30/Al_2O_3 contact. Another interesting low-friction pair appeared to be PI SP1/SS because of its easily applicable and low-cost material combination.
- The lowest wear was obtained in the PEEK CA30/Al_2O_3 contact, in accordance with the lowest friction found for this material pair.
- Detailed surface analyses are in progress and comparison with more materials is planned for the future to understand the wear and friction mechanisms.

ACKNOWLEDGEMENTS
For full support of this research we are sincerely grateful to Prof. Dr. Jože Vižintin, Head of CTD.
The authors are sincerely grateful to Slovenian company Tajfun, the greatest producer of forestry machinery in Europe, for financial and technical support.
For financial support of this research we are sincerely grateful to Slovenian Research Agency.
The majority of the components of the oil test rig were donated by the leading producer of hydraulic components in Slovenia, Kladivar d.o.o. The authors are sincerely grateful for this support.

REFERENCES

[1] M. Kalin, J. Vižintin, A comparison of the tribological behaviour of steel/steel, steel/DLC and DLC/DLC contact when lubricated with mineral and biodegradable oils. Wear 261 [1] (2006) 22-31.

[2] J. Barriga, M. Kalin, K. Van Acker, K. Vercammen, A. Ortega, L. Leiaristi. Tribological performance of titanium doped and pure DLC coatings combined with a synthetic bio-lubricant. Wear 261 [1] (2006) 9-14.

[3] Kalin, M., Vižintin, J., Vercammen, K., Arnšek, A., Barriga, J., Van Acker, K. Tribological performance of lubricated DLC coatings using biodegradable oils. The coatings in Manufacturing Engineering (2004) 457-465.

[4] J. Barriga, M. Kalin, K. Van Acker, K. Vercammen, A. Ortega, L. Leiaristi. Tribological characterisation and validation of carbon based coatings combined with bio-lubricants. Proceedings of the 11th Nordic Symposium on Tribology. Norway, June 2004. Pg. 508-517.

[5] M. Kalin, F. Majdič, J. Vižintin, J. Pezdirnik. Performance of axial piston pump using DLC-coated piston shoes and biodegradable oil. in: The 12th Nordic Symposium on Tribology, Helsingor, Denmark, June 7-9, 2006. *Nordtrib 2006*. (2006), 10 Pgs.

[6] Nessie – Sauer Danfos: http://nessie.danfoss.com/

[7] Tiefenbach Wasserhyraulik GmbH: http://www.ft-tiefenbach.de/

[8] Water Hydraulics Lth: www.waterhydraulics.co.uk

[9] Hauhinco Maschinenfabrik G. Hausherr, Jochums GmbH & Co. KG: *www.hauhinco.de*

[10] E. Trostmann: *WATER HYDRAULICS CONTROL TECHNOLOGY*; Lyngby 1996, Technical University of Denmark; ISBN: 0-8247-9680-2

[11] Y. Huayong, J. Sujuan, G. Guofang, Z. Hua: *Investigation on the tribological properties of new materials and its application in water hydraulic piston pump*, SICFP'05, Linköping, Sweden, 2005

[12] J. Pezdirnik, F. Majdič, Transient Phenomena in Gradual Changes of Hydraulic Fluid Flow, 5. IFK, Aachen, 2006,

[13] J. Pezdirnik**:** Prehodni pojavi pri hidravličnih napravah v železarstvu (Transient Phenomena in Ironworks Hydraulic Systems), M. Sc. Thesis, Faculty of Mechanical Engineering, Ljubljana 1984

[14] Y. Yamamoto, T. Takashima, Friction and wear of water lubricated PEEK and PPS sliding contacts, Wear 253 (2002) 820-826.

[15] Y. Yamamoto, T. Takashima, Friction and wear of water lubricated PEEK and PPS sliding contacts Part 2. Composites with carbon or glass fibre, Wear 253 (2002) 820-826.

[16] J.P. Davim, N. Marques, A.M. Baptista, Effect of carbon fibre reinforcement in the frictional behaviour of Peek in a water lubricated environment, Wear 251 (2001) 1100-1104.